



Technical Note: Large overestimation of $p\text{CO}_2$ calculated from pH and alkalinity in acidic, organic-rich freshwaters

G. Abril^{1,2}, S. Bouillon³, F. Darchambeau⁴, C. R. Teodoru³, T. R. Marwick³, F. Tamooh³, F. Ochieng Omengo³, N. Geeraert³, L. Deirmendjian¹, P. Polensaere¹, and A. V. Borges⁴

¹Laboratoire EPOC, Environnements et Paléoenvironnements Océaniques et Continentaux, CNRS, Université de Bordeaux, France

²Programa de Geoquímica, Universidade Federal Fluminense, Niterói, Rio de Janeiro, Brazil

³Katholieke Universiteit Leuven, Department of Earth & Environmental Sciences, Leuven, Belgium

⁴Unité d'Océanographie Chimique, Université de Liège, Belgium

Correspondence to: G. Abril (g.abril@epoc.u-bordeaux1.fr)

Received: 23 June 2014 – Published in Biogeosciences Discuss.: 31 July 2014

Revised: 18 November 2014 – Accepted: 24 November 2014 – Published: 6 January 2015

Abstract. Inland waters have been recognized as a significant source of carbon dioxide (CO_2) to the atmosphere at the global scale. Fluxes of CO_2 between aquatic systems and the atmosphere are calculated from the gas transfer velocity and the water–air gradient of the partial pressure of CO_2 ($p\text{CO}_2$). Currently, direct measurements of water $p\text{CO}_2$ remain scarce in freshwaters, and most published $p\text{CO}_2$ data are calculated from temperature, pH and total alkalinity (TA). Here, we compare calculated (pH and TA) and measured (equilibrator and headspace) water $p\text{CO}_2$ in a large array of temperate and tropical freshwaters. The 761 data points cover a wide range of values for TA (0 to 14 200 $\mu\text{mol L}^{-1}$), pH (3.94 to 9.17), measured $p\text{CO}_2$ (36 to 23 000 ppmv), and dissolved organic carbon (DOC) (29 to 3970 $\mu\text{mol L}^{-1}$). Calculated $p\text{CO}_2$ were > 10 % higher than measured $p\text{CO}_2$ in 60 % of the samples (with a median overestimation of calculated $p\text{CO}_2$ compared to measured $p\text{CO}_2$ of 2560 ppmv) and were > 100 % higher in the 25 % most organic-rich and acidic samples (with a median overestimation of 9080 ppmv). We suggest these large overestimations of calculated $p\text{CO}_2$ with respect to measured $p\text{CO}_2$ are due to the combination of two cumulative effects: (1) a more significant contribution of organic acids anions to TA in waters with low carbonate alkalinity and high DOC concentrations; (2) a lower buffering capacity of the carbonate system at low pH, which increases the sensitivity of calculated $p\text{CO}_2$ to TA in acidic and organic-rich waters. No empirical relationship could be derived from our data set in order to correct calculated $p\text{CO}_2$ for this bias.

Owing to the widespread distribution of acidic, organic-rich freshwaters, we conclude that regional and global estimates of CO_2 outgassing from freshwaters based on pH and TA data only are most likely overestimated, although the magnitude of the overestimation needs further quantitative analysis. Direct measurements of $p\text{CO}_2$ are recommended in inland waters in general, and in particular in acidic, poorly buffered freshwaters.

1 Introduction

Inland waters (streams, rivers, lakes, reservoirs, wetlands) receive carbon from terrestrial landscapes, usually have a net heterotrophic metabolism, and emit significant amounts of CO_2 to the atmosphere (Kempe 1984; Cole et al., 1994; Raymond et al., 2013). This terrestrial–aquatic–atmosphere link in the global carbon cycle is controlled by complex biogeographical drivers that generate strong spatial and temporal variations in the chemical composition of freshwaters and the intensity of CO_2 outgassing at the water–air interface (e.g. Tamooh et al., 2013; Dinsmore et al., 2013; Abril et al., 2014; Borges et al., 2014). Hence, large data sets are necessary in order to describe the environmental factors controlling these CO_2 emissions and to quantify global CO_2 fluxes from inland waters (Sobek et al., 2005; Barros et al., 2011; Raymond et al., 2013). Dissolved inorganic carbon (DIC) concentration and speciation in freshwaters greatly depend

on the lithological nature of watersheds (Meybeck 1987). For instance, rivers draining watersheds rich in carbonate rocks have a high DIC concentration, generally well above $1000 \mu\text{mol L}^{-1}$. Bicarbonate ions contribute to most of the total alkalinity (TA) in these waters, which have high conductivities and high pH. In these hard waters, dissolved CO_2 represents a minor fraction (5–15 %) of the DIC compared to bicarbonates. In rivers draining organic-rich soils and non-carbonate rocks, DIC concentrations are lower (typically a few hundred $\mu\text{mol L}^{-1}$) but dissolved organic carbon (DOC) concentrations are higher, and commonly exceed the DIC concentrations. Organic acid anions significantly contribute to TA of these soft waters (Driscoll et al., 1989; Hemond 1990), which have low conductivities and low pH. Dissolved CO_2 represents a large, generally dominant, fraction of DIC in these acidic, organic-rich waters.

Fluxes of CO_2 between aquatic systems and the atmosphere can be computed from the water–air gradient of the concentration of CO_2 and the gas transfer velocity (Liss and Slater, 1974) at local (e.g. Raymond et al., 1997), regional (e.g. Teodoru et al., 2009), and global scales (e.g. Cole et al., 1994; Raymond et al., 2013). The partial pressure of CO_2 ($p\text{CO}_2$) is relatively constant in the atmosphere compared to surface freshwaters $p\text{CO}_2$ that can vary by more than 4 orders of magnitude spatially and temporally (Sobek et al., 2005; Abril et al., 2014). Consequently, water $p\text{CO}_2$ controls the intensity of the air–water flux, together with the gas transfer velocity. At present, both measured and calculated water $p\text{CO}_2$ data are used to compute CO_2 fluxes from freshwater systems, although calculated $p\text{CO}_2$ is overwhelmingly more abundant than directly measured $p\text{CO}_2$ (e.g. Cole et al., 1994; Raymond et al., 2013). $p\text{CO}_2$ can be calculated from the dissociation constants of carbonic acid (which are a function of temperature) and any of the following couples of measured variables: pH/TA, pH/DIC, DIC/TA (Park, 1969). In a majority of cases, calculated $p\text{CO}_2$ is based on the measurements of pH/TA and water temperature. These three parameters are routinely measured by many environmental agencies, and constitute a very large database available for the scientific community. Calculation of $p\text{CO}_2$ from pH and TA was initiated in world rivers in the 1970s (Kempe, 1984) and relies on the dissociation constants of carbonic acid, and the solubility of CO_2 , all of which are temperature-dependent (Harned and Scholes, 1941; Harned and Davis, 1943; Millero, 1979; Stumm and Morgan, 1996). Measured $p\text{CO}_2$ is based on water–air phase equilibration either on discrete samples (headspace technique, e.g. Weiss, 1981) or continuously (equilibrator technique, e.g. Frankignoulle et al., 2001) using various systems and devices, followed by direct, generally infrared (IR), detection of CO_2 in the equilibrated gas. Commercial IR gas analysers are becoming cheaper and more accurate, stable and compact, and provide a large range of linear response well adapted to variability of $p\text{CO}_2$ found in freshwaters.

A limited number of studies have compared directly measured $p\text{CO}_2$ to computed $p\text{CO}_2$. Earlier examples provided a comparison between $p\text{CO}_2$ measured by headspace equilibration coupled to gas chromatography (GC) and $p\text{CO}_2$ calculated from pH and DIC (Kratz et al., 1997; Raymond et al., 1997). Reports by these authors in Wisconsin lakes and the Hudson River show that the $p\text{CO}_2$ values were linearly correlated but showed a variability of ± 500 ppmv around the 1:1 line, over a range of measured $p\text{CO}_2$ from 300 to 4000 ppmv. Later, Frankignoulle and Borges (2001) reported the first comparison of $p\text{CO}_2$ calculated from pH and TA and $p\text{CO}_2$ measured by equilibration coupled to an IR analyser in an estuary in Belgium. In this high TA ($2500\text{--}4800 \mu\text{mol L}^{-1}$) and high pH (> 7.4) system, they found a good agreement between the two approaches, calculated $p\text{CO}_2$ being either overestimated or underestimated, but always by less than 7 %. In 2003, concomitant measurements of pH, TA and $p\text{CO}_2$ were performed in acidic, humic-rich (“black” type) waters of the Sinnamary River in French Guiana (Abril et al., 2005, 2006). Calculation of $p\text{CO}_2$ from pH (~ 5) and TA ($\sim 200 \mu\text{mol L}^{-1}$) gave unrealistically high values compared to those measured directly with a headspace technique (typically 30000 ppmv vs. 5000 ppmv). Direct measurements of CO_2 and CH_4 outgassing fluxes with floating chambers and the computation of the respective gas transfer velocities of these two gases (Guérin et al., 2007) confirmed that $p\text{CO}_2$ values calculated from pH and TA were overestimated compared to direct measurements in the Sinnamary River. More recently, Hunt et al. (2011) and Wang et al. (2013) provided evidence that organic acid anions in DOC may significantly contribute to TA in some rivers and generate an overestimation of calculated $p\text{CO}_2$. Butman and Raymond (2011) reported higher calculated than measured $p\text{CO}_2$ in some US streams and rivers, but no information was available on the potential role of organic acids in this overestimation. These authors concluded that the low number of samples in their study reflected the need for more research on this topic.

With the growing interest on $p\text{CO}_2$ determination in freshwaters globally, and given the apparent simplicity and low cost of pH and TA measurements, the number of publications that report calculated $p\text{CO}_2$ in freshwaters has increased dramatically in the past decade. Some of these publications report extremely high and potentially biased $p\text{CO}_2$ values in low-alkalinity and high-DOC systems. It has thus become necessary to pay attention to this issue and investigate the occurrence of such potential bias and its magnitude in the different types of freshwaters. Here, we present a large data set of concomitant measurements of temperature, pH, TA, $p\text{CO}_2$, and DOC in freshwaters. This is the first comprehensive data set to investigate the magnitude of the bias between calculated and measured $p\text{CO}_2$, as it covers the entire range of variation of most parameters of the carbonate system in freshwaters. The objective of this paper is to alert the scientific community to the occurrence of a bias in $p\text{CO}_2$

Table 1. Summary of the presented data set. Average, minimum, and maximum values of temperature, DOC, pH (measured on the NBS scale), total alkalinity (TA), and measured partial pressure of CO_2 ($p\text{CO}_2$) in the different freshwater ecosystems.

Country	Watersheds	Temperature (°C)			DOC ($\mu\text{mol L}^{-1}$)			pH (NBS scale)			TA ($\mu\text{mol L}^{-1}$)			Measured $p\text{CO}_2$ (ppmv)			N
		Av.	Min.	Max.	Av.	Min.	Max.	Av.	Min.	Max.	Av.	Min.	Max.	Av.	Min.	Max.	
Brazil	Amazon	30.3	27.4	34.3	352	118	633	6.60	4.53	7.60	385	30	1092	4204	36	18400	155
Kenya	Athi-Galana-Sabaki	25.9	19.8	36.0	307	29	1133	7.69	6.49	8.57	2290	407	5042	2811	608	10 405	44
DRC	Congo	26.3	22.6	28.2	1002	149	3968	6.01	3.94	7.22	212	0	576	6093	1582	15 571	97
DRC/Rwanda	Lake Kivu	24.0	23.0	24.7	162	142	201	9.05	8.99	9.17	13 037	12 802	13 338	660	537	772	53
France	Leyre	12.5	7.9	19.2	588	142	3625	6.20	4.40	7.41	280	38	1082	4429	901	23 047	92
France	Loire	15.5	8.8	19.3	195	167	233	8.70	8.07	9.14	1768	1579	1886	284	65	717	18
Belgium	Meuse	18.1	13.3	25.9	229	102	404	7.89	6.95	8.59	2769	360	7141	2292	176	10 033	50
Madagascar	Rianila and Betsiboka	25.4	20.2	29.5	138	33	361	6.84	5.83	7.62	233	76	961	1701	508	3847	36
Kenya	Shimba Hills	25.1	21.9	31.8	214	36	548	7.37	6.22	8.93	1989	227	14 244	2751	546	9497	9
French Guiana	Sinnamary	27.1	24.1	28.7	419	213	596	5.50	5.08	6.30	143	66	290	7770	1358	15 622	49
Kenya	Tana	26.6	25.0	27.9	321	193	651	7.65	7.32	8.02	1619	1338	2009	2700	845	6014	51
Zambia/Mozambique	Zambezi	26.9	18.8	31.8	252	103	492	7.59	5.06	9.08	1245	52	3134	2695	151	14 004	107
Entire data set		24.6	7.9	36.0	408	29	3968	7.00	3.94	9.17	1731	0	14 244	3707	36	23 047	761

calculation from pH and TA in acidic, poorly buffered and organic-rich freshwaters, to briefly discuss its origin in terms of water chemistry, and to provide the range of pH, TA, and DOC values where $p\text{CO}_2$ calculation should be abandoned and the range where it still gives relatively accurate results.

2 Material and methods

2.1 Sample collection

Our data set consists of 761 concomitant measurements of temperature, pH, TA, water $p\text{CO}_2$, and DOC in 12 contrasting tropical and temperate systems in Europe, Amazonia, and Africa (Fig. 1; Table 1). These samples were obtained in the Central Amazon River and floodplains system in Brazil, the Athi-Galana-Sabaki River in Kenya, the Tana River (Kenya), small rivers draining the Shimba Hills in southeastern Kenya, the Congo River and tributaries in the Democratic Republic of the Congo (DRC), Lake Kivu in Rwanda and DRC, the Leyre River and tributaries in France, the Loire River in France, the Meuse River in Belgium, the Rianila and Betsiboka rivers in Madagascar, the Sinnamary River downstream of the Petit Saut Reservoir in French Guiana, and the Zambezi River in Zambia and Mozambique (Fig. 1). Details on some of the sampling sites can be found in Abril et al. (2005, 2014), Borges et al. (2012, 2014), Marwick et al. (2014a, b), Polsenaere et al. (2013), Tamooch et al. (2013), Teodoru et al. (2014). These watersheds span a range of climates and are occupied by different types of land cover, which include tropical rainforest (Amazon, Congo, Rianila), dry savannah (Tana, Athi-Galana-Sabaki, Betsiboka, Zambezi), temperate pine forest growing on podzols (Leyre), mixed temperate forest, grassland, and cropland (Meuse), and cropland (Loire). Lithology is also extremely contrasted as it includes for instance carbonate-rocks-dominated watershed as for the Meuse, sandstone-dominated silicates (Leyre), and precambrian crystalline magmatic and metamorphic rocks

with a small proportion of carbonate and evaporite rocks for the Congo river.

2.2 Field and laboratory measurements

Although pH measurements might seem almost trivial, highly accurate and precise pH data are in fact not easy to obtain, especially in low-ionic strength waters, where electrode readings are generally less stable. Even though pH measurements in the laboratory might be more accurate, it is crucial to measure pH in situ or immediately after sampling, as pH determination several hours or days after sampling will be affected by CO_2 degassing and/or microbial respiration (Frankignoulle and Borges, 2001). In this work, water temperature and pH were measured in the field with different probes depending on the origin of the data set. However, all the pH data were obtained with glass electrodes and rely on daily calibration with two-point United States National Bureau of Standards (NBS) standards (4 and 7). Measurements were performed directly in the surface water, or in collected water immediately after sampling.

Several techniques were used to measure water $p\text{CO}_2$. Water–gas equilibration was performed with a marbles-type equilibrator (Frankignoulle et al., 2001) for the Amazon, Loire, Leyre, Sinnamary, and Congo rivers (December 2013) as well for Lake Kivu, or with a Liqui-Cel MiniModule membrane contactor equilibrator (see Teodoru et al., 2009, 2014) for the Zambezi and some sites within the Congo basin (December 2012): water was pumped either continuously from a ship, or on an ad hoc basis from the bank of the rivers after waiting ~ 15 min for complete equilibration; air was continuously pumped from the equilibrator to the gas analyser (see e.g. Abril et al., 2014 for a more detailed description of the system). A syringe-headspace technique (Kratz et al., 1997; Teodoru et al., 2009) was used in the field in all African rivers and in the Meuse River: 30 mL volume of atmospheric air was equilibrated with 30 mL volume of river water by vigorously shaking during 5–10 min in four

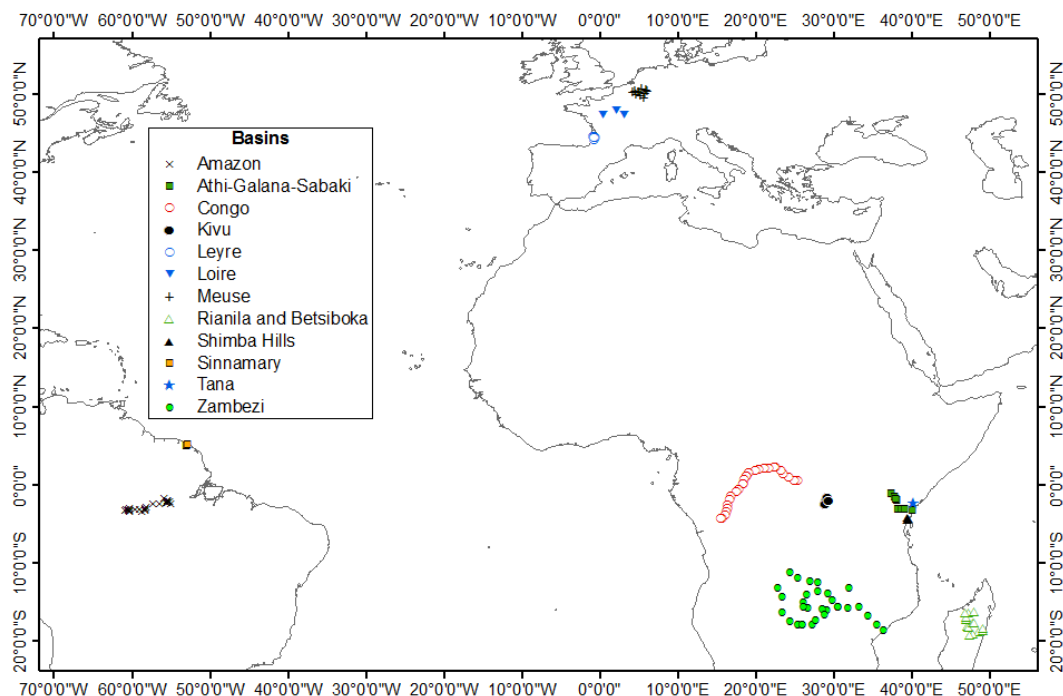


Figure 1. Location of the sampling sites in Africa, Amazonia, and Europe.

replicate gas-tight syringes. The four replicates 30 mL of equilibrated gas and a sample of atmospheric air were injected in an IR gas analyser (Li-Cor[®] models 820 or 840, or PP systems[®] model EGM-4); the first gas injection served as a purge for the air circuit and cell and the three other injections were used as triplicate $p\text{CO}_2$ determination (average repeatability of $\pm 1\%$). The $p\text{CO}_2$ in the river water was deduced from that measured in the headspace accounting for the initial $p\text{CO}_2$ in the air used for equilibration, water temperature in the river and in the water at equilibrium in the syringe, and based on Henry's law. Comparison between syringe-headspace and marbles or membrane equilibrators was made during two cruises on the Congo River and three cruises in the Zambezi basin and gave very consistent results, deviation from the 1 : 1 line being always less than 15% (see Fig. 2). This highlights the consistency of the present data set of direct $p\text{CO}_2$ measurements although different techniques were used. A serum bottle-headspace technique (Hope et al., 1995) was also used on the Sinnamary River; surface water was sampled in 120 mL serum bottles that were poisoned with HgCl_2 and sealed excluding air bubbles. Back in the laboratory, a 40 mL headspace was created with pure N_2 (Abril et al., 2005). The CO_2 concentration of equilibrated gas in the headspace was analysed by injecting small volumes (0.5 mL) of gas in a gas chromatograph calibrated with certified gas mixtures.

Immediately after water–gas phase equilibration, CO_2 was detected and quantified in most samples with non-dispersive IR gas analysers (Frankignoulle et al., 2001; Abril et al.,

2014). The gas analysers were calibrated before each field cruise, with air circulating through soda lime or pure N_2 for zero and with a certified gas standard for the span. Depending on the cruises and expected $p\text{CO}_2$ ranges, we used gas standard concentration of 1000–2000 ppmv, or a set of calibration gases at 400, 800, 4000 and 8000 ppmv. Stability of the instrument was checked after the cruise, and deviation of the signal was always less than 5%. These instruments offer a large range of linear response, depending on manufacturer and model: 0–20 000 ppmv or 0–60 000 ppmv. The linearity of an Li-COR[®] Li-820 gas analyser was verified by connecting it to a closed circuit of gas equipped with a rubber septum to allow injection of pure CO_2 with a syringe. Linearity was checked by injecting increasing volumes of CO_2 in order to cover the whole range of measurement and was excellent between zero and ~ 20000 ppmv. In addition to the IR analysers generally used in this work, in the Sinnamary River, $p\text{CO}_2$ was also measured with an INNOVA[®] 1312 optical filter IR photoacoustic gas analyser (range 0–25 000 ppmv) connected to an equilibrator and with a Hewlett Packard[®] 5890 gas chromatograph equipped with a thermal conductivity detector (TCD); both analysers were calibrated with a gas mixture of 5000 ppmv of CO_2 . Both methods gave results consistent at $\pm 15\%$ in the 0–13 000 ppmv range (Abril et al., 2006). Sinnamary data reported here are from headspace and GC determination.

TA was analysed by automated electro-titration on 50 mL filtered samples with 0.1N HCl as titrant. Equivalence point was determined with a Gran method from pH between 4

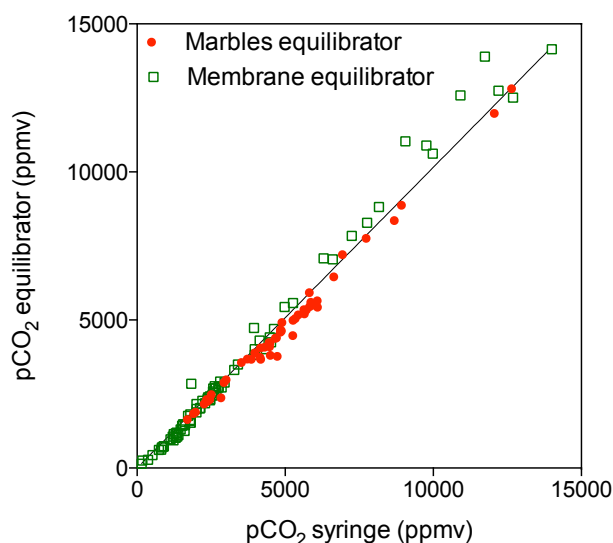


Figure 2. Comparison of results of different water–air equilibration designs for direct $p\text{CO}_2$ measurements; $p\text{CO}_2$ measured with a marbles equilibrator (Congo) and with a membrane equilibrator (Congo and Zambezi) are plotted against $p\text{CO}_2$ measured with a syringe headspace technique. Detection was made with an IR gas analyser.

and 3 (Gran, 1952). Precision based on replicate analyses was better than $\pm 5 \mu\text{mol L}^{-1}$. TA measurements should be done on filtered samples; otherwise some overestimation would occur in turbid samples, which may contain significant amounts of acid-neutralizing particles (e.g. calcium carbonate). In contrast to TA measurements based on titration to an endpoint of 5.6 (e.g. Wallin et al., 2014), the Gran titration method allows the determination of TA values in samples with in situ pH down to ~ 4.5 , i.e. very close to the dissociation constant of $\text{HCO}_3^- / \text{H}_2\text{CO}_3$. In most acidic samples with low TA, reproducibility was improved by slightly increasing the pH by up to 0.2 units by vigorously stirring during ~ 15 min in order to degas as much CO_2 as possible before starting the titration. DOC was measured on samples filtered through pre-combusted (490°C) glass fibre filter with a porosity of $0.7 \mu\text{m}$ and stored acidified with ultra-pure H_3PO_4 in borosilicate vials capped with polytetrafluoroethylene stoppers. Analysis was performed with a Shimadzu TOC5000 analyser based on high-temperature catalytic oxidation, after removal of dissolved CO_2 for samples from Amazon, Loire, Leyre, and Sinnamary rivers. DOC concentrations were measured with a customized wet oxidation TOC analyser (Thermo HiperTOC, or IO Analytical Aurora 1030W) coupled to a Delta+XL or Delta V IRMS.

2.3 $p\text{CO}_2$ calculation from pH and TA

We calculated $p\text{CO}_2$ from TA, pH, and temperature measurements using carbonic acid dissociation constants of Millero (1979) (based on those of Harned and Scholes, 1941

and Harned and Davis, 1943) and the CO_2 solubility from Weiss (1974) as implemented in the CO2SYS program. Hunt et al. (2011) reported discrepancy lower than 2 % for $p\text{CO}_2$ computed this way with those obtained with the PHREEQC program (Parkhurst and Appelo, 1999). Differences in software or dissociation constants cannot account for the large bias in calculated $p\text{CO}_2$ compared to measured $p\text{CO}_2$ we report in this paper.

3 Results

3.1 Data ranges and patterns in the entire data set

Measured $p\text{CO}_2$ varied between 36 ppmv in a floodplain of the Amazon River and 23 000 ppmv in a first-order stream of the Leyre River (Table 1). Minimum values of pH and TA occurred in the Congo River (pH=3.94 and TA=0) and maximum values in Lake Kivu (pH=9.16 and TA=14200 $\mu\text{mol L}^{-1}$). Highest DOC concentrations ($> 3000 \mu\text{mol L}^{-1}$) were observed in small streams in the Congo basin and in first-order streams draining podzolized soils in the Leyre basin. Lowest DOC concentrations ($< 40 \mu\text{mol L}^{-1}$) occurred in some tributaries of the Athi-Galana-Sabaki, in the Rianila and Betsiboka rivers, and in the Shimba Hills streams. When considering the whole data set, measured $p\text{CO}_2$ and DOC were negatively correlated with pH, whereas TA was positively correlated with pH (Fig. 3, $p < 0.0001$ for the three variables). This illustrates the large contrast in acid–base properties between acidic, organic-rich, and poorly buffered samples on one hand, and basic, carbonate-buffered samples on the other.

3.2 Comparison between measured and calculated $p\text{CO}_2$

Calculated $p\text{CO}_2$ was more than 10 % lower than measured $p\text{CO}_2$ in 16 % of the samples; the two methods were consistent at ± 10 % in 24 % of the samples; calculated $p\text{CO}_2$ was more than 10 % higher than measured $p\text{CO}_2$ in 60 % of the samples and more than 100 % higher in 26 % of the samples. Absolute values, as expressed in ppmv, were largely shifted towards overestimation, calculated vs. measured $p\text{CO}_2$ data being well above the 1 : 1 line, and calculated minus measured $p\text{CO}_2$ values ranging between -6180 and $+882\,022$ ppmv (Fig. 4). The largest overestimation of calculated $p\text{CO}_2$ occurred in the most acidic samples, whereas underestimations of calculated $p\text{CO}_2$ occurred in neutral or slightly basic samples (Fig. 4b). Ranking the data according to the pH, TA and DOC reveals that overestimation of calculated $p\text{CO}_2$ compared to measured $p\text{CO}_2$ increased in acidic, poorly buffered waters in parallel with an increase in the DOC concentration (Table 2). Discrepancies between calculated and measured $p\text{CO}_2$ were very different from one system to another, depending on the chemical status of the waters. On average at each sampled site, the

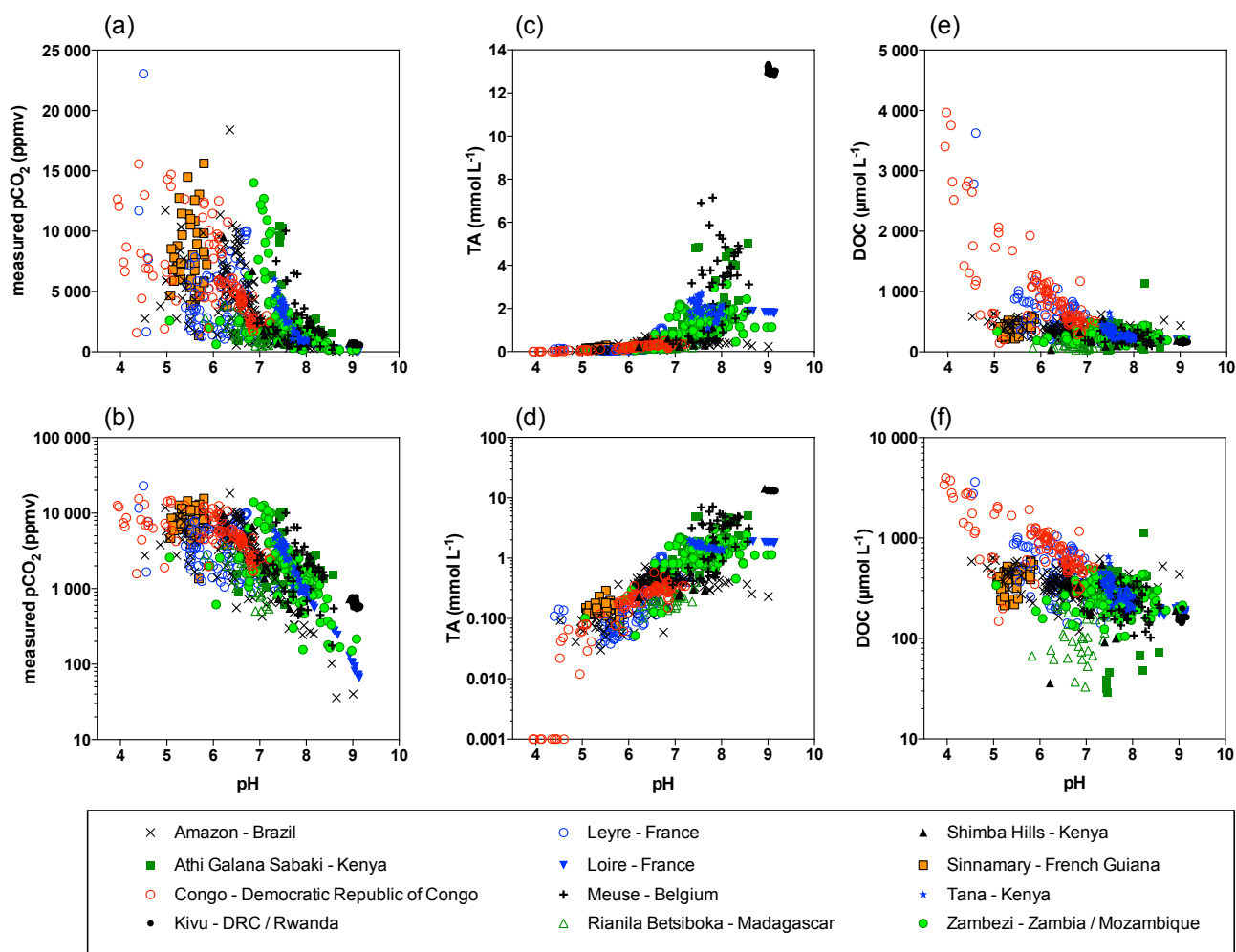


Figure 3. Plot of carbon variables vs. pH in the studied freshwater systems. Top panels are shown with a linear scale and bottom panels with a logarithmic scale; (a, b): measured $p\text{CO}_2$; (c, d) total alkalinity; (e, f) DOC. Zero TA values are plotted as 0.001 in order to be visible on the log $p\text{CO}_2$ scale. Rianila and Betsiboka are plotted together although they belong to different watersheds in Madagascar.

relative overestimation of calculated $p\text{CO}_2$ decreased with pH and TA and increased with DOC (Fig. 5). Overestimation of calculated $p\text{CO}_2$ was on average $< 10\%$ in the Kivu Lake, and the Meuse, Loire, Shimba Hills and Tana rivers, which all have neutral or basic pH, $\text{TA} > 1000 \mu\text{mol L}^{-1}$ and low to moderate DOC concentrations ($< 400 \mu\text{mol L}^{-1}$) (Fig. 5). In contrast, calculated $p\text{CO}_2$ was overestimated by $> 200\%$ on average in the Congo, Leyre, Sinnamary and Amazon rivers, which have acidic pH, $\text{TA} < 500 \mu\text{mol L}^{-1}$ and highest DOC concentration, reaching $1000 \mu\text{mol L}^{-1}$ on average in the Congo. The cases of Athi-Galana-Sabaki, Rianila, Betsiboka, and Zambezi rivers were intermediate in pH, TA and DOC, and with average overestimations of calculated $p\text{CO}_2$ of 50–90% (Fig. 5).

4 Discussion

4.1 Origin of overestimation of calculated $p\text{CO}_2$

Our data set (Fig. 3; Table 1) probably covers the full range of conditions of carbon speciation that can be encountered in continental surface waters. A $p\text{CO}_2$ overestimation negatively correlated with pH ($p = 0.001$) and TA ($p = 0.005$) and positively correlated with DOC ($p < 0.001$) (Fig. 5) is consistent with the observations of Cai et al. (1998) in the freshwater end-members of some estuaries in Georgia, USA, and of Hunt et al. (2011) in rivers in New England (USA) and New Brunswick (Canada). These authors performed NaOH back-titration in order to measure non-carbonate alkalinity (NCA). They found that NCA accounted for a large fraction (in some cases the greater part) of TA; in addition, the contribution of inorganic species other than carbonate was assumed negligible and most of the NCA was attributed to organic

Table 2. Median and average values of DOC, pH (measured on the NBS scale), total alkalinity (TA), and calculated minus measured $p\text{CO}_2$ in the data set.

	N	% of samples	cal – meas $p\text{CO}_2$ (ppmv)		cal – meas $p\text{CO}_2$ (% of meas $p\text{CO}_2$)		pH		TA ($\mu\text{mol L}^{-1}$)		DOC ($\mu\text{mol L}^{-1}$)	
			Med.	Av.	Med.	Av.	Med.	Av.	Med.	Av.	Med.	Av.
All samples	761	100 %	+611	+10692	+23%	+194%	6.94	7.00	467	1731	315	408
Ranked by calculated – measured $p\text{CO}_2$ as % of measured $p\text{CO}_2$												
< -10 %	122	16 %	-540	-890	-34 %	-36 %	7.89	7.85	1269	1766	259	275
± 10 %	174	23 %	+15	+50	+2%	+1%	7.67	7.78	1576	3735	228	273
> +10 %	465	61 %	+2430	+17710	+72%	+327%	6.52	6.49	308	972	360	497
> +50 %	280	37 %	+5490	+28660	+162%	+526%	6.18	6.14	192	460	375	567
> +100 %	199	26 %	+9080	+39120	+270%	+710%	5.89	5.96	166	364	389	602
Ranked by pH												
pH > 7	368	48 %	+1	+82	+1%	+15%	7.82	7.92	1572	3284	231	255
pH < 7	393	52 %	+3280	+20630	+71%	+362%	6.30	6.13	232	277	413	558
pH 6–7	256	34 %	+1580	+2710	+40%	+96%	6.58	6.55	334	370	350	427
pH < 6	136	18 %	+18410	+54486	+308%	+864%	5.50	5.35	93	101	487	828
pH < 5	25	3 %	+115580	+209910	+1645%	+3180%	4.53	4.53	41	45	1427	1,843
Ranked by TA												
TA > 2000 $\mu\text{mol L}^{-1}$	110	14 %	+20	+340	+2%	+12%	8.58	8.47	7023	8326	163	202
TA 1000–2000 $\mu\text{mol L}^{-1}$	157	21 %	-8	-163	-2 %	-9 %	7.81	7.83	1566	1534	271	295
TA 500–1000 $\mu\text{mol L}^{-1}$	99	13 %	+1307	+1900	+28%	+72%	6.97	7.11	651	697	304	318
TA < 500 $\mu\text{mol L}^{-1}$	395	52 %	+2070	+20090	+64%	+350%	6.30	6.24	222	232	400	538
TA < 100 $\mu\text{mol L}^{-1}$	82	11 %	+6840	+60560	+230%	+1040%	5.50	5.35	59	56	603	988
Ranked by DOC												
DOC < 200 $\mu\text{mol L}^{-1}$	179	24 %	+40	+776	+5%	+62%	7.89	7.92	1579	4807	163	149
DOC 200–300 $\mu\text{mol L}^{-1}$	167	22 %	+102	+2755	+5%	+69%	7.56	7.37	1132	1259	258	252
DOC 300–400 $\mu\text{mol L}^{-1}$	165	22 %	+887	+4473	+25%	+101%	6.90	6.93	499	866	341	344
DOC > 400 $\mu\text{mol L}^{-1}$	250	33 %	+3070	+27197	+59%	+434%	6.15	6.14	200	415	555	765
DOC > 800 $\mu\text{mol L}^{-1}$	79	10 %	+4995	+62784	+92%	+886%	5.80	5.62	94	180	1099	1438

acid anions. Hunt et al. (2011) also showed that in the absence of direct titration of NCA, which is labour-intensive and whose precision may be poor, this parameter could be calculated as the difference between the measured TA and the alkalinity calculated from measurements of pH and DIC and the dissociation constants of carbonic acid. Using the latter approach, Wang et al. (2013) obtained a positive correlation between NCA and DOC concentrations in the Congo River, evidencing the predominant role of organic acids in DIC speciation and pH in such acidic system. Because we did not directly measure DIC in this study, we could not calculate NCA with the same procedure as these studies. We attempted to calculate TA from our measured pH and $p\text{CO}_2$ with the CO2SYS program. However, TA values calculated this way were inconsistent with other measured variables (with sometimes negative values). Indeed, because pH and $p\text{CO}_2$ are too interdependent in the carbonate system, very small analytical errors on these variables lead to large uncertainties in the calculated TA (Cullison Gray et al., 2011). A second attempt to correct our TA data from NCA consisted in calculating organic alkalinity using pH and DOC as input parameters.

We compared the model of Driscoll et al. (1989), which assumes a single pK value for all organic acids, and the triprotic model of Hruska et al. (2003), which assumes three apparent pK values for organic acids. These two models applied to our pH and DOC gave very similar organic alkalinity values, which could be subtracted from the measured TA. In the most acidic samples (e.g. some sites from the Congo basin), modelled organic alkalinity values were larger than measured TA and the difference was thus negative. Nevertheless, we then recalculated $p\text{CO}_2$ from the measured pH and the TA corrected from organic alkalinity. Calculated $p\text{CO}_2$ values corrected with that method were, however, still very different from those measured in the field, being sometimes higher and sometimes lower than the measured $p\text{CO}_2$, without any meaningful pattern (indeed, corrected $p\text{CO}_2$ was negatively correlated ($p < 0.001$) with measured $p\text{CO}_2$). Consequently, we were unable to derive any empirical relationship to correct for the bias in $p\text{CO}_2$ calculation from pH and TA. Nevertheless, the negative correlation between pH and DOC and positive correlation between pH and TA (Fig. 3) confirm a

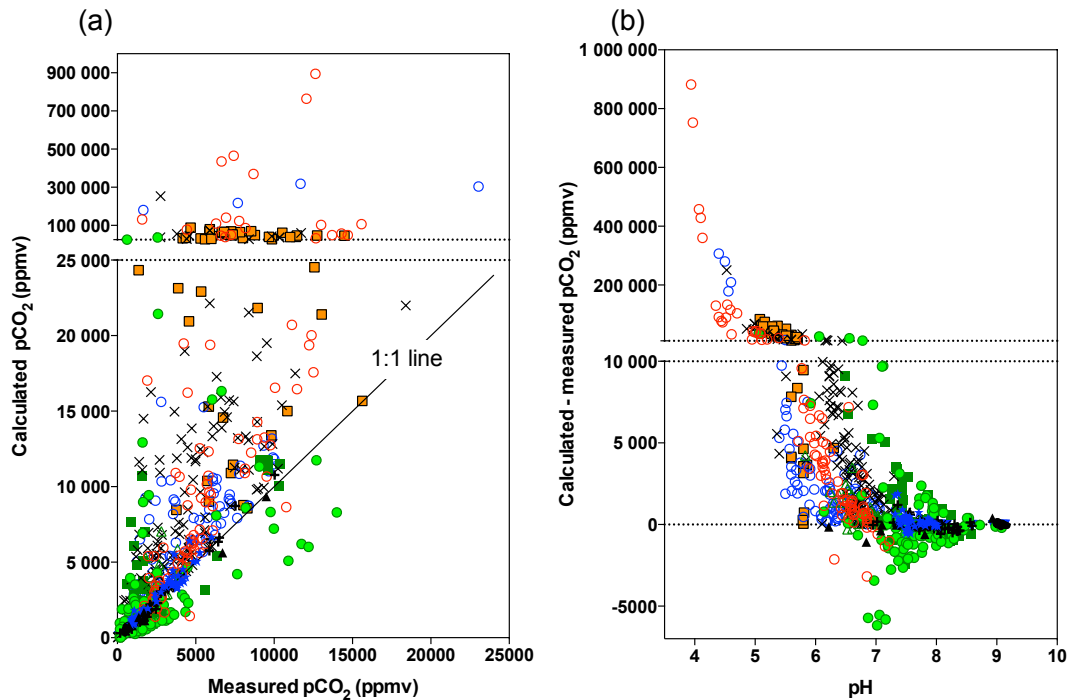


Figure 4. Comparison between measured and calculated $p\text{CO}_2$ for the whole data set: (a) calculated vs. measured $p\text{CO}_2$, the line shows when measured $p\text{CO}_2$ equals calculated $p\text{CO}_2$; (b) the difference between calculated and measured $p\text{CO}_2$ as a function of pH; same symbols as in Fig. 3.

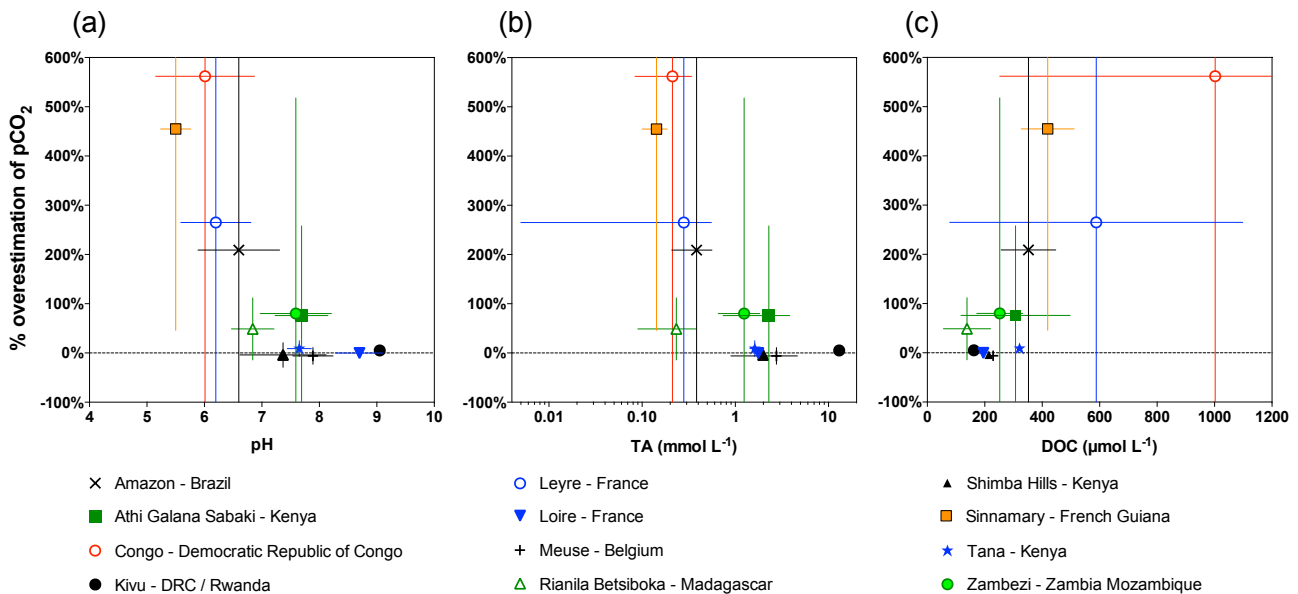


Figure 5. Average percentages of $p\text{CO}_2$ overestimation, calculated as $100 \times (\text{calculated } p\text{CO}_2 - \text{measured } p\text{CO}_2) / \text{measured } p\text{CO}_2$, as a function of (a) pH, (b) TA, and (c) DOC, for the 12 studied sites. Error bars indicate the standard deviation from the mean for each freshwater system.

strong control of organic acids on pH and DIC speciation across the entire data set.

As discussed by Hunt et al. (2011), a significant contribution of organic acids to TA leads to an overestimation of cal-

culated $p\text{CO}_2$ with the CO2SYS program, or with any program that accounts only for the inorganic species that contribute to TA. It is thus obvious that the observed increase in $p\text{CO}_2$ overestimation when pH decreases (Figs. 4b and

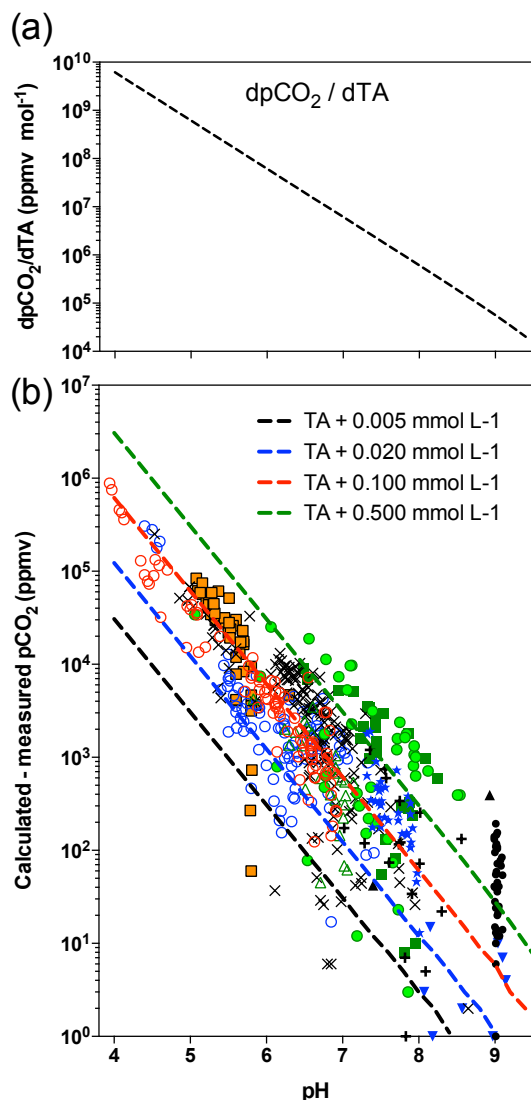


Figure 6. Sensitivity of $p\text{CO}_2$ overestimation to pH: (a) theoretical factor $dp\text{CO}_2/d\text{TA}$, which describes the sensitivity of calculated $p\text{CO}_2$ to the TA value; (b) the solid lines show the increase in calculated $p\text{CO}_2$ induced by various increases in TA, as functions of pH; these lines mimic the overestimation of calculated $p\text{CO}_2$ generated by increasing contributions of organic alkalinity to the TA; field data (as calculated – measured $p\text{CO}_2$) have been plotted for comparison; same symbols as in Fig. 3. Note that negative values do not appear in the logarithmic scale.

5; Table 2) is due to an increasing contribution of organic acid anions to TA. However, this effect is not the only driver of the observed overestimation of $p\text{CO}_2$, which is also due to a decrease in the buffering capacity of the carbonate system at acidic pH. To investigate the magnitude of this second effect, we calculated the factor $dp\text{CO}_2/d\text{TA}$ (in ppmv mol^{-1}), which describes the change in calculated $p\text{CO}_2$ induced by a change in TA. This factor, which is the opposite of a buffer factor as it reflects the sensitivity of $p\text{CO}_2$

calculation to the TA, increases exponentially when pH decreases (Fig. 6a), i.e. it is proportional to the H^+ concentration. To go further in this theoretical analysis, we computed the difference between the $p\text{CO}_2$ calculated at a given TA value and the one calculated at a slightly higher TA value ($\text{TA} + X \mu\text{mol L}^{-1}$). These calculations reveal an extreme sensitivity of calculated $p\text{CO}_2$ to TA at acidic pH (Fig. 6b). For instance, increasing TA by $5 \mu\text{mol L}^{-1}$ (a value close to the precision of TA titrations) increases the calculated $p\text{CO}_2$ by 31 ppmv at pH 7, by 307 ppmv at pH 6 and by 3070 at pH 5. Increasing TA by $100 \mu\text{mol L}^{-1}$ (a typical value of NCA found in freshwaters; Driscoll et al., 1994; Cai et al., 1998; Hunt et al., 2011), increases the calculated $p\text{CO}_2$ by 615 ppmv at pH 7, by 6156 ppmv at pH 6 and by 61560 ppmv at pH 5. Note that this increase in calculated $p\text{CO}_2$ is independent of the chosen initial TA value. The difference between calculated and measured $p\text{CO}_2$ from our data set shows that an NCA contribution around $100 \mu\text{mol L}^{-1}$ is sufficient to explain the overestimation of calculated $p\text{CO}_2$ of most samples at $\text{pH} < 6$, whereas an NCA contribution higher than $500 \mu\text{mol L}^{-1}$ would be necessary for several samples at circumneutral and slightly basic pH (Fig. 5b). Samples requiring this high NCA contribution are from the Athi-Galana-Sabaki and Zambezi watersheds, and correspond to TA values well above $1000 \mu\text{mol L}^{-1}$. An NCA value of $500 \mu\text{mol L}^{-1}$ in these samples is thus plausible.

We have no definitive explanation for lower calculated than measured $p\text{CO}_2$, which is observed mainly at neutral to slightly basic pH, for example in the Zambezi River (Fig. 4). In most of these samples, owing to the relatively high TA value, an overestimation of pH of less than 0.2 units is sufficient to account for the low calculated $p\text{CO}_2$ compared to measured values. In general, it is not easy to judge the accuracy of pH measurements, especially when data come from environmental agencies. Thus, one factor of variability throughout the data set as well as in literature data is the accuracy of pH measurements – despite the care taken (e.g. calibrations with NBS buffers for each day of measurements), we cannot rule out that drift or malfunction of pH electrodes contributes to the observed variability, constituting an additional disadvantage compared to direct $p\text{CO}_2$ measurements with very stable gas analysers.

4.2 Impact on estimates of CO_2 emissions from freshwaters

According to our analysis, overestimation of calculated $p\text{CO}_2$ is largest in acidic, poorly buffered and organic-rich waters. Consequently, the overestimation of regional and global CO_2 emissions computed from calculated $p\text{CO}_2$ depends on the relative contribution of these types of waters worldwide. In their analysis, Raymond et al. (2013) have discarded all calculated $p\text{CO}_2$ values with a pH value of less than 5.4, as well as all $p\text{CO}_2$ values above 100 000 ppmv . These criteria would exclude only 8 % of samples from our

data set. Indeed, from our analysis, it appears that overestimation of calculated $p\text{CO}_2$ occurs at pH much higher than 5.4 (Figs. 4, 5 and 6; Table 2). The two techniques were consistent at $\pm 10\%$ on average in only 5 of the 12 studied systems, which combine a circumneutral to basic pH with a TA concentration well above $1000\ \mu\text{mol L}^{-1}$ (Fig. 5). Although it would not be sufficient for the cases of the Zambezi and Athi-Galana-Sabaki rivers, where overestimation is still significant, a TA value above $1000\ \mu\text{mol L}^{-1}$ appears as a more robust criterion than a pH threshold to separate calculated $p\text{CO}_2$ values affected by bias from those consistent with measured $p\text{CO}_2$ (Table 2). In fact, $p\text{CO}_2$ calculation from pH and TA in freshwaters historically relies on theoretical background and validation data in high-alkalinity waters (Neal et al., 1998), including karstic waters (Kempe, 1975). At the global scale, high TA typically occurs in rivers draining watersheds with a significant proportion of carbonate rocks, typically $> 30\%$ of their surface area if the criterion of $\text{TA} > 1000\ \mu\text{mol L}^{-1}$ is chosen and the normalized weathering rates of Meybeck (1987) are applied. According to Meybeck (1987), the average and discharge-weighted TA is around $900\ \mu\text{mol L}^{-1}$ for world rivers and around $600\ \mu\text{mol L}^{-1}$ for tropical rivers. Among the 25 largest rivers in the world, 15 have a $\text{TA} > 1000\ \mu\text{mol L}^{-1}$ according to Cai et al. (2008). The two largest rivers in the world in terms of discharge, the Amazon and the Congo, are also well below this limit of $1000\ \mu\text{mol L}^{-1}$ and have large overestimation in calculated $p\text{CO}_2$ (on average 200 and 360%, respectively). Very low TA and pH and high DOC values have also been reported in boreal streams and rivers (Humborg et al., 2010; Dinsmore et al., 2012; Wallin et al., 2014).

In lakes, the highest $p\text{CO}_2$ values in the literature come from tropical black water lakes and were also calculated rather than directly measured (Sobek et al., 2005). Calculated $p\text{CO}_2$ was 65 250 ppmv in Lago Tupé in the Brazilian Amazon, a Ria lake connected to the Rio Negro, where, according to our own data set, pH is below 5 and TA is around $70\ \mu\text{mol L}^{-1}$. It was 18 950 ppmv in Kambanain Lake in Papua New Guinea, corresponding to a pH value of 6.1 and a TA value of $350\ \mu\text{mol L}^{-1}$ (Vyverman, 1994). This suggests a widespread overestimation of calculated $p\text{CO}_2$ that significantly impacts the estimation of global CO_2 emissions from inland waters. However, a precise analysis based on exact quantitative information on the relative contribution of acidic and high- and low-alkalinity waters to the total surface area of inland waters is necessary in order to evaluate the exact magnitude of the overestimation.

5 Conclusions

From our analysis, it appears that the validity of calculating $p\text{CO}_2$ from pH, TA and temperature is most robust in freshwaters with circumneutral to basic pH and with TA exceeding $1000\ \mu\text{mol L}^{-1}$. At lower TA and pH, however, cal-

culated $p\text{CO}_2$ (and hence, CO_2 degassing rates) are overestimated by 50 to 300% relative to direct, in situ $p\text{CO}_2$ measurements. Since a large majority of freshwater systems globally have characteristics outside the range of applicability of $p\text{CO}_2$ calculation, it appears reasonable to assume that recent estimates of global CO_2 emission from lakes and rivers, which are based exclusively on calculated $p\text{CO}_2$ data, are too high. We propose that while TA and pH measurements remain useful to describe the aquatic chemistry, data on $p\text{CO}_2$ should in the future rely on direct measurements of $p\text{CO}_2$. Even if some studies report relatively robust calculation of $p\text{CO}_2$ from pH and DIC measurements (Raymond et al., 1997; Kratz et al., 1997; Aberg and Wallin, 2014), direct $p\text{CO}_2$ values in the field are stable, precise and straightforward and do not depend on the quality of pH measurements, which are often uncertain. Further, high-quality DIC measurements are very time-consuming, fairly complicated to set up and do not allow continuous measurements to be carried out in a simple and straightforward fashion. Although there are some practical limitations to their use in the field, submerged IR sensors, which allow high temporal resolution, are also promising (Johnson et al., 2010). Long-term instrument stability and accuracy based on newly developed off-axis integrated cavity output spectroscopy and cavity ring-down spectroscopy technologies seem to improve in comparison to traditional IR instruments, although the latter are more affordable, more compact and have lower power requirements. Joint international efforts are necessary to define the most appropriate protocols for the measurement of DIC parameters in freshwaters.

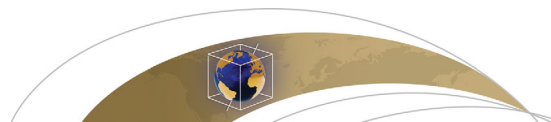
Acknowledgements. The data set used in this study was collected in the framework of projects funded by the Cluster of Excellence COTE at the Université de Bordeaux (ANR-10-LABX-45, CNP-Leyre project), the European Research Council (ERC-StG 240002, AFRIVAL: African river basins: Catchment-scale carbon fluxes and transformations, <http://ees.kuleuven.be/project/afriaval/>), the Fonds National de la Recherche Scientifique (FNRS, CAKI, 2.4.598.07, TransCongo, 14711103), the French national agency for research (ANR 08-BLAN-0221, CARBAMA project <http://carbama.epoc.u-bordeaux1.fr/>), the Research Foundation Flanders (FWO-Vlaanderen), the Belgian Federal Science Policy (BELSPO-SSD projects COBAFISH and EAGLES), the Research Council of the KU Leuven, and the Institut de Radioprotection et Sûreté Nucléaire, France (FLORE project). We thank the Hydreco Laboratory in French Guiana, and Patrick Albéric (ISTO Orléans) who analysed some of the data reported here, Aurore Beulen (ULg) for collection of Meuse data set, Marc-Vincent Commarieu (ULg) for analytical support, two anonymous reviewers and C. W. Hunt (reviewer) for constructive comments on the previous version of the paper. AVB is a senior research associate at the FNRS.

Edited by: J. Middelburg

References

- Åberg, J. and Wallin M. B.: Evaluating a fast headspace method for measuring DIC and subsequent calculation of $p\text{CO}_2$ in freshwater systems, *Inland Wat.*, 4, 157–166, 2014.
- Abril, G., Guérin, F., Richard, S., Delmas, R., Galy-Lacaux, C., Gosse, P., Tremblay, A., Varfalvy, L., Dos Santos, M. A., and Matvienko, B.: Carbon dioxide and methane emissions and the carbon budget of a 10-year old tropical reservoir (Petit-Saut, French Guiana), *Global Biogeochem. Cy.*, 19, GB4007, doi:10.1029/2005GB002457, 2005.
- Abril, G., Richard, S., and Guérin, F.: In-Situ measurements of dissolved gases (CO_2 and CH_4) in a wide range of concentrations in a tropical reservoir using an equilibrator, *Sc. Total Envir.*, 354, 246–251, 2006.
- Abril, G., Martinez, J.-M., Artigas, L. F., Moreira-Turcq, P., Benedetti, M. F., Vidal L., Meziane, T., Kim, J.-H., Bernardes, M. C., Savoye, N., Deborde, J., Albéric, P., Souza, M. F. L., Souza, E. L., and Roland, F.: Amazon River Carbon Dioxide Outgassing fuelled by Wetlands, *Nature*, 505, 395–398, 2014.
- Barros, N., Cole, J. J., Tranvik L. J., Prairie Y. T., Bastviken D., Huszar V. L. M., del Giorgio P., and Roland F.: Carbon emission from hydroelectric reservoirs linked to reservoir age and latitude, *Nat. Geosci.*, 4, 593–596, doi:10.1038/NNGEO1211, 2011.
- Borges, A. V., Bouillon, S., Abril, G., Delille, B., Poirier, D., Commarieu, M.-V., Lepoint, G., Morana, C., Servais, P., Descy, J.-P., and Darchambeau, F.: Variability of carbon dioxide and methane in the epilimnion of Lake Kivu, in: *Lake Kivu: Limnology and biogeochemistry of a tropical great lake*, edited by: Descy, J.-P., Darchambeau, F., and Schmid, M., *Aquatic Ecology Series 5*, Springer, 47–66, 2012.
- Borges, A. V., Morana, C., Bouillon, S., Servais, P., Descy, J.-P., and Darchambeau, F.: Carbon cycling of Lake Kivu (East Africa): net autotrophy in the epilimnion and emission of CO_2 to the atmosphere sustained by geogenic inputs, *PLoS ONE*, 9, e109500, doi:10.1371/journal.pone.0109500, 2014.
- Butman, D. and Raymond, P.A.: Significant efflux of carbon dioxide from streams and rivers in the United States, *Nature Geosci.*, 4, 839–842, 2011.
- Cai, W.-J., Wang, Y., and Hodson, R. E.: Acid-base properties of dissolved organic matter in the estuarine waters of Georgia, USA, *Geochim. Cosmochim. Ac.*, 62, 473–483, 1998.
- Cai, W.-J., Guo, X., Chen, C. T. A., Dai, M., Zhang, L., Zhai, W., Lohrenz, S. E., Yin, K., Harrison, P. J., and Wang, Y.: A comparative overview of weathering intensity and HCO_3^- flux in the world's major rivers with emphasis on the Changjiang, Huanghe, Zhujiang (Pearl) and Mississippi Rivers, *Cont. Shelf Res.*, 28, 1538–1549, 2008.
- Cole, J. J., Caraco, N., Kling, G. W., and Kratz, T. K.: Carbon dioxide supersaturation in the surface waters of lakes, *Science*, 265, 1568–1570, 1994.
- Cullison Gray, S. E., DeGranpre, M. E., Moore, T. S., Martz, T. R., Friedrich, G. E., and Johnson, K. S.: Applications of in situ pH measurements for inorganic carbon calculations, *Mar. Chem.*, 125, 82–90, 2011.
- Dinsmore, K. J., Wallin M. B., Johnson, M. S., Billett M. F., Bishop, K., Pumpanen, J., and Ojala, A.: Contrasting CO_2 concentration discharge dynamics in headwater streams: A multi-catchment comparison, *J. Geophys. Res. Biogeosci.*, 118, 445–461, doi:10.1002/jgrg.20047, 2012.
- Driscoll, C. T., Fuller, R., D., and Schecher, W. D.: The role of organic acids in the acidification of surface waters in the eastern US, *Water Air Soil Pollut.*, 43, 21–40, 1989.
- Frankignoulle, M. and Borges, A. V.: Direct and indirect $p\text{CO}_2$ measurements in a wide range of $p\text{CO}_2$ and salinity values, *Aquat. Geochem.*, 7, 267–273, 2001.
- Frankignoulle, M., Borges, A. V., and Biondo, R.: A new design of equilibrator to monitor carbon dioxide in highly dynamic and turbid environments, *Water Res.*, 35, 1344–1347, 2001.
- Gran, G.: Determination of the equivalence point in potentiometric titrations of seawater with hydrochloric acid, *Oceanol. Acta*, 5, 209–218, 1952.
- Guérin, F., Abril, G., Serça, D., Delon, C., Richard, S., Delmas, R., Tremblay, A., and Varfalvy, L.: Gas transfer velocities of CO_2 and CH_4 in a tropical reservoir and its river downstream, *J. Mar. Syst.*, 66, 161–172, 2007.
- Harned, H. S. and Scholes, S. R.: The ionization constant of HCO_3^- from 0 to 50 °C, *J. Am. Chem. Soc.*, 63, 1706–1709, 1941.
- Harned, H. S. and Davis, R. D.: The ionization constant of carbonic acid in water and the solubility of carbon dioxide in water and aqueous salt solutions from 0 to 50 °C, *J. Am. Chem. Soc.*, 65, 2030–2037, 1943.
- Hemond, H. F.: Acid neutralizing capacity, alkalinity, and acid-base status of natural waters containing organic acids, *Environ. Sci. Technol.*, 24, 1486–1489, 1990.
- Hope, D., Dawson, J. J. C., Cresser, M. S., and Billett, M. F.: A method for measuring free CO_2 in upland streamwater using headspace analysis, *J. Hydrol.*, 166, 1–14, 1995.
- Hruska, J., Köhler, S., Laudon, H., and Bishop, K.: Is a universal model of organic acidity possible: Comparison of the acid/base properties of dissolved organic carbon in the boreal and temperate zones, *Environ. Sci. Technol.*, 37, 1726–1730, 2003.
- Humborg, C., Mörth, C. M., Sundbom, M., Borg, H., Blenckner, T., Giesler, R., and Ittekkot, V.: CO_2 supersaturation along the aquatic conduit in Swedish watersheds as constrained by terrestrial respiration, aquatic respiration and weathering, *Glob. Change Biol.*, 16, 1966–1978, 2010.
- Hunt, C. W., Salisbury, J. E., and Vandemark, D.: Contribution of non-carbonate anions to total alkalinity and overestimation of $p\text{CO}_2$ in New England and New Brunswick rivers, *Biogeochemistry*, 8, 3069–3076, 2011, <http://www.biogeosciences.net/8/3069/2011/>.
- Johnson, M. J., Billett, M. F., Dinsmore, K. J., Wallin, M., Dyson, K. E., and Jassal, R. S.: Direct and continuous measurement of dissolved carbon dioxide in freshwater aquatic systems-method and applications, *Ecohydrol.*, 3, 68–78, 2010.
- Kempe, S.: A computer program for hydrochemical problems in karstic water. *Annales de Spéléologie* 30, 699–702, 1975.
- Kempe, S.: Sinks of the anthropogenically enhanced carbon cycle in surface freshwaters, *J. Geophys. Res.*, 89, 4657–4676, 1984.
- Kratz, T. K., Schindler, J., Hope, D., Riera, J. L., and Bowser, C. J.: Average annual carbon dioxide concentrations in eight neighboring lakes in northern Wisconsin, USA. *Verh. Internat. Verein. Limnol.*, 26, 335–338, 1997.
- Liss, P. S. and Slater P. G.: Flux of gases across the air-sea interface. *Nature*, 233, 327–329, 1974.
- Marwick, T. R., Tamooh, F., Ogwoka, B., Teodoru, C., Borges, A. V., Darchambeau, F., and Bouillon S.: Dynamic seasonal nitrogen cycling in response to anthropogenic N loading in a tropical

- catchment, Athi–Galana–Sabaki River, Kenya, *Biogeosciences*, 11, 1–18, doi:10.5194/bg-11-1-2014, 2014a
- Marwick, T. R., Borges A. V., Van Acker K., Darchambeau F., and Bouillon S.: Disproportionate contribution of riparian inputs to organic carbon pools in freshwater systems, *Ecosystems*, 17, 974–989, 2014b.
- Meybeck, M.: Global chemical weathering of surficial rocks estimated from river dissolved loads, *American J. Science*, 287, 401–428, 1987.
- Millero, F. J.: The thermodynamics of the carbonic acid system in seawater, *Geochim. Cosmochim. Ac.*, 43, 1651–1661, 1979.
- Neal, C., House, W. A., and Down, K.: An assessment of excess carbon dioxide partial pressures in natural waters based on pH and alkalinity measurements, *Sc. Total Envir.*, 210/211, 173–185, 1998.
- Park, P. K.: Oceanic CO_2 system: An evaluation of ten methods of investigation, *Limnol. Oceanogr.*, 14, 179–186, 1969.
- Parkhurst, D. L. and Appelo, C. A. J.: User's guide to PHREEQC (version 2) – A computer program for speciation, batch-reaction, one-dimensional transport, and inverse geochemical calculations: US Geol. Surv. Water-Resour. Investigat. Report, 99–4259, 312 pp., 1999.
- Polsenaere, P., Savoye, N., Etcheber, H., Canton, M., Poirier, D., Bouillon, S., and Abril, G.: Export and degassing of terrestrial carbon through watercourses draining a temperate podsolised catchment, *Aquatic Sciences*, 75, 299–319, 2013.
- Raymond, P. A., Caraco, N. F., and Cole J. J.: Carbon dioxide concentration and atmospheric flux in the Hudson River, *Estuaries*, 20, 381–390, 1997.
- Raymond, P. A., Hartmann, J., Lauerwald R., Sobek, S., McDonald, C., Hoover, M., Butman, D., Striegl R., Mayorga, E., Humborg, C., Kortelainen, P., Dürr, H., Meybeck, M., Ciais, P., and Guth, P.: Global carbon dioxide emissions from inland waters, *Nature*, 503, 355–359, 2013.
- Sobek, S., Tranvik L. J., and Cole, J. J.: Temperature independence of carbon dioxide supersaturation in global lakes, *Global Biogeochem. Cy.*, 19, GB2003, doi:10.1029/2004GB002264, 2005.
- Stumm, W. and Morgan, J. J.: *Aquatic Chemistry*, Wiley-Interscience, New York, 1996.
- Tamooh, F., Borges, A. V., Meysman, F. J. R., Van Den Meersche, K., Dehairs, F., Merckx, R., and Bouillon, S.: Dynamics of dissolved inorganic carbon and aquatic metabolism in the Tana River basin, Kenya, *Biogeosciences*, 10, 6911–6928, doi:10.5194/bg-10-6911-2013, 2013.
- Teodoru, C. R., del Giorgio P. A., Prairie Y. T., and Camire M.: Patterns in $p\text{CO}_2$ in boreal streams and rivers of northern Quebec, Canada, *Global Biogeochem. Cy.*, 23, GB2012, doi:10.1029/2008GB003404, 2009.
- Teodoru, C. R., Nyoni, F. C., Borges, A. V., Darchambeau, F., Nyambe, I., and Bouillon, S.: Spatial variability and temporal dynamics of greenhouse gas (CO_2 , CH_4 , N_2O) concentrations and fluxes along the Zambezi River mainstem and major tributaries, *Biogeosciences Discuss.*, 11, 16391–16445, doi:10.5194/bgd-11-16391-2014, 2014.
- Vyverman, W.: Limnological Features of Lakes on the Sepik-Ramu Floodplain, Papua New Guinea Aust, *J. Mar. Freshwater Res.*, 45, 1209–1224, 1994.
- Wallin, M. B., Löfgren, S., Erlandsson, M., and Bishop, K.: Representative regional sampling of carbon dioxide and methane concentrations in hemiboreal headwater streams reveal underestimates in less systematic approaches, *Glob. Biogeochem. Cy.*, 28, 465–479, 2014.
- Wang, Z. A., Bienvenu, D. J., Mann, P. J., Hoering, K. A., Poulsen, J. R., Spencer, R. G. M., and Holmes, R. M.: Inorganic carbon speciation and fluxes in the Congo River. *Geophys. Res. Lett.*, 40, 511–516, 2013.
- Weiss, R. F.: Carbon dioxide in water and seawater: the solubility of a non-ideal gas, *Mar. Chem.*, 2, 203–215, 1974.
- Weiss, R. F.: Determinations of carbon dioxide and methane by dual catalyst flame ionization chromatography and nitrous oxide by electron capture chromatography, *J. Chromatogr. Sci.*, 19, 611–616, 1981.



RESEARCH ARTICLE

10.1002/2015GC005999

Key Points:

- CH₄ concentrations were consistently above atmospheric equilibrium
- Most parameters showed no pronounced seasonal variation
- The ¹³C-DIC data indicate that part of the CO₂ involved in chemical weathering is geogenic

Supporting Information:

- Supporting Information S1
- Data Set S1
- Data Set S2

Correspondence to:

C. M. Balagizi,
balagizi.charles@gmail.com

Citation:

Balagizi, C. M., F. Darchambeau, S. Bouillon, M. M. Yalire, T. Lambert, and A. V. Borges (2015), River geochemistry, chemical weathering, and atmospheric CO₂ consumption rates in the Virunga Volcanic Province (East Africa), *Geochem. Geophys. Geosyst.*, 16, doi:10.1002/2015GC005999.

Received 9 JUL 2015

Accepted 12 JUL 2015

Accepted article online 16 JUL 2015

River geochemistry, chemical weathering, and atmospheric CO₂ consumption rates in the Virunga Volcanic Province (East Africa)

Charles M. Balagizi^{1,2,3}, François Darchambeau², Steven Bouillon⁴, Mathieu M. Yalire¹, Thibault Lambert², and Alberto V. Borges²

¹Geochemistry and Environmental Department, Goma Volcano Observatory, Goma, RD Congo, ²Chemical Oceanography Unit, Université de Liège, Liège, Belgium, ³Department of Environmental, Biological and Pharmaceutical Sciences and Technologies, Second University of Naples, Caserta, Italy, ⁴Department of Earth and Environmental Sciences, Katholieke Universiteit Leuven, Leuven-Heverlee, Belgium

Abstract We report a water chemistry data set from 13 rivers of the Virunga Volcanic Province (VVP) (Democratic Republic of Congo), sampled between December 2010 and February 2013. Most parameters showed no pronounced seasonal variation, whereas their spatial variation suggests a strong control by lithology, soil type, slope, and vegetation. High total suspended matter (289–1467 mg L⁻¹) was recorded in rivers in the Lake Kivu catchment, indicating high soil erodibility, partly as a consequence of deforestation and farming activities. Dissolved and particulate organic carbon (DOC and POC) were lower in rivers from lava fields, and higher in nonvolcanic subcatchments. Stable carbon isotope signatures ($\delta^{13}\text{C}$) of POC and DOC mean $\delta^{13}\text{C}$ of -22.5‰ and -23.5‰ , respectively, are the first data to be reported for the highland of the Congo River basin and showed a much higher C4 contribution than in lowland areas. Rivers of the VVP were net sources of CH₄ to the atmosphere (4–5052 nmol L⁻¹). Most rivers show N₂O concentrations close to equilibrium, but some rivers showed high N₂O concentrations related to denitrification in groundwaters. $\delta^{13}\text{C}$ signatures of dissolved inorganic carbon suggested magmatic CO₂ inputs to aquifers/soil, which could have contributed to increase basalt weathering rates. This magmatic CO₂-mediated basalt weathering strongly contributed to the high major cation concentrations and total alkalinity. Thus, chemical weathering (39.0–2779.9 t km⁻² yr⁻¹) and atmospheric CO₂ consumption (0.4–37.0 × 10⁶ mol km⁻² yr⁻¹) rates were higher than previously reported in the literature for basaltic terrains.

1. Introduction

Rivers transport dissolved and particulate matter from land to the oceans. Part of the solutes transported by rivers are derived from chemical weathering processes in the catchment that is a function of local lithology, climate, and topography [Ludwig *et al.*, 1996; Gaillardet *et al.*, 1999; Hartmann *et al.*, 2014]. Part of the particulate load is derived from mechanical weathering. The terrestrial biosphere and in particular soils provide particulate (POC) and dissolved (DOC) organic carbon to rivers. Groundwaters carry the products of aerobic and anaerobic mineralization in soils toward the river network, and along with mineralization of POC and DOC within the river system, this typically leads to large emissions of greenhouse gases (GHGs) such as carbon dioxide (CO₂) [Raymond *et al.*, 2013; Lauerwald *et al.*, 2015; Borges *et al.*, 2015] and methane (CH₄) [Bastviken *et al.*, 2011; Borges *et al.*, 2015]. Anthropogenic inputs of nitrogen from fertilizers or wastewater can lead to high N₂O emissions from rivers to the atmosphere that are commonly attributed to denitrification [Beaulieu *et al.*, 2010a; Baulch *et al.*, 2011; Marwick *et al.*, 2014]. Nitrogen-poor rivers on the other hand have low N₂O levels [Baulch *et al.*, 2011; Borges *et al.*, 2015].

The annual global CH₄ emissions to the atmosphere between 2000 and 2009 have been estimated at ~548 Tg CH₄ yr⁻¹; of which 218 Tg CH₄ yr⁻¹ were from natural sources and 335 Tg CH₄ yr⁻¹ from anthropogenic sources [Kirschke *et al.*, 2013]. Of the fluxes from natural sources, 175 Tg CH₄ yr⁻¹ were from natural wetlands and 43 Tg CH₄ yr⁻¹ from other natural sources, i.e., freshwater, geological processes, oceans, wild animals, wildfire, and termites [Pison *et al.*, 2009; Bousquet *et al.*, 2011; Beck *et al.*, 2012; Fraser *et al.*, 2013]. Approximately 49% of the global CH₄ emissions from freshwater ecosystems is thought to occur in the tropics [Bastviken *et al.*, 2011].

Raymond *et al.* [2013] provided global CO₂ evasion rates of 1.8 Pg C yr⁻¹ from streams and rivers, and 0.3 Pg C yr⁻¹ from lakes and reservoirs which is highly significant when compared to the land biosphere and oceanic carbon sink of 2.0 Pg C yr⁻¹, respectively [Le Quéré *et al.*, 2014]. The emission from rivers and streams has been recently revised downward to <0.7 Pg C yr⁻¹ by Lauerwald *et al.* [2015]. Yet in both these studies, the CO₂ data distribution in rivers and streams is skewed toward temperate and boreal systems in the Northern Hemisphere, while little data are available at tropical latitudes. There has been a growing number of studies of GHG fluxes in African rivers [Koné *et al.*, 2010; Bouillon *et al.*, 2009; 2012, 2014; Mann *et al.*, 2014; Marwick *et al.*, 2014; Teodoru *et al.*, 2015], that combined with new data have contributed to evaluate for the first time the emissions of GHGs from inland water at the African continental scale [Borges *et al.*, 2015]. The CO₂ and CH₄ emissions from African inland waters were found to be significant at both regional and global scales, totaling 0.4 Pg C yr⁻¹ for river channels alone, and 0.9 Pg C yr⁻¹ for river channels and wetlands of the Congo [Borges *et al.*, 2015].

Volcanic fields are characterized by dry gas emissions which dissolve in the near-surface groundwaters and could thus contribute to the regional aquatic C pool. Despite this distinctive feature, streams and rivers of volcanic zones are still under-investigated for GHG evasion estimates. Volcanic terrains also act as an atmospheric C sink through chemical weathering. Thus, chemical and physical weathering is an important part of many elements cycles. On a global scale, atmospheric CO₂ consumption by chemical weathering leads to the storage of 237–288 Mt C yr⁻¹ in surface waters and the oceans [Amiotte-Suchet and Probst, 1995; Amiotte-Suchet *et al.*, 2003; Gaillardet *et al.*, 1999; Munhoven, 2002; Hartmann *et al.*, 2009; Moon *et al.*, 2014]. About 63% of this global estimate is due to silicate weathering [Hartmann *et al.*, 2009]. Basalt weathering represents 30–35% of CO₂ sequestered by silicate weathering [Gaillardet *et al.*, 1999; Dessert *et al.*, 2003], although basalts correspond to only 4–6% of the global continent area [Meybeck, 1987; Amiotte-Suchet *et al.*, 2003; Hartmann *et al.*, 2009]. Given the large quantity of sequestered C and the subsequently significant role on climate regulation, more studies are needed to improve the quantification of chemical weathering and CO₂ consumption in basaltic formations. Investigating weathering rates in basaltic terrains at the regional scale contributes to reduce uncertainties in the modeling of the global atmospheric CO₂ consumption rate.

This study focuses on the geochemistry of rivers of the Virunga Volcanic Province (VVP) (Figure 1), characterized by high volcanic activity, located in a tropical climate zone, and with a dense hydrographic network, but which remains poorly studied from a geochemical point of view. We concentrated on the geochemical characterization of the major rivers of the VVP by: (1) quantifying concentrations of nutrients, major cations, organic and inorganic carbon and their stable carbon isotope composition ($\delta^{13}\text{C}$); (2) the quantification of riverine CH₄ and N₂O concentrations and (3) the estimation of spatial variations of these parameters. We additionally quantified solutes and suspended material fluxes, the chemical weathering rates and the associated atmospheric CO₂ consumption during basalt weathering. Finally, the dependence at regional scale of chemical weathering on climatic factors (temperature and runoff) was discussed.

2. Study Area

2.1. Geological and Hydrological Settings

The VVP is located in the western branch of the East African Rift and is bounded on the north by Lake Edward, on the south by Lake Kivu, the Rwandan dorsal on the east and the Mitumba Range on the west (Figure 1). Virunga volcanic activity started during the mid-Miocene [Poucllet, 1977] and consists of eight major volcanic edifices perpendicularly aligned to the position of the rift. Most edifices are dormant except Mount Nyiragongo (4370 m) and Mount Nyamulagira (3058 m), both located in the Democratic Republic of the Congo (DRC) and are the Africa's most active volcanoes. The edges of the rift are difficult to detect due to intense erosion, important vegetation cover and frequent lava flows [Smets, 2007] especially in the east. Nearly all the Virunga lavas are of alkalic to highly alkalic composition (Table 1), the alkalic character varies from a relatively sodic pole [Na₂O > K₂O] to a potassic or hyperpotassic pole [K₂O ≫ Na₂O]. The VVP consists of plains, shelf, and mountain ranges with altitudes of 900 m in the basin of Lake Edward and 1460 m in the Lake Kivu basin. The highest point is the Mount Karisimbi summit at 4508 m (Figure 1). The alluvial plain extends over the south basin of Lake Edward (i.e., lacustrine of Figure 2b), and then steadily rises up toward the Nyamulagira and Nyiragongo lava flows (i.e., basalt/volcanic ash of Figure 2b). The boundary

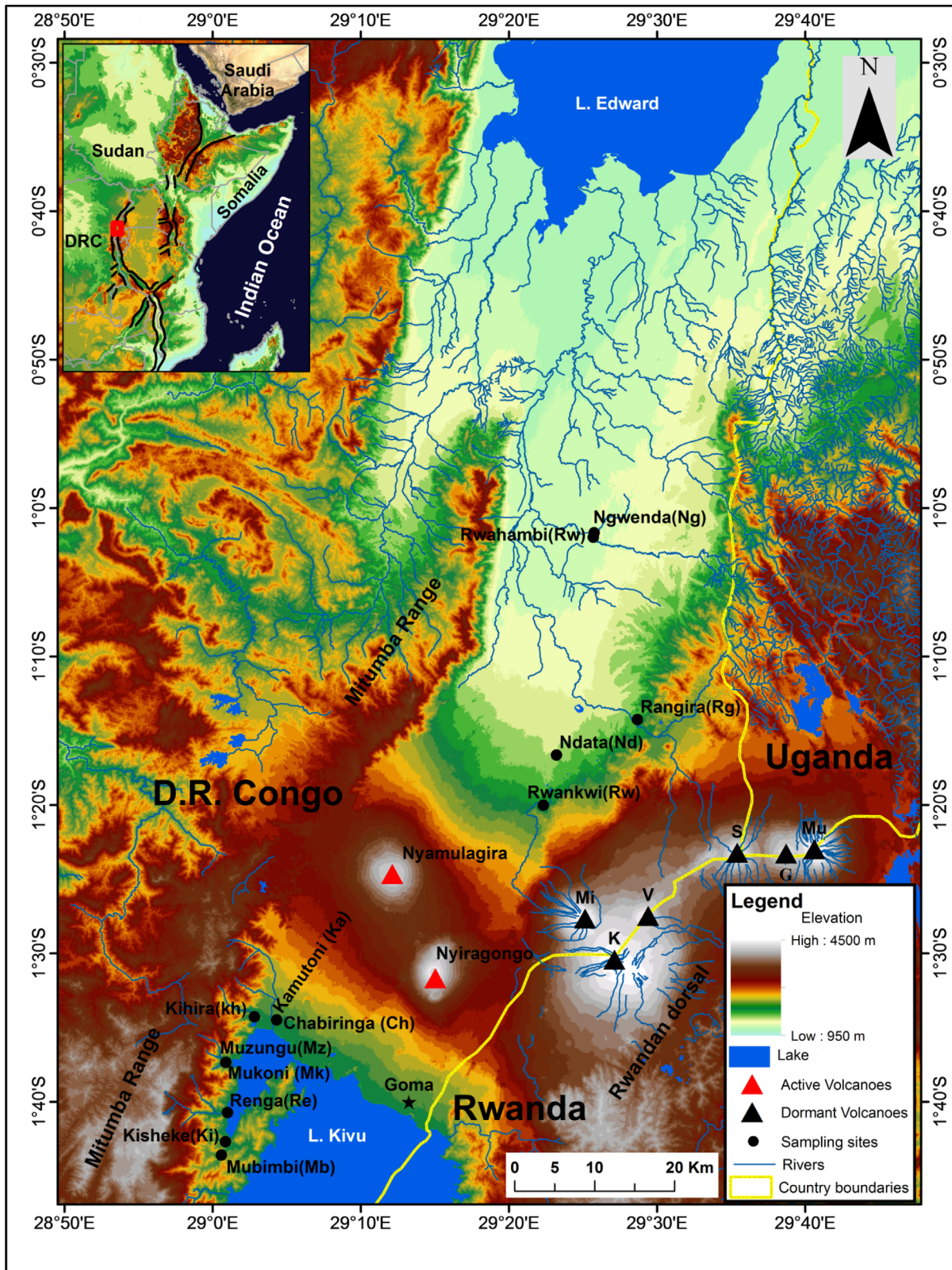


Figure 1. Map of the Virunga Volcanic Province (VVP) showing the sampling sites. Eight of the 13 sampled rivers drain into the Kabuno bay (a subbasin of Lake Kivu), i.e., Mubimbi (Mb), Kisheke (Ki), Renga (Re), Mukoni (Mk), Muzungu (Mz), Kihira (Kh), Kamutoni (Ka), and Chabiringa (Cha). The five others rivers drain into Lake Edward catchment, i.e., Rwankwi (Rk), Ndata (Nd), Rangira (Ra), Rwahambi (Rw), and Ngwenda (Ng). The blue lines represent the hydrographic network by BEGo (*Synoptics, Keyobs, Royal Museum for Central Africa, Catholic University of Louvain*) [2005]. The map also shows the six dormant volcanoes of the Virunga, i.e., Mikeno (Mi), Karisimbi (K), Visoke (V), Sabinyo (S), Gahinga (G), and Muhabura (Mu) while Nyiragongo and Nyamulagira are still active. The black lines in the inset map display the boundaries of the East African Rift System.

Table 1. Major Elements Composition (wt %) of the Virunga Lavas

	Nyiragongo ^a Mean (Range)	Nyamulagira ^b Mean (Range)	Mikeno ^c
SiO ₂	38.92 (29.72–48.38)	45.59 (37.88–47.83)	47.23
Al ₂ O ₃	14.22 (10.60–19.90)	14.08 (8.42–18.68)	15.01
Fe ₂ O ₃	11.73 (4.88–17.50)	5.07 (0.24–10.8)	9.91
FeO	6.46 (0.97–9.33)	8.64 (3.07–10.59)	
MnO	1.30 (0.16–6.30)	0.19 (0.03–0.35)	0.18
MgO	3.89 (0.16–6.30)	7.82 (0.19–14.9)	3.49
CaO	12.88 (8.11–18.86)	11.26 (5.16–18.09)	9.25
Na ₂ O	5.26 (1.90–7.28)	2.62 (1.5–11.38)	4.05
K ₂ O	5.11 (2.04–7.34)	2.93 (1.05–5.85)	6.28
TiO ₂	2.87 (1.98–4.30)	3.27 (1.25–5.14)	3.04
P ₂ O ₃	1.55 (0.44–2.39)	0.42 (0.13–2.09)	0.77
CO ₂	1.69 (0.40–3.16)	0.11 (0–0.33)	
H ₂ O ⁺	0.52 (0.35–0.68)	0.33 (0–0.84)	0.69
H ₂ O ⁻	0.18 (0.12–0.24)	0.10 (0–0.64)	
K ₂ O + Na ₂ O	10.38	5.55	10.33
K ₂ O/Na ₂ O	0.97	1.11	1.55
Mg#	29.89 (22.80–32.74)	39.08 (34.53–43.3)	28.13

^aUndated lavas, lava from the 1977 and 2002 eruptions, after Demant *et al.* [1994], Platz *et al.* [2004], Chakrabarti *et al.* [2009], and Andersen *et al.* [2012, 2014].

^bUndated lavas, lava from the 1912, 1938, 1948, 1977, 1982, 1986, 2006, and 2010 eruptions after Denaeeyr [1972, 1975], Poucllet [1974], Aoki and Kurasawa [1984], Aoki *et al.* [1985], Hertogen *et al.* [1985], Marcelot *et al.*, 1989, Head *et al.* [2011], and Smets *et al.* [2013].

^cGuibert [1978].

between the Lake Edward and Lake Kivu watersheds is located on the line connecting the Nyamulagira-Nyiragongo-Karisimbi volcanoes (W to E oriented line; Figure 1). This boundary also corresponds to the limit between the Congo River basin to the south and the Nile River in the North. The mountain climate that marks the region is controlled by the nearby equatorial forest of the Virunga National Park and the mountain range. Precipitation is estimated at 1400–1500 mm yr⁻¹ [Muvundja *et al.*, 2009], and the mean annual temperature at ~19.2°C. The region experiences a long wet season (September–May) and a dry season (June–August), with a short occasional dry season from mid-January to February. Lake Kivu (1460 m) and the hundreds of tributaries dominate the hydrography in the south of Virunga. The center and the north consist of a river network that feeds the Rutshuru River which flows into Lake Edward.

2.2. Soil Type and Land Uses

Three classes of soil are distinguished in the VVP (Figure 2a). The first lies on the area of presently active volcanoes and is composed of umbric and mollic andosols; the second covers the area of extinct volcanoes and composed of mollic andosols. The third consist of soil of alluvial and metamorphic rocks parent materials, formed by luvic phaeozems, haplic acrosols, and mubic cambisols (Figure 2a). The soils of presently active volcanic areas contain a thin humus layer covering lava flows on which mosses and lichens grow. A thick and slightly compact and humus-rich soil has developed on old lava flows; while the soil of the alluvial plain derives from sedimentary deposits. Local people practice traditional agriculture and livestock but an important area of the Virunga area is part of the Virunga National Park. No chemical fertilizers are used in the region. The lack of agricultural management on lands with steep slopes and the significant deforestation have generated substantial soil movements. They mainly include soil erosion and landslides, particularly in the mountainous watershed of Lake Kivu. The region is experiencing significant urbanization due to rural exodus triggered by repeated wars, causing Goma and the other small cities to host 4.2% of the population of the North Kivu province [Document stratégique de réduction de la pauvreté (DSRP), 2005].

3. Materials and Methods

3.1. Sampling Techniques

We carried out monthly sampling on 13 rivers in the VVP (all located in the DRC) from December 2010 to February 2013; eight are located in the Kabuno bay basin (a subbasin of Lake Kivu) while the five others drain into Lake Edward (Figure 1). Temperature, specific conductivity, pH, and dissolved oxygen (%O₂) were measured in situ with a Hanna (Hi 9828) multiparameter probe between December 2010 and December 2011,

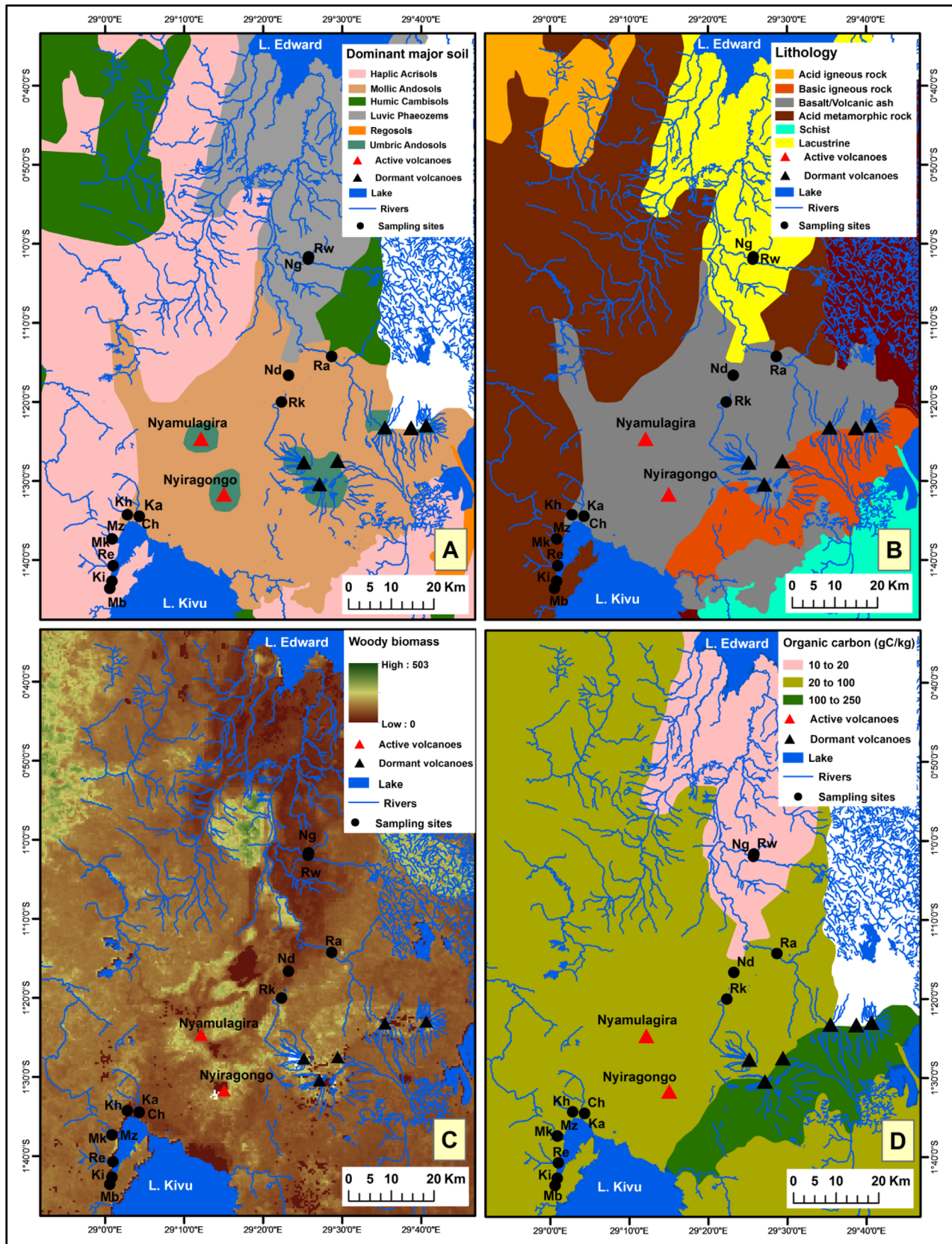


Figure 2. (a) Map of the major dominant soil groups, (b) lithology, (c) biomass, and (d) organic carbon distribution in the Virunga Volcanic Province.

and with an YSI ProPlus probe for the rest of the measurement period. The same calibration procedures were applied for both probes ensuring data continuity. Calibration of the pH electrode was carried out the evening prior to field measurements using pH 7.00 and pH 10.00 (25°C) standard buffers. The oxygen probes were calibrated with humidity-saturated ambient air in the field. Precision of conductivity, water temperature, pH, and %O₂ was estimated to 1 μS/cm, 0.1°C, 0.01 pH units, and 0.5%, respectively. Water for the analysis of dissolved gases (CH₄ and N₂O) was collected in two glass serum bottles of 50 mL and poisoned with 200 μL of a saturated HgCl₂ solution, and sealed with butyl stoppers and aluminum caps. Samples for the measurement of the carbon isotopic composition in the dissolved inorganic carbon ($\delta^{13}\text{C-DIC}$) were stored in 12 mL Exetainer vials and preserved with 100 μL of saturated HgCl₂ solution. Water for total alkalinity (TA), major elements, dissolved organic carbon (DOC), and its $\delta^{13}\text{C}$ signature was filtered through a 0.2 μm pore size polysulfone syringe filters, after prefiltration on 0.7 μm glass fiber filters. TA samples were collected in 50 mL high-density polyethylene bottles, 20 mL scintillation vials were used for major ions and preserved with 50 μL of HNO₃ 65%, while samples for DOC and $\delta^{13}\text{C}_{\text{DOC}}$ were collected in 50 mL Supelco glass bottles with polytetrafluoroethylene-coated septa, and preserved with 50 μL concentrated H₃PO₄. Samples for total suspended matter (TSM), particulate organic carbon (POC) and its $\delta^{13}\text{C}$ signature, and for particulate nitrogen (PN) were obtained by filtering a known volume of water (between 700 and 1700 mL depending on the turbidity of the river) through Macherey-Nagel GF-5 47mm precombusted (5 h at 500°C) glass fiber filters. Two 50 mL plastic bottles were filled with water from the Macherey-Nagel GF-5 filtration, preserved with 200 μL of H₂SO₄ 4 N for nitrates (NO₃⁻), nitrites (NO₂⁻), ammonium (NH₄⁺), and soluble reactive phosphorus (SRP) determination. For total phosphorus (TP) determination, a 50 mL plastic bottle was filled with unfiltered water and preserved with 200 μL of 4 N H₂SO₄.

3.2. Analytical Techniques

Concentrations of CH₄ and N₂O were determined by gas chromatography (GC) with flame ionization detection (SRI 8610C), after creating a 20 mL headspace with N₂ in the 50 mL glass serum bottle. A Flame Ionization Detector (FID) coupled to a Hayesep D column was used for CH₄ measurements, while an Electron Capture Detector (ECD) coupled to a Hayesep N column was used for N₂O measurements. The two detectors were calibrated at the start and end of each series with certified gas mixtures of 1, 10, and 30 μatm of CH₄ and 0.2, 2, and 6 μatm of N₂O (Air Liquide Belgium). The overall precision of measurements was ±3.9% and ±3.2% for CH₄ and N₂O, respectively [Borges *et al.*, 2015]. Concentrations of dissolved CH₄ and N₂O were calculated based on the partial pressure of the gas, its volume in the headspace and the water volume according to standard procedures by Weiss [1981]. $\delta^{13}\text{C-DIC}$ was analyzed using an elemental analyzer-isotope ratio mass spectrometer (EA-IRMS, Thermo Flash EA/HT and DeltaV Advantage). First, a 2 mL Helium headspace was created in the sample which was then acidified with H₃PO₄ and equilibrated overnight. A subsample from the headspace was injected into the EA-IRMS, and data were corrected for isotopic fractionation between dissolved and gaseous CO₂ as described by Gillikin and Bouillon [2007]. Measurements were calibrated with LSVEC and either NBS-19 or IAEA-CO-1 reference materials. The reproducibility of $\delta^{13}\text{C-DIC}$ measurement was typically better than ±0.2‰. TA was determined by Gran titration method with 0.1 M HCl as titrant using an automated titrator (Metrohm 725 Dosimat) equipped with a pH probe (ORION 8102 SC). Data were quality checked with certified reference material obtained from Andrew Dickinson (Scripps Institution of Oceanography, University of California, San Diego, USA). Typical reproducibility of TA measurements was better than ±3 μmol L⁻¹. For DOC and $\delta^{13}\text{C}_{\text{DOC}}$ analysis, 9–15 mL of sample were analyzed using a wet oxidation DOC analyzer (Thermo Hiper TOC or Aurora 1030W) coupled to an IRMS (Delta +XL or Delta V Advantage), calibrated with IAEA-C6 and an internal sucrose standard ($\delta^{13}\text{C} = -26.99 \pm 0.04\text{‰}$) calibrated against international reference materials. Reproducibility of $\delta^{13}\text{C-DIC}$ was typically better than ±0.2‰ and relative standard deviation for DOC concentration measurement was always below ±5%. Major elements were measured with inductively coupled plasma mass spectrometry (ICP-MS; Agilent 7700x) calibrated with the following standards: SRM1640a from National Institute of Standards and Technology, TM-27.3 (lot 0412) and TMRain-04 (lot 0913) from Environment Canada, and SPS-SW2 Batch 130 from Spectrapure Standard. Limit of quantification was 0.5 μmol L⁻¹ for Na⁺, Mg²⁺, and Ca²⁺, 1.0 μmol L⁻¹ for K⁺ and 8 μmol L⁻¹ for Si. TSM values were obtained as the ratio of sediment load to the filtered water volume, the sediment load being determined as the net weight of sediment collected on the precombusted GF-5 filters, after redrying, with a precision of ±0.2 mg L⁻¹. To measure the POC, $\delta^{13}\text{C-POC}$ and particulate nitrogen (PN), a cutout of 11 mm diameter was made in the GF-5 filter, carbonates were removed by exposure to concentrated HCl

fumes for at least 4 h, and these were redried and packed in Ag cups. Calibration of $\delta^{13}\text{C}$ -POC, $\delta^{15}\text{N}$ -PN, POC, and PN measurements was performed with acetanilide ($\delta^{13}\text{C} = -27.65 \pm 0.05\text{‰}$; $\delta^{15}\text{N} = 1.34 \pm 0.04\text{‰}$) and leucine ($\delta^{13}\text{C} = -13.47 \pm 0.07\text{‰}$; $\delta^{15}\text{N} = 0.92 \pm 0.06\text{‰}$) as standards. All standards were internally calibrated against the international standard IAEA-C6 and IAEA-N1. Reproducibility of $\delta^{13}\text{C}$ -POC and $\delta^{15}\text{N}$ -PN measurement was typically better than $\pm 0.2\text{‰}$ and relative standard deviation for POC and PN measurement was always below 5%. Nutrients (NO_2^- , NO_3^- , NH_4^+ , SRP, and TP) analysis was performed using a GENESIS 20 single beam spectrophotometer, according to standard colorimetric protocols following *Rodier and Bazin* [2005] and *American Public Health Association* [1998]. The detection limits were 0.3, 0.03, and $0.15 \mu\text{mol L}^{-1}$ for NH_4^+ , NO_2^- , and NO_3^- , respectively.

3.3. GIS Analysis and Discharge Estimation

SRTM DEM (Shuttle Radar Topography Mission-Digital Elevation Model) data sampled at 3 arc sec (~ 30 m) pixel size were used to generate the topographical map of the VVP (Figure 1). The SRTM DEM data were collected by the NASA, the USA National Geospatial-Intelligence Agency, and the German and Italian space agencies joint team. A full description of the SRTM DEM data can be found in *Farr et al.* [2007]. Maps of the dominant major soil groups (Figure 2a) and organic carbon distribution (Figure 2d) were produced using data from the FAO SOTWIScaf, ver. 1.0, a central Africa soil features described in *Batjes* [2008]. The spatial distribution of the aboveground live woody biomass (Figure 2c) was extracted from the Pantropical National Level Carbon Stock Dataset for tropical countries [*Baccini et al.*, 2008]. Land cover (supporting information Figure S1) data were extracted from the FAO GLCN2000 [*Global Land Cover 2000 database*, 2003] (Global Land Cover Network) database for Africa, which is at ~ 300 m resolution and described in *Mayaux et al.* [2004]. The hydrographic network (Lake and rivers) is taken from the Building Environment for the Gorilla's [*BEGo (Synoptics, Keyobs, Royal Museum for Central Africa, Catholic University of Louvain)*, 2005]. Lithology (Figure 2b) is based on the GLiM (Global lithological map) from *Hartmann and Moosdorf* [2012].

The drainage areas (supporting information Figure S2) were derived from a high-resolution DEM computed by the HydroSHEDS mapping product (<http://hydrosheds.cr.usgs.gov/index.php>) and using the ArcHydro 2.0 Toolbox for ArcGis 10.2 software. Monthly discharges (supporting information Data Set S1) were estimated using an approach based on DEM and local precipitation data. The DEM grid was used to successively extract flow direction and flow accumulation grids. The latter represents the number of upslope cells that flow into each cell, and thus can be used to derive stream networks. The flow accumulation grid was converted into an accumulated area grid by multiplying the flow accumulation grid by the DEM grid resolution (here 92.43 m^2). Then, multiplying the value of the accumulated area determined at the outlet of a basin by a value of precipitation results in a measure of accumulated runoff per unit of time. Average monthly precipitations (supporting information Data Set S1) for each basin are derived from the 1 km^2 resolution WorldClim Database [*Hijmans et al.*, 2005]. A comparison of the results obtained using this approach with the data from 10 USGS gauges across the U.S.A. provided satisfactory results [*Wieczorek*, 2012].

3.4. Annual Load and Weathering Rate Estimation

Discharge-weighted mean concentrations were calculated in order to avoid dilution and evaporation effects on the annual loads and weathering rates. For a given parameter, the discharge-weighted mean concentration (C_w) was calculated as follows:

$$C_w = \frac{\sum_{i=1}^n C_i \times Q_i}{\sum_{i=1}^n Q_i}$$

where C_i is the monthly measured concentration and Q_i the calculated monthly discharge.

The estimated monthly discharges can be found in the supporting information. The annual load was then obtained by multiplying the discharge-weighted mean concentration (C_w) with the annual discharge. Following the same procedure, atmospheric CO_2 consumption rate was estimated from the discharge-weighted mean HCO_3^- (TA) concentration, based on the assumption that HCO_3^- is generated by silicate rock weathering, as confirmed by analysis of major element property-property plots (see hereafter). The mechanical weathering rate was estimated from discharge-weighted mean TSM concentration. The cationic weathering rate was estimated from the sum of major cations ($\text{TDS}_{\text{cat}} = \sum \text{Ca, Mg, Na, and K}$). The chemical weathering rate was estimated from the total dissolved solid (TDS_{cond}), the latter calculated from specific

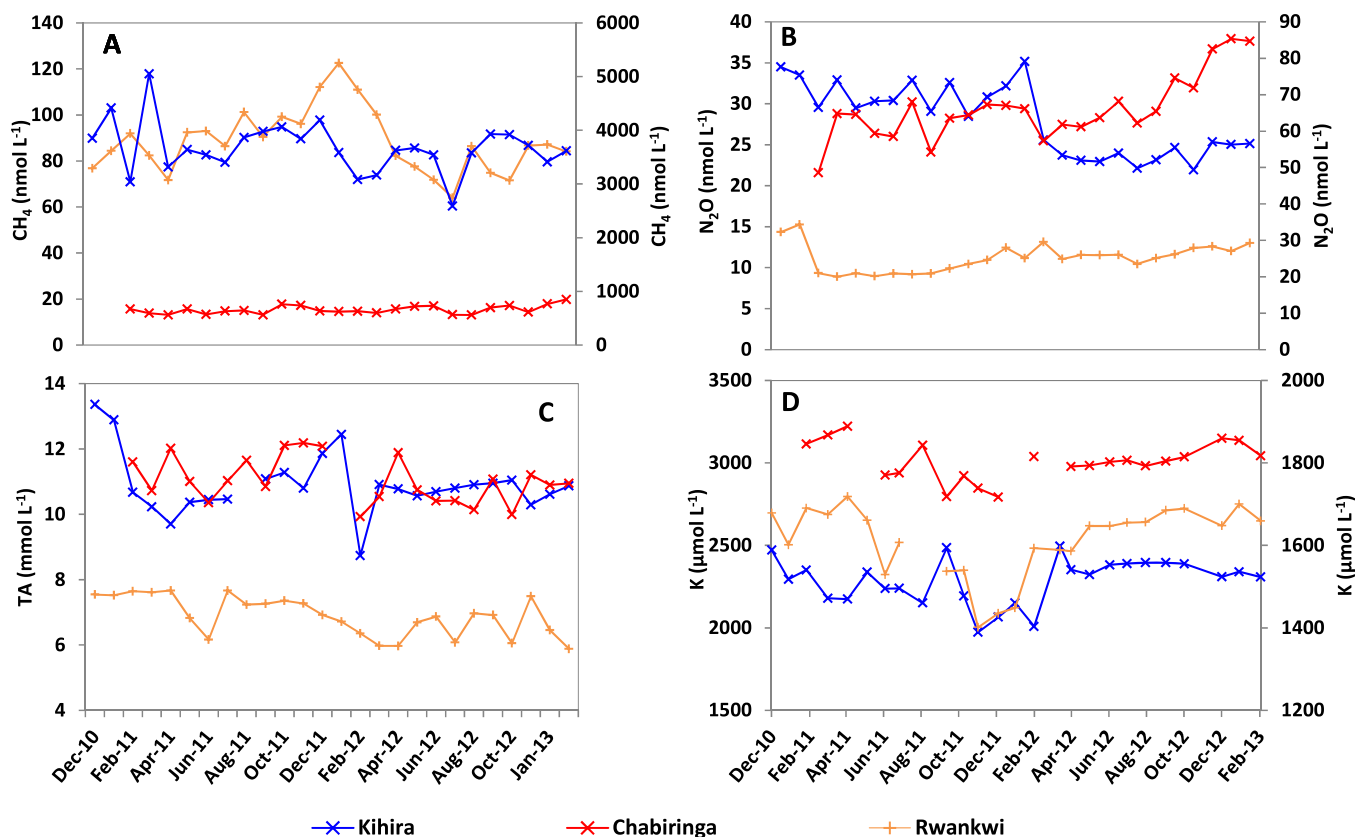


Figure 3. (a) Temporal variation of methane, (b) nitrous oxide, (c) total alkalinity, and (d) K⁺ concentrations in a selection of the sampled rivers of the Virunga Volcanic Province between December 2010 and February 2013. Kihira in Figure 3a, Chabiringa in Figure 3b, and Rwankwi in Figure 3d are referred to the right axes.

conductivity as described in *Atekwana et al.* [2004]. All fluxes and weathering rates are expressed on an areal basis, i.e., by dividing the annual load with the river catchment area.

Major cations concentrations were corrected for atmospheric inputs using data from *Cuoco et al.* [2012a] which studied rainwater chemistry in the VVP between 2004 and 2010. Only data from rain samples collected to the N-NE and the W-SW of Mt Nyiragongo were considered. Samples from Nyiragongo crater and surrounding were not considered as they were not included in the drainage basins of this study. Furthermore, this area is impacted by the plume from Nyiragongo's permanent lava lake, and would thus only represent a source of error.

4. Results and Discussion

Most measured physicochemical and chemical features showed no well-defined seasonality (e.g., Figure 3 and supporting information Data Set S2). The mean temperature for each river throughout the study period ranged between 17 and 29.4°C (Figure 4a). Temperature was almost constant in Chabiringa and Kamutoni, while the other rivers showed a relative increase during dry season period, i.e., mid June to August. Shallow rivers showed important temperature fluctuations except for the Rwankwi which is supplied with high altitude water. No large DOC and POC increases were observed during the rising stage of runoff (mid-September to October) after the dry season, in contrast to what was observed in very large rivers such as the Oubangi River in the Congo River basin or other large tropical rivers [*Meybeck, 2005; Bouillon et al., 2012*]. Thus, the POC/DOC, HCO₃⁻/DOC, and POC/PN ratios showed only minor variations over time.

Given the general lack of marked seasonal variations, we principally focus on spatial variations of parameters. Mean concentrations of studied parameters are presented in Figures 4 and 6, the full database can be found in supporting information Data Set S2.

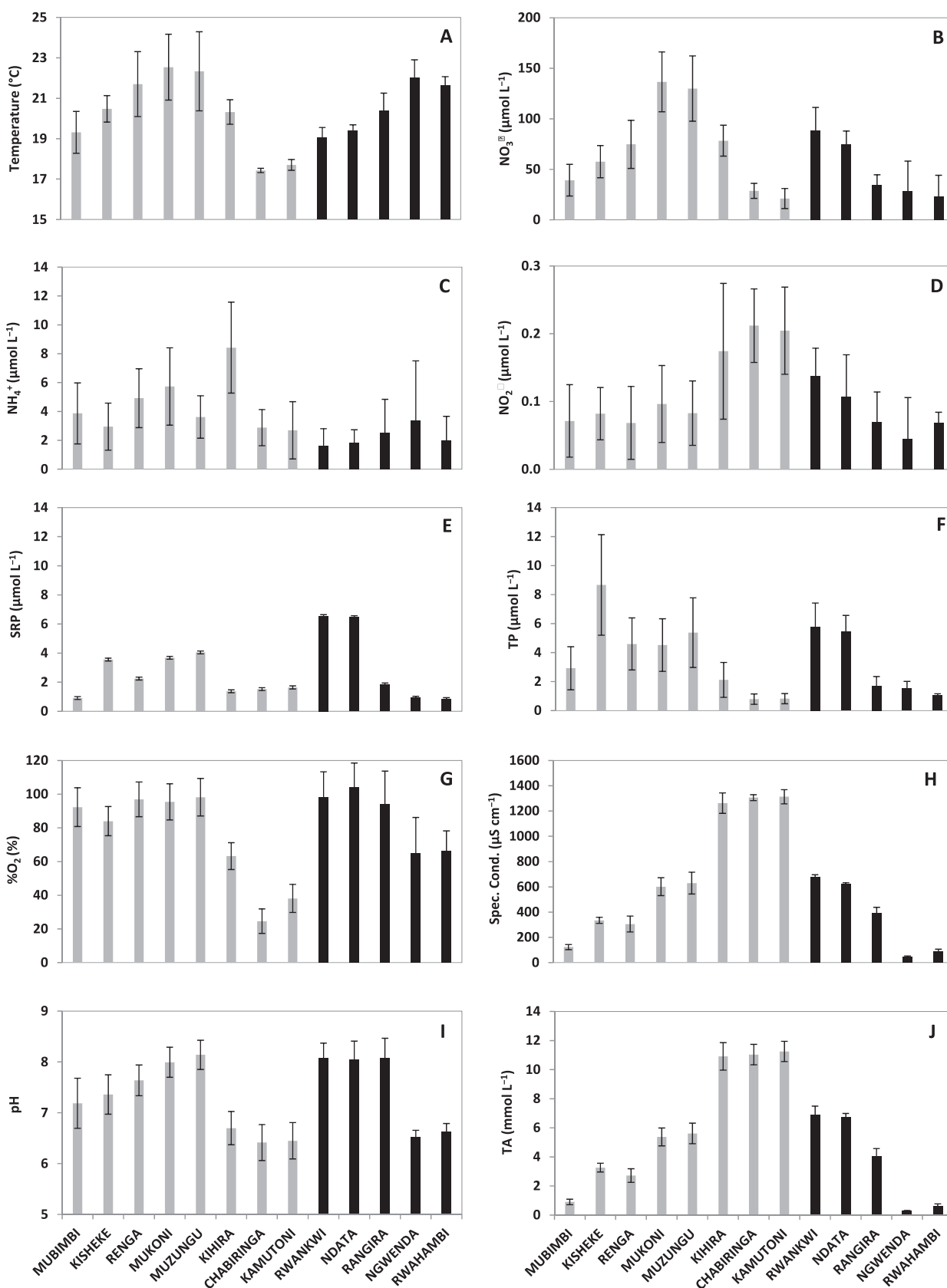


Figure 4. (a) Mean temperature, (b) nitrate, (c) ammonium, (d) nitrite, (e) soluble reactive phosphorus, (f) total phosphorus, (g) dissolved oxygen, (h) specific conductivity, (i) pH, and (j) total alkalinity in rivers of the Virunga Volcanic Province between December 2010 and February 2013. The gray and black bars represent rivers of Kabungo bay and Lake Edward catchment, respectively. The error bars represent one standard deviation.

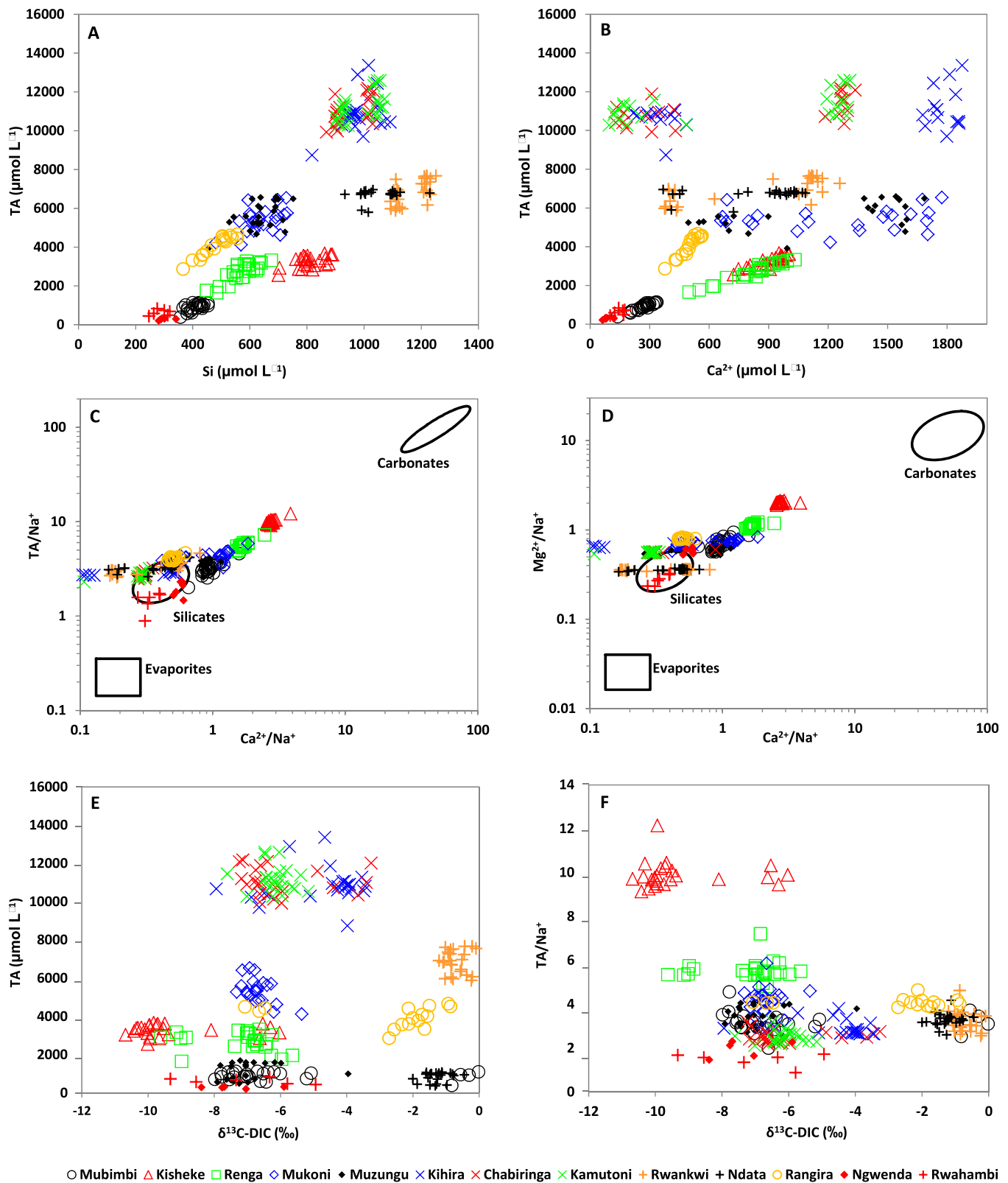


Figure 5. (a) Relationships between total alkalinity (TA) and Si, (b) TA and calcium, (c) TA/Na^{+} and $\text{Ca}^{2+}/\text{Na}^{+}$, (d) $\text{Mg}^{2+}/\text{Na}^{+}$ and $\text{Ca}^{2+}/\text{Na}^{+}$, (e) TA and $\delta^{13}\text{C}_{\text{DIC}}$ and (f) TA/Na^{+} and $\delta^{13}\text{C}_{\text{DIC}}$ in rivers of the Virunga Volcanic Province between December 2010 and February 2013. The Na^{+} normalized plots show the composition fields for rivers draining different lithologies from a global compilation of the 60 largest rivers in the World [Gaillardet et al., 1999].

4.1. Spatial Variations in Nutrient Concentrations

Monthly NO_3^- concentrations in the VVP rivers spanned a wide range (7–178 $\mu\text{mol L}^{-1}$), with large spatial variations (Figure 4b), and did not reach levels indicative of significant pollution or eutrophication. In parallel, the NH_4^+ and NO_2^- (Figures 4c and 4d, respectively) remained below the ranges normally found in unpolluted rivers (18 and 1.2 $\mu\text{mol L}^{-1}$, respectively) [Meybeck, 1982, 1983a]. The observed variations in the NO_3^- , NH_4^+ , and NO_2^- concentrations were therefore of natural origin. On the other hand, mean SRP concentrations (Figure 4e) are higher compared to those of unpolluted rivers (10 $\mu\text{g L}^{-1}$) [Meybeck, 1982, 1993a], a discrepancy which could be related to a high degree of P mobilization during weathering of basaltic rocks (see below).

In rivers of the VVP, NH_4^+ represented between 1.5% and 11.9% of the total inorganic N pool, whereas NO_3^- largely dominated and accounted for 87.9–98.3%. This might suggest the conversion of NH_4^+ into NO_3^- through nitrification, leading to the dominance of NO_3^- over NH_4^+ . The TP mean (Figure 4f) were slightly correlated to the SRP ($r^2 = 0.54$) and to NO_3^- ($r^2 = 0.33$). This implies the dominance of SRP in the P pool as SRP additionally represent >50% of TP in most rivers, and a possible common source for both P and N. In fact, P and N can be jointly mobilized from land runoff and groundwater.

Volcanic emissions are a possible source of nitrate and phosphate in active volcanic areas [Julley *et al.*, 2008], and reach surface water through wet and dry deposits on the catchment. In the Virunga atmospheric inputs are important source of N and P, indeed Muvundja *et al.* [2009] found that total-N and total-P concentrations in atmospheric deposits were equal or larger than riverine values. P can also be produced in bioavailable form (P_4O_{10}) when hot lava reacts with water [Vitousek, 2004]. Like many other elements, P is released during chemical weathering. In the Japanese archipelago, P-release from silica-dominated lithology is estimated at a rate of 1–390 $\text{kg}^{-1} \text{km}^{-2} \text{yr}^{-1}$ [Hartmann and Moosdorf, 2011]. Thus, even though P is a minor constituent of igneous rocks (mean from 0.42 to 1.55 wt % for the Virunga basalt; Table 1), volcanic products could be a minor source of P of VVP rivers.

Muvundja *et al.* [2009] reported nutrient data in Mukoni, Muzungu, Kihira, Chabiringa, and Kamutoni rivers during a monthly monitoring between October 2006 and July 2008. The SRP, Si, and TSM are comparable for both data sets. The higher NH_4^+ and TP values given by Muvundja *et al.* [2009] are possibly due to the difference in the sampling location, as they collected samples close to the mouth (near Kabuno bay) where contamination by wastewaters from villages along the course of the rivers may occur.

4.2. Major Cations and DIC Chemistry

Most rivers had mean O_2 concentrations near saturation, except Kamutoni and Chabiringa which were the most O_2 -depleted waters, with means of 38.1% and 24.6%, respectively (Figure 4g), typical of high groundwater contributions as confirmed also by low temperature (Figure 4a) since they were sampled close to the resurgence points. The activity of the Nyamulagira seems to not influence temperatures of both rivers. The other rivers showed $\% \text{O}_2 > 60\%$ which implies important water oxygenation, given the steep slopes and shallow depths. Rwankwi, Ndata, and Mubimbi showed lower temperature (mean of $\sim 19^\circ\text{C}$) associated with their high altitude origin on Mt Mikeno of the Virunga Nation Park (Rwankwi and Ndata) and the Mitumba Range (Mubimbi) (Figure 1). Specific conductivity data allow us to define three groups of rivers in the VVP: (1) the low mineralized ($< 150 \mu\text{S cm}^{-1}$), (2) moderately mineralized (200–800 $\mu\text{S cm}^{-1}$), and (3) highly mineralized rivers with $> 800 \mu\text{S cm}^{-1}$ (Figure 4h).

The highly mineralized rivers, i.e., Kihira, Chabiringa, and Kamutoni are located on basaltic lithology in the field of active volcanoes, with a high major cation content and where the dominant cations are $\text{Na}^+ > \text{K}^+ > \text{Mg}^{2+} > \text{Ca}^{2+}$ (Table 2). This is a result of the intense weathering of basalt, mediated by magmatic CO_2 and the subsequent release of major cations to groundwater. The high alkalic composition of Virunga basalt promotes the dominance of Na^+ and K^+ in the cation composition of Kihira, Chabiringa and Kamutoni.

The moderately mineralized rivers are located in the field of dormant volcanoes to the NE and on nonvolcanic fields to the west (Figure 2b), where eruptive materials (i.e., ash, volcanic plume) were frequently deposited especially during Nyiragongo and Nyamulagira eruptions. Rwankwi and Ndata to the North-East, Mukoni and Muzungu to the West have similar specific conductivities (616–682 $\mu\text{S cm}^{-1}$) despite their location on different lithologies. The North-Eastern and Western rivers had different dominant cations

Table 2. Mean Cation Concentrations (Min-Max Between Parentheses) in Rivers of the Virunga Volcanic Province, Between December 2010 and February 2013

	Na (mM) Mean (Min-Max)	K (mM) Mean (Min-Max)	Mg (mM) Mean (Min-Max)	Ca (mM) Mean (Min-Max)	Si (mM) Mean (Min-Max)
Mubimbi	0.29 (0.15–0.39)	0.10 (0.07–0.16)	0.19 (0.12–0.23)	0.27 (0.14–0.34)	0.41 (0.36–0.45)
Kisheke	0.33 (0.23–0.37)	0.24 (0.12–0.30)	0.67 (0.47–0.74)	0.91 (0.72–1.00)	0.81 (0.70–0.89)
Renga	0.49 (0.29–0.69)	0.27 (0.20–0.33)	0.54 (0.34–0.71)	0.83 (0.50–1.03)	0.57 (0.45–0.68)
Mukoni	1.27 (0.83–1.66)	0.69 (0.53–1.00)	0.92 (0.69–1.05)	1.24 (0.66–1.77)	0.64 (0.48–0.73)
Muzungu	1.63 (1.03–1.92)	0.95 (0.72–1.13)	0.97 (0.54–1.14)	1.17 (0.50–1.69)	0.64 (0.45–0.75)
Kihira	3.72 (3.11–4.09)	2.28 (1.97–2.50)	2.49 (2.04–2.86)	1.12 (0.22–1.88)	0.99 (0.82–1.09)
Chabiringa	4.26 (1.62–4.71)	2.91 (0.88–3.22)	2.31 (0.97–2.55)	0.76 (0.13–1.43)	0.95 (0.69–1.03)
Kamutoni	4.49 (3.94–4.97)	3.08 (2.85–3.26)	2.44 (2.21–2.58)	0.73 (0.10–1.31)	0.99 (0.90–1.07)
Rwankwi	2.15 (0.26–0.55)	1.61 (0.04–0.11)	0.77 (0.08–0.14)	0.81 (0.10–0.17)	1.17 (0.25–0.32)
Ndata	2.05 (1.62–2.25)	1.41 (1.28–1.49)	0.73 (0.58–0.78)	0.84 (0.37–1.09)	1.05 (0.93–1.23)
Rangira	0.99 (0.74–1.15)	0.69 (0.53–0.81)	0.79 (0.60–0.93)	0.50 (0.38–0.56)	0.48 (0.37–0.56)
Ngwenda	0.15 (0.13–0.20)	0.05 (0.03–0.08)	0.09 (0.07–0.11)	0.08 (0.06–0.12)	0.30 (0.28–0.34)
Rwahambi	0.44 (1.57–2.34)	0.06 (1.40–1.72)	0.12 (0.56–0.83)	0.15 (0.38–1.26)	0.29 (1.09–1.25)

depending on the soil and the lithology of each watershed (Figures 2a and 2b). This highlights the secondary role of soil weathering to the river chemical composition in the VVP. Thus, Mukoni and Muzungu flowing on haplic acrisols (Figure 2a) were Na^+ and Ca^{2+} dominated; followed by K^+ and Mg^{2+} whose concentrations compete (Table 2). In contrast, Rwankwi and Ndata kept the K^+ - Na^+ dominance related to the presence of extinct volcanoes in the catchments (Figure 2b). The low mineralized rivers are found on haplic acrisols to the West and luvic phaeozems to the North (Figure 2a) with the most diluted water at both extremities of the sampling zone, away from the influence of active volcanoes.

Mean pH varied from neutral to relatively acid or basic (6.4–8.1; Figure 4i). The mean TA ranged from low ($<1.0 \text{ mmol L}^{-1}$) to exceptionally high ($>10.0 \text{ mmol L}^{-1}$) values (Figure 4j). The TA was overall positively correlated to Si (Figure 5a), and showed a larger scatter as a function of Ca^{2+} (Figure 5b). This is indicative of a strong contribution of silicate rock weathering to TA (Figure 5a), and this is confirmed by the Na^+ normalized plots (Figures 5c and 5d). Both TA/Na^+ and $\text{Mg}^{2+}/\text{Na}^+$ versus $\text{Ca}^{2+}/\text{Na}^+$ (Figures 5c and 5d, respectively) are aggregated to values close to those expected for silicate rock weathering based on the average values proposed by Gaillardet *et al.* [1999]. The rivers with a lithology dominated by acid metaphoric rocks (Mubimbi, Kisheke, Renga, Mukoni, and Muzungu) had a $\text{Ca}^{2+}/\text{Na}^{2+} > 1$, while the rivers with a lithology dominated by basalt/volcanic ash (i.e., Kihira, Chabiringa, Kamutoni, Rwankwi, Ndata, and Rangira; Figure 2b) were characterized by a $\text{Ca}^{2+}/\text{Na}^{2+} < 1$ and a TA/Na^+ close to 3. A few rivers (Kihira, Rwankwi, and Ndata) had $\text{Ca}^{2+}/\text{Na}^+$ values lower than the envelope of silicate rock end-member proposed by Gaillardet *et al.* [1999] (Figure 5c). This is probably related to the fact that Gaillardet *et al.* [1999] reported the chemical composition of the 60 largest rivers in the World, hence, excluding low mineralized small rivers such as some of those studied here. Another reason could be the atypical strong dominance of Na in the Virunga basalt, and consequently in the major cation composition of the stream network. The Na-normalized Ca^{2+} and Mg^{2+} ratios are consistent with high dissolution of Ca and Mg-rich silicate minerals, such as clinopyroxenes, mostly formed of diopside ($\text{CaMgSi}_2\text{O}_6$) [Morimoto, 1989] and which have been identified in Nyiragono's basalt [Platz, 2002; Platz *et al.*, 2004].

No consistent simple relationship was observed between TA and $\delta^{13}\text{C}$ -DIC (Figure 5e), but the river with the highest TA/Na^+ (Kisheke) was also characterized by the lowest $\delta^{13}\text{C}$ -DIC values (Figure 5f). Silicate weathering leads to the formation of HCO_3^- that has the isotopic signature of the CO_2 driving the weathering reaction. Since in freshwaters, DIC is usually dominated by HCO_3^- , especially in high TA systems, the $\delta^{13}\text{C}$ -DIC is close to the one of HCO_3^- , hence of the CO_2 initially involved in the dissolution of silicate rocks. Considering the evidence discussed above that silicate weathering is a strong contributor to TA in the region, the observed range of $\delta^{13}\text{C}$ -DIC (between -10.7‰ and 0‰ ; Figure 6a) indicates that the CO_2 driving silicate weathering was not derived from organic matter mineralized in soils. Indeed, DOC and POC have a $\delta^{13}\text{C}$ signature ranging between -28‰ and -18‰ (Figures 6b and 6c, respectively). However, the range of river $\delta^{13}\text{C}$ -DIC matches well with the range of $\delta^{13}\text{C}$ of CO_2 in volcanic gases reported by Deines [2002]. We thus conclude that the $\delta^{13}\text{C}$ -DIC signatures are to a large extent influenced by volcanic CO_2 dissolution in groundwaters and involved in silicate rock weathering. This pattern is quite different from those observed

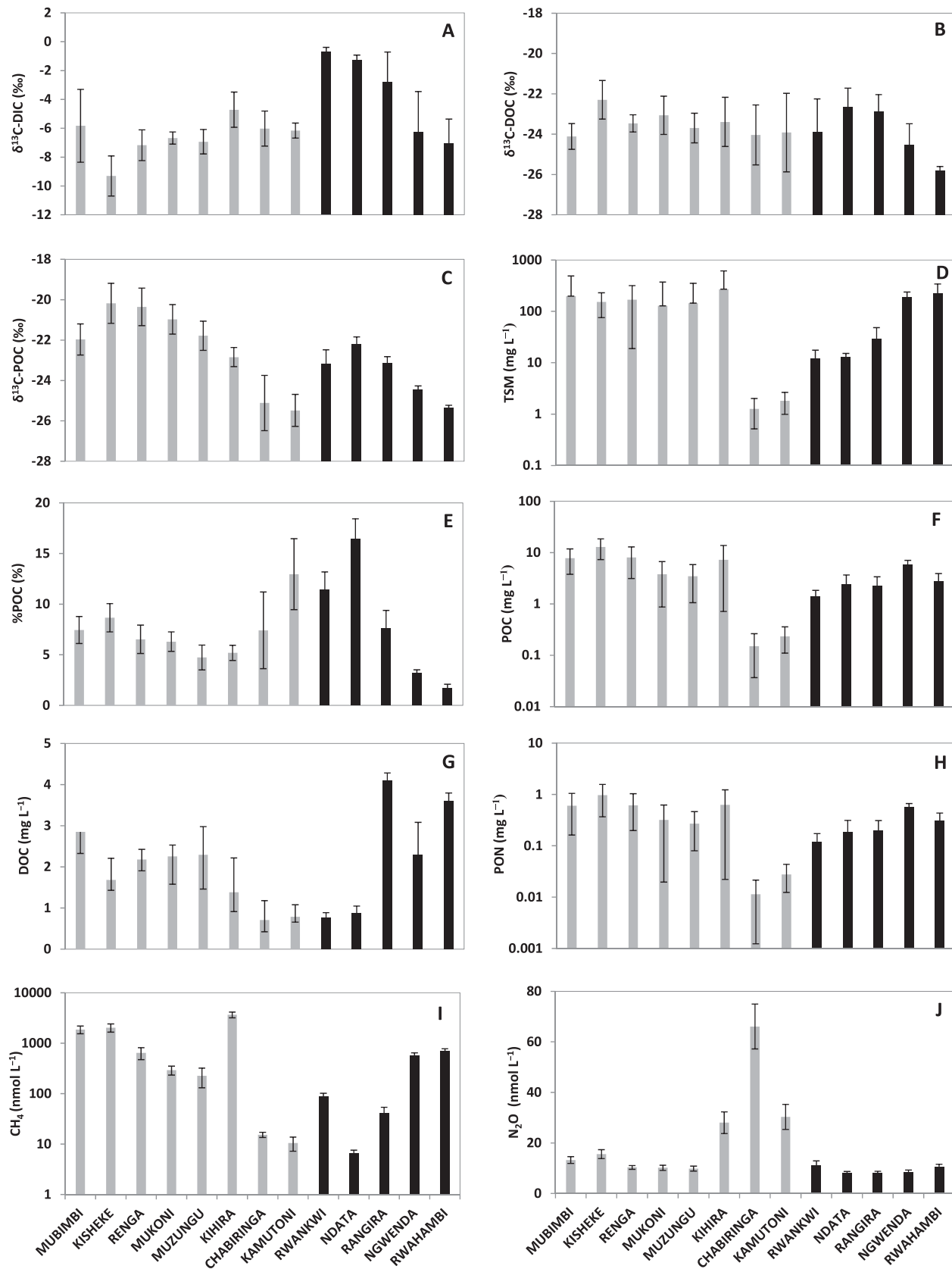


Figure 6. (a) Mean values of $\delta^{13}\text{C}_{\text{DIC}}$, (b) $\delta^{13}\text{C}_{\text{DOC}}$, (c) $\delta^{13}\text{C}_{\text{POC}}$, (d) total suspended matter, (e) %POC, (f) particulate organic carbon, (g) dissolved organic carbon, (h) particulate organic nitrogen, (i) methane, and (j) nitrous oxide in rivers of the Virunga Volcanic Province between December 2010 and February 2013. The gray and black bars represent rivers of Kabuno bay catchment and those of Lake Edward catchment, respectively. The error bars represent one standard deviation.

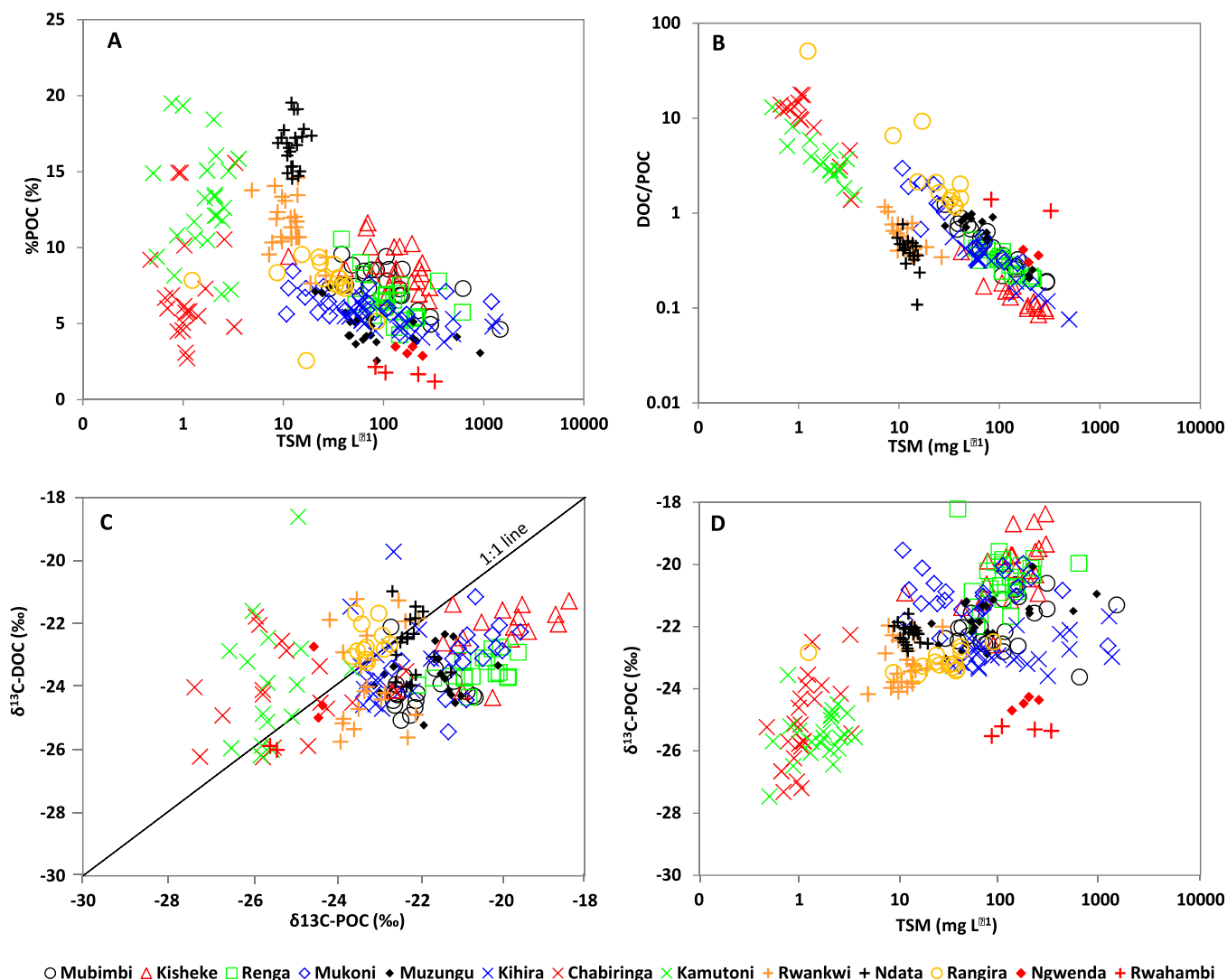


Figure 7. (a) Relationships between the %POC and total suspended matter, (b) DOC/POC and total suspended matter, (c) $\delta^{13}\text{C}_{\text{DOC}}$ and $\delta^{13}\text{C}_{\text{POC}}$ and (d) $\delta^{13}\text{C}_{\text{POC}}$ and TSM in rivers of the Virunga Volcanic Province between December 2010 and February 2013.

in the lower Congo basin, where $\delta^{13}\text{C}\text{-DIC}$ values as low as $\sim -26\text{‰}$ are found in rivers where silicate weathering also dominates, but where the CO_2 driving silicate weathering is produced by mineralization of organic matter derived from C3 vegetation [Bouillon *et al.*, 2014].

Silicate weathering also strongly affected the SRP distribution as shown by the highly significant correlation between SRP and dissolved Si (when the three headwater rivers Kihira, Chabiringa and Kamutoni are excluded) (Figure 8a). This is in line with the general link between P release and rock weathering [Hartmann *et al.*, 2014].

4.3. Organic Matter Dynamics and Origin

Large differences in the TSM load were observed in the VVP rivers. Higher TSM ($289\text{--}1467\text{ mg L}^{-1}$) was found in rivers located in the west of Kabuno bay basin, i.e., in Mubimbi, Kisheke, Renga, Mukoni, Muzungu, and Kihira (Figure 6d). These are second-order rivers draining a basin where steep slopes (supporting information Data Set S2), combined with high rainfall and agricultural land use practices, result in high erosion rates. The TSM load of these rivers is characterized by a relatively low organic matter content (mean %POC $< 9\%$, Figure 6e). The catchment of Kabuno bay is composed of haplic acrisols (Figure 2a) which are clay-enriched soils. The land is mainly used for farming (crops and pastures; supporting information Figure S1) which

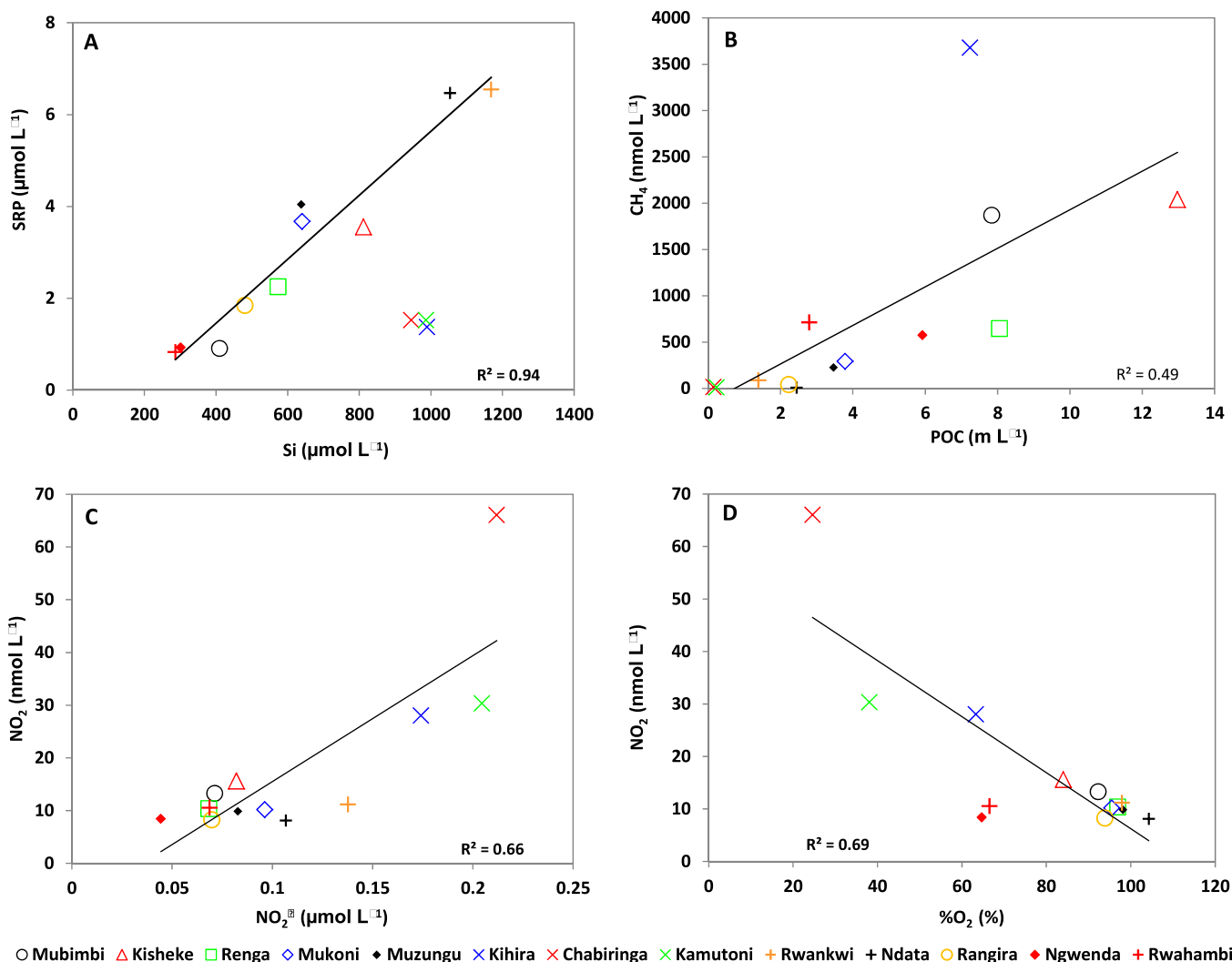


Figure 8. (a) Relationships between mean soluble reactive phosphorus and silicon, (b) mean methane and particulate organic carbon, (c) mean nitrous oxide and nitrite, and (d) between mean nitrous oxide and dissolved oxygen in rivers of the Virunga Volcanic Province between December 2010 and February 2013.

promotes soil erosion. Chabiringa, Kamutoni, Rwankwi, Ndata, and Rangira showed the lowest TSM, with values ranging from 0.5 to 86.3 mg L⁻¹ (Figure 6d). These rivers flow on mollic andosols of volcanic parent material from the Nyamulagira and Mikeno volcanoes (Figure 2a), with shrubs or forest cover (supporting information Figure S1). Thus, the lower TSM observed in the rivers draining volcanic fields are a result of the lower sensitivity of volcanic rocks toward mechanical erosion processes. The TSM could however be potentially enriched in organic matter (%POC > 10, e.g., in Kamutoni, Rwankwi, and Ndata; Figure 7a) from the dense vegetation cover. Ngwenda and Rwahambi flow on luvic phaeozems which are humic-rich and highly productive soils. The latter have favored the development of farming activities that generate high TSM with a low %POC (Figure 7a) found in Ngwenda and Rwahambi.

Most Virunga rivers have mean TSM and POC (Figure 6f) that are higher than main stem Congo River (26.3 mg/L for TSM, 1.7 mg/L for POC) [Coynel *et al.*, 2005] or other large rivers [Meybeck, 1982; Spitzy and Leenheer, 1991; Martins and Probst, 1991]. Mean TSM loads in the VVP rivers draining mountainous catchments (128.3–270.4 mg L⁻¹) were also higher compared to volcanic mountainous rivers of Guadeloupe (11.8–56.2 mg L⁻¹) [Lloret *et al.*, 2013]. Nevertheless, Guadeloupe rivers have mean TSM somewhat high than that of Virunga rivers draining basaltic field (1.3–29.8 mg L⁻¹). POC concentrations were extremely variable among rivers, while DOC showed lower spatial variability (Figure 6g). In the majority of rivers, POC dominated the organic C pool. Differences in the POC/DOC ratios can be explained by differences in soil type, soil leaching and/or erosion and the relief. Both lower mean DOC (<0.9 mg L⁻¹) and POC

(<2.5 mg L⁻¹) were observed in rivers draining volcanic fields (Figure 2a). These rivers (i.e., Chabiringa, Kamutoni, Rwankwi, and Ndata rivers) are characterized by low terrestrial biomass (Figure 2c) and low organic C soil content (Figure 2d).

The total organic C (TOC = DOC + POC) generally increased as one moves away from the volcanic area toward the NE and W. Thus, the TOC was found to be 6 to ~20 times higher in the most remote rivers. While DOC has typically been suggested to be the dominant C pool in large tropical rivers [Meybeck, 1993b], C of rivers of the VVP was largely DIC dominated. This is due to the high rates of silicate weathering and magmatic CO₂ inputs. The DOC/DIC ratios were below those of rivers draining carbonate rocks (<0.2) [Meybeck, 2005].

There was no straightforward relationship between the riverine POC and DOC and the vegetation or soil organic carbon distribution in the catchments. For instance, Rwahambi had among the highest mean DOC, and yet was draining catchment of both low organic C soil (Figure 2d) and woody biomass (Figure 2c). In contrast, DOC/POC ratios were well correlated to TSM (Figure 7b), with ratios above 1 (dominance of the DOC in the TOC pool) in the headwater streams (e.g., Chabiringa and Kamutoni). POC became dominant in more erosive and turbid systems as previously described in other studies [e.g., Meybeck, 1982; Ittekkot and Laane, 1991; Ralison et al., 2008; Bouillon et al., 2009]. Mean DOC, POC, and PN (Figure 6h) in the VVP rivers were almost similar to those reported by Lloret et al. [2013] for Guadeloupan rivers of volcanic fields (0.69–2.25, 0.98–6.70, 0.1–2.31 mg L⁻¹, respectively, for DOC, POC, and PN). Natural vegetation in the Virunga consists of a mixture of Hatch-Slack photosynthetic pathway plants (C4) and grasslands employing Calvin pathway (C3), with the former dominating in quantity [Still and Powell, 2010] (supporting information Figure S1). Agricultural practices have introduced both new C4 (e.g., maize, sorghum, sugar cane, etc.) and C3 (e.g., banana, potato, cassava, etc.) plants. Thus, Virunga riverine $\delta^{13}\text{C}$ -DOC (Figure 6b) and $\delta^{13}\text{C}$ -POC (Figure 6c) showed a mixed origin for organic C, from both C3 and C4: C3 plants have a typical $\delta^{13}\text{C}$ around -30‰ to -26‰ , while C4 plants show a $\delta^{13}\text{C}$ of $\sim -12\text{‰}$ (-10‰ to -14‰) [Ehleringer, 1991]. We found however a slight dominance of C3-derived C to the riverine organic C pool, with mean $\delta^{13}\text{C}$ -DOC and $\delta^{13}\text{C}$ -POC of -23.5‰ and -22.5‰ respectively. There were no clear relationships between individual paired $\delta^{13}\text{C}$ -DOC and $\delta^{13}\text{C}$ -POC data, indicating both C pools were not closely coupled (Figure 7c). Literature data on the $\delta^{13}\text{C}$ of riverine POC and DOC in the Congo Basin are only available for low-altitude regions [e.g., Mariotti et al., 1991, Spencer et al., 2012, Bouillon et al., 2012, 2014], and show much more limited C4 contributions than those found in Virunga highlands, with the majority of data ranging between -30‰ and -26‰ .

As also reported in the lowland Congo [Bouillon et al., 2014], the $\delta^{13}\text{C}$ -POC was positively correlated to TSM (Figure 7d) and might indicate higher sediment inputs in catchments where C4 vegetation (grassland) is more substantial. The negative relationship between %POC and TSM (Figure 7a) has been previously observed within a given catchment [Tamooh et al., 2012; Bouillon et al., 2014] or globally across catchments [Meybeck, 1982]. This pattern is typically driven by the combination of inputs from direct litter or organic-rich surface soil layers (high %POC-low TSM) and more soil-derived sediments (low %POC-high TSM).

4.4. CH₄ and N₂O

Virunga rivers were sources of methane to the atmosphere as most rivers of the world [Bastviken et al., 2011], the observed CH₄ concentrations (Figure 6i) were above atmospheric equilibrium (~ 2 nmol L⁻¹). Overall there was a positive relationship between CH₄ and POC (Figure 8b) driven by enhanced in situ CH₄ production fuelled by the availability of organic matter and the removal of both POC and CH₄ in groundwaters.

In contrast, only Chabiringa, Kamutoni, and Kihira were sources of N₂O to the atmosphere as they showed concentrations (Figure 6j) above the atmospheric equilibrium (~ 10 nmol L⁻¹). Two of these rivers (Chabiringa and Kamutoni) showed low CH₄, while the third (Kihira) had the highest CH₄ of all rivers sampled. Chabiringa and Kamutoni were sampled close to springs, and therefore have chemical characteristics close to those of groundwaters such as high TA, conductivity and major cation concentrations, and low pH, temperature, DOC, and POC concentrations. These rivers were also characterized by low NO₂⁻ and high N₂O which might be indicative of denitrification in the groundwaters. These features drive the positive correlation between N₂O and NO₂⁻ (Figure 8c) and the negative correlation between N₂O and %O₂ (Figure 8d). Chabiringa and Kamutoni were also characterized by lower CH₄ concentrations indicative of CH₄ removal by bacterial oxidation in the groundwaters [Borges et al., 2015].

Table 3. Estimated Annual TSM, POC, PON, DOC, Si, and Nutrient Fluxes in Rivers of the Virunga Volcanic Province

	TSM (10 ³ t/yr)	POC (t/yr)	PON (t/yr)	DOC (t/yr)	Si (t/yr)	NO ₃ ⁻ (t/yr)	NO ₂ ⁻ (t/yr)	NH ₄ ⁺ (t/yr)	SRP (t/yr)	Total P (t/yr)
Mubimbi	20.79	793.33	60.38	290.56	1061.75	231.31	0.34	6.63	2.55	8.67
Kisheke	1.47	121.56	9.03	15.23	196.87	29.43	0.03	0.48	0.84	2.37
Renga	13.10	661.38	46.96	162.07	1145.21	319.94	0.19	6.43	4.38	10.39
Mukoni	2.52	71.10	5.64	40.20	305.96	127.75	0.08	1.94	1.65	2.40
Muzungu	6.86	159.71	14.62	99.84	711.54	340.54	0.37	2.90	5.44	7.81
Kihira	15.06	411.68	36.01	70.77	1368.97	245.06	0.42	7.49	1.80	2.73
Chabiringa	0.04	3.20	0.35	20.22	752.99	49.59	0.27	1.47	1.08	0.64
Kamutoni	0.03	3.20	0.41	11.55	406.14	20.36	0.14	0.84	0.67	0.35
Rwankwi	1.76	196.10	16.37	107.42	4696.05	776.76	0.87	4.92	27.62	24.89
Ndata	0.74	138.19	10.11	51.96	1726.19	277.44	0.30	1.85	12.07	9.85
Rangira	56.17	4206.60	379.14	7437.30	23689.23	3651.04	6.49	92.32	96.75	90.73
Ngwenda	56.47	1737.54	163.21	687.11	2516.19	518.14	0.52	17.58	8.67	13.53
Rwahambi	28.11	356.82	39.71	431.45	970.14	153.30	0.39	3.85	3.15	3.97
Virunga total	203.12	8860.42	781.94	9425.68	39547.22	6740.68	10.42	148.69	166.67	178.32

Kihira was sampled downstream of a confluence, one river is from the west in the Mitumba range (Figure 1) and the other from the east. During the last three sampling campaigns, the two tributaries of Kihira were also sampled, and the eastern was found to bring in O₂-deficient water, of high specific conductivity, TA, CH₄, and N₂O. Except for CH₄, these previous parameters (%O₂, TA, and N₂O) showed similar patterns as Chabiringa and Kamutoni. The eastern tributary collects inflowing water containing CH₄ produced in a small swamp (supporting information Figure S1), which could explain the elevated CH₄ found in Kihira. In contrast, the western tributary brought almost the entire TSM and POC load, as a consequence of its mountainous origin in the Mitumba range and its course along a clayey and steep catchment.

As mentioned above, most rivers were only small sources of N₂O to the atmosphere, as observed in other near-pristine tropical rivers with low NO₃⁻ and NH₄⁺ [Bouillon et al., 2012; Borges et al., 2015] and unlike most nitrogen-enriched temperate rivers that have high N₂O concentrations [Beaulieu et al., 2010a, 2010b; Baulch et al., 2011]. The higher N₂O in Chabiringa, Kamutoni and Kihira were associated with high NO₃⁻ and low NO₂⁻ and O₂ (Figures 8c and 8d; respectively) that suggests active denitrification in the groundwaters. Such correlations between N₂O and NO₂⁻ were also observed in some temperate rivers [Dong et al., 2004].

The CH₄ concentration of Virunga rivers (4–5052 nmol L⁻¹) have a broader range than previous data from African rivers such as Comoé, Bia, and Tanoé rivers in West Africa (50–870 nmol L⁻¹) [Koné et al., 2010], Tana river in Kenya (50–500 nmol L⁻¹) [Bouillon et al., 2009], the Oubangui river in Central Africa (50–300 nmol L⁻¹) [Bouillon et al., 2012], but similar to the Athi-Galana-Sabaki rivers in Kenya (2–6729 μmol L⁻¹) [Marwick et al., 2014], although for the latter the highest values were related to organic matter inputs from the city of Nairobi. CH₄ of rivers of the VVP were also characterized by higher values than the adjacent Lake Kivu where CH₄ in surface waters varied from 18 to 197 nmol L⁻¹ in the main basins of the lake and 89–303 in the Kabuno bay [Borges et al., 2011, 2012]. On the other hand, rivers of the VVP contain N₂O close to that observed in the Oubangui river [Bouillon et al., 2012] and the Athi-Galana-Sabaki rivers (18–198 nmol L⁻¹) [Marwick et al., 2014] but remain largely below concentrations normally found in temperate rivers where human activities have increased the DIN concentrations (see compilation by Zhang et al. [2010]).

4.5. Riverine Material Fluxes

Our estimated annual TSM, Si, NH₄⁺, and SRP fluxes for Kihira (Table 3) are comparable with fluxes reported by Muvundja et al. [2009], except for the TP fluxes which were ~90 times higher in their study compared to our estimate. For Chabiringa-Kamutoni, the TSM and SRP annual fluxes are similar for both studies, but our mean TP flux is 48 times higher, and our NH₄⁺ flux is 23 times lower. In Mukoni-Muzungu, our TSM, Si, NH₄⁺, and SRP fluxes are 18, 10, 12, and 8 times higher, respectively, while their mean TP flux is 4 times higher. The observed dissimilarities in fluxes between the two studies are due to differences already discussed among TSM and nutrients concentrations, and are even more pronounced due to differences in the annual discharges used. Muvundja et al. [2009] estimated their annual discharge using the float method described in Harrelson et al. [1994], which assumes a steady and uniform flow and does not offset flood and low flow conditions. For rivers of mountainous catchments (e.g., Kabuno bay), such a method results in discharges with errors of 30% or greater [Bathurst, 1990].

Table 4. Drainage Areas, Climatic Settings, Mean Solute Concentrations and Rates for Rivers in the Virunga Volcanic Province

	Drainage Area (km ²)	Runoff ^d (mm/year)	T (°C)	HCO ₃ ⁻ (mmol/L)	TSM (mg/L)	TDS _{cat} (mg/L)	TDS _{cond} (mg/L)	CO ₂ Consumption Rate (10 ⁶ mol/km ² /year)	Si Weathering Rate (t/km ² /year)	Cationic Weathering Rate (t/km ² /year)	Chemical Weathering Rate (t/km ² /year)	Mechanical Weathering Rate (t/km ² /year)
Mubimbi ^a	55.7	1670	19.3	0.9	223.3	20.7	78.8	1.5	19.0	34.5	131.6	372.9
Kisheke ^a	5.8	1508	20.5	3.2	168.6	65.0	214.0	4.9	34.1	98.0	322.7	254.3
Renga ^a	43.6	1651	21.7	2.6	181.7	61.6	195.6	4.4	26.2	101.7	323.1	300.1
Mukoni ^a	15.4	1119	22.5	5.2	146.0	118.6	384.9	5.8	19.8	132.8	430.9	163.4
Muzungu ^a	16.1	2637	22.3	5.4	161.3	130.8	402.7	14.2	44.1	345.0	1062.0	425.5
Kihira ^b	31.7	1559	20.3	10.9	304.4	275.2	808.1	17.0	43.1	428.9	1259.5	474.5
Chabiringa ^b	8.5	3326	17.4	11.1	1.3	294.3	835.9	37.0	88.4	978.7	2779.9	4.3
Kamutoni ^b	10.2	1430	17.7	11.3	1.7	308.1	840.7	16.1	39.6	440.6	1202.4	2.5
Rwankwi ^b	95.0	1505	19.1	6.9	12.3	159.1	433.1	10.4	49.4	239.4	651.8	18.5
Ndata ^b	70.5	829	19.4	6.7	12.7	149.6	398.0	5.6	24.5	124.0	329.8	10.5
Rangira ^a	1351.0	1313	20.4	4.0	31.7	83.5	250.3	5.2	17.5	109.6	328.7	41.6
Ngwenda ^c	231.8	1297	22.0	0.3	187.7	6.1	30.1	0.4	10.9	7.9	39.0	243.6
Rwahambi ^c	107.3	1120	21.6	0.6	233.8	16.6	55.5	0.7	9.0	18.6	62.1	261.9

^aRivers draining basaltic formations.

^bRivers draining acid metamorphic rock formations.

^cRivers draining lacustrine formations.

^dEstimated runoff.

The estimated mean TSM (198.0 t km⁻² yr⁻¹) and POC (7.43 t km⁻² yr⁻¹) yields of VVP rivers were much higher when compared to those of the Congo River (8.8 t km⁻² yr⁻¹ for TSM and 0.6 t km⁻² yr⁻¹ for POC) [Coynel *et al.*, 2005], the Oubangui River (4.8–5.1 t km⁻² yr⁻¹ for TSM and ~0.3 t km⁻² yr⁻¹ for POC) [Coynel *et al.*, 2005; Bouillon *et al.*, 2012], and the world largest rivers (see compilation by Meybeck [1982], Spitzy and Leenheer [1991], and Coynel *et al.* [2005]). The estimated mean DOC yields (3.11 t km⁻² yr⁻¹) were similar to that of the Congo River (3.5 t km⁻² yr⁻¹) [Coynel *et al.*, 2005], but higher compared to the Oubangui River (1.1–1.4 t km⁻² yr⁻¹) [Coynel *et al.*, 2005; Bouillon *et al.*, 2012].

The estimated DOC (0.74–6.19 t km⁻² yr⁻¹) and POC (0.31–21.08 t km⁻² yr⁻¹) yields in the VVP were almost in the same range with those reported for Guadeloupan volcanic islands [1.9–8.9 t km⁻² yr⁻¹ and 8.1–25.5 t km⁻² yr⁻¹, respectively, for DOC and POC] [Lloret *et al.*, 2011, 2013]. This could partly be explained by two major similarities between the areas. First, both fields experience tropical wet season, and second; their organic C soil content are similar: 1–25% for Virunga and 10–15% for Guadeloupe [Lloret, 2010].

4.6. Weathering and Atmospheric CO₂ Consumption Rates

The discharge-weighted mean TDS_{cat}, TDS_{cond}, and TSM yielded cationic weathering rates from 7.9 to 978.7 t km⁻² yr⁻¹, chemical weathering rates from 39.0 to 2779.9 t km⁻² yr⁻¹, and mechanical weathering rates between 2.5 and 474.5 t km⁻² yr⁻¹ (Table 4). The Si weathering rates and CO₂ consumption rates ranged from 9.0 to 88.4 t km⁻² yr⁻¹, and 0.4 × 10⁶ to 37.0 × 10⁶ mol km⁻² yr⁻¹, respectively. Chemical weathering was more important in rivers draining basaltic fields, whereas mechanical weathering was prevailing in others lithological formations; i.e., acid metamorphic and lacustrine (Table 4). An opposite trend, with higher mechanical than chemical weathering rates, has been observed in the tropical basaltic field of Réunion, [Louvât and Allègre, 1997]. The large influence of lithology on the chemical weathering and CO₂ consumption rates in the Virunga is evident, and illustrated, for example, by comparing Chabiringa (basaltic terrain) with Ngwenda (lacustrine terrain). Thus, Chabiringa (drainage area of 8.5 km²) showed the highest weathering (Si, cationic, and chemical) and CO₂ consumption rates; whereas Ngwenda (231.8 km² drainage area) showed the lowest. Similar trends are observed when comparing rivers draining basaltic terrain (i.e., Kihira, Chabiringa, Kamutoni, Rwankwi, and Ndata) with those of lacustrine and metamorphic rocks. As a result, the five rivers of basaltic terrain cover only 10.6% of the total studied drainage area, but are responsible for 23.4% of the total CO₂ consumed, 22.6% of the total Si weathered, and 25.8% of the total major cations weathered. Basalt was characterized by a mean chemical weathering rate and mean CO₂ consumption rate 2.87 and 2.88 times higher, respectively, compared to values in acid metamorphic rocks terrain; and 24.6 and 32.7 times higher than in lacustrine terrain.

Chemical weathering rates were found to depend strongly on runoff, since there were strong linear relationships between runoff and CO₂ consumption rates ($r^2 = 0.63$; Figure 9a), cationic weathering rates ($r^2 = 0.62$; Figure 9b), and Si weathering rates ($r^2 = 0.66$; Figure 9c). In contrast, no positive temperature dependency

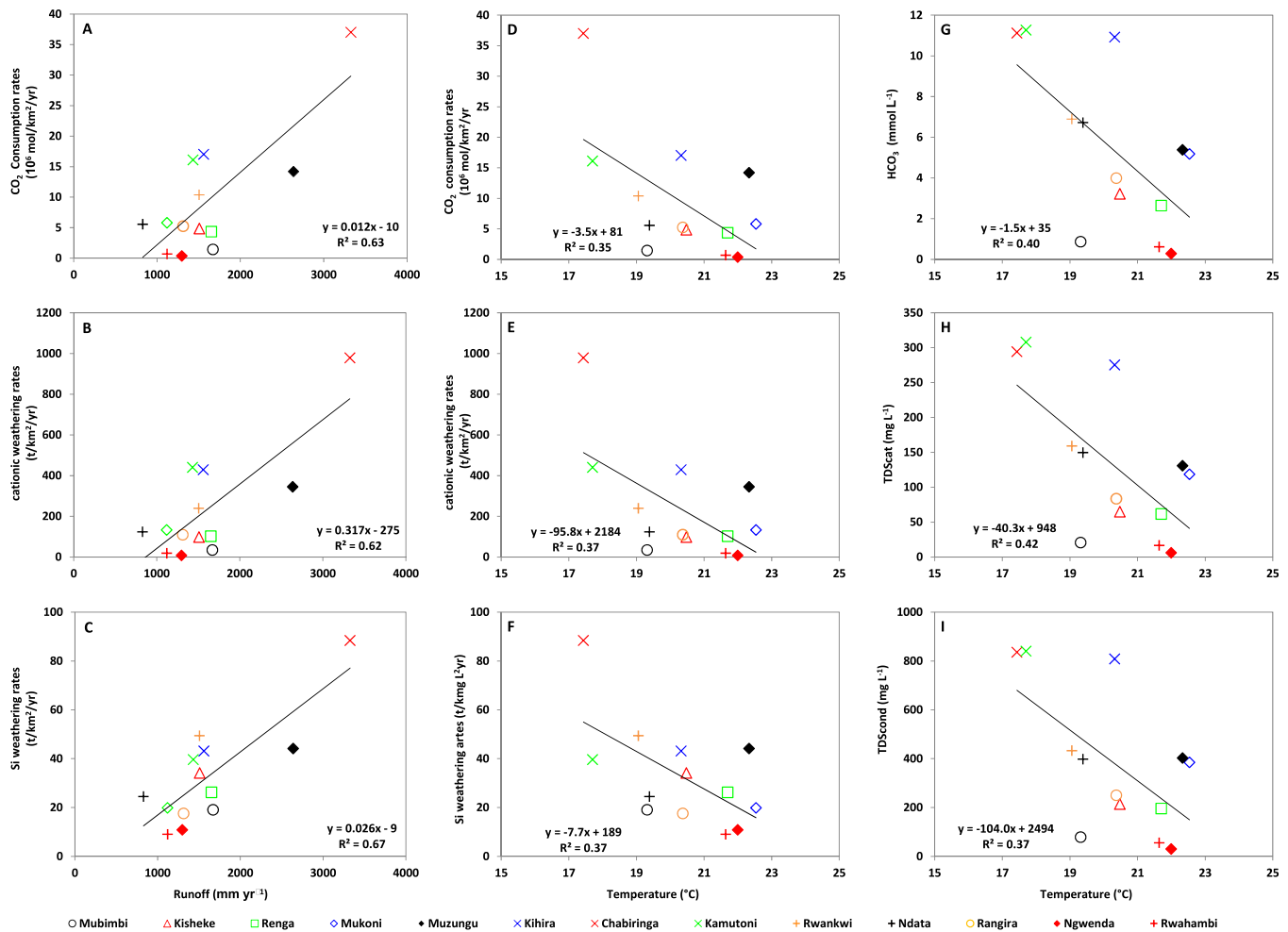


Figure 9. (a-c) Mean riverine CO₂ consumption rates, cationic weathering rates, and Si weathering rates versus runoff; (d-f) mean riverine CO₂ consumption rates, cationic weathering rates and Si weathering rates versus temperature; and (g-i) mean HCO₃⁻, TDS_{cat}, TDS_{cond} concentrations versus corresponding mean water temperature.

was found for either the CO₂ consumption rate (Figure 9d), cationic weathering rate (Figure 9e), and Si weathering rate (Figure 9f). In addition, no dependency on temperature was found for elements released during chemical weathering (Figures 9h and 9i), or for the HCO₃⁻ ions which balance the major cation charge (Figure 9g), as previously noted by *Amiotte-Suchet and Probst* [1995] and *Bluth and Kump* [1994] in the French basaltic basins. *Dessert et al.* [2003] attributed this pattern to the relative similarity among temperatures of neighboring watersheds, and thus only the effect of runoff could be observed.

The mean CO₂ consumption rate estimated for the study area ($9.46 \times 10^6 \text{ mol km}^{-2} \text{ yr}^{-1}$, or $1.72 \times 10^7 \text{ mol km}^{-2} \text{ yr}^{-1}$ if only considering the basaltic fields) is markedly higher than data reported in the literature for other tropical basaltic regions (Figure 10). On the other hand, the measured mean atmospheric C yield ($113.68 \text{ t C km}^{-2} \text{ yr}^{-1}$) is much higher than previous model estimates for the Virunga ($0.5\text{--}5 \text{ t C km}^{-2} \text{ yr}^{-1}$) [*Hartmann et al.*, 2009]. Since the Virunga mean CO₂ consumption rate is >10 times the global average ($1.99 \text{ t C km}^{-2} \text{ yr}^{-1}$) [*Hartmann et al.*, 2009], the VVP can thereby be considered as CO₂ consumption “hot spot zone” according to a classification by *Meybeck et al.* [2006].

Factors contributing to the high CO₂ consumption rates in the VVP include the high chemical weathering rate of volcanic rocks [*Dessert et al.*, 2001], the high reactivity of basaltic glasses and minerals [*Berner and Berner*, 1996; *Oelkers and Gislason*, 2001; *Gislason and Oelkers*, 2003], and the high annual mean runoff (1613 mm yr^{-1}) and temperature (20.3°C).

Furthermore, the CO₂ consumption rates that can be calculated with the model of *Dessert et al.* [2003] based on a compilation of data in other basalt dominated areas are lower than those we computed (Figure 11).

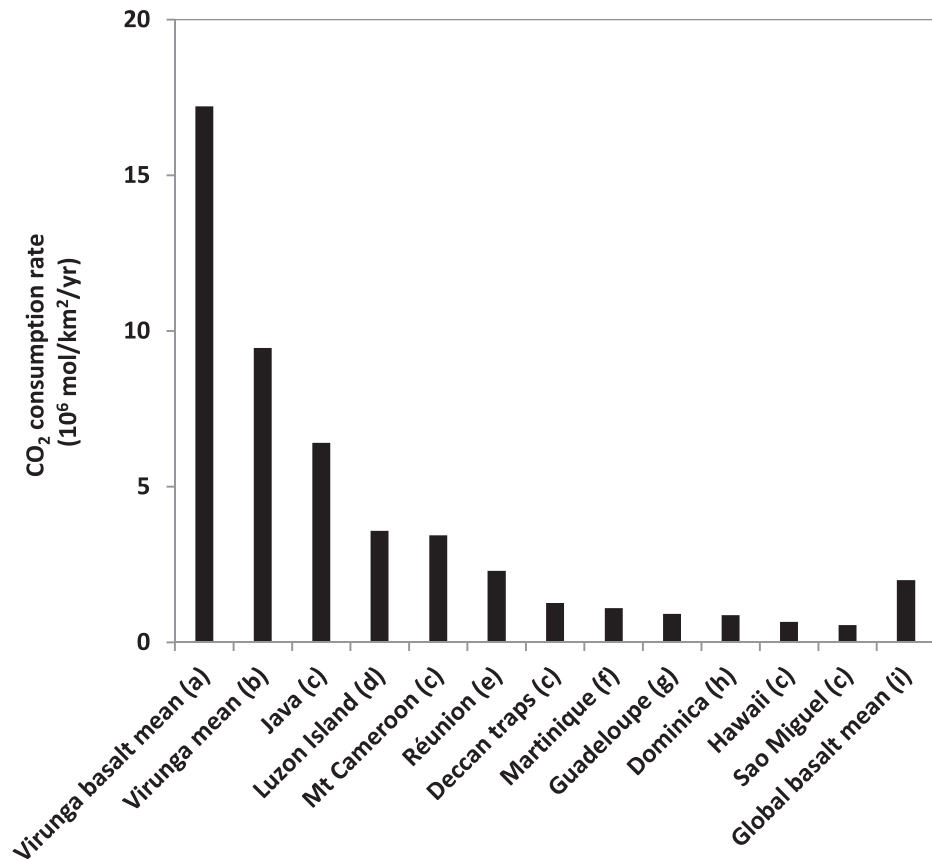


Figure 10. Comparison of Virunga basalt mean and Virunga mean CO₂ consumption rates with the rates of other tropical basaltic provinces, and the Caribbean basalt-andesite formations. (a) represents the mean CO₂ consumption rate for the rivers draining Virunga basalt, (b) the mean CO₂ consumption rate for the whole Virunga, i.e., basalt, metamorphic rocks and lacustrine; (c) is from Dessert *et al.* [2003], (d) Schopka *et al.* [2011], (e) Louvat and Allègre [1997], (f) Rad *et al.* [2006], (g) Lloret *et al.* [2011], (h) Goldsmith *et al.* [2010], and (i) is from Louvat [1997].

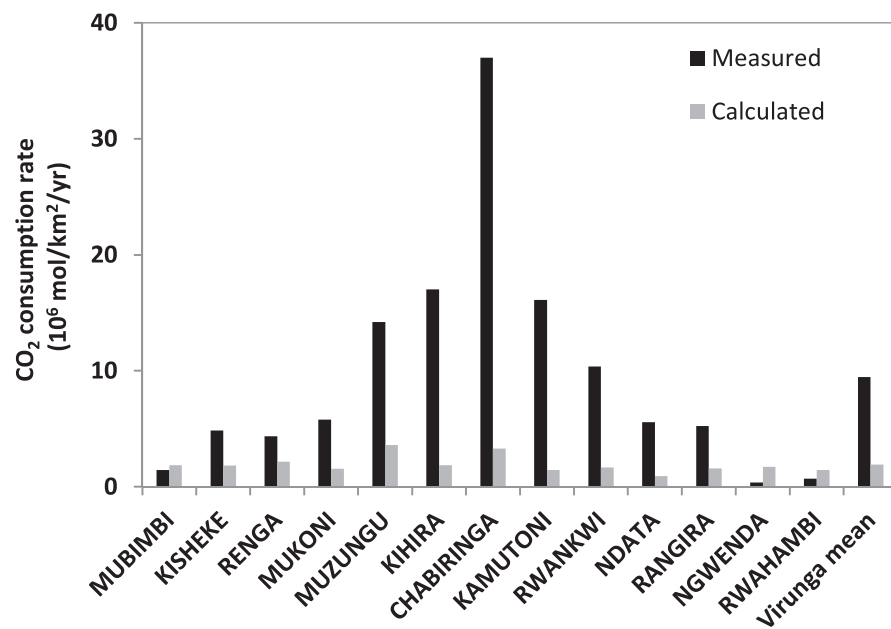


Figure 11. Comparison between the CO₂ consumption rates from field data (measured) and calculated CO₂ consumption (calculated) rates applying the regression model as a function of runoff and temperature as suggested by Dessert *et al.* [2003].

This is indicative of the high solubility of the rocks in the watershed which is probably related to the fact that the VVP is a young active tectonic and volcanic area.

5. Conclusions

The present study offers the first geochemical data set from an under-documented area, in terms of river GHGs and major cations concentrations, DOC, POC, and DIC concentrations and their respective $\delta^{13}\text{C}$ signatures, chemical weathering rates, and atmospheric CO_2 consumption rates. The VVP is a tropical, young active tectonic and volcanic area, relatively undisturbed by anthropogenic activities.

Our results showed that soil, land use, and morphology control the spatial distribution of riverine organic matter (POC and DOC concentrations and origin), TSM, and nutrient concentrations. The DIC was found to largely dominate the C pool. Intense soil erosion leads to high TSM yields in the mountainous rivers draining into Kabuno bay. Lithology and volcanism exert a strong control on the major cation and DIC concentrations, and their spatial distribution. Thus, high basalt (and secondary soil) chemical weathering and leaching mediated by magmatic CO_2 inputs yielded markedly high Na^+ , K^+ , Mg^{2+} , and Si; particularly in basaltic fields. CH_4 concentrations were consistently above atmospheric equilibrium, and thus Virunga rivers were sources of CH_4 to the atmosphere. In contrast, only a few rivers were a net source of N_2O to the atmosphere, as denitrification in groundwaters depleted N_2O concentrations below their atmospheric equilibrium levels in other rivers.

The multilithological state of the VVP highlights the strong influence of lithology on the chemical weathering rates, and the associated atmospheric CO_2 consumption rate under the same climatic conditions. In fact, we noticed that the mean chemical weathering rate and mean CO_2 consumption rate in basalt terrain were respectively ~ 3 higher compared to values in acid metamorphic rocks terrain; and ~ 25 and ~ 33 higher compared to lacustrine terrain. Our study additionally showed that runoff and lithology are the main factors controlling the rates of local chemical weathering and atmospheric CO_2 consumption rates. The $\delta^{13}\text{C}$ -DIC data indicate that part of the CO_2 involved in chemical weathering is geogenic, and thus the active volcanism may partly explain the higher CO_2 consumption and weathering rates reported in this study compared to the literature data.

Note that much of the Virunga lava field is not drained by rivers. This zone is composed of macroporous materials, slightly fractured, and therefore considerably permeable. Rainfall is influenced by the Nyiragongo and Nyamulagira emissions and pH values as low as three have been recorded [Cuoco *et al.*, 2012a, 2012b]. The precipitation interacts with surface and deep basalts, but the resulting atmospheric CO_2 consumption rate is not included in the data we report.

Acknowledgments

We are grateful to Stephane Hoornaert, Marc-Vincent Commarieu and Sandro Petrovic (Université de Liège), and Zita Kelemen (KU Leuven) for their support during sample analysis, Trent Marwick and Cristian Teodoru (KU Leuven) for help and advice with the GIS analysis, Jens Hartmann for kindly providing access to the GLIM database, Marcellin Kasereka for help in field sampling, and Bernhard Peucker-Ehrenbrink (reviewer) and two additional anonymous reviewers for constructive comments on a previous version of the manuscript. This work was funded by the European Research Council starting grant project AFRIVAL (African river basins: Catchment-scale carbon fluxes and transformations, StG 240002) and the Belgian Federal Science Policy Office EAGLES (East African Great Lake Ecosystem Sensitivity to changes, SD/AR/02A) projects. AVB is a senior research associate at the FRS-FNRS. The full data set is provided as supporting information (SI) (Balagizal-ds01 and Balagizal-ds02; XLS).

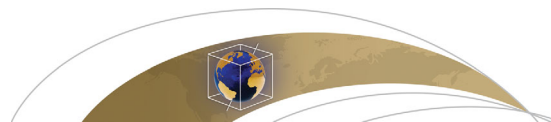
References

- American Public Health Association (1998), *Standard Methods for the Examination of Water and Wastewater*, 20th ed., Washington, D. C.
- Amiotte-Suchet, P., and J. L. Probst (1995), A global model for present-day atmospheric/soil CO_2 consumption by chemical erosion of continental rocks (GEM- CO_2), *Tellus, Ser. A*, 47, 273–280.
- Amiotte-Suchet, P., J. L. Probst, and W. Ludwig (2003), Worldwide distribution of continental rock lithology: Implications for the atmospheric/soil CO_2 uptake by continental weathering and alkalinity river transport to the oceans, *Global Biogeochem. Cycles*, 17(2), 1038, doi:10.1029/2002GB001891.
- Andersen, T., A. E. Marlina, and E. Muriel (2012), Petrology of combeite- and götzenite-bearing nephelinite at Nyiragongo, Virunga Volcanic Province in the East African Rift, *Lithos*, 152, 105–121, doi:10.1016/j.lithos.2012.04.018.
- Andersen, T., A. E. Marlina, and E. Muriel (2014), Extreme peralkalinity in delhayelite- and andremeyerite-bearing nephelinite from Nyiragongo volcano, East African Rift, *Lithos*, 206–207, 164–178, doi:10.1016/j.lithos.2014.07.025.
- Aoki, K., and H. Kurasawa (1984), Sr isotope study of the tephrite series from Nyamuragira volcano, Zaire, *Geochem. J.*, 18, 95–100.
- Aoki, K., T. Yoshida, K. Yusa, and Y. Nakamura (1985), Petrology and geochemistry of the Nyamuragira volcano, Zaire, *J. Volcanol. Geotherm. Res.*, 25, 1–28.
- Atekwana, E. A., E. A. Atekwana, R. S. Rowe, D. D. Werkema Jr., and F. D. Legall (2004), the relationship of total dissolved solids measurements to bulk electrical conductivity in an aquifer contaminated with hydrocarbon, *J. Appl. Geophys.*, 56, 281–294, doi:10.1016/j.jappgeo.2004.08.003.
- Baccini, A., N. Laporte, S. J. Goetz, M. Sun, and H. Dong (2008), A first map of tropical Africa's above-ground biomass derived from satellite imagery, *Environ. Res. Lett.*, 3, 045011, doi:10.1088/1748-9326/3/4/045011.
- Bastviken, D., L. J. Tranvik, J. A. Downing, P. M. Crill, and A. E. Prast (2011), Freshwater methane emissions offset the continental carbon sink, *Science*, 331, 50, doi:10.1126/science.1196808.
- Bathurst, J. C. (1990), Tests of three discharge gauging techniques in mountain rivers, in *Hydrology of Mountainous Areas*, IAHS Publ. no 190, pp. 93–100, Wallingford, U. K.
- Batjes, N. H. (2008), Mapping soil carbon stocks of Central Africa using SOTER, *Geoderma*, 146, 58–65, doi:10.1016/j.geoderma.2008.05.006.
- Baulch, H. M., S. L. Schiff, R. Maranger, and P. J. Dillon (2011), Nitrogen enrichment and the emission of nitrous oxide from streams, *Global Biogeochem. Cycles*, 25, GB4013, doi:10.1029/2011GB004047.
- Beaulieu, J. J., et al. (2010a), Nitrous oxide emission from denitrification in stream and river networks, *Proc. Natl. Acad. Sci. U. S. A.*, 108, 214–219, doi:10.1073/pnas.1011464108.

- Beaulieu, J. J., W. D. Huster, and J. A. Rebold (2010b), Nitrous oxide emissions from a large, impounded river: The Ohio River, *Environ. Sci. Technol.*, *44*(19), 7527–7533, doi:10.1021/es1016735.
- Beck, V., et al. (2012), Methane airborne measurements and comparison to global models during BARCA, *J. Geophys. Res.*, *117*, D15310, doi:10.1029/2011JD017345.
- BEGo (Synoptics, Keyobs, Royal Museum for Central Africa, Catholic University of Louvain) (2005), Parc National des Virunga, République Démocratique du Congo, 1/260,000, Map realized in the framework of the BEGo (Building Environment for the Gorilla's) project, co-financed by ESA and UNESCO-WHC, Belgium.
- Berner, E. K., and R. A. Berner (1996), *Global Environment: Water, Air, and Geochemical Cycles*, Prentice-Hall, N. J.
- Bluth, G. J. S., and L. R. Kump (1994), Lithologic and climatologic controls of river chemistry, *Geochim. Cosmochim. Acta*, *58*, 2341–2359.
- Borges, A. V., G. Abril, B. Delille, J.-P. Descy, and F. Darchambeau (2011), Diffusive methane emissions to the atmosphere from Lake Kivu (Eastern Africa), *J. Geophys. Res.*, *116*, G03032, doi:10.1029/2011JG001673.
- Borges, A. V., et al. (2012), Variability of carbon dioxide and methane in the epilimnion of Lake Kivu, in *Lake Kivu: Limnology and Biogeochemistry of a Tropical Great Lake*, *Aquat. Ecol.*, vol. 5, edited by J. P. Descy, pp. 47–66, Springer, Dordrecht, Netherlands, doi:10.1007/978-94-007-4243-7_4.
- Borges, A. V., et al. (2015), Globally significant greenhouse gas emissions from African inland waters, *Nat. Geosci.*, doi:10.1038/NGEO2486.
- Bouillon, S., et al. (2009), Distribution, origin and cycling of carbon in the Tana River (Kenya): A dry season basin-scale survey from headwaters to the delta, *Biogeosciences*, *6*, 2475–2493, doi:10.5194/bg-6-2475-2009.
- Bouillon, S., A. Yambélé, R. G. M. Spencer, D. P. Gillikin, P. J. Hernes, J. J. Six, R. Merckx, and A. V. Borges (2012), Organic matter sources, fluxes and greenhouse gas exchange in the Oubangui River (Congo River basin), *Biogeosciences*, *9*, 2045–2062, doi:10.5194/bg-9-2045-2012.
- Bouillon, S., A. Yambélé, D. P. Gillikin, C. Teodoru, F. Darchambeau, T. Lambert, and A. V. Borges (2014), Contrasting biogeochemical characteristics of right-bank tributaries and a comparison with the mainstem Oubangui River, Central African Republic (Congo River basin), *Sci. Rep.*, *4*, 5402, doi:10.1038/srep05402.
- Bousquet, P., et al. (2011), Source attribution of the changes in atmospheric methane for 2006–2008 *Atmos. Chem. Phys.*, *11*, 3689–3700, doi:10.5194/acp-11-3689-2011.
- Chakrabarti R., A. R. Basu, A. P. Santo, D. Tedesco, and O. Vaselli (2009), Isotopic and geochemical evidence for a heterogeneous mantle plume origin of the Virunga volcanics, Western rift, East African Rift system, *Chem. Geol.*, *259*, 273–289, doi:10.1016/j.chemgeo.2008.11.010.
- Coynel, A., P. Seyler, H. Etcheber, M. Meybeck and D. Orange (2005), Spatial and seasonal dynamics of total suspended sediment and organic carbon species in the Congo River, *Global Biogeochem. Cycles*, *19*, GB4019, doi:10.1029/2004GB002335.
- Cuomo, E., A. Spagnuolo, C. Balagizi, S. Francesco, F. Tassi, O. Vaselli, and D. Tedesco (2012a), Impact of volcanic emissions on rainwater chemistry: The case of Mt. Nyiragongo in the Virunga volcanic region (DRC), *J. Geochem. Explor.*, *125*, 69–79, doi:10.1016/j.jgexplo.2012.11.008.
- Cuomo, E., D. Tedesco, R. J. Poreda, J. C. Williams, S. De Francesco, C. Balagizi, and T. H. Darrah (2012b), Impact of volcanic plume emissions on rain water chemistry during the January 2010 Nyamuragira eruptive event: Implications for essential potable water resources, *J. Hazard. Mater.*, *244–245*, 570–581, doi:10.1016/j.jhazmat.2012.10.055.
- Deines, P. (2002), The carbon isotope geochemistry of mantle xenoliths, *Earth Sci. Rev.*, *58*, 247–278, doi:10.1016/S0012-8252(02)00064-8.
- Demant, A., P. Lestrade, T. R. Lubala, A. B. Kampunzu, and J. Durieux (1994), Volcanological and petrological evolution of Nyiragongo volcano, Virunga volcanic field, Zaire, *Bull. Volcanol.*, *56*, 47–61.
- Denaeyer, M. E. (1972), Les laves du fossé tectonique de l'Afrique Centrale. II: Magmatologie, *Ann. Musée R. Afrique Cent.*, *72*, 250.
- Denaeyer, M. E. (1975), *Le glacis des volcans actifs au nord du Lac Kivu (république du Zaïre)*, Ed. du Museum, Sér. C, Sci. de la terre, Paris.
- Dessert, C., B. Dupré, L. M. François, J. Schott, J. Gaillardet, G. Chakrapani and S. Bajpai (2003), Erosion of Deccan Traps determined by river geochemistry, impact on the global climate and the ⁸⁷Sr/⁸⁶Sr ratio of seawater, *Earth Planet. Sci. Lett.*, *188*, 459–474.
- Dessert, C., B. Dupré, J. Gaillardet, L. M. François, and C. J. Allègre (2003), Basalt weathering laws and the impact of basalt weathering on the global carbon cycle, *Chem. Geol.*, *202*, 257–273, doi:10.1016/j.chemgeo.2002.10.001.
- Document stratégique de réduction de la pauvreté (2005), *Province du Nord-Kivu*, SRP-Nord-Kivu, Goma, RD Congo.
- Dong, L. F., D. B. Nedwell, I. Colbeck, and J. Finch (2004), Nitrous oxide emission from some English and Welsh rivers and estuaries, *Water Air Soil Pollut.*, *4*(6), 127–134, doi:10.1007/s11267-005-3022-z.
- Ehleringer, J. R. (1991), ¹³C/¹²C Fractionation and its utility in terrestrial plant studies, in *Carbon Isotope Techniques*, edited by B. Fry, pp. 187–200, Academic, N. Y.
- Farr, T. G., et al. (2007), The shuttle radar topography mission, *Rev. Geophys.*, *45*, RG2004, doi:10.1029/2005RG000183.
- Fraser, A., et al. (2013), Estimating regional methane surface fluxes: The relative importance of surface and GOSAT mole fraction measurements, *Atmos. Chem. Phys.*, *13*, 5697–5713, doi:10.5194/acp-13-5697-2013.
- Gaillardet, J., B. Dupré, P. Louvat, and C. J. Allègre (1999), Global silicate weathering and CO₂ consumption rates deduced from the chemistry of large rivers, *Chem. Geol.*, *159*(1–4), 3–30.
- Gillikin, D. P., and S. Bouillon (2007), Determination of δ¹⁸O of water and δ¹³C of dissolved inorganic carbon using a simple modification of an elemental analyzer-isotope ratio mass spectrometer (EA-IRMS): An evaluation, *Rapid Commun. Mass Spectrom.*, *21*, 1475–1478, doi:10.1002/rcm.2968.
- Gislason, S. R., and E. H. Oelkers (2003), Mechanism, rates and consequences of basaltic glass dissolution. II: An experimental study of the dissolution rates of basaltic glass as a function of pH and temperature, *Geochim. Cosmochim. Acta*, *67*, 3817–3832, doi:10.1016/S0016-7037(03)00176-5.
- Global Land Cover 2000 database (2003), *European Commission*, Joint Res. Cent. [Available at <http://bioval.jrc.ec.europa.eu/products/glc2000/glc2000.php>, last accessed 20 Jan. 2015.]
- Goldsmith, S. T., A. E. Carey, B. M. Johnson, S. A. Welch, W. B. Lyons, W. H. McDowell, and J. S. Pigott (2010), Stream geochemistry, chemical weathering and CO₂ consumption potential of andesitic terrains, Dominica, Lesser Antilles, *Geochim. Cosmochim. Acta*, *74*, 85–103, doi:10.1016/j.gca.2009.10.009.
- Guibert, P. (1978), Contribution à l'étude du volcanisme de la chaîne des Virunga (République du Zaïre): Le volcan Mikeno, PhD thesis, Univ. de Genève, Geneva, Switzerland.
- Harrelson, C. C., C. L. Rawlins, and J. P. Potyondy (1994), Stream channel reference sites: An illustrated guide to field technique, *Gen. Tech. Rep. RM-245*, 61 pp., Dep. of Agric., For. Serv., Rocky Mt. For. and Range Exp. Str., Fort Collins, Colo.
- Hartmann, J., and N. Moosdorf (2011), Chemical weathering rates of silicate-dominated lithological classes and associated liberation rates of phosphorus on the Japanese Archipelago-Implications for global scale analysis, *Chem. Geol.*, *287*, 125–157, doi:10.1016/j.chemgeo.2010.12.004.

- Hartmann, J., and N. Moosdorf (2012), The new global lithological map database GLiM: A representation of rock properties at the Earth surface, *Geochem. Geophys. Geosyst.*, *13*, Q12004, doi:10.1029/2012GC004370.
- Hartmann, J., N. Jansen, H. H. Dürr, S. Kempe, and P. Köhler (2009), Global CO₂-consumption by chemical weathering: What is the contribution of highly active weathering regions?, *Global Planet. Change*, *69*, 185–194, doi:10.1016/j.gloplacha.2009.07.007.
- Hartmann, J., N. Moosdorf, R. Lauerwald, M. Hinderer, and A. J. West (2014), Global chemical weathering and associated P-release—The role of lithology, temperature and soil properties, *Chem. Geol.*, *363*, 145–163, doi:10.1016/j.chemgeo.2013.10.025.
- Head, E. M., A. M. Shaw, P. J. Wallace, K. W. W. Sims, and S. A. Carn (2011), Insight into volatile behavior at Nyamuragira volcano (D.R. Congo, Africa) through olivine-hosted melt inclusions, *Geochem. Geophys. Geosyst.*, *12*, Q0AB11, doi:10.1029/2011GC003699.
- Hertogen, J., L. Vanlerberghe, and M. R. Namegabe (1985), Geochemical evolution of the Nyiragongo volcano (Virunga, Western African Rift, Zaire), *Bull. Geol. Soc.*, *57*(1–2), 21–35.
- Hijmans, R. J., S. E. Cameron, J. L. Parra, P. G. Jones, and A. Jarvis (2005), Very high resolution interpolated climate surfaces for global land areas, *Int. J. Climatol.*, *25*, 1965–1978, doi:10.1002/joc.1276.
- Ittekkot, V., and R. W. P. M. Laane (1991), Fate of riverine particulate organic matter, in *Biogeochemistry of Major World Rivers*, edited by E. T. Degens, S. Kempe, and J. E. Richey, chap. 6, pp. 233–243, John Wiley, N. Y.
- Julley, D. W., M. Windowson, and S. Self (2008), Volcanogenic nutrient fluxes and plant ecosystems in large igneous provinces: An example from the Columbia River Basalt Group, *J. Geol. Soc.*, *165*, 955–966, doi:10.1144/0016-76492006-199.
- Kirschke, S., et al. (2013), Three decades of global methane sources and sinks, *Nat. Geosci.*, *6*, 813–823, doi:10.1038/NGEO1955.
- Koné, Y. J. M., G. Abril, B. Delille, and A. V. Borges (2010), Seasonal variability of methane in the rivers and lagoons of Ivory Coast (West Africa), *Biogeochemistry*, *100*, 21–37, doi:10.1007/s10533-009-9402-0.
- Lauerwald, R., G. G. Laruelle, J. Hartmann, P. Ciais, and P. A. G. Regnier (2015), Spatial patterns in CO₂ evasion from the global river network, *Global Biogeochem. Cycles*, *29*, 534–554, doi:10.1002/2014GB004941.
- Le Quéré, C., et al. (2014), Global carbon budget 2014, *Earth Syst. Sci. Data Discuss.*, *7*, 521–610, doi:10.5194/essdd-7-521-2014.
- Loret, E. (2010), Dynamique du carbone dans des petits bassins versants tropicaux, exemple de la Guadeloupe, PhD thesis, Univ. of Paris, Paris.
- Loret, E., C. Dessert, J. Gaillardet, P. Albéric, O. Crispi, C. Chaduteau, and M. F. Benedetti (2011), Comparison of dissolved inorganic and organic carbon yields and fluxes in the watersheds of tropical volcanic islands, examples from Guadeloupe, *Chem. Geol.*, *280*, 65–78, doi:10.1016/j.chemgeo.2010.10.016.
- Lloret, E., C. Dessert, L. Pastor, E. Lajeunesse, O. Crispi, J. Gaillardet, and M. F. Benedetti (2013), Dynamic of particulate and dissolved organic carbon in small volcanic mountainous tropical watersheds, *Chem. Geol.*, *351*, 229–244, doi:10.1016/j.chemgeo.2013.05.023.
- Louvat, P. (1997), Etude géochimique de l'érosion fluviale d'îles volcaniques à l'aide des bilans d'éléments majeurs et traces, PhD thesis, 322 pp., Univ. of Paris, Paris.
- Louvat, P., and C. J. Allègre (1997), Present denudation rates at Réunion Island determined by river geochemistry: Basalt weathering and mass budget between chemical and mechanical erosions, *Geochim. Cosmochim. Acta*, *61*, 3645–3669.
- Ludwig, W., J. L. Probst, and S. Kempe (1996), Predicting the oceanic input of organic carbon by continental erosion, *Global Biogeochem. Cycles*, *10*(1), 23–41, doi:10.1029/95GB02925.
- Mann, P. J., et al. (2014), The biogeochemistry of carbon across a gradient of streams and rivers within the Congo Basin, *J. Geophys. Res. Biogeosci.*, *119*, 687–702, doi:10.1002/2013JG002442.
- Marcelot, G., C. Dupuy, J. Dostal, J. P. Rancon, and A. Pouclet (1989), Geochemistry of mafic volcanic rocks from Lake Kivu (Zaire and Rwanda) section of the Western Branch of the African Rift, *J. Volcanol. Geotherm. Res.*, *39*, 73–88.
- Mariotti, A., F. Gadel, P. Giresse, and Kinga-Mouzeo (1991), Carbon isotope composition and geochemistry of particulate organic matter in the Congo River (Central Africa): Application to the study of Quaternary sediments off the mouth of the river, *Chem. Geol.*, *86*, 345–357.
- Martins, O., and J. L. Probst (1991), Biogeochemistry of major African Rivers: Carbon and mineral transport, in *Biogeochemistry of Major World Rivers*, edited by E. T. Degens, S. Kempe, and J. E. Richey, chap. 6, pp. 129–155, John Wiley, N. Y.
- Marwick, T. R., F. Tamooh, B. Ogwoka, C. Teodoru, A. V. Borges, F. Darchambeau, and S. Bouillon (2014), Dynamic seasonal nitrogen cycling in response to anthropogenic N loading in a tropical catchment, Athi-Galana-Sabaki River, Kenya, *Biogeosciences*, *11*, 1–18, doi:10.5194/bg-11-1-2014.
- Mayaux, P., E. Bartholomé, S. Fritz, and A. Belward (2004), A new land-cover map of Africa for the year 2000, *J. Biogeogr.*, *31*, 861–877, doi:10.1111/j.1365-2699.2004.01073.x.
- Meybeck, M. (1982), Carbon, nitrogen and phosphorus transport by world rivers, *Am. J. Sci.*, *282*, 401–450.
- Meybeck, M. (1987), Global chemical weathering of surficial rocks estimated from river dissolved loads, *Am. J. Sci.*, *287*, 401–428.
- Meybeck, M. (1993a), Natural sources of C, N, P and S, in *Interactions of C, N, P and S Biogeochemical Cycles and Global Change*, edited by R. Wollast, F. T. Mackenzie, and L. Chou, pp. 163–193, Springer, Berlin.
- Meybeck, M. (1993b), Riverine transport of atmospheric carbon: Sources, global typology and budget, *Water Air Soil Pollut.*, *70*, 443–464.
- Meybeck, M. (2005), Origins and behaviours of carbon species in World rivers, in *Erosion and Carbon Dynamics*, *Adv. Soil Sci.*, edited by E. Roose and R. Lal, pp. 209–238, CRC Press, Boca Raton, Fla.
- Meybeck, M., H. H. Dürr and C. J. Vörösmarty (2006), Global coastal segmentation and its river catchment contributors: A new look at land-ocean linkage, *Glob. Biogeochem. Cycles*, *20*, GB1590, doi:10.1029/2005GB002540.
- Moon, S., C. P. Chamberlain, and G. E. Hilley (2014), New estimates of silicate weathering rates and their uncertainties in global rivers, *Geochim. Cosmochim. Acta*, *134*, 257–274, doi:10.1016/j.gca.2014.02.033.
- Morimoto, N. (1989), Nomenclature of pyroxenes, *Can. Mineral.*, *27*, 143–156.
- Munhoven, G. (2002), Glacial-interglacial changes of continental weathering: Estimates of the related CO₂ and HCO₃⁻ flux variations and their uncertainties, *Global Planet. Change*, *33*(1–2), 155–176.
- Muvundja, A. F., et al. (2009), Balancing nutrient inputs to Lake Kivu, *J. Great Lakes Res.*, *35*(3), 406–418, doi:10.1016/j.jglr.2009.06.002.
- Oelkers, E. H., and S. R. Gislason (2001), The mechanism, rates and consequences of basaltic glass dissolution. I: An experimental study of the dissolution rates of basaltic glass as function of aqueous Al, Si and oxalic acid concentration at 25°C and pH = 3 and 11, *Geochim. Cosmochim. Acta*, *65*, 3671–3681.
- Platz, T. (2002), Nyiragongo volcano, DR Congo-mineral chemistry and petrology, PhD thesis, Univ. of Greifswald, Inst. of Geol. Sci., Greifswald, Germany.
- Pison, I., P. Bousquet, F. Chevallier, S. Szopa, and D. Hauglustaine (2009), Multi-species inversion of CH₄, CO and H₂ emissions from surface measurements, *Atmos. Chem. Phys.*, *9*, 5281–5297, doi:10.5194/acp-9-5281-2009.

- Platz, T., S. F. Foley, and L. Andre (2004), Low-pressure fractionation of the Nyiragongo volcanic rocks, Virunga Province, D.R. Congo, *J. Volcanol. Geotherm. Res.*, *136*, 269–295, doi:10.1016/j.jvolgeores.2004.05.020.
- Poucllet, A. (1974), Pétrographie du Rugarama, dernier cône adventif du volcan Nyamuragira (1971), (Rift W.-Africain), *Publ. Spéc.*, 1–28.
- Poucllet, A. (1977), Contribution à l'étude structurale de l'aire volcanique des Virunga, rift de l'Afrique Centrale, *Rev. Géogr. Phys. Géol. Dyn.*, *19*(2), 115–124.
- Rad, S., P. Louvat, C. Gorge, J. Gaillardet, and C. J. Allègre (2006), River dissolved and solid loads in the Lesser Antilles: New insight into basalt weathering processes, *J. Geochem. Explor.*, *88*, 308–312, doi:10.1016/j.gexplo.2005.08.063.
- Ralison, O., F. Dehairs, J. J. Middelburg, A. V. Borges, and S. Bouillon (2008), Carbon biogeochemistry in the Betsiboka estuary (northwestern Madagascar), *Org. Geochem.*, *39*, 1649–1658, doi:10.1016/j.orggeochem.2008.01.010.
- Raymond, P. A., et al. (2013), Global carbon dioxide emissions from inland waters, *Nature*, *503*, 355–359, doi:10.1038/nature12760.
- Rodier, J., and C. Bazin (2005), *Analyse de l'eau: Eaux naturelles, eaux résiduelles et eaux de mer*, 8 éd., Dunod, Paris.
- Schopka, H. H., L. A. Derry, and C. A. Arcilla (2011), Chemical weathering, river geochemistry and atmospheric carbon fluxes from volcanic and ultramafic regions on Luzon Island, the Philippines, *Geochim. Cosmochim. Acta*, *75*, 978–1002, doi:10.1016/j.gca.2010.11.014.
- Smets, B. (2007), *Etude des mazokus dans la région de Goma (République Démocratique du Congo) et gestion des risques, Mémoire de Master en Gestion des Risques Naturels*, Univ. de Liège, Liège, Belgium.
- Smets, B., et al. (2013), Detailed multidisciplinary monitoring reveals pre- and co-eruptive signals at Nyamulagira volcano (North Kivu, Democratic Republic of Congo), *Bull. Volcanol.*, *76*(1), 1–35, doi:10.1007/s00445-013-0787-1.
- Spencer, R. G. M., et al. (2012), An initial investigation into the organic matter biogeochemistry of the Congo River, *Geochim. Cosmochim. Acta*, *84*, 614–627, doi:10.1016/j.gca.2012.01.013.
- Spitz, A., and J. Leenheer (1991), dissolved organic carbon in rivers, in *Biogeochemistry of Major World Rivers*, edited by E. T. Degens, S. Kempe, and J. E. Richey, chap. 9, pp. 213–232, John Wiley, N. Y.
- Still, C. J., and R. L. Powell (2010), Continental-scale distributions of vegetation stable carbon isotope ratios, in *Isoscapes: Understanding Movement, Pattern, and Process on Earth Through Isotope Mapping*, edited by J. B. West, et al., pp. 179–193, Springer, Netherlands, doi:10.1007/978-90-481-3354-3_9.
- Tamooch, F. K., et al. (2012), Distribution and origin of suspended matter and organic carbon pools in the Tana River Basin, Kenya, *Biogeosciences*, *9*, 2905–2920, doi:10.5194/bg-9-2905-2012.
- Teodoru, C. R., F. C. Nyoni, A. V. Borges, F. Darchambeau, I. Nyambe, and S. Bouillon (2015), Spatial variability and temporal dynamics of greenhouse gas (CO₂, CH₄, N₂O) concentrations and fluxes along the Zambezi River main stem and major tributaries, *Biogeosciences*, *12*, 2431–2453, doi:10.5194/bg-12-2431-2015.
- Vitousek, P. M. (2004), *Nutrient Cycling and Limitation: Hawaii as a Model System*, Princeton Univ. Press, Princeton, N. J.
- Weiss, R. F. (1981), Determinations of carbon dioxide and methane by dual catalyst flame ionization chromatography and nitrous oxide by electron capture chromatography, *J. Chromatogr. Sci.*, *19*, 611–616.
- Wieczorek, M. E. (2012), *Flow-Based Method for Stream Generation in a GIS*, USGS Water Sci. Cent. for Md., Delaware and the Dist. of Columbia, USGS. [Available at <http://md.water.usgs.gov/posters/flowGIS/index.html>].
- Zhang, G. L., J. Zhang, S. M. Liu, J. L. Ren, and Y. C. Zhao (2010), Nitrous oxide in the Changjiang (Yangtze River) Estuary and its adjacent marine area: Riverine input, sediment release and atmospheric fluxes, *Biogeosciences*, *7*, 3505–3516, doi:10.5194/bg-7-3505-2010.



RESEARCH ARTICLE

10.1002/2015GC005999

Key Points:

- CH₄ concentrations were consistently above atmospheric equilibrium
- Most parameters showed no pronounced seasonal variation
- The ¹³C-DIC data indicate that part of the CO₂ involved in chemical weathering is geogenic

Supporting Information:

- Supporting Information S1
- Data Set S1
- Data Set S2

Correspondence to:

C. M. Balagizi,
balagizi.charles@gmail.com

Citation:

Balagizi, C. M., F. Darchambeau, S. Bouillon, M. M. Yalire, T. Lambert, and A. V. Borges (2015), River geochemistry, chemical weathering, and atmospheric CO₂ consumption rates in the Virunga Volcanic Province (East Africa), *Geochem. Geophys. Geosyst.*, 16, doi:10.1002/2015GC005999.

Received 9 JUL 2015

Accepted 12 JUL 2015

Accepted article online 16 JUL 2015

River geochemistry, chemical weathering, and atmospheric CO₂ consumption rates in the Virunga Volcanic Province (East Africa)

Charles M. Balagizi^{1,2,3}, François Darchambeau², Steven Bouillon⁴, Mathieu M. Yalire¹, Thibault Lambert², and Alberto V. Borges²

¹Geochemistry and Environmental Department, Goma Volcano Observatory, Goma, RD Congo, ²Chemical Oceanography Unit, Université de Liège, Liège, Belgium, ³Department of Environmental, Biological and Pharmaceutical Sciences and Technologies, Second University of Naples, Caserta, Italy, ⁴Department of Earth and Environmental Sciences, Katholieke Universiteit Leuven, Leuven-Heverlee, Belgium

Abstract We report a water chemistry data set from 13 rivers of the Virunga Volcanic Province (VVP) (Democratic Republic of Congo), sampled between December 2010 and February 2013. Most parameters showed no pronounced seasonal variation, whereas their spatial variation suggests a strong control by lithology, soil type, slope, and vegetation. High total suspended matter (289–1467 mg L⁻¹) was recorded in rivers in the Lake Kivu catchment, indicating high soil erodibility, partly as a consequence of deforestation and farming activities. Dissolved and particulate organic carbon (DOC and POC) were lower in rivers from lava fields, and higher in nonvolcanic subcatchments. Stable carbon isotope signatures ($\delta^{13}\text{C}$) of POC and DOC mean $\delta^{13}\text{C}$ of -22.5‰ and -23.5‰ , respectively, are the first data to be reported for the highland of the Congo River basin and showed a much higher C4 contribution than in lowland areas. Rivers of the VVP were net sources of CH₄ to the atmosphere (4–5052 nmol L⁻¹). Most rivers show N₂O concentrations close to equilibrium, but some rivers showed high N₂O concentrations related to denitrification in groundwaters. $\delta^{13}\text{C}$ signatures of dissolved inorganic carbon suggested magmatic CO₂ inputs to aquifers/soil, which could have contributed to increase basalt weathering rates. This magmatic CO₂-mediated basalt weathering strongly contributed to the high major cation concentrations and total alkalinity. Thus, chemical weathering (39.0–2779.9 t km⁻² yr⁻¹) and atmospheric CO₂ consumption (0.4–37.0 × 10⁶ mol km⁻² yr⁻¹) rates were higher than previously reported in the literature for basaltic terrains.

1. Introduction

Rivers transport dissolved and particulate matter from land to the oceans. Part of the solutes transported by rivers are derived from chemical weathering processes in the catchment that is a function of local lithology, climate, and topography [Ludwig *et al.*, 1996; Gaillardet *et al.*, 1999; Hartmann *et al.*, 2014]. Part of the particulate load is derived from mechanical weathering. The terrestrial biosphere and in particular soils provide particulate (POC) and dissolved (DOC) organic carbon to rivers. Groundwaters carry the products of aerobic and anaerobic mineralization in soils toward the river network, and along with mineralization of POC and DOC within the river system, this typically leads to large emissions of greenhouse gases (GHGs) such as carbon dioxide (CO₂) [Raymond *et al.*, 2013; Lauerwald *et al.*, 2015; Borges *et al.*, 2015] and methane (CH₄) [Bastviken *et al.*, 2011; Borges *et al.*, 2015]. Anthropogenic inputs of nitrogen from fertilizers or wastewater can lead to high N₂O emissions from rivers to the atmosphere that are commonly attributed to denitrification [Beaulieu *et al.*, 2010a; Baulch *et al.*, 2011; Marwick *et al.*, 2014]. Nitrogen-poor rivers on the other hand have low N₂O levels [Baulch *et al.*, 2011; Borges *et al.*, 2015].

The annual global CH₄ emissions to the atmosphere between 2000 and 2009 have been estimated at ~548 Tg CH₄ yr⁻¹; of which 218 Tg CH₄ yr⁻¹ were from natural sources and 335 Tg CH₄ yr⁻¹ from anthropogenic sources [Kirschke *et al.*, 2013]. Of the fluxes from natural sources, 175 Tg CH₄ yr⁻¹ were from natural wetlands and 43 Tg CH₄ yr⁻¹ from other natural sources, i.e., freshwater, geological processes, oceans, wild animals, wildfire, and termites [Pison *et al.*, 2009; Bousquet *et al.*, 2011; Beck *et al.*, 2012; Fraser *et al.*, 2013]. Approximately 49% of the global CH₄ emissions from freshwater ecosystems is thought to occur in the tropics [Bastviken *et al.*, 2011].

Raymond *et al.* [2013] provided global CO₂ evasion rates of 1.8 Pg C yr⁻¹ from streams and rivers, and 0.3 Pg C yr⁻¹ from lakes and reservoirs which is highly significant when compared to the land biosphere and oceanic carbon sink of 2.0 Pg C yr⁻¹, respectively [Le Quéré *et al.*, 2014]. The emission from rivers and streams has been recently revised downward to <0.7 Pg C yr⁻¹ by Lauerwald *et al.* [2015]. Yet in both these studies, the CO₂ data distribution in rivers and streams is skewed toward temperate and boreal systems in the Northern Hemisphere, while little data are available at tropical latitudes. There has been a growing number of studies of GHG fluxes in African rivers [Koné *et al.*, 2010; Bouillon *et al.*, 2009; 2012, 2014; Mann *et al.*, 2014; Marwick *et al.*, 2014; Teodoru *et al.*, 2015], that combined with new data have contributed to evaluate for the first time the emissions of GHGs from inland water at the African continental scale [Borges *et al.*, 2015]. The CO₂ and CH₄ emissions from African inland waters were found to be significant at both regional and global scales, totaling 0.4 Pg C yr⁻¹ for river channels alone, and 0.9 Pg C yr⁻¹ for river channels and wetlands of the Congo [Borges *et al.*, 2015].

Volcanic fields are characterized by dry gas emissions which dissolve in the near-surface groundwaters and could thus contribute to the regional aquatic C pool. Despite this distinctive feature, streams and rivers of volcanic zones are still under-investigated for GHG evasion estimates. Volcanic terrains also act as an atmospheric C sink through chemical weathering. Thus, chemical and physical weathering is an important part of many elements cycles. On a global scale, atmospheric CO₂ consumption by chemical weathering leads to the storage of 237–288 Mt C yr⁻¹ in surface waters and the oceans [Amiotte-Suchet and Probst, 1995; Amiotte-Suchet *et al.*, 2003; Gaillardet *et al.*, 1999; Munhoven, 2002; Hartmann *et al.*, 2009; Moon *et al.*, 2014]. About 63% of this global estimate is due to silicate weathering [Hartmann *et al.*, 2009]. Basalt weathering represents 30–35% of CO₂ sequestered by silicate weathering [Gaillardet *et al.*, 1999; Dessert *et al.*, 2003], although basalts correspond to only 4–6% of the global continent area [Meybeck, 1987; Amiotte-Suchet *et al.*, 2003; Hartmann *et al.*, 2009]. Given the large quantity of sequestered C and the subsequently significant role on climate regulation, more studies are needed to improve the quantification of chemical weathering and CO₂ consumption in basaltic formations. Investigating weathering rates in basaltic terrains at the regional scale contributes to reduce uncertainties in the modeling of the global atmospheric CO₂ consumption rate.

This study focuses on the geochemistry of rivers of the Virunga Volcanic Province (VVP) (Figure 1), characterized by high volcanic activity, located in a tropical climate zone, and with a dense hydrographic network, but which remains poorly studied from a geochemical point of view. We concentrated on the geochemical characterization of the major rivers of the VVP by: (1) quantifying concentrations of nutrients, major cations, organic and inorganic carbon and their stable carbon isotope composition ($\delta^{13}\text{C}$); (2) the quantification of riverine CH₄ and N₂O concentrations and (3) the estimation of spatial variations of these parameters. We additionally quantified solutes and suspended material fluxes, the chemical weathering rates and the associated atmospheric CO₂ consumption during basalt weathering. Finally, the dependence at regional scale of chemical weathering on climatic factors (temperature and runoff) was discussed.

2. Study Area

2.1. Geological and Hydrological Settings

The VVP is located in the western branch of the East African Rift and is bounded on the north by Lake Edward, on the south by Lake Kivu, the Rwandan dorsal on the east and the Mitumba Range on the west (Figure 1). Virunga volcanic activity started during the mid-Miocene [Poucllet, 1977] and consists of eight major volcanic edifices perpendicularly aligned to the position of the rift. Most edifices are dormant except Mount Nyiragongo (4370 m) and Mount Nyamulagira (3058 m), both located in the Democratic Republic of the Congo (DRC) and are the Africa's most active volcanoes. The edges of the rift are difficult to detect due to intense erosion, important vegetation cover and frequent lava flows [Smets, 2007] especially in the east. Nearly all the Virunga lavas are of alkalic to highly alkalic composition (Table 1), the alkalic character varies from a relatively sodic pole [Na₂O > K₂O] to a potassic or hyperpotassic pole [K₂O ≫ Na₂O]. The VVP consists of plains, shelf, and mountain ranges with altitudes of 900 m in the basin of Lake Edward and 1460 m in the Lake Kivu basin. The highest point is the Mount Karisimbi summit at 4508 m (Figure 1). The alluvial plain extends over the south basin of Lake Edward (i.e., lacustrine of Figure 2b), and then steadily rises up toward the Nyamulagira and Nyiragongo lava flows (i.e., basalt/volcanic ash of Figure 2b). The boundary

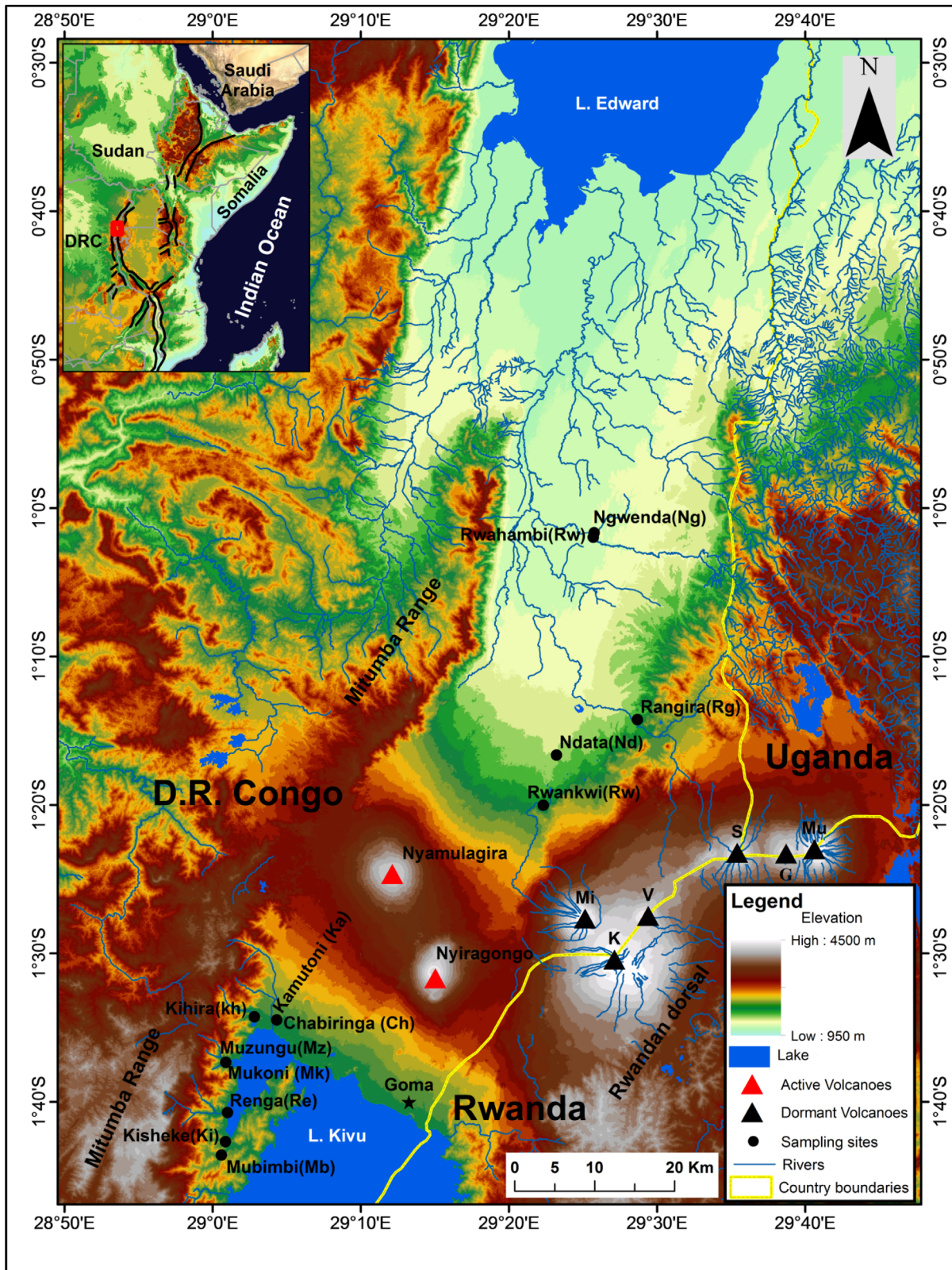


Figure 1. Map of the Virunga Volcanic Province (VVP) showing the sampling sites. Eight of the 13 sampled rivers drain into the Kabuno bay (a subbasin of Lake Kivu), i.e., Mubimbi (Mb), Kisheke (Ki), Renga (Re), Mukoni (Mk), Muzungu (Mz), Kihira (Kh), Kamutoni (Ka), and Chabiringa (Cha). The five others rivers drain into Lake Edward catchment, i.e., Rwankwi (Rk), Ndata (Nd), Rangira (Ra), Rwahambi (Rw), and Ngwenda (Ng). The blue lines represent the hydrographic network by BEGo (*Synoptics, Keyobs, Royal Museum for Central Africa, Catholic University of Louvain*) [2005]. The map also shows the six dormant volcanoes of the Virunga, i.e., Mikeno (Mi), Karisimbi (K), Visoke (V), Sabinyo (S), Gahinga (G), and Muhabura (Mu) while Nyiragongo and Nyamulagira are still active. The black lines in the inset map display the boundaries of the East African Rift System.

Table 1. Major Elements Composition (wt %) of the Virunga Lavas

	Nyiragongo ^a Mean (Range)	Nyamulagira ^b Mean (Range)	Mikeno ^c
SiO ₂	38.92 (29.72–48.38)	45.59 (37.88–47.83)	47.23
Al ₂ O ₃	14.22 (10.60–19.90)	14.08 (8.42–18.68)	15.01
Fe ₂ O ₃	11.73 (4.88–17.50)	5.07 (0.24–10.8)	9.91
FeO	6.46 (0.97–9.33)	8.64 (3.07–10.59)	
MnO	1.30 (0.16–6.30)	0.19 (0.03–0.35)	0.18
MgO	3.89 (0.16–6.30)	7.82 (0.19–14.9)	3.49
CaO	12.88 (8.11–18.86)	11.26 (5.16–18.09)	9.25
Na ₂ O	5.26 (1.90–7.28)	2.62 (1.5–11.38)	4.05
K ₂ O	5.11 (2.04–7.34)	2.93 (1.05–5.85)	6.28
TiO ₂	2.87 (1.98–4.30)	3.27 (1.25–5.14)	3.04
P ₂ O ₃	1.55 (0.44–2.39)	0.42 (0.13–2.09)	0.77
CO ₂	1.69 (0.40–3.16)	0.11 (0–0.33)	
H ₂ O ⁺	0.52 (0.35–0.68)	0.33 (0–0.84)	0.69
H ₂ O [−]	0.18 (0.12–0.24)	0.10 (0–0.64)	
K ₂ O + Na ₂ O	10.38	5.55	10.33
K ₂ O/Na ₂ O	0.97	1.11	1.55
Mg#	29.89 (22.80–32.74)	39.08 (34.53–43.3)	28.13

^aUndated lavas, lava from the 1977 and 2002 eruptions, after Demant *et al.* [1994], Platz *et al.* [2004], Chakrabarti *et al.* [2009], and Andersen *et al.* [2012, 2014].

^bUndated lavas, lava from the 1912, 1938, 1948, 1977, 1982, 1986, 2006, and 2010 eruptions after Denaeeyr [1972, 1975], Poucllet [1974], Aoki and Kurasawa [1984], Aoki *et al.* [1985], Hertogen *et al.* [1985], Marcelot *et al.*, 1989, Head *et al.* [2011], and Smets *et al.* [2013].

^cGuibert [1978].

between the Lake Edward and Lake Kivu watersheds is located on the line connecting the Nyamulagira-Nyiragongo-Karisimbi volcanoes (W to E oriented line; Figure 1). This boundary also corresponds to the limit between the Congo River basin to the south and the Nile River in the North. The mountain climate that marks the region is controlled by the nearby equatorial forest of the Virunga National Park and the mountain range. Precipitation is estimated at 1400–1500 mm yr^{−1} [Muvundja *et al.*, 2009], and the mean annual temperature at ~19.2°C. The region experiences a long wet season (September–May) and a dry season (June–August), with a short occasional dry season from mid-January to February. Lake Kivu (1460 m) and the hundreds of tributaries dominate the hydrography in the south of Virunga. The center and the north consist of a river network that feeds the Rutshuru River which flows into Lake Edward.

2.2. Soil Type and Land Uses

Three classes of soil are distinguished in the VVP (Figure 2a). The first lies on the area of presently active volcanoes and is composed of umbric and mollic andosols; the second covers the area of extinct volcanoes and composed of mollic andosols. The third consist of soil of alluvial and metamorphic rocks parent materials, formed by luvic phaeozems, haplic acrosols, and mubic cambisols (Figure 2a). The soils of presently active volcanic areas contain a thin humus layer covering lava flows on which mosses and lichens grow. A thick and slightly compact and humus-rich soil has developed on old lava flows; while the soil of the alluvial plain derives from sedimentary deposits. Local people practice traditional agriculture and livestock but an important area of the Virunga area is part of the Virunga National Park. No chemical fertilizers are used in the region. The lack of agricultural management on lands with steep slopes and the significant deforestation have generated substantial soil movements. They mainly include soil erosion and landslides, particularly in the mountainous watershed of Lake Kivu. The region is experiencing significant urbanization due to rural exodus triggered by repeated wars, causing Goma and the other small cities to host 4.2% of the population of the North Kivu province [Document stratégique de réduction de la pauvreté (DSRP), 2005].

3. Materials and Methods

3.1. Sampling Techniques

We carried out monthly sampling on 13 rivers in the VVP (all located in the DRC) from December 2010 to February 2013; eight are located in the Kabuno bay basin (a subbasin of Lake Kivu) while the five others drain into Lake Edward (Figure 1). Temperature, specific conductivity, pH, and dissolved oxygen (%O₂) were measured in situ with a Hanna (Hi 9828) multiparameter probe between December 2010 and December 2011,

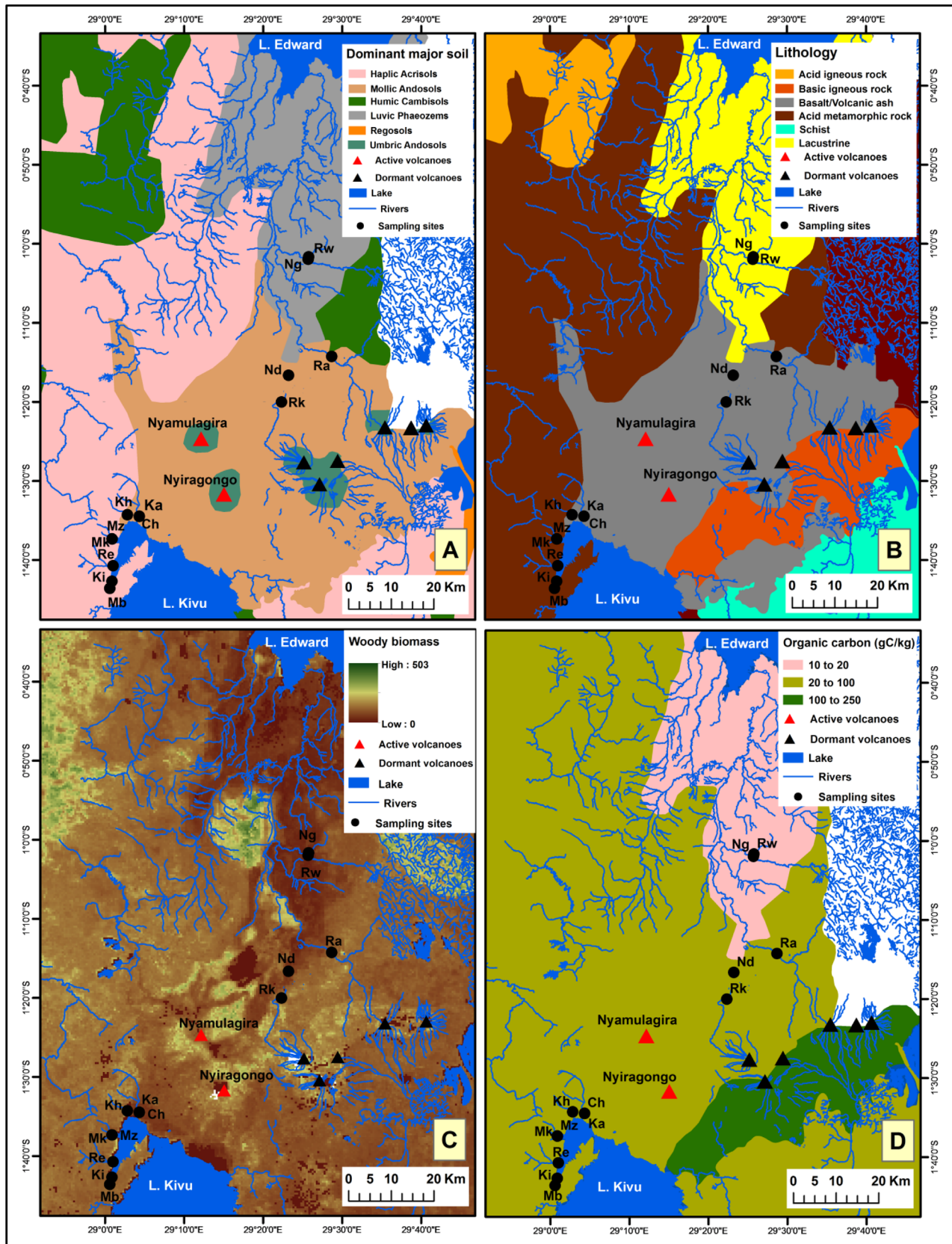


Figure 2. (a) Map of the major dominant soil groups, (b) lithology, (c) biomass, and (d) organic carbon distribution in the Virunga Volcanic Province.

and with an YSI ProPlus probe for the rest of the measurement period. The same calibration procedures were applied for both probes ensuring data continuity. Calibration of the pH electrode was carried out the evening prior to field measurements using pH 7.00 and pH 10.00 (25°C) standard buffers. The oxygen probes were calibrated with humidity-saturated ambient air in the field. Precision of conductivity, water temperature, pH, and %O₂ was estimated to 1 μS/cm, 0.1°C, 0.01 pH units, and 0.5%, respectively. Water for the analysis of dissolved gases (CH₄ and N₂O) was collected in two glass serum bottles of 50 mL and poisoned with 200 μL of a saturated HgCl₂ solution, and sealed with butyl stoppers and aluminum caps. Samples for the measurement of the carbon isotopic composition in the dissolved inorganic carbon ($\delta^{13}\text{C-DIC}$) were stored in 12 mL Exetainer vials and preserved with 100 μL of saturated HgCl₂ solution. Water for total alkalinity (TA), major elements, dissolved organic carbon (DOC), and its $\delta^{13}\text{C}$ signature was filtered through a 0.2 μm pore size polysulfone syringe filters, after prefiltration on 0.7 μm glass fiber filters. TA samples were collected in 50 mL high-density polyethylene bottles, 20 mL scintillation vials were used for major ions and preserved with 50 μL of HNO₃ 65%, while samples for DOC and $\delta^{13}\text{C}_{\text{DOC}}$ were collected in 50 mL Supelco glass bottles with polytetrafluoroethylene-coated septa, and preserved with 50 μL concentrated H₃PO₄. Samples for total suspended matter (TSM), particulate organic carbon (POC) and its $\delta^{13}\text{C}$ signature, and for particulate nitrogen (PN) were obtained by filtering a known volume of water (between 700 and 1700 mL depending on the turbidity of the river) through Macherey-Nagel GF-5 47mm precombusted (5 h at 500°C) glass fiber filters. Two 50 mL plastic bottles were filled with water from the Macherey-Nagel GF-5 filtration, preserved with 200 μL of H₂SO₄ 4 N for nitrates (NO₃⁻), nitrites (NO₂⁻), ammonium (NH₄⁺), and soluble reactive phosphorus (SRP) determination. For total phosphorus (TP) determination, a 50 mL plastic bottle was filled with unfiltered water and preserved with 200 μL of 4 N H₂SO₄.

3.2. Analytical Techniques

Concentrations of CH₄ and N₂O were determined by gas chromatography (GC) with flame ionization detection (SRI 8610C), after creating a 20 mL headspace with N₂ in the 50 mL glass serum bottle. A Flame Ionization Detector (FID) coupled to a Hayesep D column was used for CH₄ measurements, while an Electron Capture Detector (ECD) coupled to a Hayesep N column was used for N₂O measurements. The two detectors were calibrated at the start and end of each series with certified gas mixtures of 1, 10, and 30 μatm of CH₄ and 0.2, 2, and 6 μatm of N₂O (Air Liquide Belgium). The overall precision of measurements was ±3.9% and ±3.2% for CH₄ and N₂O, respectively [Borges *et al.*, 2015]. Concentrations of dissolved CH₄ and N₂O were calculated based on the partial pressure of the gas, its volume in the headspace and the water volume according to standard procedures by Weiss [1981]. $\delta^{13}\text{C-DIC}$ was analyzed using an elemental analyzer-isotope ratio mass spectrometer (EA-IRMS, Thermo Flash EA/HT and DeltaV Advantage). First, a 2 mL Helium headspace was created in the sample which was then acidified with H₃PO₄ and equilibrated overnight. A subsample from the headspace was injected into the EA-IRMS, and data were corrected for isotopic fractionation between dissolved and gaseous CO₂ as described by Gillikin and Bouillon [2007]. Measurements were calibrated with LSVEC and either NBS-19 or IAEA-CO-1 reference materials. The reproducibility of $\delta^{13}\text{C-DIC}$ measurement was typically better than ±0.2‰. TA was determined by Gran titration method with 0.1 M HCl as titrant using an automated titrator (Metrohm 725 Dosimat) equipped with a pH probe (ORION 8102 SC). Data were quality checked with certified reference material obtained from Andrew Dickinson (Scripps Institution of Oceanography, University of California, San Diego, USA). Typical reproducibility of TA measurements was better than ±3 μmol L⁻¹. For DOC and $\delta^{13}\text{C}_{\text{DOC}}$ analysis, 9–15 mL of sample were analyzed using a wet oxidation DOC analyzer (Thermo Hiper TOC or Aurora 1030W) coupled to an IRMS (Delta +XL or Delta V Advantage), calibrated with IAEA-C6 and an internal sucrose standard ($\delta^{13}\text{C} = -26.99 \pm 0.04\text{‰}$) calibrated against international reference materials. Reproducibility of $\delta^{13}\text{C-DIC}$ was typically better than ±0.2‰ and relative standard deviation for DOC concentration measurement was always below ±5%. Major elements were measured with inductively coupled plasma mass spectrometry (ICP-MS; Agilent 7700x) calibrated with the following standards: SRM1640a from National Institute of Standards and Technology, TM-27.3 (lot 0412) and TMRain-04 (lot 0913) from Environment Canada, and SPS-SW2 Batch 130 from Spectrapure Standard. Limit of quantification was 0.5 μmol L⁻¹ for Na⁺, Mg²⁺, and Ca²⁺, 1.0 μmol L⁻¹ for K⁺ and 8 μmol L⁻¹ for Si. TSM values were obtained as the ratio of sediment load to the filtered water volume, the sediment load being determined as the net weight of sediment collected on the precombusted GF-5 filters, after redrying, with a precision of ±0.2 mg L⁻¹. To measure the POC, $\delta^{13}\text{C-POC}$ and particulate nitrogen (PN), a cutout of 11 mm diameter was made in the GF-5 filter, carbonates were removed by exposure to concentrated HCl

fumes for at least 4 h, and these were redried and packed in Ag cups. Calibration of $\delta^{13}\text{C}$ -POC, $\delta^{15}\text{N}$ -PN, POC, and PN measurements was performed with acetanilide ($\delta^{13}\text{C} = -27.65 \pm 0.05\text{‰}$; $\delta^{15}\text{N} = 1.34 \pm 0.04\text{‰}$) and leucine ($\delta^{13}\text{C} = -13.47 \pm 0.07\text{‰}$; $\delta^{15}\text{N} = 0.92 \pm 0.06\text{‰}$) as standards. All standards were internally calibrated against the international standard IAEA-C6 and IAEA-N1. Reproducibility of $\delta^{13}\text{C}$ -POC and $\delta^{15}\text{N}$ -PN measurement was typically better than $\pm 0.2\text{‰}$ and relative standard deviation for POC and PN measurement was always below 5%. Nutrients (NO_2^- , NO_3^- , NH_4^+ , SRP, and TP) analysis was performed using a GENESIS 20 single beam spectrophotometer, according to standard colorimetric protocols following *Rodier and Bazin* [2005] and *American Public Health Association* [1998]. The detection limits were 0.3, 0.03, and $0.15 \mu\text{mol L}^{-1}$ for NH_4^+ , NO_2^- , and NO_3^- , respectively.

3.3. GIS Analysis and Discharge Estimation

SRTM DEM (Shuttle Radar Topography Mission-Digital Elevation Model) data sampled at 3 arc sec (~ 30 m) pixel size were used to generate the topographical map of the VVP (Figure 1). The SRTM DEM data were collected by the NASA, the USA National Geospatial-Intelligence Agency, and the German and Italian space agencies joint team. A full description of the SRTM DEM data can be found in *Farr et al.* [2007]. Maps of the dominant major soil groups (Figure 2a) and organic carbon distribution (Figure 2d) were produced using data from the FAO SOTWIScaf, ver. 1.0, a central Africa soil features described in *Batjes* [2008]. The spatial distribution of the aboveground live woody biomass (Figure 2c) was extracted from the Pantropical National Level Carbon Stock Dataset for tropical countries [*Baccini et al.*, 2008]. Land cover (supporting information Figure S1) data were extracted from the FAO GLCN2000 [*Global Land Cover 2000 database*, 2003] (Global Land Cover Network) database for Africa, which is at ~ 300 m resolution and described in *Mayaux et al.* [2004]. The hydrographic network (Lake and rivers) is taken from the Building Environment for the Gorilla's [*BEGo (Synoptics, Keyobs, Royal Museum for Central Africa, Catholic University of Louvain)*, 2005]. Lithology (Figure 2b) is based on the GLiM (Global lithological map) from *Hartmann and Moosdorf* [2012].

The drainage areas (supporting information Figure S2) were derived from a high-resolution DEM computed by the HydroSHEDS mapping product (<http://hydrosheds.cr.usgs.gov/index.php>) and using the ArcHydro 2.0 Toolbox for ArcGis 10.2 software. Monthly discharges (supporting information Data Set S1) were estimated using an approach based on DEM and local precipitation data. The DEM grid was used to successively extract flow direction and flow accumulation grids. The latter represents the number of upslope cells that flow into each cell, and thus can be used to derive stream networks. The flow accumulation grid was converted into an accumulated area grid by multiplying the flow accumulation grid by the DEM grid resolution (here 92.43 m^2). Then, multiplying the value of the accumulated area determined at the outlet of a basin by a value of precipitation results in a measure of accumulated runoff per unit of time. Average monthly precipitations (supporting information Data Set S1) for each basin are derived from the 1 km^2 resolution WorldClim Database [*Hijmans et al.*, 2005]. A comparison of the results obtained using this approach with the data from 10 USGS gauges across the U.S.A. provided satisfactory results [*Wieczorek*, 2012].

3.4. Annual Load and Weathering Rate Estimation

Discharge-weighted mean concentrations were calculated in order to avoid dilution and evaporation effects on the annual loads and weathering rates. For a given parameter, the discharge-weighted mean concentration (C_w) was calculated as follows:

$$C_w = \frac{\sum_{i=1}^n C_i \times Q_i}{\sum_{i=1}^n Q_i}$$

where C_i is the monthly measured concentration and Q_i the calculated monthly discharge.

The estimated monthly discharges can be found in the supporting information. The annual load was then obtained by multiplying the discharge-weighted mean concentration (C_w) with the annual discharge. Following the same procedure, atmospheric CO_2 consumption rate was estimated from the discharge-weighted mean HCO_3^- (TA) concentration, based on the assumption that HCO_3^- is generated by silicate rock weathering, as confirmed by analysis of major element property-property plots (see hereafter). The mechanical weathering rate was estimated from discharge-weighted mean TSM concentration. The cationic weathering rate was estimated from the sum of major cations ($\text{TDS}_{\text{cat}} = \sum \text{Ca, Mg, Na, and K}$). The chemical weathering rate was estimated from the total dissolved solid (TDS_{cond}), the latter calculated from specific

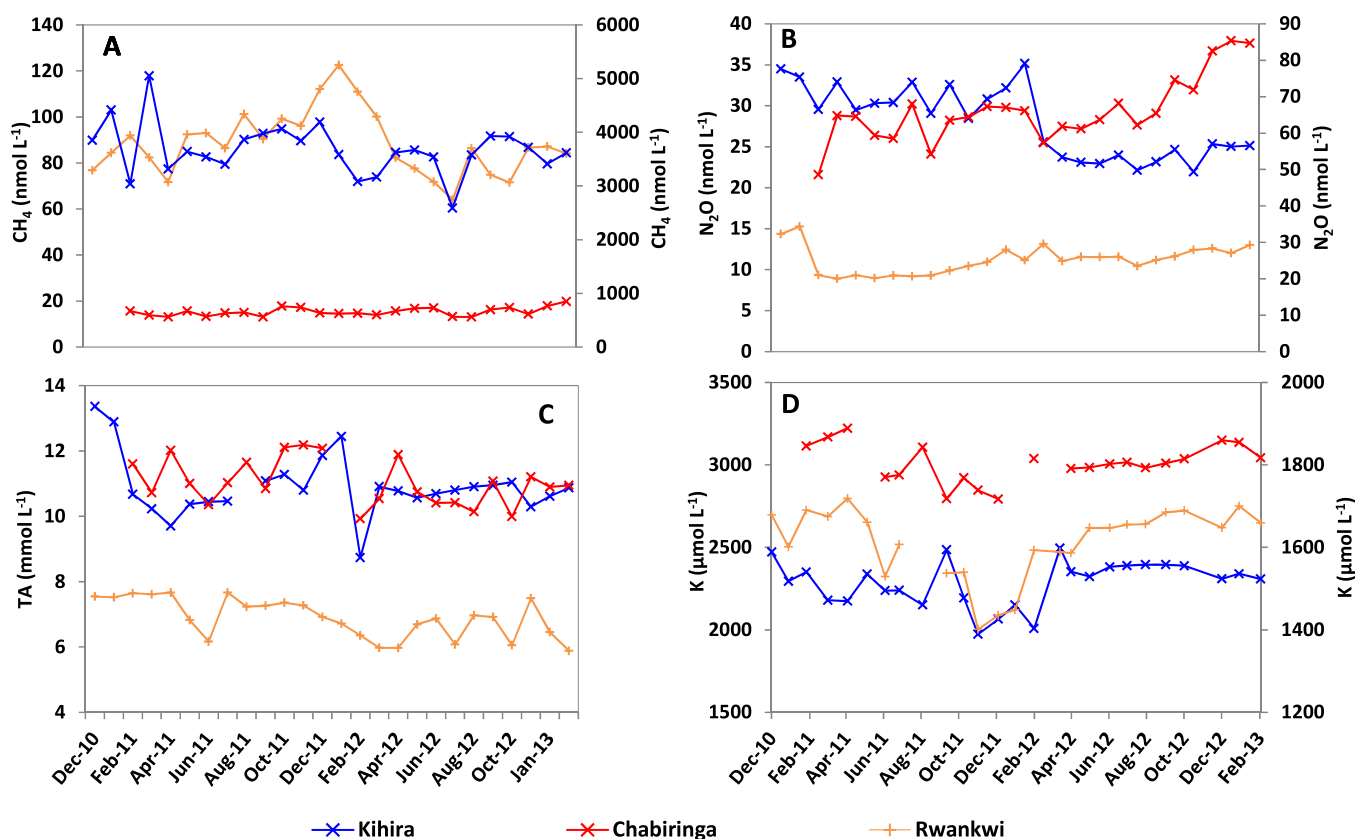


Figure 3. (a) Temporal variation of methane, (b) nitrous oxide, (c) total alkalinity, and (d) K⁺ concentrations in a selection of the sampled rivers of the Virunga Volcanic Province between December 2010 and February 2013. Kihira in Figure 3a, Chabiringa in Figure 3b, and Rwankwi in Figure 3d are referred to the right axes.

conductivity as described in *Atekwana et al.* [2004]. All fluxes and weathering rates are expressed on an areal basis, i.e., by dividing the annual load with the river catchment area.

Major cations concentrations were corrected for atmospheric inputs using data from *Cuoco et al.* [2012a] which studied rainwater chemistry in the VVP between 2004 and 2010. Only data from rain samples collected to the N-NE and the W-SW of Mt Nyiragongo were considered. Samples from Nyiragongo crater and surrounding were not considered as they were not included in the drainage basins of this study. Furthermore, this area is impacted by the plume from Nyiragongo's permanent lava lake, and would thus only represent a source of error.

4. Results and Discussion

Most measured physicochemical and chemical features showed no well-defined seasonality (e.g., Figure 3 and supporting information Data Set S2). The mean temperature for each river throughout the study period ranged between 17 and 29.4°C (Figure 4a). Temperature was almost constant in Chabiringa and Kamutoni, while the other rivers showed a relative increase during dry season period, i.e., mid June to August. Shallow rivers showed important temperature fluctuations except for the Rwankwi which is supplied with high altitude water. No large DOC and POC increases were observed during the rising stage of runoff (mid-September to October) after the dry season, in contrast to what was observed in very large rivers such as the Oubangi River in the Congo River basin or other large tropical rivers [*Meybeck, 2005; Bouillon et al., 2012*]. Thus, the POC/DOC, HCO₃⁻/DOC, and POC/PN ratios showed only minor variations over time.

Given the general lack of marked seasonal variations, we principally focus on spatial variations of parameters. Mean concentrations of studied parameters are presented in Figures 4 and 6, the full database can be found in supporting information Data Set S2.

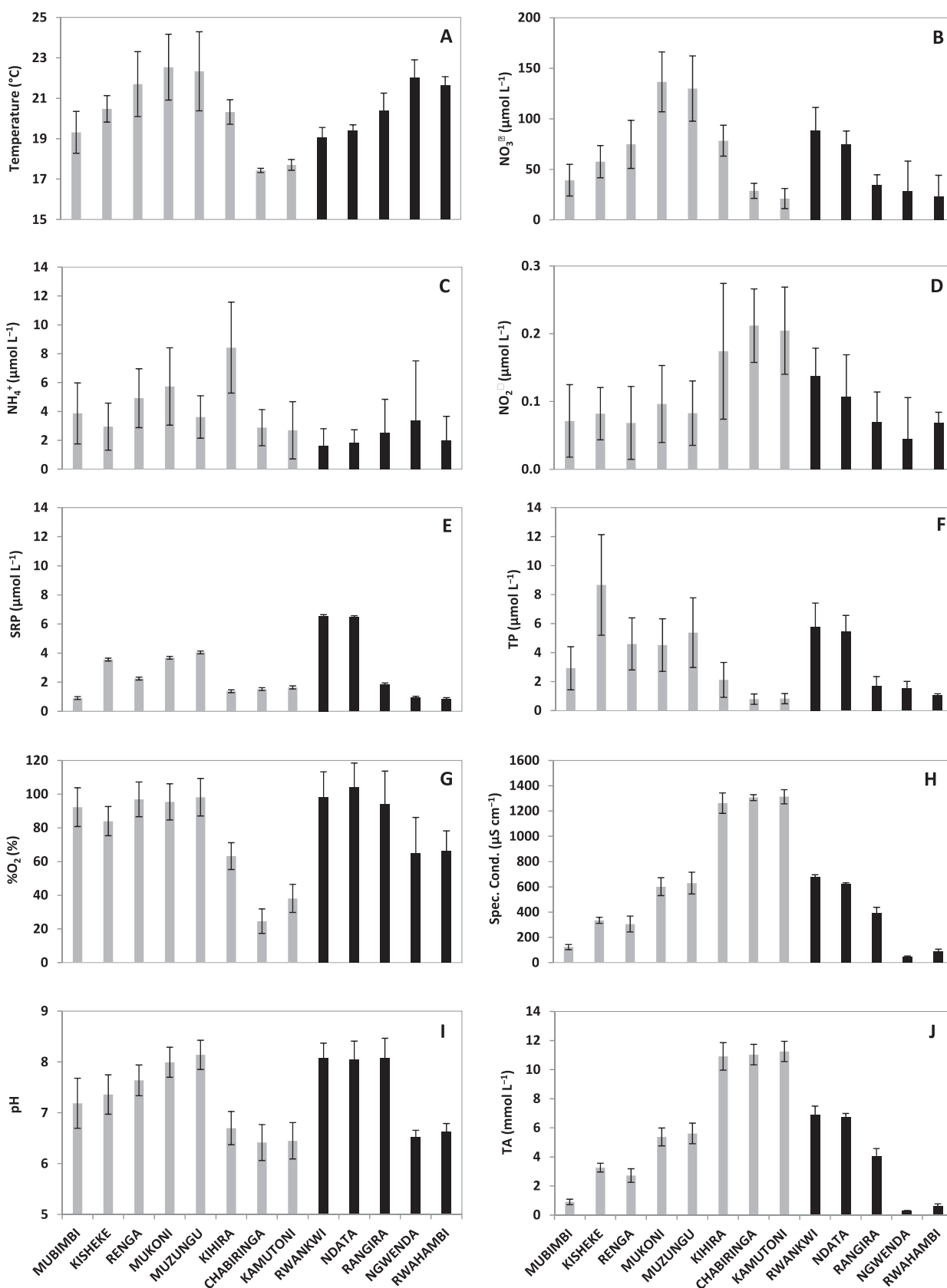


Figure 4. (a) Mean temperature, (b) nitrate, (c) ammonium, (d) nitrite, (e) soluble reactive phosphorus, (f) total phosphorus, (g) dissolved oxygen, (h) specific conductivity, (i) pH, and (j) total alkalinity in rivers of the Virunga Volcanic Province between December 2010 and February 2013. The gray and black bars represent rivers of Kabungo bay and Lake Edward catchment, respectively. The error bars represent one standard deviation.

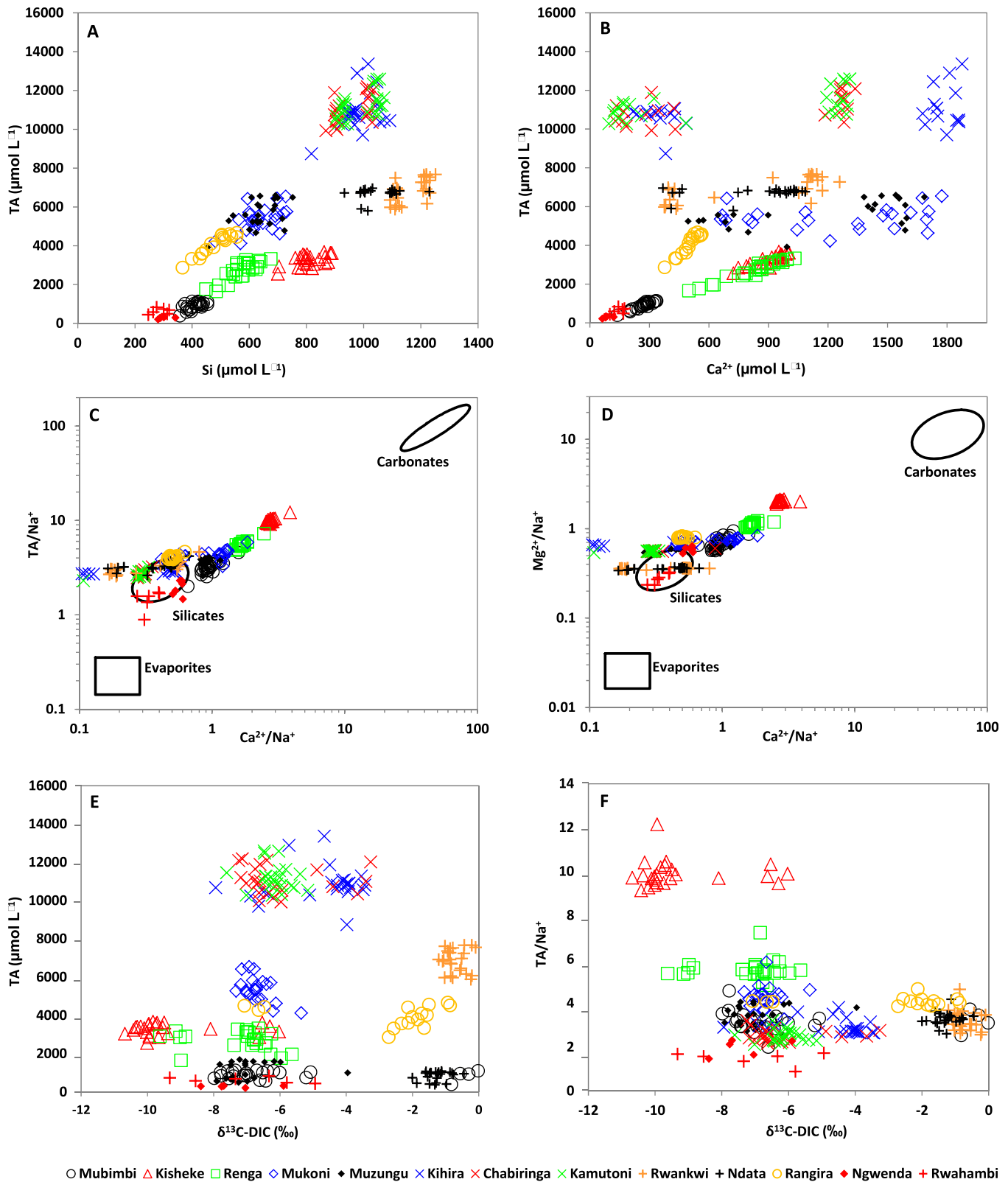


Figure 5. (a) Relationships between total alkalinity (TA) and Si, (b) TA and calcium, (c) TA/Na^+ and Ca^{2+}/Na^+ , (d) Mg^{2+}/Na^+ and Ca^{2+}/Na^+ , (e) TA and $\delta^{13}C_{DIC}$, and (f) TA/Na^+ and $\delta^{13}C_{DIC}$ in rivers of the Virunga Volcanic Province between December 2010 and February 2013. The Na^+ normalized plots show the composition fields for rivers draining different lithologies from a global compilation of the 60 largest rivers in the World [Gaillardet et al., 1999].

4.1. Spatial Variations in Nutrient Concentrations

Monthly NO_3^- concentrations in the VVP rivers spanned a wide range (7–178 $\mu\text{mol L}^{-1}$), with large spatial variations (Figure 4b), and did not reach levels indicative of significant pollution or eutrophication. In parallel, the NH_4^+ and NO_2^- (Figures 4c and 4d, respectively) remained below the ranges normally found in unpolluted rivers (18 and 1.2 $\mu\text{mol L}^{-1}$, respectively) [Meybeck, 1982, 1983a]. The observed variations in the NO_3^- , NH_4^+ , and NO_2^- concentrations were therefore of natural origin. On the other hand, mean SRP concentrations (Figure 4e) are higher compared to those of unpolluted rivers (10 $\mu\text{g L}^{-1}$) [Meybeck, 1982, 1993a], a discrepancy which could be related to a high degree of P mobilization during weathering of basaltic rocks (see below).

In rivers of the VVP, NH_4^+ represented between 1.5% and 11.9% of the total inorganic N pool, whereas NO_3^- largely dominated and accounted for 87.9–98.3%. This might suggest the conversion of NH_4^+ into NO_3^- through nitrification, leading to the dominance of NO_3^- over NH_4^+ . The TP mean (Figure 4f) were slightly correlated to the SRP ($r^2 = 0.54$) and to NO_3^- ($r^2 = 0.33$). This implies the dominance of SRP in the P pool as SRP additionally represent >50% of TP in most rivers, and a possible common source for both P and N. In fact, P and N can be jointly mobilized from land runoff and groundwater.

Volcanic emissions are a possible source of nitrate and phosphate in active volcanic areas [Julley *et al.*, 2008], and reach surface water through wet and dry deposits on the catchment. In the Virunga atmospheric inputs are important source of N and P, indeed Muvundja *et al.* [2009] found that total-N and total-P concentrations in atmospheric deposits were equal or larger than riverine values. P can also be produced in bioavailable form (P_4O_{10}) when hot lava reacts with water [Vitousek, 2004]. Like many other elements, P is released during chemical weathering. In the Japanese archipelago, P-release from silica-dominated lithology is estimated at a rate of 1–390 $\text{kg}^{-1} \text{km}^{-2} \text{yr}^{-1}$ [Hartmann and Moosdorf, 2011]. Thus, even though P is a minor constituent of igneous rocks (mean from 0.42 to 1.55 wt % for the Virunga basalt; Table 1), volcanic products could be a minor source of P of VVP rivers.

Muvundja *et al.* [2009] reported nutrient data in Mukoni, Muzungu, Kihira, Chabiringa, and Kamutoni rivers during a monthly monitoring between October 2006 and July 2008. The SRP, Si, and TSM are comparable for both data sets. The higher NH_4^+ and TP values given by Muvundja *et al.* [2009] are possibly due to the difference in the sampling location, as they collected samples close to the mouth (near Kabuno bay) where contamination by wastewaters from villages along the course of the rivers may occur.

4.2. Major Cations and DIC Chemistry

Most rivers had mean O_2 concentrations near saturation, except Kamutoni and Chabiringa which were the most O_2 -depleted waters, with means of 38.1% and 24.6%, respectively (Figure 4g), typical of high groundwater contributions as confirmed also by low temperature (Figure 4a) since they were sampled close to the resurgence points. The activity of the Nyamulagira seems to not influence temperatures of both rivers. The other rivers showed $\% \text{O}_2 > 60\%$ which implies important water oxygenation, given the steep slopes and shallow depths. Rwankwi, Ndata, and Mubimbi showed lower temperature (mean of $\sim 19^\circ\text{C}$) associated with their high altitude origin on Mt Mikeno of the Virunga Nation Park (Rwankwi and Ndata) and the Mitumba Range (Mubimbi) (Figure 1). Specific conductivity data allow us to define three groups of rivers in the VVP: (1) the low mineralized ($< 150 \mu\text{S cm}^{-1}$), (2) moderately mineralized (200–800 $\mu\text{S cm}^{-1}$), and (3) highly mineralized rivers with $> 800 \mu\text{S cm}^{-1}$ (Figure 4h).

The highly mineralized rivers, i.e., Kihira, Chabiringa, and Kamutoni are located on basaltic lithology in the field of active volcanoes, with a high major cation content and where the dominant cations are $\text{Na}^+ > \text{K}^+ > \text{Mg}^{2+} > \text{Ca}^{2+}$ (Table 2). This is a result of the intense weathering of basalt, mediated by magmatic CO_2 and the subsequent release of major cations to groundwater. The high alkalic composition of Virunga basalt promotes the dominance of Na^+ and K^+ in the cation composition of Kihira, Chabiringa and Kamutoni.

The moderately mineralized rivers are located in the field of dormant volcanoes to the NE and on nonvolcanic fields to the west (Figure 2b), where eruptive materials (i.e., ash, volcanic plume) were frequently deposited especially during Nyiragongo and Nyamulagira eruptions. Rwankwi and Ndata to the North-East, Mukoni and Muzungu to the West have similar specific conductivities (616–682 $\mu\text{S cm}^{-1}$) despite their location on different lithologies. The North-Eastern and Western rivers had different dominant cations

Table 2. Mean Cation Concentrations (Min-Max Between Parentheses) in Rivers of the Virunga Volcanic Province, Between December 2010 and February 2013

	Na (mM) Mean (Min-Max)	K (mM) Mean (Min-Max)	Mg (mM) Mean (Min-Max)	Ca (mM) Mean (Min-Max)	Si (mM) Mean (Min-Max)
Mubimbi	0.29 (0.15–0.39)	0.10 (0.07–0.16)	0.19 (0.12–0.23)	0.27 (0.14–0.34)	0.41 (0.36–0.45)
Kisheke	0.33 (0.23–0.37)	0.24 (0.12–0.30)	0.67 (0.47–0.74)	0.91 (0.72–1.00)	0.81 (0.70–0.89)
Renga	0.49 (0.29–0.69)	0.27 (0.20–0.33)	0.54 (0.34–0.71)	0.83 (0.50–1.03)	0.57 (0.45–0.68)
Mukoni	1.27 (0.83–1.66)	0.69 (0.53–1.00)	0.92 (0.69–1.05)	1.24 (0.66–1.77)	0.64 (0.48–0.73)
Muzungu	1.63 (1.03–1.92)	0.95 (0.72–1.13)	0.97 (0.54–1.14)	1.17 (0.50–1.69)	0.64 (0.45–0.75)
Kihira	3.72 (3.11–4.09)	2.28 (1.97–2.50)	2.49 (2.04–2.86)	1.12 (0.22–1.88)	0.99 (0.82–1.09)
Chabiringa	4.26 (1.62–4.71)	2.91 (0.88–3.22)	2.31 (0.97–2.55)	0.76 (0.13–1.43)	0.95 (0.69–1.03)
Kamutoni	4.49 (3.94–4.97)	3.08 (2.85–3.26)	2.44 (2.21–2.58)	0.73 (0.10–1.31)	0.99 (0.90–1.07)
Rwankwi	2.15 (0.26–0.55)	1.61 (0.04–0.11)	0.77 (0.08–0.14)	0.81 (0.10–0.17)	1.17 (0.25–0.32)
Ndata	2.05 (1.62–2.25)	1.41 (1.28–1.49)	0.73 (0.58–0.78)	0.84 (0.37–1.09)	1.05 (0.93–1.23)
Rangira	0.99 (0.74–1.15)	0.69 (0.53–0.81)	0.79 (0.60–0.93)	0.50 (0.38–0.56)	0.48 (0.37–0.56)
Ngwenda	0.15 (0.13–0.20)	0.05 (0.03–0.08)	0.09 (0.07–0.11)	0.08 (0.06–0.12)	0.30 (0.28–0.34)
Rwahambi	0.44 (1.57–2.34)	0.06 (1.40–1.72)	0.12 (0.56–0.83)	0.15 (0.38–1.26)	0.29 (1.09–1.25)

depending on the soil and the lithology of each watershed (Figures 2a and 2b). This highlights the secondary role of soil weathering to the river chemical composition in the VVP. Thus, Mukoni and Muzungu flowing on haplic acrisols (Figure 2a) were Na^+ and Ca^{2+} dominated; followed by K^+ and Mg^{2+} whose concentrations compete (Table 2). In contrast, Rwankwi and Ndata kept the K^+ - Na^+ dominance related to the presence of extinct volcanoes in the catchments (Figure 2b). The low mineralized rivers are found on haplic acrisols to the West and luvic phaeozems to the North (Figure 2a) with the most diluted water at both extremities of the sampling zone, away from the influence of active volcanoes.

Mean pH varied from neutral to relatively acid or basic (6.4–8.1; Figure 4i). The mean TA ranged from low ($<1.0 \text{ mmol L}^{-1}$) to exceptionally high ($>10.0 \text{ mmol L}^{-1}$) values (Figure 4j). The TA was overall positively correlated to Si (Figure 5a), and showed a larger scatter as a function of Ca^{2+} (Figure 5b). This is indicative of a strong contribution of silicate rock weathering to TA (Figure 5a), and this is confirmed by the Na^+ normalized plots (Figures 5c and 5d). Both TA/Na^+ and $\text{Mg}^{2+}/\text{Na}^+$ versus $\text{Ca}^{2+}/\text{Na}^+$ (Figures 5c and 5d, respectively) are aggregated to values close to those expected for silicate rock weathering based on the average values proposed by Gaillardet *et al.* [1999]. The rivers with a lithology dominated by acid metaphoric rocks (Mubimbi, Kisheke, Renga, Mukoni, and Muzungu) had a $\text{Ca}^{2+}/\text{Na}^{2+} > 1$, while the rivers with a lithology dominated by basalt/volcanic ash (i.e., Kihira, Chabiringa, Kamutoni, Rwankwi, Ndata, and Rangira; Figure 2b) were characterized by a $\text{Ca}^{2+}/\text{Na}^{2+} < 1$ and a TA/Na^+ close to 3. A few rivers (Kihira, Rwankwi, and Ndata) had $\text{Ca}^{2+}/\text{Na}^+$ values lower than the envelope of silicate rock end-member proposed by Gaillardet *et al.* [1999] (Figure 5c). This is probably related to the fact that Gaillardet *et al.* [1999] reported the chemical composition of the 60 largest rivers in the World, hence, excluding low mineralized small rivers such as some of those studied here. Another reason could be the atypical strong dominance of Na in the Virunga basalt, and consequently in the major cation composition of the stream network. The Na-normalized Ca^{2+} and Mg^{2+} ratios are consistent with high dissolution of Ca and Mg-rich silicate minerals, such as clinopyroxenes, mostly formed of diopside ($\text{CaMgSi}_2\text{O}_6$) [Morimoto, 1989] and which have been identified in Nyiragono's basalt [Platz, 2002; Platz *et al.*, 2004].

No consistent simple relationship was observed between TA and $\delta^{13}\text{C}$ -DIC (Figure 5e), but the river with the highest TA/Na^+ (Kisheke) was also characterized by the lowest $\delta^{13}\text{C}$ -DIC values (Figure 5f). Silicate weathering leads to the formation of HCO_3^- that has the isotopic signature of the CO_2 driving the weathering reaction. Since in freshwaters, DIC is usually dominated by HCO_3^- , especially in high TA systems, the $\delta^{13}\text{C}$ -DIC is close to the one of HCO_3^- , hence of the CO_2 initially involved in the dissolution of silicate rocks. Considering the evidence discussed above that silicate weathering is a strong contributor to TA in the region, the observed range of $\delta^{13}\text{C}$ -DIC (between -10.7‰ and 0‰ ; Figure 6a) indicates that the CO_2 driving silicate weathering was not derived from organic matter mineralized in soils. Indeed, DOC and POC have a $\delta^{13}\text{C}$ signature ranging between -28‰ and -18‰ (Figures 6b and 6c, respectively). However, the range of river $\delta^{13}\text{C}$ -DIC matches well with the range of $\delta^{13}\text{C}$ of CO_2 in volcanic gases reported by Deines [2002]. We thus conclude that the $\delta^{13}\text{C}$ -DIC signatures are to a large extent influenced by volcanic CO_2 dissolution in groundwaters and involved in silicate rock weathering. This pattern is quite different from those observed

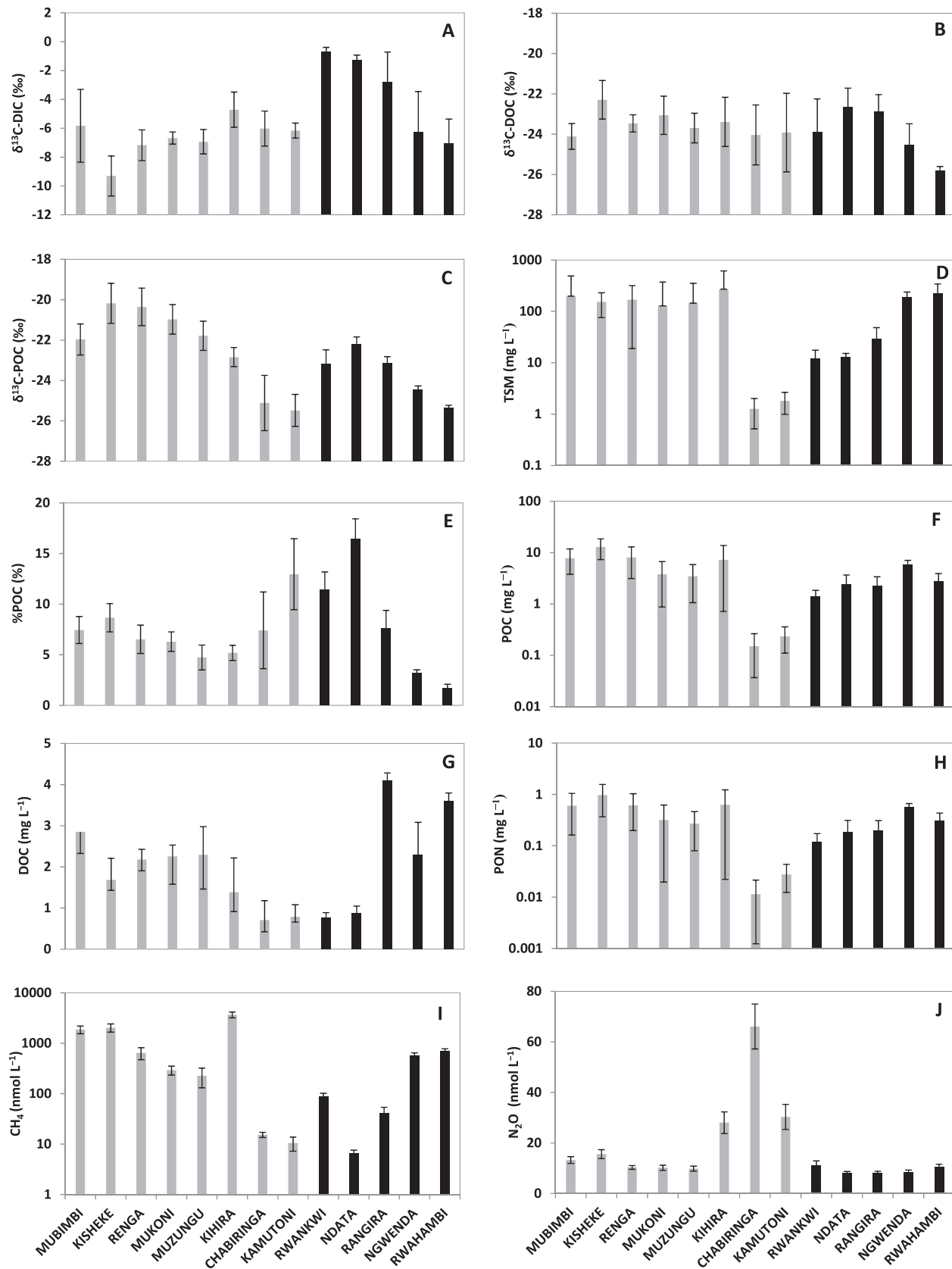


Figure 6. (a) Mean values of $\delta^{13}\text{C}_{\text{DIC}}$, (b) $\delta^{13}\text{C}_{\text{DOC}}$, (c) $\delta^{13}\text{C}_{\text{POC}}$, (d) total suspended matter, (e) %POC, (f) particulate organic carbon, (g) dissolved organic carbon, (h) particulate organic nitrogen, (i) methane, and (j) nitrous oxide in rivers of the Virunga Volcanic Province between December 2010 and February 2013. The gray and black bars represent rivers of Kabuno bay catchment and those of Lake Edward catchment, respectively. The error bars represent one standard deviation.

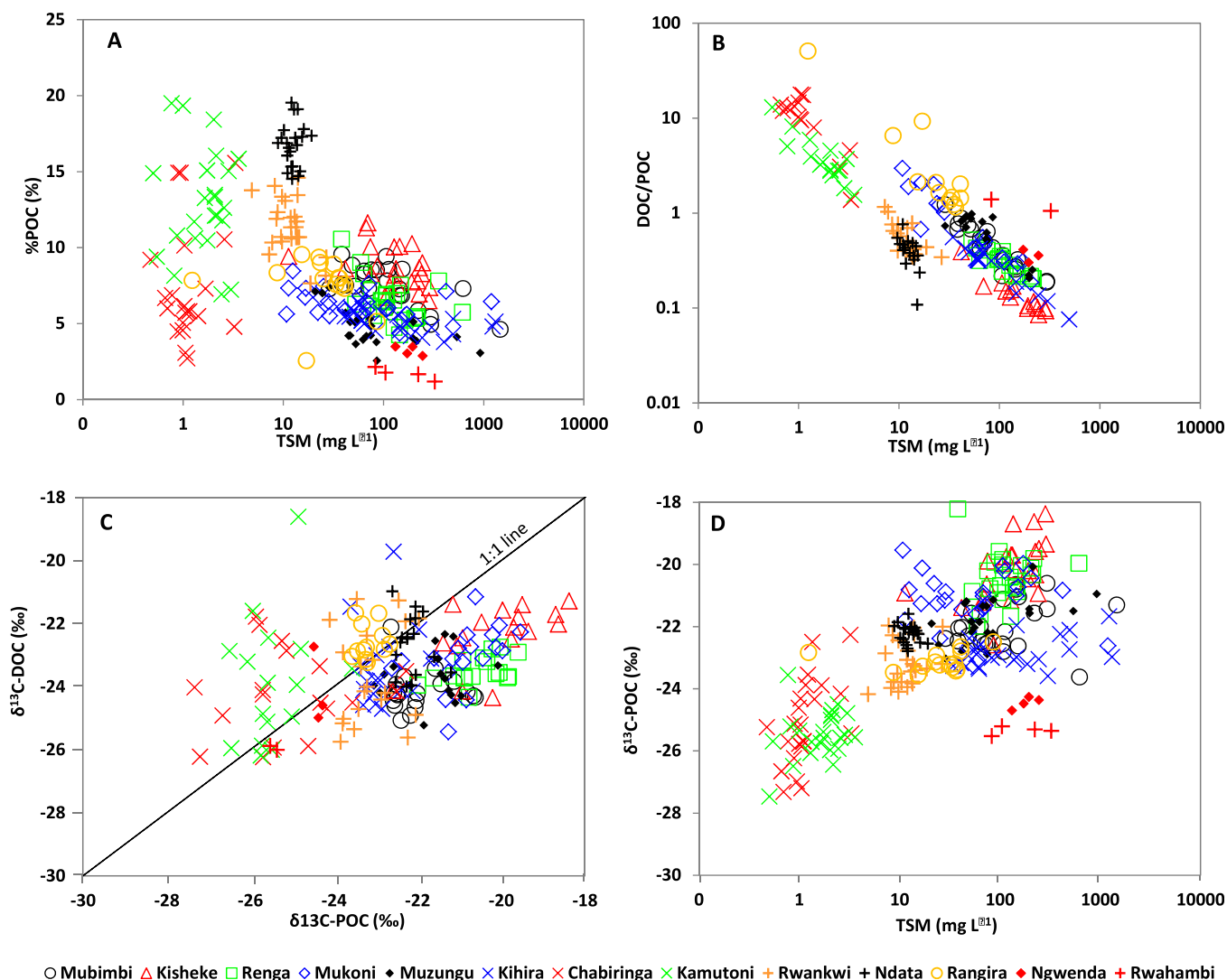


Figure 7. (a) Relationships between the %POC and total suspended matter, (b) DOC/POC and total suspended matter, (c) $\delta^{13}\text{C}_{\text{DOC}}$ and $\delta^{13}\text{C}_{\text{POC}}$ and (d) $\delta^{13}\text{C}_{\text{POC}}$ and TSM in rivers of the Virunga Volcanic Province between December 2010 and February 2013.

in the lower Congo basin, where $\delta^{13}\text{C}\text{-DIC}$ values as low as $\sim -26\text{‰}$ are found in rivers where silicate weathering also dominates, but where the CO_2 driving silicate weathering is produced by mineralization of organic matter derived from C3 vegetation [Bouillon *et al.*, 2014].

Silicate weathering also strongly affected the SRP distribution as shown by the highly significant correlation between SRP and dissolved Si (when the three headwater rivers Kihira, Chabiringa and Kamutoni are excluded) (Figure 8a). This is in line with the general link between P release and rock weathering [Hartmann *et al.*, 2014].

4.3. Organic Matter Dynamics and Origin

Large differences in the TSM load were observed in the VVP rivers. Higher TSM ($289\text{--}1467\text{ mg L}^{-1}$) was found in rivers located in the west of Kabuno bay basin, i.e., in Mubimbi, Kisheke, Renga, Mukoni, Muzungu, and Kihira (Figure 6d). These are second-order rivers draining a basin where steep slopes (supporting information Data Set S2), combined with high rainfall and agricultural land use practices, result in high erosion rates. The TSM load of these rivers is characterized by a relatively low organic matter content (mean %POC $< 9\%$, Figure 6e). The catchment of Kabuno bay is composed of haplic acrisols (Figure 2a) which are clay-enriched soils. The land is mainly used for farming (crops and pastures; supporting information Figure S1) which

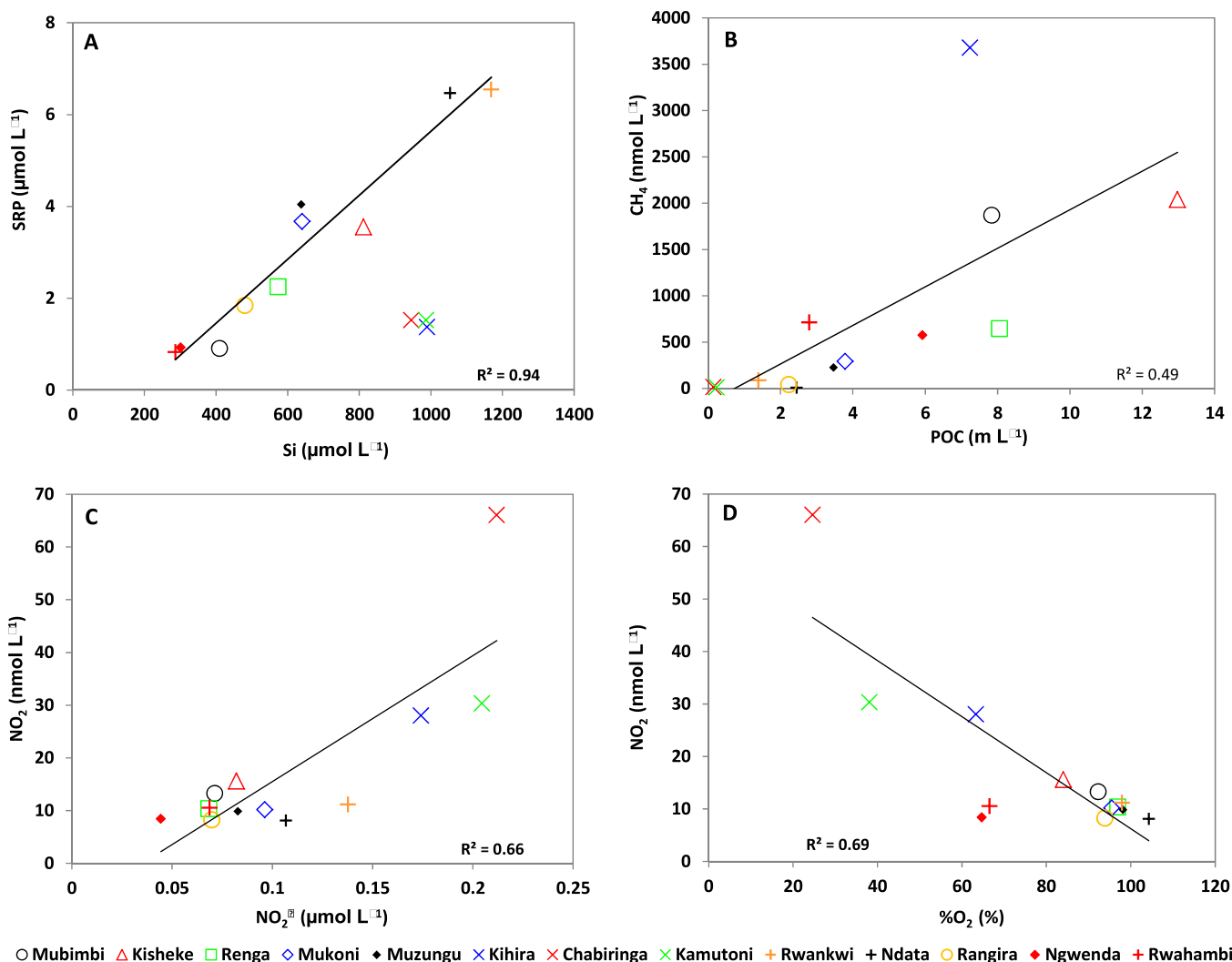


Figure 8. (a) Relationships between mean soluble reactive phosphorus and silicon, (b) mean methane and particulate organic carbon, (c) mean nitrous oxide and nitrite, and (d) between mean nitrous oxide and dissolved oxygen in rivers of the Virunga Volcanic Province between December 2010 and February 2013.

promotes soil erosion. Chabiringa, Kamutoni, Rwankwi, Ndata, and Rangira showed the lowest TSM, with values ranging from 0.5 to 86.3 mg L⁻¹ (Figure 6d). These rivers flow on mollic andosols of volcanic parent material from the Nyamulagira and Mikeno volcanoes (Figure 2a), with shrubs or forest cover (supporting information Figure S1). Thus, the lower TSM observed in the rivers draining volcanic fields are a result of the lower sensitivity of volcanic rocks toward mechanical erosion processes. The TSM could however be potentially enriched in organic matter (%POC > 10, e.g., in Kamutoni, Rwankwi, and Ndata; Figure 7a) from the dense vegetation cover. Ngwenda and Rwahambi flow on luvisc phaeozems which are humic-rich and highly productive soils. The latter have favored the development of farming activities that generate high TSM with a low %POC (Figure 7a) found in Ngwenda and Rwahambi.

Most Virunga rivers have mean TSM and POC (Figure 6f) that are higher than main stem Congo River (26.3 mg/L for TSM, 1.7 mg/L for POC) [Coynel *et al.*, 2005] or other large rivers [Meybeck, 1982; Spitzy and Leenheer, 1991; Martins and Probst, 1991]. Mean TSM loads in the VVP rivers draining mountainous catchments (128.3–270.4 mg L⁻¹) were also higher compared to volcanic mountainous rivers of Guadeloupe (11.8–56.2 mg L⁻¹) [Lloret *et al.*, 2013]. Nevertheless, Guadeloupe rivers have mean TSM somewhat high than that of Virunga rivers draining basaltic field (1.3–29.8 mg L⁻¹). POC concentrations were extremely variable among rivers, while DOC showed lower spatial variability (Figure 6g). In the majority of rivers, POC dominated the organic C pool. Differences in the POC/DOC ratios can be explained by differences in soil type, soil leaching and/or erosion and the relief. Both lower mean DOC (<0.9 mg L⁻¹) and POC

(<2.5 mg L⁻¹) were observed in rivers draining volcanic fields (Figure 2a). These rivers (i.e., Chabiringa, Kamutoni, Rwankwi, and Ndata rivers) are characterized by low terrestrial biomass (Figure 2c) and low organic C soil content (Figure 2d).

The total organic C (TOC = DOC + POC) generally increased as one moves away from the volcanic area toward the NE and W. Thus, the TOC was found to be 6 to ~20 times higher in the most remote rivers. While DOC has typically been suggested to be the dominant C pool in large tropical rivers [Meybeck, 1993b], C of rivers of the VVP was largely DIC dominated. This is due to the high rates of silicate weathering and magmatic CO₂ inputs. The DOC/DIC ratios were below those of rivers draining carbonate rocks (<0.2) [Meybeck, 2005].

There was no straightforward relationship between the riverine POC and DOC and the vegetation or soil organic carbon distribution in the catchments. For instance, Rwahambi had among the highest mean DOC, and yet was draining catchment of both low organic C soil (Figure 2d) and woody biomass (Figure 2c). In contrast, DOC/POC ratios were well correlated to TSM (Figure 7b), with ratios above 1 (dominance of the DOC in the TOC pool) in the headwater streams (e.g., Chabiringa and Kamutoni). POC became dominant in more erosive and turbid systems as previously described in other studies [e.g., Meybeck, 1982; Ittekkot and Laane, 1991; Ralison et al., 2008; Bouillon et al., 2009]. Mean DOC, POC, and PN (Figure 6h) in the VVP rivers were almost similar to those reported by Lloret et al. [2013] for Guadeloupan rivers of volcanic fields (0.69–2.25, 0.98–6.70, 0.1–2.31 mg L⁻¹, respectively, for DOC, POC, and PN). Natural vegetation in the Virunga consists of a mixture of Hatch-Slack photosynthetic pathway plants (C4) and grasslands employing Calvin pathway (C3), with the former dominating in quantity [Still and Powell, 2010] (supporting information Figure S1). Agricultural practices have introduced both new C4 (e.g., maize, sorghum, sugar cane, etc.) and C3 (e.g., banana, potato, cassava, etc.) plants. Thus, Virunga riverine δ¹³C-DOC (Figure 6b) and δ¹³C-POC (Figure 6c) showed a mixed origin for organic C, from both C3 and C4: C3 plants have a typical δ¹³C around -30‰ to -26‰, while C4 plants show a δ¹³C of ~-12‰ (-10‰ to -14‰) [Ehleringer, 1991]. We found however a slight dominance of C3-derived C to the riverine organic C pool, with mean δ¹³C-DOC and δ¹³C-POC of -23.5‰ and -22.5‰ respectively. There were no clear relationships between individual paired δ¹³C-DOC and δ¹³C-POC data, indicating both C pools were not closely coupled (Figure 7c). Literature data on the δ¹³C of riverine POC and DOC in the Congo Basin are only available for low-altitude regions [e.g., Mariotti et al., 1991, Spencer et al., 2012, Bouillon et al., 2012, 2014], and show much more limited C4 contributions than those found in Virunga highlands, with the majority of data ranging between -30‰ and -26‰.

As also reported in the lowland Congo [Bouillon et al., 2014], the δ¹³C-POC was positively correlated to TSM (Figure 7d) and might indicate higher sediment inputs in catchments where C4 vegetation (grassland) is more substantial. The negative relationship between %POC and TSM (Figure 7a) has been previously observed within a given catchment [Tamooh et al., 2012; Bouillon et al., 2014] or globally across catchments [Meybeck, 1982]. This pattern is typically driven by the combination of inputs from direct litter or organic-rich surface soil layers (high %POC-low TSM) and more soil-derived sediments (low %POC-high TSM).

4.4. CH₄ and N₂O

Virunga rivers were sources of methane to the atmosphere as most rivers of the world [Bastviken et al., 2011], the observed CH₄ concentrations (Figure 6i) were above atmospheric equilibrium (~2 nmol L⁻¹). Overall there was a positive relationship between CH₄ and POC (Figure 8b) driven by enhanced in situ CH₄ production fuelled by the availability of organic matter and the removal of both POC and CH₄ in groundwaters.

In contrast, only Chabiringa, Kamutoni, and Kihira were sources of N₂O to the atmosphere as they showed concentrations (Figure 6j) above the atmospheric equilibrium (~10 nmol L⁻¹). Two of these rivers (Chabiringa and Kamutoni) showed low CH₄, while the third (Kihira) had the highest CH₄ of all rivers sampled. Chabiringa and Kamutoni were sampled close to springs, and therefore have chemical characteristics close to those of groundwaters such as high TA, conductivity and major cation concentrations, and low pH, temperature, DOC, and POC concentrations. These rivers were also characterized by low NO₂⁻ and high N₂O which might be indicative of denitrification in the groundwaters. These features drive the positive correlation between N₂O and NO₂⁻ (Figure 8c) and the negative correlation between N₂O and %O₂ (Figure 8d). Chabiringa and Kamutoni were also characterized by lower CH₄ concentrations indicative of CH₄ removal by bacterial oxidation in the groundwaters [Borges et al., 2015].

Table 3. Estimated Annual TSM, POC, PON, DOC, Si, and Nutrient Fluxes in Rivers of the Virunga Volcanic Province

	TSM (10 ³ t/yr)	POC (t/yr)	PON (t/yr)	DOC (t/yr)	Si (t/yr)	NO ₃ ⁻ (t/yr)	NO ₂ ⁻ (t/yr)	NH ₄ ⁺ (t/yr)	SRP (t/yr)	Total P (t/yr)
Mubimbi	20.79	793.33	60.38	290.56	1061.75	231.31	0.34	6.63	2.55	8.67
Kisheke	1.47	121.56	9.03	15.23	196.87	29.43	0.03	0.48	0.84	2.37
Renga	13.10	661.38	46.96	162.07	1145.21	319.94	0.19	6.43	4.38	10.39
Mukoni	2.52	71.10	5.64	40.20	305.96	127.75	0.08	1.94	1.65	2.40
Muzungu	6.86	159.71	14.62	99.84	711.54	340.54	0.37	2.90	5.44	7.81
Kihira	15.06	411.68	36.01	70.77	1368.97	245.06	0.42	7.49	1.80	2.73
Chabiringa	0.04	3.20	0.35	20.22	752.99	49.59	0.27	1.47	1.08	0.64
Kamutoni	0.03	3.20	0.41	11.55	406.14	20.36	0.14	0.84	0.67	0.35
Rwankwi	1.76	196.10	16.37	107.42	4696.05	776.76	0.87	4.92	27.62	24.89
Ndata	0.74	138.19	10.11	51.96	1726.19	277.44	0.30	1.85	12.07	9.85
Rangira	56.17	4206.60	379.14	7437.30	23689.23	3651.04	6.49	92.32	96.75	90.73
Ngwenda	56.47	1737.54	163.21	687.11	2516.19	518.14	0.52	17.58	8.67	13.53
Rwahambi	28.11	356.82	39.71	431.45	970.14	153.30	0.39	3.85	3.15	3.97
Virunga total	203.12	8860.42	781.94	9425.68	39547.22	6740.68	10.42	148.69	166.67	178.32

Kihira was sampled downstream of a confluence, one river is from the west in the Mitumba range (Figure 1) and the other from the east. During the last three sampling campaigns, the two tributaries of Kihira were also sampled, and the eastern was found to bring in O₂-deficient water, of high specific conductivity, TA, CH₄, and N₂O. Except for CH₄, these previous parameters (%O₂, TA, and N₂O) showed similar patterns as Chabiringa and Kamutoni. The eastern tributary collects inflowing water containing CH₄ produced in a small swamp (supporting information Figure S1), which could explain the elevated CH₄ found in Kihira. In contrast, the western tributary brought almost the entire TSM and POC load, as a consequence of its mountainous origin in the Mitumba range and its course along a clayey and steep catchment.

As mentioned above, most rivers were only small sources of N₂O to the atmosphere, as observed in other near-pristine tropical rivers with low NO₃⁻ and NH₄⁺ [Bouillon et al., 2012; Borges et al., 2015] and unlike most nitrogen-enriched temperate rivers that have high N₂O concentrations [Beaulieu et al., 2010a, 2010b; Baulch et al., 2011]. The higher N₂O in Chabiringa, Kamutoni and Kihira were associated with high NO₃⁻ and low NO₂⁻ and O₂ (Figures 8c and 8d; respectively) that suggests active denitrification in the groundwaters. Such correlations between N₂O and NO₂⁻ were also observed in some temperate rivers [Dong et al., 2004].

The CH₄ concentration of Virunga rivers (4–5052 nmol L⁻¹) have a broader range than previous data from African rivers such as Comoé, Bia, and Tanoé rivers in West Africa (50–870 nmol L⁻¹) [Koné et al., 2010], Tana river in Kenya (50–500 nmol L⁻¹) [Bouillon et al., 2009], the Oubangui river in Central Africa (50–300 nmol L⁻¹) [Bouillon et al., 2012], but similar to the Athi-Galana-Sabaki rivers in Kenya (2–6729 μmol L⁻¹) [Marwick et al., 2014], although for the latter the highest values were related to organic matter inputs from the city of Nairobi. CH₄ of rivers of the VVP were also characterized by higher values than the adjacent Lake Kivu where CH₄ in surface waters varied from 18 to 197 nmol L⁻¹ in the main basins of the lake and 89–303 in the Kabuno bay [Borges et al., 2011, 2012]. On the other hand, rivers of the VVP contain N₂O close to that observed in the Oubangui river [Bouillon et al., 2012] and the Athi-Galana-Sabaki rivers (18–198 nmol L⁻¹) [Marwick et al., 2014] but remain largely below concentrations normally found in temperate rivers where human activities have increased the DIN concentrations (see compilation by Zhang et al. [2010]).

4.5. Riverine Material Fluxes

Our estimated annual TSM, Si, NH₄⁺, and SRP fluxes for Kihira (Table 3) are comparable with fluxes reported by Muvundja et al. [2009], except for the TP fluxes which were ~90 times higher in their study compared to our estimate. For Chabiringa-Kamutoni, the TSM and SRP annual fluxes are similar for both studies, but our mean TP flux is 48 times higher, and our NH₄⁺ flux is 23 times lower. In Mukoni-Muzungu, our TSM, Si, NH₄⁺, and SRP fluxes are 18, 10, 12, and 8 times higher, respectively, while their mean TP flux is 4 times higher. The observed dissimilarities in fluxes between the two studies are due to differences already discussed among TSM and nutrients concentrations, and are even more pronounced due to differences in the annual discharges used. Muvundja et al. [2009] estimated their annual discharge using the float method described in Harrelson et al. [1994], which assumes a steady and uniform flow and does not offset flood and low flow conditions. For rivers of mountainous catchments (e.g., Kabuno bay), such a method results in discharges with errors of 30% or greater [Bathurst, 1990].

Table 4. Drainage Areas, Climatic Settings, Mean Solute Concentrations and Rates for Rivers in the Virunga Volcanic Province

	Drainage Area (km ²)	Runoff ^d (mm/year)	T (°C)	HCO ₃ ⁻ (mmol/L)	TSM (mg/L)	TDS _{cat} (mg/L)	TDS _{cond} (mg/L)	CO ₂ Consumption Rate (10 ⁶ mol/km ² /year)	Si Weathering Rate (t/km ² /year)	Cationic Weathering Rate (t/km ² /year)	Chemical Weathering Rate (t/km ² /year)	Mechanical Weathering Rate (t/km ² /year)
Mubimbi ^a	55.7	1670	19.3	0.9	223.3	20.7	78.8	1.5	19.0	34.5	131.6	372.9
Kisheke ^a	5.8	1508	20.5	3.2	168.6	65.0	214.0	4.9	34.1	98.0	322.7	254.3
Renga ^a	43.6	1651	21.7	2.6	181.7	61.6	195.6	4.4	26.2	101.7	323.1	300.1
Mukoni ^a	15.4	1119	22.5	5.2	146.0	118.6	384.9	5.8	19.8	132.8	430.9	163.4
Muzungu ^a	16.1	2637	22.3	5.4	161.3	130.8	402.7	14.2	44.1	345.0	1062.0	425.5
Kihira ^b	31.7	1559	20.3	10.9	304.4	275.2	808.1	17.0	43.1	428.9	1259.5	474.5
Chabiringa ^b	8.5	3326	17.4	11.1	1.3	294.3	835.9	37.0	88.4	978.7	2779.9	4.3
Kamutoni ^b	10.2	1430	17.7	11.3	1.7	308.1	840.7	16.1	39.6	440.6	1202.4	2.5
Rwankwi ^b	95.0	1505	19.1	6.9	12.3	159.1	433.1	10.4	49.4	239.4	651.8	18.5
Ndata ^b	70.5	829	19.4	6.7	12.7	149.6	398.0	5.6	24.5	124.0	329.8	10.5
Rangira ^a	1351.0	1313	20.4	4.0	31.7	83.5	250.3	5.2	17.5	109.6	328.7	41.6
Ngwenda ^c	231.8	1297	22.0	0.3	187.7	6.1	30.1	0.4	10.9	7.9	39.0	243.6
Rwahambi ^c	107.3	1120	21.6	0.6	233.8	16.6	55.5	0.7	9.0	18.6	62.1	261.9

^aRivers draining basaltic formations.

^bRivers draining acid metamorphic rock formations.

^cRivers draining lacustrine formations.

^dEstimated runoff.

The estimated mean TSM (198.0 t km⁻² yr⁻¹) and POC (7.43 t km⁻² yr⁻¹) yields of VVP rivers were much higher when compared to those of the Congo River (8.8 t km⁻² yr⁻¹ for TSM and 0.6 t km⁻² yr⁻¹ for POC) [Coynel *et al.*, 2005], the Oubangui River (4.8–5.1 t km⁻² yr⁻¹ for TSM and ~0.3 t km⁻² yr⁻¹ for POC) [Coynel *et al.*, 2005; Bouillon *et al.*, 2012], and the world largest rivers (see compilation by Meybeck [1982], Spitzy and Leenheer [1991], and Coynel *et al.* [2005]). The estimated mean DOC yields (3.11 t km⁻² yr⁻¹) were similar to that of the Congo River (3.5 t km⁻² yr⁻¹) [Coynel *et al.*, 2005], but higher compared to the Oubangui River (1.1–1.4 t km⁻² yr⁻¹) [Coynel *et al.*, 2005; Bouillon *et al.*, 2012].

The estimated DOC (0.74–6.19 t km⁻² yr⁻¹) and POC (0.31–21.08 t km⁻² yr⁻¹) yields in the VVP were almost in the same range with those reported for Guadeloupan volcanic islands [1.9–8.9 t km⁻² yr⁻¹ and 8.1–25.5 t km⁻² yr⁻¹, respectively, for DOC and POC] [Lloret *et al.*, 2011, 2013]. This could partly be explained by two major similarities between the areas. First, both fields experience tropical wet season, and second; their organic C soil content are similar: 1–25% for Virunga and 10–15% for Guadeloupe [Lloret, 2010].

4.6. Weathering and Atmospheric CO₂ Consumption Rates

The discharge-weighted mean TDS_{cat}, TDS_{cond}, and TSM yielded cationic weathering rates from 7.9 to 978.7 t km⁻² yr⁻¹, chemical weathering rates from 39.0 to 2779.9 t km⁻² yr⁻¹, and mechanical weathering rates between 2.5 and 474.5 t km⁻² yr⁻¹ (Table 4). The Si weathering rates and CO₂ consumption rates ranged from 9.0 to 88.4 t km⁻² yr⁻¹, and 0.4 × 10⁶ to 37.0 × 10⁶ mol km⁻² yr⁻¹, respectively. Chemical weathering was more important in rivers draining basaltic fields, whereas mechanical weathering was prevailing in others lithological formations; i.e., acid metamorphic and lacustrine (Table 4). An opposite trend, with higher mechanical than chemical weathering rates, has been observed in the tropical basaltic field of Réunion, [Louvât and Allègre, 1997]. The large influence of lithology on the chemical weathering and CO₂ consumption rates in the Virunga is evident, and illustrated, for example, by comparing Chabiringa (basaltic terrain) with Ngwenda (lacustrine terrain). Thus, Chabiringa (drainage area of 8.5 km²) showed the highest weathering (Si, cationic, and chemical) and CO₂ consumption rates; whereas Ngwenda (231.8 km² drainage area) showed the lowest. Similar trends are observed when comparing rivers draining basaltic terrain (i.e., Kihira, Chabiringa, Kamutoni, Rwankwi, and Ndata) with those of lacustrine and metamorphic rocks. As a result, the five rivers of basaltic terrain cover only 10.6% of the total studied drainage area, but are responsible for 23.4% of the total CO₂ consumed, 22.6% of the total Si weathered, and 25.8% of the total major cations weathered. Basalt was characterized by a mean chemical weathering rate and mean CO₂ consumption rate 2.87 and 2.88 times higher, respectively, compared to values in acid metamorphic rocks terrain; and 24.6 and 32.7 times higher than in lacustrine terrain.

Chemical weathering rates were found to depend strongly on runoff, since there were strong linear relationships between runoff and CO₂ consumption rates ($r^2 = 0.63$; Figure 9a), cationic weathering rates ($r^2 = 0.62$; Figure 9b), and Si weathering rates ($r^2 = 0.66$; Figure 9c). In contrast, no positive temperature dependency

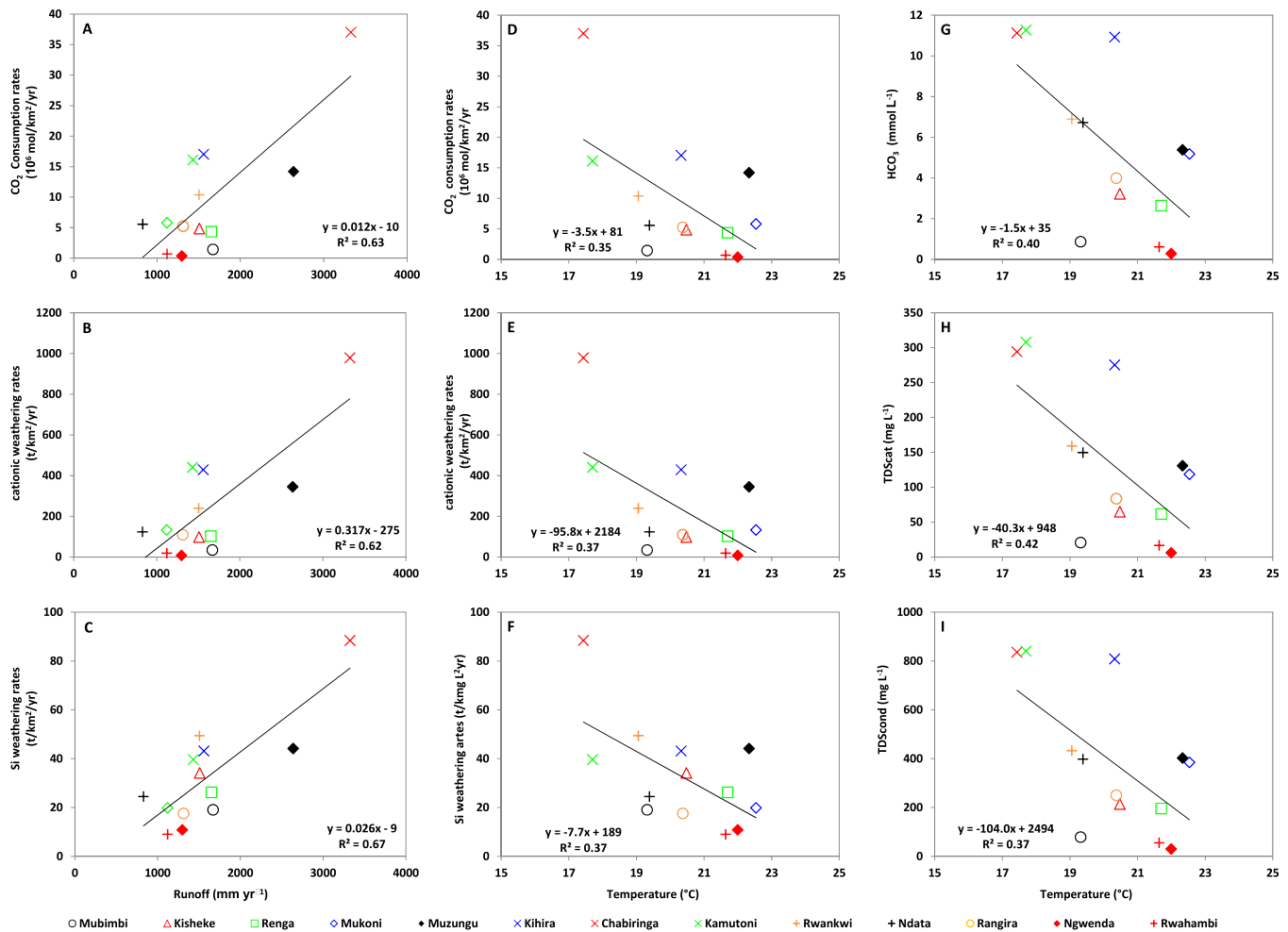


Figure 9. (a-c) Mean riverine CO₂ consumption rates, cationic weathering rates, and Si weathering rates versus runoff; (d-f) mean riverine CO₂ consumption rates, cationic weathering rates and Si weathering rates versus temperature; and (g-i) mean HCO₃⁻, TDScat, TDScond concentrations versus corresponding mean water temperature.

was found for either the CO₂ consumption rate (Figure 9d), cationic weathering rate (Figure 9e), and Si weathering rate (Figure 9f). In addition, no dependency on temperature was found for elements released during chemical weathering (Figures 9h and 9i), or for the HCO₃⁻ ions which balance the major cation charge (Figure 9g), as previously noted by *Amiotte-Suchet and Probst* [1995] and *Bluth and Kump* [1994] in the French basaltic basins. *Dessert et al.* [2003] attributed this pattern to the relative similarity among temperatures of neighboring watersheds, and thus only the effect of runoff could be observed.

The mean CO₂ consumption rate estimated for the study area ($9.46 \times 10^6 \text{ mol km}^{-2} \text{ yr}^{-1}$, or $1.72 \times 10^7 \text{ mol km}^{-2} \text{ yr}^{-1}$ if only considering the basaltic fields) is markedly higher than data reported in the literature for other tropical basaltic regions (Figure 10). On the other hand, the measured mean atmospheric C yield ($113.68 \text{ t C km}^{-2} \text{ yr}^{-1}$) is much higher than previous model estimates for the Virunga ($0.5\text{--}5 \text{ t C km}^{-2} \text{ yr}^{-1}$) [*Hartmann et al.*, 2009]. Since the Virunga mean CO₂ consumption rate is >10 times the global average ($1.99 \text{ t C km}^{-2} \text{ yr}^{-1}$) [*Hartmann et al.*, 2009], the VVP can thereby be considered as CO₂ consumption “hot spot zone” according to a classification by *Meybeck et al.* [2006].

Factors contributing to the high CO₂ consumption rates in the VVP include the high chemical weathering rate of volcanic rocks [*Dessert et al.*, 2001], the high reactivity of basaltic glasses and minerals [*Berner and Berner*, 1996; *Oelkers and Gislason*, 2001; *Gislason and Oelkers*, 2003], and the high annual mean runoff (1613 mm yr^{-1}) and temperature (20.3°C).

Furthermore, the CO₂ consumption rates that can be calculated with the model of *Dessert et al.* [2003] based on a compilation of data in other basalt dominated areas are lower than those we computed (Figure 11).

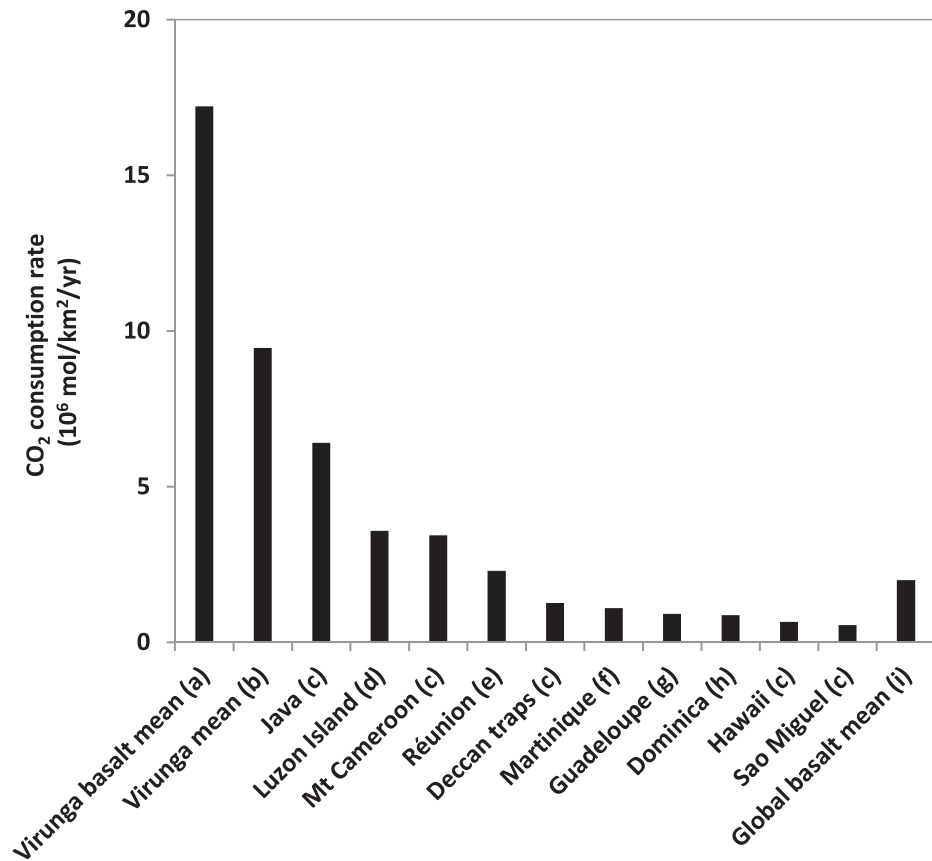


Figure 10. Comparison of Virunga basalt mean and Virunga mean CO₂ consumption rates with the rates of other tropical basaltic provinces, and the Caribbean basalt-andesite formations. (a) represents the mean CO₂ consumption rate for the rivers draining Virunga basalt, (b) the mean CO₂ consumption rate for the whole Virunga, i.e., basalt, metamorphic rocks and lacustrine; (c) is from Dessert *et al.* [2003], (d) Schopka *et al.* [2011], (e) Louvat and Allègre [1997], (f) Rad *et al.* [2006], (g) Lloret *et al.* [2011], (h) Goldsmith *et al.* [2010], and (i) is from Louvat [1997].

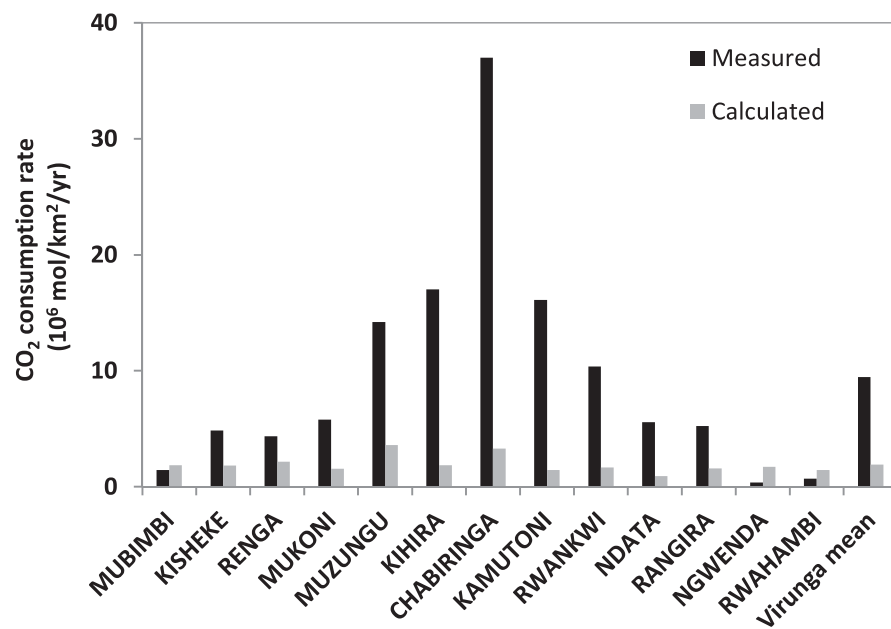


Figure 11. Comparison between the CO₂ consumption rates from field data (measured) and calculated CO₂ consumption (calculated) rates applying the regression model as a function of runoff and temperature as suggested by Dessert *et al.* [2003].

This is indicative of the high solubility of the rocks in the watershed which is probably related to the fact that the VVP is a young active tectonic and volcanic area.

5. Conclusions

The present study offers the first geochemical data set from an under-documented area, in terms of river GHGs and major cations concentrations, DOC, POC, and DIC concentrations and their respective $\delta^{13}\text{C}$ signatures, chemical weathering rates, and atmospheric CO_2 consumption rates. The VVP is a tropical, young active tectonic and volcanic area, relatively undisturbed by anthropogenic activities.

Our results showed that soil, land use, and morphology control the spatial distribution of riverine organic matter (POC and DOC concentrations and origin), TSM, and nutrient concentrations. The DIC was found to largely dominate the C pool. Intense soil erosion leads to high TSM yields in the mountainous rivers draining into Kabuno bay. Lithology and volcanism exert a strong control on the major cation and DIC concentrations, and their spatial distribution. Thus, high basalt (and secondary soil) chemical weathering and leaching mediated by magmatic CO_2 inputs yielded markedly high Na^+ , K^+ , Mg^{2+} , and Si; particularly in basaltic fields. CH_4 concentrations were consistently above atmospheric equilibrium, and thus Virunga rivers were sources of CH_4 to the atmosphere. In contrast, only a few rivers were a net source of N_2O to the atmosphere, as denitrification in groundwaters depleted N_2O concentrations below their atmospheric equilibrium levels in other rivers.

The multilithological state of the VVP highlights the strong influence of lithology on the chemical weathering rates, and the associated atmospheric CO_2 consumption rate under the same climatic conditions. In fact, we noticed that the mean chemical weathering rate and mean CO_2 consumption rate in basalt terrain were respectively ~ 3 higher compared to values in acid metamorphic rocks terrain; and ~ 25 and ~ 33 higher compared to lacustrine terrain. Our study additionally showed that runoff and lithology are the main factors controlling the rates of local chemical weathering and atmospheric CO_2 consumption rates. The $\delta^{13}\text{C}$ -DIC data indicate that part of the CO_2 involved in chemical weathering is geogenic, and thus the active volcanism may partly explain the higher CO_2 consumption and weathering rates reported in this study compared to the literature data.

Note that much of the Virunga lava field is not drained by rivers. This zone is composed of macroporous materials, slightly fractured, and therefore considerably permeable. Rainfall is influenced by the Nyiragongo and Nyamulagira emissions and pH values as low as three have been recorded [Cuoco *et al.*, 2012a, 2012b]. The precipitation interacts with surface and deep basalts, but the resulting atmospheric CO_2 consumption rate is not included in the data we report.

Acknowledgments

We are grateful to Stephane Hoornaert, Marc-Vincent Commarieu and Sandro Petrovic (Université de Liège), and Zita Kelemen (KU Leuven) for their support during sample analysis, Trent Marwick and Cristian Teodoru (KU Leuven) for help and advice with the GIS analysis, Jens Hartmann for kindly providing access to the GLIM database, Marcellin Kasereka for help in field sampling, and Bernhard Peucker-Ehrenbrink (reviewer) and two additional anonymous reviewers for constructive comments on a previous version of the manuscript. This work was funded by the European Research Council starting grant project AFRIVAL (African river basins: Catchment-scale carbon fluxes and transformations, StG 240002) and the Belgian Federal Science Policy Office EAGLES (East African Great Lake Ecosystem Sensitivity to changes, SD/AR/02A) projects. AVB is a senior research associate at the FRS-FNRS. The full data set is provided as supporting information (SI) (Balagizal-ds01 and Balagizal-ds02; XLS).

References

- American Public Health Association (1998), *Standard Methods for the Examination of Water and Wastewater*, 20th ed., Washington, D. C.
- Amiotte-Suchet, P., and J. L. Probst (1995), A global model for present-day atmospheric/soil CO_2 consumption by chemical erosion of continental rocks (GEM- CO_2), *Tellus, Ser. A*, 47, 273–280.
- Amiotte-Suchet, P., J. L. Probst, and W. Ludwig (2003), Worldwide distribution of continental rock lithology: Implications for the atmospheric/soil CO_2 uptake by continental weathering and alkalinity river transport to the oceans, *Global Biogeochem. Cycles*, 17(2), 1038, doi:10.1029/2002GB001891.
- Andersen, T., A. E. Marlina, and E. Muriel (2012), Petrology of combeite- and götzenite-bearing nephelinite at Nyiragongo, Virunga Volcanic Province in the East African Rift, *Lithos*, 152, 105–121, doi:10.1016/j.lithos.2012.04.018.
- Andersen, T., A. E. Marlina, and E. Muriel (2014), Extreme peralkalinity in delhayelite- and andremeyerite-bearing nephelinite from Nyiragongo volcano, East African Rift, *Lithos*, 206–207, 164–178, doi:10.1016/j.lithos.2014.07.025.
- Aoki, K., and H. Kurasawa (1984), Sr isotope study of the tephrite series from Nyamuragira volcano, Zaire, *Geochem. J.*, 18, 95–100.
- Aoki, K., T. Yoshida, K. Yusa, and Y. Nakamura (1985), Petrology and geochemistry of the Nyamuragira volcano, Zaire, *J. Volcanol. Geotherm. Res.*, 25, 1–28.
- Atekwana, E. A., E. A. Atekwana, R. S. Rowe, D. D. Werkema Jr., and F. D. Legall (2004), the relationship of total dissolved solids measurements to bulk electrical conductivity in an aquifer contaminated with hydrocarbon, *J. Appl. Geophys.*, 56, 281–294, doi:10.1016/j.jappgeo.2004.08.003.
- Baccini, A., N. Laporte, S. J. Goetz, M. Sun, and H. Dong (2008), A first map of tropical Africa's above-ground biomass derived from satellite imagery, *Environ. Res. Lett.*, 3, 045011, doi:10.1088/1748-9326/3/4/045011.
- Bastviken, D., L. J. Tranvik, J. A. Downing, P. M. Crill, and A. E. Prast (2011), Freshwater methane emissions offset the continental carbon sink, *Science*, 331, 50, doi:10.1126/science.1196808.
- Bathurst, J. C. (1990), Tests of three discharge gauging techniques in mountain rivers, in *Hydrology of Mountainous Areas*, IAHS Publ. no 190, pp. 93–100, Wallingford, U. K.
- Batjes, N. H. (2008), Mapping soil carbon stocks of Central Africa using SOTER, *Geoderma*, 146, 58–65, doi:10.1016/j.geoderma.2008.05.006.
- Baulch, H. M., S. L. Schiff, R. Maranger, and P. J. Dillon (2011), Nitrogen enrichment and the emission of nitrous oxide from streams, *Global Biogeochem. Cycles*, 25, GB4013, doi:10.1029/2011GB004047.
- Beaulieu, J. J., et al. (2010a), Nitrous oxide emission from denitrification in stream and river networks, *Proc. Natl. Acad. Sci. U. S. A.*, 108, 214–219, doi:10.1073/pnas.1011464108.

- Beaulieu, J. J., W. D. Huster, and J. A. Rebold (2010b), Nitrous oxide emissions from a large, impounded river: The Ohio River, *Environ. Sci. Technol.*, *44*(19), 7527–7533, doi:10.1021/es1016735.
- Beck, V., et al. (2012), Methane airborne measurements and comparison to global models during BARCA, *J. Geophys. Res.*, *117*, D15310, doi:10.1029/2011JD017345.
- BEGo (Synoptics, Keyobs, Royal Museum for Central Africa, Catholic University of Louvain) (2005), Parc National des Virunga, République Démocratique du Congo, 1/260,000, Map realized in the framework of the BEGo (Building Environment for the Gorilla's) project, co-financed by ESA and UNESCO-WHC, Belgium.
- Berner, E. K., and R. A. Berner (1996), *Global Environment: Water, Air, and Geochemical Cycles*, Prentice-Hall, N. J.
- Bluth, G. J. S., and L. R. Kump (1994), Lithologic and climatologic controls of river chemistry, *Geochim. Cosmochim. Acta*, *58*, 2341–2359.
- Borges, A. V., G. Abril, B. Delille, J.-P. Descy, and F. Darchambeau (2011), Diffusive methane emissions to the atmosphere from Lake Kivu (Eastern Africa), *J. Geophys. Res.*, *116*, G03032, doi:10.1029/2011JG001673.
- Borges, A. V., et al. (2012), Variability of carbon dioxide and methane in the epilimnion of Lake Kivu, in *Lake Kivu: Limnology and Biogeochemistry of a Tropical Great Lake*, *Aquat. Ecol.*, vol. 5, edited by J. P. Descy, pp. 47–66, Springer, Dordrecht, Netherlands, doi:10.1007/978-94-007-4243-7_4.
- Borges, A. V., et al. (2015), Globally significant greenhouse gas emissions from African inland waters, *Nat. Geosci.*, doi:10.1038/NGEO2486.
- Bouillon, S., et al. (2009), Distribution, origin and cycling of carbon in the Tana River (Kenya): A dry season basin-scale survey from headwaters to the delta, *Biogeosciences*, *6*, 2475–2493, doi:10.5194/bg-6-2475-2009.
- Bouillon, S., A. Yambélé, R. G. M. Spencer, D. P. Gillikin, P. J. Hernes, J. J. Six, R. Merckx, and A. V. Borges (2012), Organic matter sources, fluxes and greenhouse gas exchange in the Oubangui River (Congo River basin), *Biogeosciences*, *9*, 2045–2062, doi:10.5194/bg-9-2045-2012.
- Bouillon, S., A. Yambélé, D. P. Gillikin, C. Teodoru, F. Darchambeau, T. Lambert, and A. V. Borges (2014), Contrasting biogeochemical characteristics of right-bank tributaries and a comparison with the mainstem Oubangui River, Central African Republic (Congo River basin), *Sci. Rep.*, *4*, 5402, doi:10.1038/srep05402.
- Bousquet, P., et al. (2011), Source attribution of the changes in atmospheric methane for 2006–2008 *Atmos. Chem. Phys.*, *11*, 3689–3700, doi:10.5194/acp-11-3689-2011.
- Chakrabarti R., A. R. Basu, A. P. Santo, D. Tedesco, and O. Vaselli (2009), Isotopic and geochemical evidence for a heterogeneous mantle plume origin of the Virunga volcanics, Western rift, East African Rift system, *Chem. Geol.*, *259*, 273–289, doi:10.1016/j.chemgeo.2008.11.010.
- Coyne, A., P. Seyler, H. Etcheber, M. Meybeck and D. Orange (2005), Spatial and seasonal dynamics of total suspended sediment and organic carbon species in the Congo River, *Global Biogeochem. Cycles*, *19*, GB4019, doi:10.1029/2004GB002335.
- Cuomo, E., A. Spagnuolo, C. Balagizi, S. Francesco, F. Tassi, O. Vaselli, and D. Tedesco (2012a), Impact of volcanic emissions on rainwater chemistry: The case of Mt. Nyiragongo in the Virunga volcanic region (DRC), *J. Geochem. Explor.*, *125*, 69–79, doi:10.1016/j.jgexplo.2012.11.008.
- Cuomo, E., D. Tedesco, R. J. Poreda, J. C. Williams, S. De Francesco, C. Balagizi, and T. H. Darrah (2012b), Impact of volcanic plume emissions on rain water chemistry during the January 2010 Nyamuragira eruptive event: Implications for essential potable water resources, *J. Hazard. Mater.*, *244–245*, 570–581, doi:10.1016/j.jhazmat.2012.10.055.
- Deines, P. (2002), The carbon isotope geochemistry of mantle xenoliths, *Earth Sci. Rev.*, *58*, 247–278, doi:10.1016/S0012-8252(02)00064-8.
- Demant, A., P. Lestrade, T. R. Lubala, A. B. Kampunzu, and J. Durieux (1994), Volcanological and petrological evolution of Nyiragongo volcano, Virunga volcanic field, Zaire, *Bull. Volcanol.*, *56*, 47–61.
- Denaeyer, M. E. (1972), Les laves du fossé tectonique de l'Afrique Centrale. II: Magmatologie, *Ann. Musée R. Afrique Cent.*, *72*, 250.
- Denaeyer, M. E. (1975), *Le glacis des volcans actifs au nord du Lac Kivu (république du Zaïre)*, Ed. du Museum, Sér. C, Sci. de la terre, Paris.
- Dessert, C., B. Dupré, L. M. François, J. Schott, J. Gaillardet, G. Chakrapani and S. Bajpai (2003), Erosion of Deccan Traps determined by river geochemistry, impact on the global climate and the ⁸⁷Sr/⁸⁶Sr ratio of seawater, *Earth Planet. Sci. Lett.*, *188*, 459–474.
- Dessert, C., B. Dupré, J. Gaillardet, L. M. François, and C. J. Allègre (2003), Basalt weathering laws and the impact of basalt weathering on the global carbon cycle, *Chem. Geol.*, *202*, 257–273, doi:10.1016/j.chemgeo.2002.10.001.
- Document stratégique de réduction de la pauvreté (2005), *Province du Nord-Kivu*, SRP-Nord-Kivu, Goma, RD Congo.
- Dong, L. F., D. B. Nedwell, I. Colbeck, and J. Finch (2004), Nitrous oxide emission from some English and Welsh rivers and estuaries, *Water Air Soil Pollut.*, *4*(6), 127–134, doi:10.1007/s11267-005-3022-z.
- Ehleringer, J. R. (1991), ¹³C/¹²C Fractionation and its utility in terrestrial plant studies, in *Carbon Isotope Techniques*, edited by B. Fry, pp. 187–200, Academic, N. Y.
- Farr, T. G., et al. (2007), The shuttle radar topography mission, *Rev. Geophys.*, *45*, RG2004, doi:10.1029/2005RG000183.
- Fraser, A., et al. (2013), Estimating regional methane surface fluxes: The relative importance of surface and GOSAT mole fraction measurements, *Atmos. Chem. Phys.*, *13*, 5697–5713, doi:10.5194/acp-13-5697-2013.
- Gaillardet, J., B. Dupré, P. Louvat, and C. J. Allègre (1999), Global silicate weathering and CO₂ consumption rates deduced from the chemistry of large rivers, *Chem. Geol.*, *159*(1–4), 3–30.
- Gillikin, D. P., and S. Bouillon (2007), Determination of δ¹⁸O of water and δ¹³C of dissolved inorganic carbon using a simple modification of an elemental analyzer-isotope ratio mass spectrometer (EA-IRMS): An evaluation, *Rapid Commun. Mass Spectrom.*, *21*, 1475–1478, doi:10.1002/rcm.2968.
- Gislason, S. R., and E. H. Oelkers (2003), Mechanism, rates and consequences of basaltic glass dissolution. II: An experimental study of the dissolution rates of basaltic glass as a function of pH and temperature, *Geochim. Cosmochim. Acta*, *67*, 3817–3832, doi:10.1016/S0016-7037(03)00176-5.
- Global Land Cover 2000 database (2003), *European Commission*, Joint Res. Cent. [Available at <http://bioval.jrc.ec.europa.eu/products/glc2000/glc2000.php>, last accessed 20 Jan. 2015.]
- Goldsmith, S. T., A. E. Carey, B. M. Johnson, S. A. Welch, W. B. Lyons, W. H. McDowell, and J. S. Pigott (2010), Stream geochemistry, chemical weathering and CO₂ consumption potential of andesitic terrains, Dominica, Lesser Antilles, *Geochim. Cosmochim. Acta*, *74*, 85–103, doi:10.1016/j.gca.2009.10.009.
- Guibert, P. (1978), Contribution à l'étude du volcanisme de la chaîne des Virunga (République du Zaïre): Le volcan Mikeno, PhD thesis, Univ. de Genève, Geneva, Switzerland.
- Harrelson, C. C., C. L. Rawlins, and J. P. Potyondy (1994), Stream channel reference sites: An illustrated guide to field technique, *Gen. Tech. Rep. RM-245*, 61 pp., Dep. of Agric., For. Serv., Rocky Mt. For. and Range Exp. Str., Fort Collins, Colo.
- Hartmann, J., and N. Moosdorf (2011), Chemical weathering rates of silicate-dominated lithological classes and associated liberation rates of phosphorus on the Japanese Archipelago-Implications for global scale analysis, *Chem. Geol.*, *287*, 125–157, doi:10.1016/j.chemgeo.2010.12.004.

- Hartmann, J., and N. Moosdorf (2012), The new global lithological map database GLiM: A representation of rock properties at the Earth surface, *Geochem. Geophys. Geosyst.*, *13*, Q12004, doi:10.1029/2012GC004370.
- Hartmann, J., N. Jansen, H. H. Dürr, S. Kempe, and P. Köhler (2009), Global CO₂-consumption by chemical weathering: What is the contribution of highly active weathering regions?, *Global Planet. Change*, *69*, 185–194, doi:10.1016/j.gloplacha.2009.07.007.
- Hartmann, J., N. Moosdorf, R. Lauerwald, M. Hinderer, and A. J. West (2014), Global chemical weathering and associated P-release—The role of lithology, temperature and soil properties, *Chem. Geol.*, *363*, 145–163, doi:10.1016/j.chemgeo.2013.10.025.
- Head, E. M., A. M. Shaw, P. J. Wallace, K. W. W. Sims, and S. A. Carn (2011), Insight into volatile behavior at Nyamuragira volcano (D.R. Congo, Africa) through olivine-hosted melt inclusions, *Geochem. Geophys. Geosyst.*, *12*, Q0AB11, doi:10.1029/2011GC003699.
- Hertogen, J., L. Vanlerberghe, and M. R. Namegabe (1985), Geochemical evolution of the Nyiragongo volcano (Virunga, Western African Rift, Zaire), *Bull. Geol. Soc.*, *57*(1–2), 21–35.
- Hijmans, R. J., S. E. Cameron, J. L. Parra, P. G. Jones, and A. Jarvis (2005), Very high resolution interpolated climate surfaces for global land areas, *Int. J. Climatol.*, *25*, 1965–1978, doi:10.1002/joc.1276.
- Ittekkot, V., and R. W. P. M. Laane (1991), Fate of riverine particulate organic matter, in *Biogeochemistry of Major World Rivers*, edited by E. T. Degens, S. Kempe, and J. E. Richey, chap. 6, pp. 233–243, John Wiley, N. Y.
- Julley, D. W., M. Windowson, and S. Self (2008), Volcanogenic nutrient fluxes and plant ecosystems in large igneous provinces: An example from the Columbia River Basalt Group, *J. Geol. Soc.*, *165*, 955–966, doi:10.1144/0016-76492006-199.
- Kirschke, S., et al. (2013), Three decades of global methane sources and sinks, *Nat. Geosci.*, *6*, 813–823, doi:10.1038/NGEO1955.
- Koné, Y. J. M., G. Abril, B. Delille, and A. V. Borges (2010), Seasonal variability of methane in the rivers and lagoons of Ivory Coast (West Africa), *Biogeochemistry*, *100*, 21–37, doi:10.1007/s10533-009-9402-0.
- Lauerwald, R., G. G. Laruelle, J. Hartmann, P. Ciais, and P. A. G. Regnier (2015), Spatial patterns in CO₂ evasion from the global river network, *Global Biogeochem. Cycles*, *29*, 534–554, doi:10.1002/2014GB004941.
- Le Quéré, C., et al. (2014), Global carbon budget 2014, *Earth Syst. Sci. Data Discuss.*, *7*, 521–610, doi:10.5194/essdd-7-521-2014.
- Loret, E. (2010), Dynamique du carbone dans des petits bassins versants tropicaux, exemple de la Guadeloupe, PhD thesis, Univ. of Paris, Paris.
- Loret, E., C. Dessert, J. Gaillardet, P. Albéric, O. Crispi, C. Chaduteau, and M. F. Benedetti (2011), Comparison of dissolved inorganic and organic carbon yields and fluxes in the watersheds of tropical volcanic islands, examples from Guadeloupe, *Chem. Geol.*, *280*, 65–78, doi:10.1016/j.chemgeo.2010.10.016.
- Lloret, E., C. Dessert, L. Pastor, E. Lajeunesse, O. Crispi, J. Gaillardet, and M. F. Benedetti (2013), Dynamic of particulate and dissolved organic carbon in small volcanic mountainous tropical watersheds, *Chem. Geol.*, *351*, 229–244, doi:10.1016/j.chemgeo.2013.05.023.
- Louvat, P. (1997), Etude géochimique de l'érosion fluviale d'îles volcaniques à l'aide des bilans d'éléments majeurs et traces, PhD thesis, 322 pp., Univ. of Paris, Paris.
- Louvat, P., and C. J. Allègre (1997), Present denudation rates at Réunion Island determined by river geochemistry: Basalt weathering and mass budget between chemical and mechanical erosions, *Geochim. Cosmochim. Acta*, *61*, 3645–3669.
- Ludwig, W., J. L. Probst, and S. Kempe (1996), Predicting the oceanic input of organic carbon by continental erosion, *Global Biogeochem. Cycles*, *10*(1), 23–41, doi:10.1029/95GB02925.
- Mann, P. J., et al. (2014), The biogeochemistry of carbon across a gradient of streams and rivers within the Congo Basin, *J. Geophys. Res. Biogeosci.*, *119*, 687–702, doi:10.1002/2013JG002442.
- Marcelot, G., C. Dupuy, J. Dostal, J. P. Rancon, and A. Pouclet (1989), Geochemistry of mafic volcanic rocks from Lake Kivu (Zaire and Rwanda) section of the Western Branch of the African Rift, *J. Volcanol. Geotherm. Res.*, *39*, 73–88.
- Mariotti, A., F. Gadel, P. Giresse, and Kinga-Mouzeo (1991), Carbon isotope composition and geochemistry of particulate organic matter in the Congo River (Central Africa): Application to the study of Quaternary sediments off the mouth of the river, *Chem. Geol.*, *86*, 345–357.
- Martins, O., and J. L. Probst (1991), Biogeochemistry of major African Rivers: Carbon and mineral transport, in *Biogeochemistry of Major World Rivers*, edited by E. T. Degens, S. Kempe, and J. E. Richey, chap. 6, pp. 129–155, John Wiley, N. Y.
- Marwick, T. R., F. Tamooh, B. Ogwoka, C. Teodoru, A. V. Borges, F. Darchambeau, and S. Bouillon (2014), Dynamic seasonal nitrogen cycling in response to anthropogenic N loading in a tropical catchment, Athi-Galana-Sabaki River, Kenya, *Biogeosciences*, *11*, 1–18, doi:10.5194/bg-11-1-2014.
- Mayaux, P., E. Bartholomé, S. Fritz, and A. Belward (2004), A new land-cover map of Africa for the year 2000, *J. Biogeogr.*, *31*, 861–877, doi:10.1111/j.1365-2699.2004.01073.x.
- Meybeck, M. (1982), Carbon, nitrogen and phosphorus transport by world rivers, *Am. J. Sci.*, *282*, 401–450.
- Meybeck, M. (1987), Global chemical weathering of surficial rocks estimated from river dissolved loads, *Am. J. Sci.*, *287*, 401–428.
- Meybeck, M. (1993a), Natural sources of C, N, P and S, in *Interactions of C, N, P and S Biogeochemical Cycles and Global Change*, edited by R. Wollast, F. T. Mackenzie, and L. Chou, pp. 163–193, Springer, Berlin.
- Meybeck, M. (1993b), Riverine transport of atmospheric carbon: Sources, global typology and budget, *Water Air Soil Pollut.*, *70*, 443–464.
- Meybeck, M. (2005), Origins and behaviours of carbon species in World rivers, in *Erosion and Carbon Dynamics*, *Adv. Soil Sci.*, edited by E. Roose and R. Lal, pp. 209–238, CRC Press, Boca Raton, Fla.
- Meybeck, M., H. H. Dürr and C. J. Vörösmarty (2006), Global coastal segmentation and its river catchment contributors: A new look at land-ocean linkage, *Glob. Biogeochem. Cycles*, *20*, GB1590, doi:10.1029/2005GB002540.
- Moon, S., C. P. Chamberlain, and G. E. Hilley (2014), New estimates of silicate weathering rates and their uncertainties in global rivers, *Geochim. Cosmochim. Acta*, *134*, 257–274, doi:10.1016/j.gca.2014.02.033.
- Morimoto, N. (1989), Nomenclature of pyroxenes, *Can. Mineral.*, *27*, 143–156.
- Munhoven, G. (2002), Glacial-interglacial changes of continental weathering: Estimates of the related CO₂ and HCO₃⁻ flux variations and their uncertainties, *Global Planet. Change*, *33*(1–2), 155–176.
- Muvundja, A. F., et al. (2009), Balancing nutrient inputs to Lake Kivu, *J. Great Lakes Res.*, *35*(3), 406–418, doi:10.1016/j.jglr.2009.06.002.
- Oelkers, E. H., and S. R. Gislason (2001), The mechanism, rates and consequences of basaltic glass dissolution. I: An experimental study of the dissolution rates of basaltic glass as function of aqueous Al, Si and oxalic acid concentration at 25°C and pH = 3 and 11, *Geochim. Cosmochim. Acta*, *65*, 3671–3681.
- Platz, T. (2002), Nyiragongo volcano, DR Congo—mineral chemistry and petrology, PhD thesis, Univ. of Greifswald, Inst. of Geol. Sci., Greifswald, Germany.
- Pison, I., P. Bousquet, F. Chevallier, S. Szopa, and D. Hauglustaine (2009), Multi-species inversion of CH₄, CO and H₂ emissions from surface measurements, *Atmos. Chem. Phys.*, *9*, 5281–5297, doi:10.5194/acp-9-5281-2009.

- Platz, T., S. F. Foley, and L. Andre (2004), Low-pressure fractionation of the Nyiragongo volcanic rocks, Virunga Province, D.R. Congo, *J. Volcanol. Geotherm. Res.*, *136*, 269–295, doi:10.1016/j.jvolgeores.2004.05.020.
- Poucllet, A. (1974), Pétrographie du Rugarama, dernier cône adventif du volcan Nyamuragira (1971), (Rift W.-Africain), *Publ. Spéc.*, 1–28.
- Poucllet, A. (1977), Contribution à l'étude structurale de l'aire volcanique des Virunga, rift de l'Afrique Centrale, *Rev. Géogr. Phys. Géol. Dyn.*, *19*(2), 115–124.
- Rad, S., P. Louvat, C. Gorge, J. Gaillardet, and C. J. Allègre (2006), River dissolved and solid loads in the Lesser Antilles: New insight into basalt weathering processes, *J. Geochem. Explor.*, *88*, 308–312, doi:10.1016/j.gexplo.2005.08.063.
- Ralison, O., F. Dehairs, J. J. Middelburg, A. V. Borges, and S. Bouillon (2008), Carbon biogeochemistry in the Betsiboka estuary (northwestern Madagascar), *Org. Geochem.*, *39*, 1649–1658, doi:10.1016/j.orggeochem.2008.01.010.
- Raymond, P. A., et al. (2013), Global carbon dioxide emissions from inland waters, *Nature*, *503*, 355–359, doi:10.1038/nature12760.
- Rodier, J., and C. Bazin (2005), *Analyse de l'eau: Eaux naturelles, eaux résiduelles et eaux de mer*, 8 éd., Dunod, Paris.
- Schopka, H. H., L. A. Derry, and C. A. Arcilla (2011), Chemical weathering, river geochemistry and atmospheric carbon fluxes from volcanic and ultramafic regions on Luzon Island, the Philippines, *Geochim. Cosmochim. Acta*, *75*, 978–1002, doi:10.1016/j.gca.2010.11.014.
- Smets, B. (2007), *Etude des mazokus dans la région de Goma (République Démocratique du Congo) et gestion des risques, Mémoire de Master en Gestion des Risques Naturels*, Univ. de Liège, Liège, Belgium.
- Smets, B., et al. (2013), Detailed multidisciplinary monitoring reveals pre- and co-eruptive signals at Nyamulagira volcano (North Kivu, Democratic Republic of Congo), *Bull. Volcanol.*, *76*(1), 1–35, doi:10.1007/s00445-013-0787-1.
- Spencer, R. G. M., et al. (2012), An initial investigation into the organic matter biogeochemistry of the Congo River, *Geochim. Cosmochim. Acta*, *84*, 614–627, doi:10.1016/j.gca.2012.01.013.
- Spitz, A., and J. Leenheer (1991), dissolved organic carbon in rivers, in *Biogeochemistry of Major World Rivers*, edited by E. T. Degens, S. Kempe, and J. E. Richey, chap. 9, pp. 213–232, John Wiley, N. Y.
- Still, C. J., and R. L. Powell (2010), Continental-scale distributions of vegetation stable carbon isotope ratios, in *Isoscapes: Understanding Movement, Pattern, and Process on Earth Through Isotope Mapping*, edited by J. B. West, et al., pp. 179–193, Springer, Netherlands, doi:10.1007/978-90-481-3354-3_9.
- Tamooch, F. K., et al. (2012), Distribution and origin of suspended matter and organic carbon pools in the Tana River Basin, Kenya, *Biogeosciences*, *9*, 2905–2920, doi:10.5194/bg-9-2905-2012.
- Teodoru, C. R., F. C. Nyoni, A. V. Borges, F. Darchambeau, I. Nyambe, and S. Bouillon (2015), Spatial variability and temporal dynamics of greenhouse gas (CO₂, CH₄, N₂O) concentrations and fluxes along the Zambezi River mains tem and major tributaries, *Biogeosciences*, *12*, 2431–2453, doi:10.5194/bg-12-2431-2015.
- Vitousek, P. M. (2004), *Nutrient Cycling and Limitation: Hawai'i as a Model System*, Princeton Univ. Press, Princeton, N. J.
- Weiss, R. F. (1981), Determinations of carbon dioxide and methane by dual catalyst flame ionization chromatography and nitrous oxide by electron capture chromatography, *J. Chromatogr. Sci.*, *19*, 611–616.
- Wieczorek, M. E. (2012), *Flow-Based Method for Stream Generation in a GIS*, USGS Water Sci. Cent. for Md., Delaware and the Dist. of Columbia, USGS. [Available at <http://md.water.usgs.gov/posters/flowGIS/index.html>].
- Zhang, G. L., J. Zhang, S. M. Liu, J. L. Ren, and Y. C. Zhao (2010), Nitrous oxide in the Changjiang (Yangtze River) Estuary and its adjacent marine area: Riverine input, sediment release and atmospheric fluxes, *Biogeosciences*, *7*, 3505–3516, doi:10.5194/bg-7-3505-2010.

Diffusive methane emissions to the atmosphere from Lake Kivu (Eastern Africa)

A. V. Borges,¹ G. Abril,^{2,3} B. Delille,¹ J.-P. Descy,⁴ and F. Darchambeau^{1,4}

Received 1 February 2011; revised 24 May 2011; accepted 7 June 2011; published 9 September 2011.

[1] We report a data set of methane (CH₄) concentrations in the surface waters of Lake Kivu obtained during four cruises (March 2007, September 2007, June 2008, and April 2009) covering the two main seasons, rainy (October to May) and dry (June to September). Spatial gradients of CH₄ concentrations were modest in the surface waters of the main basin. In Kabuno Bay (a small subbasin), CH₄ concentrations in surface waters were significantly higher than in the main basin. Seasonal variations of CH₄ in the main basin were strongly driven by deepening of the mixolimnion and mixing of surface waters with deeper waters rich in CH₄. On an annual basis, both Kabuno Bay and the main basin of Lake Kivu were over-saturated in CH₄ with respect to atmospheric equilibrium (7330% and 2510%, respectively), and emitted CH₄ to the atmosphere (39 mmol m⁻² yr⁻¹ and 13 mmol m⁻² yr⁻¹, respectively). The source of CH₄ to atmosphere was two orders of magnitude lower than the CH₄ upward flux. The source of CH₄ to the atmosphere from Lake Kivu corresponded to ~60% of the terrestrial sink of atmospheric CH₄ over the lake's catchment. A global cross-system comparison of CH₄ in surface waters of lakes shows that both Kabuno Bay and the main basin are at the lower end of values in lakes globally, despite the huge amounts of CH₄ in the deeper layers of the lake. This is related to the strongly meromictic nature of the lake that promotes an intense removal of CH₄ by bacterial oxidation.

Citation: Borges, A. V., G. Abril, B. Delille, J.-P. Descy, and F. Darchambeau (2011), Diffusive methane emissions to the atmosphere from Lake Kivu (Eastern Africa), *J. Geophys. Res.*, 116, G03032, doi:10.1029/2011JG001673.

1. Introduction

[2] Freshwater environments are important components of the global carbon (C) cycle, as they transport organic and inorganic C from the terrestrial biosphere to the oceans. This transport of C is not passive, and freshwater ecosystems produce, degrade, store organic C and exchange C with the atmosphere [Cole and Caraco, 2001; Cole et al., 2007; Battin et al., 2008; Tranvik et al., 2009]. Degradation of organic C in freshwater environments is partly mediated by anaerobic processes, including methanogenesis, which leads to the emission of methane (CH₄) to the atmosphere. The global emission of CH₄ to the atmosphere from freshwater ecosystems has been recently reevaluated by Bastviken et al. [2011] to 103 Tg CH₄ yr⁻¹ which is significant when compared to other natural (168 Tg CH₄ yr⁻¹) and anthropogenic (428 Tg CH₄ yr⁻¹) CH₄ emissions [Chen and Prinn, 2006].

The CH₄ emission from freshwater ecosystems is broken down into 72 Tg CH₄ yr⁻¹ from lakes, 20 Tg CH₄ yr⁻¹ from reservoirs, 1 Tg CH₄ yr⁻¹ from rivers, and 10 Tg CH₄ yr⁻¹ plant mediated (all aquatic systems). About 49% of the CH₄ emission to the atmosphere from freshwater ecosystems occurs in the tropics, although tropical lakes are under-sampled. In the Bastviken et al. [2011] compilation, only 9 out of 36 publications, and only 7 out of 106 data entries deal with tropical lakes.

[3] We report the seasonal and spatial variability of CH₄ in the epilimnion of Lake Kivu [2.50°S 1.59°S 29.37°E 28.83°E] one of the East African great lakes (2370 km² surface area, 550 km³ volume). Lake Kivu is a deep (maximum depth of 485 m) meromictic lake, with an oxic mixolimnion down to 70 m, and a deep monolimnion rich in dissolved gases and nutrients [Degens et al., 1973; Schmid et al., 2005]. Lake Kivu is permanently stratified and deep layers receive heat, salts, and CO₂ from deep geothermal springs [Schmid et al., 2005]. Seasonality of the physical and chemical vertical structure and biological activity in surface waters of Lake Kivu is driven by the oscillation between the dry season (June–September) and the rainy season (October–May), the former characterized by a deepening of the mixolimnion [Sarmiento et al., 2006]. This seasonal mixing favors the input of dissolved nutrients and the development of diatoms, while, during the rest of the

¹Unité d'Océanographie Chimique, Université de Liège, Liège, Belgium.

²Laboratoire Environnements et Paléoenvironnements Océaniques, UMR CNRS 5805, Université de Bordeaux 1, Talence, France.

³Institut de Recherche pour le Développement, Laboratório de Potamologia Amazônica, Universidade Federal do Amazonas, Manaus, Brazil.

⁴Laboratoire d'écologie des Eaux Douces, URBE, University of Namur, Namur, Belgium.

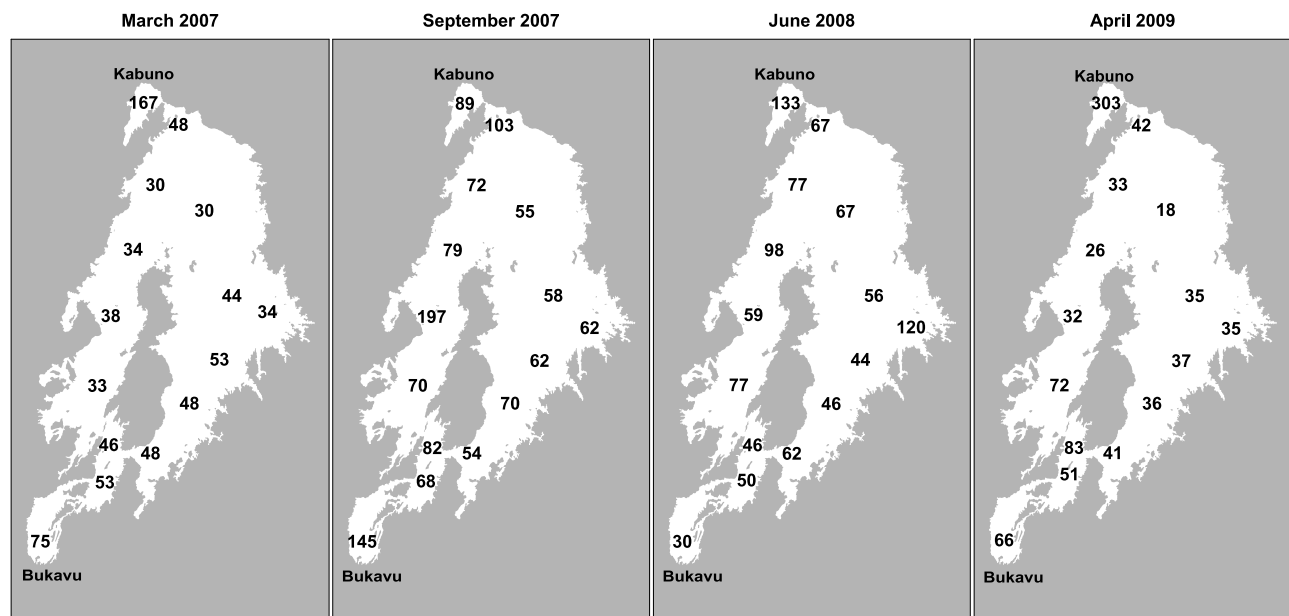


Figure 1. Distribution of the CH₄ concentration (nM) in surface waters of Lake Kivu (10 m depth in the main basin and 5 m depth in Kabuno Bay) in March 2007, September 2007, June 2008, and April 2009.

year, the phytoplankton assemblage is dominated by cyanobacteria, chrysophytes and cryptophytes.

[4] Huge amounts of carbon dioxide (CO₂) and CH₄ (300 km³ and 60 km³, respectively, at 0°C and 1 atm) [Schmid *et al.*, 2005] are dissolved in the deep layers of Lake Kivu. While CO₂ is mainly geogenic, two thirds of the CH₄ originates from anoxic bacterial reduction of CO₂ and one third from anaerobic degradation of settling organic material [Schoell *et al.*, 1988; Pasche *et al.*, 2011]. Large scale industrial extraction of CH₄ from the deep layers of Lake Kivu is planned [Nayar, 2009] which could affect the ecology and biogeochemical cycling of C of the lake and change for instance the emission of greenhouse gases such as CH₄ and CO₂. To monitor, understand and quantify the consequences of the industrial extraction of CH₄ it is required to establish the baseline of ecological and biogeochemical settings.

2. Material and Methods

[5] In order to capture the seasonal and spatial variations of CH₄ in surface waters, four cruises were carried out in Lake Kivu on 15–29 March 2007 (middle of the rainy season), 28 August to 10 September 2007 (late dry season), 21 June to 3 July 2008 (early dry season), and 21 April to 5 May 2009 (late rainy season). Sampling was carried out at 15 stations distributed in a relatively regular grid covering the whole lake (Figure 1).

[6] Vertical profiles of temperature, conductivity, oxygen and pH were obtained with a Yellow Springs Instrument (YSI) 6600 V2 probe. Calibration of sensors was carried out prior to the cruises and regularly checked during the cruises. Conductivity cell was calibrated with a 1000 μS cm⁻¹ (25°C) YSI standard, pH electrode was calibrated with pH 4.00 (25°C) and pH 7.00 (25°C) National Institute of Standards

and Technology (YSI) buffers, oxygen membrane probe was calibrated with humidity saturated ambient air. Water was sampled with a 5 L Niskin bottle (Hydro-Bios) at 5 m in Kabuno Bay (48 km²) and at 10 m in the rest of the lake (hereafter referred to as main basin, 2322 km²). During the April 2009 cruise, samples were also collected at all stations at 0.5 m, and vertical profiles were made down to 80 m depth at two stations. Water was collected in glass serum bottles from the Niskin bottle with tubing, left to overflow, poisoned with 100 μl of saturated HgCl₂ and sealed with butyl stoppers and aluminum caps.

[7] Concentrations of CH₄ were determined by gas chromatography (GC) with flame ionization detection (GC-FID, Hewlett Packard HP 5890A), after creating a 12 ml headspace with N₂ in 40 ml glass serum bottles, as described by Abril and Iversen [2002]. Certified CH₄:N₂ mixture (Air Liquide France) of 10.0 ± 0.2 ppm CH₄ was used as standard. For the April 2009 cruise, CH₄ measurements were carried out with the same procedures but using 30 ml headspace with N₂ in 70 ml serum bottles, and a SRI 8610C GC-FID calibrated with CH₄:CO₂:N₂O:N₂ mixtures (Air Liquide Belgium) of 1.05 ± 0.02, 10.2 ± 0.2 and 509 ± 10 ppm CH₄. Precision estimated from multiple injections of gas standards was on average ±4% for the 10.0 ppm standard with the HP 5890A GC-FID. Precision was better than ±3% for the 1.05 ppm standard and better than ±0.5% for both the 10.2 ppm and 509 ppm standards with the SRI 8610C GC-FID. The concentrations were computed using the CH₄ solubility coefficient given by Yamamoto *et al.* [1976].

[8] During the April 2009 cruise, on all stations, CH₄ data were acquired at two depths, near surface (~0.5 m) and below (10 m in the main basin and 5 m in Kabuno Bay), and were not significantly different (paired *t* test, *p* = 0.125, *n* = 15). Hence, CH₄ concentrations at 10 m in the main basin and at 5 m in Kabuno Bay were used for the 4 cruises to

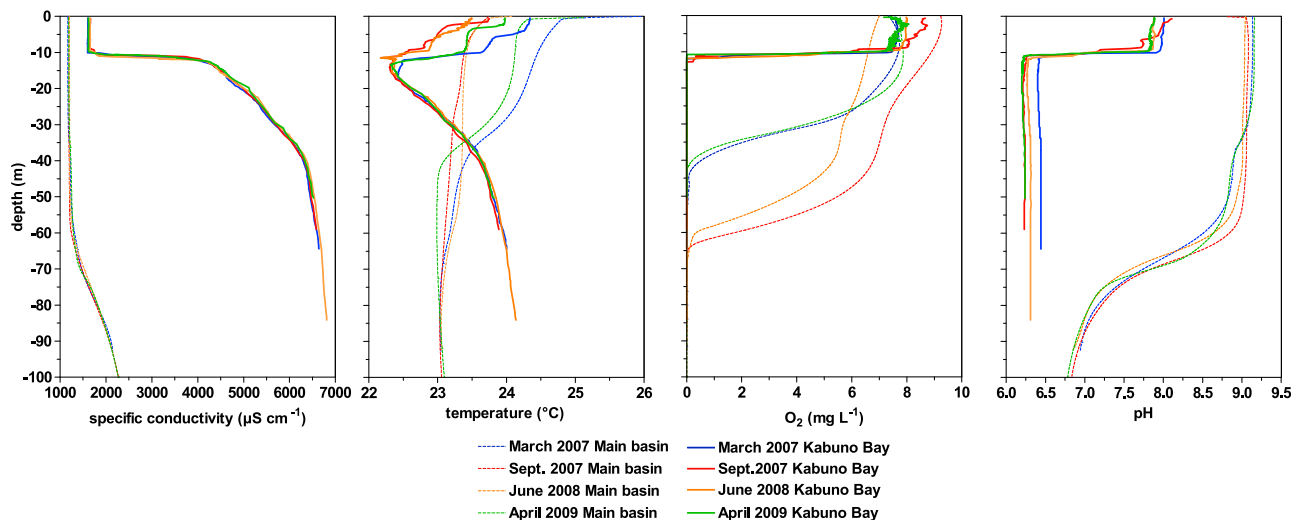


Figure 2. Vertical profiles of specific conductivity (25°C , $\mu\text{S cm}^{-1}$), temperature ($^{\circ}\text{C}$), dissolved O_2 (mg L^{-1}), and pH in the main basin of Lake Kivu (average of all stations) and Kabuno Bay in March 2007, September 2007, June 2008, and April 2009.

compute the diffusive air-water CH_4 flux (FCH_4), according to

$$\text{FCH}_4 = k \Delta[\text{CH}_4]$$

where k is the gas transfer velocity of CH_4 and $\Delta[\text{CH}_4]$ is the air-water gradient of CH_4 computed from CH_4 concentration in the water and a constant atmospheric CH_4 concentration of 1.8 ppm (corresponding to the global average mixing ratio).

[9] The value k was computed from wind speed using the parameterization of *Cole and Caraco* [1998] and the Schmidt number of CH_4 in freshwater according to the algorithm given by *Wanninkhof* [1992]. Wind speed data were acquired with a Davis Instruments meteorological station in Bukavu (2.51°S 28.86°E). During the April 2009 cruise, wind speed was measured at 11 stations on the lake with a THIES anemometer, and data were not significantly different from those acquired at Bukavu (paired t test, $p = 0.593$, $n = 11$). FCH_4 was computed with daily wind speed averages for a time period of one month centered on the date of the middle of each field cruise. Such an approach allows to account for the day-to-day variability of wind speed, and to provide FCH_4 values that are seasonally representative.

3. Results and Discussion

[10] In the main basin of Lake Kivu, the seasonal variation of temperature in surface waters was modest, ranging between 23.35 ± 0.18 (standard deviation) $^{\circ}\text{C}$ in September 2007 and $24.43 \pm 0.18^{\circ}\text{C}$ in March 2007. The oxycline varied seasonally between ~ 35 m in March 2007 and April 2009 and ~ 60 m in September 2007 and June 2008, while the chemocline (conductivity, pH) was relatively stable and started at 60 m (Figure 2). In Kabuno Bay, the amplitude of the seasonal variations of temperature in surface waters was similar ($\sim 1.1^{\circ}\text{C}$) but values were systematically lower than in the main basin between 0.3°C and 0.7°C depending on the cruise. Kabuno Bay was characterized by a very stable

chemocline (conductivity, pH) and oxycline at ~ 10.5 m, irrespective of the sampling period. At 60 m, conductivity and water temperature were markedly higher in Kabuno Bay than in the main basin. These vertical patterns and their lack of seasonality indicate that Kabuno Bay is distinct from the main basin. There seems to be a much larger contribution of internal geothermal inputs to the whole water column including surface waters in Kabuno Bay than in the main basin of Lake Kivu (not necessarily in terms of absolute inputs but possibly in terms of the ratio of inputs to volume). This is related to the different geomorphology, since Kabuno Bay is shallower than the main basin (maximum depth of 110 m versus 485 m) and exchanges little water with the main basin (narrow connection ~ 10 m deep).

[11] In surface waters of the main basin of Lake Kivu, CH_4 concentrations were systematically above atmospheric equilibrium (~ 2 nM), and varied within relatively narrow ranges of 30–75 nM in March 2007, 54–197 nM in September 2007, 30–120 nM in June 2008, and 18–83 nM in April 2009 (Figure 1). The coefficient of variation of CH_4 in surface waters of the main basin ranged between 26% in March 2007 and 46% in September 2007. We cannot provide a straightforward explanation for these small spatial variations of CH_4 concentrations. For a given cruise, CH_4 concentrations did not correlate with mixed layer depth nor water temperature. For the whole data set, CH_4 concentrations in surface waters of Kabuno Bay were significantly higher than in the main basin (repeated measures ANOVA, $f_{4,10} = 61.85$, $p < 0.0001$). The CH_4 concentrations in surface waters of lakes result from the balance of inputs from depth or laterally from the littoral zone, and of loss terms (bacterial oxidation and evasion to the atmosphere) [*Bastviken et al.*, 2004]. *Tietze et al.* [1980] showed that CH_4 concentrations in deep waters of Kabuno Bay are similar to the ones for similar depths in the main basin of Lake Kivu. The likely higher contribution of deepwater springs in Kabuno Bay than in the main basin increases the upward flux of solutes and might explain the higher CH_4 concentrations we observed in Kabuno Bay than in the main basin. Also, the

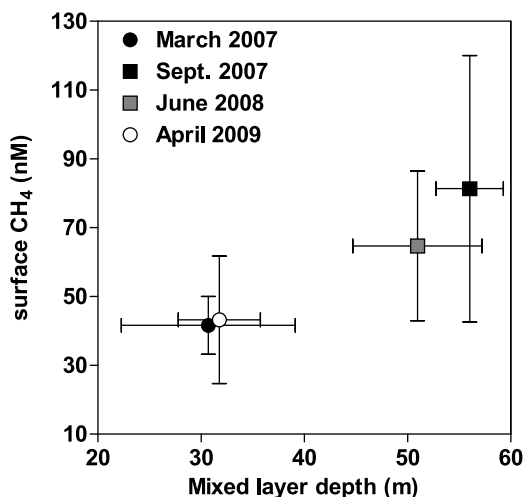


Figure 3. Mean values in the main basin of Lake Kivu of CH₄ concentration in surface waters (10 m, nM) versus mixed layer depth in March 2007, September 2007, June 2008, and April 2009. Error bars correspond to standard deviation on the mean.

shallower oxycline in Kabuno Bay (Figure 2) than in the main basin could promote less removal of CH₄ by aerobic bacterial oxidation in the oxic layer.

[12] Seasonal variations of CH₄ in the main basin of Lake Kivu were significant (one-way ANOVA, log-transformed data, $f_{3,52} = 10.55$, $p < 0.0001$). Average CH₄ concentrations for each cruise were positively correlated (Pearson $r^2 = 0.96$, $p = 0.0214$) to mixed layer depth (Figure 3). This suggests that the deepening of the mixed layer and mixing of deeper waters rich in CH₄ with surface waters was a major driver of seasonal variability of CH₄ concentrations in surface waters of the main basin of Lake Kivu. Vertical profiles obtained in April 2009 in the main basin, show that CH₄ concentrations at 60 m are ~2100 to ~2600 times higher than in surface waters (Figure 4).

[13] Deepening of the mixed layer is induced by enhanced turbulence in surface waters which will also increase k and the loss of CH₄ to the atmosphere. However, CH₄ is a sparingly soluble gas and the exchange of CH₄ across the air-water interface is a slow process. For the conditions in September 2007, the reduction by 50% of the initial surface average CH₄ concentration (81 nM) by loss to the atmosphere would require about 67 days and the reduction by 95% would require 354 days (with a constant wind speed of 1.2 m s⁻¹ and a mixed layer of 56 m). As the loss of CH₄ to

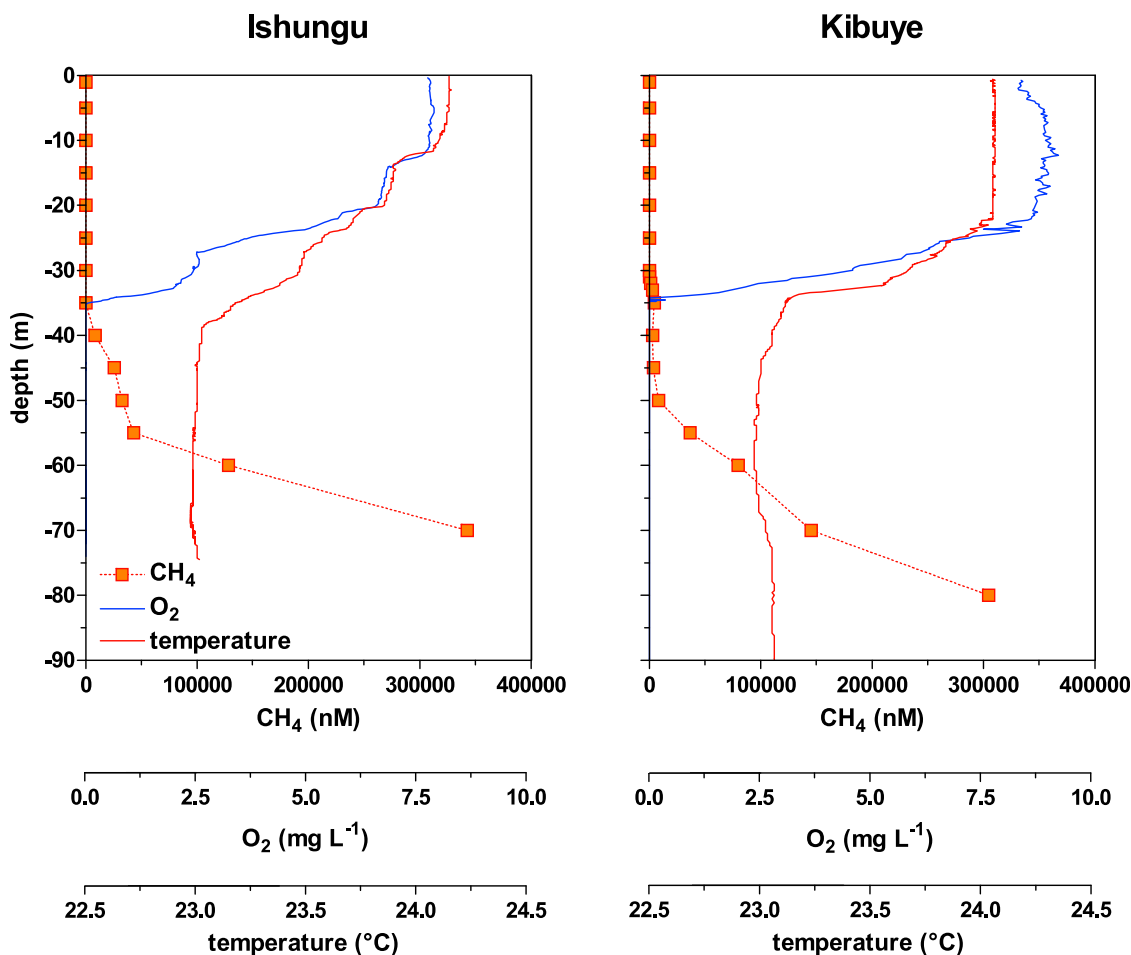


Figure 4. Vertical profiles of CH₄ (nM), temperature (°C), and dissolved O₂ (mg L⁻¹) in April 2009 at two stations in the main basin of Lake Kivu (Ishungu (2.34°S, 28.98°E) and Kibuye (2.05°S, 29.29°E)).

Table 1. Average of Wind Speed, CH₄ Saturation and FCH₄ in the Main Basin of Lake Kivu and Kabuno Bay During Four Cruises and Overall Average^a

	Wind Speed (m s ⁻¹)	CH ₄ Saturation (%)	FCH ₄ (μmol m ⁻² d ⁻¹)
<i>March 2007</i>			
Kabuno Bay	1.3 ± 0.4	7143	103 ± 7
Main basin	1.3 ± 0.4	1897 ± 494	26 ± 7
<i>September 2007</i>			
Kabuno Bay	1.2 ± 0.4	3736	53 ± 4
Main basin	1.2 ± 0.4	3552 ± 1642	50 ± 24
<i>June 2008</i>			
Kabuno Bay	1.6 ± 0.2	5593	85 ± 4
Main basin	1.6 ± 0.2	2722 ± 957	41 ± 15
<i>April 2009</i>			
Kabuno Bay	1.3 ± 0.2	12840	185 ± 8
Main basin	1.3 ± 0.2	1887 ± 772	26 ± 11
<i>Average</i>			
Kabuno Bay	1.4 ± 0.4	7328 ± 3930	106 ± 57
Main basin	1.4 ± 0.4	2514 ± 795	36 ± 12

^aAverage is plus or minus the standard deviation. Lake Kivu main basin at ~2322 km²; Kabuno Bay at ~48 km².

the atmosphere is a slow process and does not balance at short time scales the input of CH₄ by vertical mixing, the net effect of enhanced turbulence in Lake Kivu is an increase of CH₄ in the mixed layer.

[14] In Kabuno Bay, seasonal variations were opposed to those observed in the main lake with values lower during the dry season (September 2007, June 2008) than during the wet season (March 2007, April 2009). We cannot provide a straightforward explanation for the seasonal variations of CH₄ in surface waters of Kabuno Bay, that are probably related to variations of input terms (the upward flux of CH₄) and/or loss terms (performance and abundance of methanotrophic bacteria or emission of CH₄ to the atmosphere).

[15] Average wind speed values were significantly different among the four cruises (one-way ANOVA, $f_{3,81} = 5.93$, $p = 0.00104$), and average value in June 2008 was significantly higher than during the other cruises (post hoc Tukey's honestly significant difference test, $p < 0.05$). Yet, seasonal variations of wind speed were rather modest (coefficient of variation of 13%), hence, seasonal FCH₄ variations closely tracked those of CH₄ concentrations with FCH₄ values ranging between 26 and 50 μmol m⁻² d⁻¹ in the main basin, and between 53 and 185 μmol m⁻² d⁻¹ in Kabuno Bay (Table 1).

[16] Vertical mixing in surface of Lake Kivu follows a regular bimodal seasonal cycle according to the two main seasons (wet and dry). Mixed layer is shallowest in April (late wet season) and deepest in August–September (late dry season) [Sarmiento *et al.*, 2006]. Hence, our four cruises bracket reasonably well the seasonality of physical structure of surface waters in Lake Kivu. Since vertical mixing seems to be the main driver of CH₄ seasonal variations in surface waters of Lake Kivu (Figure 3), this allows evaluating robustly annual CH₄ emission rates. The annually integrated CH₄ emission to the atmosphere was 13 mmol m⁻² yr⁻¹ (30.5 10⁶ mol yr⁻¹) for the main basin of Lake Kivu and 39 mmol m⁻² yr⁻¹ (1.9 10⁶ mol yr⁻¹) for Kabuno Bay (Table 1).

The total emission of CH₄ to the atmosphere (32.4 10⁶ mol yr⁻¹) was extremely small compared to the total inventory of CH₄ predominantly in deeper layers of 2.7 10¹² mol (based on values reported by Schmid *et al.* [2005]). The emission of CH₄ to the atmosphere (14 mmol m⁻² yr⁻¹) was also very small compared to the upward flux of CH₄ of 2917 mmol m⁻² yr⁻¹ [Pasche *et al.*, 2011], consistent with a comparable CH₄ oxidation rate of 2628 mmol m⁻² yr⁻¹ [Jannasch, 1975].

[17] Air-soil CH₄ fluxes were scaled to the lake's catchment using the total catchment area of 5097 km² with a 72% coverage by cropland and pasture, and a 28% coverage by shrubland and evergreen forest [Muvundja *et al.*, 2009]. We used for the air-soil CH₄ fluxes a value of -1 μmol m⁻² d⁻¹ for cropland based on measurements in Burkina Faso [Brümmer *et al.*, 2009] and a value of -95 μmol m⁻² d⁻¹ for forests derived from the average from several sites (excluding flooded forests) across East, Central and West Africa [Delmas *et al.*, 1992; Tathy *et al.*, 1992; Macdonald *et al.*, 1998, 1999; Werner *et al.*, 2007]. Potential terrestrial sources of CH₄ related to biomass burning, termites and cattle could not be quantified due to lack of appropriate information. The sink of atmospheric CH₄ on the catchment of Lake Kivu can be evaluated on first approximation at -51 10⁶ mol yr⁻¹. Hence, the emission of CH₄ from the lake's surface to the atmosphere (32 10⁶ mol yr⁻¹) corresponds to 63% of the terrestrial sink of CH₄ on the lake's catchment area.

[18] When compared to other lakes globally as reported by Bastviken *et al.* [2004], the main basin of Lake Kivu ranks 47th and Kabuno Bay ranks 30th in terms of CH₄ concentration in surface waters (out of 49 lakes). Cross-system comparison of CH₄ in surface waters of lakes was carried out as function of lake surface area (Figure 5). Both Kabuno Bay and the main basin of Lake Kivu fall on the negative relationship between CH₄ and lake surface area. There is probably no unique explanation of the negative relationship between CH₄ concentrations and lake surface area, but rather a combination of several factors. In smaller

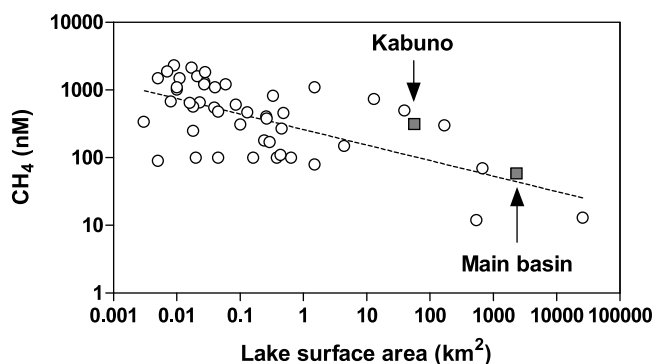


Figure 5. CH₄ concentration (nM) versus lake surface area (km²) in the main basin of Lake Kivu and Kabuno Bay and from the compilation by Bastviken *et al.* [2004]. Relationship between CH₄ concentration and lake surface area ($\log(\text{CH}_4) = 2.42 - 0.229 \log(\text{lake surface area})$; $r^2 = 0.40$; $p < 0.0001$; $n = 47$) was not originally reported by Bastviken *et al.* [2004] but is based on the same data set. Note the higher number of observations of CH₄ in lakes smaller than 10 km².

systems there is a higher supply of allochthonous inputs (from catchment and littoral zone) of nutrients and organic C relative to volume of lake (i.e., large ratio of catchment area to lake surface area). Hence, in smaller systems, higher levels of benthic degradation of organic C should occur in relation to higher availability of allochthonous organic carbon and of autochthonous organic carbon (the former sustained by higher allochthonous nutrient inputs) [Schindler, 1971; Rasmussen et al., 1989; Fee et al., 1992, 1994; Curtis and Schindler, 1997; Cole et al., 2006; Weidel et al., 2008]. This will promote a higher flux of CH₄ from sediments to the water column in smaller systems. As a first approximation, we can also assume that the smaller systems are shallower than larger ones. In shallow systems, there will be a lower removal of CH₄ by bacterial oxidation, due to a shorter distance between sediments and the air-water interface. Finally, in larger systems, there will be a lower fetch limitation of wind induced turbulence and *k* [Wanninkhof, 1992; Fee et al., 1996] leading to a higher loss of CH₄ by emission to the atmosphere (for an identical air-water gradient of CH₄). The lower fetch limitation of wind induced turbulence in larger systems will also promote deeper oxygenated mixed layers, promoting CH₄ loss by bacterial aerobic CH₄ oxidation.

4. Conclusions

[19] Surface waters of Lake Kivu were oversaturated with respect to CH₄ atmospheric equilibrium, with saturation levels ranging seasonally between 1887% and 3552% in the main basin, and between 3736% and 12840% in Kabuno Bay (Table 1). Yet, the CH₄ concentrations in surface waters of Lake Kivu are surprisingly low compared to lakes globally (Figure 5), considering the huge amounts of CH₄ contained in the deep layer of the lake, i.e., concentrations up to 10⁶ higher than in surface waters [Schmid et al., 2005]. This is related to highly stratified conditions of the lake that promote a very strong removal of CH₄ by bacterial oxidation [Jannasch, 1975] leading to low CH₄ concentrations in surface waters. Indeed, the average CH₄ oxidation rate (2628 mmol m⁻² yr⁻¹) reported by Jannasch [1975] in the main basin of Lake Kivu is 200 times higher than the average CH₄ emission to the atmosphere in the main basin (Table 1). The annually integrated CH₄ emissions to the atmosphere from the main basin of Lake Kivu (13 mmol m⁻² yr⁻¹; 30.5 10⁶ mol yr⁻¹) and Kabuno Bay (39 mmol m⁻² yr⁻¹; 1.9 10⁶ mol yr⁻¹, Table 1) are minimal estimates since we did not quantify plant mediated and ebullition CH₄ fluxes. Plant mediated CH₄ fluxes and shallow sediment CH₄ ebullition fluxes are expected to be marginal in Lake Kivu, since the littoral zone is very narrow owing to the steep shores [Degens et al., 1973]. Ebullition CH₄ fluxes remain to be determined in the deeper areas of the lake, however, since Lake Kivu is very deep, it can be expected that if CH₄ bubbles occur, they dissolve before reaching surface waters [e.g., McGinnis et al., 2006].

[20] **Acknowledgments.** We are grateful to Boniface Kaningini and Pascal Mwapu Isumbisho (Institut Supérieur Pédagogique, Bukavu, République Démocratique du Congo) and Laetitia Nyinawamwiza (National University of Rwanda, Butare, Rwanda) and their respective teams for logistic support during the cruises; to M.-V. Commarieu, C. Morana, G. Lepoint,

and M. K. Živadinović for help in field sampling; to D. Poirier for analytical assistance; and to the Editor (D. Baldocchi), the Associate Editor (P. Raymond), and one anonymous reviewer for constructive comments on a previous version of the manuscript. This work was funded by the Fonds National de la Recherche Scientifique (FNRS) under the CAKI (Cycle du carbone et des nutriments au Lac Kivu, contract 2.4.598.07) and MICKI (Microbial diversity and processes in Lake Kivu, contract 2.4.515.11) projects and contributes to the European Research Council starting grant project AFRIVAL (African river basins: Catchment-scale carbon fluxes and transformations, 240002) and to the Belgian Federal Science Policy Office EAGLES (East African Great Lake Ecosystem Sensitivity to changes, SD/AR/02A) project. A.V.B. and B.D. are research associates at the F.R.S-FNRS.

References

- Abril, G., and N. Iversen (2002), Methane dynamics in a shallow, non-tidal, estuary (Randers Fjord, Denmark), *Mar. Ecol. Prog. Ser.*, **230**, 171–181, doi:10.3354/meps230171.
- Bastviken, D., J. Cole, M. Pace, and L. Tranvik (2004), Methane emissions from lakes: Dependence of lake characteristics, two regional assessments, and a global estimate, *Global Biogeochem. Cycles*, **18**, GB4009, doi:10.1029/2004GB002238.
- Bastviken, D., L. J. Tranvik, J. A. Downing, P. M. Crill, and A. Enrich-Prast (2011), Freshwater methane emissions offset the continental carbon sink, *Science*, **331**, 50, doi:10.1126/science.1196808.
- Battin, T. J., L. A. Kaplan, S. Findlay, C. S. Hopkinson, E. Marti, A. I. Packman, J. D. Newbold, and F. Sabater (2008), Biophysical controls on organic carbon fluxes in fluvial networks, *Nat. Geosci.*, **1**, 95–100, doi:10.1038/ngeo101.
- Brümmer, C., H. Papen, R. Wassmann, and N. Brüggemann (2009), Fluxes of CH₄ and CO₂ from soil and termite mounds in south Sudanian savanna of Burkina Faso (West Africa), *Global Biogeochem. Cycles*, **23**, GB1001, doi:10.1029/2008GB003237.
- Chen, Y.-H., and R. G. Prinn (2006), Estimation of atmospheric methane emission between 1996–2001 using a 3-D global chemical transport model, *J. Geophys. Res.*, **111**, D10307, doi:10.1029/2005JD006058.
- Cole, J. J., and N. F. Caraco (1998), Atmospheric exchange of carbon dioxide in a low-wind oligotrophic lake measured by the addition of SF₆, *Limnol. Oceanogr.*, **43**, 647–656, doi:10.4319/lo.1998.43.4.0647.
- Cole, J. J., and N. F. Caraco (2001), Carbon in catchments: Connecting terrestrial carbon losses with aquatic metabolism, *Mar. Freshwater Res.*, **52**, 101–110, doi:10.1071/MF00084.
- Cole, J., S. Carpenter, M. Pace, M. Van de Bogert, J. Kitchell, and J. Hodgson (2006), Differential support of lake food webs by three types of terrestrial organic carbon, *Ecol. Lett.*, **9**, 558–568, doi:10.1111/j.1461-0248.2006.00898.x.
- Cole, J. J., et al. (2007), Plumbing the global carbon cycle: Integrating inland waters into the terrestrial carbon budget, *Ecosystems*, **10**, 172–185, doi:10.1007/s10021-006-9013-8.
- Curtis, P. J., and D. W. Schindler (1997), Hydrologic control of dissolved organic matter in low-order Precambrian Shield lakes, *Biogeochemistry*, **36**, 125–138, doi:10.1023/A:1005787913638.
- Degens, E. T., R. P. von Herzen, H.-K. Wong, W. G. Deuser, and H. W. Jannasch (1973), Lake Kivu: Structure, chemistry and biology of an East African rift lake, *Geol. Rundsch.*, **62**, 245–277, doi:10.1007/BF01826830.
- Delmas, R. A., J. Servant, J. P. Tathy, B. Cros, and M. Labat (1992), Sources and sinks of methane and carbon dioxide exchanges in mountain forest in Equatorial Africa, *J. Geophys. Res.*, **97**(D6), 6169–6179, doi:10.1029/90JD02575.
- Fee, E. J., J. A. Shearer, E. R. Debruyne, and E. U. Schindler (1992), Effects of lake size on phytoplankton photosynthesis, *Can. J. Fish. Aquat. Sci.*, **49**, 2445–2459, doi:10.1139/f92-270.
- Fee, E. J., R. E. Hecky, G. W. Regehr, L. L. Hendzel, and P. Wilkinson (1994), Effects of lake size on nutrient availability in the mixed layer during summer stratification, *Can. J. Fish. Aquat. Sci.*, **51**, 2756–2768, doi:10.1139/f94-276.
- Fee, E. J., R. E. Hecky, S. E. M. Kasian, and D. R. Cruikshank (1996), Effects of lake size, water clarity, and climatic variability on mixing depths in Canadian Shield lakes, *Limnol. Oceanogr.*, **41**, 912–920, doi:10.4319/lo.1996.41.5.0912.
- Jannasch, H. W. (1975), Methane oxidation in Lake Kivu (central Africa), *Limnol. Oceanogr.*, **20**, 860–864, doi:10.4319/lo.1975.20.5.0860.
- Macdonald, J. A., P. Eggleton, D. E. Bignell, F. Forzi, and D. Fowler (1998), Methane emission by termites and oxidation by soils, across a forest disturbance gradient in the Mbalmayo Forest Reserve, Cameroon, *Global Change Biol.*, **4**, 409–418, doi:10.1046/j.1365-2486.1998.00163.x.
- Macdonald, J. A., D. Jeeva, P. Eggleton, R. Davies, D. E. Bignell, D. Fowler, J. Lawton, and M. Maryati (1999), The effect of termite biomass and

- anthropogenic disturbance on the CH₄ budgets of tropical forests in Cameroon and Borneo, *Global Change Biol.*, *5*, 869–879, doi:10.1046/j.1365-2486.1999.00279.x.
- McGinnis, D. F., J. Greinert, Y. Artemov, S. E. Beaubien, and A. Wüest (2006), Fate of rising methane bubbles in stratified waters: How much methane reaches the atmosphere?, *J. Geophys. Res.*, *111*, C09007, doi:10.1029/2005JC003183.
- Muvundja, F., N. Pasche, F. W. B. Bugenyi, M. Isumbusho, B. Müller, J. N. Namugize, P. Rinta, M. Schmid, R. Stierli, and A. Wüest (2009), Balancing nutrient inputs to Lake Kivu, *J. Great Lakes Res.*, *35*(3), 406–418, doi:10.1016/j.jglr.2009.06.002.
- Nayar, A. (2009), A lakeful of trouble, *Nature*, *460*, 321–323, doi:10.1038/460321a.
- Pasche, N., M. Schmid, F. Vazquez, C. Schubert, A. Wüest, J. D. Kessler, M. A. Pack, W. S. Reebergh, and H. Bürgmann (2011), Methane sources and sinks in Lake Kivu, *J. Geophys. Res.*, *116*, G03006, doi:10.1029/2011JG001690.
- Rasmussen, J. B., L. Godbout, and M. Schallenberg (1989), The humic content of lake water and its relationship to watershed and lake morphology, *Limnol. Oceanogr.*, *34*, 1336–1343, doi:10.4319/lo.1989.34.7.1336.
- Sarmiento, H., M. Isumbusho, and J.-P. Descy (2006), Phytoplankton ecology of Lake Kivu (Eastern Africa), *J. Plankton Res.*, *28*, 815–829, doi:10.1093/plankt/fbl017.
- Schindler, D. W. (1971), A hypothesis to explain differences and similarities among lakes in the Experimental Lakes Area, northwestern Ontario, *J. Fish. Res. Board Can.*, *28*, 295–301, doi:10.1139/f71-039.
- Schmid, M., M. Halbwachs, B. Wehrli, and A. Wüest (2005), Weak mixing in Lake Kivu: New insights indicate increasing risk of uncontrolled gas eruption, *Geochem. Geophys. Geosyst.*, *6*, Q07009, doi:10.1029/2004GC000892.
- Schoell, M., K. Tietze, and S. M. Schoberth (1988), Origin of methane in Lake Kivu (East-Central Africa), *Chem. Geol.*, *71*, 257–265, doi:10.1016/0009-2541(88)90119-2.
- Tathy, J. P., B. Cros, R. A. Delmas, A. Marengo, J. Servant, and M. Labat (1992), Methane emission from flooded forest in Central Africa, *J. Geophys. Res.*, *97*(D6), 6159–6168, doi:10.1029/90JD02555.
- Tietze, K., M. Geyh, H. Müller, L. Schröder, W. Stahl, and H. Wehner (1980), The genesis of the methane in Lake Kivu (Central Africa), *Geol. Rundsch.*, *69*, 452–472, doi:10.1007/BF02104549.
- Tranvik, L. J., et al. (2009), Lakes and reservoirs as regulators of carbon cycling and climate, *Limnol. Oceanogr.*, *54*, 2298–2314, doi:10.4319/lo.2009.54.6_part_2.2298.
- Wanninkhof, R. (1992), Relationship between wind speed and gas exchange over the ocean, *J. Geophys. Res.*, *97*, 7373–7382, doi:10.1029/92JC00188.
- Weidel, B., S. Carpenter, J. Cole, J. Hodgson, J. Kitchell, M. Pace, and C. Solomon (2008), Carbon sources supporting fish growth in a north temperate lake, *Aquat. Sci.*, *70*, 446–458, doi:10.1007/s00027-008-8113-2.
- Werner, C., R. Kiese, and K. Butterbach-Bahl (2007), Soil-atmosphere exchange of N₂O, CH₄, and CO₂ and controlling environmental factors for tropical rain forest sites in western Kenya, *J. Geophys. Res.*, *112*, D03308, doi:10.1029/2006JD007388.
- Yamamoto, S., J. B. Alcauskas, and T. E. Crozier (1976), Solubility of methane in distilled water and seawater, *J. Chem. Eng. Data*, *21*, 78–80, doi:10.1021/je60068a029.
- G. Abril, Laboratoire Environnements et Paléoenvironnements Océaniques, UMR CNRS 5805, Université de Bordeaux 1, Avenue des Facultés, F-33405 Talence, France.
- A. V. Borges, F. Darchambeau, and B. Delille, Unité d'Océanographie Chimique, Université de Liège, Bât B5, Liège B-4000, Belgium. (alberto.borges@ulg.ac.be)
- J.-P. Descy, Laboratoire d'Écologie des Eaux Douces, URBE, University of Namur, Rue des Bruxelles 61, Namur B-5000, Belgium.



Carbon Cycling of Lake Kivu (East Africa): Net Autotrophy in the Epilimnion and Emission of CO₂ to the Atmosphere Sustained by Geogenic Inputs

Alberto V. Borges^{1*}, Cédric Morana², Steven Bouillon², Pierre Servais³, Jean-Pierre Descy⁴, François Darchambeau¹

1 Chemical Oceanography Unit, Université de Liège, Liège, Belgium, **2** Department of Earth and Environmental Sciences, KU Leuven, Leuven, Belgium, **3** Ecologie des Systèmes Aquatiques, Université Libre de Bruxelles, Bruxelles, Belgium, **4** Research Unit in Environmental and Evolutionary Biology, University of Namur, Namur, Belgium

Abstract

We report organic and inorganic carbon distributions and fluxes in a large (>2000 km²) oligotrophic, tropical lake (Lake Kivu, East Africa), acquired during four field surveys, that captured the seasonal variations (March 2007–mid rainy season, September 2007–late dry season, June 2008–early dry season, and April 2009–late rainy season). The partial pressure of CO₂ (pCO₂) in surface waters of the main basin of Lake Kivu showed modest spatial (coefficient of variation between 3% and 6%), and seasonal variations with an amplitude of 163 ppm (between 579±23 ppm on average in March 2007 and 742±28 ppm on average in September 2007). The most prominent spatial feature of the pCO₂ distribution was the very high pCO₂ values in Kabuno Bay (a small sub-basin with little connection to the main lake) ranging between 11213 ppm and 14213 ppm (between 18 and 26 times higher than in the main basin). Surface waters of the main basin of Lake Kivu were a net source of CO₂ to the atmosphere at an average rate of 10.8 mmol m⁻² d⁻¹, which is lower than the global average reported for freshwater, saline, and volcanic lakes. In Kabuno Bay, the CO₂ emission to the atmosphere was on average 500.7 mmol m⁻² d⁻¹ (~46 times higher than in the main basin). Based on whole-lake mass balance of dissolved inorganic carbon (DIC) bulk concentrations and of its stable carbon isotope composition, we show that the epilimnion of Lake Kivu was net autotrophic. This is due to the modest river inputs of organic carbon owing to the small ratio of catchment area to lake surface area (2.15). The carbon budget implies that the CO₂ emission to the atmosphere must be sustained by DIC inputs of geogenic origin from deep geothermal springs.

Citation: Borges AV, Morana C, Bouillon S, Servais P, Descy J-P, et al. (2014) Carbon Cycling of Lake Kivu (East Africa): Net Autotrophy in the Epilimnion and Emission of CO₂ to the Atmosphere Sustained by Geogenic Inputs. PLoS ONE 9(10): e109500. doi:10.1371/journal.pone.0109500

Editor: Moncho Gomez-Gesteira, University of Vigo, Spain

Received: April 1, 2014; **Accepted:** September 11, 2014; **Published:** October 14, 2014

Copyright: © 2014 Borges et al. This is an open-access article distributed under the terms of the Creative Commons Attribution License, which permits unrestricted use, distribution, and reproduction in any medium, provided the original author and source are credited.

Data Availability: The authors confirm that all data underlying the findings are fully available without restriction. All relevant data are within the paper and its Supporting Information files.

Funding: This work was funded by the Fonds National de la Recherche Scientifique (FNRS) under the CAKI (Cycle du carbone et des nutriments au Lac Kivu, 2.4.598.07) and the MICKI (Microbial diversity and processes in Lake Kivu, 1715859) projects, and contributes to the European Research Council Starting Grant AFRIVAL (African river basins: catchment-scale carbon fluxes and transformations, 240002) and to the Belgian Federal Science Policy Office EAGLES (East African Great Lake Ecosystem Sensitivity to changes, SD/AR/02A) projects. The funders had no role in study design, data collection and analysis, decision to publish, or preparation of the manuscript.

Competing Interests: AVB is a senior research associate at the FRS-FNRS. There are no patents, products in development or marketed products to declare. This does not alter the authors' adherence to all PLOS ONE policies on sharing data and materials.

* Email: alberto.borges@ulg.ac.be

Introduction

Freshwater ecosystems are frequently considered to be net heterotrophic, whereby the consumption of organic carbon (C) is higher than the autochthonous production of organic C, and excess organic C consumption is maintained by inputs of allochthonous organic C [1]. Net heterotrophy in freshwater ecosystems promotes the emission of carbon dioxide (CO₂) to the atmosphere [2], [3], [4], [5], [6], [7], [9], [10], with the global emission from continental waters estimated at ~0.75 PgC yr⁻¹ [4] (0.11 PgC yr⁻¹ from lakes, 0.28 PgC yr⁻¹ from reservoirs, 0.23 PgC yr⁻¹ from rivers, 0.12 PgC yr⁻¹ from estuaries, and 0.01 PgC yr⁻¹ from ground waters). More recent studies provided even higher CO₂ emission estimates. Tranvik et al. [7] revised the CO₂ emission from lakes to 0.53 PgC yr⁻¹, while Battin et al. [6] estimated CO₂ emission from streams at 0.32 PgC yr⁻¹.

Aufdenkampe et al. [8] estimated a total CO₂ emission of 0.64 PgC yr⁻¹ for lakes and reservoirs, a total of 0.56 PgC yr⁻¹ for rivers and streams, and a massive 2.08 PgC yr⁻¹ for wetlands. Raymond et al. [10] estimated an emission of 1.8 PgC yr⁻¹ for streams and rivers and 0.32 PgC yr⁻¹ for lakes and reservoirs. Such emissions of CO₂ from continental waters exceed the net sink of C by terrestrial vegetation and soils of ~1.3 PgC yr⁻¹ [4] as well as the sink of CO₂ in open oceans of ~1.4 PgC yr⁻¹ [11].

However, our present understanding of the role of lakes on CO₂ emissions could be biased because most observations were obtained in temperate and boreal (humic) systems, and mostly in medium to small sized lakes, during open-water (ice-free) periods. Much less observations are available from hard-water, saline, large, or tropical lakes. Tropical freshwater environments are indeed under-sampled compared to temperate and boreal systems in terms of C dynamics in general, and specifically in terms of CO₂

dynamics. In an extensive compilation of CO₂ concentration data from 4902 lakes globally [12], there were only 148 data entries for tropical systems (~3%). Yet, about 50% of freshwater and an equivalent fraction of organic C is delivered by rivers to the oceans at tropical latitudes [13]. Tropical lakes represent about 16% of the total surface of lakes [14], and Lakes Victoria, Tanganyika, and Malawi belong to the seven largest lakes by area in the world. Current estimates assume that areal CO₂ fluxes are substantially higher in tropical systems than in temperate or boreal regions (often ascribed to higher temperatures) [8]. Thus, according to the zonal distribution given by Aufdenkampe et al. [8], tropical inland waters account for ~60% of the global emission of CO₂ from inland waters (0.45 PgC yr⁻¹ for lakes and reservoirs, 0.39 PgC yr⁻¹ for rivers and streams, and 1.12 PgC yr⁻¹ for wetlands). It is clear that additional data are required to verify and re-evaluate more accurately the CO₂ fluxes from tropical systems.

Pelagic particulate primary production (PP) of East African great lakes, as reviewed by Darchambeau et al. [15], ranges from ~30 mmol m⁻² d⁻¹ for the most oligotrophic conditions (north basin of Lake Tanganyika) to ~525 mmol m⁻² d⁻¹ for the most eutrophic conditions (Lake Victoria). The comparatively fewer data on bacterial production (BP), available only for Lake Tanganyika, suggest that PP and BP are seasonally closely coupled [16]. However, with an average pelagic BP of ~25 mmol m⁻² d⁻¹ [16], the bacterial C demand would exceed the production of particulate organic C (POC) by phytoplankton in Lake Tanganyika. This has led to speculate about additional C supply to bacterioplankton, for instance, from dissolved organic C (DOC) exudation by phytoplankton [16].

Lake Kivu (2.50°S 1.59°S 29.37°E 28.83°E) is one of the East African great lakes (2370 km² surface area, 550 km³ volume). It is a deep (maximum depth of 485 m) meromictic lake, with an oxic mixolimnion down to 70 m maximum, and a deep monolimnion rich in dissolved gases and nutrients [17], [18], [19]. Deep layers receive heat, salts, and CO₂ from deep geothermal springs [19]. Seasonality of the physical and chemical vertical structure and biological activity in surface waters of Lake Kivu is driven by the oscillation between the dry season (June-September) and the rainy season (October-May), the former characterized by a deepening of the mixolimnion [20]. This seasonal mixing favours the input of dissolved nutrients and the development of diatoms, while, during the rest of the year, the phytoplankton assemblage is dominated by cyanobacteria, chrysophytes and cryptophytes [15], [21], [22]. Surface waters of Lake Kivu are oligotrophic, and, consequently, PP is at the lower end of the range for East African great lakes (on average ~50 mmol m⁻² d⁻¹) [15].

Extremely high amounts of CO₂ and methane (CH₄) (300 km³ and 60 km³, respectively, at 0°C and 1 atm) [19] are dissolved in the deep layers of Lake Kivu. This is due to a steep density gradient at 260 m depth that leads to residence times in the order of 1000 yr in the deepest part of the lake [19], [23]. Stable isotope and radiocarbon data suggest that the CO₂ is mainly geogenic [24]. While the risk of a limnic eruption is minimal [25], large scale industrial extraction of CH₄ from the deep layers of Lake Kivu is planned [26], [27] which could affect the ecology and biogeochemical cycling of C of the lake and change for instance the emission of greenhouse gases such as CH₄ and CO₂. The net emission of CH₄ to the atmosphere from Lake Kivu was quantified by Borges et al. [28], and was surprisingly low - among the lowest ever reported in lakes globally - considering the large amounts of CH₄ stored in deep waters. Here, we report a data-set obtained during four surveys covering the seasonality of CO₂ dynamics and fluxes, in conjunction with mass balances of C, and process rate measurements (PP and BP) in the epilimnion of Lake Kivu, with

the aim of quantifying the exchange of CO₂ with the atmosphere and determining the underlying drivers, in particular, the net metabolic status.

Materials and Methods

Official permission was not required for sampling in locations where measurements were made and samples acquired. The field studies did not involve endangered or protected species. The full data-set is available in Table S1.

2.1 Field sampling and chemical analysis

In order to capture the seasonal variations of the studied quantities, four cruises were carried out in Lake Kivu on 15/03-29/03/2007 (mid rainy season), 28/08-10/09/2007 (late dry season), 21/06-03/07/2008 (early dry season), 21/04-05/05/2009 (late rainy season), and 19/10/10-27/10/10 (early rainy season) for a selection of variables. Sampling was carried out at 15 stations distributed over the whole lake and in Kabuno Bay, and at 12 rivers draining into Lake Kivu and representing the outflow of the lake (Ruzizi River, Fig. 1). The core of data presented hereafter was obtained in 2007–2009, while from the 2010 cruise only vertical DOC and POC data obtained at two stations are presented.

Vertical profiles of temperature, conductivity and oxygen were obtained with a Yellow Springs Instrument (YSI) 6600 V2 probe. Calibration of sensors was carried out prior to the cruises and regularly checked during the cruises. The conductivity cell was

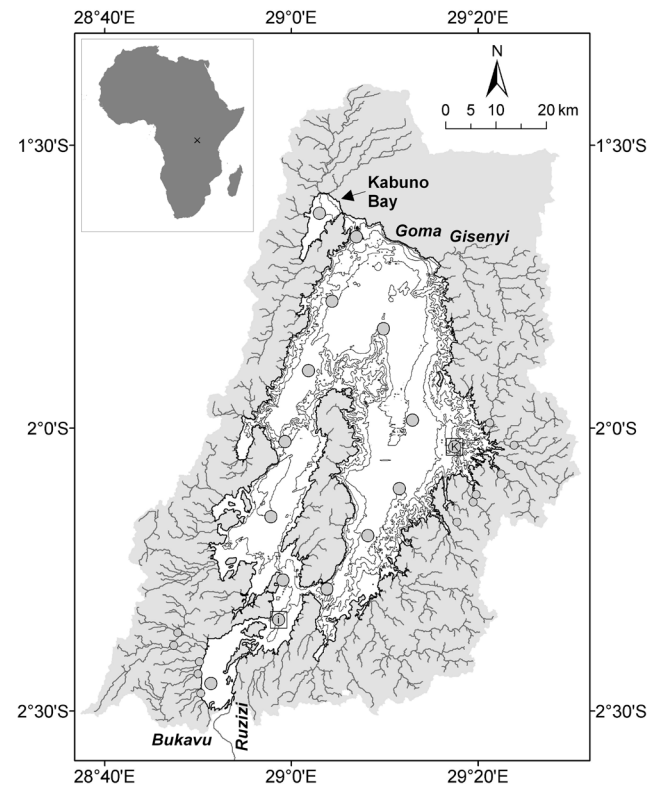


Figure 1. Map of Lake Kivu, showing bathymetry (isobaths at 100 m intervals), catchment area (shaded in grey), rivers, and sampling stations (small circles indicate the rivers). Primary production and bacterial production measurements were made at the stations identified with a square (I = Ishungu; K = Kibuye), adapted from [29].

doi:10.1371/journal.pone.0109500.g001

calibrated with a 1000 $\mu\text{S cm}^{-1}$ (25°C) YSI standard. The oxygen membrane probe was calibrated with humidity saturated ambient air. Salinity was computed from specific conductivity according to Schmid and Wüest [29].

Sampling for the partial pressure of CO_2 ($p\text{CO}_2$) was carried out at 1 m depth. Measurements of $p\text{CO}_2$ were carried out with a non-dispersive infra-red (NDIR) analyzer coupled to an equilibrator [30] through which water was pumped with a peristaltic pump (Masterflex E/S portable sampler). In-situ temperature and temperature at the outlet of the equilibrator were determined with Li-Cor 1000-15 probes. The NDIR analyzer (Li-Cor, Li-820) was calibrated with five gas standards: pure N_2 and four $\text{CO}_2:\text{N}_2$ mixtures with a CO_2 molar fraction of 363, 819, 3997 and 8170 ppm (Air Liquide Belgium).

For the determination of pH, CH_4 concentrations, $\delta^{13}\text{C}$ of dissolved inorganic C (DIC) ($\delta^{13}\text{C}\text{-DIC}$), and total alkalinity (TA), water was sampled with a 5 L Niskin bottle (Hydro-Bios). Samples were collected every 10 m from 10 to 60–80 m depending on the cruise and station, except for CH_4 which was only sampled at 10 m. Additional samples for pH, $\delta^{13}\text{C}_{\text{DIC}}$ and TA were collected at 5 m in Kabuno Bay. Water for CH_4 analysis was collected in 50 ml glass serum bottles from the Niskin bottle with tubing, left to overflow, poisoned with 100 μl of a saturated HgCl_2 solution, and sealed with butyl stoppers and aluminium caps. Water samples for the analysis of $\delta^{13}\text{C}_{\text{DIC}}$ were taken from the same Niskin bottle by gently overfilling 12 ml glass Exetainer vials, poisoned with 20 μl of a saturated HgCl_2 solution, and gas-tight capped. A water volume of 50 ml was filtered through a 0.2 μm pore size polyethersulfone (PES) syringe filters and was stored at ambient temperature in polyethylene bottles for the determination of TA. POC and DOC samples were obtained from surface waters in June 2008 and April 2009, and along a depth profile in October 2010. DOC was filtered on 0.2 μm PES syringe filters, stored at ambient temperature in 40 mL glass vials with polytetrafluoroethylene coated septa, and poisoned with 50 μL of H_3PO_4 (85%). POC was filtered on 0.7 μm pore 25 mm diameter Whatman GF/F glass fiber filters (pre-combusted 5 h at 500°C), stored dry. Sampling of river surface waters followed the same procedures outlined above (sampling depth ~ 20 cm) with the addition of water sampling for total suspended matter (TSM). Samples for TSM were obtained by filtering 50–200 mL of water on pre-combusted pre-weighted 47 mm diameter GF/F glass fiber filters, stored dry.

Measurements of pH in water sampled from the Niskin bottle were carried out with a Metrohm (6.0253.100) combined electrode calibrated with US National Bureau of Standards (NBS) buffers of pH 4.002 (25°C) and pH 6.881 (25°C) prepared according to Frankignoulle and Borges [31]. Measurements of TA were carried out by open-cell titration with HCl 0.1 M according to Gran [32] on 50 ml water samples, and data were quality checked with Certified Reference Material acquired from Andrew Dickson (Scripps Institution of Oceanography, University of California, San Diego). DIC was computed from pH and TA measurements using the carbonic acid dissociation constants of Millero et al. [33]. For the analysis of $\delta^{13}\text{C}\text{-DIC}$, a He headspace was created in 12 ml glass vials, and ~ 300 μl of H_3PO_4 (99%) was added to convert all DIC species to CO_2 . After overnight equilibration, part of the headspace was injected into the He stream of an elemental analyser – isotope ratio mass spectrometer (EA-IRMS) (ThermoFinnigan Flash1112 and ThermoFinnigan Delta+XL, or Thermo FlashEA/HT coupled to Thermo Delta V) for $\delta^{13}\text{C}$ measurements. The obtained $\delta^{13}\text{C}$ data were corrected for the isotopic equilibration between gaseous and dissolved CO_2 using an algorithm similar to that presented by Miyajima et al. [34], and

calibrated with LSVEC and NBS-19 certified standards or internal standards calibrated with the former. Concentrations of CH_4 were determined by gas chromatography with flame ionization detection, as described by Borges et al. [28]. DOC and $\delta^{13}\text{C}\text{-DOC}$ were measured with a customized Thermo HiperTOC coupled to a Delta+XL IRMS. POC and $\delta^{13}\text{C}\text{-POC}$ from filters were determined on a Thermo EA-IRMS (various configurations, either Flash1112, FlashHT with Delta+XL or DeltaV Advantage). Quantification and calibration of $\delta^{13}\text{C}$ data was performed with IAEA-C6 and acetanilide which was internally calibrated versus international standards.

PP and BP were measured at 2 stations: Kibuye (2.05°S 29.29°E) and Ishungu (2.34°S 28.98°E) (Fig. 1). PP was measured using the ^{14}C method [35] as described by Darchambeau et al. [15] in a pooled sample prepared from discrete samples (2 L) spaced every 5 m in the mixed layer. The mixed layer depth (MLD) was determined from vertical profiles of temperature and oxygen. The ^{14}C incubations were assumed to provide an estimate of net PP of the particulate phase (PNPP). Chlorophyll a (Chl-*a*) of the pooled sample was measured according to Descy et al. [36] by high-performance liquid chromatography analysis of extracts in 90% acetone from samples filtered on Macherey-Nägel GF5 (0.7 μm nominal pore size) filters (3–4 L). BP was estimated every 5 m in the mixed layer from tritiated thymidine ($^3\text{H}\text{-Thy}$) incorporation rates [37]. Samples (20 mL) were incubated in duplicate for 2 h in the dark at in-situ temperature in the presence of $^3\text{H}\text{-Thy}$ (~ 80 Ci mmol) at saturating concentration (~ 50 nmol L^{-1}). After incubation, cold trichloroacetic acid (TCA) was added (final concentration 5%) and the samples were kept cold until filtration through a 0.2 μm pore-size cellulose nitrate membrane. Filters were preserved in the dark at -20°C . The radioactivity associated with the filters was estimated by liquid scintillation using a Beckman counter LS 6000. Cell production was calculated from the $^3\text{H}\text{-Thy}$ incorporation rate using a conversion factor of 1.2×10^{18} cells produced per mole of $^3\text{H}\text{-Thy}$ incorporated into cold TCA insoluble material. This conversion factor was determined experimentally in batch experiments in which the increase of bacterial abundance and $^3\text{H}\text{-Thy}$ incorporation were followed simultaneously (data not shown) and was similar to the one used by Stenuite et al. [16] to calculate BP in Lake Tanganyika. Cellular production was multiplied by the average bacterial C content per cell (15 fgC cell $^{-1}$) [16] to obtain BP data. Daily BP was estimated from the experimental values considering constant activity over 24 h, and expressed per unit area (mmol $\text{m}^{-2} \text{d}^{-1}$), by integrating over the euphotic zone. Bacterial respiration (BR) rates were computed from BP using a bacterial growth efficiency computed from BP according to the model of Del Giorgio and Cole [38].

2.2 Bulk DIC mass balance model

TA and DIC mass balance models were constructed in order to determine the major processes controlling CO_2 dynamics in surface waters, and to evaluate the net metabolic balance of the epilimnion (net autotrophy or net heterotrophy).

The TA mass balance was constructed assuming a steady-state, according to:

$$F_{TA_river} + F_{TA_70m_10m} + F_{TA_upwelling} = F_{TA_Ruzizi} + F_{TA*} \quad (1)$$

where F_{TA_river} is the input of TA from rivers, F_{TA_Ruzizi} is the output of TA by the Ruzizi river, $F_{TA_70m_10m}$ is the flux of TA from the monimolimnion to the mixolimnion by eddy diffusion, $F_{TA_upwelling}$ is the flux of TA from the monimolimnion to the mixolimnion by upwelling, and F_{TA*} is the closing term.

F_{TA_river} was computed from discharge-weighted average TA in the 12 sampled rivers draining into Lake Kivu (TA_{river}), and total freshwater discharge from rivers (Q_{river}), according to:

$$F_{TA_river} = TA_{river} Q_{river} \quad (2)$$

F_{TA_Ruzizi} was computed from TA measured in the Ruzizi River (TA_{Ruzizi}), and the flow of the Ruzizi River (Q_{Ruzizi}), according to:

$$F_{TA_Ruzizi} = TA_{Ruzizi} Q_{Ruzizi} \quad (3)$$

$F_{TA_70m_10m}$ was computed from the gradient of TA across the pycnocline ($\delta_{TA_70m_10m}/\delta z$, where δz represents the depth interval) and the eddy diffusion coefficient (E) according to:

$$F_{TA_70m_10m} = -E \frac{\delta_{TA_70m_10m}}{\delta z} \quad (4)$$

$F_{TA_upwelling}$ was computed from the TA at 70 m (TA_{70m}) and the upwelling flow ($Q_{upwelling}$), according to:

$$F_{TA_upwelling} = TA_{70m} Q_{upwelling} \quad (5)$$

A DIC mass balance was constructed assuming a steady-state, according to:

$$F_{DIC_river} + F_{DIC_70m_10m} + F_{DIC_upwelling} = F_{DIC_Ruzizi} + F_{CO_2} + F_{CaCO_3} + F_{POC} \quad (6)$$

where F_{DIC_river} is the input of DIC from rivers, F_{DIC_Ruzizi} is the output of DIC by the Ruzizi river, $F_{DIC_70m_10m}$ is the flux of DIC from the monimolimnion to the mixolimnion by eddy diffusion, $F_{DIC_upwelling}$ is the flux of DIC from the monimolimnion to the mixolimnion by upwelling, F_{CO_2} is the exchange of CO_2 with the atmosphere, F_{CaCO_3} is the precipitation and subsequent export to depth of $CaCO_3$, and F_{POC} is the closing term and represents the export of POC from surface to depth.

F_{DIC_river} was computed from discharge-weighted average DIC in the 12 sampled rivers draining into Lake Kivu (DIC_{river}), and Q_{river} , according to:

$$F_{DIC_river} = DIC_{river} Q_{river} \quad (7)$$

F_{DIC_Ruzizi} was computed from DIC measured in the Ruzizi River (DIC_{Ruzizi}), and Q_{Ruzizi} , according to:

$$F_{DIC_Ruzizi} = DIC_{Ruzizi} Q_{Ruzizi} \quad (8)$$

$F_{DIC_70m_10m}$ was computed from the gradient of DIC across the metalimnion ($\delta_{DIC_70m_10m}/\delta z$) and E according to:

$$F_{DIC_70m_10m} = -E \frac{\delta_{DIC_70m_10m}}{\delta z} \quad (9)$$

$F_{DIC_upwelling}$ was computed from the DIC at 70 m (DIC_{70m}) and $Q_{upwelling}$, according to:

$$F_{DIC_upwelling} = DIC_{70m} Q_{upwelling} \quad (10)$$

F_{CO_2} was computed according to:

$$F_{CO_2} = k \alpha \Delta p CO_2 \quad (11)$$

where k is the gas transfer velocity, α is the CO_2 solubility coefficient, and $\Delta p CO_2$ is the air-water gradient of pCO_2 computed from water pCO_2 (1 m depth) and an atmospheric pCO_2 value ranging from ~ 372 ppm to ~ 376 ppm (depending on the cruise), corresponding to the monthly average at Mount Kenya (Kenya, 0.05°S 37.30°E) obtained from GLOBALVIEW-CO2 (Carbon Cycle Greenhouse Gases Group of the National Oceanic and Atmospheric Administration, Earth System Research Laboratory), and converted into wet air using the water vapour algorithm of Weiss and Price [39].

α was computed from temperature and salinity using the algorithm of Weiss [40], k was computed from wind speed using the parameterization of Cole and Caraco [41] and the Schmidt number of CO_2 in fresh water according to the algorithm given by Wanninkhof [42]. Wind speed data were acquired with a Davis Instruments meteorological station in Bukavu (2.51°S 28.86°E). The wind speed data were adjusted to be representative of wind conditions over the lake by adding 2 m s^{-1} according to Thiery et al. [20]. F_{CO_2} was computed with daily wind speed averages for a time period of one month centred on the date of the middle of each field cruise. Such an approach allows to account for the day-to-day variability of wind speed, and to provide F_{CO_2} values that are seasonally representative.

F_{CaCO_3} was computed according to:

$$F_{CaCO_3} = \frac{F_{TA*}}{2} \quad (12)$$

The average value of Q_{river} ($76.1 \text{ m}^3 \text{ s}^{-1}$) was given by Muvundja et al. [43], the average Q_{Ruzizi} for 2007–2009 ($87.8 \text{ m}^3 \text{ s}^{-1}$) measured at Ruzizi I Hydropower Plant was provided by the Société Nationale d'Electricité. A value of $Q_{upwelling}$ of $42 \text{ m}^3 \text{ s}^{-1}$ and a value of E of $0.06 \text{ cm}^2 \text{ s}^{-1}$ were given by Schmid et al. [19].

2.3 $\delta^{13}C$ -DIC mass balance model

The combination of the DIC and $\delta^{13}C$ -DIC budget for the mixed layer allows to estimate independently the total DIC vertical input by upwelling and by eddy diffusion (F_{DIC_upward}) and F_{POC} [44]. At steady-state, DIC and $\delta^{13}C$ -DIC mass balances are given by the following equations:

$$F_{DIC_river} + F_{upward} = F_{DIC_Ruzizi} + F_{CO_2} + F_{CaCO_3} + F_{POC} \quad (13)$$

$$\begin{aligned} & F_{DIC_river} (^{13}C/^{12}C)_{DIC_river} + F_{DIC_Ruzizi} (^{13}C/^{12}C)_{DIC_Lake} \\ & + F_{DIC_upward} (^{13}C/^{12}C)_{DIC_upward} \\ & + F_{CO_2} (^{13}C/^{12}C)_{CO_2} + F_{CaCO_3} (^{13}C/^{12}C)_{CaCO_3} \\ & + F_{POC} (^{13}C/^{12}C)_{POC} = 0 \end{aligned} \quad (14)$$

$$F_{upward} = F_{DIC_{70m-10m}} + F_{DIC_{upwelling}} \quad (15)$$

The $(^{13}\text{C}/^{12}\text{C})$ in the equation (14) represents the ^{13}C to ^{12}C ratio of net C fluxes, and can be expressed using the classical $\delta^{13}\text{C}$ notation [45]. 10 out of the 12 different terms in equations (13) and (14) were measured or can be computed from measured variables, and then the two equations can be solved in order to estimate the $F_{DIC_{upward}}$ and F_{POC} fluxes. $F_{DIC_{river}}$, $F_{DIC_{Ruzizi}}$, F_{CaCO_3} and F_{CO_2} were calculated as described above. $(^{13}\text{C}/^{12}\text{C})_{DIC_{river}}$, $(^{13}\text{C}/^{12}\text{C})_{DIC_{lake}}$ and $(^{13}\text{C}/^{12}\text{C})_{POC}$ were measured during the 4 field surveys. $(^{13}\text{C}/^{12}\text{C})_{CaCO_3}$ was computed from the measured $\delta^{13}\text{C}_{DIC}$ in surface and the fractionation factor $\epsilon_{CaCO_3-HCO_3}$ of 0.88 ‰ [46].

The $(^{13}\text{C}/^{12}\text{C})_{DIC_{upward}}$ which represents the $\delta^{13}\text{C}$ signature of the net upward DIC input, was estimated from the $\delta^{13}\text{C}$ -DIC vertical gradient as follows:

$$(^{13}\text{C}/^{12}\text{C})_{DIC_{upward}} = \frac{DIC_z(^{13}\text{C}/^{12}\text{C})_{DIC_{z+1}} - DIC_{z+1}(^{13}\text{C}/^{12}\text{C})_{DIC_z}}{DIC_{z+1} - DIC_z} \quad (16)$$

where z is the depth, DIC_z and DIC_{z+1} are the DIC concentration at the depth z and $z+1$, $(^{13}\text{C}/^{12}\text{C})_{DIC_z}$ and $(^{13}\text{C}/^{12}\text{C})_{DIC_{z+1}}$ are the $\delta^{13}\text{C}$ signature of DIC at the depth z and $z+1$.

The $\delta^{13}\text{C}$ signature of the net flux of CO_2 at the air-water interface was calculated from the $\delta^{13}\text{C}$ signature of the different DIC species in surface water and the atmospheric CO_2 (-8.0‰) according to:

$$(^{13}\text{C}/^{12}\text{C})_{CO_2} = \alpha_{am}\alpha_{sol} \frac{pCO_{2w}(^{13}\text{C}/^{12}\text{C})_{DIC_{lake}}\alpha_{DIC-g}}{pCO_{2atm} - pCO_{2w}} - pCO_{2atm}(^{13}\text{C}/^{12}\text{C})_{CO_{2atm}} \quad (17)$$

where $(^{13}\text{C}/^{12}\text{C})_{CO_{2atm}}$ and $(^{13}\text{C}/^{12}\text{C})_{DIC_{lake}}$ are the $\delta^{13}\text{C}$ signature of atmospheric CO_2 and lake surface DIC, respectively, α_{am} and α_{sol} are respectively the kinetic fractionation effect during CO_2 gas transfer, and the equilibrium fractionation during CO_2 dissolution measured by Zhang et al. [47] in distilled water. α_{DIC-g} is the equilibrium fractionation factor between aqueous DIC and gaseous CO_2 and is defined by:

$$\alpha_{DIC-g} = \frac{(^{13}\text{C}/^{12}\text{C})_{CO_{2atm}} - (^{13}\text{C}/^{12}\text{C})_{diseq}}{(^{13}\text{C}/^{12}\text{C})_{DIC_{lake}}} \quad (18)$$

where $(^{13}\text{C}/^{12}\text{C})_{diseq}$ is the air-water $\delta^{13}\text{C}$ disequilibrium, that is the difference between the $\delta^{13}\text{C}$ -DIC expected at equilibrium with atmosphere CO_2 minus the measured $\delta^{13}\text{C}$ -DIC in surface water of the lake.

2.4 Bulk DIC mixing models

A mixing model was developed to compute the theoretical evolution of TA, DIC, and $p\text{CO}_2$ between March 2007 and September 2007, when the mixed layer deepened. The aim of this model is to compare theoretical evolution considering conservative mixing (no biology or other in/outputs) with observational data to infer the importance of certain processes. The model was computed by daily time steps assuming the conservative mixing (no biological activity) of surface waters with deep waters for TA and DIC. At each time step, $p\text{CO}_2$ was calculated from TA, DIC,

salinity and temperature, allowing the computation of F_{CO_2} and correcting DIC for F_{CO_2} . The mixing model was also run without correcting DIC for F_{CO_2} . The MLD, salinity and temperature were interpolated linearly between March and September 2007.

At each time step, TA was computed according to:

$$TA_{i+1_ML} = \frac{TA_{deep}(MLD_{i+1} - MLD_i) + TA_{i_ML}MLD_i}{MLD_{i+1}} \quad (19)$$

where TA_{i_ML} is TA in the mixed layer at time step i , TA_{i+1_ML} is TA in the mixed layer at time step $i+1$, MLD_i is the MLD at time step i , MLD_{i+1} is the MLD at time step $i+1$, and TA_{deep} is TA in the deep waters.

At each time step, DIC corrected for F_{CO_2} was computed according to:

$$DIC_{i+1_ML} = \frac{DIC_{deep}(MLD_{i+1} - MLD_i) + DIC_{i_ML}MLD_i - F_{CO_2i}\delta t}{MLD_{i+1}} \quad (20)$$

where DIC_{i_ML} is DIC in the mixed layer at time step i , DIC_{i+1_ML} is DIC in the mixed layer at time step $i+1$, F_{CO_2i} is F_{CO_2} at time step i , δt is the time interval between each time step (1 d), and DIC_{deep} is DIC in the deep waters.

At each time step, DIC not corrected for F_{CO_2} was computed according to:

$$DIC_{i+1_ML} = \frac{DIC_{deep}(MLD_{i+1} - MLD_i) + DIC_{i_ML}MLD_i}{MLD_{i+1}} \quad (21)$$

Results

In surface waters (1 m depth) of the main basin of Lake Kivu (excluding Kabuno Bay), $p\text{CO}_2$ values were systematically above atmospheric equilibrium (~ 372 ppm to ~ 376 ppm depending on the cruise), and varied within narrow ranges of 534–605 ppm in March 2007, 701–781 ppm in September 2007, 597–640 ppm in June 2008, and 583–711 ppm in April 2009 (Fig. 2). The most prominent feature of the spatial variations was the much higher $p\text{CO}_2$ values in Kabuno Bay, ranging between 11213 ppm and 14213 ppm (i.e., between 18 and 26 times higher than in the main basin). Wind speed showed little seasonal variability (ranging between 3.2 and 3.6 m s^{-1}), hence, the seasonal variations of the CO_2 emission rates followed those of $\Delta p\text{CO}_2$ with higher F_{CO_2} values in September 2007 (14.2 $\text{mmol m}^{-2} \text{d}^{-1}$) and lowest F_{CO_2} values in March 2007 (8.0 $\text{mmol m}^{-2} \text{d}^{-1}$) in the main basin (Table 1). In Kabuno Bay, the F_{CO_2} values ranged between 414.2 and 547.7 $\text{mmol m}^{-2} \text{d}^{-1}$, and were on average ~ 46 times higher than in the main basin.

Compared to the main basin, surface and deep waters of Kabuno Bay were characterized by higher salinity, DIC and TA values and by lower pH and $\delta^{13}\text{C}$ -DIC values (Fig. 3). Comparison of DIC and TA profiles shows that the relative contribution of CO_2 to DIC was more important in Kabuno Bay than in the main lake, since TA is mainly as HCO_3^- , and if the CO_2 contribution to DIC is low, then DIC and TA should be numerically close. At 60 m depth, CO_2 contributes $\sim 30\%$ to DIC in Kabuno Bay, and only $\sim 1\%$ in the main basin. Kabuno Bay was also characterized by a very stable chemocline (salinity, pH) and oxycline at ~ 11 m irrespective of the sampling period [28]. In the main basin of Lake Kivu, the oxycline varied seasonally between ~ 35 m in March

and September 2007 and ~60 m in June 2008 [28]. The deepening of the mixed layer and entrainment of deeper waters to the surface mixed layer was shown to be main driver of the seasonal variations of CH₄ [28]. The positive correlations between pCO₂ and CH₄ and between pCO₂ and the MLD also show that the mixing of deep and surface waters was a major driver of the seasonal variability of pCO₂ (Fig. 4). This is also consistent with the negative relation between pCO₂ and δ¹³C-DIC (Fig. 4), as DIC in deeper waters is more ¹³C-depleted than that in surface waters (Fig. 3).

DIC concentrations in surface waters averaged 13.0 mmol L⁻¹ and 16.9 mmol L⁻¹ in the main basin of Lake Kivu and in Kabuno Bay, respectively, but were much lower in the inflowing rivers (on average ~0.5 mmol L⁻¹). The comparison with the lake values shows that the δ¹³C-DIC were always more negative in rivers (mean -7.0±2.1‰) than in the main basin (mean 3.4±0.5‰) and Kabuno Bay (mean 0.8±0.5‰) (Fig. 5). This difference suggests that the DIC in surface waters of Lake Kivu originates from a different source than that in the rivers. POC concentrations in surface waters of the main basin averaged 32 μmol L⁻¹ in June 2008, 24 μmol L⁻¹ in April 2009 and 42 μmol L⁻¹ in October 2010. In the rivers, POC concentration was higher, 358 μmol L⁻¹ in June 2008 and 499 μmol L⁻¹ in April 2009. However, POC in the rivers never contributed more than 4.4% of TSM. δ¹³C-POC and δ¹³C-DIC signatures appeared uncoupled in rivers (Fig. 6), but a positive relationship between δ¹³C-DIC and δ¹³C-POC was found in the lake when combining the data from the main lake and Kabuno Bay (model I linear regression, $p < 0.001$, $r^2 = 0.71$, $n = 15$). Furthermore, the δ¹³C-POC in the main basin and Kabuno Bay (mean -24.1±2.0‰, $n = 15$) was significantly lower than the δ¹³C-POC in rivers (mean = -22.9±1.5‰, $n = 21$) (t -test; $p < 0.05$), but the δ¹³C-DOC in the main lake (mean -23.1±1.1‰, $n = 15$) did not differ from the δ¹³C-DOC in rivers (mean -23.9±1.4‰, $n = 21$) (Fig. 7) and was vertically uncoupled from δ¹³C-POC (Fig. 8).

In order to test if vertical mixing was the only driver of seasonal variations of pCO₂, we applied the mixing model to the March 2007 data in order to predict the evolution of TA, DIC, and pCO₂ up to September 2007 and we compared the predicted values to the actual data obtained at that period (Fig. 9). The TA value predicted by the mixing model was higher than the observations in September 2007 by 108 μmol L⁻¹. We assumed that the process removing TA was CaCO₃ precipitation in the mixolimnion and subsequent export to depth (F_{CaCO_3}). In order to account for the difference between the mixing model prediction and the observations, F_{CaCO_3} was estimated to be 14.2 mmol m⁻² d⁻¹ between March and September 2007.

The DIC value predicted by the mixing model was higher than the observations in September 2007 by 108 μmol L⁻¹. The emission of CO₂ to the atmosphere only accounted for 19% of the DIC removal. We assumed that the remaining DIC was removed by the combination of F_{CaCO_3} and POC production in the epilimnion and export to depth (F_{POC}) that was estimated to be 11.5 mmol m⁻² d⁻¹, using the F_{CaCO_3} value estimated above from the TA data. The modeled pCO₂ was above the observed pCO₂ and the CO₂ emission only accounted for 27% of the difference. This implies that the decrease of pCO₂ was mainly related to F_{POC} .

To further investigate the drivers of CO₂ dynamics in Lake Kivu, we computed the TA and DIC whole-lake (bulk concentration) mass balances based on averages for the cruises (Fig. 10). The major flux of TA was the vertical input from deeper waters (50.9 mmol m⁻² d⁻¹) and the outflow by the Ruzizi (42.6 mmol m⁻² d⁻¹), which was higher than the inputs from rivers by one

order of magnitude (1.2 mmol m⁻² d⁻¹). The closing term of the TA mass balance was 9.5 mmol m⁻² d⁻¹. We assume that this was related to F_{CaCO_3} (4.7 mmol m⁻² d⁻¹). Similarly, the major fluxes of DIC were the vertical input (63.5 mmol m⁻² d⁻¹) and the outflow of the Ruzizi (39.3 mmol m⁻² d⁻¹), which were higher than the inputs from rivers by one order of magnitude (1.3 mmol m⁻² d⁻¹), and than the emission of CO₂ to the atmosphere (10.8 mmol m⁻² d⁻¹). The closing term of the DIC mass balance was 14.8 mmol m⁻² d⁻¹. We assume that this was related to the sum of F_{CaCO_3} and F_{POC} , allowing to compute F_{POC} using the F_{CaCO_3} values computed from the TA mass balance. The estimated F_{POC} values was 10.0 mmol m⁻² d⁻¹. The whole-lake DIC stable isotope mass balance provided a F_{POC} value of 25.4 mmol m⁻² d⁻¹, and vertical inputs of DIC of 78.0 mmol m⁻² d⁻¹.

Planktonic metabolic rates in the epilimnion (PNPP and BP) were measured during each cruise (Table 2). The PNPP values ranged from 14.2 to 49.7 mmol m⁻² d⁻¹, and were relatively similar in March 2007, September 2007 and June 2008, but distinctly lower in April 2009. The BP values ranged from 3.9 to 49.8 mmol m⁻² d⁻¹. This range encompasses the one reported for BP in the euphotic layer (~40 m) of Lake Tanganyika (3.0 to 20.0 mmol m⁻² d⁻¹) [16]. The BR values estimated from BP ranged from 13.6 to 61.2 mmol C m⁻² d⁻¹. PNPP was markedly in excess of BR only in June 2008. In March 2007 and September 2007, BR was balanced by PNPP or slightly in excess of PNPP. In April 2009, BR was markedly in excess of PNPP.

Discussion

The amplitude of the seasonal variations of mean pCO₂ across the main basin of Lake Kivu was 163 ppm (between 579±23 ppm on average in March 2007 and 742±28 ppm on average in September 2007). Such pCO₂ seasonal amplitude is low compared to temperate and boreal lakes, where it is usually between ~500 ppm [48] and >1000 ppm [49],[50],[51],[52],[53],[54], and even up to ~10,000 ppm in small bog lakes [53]. The lower amplitude of seasonal variations of the pCO₂ in Lake Kivu might be related to the tropical climate leading only to small surface water temperature seasonal variations (from 23.6°C in September 2007 to 24.6°C in March 2007 on average), and also for relatively modest variations in mixing (MLD changed from 20 m to 70 m). Hence, compared to temperate and boreal lakes, the seasonal variations of biological activity are less marked (due to relatively constant temperature and light, and modest changes in mixing), and also there is an absence of large episodic CO₂ inputs to surface waters such as those occurring in temperate or boreal systems during lake overturns or of CO₂ accumulation during ice covered periods.

The spatial variations of pCO₂ in the main basin of Lake Kivu were also low. The coefficient of variation of pCO₂ in surface waters of the main basin ranged for each cruise between 3% and 6%, below the range reported by Kelly et al. [54] in five large boreal lakes (range 5% to 40%). The relative horizontal homogeneity of pCO₂ could be in part related to the absence of extensive shallow littoral zones, owing to the steep shores [18], and also due to very small influence of C inputs from rivers in the overall DIC budget (Fig. 10). The most prominent spatial feature in Lake Kivu was the much larger pCO₂ values in surface waters of Kabuno Bay compared to the main basin. Furthermore, surface and deep waters of Kabuno Bay were characterized by higher salinity, DIC and TA values and by lower pH and δ¹³C-DIC values. These vertical patterns indicate that there is a much larger contribution of subaquatic springs to the whole water column

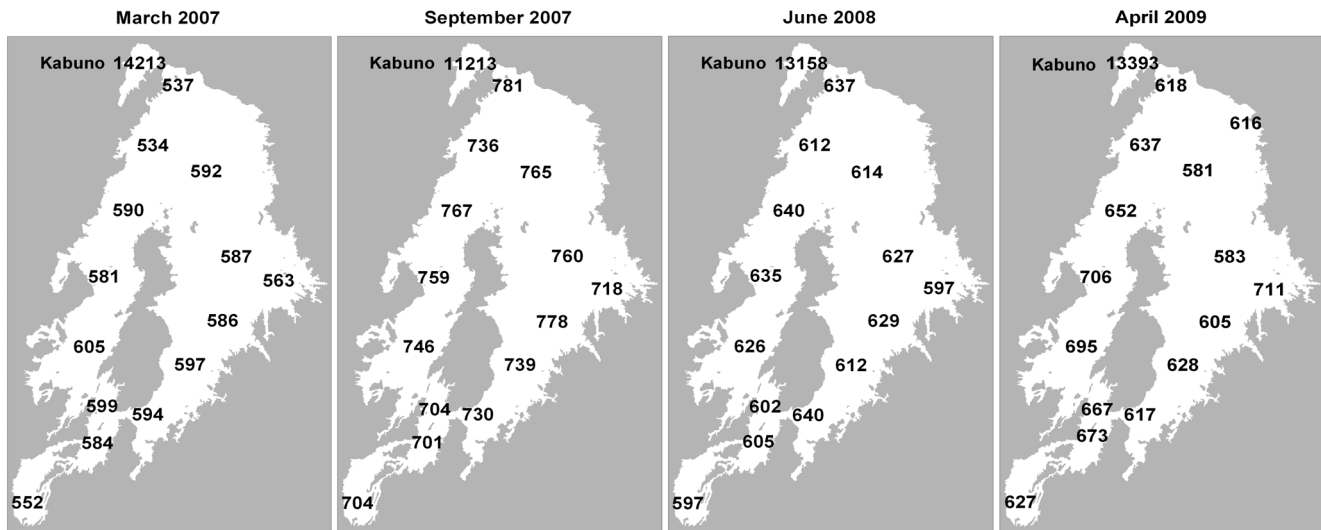


Figure 2. Spatial distribution of the partial pressure of CO₂ (pCO₂, ppm) in the surface waters of Lake Kivu (1 m depth) in March 2007, September 2007, June 2008 and April 2009.
doi:10.1371/journal.pone.0109500.g002

including surface waters in Kabuno Bay than in the main basin of Lake Kivu relative to their respective volumes. This is related to the different geomorphology, since Kabuno Bay is shallower than the main basin (maximum depth of 110 m versus 485 m) and exchanges little water with the main basin (narrow connection ~10 m deep). Also, Kabuno Bay is smaller (~48 km²) than the main basin (~2322 km²). Hence, there is a stronger fetch limitation of wind induced turbulence that also contributes to the stability of the vertical water column structure in Kabuno Bay irrespective of the season [28].

The overall average of pCO₂ for the 4 cruises in the main basin of Lake Kivu (646 ppm) is lower than the average of 41 large lakes (>500 km²) of the world (850 ppm) [5], than the global average for freshwater lakes (1287 ppm) [12], than the average of tropical freshwater lakes (1804 ppm) [55], and than the average for tropical African freshwater lakes (2296 ppm) [49]. Lake Kivu

corresponds to a saline lake according to the definition of Duarte et al. [56] (specific conductivity >1000 μS cm⁻¹; salinity >0.68) that collectively have a global average pCO₂ of 1900 ppm (derived from carbonic acid dissociation constants for freshwater) or 3040 ppm (derived from carbonic acid dissociation constants for seawater). Kabuno Bay, in contrast, was characterized by an exceptionally high average pCO₂ value (12994 ppm) compared to other freshwater lakes, tropical (African) freshwater lakes, and saline lakes globally.

The average F_{CO_2} of the 4 cruises in the main basin of Lake Kivu was 10.8 mmol m⁻² d⁻¹, which is lower than the global average for freshwater lakes of 16.0 mmol m⁻² d⁻¹ reported by Cole et al. [49], and the average for saline lakes ranging between 81 and 105 mmol m⁻² d⁻¹ reported by Duarte et al. [56]. The average F_{CO_2} in Kabuno Bay (500.7 mmol m⁻² d⁻¹) is distinctly higher than the F_{CO_2} global averages for freshwater and saline

Table 1. Average wind speed (m s⁻¹), air-water gradient of the partial pressure of CO₂ (ΔpCO₂, ppm), and air-water CO₂ flux (F_{CO_2} , mmol m⁻² d⁻¹) in the main basin of Lake Kivu and Kabuno Bay in March 2007, September 2007, June 2008, and April 2009.

	wind speed (m s ⁻¹)	ΔpCO ₂ (ppm)	F_{CO_2} (mmol m ⁻² d ⁻¹)
March 2007			
Main basin	3.3±0.4	207±22	8.0±1.3
Kabuno Bay		13841	536.4±61.8
September 2007			
Main basin	3.2±0.4	370±27	14.2±2.0
Kabuno Bay		10841	547.7±38.7
June 2008			
Main basin	3.6±0.2	245±15	10.5±1.0
Kabuno Bay		12783	547.7±38.7
April 2009			
Main basin	3.3±0.2	267±41	10.3±1.8
Kabuno Bay		13016	504.5±36.7

doi:10.1371/journal.pone.0109500.t001

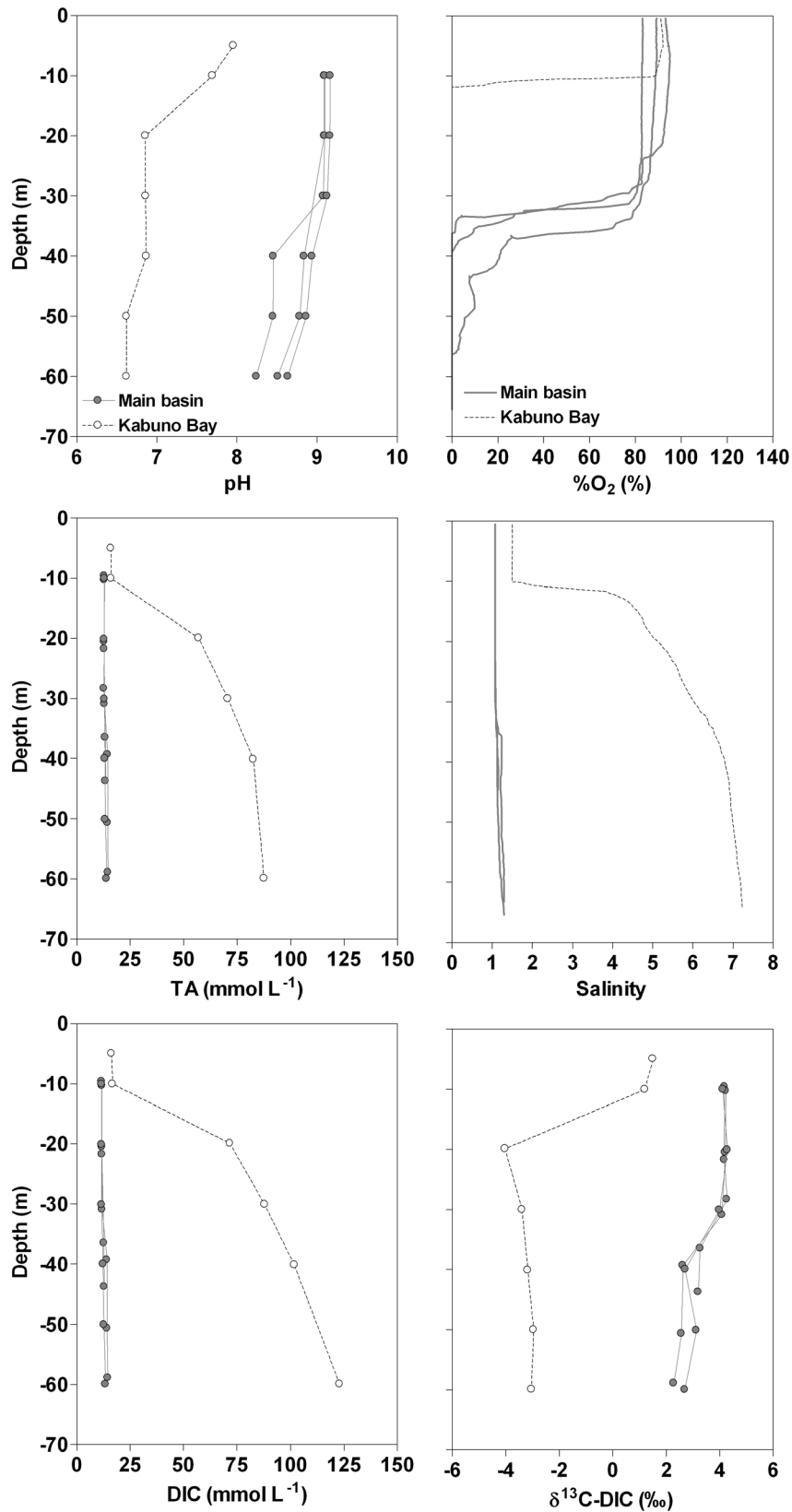


Figure 3. Vertical profiles in March 2007 of pH, oxygen saturation level (%O₂, %), total alkalinity (TA, mmol L⁻¹), salinity, dissolved inorganic carbon (DIC, mmol L⁻¹), δ¹³C signature of DIC (δ¹³C-DIC, ‰) in Kabuno Bay and in the three northernmost stations in the main basin of Lake Kivu.

doi:10.1371/journal.pone.0109500.g003

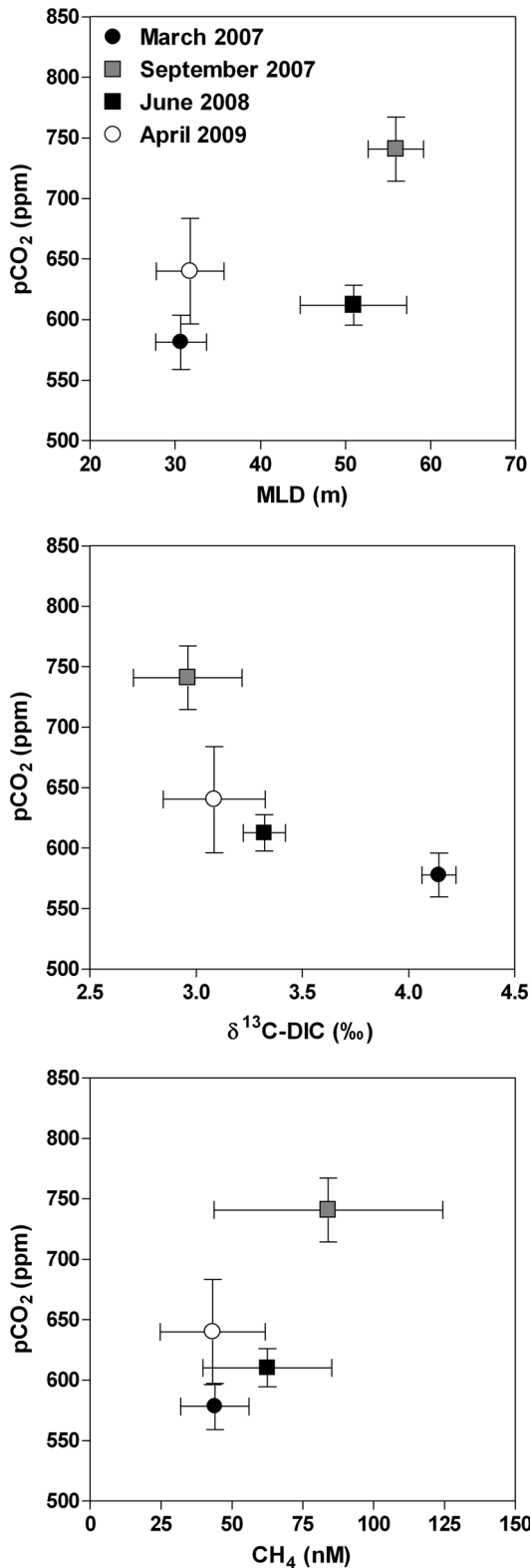


Figure 4. Average partial pressure of CO_2 ($p\text{CO}_2$, ppm) in the surface waters of the main basin of Lake Kivu (1 m depth) versus mixed layer depth (MLD, m), $\delta^{13}\text{C}$ signature of dissolved inorganic carbon (DIC) ($\delta^{13}\text{C-DIC}$, ‰), and methane concentration (CH_4 , nmol L^{-1}) in March 2007, September 2007, June 2008, and April 2009. Vertical and horizontal bars represent standard deviations.

doi:10.1371/journal.pone.0109500.g004

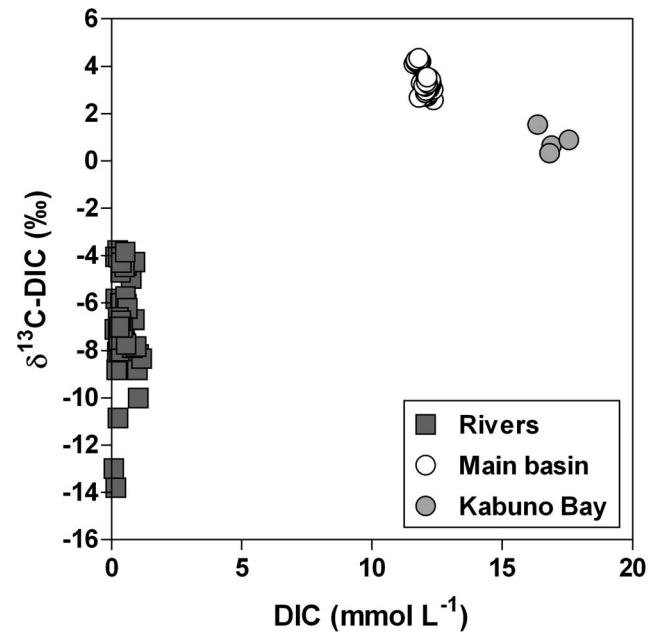


Figure 5. Relation between $\delta^{13}\text{C}$ signature of dissolved inorganic carbon (DIC) ($\delta^{13}\text{C-DIC}$, ‰) and DIC concentration (mmol L^{-1}), in the mixed layer of the main basin of Lake Kivu, Kabuno Bay, and various inflowing rivers, in March 2007, September 2007, June 2008, and April 2009.

doi:10.1371/journal.pone.0109500.g005

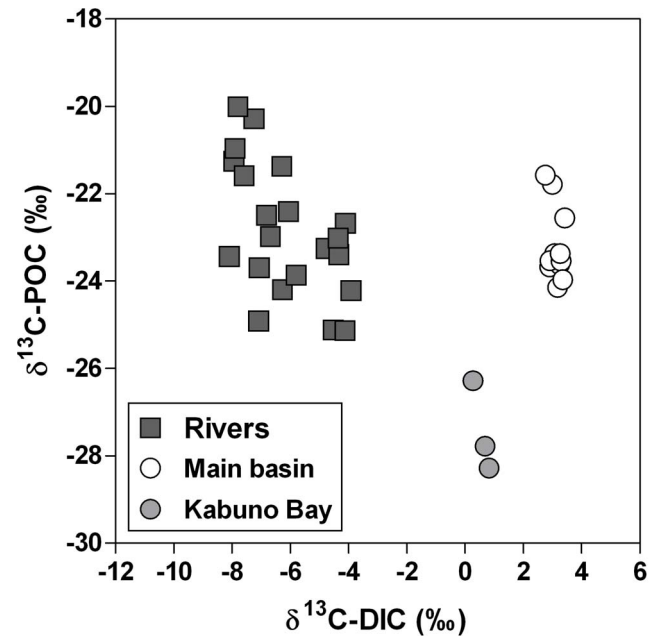


Figure 6. Relation between $\delta^{13}\text{C}$ signature of particulate organic carbon (POC) ($\delta^{13}\text{C-POC}$, ‰) and $\delta^{13}\text{C}$ signature of dissolved inorganic carbon (DIC) ($\delta^{13}\text{C-DIC}$, ‰), in the mixed layer of the main basin of Lake Kivu, Kabuno Bay and various inflowing rivers, in June 2008, April 2009, and October 2010.

doi:10.1371/journal.pone.0109500.g006

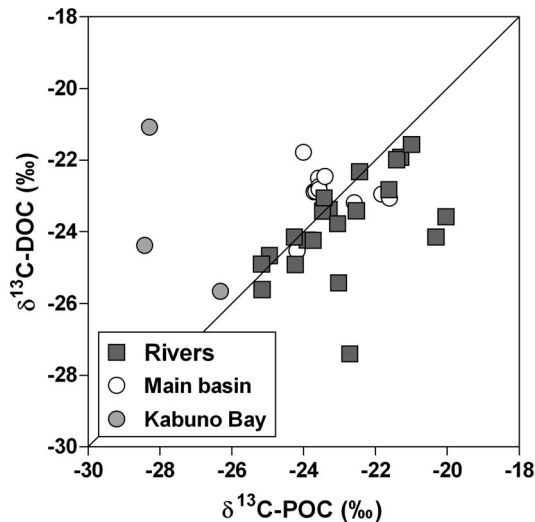


Figure 7. Relation between $\delta^{13}\text{C}$ signature of dissolved organic carbon (DOC) ($\delta^{13}\text{C}\text{-DOC}$, ‰) and $\delta^{13}\text{C}$ signature of particulate organic carbon (POC) ($\delta^{13}\text{C}\text{-POC}$, ‰), in the mixed layer of the main basin of Lake Kivu, Kabuno Bay and various inflowing rivers, in June 2008, April 2009, and October 2010. Solid line is the 1:1 line.

doi:10.1371/journal.pone.0109500.g007

lakes. However, the average F_{CO_2} in Kabuno Bay is equivalent to average of F_{CO_2} value of alkaline volcanic lakes ($458 \text{ mmol m}^{-2} \text{ d}^{-1}$) but lower than average of F_{CO_2} of acid volcanic lakes ($51183 \text{ mmol m}^{-2} \text{ d}^{-1}$) reported by Pérez et al. [57].

Cross system regional analyses show a general negative relationship between pCO_2 and lake surface area [5], [54], [58], [59], [60] and a positive relationship between pCO_2 and DOC [61] (and reference therein). The low pCO_2 and F_{CO_2} values in Lake Kivu are consistent with these general patterns, since this is a large ($>2000 \text{ km}^2$) and organic poor ($\text{DOC} \sim 0.2 \text{ mmol L}^{-1}$) system. However, the low seasonal amplitude of pCO_2 and relative horizontal homogeneity of pCO_2 in Lake Kivu are not necessarily linked to its large size. Indeed, spatial and temporal variability of pCO_2 within a single lake have been found to be no greater nor smaller in larger lakes than in smaller lakes, in cross system analyses in Northwest Ontario [54] and northern Québec [60].

Borges et al. [28] reported diffusive CH_4 emissions of $0.04 \text{ mmol m}^{-2} \text{ d}^{-1}$ and $0.11 \text{ mmol m}^{-2} \text{ d}^{-1}$ for the main basin of Lake Kivu and Kabuno Bay, respectively. Using a global warming potential of 72 for a time horizon of 20 yr [62], the CH_4 diffusive emissions in CO_2 equivalents correspond to $0.26 \text{ mmol m}^{-2} \text{ d}^{-1}$ and $0.77 \text{ mmol m}^{-2} \text{ d}^{-1}$ for the main basin of Lake Kivu and Kabuno Bay, respectively, hence 41 to 650 times lower than the actual F_{CO_2} values.

DIC concentrations in surface waters of the main basin of Lake Kivu and Kabuno Bay averaged 13.0 and 16.8 mmol L^{-1} , respectively, and were well within the range of DIC reported for saline lakes by Duarte et al. [56], which range from 0.1 to 2140 mmol L^{-1} , but are lower than the global average for saline lakes of 59.5 mmol L^{-1} . DOC averaged in surface waters 0.15 mmol L^{-1} and 0.20 mmol L^{-1} in the main basin of Lake Kivu and in Kabuno Bay, respectively. Hence, DIC strongly dominated the dissolved C pool, with DIC:DOC ratios of 82 and 87 in the main basin of Lake Kivu and in Kabuno Bay, respectively. These DIC:DOC ratios are higher than those in 6 hard-water lakes of the northern Great Plains ranging from 3 to 6 [63], and higher than those in boreal lakes where DOC is the

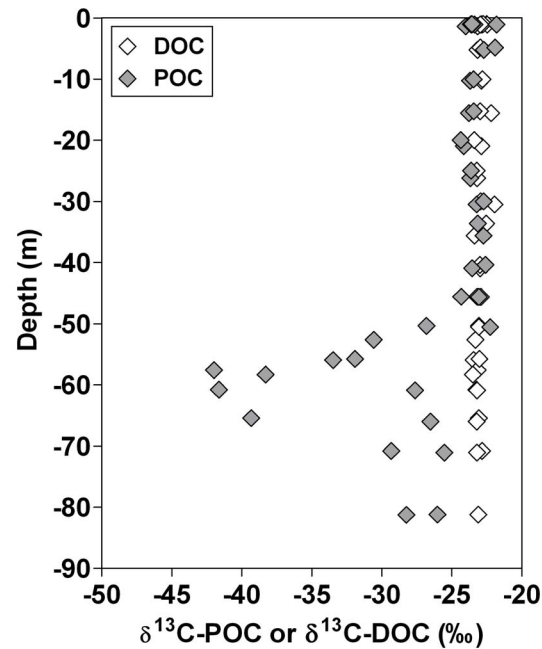


Figure 8. Vertical profiles of $\delta^{13}\text{C}$ signature of dissolved organic carbon (DOC) ($\delta^{13}\text{C}\text{-DOC}$, ‰) and $\delta^{13}\text{C}$ signature of particulate organic carbon (POC) ($\delta^{13}\text{C}\text{-POC}$, ‰) in the main basin of Lake Kivu in October 2010.

doi:10.1371/journal.pone.0109500.g008

dominant form of the dissolved C pool, with DIC:DOC ratios ranging from 0.01 to 0.68 *e.g.* [64], [65], this range reflecting both seasonal changes [59] and differences in catchment characteristics [66]. Unlike the 6 hard-water lakes of the northern Great Plains, where the high DIC concentrations are due to river inputs [67], the high DIC concentrations in Lake Kivu were related to vertical inputs of DIC from deep waters that were on average 49 times larger than the DIC inputs from rivers (Fig. 10), as confirmed by $\delta^{13}\text{C}\text{-DIC}$ values clearly more positive in the lake than in the rivers (Fig. 5). The difference in C stable isotope composition of POC between the lake and rivers indicates that these two pools of organic C do not share the same origin. In the small, turbid rivers flowing to Lake Kivu, we expect the POC and DOC pools to be derived from terrestrial inputs, as reflected by the low contribution of POC to TSM *e.g.* [68]. In contrast, the positive relationship between the $\delta^{13}\text{C}\text{-DIC}$ and $\delta^{13}\text{C}\text{-POC}$ in surface waters (Fig. 6) suggests that DIC is the main C source for POC in surface waters of Lake Kivu, implying that the whole microbial food web could be supported by autochthonous organic C. However, the $\delta^{13}\text{C}$ data indicate a surprising difference between the origin of DOC and POC in the lake (Figs. 7, 8). The $\delta^{13}\text{C}\text{-POC}$ signatures were constant from the surface to the oxic-anoxic interface, then showed a local and abrupt excursion to values as low as -40‰ , reflecting the incorporation of a ^{13}C -depleted source in the POC (Fig. 8). Indeed, while the large pool of DIC is the main C source for POC in surface waters, it appears that CH_4 with a $\delta^{13}\text{C}$ signature of approximately -60‰ (own data not shown) contributes significantly to C fixation at the oxic-anoxic interface, as also shown in Lake Lugano [69]. In contrast, the $\delta^{13}\text{C}$ signature of the DOC pool in the mixolimnion showed little seasonal and spatial variations and appeared to be uncoupled from the POC pool (Figs. 7, 8). Heterotrophic bacteria quickly mineralized the labile autochthonous DOC that reflects the $\delta^{13}\text{C}$ signature of POC, produced by cell lysis, grazing, or phytoplankton excretion

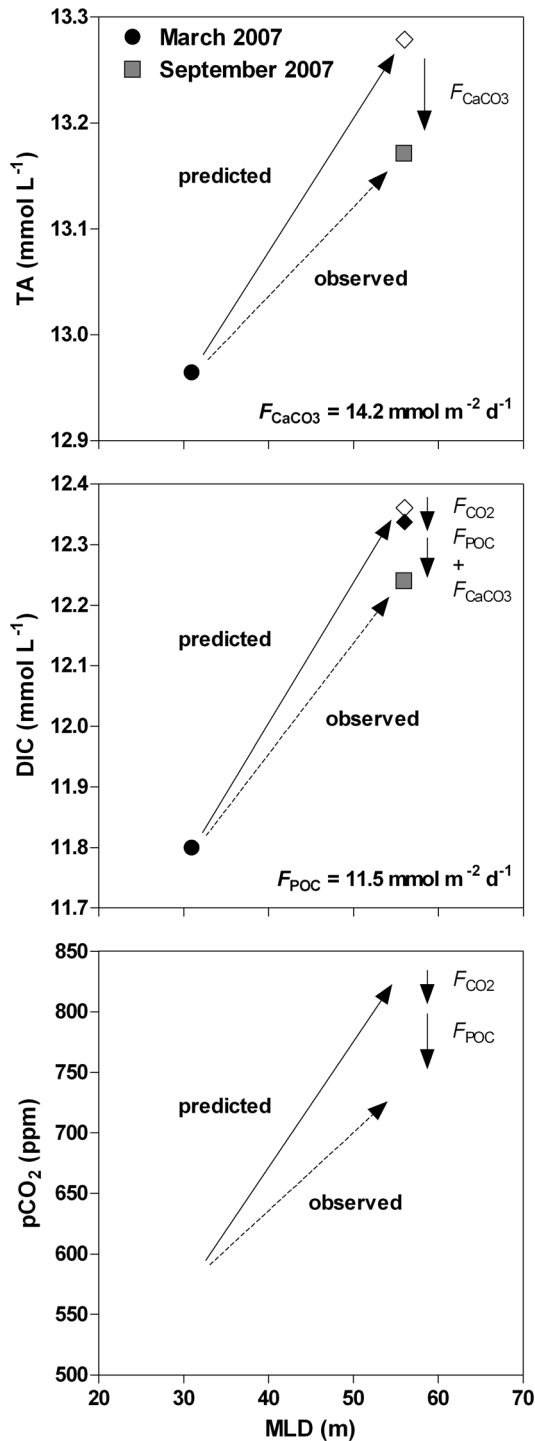


Figure 9. Observed data (circles and squares) and predicted values from a mixing model (diamonds) from March 2007 to September 2007 of total alkalinity (TA, mmol L⁻¹), dissolved inorganic carbon (DIC, mmol L⁻¹), and the partial pressure of CO₂ (pCO₂, ppm) as a function of mixed layer depth (MLD, m) in the main basin of Lake Kivu. F_{CO_2} = air-water CO₂ flux; F_{POC} = export of particulate organic carbon to depth; F_{CaCO_3} = export of CaCO₃ to depth.

doi:10.1371/journal.pone.0109500.g009

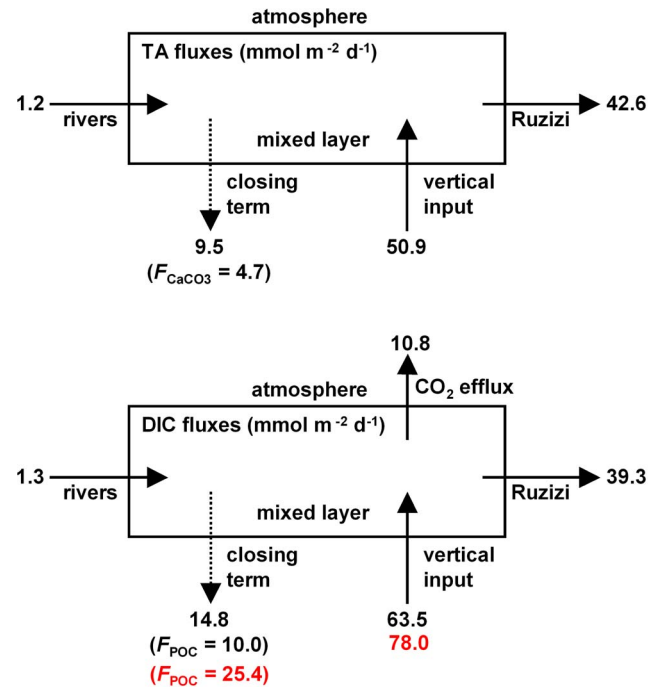


Figure 10. Average mass balance of total alkalinity (TA) and dissolved inorganic carbon (DIC) in the mixed layer of the main basin of Lake Kivu based on data collected in March 2007, September 2007, June 2008 and April 2009. F_{POC} = export of particulate organic carbon to depth; F_{CaCO_3} = export of CaCO₃ to depth. Numbers in black correspond to the mass balance based on bulk concentrations, and numbers in red correspond to the mass balance based on DIC stable isotopes. All fluxes are expressed in mmol m⁻² d⁻¹. doi:10.1371/journal.pone.0109500.g010

[70]. Hence, standing stocks of autochthonous DOC are small, and older refractory compounds constitute the major part of the DOC pool.

The F_{CaCO_3} value computed from the whole-lake TA budget was 4.7 mmol m⁻² d⁻¹, higher than the total inorganic C (TIC) annual average fluxes in sediment traps ranging from 0.3 mmol m⁻² d⁻¹ (at 50 m depth) to 0.5 mmol m⁻² d⁻¹ (at 130 m depth) reported by Pasche et al. [71] at Ishungu. The maximum individual monthly TIC flux from sediment traps at Ishungu reported by Pasche et al. [71] was 4.0 mmol m⁻² d⁻¹. However, the F_{CaCO_3} value was closer to the TIC deposition fluxes in the top cm of sediment cores ranging from 1.4 mmol m⁻² d⁻¹ (at Ishungu) to 4.8 mmol m⁻² d⁻¹ (at Gisenyi) also reported by Pasche et al. [71]. The F_{POC} computed from the DIC whole-lake budget was 10.0 mmol m⁻² d⁻¹ close to the total organic C (TOC) average fluxes in sediment traps ranging from 8.7 mmol m⁻² d⁻¹ (at 50 m depth) to 9.8 mmol m⁻² d⁻¹ (at 172 m depth) reported by Pasche et al. [71] at Ishungu.

Due to thermodynamic equilibria of the dissolved carbonate system, CaCO₃ precipitation leads to a shift from the HCO₃⁻ to the CO₂ pool according to:



However, CaCO₃ precipitation has frequently been reported in lakes as biologically mediated by primary producers [50], [72], [73], whereby the CO₂ produced by the precipitation of CaCO₃ is fixed into organic matter by photosynthesis and does not accumulate in the water [50], [74].

Table 2. Photic depth (Z_e , m), chlorophyll-*a* concentration in the mixed layer ($\text{Chl-}a$, mg m^{-2}), particulate net primary production (PNPP, $\text{mmol m}^{-2} \text{d}^{-1}$), bacterial production integrated over Z_e (BP, $\text{mmol m}^{-2} \text{d}^{-1}$), bacterial respiration (BR, $\text{mmol m}^{-2} \text{d}^{-1}$), and percent of extracellular release (PER, %), at two stations in the main basin of Lake Kivu (Kibuye, Ishungu) in March 2007, September 2007, June 2008, and April 2009.

	Z_e (m)	Chl- <i>a</i> (mg m^{-2})	PNPP ($\text{mmol m}^{-2} \text{d}^{-1}$)	BP ($\text{mmol m}^{-2} \text{d}^{-1}$)	BR ($\text{mmol m}^{-2} \text{d}^{-1}$)	PNPP-BR ($\text{mmol m}^{-2} \text{d}^{-1}$)	PER (%)
March 2007							
15/03/2007	18	38.3	27.0	23.2	35.7	-8.7	54
17/03/2007	20	48.4	42.5	25.8	39.9	2.6	33
23/03/2007	17	36.1	49.7	40.5	49.6	0.1	32
September 2007							
09/09/2007	19	56.4	42.9	35.9	47.9	-5.0	42
12/09/2007	18	55.1	45.9	34.0	45.9	0.1	36
04/09/2007	20	48.2	<i>n.d.</i>	16.0	29.9	<i>n.d.</i>	<i>n.d.</i>
June 2008							
23/06/2008	24	42.8	46.0	7.7	21.6	24.4	3
11/07/2008	20	37.8	42.0	11.1	24.3	17.7	17
03/07/2008	19	28.1	40.7	3.9	13.6	27.1	-4
April 2009							
04/05/2009	21	22.9	14.2	49.8	61.2	-47.0	82
21/04/2009	24	39.3	24.5	43.5	58.9	-34.4	68

PNPP and BP were derived from experimental measurements. BR was computed from BP (see material and methods), and PER was computed from PNPP, BR, river inputs and vertical export of organic matter according to equation (24).
doi:10.1371/journal.pone.0109500.t002

Precipitation and preservation of CaCO_3 in lakes are not considered in global compilations of C fluxes in lakes, that focus exclusively on organic C and CO_2 fluxes *e.g.* [4], [7]. However, in Lake Kivu, F_{CaCO_3} was found to be a major flux term in the C budgets, 3.6 times larger than the DIC inputs from rivers, and comparable to the emission of CO_2 to the atmosphere and F_{POC} (~ 2 times lower). The $F_{\text{POC}}:F_{\text{CaCO}_3}$ ratio in the main basin of Lake Kivu was 2.1, which is consistent with the values reported in 6 hard-water lakes of the northern Great Plains, ranging from 1.0 to 4.0 [63], and with the values in Lake Malawi ranging from 0.2 to 7.3 (on average 2.5) [75]. As a comparison, the average $F_{\text{POC}}:F_{\text{CaCO}_3}$ in the ocean (so called rain ratio) has been estimated from models of varying complexity to be 4.0 [76], 3.5 to 7.5 [77], and 11.0 [78].

The export ratio (ER) is the fraction of PP that is exported from surface waters to depth and is an important metric of the net metabolism and overall C fluxes in aquatic systems. We computed ER as defined by Baines et al. [79], according to:

$$ER = \frac{F_{\text{POC}}}{\text{PNPP}_i} 100 \quad (23)$$

where F_{POC} is derived from the DIC mass balance (Fig. 10), and PNPP_i is the average PNPP for a given cruise i measured by incubations (Table 2).

ER was 25%, 23%, 23%, and 52% in March 2007, September 2007, June 2008, and April 2009, respectively. These values are consistent with the fact that the ER in lakes is negatively related to lake primary production based on the analysis of Baines et al. [79]. These authors reported ER values as high as 50% for oligotrophic lakes such as Lake Kivu.

The general agreement between the F_{CaCO_3} computed from the TA budget and the TIC deposition fluxes derived from sediment cores reported by Pasche et al. [71], and the F_{POC} computed from the DIC budget and TOC average fluxes in sediment traps reported by Pasche et al. [71], give confidence on the overall robustness of the TA and DIC whole-lake budget we computed. Also, the F_{CaCO_3} and F_{POC} values computed from whole-lake budget are consistent with those derived independently from a mixing model based on the March and September 2007 data (Fig. 9). The whole-lake DIC stable isotope mass balance budgets give F_{POC} and upward DIC inputs estimates that are of same order of magnitude as those derived from whole-lake bulk DIC mass balance budget. The difference in the two approaches is that in the DIC stable isotope mass balance the upward DIC inputs were computed from vertical distributions of DIC and $\delta^{13}\text{C}$ -DIC while in the bulk DIC mass balance they are computed from the E and $Q_{\text{upwelling}}$ values from the model of Schmid et al. [19] and the DIC vertical distribution. This can explain the mismatch between both approaches in the upward DIC input estimates (difference of 23%) that propagated into a relatively larger mismatch in the F_{POC} estimates (difference of 61%) computed as a closing term in both approaches.

Based on the POC and DOC data acquired during the June 2008 and April 2009 cruises in 12 rivers flowing into Lake Kivu (Fig. 1), we computed an overall TOC input from rivers of $0.7 \text{ mmol m}^{-2} \text{ d}^{-1}$ and $3.3 \text{ mmol m}^{-2} \text{ d}^{-1}$, respectively. The F_{POC} was $10 \text{ mmol m}^{-2} \text{ d}^{-1}$, implying a net organic C production in the epilimnion (net autotrophic community metabolic status). This would mean that the fraction of PNPP that does not sediment out of the epilimnion cannot meet BR, and that BR must then rely on other organic C sources. We assume these other organic C sources to be dissolved primary production (DPP), that was estimated assuming steady-state, according to:

$$DPP = F_{\text{POC}} + BR - \text{PNPP} - F_{\text{TOC}_{\text{river}}} \quad (24)$$

where $F_{\text{TOC}_{\text{river}}}$ is the input of TOC from rivers that was computed from the discharge weighted average TOC concentrations from the June 2008 and April 2009 cruises.

The percent of extracellular release (PER) allows to determine the relative importance of DPP in overall C flows in an aquatic system. PER as defined by Baines and Pace [80] was computed according:

$$PER = \frac{DPP}{DPP + \text{PNPP}} 100 \quad (25)$$

In June 2008, for two stations, the sum of organic C inputs ($\text{PNPP} + F_{\text{TOC}_{\text{river}}}$) exceeded the sum of organic C outputs ($F_{\text{POC}} + BR$), leading to negative DPP and PER estimates. If we exclude these values, PER estimates ranged from 3% to 80% (Table 2) encompassing the range reported by Baines and Pace [80] for freshwater lakes from $\sim 0\%$ to $\sim 75\%$. PNPP in April 2009 was distinctly lower than during the other cruises, leading to high PER estimates. The average PER for all cruises was 32%, and if the April 2009 data are excluded, the average PER was 19%. During the April 2009 field survey, we carried 6 h incubations using the ^{14}C incorporation method [81] in light controlled ($200 \mu\text{E m}^{-2} \text{ s}^{-1}$) conditions, allowing to measure PNPP and to compute DPP using the model of Moran et al. [82]. Experimentally-derived PER estimates were 57% at Ishungu, 62% at Kibuye, and 50% in Kabuno Bay [70]. These experimentally determined PER values are within the range of those determined from the mass balance (3% to 80%) and above the average for all cruises (32%). This confirms that a substantial part of the BR is subsidised by DPP, that part of the PNPP is available for export to depth, and consequently that the epilimnion of Lake Kivu is net autotrophic, although a source of CO_2 to the atmosphere.

Conclusions

Surface waters of 93% of the lakes in the compilation of Sobek et al. [12] were over-saturated in CO_2 with respect to the atmospheric equilibrium. Hence, the overwhelming majority of lakes globally act as a CO_2 source to the atmosphere. These emissions to the atmosphere have been frequently explained by the net heterotrophic nature of lakes sustained by terrestrial organic C inputs mainly as DOC [1], [6], [7], [12], [49], [83], [84], [85], [86], [87]. While this paradigm undoubtedly holds true for boreal humic lakes, several exceptions have been put forward in the literature. For instance, Balmer and Downing [88] showed that the majority (60%) of eutrophic agriculturally impacted lakes are net autotrophic and CO_2 sinks. Karim et al. [89] showed that surface waters of very large lakes such as the Laurentian Great Lakes are at equilibrium with atmospheric CO_2 and O_2 . This is consistent with the negative relationship between pCO_2 and lake size reported in several regional analyses [5], [54], [58], [59], [60], and with the positive relationship between pCO_2 and catchment area: lake area reported for Northern Wisconsin lakes [90]. Also, in some lakes among which hard-water lakes, the magnitude of CO_2 emissions to the atmosphere seems to depend mainly on hydrological inputs of DIC from rivers and streams [67], [91], [92], [93] or ground-water [52], [94], [95], rather than on lake metabolism. Some of these hard-water lakes were actually found to be net autotrophic, despite acting as a source of CO_2 to the atmosphere [67], [91], [93].

Here, we demonstrate that Lake Kivu represents an example of a large, oligotrophic, tropical lake acting as a source of CO₂ to the atmosphere, despite having a net autotrophic epilimnion. The river inputs of TOC were modest, and were on average 11 times lower than the export of POC to depth. This is probably related to the very low ratio of catchment surface area: lake surface area (5100:2370 km²:km²) that is among the lowest in lakes globally [96]. We showed that BR was in part subsidized by DPP, based on mass balance considerations and incubations. Since the epilimnion of Lake Kivu is net autotrophic, the CO₂ emission to the atmosphere must be sustained by DIC inputs. The river DIC inputs are also low owing to very low ratio of catchment surface area: lake surface area, and cannot sustain the CO₂ emission to the atmosphere unlike the hard water lakes studied by Finlay et al. [67] and Stets et al. [91]. In Lake Kivu, the CO₂ emission is sustained by DIC inputs from depth, and this DIC is mainly geogenic [24] and originates from deep geothermal springs [19].

Carbonate chemistry in surface waters of Lake Kivu is unique from other points of view. The dissolved C pool is largely dominated by DIC, with DIC:DOC ratios distinctly higher than in hard-water lakes and humic lakes. The high DIC content in surface water results in CaCO₃ over-saturation, in turn leading to CaCO₃ precipitation and export to depth. This flux was found to be significant, being 4 times larger than the river inputs of DIC and of similar magnitude than the CO₂ emission to the atmosphere.

References

- Cole JJ, Caraco NF (2001) Carbon in catchments: connecting terrestrial carbon losses with aquatic metabolism. *Mar Fresh Res* 52: 101–110.
- Kempe S (1984) Sinks of the anthropogenically enhanced carbon cycle in surface fresh waters. *J Geophys Res* 89: 4657–4676.
- Richey JE, Melack JM, Aufdenkampe AK, Ballester VM, Hess LL (2002) Outgassing from Amazonian rivers and wetlands as a large tropical source of atmospheric CO₂. *Nature* 416: 617–620.
- Cole JJ, Prairie YT, Caraco NF, McDowell WH, Tranvik IJ, et al. (2007) Plumbing the global carbon cycle: Integrating inland waters into the terrestrial carbon budget. *Ecosystems* 10: 171–184.
- Alin SR, Johnson TC (2007) Carbon cycling in large lakes of the world: A synthesis of production, burial, and lake-atmosphere exchange estimates. *Global Biogeochem Cycles* 21(GB3002): doi:10.1029/2006GB002881.
- Battin TJ, Kaplan LA, Findlay S, Hopkinson CS, Marti E, et al. (2008) Biophysical controls on organic carbon fluxes in fluvial networks. *Nature Geosc* 1: 95–100.
- Tranvik IJ, Downing JA, Cotner JB, Loiselle SA, Striegl RG, et al. (2009) Lakes and reservoirs as regulators of carbon cycling and climate. *Limnol Oceanogr* 54: 2298–2314.
- Aufdenkampe AK, Mayorga E, Raymond PA, Melack JM, Doney SC, et al. (2011) Riverine coupling of biogeochemical cycles between land, oceans, and atmosphere. *Front Ecol Environ* 9: 53–60.
- Butman D, Raymond PA (2011) Significant efflux of carbon dioxide from streams and rivers in the United States. *Nature Geosc* 4: 839–842.
- Raymond PA, Hartmann J, Lauerwald R, Sobek S, McDonald C, et al. (2013) Global carbon dioxide emissions from inland waters. *Nature* 503: 355–359.
- Takahashi T, Sutherland SC, Wanninkhof R, Sweeney C, Feely RA, et al. (2009) Climatological mean and decadal change in surface ocean pCO₂, and net sea-air CO₂ flux over the global oceans. *Deep-Sea Res. II* 56: 554–577.
- Sobek S, Tranvik IJ, Cole JJ (2005) Temperature independence of carbon dioxide supersaturation in global lakes. *Global Biogeochem Cycles* 19(GB2003): doi:10.1029/2004GB002264.
- Ludwig W, Probst JL, Kempe S (1996) Predicting the oceanic input of organic carbon by continental erosion. *Global Biogeochem Cycles* 10: 23–41.
- Lehner B, Döll P (2004) Development and validation of a global database of lakes, reservoirs and wetlands. *J Hydrol* 296: 1–22.
- Darchambeau F, Sarmiento H, Descy J-P (2014) Primary production in a tropical large lake: The role of phytoplankton composition. *Sci Total Environ* 473–474: 178–188.
- Stenuite S, Pirlot S, Tarbe AL, Sarmiento H, Lecomte M, et al. (2009) Abundance and production of bacteria, and relationship to phytoplankton

Supporting Information

Table S1 Data-set of depth (m), water temperature (°C), specific conductivity at 25°C (μS cm⁻¹), oxygen saturation level (%O₂, %), δ¹³C signature of dissolved inorganic carbon (DIC) (δ¹³C-DIC, ‰), total alkalinity (TA, mmol L⁻¹), pH, partial pressure of CO₂ (pCO₂, ppm), dissolved methane concentration (CH₄, mmol L⁻¹), particulate organic carbon (POC, mg L⁻¹), δ¹³C signature of POC (δ¹³C-POC, ‰), dissolved organic carbon (DOC, mg L⁻¹), δ¹³C signature of DOC (δ¹³C-DOC, ‰), total suspended matter (TSM, mg L⁻¹) in Lake Kivu and 12 rivers flowing into Lake Kivu, in March 2007, September 2007, June 2008, April 2009 and October 2010. (XLS)

Acknowledgments

We are grateful to Pascal Isumbisho Mwapu (Institut Supérieur Pédagogique, Bukavu, République Démocratique du Congo) and Laetitia Nyinawamwiza (National University of Rwanda, Butare, Rwanda) and their respective teams for logistical support during the cruises, to Bruno Delille, Gilles Lepoint, Bruno Leporcq, and Marc-Vincent Commarieu for help in field sampling, to an anonymous reviewer and Pirkko Kortelainen (reviewer) for constructive comments on a previous version of the manuscript.

Author Contributions

Conceived and designed the experiments: AVB SB PS JPD FD. Performed the experiments: AVB CM FD. Analyzed the data: AVB CM SB PS JPD FD. Contributed reagents/materials/analysis tools: AVB CM SB PS JPD FD. Wrote the paper: AVB CM SB PS JPD FD.

- production, in a large tropical lake (Lake Tanganyika). *Freshwater Biol* 54: 1300–1311.
- Damas H (1937) La stratification thermique et chimique des lacs Kivu, Edouard et Ndalaga (Congo Belge). *Verh Internat Verein Theor Angew Limnol* 8: 51–68.
- Degens ET, vos Herzes RP, Wosg H-K, Deuser WG, Jannasch HW (1973) Lake Kivu: Structure, chemistry and biology of an East African rift lake. *Geol Rundsch* 62: 245–277.
- Schmid M, Halbwachs M, Wehrli B, Wüest A (2005) Weak mixing in Lake Kivu: new insights indicate increasing risk of uncontrolled gas eruption. *Geochem Geophys Geosyst* 6(Q07009): doi:10.1029/2004GC000892.
- Thierry W, Stepanenko VM, Fang X, Jöhnk KD, Li Z, et al. (2014) LakeMIP Kivu: Evaluating the representation of a large, deep tropical lake by a set of one-dimensional lake models. *Tellus A* 66(21390): doi:10.3402/tellusa.v66.21390.
- Sarmiento H, Isumbisho M, Descy J-P (2006) Phytoplankton ecology of Lake Kivu (Eastern Africa). *J Plankton Res* 28: 815–829.
- Sarmiento H, Darchambeau F, Descy J-P (2012) Phytoplankton of Lake Kivu. In: *Lake Kivu - Limnology and biogeochemistry of a tropical great lake*: Springer. pp. 67–83.
- Schmid M, Busbridge M, Wüest A (2010) Double-diffusive convection in Lake Kivu. *Limnol Oceanogr* 55: 225–238.
- Schoell M, Tietze K, Schoberth SM (1988) Origin of methane in Lake Kivu (East-Central Africa). *Chem Geol* 71: 257–265.
- Schmid M, Tietze K, Halbwachs M, Lorke A, McGinnis D, et al. (2004) How hazardous is the gas accumulation in Lake Kivu? Arguments for a risk assessment in light of the Nyiragongo Volcano eruption of 2002. *Acta Vulcanol* 14/15: 115–121.
- Nayar A (2009) A lakeful of trouble. *Nature* 460: 321–323.
- Wüest A, Jarc L, Bürgmann H, Pasche N, Schmid M (2012) Methane Formation and Future Extraction in Lake Kivu. In: *Lake Kivu - Limnology and biogeochemistry of a tropical great lake*: Springer. pp. 165–180.
- Borges AV, Abril G, Delille B, Descy J-P, Darchambeau F (2011) Diffusive methane emissions to the atmosphere from Lake Kivu (Eastern Africa) *J Geophys Res* 116(G03032): doi:10.1029/2011JG001673.
- Schmid M, Wüest A (2012) Stratification, Mixing and Transport Processes in Lake Kivu. In: *Lake Kivu - Limnology and biogeochemistry of a tropical great lake*: Springer. pp. 13–29.
- Frankignoulle M, Borges A, Biondo R (2001) A new design of equilibrator to monitor carbon dioxide in highly dynamic and turbid environments. *Water Res* 35: 1344–1347.
- Frankignoulle M, Borges AV (2001) Direct and indirect pCO₂ measurements in a wide range of pCO₂ and salinity values (the Scheldt estuary). *Aquat Geochem* 7: 267–273.

32. Gran G (1952) Determination of the equivalence point in potentiometric titrations of seawater with hydrochloric acid. *Oceanol Acta* 5: 209–218.
33. Millero FJ, Graham TB, Huang F, Bustos-Serrano H, Pierrot D (2006) Dissociation constants of carbonic acid in sea water as a function of salinity and temperature. *Mar Chem* 100: 80–94.
34. Miyajima T, Yamada Y, Hanba YT, Yoshii K, Koitabashi T, et al. (1995) Determining the stable-isotope ratio of total dissolved inorganic carbon in lake water by GC/C/IRMS. *Limnol Oceanogr* 40: 994–1000.
35. Steemann-Nielsen E (1951) Measurement of production of organic matter in sea by means of carbon-14. *Nature* 267: 684–685.
36. Descy J-P, Higgins HW, Mackey DJ, Hurley JP, Frost TM (2000) Pigment ratios and phytoplankton assessment in northern Wisconsin lakes. *J Phycol* 36: 274–286.
37. Fuhrman JA, Azam F (1982) Thymidine incorporation as a measure of heterotrophic bacterioplankton production in marine surface waters: Evaluation and field results. *Mar Biol* 66: 109–120.
38. Del Giorgio PA, Cole JJ (1998) Bacterial growth efficiency in natural aquatic systems. *Annu Rev Ecol Syst* 29: 503–41.
39. Weiss RF, Price BA (1980) Nitrous oxide solubility in water and seawater. *Mar Chem* 8: 347–359.
40. Weiss RF (1974) Carbon dioxide in water and seawater: the solubility of a non-ideal gas. *Mar Chem* 2: 203–215.
41. Cole JJ, Caraco NF (1998) Atmospheric exchange of carbon dioxide in a low-wind oligotrophic lake measured by the addition of SF₆. *Limnol Oceanogr* 43: 647–656.
42. Wanninkhof R (1992) Relationship between wind speed and gas exchange over the ocean. *J Geophys Res* 97: 7373–7382.
43. Muvundja FA, Pasche N, Bugenyi FWB, Isumbiso M, Müller B, et al. (2009) Balancing nutrient inputs to Lake Kivu. *J Great Lakes Res* 35: 406–418.
44. Quay PD, Stutsman J, Feely RA, Juranek W (2009) Net community production rates across the subtropical and equatorial Pacific Ocean estimated from air-sea $\delta^{13}\text{C}$ disequilibrium. *Global Biogeochem Cycles* 23 (GB2006): doi:10.1029/2008GB003193.
45. Quay PD, Stutsman J (2003) Surface layer carbon budget for the subtropical N. Pacific: $\delta^{13}\text{C}$ constraints at station ALOHA. *Deep-Sea Res I* 50: 1045–1061.
46. Emrich K, Ehhalt DH, Vogel JC (1970) Carbon isotope fractionation during the precipitation of calcium carbonate. *Earth Planet Sci Lett* 8: 363–371.
47. Zhang J, Quay PD, Wilbur DO (1995) Carbon isotope fractionation during gas-water exchange and dissolution of CO₂. *Geochim Cosmochim Acta* 59: 107–114.
48. Atilla N, McKinley GA, Bennington V, Baehr M, Urban N, et al. (2011) Observed variability of Lake Superior pCO₂. *Limnol Oceanogr* 56: 775–786.
49. Cole JJ, Caraco NF, Kling GW, Kratz TK (1994) Carbon dioxide supersaturation in the surface waters of lakes. *Science* 265: 1568–1570.
50. McConnaughey TA, LaBaugh JW, Rosenberry DO, Striegl RG, Reddy MM, et al. (1994) Carbon budget for a groundwater-fed lake: Calcification supports summer photosynthesis. *Limnol Oceanogr* 39: 1319–1332.
51. Gelbrecht J, Fait M, Dittrich M, Steinberg C (1998) Use of GC and equilibrium calculations of CO₂ saturation index to indicate whether freshwater bodies in north-eastern Germany are net sources or sinks for atmospheric CO₂. *Fresenius J Anal Chem* 361: 47–53.
52. Striegl RG, Michmerhuizen CM (1998) Hydrologic influence on methane and carbon dioxide dynamics at two north-central Minnesota lakes. *Limnol Oceanogr* 43: 1519–1529.
53. Riera JL, Schindler JE, Kratz TK (1999) Seasonal dynamics of carbon dioxide and methane in two clear-water lakes and two bogs lakes in northern Wisconsin, U.S.A. *Can J Fish Aquat Sci* 56: 265–274.
54. Kelly CA, Fee E, Ramlal PS, Rudd JWM, Hesslein RH, et al. (2001) Natural variability of carbon dioxide and net epilimnetic production in the surface waters of boreal lakes of different sizes. *Limnol Oceanogr* 46: 1054–1064.
55. Marotta H, Duarte CM, Sobek S, Enrich-Prast A (2009) Large CO₂ disequilibria in tropical lakes. *Global Biogeochem Cycles*, 23(GB4022): doi:10.1029/2008GB003434.
56. Duarte CM, Prairie YT, Montes C, Cole JJ, Striegl R, et al. (2008) CO₂ emissions from saline lakes: A global estimate of a surprisingly large flux. *J Geophys Res* 113 (G04041): doi:10.1029/2007JG000637.
57. Pérez NM, Hernández PA, Padilla G, Nolasco D, Barrancos J, et al. (2011) Global CO₂ emission from volcanic lakes. *Geology* 39: 235–238.
58. Kortelainen P, Rantakari M, Huttunen JT, Mattsson T, Alm J, et al. (2006) Sediment respiration and lake trophic state are important predictors of large CO₂ evasion from small boreal lakes. *Global Change Biol* 12: 1554–1567.
59. Kortelainen P, Rantakari M, Pajunen H, Huttunen JT, Mattsson T, et al. (2013) Carbon evasion/accumulation ratio in boreal lakes is linked to nitrogen. *Global Biogeochem Cycles* 27: 363–374.
60. Roehm CL, Prairie YT, del Giorgio PA (2009) The pCO₂ dynamics in lakes in the boreal region of northern Quebec, Canada. *Global Biogeochem Cycles* 23(GB3013): doi:10.1029/2008GB003297.
61. Lapierre J-F, del Giorgio PA (2012) Geographical and environmental drivers of regional differences in lake pCO₂ versus DOC relationship across northern landscapes. *J Geophys Res* 117(G03015): doi:10.1029/2012JG001945.
62. IPCC (2007) Climate Change 2007: The Physical Science Basis. Contribution of Working Group I In: Fourth Assessment Report of the Intergovernmental Panel on Climate: Cambridge University Press. pp. 1–996
63. Finlay K, Leavitt PR, Wissel B, Prairie YT (2009) Regulation of spatial and temporal variability of carbon flux in six hard-water lakes of the northern Great Plains. *Limnol Oceanogr* 54: 2553–2564.
64. Whitfield PH, van der Kamp G, St-Hilaire A (2009) Predicting the partial pressure of carbon dioxide in boreal lakes. *Can Water Resour J* 34: 303–310.
65. Einola E, Rantakari M, Kankaala P, Kortelainen P, Ojala A, et al. (2011) Carbon pools and fluxes in a chain of five boreal lakes: A dry and wet year comparison. *J Geophys Res* 116(G03009): doi:10.1029/2010JG001636.
66. Rantakari M, Kortelainen P (2008) Controls of total organic and inorganic carbon in randomly selected Boreal lakes in varied catchments. *Biogeochemistry* 91: 151–162.
67. Finlay K, Leavitt PR, Patoine A, Wissel B (2010) Magnitudes and controls of organic and inorganic carbon flux through a chain of hardwater lakes on the northern Great Plains. *Limnol Oceanogr* 55: 1551–1564.
68. Tamoooh F, Van den Meersche K, Meysman F, Marwick TR, Borges AV, et al. (2012) Distribution and origin of suspended matter and organic carbon pools in the Tana River Basin, Kenya. *Biogeochemistry* 9: 2905–2920.
69. Lehmann MF, Bernasconi SM, McKenzie JA, Barbieri A, Simona M, et al. (2004) Seasonal variation of the $\delta^{13}\text{C}$ and $\delta^{15}\text{N}$ of particulate and dissolved carbon and nitrogen in Lake Lugano: Constraints on biogeochemical cycling in a eutrophic lake. *Limnol Oceanogr* 49: 415–429.
70. Morana C, Sarmiento H, Descy J-P, Gasol JM, Borges AV, et al. (2014) Production of dissolved organic matter by phytoplankton and its uptake by heterotrophic prokaryotes in large tropical lakes. *Limnol Oceanogr* 59: 1364–1375.
71. Pasche N, Alunga G, Mills K, Muvundja F, Ryves DB, et al. (2010) Abrupt onset of carbonate deposition in Lake Kivu during the 1960s: response to recent environmental changes. *J Paleolimnol* 44: 931–946.
72. Dittrich M, Obst M (2004) Are picoplankton responsible for calcite precipitation in lakes? *Ambio* 33: 559–564.
73. Obst M, Wehrli B, Dittrich M (2009) CaCO₃ nucleation by cyanobacteria: laboratory evidence for a passive, surface-induced mechanism. *Geobiology* 7: 324–347.
74. Nimick DA, Gammons CH, Parker SR (2011) Diel biogeochemical processes and their effect on the aqueous chemistry of streams: A review. *Chem Geol* 283: 3–17.
75. Pilskaln CH (2004) Seasonal and interannual particle export in an African rift valley lake: A 5-yr record from Lake Malawi, southern East Africa. *Limnol Oceanogr* 49: 964–977.
76. Broecker WS, Peng TH (1982) Tracers in the sea. Eldigio Press.
77. Shaffer G (1993) Effects of the marine carbon biota on global carbon cycling. In: *The Global Carbon Cycle*. Berlin: Springer Verlag. pp. 431–455.
78. Yamanaka Y, Tajika E (1996) The role of the vertical fluxes of particulate organic matter and calcite in the oceanic carbon cycle: Studies using an ocean biogeochemical general circulation model. *Global Biogeochem Cycles* 10: 361–382.
79. Baines SB, Pace ML, Karl DM (1994) Why does the relationship between sinking flux and planktonic primary production differ between lakes and the ocean? *Limnol Oceanogr* 39: 213–226.
80. Baines SB, Pace ML (1991) The production of dissolved organic matter by phytoplankton and its importance to bacteria: patterns across marine and freshwater systems. *Limnol Oceanogr* 36: 1078–1090.
81. Moran XAG, Gasol JM, Pedros-Alio C, Estrada M (2001) Dissolved and particulate primary production and bacterial production in offshore Antarctic waters during austral summer: coupled or uncoupled? *Mar Ecol Prog Ser* 222: 25–30.
82. Moran XAG, Estrada M, Gasol JM, Pedros-Alio C (2002) Dissolved primary production and the strength of phytoplankton-bacterioplankton coupling in constraining marine regions. *Microb Ecol* 44: 217–223.
83. Del Giorgio PA, Cole JJ, Caraco NF, Peters RH (1999) Linking planktonic biomass and metabolism to net gas fluxes in northern temperate lakes. *Ecology* 80: 1422–1431.
84. Prairie YT, Bird DF, Cole JJ (2002) The summer metabolic balance in the epilimnion of southeastern Quebec lakes. *Limnol Oceanogr* 47: 316–321.
85. Algesten G, Sobek S, Bergstrom A-K, Agren A, Tranvik IJ, et al. (2004) Role of lakes for organic carbon cycling in the boreal zone. *Global Change Biol* 10: 141–147.
86. Hanson PC, Bade DL, Carpenter SR, Kratz TK (2003) Lake metabolism: Relationships with dissolved organic carbon and phosphorus. *Limnol Oceanogr* 48: 1112–1119.
87. Kosten S, Roland F, Da Motta Marques DML, Van Nes EH, Mazzeo N, et al. (2010) Climate-dependent CO₂ emissions from lakes. *Global Biogeochem Cycles* 24(GB2007): doi:10.1029/2009GB003618.
88. Balmer MB, Downing JA (2011) Carbon dioxide concentrations in eutrophic lakes: undersaturation implies atmospheric uptake. *Inland Waters* 1: 125–132.
89. Karim A, Dubois K, Veizer J (2011) Carbon and oxygen dynamics in the Laurentian Great Lakes: Implications for the CO₂ flux from terrestrial aquatic systems to the atmosphere. *Chem Geol* 281: 133–141.
90. Hope D, Kratz TK, Riera JL (1996) The relationship between pCO₂ and dissolved organic carbon in the surface waters of 27 northern Wisconsin lakes. *J Environ Qual* 49: 1442–1445.
91. Stets EG, Striegl RG, Aiken GR, Rosenberry DO, Winter TC (2009) Hydrologic support of carbon dioxide flux revealed by whole-lake carbon budgets. *J Geophys Res* 114(G01008): doi:10.1029/2008JG000783.

92. Maberly SC, Barker PA, Stott AW, De Ville MM (2012) Catchment productivity controls CO₂ emissions from lakes. *Nat Clim Chang* doi:10.1038/NCLIMATE1748.
93. McDonald CP, Stets EG, Striegl RG, Butman D (2013) Inorganic carbon loading as a primary driver of dissolved carbon dioxide concentrations in the lakes and reservoirs of the contiguous United States. *Global Biogeochem Cycles* 27: doi:10.1002/gbc.20032.
94. Dubois K, Carignan R, Veizer J (2009) Can pelagic net heterotrophy account for carbon fluxes from eastern Canadian lakes? *Appl Geochem* 24: 988–998.
95. Humborg C, Mörth C-M, Sundbom M, Borg H, Blenckner T, et al. (2010) CO₂ supersaturation along the aquatic conduit in Swedish watersheds as constrained by terrestrial respiration, aquatic respiration and weathering. *Global Change Biol* 16: 1966–1978.
96. Spigel RH, Coulter GW (1996) Comparison of hydrology and physical limnology of the East African Great Lakes: Tanganyika, Malawi, Victoria, Kivu and Turkana (with reference to some North American Great Lakes). In: Johnson TC, Odada EO, editors. *The limnology, climatology and paleoclimatology of the East African lakes*. Boca Raton, FL: Gordon and Breach Publishers. pp. 103-139.

Globally significant greenhouse-gas emissions from African inland waters

Alberto V. Borges^{1*}, François Darchambeau¹, Cristian R. Teodoru², Trent R. Marwick², Fredrick Tamooch^{2,3}, Naomi Geeraert², Fredrick O. Omengo², Frédéric Guérin⁴, Thibault Lambert¹, Cédric Morana², Eric Okuku^{2,5} and Steven Bouillon²

Carbon dioxide emissions to the atmosphere from inland waters—streams, rivers, lakes and reservoirs—are nearly equivalent to ocean and land sinks globally. Inland waters can be an important source of methane and nitrous oxide emissions as well, but emissions are poorly quantified, especially in Africa. Here we report dissolved carbon dioxide, methane and nitrous oxide concentrations from 12 rivers in sub-Saharan Africa, including seasonally resolved sampling at 39 sites, acquired between 2006 and 2014. Fluxes were calculated from published gas transfer velocities, and upscaled to the area of all sub-Saharan African rivers using available spatial data sets. Carbon dioxide-equivalent emissions from river channels alone were about 0.4 Pg carbon per year, equivalent to two-thirds of the overall net carbon land sink previously reported for Africa. Including emissions from wetlands of the Congo river increases the total carbon dioxide-equivalent greenhouse-gas emissions to about 0.9 Pg carbon per year, equivalent to about one quarter of the global ocean and terrestrial combined carbon sink. Riverine carbon dioxide and methane emissions increase with wetland extent and upland biomass. We therefore suggest that future changes in wetland and upland cover could strongly affect greenhouse-gas emissions from African inland waters.

Climate predictions necessitate a full and robust account of natural and anthropogenic greenhouse-gas (GHG) fluxes, especially for CO₂ (refs 1–3), CH₄ (ref. 4) and N₂O (ref. 5), which together accounted for 94% of the anthropogenic global radiative forcing by well-mixed GHGs in 2011 relative to 1750 (ref. 6). Inland waters (streams, rivers, lakes and reservoirs) are increasingly recognized as important sources of GHGs to the atmosphere, with global CO₂ and CH₄ emissions estimated at 2.1 PgC yr⁻¹ (ref. 3) and 0.7 PgC yr⁻¹ (CO₂-equivalents; CO₂e) (ref. 4) (1 Pg = 10¹⁵ g), respectively. Considering that the oceanic and land carbon (C) sinks correspond to ~1.5 and ~2.0 PgC yr⁻¹ (ref. 7), respectively, the GHG flux from inland waters is significant in the global C budget.

In a recent global compilation of inland CO₂ data³, <20 data points (out of 6,708, that is, <0.3%) represented African inland waters (with the exception of South Africa, which has been densely sampled), even though they account for ~12% of both global freshwater discharge⁸ and riverine surface area³, and include some of the largest rivers and lakes in the world. Equally for the global CH₄ database, there is a strong under-representation of tropical inland waters, whereby a recent synthesis⁴ resorted to extrapolating CH₄ fluxes from temperate rivers.

The prevailing large uncertainty involved in GHG flux estimates for inland waters, essentially due to the paucity of available data, is coupled to a poor understanding of underlying processes, both of which preclude gauging of future fluxes in response to human pressures. In particular, there is a need to further understand the link between inland water GHG fluxes and catchment characteristics, in particular regarding their connectivity with upland terrestrial^{9,10}

and wetland^{11–13} C production and stocks. The CO₂ emissions from inland waters have been traditionally interpreted as fuelled by organic C from upland terrestrial biomass^{1,14}. In the Amazon basin, CO₂ emissions from floodplain lakes¹¹ and from river channels^{12,13} have been attributed to organic and inorganic C from wetlands (flooded forest and macrophytes). Finally, recently recognized biases in computed CO₂ data traditionally used in inland water studies^{15,16} highlight the requirement for careful data-quality checking and future emphasis on high-quality direct CO₂ measurements.

In this study, we report an extensive compilation of dissolved CO₂, CH₄ and N₂O concentrations (Supplementary Table 1) gathered in 12 river basins in sub-Saharan Africa (SSA; Fig. 1 and Supplementary Fig. 1). The rivers range from 7.8 × 10³ to 3.7 × 10⁶ km² in watershed area and from 1.9 to 1.3 × 10³ km³ yr⁻¹ in discharge, including the largest in Africa (Supplementary Table 2). A wide size range was sampled, from <1 m width (headwaters) to ~10 km width (mainstem Congo).

Variability of GHG concentrations and fluxes

The partial pressure of CO₂ (p_{CO_2}) values spanned two orders of magnitude, ranging between 300 and 16,942 ppm, CH₄ concentrations varied over five orders of magnitude, ranging between 2 and 62,966 nmol l⁻¹, whereas N₂O spanned three orders of magnitude, ranging between 0.2 and 85.4 nmol l⁻¹ (Supplementary Fig. 2). The Congo River was the most variable in GHG concentrations, with distinct differences between streams (<100 m width) and rivers (>100 m width): p_{CO_2} and CH₄ values were higher in streams than rivers, whereas the opposite was observed for N₂O and oxygen saturation level

¹Université de Liège, Unité d'Océanographie Chimique, Institut de Physique (B5), B-4000, Belgium. ²Katholieke Universiteit Leuven, Department of Earth and Environmental Sciences, Celestijnenlaan 200E, B-3001 Leuven, Belgium. ³Kenyatta University, Department of Zoological Sciences, PO Box 16778-80100, Mombasa, Kenya. ⁴Geosciences Environnement Toulouse UMR 5563 & UR 234 IRD, Université Paul-Sabatier, Avenue Edouard Belin 14, F-31400 Toulouse, France. ⁵Kenya Marine and Fisheries Research Institute, PO Box 81651, Mombasa-80100, Kenya.

*e-mail: alberto.borges@ulg.ac.be

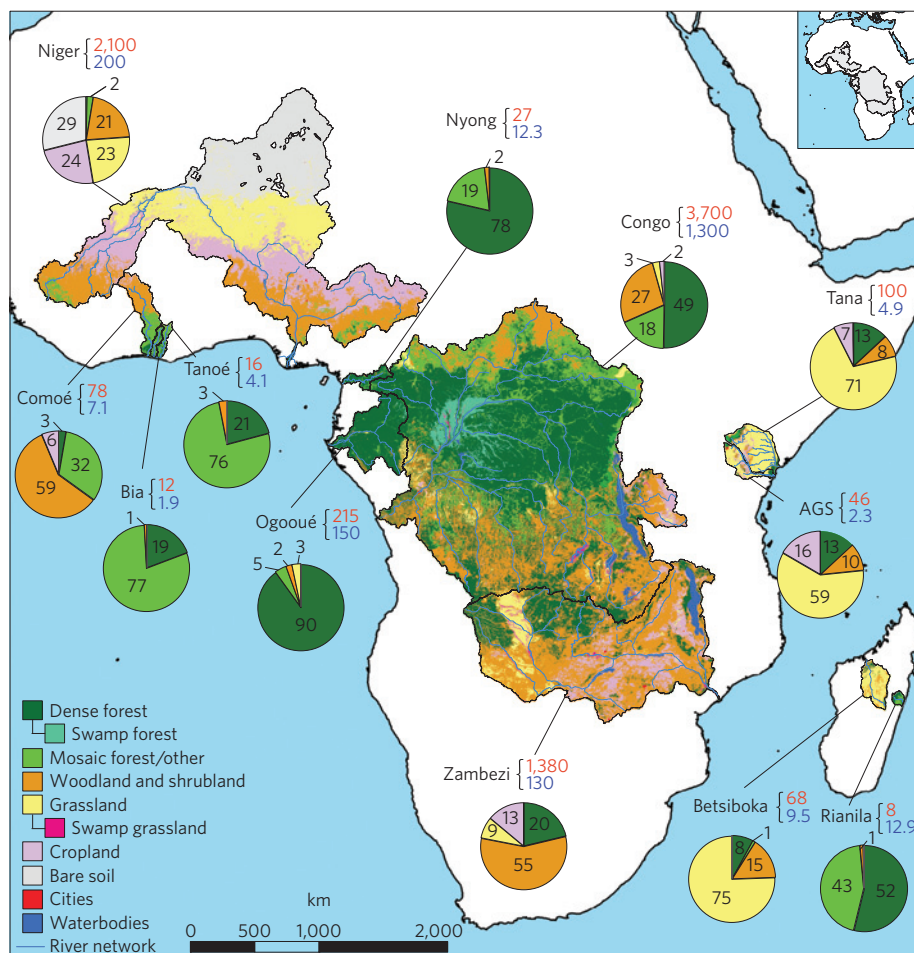


Figure 1 | The 12 studied rivers cover a wide range of discharge, catchment size and land cover. The red numbers correspond to the catchment surface area (10^3 km^2) and the blue numbers correspond to the annual freshwater discharge ($\text{km}^3 \text{ yr}^{-1}$). Refer to Methods for data sources. AGS, Athi-Galana-Sabaki River.

(% O_2) (Supplementary Fig. 2). The overall average p_{CO_2} and CH_4 in rivers was $6,415 \text{ ppm}$ and $2,205 \text{ nmol l}^{-1}$, respectively, corresponding to large over-saturation of surface waters with respect to atmospheric equilibrium of CO_2 and CH_4 (on average $\sim 395 \text{ ppm}$ and $\sim 2 \text{ nmol l}^{-1}$, respectively). The N_2O values oscillated between under- and over-saturation, with an overall average of 9.2 nmol l^{-1} , only slightly above the atmospheric equilibrium of $\sim 6.6 \text{ nmol l}^{-1}$.

The fluxes were computed from the gas transfer velocity (k) using two approaches. The Aufdenkampe *et al.* (Auf) approach² relies on constant k values across basins separated into streams and rivers ($<100 \text{ m}$ and $>100 \text{ m}$ width, respectively). The Raymond *et al.* (Ray) approach³ uses basin-specific k values computed from hydraulic equations and basin characteristics. We present both estimates to provide a range of flux values, allowing a comparison with published fluxes. An error analysis is provided in the Supplementary Methods and Methods. Among river systems, the air–water CO_2 fluxes computed with the Auf approach ($\text{FCO}_{2\text{Auf}}$) ranged between 186 ± 9 and $1,149 \pm 53 \text{ mmol m}^{-2} \text{ d}^{-1}$, the air–water CH_4 fluxes ($\text{FCH}_{4\text{Auf}}$) ranged between 0.5 ± 0.1 and $18 \pm 1 \text{ mmol m}^{-2} \text{ d}^{-1}$, and the air–water N_2O fluxes ($\text{FN}_{2\text{O}\text{Auf}}$) ranged between 2.0 ± 0.1 and $16 \pm 1 \mu\text{mol m}^{-2} \text{ d}^{-1}$ (Supplementary Table 3). The fluxes computed using the Ray approach were ~ 1.34 times higher, as it accounts for lower-order streams that are more turbulent and have higher k values. The average FCO_2 for all rivers was 11 times higher than FCH_4 (in CO_2e) and 273 times higher than $\text{FN}_{2\text{O}}$ (in CO_2e). For individual basins, the $\text{FCO}_2:\text{FCH}_4$ ratio

ranged between 4 (Zambezi) and 39 (Tana). This is in contrast to other concurrent FCO_2 , FCH_4 and $\text{FN}_{2\text{O}}$ estimates in temperate rivers (Supplementary Table 4), where $\text{FCO}_2:\text{FCH}_4$ ratios are higher (between 9 and 411, average 108) and $\text{FCO}_2:\text{FN}_{2\text{O}}$ ratios are lower (between 10 and 71, average 35). This reflects the less extensive flooded areas in these temperate rivers (floodplains promote FCH_4 compared to FCO_2), and higher inputs of fertilizer- or wastewater-derived nitrogen, which promote $\text{FN}_{2\text{O}}$ (ref. 5) compared to FCO_2 .

The $\text{FCO}_{2\text{Ray}}$ we report were 1.1–4.7 times (on average 2.6 times) higher than those given by Raymond *et al.*³ for the same basins (Supplementary Fig. 3), suggesting that the reliance of the latter on a very limited African p_{CO_2} database resulted in underestimating the riverine FCO_2 for the African continent. When comparing the surface-area-integrated FCO_2 per basin (Supplementary Table 3) to the flux of total organic C (TOC) and dissolved inorganic C (DIC) to the ocean for the Congo, the Zambezi and the Tana (data are unavailable for other rivers sampled), FCO_2 was, respectively, 8.6, 2.1 and 9.9 times higher than the TOC+DIC export to the ocean, or 13.3, 16.5 and 23.0 times higher than the TOC export to the ocean. By comparison, in the Amazon River, the total FCO_2 is 6.6 and 13.1 times higher than the TOC+DIC and TOC export to the ocean¹⁴. This clearly highlights the significance of vertical C fluxes from inland waters to the atmosphere.

Regional and global significance of GHG fluxes

The FCO_2 integrated for all SSA rivers ranged between 0.27 ± 0.05 (Auf) and 0.37 ± 0.07 (Ray) PgC yr^{-1} . Such values are of the same

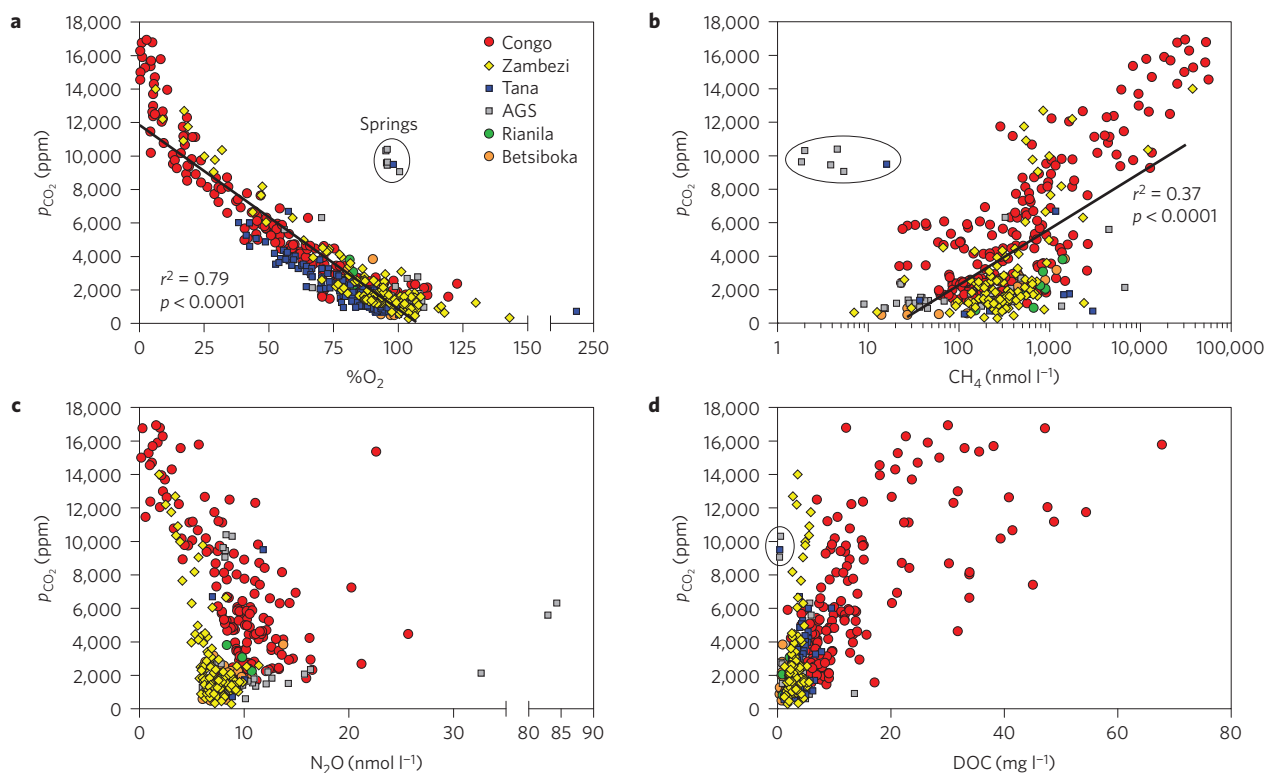


Figure 2 | Complex interplay of biogeochemical processes is revealed by GHGs property-property relations. p_{CO_2} as functions of % O_2 (a), log CH_4 (b), N_2O (c) and DOC (d) in six African river systems. The encircled data points correspond to water from springs that are enriched in CO_2 , depleted in CH_4 and DOC owing to bacterial removal in groundwaters and at O_2 saturation owing to rapid equilibration with the atmosphere. Lines correspond to a linear regression fit.

order of magnitude as the integrated FCO_2 for the Amazon River of 0.47 PgC yr^{-1} (ref. 14), although the latter estimate included wetlands that accounted for 86% of flooded land whereas river channels only occupied 14% (ref. 13). The FCH_4 integrated for all rivers in SSA ranged between 2.9 ± 0.1 (Auf) and 3.9 ± 0.1 (Ray) TgC yr^{-1} . This is roughly five times higher than the FCH_4 recently attributed for all tropical rivers (0.7 TgC yr^{-1}) in a recent data synthesis⁴, where, in the absence of empirical data from the tropics, the average CH_4 flux from temperate rivers was upscaled. The sum of integrated FCO_2 and FCH_4 ranged between 0.29 ± 0.05 (Auf) and 0.39 ± 0.07 (Ray) $\text{PgCO}_2\text{e yr}^{-1}$. These values are highly significant when compared to other fluxes at the scale of the African continent given by the most recent overarching synthesis⁸, such as the C emission from fossil fuel ($\sim 1.25 \text{ PgC yr}^{-1}$), terrestrial net ecosystem production (NEP) ($1.2\text{--}2.9 \text{ PgC yr}^{-1}$), or TOC+DIC export to the ocean (0.06 PgC yr^{-1}). The emission of CO_2 and CH_4 in CO_2e from SSA rivers would thus balance two-thirds of the reported net C sink for continental Africa ($0.6 \pm 0.6 \text{ PgC yr}^{-1}$; ref. 8). Note that the net C sink estimate of the latter did not account for the fluxes from inland waters.

We propose that our emission estimates of CO_2 and CH_4 from SSA rivers may be conservative for two reasons. First, the FCH_4 values correspond only to diffusive emissions and do not account for CH_4 ebullition, which can be highly significant in tropical aquatic environments^{17–19}. Based on floating chamber flux measurements in the Congo and Zambezi rivers ($n = 68$), we found CH_4 ebullition rates to be on average 0.25 times the diffusive CH_4 flux (Supplementary Fig. 4). This compares well with data from six Amazon river channels, where CH_4 ebullition was 0.33 times the diffusive CH_4 flux¹⁹. Applying a factor of 0.25 to estimate the CH_4 ebullition, the sum of integrated FCO_2 and FCH_4 would then range between 0.30 ± 0.05 (Auf) and 0.40 ± 0.07 (Ray)

$\text{PgCO}_2\text{e yr}^{-1}$. Second, our estimates do not account for extensive tropical wetlands, which in the Amazon are known to show CH_4 fluxes two orders of magnitude higher than river channels¹⁷. The Congolese ‘Cuvette Centrale’, with a flooded surface area of $360 \times 10^3 \text{ km}^2$ (ref. 20), is the second largest tropical wetland area after the Amazon. The sum of FCO_2 and FCH_4 from the ‘Cuvette Centrale’ would correspond to $0.48 \pm 0.08 \text{ PgCO}_2\text{e yr}^{-1}$ (based on the scaling of a subset of fluxes from the rivers, streams and navigation channels draining the ‘Cuvette Centrale’ and computed with the k recommended for flooded areas²). The above FCH_4 estimate for the ‘Cuvette Centrale’ does not include the ebullition of CH_4 ; using a reported ebullition:diffusion ratio of 0.73 for tropical wetlands¹⁸ would bring the total FCO_2 and FCH_4 from SSA rivers and wetlands to range between 0.85 ± 0.10 (Auf) and 0.95 ± 0.11 (Ray) $\text{PgCO}_2\text{e yr}^{-1}$. These fluxes are significant beyond the African continental scale, considering that the global net CO_2 sink is at present estimated at 1.5 and 2.0 PgC yr^{-1} for the oceans and the terrestrial biosphere, respectively⁷.

Processes underlying GHG dynamics

Although it is crucial to quantify GHG fluxes, unravelling the underlying processes is equally important. This can be attempted with a correlation analysis with other biogeochemical variables and catchment characteristics. The p_{CO_2} data were well correlated to % O_2 and to the log of CH_4 (Fig. 2a,b), suggesting that the dynamics of the three variables were driven by net heterotrophy¹. The lowest N_2O values (below atmospheric equilibrium) were observed at the highest p_{CO_2} (Fig. 2c) and lowest % O_2 levels (Supplementary Fig. 5), suggesting the removal of N_2O by denitrification, as also reported in the Amazon floodplains²¹. No distinct relationship could be established between N_2O and either nitrate (NO_3^-), ammonium (NH_4^+), or dissolved inorganic nitrogen ($\text{DIN} = \text{NO}_3^- + \text{NH}_4^+$)

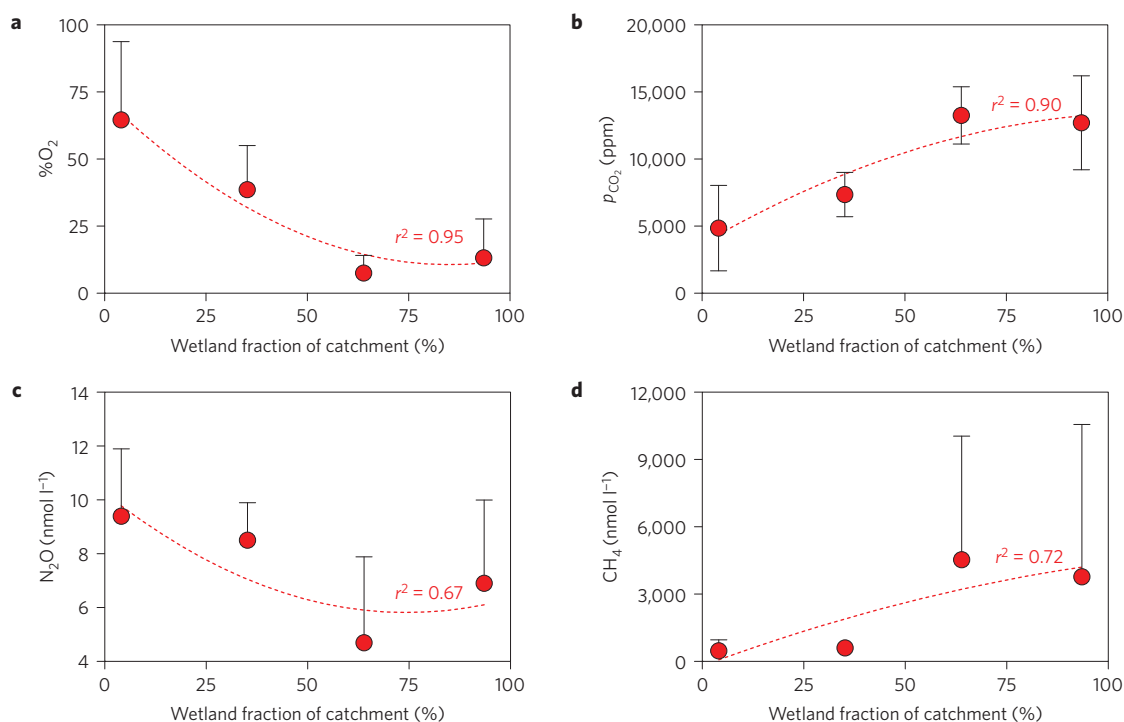


Figure 3 | Wetland presence drives the pattern of GHGs and O₂ in the Congo River. %O₂ (a), *p*CO₂ (b), N₂O (c) and CH₄ (d) in 46 rivers of the Congo basin as a function of wetland fraction of catchment surface. Data were bin-averaged in intervals of 25%. Two extreme CH₄ values (>25,000 nmol l⁻¹) were removed from the analysis. Error bars show mean ± s.d. Lines correspond to a second-degree polynomial fit.

(Supplementary Fig. 5), unlike in some temperate rivers⁵. In three of the sampled rivers, data sets from long-term fixed station monitoring showed a positive relationship between N₂O and NO₃⁻ (Supplementary Fig. 6). The sampled rivers had relatively low DIN values²², as fertilizer use is minimal within the catchments studied²³, and samples were not directly impacted by wastewaters from major cities; the only exception being the upper reaches of the Athi River, which are strongly influenced by wastewater inputs from Nairobi²² and where the highest N₂O concentrations were recorded (Supplementary Fig. 3).

No relationship could be established between GHGs and elevation or water temperature (Supplementary Fig. 7). There was a general positive relationship between *p*CO₂ and dissolved organic C (DOC) (Fig. 2d) that has been used to infer the role of terrestrial organic matter inputs in sustaining net heterotrophy and CO₂ production within inland waters⁹, although this can also be interpreted as an indication of concurrent DOC and CO₂ inputs from soils or wetlands. The *p*CO₂ in the Congo River levelled off for DOC concentrations >15 mg l⁻¹, which may indicate a limitation of bacterial growth (and subsequent CO₂ production) by the low pH in these very acidic organic environments (so called ‘black waters’, with pH between 3.6 and 5.9 and averaged 4.4), O₂ availability (%O₂ ranged between 0.3% and 93.5% and averaged 23.4%; Supplementary Fig. 8), or phosphorus availability as reported in other tropical black water rivers²⁴.

Concentrations of GHGs increased as the wetland fraction of the catchment surface increased for individual catchments (Congo River) and across river systems (Figs 3 and 4). In the Congo River, *p*CO₂ and CH₄ were positively related to wetland fraction, whereas %O₂ and N₂O were negatively related to the latter (Fig. 3). The CO₂, CH₄ and %O₂ patterns in the Congo tributaries along a 1,700 km river stretch (Supplementary Fig. 9) and in the Zambezi River²⁵ also follow the presence of wetlands. Similarly, a relationship between CH₄, *p*CO₂ and %O₂ with wetland fraction was also found across river systems (Fig. 4), consistent with findings in the Amazon basin,

where CO₂ emissions from wetland lakes and river channels have been attributed to organic C from wetlands^{11–13} that also sustain intense CH₄ evasion¹⁷.

However, basins that are virtually devoid of wetlands, such as the Tana (<0.5% of the catchment), were also found to be sources of CO₂, although admittedly lower than other SSA rivers. This suggests that part of the CO₂ emissions from SSA rivers are partly sustained by upland biomass. The increase of CO₂ and CH₄ and decrease of %O₂ in the Congo tributaries also follow the downstream increase of aboveground biomass and of the relative dense forest cover (Supplementary Figs 9 and 10). These patterns were also observed across river systems, although the Rianila catchment deviated from the general pattern owing to much steeper slopes within the basin (Supplementary Fig. 11). This highlights the role of relief, whereby gentle slopes increase water residence time and the extent of flooded areas, and steeper slopes enhance *k*, which drives dissolved GHG concentrations closer to saturation²⁶. Precipitation has been previously used to model river CO₂ regionally²⁶. We indeed found a positive relationship between *p*CO₂ and CH₄ and precipitation across SSA rivers, with the exception of the two Malagasy rivers (Supplementary Fig. 11). For the Rianila, this might also be related to the steeper slope. In the Betsiboka, nearly all of the yearly precipitation occurs from December to March, the rest of the year being extremely dry, leading to vegetation typical of a semi-arid climate. This suggests that models to predict *p*CO₂ from precipitation should also account for the regional differences in seasonal patterns.

Lateral inputs versus *in situ* respiration as CO₂ drivers

In addition to our GHG concentration measurements, we acquired 812 aquatic community respiration (*R*) data (Supplementary Fig. 12). The *R* values ranged between 0.3 and 404.0 mmolC m⁻³ d⁻¹, with a median of 20.0 mmolC m⁻³ d⁻¹, which is close to the median value of pelagic bacterial respiration reported in a recent data synthesis in tropical inland waters²⁷. On individual paired mea-

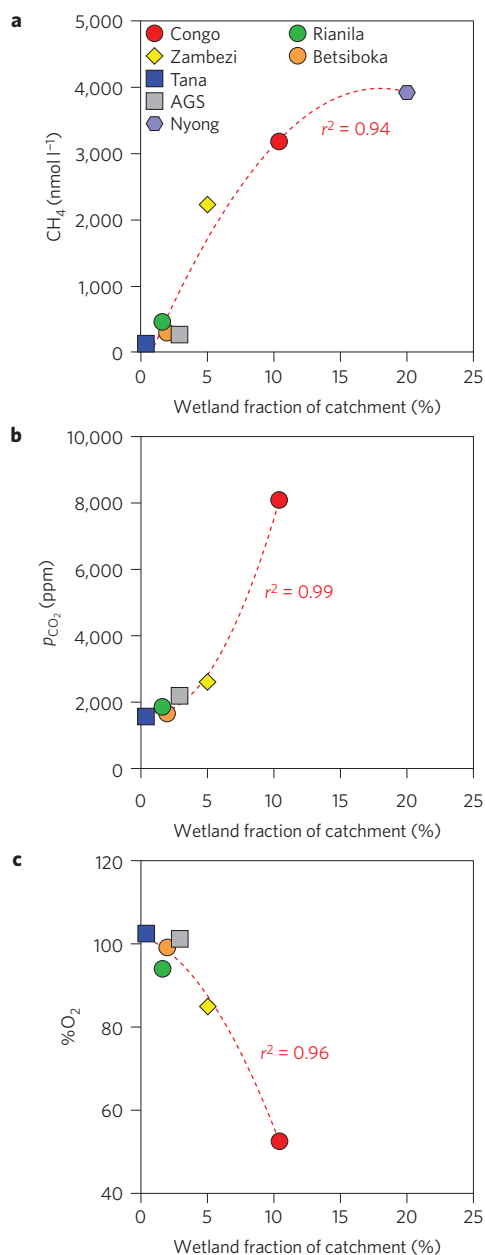


Figure 4 | Wetland presence drives the pattern of CO₂ and CH₄ concentrations across sub-Saharan African Rivers. p_{CO_2} (a), CH₄ (b) and %O₂ (c), as a function of the wetland fraction of catchment surface (%) in seven African rivers. Only the data sets that capture spatial variations were included in the analysis (excluding fixed time series in the mainstem of rivers). Lines correspond to a second-degree polynomial fit.

measurements, the FCO₂ was on average 8 times (Auf) to 12 times (Ray) higher than vertically integrated R ($n = 602$). The median R was 99.4 mmol C m⁻² d⁻¹, which, when upscaled to all SSA rivers, can account only for 11% of the FCO₂ (0.27 Pg C yr⁻¹). Although benthic respiration was not measured during our study, using the average value from a recent data synthesis for tropical rivers and streams (50.8 mmol C m⁻² d⁻¹; ref. 28), we find that pelagic and benthic R combined still account for only <14% of the FCO₂. Furthermore, these estimates do not account for pelagic and benthic aquatic primary production, which would decrease the dissolved CO₂ concentration. These calculations imply that lateral inputs of CO₂ from soils, groundwaters and wetlands would be the largest contributors of the CO₂ emitted from rivers and streams.

Implications for understanding global C fluxes

Large CO₂ fluxes from inland waters have significant implications for our understanding of overall C fluxes and cycling at the landscape or catchment scale. The CO₂ emitted to the atmosphere from inland waters can be considered as a component of the respiration of upland and wetland vegetation, whether it is related to lateral transport of soil/wetland CO₂ (that is, respiration taking place in terrestrial or wetland habitats) or lateral transport of soil or wetland DOC and POC that is mineralized to CO₂ within the aquatic domain. Hence, the lateral transport of C from the upland terrestrial biosphere and wetlands to inland waters and its subsequent emission to the atmosphere offsets the estimates of terrestrial NEP. Furthermore, lateral transport of soil DOC leads to an underestimation of NEP based on biomass accumulation techniques, whereas the lateral transport of soil CO₂ leads to an overestimation of NEP derived from atmospheric measurements (eddy-covariance or flux towers). The significant FCO₂ from African inland waters at the continental scale is particularly important in the context of the mitigation of, and accounting for, GHG emissions, as C emissions related to tropical deforestation are only partially offset by C sequestration from forest regrowth²⁹. Accounting for the additional C emissions from inland waters could further offset this balance. Alternatively, if most of the CO₂ emissions from SSA river channels are derived from wetland C, the net balance would be nearly neutral as it is balanced by the atmospheric CO₂ fixation by the emergent vegetation, as shown in the Amazon lowland areas^{11–13}. Untangling the relative contributions of wetland and upland C in sustaining CO₂ and CH₄ emissions from inland waters is essential to better understand the role of tropical inland waters in the global C cycle and related potential feedbacks on a warming climate. Our results in SSA rivers show that this relative contribution is variable both within individual catchments and across catchments.

Methods

Methods and any associated references are available in the [online version of the paper](#).

Received 19 February 2015; accepted 10 June 2015; published online 20 July 2015

References

- Cole, J. J. *et al.* Plumbing the global carbon cycle: Integrating inland waters into the terrestrial carbon budget. *Ecosystems* **10**, 171–184 (2007).
- Aufdenkampe, A. K. *et al.* Riverine coupling of biogeochemical cycles between land, oceans, and atmosphere. *Front. Ecol. Environ.* **9**, 53–60 (2011).
- Raymond, P. A. *et al.* Global carbon dioxide emissions from inland waters. *Nature* **503**, 355–359 (2013).
- Bastviken, D., Tranvik, L. J., Downing, J. A., Crill, P. M. & Enrich-Prast, A. Freshwater methane emissions offset the continental carbon sink. *Science* **331**, 50 (2011).
- Baulch, H. M., Schiff, S. L., Maranger, R. & Dillon, P. J. Nitrogen enrichment and the emission of nitrous oxide from streams. *Glob. Biogeochem. Cycles* **25**, GB4013 (2011).
- IPCC *Climate Change 2013: The Physical Science Basis* (eds Stocker, T. F. *et al.*) (Cambridge Univ. Press, 2013).
- Le Quéré, C. *et al.* Global carbon budget 2014. *Earth Syst. Sci. Data Discuss.* **7**, 521–610 (2014).
- Valentini, R. *et al.* A full greenhouse gases budget of Africa: Synthesis, uncertainties, and vulnerabilities. *Biogeosciences* **11**, 381–407 (2014).
- Lapierre, J.-F. & del Giorgio, P. A. Geographical and environmental drivers of regional differences in the lake p_{CO_2} versus DOC relationship across northern landscapes. *J. Geophys. Res.* **117**, G03015 (2012).
- Maberly, S. C., Barker, P. A., Stott, A. W. & De Ville, M. M. Catchment productivity controls CO₂ emissions from lakes. *Nature Clim. Change* **3**, 391–394 (2013).
- Melack, J. M. & Engle, D. L. An organic carbon budget for an Amazon floodplain lake. *Verh. Int. Verein. Limnol.* **30**, 1179–1182 (2009).

12. Engle, D. L., Melack, J. M., Doyle, R. D. & Fisher, T. R. High rates of net primary production and turnover of floating grasses on the Amazon floodplain: Implications for aquatic respiration and regional CO₂ flux. *Glob. Change Biol.* **14**, 369–381 (2008).
13. Abril, G. *et al.* Amazon River carbon dioxide outgassing fuelled by wetlands. *Nature* **505**, 395–398 (2014).
14. Richey, J. E., Melack, J. M., Aufdenkampe, A. K., Ballester, V. M. & Hess, L. Outgassing from Amazonian rivers and wetlands as a large tropical source of atmospheric CO₂. *Nature* **416**, 617–620 (2002).
15. Wang, Z. A. *et al.* Inorganic carbon speciation and fluxes in the Congo River. *Geophys. Res. Lett.* **40**, 511–516 (2013).
16. Abril, G. *et al.* Technical Note: Large overestimation of calculated pCO₂ in acidic, organic-rich freshwaters. *Biogeosciences* **12**, 67–78 (2015).
17. Melack, J. M. *et al.* Regionalization of methane emissions in the Amazon Basin with microwave remote sensing. *Glob. Change Biol.* **10**, 530–544 (2004).
18. Bastviken, D. *et al.* Methane emissions from Pantanal, South America, during the low water season: Toward more comprehensive sampling. *Environ. Sci. Technol.* **44**, 5450–5455 (2010).
19. Sawakuchi, H. O. *et al.* Methane emissions from Amazonian Rivers and their contribution to the global methane budget. *Glob. Change Biol.* **20**, 2829–2840 (2014).
20. Bwagoy, J.-R. B., Hansen, M. C., Roy, D. P., De Grandi, G. & Justice, C. O. Wetland mapping in the Congo Basin using optical and radar remotely sensed data and derived topographical indices. *Remote Sens. Environ.* **114**, 73–86 (2010).
21. Richey, J. E., Devol, A. H., Wofsy, S. C., Victoria, R. & Riberio, M. N. G. Biogenic gases and the oxidation and reduction of carbon in Amazon River and floodplain waters. *Limnol. Oceanogr.* **33**, 551–561 (1988).
22. Marwick, T. R. *et al.* Dynamic seasonal nitrogen cycling in response to anthropogenic N loading in a tropical catchment, Athi–Galana–Sabaki River, Kenya. *Biogeosciences* **11**, 1–18 (2014).
23. Yasin, J. A., Kroeze, C. & Mayorga, E. Nutrients export by rivers to the coastal waters of Africa: Past and future trends. *Glob. Biogeochem. Cycles* **24**, GB0A07 (2010).
24. Castillo, M. M., Kling, G. W. & Allan, J. D. Bottom-up controls on bacterial production in tropical lowland rivers. *Limnol. Oceanogr.* **48**, 1466–1475 (2003).
25. Teodoru, C. *et al.* Spatial variability and temporal dynamics of greenhouse gas (CO₂, CH₄, N₂O) concentrations and fluxes along the Zambezi River mainstem and major tributaries. *Biogeosciences* **12**, 2431–2453 (2015).
26. Butman, D. & Raymond, P. A. Significant efflux of carbon dioxide from streams and rivers in the United States. *Nature Geosci.* **4**, 839–842 (2011).
27. Amado, A. M. *et al.* Tropical freshwater ecosystems have lower bacterial growth efficiency than temperate ones. *Front. Microbiol.* **4**, 167 (2014).
28. Cardoso, S. J., Enrich-Prast, A., Pace, M. L. & Roland, F. Do models of organic carbon mineralization extrapolate to warmer tropical sediments? *Limnol. Oceanogr.* **59**, 48–54 (2014).
29. Pan, Y. *et al.* A Large and persistent carbon sink in the World's forests. *Science* **333**, 988–993 (2011).

Acknowledgements

This work was funded by the European Research Council (ERC-StG 240002 AFRIVAL), the Fonds National de la Recherche Scientifique (FNRS, CAKI 2.4.598.07, TransCongo, 14711103), the Belgian Federal Science Policy (BELSPO) (projects COBAFISH SD/AR/05A and EAGLES SD/AR/02A), the Research Foundation Flanders (FWO-Vlaanderen), the Research Council of the KU Leuven, the IRD and INSU/CNRS (SOERE BVET and LIMON projects). The Boyekoli-Ebale-Congo Expedition (2010) was funded by the Belgian Development Cooperation, BELSPO, and Belgian National Lottery. A.V.B. and T.L. are a senior research associate and a postdoctoral researcher at the FNRS, respectively. We are very grateful for help in sampling from A. Yambélé (Direction de la Météorologie Nationale, Central African Republic), J.-D. Mbega (Institut de Recherches Agronomiques et Forestières, Gabon), B. Alhou (Université de Niamey, Niger), F. C. Nyoni and I. Nyambe (University of Zambia, Zambia), B. Ogwoka (Kenya Wildlife Service, Kenya), T. Mambo Baba and E. Tambwe Lukosha (Université de Kisangani, DRC), T. Kisekelwa (Institut Supérieur Pédagogique de Bukavu, DRC), J. N. Wabakghanzi (Congo Atomic Energy Commission, DRC), C. M. Balagizi (Goma Volcano Observatory, DRC) and J. L. Boeglin (Géosciences Environnement Toulouse – GET, France), for analytical support from M.-V. Commarieu, S. Hoornaert, S. Petrovic (University of Liège (ULg)) and C. Deshmukh (GET), for advice and help in setting up the GCs at ULg from J. Barnes, G. Abril, B. Delille and W. Champenois, and for feedback and input on modelled basin-wide *k* values from P. Raymond.

Author contributions

A.V.B. and S.B. conceived and designed the study and coordinated the project and fieldwork. Field data collection was carried out by all co-authors. T.L. carried out the geographical system information (GIS) analysis. A.V.B. drafted the manuscript, which was substantially commented upon and amended by S.B., C.R.T., T.R.M., N.G., T.L. and E.G. All co-authors approved the manuscript.

Additional information

Supplementary information is available in the [online version of the paper](#). Reprints and permissions information is available online at www.nature.com/reprints. Correspondence and requests for materials should be addressed to A.V.B.

Competing financial interests

The authors declare no competing financial interests.

Methods

We acquired 1,880 data for CH₄, 1,625 data for N₂O and 693 data for *p*_{CO₂} from June 2006 to September 2014 in 12 river basins (Supplementary Table 1). The dissolved gases were measured with a uniform method based on the headspace technique, either directly in the field by infrared gas analysis (IRGA; for CO₂), or on return in the laboratory by gas chromatography (GC; for CH₄ and N₂O). Our analysis excludes *p*_{CO₂} data computed from pH and total alkalinity, because of strong biases due to the interference from organic acids, in particular in organic C rich black waters^{15,16}.

Sampling and field measurements. Two approaches were used during this study (Supplementary Table 1). First, a 'survey' approach aimed at sampling the mainstem of a river network over the longest possible stretch, as well as a maximum number of contributing tributaries, typically during a short period of time (2–60 d). In most cases, the surveys were done by car, with sampling from boats, bridges, or from the shore. In other cases, travel and sampling were carried out by boat (Congo River). Second, a 'monitoring' approach was applied at various fixed stations during a 1–2 yr period, with sampling taking place at monthly or fortnightly intervals in the mainstem of one or several rivers. The two approaches are highly complementary as the 'survey' approach provides a snapshot of the spatial variability, whereas the 'monitoring' approach provides the range of seasonal variability, but with little or no description of the spatial heterogeneity.

Water was collected with a Niskin bottle just below the surface (<0.5 m) and two serum bottles (50 ml) for the determination of CH₄ and N₂O were filled through tubing, allowed to overflow, poisoned with a saturated solution of HgCl₂ (50–100 µl), sealed with butyl stoppers, crimped with aluminium caps, and stored at ambient temperature in the dark. Samples for the determination of *p*_{CO₂} were directly collected in surface waters in four plastic 60 ml syringes and 30 ml of sample water was equilibrated with 30 ml of ambient air (5–10 min of vigorous shaking). The *p*_{CO₂} in ambient air and in the equilibrated gas phase were determined with a portable IRGA, from which the *in situ* *p*_{CO₂} was computed using the temperature values *in situ* and in the equilibrated water (that is, in the syringe), and Henry's constant. The IRGAs were calibrated with N₂ and a CO₂:N₂ commercial mixture (Air Liquide Belgium) with a mixing ratio of 1,017 ppm of CO₂ (PP Systems EGM-4 and Li-Cor Li-820) or with N₂ and a suite of CO₂:N₂ commercial mixtures (Air Liquide Belgium) with mixing ratios of 388, 813, 3,788 and 8,300 ppm CO₂ (Li-Cor Li-840). The Li-840 was used on the Congo in December 2013 and June 2014, the EGM-4 was used on the Congo in December 2012 and September 2013 and on the Zambezi, whereas the Li-820 was used on the Malagasy, Tana and Athi-Galana-Sabaki rivers. In the Congo in March 2013, the headspace was injected in pre-evacuated 12 ml Exetainer (Labco) vials and the CO₂ content was analysed by GC back in the laboratory (see hereafter). The overall precision of *p*_{CO₂} measurements was ±2.0% (*n*=447 replications of three to four measurements).

Water temperature, conductivity, %O₂ and pH were measured *in situ* with portable field probes calibrated using standard protocols (in most cases using an YSI Proplus probe). Pelagic *R* was determined from the decrease of O₂ in 60 ml biological oxygen demand bottles over ~24 h incubation periods. The bottles were kept in the dark and close to *in situ* temperature in a cool box filled with *in situ* water. The O₂ decrease was determined from triplicate measurements at the start and the end of the incubation with an optical O₂ probe (YSI ProODO), and *R* data were converted into carbon units using a respiratory quotient of 1.3 (ref. 30). Samples for the DOC determination were preserved in 40 ml borosilicate vials with polytetrafluoroethylene-coated stoppers and preserved with H₃PO₄ (85% after filtration through 0.2 µm pore size polyethersulphone (PES) syringe filters. Samples for nitrate (NO₃⁻) and ammonium (NH₄⁺) were filtered on a 0.2 µm PES syringe filter, collected in 50 ml plastic vials, to which was added 200 µl of H₂SO₄ 5N.

Laboratory chemical analysis. Concentrations of CH₄ and N₂O were determined via the headspace equilibration technique (20 ml N₂ headspace in 50 ml serum bottles) and measured by GC (ref. 31) with flame ionization detection (GC-FID) and electron capture detection (GC-ECD) with a SRI 8610C GC-FID-ECD calibrated with CH₄:CO₂:N₂O:N₂ mixtures (Air Liquide Belgium) of 1, 10 and 30 ppm CH₄ and of 0.2, 2.0 and 6.0 ppm N₂O, and using the solubility coefficients of CH₄ (ref. 32) and N₂O (ref. 33). For the Nyong, the CH₄ was determined with a SRI 8610C GC-FID calibrated with CH₄:N₂ mixtures (Air Liquide France) of 2, 10 and 100 ppm CH₄. For the Ivory Coast rivers, the CH₄ was determined by GC-FID, as described elsewhere³⁴. The overall precision of measurements was ±3.9% (*n*=1,057 duplicate measurements) and ±3.2% (*n*=900 duplicate measurements) for CH₄ and N₂O, respectively. DOC was analysed according either on a Thermo HiPerTOC-isotope ratio mass spectrometer (IRMS) or with an Aurora 1030 TOC analyser (OI Analytical) coupled to a Delta V Advantage IRMS, with a precision better than ±5% (ref. 35). NO₃⁻ and NH₄⁺ concentrations were estimated by spectrophotometry, using the dichloroisocyanurate-salicylate-nitroprussiate colorimetric method for NH₄⁺ (ref. 36) and the sulphanilamide colorimetric method for NO₃⁻ (refs 37,38). The detection limits were 0.30 and 0.15 µmol l⁻¹ for NH₄⁺ and NO₃⁻, respectively.

GHG flux computations. The air–water gas flux (*F*) was computed according to

$$F = k\Delta C$$

where *k* is the gas transfer velocity and ΔC is the air–water gas concentration gradient³⁹, whereby a positive value corresponds by convention to an emission of gas from the water to the atmosphere.

We used the monthly average corresponding to time of sampling of atmospheric *p*_{CO₂} from Mount Kenya (Kenya, -0.05° N 37.80° E), retrieved from the GLOBALVIEW-CO₂ database (Carbon Cycle Greenhouse Gases Group of the National Oceanic and Atmospheric Administration (NOAA), Earth System Research Laboratory (ESRL)) and of N₂O from Mauna Loa (Hawaii, 19.54° N–155.85° E) from the NOAA/ESRL Chromatograph for Atmospheric Trace Species (CATS) Program. For atmospheric CH₄, a constant mixing ratio of 1.9 ppm was used. Atmospheric mixing ratios were converted from dry air to wet air using the water vapour computed from temperature³³ and into corresponding dissolved concentrations using solubility coefficients of CO₂ (ref. 40), CH₄ (ref. 32) and N₂O (ref. 33). Fluxes of CH₄ and N₂O were converted into CO₂ equivalents based on the assumption that over a 100-year period the emissions of 1 kg of CH₄ and 1 kg of N₂O correspond to 34 kg and 298 kg of CO₂, respectively⁶. For *k*, we used two approaches. The first approach² uses a constant *k* normalized to a Schmidt number (*Sc*) of 600 (*k*₆₀₀) of 17.2 cm h⁻¹ for streams and small rivers (<100 m width), of 12.3 cm h⁻¹ for larger rivers (>100 m width) and of 2.4 cm h⁻¹ for wetlands. The second approach³ provides *k*₆₀₀ values per river basin corresponding to the average value for the whole river network up to stream order 1 derived from hydraulic equations⁴¹ and a geographical information system (GIS) description of corresponding input hydraulic variables for each catchment. The *Sc* numbers of CO₂, N₂O and CH₄ were computed from water temperature⁴². The *F* data were aggregated to derive one value per tributary and per river mainstem, before averaging for a given river system. The global *F* values were computed as averages weighted by water body surface area for each river catchment derived from the percentage of river/stream effective surface area per catchment given in ref. 3. The *F* values were similarly upscaled to SSA using the river/stream surface areas given in ref. 3.

FCO₂ and FCH₄ were measured in parallel with a floating chamber in 25 stations in the Congo basin, and 43 stations in the Zambezi basin. The floating chamber consisted of an opaque polyvinyl chloride cylinder 15 cm in height with a 38 cm internal diameter holding a volume of 17 l, and a 7-cm-long underwater skirt. The chamber was deployed for 30 min and the *p*_{CO₂} change inside the chamber was determined directly with an IRGA (30 s logging), whereas 30 ml gas samples for CH₄ extracted from inside the chamber at 0, 5, 10, 20 and 30 min interval were injected into 50 ml serum vials full of a hyper-saline solution (saturated solution of NaCl) for analysis in the laboratory by GC-FID. The fluxes were computed from the temporal change of the partial pressure of the gases, the law of perfect gases, and the geometry of the chamber⁴³. The *k*₆₀₀ of CO₂ was computed based on the measured FCO₂ and the *p*_{CO₂} in water and air. Assuming that the FCO₂ is exclusively diffusive (that is, that the CO₂ ebullition flux is negligible), this *k*₆₀₀ of CO₂ allows the computation of the diffusive CH₄ flux from the dissolved CH₄ concentration. This in turn allows the computation of the ebullition CH₄ flux from the chamber CH₄ measurement that captures both ebullition and diffusive CH₄ fluxes. Chamber measurements have been assumed to provide biased *k* values⁴⁴, although often comparing satisfactorily with atmospheric flux measurements^{45,46} or infrared imaging of the water surface⁴⁷. The obtained average *k*₆₀₀ in the Congo (12 ± 11 cm h⁻¹) was not significantly different from the average in the Zambezi (10 ± 11 cm h⁻¹) (unpaired *t*-test, *p* < 0.05). These values are distinctly lower than those computed by Raymond *et al.*³ of 22 and 20 cm h⁻¹ for the Congo and Zambezi, respectively. This is related to the fact that Raymond *et al.*³ provide *k*₆₀₀ values for the whole basin, including low-order streams that are more turbulent than higher-order streams and rivers, and characterized by higher *k*₆₀₀ values⁴¹. Our data were acquired in the mainstem of rivers and adjacent large tributaries, typically high-order systems. The *k*₆₀₀ values in the highest stream order in the Congo (9) and Zambezi (8) given by Raymond *et al.*³ are, respectively, 14.5 and 13.3 cm h⁻¹—closer to those derived from our chamber measurements. The Congo and Zambezi streams (<100 m width) had *k*₆₀₀ values (11 ± 10 cm h⁻¹) that were not significantly different from those (10 ± 7 cm h⁻¹) in rivers (>100 m width) (unpaired *t*-test, *p* < 0.05). These values were close to the *k*₆₀₀ value for rivers (>100 m width) of 12 cm h⁻¹, but lower than the value for streams (<100 m width) of 17 cm h⁻¹ given by Aufdenkampfe and colleagues⁷. This reflects the fact that our data in the Congo and Zambezi were obtained in high-order streams, mainly in regions with gentle slopes (lowlands). Nevertheless, the actual accuracy of the chamber *k* values is irrelevant in the present case because we aimed at determining the CH₄ ebullition from the chamber measurements. Yet, these CH₄ ebullition estimates are probably conservative and provide underestimates, as for logistical reasons there was no replication of chambers and the deployment was short relative other studies, where it varies between 1 h (ref. 19) and 24 h (ref. 18). Indeed, CH₄ ebullition is notoriously heterogeneous both in space and time (across different timescales from

daily to seasonal)^{48–51}, and adequately capturing this heterogeneity would require a sampling effort and design incompatible with other aims of our research.

GHG flux error analysis. An error analysis on the GHG flux computation and upscaling was carried out by error propagation of the GHG concentration measurements, the *k* value estimates, and the estimate of surface areas of river channels to scale the areal fluxes, using a Monte Carlo simulation with 1,000 iterations. The uncertainty on the GHG concentrations led to an uncertainty of areal fluxes of $\pm 1.2\%$, $\pm 2.3\%$ and $\pm 5.2\%$ for CO₂, CH₄ and N₂O, respectively. Whereas no information is available in Aufdenkampe *et al.*² regarding the uncertainty on *k* values, the uncertainty on *k* given by Raymond *et al.*³ was estimated to be $\pm 10.0\%$, based on the errors on slope and constant of the parameterization⁴¹. This leads to a cumulated uncertainty of areal fluxes of $\pm 4.6\%$, $\pm 4.9\%$ and $\pm 6.7\%$ for CO₂, CH₄ (diffusive) and N₂O, respectively. Ebullition of CH₄ is highly heterogeneous spatially and temporally^{48–51}, and it is difficult to quantify this uncertainty. We arbitrarily assigned an uncertainty of $\pm 50\%$ for CH₄ ebullition. This leads to a cumulated uncertainty of total areal fluxes of $\pm 29.4\%$ for CH₄ (diffusive + ebullitive). The river/stream surface areas reported by Raymond *et al.*³ were estimated using two different hydraulic equations, which allow one to estimate an uncertainty of $\pm 31.0\%$. The overall uncertainty of integrated fluxes in river channels is $\pm 18.8\%$, $\pm 18.3\%$, $\pm 34.2\%$ and $\pm 19.2\%$ for CO₂, CH₄ (diffusive only), CH₄ (diffusive + ebullitive) and N₂O, respectively. The comparison of the wetland mapping of Bwangoy *et al.*²⁰ and of the Africover vegetation map, allows one to evaluate the uncertainty of the surface area of Congolese ‘Cuvette Centrale’ to $\pm 10\%$. The overall uncertainty of integrated fluxes in the Congolese ‘Cuvette Centrale’ is $\pm 7.0\%$ and $\pm 30.6\%$ for CO₂ and CH₄ (diffusive + ebullitive), respectively.

Other sources of uncertainty that are not straightforward to quantify relate to seasonal and spatial representativeness. For all spatial surveys, we paid particular attention to cover the widest possible spectrum of systems from mainstem to headwaters, to capture spatial variations in the most comprehensive way given logistical constraints. Data from all basins cover different hydrologic conditions and average fluxes capture seasonality. Spatial and seasonal variations have been presented and discussed for some basins in site-specific studies^{22,25,34,52–54}.

GIS analysis of catchment characteristics. Mean slope and drainage area were extracted from the HYDRO1K global hydrologic data set⁵⁵. The fractional land cover type of the watershed was extracted from the Global Land Cover (GLC) 2000 database of Africa⁵⁶. In total, 27 different land sub-classes are defined in the GLC database, taking into account the dominant vegetation class (namely trees, shrubs and grasses), phenology, seasonality, flooding regime and altitude. These sub-classes were aggregated in seven first-level classes based on vegetation structural categories: dense forest, mosaic forest/other, woodlands and shrublands, grasslands, agricultural lands, bare soils and others (water bodies, urban). Aboveground biomass in Mg km⁻² (Mg = 10⁹ g) was extracted from the Woods Hole Research Center (WHRC) pantropical national level C stock data set⁵⁷. The extent of wetland and floodplain areas was extracted from the Global Lakes and Wetlands Database⁵⁸, except for the Nyong⁵⁹ and the Tana (Omengo, F. O. Based on a GIS Analysis of Landsat Images). Annual precipitation was extracted from the WorldClim Global Climate Database⁶⁰.

Data availability. The full data set of CO₂, CH₄ and N₂O concentrations is available as Supplementary Information.

Data sources. Several publicly available data sources were used: HYDRO1K global hydrologic data set: <https://lta.cr.usgs.gov/HYDRO1K> GLC 2000 database of Africa: <http://forobs.jrc.ec.europa.eu/products/glc2000/products.php> WHRC pantropical national level C stock data set: http://www.whrc.org/mapping/pantropical/carbon_dataset.html Global Lakes and Wetlands Database: <https://www.worldwildlife.org/pages/global-lakes-and-wetlands-database> WorldClim—Global Climate Data: <http://www.worldclim.org> Data on river/stream surface and *k* values from: <http://www.nature.com/nature/journal/v503/n7476/abs/nature12760.html#supplementary-information>

References

- Richardson, D. C., Newbold, J. D., Aufdenkampe, A. K., Taylor, P. G. & Kaplan, L. A. Measuring heterotrophic respiration rates of suspended particulate organic carbon from stream ecosystems. *Limnol. Oceanogr.* **11**, 247–261 (2013).
- Weiss, R. F. Determinations of carbon dioxide and methane by dual catalyst flame ionization chromatography and nitrous oxide by electron capture chromatography. *J. Chromatogr. Sci.* **19**, 611–616 (1981).
- Yamamoto, S., Alcauskas, J. B. & Crozier, T. E. Solubility of methane in distilled water and seawater. *J. Chem. Eng. Data* **21**, 78–80 (1976).
- Weiss, R. F. & Price, B. A. Nitrous oxide solubility in water and seawater. *Mar. Chem.* **8**, 347–359 (1980).
- Koné, Y. J. M., Abril, G., Delille, B. & Borges, A. V. Seasonal variability of methane in the rivers and lagoons of Ivory Coast (West Africa). *Biogeochemistry* **100**, 21–37 (2010).
- Bouillon, S., Korntheuer, M., Baeyens, W. & Dehairs, F. A new automated setup for stable isotope analysis of dissolved organic carbon. *Limnol. Oceanogr.* **4**, 216–226 (2006).
- Standing Committee of Analysts *Methods for the Examination of Waters and Associated Materials* (HMSO, 1981).
- Standard Methods for the Examination of Water and Wastewater* (APHA, 1998).
- Miranda, K. M. *et al.* A rapid, simple spectrophotometric method for simultaneous detection of nitrate and nitrite. *Nitric Oxide* **5**, 62–71 (2001).
- Liss, P. S. & Slater, P. G. Flux of gases across the air–sea interface. *Nature* **247**, 181–184 (1974).
- Weiss, R. F. Carbon dioxide in water and seawater: The solubility of a non-ideal gas. *Mar. Chem.* **2**, 203–215 (1974).
- Raymond, P. A. *et al.* Scaling the gas transfer velocity and hydraulic geometry in streams and small rivers. *Limnol. Oceanogr.* **2**, 41–53 (2012).
- Wanninkhof, R. Relationship between wind speed and gas exchange over the ocean. *J. Geophys. Res.* **97**, 7373–7382 (1992).
- Frankignoulle, M. Field measurements of air–sea CO₂ exchange. *Limnol. Oceanogr.* **33**, 313–322 (1988).
- Raymond, P. A. & Cole, J. J. Gas exchange in rivers and estuaries: Choosing a gas transfer velocity. *Estuaries* **24**, 312–317 (2001).
- Guérin, F. *et al.* Gas transfer velocities of CO₂ and CH₄ in a tropical reservoir and its river downstream. *J. Mar. Syst.* **66**, 161–172 (2007).
- Huotari, J., Haapanala, S., Pumpanen, J., Vesala, T. & Ojala, A. Efficient gas exchange between a boreal river and the atmosphere. *Geophys. Res. Lett.* **40**, 5683–5686 (2013).
- Gålfalk, M., Bastviken, D., Fredriksson, S. & Arneborg, L. Determination of the piston velocity for water–air interfaces using flux chambers, acoustic Doppler velocimetry, and IR imaging of the water surface. *J. Geophys. Res.* **118**, 770–782 (2013).
- Crawford, J. T. *et al.* Ebullitive methane emissions from oxygenated wetland streams. *Glob. Change Biol.* **20**, 3408–3422 (2014).
- DelSontro, T. *et al.* Spatial Heterogeneity of methane ebullition in a large tropical reservoir. *Environ. Sci. Technol.* **45**, 9866–9873 (2011).
- Deshmukh, C. *et al.* Physical controls on CH₄ emissions from a newly flooded subtropical freshwater hydroelectric reservoir: Nam Theun 2. *Biogeosciences* **11**, 4251–4269 (2014).
- Maeck, A., Hofmann, H. & Lorke, A. Pumping methane out of aquatic sediments – ebullition forcing mechanisms in an impounded river. *Biogeosciences* **11**, 2925–2938 (2014).
- Bouillon, S. *et al.* Organic matter sources, fluxes and greenhouse gas exchange in the Oubangui River (Congo River basin). *Biogeosciences* **9**, 2045–2062 (2012).
- Bouillon, S. *et al.* Contrasting biogeochemical characteristics of right-bank tributaries and a comparison with the mainstem Oubangui River, Central African Republic (Congo River basin). *Sci. Rep.* **4**, 5402 (2014).
- Bouillon, S. *et al.* Distribution, origin and cycling of carbon in the Tana River (Kenya): A dry season basin-scale survey from headwaters to the delta. *Biogeosciences* **6**, 2475–2493 (2009).
- HYDRO1K Elevation Derivative Database* (US Geological Survey, 2000).
- Mayaux, P., Bartholomé, E., Fritz, S. & Belward, A. A new land-cover map of Africa for the year 2000. *J. Biogeogr.* **31**, 861–877 (2004).
- Baccini, A., Laporte, N., Goetz, S. J., Sun, M. & Dong, H. A first Map of tropical Africa’s above-ground biomass derived from satellite imagery. *Environ. Res. Lett.* **3**, 045011 (2008).
- Lehner, B. & Döll, P. Development and validation of a global database of lakes, reservoirs and wetlands. *J. Hydrol.* **296**, 1–22 (2004).
- Olivry, J. C. *Fleuves et Rivières du Cameroun* (MESCES – ORSTOM, 1986).
- Hijmans, R. J., Cameron, S. E., Parra, J. L., Jones, P. G. & Jarvis, A. Very high resolution interpolated climate surfaces for global land areas. *Int. J. Clim.* **25**, 1965–1978 (2005).

Globally significant greenhouse-gas emissions from African inland waters

Alberto V. Borges, François Darchambeau, Cristian R. Teodoru, Trent R. Marwick, Fredrick Tamooh,
Naomi Geeraert, Fredrick O. Omengo, Frédéric Guérin, Thibault Lambert, Cédric Morana, Eric Okuku
and Steven Bouillon

Figure S1. Sampling stations, catchment and river network of the studied Sub-Saharan rivers.

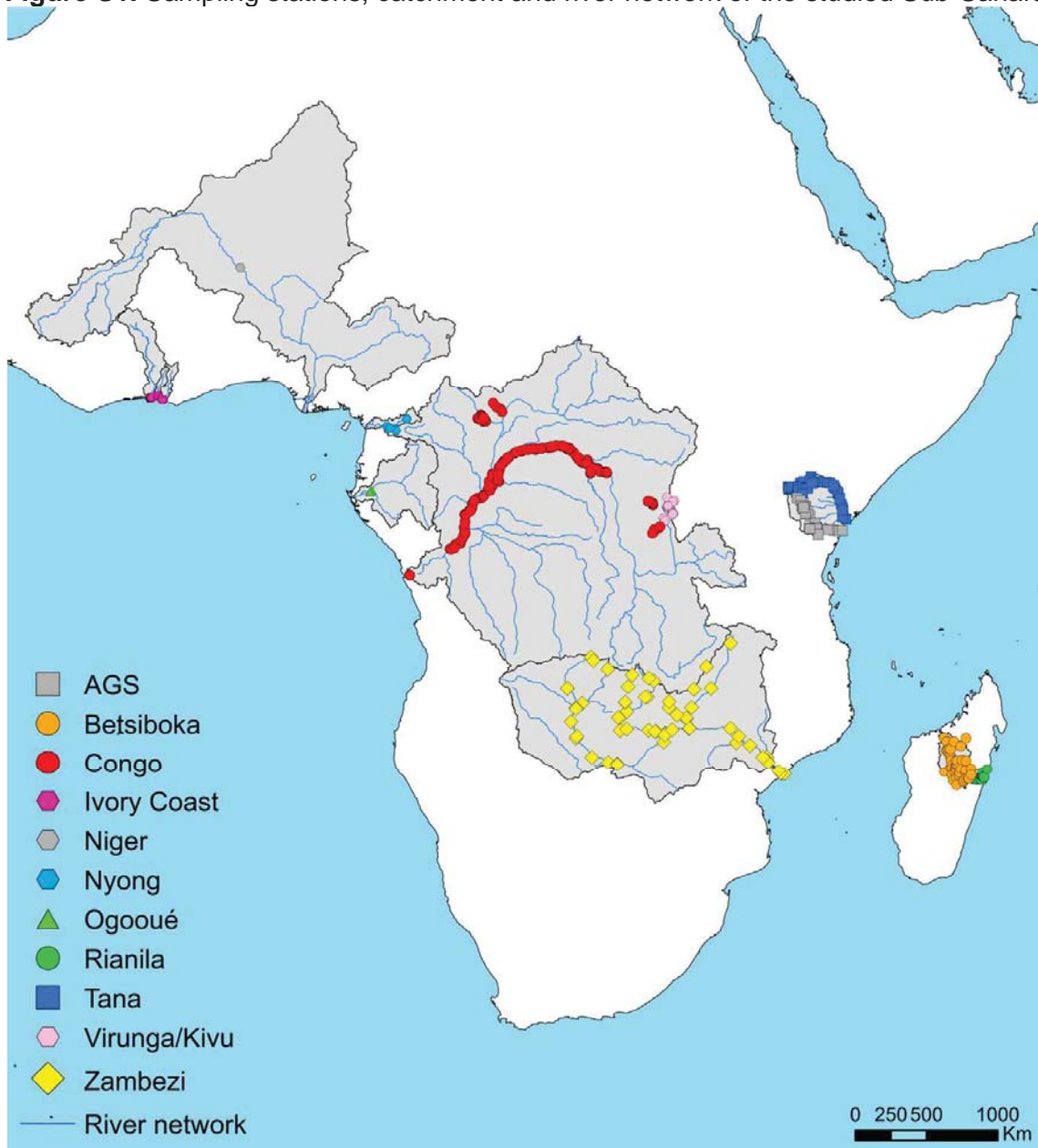


Figure S2. Box and whisker plots of pCO₂, CH₄, N₂O and %O₂ in the studied Sub-Saharan rivers. Data were categorized into small (<100 m width) and larger (>100 m width) rivers/streams. The horizontal line corresponds to the median, the cross to the average, error bars correspond to the 5 and 95 percentile, symbols to outliers.

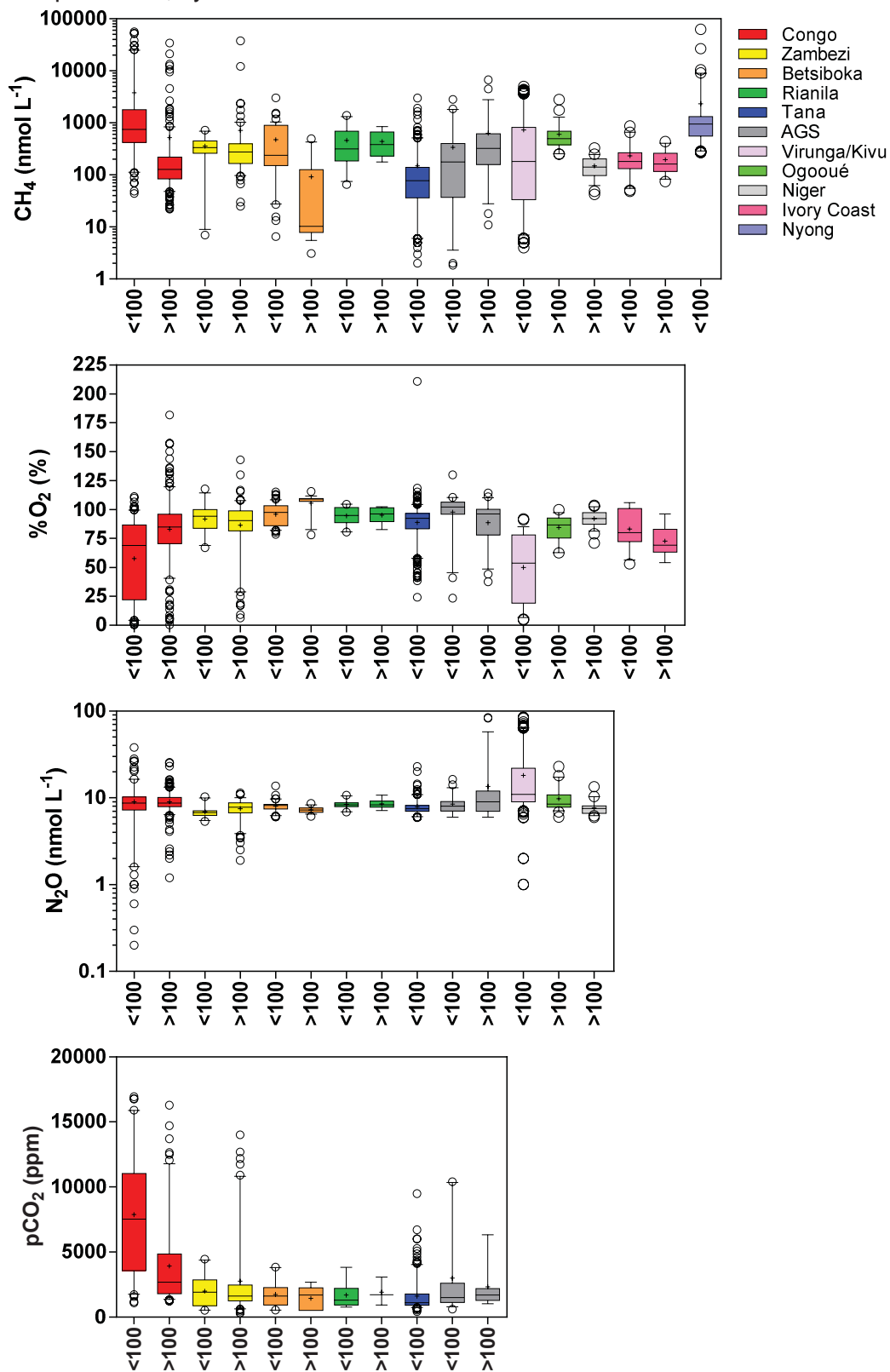


Figure S3. Comparison of the basin-wide averages of $p\text{CO}_2$ and FCO_2 reported in the present study and by³ for the Congo, Zambezi, Tana, Rianila and Betsiboka Rivers. The strongest deviations in $p\text{CO}_2$ between data from this study and the modelled data from³ were observed for the rivers (Zambezi and Congo) with extensive wetland coverage (5 and 10% of the total catchment, respectively).

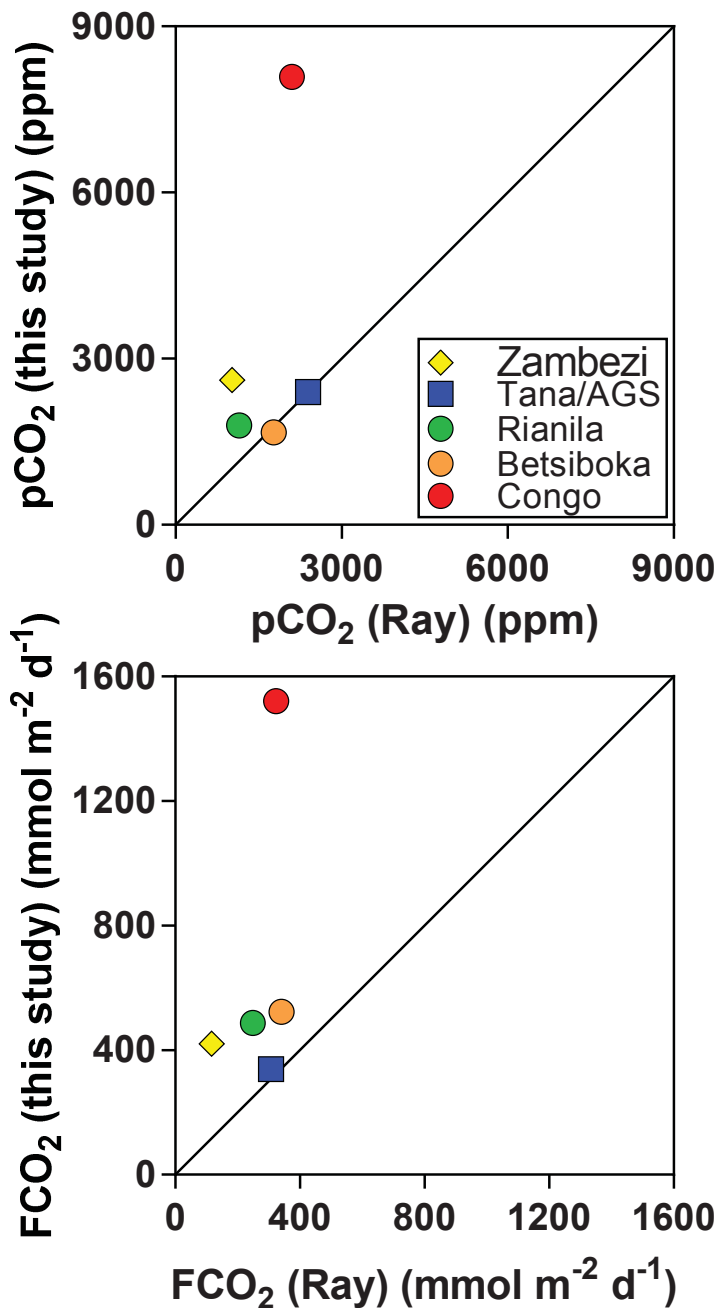


Figure S4. Comparison of the CH₄ flux calculated from the k_{600} derived from the corresponding chamber FCO₂ (that should correspond exclusively to the diffusive CH₄ flux) and the CH₄ flux measured with the floating chamber (that integrates the ebullition CH₄ flux and the diffusive CH₄ flux). The difference between both approaches corresponds to the ebullition CH₄ flux. The highest ebullition flux (2575 times higher than the diffusive CH₄ flux) was measured in a *Vossia cuspidata* patch in Congo River.

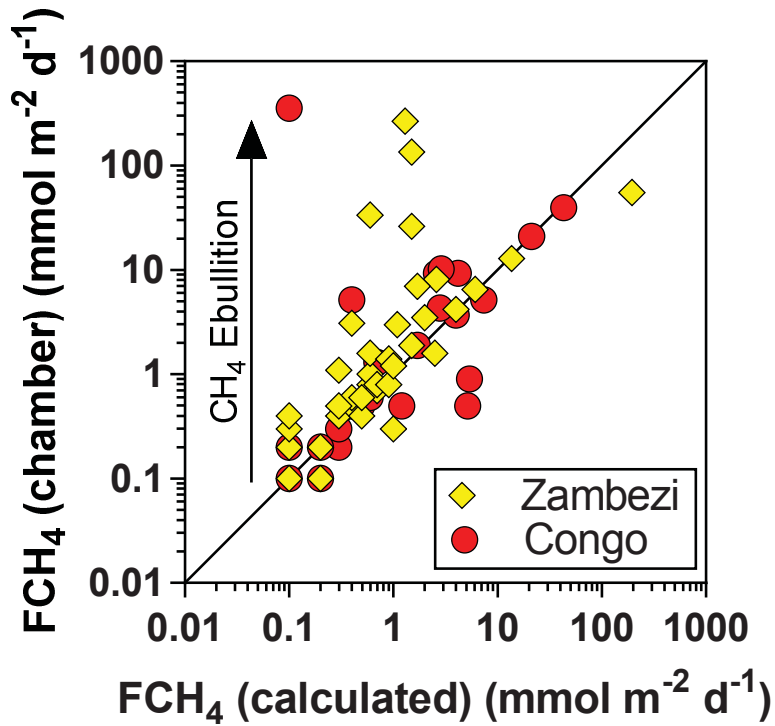


Figure S5. N_2O as a function of $\% \text{O}_2$, NO_3^- , NH_4^+ and DIN in the studied African rivers.

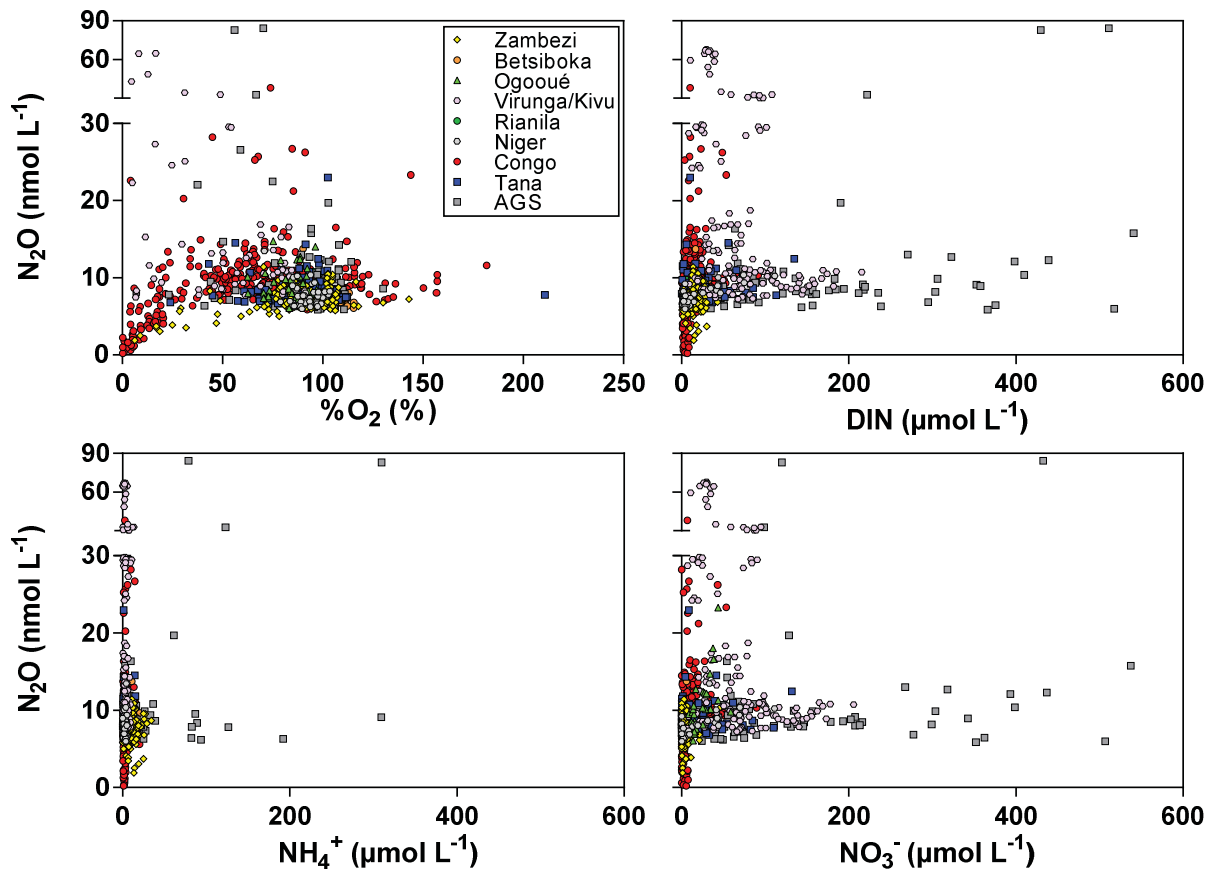


Figure S6. N₂O as a function of NO₃⁻ from seasonal monitoring on the mainstem (fixed station) in the Oubangui (Congo River), Niger and Ogooué.

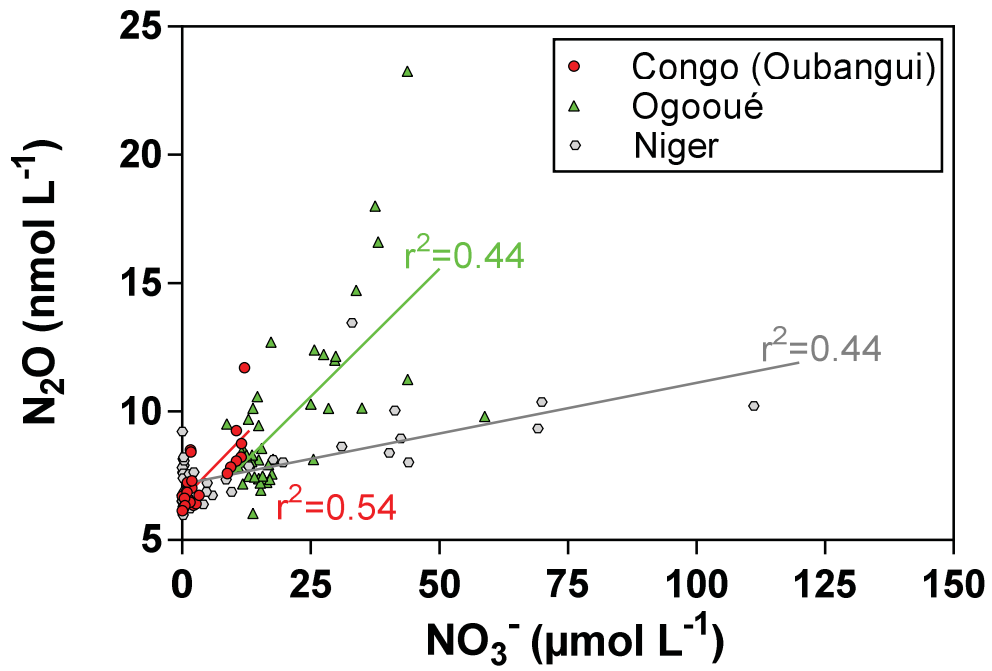


Figure S7. CH₄, pCO₂, N₂O and %O₂ as a function of water temperature and altitude in the studied African rivers.

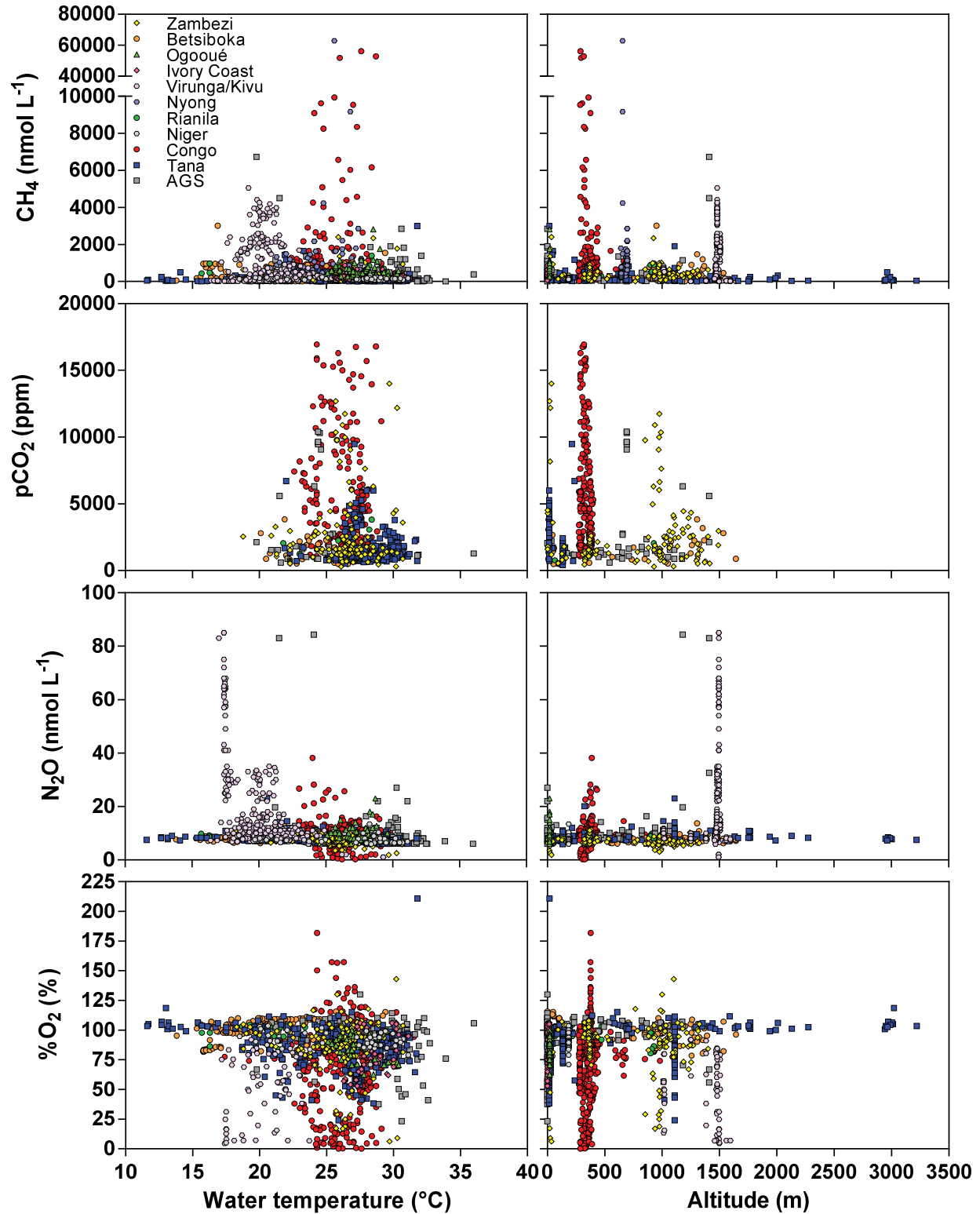


Figure S8. pH and %O₂ as a function of DOC in the studied African rivers.

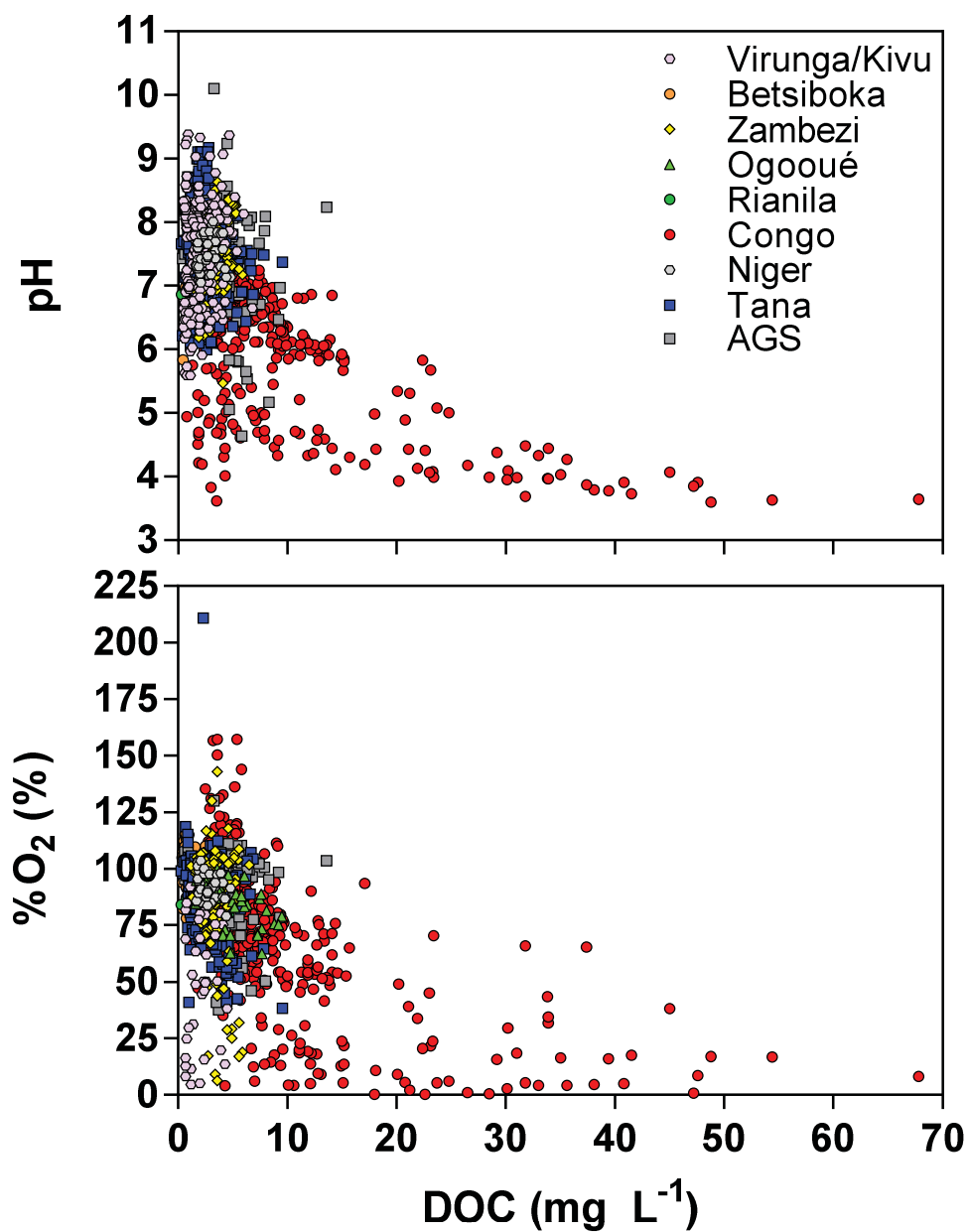


Fig. S9. Longitudinal variations in the Congo mainstem and tributaries along a transect in December 2013 (high water) from Kisangani to Kinshasa of $p\text{CO}_2$ (ppm), CH_4 (nmol L^{-1}) and $\% \text{O}_2$ (%), and aboveground woody biomass (Mg km^{-2})⁵⁷, % of dense forest cover (%)⁵⁶, and wetland surface (cumulated surface and fraction of catchment)⁵⁸. The strong increase in cumulated wetland surface between 200 and 700 km upstream of Kinshasa corresponds to the core of the “Cuvette Centrale”. About 200 km upstream of Kinshasa, the catchment becomes dominated by shrubby savannah. Aboveground biomass and dense forest cover increase gradually along the transect and decrease 200 km above Kinshasa with savannahs becoming more prevalent. The $p\text{CO}_2$ and CH_4 concentration increase downstream towards the “Cuvette Centrale” and collapse in the savannah area upstream of Kinshasa. These patterns are mirrored by $\% \text{O}_2$ (%).

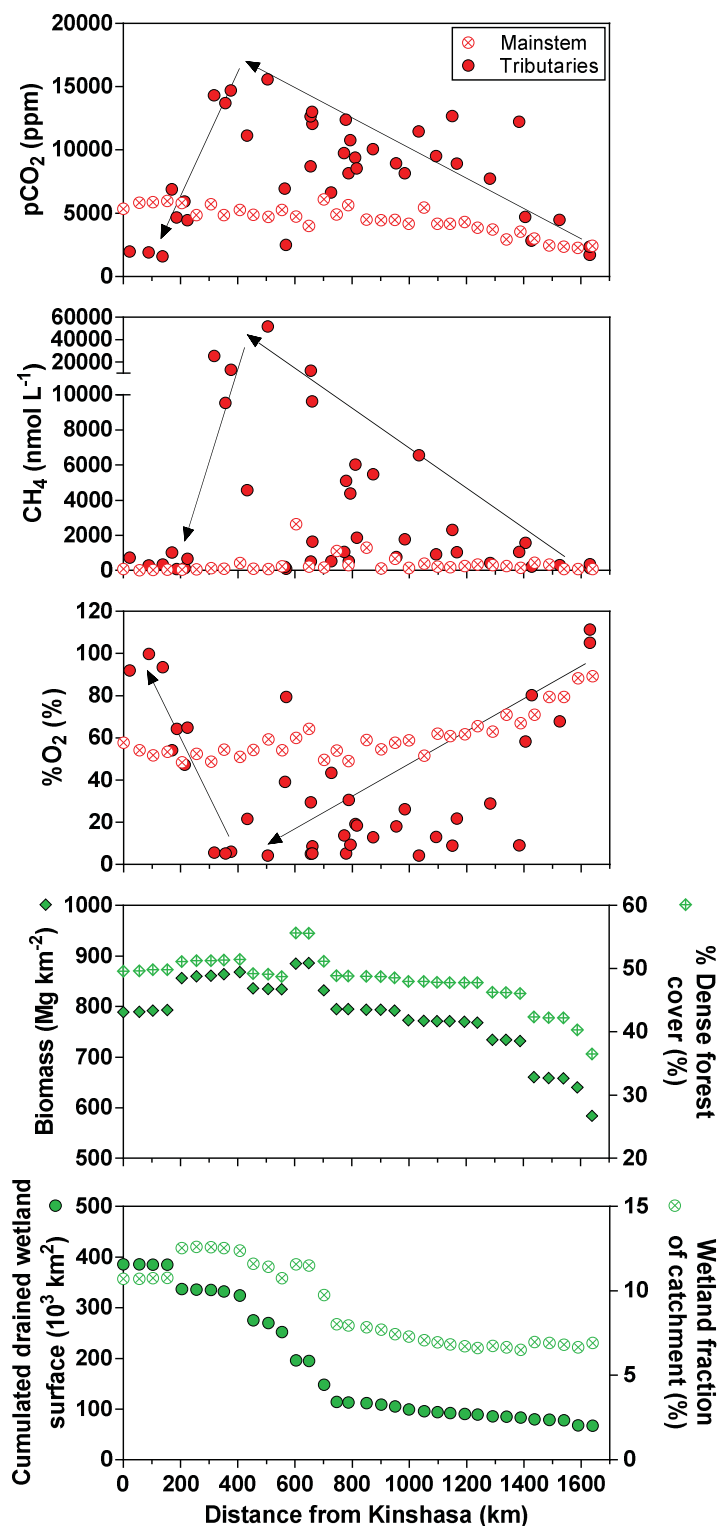


Fig. S10. pCO₂ (ppm), CH₄ (nmol L⁻¹), N₂O (nmol L⁻¹) and %O₂ (%) in 46 rivers of the Congo basin as function of dense forest cover⁵⁶ and aboveground woody biomass (Mg km⁻²)⁵⁷ on the catchment⁵⁵. Data were bin-averaged by intervals of 25% of dense forest cover and by intervals of 400 Mg km⁻² of biomass. Two extreme CH₄ values (>25000 nmol L⁻¹) were removed from the analysis. Error bars correspond to the standard deviation on the mean.

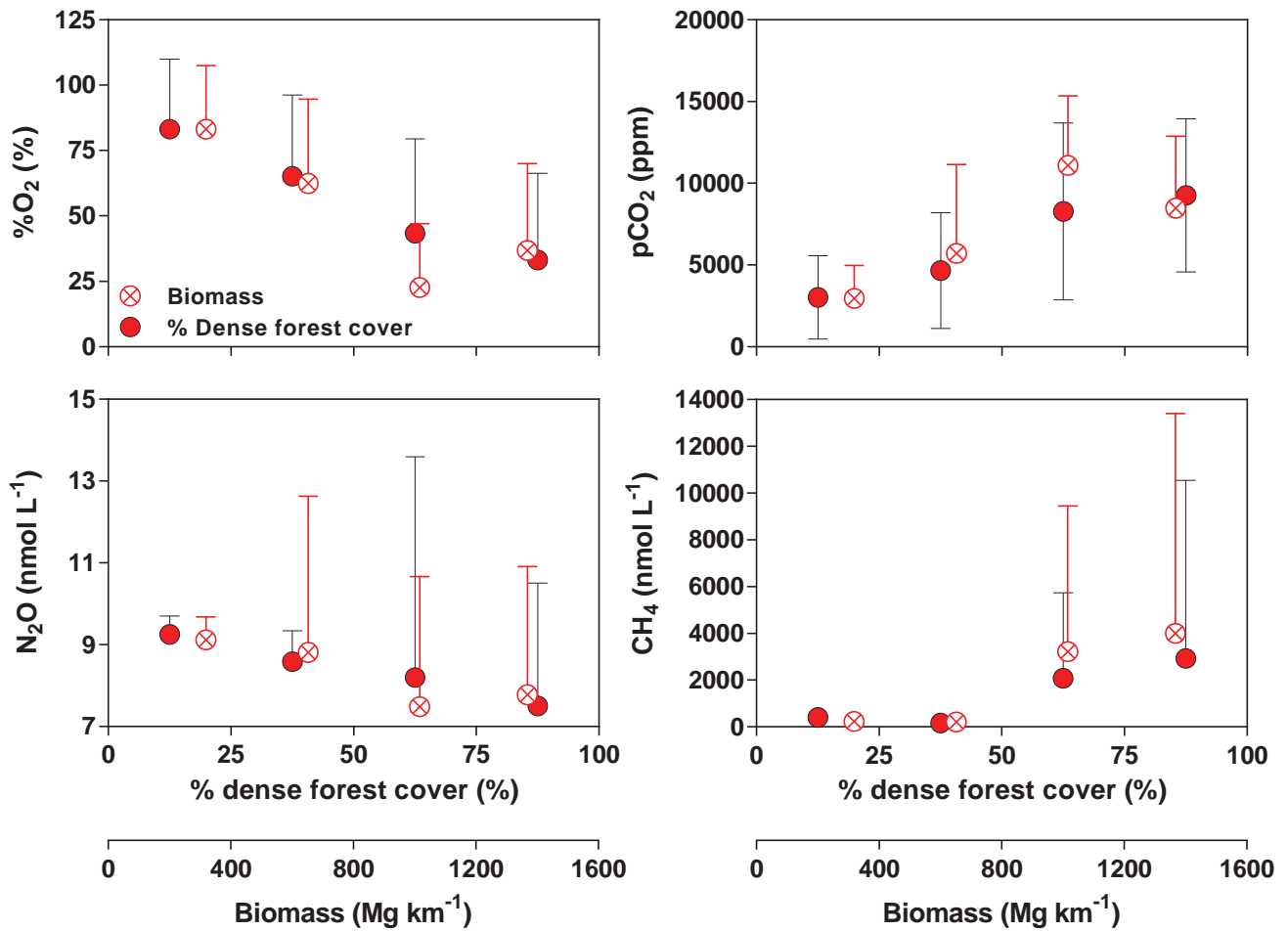


Figure S11. $p\text{CO}_2$ (ppm), CH_4 (nmol L^{-1}) and $\% \text{O}_2$ (%) as function of dense forest cover (%)⁵⁶, of aboveground living biomass (Mg km^{-2})⁵⁷, average catchment slope⁵⁵, and precipitation⁶¹. Only the data-sets that capture spatial variations were included in the analysis (excluding fixed time-series in the mainstem of rivers).

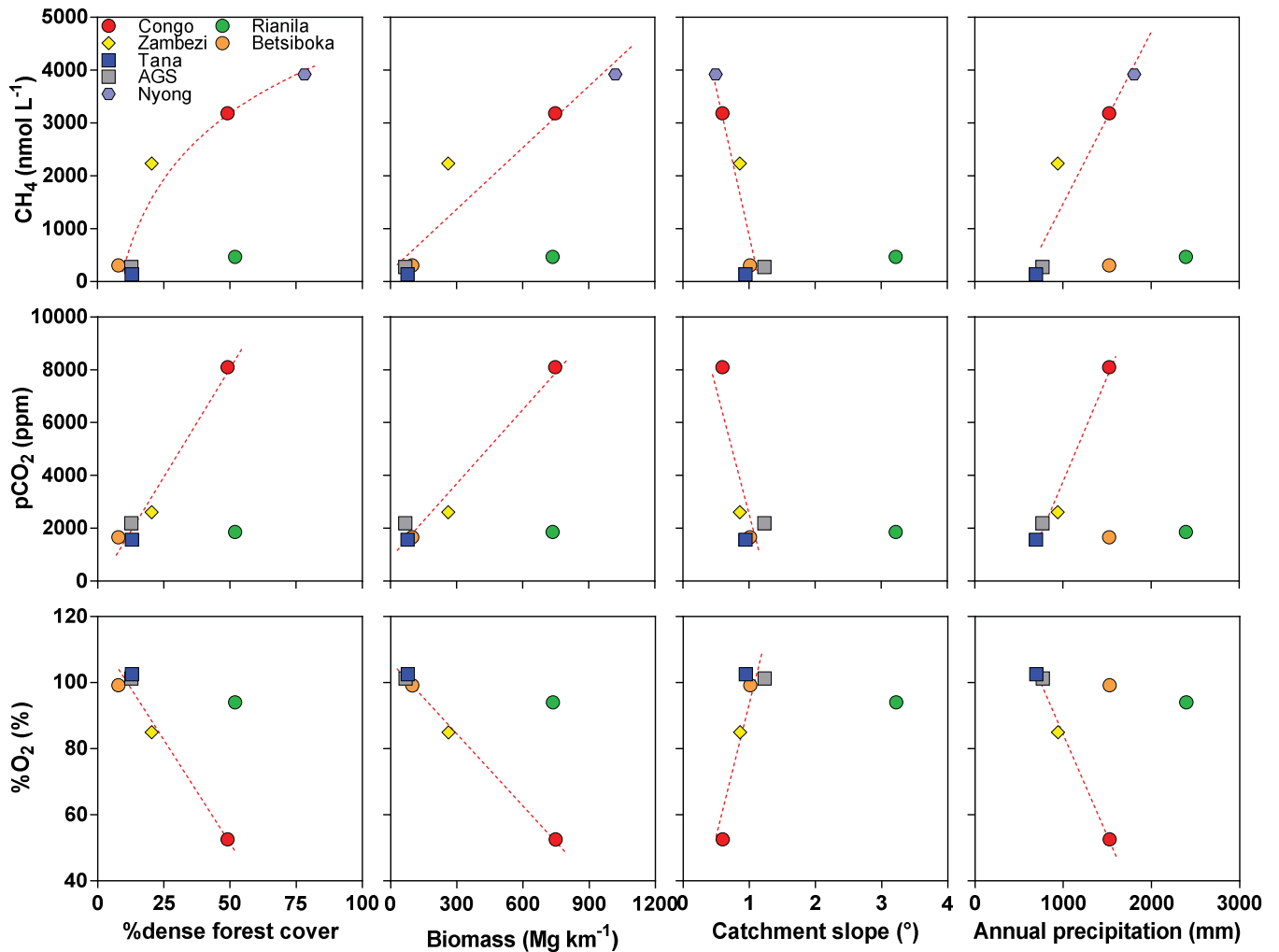


Figure S12. Frequency distribution of the pelagic R measurements gathered in the studied Sub-Saharan rivers.

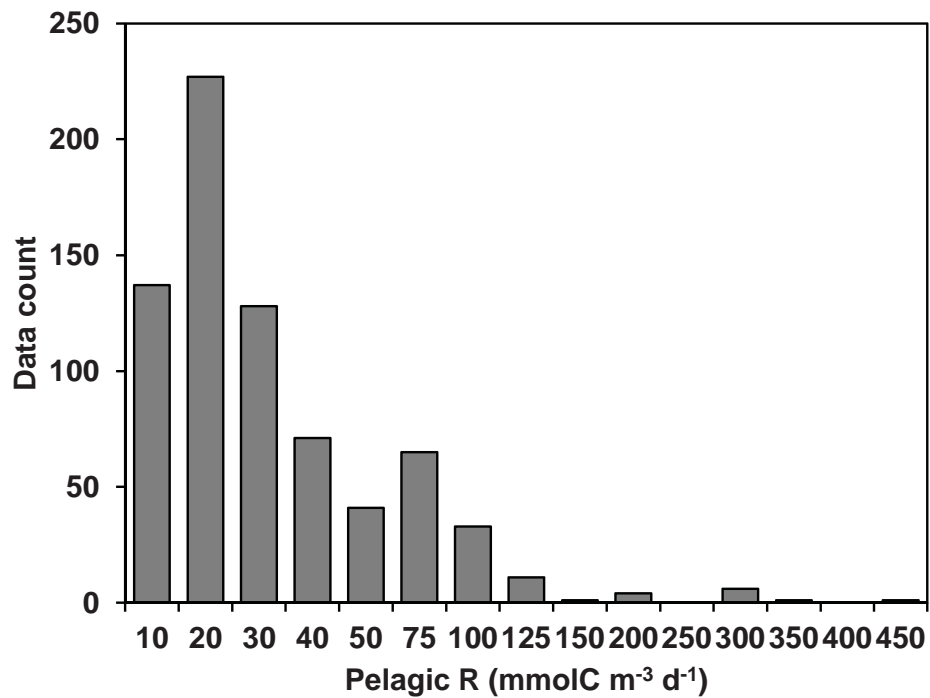


Table S1. Summary of sample collection for GHGs and pelagic respiration (R) in African rivers and streams. Unpubl. = unpublished

	Approach	Dates	Longitude (°E)	Latitude (°N)	<i>n</i> pCO ₂	<i>n</i> CH ₄	<i>n</i> N ₂ O	<i>n</i> R	Reference
Congo	Survey	03/12/2013 - 19/12/2013	15.350 ; 25.187	-4.307 ; 2.206	75	75	75	67	Unpubl.
Congo	Survey	10/06/2014 - 30/06/2014	15.357 ; 25.187	-4.306 ; 2.217	89	89	89	69	Unpubl.
Congo	Survey	13/03/2014 - 21/03/2014	24.170 ; 24.604	0.493 ; 0.784	20	20	20	2	Unpubl.
Congo	Survey	17/09/2013 - 26/09/2013	24.169 ; 24.599	0.494 ; 0.775	6	7	7	7	Unpubl.
Congo	Survey	20/11/2012 - 08/12/2012	24.170 ; 25.196	0.490 ; 0.795	32	32	32	21	Unpubl.
Congo	Monitoring	10/12/2012 - 29/05/2014	25.200	0.499		37	37		Unpubl.
Congo	Monitoring	11/12/2012 - 29/05/2014	25.186	0.542		36	36		Unpubl.
Congo	Survey	20/12/2010 - 31/12/2010	27.803 ; 28.574	-3.310 ; -1.283		15	15		Unpubl.
Congo	Survey	21/03/2010 - 23/03/2010	17.025 ; 18.469	3.945 ; 4.919		7	7		[52;53]
Congo	Survey	20/03/2011 - 23/03/2011	17.110 ; 17.529	3.754 ; 4.105		16	16		[52;53]
Congo	Survey	20/11/2012 - 24/11/2012	17.157 ; 17.535	3.755 ; 4.081		14	14		[52;53]
Congo	Monitoring	20/03/2010 - 31/03/2012	18.567	4.350		54	54		[52;53]
Congo	Survey	01/05/2010 - 06/06/2010	22.458 ; 25.181	0.475 ; 2.172		52	52	41	Unpubl.
Congo	Monitoring	22/07/2011 - 23/11/2012	15.276	-4.296		29	28		Unpubl.
Congo	Survey	02/05/2010 - 22/07/2011	15.276 ; 25.181	-4.296 ; 2.172		52	52	40	Unpubl.
Congo	Survey	22/06/2012 - 24/06/2012	12.705 ; 12.733	-5.964 ; -5.956		2	2		Unpubl.
Congo	Survey	22/06/2012 - 24/06/2012	12.705 ; 12.733	-5.964 ; -5.964		2	2		Unpubl.
Virunga Rivers (12)	Monitoring	18/12/2010 - 20/02/2013	29.004 ; 29.478	-1.727 ; -1.028		291	290		Unpubl.
Kivu Rivers	Survey	17/03/2007 - 22/03/2007	28.788 ; 29.411	-2.470 ; -1.991		12			Unpubl.
Kivu Rivers	Survey	28/08/2007 - 10/09/2007	28.788 ; 29.411	-2.505 ; -1.992		13			Unpubl.
Kivu Rivers	Survey	21/06/2008 - 26/06/2008	28.788 ; 29.411	-2.505 ; -1.992		12			Unpubl.
Kivu Rivers	Survey	22/04/2009 - 05/05/2009	28.788 ; 29.411	-2.505 ; -1.991		12	12		Unpubl.
Kivu Rivers	Survey	20/10/2010 - 24/10/2010	28.789 ; 29.072	-2.505 ; -1.574		8	8		Unpubl.
Kivu Rivers	Survey	25/06/2011 - 25/06/2011	28.788 ; 28.837	-2.470 ; -2.362		5	5	5	Unpubl.
Kivu Rivers	Survey	27/01/2012 - 27/01/2012	28.788 ; 28.837	-2.470 ; -2.362		5	5	5	Unpubl.
Ivory Coast (Comoé)	Monitoring	22/06/2006 - 21/03/2007	-3.669	5.241		31			[34]
Ivory Coast (Bia)	Monitoring	08/06/2006 - 08/03/2007	-3.210	5.370		30			[34]
Ivory Coast (Tanoé)	Monitoring	13/06/2006 - 13/03/2007	-2.920	5.123		25			[34]
Ogooué	Monitoring	19/04/2012 - 18/04/2014	10.225	-0.706		55	53		Unpubl.
Niger	Monitoring	03/04/2011 - 17/03/2013	2.006	13.567		49	49		Unpubl.
Zambezi	Survey	04/02/2012 - 27/04/2012	22.688 ; 36.193	-18.549 ; -11.122	50	52	52	44	[25]
Zambezi	Survey	12/01/2013 - 15/03/2013	22.689 ; 36.445	-18.579 ; -8.596	55	45	45	37	[25]
Zambezi	Survey	19/10/2013 - 24/11/2013	22.685 ; 30.414	-17.887 ; -11.350	32	30	30	16	[25]
Zambezi (2 rivers)	Monitoring	19/02/2012 - 24/11/2013	28.858 ; 28.875	-16.035 ; -15.946	16	55	55	57	Unpubl.
Madagascar	Survey	04/07/2010 - 03/09/2010	46.547 ; 49.268	-19.295 ; -16.233		121	121	56	Unpubl.
Madagascar	Survey	21/01/2012 - 01/03/2012	46.547 ; 49.026	-19.295 ; -16.233	36	49	49	43	Unpubl.
Tana	Survey	03/09/2012 - 09/09/2012	39.340 ; 39.472	-4.422 ; -4.158	9	10	10	9	Unpubl.
Tana	Survey	12/02/2008 - 24/02/2008	36.708 ; 40.352	-2.410 ; -0.062		24			[54]
Tana	Survey	03/06/2010 - 22/07/2010	36.674 ; 40.352	-2.410 ; 0.269		98	98		Unpubl.
Tana (1 river)	Monitoring	14/12/2010 - 16/07/2013	37.269	-0.787		51	51		Unpubl.
Tana (5 sites)	Monitoring	25/06/2010 - 02/01/2012	38.311 ; 40.115	-1.851 ; -0.055		78	76		Unpubl.
Tana (2 sites)	Monitoring	11/09/2011 - 16/12/2013	39.636 ; 40.115	-1.851 ; -0.464		106	102		Unpubl.
Tana (2 sites)	Monitoring	13/10/2012 - 20/05/2014	39.636 ; 40.117	-2.269 ; -0.464	247			245	Unpubl.
Athi-Galana-Sabaki	Survey	01/11/2011 - 21/11/2011	37.253 ; 40.108	-3.391 ; -1.078	28	29	30	26	[22]
Athi-Galana-Sabaki	Survey	17/04/2012 - 01/05/2012	37.253 ; 40.108	-3.144 ; -1.078	16	22	22	22	[22]
Athi-Galana-Sabaki	Monitoring	08/09/2011 - 14/12/2013	40.108	-3.144		57	53		Unpubl.
Nyong (6 sites)	Monitoring	26/02/2009 - 15/05/2010	11.283 ; 12.533	3.167 ; 3.900		100			Unpubl.

Table S2. Characteristics of the 12 studied African rivers. AGS = Athi–Galana–Sabaki River.

	AGS	Betsiboka	Bia	Comoé	Congo	Niger	Nyong	Ogooué	Rianila	Tana	Tanoé	Zambezi
Catchment area (km ²) ⁵⁵	40300	68311	11917	78474	3705222	2098640	27415	215216	7844	100608	15608	1378102
Slope (°) ⁵⁶	1.23	1.02	0.36	0.48	0.60	0.44	0.50	0.49	3.22	0.95	0.58	0.86
Discharge (km ³ yr ⁻¹)	2.30	9.49	1.86	7.06	1292.98	200.00	12.30	148.22	12.87	4.92	4.16	130.37
Precipitation (mm) ⁵⁹	769	1527	1545	1174	1527	646	1809	1794	2397	696	1529	940
River-stream surface (km ²) ³	359	1105	105	690	26517	4118	222	4261	1125	895	137	7325
Wetland surface (km ²) ^{58,59,60}	1181	1354	0	150	358756	119734	5483	12612	128	402	126	69254
Aboveground biomass (Mg km ⁻²) ⁵⁷	67	98	479	279	7488	59	1022	984	736	77	489	262
Land cover ⁵⁶												
Dense Forest (%)	12.8	7.9	18.6	2.7	49.1	0.4	78.2	89.8	52.0	12.9	20.7	20.4
Mosaic Forest (%)	0.1	0.9	77.4	32.3	17.8	2.2	19.5	4.4	43.2	0.1	75.6	0.0
Woodland and shrubland (%)	10.2	15.5	0.8	58.7	26.6	21.1	1.6	2.2	1.0	8.1	3.0	54.6
Grassland (%)	59.5	75.3	0.0	0.0	2.9	23.4	0.2	3.2	0.4	71.2	0.0	8.7
Cropland / Bare soil (%)	16.5	0.0	0.0	6.3	1.7	52.2	0.0	0.1	0.0	7.4	0.0	13.4

Table S3. Average values per river of pCO₂, CH₄, N₂O, FCO₂, FCH₄ and FN₂O computed according to² (Auf) and ³ (Ray), integrated at basin and Sub-Saharan continental scaled using the river/stream surface areas reported by³, and the export of TOC and DIC reported in literature for the Congo, the Zambezi and the Tana. AGS = Athi-Galana-Sabaki River

		Congo	Ivory Coast	Ogooué	Niger	Zambezi	Betsiboka	Rianila	Tana	AGS	Nyong	Total
pCO ₂	(ppm)	8092				2612	1665	1861	1571	2197		6415
CH ₄	(nmol L ⁻¹)	3184	223	606	149	2235	305	469	140	277	3922	2205
N ₂ O	(nmol L ⁻¹)	10		10	8	7	8	9	8	10		9.2
FCH ₄ (Aufd)	(μmol m ⁻² d ⁻¹)	14296	1003	2115	502	8348	1305	1923	568	1156	18019	9607
FCH ₄ (Ray)	(μmol m ⁻² d ⁻¹)	18534	1667	4668	583	13597	3493	4537	604	1374	28579	13164
FN ₂ O (Aufd)	(μmol m ⁻² d ⁻¹)	15		13	4	2	4	5	6	16		11
FN ₂ O (Ray)	(μmol m ⁻² d ⁻¹)	19		28	5	2	9	12	6	19		15
FCO ₂ (Aufd)	(mmol m ⁻² d ⁻¹)	1149				283	194	214	186	274		894
FCO ₂ (Ray)	(mmol m ⁻² d ⁻¹)	1520				421	523	509	198	306		1205
FCO ₂ (Aufd)	(TgC yr ⁻¹)	133.41				9.08	0.94	1.06	1.02	0.04		145.5
FCO ₂ (Ray)	(TgC yr ⁻¹)	176.52				13.52	2.53	2.51	1.09	0.05		196.2
TOC export to sea	(TgC yr ⁻¹)	10.00-14.40 ^[62,63]				0.55 ^[25]			0.04 ^[65]			
DIC export to sea	(TgC yr ⁻¹)	3.20-3.46 ^[15,64]				3.69 ^[25]			0.06 ^[65]			
TOC+DIC export to sea	(TgC yr ⁻¹)	15.53				4.24			0.10			

Table S4. FCO₂, FCH₄ and FN₂O in CO₂ equivalents in temperate rivers, the Ohio⁶⁶ and four Belgian⁶⁷ (BE) rivers. The sampled African rivers (Fig. 1) were characterized by lower FCO₂:FCH₄(CO₂ equ) ratios and higher FCO₂:FN₂O(CO₂ equ) than temperate rivers.

	FCO ₂ mmol m ⁻² d ⁻¹	FCH ₄ μmol m ⁻² d ⁻¹	FN ₂ O μmol m ⁻² d ⁻¹	FCO ₂ gC m ⁻² d ⁻¹	FCH ₄ gC m ⁻² d ⁻¹ (CO ₂ equ)	FN ₂ O gC m ⁻² d ⁻¹ (CO ₂ equ)
Ohio (USA)	194	1188	23	2.33	0.12	0.08
Ourthe (BE)	67	110	7	0.80	0.01	0.03
Meuse (BE)	224	1060	22	2.69	0.11	0.08
Geer (BE)	1662	22460	550	19.94	2.25	1.97
Blanc Gravier (BE)	275	80	13	3.30	0.01	0.05

Full data-set available from :

<http://www.nature.com/ngeo/journal/vaop/ncurrent/extref/ngeo2486-s2.xlsx>

Provided for non-commercial research and education use.
Not for reproduction, distribution or commercial use.



This article appeared in a journal published by Elsevier. The attached copy is furnished to the author for internal non-commercial research and education use, including for instruction at the authors institution and sharing with colleagues.

Other uses, including reproduction and distribution, or selling or licensing copies, or posting to personal, institutional or third party websites are prohibited.

In most cases authors are permitted to post their version of the article (e.g. in Word or Tex form) to their personal website or institutional repository. Authors requiring further information regarding Elsevier's archiving and manuscript policies are encouraged to visit:

<http://www.elsevier.com/authorsrights>



Contents lists available at ScienceDirect

Science of the Total Environment

journal homepage: www.elsevier.com/locate/scitotenv

Primary production in a tropical large lake: The role of phytoplankton composition

F. Darchambeau^a, H. Sarmento^b, J.-P. Descy^{c,*}^a Chemical Oceanography Unit, University of Liège, Liège, Belgium^b Department of Hydrobiology, Federal University of São Carlos, 13565-905 São Carlos, São Paulo, Brazil^c Research Unit in Environmental and Evolutionary Biology, University of Namur, Namur, Belgium

HIGHLIGHTS

- We provide a 7-year dataset of primary production in a tropical great lake.
- Specific photosynthetic rate was determined by community composition.
- Annual primary production varied between 143 and 278 mg C m⁻² y⁻¹.
- Pelagic production was highly sensitive to climate variability.

ARTICLE INFO

Article history:

Received 17 July 2013

Received in revised form 9 December 2013

Accepted 9 December 2013

Available online 24 December 2013

Keywords:

Phytoplankton
 Photosynthetic parameters
 Diatoms
 Cyanobacteria
 Tropical limnology
 Predictive model

ABSTRACT

Phytoplankton biomass and primary production in tropical large lakes vary at different time scales, from seasons to centuries. We provide a dataset made of 7 consecutive years of phytoplankton biomass and production in Lake Kivu (Eastern Africa). From 2002 to 2008, bi-weekly samplings were performed in a pelagic site in order to quantify phytoplankton composition and biomass, using marker pigments determined by HPLC. Primary production rates were estimated by 96 in situ ¹⁴C incubations. A principal component analysis showed that the main environmental gradient was linked to a seasonal variation of the phytoplankton assemblage, with a clear separation between diatoms during the dry season and cyanobacteria during the rainy season. A rather wide range of the maximum specific photosynthetic rate (P_{Bm}) was found, ranging between 1.15 and 7.21 g carbon g⁻¹ chlorophyll *a* h⁻¹, and was best predicted by a regression model using phytoplankton composition as an explanatory variable. The irradiance at the onset of light saturation (I_k) ranged between 91 and 752 μE m⁻² s⁻¹ and was linearly correlated with the mean irradiance in the mixed layer. The inter-annual variability of phytoplankton biomass and production was high, ranging from 53 to 100 mg chlorophyll *a* m⁻² (annual mean) and from 143 to 278 g carbon m⁻² y⁻¹, respectively. The degree of seasonal mixing determined annual production, demonstrating the sensitivity of tropical lakes to climate variability. A review of primary production of other African great lakes allows situating Lake Kivu productivity in the same range as that of lakes Tanganyika and Malawi, even if mean phytoplankton biomass was higher in Lake Kivu.

© 2013 Elsevier B.V. All rights reserved.

1. Introduction

Contrary to common assumptions on the constancy of ecological conditions in tropical lakes, pelagic primary production may vary considerably in African great lakes, at different time scales, from seasons to centuries (Melack, 1979; Cohen et al., 2006). At long time scales, Indian Ocean surface temperatures, determining rainfall, are the primary influence on East African climate (Tierney et al., 2013), which largely determines water column processes in the great Rift lakes (e.g. Johnson

and Odada, 1996; Plisnier, 2000; MacIntyre, 2012). At a seasonal scale, the main driver of pelagic primary production is the alternation of wet and dry seasons, with changes in relative humidity and wind velocities: typical wet season conditions induce thermal stratification of the water column, which reduces nutrient supply in the euphotic zone. Dry season conditions tend to reduce the temperature–density gradient and higher wind velocities result in deep vertical mixing of the water column, increasing nutrient supply in the euphotic zone, inducing a dry season phytoplankton peak (Hecky and Kling, 1987; Spigel and Coulter, 1996).

Phytoplankton composition also depends on the alternation of stratified conditions in the rainy season with the deep mixing that occurs in the dry season: the seasonal mixing event not only increases the supply of dissolved nutrients in the euphotic zone, but also results in a rise of the ratio between mixed layer depth (Z_m) to the euphotic layer depth

* Corresponding author. Tel.: +32 81724405.

E-mail addresses: francois.darchambeau@ulg.ac.be (F. Darchambeau), hugo.sarmento@gmail.com (H. Sarmento), jean-pierre.descy@unamur.be (J.-P. Descy).

(Zeu) (Sarmiento et al., 2006). In these conditions, phytoplankton is subjected to potential light limitation, leading to diatom dominance (Reynolds, 2006a). By contrast, in the shallow mixed layer of the rainy season, the lower Zm:Zeu ratio selects for high-light adapted phytoplankton such as green algae and cyanobacteria. The trade-off between high light and nutrient limitation in the rainy season and low light and high nutrients during the dry season has been documented in classic studies in African lakes (e.g. Hecky and Kling, 1987; Kilham et al., 1986) and is a key to understanding shifts in phytoplankton composition in these lakes.

Estimates of annual primary productivity in tropical lakes have been usually based on measurements of phytoplankton photosynthesis carried out over sufficiently long periods to capture the seasonal variations of incident light, water transparency, temperature, nutrients and phytoplankton biomass. Examples of this approach can be found in Lewis (1974) in Lake Lanao (Philippines), in Talling (1965) for several East African lakes, in Hecky and Fee (1981), Sarvala et al. (1999) and Stenuite et al. (2007) for Lake Tanganyika, in Guildford et al. (2007) for Lake Malawi and in Silsbe et al. (2006) for Lake Victoria. Such studies derived photosynthetic parameters (P_{Bm} , the maximum specific photosynthetic rate, and lk or α , a measure of the photosynthetic efficiency) from in situ incubations. If the irradiance at the onset of light saturation (lk) describes the regulatory response of the phytoplankton photosynthesis to the light climate, P_{Bm} relates to the efficiency of the light harvesting system. Main environmental factors influencing P_{Bm} in cultures are temperature and nutrient availability (Geider and MacIntyre, 2002). A reduction of P_{Bm} is observed in nutrient-limited algae (Geider et al., 1998; Greene et al., 1991). At the community level, it has occasionally been demonstrated that larger cells sustain higher P_{Bm} than smaller cells (Cermeño et al., 2005; Peltomaa and Ojala, 2010), but field studies attempting to relate the compound photosynthetic response on the taxonomic composition of the phytoplankton assemblage are rare (Segura et al., 2013). However, phytoplankton composition matters, as

shown by experimental studies on pure cultures, which have provided evidence of significant variation of photosynthetic parameters among taxonomic groups (Falkowski and Raven, 2007; Kirk, 1994; Reynolds, 2006a).

Pigment-based analysis of phytoplankton composition may provide an adequate framework to relate community composition to photosynthesis parameters. Phytoplankton pigments, determined by high performance liquid chromatography (HPLC) analysis, have been used widely for assessing biomass at the class level, with many applications in marine, estuarine, and freshwater environments (e.g., review in Sarmiento and Descy, 2008). The assessment of algal abundance from pigment concentrations uses different techniques, involving ratios of marker pigments to chlorophyll *a* (Chl*a*) (Mackey et al., 1996). As it is based on a fast, automatic and reliable analytical technique, the pigment approach has been largely used in oceanographic studies and monitoring programs (Jeffrey et al., 1997), as well as in large lake studies (Descy et al., 2005; Fietz and Nicklish, 2004; Fietz et al., 2005; Sarmiento et al., 2006).

We applied a pigment approach in Lake Kivu, a great and deep (maximum depth of 489 m) meromictic lake of the East African Rift (Fig. 1). Lake Kivu is located north of Lake Tanganyika, at 1463 m above sea level. The mixolimnion (i.e. the upper layer of a meromictic lake) alternates between periods of complete mixing down to maximum 65 m and periods of stratification during which nutrients become depleted in the euphotic zone (Sarmiento et al., 2006; Schmid and Wüest, 2012). Whereas moderate to severe P-limitation of phytoplankton prevails during most of the year (Sarmiento et al., 2009, 2012), N-limitation may occur in the stratified rainy season, as denitrification takes place within the oxic–anoxic transition zone (Llirós et al., 2012). By contrast, the monimolimnion, i.e. the lower layer that never mixes with surface waters, is rich in nutrients and dissolved gases (Degens et al., 1973; Schmid et al., 2005). Pelagic primary production in Lake Kivu exhibits substantial variation at the seasonal scale, but also between years

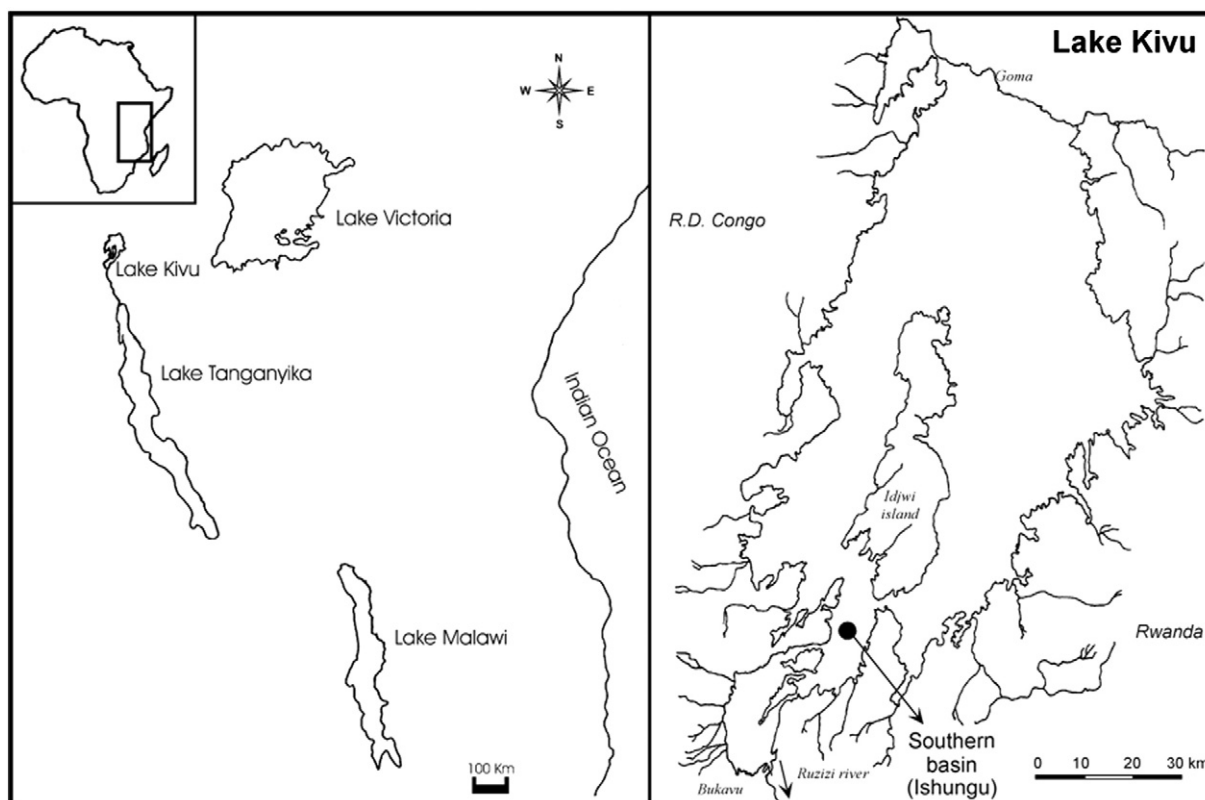


Fig. 1. Location of Lake Kivu in East Africa (left panel) and the sampling site (Ishungu, southern basin).

(Sarmiento et al., 2012), as shown by the variable height of the dry season Chla peak. Phytoplankton composition also varies seasonally in a typical way, with diatoms and cryptophytes being more abundant in the dry season, and cyanobacteria better developed in the rainy season (Sarmiento et al., 2006, 2007).

Our working hypothesis was that in this tropical great lake, phytoplankton composition, along with water transparency and depth of the mixed layer, is a key factor determining pelagic photosynthesis. We used a long-term database of in situ photosynthesis measurements and phytoplankton composition, determined by HPLC analysis of marker pigments, to demonstrate that the photosynthetic parameters, P_{Bm} and I_k , can be derived from quantitative composition of the phytoplankton assemblage, allowing accurate prediction of daily and annual primary production.

2. Material and methods

2.1. Sampling

The study site was located in the southern basin (Ishungu) of Lake Kivu (2.34°S, 28.98°E) (Fig. 1). General physico-chemical characteristics of the lake's water are described elsewhere (e.g. Borges et al., 2011; Descy et al., 2012; Sarmiento et al., 2006; Schmid et al., 2005). Limnological observations were made twice a month from March 2002 to November 2009. First, vertical profiles of temperature were obtained with a Hydrolab DS4a probe or a Yellow Springs Instrument 6600 V2 probe. The mixed layer depth, Z_m , was determined at each occasion as the depth with the maximum downward temperature change per meter, based on the fact that salinity has a marginal effect on density gradient in the top 65 m (Schmid and Wüest, 2012). Water samples were collected at discrete depth intervals (0, 5, 10, 15, 20, 25, 30, 40, 50 and 60 m depth) using a 6 L Van Dorn bottle. For each sampling depth, at least 3 L of water were filtered on Macherey-Nägel (Düren, Germany) GF5 filters (average retention capacity of 0.4 μm) which were immediately frozen at -20 °C for pigment analysis. For the primary production incubation (see below), a pooled sample was constituted on each sampling occasion from discrete samples (2 L) spaced every 5 m in the mixed layer. In addition, at least 3 L of water was filtered from the pooled mixed layer sample for pigment analysis and 2 L was filtered on a pre-combusted GF5 filter for particulate carbon (C), nitrogen (N) and phosphorus (P) analyses. Filters were kept frozen until analysis.

2.2. Phytoplankton biomass

Chla was used as an index of phytoplankton biomass (Reynolds, 2006a). Total phytoplankton biomass and the contribution of the different algal groups were achieved by HPLC analysis of marker pigments. It was demonstrated that the accuracy of Chla and chemotaxonomic carotenoid quantification by HPLC is less than 10 and 25%, respectively (Claustre et al., 2004). Data were subsequently processed with CHEMTAX (for CHEmical TAXonomy) (Mackey et al., 1996), as described in Descy et al. (2005) and Sarmiento et al. (2006). CHEMTAX is a computer program that allows allocating Chla among different algal groups defined by a suite of markers. From an initial ratio matrix (or input matrix) usually derived from pure cultures of phytoplankton, the program uses an iterative process to find the optimal pigment:Chla ratios and generates the fraction of the total Chla pool belonging to each pigment-determined group (Mackey et al., 1996). A supplementary 50 mL sample was preserved immediately after collection with Lugol's solution and neutral formaldehyde (2–4% final concentration) for microscopic identification of main taxa, according to Sarmiento et al. (2007). Phytoplankton biomass was expressed either as mg Chla m⁻³ or as mg Chla m⁻², by integrating the Chla measurements at the different sampled depths over the whole mixolimnion (0–65 m).

2.3. Primary production

The primary production rate was determined in 96 field photosynthesis-irradiance incubations. Eighteen 120-mL (from 2003 to 2005) or 20 180-mL (from 2006 to 2008) glass flasks were filled with water from the pooled mixed layer sample and 50 μCi of NaH¹⁴CO₃ was added into each flask. Duplicate sets of bottles were placed into a ten-case floating incubator providing a range from 0 to 90% of natural light energy and incubated in situ at mid-day for ~2 h just below the surface. Incident light was monitored by a Li-Cor (Lincoln, Nebraska, USA) quantum sensor throughout the incubations.

The incubation was stopped by adding neutral formaldehyde and the phytoplankton was collected on Macherey-Nägel GF5 filters. Filters were rinsed with HCl 0.1 N and the radioactivity of the filters was measured using a Beckman scintillation counter (LS 6000 SC) with Filter-Count (Packard) as scintillation cocktail and the external standard method for quench correction. The specific photosynthetic rate of individual bottle i , P_i (in mg C mg⁻¹ Chla h⁻¹), was calculated following Steeman-Nielsen (1952). Dissolved inorganic carbon (DIC, in mg C L⁻¹) was computed from pH and total alkalinity (TA) measurements using the carbonic acid dissociation constants of Millero et al. (2006). Measurements of TA were carried out by open-cell titration with HCl 0.1 M according to Gran (1952) on 50 mL water samples.

For each experiment, the maximum specific photosynthetic rate P_{Bm} (in mg C mg⁻¹ Chla h⁻¹) and the irradiance at the onset of light saturation I_k (μE m⁻² s⁻¹) were determined by fitting P_i to the irradiance gradient provided by the incubator I_i (μE m⁻² s⁻¹), using the Vollenweider's (1965) equation, with the photo inhibition parameters set to 1:

$$P_i = 2P_{Bm} \frac{I_i}{2I_k} \frac{1}{1 + \left(\frac{I_i}{2I_k}\right)^2} \quad (1)$$

Fitting was performed using the Gauss-Newton algorithm for non-linear least squares regression with the help of the STATISTICA 10[®] software (StatSoft France). The vertical light attenuation coefficient (Kirk, 1994), K_e (m⁻¹), was calculated from simultaneous measurements of surface irradiance with a Li-Cor LI-190 Quantum Sensor and underwater PAR measurements with a submersible Li-Cor LI-193SA Spherical Quantum Sensor. K_e was derived from the slope of the semi-logarithmic regression between relative quantum irradiance and depth (from 0 to 20 m). From 2003 to 2006, K_e was derived from Secchi depth, SD (m), using a conversion factor $K_e = -\ln(0.25)/SD$ obtained by calibration with PAR downward attenuation ($n = 16$, Pearson $r = 0.81$, $p < 0.001$). The euphotic depth, Z_{eu} , was defined as the depth at which light is 1% of subsurface light. The average light in the mixed layer, I_{Zm} (in μE m⁻² s⁻¹), was calculated according to Riley (1957):

$$I_{Zm} = \frac{I_s(1 - e^{-Z_m K_e})}{Z_m \cdot K_e} \quad (2)$$

where I_s is the mean solar flux at the surface of the lake (24 h average) and Z_m is the depth of the mixed layer. I_s was calculated for a theoretical cloudless atmosphere for the appropriate latitude (Fee, 1990).

Daily depth-integrated primary production (DPP, in g C m⁻² d⁻¹) was determined using photosynthetic parameters P_{Bm} and I_k , Chla biomass vertical profile, vertical light attenuation coefficient K_e and continuous surface irradiance data (Kirk, 1994), calculated for a theoretical cloudless atmosphere for the appropriate latitude (Fee, 1990):

$$DPP = \int_0^{24h} \int_0^{Z_m} 2P_{Bm} B_z \frac{I_{z,t}}{1 + \left(\frac{I_{z,t}}{2I_k}\right)^2} dz dt \quad (3)$$

Table 1
Description of the variables used for modeling primary production.

Symbol	Description	Unit	Data source
B_z	Chlorophyll <i>a</i> biomass at depth <i>z</i>	mg Chla m^{-3}	Field observations
DPP	Daily depth-integrated primary production	$g\ C\ m^{-2}\ d^{-1}$	Eq. (3)
$I_{0,t}$	Surface irradiance at time <i>t</i>	$\mu E\ m^{-2}\ s^{-1}$	Solar modeling (Fee, 1990)
I_k	Irradiance at the onset of light saturation	$\mu E\ m^{-2}\ s^{-1}$	Field experiment or Eq. (5)
I_s	Mean solar flux at the surface of the lake during the day (24 h average)	$\mu E\ m^{-2}\ s^{-1}$	Solar modeling (Fee, 1990)
I_{zm}	Average light in the mixed layer	$\mu E\ m^{-2}\ s^{-1}$	Eq. (2)
I_{zt}	Irradiance at depth <i>z</i> and time <i>t</i>	$\mu E\ m^{-2}\ s^{-1}$	Eq. (4)
K_e	Vertical light attenuation coefficient	m^{-1}	Field observations
P_{Bm}	Maximum specific photosynthetic rate	$mg\ C\ mg^{-1}\ Chla\ h^{-1}$	Field experiment or Eq. (6)
PCAaxis1	Score of pigment-based phytoplankton composition on the 1st axis of the PCA	No unit	HPLC analyses of field samples
PCAaxis2	Score of pigment-based phytoplankton composition on the 2nd axis of the PCA	No unit	HPLC analyses of field samples
Z_m	Mixed layer depth	m	Field observations

with:

$$I_{z,t} = 0.95 I_{0,t} e^{-K_e z} \quad (4)$$

All symbols and units are described in Table 1.

2.4. Particulate CNP

Particulate C and N were analyzed using a Carlo-Erba NA1500 elemental analyzer. Particulate P was analyzed by spectrophotometric determination of phosphate after digestion with potassium persulfate and boric acid (Valderrama, 1981). The elemental ratios were expressed as the mean ratio in molar units of the different sampling dates.

2.5. Statistical analysis

A principal component analysis (PCA) was performed on the relative contribution of the different phytoplankton groups to Chla resulting from the CHEMTAX processing. In total, 1387 individual HPLC samples from Lake Kivu were used. The PCA was carried out with the help of the CANOCO software (ter Braak and Šmilauer, 2002) after centering and standardization of the relative contributions to total Chla biomass. Results of the PCA ordination, i.e. sample scores along the first factorial axis, were used as independent variables to explain the maximum specific photosynthetic rate, P_{Bm} , of the different photosynthesis experiments. The reason for using the PCA axes instead of phytoplankton relative class abundances was to avoid autocorrelation between independent variables (Legendre and Legendre, 1998). The effects of the season along PCA axes were tested using Student's *t* statistical tests. Simple and multiple linear regressions were performed to explain variations of photosynthetic parameters, I_k and P_{Bm} , with, respectively, light conditions in the water column and phytoplankton community composition and CNP ratios. Multiple linear regressions were achieved using a forward stepwise selection of explanatory variables. Statistical tests, i.e. simple and multiple linear regressions and Student's *t*-test, were carried out with the help of the STATISTICA 10[®] software (StatSoft France). Daily primary production was calculated using Eq. (4) with observed or statistically-derived photosynthetic parameters. A sensitivity analysis of the primary production model was performed by replacing each variable by its mean in turn, while holding all other variables at their original values. The mean absolute relative error of daily primary production was then computed for each variable.

3. Results

Phytoplankton composition and biomass are presented in Fig. 2. The community was dominated by cyanobacteria, diatoms and cryptophytes. A seasonal peak higher than 100 mg Chla m^{-2} was observed at the end of the dry season (July–August) in 2003, 2004 and more spectacularly in 2008. A lower dry season peak was observed in

2006 and 2007. These peaks were mainly constituted of diatoms (essentially *Nitzschia bacata* Hust. and *Fragilaria danica* Lange Bert.). By contrast, cyanobacteria developed best during the rainy season, from October to May. The most common cyanobacteria taxa present in Lake Kivu were *Planktolyngbya limnetica* Lemm., *Synechococcus* spp. and various *Microcystis* species. The cryptophyte *Rhodomonas* was present throughout the year.

The inter-annual variability of phytoplankton biomass was relatively high, with the lowest mean annual biomass observed in 2005 with 53 mg Chla m^{-2} and the highest in 2008 with 100 mg Chla m^{-2} . The inter-annual coefficient of variation (CV) from 2002 to 2008 was 21%.

The seasonal variation of the mixed layer depth is presented in Fig. 2C. The dry season (from June to August) was characterized by a deeper mixed layer, although this pattern was not consistent over the years.

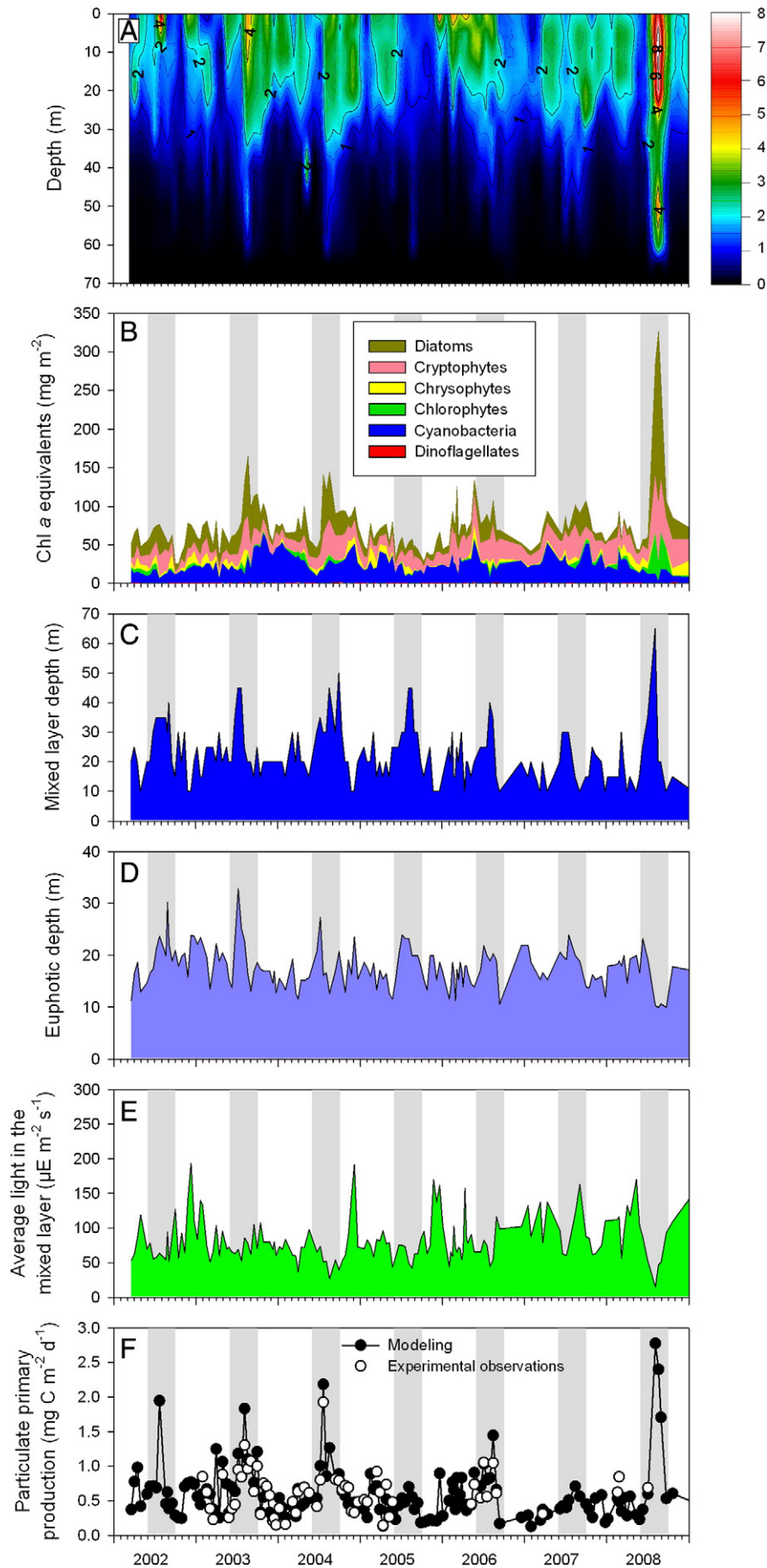
The PCA carried out on the relative contribution of each phytoplankton group to the total Chla biomass confirmed that the first component was linked to the seasonal variations (Fig. 3). The first axis, which represents 30.5% of the total variance, separates diatoms and chlorophytes from cyanobacteria. This axis clearly separates rainy season samples, with generally negative values (mean value, -0.19), from dry season samples, with positive values (mean value, $+0.31$) (Student's *t*-test, $p < 0.001$). The second axis collects 22.0% of the total variance and dissociates cryptophytes from the other groups. This axis is independent on the seasonal succession (Student's *t*-test, $p = 0.112$).

The depth of the euphotic zone, Z_{eu} , ranged between 8.3 and 28.5 m (median, 17.6 m) (Fig. 2D). The highest transparencies were observed at the end of the rainy season, in June, and sometimes in July and August, depending on the year. As expected, phytoplankton biomass directly influenced water transparency (Fig. 4).

Mean (\pm standard deviation) seston C, N and P concentrations were 458 (± 113) $\mu g\ C\ L^{-1}$, 56 (± 12) $\mu g\ N\ L^{-1}$ and 5.2 (± 1.8) $\mu g\ P\ L^{-1}$. Seasonal variations of the seston C:N:P molar ratios are presented in Fig. 5. The C:N ratio (mean 10.1, min–max 6.3–14.4) was largely influenced by season, with lower values at the end of dry season (July–August) than in the rest of year ($p < 0.005$). Nevertheless, dry season values (June–August) were the most variable, depending on the year. The C:P ratio (mean 263, min–max 130–447) was also largely influenced by season, with decreasing values from December to June and increasing values from July to November. The seasonal pattern was consistent over the years.

The photosynthetic parameters were estimated at 96 occasions from 2002 to 2008. An example of the photosynthesis vs irradiance curve we usually obtained is illustrated in Fig. 6. The fitting to the Vollenweider's model (Eq. (1)) was usually good, with a $R^2 > 0.95$. The irradiance at the onset of light saturation, I_k , ranged between 91 and 752 $\mu E\ m^{-2}\ s^{-1}$ (mean 318 $\mu E\ m^{-2}\ s^{-1}$). It was linearly correlated to the mean irradiance in the mixed layer, I_{zm} (Fig. 7).

The maximum specific photosynthetic rate, P_{Bm} , ranged between 1.15 and 7.21 $g\ C\ g^{-1}\ Chla\ h^{-1}$ (mean 3.57 $g\ C\ g^{-1}\ Chla\ h^{-1}$). Simple and multiple linear regressions were tested to explain the variability of



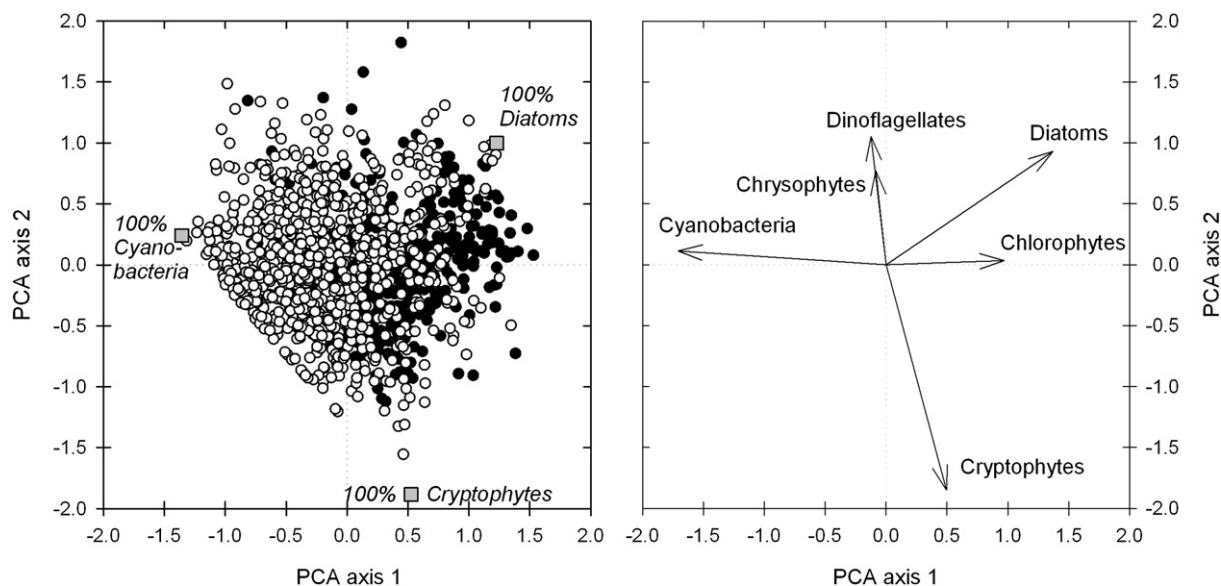


Fig. 3. Principal component analysis (PCA) of the relative contribution of the main phytoplankton groups to chlorophyll *a* from Lake Kivu, Ishungu station (southern basin); left panel: diagram of the samples on the two first axes of the PCA, showing a clear separation depending on season (open circles: samples from the rainy season; black circles: dry season) and the position of hypothetical “pure” phytoplankton group samples; right panel: diagram of the phytoplankton groups on the two first axes of the PCA.

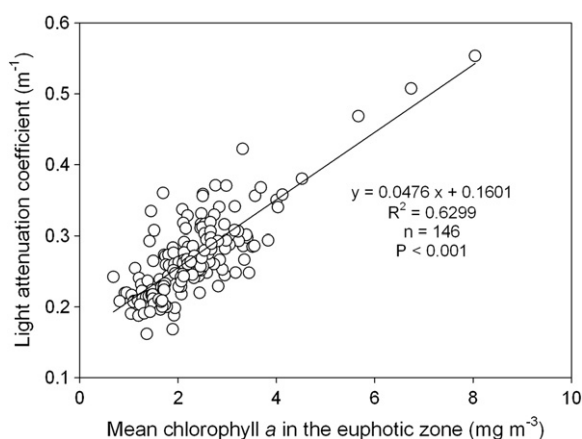


Fig. 4. Linear regression of the vertical attenuation of light against mean chlorophyll *a* concentration in the euphotic layer in Lake Kivu, Ishungu station (southern basin), 2002–2008.

P_{Bm} using phytoplankton composition, represented by the sample position along the first 4 axes of the PCA, and C:N and C:P ratios as explanatory variables. P_{Bm} was significantly correlated with axis 1 ($r = 0.779$; $p < 0.001$) and axis 2 ($r = 0.321$; $p = 0.001$) of the PCA. P_{Bm} was also negatively correlated with seston C:P ratios ($r = -0.448$; $p < 0.001$). A multiple linear regression was constructed with a forward stepwise selection of significant variables (Table 2). A single model with the first two axes of the PCA, significant at the 0.05 probability level, explained around 66% of the P_{Bm} variance (Table 2 and Fig. 8). As the C:P ratios were negatively correlated with the first PCA axis ($r = -0.49$, $p < 0.001$), both variables explained a common variance of P_{Bm} . This explains why the C:P ratio was not significant to explain P_{Bm} when the first PCA axis was already included in the regression model.

P_{Bm} was positively correlated with the sample score along the first and the second axes of the PCA: this results from the fact that P_{Bm} was

higher for a phytoplankton assemblage dominated by diatoms than when phytoplankton was dominated by cyanobacteria and/or cryptophytes. Three fictive HPLC samples with communities composed exclusively of cyanobacteria, diatoms or cryptophytes were added as passive samples in the PCA (see Fig. 3). The position of these communities along the first 2 axes was used within the multiple linear regression model presented in Table 2, to calculate the P_{Bm} values for “pure” communities in Lake Kivu. The calculated P_{Bm} was $1.13 \text{ g C g}^{-1} \text{ Chla h}^{-1}$ for cyanobacteria, $2.36 \text{ g C g}^{-1} \text{ Chla h}^{-1}$ for cryptophytes, and $7.21 \text{ g C g}^{-1} \text{ Chla h}^{-1}$ for diatoms.

The daily primary production was calculated based upon observed and statistically-derived photosynthetic parameters. I_k was modeled using the linear regression model including I_{zm} as single explanatory variable (Fig. 7):

$$I_k = 43.7 + 3.67I_{zm} \quad (5)$$

and P_{Bm} values were obtained from the multiple linear regression model presented in Table 2:

$$P_{Bm} = 3.56 + 2.001 \text{ PCAaxis1} + 1.196 \text{ PCAaxis2}. \quad (6)$$

Daily primary production results are presented in Fig. 2F. The mean daily primary production based upon observed photosynthetic parameters was $0.620 \text{ g C m}^{-2} \text{ d}^{-1}$ (range 0.142–1.924). Daily primary production values calculated from observed or statistically-derived photosynthetic parameters were highly correlated ($R^2 = 0.787$) and not statistically different (Student’s t-test for paired samples, $n = 59$, $P = 0.206$). Annual primary production was then calculated based on statistically-derived photosynthetic parameters. The mean annual primary production from 2002 to 2008 was $213 \text{ g C m}^{-2} \text{ y}^{-1}$. The inter-annual variation was important (CV = 25%), with a minimum value of $143 \text{ g C m}^{-2} \text{ y}^{-1}$ in 2007 and a maximum value of $278 \text{ g C m}^{-2} \text{ y}^{-1}$ in 2008.

Input variables of the primary production model are the phytoplankton biomass (Chla), the photosynthetic parameters (P_{Bm} and I_k), the

Fig. 2. (A) Vertical distribution of phytoplankton biomass (Chlorophyll *a*, mg m^{-3}), (B) areal chlorophyll *a* concentrations and biomass composition from marker pigment analysis, (C) depth of the mixed layer, (D) depth of the euphotic layer, (E) average light in the mixed layer, (F) daily depth-integrated primary production with photosynthetic parameters estimated from in situ ^{14}C incubations (white circles) or with photosynthetic parameters calculated from Eqs. (5) and (6) (black circles with lines), during the 2002–2008 period in Lake Kivu, Ishungu station (southern basin). The gray boxes identify the main dry season periods.

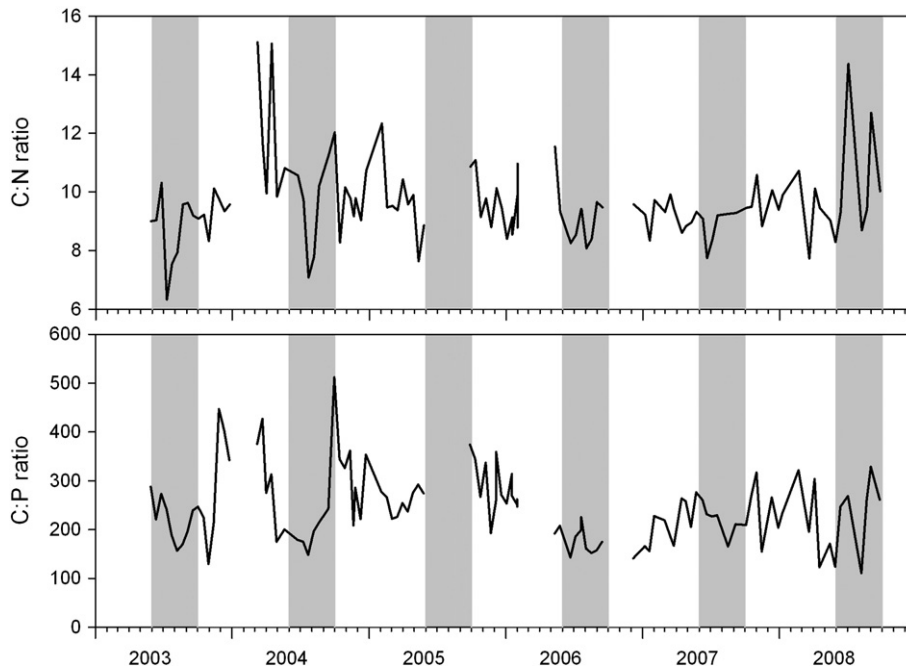


Fig. 5. C:N:P elemental ratios (atomic values) of epilimnetic seston in Ishungu station (southern basin) of Lake Kivu from 2003 to 2008. The gray boxes identify the main dry season periods.

depth of the mixed layer (Z_m), the vertical light attenuation coefficient (K_e), and indirectly (via its influence on P_{Bm}) the phytoplankton community composition (PCAaxis1). Results of the sensitivity analysis of the primary production model are presented in Table 3. Chla was the most influential variable of the daily primary production, followed by the photosynthetic parameters. The physical variables, such as Z_m and K_e had only minor influence.

4. Discussion

In this study, we present results on phytoplankton assemblage, biomass and production obtained during a 7-year continuous survey in Lake Kivu, a large tropical lake of East Africa. Such a dataset is unique for East African Great lakes and provides evidence for substantial variations of phytoplankton biomass and production between years. From these data, we developed an empirical model of planktonic primary

production which can be used for deriving photosynthetic parameters based upon phytoplankton community composition and light conditions.

In Lake Kivu, phytoplankton generally peaks in the main dry season (June–September) (Fig. 2), when enhanced lake evaporation causes a significant heat loss from the lake surface, allowing a reduction of the thermal gradient in the mixolimnion (Sarmiento et al., 2006). Surface waters are then mixed with deeper waters enriched in nutrients, allowing adequate conditions for phytoplankton development. Community is then dominated by diatoms, which sustained a higher specific photosynthetic rate, P_{Bm} ($7.21 \text{ g C g Chla}^{-1} \text{ h}^{-1}$), than the other taxonomic groups. During the rest of the year, i.e. from September to June, stable density stratification is usually observed within the mixolimnion, with varying depths of the surface mixed layer of typically around 10–30 m (Fig. 2). During this time, nutrient supply for primary production is scarce (Pasche et al., 2012; Sarmiento et al., 2012) and phytoplankton becomes nutrient-limited (Fig. 5). Cyanobacteria with a low P_{Bm} ($1.13 \text{ g C g Chla}^{-1} \text{ h}^{-1}$) then dominated the community.

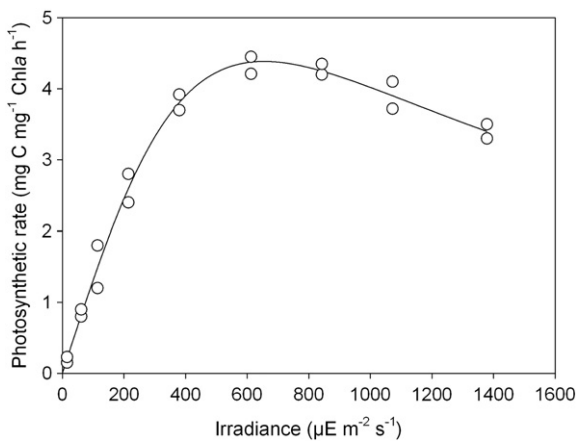


Fig. 6. Example of a photosynthesis–light relationship obtained from an in situ radiocarbon incubation under light saturation in Lake Kivu (July 3rd, 2008). White circles are for the rates estimated from the incubated bottles while the line shows the rates estimated from Vollenweider's equation (Eq. (1)) fitted to the incubation results ($R^2 = 0.989$).

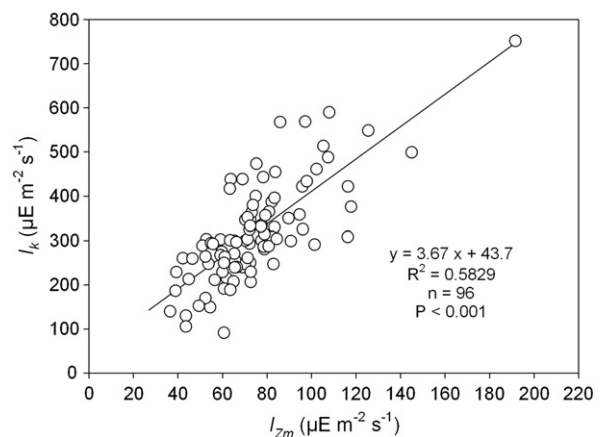


Fig. 7. Linear regression of the onset of light saturation of the phytoplankton (I_k) against average light in the mixed layer (I_{zm}); data from ^{14}C incubations in Lake Kivu, Ishungu station (southern basin), 2002–2008.

Table 2

Results of multiple linear regressions with forward stepwise selection between P_{Bm} as dependent variable and sample coordinates along the first 4 axes of the PCA with HPLC results and seston C:P and C:N ratios as explanatory variables, $n = 96$.

Variables	Coefficient	P	R ²
Origin	+3.560	<0.001	0.658
PCAaxis1	+2.001	<0.001	
PCAaxis2	+1.196	<0.001	

P_{Bm} was significantly correlated to both intracellular nutrient quota and phytoplankton taxonomic composition described by the principal components of a PCA. As the effects of nutrient supply and phytoplankton taxonomic composition are confounded in our field study, we cannot distinguish their respective role in controlling P_{Bm} . It was demonstrated that N limitation in microalgae limits the amount of Chla and RubisCO, the key enzyme involved in photosynthetic fixation of carbon dioxide (CO₂) (Geider and MacIntyre, 2002; Turpin, 1991) and that P_{Bm} parallels N content in N-limited algae (Geider et al., 1998). Moreover, P starvation limited also P_{Bm} and the contribution of RubisCO to cell protein in *Dunaliella tertiolecta* Butcher (Geider et al., 1998).

Nevertheless, the best prediction of P_{Bm} in Lake Kivu was obtained by a regression model including the first principal component of a PCA analysis, used as synthetic descriptor of the phytoplankton taxonomic composition. This approach generated estimates of P_{Bm} which depended primarily on the dominant phytoplankton groups according to season. We were able to calculate P_{Bm} specific to each important taxonomic group: 1.13 g C g Chla⁻¹ h⁻¹ for cyanobacteria, 2.36 for cryptophytes, and 7.21 for diatoms. The physiological basis for these large differences among phytoplankton depends on inorganic C fixation mechanisms and therefore on the specific properties of RubisCO, as discussed by Tortell (2000). Indeed, RubisCO exists in different forms in photosynthetic organisms (Falkowski and Raven, 2007) and differs largely in affinity and specificity for CO₂. The specificity is measured by the ratio between the CO₂ fixation rate and the O₂ fixation rate when CO₂ and O₂ are at limiting concentrations: the higher the value of the ratio, the higher the affinity for CO₂ relative to O₂ (Falkowski and Raven, 2007). Most cyanobacteria, including *Synechococcus* sp., abundant in tropical lakes (Sarmiento, 2012), have high affinity and low specificity, whereas diatoms are among the eukaryotes having the lowest affinity and highest specificity (Falkowski and Raven, 2007; Tortell, 2000). This would give diatoms a higher inherent capacity for C-fixation relative to photorespiration and may explain the high P_{Bm} we found for this phytoplankton group.

The irradiance at the onset of light saturation, I_k , was highly correlated to the average light in the mixed layer, I_{Zm} (Fig. 7). For a given taxon,

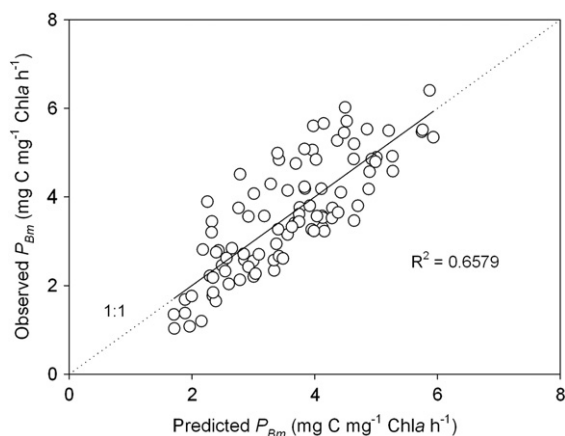


Fig. 8. Plot of observed vs predicted photosynthetic capacity (P_{Bm}) of the phytoplankton in Lake Kivu, Ishungu station (southern basin), 2002–2008.

Table 3

Sensitivity analysis of the daily primary production model. Each variable was replaced by its mean in turn while holding all other variables at their original values. The main absolute relative error of daily primary production (MARE, in %) was computed for each variable. A high value indicates that the model is sensitive to the variable. Variables are classified by decreasing order of MARE.

Variables	Mean	MARE
Biomass	0 m: 2.44 mg Chla m ⁻³ 10 m: 2.26 mg Chla m ⁻³ 20 m: 1.95 mg Chla m ⁻³ 30 m: 1.12 mg Chla m ⁻³ 40 m: 0.55 mg Chla m ⁻³ 50 m: 0.32 mg Chla m ⁻³ 60 m: 0.17 mg Chla m ⁻³	38%
P_{Bm}^a	3.57 mg C mg ⁻¹ Chla h ⁻¹	27%
K_e (only directly) ^b	0.26 m ⁻¹	18%
I_k^c	318 μE m ⁻² s ⁻¹	17%
Z_m^d	21.6 m	17%
K_e^e	0.26 m ⁻¹	10%

^a P_{Bm} in the model is predicted by the algae community composition.

^b K_e influences the daily primary production both directly and indirectly (through its influence on I_k); in this line only the direct effect is evaluated.

^c I_k in the model is predicted by I_{Zm} , which is calculated from Z_m and K_e .

^d Z_m in the model influences I_{Zm} and therefore I_k .

^e The direct and indirect effects of K_e on the daily primary production is evaluated.

I_k is influenced by both temperature and available light (Kirk, 1994). Given the small range of temperature variation in tropical lakes, it is expected that I_k would be best predicted by available light in the mixed layer, which is itself, given by the relative constancy of I_0 in tropical regions, governed by the depth of the mixed layer (Z_m) and by the vertical light attenuation coefficient (K_e). A low I_k is characteristic of phytoplankton adapted to low light, i.e. able of developing their maximal photosynthetic rate at low mean irradiance induced by deep mixing, and having accessory photosynthetic pigments. This situation occurs in deep tropical lakes in the dry season conditions, selecting for diatoms, which are also favored by increased nutrient supply and reduced sedimentation losses (Reynolds, 2006b). In contrast, high I_k occurred in Lake Kivu when I_{Zm} was high due to stratification of the mixolimnion reducing the mixing depth, selecting for high-light-adapted phytoplankton, able to face N depletion, such as cyanobacteria. So, to a large extent, the variation of I_k in deep tropical lakes reflects seasonal variations of the environmental factors that contribute to determine the phytoplankton assemblage (Stenuite et al., 2007).

A key feature of Lake Kivu, already pointed out by Spigel and Coulter (1996), is the weak thermal gradient in the mixolimnion, due to its location at high altitude, where air temperature is lower than in the regions of the other East African great lakes. Then the density gradient in surface waters is always weak (Schmid and Wüest, 2012). Stratification conditions are therefore not constant during the rainy season and short mixing events may alternate with episodes of stratification (Fig. 2C). This leads to short periods of phytoplankton development out of the dry season, as observed by example during the rainy season 2006. On average, half of the annual primary production occurred nevertheless during the 4 months of the dry season. But exceptions to this general pattern are not rare: dry season phytoplankton peaks were not observed during 3 years (2002, 2005 and 2007) out of 7 (Fig. 2). Consequently, the absence of the dry season peak directly heavily impacted the mean annual primary production. For example, the absence of a complete mixing within the mixolimnion during the dry season 2007 led to a low annual primary production (143 g C m⁻² y⁻¹) compared to the situation in 2008 where a complete overturn of the mixolimnion was observed during the dry season, producing a high phytoplankton biomass over the whole mixed layer and an annual production of 278 g C m⁻² y⁻¹.

This demonstrates the sensitivity of tropical lakes to climate variability, as emphasized by several authors (e.g. Johnson and Odada, 1996; Descy and Sarmiento, 2008). If the weather conditions leading to the

Table 4

Volumetric (average in the euphotic zone) and total areal chlorophyll *a* (Chl_a) concentrations, mean annual primary production (PP) in the pelagic zone of the East African great lakes. ⁽¹⁾ Sarmento et al. (2012) and unpublished results (Jean-Pierre Descy, pers. comm.), ⁽²⁾ volumetric Chl_a from Descy et al. (2005), areal Chl_a and CNP data from Descy et al. (2006), PP data from Stenuite et al. (2007); ⁽³⁾ Bergamino et al. (2010) and unpublished results (Nadia Bergamino, pers. comm.); ⁽⁴⁾ Degenbol (1993); ⁽⁵⁾ Guildford et al. (2000); ⁽⁶⁾ Patterson et al. (2000); ⁽⁷⁾ Guildford et al. (2007); ⁽⁸⁾ Mugidde (1993); ⁽⁹⁾ Guildford and Hecky (2000); ⁽¹⁰⁾ Mugidde (2001); ⁽¹¹⁾ Silsbe (2004) using a photosynthetic quotient of 1.

		Chl _a (mg m ⁻³)	Chl _a (mg m ⁻²)	PP (g C m ⁻² y ⁻¹)
L. Kivu (southern basin)	2002	1.77	57	223
	2003	2.31	80	264
	2004	2.55	83	236
	2005	1.63	53	153
	2006	2.58	74	192
	2007	2.04	73	143
	2008	2.89	100	278
	Mean	2.23	74	213
L. Kivu (eastern basin) ⁽¹⁾	2005	2.11	91	
	2006	1.94	63	
	2007	2.03	65	
	2008	2.10	88	
	Mean	2.03	77	
L. Tanganyika (off Kigoma) ⁽²⁾	2002	0.64	36.4	123
	2003	0.59	37.3	130
	2004		35.8	
L. Tanganyika (off Mpulungu) ⁽²⁾	2002	0.71	38.3	175
	2003	0.73	41.3	205
	2004		34.4	
L. Tanganyika (whole lake) ⁽³⁾	2003	1.06	42.9	236
L. Malawi (pelagic) ⁽⁴⁾	1977–1981		27.0	271
	1990–1991	0.51	23.0	
	1992			329
	1993			518
	1997–2000	0.86	34.4	169
L. Victoria (near offshore) ⁽⁸⁾	1989–1991	24.5	330.8	1903 ^a
	1990	26.5		
	1992–1996			
	1994–1998	13.5		
L. Victoria (lake-wide averages) ⁽¹¹⁾	2000 ^b	10.7	116.5	1302/366 ^c
	2001 ^d	10.5	106.9	1350/236 ^c

^a Gross primary production estimated by the O₂ light and dark technique and converted into C using a photosynthetic quotient of 1.

^b Mean of the February and August 2000 cruises.

^c Respectively, gross and net primary productions estimated by the O₂ light and dark technique and converted into C using a photosynthetic quotient of 1.

^d Mean of the February and August 2001 cruises.

seasonal mixolimnion cooling and overturn are well understood, regional drivers of the inter-annual variability of the limnology of Lake Kivu are not yet explored. The East African climate was shown to be highly sensitive to sea-surface temperatures in the tropical Atlantic and Indian Oceans (Nicholson, 1996; Tierney et al., 2013). For example, the weather of the area centered around Lake Tanganyika is influenced by the El-Niño Southern Oscillation but timing and magnitude of this teleconnection are controlled by the local climate system (Plisnier et al., 2000).

Table 5

P values from Mann–Whitney *U* tests performed between individual East African great lakes for the variables and data presented in Table 4. Significant values at the 0.05 level are in bold.

	Volumetric Chl _a	Areal Chl _a	Net PP
Lake Kivu vs Lake Tanganyika	0.003	<0.001	0.234
Lake Kivu vs Lake Malawi	0.041	0.014	0.165
Lake Kivu vs Lake Victoria	0.003	0.014	0.241
Lake Tanganyika vs Lake Malawi	0.846	0.030	0.111
Lake Tanganyika vs Lake Victoria	0.012	0.023	0.118
Lake Malawi vs Lake Victoria	0.081	0.081	0.817

A comparison of phytoplankton biomass and production data from East African Great Lakes shows that volumetric and areal biomass in Lake Kivu was higher than in lakes Tanganyika or Malawi but lower than in Lake Victoria (Tables 4 and 5). However, the annual primary production in Lake Kivu was in the same range as that in lakes Tanganyika or Malawi and no statistical difference can be observed between the phytoplankton production of these lakes (Table 5). Severe eutrophication of Lake Victoria, resulting into the highest pelagic Chl_a biomass for the East African great lakes (Table 4), arose from an important increase of human-population and agricultural activity from the 1930s onwards in its drainage basin (Verschuren et al., 2002). Higher phytoplankton biomass is still observed in the littoral areas and in closed bays (see e.g. Silsbe et al., 2006). Despite this higher Chl_a concentration in Lake Victoria, the net particulate primary production in the pelagic of Lake Victoria is surprisingly in the same range as those of the other East African Great Lakes (Tables 4 and 5). This low net productivity is most probably caused by self-shading, reducing the euphotic layer and inducing low light availability, as described for many other eutrophic lakes (e.g. Hubble and Harper, 2001; Vareschi, 1982).

Higher nutrient concentrations are usually observed in surface waters of Lake Kivu than in Lake Tanganyika (Sarmento et al., 2006). Soluble reactive phosphorus (SRP) in the euphotic zone of Lake Kivu was on average 0.44 μM in rainy season and 0.75 μM in dry season in 2002–2005; mean SRP in the euphotic layer of Lake Tanganyika was 0.19 and 0.43 in rainy season and dry season, respectively, in 2002 off Kigoma (Sarmento et al., 2006). The average dissolved inorganic nitrogen (DIN) in Lake Kivu was 2.42 and 3.29 μM in the rainy season and the dry season, respectively. This contrast with lower DIN in Lake Tanganyika off Kigoma (mean rainy season DIN: 0.48 μM; mean dry season DIN: 0.69 μM). In Lake Malawi, annual means of total P and total N were 0.25 and 6.7 μM, respectively (Guildford et al., 2000). So, if Lake Kivu presents higher P concentrations in surface waters than in lakes Tanganyika and Malawi, Lake Malawi presents higher N concentrations than the other two lakes. Nevertheless phytoplankton of the three lakes present periods of single or combined N and/or P limitations (De Wever et al., 2008; Guildford et al., 2003; Sarmento et al., 2012). Differences in nutrient concentrations, and especially P, between these lakes may help to explain the higher phytoplankton biomass we observed in Lake Kivu compared to lakes Tanganyika and Malawi.

An alternative but not exclusive hypothesis is linked to the food web structure, which allows a lower grazing pressure from the metazooplankton in Lake Kivu than in the other large Rift lakes. In 1959, *Limnothrissa miodon* Boulenger, a clupeid endemic to Lake Tanganyika, was introduced into Lake Kivu (Snoeks et al., 2012) in order to fill the empty pelagic niche and provide proteins for the local population. The planktivorous “Tanganyika sardine” may have led to the extinction of the cladoceran *Daphnia curvirostris* Eylmann, an efficient grazer and nutrient recycler (Dumont, 1986), which was presumably present in the lake in the 1950s. The current zooplankton is dominated by cyclopoid copepods, which are less efficient grazers (Isumbusho et al., 2006). Further, predation by the sardine has led to a reduction of zooplankton biomass, which has reduced the top-down control over phytoplankton (Darchambeau et al., 2012). The absence of an efficient grazer in Lake Kivu, as those present in lakes Tanganyika and Malawi, may help to explain why phytoplankton biomass observed in Lake Kivu is relatively high, despite phytoplankton productivity is of the same magnitude as in lakes Malawi and Tanganyika.

Huge amounts of CO₂ and methane (CH₄) (300 km³ and 60 km³, respectively, at 0 °C and 1 atm) are dissolved in the deep water layers of Lake Kivu (Degens et al., 1973; Schmid et al., 2005). Around one third of CH₄ originates from acetoclastic methanogenesis of sedimentary organic material, the other two thirds is produced by reduction of geogenic CO₂ (Schoell et al., 1988; Pasche et al., 2011). Deep gas concentrations increased by 15–20% for CH₄ and 10% for CO₂ in the past 30 years (Schmid et al., 2005). In an attempt to explain the increase of CH₄ concentrations in deep waters, Schmid et al. (2005) simulated the

CH₄ production along the 990 last years. They concluded that the historical CH₄ production rate rose from an historical constant production rate of 30 g C m⁻² y⁻¹ to 100 g C m⁻² y⁻¹ between 1974 and 2004. Such a 3-fold increase would have been possible if an equivalent increase of primary production in the mixolimnion had occurred. In order to evaluate a possible increase of primary production in the lake, few historical data are available: Degens et al. (1973) and Jannasch (1975) reported a range of mean daily production of, respectively, 1.03–1.44 g C m⁻² d⁻¹ and 0.66–1.03 g C m⁻² d⁻¹, whereas Descy (1990) measured a rate of 0.33 g C m⁻² d⁻¹ in the pelagic zone. According to our estimates, the present daily primary production in Lake Kivu spans over a wide range of values, from 0.14 to 1.92 g C m⁻² d⁻¹, with a mean of 0.62 g C m⁻² d⁻¹. This range of variation covers well the few historic observations, allowing the conclusion that there was no important change of the lake's primary production in the pelagic zone over the last 40 years.

Other hypotheses than lake eutrophication for explaining the CH₄ increase should then be envisaged. These hypotheses would involve an increased net sedimentation flux of C and nutrients due to environmental modifications as observed from analyses of sediments cores (Pasche et al., 2010, 2011). Among these modifications, the introduction of the Tanganyika sardine, *L. miodon*, at the end of the 1950s might have been a key event leading to ecological and geochemical changes. The possible consequences of this introduction, involving a trophic cascade effect with a reduction of the grazing pressure on phytoplankton and a subsequent increase of net sedimentation of organic matter, are further discussed by Darchambeau et al. (2012) and Descy et al. (2012). However, the extent of the changes in the food web is still difficult to evaluate from the present data, and an improved understanding will likely result from further paleolimnological studies based on various proxies of past productivity and phytoplankton composition.

Conflict of interest

There is no conflict of interest.

Acknowledgments

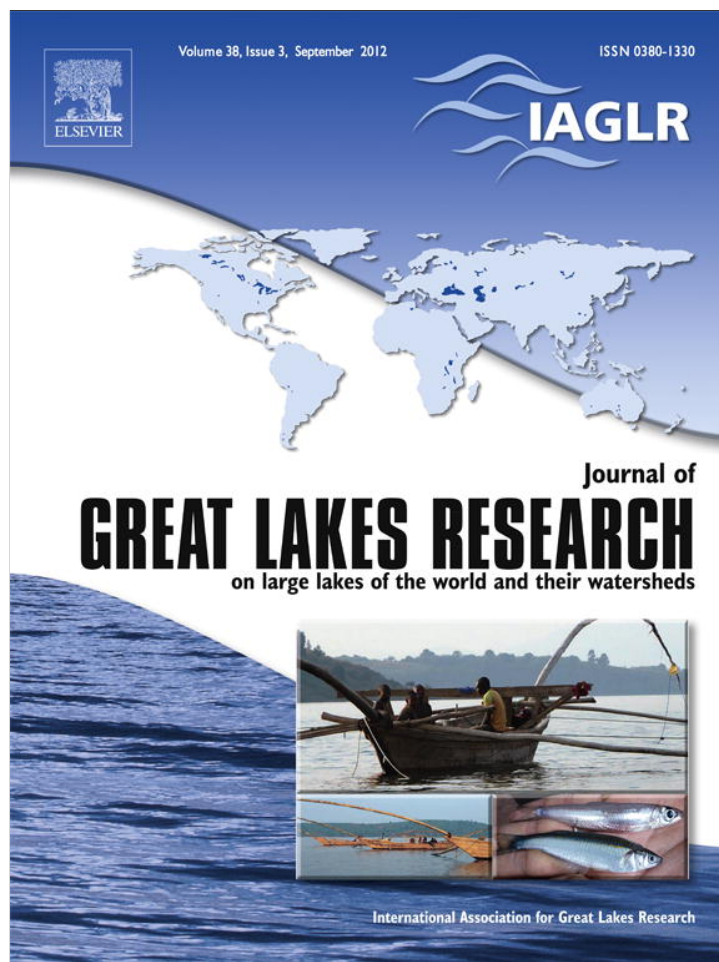
We are grateful to Mwapu Isumbisho, Georges Alunga, Pascal Masilya and Bruno Leporcq for field and laboratory assistance. H.S. benefited from fellowships from Brazilian “Ciências sem Fronteiras” Program from CAPES (BJT 013/2012). The study was supported by projects and grants from different Belgian institutions: CUD (“Commission Universitaire pour le Développement”), FRS-FNRS (“Fonds de la Recherche Scientifique”). The study is a contribution to EAGLES (East African Great Lakes Sensitivity to changes, SD/AR/02A), supported by BELSPO, the Belgian Federal Science Policy Office. FD was a postdoctoral researcher at FRS-FNRS.

References

- Bergamino N, Horion S, Stenuite S, Cornet Y, Loisselle S, Plisnier P-D, et al. Spatio-temporal dynamics of phytoplankton and primary production in Lake Tanganyika using a MODIS based bio-optical time series. *Remote Sens Environ* 2010;114:772–80.
- Borges AV, Abril G, Delille B, Descy J-P, Darchambeau F. Diffusive methane emissions to the atmosphere from Lake Kivu (Eastern Africa). *J Geophys Res* 2011;116:G03032.
- Cermeño P, Marañón E, Rodríguez J, Fernández E. Large-sized phytoplankton sustain higher carbon-specific photosynthesis than smaller cells in a coastal eutrophic ecosystem. *Mar Ecol Prog Ser* 2005;297:51–60.
- Claustre H, Hooker SB, Van Heukelem L, Berthon J-F, Barlow R, Ras J, et al. An intercomparison of HPLC phytoplankton pigment methods using in situ samples: application to remote sensing and database activities. *Mar Chem* 2004;85:41–61.
- Cohen AS, Lezzar KE, Cole J, Dettman D, Ellis GS, Gonnea ME, et al. Late Holocene linkages between decade-century scale climate variability and productivity at Lake Tanganyika, Africa. *J Paleolimnol* 2006;36:189–209.
- Darchambeau F, Isumbisho M, Descy J-P. Zooplankton of Lake Kivu. In: Descy J-P, Darchambeau F, Schmid M, editors. *Lake Kivu: limnology and geochemistry of a tropical great lake*. Dordrecht: Springer; 2012. p. 107–26.
- De Wever A, Muylaert K, Langlet D, Alleman L, Descy J-P, André L, et al. Differential responses of phytoplankton additions of nitrogen, phosphorus and iron in Lake Tanganyika. *Freshw Biol* 2008;53:264–77.
- Degens ET, von Herzen RP, Wong H-K, Deuser WG, Jannasch HW. Lake Kivu: structure, chemistry and biology of an East African Rift Lake. *Geol Rundsch* 1973;62:245–77.
- Degnbol P. The pelagic zone of central Lake Malawi—a trophic box model. In: Christensen V, Pauly D, editors. *Trophic models of aquatic ecosystems*. Makati: ICLARM; 1993. p. 110–5.
- Descy J-P. Etude de la production planctonique au lac Kivu—Rapport de mission. *Projet PNUD/FAO—RWA/87/012*. Namur: UNCED; 1990.
- Descy JP, Sarmento H. Microorganisms of the East African Great Lakes and their response to environmental changes. *Freshw Rev* 2008;1:59–73.
- Descy J-P, Hardy M-A, Stenuite S, Pirlot S, Leporcq B, Kimirei I, et al. Phytoplankton pigments and community composition in Lake Tanganyika. *Freshw Biol* 2005;50:668–84.
- Descy J-P, Plisnier P-D, Leporcq B, Stenuite S, Pirlot S, Stimart J, et al. Climate variability as recorded in Lake Tanganyika (CLIMLAKE). Final report. Brussels: Belgian Science Policy; 2006.
- Descy J-P, Darchambeau F, Schmid M. Lake Kivu research: conclusions and perspectives. In: Descy J-P, Darchambeau F, Schmid M, editors. *Lake Kivu: limnology and geochemistry of a tropical great lake*. Dordrecht: Springer; 2012. p. 181–90.
- Dumont HJ. The Tanganyika sardine in Lake Kivu: another ecodisaster for Africa? *Environ Conserv* 1986;13:143–8.
- Falkowski PG, Raven JA. *Aquatic photosynthesis*. Princeton: Princeton University Press; 2007.
- Fee EJ. Computer programs for calculating in situ phytoplankton photosynthesis. *Can Technol Rep Fish Aquat Sci* 1990;1740:1–27.
- Fietz S, Nicklisch A. An HPLC analysis of the summer phytoplankton assemblage in Lake Baikal. *Freshw Biol* 2004;49:332–45.
- Fietz S, Kobanova G, Izmeteva L, Nicklisch A. Regional, vertical and seasonal distribution of phytoplankton and photosynthetic pigments in Lake Baikal. *J Plankton Res* 2005;27:793–810.
- Geider RJ, MacIntyre HL. Physiology and biochemistry of photosynthesis and algal carbon acquisition. In: Williams PJ, le B, Thomas DN, Reynolds CS, editors. *Phytoplankton productivity: carbon assimilation in marine and freshwater ecosystems*. Oxford: Blackwell; 2002. p. 44–77.
- Geider RJ, MacIntyre HL, Kana TM. A dynamic regulatory model of phytoplankton acclimation to light, nutrients, and temperature. *Limnol Oceanogr* 1998;43:679–94.
- Gran G. Determination of the equivalence point in potentiometric titrations of seawater with hydrochloric acid. *Oceanol Acta* 1952;5:209–18.
- Greene RM, Geider RJ, Falkowski PG. Effect of iron limitation on photosynthesis in a marine diatom. *Limnol Oceanogr* 1991;36:1772–82.
- Guilford SJ, Hecky RE. Total nitrogen, total phosphorus, and nutrient limitation in lakes and oceans: is there a common relationship? *Limnol Oceanogr* 2000;45:1213–23.
- Guilford SJ, Bootsma HA, Fee EJ, Hecky RE, Patterson G. Phytoplankton nutrient status and mean water column irradiance in Lakes Malawi and Superior. *Aquat Ecosyst Health* 2000;3:35–45.
- Guilford SJ, Hecky RE, Taylor WD, Mugidde R, Bootsma HA. Nutrient enrichment experiments in tropical great lakes Malawi/Nyasa and Victoria. *J Great Lakes Res* 2003;29(Suppl. 2):89–106.
- Guilford SJ, Bootsma HA, Taylor WD, Hecky RE. High variability of phytoplankton photosynthesis in response to environmental forcing in oligotrophic Lake Malawi/Nyasa. *J Great Lakes Res* 2007;33:170–85.
- Hecky RE, Fee EJ. Primary production and rates of algal growth in Lake Tanganyika. *Limnol Oceanogr* 1981;26:532–47.
- Hecky RE, Kling HJ. Phytoplankton ecology of the great lakes in the rift valleys of Central Africa. *Arch Hydrobiol Beih Ergeb Limnol* 1987;25:197–228.
- Hubble DS, Harper DM. Impact of light regimen and self-shading by algal cells on primary productivity in the water column of a shallow tropical lake (Lake Naivasha, Kenya). *Lakes Reserv Res Manag* 2001;6:143–50.
- Isumbisho M, Sarmento H, Kaningini B, Micha JC, Descy JP. Zooplankton of Lake Kivu, East Africa, half a century after the Tanganyika sardine introduction. *J Plankton Res* 2006;28:971–89.
- Jannasch HW. Methane oxidation in Lake Kivu (central Africa). *Limnol Oceanogr* 1975;20:860–4.
- Jeffrey SW, Mantoura RFC, Wright SW. *Phytoplankton pigments in oceanography*. Paris: SCOR—UNESCO; 1997.
- Johnson TC, Odada EO. *The limnology, climatology and paleoclimatology of the East African lakes*. Amsterdam: Gordon and Breach Publishers; 1996.
- Kilham P, Kilham SS, Hecky RE. Hypothesized resource relationships among African planktonic diatoms. *Limnol Oceanogr* 1986;31:1169–81.
- Kirk J. *Light and photosynthesis in aquatic ecosystems*. 2nd ed. Cambridge: Cambridge University Press; 1994.
- Legendre P, Legendre L. *Numerical ecology*. 2nd ed. Amsterdam: Elsevier; 1998.
- Lewis WMJ. Primary production in the plankton community of a tropical lake. *Ecol Monogr* 1974;44:377–409.
- Llirós M, Descy J-P, Libert X, Morana C, Schmitz M, Wimba L, et al. Microbial ecology and geochemistry of a tropical great lake. Dordrecht: Springer; 2012. p. 67–83.
- MacIntyre S. Climatic variability, mixing dynamics, and ecological consequences in the African Great Lakes. In: Goldman CR, Kumagai M, Robarts RD, editors. *Climate change and global warming of inland waters*. John Wiley & Sons; 2012. p. 311–34.
- Mackey MD, Mackey DJ, Higgins HW, Wright SW. CHEMTAX—a program for estimating class abundances from chemical markers: application to HPLC measurements of phytoplankton. *Mar Ecol Prog Ser* 1996;144:265–83.
- Melack JM. Temporal variability of phytoplankton in tropical lakes. *Oecologia* 1979;44:1–7.

- Millero FJ, Graham TB, Huang F, Bustos-Serrano H, Pierrot D. Dissociation constants of carbonic acid in sea water as a function of salinity and temperature. *Mar Chem* 2006;100:80–94.
- Mugidde R. The increase in phytoplankton primary productivity and biomass in Lake Victoria (Uganda). *Verh. Int. Ver. Limnol.* 1993;25:846–9.
- Mugidde R. Nutrient status and planktonic nitrogen fixation in Lake Victoria, Africa. [PhD thesis] Waterloo: University of Waterloo; 2001.
- Nicholson SE. A review of climate dynamics and climate variability in Eastern Africa. In: Johnson TC, Odada EO, editors. *The limnology, climatology and paleoclimatology of the East African lakes*. Amsterdam: Gordon and Breach Publishers; 1996. p. 25–56.
- Pasche N, Alunga G, Mills K, Muvundja F, Ryves DB, Schurter M, et al. Abrupt onset of carbonate deposition in Lake Kivu during the 1960s: response to recent environmental changes. *J Paleolimnol* 2010;44:931–46.
- Pasche N, Schmid M, Vazquez F, Schubert CJ, Wüest A, Kessler JD, et al. Methane sources and sinks in Lake Kivu. *J Geophys Res* 2011;116:G03006.
- Pasche N, Muvundja FA, Schmid M, Wüest A, Müller B. Nutrient cycling in Lake Kivu. In: Descy J-P, Darchambeau F, Schmid M, editors. *Lake Kivu: limnology and geochemistry of a tropical great lake*. Dordrecht: Springer; 2012. p. 31–45.
- Patterson G, Hecky RE, Fee EJ. Effect of hydrological cycles on planktonic primary production in Lake Malawi/Niassa. In: Rossiter A, Kawanabe H, editors. *Ancient lakes: biodiversity, ecology and evolution*. London: Academic Press; 2000. p. 421–30.
- Peltomaa E, Ojala A. Size-related photosynthesis of algae in a strongly stratified humic lake. *J Plankton Res* 2010;32:341–55.
- Plisnier PD. Recent climate and limnology changes in Lake Tanganyika. *Verh internat Verein Limnol* 2000;27:2670–3.
- Plisnier P-D, Serneels S, Lambin EF. Impact of ENSO on East African ecosystems: a multivariate analysis based on climate and remote sensing data. *Glob Ecol Biogeogr* 2000;9:481–97.
- Reynolds CS. *Ecology of phytoplankton*. Cambridge: Cambridge University Press; 2006a.
- Reynolds CS. *The Ecology of Phytoplankton*. New York: Cambridge University Press; 2006b. p. 535.
- Riley GA. Phytoplankton of the north central Sargasso Sea. *Limnol Oceanogr* 1957;2:252–70.
- Sarmento H. New paradigms in tropical limnology: the importance of the microbial food web. *Hydrobiologia* 2012;686:1–14.
- Sarmento H, Descy J-P. Use of marker pigments and functional groups for assessing the status of phytoplankton assemblages in lakes. *J Appl Phycol* 2008;20:1001–11.
- Sarmento H, Isumbisho M, Descy J-P. Phytoplankton ecology of Lake Kivu (eastern Africa). *J Plankton Res* 2006;28:815–29.
- Sarmento H, Leitao M, Stoyneva M, Couté A, Compère P, Isumbisho, et al. Diversity of pelagic algae of Lake Kivu (East Africa). *Cryptogam Algal* 2007;28:245–69.
- Sarmento H, Isumbisho M, Stenuite S, Darchambeau F, Leporcq B, Descy JP. Phytoplankton ecology of Lake Kivu (eastern Africa): biomass, production and elemental ratios. *Int. Assoc. Theor. Appl. Limnol.* 2009;30:709–13.
- Sarmento H, Darchambeau F, Descy J-P. Phytoplankton of Lake Kivu. In: Descy J-P, Darchambeau F, Schmid M, editors. *Lake Kivu: limnology and geochemistry of a tropical great lake*. Dordrecht: Springer; 2012. p. 67–83.
- Sarvala J, Salonen K, Jarvinen M, Aro E, Huttula T, Kotilainen P, et al. Trophic structure of Lake Tanganyika: carbon flows in the pelagic food web. *Hydrobiologia* 1999;407:140–73.
- Schmid M, Wüest A. Stratification, mixing and transport processes in Lake Kivu. In: Descy J-P, Darchambeau F, Schmid M, editors. *Lake Kivu: limnology and geochemistry of a tropical great lake*. Dordrecht: Springer; 2012. p. 13–29.
- Schmid M, Halbwachs M, Wehrli B, Wüest A. Weak mixing in Lake Kivu: new insights indicate increasing risk of uncontrolled gas eruption. *Geochem Geophys Geosyst* 2005;6:1–11.
- Schoell M, Tietze K, Schoberth SM. Origin of methane in Lake Kivu (East-Central Africa). *Chem Geol* 1988;71:257–65.
- Segura V, Lutz VA, Dogliotti A, Silva RI, Negri RM, Akselman R, et al. Phytoplankton types and primary production in the Argentine Sea. *Mar Ecol Prog Ser* 2013;491:15–31.
- Silsbe GM. Phytoplankton production in Lake Victoria, East Africa. [MSc thesis] Waterloo: University of Waterloo; 2004.
- Silsbe GM, Hecky RE, Guildford SJ, Mugidde R. Variability of chlorophyll *a* and photosynthetic parameters in a nutrient-saturated tropical great lake. *Limnol Oceanogr* 2006;51:2052–63.
- Snoeks J, Kaningini B, Masilya P, Nyina-wamwiza L, Guillard J. Fishes in Lake Kivu: diversity and fisheries. In: Descy J-P, Darchambeau F, Schmid M, editors. *Lake Kivu: limnology and geochemistry of a tropical great lake*. Dordrecht: Springer; 2012. p. 127–52.
- Spigel RH, Coulter GW. Comparison of hydrology and physical limnology of the East African Great Lakes: Tanganyika, Malawi, Victoria, Kivu and Turkana (with references to some North American great lakes). In: Johnson TC, Odada EO, editors. *The limnology, climatology and paleoclimatology of the East African lakes*. Amsterdam: Gordon and Breach Publishers; 1996. p. 103–40.
- Steehan-Nielsen E. The use of radioactive carbon (^{14}C) for measuring organic production in the sea. *J Cons Perm Int. Explor Mer* 1952;18:117–40.
- Stenuite S, Pirlot S, Hardy M-A, Sarmento H, Tarbe A-L, Leporcq B, et al. Phytoplankton production and growth rate in Lake Tanganyika: evidence of a decline in primary productivity in recent decades. *Freshw Biol* 2007;52:2226–39.
- Talling JF. Photosynthetic activity of phytoplankton in East African lakes. *Int Rev Ges Hydrobiol* 1965;50:1–32.
- ter Braak CJF, Šmilauer P. *CANOCO reference manual and CanoDraw for Windows user's guide: software for canonical community ordination (version 4.5)*. Ithaca: Microcomputer Power; 2002.
- Tierney JE, Smerdon JE, Anchukaitis KJ, Seager R. Multidecadal variability in East African hydroclimate controlled by the Indian Ocean. *Nature* 2013;493:389–92.
- Tortell PD. Evolutionary and ecological perspectives on carbon acquisition in phytoplankton. *Limnol Oceanogr* 2000;45:744–50.
- Turpin DH. Effects of inorganic N availability on algal photosynthesis and carbon metabolism. *J Phycol* 1991;27:14–20.
- Valderrama JC. The simultaneous analysis of total nitrogen and total phosphorus in natural waters. *Mar Chem* 1981;10:109–22.
- Vareschi E. The ecology of Lake Nakuru (Kenya). III. Abiotic factors and primary production. *Oecologia* 1982;55:81–101.
- Verschuren D, Johnson TC, Kling HJ, Edgington DN, Leavitt PR, Brown ET, et al. History and timing of human impact on Lake Victoria, East Africa. *Proc R Soc Lond B* 2002;269:289–94.
- Vollenweider RA. Calculations models of photosynthesis-depth curves and some implications regarding day rate estimates in primary production measurements. *Mem Ist Italo Idrobiol* 1965;18:425–57.

Provided for non-commercial research and education use.
Not for reproduction, distribution or commercial use.



This article appeared in a journal published by Elsevier. The attached copy is furnished to the author for internal non-commercial research and education use, including for instruction at the authors institution and sharing with colleagues.

Other uses, including reproduction and distribution, or selling or licensing copies, or posting to personal, institutional or third party websites are prohibited.

In most cases authors are permitted to post their version of the article (e.g. in Word or Tex form) to their personal website or institutional repository. Authors requiring further information regarding Elsevier's archiving and manuscript policies are encouraged to visit:

<http://www.elsevier.com/copyright>



Contents lists available at SciVerse ScienceDirect

Journal of Great Lakes Research

journal homepage: www.elsevier.com/locate/jglr

Is the fishery of the introduced Tanganyika sardine (*Limnothrissa miodon*) in Lake Kivu (East Africa) sustainable?

Jean Guillard ^{a,*}, François Darchambeau ^b, Pascal Masilya Mulungula ^{c,d}, Jean-Pierre Descy ^d

^a INRA, UMR CARRTEL, Centre Alpin de Recherche sur les Réseaux Trophiques et Ecosystèmes Limniques, 75, avenue de Corzent, F-74203 Thonon-les-Bains cedex, France

^b Unité d'Océanographie Chimique, Département d'Astrophysique, Géophysique et Océanographie, Université de Liège, Allée du 6-Août 17, 4000 Liège, Belgique

^c Unité d'Enseignement et de Recherche en Hydrobiologie Appliquée (UERHA) – Dpt. de Biologie – Chimie, I.S.P., Bukavu, Congo

^d Laboratoire d'Ecologie des Eaux Douces, URBE, Département de Biologie, Université de Namur, Rue de Bruxelles 61, 5000 Namur, Belgique

ARTICLE INFO

Article history:

Received 16 November 2011

Accepted 9 May 2012

Available online 19 June 2012

Communicated by Lars Rudstam

Keywords:

Echo-integration

Hydroacoustic

Lake Kivu

Limnothrissa miodon

Pelagic fish

Stock assessment

ABSTRACT

Limnothrissa miodon, a small pelagic clupeid fish introduced at the end of the 1950s into Lake Kivu, became an important resource for the human populations of this area. The total stock of pelagic fish populations of this lake was estimated in 2008 by two hydroacoustic surveys, using an EK60 split-beam sounder (frequency 70 kHz). The total fish stocks were estimated to be approximately 5000 t in the rainy season and 6000 tons in the dry season. These values are similar to previous estimations performed in the 1980s. During 2008, the stock did not fluctuate throughout the seasons; however, the spatial distributions were different in the two hydrological seasons. Interestingly, the *L. miodon* stock has appeared to remain stable over the last two decades, which suggests that the pelagic fishery in Lake Kivu has not been overexploited and that it is sustainable.

© 2012 International Association for Great Lakes Research. Published by Elsevier B.V. All rights reserved.

Introduction

Introductions of species are widely regarded as detrimental (Gozlan, 2008; Leprieur et al., 2009; Vitule et al., 2009) and are considered as a major threat to biodiversity (Sala et al., 2000; Vitousek et al., 1997). Worldwide, but particularly in the African continent, introductions have been aimed to develop fisheries (Moreau et al., 1988). Often, the consequences have been reported as catastrophic for the native fauna, for the ecosystems, and for the well-being of the human populations, such as in the African Great Lakes (Ogutu-Ohwayo et al., 1997). However, some cases have been reported as successful, as far as the fishery is concerned (Gozlan, 2008). For instance, the introduction of Tanganyika sardines, *Limnothrissa miodon* (Boulenger, 1906), in Lake Kivu (Spliethoff et al., 1983) seems to be productive even though the effects on the ecosystem and on the geochemistry of the whole lake are still matter of debate (Dumont, 1986; Isumbisho et al., 2006; Pasche et al., 2010).

Lake Kivu has a species-poor fish fauna compared to other large lakes of the East-African Rift valley (Beadle, 1981). While Lake Tanganyika and Lake Malawi harbour hundreds of endemic species,

mostly Cichlidae, only 29 species have been described from Lake Kivu. Four of these species have been accidentally or deliberately introduced (Collart, 1960; Marshall, 1993; Snoeks et al., in press): three cichlids [*Oreochromis macrochir* (Boulenger, 1912), *Oreochromis leucostictus* (Trewavas, 1933) and *Tilapia rendalli* (Boulenger, 1897)], and one clupeid *L. miodon* (Boulenger, 1906). Recently, a fifth species, *Lamprichthys tanganicanus* (Boulenger, 1898), endemic to Lake Tanganyika (Coulter, 1991) has appeared in the commercial catches from several sites in Lake Kivu (Muderhwa and Matabaro, 2010), but with low occurrence in the pelagic area (Masilya, 2011). The species-poor fish fauna of Lake Kivu is due to profound geologic disturbances that occurred approximately 11,000 years BP (Haberyan and Hecky, 1987). Snoeks et al. (1997) gave a detailed account of the history and status of the ichthyofauna of Lake Kivu, providing evidence for the existence of 15 endemic haplochromines.

Among the introduced species, the most famous is the Tanganyika sardine, locally known as “Isambaza”, *L. miodon*, which was deliberately introduced in 1959 (Collart, 1960) from Lake Tanganyika to occupy the pelagic area of Lake Kivu, which previously lacked pelagic fish species. *L. miodon* was introduced in an attempt to establish a pelagic fishery in Lake Kivu based on the pelagic planktonic food web. Despite the fact that this introduction might be considered as a disturbance of the pelagic ecosystem (Darchambeau et al., in press; Dumont, 1986; Isumbisho et al., 2004; Kaningini et al., 2003), it permitted the development of an important pelagic fishery with an

* Corresponding author. Tel.: +33 450267851.

E-mail addresses: jean.guillard@thonon.inra.fr (J. Guillard), Francois.Darchambeau@ulg.ac.be (F. Darchambeau), pascalmasilya@yahoo.com (P.M. Mulungula), jean-pierre.descy@fundp.ac.be (J.-P. Descy).

annual exploitable stock that was estimated at approximately 7000 t (FAO, 1992; Roest, 1999). However, rather pessimistic predictions on the sustainability of the *L. miodon* fishery were made by Dumont (1986), based on observed changes in the composition and biomass decline of mesozooplankton in the lake.

Major projects were enacted to manage the pelagic fishery of Lake Kivu, including the “*Isambaza*” project conducted by PNUD-FAO in Rwanda in the 1980s and the “*Pêche du Sambaza au filet maillant dans le lac Kivu*” conducted in Congo (Kaningini et al., 1999). Despite the systematic collection of data on total fishery yield by the Rwandan administration, the fishery pressure on different species is poorly known. Furthermore, no fishery independent survey has been conducted since the study of Lamboeuf (1991). Thus, a pelagic fishery management plan based on reliable data cannot be proposed. Therefore, the only way to assess the sustainability of the pelagic fishery was to conduct a comprehensive stock assessment of the *L. miodon* with hydroacoustic methods, and compare our results with estimates reported by Lamboeuf (1991) 20 years earlier.

The use of hydroacoustic methods to estimate fish abundance in aquatic ecosystems is well accepted (Simmonds and MacLennan, 2005), particularly for the pelagic zones of lakes (Dunlop et al., 2010; Guillard et al., 2006; Johnson et al., 2004). By contrast, the use of gillnets for assessing fish stocks is likely to provide a biased picture of species composition and size-structure because of known issues with capturing small (<10 cm) fishes using this equipment (Kurkilahti et al., 2002; Prachalová et al., 2009).

We conducted two hydroacoustic stock estimation surveys, during both rainy (February 2008) and dry (July 2008) seasons using a sampling design similar to that of Lamboeuf (1991), in order to determine whether or not the pelagic fish population has declined as predicted by Dumont (1986). In addition to the comparison with historical data, fish distributions across seasons were also studied.

Material and methods

Lake Kivu is a large (surface area 2370 km²), deep (maximum depth 489 m), oligotrophic lake that belongs to the African Eastern Rift. The lake is meromictic, with oxygenated waters limited to the

upper 60 m and permanently separated from deep waters by several steep salinity gradients (Degens et al., 1973). Given the location of Lake Kivu, just 2° south of the Equator, but at relatively high elevation (1463 m), the average surface temperature ranges from 23 to 24 °C and the temperature gradient is only 1 to 2 °C between the surface and the bottom of the mixolimnion. Therefore, surface cooling occurring in the dry season reduces the temperature gradient and promotes mixing of the first 60 m, which increases the nutrient availability in the euphotic zone (ca. 18 m on average) and promotes phytoplankton development (Sarmiento et al., 2006). The dry season mixing also oxygenates the water over the whole mixolimnion. Thus, mixing events extend the oxic layer, and provide the pelagic fish with access to increased planktonic resources, whereas the rainy season conditions reduce both the depth of the oxic layer and food resources for planktivores (Isumbisho et al., 2006; Sarmiento et al., 2006).

The lake can be divided into four large basins (Fig. 1, Table 1) and two bays, the Bukavu Bay in the south and Kabuno Bay in the north. Kabuno Bay was not included in our surveys. The basins have different patterns of wind and precipitation resulting shift of several weeks of the dry season between the North and the South basins (Kwetuenda et al., 1989). The inshore area represents less than 10% of the area of Lake Kivu and was considered separately in our analyses. The two 2008 surveys were performed in two contrasted seasons: from February 15–22 (rainy season), and from July 05–11 (dry season), before the occurrence of the two seasonal peaks in fish reproduction (August to October and March to May, Kaningini et al., 1999). Surveys were performed during the daytime for both safety reasons and to be consistent with historical surveys (Lamboeuf, 1991). The routes (Fig. 1) covering 252 km in February and 345 km in July, were designed to cover all areas of the lake and have a cover ratio as defined by Aglen (1989) of approximately 6 (5.37 in February and 7.35 in July). Some transects were shortened due to periods of strong winds and for logistic reasons (mainly safe places to rest for the night). In the analyses, samples recorded in areas with bottom depths of <50 m were considered as inshore areas. In addition, a night survey was repeated on a single daytime transect to highlight the variation between night and day. Temperature and oxygen vertical profiles (Fig. 1) were obtained using an YSI 6600 multiparameter probe.

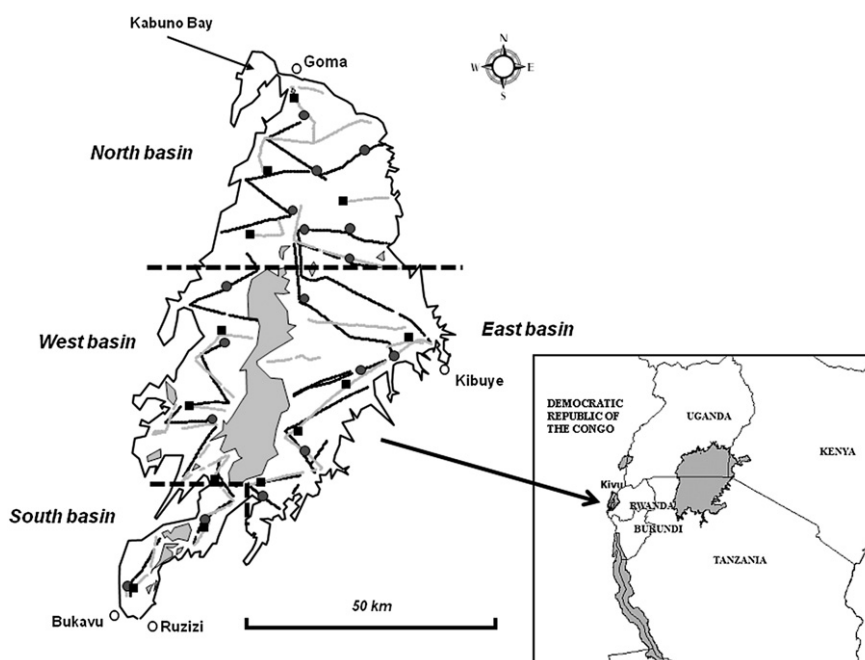


Fig. 1. Map of Lake Kivu showing the February 2008 (grey line) and July 2008 (black line) tracks and localization of the YSI profiles (February, black squares, July black circles). The dotted black lines showed the limit of the basins.

Table 1
Morphometry of the pelagic area of the four main basins, and of the inshore area of Lake Kivu (from Kaningini et al., 1999).

Basin	North	East	West	South	Inshore area
Surface (km ²)	900 ^a	900 ^a	320	97	50 ^a
Depth max (m)	489	400	225	105	50

^a Estimated.

The echosounder used was a Simrad EK60 equipped with a 70 kHz split-beam transducer with a half-power beam angle of 11°. A GPS system was used to record boat positions. The collection parameters were a pulse-length of 0.256 ms (Godlewska et al., 2011) and 5 pulses per second. Sounder calibrations were performed annually in a large basin (IFREMER, Brest) according to the standard protocol of Foote et al. (1987), and the system was stable (gain variation < 0.4 dB). The sound speed parameter and the attenuation coefficient α were adjusted for temperature based on collected profiles. Surveys were performed from a wooden boat, at a mean speed of 8 km h⁻¹; the transducer was vertically attached to a pole along the boat at a depth of 0.5 m. The acoustic data were analyzed using the Sonar5-Pro software (Balk and Lindem, 2006) to calculate the total acoustic fish biomass in each depth layer and the acoustic size distributions. The processing thresholds were set at -60 dB for single targets and -55 dB for echointegration data, for consistency with those of Lamboeuf (1991). The Elementary Sampling Distance Unit (ESDU) was *a priori* fixed to 250 m, according to previous analyses in other lake ecosystems (Guillard and Marchal, 2001). Previous studies on Lake Kivu (Lamboeuf, 1989) have demonstrated that fishes are not present at depths > 60 m due to the permanent lack of oxygen: therefore, data were recorded below this lower limit with *in situ* checking. Data were analyzed by vertical layers of 15 m, like in the surveys carried out by Lamboeuf (1991): surface to 15 m, 15 to 30 m, 30 to 45 m, and 45 to 60 m. Fish area being proportional to acoustics back-scattering (Simmonds and MacLennan, 2005), values were initially expressed in acoustic energy (s_a expressed m² ha⁻¹) (MacLennan et al., 2002) reflected per layer and per unit of area, hereafter called acoustic biomass. Layered acoustic energy values were summed up by ESDU and the arithmetic mean acoustic biomass was computed for each basin. The arithmetic mean can be regarded as an unbiased estimate of the average in the area, if the effort is distributed in a homogeneous way, without initial statistical assumption (Smith, 1990). This estimator is similar to estimators obtained by other methods of calculation if the sampling effort is close to that recommended by Aglen (1989) (Guillard and Vergés, 2007). The whole lake acoustic biomass was given by the sum of each basin-specific mean acoustic biomass multiplied by the respective area of each basin. To estimate lake biomass, individual fish length and biomass were computed from single-echo observations. Single-echo detections criteria included echoes having 0.8–1.6 relative pulse widths, one-way beam compensation < 3 dB, and a maximum phase deviation of 0.3. To be classified as a tracked fish, traces had to include at least three echoes of the same target, separated by a maximum of one missing ping within a 0.3 m gating range (Balk and Lindem, 2006). From each tracked fish (see Fig. 4D), the average target strength (TS, dB) (MacLennan et al., 2002) was calculated in the linear domain. Frequency distribution of TS values was computed for each basin *i*. Each TS distribution was then split into 10 even-spaced frequency classes *c* (i.e., decile classes). Due to the non normality of the distributions, median TS values by frequency class, $TS_{c,i}$, were calculated for each basin and individual scattering cross-section (σ , m²) was calculated following MacLennan et al. (2002):

$$\sigma_{c,i} = 10 \left(\frac{TS_{c,i}}{10} \right) * 4\pi$$

Median individual fish lengths were calculated by basin for each TS frequency class using the TS-length relationship given by Lamboeuf (1991) for *L. miodon* in Lake Kivu:

$$TS_{c,i} = 20 \log_{10} L_{c,i} - 67.6$$

where *L* = total fish length (cm). Median individual fish weights (*W*, g) were calculated by basin for each TS frequency class using the length-weight relationship given by Lamboeuf (1989) for *L. miodon* in Lake Kivu:

$$W_{c,i} = 0.055 L_{c,i}^{2.27}$$

The whole biomass per basin was calculated using the following equation:

$$W_i = \sum_{c=1}^{10} \frac{p_{c,i} s_{a,i}}{\sigma_{c,i}} W_{c,i}$$

where $s_{a,i}$ is the mean acoustic biomass of basin *i* and $p_{c,i}$ is the proportion of the acoustic biomass for the TS frequency class *c* in basin *i* and is given by:

$$p_{c,i} = \frac{\sigma_{c,i}}{\sum_{c=1}^{10} \sigma_{c,i}}$$

To generate confidence intervals for the fish biomass per basin and for the whole lake, we used a bootstrap approach that incorporated uncertainty in each of the following two estimates used to calculate the fish biomass: the mean s_a per basin, the fish size structure. First, we randomly selected s_a per basin with replacement and calculated a mean acoustic biomass, $s_{a,i}$. Next, we randomly selected target strengths with replacement and calculated median TS values by frequency class, $TS_{c,i}$. We then applied above-mentioned equations for calculating the whole biomass per basin, W_i . This process was repeated 2500 times to generate a distribution of biomass estimates and calculate 95% confidence interval. The whole lake biomass was obtained by summing the four basin biomass plus the biomass observed in littoral areas.

The parametric one-way analysis of variance and post-hoc Tukey's HSD tests were used to compare acoustic biomass between basins and seasons. The heterogeneity of spatial distribution was given by the coefficient of variation ($CV = SD/mean$) of acoustic biomass. Multiple CV were compared using the Bennett's test as modified by Shafer and Sullivan (1986). The Kruskal-Wallis one-way analysis of variance was used to compare the estimated fish length distributions between seasons and areas. Bootstrap confidence intervals of biomass estimates were compared using Student's *t* test.

Results

Temperature and oxygen

The water temperatures in the surface layer varied between 23.5 and 24.0 °C regardless of the season (Fig. 2). In February, a thermocline around 30–40 m was recorded, while temperatures were almost constant in the mixolimnion during July (Fig. 2). During each survey, no difference in temperature and oxygen profiles was observed between basins: only the two profiles in the Bukavu Bay had a significantly lower surface temperature (23.0 °C). In February, the oxygen concentration rapidly decreased below 30 m, with an oxycline ending at 35 to 50 m depending on the location (Fig. 3). In July, the oxycline was located at greater depths, ending between 50 and 60 m. Waters below the oxycline were always anoxic.

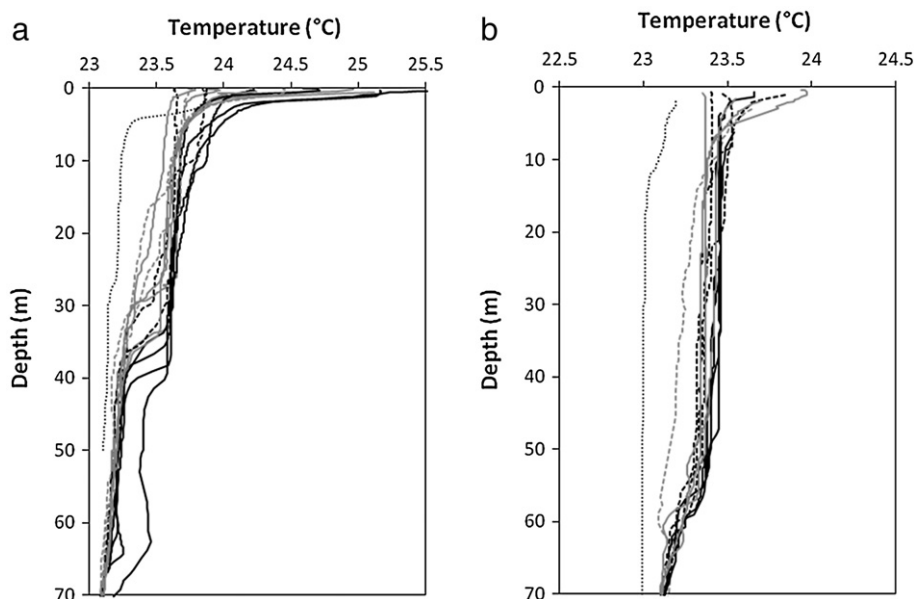


Fig. 2. Vertical temperature profiles in February (a) and July (b) 2008 in Lake Kivu. The continuous black lines represent the vertical profiles of the North basin, the continuous grey lines of the East basin, the dashed black lines of the West basin, the dashed grey lines of the South basin and the dotted black line of Bukavu Bay.

Detected biomass

Echograms

Observations performed during the daytime showed no target in layers close to the surface and in layers below 60 m. Several kinds of structures were identified (Fig. 4) including individual fish, aggregations and more or less dense schools. High-density schools (Fig. 4A) were mainly observed in the inshore area or in pelagic areas close to shallows. Large differences in the nature of aggregations were observed in different areas and in various vertical strata. During the night survey, fishes were scattered and no aggregations structures were observed (Fig. 4C).

Acoustic biomass

The acoustic biomass detected per sampling unit showed spatial and seasonal heterogeneities (Figs. 5 and 6). Regarding the vertical

distribution, fishes were mainly observed in the intermediate layers (15–30 and 30–45 m) in February (layer effect $F_{3,4016} = 85.81$, $p < 0.001$); however, fishes were more abundant in the upper layers (3–15 and 15–30 m) in July (layer effect $F_{3,5504} = 352.5$, $p < 0.001$). Furthermore the acoustic biomass was always low in the deepest layer (45–60 m) with 84% and 61% of ESDUs without fish in February and July 2008, respectively (Fig. 6). However, when considering all of the layers, the percentage of units without fish detection became negligible, <1% during both seasons. The highest acoustic biomass were observed in February in the southern and western basins (one-way ANOVA and post-hoc Tukey test, basin-effect $F_{3,1001} = 45.66$, $p < 0.001$) while in July only the South basin showed higher values than the others (basin effect $F_{3,1373} = 6.739$, $p < 0.001$).

The acoustic biomass detected in inshore areas were 3 to 8 times greater than in pelagic areas during both seasons ($F_{1,2611} = 565.4$, $p < 0.001$; Table 2). The coefficients of variation (CV) of acoustic

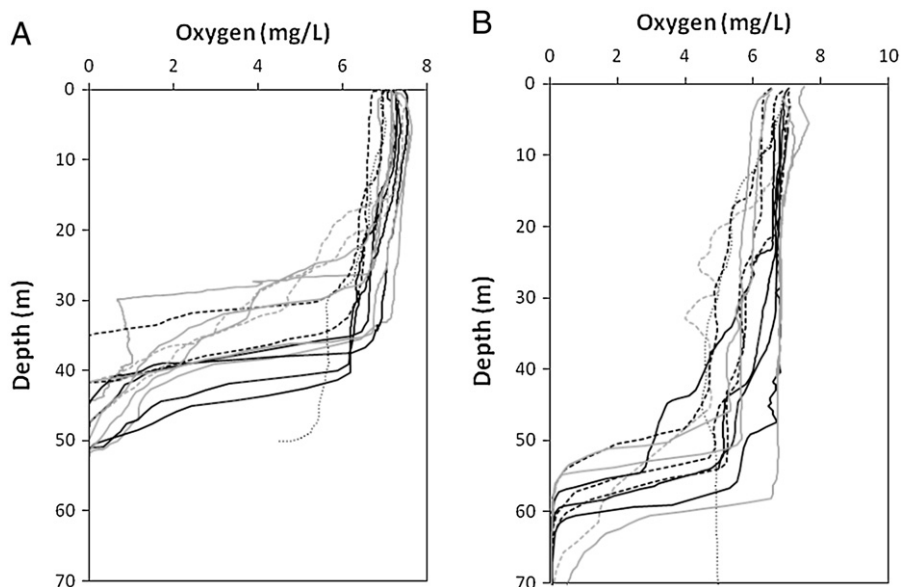


Fig. 3. Vertical profiles of dissolved oxygen in February (A) and July (B) 2008 in Lake Kivu. The continuous black lines represent vertical profiles of the North basin, the continuous grey lines of the East basin, the dashed black lines of the West basin, the dashed grey lines of the South basin and the dotted black line of Bukavu Bay.

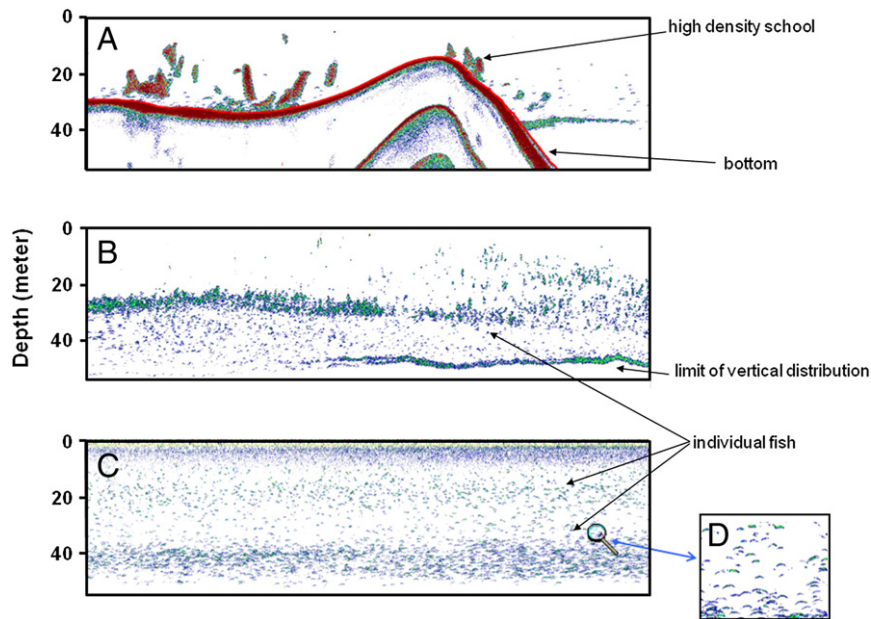


Fig. 4. Examples of echograms captured in the inshore area (A) and in the pelagic area (B) of Lake Kivu during daylight, in the pelagic area at night (C), and a zoom on individual fishes (D).

biomass by basin, which is a measure of spatial heterogeneity, ranged between 0.80 and 1.38, depending on basin and survey (Table 2). The fish population showed a greater heterogeneous dispersion (higher CV) at both basin and whole-lake scales in February than in July 2008. Indeed, at whole-lake scale, the CV of acoustic biomass was higher in February than in July 2008 (modified Bennett's statistic = 29.452, $p < 0.001$), and at basin scale there was a significant difference between basin-specific CVs during the February survey (modified

Bennett's statistic = 4.218, $p = 0.040$) but not during the July survey (statistic = 1.292, $p = 0.256$).

Size assessment

Individual fish lengths, converted from TS data, ranged from 2 to 20 cm (Fig. 7). Some differences in fish length distributions were observed between basins or seasons (Kruskal-Wallis one-way analysis of variance, statistic = 1609.7, $p < 0.001$; Fig. 7). Particularly, fishes

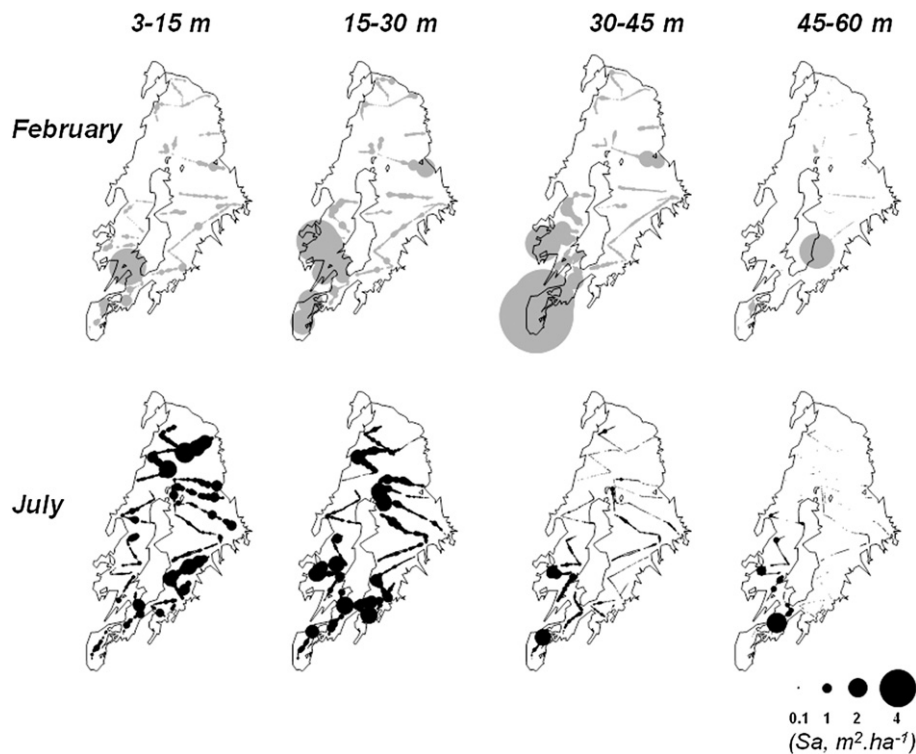


Fig. 5. Fish acoustic biomass detected by ESDU in the four vertical layers (3–15, 15–30, 30–45, 45–60 m) in February (grey) and July (black) 2008. The values are in $m^2 ha^{-1}$.

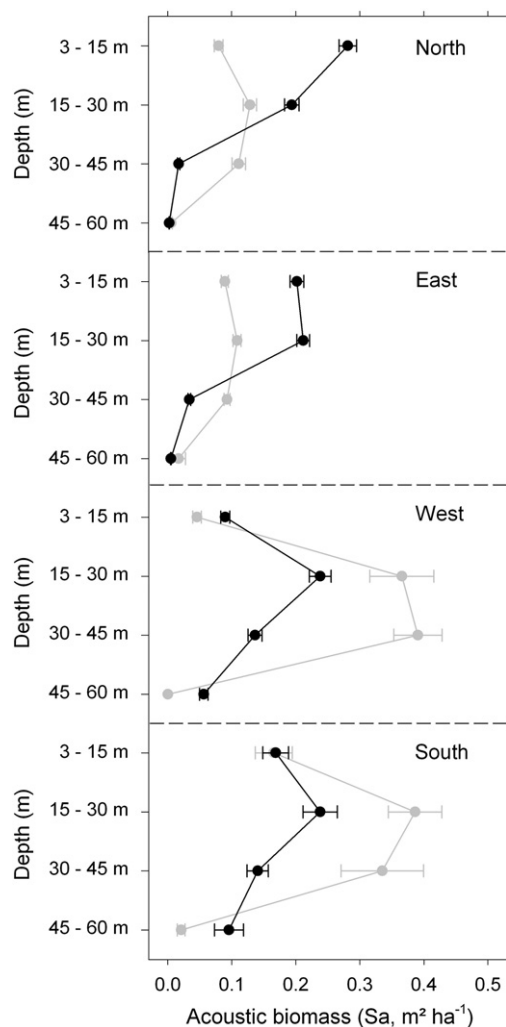


Fig. 6. Mean acoustic biomass (\pm standard deviation) of the four vertical layers per basin in February (grey line) and July (black line) 2008.

longer than 10 cm were relatively more abundant in July than in February ($p < 0.001$): they represented 25% (acoustic biomass-weighted mean) of total numbers of fishes in February for 34% in July.

Calculation of biomass

The fish biomass per basin was determined using the mean acoustic biomass, s_{ai} , and TS frequency distribution of the considered basin. Results are given in Table 3. Due to their greater areas, the fish biomass was highest in the northern and eastern basins whatever the season. The western basin showed also a high biomass in February. The littoral areas counted for 12–13% of the total fish biomass while they represent only 2% of the total surface area. There was no difference of total fish biomass between both seasons, with a mean

Table 2 Mean and coefficient of variation (CV) of acoustic energy (s_a m² ha⁻¹) in the different lake areas and seasons.

	North	East	West	South	Whole pelagic area	Inshore area
February						
Mean s_a (m ² .ha ⁻¹)	0.324	0.306	0.802	0.908	0.497	2.336
CV	1.13	0.90	1.18	1.38	1.49	1.74
July						
Mean s_a (m ² .ha ⁻¹)	0.495	0.452	0.520	0.642	0.497	2.989
CV	0.85	0.80	0.92	0.84	0.86	1.04

estimation of 5004 tons and 6036 tons, respectively in February and July (Table 3).

Diel vertical migration

In February, a survey was performed before and after dusk on a similar track (Fig. 8) to observe and quantify vertical distributions and changes in aggregation structures. On the echograms (Fig. 8), fish dispersion and migration at dusk to the 10–15 m layer were observed. Before dusk, the percentage of single echoes in each ESDU was near 22%, whereas it was more than 40% during the night, showing a change from aggregations to scattered fish.

Discussion

Our surveys were performed during the daytime, similar to those conducted in the 1980s (Lamboeuf, 1991), with a sampling effort close to that recommended by Aglen (1989). Schooling of fish during daylight (Fréon and Misund, 1999) was observed, similarly to previous observations (Kaningini et al., 1999). Fish dispersion at dusk (Fréon et al., 1996) was also noted in the lake. This behaviour is often interpreted as an anti-predatory mechanism (Parrish et al., 2002; Pitcher and Parrish, 1993), but Lake Kivu has no predatory fish species in the pelagic zone, except large *L. miodon* for which predation upon its own fry in Lake Kivu has been reported (Kaningini, 1995). Acoustic surveys performed during the night, when distributions are more homogeneous, are typically more reliable than those performed during daylight (Simmonds and MacLennan, 2005). In our study, we assumed that daylight surveys were also reliable due to the relatively homogeneous distribution during daytime and because no fish were detected close to the surface. In Lake Kivu, the inshore area is limited due to its steep banks; therefore hydroacoustic sampling in the pelagic area allows reliable estimation of the vast majority of the stock (Brehmer et al., 2006). Nevertheless, although the inshore area of Lake Kivu represented ~2% of the surface area, 12–13% of total biomass resided in this area. In these inshore zones, contrary to offshore zones where *L. miodon* was the dominant species (Kaningini et al., 1999), other fish species are present, especially *L. tanganicanus* (Masilya et al., 2011), leading to a possible over-estimation of the *L. miodon* stock. Therefore additional samplings by complementary fishing methods should be conducted in future surveys to check for the abundances of *L. tanganicanus* in this area. Nevertheless, since the occurrence of *L. tanganicanus* is low in the pelagic zone (Masilya, 2011), their presence likely did not significantly biased our assessment of the *L. miodon* stock.

Notable differences in fish distributions in the pelagic zone were found. The biomass were higher in the western and southern basins in February, while only the South basin had higher biomass in July. However, fish biomass was more homogenous among basins during July than during February. Notably, the biomass of the southern and western basins significantly decreased between February and July, while values in the northern and eastern basins increased. Marshall (1991) noted a similar pattern, i.e. CPUE was higher in the South in February and in the North in July, and concluded that *L. miodon* undertook South to North migrations in Lake Kivu. However, due to a high variation in fishery activities (Kaningini et al., 1999) related to seasonal wind and waves conditions, the differences highlighted by Marshall (1991) might be questionable. High concentrations in the South basin in February were also described by Marshall (1991), who hypothesized that the morphology of this basin, with well-developed coastal zones were favorable to *L. miodon* reproduction. Past and present surveys show that fish were always limited to the upper 60 m of the water column (i.e. to the mixolimnion), but the deepest layer, 45–60 m, was devoid of fish in February. In July, this deepest layer supported low fish biomass, despite the whole mixolimnion was well oxygenated, and fishes were closer to the surface than in February. Fishes were not present in the surface layers,

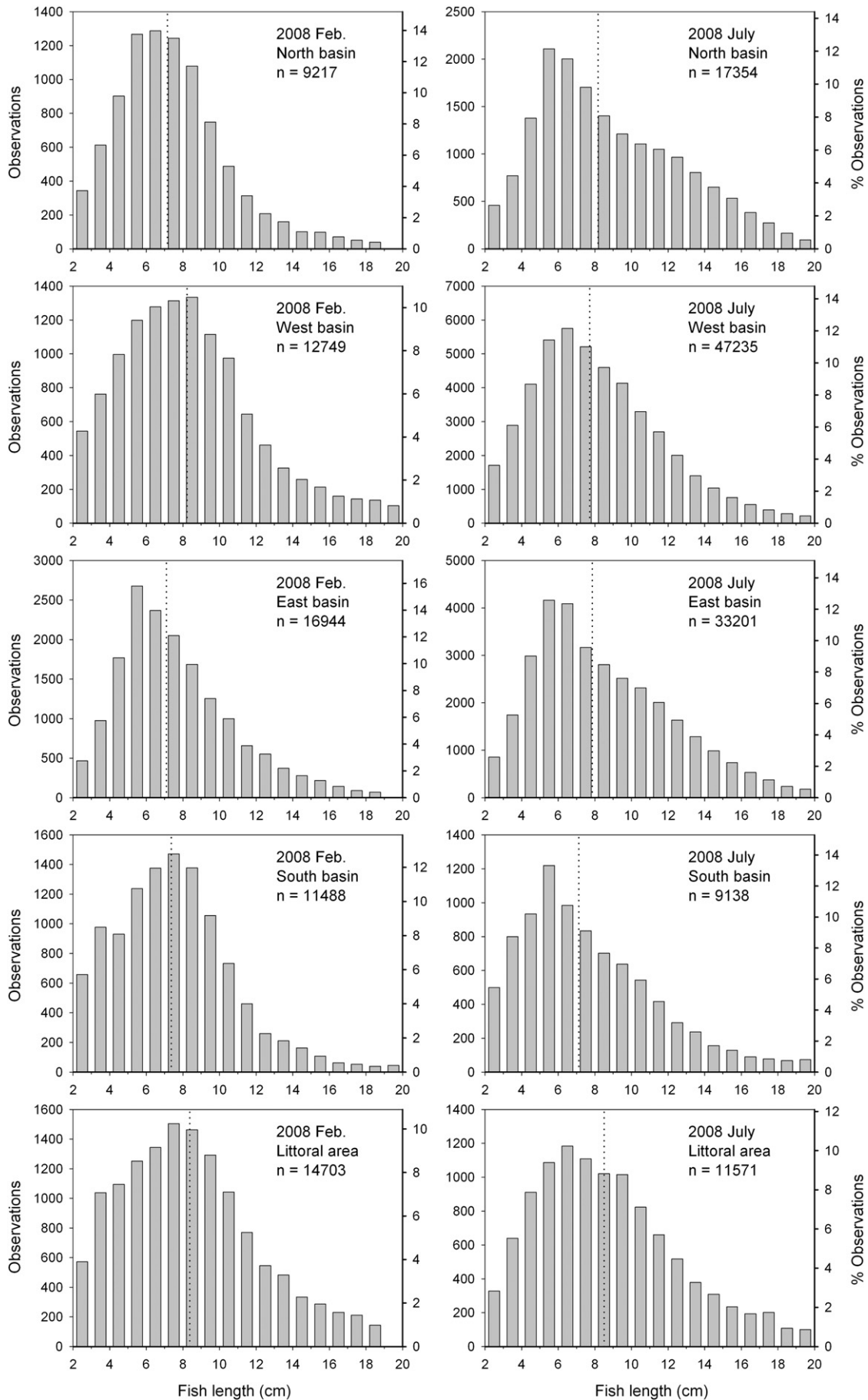


Table 3

Fish biomass in the different lake areas and seasons. 95% confidence intervals (C.I.) were estimated by a bootstrap procedure.

	North	East	West	South	Whole pelagic area	Inshore area	Whole lake
February							
Biomass (T)	1367	1295	1324	414	4399	605	5004
(95% C.I.)	(1210–1549)	(1184–1426)	(1100–1564)	(338–510)	(3832–5049)	(450–800)	(4283–5848)
July							
Biomass (T)	2183	1969	797	313	5263	773	6036
95% C.I. (T)	(2021–2352)	(1832–2113)	(715–882)	(268–365)	(4836–5712)	(615–945)	(5451–6657)

thus escape behaviours observed elsewhere (Guillard et al., 2010; Knudsen and Saegrov, 2002) should not be an issue. No spatial pattern of fish size distribution was observed in pelagic areas, which is consistent with the previous findings of Lamboeuf (1991). However, the proportion of small fish in the inshore areas was lower than in the pelagic zone whatever the season. Fish sizes were estimated using tracked fish, smoothing the variability due to behaviour and position. The number of detected targets was always considerable and the Sawada indexes were less than 0.1 as recommended by Rudstam et al. (2009). The size distributions were always unimodal (Fig. 7), which is representative of only one fish species, without marked cohorts. As *L. miodon* is by far the major pelagic fish species in Lake Kivu (Masilya, 2011), the transformation of TS to fish length was straightforward. In our study, the percentage of small targets representing juvenile fish (1–6 cm) (Kaningini, 1995), did not vary much in different basins and seasons and was approximately 30% of the total population based on the number of fish detected. Seasonal variation in the abundance of different size classes were noticed by Lamboeuf (1991) who used a single-beam sonar (EY200).

The two fish stock assessments were performed before the two main periods of *L. miodon* reproduction in Lake Kivu, i.e. March to May and August to October (Kaningini et al., 1999). The surveys led to an estimate of total fish stock of 5004 tons in February and of 6036 tons in July. Previous surveys (Kaningini et al., 1999) estimated the total fish biomass to be between 6000 and 10,000 t, while Lamboeuf (1991) estimated the biomass of *L. miodon* at 3445 to 5351 t between April 1989 and June 1991. Also, the mean areal density we observed (23 kg ha^{-1}) was similar to that described by Lamboeuf (1991). Given the similarity of the approaches used and the comparable sampling design, we conclude that there has been no difference in the sardine stock between the end of the 1980s and 2008. It is worth noting that estimates made at the end of the 1980s followed a period of stock decrease from 1981 to 1988, followed by a sharp increase in 1989 and 1990 (Lamboeuf, 1991; Marshall, 1991) and we cannot exclude that fish biomass varied during the two survey periods. While not significant, an approximately 20% increase in fish biomass was noted between February and July 2008. Actually, such a rise in fish biomass is within the range of natural stock fluctuations for this small pelagic fish (Marshall, 1993), and given the estimation errors, it should not be interpreted as a long-term trend. More frequent surveys, complementary with estimates of fisheries catches, should be performed to better understand the natural and human-caused fluctuations, as recently illustrated in Lake Kariba (Magadza, 2011).

A collapse of the *L. miodon* stock in Lake Kivu was predicted by Dumont (1986) due to a drop in the zooplankton size and abundance following the *L. miodon* introduction. Our hydroacoustic surveys demonstrate that the predicted collapse of *L. miodon* did not occur. The capacity of zooplankton communities to recover after a fish introduction has been reported in other lentic systems (see e.g. Harig and Bain, 1998; Knapp et al., 2001). Successful populations of alien species often rapidly increase in abundance, but then decline to what might

be called an “equilibrium level” (Strayer and Malcom, 2007; Williamson, 1996). The *L. miodon* introduction in Lake Kivu might have followed this “boom-and-bust” dynamic, and we can reasonably assume that the zooplankton biomass decrease detected in the 1980s was observed during the boom phase of *L. miodon* invasion. Unfortunately, data on the *L. miodon* dynamics in the years following the introduction are lacking. It is possible that the low zooplankton biomass reported by Dumont (1986) was a short-term effect, and that after some time both zooplankton and fish communities reached a more stable system state in Lake Kivu. This is in accordance to recent observations on the zooplankton community in Lake Kivu (Darchambeau et al., in press; Isumbusho et al., 2006). Re-analysis of past and recent zooplankton records indicates that zooplankton biomass before the sardine introduction may have been as high as 3 g Cm^{-2} , whereas the biomass in 2003–2004 was $\sim 1 \text{ g Cm}^{-2}$, suggesting a strong decline from the past situation without a planktivore fish. However, the present zooplankton biomass in lake Kivu is comparable to that of other great lakes of the East African rift (Darchambeau et al., in press), and may represent a new equilibrium biomass for zooplankton in the presence of planktivorous fish.

As already outlined (Lamboeuf, 1991; Marshall, 1993; Roest, 1999), *L. miodon* densities in Lake Kivu are low in comparison with lakes or reservoirs where the species is naturally present (Lake Tanganyika) or was introduced (Lakes Kariba and Cahora Bassa). The mean *L. miodon* biomass in 2008 in Lake Kivu (23 kg ha^{-1}) is notably lower than the sardine biomass in Lake Tanganyika, where estimates range from 60 kg ha^{-1} (Szczycka, 1998) to 300 kg ha^{-1} (Moreau and Nyakageni, 1988). Worth noticing, however, is that these figures are based on the fishery yield of the two sardine species inhabiting Lake Tanganyika, *Stolothrissa tanganyicae* and *L. miodon*. The reasons for the low *L. miodon* density in Lake Kivu are not known (Descy et al., 2012). Indeed, total phytoplankton and zooplankton productions are comparable across East African Great lakes (Darchambeau et al., 2012; Sarmento et al., 2012). Among the possible explanations, large fluctuations in clupeid stocks have been reported from other systems, in which variations of recruitment and larval survival may play a significant role (Kimirei and Mgaya, 2007; Mölsä et al., 2002). In addition local people around Lake Kivu often use illegal fishing techniques for catching young fish in the inshore areas (Kaningini et al., 1999) where the growth of *L. miodon* larvae and juveniles takes place (Masilya, 2011). This potentially harmful practice, coupled with the incidence of predation by *L. miodon* adults and other fish species in the inshore areas (De longh et al., 1983; Masilya, 2011), might significantly reduce larvae survival. Moreover, strong competition for resources may occur in these inshore zones (Masilya, 2011) which harbour almost all the fish diversity in Lake Kivu, with several haplochromine species (Snoeks et al., 1997).

Conclusion

Given that the pelagic area of Lake Kivu is dominated by *L. miodon* (Kaningini et al., 1999; Masilya, 2011) the two hydroacoustic surveys

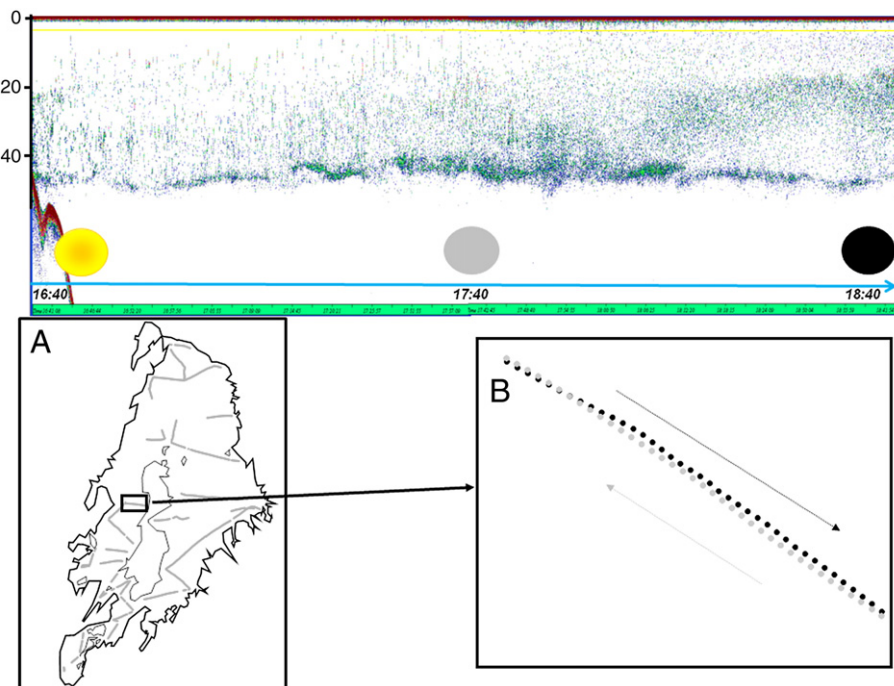


Fig. 8. Echogram recorded continuously from 16:40 to 19:00 GMT (dusk from 17:30 to 17:50 GMT), showing the detected fish (see Fig. 4) with the area (A) where the survey was performed indicated by a black rectangle, and a zoom (B) with the way forward, in grey, and the way back, in black.

performed in 2008 in Lake Kivu provided estimates of *L. miodon* biomass of 5004 tons (February) and 6036 tons (July). These results are similar to those reported at the end of the 1980s. Thus, contrary to predictions based on changes in the zooplankton assemblage, the stock of *L. miodon* did not collapse, but remained stable, despite a likely increase in the fishing effort. Based on the data presented here, the pelagic fishery on *L. miodon* in Lake Kivu appears sustainable. However, further hydroacoustic studies should examine the variations of the fish stocks in the lake. These surveys should be complemented by an assessment of the fishing effort over the whole lake in order to define management strategies for ensuring sustainability in the future. This becomes all the more relevant in the context of the methane exploitation (Nayar, 2009), which may in the long term affect both the environmental conditions and the resources available to the pelagic fish in Lake Kivu (Descy et al., 2012)

Acknowledgments

We are grateful to Boniface Kaningini and Pascal Isumbisho Mwapu (Institut Supérieur Pédagogique, Bukavu, République Démocratique du Congo), to Laetitia Nyinawamwiza (National University of Rwanda, Butare, Rwanda) and their respective teams for their logistic support during the trips, and to Bruno Leporcq for his help during field sampling. This work was funded by the Commission Universitaire pour le Développement (CUD) under the ECOSYKI (Etude du fonctionnement de l'écosystème du lac Kivu en vue de son exploitation durable) project and by the Fonds National de la Recherche Scientifique (FNRS) under the CAKI (Cycle du carbone et des nutriments au Lac Kivu, contract n° 2.4.598.07) project. Likewise, this study contributes to the Belgian Federal Science Policy Office EAGLES (East African Great Lake Ecosystem Sensitivity to changes, SD/AR/02A) project. FD was a postdoctoral researcher at the FNRS. In addition, we thank two anonymous referees for their helpful comments.

References

Aglen, A., 1989. Empirical results on precision-effort relationships for acoustic surveys. ICES CM B/30.

- Balk, H., Lindem, T., 2006. Sonar 4, Sonar 5, Sonar 6 — post-processing systems. Operator Manual. University of Oslo, Norway.
- Beadle, L.C., 1981. The inland waters of tropical Africa, an introduction to tropical limnology. Longman, London.
- Brehmer, P., Guillard, J., Guennégan, Y., Bigot, J.L., Liorzou, B., 2006. Evidence of a variable "unsampled" biomass along the shallow water (<20 m) coastline in small pelagic fish stock assessment method. ICES J. Mar. Sci. 63, 444–451.
- Collart, A., 1960. L'introduction du *Stolothrissa tanganyicae* (Ndagala) au lac Kivu. Bull. Agric. Congo Belge 51 (4), 975–985.
- Coulter, G.W., 1991. Lake Tanganyika and its life. Oxford University Press, London.
- Darchambeau, F., Isumbisho, M., Descy, J.-P., 2012. Zooplankton of Lake Kivu. In: Descy, J.-P., Darchambeau, F., Schmid, M. (Eds.), Lake Kivu — Limnology and biogeochemistry of a tropical great lake: Aquatic Ecology Series, vol. 5, Springer, pp. 107–126.
- De longh, H.H., Spliethoff, P.C., Frank, V.G., 1983. Feeding habits of the clupeid *Limnothrissa miodon* (Boulenger), in Lake Kivu. Hydrobiologia 102, 113–122.
- Degens, E.T., Von Herzen, R.P., Wong, H.-K., Deuser, W.G., Jannasch, H.W., 1973. Lake Kivu: structure, chemistry and biology of an East African Rift Lake. Geol. Rundsch. 62, 245–277.
- Descy, J.-P., Darchambeau, F., Schmid, M., 2012. Lake Kivu — limnology and biogeochemistry of a tropical great lake. Aquatic Ecology Series, vol. 5. Springer.
- Dumont, H.J., 1986. The Tanganyika Sardine in Lake Kivu: another ecodisaster for Africa? Environ. Conserv. 13 (2), 143–148.
- Dunlop, E.S., Milne, S.W., Ridgway, M.S., 2010. Temporal trends in the numbers and characteristics of Lake Huron fish schools between 2000 and 2004. J. Great Lakes Res. 36 (1), 74–85.
- FAO, 1992. Développement de la pêche au lac Kivu, Rwanda. Conclusions et recommandations du projet. FAO Fi:DP/RWA/87/012.
- Foot, K.G., Knudsen, H.P., Vestnes, G., MacLennan, D.N., Simmonds, E.J., 1987. Calibration of acoustic instruments for fish-density estimation: a practical guide. ICES Cooper. Res. Rep.
- Fréon, P., Misund, O.A., 1999. Dynamics of pelagic fish distribution and behaviour: effects on fisheries and stock assessment. Fishing news books. Blackwell Science, Oxford, U.K.
- Fréon, P., Gerlotto, F., Soria, M., 1996. Diel variability of school structure with special reference to transition. ICES J. Mar. Sci. 53, 459–464.
- Godlewska, M., Colon, M., Jozwika, A., Guillard, J., 2011. How pulse lengths impact fish stock estimations during hydroacoustic measurements at 70 kHz. Aquat. Living Resour. 24, 71–78.
- Gozlan, R.E., 2008. Introduction of non-native freshwater fish: is it all bad? Fish Fish. 9, 106–115.
- Guillard, J., Marchal, E., 2001. L'hydroacoustique, méthode d'étude de la distribution spatiale et de l'abondance des peuplements pisciaires lacustres. In: Gerdeaux, D. (Ed.), La gestion piscicole des grands plans d'eau, INRA Paris, pp. 215–239.
- Guillard, J., Vergés, C., 2007. The repeatability of fish biomass and size distribution estimates obtained by hydroacoustic surveys using various survey designs and statistical analyses. Int. Rev. Hydrobiol. 92 (6), 605–617.
- Guillard, J., Perga, M.-E., Colon, M., Angeli, N., 2006. Hydroacoustic assessment of young-of-year perch, *Perca fluviatilis*, population dynamics in an oligotrophic lake (Lake Annecy, France). Fish. Manag. Ecol. 13, 319–327.

- Guillard, J., Balay, P., Colon, M., Brehmer, P., 2010. Survey boat effect on YOY fish schools in a pre-alpine lake: evidence from multibeam sonar and split-beam echosounder data. *Ecol. Freshw. Fish* 19, 373–380.
- Haberyan, K.A., Hecky, R.E., 1987. The late Pleistocene and Holocene stratigraphy and paleolimnology of Lakes Kivu and Tanganyika. *Palaeogeogr. Palaeoclimatol. Palaeoecol.* 61, 169–197.
- Harig, A.L., Bain, M.B., 1998. Defining and restoring biological integrity in wilderness lakes. *Ecol. Appl.* 8, 71–87.
- Isumbisho, M., Kaningini, B., Descy, J.-P., Baras, E., 2004. Seasonal and diel variations in diet of the young stages of the fish *Limnothrissa miodon* in Lake Kivu, Eastern Africa. *J. Trop. Ecol.* 20, 73–83.
- Isumbisho, M., Sarmiento, H., Kaningini, B., Micha, J.-C., Descy, J.-P., 2006. Zooplankton of Lake Kivu, half a century after the Tanganyika sardine introduction. *J. Plankton Res.* 28 (10), 1–19.
- Johnson, T.B., Hoff, M.H., Trebitz, A.S., Bronte, C.R., Corry, T.D., Kitchell, J.F., Lozano, S.J., Mason, D.M., Scharold, J.V., Schram, S.T., Schreiner, D.R., 2004. Spatial patterns in assemblage structures of pelagic forage fish and zooplankton in Western Lake Superior. *J. Great Lakes Res.* 30 (1), 395–406.
- Kaningini B., 1995. Etude de la croissance, de la reproduction et de l'exploitation de *Limnothrissa miodon* au lac Kivu, bassin de Bukavu (Zaire). Thèse de Doctorat en Sciences, Biologie, F.U.N.D.P., Faculté des Sciences, Namur, Belgium.
- Kaningini, B., Micha, J.-C., Vandenhoute, J., Platteau, J.-P., Watongoka, H., Mélard, C., Wilondja, M.K., Isumbisho, M., 1999. Pêche du Sambaza au filet maillant dans le lac Kivu. Presses Universitaires de Namur, Namur, Belgium.
- Kaningini, M., Isumbisho, M., Ndayike, N., Micha, J.-C., 2003. L'étude du zooplancton du lac Kivu : composition, variations saisonnières d'abondance et distribution. *Bull. Séanc. Acad. R. Sci. Outre-Mer* 49 (2), 145–160.
- Kimirei, I.A., Mgaya, Y.D., 2007. Influence of environmental factors on seasonal changes in clupeid catches in the Kigoma area of Lake Tanganyika. *Afr. J. Aquat. Sci.* 32, 291–298.
- Knapp, R.A., Matthews, K.R., Sarnelle, O., 2001. Resistance and resilience of alpine lake fauna to fish introductions. *Ecol. Monogr.* 71, 401–421.
- Knudsen, F.R., Sægrov, H., 2002. Benefits from horizontal beaming during acoustic survey: application to three Norwegian lakes. *Fish. Res.* 56, 205–211.
- Kurkilahti, M., Appelberg, M., Hesthagen, T., Rask, M., 2002. Effect of fish shape on gillnet selectivity: a study with Fulton's condition factor. *Fish. Res.* 54, 153–170.
- Kwetuenda, M., Nakao, K., Kagogo, B., 1989. Climatic conditions in the hydrological basin of Lake Kivu during 12 years. In: Kawanabe, H., Nagoshi, M. (Eds.), *Ecological and limnological study on Lake Tanganyika and its adjacent regions*, Kyoto, Japan, pp. 55–56.
- Lamboeuf, M., 1989. Estimation de l'abondance du stock d'Isambaza (*Limnothrissa miodon*), résultats de la prospection acoustique de septembre 1989. RWA/87/012/DOC/TR/20.
- Lamboeuf, M., 1991. Abondance et répartition du *Limnothrissa miodon* du lac Kivu, résultat des prospections acoustiques d'avril 1989 à juin 1991. RWA/87/012/DOC/TR/46.
- Leprieur, F., Brosse, S., Garcia-Berthou, E., Oberdorff, T., Olden, J.D., Townsend, C.R., 2009. Scientific uncertainty and the assessment of risks posed by non-native freshwater fishes. *Fish. Fish.* 10, 88–97.
- MacLennan, D., Fernandes, P.G., Dalen, J., 2002. A consistent approach to definitions and symbols in fisheries acoustics. *ICES J. Mar. Sci.* 59, 365–369.
- Magadza, C.H.D., 2011. Indications of the effect of climate change on the pelagic fishery of Lake Kariba, Zambia-Zimbabwe. *Lakes Reservoirs Res. Manage.* 16, 15–22.
- Marshall, B.E., 1991. Seasonal and annual variations in the abundance of the clupeid *Limnothrissa miodon* in Lake Kivu. *J. Fish Biol.* 39, 641–648.
- Marshall, B.E., 1993. Biology of the African clupeid *Limnothrissa miodon* with reference to its small size in artificial lakes. *Rev. Fish Biol. Fish.* 3, 17–38.
- Masilya P., 2011. Ecologie alimentaire de *Limnothrissa miodon* au Lac Kivu (Afrique de l'Est). PhD thesis, University of Namur, Belgium.
- Masilya, M.P., Darchambeau, F., Isumbisho, M., Descy, J.-P., 2011. Diet overlap between the newly introduced *Lamprichthys tanganyicanus* and the Tanganyika sardine in Lake Kivu, Eastern Africa. *Hydrobiologia* 675, 75–86.
- Mölsä, H., Sarvala, J., Badende, S., Chitamwebwa, D., Kanyaru, R., MuliMbwa, N., Mwape, L., 2002. Ecosystem monitoring in the development of sustainable fisheries in Lake Tanganyika. *Aquat. Ecosyst. Health Manage.* 5, 267–281.
- Moreau, J., Nyakageni, B., 1988. Les relations trophiques dans la zone pélagique du lac Tanganyika (secteur Burundi). Essai d'évaluation. *Rev. Hydrobiol. Trop.* 21, 357–364.
- Moreau, J., Arrignon, J., Jubb, R.A., 1988. Les introductions d'espèces étrangères dans les eaux continentales africaines. Intérêts et limites. In: Lévêque, C., Bruton, M.N., Sentongo, G.W. (Eds.), *Biologie et écologie des poissons d'eau douce africains*. Editions de l'ORSTOM, France, pp. 221–242.
- Muderhwa, N., Matabaro, L., 2010. The introduction of the endemic fish species, *Lamprichthys tanganyicanus* (Poeciliidae), from Lake Tanganyika into Lake Kivu: Possible causes and effects. *Aquat. Ecosyst. Health Manage.* 13 (2), 203–213.
- Nayar, A., 2009. A lakeful of trouble. *Nature* 460, 321–323.
- Ogutu-Ohwayo, R., Hecky, R., Cohen, A.S., Kaufman, N.L., 1997. Human impacts on the African Great Lakes. *Environ. Biol. Fish.* 50, 117–131.
- Parrish, J., Viscido, S., Grünbaum, D., 2002. Self-Organized Fish Schools: An Examination of Emergent Properties. *Biol. Bull.* 202, 296–305.
- Pasche, N., Alunga, G., Mills, K., Muvundja, F., Ryves, D.B., Schurter, M., Wehrli, B., Schmid, M., 2010. Abrupt onset of carbonate deposition in Lake Kivu during the 1960s: response to recent environmental changes. *J. Paleolimnol.* 44, 931–946.
- Pitcher, T.J., Parrish, J.K., 1993. Function of shoaling behavior in teleosts. In: Pitcher, T.J. (Ed.), *Behaviour of Teleost Fishes*. Chapman and Hall, London, U.K., pp. 363–439.
- Prchalová, M., Kubecka, J., Říha, M., Mrkvicka, T., Vasek, M., Juza, T., Kratochvíl, M., Peterka, J., Drastik, V., Krizek, J., 2009. Size selectivity of standardized multimesh gillnets in sampling coarse European species. *Fish. Res.* 96, 51–57.
- Roest, F.C., 1999. Introduction of a pelagic fish into a large natural Lake : Lake Kivu, Central Africa. In: Van Densen, W.L.T., Morris, M.J. (Eds.), *Fish and Fisheries of Lakes and Reservoirs in Southeast Asia and Africa*. Westbury Academic and Scientific Pub, Otley (United Kingdom), pp. 327–338.
- Rudstam, L.G., Parker-Stetter, S.L., Sullivan, P.J., Warner, D.M., 2009. Towards a standard operating procedure for fishery acoustic surveys in the Laurentian Great Lakes, North America. *ICES J. Mar. Sci.* 66, 1391–1397.
- Sala, O.E., Chapin III, F.S., Armesto, J.J., Berlow, E., Bloomfield, J., Dirzo, R., Huber-Sanwald, E., Huenneke, L.F., Jackson, R.B., Kinzig, A., Leemans, R., Lodge, D.M., Mooney, H.A., Oesterheld, M., LeRoy Poff, N., Sykes, M.T., Walker, B.H., Walker, M., Wall, D.H., 2000. Global Biodiversity Scenarios for the Year 2100. *Science* 287, 1770–1774.
- Sarmiento, H., Isumbisho, M., Descy, J.-P., 2006. Phytoplankton ecology of Lake Kivu (Eastern Africa). *J. Plankton Res.* 28 (9), 815–829.
- Sarmiento, H., Darchambeau, F., Descy, J.-P., 2012. Phytoplankton of Lake Kivu. In: Descy, J.-P., Darchambeau, F., Schmid, M. (Eds.), *Lake Kivu – Limnology and biogeochemistry of a tropical great lake*, Aquatic Ecology Series, vol. 5, Springer, pp. 67–84.
- Shafer, N.J., Sullivan, J.A., 1986. A simulation study of a test for the equality of the coefficients of variation. *Commun. Stat. – Simul. Comput.* 15, 681–695.
- Simmonds, E.J., MacLennan, D.N., 2005. *Fisheries Acoustics: Theory and Practice*. Blackwell Science Ltd, Oxford.
- Smith, S., 1990. Use of statistical models for the estimation of abundance from ground-fish survey data. *Can. J. Fish. Aquat. Sci.* 47, 894–903.
- Snoeks, J., De Vos, L., Thys Van den Audenaerde, D., 1997. The ichthyogeography of Lake Kivu. *S. Afr. J. Sci.* 93, 579–584.
- Snoeks, J., Kaningini, B., Nyinawamwiza, L., Guillard, J., 2012. Fishes: diversity and fisheries. In: Descy, J.-P., Darchambeau, F., Schmid, M. (Eds.), *Lake Kivu – Limnology and biogeochemistry of a tropical great lake*, Aquatic Ecology Series, vol. 5, Springer, pp. 127–152.
- Splithoff, P.C., De longh, H.H., Frank, V., 1983. Success of the introduction of the freshwater Clupeid *Limnothrissa miodon* (Boulenger) in Lake Kivu. *Fish. Manag.* 14, 17–31.
- Strayer, D.L., Malcom, H.M., 2007. Effects of zebra mussels (*Dreissena polymorpha*) on native bivalves: the beginning of the end or the end of beginning? *J. N. Am. Benthol. Soc.* 26, 111–122.
- Szczucka, J., 1998. Acoustical estimation of fish abundance and their spatial distributions in Lake Tanganyika. FAO/FINNIDA Research for the Management of the Fisheries of Lake Tanganyika. GCP/RAF/271/FIN-TD/84.
- Vitousek, P.M., Mooney, H.A., Lubchenco, J., Melillo, J.M., 1997. Human Domination of Earth's Ecosystems. *Science* 277, 494–499.
- Vitule, J.R.S., Freire, C.A., Simberloff, D., 2009. Introduction of non-native freshwater fish can certainly be bad. *Fish. Fish.* 10, 98–108.
- Williamson, M., 1996. *Biological Invasions*. Chapman and Hall, London.

Vertical Distribution of Functional Potential and Active Microbial Communities in Meromictic Lake Kivu

Özgül İnceoğlu¹ · Marc Llíros^{2,6} · Sean A. Crowe³ · Tamara García-Armisen¹ · Cedric Morana⁴ · François Darchambeau⁵ · Alberto V. Borges⁵ · Jean-Pierre Descy² · Pierre Servais¹

Received: 4 December 2014 / Accepted: 2 April 2015
© Springer Science+Business Media New York 2015

Abstract The microbial community composition in meromictic Lake Kivu, with one of the largest CH₄ reservoirs, was studied using 16S rDNA and ribosomal RNA (rRNA) pyrosequencing during the dry and rainy seasons. Highly abundant taxa were shared in a high percentage between bulk (DNA-based) and active (RNA-based) bacterial communities, whereas a high proportion of rare species was detected only in either an active or bulk community, indicating the existence of a potentially active rare biosphere and the possible underestimation of diversity detected when using only one nucleic acid pool. Most taxa identified as generalists were abundant, and those identified as specialists were more likely to be rare in the bulk community. The overall number of environmental parameters that could explain the variation was higher for abundant taxa in comparison to rare taxa. Clustering analysis based

on operational taxonomic units (OTUs at 0.03 cutoff) level revealed significant and systematic microbial community composition shifts with depth. In the oxic zone, *Actinobacteria* were found highly dominant in the bulk community but not in the metabolically active community. In the oxic–anoxic transition zone, highly abundant potentially active *Nitrospira* and *Methylococcales* were observed. The co-occurrence of potentially active sulfur-oxidizing and sulfate-reducing bacteria in the anoxic zone may suggest the presence of an active yet cryptic sulfur cycle.

Keywords Bacteria · Archaea · Pyrosequencing · Active · Bulk · qPCR · Network · Abundant and rare · Meromictic lake

Electronic supplementary material The online version of this article (doi:10.1007/s00248-015-0612-9) contains supplementary material, which is available to authorized users.

✉ Özgül İnceoğlu
oetzguel@gmail.com

- ¹ Ecologie des Systèmes Aquatiques, Université Libre de Bruxelles, Brussel, Belgium
- ² Laboratory of Freshwater Ecology, Université de Namur, Namur, Belgium
- ³ Departments of Microbiology and Immunology, and Earth, Ocean, and Atmospheric Sciences, University of British Columbia, Vancouver, Canada
- ⁴ Department of Earth and Environmental Sciences, Katholieke Universiteit Leuven, Leuven, Belgium
- ⁵ Chemical Oceanography Unit, Université de Liège, Liège, Belgium
- ⁶ Present address: Department of Genetics and Microbiology, Universitat Autònoma de Barcelona, Bellaterra, Spain

Introduction

Meromictic lakes are good model systems for microbial ecology research due to the high vertical stability of the water masses and physicochemical gradients (in particular oxygen) that lead to relatively constant stratification of microbial populations [1–3]. Since microbes are key players in biogeochemical cycles, investigations on microbial diversity and community composition are important to understand the ecological functioning of lakes. Environmental heterogeneity was shown to produce community differences in lakes [4, 5]. According to Lennon and Jones [6], core community shifts, including active, dormant, and dead cells, may vary widely along vertical gradients, contributing to the community dynamics as well as to the maintenance of ecosystem biodiversity and ecosystem stability. Currently, high-throughput sequencing technology provides an opportunity to detect greater microbial diversity than the one detected by previous techniques [7–9]. It has revealed that the core community is composed of abundant and rare taxa that are in continuous exchange based on the

environmental gradients [10]. However, most recent studies were based on bulk community composition (i.e., DNA-based 16S ribosomal RNA (rRNA) genes) and did not distinguish between functionally active (i.e., RNA-based 16S rRNA genes) or dormant populations [11]. Even though potential biases can be introduced during DNA and RNA extraction, complementary DNA (cDNA) synthesis, and PCR amplification [12], parallel comparisons of DNA- and RNA-based pyrosequencing approaches can help differentiate whether abundant taxa are active or whether rare but active taxa exist. In addition, stronger evidence on the links between biogeochemical processes and microbial communities might be obtained if active communities are monitored rather than bulk communities [13–16].

Lake Kivu in East Africa is a meromictic lake with a permanent density stratification separating the oximixolimnion from a deep anoxic monolimnion rich in dissolved salts, carbon dioxide (CO₂), and methane (CH₄) [17]. In spite of the presence of high amounts of CH₄ at the bottom of Lake Kivu, the CH₄ concentration in the oxic zone is surprisingly low compared to other lakes globally, due to intense microbial methane oxidation [18, 19]. The vertical stratification of microbial taxa and their potential role in biogeochemical cycles in Lake Kivu were recently studied for both archaeal and bacterial counterparts using DNA-based analysis, and important key players of carbon, nitrogen, and sulfur cycles were identified [20, 21]. Furthermore, evaluation of the effect of temporal variations on abundant versus rare taxa in different layers revealed that abundant taxa were more stable between two sampling times than rare ones, indicating a potentially higher contribution of rare taxa to biogeochemical processes [20]. Therefore, in the present study, Lake Kivu was investigated as a model ecosystem by comparative DNA- and RNA-based pyrosequencing of bacterial and archaeal communities in two different seasons (i) to check if bulk (DNA) and potentially active (RNA) microbial communities have the same composition through the water column and (ii) to explore if rare bulk and potentially active taxa respond to environmental changes as abundant taxa do in Lake Kivu. Furthermore, the abundance of key genes related to the carbon (particulate methane monooxygenase gene (*pmoA*) and methyl coenzyme-M reductase gene (*mcrA*)) and nitrogen (ammonia monooxygenase gene (*amoA*), nitrite reductase gene (*nirK*) and nitrous oxide reductase (*nosZ*)) biogeochemical cycles was measured to evaluate the functional potential and their response to environmental changes.

Materials and Methods

Study Site and Sampling Meromictic and oligotrophic Lake Kivu is located between Rwanda and the Democratic Republic of the Congo at 1463 m above sea level. It has a surface area of 2370 km², a total volume of 580 km³, and a maximum

depth of 485 m. Surface waters are considered to be oligotrophic with moderate primary production compared to other African lakes [22, 23]. Further details on the hydrology, physicochemistry, and biology of the lake are published elsewhere [22–25]. In order to study the microbial communities in the water column of Lake Kivu, water samples were collected from the upper 100 m of the water column in the North basin (off Gisenyi; 29.24° E, -1.72° N). Water samples were collected during two sampling campaigns during both rainy (RS, February 2012) and dry seasons (DS, September 2012). Up to 20 discrete depths were sampled along a vertical profile between 1 and 100 m to cover the whole gradient of oxygen concentrations (from oxic to anoxic waters). Water samples for chemical and microbiological analyses were collected using a 7.5-L Niskin bottle and stored in 4-L plastic containers for chemical analyses (except for CH₄ and HS⁻) and 2-L Nalgene plastic bottles for biological analyses. Water samples for DNA and RNA extractions were immediately passed through 5.0-μm pore size filters (ISOPORE, Millipore, MA) to remove particulate debris as well as large protozoa. Eluents were then passed through 0.22-μm pore size filters (ISOPORE, Millipore, MA) to retain free-living prokaryotes. Filters for DNA extraction were preserved in Lysis Buffer as previously described [21], whereas filters for RNA extraction were preserved in 300 μL of RNAlater (Ambion) and all stored frozen until further analyses.

Chemical Analyses Temperature, conductivity, pH, and dissolved oxygen (DO) vertical depth profiles were measured in situ with a YSI 6600 V2 (Yellow Spring Instruments, USA) multiparametric probe. According to Wright et al. [26], the upper 100 m of the water column of Lake Kivu was split into three distinct vertical layers: an oxic surface layer (DO > 90 μM), a transition zone (DO between 1 and 90 μM), and a deep anoxic zone (DO < 1 μM; Fig. 1). The concentration of methane (CH₄) was measured using the headspace technique with a gas chromatograph with a flame ionization detector as previously described [18]. Samples for NO_x and SO₄²⁻ were filtered directly through 0.2-μm pore size cellulose acetate syringe filters. NH₄⁺ concentrations were determined using the dichloroisocyanurate-salicylate-nitroprussiate colorimetric method [27]. NO₂⁻ concentrations were determined by the sulfanilamide coloration method [28]. NO₃⁻ concentrations were determined after vanadium reduction to nitrite and quantified in this form following the nitrite determination procedure [28, 29]. SO₄²⁻ concentrations were measured using ion chromatography. Samples for HS⁻ determination were not filtered but preserved instead with zinc acetate and stored frozen. HS⁻ concentrations were measured spectrophotometrically [30]. The detection limits for these methods were 0.5 nM for CH₄ and 0.3, 0.03, 0.1, 2, and 0.5 μM for NH₄⁺, NO₂⁻, NO₃⁻, SO₄²⁻, and HS⁻, respectively. Samples for particulate organic carbon concentration (POC) were filtered on precombusted

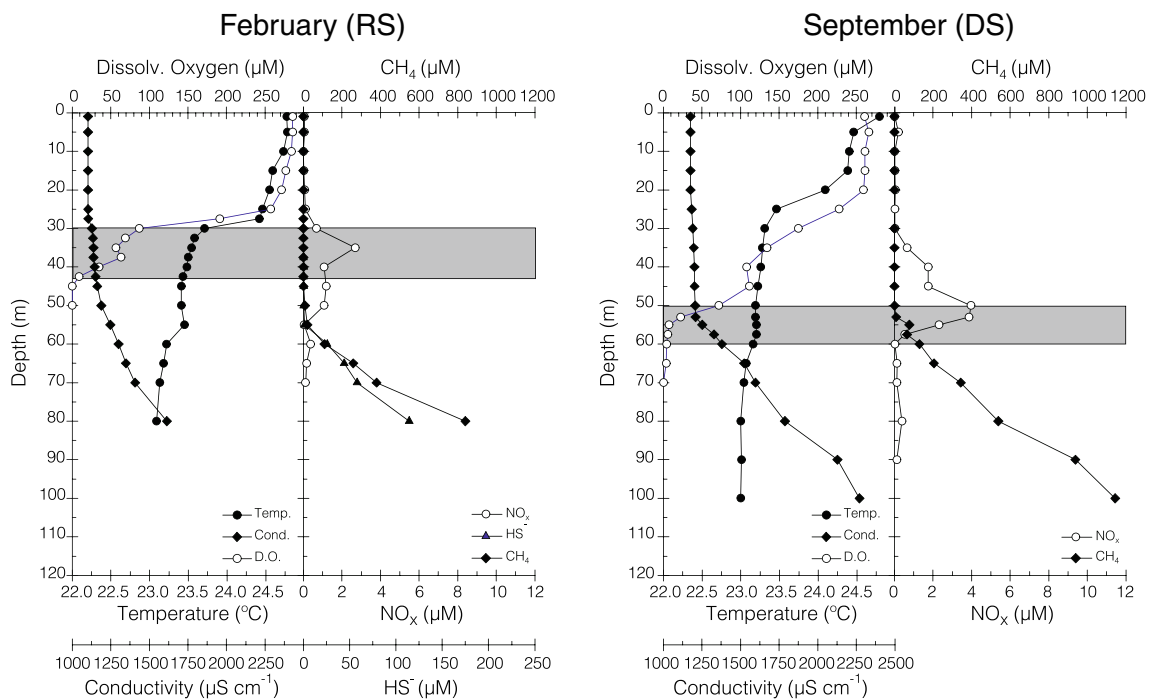


Fig. 1 Depth profiles of temperature, conductivity and dissolved oxygen (DO), nitrite and nitrite (NO_x), CH₄, and HS⁻ concentrations during the two sampling campaigns (February (RS) and September (DS)). The transition zones were indicated with a gray bar

(overnight at 450 °C) 25-mm glass fiber filters (Advantec GF-75; 0.3 µm) and dried. These filters were later decarbonated with HCl fumes for 4 h and then dried and packed in silver cups. POC was determined by elemental analysis-isotope ratio mass spectrometry (EA-IRMS, ThermoFlashHT with Thermo Delta V Advantage). POC was calibrated with International Atomic Energy Agency (IAEA-C6) and acetanilide.

Chlorophyll a (Chla) concentrations were determined using high-performance liquid chromatography (HPLC). At each sampling depth, 3 L of water were filtered on a Macherey–Nägel GF-5 filter (nominal porosity, 0.4 µm). Pigment extraction was carried out in 10 mL of 90 % HPLC grade acetone (Fisher Scientific). After two 15-min sonication steps separated by an overnight period at 4 °C, the extracts were stored in 2-mL amber vials at -25 °C. HPLC analysis was performed following the method described in Sarmento et al. [23]. Commercial external standards (DHI Lab Products) were used for calibration.

Nucleic Acid Extraction DNA was extracted using a combination of enzymatic cell lysis and the cetyltrimethyl ammonium bromide (CTAB) extraction protocol as previously described [20, 31]. Dry DNA pellets were finally rehydrated in 50 µL of 10 mM Tris–HCl buffer (pH 7.4).

Total RNA was extracted using a mirVana RNA isolation kit (Ambion, Austin, TX, USA; [32]). RNA samples were treated with the Turbo DNA-free kit (Ambion, Austin, TX, USA), and cDNA synthesis was performed with the iScript reverse transcription supermix (Bio-Rad) in a MasterCycler

5331 Gradient (Eppendorf, Hamburg, Germany). Possible DNA contamination of RNA templates was routinely monitored by PCR amplification of RNA aliquots that were not reverse transcribed. No contaminating DNA was detected in any of these reactions.

Real-Time Quantitative PCR qPCR was used to quantify the presence of distinct functional genes. The following genes were used as proxies for quantification of DNA: the bacterial alpha subunit of the particulate methane monooxygenase enzyme (*pmoA*) for methanotrophs, the archaeal alpha subunit of methyl-coenzyme M reductase enzyme gene (*mcrA*) for methanogens, the alpha subunit of the archaeal ammonia monooxygenase enzyme gene (*amoA*) for archaeal ammonia oxidation, the bacterial copper-containing nitrite reductase gene (*nirK*), and the cytochrome cd1-containing nitrite reductase gene (*nosZ*) for bacterial denitrification. All qPCR assays were performed in a StepOne Real-Time PCR system (Applied Biosystems, Foster City, CA, USA) using the primers and thermal conditions described in Table 1. All reactions were performed in triplicate for both serial dilutions of titrated standards and unknown templates using a 20 µL reaction mixture consisting of the 1× PowerSYBR green PCR master mix (Applied Biosystems), each primer (Table 1), and DNA templates of known concentrations of standards or 20 ng DNA extracted from water samples. The specificity of the amplification products was further confirmed by melting curve analyses, and the expected sizes of the amplified fragments were checked on a 1 % agarose gel. Overall, average efficiencies for

Table 1 PCR and thermal cycling conditions for real-time quantification of functional genes used in the present study

Primer pair ^a	Sequence (5'–3')	Cycles ^b	Denaturation		Annealing		Elongation		Signal detect.		Reference
			C	Min	C	Min	C	Min	C	Min	
<i>pmoA</i> [200 nM]		40	95	30	56	30	72	30	72	30	[33]
A189f	GGN GAC TGGGAC TTC TGG										
mb661r	CCGGMG CAA CGT CYT TAC C										
<i>mcrA</i> [200 nM]		40	95	30	55	30	72	30	72	30	[34]
LuF	GGT GGTGTM GGA TTC ACA CAR TAY GCW ACA GC										
LuR	TTC ATT GCR TAG TTW GGR TAG TT										
<i>amoA</i> [200 nM]		60	94	39	59	40	72	40	72	32	[21]
AOA-amoAf	CTG AYT GGG CYT GGA CAT C										
AOA-amoAr	TTC TTC TTT GTT GCC CAG TA										
<i>nirK</i> [500 nM]		6/40	94	15	63–58/60	30	72	30	80	15	[35]
nirK876	ATY GGC GGV CAY GGC GA										
nirK1040	GCC TCG ATC AGR TTR TGG TT										
<i>nosZ</i> [750 nM]		6/40	94	15	65–60/60	30/20	72	20/30	80	15	[35]
nosZ2F	CGC RAC GGC AAS AAGGTS MSS GT										
nosZ2R	CAK RTG CAK SGC RTGGCA GAA										

^a Concentration for each primer pair is given in brackets

^b All quantitative PCR reactions have an initial denaturation step at 95° during 3 min

all quantification reactions ranged from 0.88 to 0.97 with R^2 values >0.99 . Standard curves were generated from serial dilutions of previously titrated suspensions of the desired genes from isolates or environmental clones, purified (QIAquick; Qiagen), and quantified. Statistical analyses (ANOVA and Tukey's HSD) were performed to compare differences between water zones (oxic, transition, anoxic) [36].

16S Tag-Encoded FLX-Titanium Amplicon Pyrosequencing Bacterial and archaeal tag-encoded FLX amplicon pyrosequencing (bTEFAP and aTEFAP, respectively), analyses by means of a Roche 454 FLX instrument with titanium reagents, were performed at the Research and Testing Laboratory (Lubbock, TX, USA) as described previously [37, 38]. The PCR primers for FLX amplicon pyrosequencing were chosen to span the variable V1–V3 regions in the 16S rRNA gene: 27 F (5'-GAGTTTGATCNTGGCTCAG-3') and 519R (5'-GWNTTACNGCGGCKGCTG-3') for bacteria and V3–V4 regions ARCH 349 F (5'-GYGCASCAGKCGMGAAW-3') and ARCH 806R (5'-GGACTACVSGGGTATCTAAT-3') for archaea. These primers cover about 78 and 70 % of publicly available 16S rRNA for bacteria and archaea, respectively (check using TestPrime tool available at SILVA webpage (<http://www.arb-silva.de/search/testprime/>)).

Pyrosequencing Data Analyses All sequences generated in this study can be downloaded from the National Center for Biotechnology Information (NCBI) Short Read Archive, accession number: SRP021176. Pyrosequencing data were processed using Mothur [40]. To minimize the effects of random sequencing errors, a denoising algorithm (shhh.flows) included in the pipeline is used and low-quality sequences were removed by eliminating those without an exact match to the forward primer, without a recognizable reverse primer, with a length shorter than 200 nucleotides, and those containing any ambiguous base calls. We trimmed the barcodes and primers from the resulting sequences. Chimeric sequences were removed using the Uchime software [39] implemented in Mothur [40]. The latest Greengenes and SILVA databases were used for classification of bacterial and archaeal 16S rRNA gene sequences, respectively, at a 80 % confidence threshold using Mothur. After taxonomic assignment of the sequences to the phylum, class, and genus level, relative abundance of a given phylogenetic group was set as the number of sequences affiliated with that group divided by the total number of sequences per sample. The sequences retrieved were grouped based on oxygen stratification as oxic, transition, and anoxic zones.

Sequences were clustered into operational taxonomic units (OTUs) by setting a 0.03 distance limit (equivalent to 97 % similarity). A data matrix was created based on the relative abundance of genus and OTU. The relative abundances were square root transformed. Dendrograms were generated based on the Bray–Curtis similarity index using complete linkage

clustering. Furthermore, the scatterplot depicted the relationship between the depths and observed species-based Bray–Curtis similarity. The discrimination of microbial assemblages based on time and stratification was tested with one-way analysis of similarities (ANOSIM). Unless otherwise stated, all the analyses were performed using PRIMER 6 [41].

To measure habitat specialization, the niche breadth approach was used, as described previously [42, 43]. The niche breadth (B_j) was calculated using the following equation:

$$B_j = \frac{1}{\sum_{i=1}^N P_{ij}^2}$$

in which P_{ij} is the proportion of individuals belonging to species j present in a given habitat i . OTUs with a high B_j value indicate a wide range of habitats, which can be considered as habitat generalists. Similarly, OTUs with a low value can be assigned as habitat specialists.

Furthermore, the data sets were split into two groups: Taxa represented by more than 15 sequences per sample were defined as abundant taxa, and taxa that had fewer than 15 sequences were considered rare. Venn diagrams of OTUs were constructed to illustrate the number of shared OTUs (both subsampled and not subsampled) for the two sampling campaigns based on DNA and RNA. A relative abundance matrix for OTUs was created for sampling times and points pooled, and those OTUs that appeared less than five times were removed from the matrix. For network inference, Pearson's rank correlations were calculated between OTUs with CoNet [44], when coefficient (r) was both above 0.8 and statistically significant (adjusted p value <0.01 with Benjamini–Hochberg). The data matrix was translated into an association network using Cytoscape 2.6.3 [44, 45]. Cytoscape depicts data sets as nodes (tribes) connected by lines that denote the positive correlation. In the network, the size of each node is proportional to the number of connections (degree) and the node border color indicates if the OTU is either abundant or rare.

We further quantified the influences of environmental variables (pH+DO+NO_x+POC+CH₄+Chl- α), depth, and season on bacterial community variation using variation partitioning analyses [46], with the varpart function of the vegan package [47, 36]. If any colinearity was present, it would be revealed by the analysis.

Results

Environmental Parameters

Lake Kivu is characterized by vertical gradients in temperature, pH, conductivity, DO, CH₄, and HS⁻ (Fig. 1). Surface waters were characterized by high DO content and low NO_x

and CH₄ concentrations, whereas the anoxic deep waters were characterized by high concentrations of NH₄⁺ and dissolved CO₂ and CH₄ [18]. NO_x⁻ showed maximum values in the oxic–anoxic transition zone, whereas increasing concentrations with depth of HS⁻ (>50 μM) and CH₄ (>100 μM) were only observed in the anoxic zone (Fig. 1). The mixed oxic zone was deeper during the DS than during the RS with a more gradual decrease in DO with depth and a steady increase in NO_x values toward the chemocline (Fig. 1). The pH decreased with depth over the first 100-m depth (data not shown). POC concentration was higher in the oxic water than in the anoxic zones during both sampling campaigns and was slightly higher in the oxic water compartments in DS than in RS (data not shown).

qPCR In the current study, functional genes involved in key processes of carbon and nitrogen cycles were measured by genomic DNA qPCR. In relation to the carbon cycle, the *pmoA* gene was used to quantify the bacterial methanotrophs and the *mcrA* gene to quantify archaeal methanogens and

methanotrophs. Concerning the N cycle, the *amoA* gene was used to quantify archaeal ammonia oxidizers (AOA) while the *nirK* and *nosZ* genes were used to quantify bacterial denitrifiers.

In RS, *pmoA* gene copies ranged between 1.13×10^3 and 2.92×10^4 gene copies mL⁻¹, whereas in DS, the values varied between 4.19×10^2 and 9.63×10^4 gene copies mL⁻¹ throughout the water column. In DS, more *pmoA* gene copies were measured in the transition zone ($p < 0.05$, Fig. 2) than in RS. Concerning archaeal methanogens and methanotrophs, *mcrA* gene copies were only detected in the anoxic zone with abundance ranging between 8.00×10^2 and 3.53×10^3 gene copies mL⁻¹ in RS (Fig. 2), whereas lower values were recovered in DS (4.15×10^2 to 2.21×10^3 gene copies mL⁻¹). The difference between sampling dates was not statistically significant.

The numbers of archaeal *amoA* gene copies were used to investigate the vertical distribution and abundance of AOA in relation to the NO_x profile available for both sampling campaigns. The quantitative distribution varied with depth, and

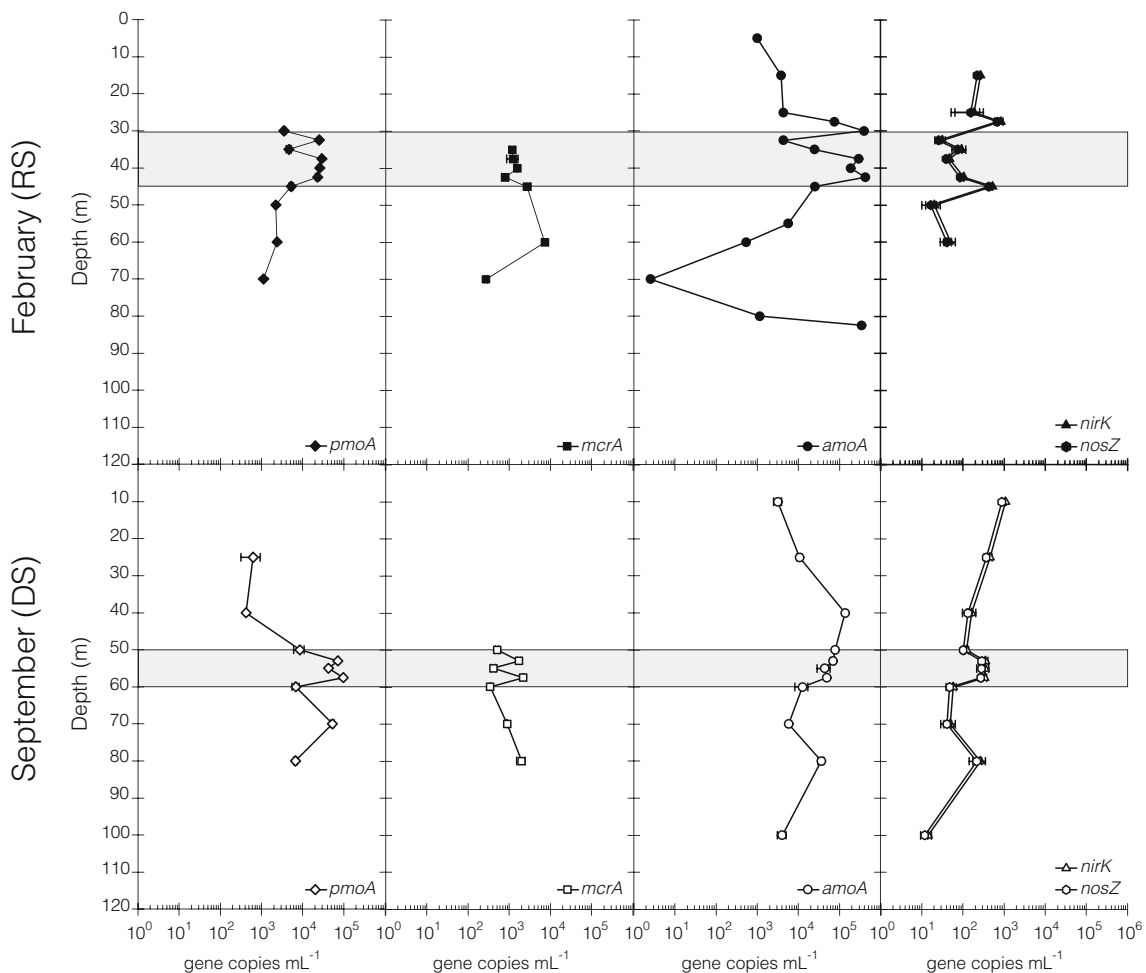


Fig. 2 Depth profiles of gene copy numbers for *pmoA*, *mcrA*, *amoA*, and *nirK/nosZ* genes determined by quantitative PCR for two sampling campaigns (February (RS) and September (DS)). Error bars represent

the standard deviation from triplicates. The transition zones were indicated with a gray bar

the highest copy numbers were mainly observed in the oxic and transition zones (from 30.0 to 42.5 m in RS and from 40.0 to 57.5 m in DS). The maximum values were 4.2×10^5 and 2.5×10^4 gene copies mL^{-1} in RS and DS, respectively (Fig. 2). Furthermore, functional genes involved in bacterial denitrification (i.e., *nirK* and *nosZ* genes) showed similar depth patterns during both seasons with rather low values (never exceeding 1×10^3 gene copies mL^{-1} ; Fig. 2). Oxic waters had significantly higher densities of *nirK* than in transition zone ($p < 0.05$) and higher densities of *nosZ* than anoxic water in September ($p < 0.05$). During the RS, no clear pattern with depth was observed, but higher values were observed at 27.5 and 45 m, whereas during the DS, maximum values were observed at 10 m and decreased regularly with depth, with a slight increase at the oxic–anoxic transition zone.

Pyrosequencing Overview and Community β -Diversity

After removing the noise and poor-quality reads with Mothur, about 34,097 bacterial DNA reads and 27,095 bacterial RNA reads were used for subsequent analyses. Rarefaction analysis indicated that most of the bacterial libraries may require deeper sequencing to avoid underestimation of microbial diversity in the samples (Table S1). Samples were randomly subsampled to the smallest sampling size using Mothur in order to reduce bias in species richness due to the differences in the number of sequences. The number of bacterial OTUs increased with depth for both DNA and RNA-based bacterial communities (Table S1). Richness estimates of the RNA-based bacterial community in the deepest anoxic waters were slightly higher than the DNA-based community in RS, whereas richness estimates of the DNA-based bacterial community in anoxic waters were higher than the estimates of the potentially active bacterial community in DS. The number of observed bacterial species per depth ranged from 127 to 240 in RS and 237 to 603 in DS for bulk and active bacterial communities, respectively (Table S1). The Chao1 estimator predicted richness values in the range of 324–988 in RS and 492–2234 in DS. Moreover, rank-abundance curves of DNA- and RNA-based bacterial communities showed a power-law distribution, which had a few abundant OTUs and a long tail of low-abundant species (Fig. S1). Venn diagrams also suggested that highly abundant taxa were common in a high percentage between DNA- and RNA-based communities. In contrast, a high proportion of rare species was determined to be specific to either DNA- and RNA-based community (Fig. 3).

In turn, 16,700 archaeal DNA reads and 2573 archaeal RNA reads were recovered for subsequent analyses. No high-quality sequences were retrieved from 15, 25, 35, and 50 m RNA samples in RS and from 10, 25, 40, 50, and 53 m DNA and RNA samples in DS. Rarefaction analysis based on OTUs indicated that most of the archaeal libraries reached the plateau level with the exception of the 40 m RNA sample in RS and the 80 m RNA sample in DS. In general

terms, richness was higher in the anoxic zone than in the oxic zone during both sampling times. During both seasons, archaeal richness estimates (i.e., Chao1 estimator) predicted lower richness values in the oxic and oxic–anoxic transition zone than in the anoxic waters (Table S2). No clear richness differences were observed between DNA- and RNA-based archaeal communities in oxic and oxic–anoxic transition zones, whereas richness estimates were higher for DNA samples than RNA samples in the anoxic zone (Table S1).

Bacterial Community Composition Analysis Between 7 and 42 % of the bacterial sequences analyzed were unclassified, with an increasing proportion toward the anoxic zone. Altogether, 34 distinct bacterial phyla were recovered from DNA samples and 29 phyla from RNA samples in RS, while 43 phyla were recovered from DNA samples and 29 phyla from RNA samples in DS. *Actinobacteria*, *Proteobacteria* (*Alphaproteobacteria*, *Betaproteobacteria*, *Epsilonproteobacteria*, and *Gammaproteobacteria*), *Cyanobacteria*, *Planctomycetes*, *Bacteroidetes*, *Chlorobi*, *Chloroflexi*, and *Nitrospirae* were detected both in the DNA- and RNA-based bacterial communities (Fig. 4, S2A–I). In DNA- and RNA-based communities, candidate bacterial phyla such as *GN02*, *OP3*, *OP8*, *NC10*, *NKB19*, *TM6*, and *WS1* were mostly detected in the anoxic zone but never exceeding relative abundance of 1 %. The comparison of the DNA- and RNA-based bacterial communities revealed similar relative abundance of the numerically dominant taxa with the exception of a lower relative abundance of *Actinobacteria* (Fig. 4, S2B) and a higher abundance of *Planctomycetes* (Fig. 4, S2C) and *Bacteroidetes* (Fig. 4) in the potentially active bacterial community composition (BCC) with respect to DNA-based bacterial community in the oxic zone. The BCC is further described in the co-occurrence patterns of the bacterial taxa section.

Bray–Curtis similarity trees were constructed based on total OTU composition of the 47 bacterial RNA and DNA samples to determine the associations among the communities. Clustering and ANOSIM analyses revealed the stratification (three zones based on DO concentrations) as the most important factor in structuring both DNA- and RNA-based BCC (Fig. 5). Although the clustering showed the grouping of the samples by DO zones, no similarity higher than 60 % was observed between samples. When the DNA- and RNA-based bacterial communities were compared based on Bray–Curtis distances against depth, significant negative correlations were observed (Fig. 6), with higher slopes (m) and linear correlation coefficients (R) for DNA- than RNA-based BCC ($m = -6.48$, $R = 0.77$ for the bulk community and $m = -3.58$, $R = 0.47$ for the potentially active community), suggesting more rapid changes in the DNA-based BCC with depth than in the RNA-based community. Moreover, the BCC differed significantly and systematically depending on whether DNA

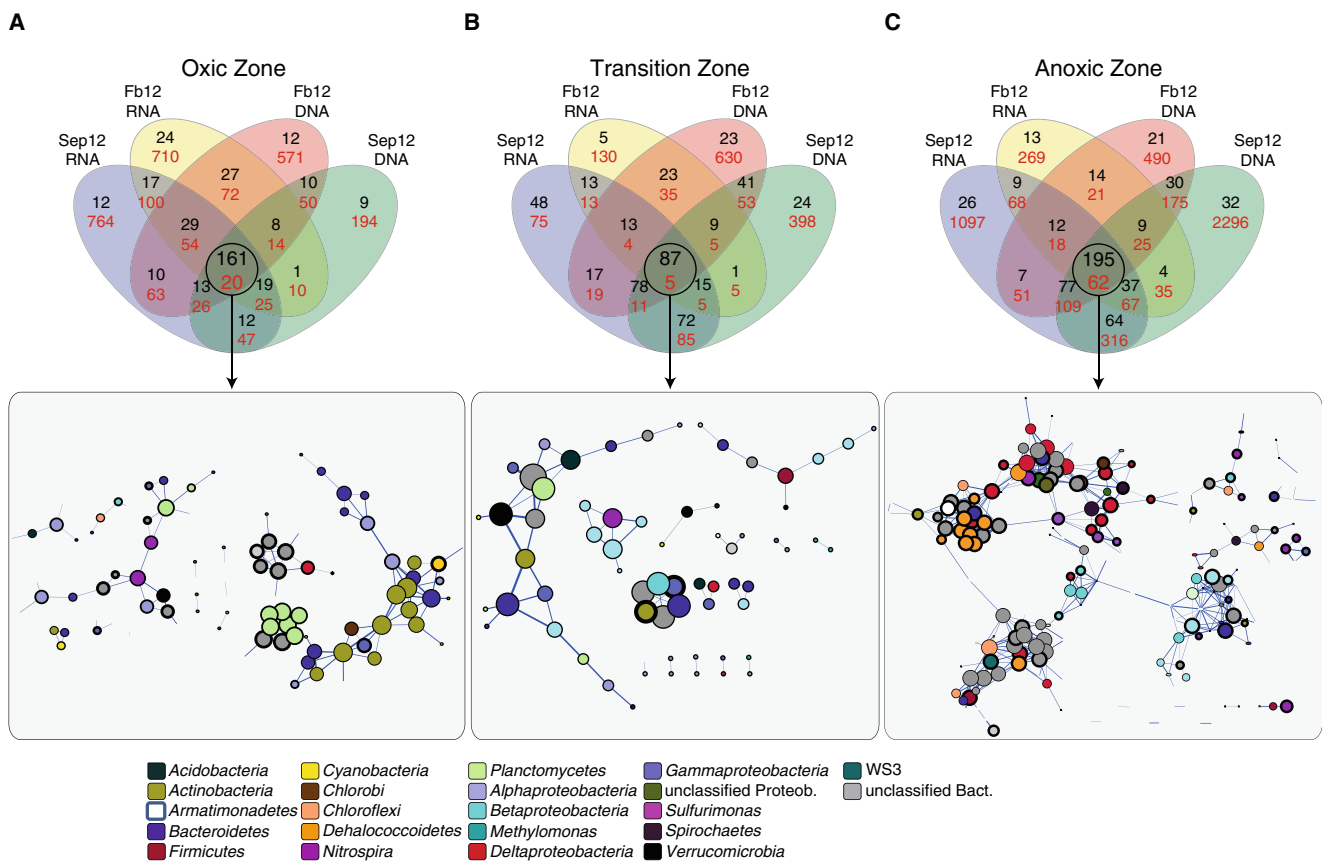


Fig. 3 Venn diagrams showing the distribution of OTUs between active and bulk communities in two campaigns in **a** oxic, **b** transition, and **c** anoxic zones. Abundant OTUs were defined as taxa represented by >15 sequences (*black*), whereas rare OTUs were defined as taxa represented by <15 sequences (*red*). Network of co-occurring shared OTUs based on

correlation analyses are shown in the *panels* below the diagrams. A connection stands for a strong (Pearson $r > 0.8$) and significant (p value 0.01) correlation. The size of each node is proportionate to the number of connections (i.e., degree)

or RNA was analyzed (Fig. 4). Based on clustering at the OTU level and ANOSIM analysis of the bulk community, a significant temporal effect (DS vs. RS) was also observed (Table 2).

Archaeal Community Composition Analysis At an 80 % confidence threshold, all of the reads could be assigned to the Archaea using the SILVA database classifier. Most of all, the nonchimeric and good-quality archaeal amplicons retrieved were affiliated with archaeal phyla, and only two samples from the deepest depths had 7 % unclassified Archaea. All archaeal amplicons retrieved spanned over archaeal lineages covering *Thaumarchaeota*, *Crenarchaeota*, and *Euryarchaeota* within both cultured (e.g., marine *Crenarchaeota* group, *Methanosaeta*, or *Candidatus Methanoregula*) and uncultured (e.g., *Miscellaneous Crenarchaeotic Group* (MCG) and GOM-Arc-I) groups.

At both sampling times, one OTU dominated the DNA- and RNA-based communities of the oxic zone, which belonged to the marine group I, tentative ammonia-oxidizing archaea (AOA). AOA were also dominant in the bulk communities in the transition zone, whereas the potentially active archaeal community composition (ACC) was mainly

composed of AOA, *Methanomicrobia*, and *Methanobacteria* in the transition zone (Fig. S2J). The DNA- and RNA-based communities thriving in the anoxic zone were dominated by the two methanogens mentioned above and by members of the MCG group.

A Bray–Curtis similarity tree was constructed based on total OTU composition of the 40 archaeal RNA and DNA samples to determine the associations among the communities. Clustering and ANOSIM analyses revealed sampling date as the main grouping factor in structuring the ACC (Fig. S3, Table 2) and nucleic acid type as the second grouping factor. Oxygen had the lowest global structuring effect on ACC, butoxic, and transition water samples clearly segregated from anoxic samples (Fig. S3).

Bacterial Abundance Classification and Overlap Estimates Bulk and potentially active bacterial taxa from oxic, transition, and anoxic zones were grouped per season (Fig. 3). Venn diagrams of OTUs were constructed to illustrate the number of shared OTUs for the two sampling campaigns based on DNA and RNA. The DNA and RNA samples over the two seasons shared less than 1 % of OTUs in the rare

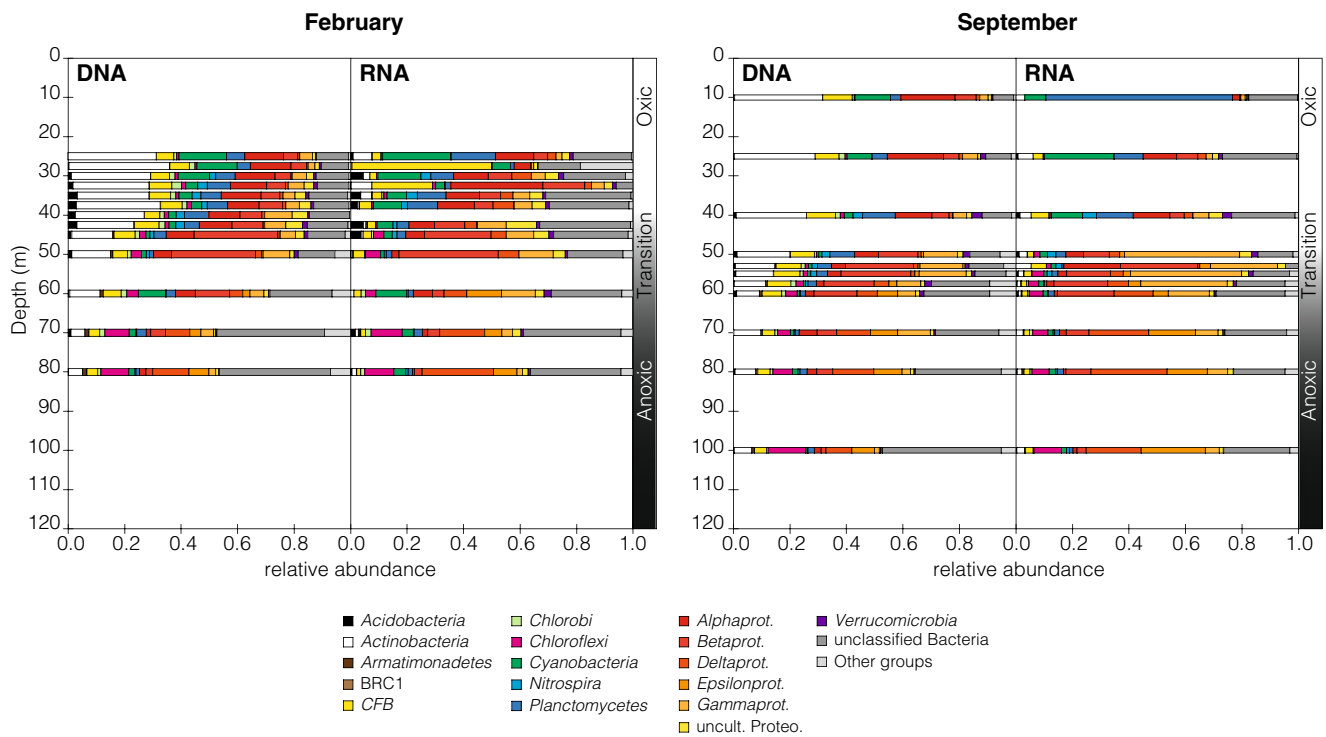


Fig. 4 Taxonomic classification of DNA and RNA bacterial reads at the phylum level in Lake Kivu for the two sampling campaigns (February (left) and September (right)). *CFB Bacteroidetes*

community. Forty-six, 19, and 35 % of the abundant OTUs were shared in the oxidic, transition, and anoxic zone, respectively. Rare species were also found to be specific to the sampling season and nucleic acid-type pool for both subsampled and not-subsampled data (i.e., DNA or RNA).

Co-occurrence Patterns of Bacteria Co-occurrence patterns of the microbes present in Lake Kivu were only analyzed with the bacterial data set due to the lack of archaeal information at some depths. The co-occurrence patterns for the potentially active core microbiome detected by Venn diagrams were

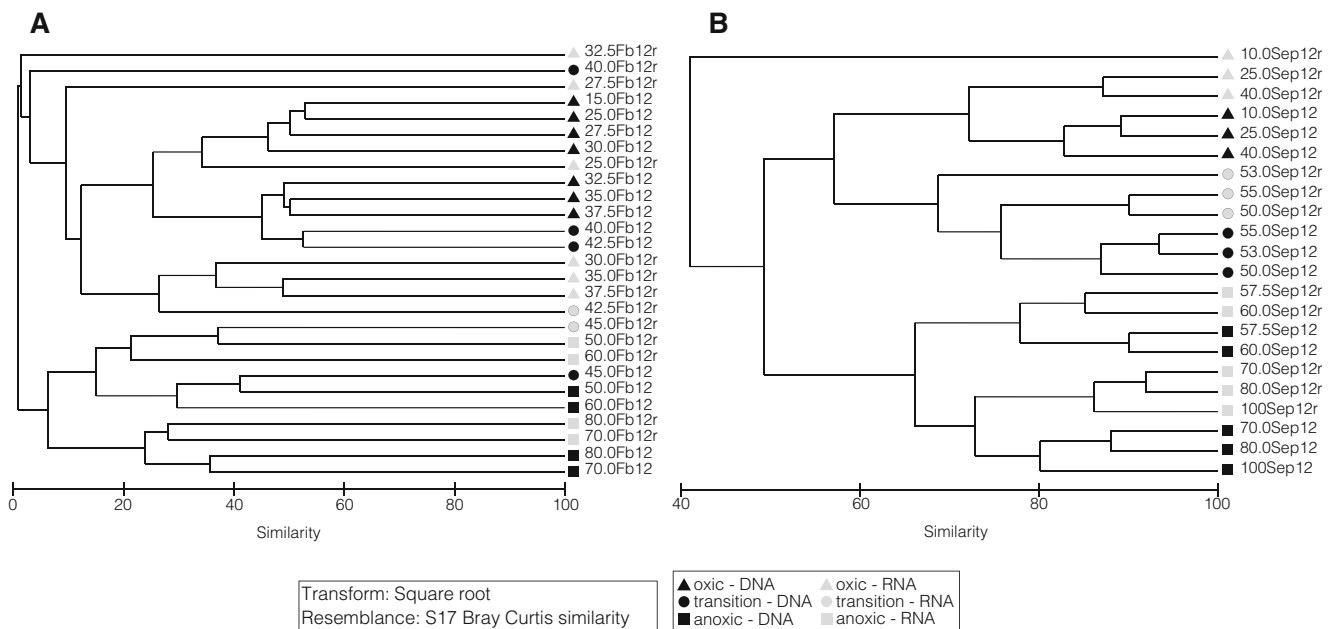


Fig. 5 Hierarchical clustering of Bray–Curtis similarities of the bacterial community composition at OTU level retrieved by pyrosequencing of both DNA (black symbols) and RNA (gray symbols) nucleic acid pools in **a** February and **b** September. Samples were grouped according to oxygen content as oxidic (triangles), transition (dots), and anoxic (squares)

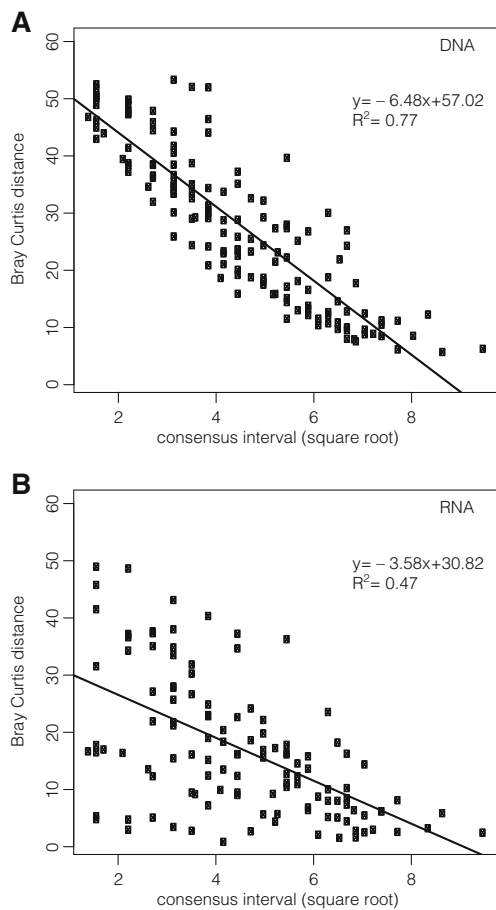


Fig. 6 Quantification of bulk and active bacterial dynamics. Patterns of change (regression of square root of depth lag (consensus interval) on Bray–Curtis distance) of **a** DNA-based and **b** RNA-based bacterial communities. The best-fit line and its equation are also shown

Table 2 ANOSIM test on bacterial and archaeal community composition at the OTU level between the three analyzed water compartments

Test for differences between DNA/RNA across all water compartments				
	Bacteria		Archaea	
	<i>R</i>	<i>p</i>	<i>R</i>	<i>p</i>
Global test	0.53	0.002	0.493	0.001
Test for differences between water compartments across all DNA/RNA				
	Bacteria		Archaea	
	<i>R</i>	<i>p</i>	<i>R</i>	<i>p</i>
Global test	0.537	0.001	0.355	0.001
Pairwise test				
Oxic–transition	0.370	0.03	0.016	0.34
Oxic–anoxic	0.735	0.001	0.553	0.001
Transition–anoxic	0.454	0.03	0.474	0.001
Test for differences between sampling dates across all DNA/RNA				
	Bacteria		Archaea	
	<i>R</i>	<i>p</i>	<i>R</i>	<i>p</i>
Global test	0.145	0.009	0.503	0.001

Significant values were indicated in bold

further assessed using network inference based on strong and significant Pearson correlations ($r > 0.8$, $p < 0.01$). The most complex interaction was found between potentially active bacteria in the anoxic zone. The microbial network for both the oxic and transition zones was composed of 66 nodes (OTUs) with moderate interconnection (2.3 edges per node on average), whereas in the network of the anoxic zone, there were *ca.* three times more nodes with a higher degree of connection (5.6 edges per node on average; Fig. 3). Aside from many unclassified bacteria, interactions between different known taxa were observed. For instance, in the oxic zone, there was a fairly complex subnetwork including *Actinobacteria*, *Bacteroidetes*, *Alphaproteobacteria*, *Betaproteobacteria*, *Gammaproteobacteria*, *Cyanobacteria*, and *OPB56*. In the transition zone, a subnetwork was observed between OTUs affiliated with N-fixing methane-oxidizing *Methylocaldum*, hydrogen-oxidizing *Hydrogenophaga*, and nitrifying bacteria *Nitrospira* with members of the unclassified proteobacterial class (Fig. 3a). In the anoxic zone, a co-occurrence pattern was observed between sulfate reducers (*Desulfobacca*, *Desulfocapsa*, and *Desulfobacterium*), sulfur oxidizers (*Sulfurimonas*), and hydrogen oxidizers (*Dehalococcoidetes*).

Co-occurrence Patterns of Potentially Active Bacteria and Archaea in the Anoxic Zone

Diverse and complex interactions between potentially active bacteria were found in the anoxic zone; therefore, their correlations with archaea were further investigated. The co-occurrence patterns of the potentially active microbiome with a relative abundance higher than 0.5 % were defined using network inference based on strong and significant Pearson correlations ($r > 0.8$, $p < 0.001$). The microbial network in the anoxic zone consisted of 31 moderately interconnected nodes (2.9 edges per node on average; Fig. S4). A clear interaction between bacterial sulfate reducers, sulfur oxidizers, nitrogen-fixing methanotrophs, archaeal methanogens, and anaerobic methane oxidizers was observed. In addition, another interaction between members of *Methanomicrobia*, *Chlorobicaea*, and *Syntrophaceae* was also observed.

Niche Breadth Comparison

Levins’ niche breadth was calculated as a proxy to understand how particular taxa relate to their environment. The bulk bacterial community had a strong linear relationship between niche breadth and their relative abundance, while generalist and specialist OTUs in the potentially active bacterial community were more equally distributed within rare and abundant taxa. In addition, niche breadth in the DNA-based bacterial community was higher than in the RNA-based community. Potentially active bacterial OTUs able to develop in either the oxic or anoxic zone were mainly assigned at different taxonomic levels to *Burkholderiales*, *Pseudanabaenaceae*, *Acidobacteria*, and *Methylocaldum*. In

contrast, no significant relationship was observed between niche breadth and DNA- and/or RNA-based archaeal relative abundance. Archaeal OTUs detected in both the oxic and anoxic zones were assigned to MGI and Miscellaneous Crenarchaeotic Group. The niche breadth observed for the RNA-based bacterial and archaeal community was narrower than for the DNA-based bacterial and archaeal community (Fig. S5).

Linking Bacterial Communities to Environmental Parameters Variance partitioning analysis (VPA) was performed to quantify the relative contribution of season, depth, and environmental parameters to the taxonomic structure of the bacterial and archaeal communities. The analysis of environmental variables was restricted to a subset of all variables acquired during the field cruises including: DO, pH, NO_x, POC, CH₄, and Chl-*a*. Clear differences were observed in variance partitioning patterns, if all bacterial OTUs or both abundance categories (abundant/rare) were considered. In all cases, the impact of the environmental parameters was found to be the highest, followed by either season or depth (Fig. 7). The parameters analyzed (depth, season, and environmental variables) in total explained 50 % of the variation observed for the bulk bacterial community, and they explained only 30 % of the variation observed for the potentially active bacterial community. Furthermore, the total relative contributions of variables increased when VPA was performed for only abundant bacterial species, whereas it clearly decreased for rare

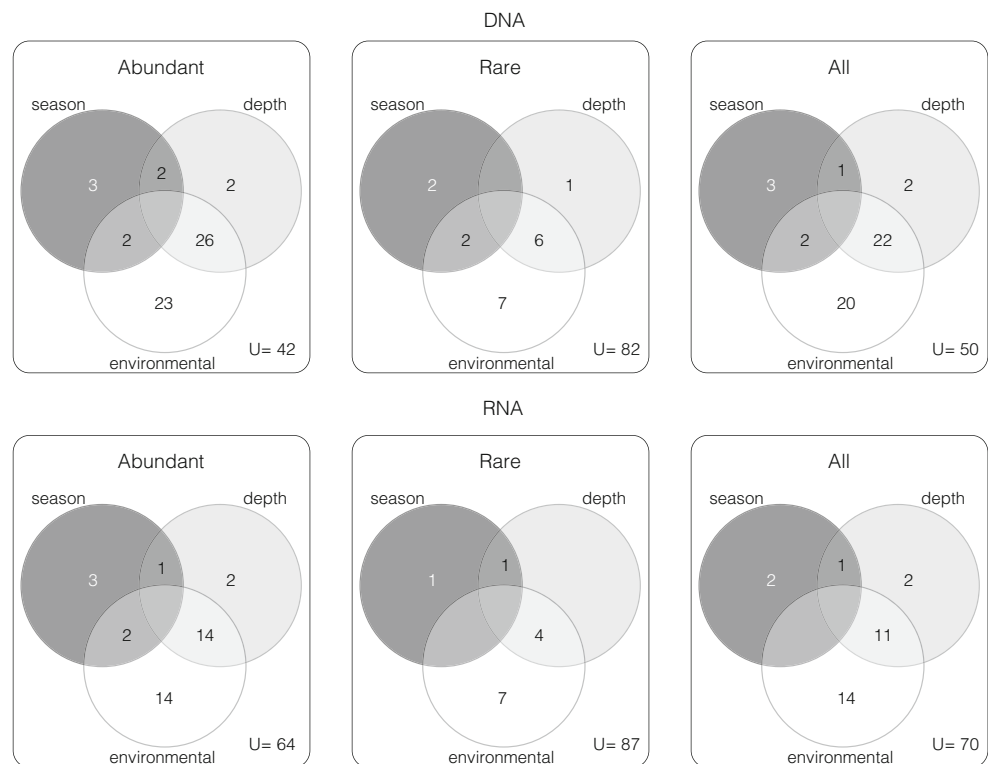
species. The sum of the parameters analyzed (depth, season, environmental variables) explained 73 % of the variation observed for the bulk archaeal community and only 18 % for the potentially active archaeal community (data not shown).

Discussion

In the present study, DNA- and RNA-based amplicon pyrosequencing was performed to further investigate the temporal and vertical effects on the bulk and potentially active microbial biosphere of Lake Kivu and to gain a more complete view of the microbial dynamics in Lake Kivu than the one afforded by analyzing either nucleic acid pool alone.

Community Composition at a High Taxonomic Level Due to the strong vertical chemical gradients and zonation of redox reactions with depth, a clear vertical stratification of microbial communities is usually observed for meromictic lakes [48–51]. In spite of the different extraction protocols used, the relative abundances of potentially active and bulk bacterial and archaeal communities were mostly similar at the phylum level, with some notable exceptions. These differences were mostly observed in the oxic zone. For instance, *Actinobacteria* were highly dominant in the bulk bacterial community of surface waters (around 30 %); however, this dominance was lower in the potentially active community, as previously shown in a eutrophic lake [52]. *Actinobacteria* might experience lower

Fig. 7 Variation partitioning of bacterial community composition. The figure depicts the fractions (%) of variation in bacterial community composition that are explained by environmental parameters (pH+DO+NO_x+POC+CH₄+Chl), depth, and season or that remain unexplained for bulk and active bacterial communities. *U* unexplained



mortality rates than other bacterial lineages due to the resistance to protozoan grazing [53] and small cell size [54]. Therefore, *Actinobacteria* might not require rapid growth to maintain high cell densities in the water column [55]. This might be also due to the difference in lysis methods used for DNA and RNA extraction. *Bacteroidetes* (CFB) and *Planctomycetes* were substantial components of potentially active BCC in the oxic waters of Lake Kivu in the rainy and dry season, respectively (Fig. 4). Many studies have reported high relative abundance of *Bacteroidetes* or *Planctomycetes* following algal blooms [56–60]. Both phyla are known to be present and attached to aggregates, and they have various extracellular enzymes that can degrade complex organic molecules and give a competitive advantage with regards to other microbial groups [61–63]. Presence of a high percentage of these two phyla in different seasons might be due to the competition between these two phyla for organic matter or dominance of different phytoplankton species in two seasons, as mainly a higher dominance of diatoms was observed in the DS and *Cyanobacteria* were more dominant in the RS (Fig. 4; [23]). Besides, *Cyanobacteria* represent a big fraction of the active microbial community in oxic and illuminated waters (Fig. 4 and Fig. S2) due to their oxic photoautotrophic metabolism. A recent study done in Lake Kivu suggested that a variety of ecological niches of heterotrophic bacteria can be supported by the diversity of molecules excreted by the phytoplankton community [64]. Detection of a low abundance of potentially active *Planctomycetes*-affiliated sequences in the anoxic zone supported the idea that members of this group have anaerobic metabolic abilities, as suggested by previous studies showing that they rely on carbohydrate fermentation and sulfur reduction for growth and survival under anaerobic conditions [65]. Furthermore, sequences affiliated to *Chlorobi* phylum were recovered from both nucleic acid pools of either oxic or anoxic waters and sampling campaigns. Their recovery from oxic waters is an interesting feature and deserves further investigations, but recent evidences pointed toward new *Chlorobi* representatives able to develop under aerobic conditions performing photoheterotrophic metabolisms [66, 67].

Furthermore, higher abundance of AOA was shown in the bulk community in comparison to the potentially active community. Such discrepancy between DNA- and RNA-based studies of surface waters has also been observed in freshwater ecosystems [4, 68]. The denitrification genes *nirK* and *nosZ* were slightly higher in the oxic zone than in the anoxic zone (Fig. 2). Previously, growth of facultative anaerobic denitrifiers in aerobic environments was demonstrated, which suggests a wider distribution of potential denitrifiers in the aerobic growth conditions of this lake [69, 70]. The good correlation found between *nirK* and *nosZ* genes might be due to the fact that these genes are usually located in the same operon [71, 72].

Detection of highly abundant potentially active *Nitrospira* in the transition zone confirmed a previous study of the nitrite-

oxidizing community in the transition zone of Lake Kivu (Figs. 4 and S2D; [20]). The CH₄ oxidation peak in the transition zone was also strongly correlated with the relative abundance of active methanotrophs and abundance of *pmoA* gene ($p < 0.05$; data not shown). Detection of potentially active *Methylococcales* and *Methyloversatilis* indicates aerobic CH₄ oxidation as the main process preventing CH₄ from escaping to the atmosphere (Fig. S2E). The co-occurrence of CH₄ oxidizing *Methylocaldum* and hydrogen-oxidizing *Hydrogenophaga* supports recent findings of CH₄ consumption in O₂-limiting conditions by *Methylocaldum*, leading to the release of several organic molecules (e.g., acetate, lactate, succinate, and hydrogen) that can be used by *Hydrogenophaga* [73].

Several archaeal groups able to produce CH₄ have also been detected in both DNA and RNA-based communities mainly in the anoxic waters. Indeed, their presence even in the transition zone is consistent with recent studies that showed the presence of potentially active methanogens in the oxygenated water column of an oligotrophic lake attached to photoautotrophic microbes that might be enabling aerobic growth and supply of methanogenic substrates [74, 75]. However, the presence of acetoclastic methanogens (*Methanosarcinales*) in the oxic–anoxic transition zone might also indicate the presence of syntrophy between methanogenic and fermentative microbes, through the occurrence of a coupled mutualistic interaction between hydrogen-/formate-producing and hydrogen-/formate-using microorganisms [76]. A consistent relationship between uncultured OTUs of *Methanomicrobia*, *Chlorobicaeae*, and *Syntrophaceae* was also observed in the anoxic zone (Fig. S3), which could indicate the presence of syntrophic relationships between these microbes in hydrocarbon or complex high molecular weight compound degradation, as previously shown in the sediments of the River Tyne [77].

Network analysis revealed a complex interaction between active *Dehalococcoidetes*, sulfate-reducing bacteria (SRB; *Desulfocapsa*, *Desulfobacca*), and sulfur-oxidizing bacteria (SOB; *Sulfurimonas*, *Sulfuricurvum*) in the anoxic zone (Fig. 3c). The co-occurrence of active SOB and SRB in the anoxic zone may further suggest the presence of an active yet cryptic sulfur cycle [20]. It has been evidenced that *Dehalococcoidetes* may have a nutritional dependence on other organisms [78, 79]; the co-occurrence of this active but rare bacterial class with SRB might thus be linked to its role in hydrocarbon degradation (Fig. 3c). Recent investigations have described complex interactions between *Dehalococcoides*, SRB, and methanogens depending on their metabolic activities and nutrient (e.g., hydrogen, acetate) or vitamin (e.g., B12) concentrations [80], suggesting their multiple metabolic capabilities.

Bulk Versus Potentially Active Community Structure

Although the samples analyzed had mostly similar taxonomic characterization at the phylum level, clustering analysis at the OTU level highlighted the importance of which nucleic acid

pool (i.e., DNA or RNA) was analyzed. The presence of sequences exclusively found in one of the two nucleic acid pools suggests that using both nucleic acids provides a more complete overview of the microbial diversity present in a given environment since on average, only 20 % of the OTUs (18–22 %) were shared per DO zone and per season. As previously suggested [81], sequences found only in the DNA pool might be related to metabolically less active, yet abundant populations, whereas sequences detected only in RNA are associated with active members of the community but may be present in relatively low numbers. The type of populations associated with shared and unshared sequences could be the result of differences in their respective overall abundance and/or a reflection on the overall metabolic status of a population within a given OTU. The detection of taxa in only one pool and not in the other can also be due to insufficient pyrosequencing in the effort to reveal complete diversity, and this had obviously more effect on the rare community.

Inactive cells are seen as a potential seed bank, which enables a rapid community adaptation to changing environments, so that the overall community always prevails [82, 83]. DNA and RNA profiles were found to be more similar in the anoxic zone than in the oxic or transition zones. The results agree with the fact that anaerobic processes are less energetic than aerobic respiration, thus suggesting slow growth rates in the anoxic water compartment of Lake Kivu. Besides, the anoxic water compartment of Lake Kivu was also more diverse in types as pointed out by the richness estimations ($p < 0.02$). It was previously suggested that anoxic environments maintain a higher diversity of energetic pathways and that this complexity permits the retention of higher metabolic and thus ecological diversity [3, 84].

Abundant and Rare Taxa Both bulk and potentially active microbial communities present in the water column of Lake Kivu comprised few very abundant OTUs and a huge number of low-abundant and rare OTUs (data not shown). The fact of even recovering a long tail of rare low-abundant OTUs within the potentially active members of the microbial community evidenced the existence of an active rare biosphere in Lake Kivu or a pool of dormant microbes with enough RNA pool to recover from this situation when necessary [6]. Venn diagrams revealed that bulk and potentially active bacterial communities shared a high fraction of those highly abundant taxa. In contrast, rare OTUs were detected in a high proportion exclusively in either bulk or potentially active bacterial communities. As suggested for estuarine and coastal ocean waters, the metabolically active rare biosphere of Lake Kivu might be potentially important for the functioning and the temporal dynamics of microbial communities as they shift between seasons [13–15].

Levins' niche width was used to classify the taxa retrieved in Lake Kivu as generalists or specialists based on the

environmental conditions in which they developed but not directly on their intrinsic biological properties [85]. Most bacterial taxa identified as generalists were abundant, whereas those identified as specialists were more likely to be rare (mainly in the bulk community), and this pattern was less evident for the potentially active community. Such a significant relationship could not be observed for archaeal taxa, which might be due to missing depths in our analysis. The detection of some OTUs in either bulk or potentially active communities in both oxic and anoxic zones might reflect some metabolic flexibility and capacity to cope with the different redox conditions present in the lake's water column.

Moreover, variation partitioning analyses were performed to assess the contributions of depth, season, and environmental parameters to microbial community structure. The pool of environmental parameters analyzed here could explain the highest part of the variation in bacterial communities. The results of this study showed that DO had the most significant effect in shaping the BCC, as shown previously [86]. In addition to DO, bacterial community variance was also significantly related to pH in the lake. Any significant deviation in environmental pH should impose stress on single-cell organisms, since intracellular pH of most microorganisms is usually within 1 pH unit of neutral [87, 88]. The significant effect of pH on the BCC was also shown in a range of aquatic environments [88]. The overall number of environmental variations that could explain the presence of taxa was also higher for abundant taxa in comparison to rare taxa. This might indicate that abundant taxa are sufficient to describe the mechanisms underlying the beta-diversity [6]. However, it is possible that rare species were more affected by environmental parameters such as concentrations of micronutrients, hydrocarbons, as well as stochastic dispersal, immigration, and predation, which were not measured in this study and thus not taken into account in the statistical analysis [6]. Furthermore, a higher degree of the variation was explained for the bulk BCC than for the potentially active BCC. It might indicate that the seed bank likely represents the species pool of the complex water habitat and enables the shift in rapidly changing environments and also potentially stabilize ecosystem.

Conclusions

Combination of complementary methods (16S rRNA, rDNA pyrosequencing, and qPCR) provided insights into the active community and functional genes present in Lake Kivu, where biogeochemical cycling appeared to be functioning synergistically. Detection of key players in biogeochemical cycles in the various water layers were also supported by the vertical chemical gradients. The experimental evaluation suggests that the quantification of functional genes by qPCR was mostly in agreement with the pyrosequencing of complex microbial

communities. This study showed that rare taxa (mainly specialists), especially in the anoxic zone, cannot solely be characterized as a seed bank or dormant cells in Lake Kivu but that a significant portion of the rare community is potentially active, which supports the results of various studies conducted in freshwater and marine environments [13, 14]. However, the impact of environmental parameters measured was stronger for the generalists (mainly abundant taxa), which indicates the presence of different ecological rules for different groups.

Acknowledgments In addition to the authors of this paper, the Lake Kivu consortium includes the following individuals: S. Bouillon (Katholieke Universiteit Leuven), M.-V. Commarieu, F. A. E. Roland (Université de Liège), B. Leporcq, K. de Saedeleer (Université de Namur), A. Anzil, S. Vanderschueren, C. Michiels (Université Libre de Bruxelles), and G. Alunga (DR Congo team). The consortium gratefully acknowledges the Rwanda Energy Company and Michel Halbwachs for free access to their industrial platform off Gisenyi. R. Trias (Institut de Physique du Globe de Paris, France) is acknowledged for supplying some of the qPCR-positive controls. This work was funded by the Fonds National de la Recherche Scientifique (FNRS) under the MICKI (Microbial diversity and processes in Lake Kivu) project and the Belgian Federal Science Policy Office EAGLES (East African Great Lake Ecosystem Sensitivity to changes, SD/AR/02A) project, and contributes the European Research Council starting grant project AFRIVAL (African river basins: Catchment-scale carbon fluxes and transformations, 240002).

Conflict of Interest The authors declare no conflict of interest.

References

- Casamayor EO, Llíros M, Picazo A, Barberán CM, Borrego CM, Camacho A (2012) Contribution of deep dark fixation processes to overall CO₂ incorporation and large vertical changes of microbial populations in stratified karstic lakes. *Aquat Sci* 74(1):61–75
- Eiler A, Heinrich F, Bertilsson S (2012) Coherent dynamics and association networks among lake bacterioplankton taxa. *ISME J* 6:330–342
- Lehours AC, Bardot C, Thenot A, Debroad D, Fonty G (2005) Anaerobic microbial communities in Lake Pavin, a unique meromictic lake in France. *Appl Environ Microbiol* 71:7389–7400
- Logue JB, Lindström ES (2010) Species sorting affects bacterioplankton community composition as determined by 16S rDNA and 16S rRNA fingerprints. *ISME J* 4:729–738
- Van der Gucht K, Cottenie K, Muylaert K, Vloemans N, Cousin S, Declerck S et al (2007) The power of species sorting: local factors drive bacterial community composition over a wide range of spatial scales. *Proc Natl Acad Sci USA* 104:20404–20409
- Lennon JJ, Jones SE (2011) Microbial seed banks: the ecological and evolutionary implications of dormancy. *Nat Rev* 9:119–130
- Huber JA, Welch DBM, Morrison HG, Huse SM, Neal PR, Butterfield DA, Sogin ML (2007) Microbial population structures in the deep marine biosphere. *Science* 318:97–100
- Huber JA, Cantin HV, Huse SM, Mark Welch DB, Sogin ML, Butterfield DA (2010) Isolated communities of Epsilonproteobacteria in hydrothermal vent fluids of the Mariana Arc sea mounts. *FEMS Microbiol Ecol* 73:538–549
- Sogin ML, Morrison HG, Huber JA et al (2006) Microbial diversity in the deep sea and the underexplored ‘rare biosphere’. *Proc Natl Acad Sci USA* 103:12115–12120
- Pedrés-Alió C (2006) Marine microbial diversity: can it be determined? *Trends Microbiol* 14:257–263
- Polymenakou PN, Lampadariou N, Mandalakis M, Tselepidis A (2009) Phylogenetic diversity of sediment bacteria from the southern Cretan margin, Eastern Mediterranean Sea. *Syst Appl Microbiol* 32:17–26
- Lanzén A, Jørgensen SL, Bengtsson MM, Jonassen I, Øvreås L, Urich T (2011) Exploring the composition and diversity of microbial communities at the Jan Mayen hydrothermal vent field using RNA and DNA. *FEMS Microbiol Ecol* 77:577–589
- Campbell BJ, Yu L, Heidelberg JF, Kirchman DL (2011) Activity of abundant and rare bacteria in a coastal ocean. *Proc Natl Acad Sci USA* 108:12776–12781
- Campbell BJ, Kirchman DL (2013) Bacterial diversity, community structure and potential growth rates along an estuarine salinity gradient. *ISME J* 7:210–220
- Jones SE, Lennon JT (2010) Dormancy contributes to the maintenance of microbial diversity. *Proc Natl Acad Sci USA* 107:5881–5886
- Moeseneder MM, Arrieta JM, Herndl GJ (2005) A comparison of DNA- and RNA-based clone libraries from the same marine bacterioplankton community. *FEMS Microbiol Ecol* 51(3):341–52
- Schmid M, Halbwachs M, Wehrli B, Wüest A (2005) Weak mixing in Lake Kivu: new insights indicate increasing risk of uncontrolled gas eruption. *Geochem Geophys Geosyst* 6, Q07009
- Borges AV, Abril G, Delille B, Descy JP, Darchambeau F (2011) Diffusive methane emissions to the atmosphere from Lake Kivu (Eastern Africa). *J Geophys Res* 116, G03032
- Pasche N, Schmid M, Vasquez F, Schubert CJ, Wüest A, Kessler JD, Pack MA, Reeburgh WS, Bürgmann H (2011) Methane sources and sinks in Lake Kivu. *J Geophys Res* 116, G03006
- İnceoğlu Ö, Llíros M, Garcia-Armisen T, Crowe SA, Michiels C, Darchambeau F, Descy JP, Servais P Distribution of bacteria and archaea in meromictic tropical Lake Kivu (Africa). *Aquat Microb Ecol*. doi:10.3354/ame01737. In press.
- Llíros M, Gich F, Plasencia A, Auguet JC, Darchambeau F, Casamayor EO, Descy JP, Borrego C (2010) Vertical distribution of ammonia-oxidizing Crenarchaeota and methanogens in the epilimnetic waters of Lake Kivu (Rwanda-Democratic Republic of the Congo). *Appl Environ Microbiol* 76(20):6853–6863
- Darchambeau F, Sarmento H, Descy J-P (2014) Primary production in a tropical large lake: the role of phytoplankton composition. *Sci Total Environ* 473–474:178–188
- Sarmento H, Isumbisho M, Descy JP (2006) Phytoplankton ecology of Lake Kivu. *J Plankton Res* 28:815–829
- Isumbisho M, Sarmento H, Kaningini B, Micha JC, Descy JP (2006) Zooplankton of Lake Kivu, East Africa, half a century after the Tanganyika sardine introduction. *J Plankton Res* 28:971–989
- Schmid M, Wüest A (2012) In: Descy JP, Darchambeau F, Schmid M (eds) Stratification mixing and transport processes in Lake Kivu. Springer, Lake Kivu, pp 13–30
- Wright JJ, Konwar KM, Hallam SJ (2012) Microbial ecology of expanding oxygen minimum zones. *Nat Rev Microbiol* 10(6):381–394
- Standing Committee of Analysts (1981) Methods for the examination of waters and associated materials Ammonia in waters. HMSO, London
- Eaton E, Archie AE, Rice EW, Clesce LS (2012) Standard Methods for the Examination of Water Wastewater, APHA 22nd Edition
- Miranda KM, Espey MG, Wink DA (2001) A rapid, simple spectrophotometric method for simultaneous detection of nitrate and nitrite. *Nitric Oxide* 5(1):62–71
- Cline JD (1969) Spectrophotometric determination of hydrogen sulfide in natural waters. *Limnol Oceanogr* 14:454–458

31. Llíros M, Casamayor E, Borrego CM (2008) High archaeal richness in the water column of a freshwater sulfurous karstic lake along an inter-annual study. *FEMS Microbiol Ecol* 66:331–342
32. Frias-Lopez J, Shi Y, Tyson GW, Coleman ML, Schuster SC, Chisholm SW, DeLong EF (2008) Microbial community gene expression in ocean surface waters. *Proc Natl Acad Sci USA* 105: 3805–10
33. Costello AM, Lidstrom ME (1999) Molecular characterization of functional and phylogenetic genes from natural populations of methanotrophs in lake sediments. *Appl Environ Microbiol* 65(11): 5066–5073
34. Luton PE, Wayne JM, Sharp RJ, Riley PW (2002) The *mcrA* gene as an alternative to 16S rRNA in the phylogenetic analysis of methanogen populations in landfill. *Microbiology* 148:3521–3530
35. Henry S, Bru D, Stres B, Hallet S, Philippot L (2006) Quantitative detection of the *nosZ* gene, encoding nitrous oxide reductase, and comparison of the abundances of 16S rRNA, *narG*, *nirK*, and 1 genes in soils. *Appl Environ Microbiol* 72(8):5181–5189
36. Development Core Team R (2011) R: A language and environment for statistical computing R Foundation for Statistical Computing. Austria, Vienna, Available at: <http://www.R-project.org>
37. Callaway TR, Dowd SE, Wolcott RD, Sun Y, McReynolds JL et al (2009) Evaluation of the bacterial diversity in cecal contents of laying hens fed various molting diets by using bacterial tag encoded FLX amplicon pyrosequencing. *Poult Sci* 88:298–302
38. Dowd SE, Wolcott RD, Sun Y, McKeenan T, Smith E, Rhoads D (2008) Polymicrobial nature of chronic diabetic foot ulcer biofilm infections determined using bacterial tag encoded FLX amplicon pyrosequencing (bTEFAP). *PLoS One* 3, e3326
39. Edgar RC, Haas BJ, Clemente JC, Quince C, Knight R (2011) UCHIME improves sensitivity and speed of chimera detection. *Bioinformatics (Oxford, England)* 27(16):2194–2200
40. Schloss PD, Westcott SL, Ryabin T, Hall JR, Hartmann M et al (2009) Introducing Mothur: open-source, platform-independent, community-supported software for describing and comparing microbial communities. *Appl Environ Microbiol* 75:7537–7541
41. Clarke KR, Gorley RN (2006) PRIMER V6: usermanual/Tutorial Plymouth. PRIMER-E, UK
42. Levins R (1968) Evolution in changing environments. Princeton University Press, Princeton
43. Logares R, Lindström ES, Langenheder S, Logue JB, Paterson H, Laybourn-Parry J, Rengefors K, Tranvik L, Bertilsson S (2013) Biogeography of bacterial communities exposed to progressive long-term environmental change. *ISME J* 7(5):937–48
44. Faust K, Sathirapongsasuti JF, Izard J, Segata N, Gevers G, Raes J, Huttenhower C (2012) Microbial co-occurrence relationships in the human microbiome. *PLoS Comput Biol* 8(7), e1002606
45. Shannon P, Markiel A, Ozier O, Baliga NS, Wang JT, Ramage D, Amin N, Schwikowski B, Ideker T, Wamecke F, Sommaruga R, Sekar R, Hofer JS, Pernthaler J (2003) Cytoscape: a software environment for integrated models of biomolecular interaction networks. *Genome Res* 13:2498–2503
46. Peres-Neto PR, Legendre P, Dray S, Borcard D (2006) Variation partitioning of species data matrices: estimation comparison of fractions. *Ecology* 87:2614–2625
47. Oksanen J, Blanchet FG, Kindt R, Legendre P, Minchin PR, O'Hara RB, Simpson GL (2012) vegan: Community Ecology Package R package version 20-5 <http://CRAN.R-project.org/package=vegan>
48. Dimitriu PA, Pinkart HC, Peyton BM, Mormile MR (2008) Spatial and temporal patterns in the microbial diversity of a meromictic soda lake in Washington State. *Appl Environ Microbiol* 74:4877–4888
49. Koizumi Y, Kojima H, Oguri K, Kitazato H, Fukui M (2004) Vertical and temporal shifts in microbial communities in the water column and sediment of saline meromictic Lake Kaiike (Japan), as determined by a 16S rDNA-based analysis, and related to physico-chemical gradients. *Environ Microbiol* 6:622–637
50. Lentini V, Gugliandolo C, Maugeri TL (2012) Vertical distribution of Archaea and Bacteria in a meromictic lake as determined by fluorescent in situ hybridization. *Curr Microbiol* 64:66–74
51. Newton RJ, Jones SE, Eiler A, McMahon KD, Bertilsson S (2011) A guide to the natural history of freshwater lake bacteria. *Microbiol Mol Biol Rev* 75(1):14–49
52. Kolmonen E, Sivonen K, Rapala J, Haukka K (2004) Diversity of Cyanobacteria and heterotrophic bacteria in cyanobacterial blooms in Lake Joutikas, Finland. *Aquat Microb Ecol* 36:201–211
53. Hahn MW, Lünsdorf H, Wu Q, Schauer M, Höfle MG, Boenigk J, Stadler P (2003) Isolation of novel ultramicrobacteria classified as Actinobacteria from five freshwater habitats in Europe and Asia. *Appl Environ Microbiol* 69:1442–1451
54. Kemp PF, Lee S, LaRoche J (1993) Estimating the growth rate of slowly growing marine bacteria from RNA content. *Appl Environ Microbiol* 59:2594–2601
55. Pernthaler J, Posch T, Simek K, Vrba J, Pernthaler A, Glöckner FO, Nübel U, Psenner R, Amann R (2001) Predator-specific enrichment of actinobacteria from a cosmopolitan freshwater clade in mixed continuous culture. *Appl Environ Microbiol* 67:2145–2155
56. Brümmer IHM, Felske ADM, Wagner-Döbler I (2004) Diversity and seasonal changes of uncultured Planctomycetales in river biofilms. *Appl Environ Microbiol* 70:5094–5101
57. Mary I, Cummings DG, Biegala IC, Burkill PH, Archer SD, Zubkov MV (2006) Seasonal dynamics of bacterioplankton community structure at a coastal station in the western English Channel. *Aquat Microb Ecol* 41:119–126
58. Pinhassi J, Sala MM, Havskum H, Peters F, Guadayol O, Malits A, Marrasé C (2004) Changes in bacterioplankton composition under different phyto-plankton regimens. *Appl Environ Microbiol* 70: 6753
59. Pizzetti I, Fuchs BM, Gerdt G, Wichels A, Wiltshire KH, Amann R (2011) Temporal variability of coastal Planctomycetes clades at Kabeltonne station, North Sea. *Appl Environ Microbiol* 77:5009–5017
60. Tadonlélé RD (2007) Strong coupling between natural Planctomycetes and changes in the quality of dissolved organic matter in freshwater samples. *FEMS Microbiol Ecol* 59:543–555
61. Bauer M, Kube M, Teeling H, Richter M, Lombardot T, Allers E, Würdemann CA, Quast C, Kuhl H, Knaust F, Wobken D, Bischof K, Mussmann M, Choudhuri JV, Meyer F, Reinhardt R, Amann RI, Glöckner FO (2006) Whole genome analysis of the marine Bacteroidetes 'Gramellaforsetii' reveals adaptations to degradation of polymeric organic matter. *Environ Microbiol* 8:2201–2213
62. DeLong EF, Franks DG, Alldredge AL (1993) Phylogenetic diversity of aggregate-attached vs. free-living marine bacterial assemblages. *Limnol Oceanogr* 38:924–934
63. Grossart HP, Levold F, Allgaier M, Simon M, Brinkhoff T (2005) Marine diatom species harbour distinct bacterial communities. *Environ Microbiol* 7:860–873
64. Morana C, Sarmento H, Descy JP, Gasol JM, Borges AV, Bouillon S, Darchambeau F (2014) Production of dissolved organic matter by phytoplankton and its uptake by heterotrophic prokaryotes in large tropical lakes. *Limnol Oceanogr* 59(4):1364–1375
65. Elshahed MS, Youssef NH, Luo Q, Najjar FZ, Roe BA, Sisk TM, Bühring SI, Hinrichs KU, Krumholz LR (2007) Phylogenetic and metabolic diversity of Planctomycetes from anaerobic, sulfide- and sulfur-rich Zedletone Spring, Oklahoma. *Appl Environ Microbiol* 73(15):4707–16
66. Bryant DA, Liu Z, Li T, Zhao F, Garcia Costas AM, Klatt CG (2012) Comparative and functional genomics of anoxygenic green bacteria from the taxa Chlorobi, Chloroflexi, and Acidobacteria. In: Burnap RL, Vermaas W (eds) *Functional Genomics and Evolution of Photosynthetic Systems*, vol 35. Springer, Dordrecht, pp 47–102

67. aaaaaaaaaaaaa
68. Troussellier M, Schäfer H, Batailler N, Bernard L, Courties L, Lebaron P, Muyzer G, Servais P, Stackebrandt E, Vives-Rego J (2002) Bacterial activity and genetic richness along an estuarine gradient (Rhône River plume, France). *Aquat Microb Ecol* 28:13–24
69. Hannig M, Braker G, Dippner J, Jürgens K (2006) Linking denitrifier community structure and prevalent biogeochemical parameters in the pelagial of the central Baltic Proper (Baltic Sea). *FEMS Microbiol Ecol* 57:260–271
70. Tiedje JM (1998) Ecology of denitrification and dissimilatory nitrate reduction to ammonium. In: Zehnder AJB (ed) *Biology of anaerobic microorganisms*. John Wiley Sons, New York, pp 179–244
71. Richardson R, Felgate H, Watmough N, Thomson A, Baggs E (2009) Mitigating release of the potent greenhouse gas N₂O from the nitrogen cycle could enzymic regulation hold the key? *Trends Biotechnol* 27(7):388–397
72. Jones CM, Stres M, Rosenquist M, Hallin S (2008) Phylogenetic analysis of nitrite, nitric oxide and nitrous oxide respiratory enzymes reveal a complex evolutionary history for denitrification. *Mol Biol Evol* 25(9):1955–1966
73. Kalhuzhnaya M (2013) Highly efficient methane biocatalysis revealed in a methanotrophic bacterium. *Nat Commun* 4:2785
74. Grossart HP, Frindte K, Dziallas C, Eckert W, Tang KW (2011) Microbial methane production in oxygenated water column of an oligotrophic lake. *Proc Natl Acad Sci USA* 108(49):19657–61
75. Tang KT, McGinnis DF, Frindte K, Brüchert V, Grossart H-P (2014) Paradox reconsidered: methane oversaturation in well-oxygenated lake waters. *Limnol Oceanogr* 59:275–284
76. Sieber JR, McInerney MJ, Gunsalus RP (2012) Genomic insights into syntrophy: the paradigm for anaerobic metabolic cooperation. *Annu Rev Microbiol* 66:429–52
77. Gray ND, Sherry A, Grant RJ, Rowan AK, Hubert CR, Callbeck CM, Aitken CM, Jones DM, Adams JJ, Larter SR, Head IM (2011) The quantitative significance of Syntrophaceae and syntrophic partnerships in methanogenic degradation of crude oil alkanes. *Environ Microbiol* 13(11):2957–75
78. He J, Holmes VF, Lee PKH, Alvarez-Cohen L (2007) Influence of vitamin B12 and cocultures on the growth of *Dehalococcoides* isolates in defined medium. *Appl Environ Microbiol* 73:2847–2853
79. Krzmarzick MJ, McNamara PJ, Crary BB, Novak PJ (2013) Abundance and diversity of organohalide-respiring bacteria in lake sediments across a geographical sulfur gradient. *FEMS Microbiol Ecol* 84(2):248–58
80. Futagami T, Okamoto F, Hashimoto H, Fukuzawa K, Higashi K, Nazir KH, Wada E, Suyama A, Takegawa K, Goto M, Nakamura K, Furukawa K (2011) Enrichment and characterization of a trichloroethene-dechlorinating consortium containing multiple "dehalococcoides" strains. *Biosci Biotechnol Biochem* 75(7):1268–74
81. Revetta RP, Matlib RS, Santo Domingo JW (2011) 16S rRNA gene sequence analysis of drinking water using RNA and DNA extracts as targets for clone library development. *Curr Microbiol* 63:50–59
82. Caporaso JG, Paszkiewicz K, Field D, Knight R, Gilbert JA (2011) The Western English Channel contains a persistent microbial seed bank. *ISME J* 6(6):1089–1093
83. O'dor RK, Fennel K, VandenBerghe E (2009) A one ocean model of biodiversity. *Deep-Sea Res II* 56:1816–1823
84. Humayoun SB, Bano N, Hollibaugh JT (2003) Depth distribution of microbial diversity in Mono Lake, a meromictic Soda Lake in California. *Appl Environ Microbiol* 69:1030–1042
85. Székely AJ, Berga M, Langenheder S (2013) Mechanisms determining the fate of dispersed bacterial communities in new environments. *ISME J* 7(1):61–71
86. Comeau AM, Harding T, Galand PE, Vincent WF, Lovejoy C (2012) Vertical distribution of microbial communities in a perennially stratified Arctic lake with saline, anoxic bottom waters. *Sci Rep* 2:604
87. Booth IR (1985) Regulation of cytoplasmic pH in bacteria. *Microbiol Rev* 49(4):359–378
88. Krause E, Wichels A, Gimenez L, Lunau M, Schilhabel MB, Gerdtz G (2012) Small changes in pH have direct effects on marine bacterial community composition: a microcosm approach. *PLoS ONE* 7(10), e47035. doi:10.1371/journal.pone.0047035

Distribution of *Bacteria* and *Archaea* in meromictic tropical Lake Kivu (Africa)

Özgül Inceoğlu¹, Marc Llíros^{2,5}, Tamara García-Armisen¹, Sean A. Crowe³,
Celine Michiels^{1,3}, François Darchambeau⁴, Jean-Pierre Descy², Pierre Servais^{1,*}

¹Ecologie des Systèmes Aquatiques, Campus Plaine, CP 221, Université Libre de Bruxelles, 1050 Brussels, Belgium

²Laboratory of Freshwater Ecology, Université de Namur, 61 rue de Bruxelles, 5000 Namur, Belgium

³Departments of Microbiology and Immunology, and Earth, Ocean and Atmospheric Sciences,
University of British Columbia, V6T 1Z4 Vancouver, Canada

⁴Chemical Oceanography Unit, Université de Liège, 4000 Liège, Belgium

⁵Present address: Department of Genetics and Microbiology, Universitat Autònoma de Barcelona, 08193 Bellesguard, Catalonia, Spain

ABSTRACT: Lake Kivu is a meromictic lake in East Africa with enormous amounts of dissolved methane (CH₄) and carbon dioxide (CO₂) in its deep waters and surprisingly low CH₄ in the surface waters. We applied 454 pyrosequencing of 16S rRNA gene fragments to study the bacterial and archaeal community compositions (BCC and ACC, respectively) to provide insight into the ecology of the microbes in Lake Kivu. The vertical distribution of electron donors and acceptors in the chemically stratified water column may be responsible for the stratified distribution of microbial populations, suggesting well-defined functional specialization. The highest microbial richness was detected in the anoxic zone, which hosted high percentages of bacterial sequences related to uncultured and poorly described phyla. This suggests an under-representation of anoxic environments in current databases and the presence of previously undescribed taxa. Microbial diversity is made up of 2 fractions: abundant species (e.g. Galand et al. 2009) and rare species. Abundant species were more stable than rare species over time. The detection of rare candidate divisions (e.g. OP3, WS3, GN02) co-occurring with sulphur-oxidising *Epsilonproteobacteria*, sulphate-reducing *Deltaproteobacteria*, hydrogen-oxidising *Dehalococcoidetes* and methanogens might indicate interactions in the carbon and sulphur cycles in the anoxic waters.

KEY WORDS: Microbial community · Stratified lake · Diversity · Network · Pyrosequencing · qPCR

Resale or republication not permitted without written consent of the publisher

INTRODUCTION

Meromictic Lake Kivu, located in the volcanic region between Rwanda and the Democratic Republic of the Congo, has a permanent vertical density stratification that separates a seasonally mixed layer (or mixolimnion) with a maximum depth of 65 m from a permanently anoxic zone (or monimolimnion) rich in dissolved salts, carbon dioxide (CO₂) and methane (CH₄). Lake Kivu has garnered attention as a unique ecosystem with one of the largest CH₄ reservoirs in the world (Schmid et al. 2002, 2005). However, the

CH₄ concentrations in the oxic zone are surprisingly low compared to other lakes worldwide (Borges et al. 2011). This might be due to intense bacterial oxidation given that CH₄ diffuses from the depths towards the surface (Borges et al. 2011, Pasche et al. 2011). Furthermore, Lake Kivu has high vertical stability of the water masses and physico-chemical gradients. Variation of the vertical position of the oxic–anoxic interface over time is driven by contrasting precipitation and wind speed regimes between rainy (October–May) and dry (June–September) seasons (Thiery et al. 2014), the latter being characterised by

*Corresponding author: pservais@ulb.ac.be

a deepening of the oxic zone. Several sources of groundwater enter the lake at various depths, which explains the strong gradients observed in the vertical profiles of salinity, temperature and concentrations of dissolved gases (Degens et al. 1973, Schmid et al. 2005, Bhattarai et al. 2012).

Hence, these contrasting conditions might influence the vertical distributions and the level of microbial abundance. However, in contrast to diversity and activity studies of phytoplankton and zooplankton in the mixolimnion of Lake Kivu (Isumbisho et al. 2006, Sarmiento et al. 2006, Darchambeau et al. 2014), very few data are available on the distribution, composition and diversity of the bacterial and archaeal communities present in the lake's water column (Llirós et al. 2010, 2012, Pasche et al. 2011). Moreover, the main focus of these studies was the most abundant members of the microbial communities due to the limitations of the molecular tools used (Llirós et al. 2010, 2012). Although the most abundant species are thought to be the most active and most important in biogeochemical cycles (Cottrell & Kirchman 2003), they account for only a small proportion of microbial diversity. It is now recognised that microbial diversity is made up of 2 fractions: abundant species (e.g. Galand et al. 2009) and rare species (seed bank; Pedrós-Alió 2006, Sogin et al. 2006). Recent advances in high-throughput sequencing technologies (e.g. 454 pyrosequencing) make it possible to describe microbial communities on a scale fine enough to account for rare taxa.

To shed light on patterns and dynamics of microbial diversity in Lake Kivu, the horizontal (2 distinct lake locations) and temporal (3 sampling periods, covering the 2 main seasons) dynamics of the bacterial (BCC) and archaeal (ACC) community composition in 3 water zones of Lake Kivu were studied by means of 16S rRNA gene amplicon 454 pyrosequencing. Network analysis was further used to show the co-occurrence patterns of abundant and rare operational taxonomic units (OTUs) and to reveal their potential roles in microbial processes controlling the main biogeochemical cycles (i.e. C and S) in Lake Kivu.

MATERIALS AND METHODS

The following sections summarise the methods used in this study. More detailed information is provided in the section 'Materials and methods' of the Supplement available at www.int-res.com/articles/suppl/a074p215_supp.pdf.

Sampling sites and chemical analyses

Lake Kivu is located between Rwanda and the Democratic Republic of the Congo at 1463 m above sea level with maximum depth of 485 m in the northern basin. It has a surface area of 2370 km² and a total volume of 580 km³. Further details on the hydrology, physico-chemistry and biology of the lake have been published previously (Isumbisho et al. 2006, Sarmiento et al. 2006, Schmid & Wüest 2012).

To cover the horizontal and vertical heterogeneity of the lake's water column, 2 stations were sampled, 1 in the northern (off Gisenyi; 29.07° E, 1.77° S) and 1 in the southern (Ishungu; 29.12° E, 1.45° S) basins. Water samples were collected on 3 occasions; 2 during the dry season (October 2010 and June 2011) and 1 during the rainy season (February 2012). Vertical depth profiles of temperature, conductivity, pH and dissolved oxygen (DO) were measured *in situ* with a YSI 6600 V2 (Yellow Spring Instruments) multiparametric probe. Up to 20 discrete depths were sampled along a vertical profile between 10 and 100 m to cover the entire gradient of oxygen concentrations, from oxic to anoxic waters; only the upper layer of the anoxic layer was thus sampled. Water samples for chemical and microbiological analyses were collected using a 7.5 l Niskin bottle and stored in 4 l plastic containers for chemical analyses and 2 l Nalgene plastic bottles for biological analyses and kept at 4°C in a portable cooling box until further processing. The concentration of CH₄ was measured using the headspace technique with a gas chromatograph combined with a flame ionisation detector as previously described (Borges et al. 2011). Samples for NO_x (NO₃⁻ and NO₂⁻) and SO₄²⁻ were filtered directly through 0.2 µm pore size cellulose acetate syringe filters and were stored frozen until analysis with no preservative. NH₄⁺ concentrations were determined using the dichloroisocyanurate-salicylate-nitroprusside colorimetric method (SCA 1981). NO₂⁻ concentrations were determined using the sulphanilamide colouration method (Eaton et al. 2012). NO₃⁻ concentrations were determined after vanadium reduction to nitrite and quantified in this form following the nitrite determination procedure (Miranda et al. 2001, Eaton et al. 2012). SO₄²⁻ concentrations were measured using ion chromatography. Samples for H₂S determination were not filtered but preserved in zinc acetate and stored frozen. H₂S concentrations were measured spectrophotometrically (Cline 1969). The detection limits for these methods were 0.5 nM for CH₄ and 0.3, 0.03, 0.1, 2 and 0.5 µM for NH₄⁺, NO₂⁻, NO₃⁻, SO₄²⁻ and H₂S, respectively.

Nucleic acid extraction and quantitative real-time PCR

Water samples (0.5–1.0 l) for nucleic acid extraction were processed as described by Llirós et al. (2010).

The abundance of 16S rRNA bacterial and archaeal genes were determined by quantitative polymerase chain reaction (qPCR) using the primer combinations 341f–534r (López-Gutiérrez et al. 2004) and 519f–915r (Coolen et al. 2007), respectively. qPCR amplifications were performed in triplicate for both standard and unknown templates in a StepOne real-time PCR system (Applied Biosystems). Standard curves were generated from serial dilutions of previously titrated suspensions of conventionally PCR-amplified environmental clones.

16S rRNA bacterial and archaeal pyrosequencing

DNA extractions from each water depth and sampling site were analysed by means of bacterial and archaeal tag-encoded FLX amplicon pyrosequencing (bTEFAP and aTEFAP, respectively) as previously described (Dowd et al. 2008, Callaway et al. 2010). The bTEFAP was based upon the variable regions V1–V3 in the 16S rRNA gene using the 27F (5'-GAG TTT GAT CNT GGC TCA G-3') and 519R (5'-GWN TTA CNG CGG CKG CTG-3') primers, whereas aTEFAP used ARCH 349F (5'-GYG CAS CAG KCG MGA AW-3') and ARCH 806R (5'-GGA CTA CVS GGG TAT CTA AT-3') primers for *Archaea*. Bacterial and archaeal pyrosequencing were done based upon procedures developed by and performed at Research and Testing Laboratory (RTL; Lubbock, TX, USA) based upon RTL protocols.

Pyrosequencing data analyses

All sequences generated in this study can be downloaded from the National Center for Biotechnology Information (NCBI) Short Read Archive, accession number: SRA062980. Pyrosequencing data were processed using Mothur (Schloss et al. 2009). To minimise the effects of random sequencing errors, a denoising algorithm included in the pipeline was used, and low-quality sequences were removed by eliminating those without an exact match to the forward primer, without a recognisable reverse primer, with a length shorter than 200 nucleotides and those containing any ambiguous base calls. We trimmed

the barcodes and primers from the resulting sequences. Chimeras (checked using Uchime software; Edgar et al. 2011) and contaminants (understood as unclassified or misclassified sequences after comparing candidate sequences against the latest SILVA or RDP training set with cutoff values of 80 for both *Bacteria* and *Archaea*, respectively) were removed from sequence collection files. After taxonomic classification of the sequences down to phylum, class and genus level, the relative abundance of a given phylogenetic group was set as the number of sequences affiliated with that group divided by the total number of sequences per sample to normalize the dataset. Due to the advantages of using the largest and most diverse sets available, the latest Greengenes and SILVA were used for classification as bacterial and archaeal 16S rRNA gene sequence databases, respectively, at 80 % confidence threshold with Mothur (Werner et al. 2012). Sequences were clustered into operational taxonomic units (OTUs) by setting a 0.03 distance limit (equivalent to 97 % similarity). Rarefaction curves based on identified OTUs, Shannon diversity index and species richness estimator of Chao1 were generated in Mothur for each sample. To test for differences between water zones and reduce sampling effort influences, all bacterial samples were randomly subsampled to the same size according to the sample with the smallest sampling size (i.e. the smallest number of reads). In turn, no random subsampling was carried out for all archaeal datasets due to the low diversity values within oxic samples and the high observed richness coverage values (see Table 2).

Statistical analyses

Unless otherwise stated, all statistical analyses were performed using PRIMER 6 (Clarke & Gorley 2006). The relative abundance of bacteria and archaea at the phylum, genus and OTU (97 % cut off) levels were square-root transformed, and dissimilarities between samples were computed using the Bray-Curtis similarity coefficient. Dendrograms were generated based on the Bray-Curtis similarity index using complete linkage clustering to visualise the relationships between communities. The effect of time, location and DO conditions on BCC and ACC were tested with 1-way analysis of similarities (ANOSIM). Relative abundances of phyla per sample were visualised as a bubble chart using the bubble.pl.program (www.cmde.science.ubc.ca/hallam/bubble.php).

For network inference, OTUs occurring fewer than 5 times in the whole data set were removed, and Pearson's rank correlations were calculated between remaining OTUs using the CoNet program (Faust et al. 2012), when the coefficient (r) was both above 0.8 and statistically significant (p value 0.01). The results were then translated into an association network using Cytoscape 2.6.3 (Shannon et al. 2003, Faust et al. 2012). Cytoscape depicts taxa as nodes connected by lines that denote the positive correlations between them. In the network, the size of each node is proportional to the number of connections (that is, the degree), and the size of each edge is proportional to the strength of the correlations.

In addition, Venn diagrams were used to show the distribution of OTUs between the 3 sampling campaigns in the oxic, transition and anoxic zones. Abundant OTUs were defined as those taxa containing more than 6 sequences at each depth, whereas rare OTUs were defined as those taxa represented by fewer than 6 sequences at each depth (Magurran & Henderson 2003). In turn, habitat generalists were defined as those OTUs appearing in more than 15 samples (i.e. depths) across the 3 sampling campaigns, and habitat specialists were those OTUs that were locally abundant ($>0.5\%$ of relative abundance) and appeared in fewer than 6 samples (Logares et al. 2013). Additionally, OTUs appearing in 6 to 15 samples were defined as imperfect generalists (able to grow under most environmental conditions and not in others) in the present study.

RESULTS

Environmental parameters along the water column

The water column of Lake Kivu is complex with vertical gradients of temperature, conductivity and DO, as well as CH_4 , NH_4 and H_2S (Fig. 1). The first 100 m of the water column of Lake Kivu were separated into 3 distinct water zones according to DO criteria established previously (Wright et al. 2012), resulting in an oxic surface zone ($\text{DO} > 90 \mu\text{M}$), a transition zone (DO between 1 and $90 \mu\text{M}$) and a deep anoxic zone ($\text{DO} < 1 \mu\text{M}$; Fig. 1). Oxic surface waters were characterised by low nitrogen and CH_4 concentrations, whereas the anoxic deep waters were characterised by high concentrations of NH_4 , and dissolved CO_2 and CH_4 . Oxidised inorganic forms of N (NO_x^-) showed maximum values in the transition zone, whereas high concentrations of H_2S (Fig. 1) and CH_4 were only observed in the anoxic waters. The mixed oxic zone appeared to

be slightly deeper in October 2010 than during the 2 other sampling campaigns (Fig. 1).

Microbial abundance analyses

The numbers of bacterial 16S rRNA gene copies ranged between ca. 10^4 and 10^6 ml^{-1} for the Gisenyi and Ishungu water samples in June 2011 and February 2012. On the other hand, the numbers of archaeal 16S rRNA gene copies ranged between ca. 10^2 and 10^5 ml^{-1} in June 2011 and February 2012 at both sampled stations (Fig. 2). No qPCR analyses were conducted on October 2010 samples due to technical problems. In general, vertical depth profiles for bacterial and archaeal 16S rRNA gene copy numbers showed similar patterns with no or slight differences between each of the 3 water zones defined at each sampling station and time. In contrast to other sampling times, no decrease was observed in the transition zone in Gisenyi in June 2011. Furthermore, 16S rRNA gene copies detected for both bacteria and archaea were fairly constant with depth in oxic and anoxic waters during June and February in Ishungu, whereas 16S rRNA gene copies showed more variation with depth in Gisenyi (Fig. 2).

Bacterial and archaeal diversity analysis

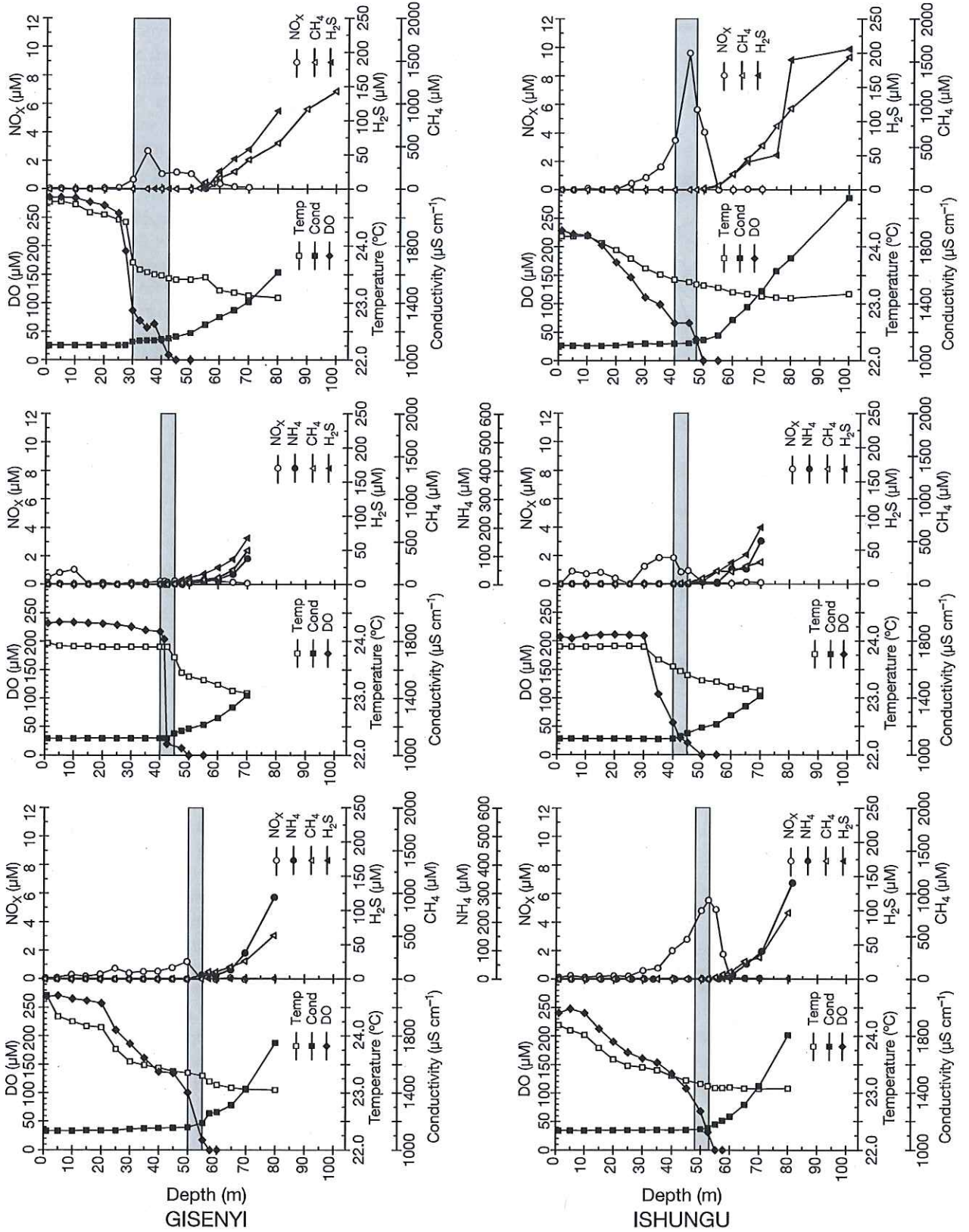
The stratification based on DO concentrations was found as the strongest predictor of the overall BCC structure (Figs. 3 & 4; $R = 0.527$, $p = 0.001$), followed by temporal and then by horizontal variation (Table 1). Clustering analysis of the BCC revealed the presence of 9 sub-clusters, 2 of which were exclusively composed of samples from the oxic zone, and 3 clusters contained only samples from anoxic depths. In turn, those samples from the transition zone occupied transitional sub-clusters containing samples from both oxic and anoxic zones. However, the results were less evident for the ACC, although anoxic water samples clearly clustered apart from oxic samples (Fig. 4). ANOSIM also highlighted the similarity between oxic and transition archaeal communities as well as

Fig. 1. Depth profiles of temperature (Temp), conductivity (Cond) and dissolved oxygen (DO) concentrations (left-hand plots) and NH_4 , NO_x ($\text{NO}_3^- + \text{NO}_2^-$), CH_4 and H_2S concentrations (right-hand plots) for Gisenyi (upper panels) and Ishungu (lower panels) from 3 sampling campaigns (October 2010, June 2011 and February 2012) in Lake Kivu (Africa). Grey shading depicts the transition zone

Feb 2012

Jun 2011

Oct 2010



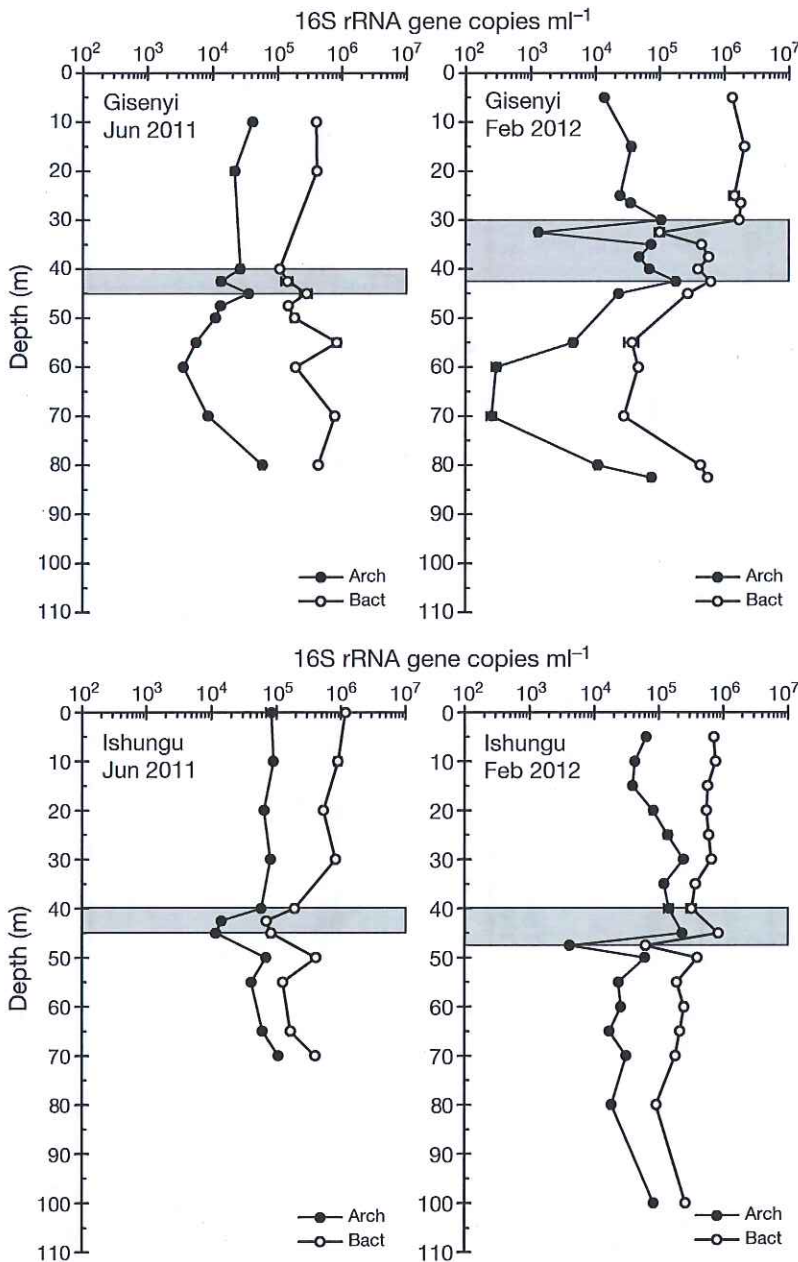


Fig. 2. Bacterial (Bact) and archaeal (Arch) abundances determined by 16S rDNA gene qPCR for 2 sampling campaigns (June 2011 and February 2012) in Lake Kivu. Grey shading depicts the transition zone

significant variations of the ACC between sampling stations, whereas no clear effects between sampling seasons were observed (Table 1).

Richness and diversity estimates

Based upon hierarchical clustering analysis, those samples corresponding to previously defined water

compartments (i.e. oxic, transition and anoxic zones) were pooled for each location and each sampling campaign (18 groups of sequences). We used 44 883 (between 842 and 7513 per group) bacterial and 10 323 (between 1 and 1498 per group) archaeal reads for richness and diversity estimates (Table 2).

Across all samples, rank abundance distributions best fitted the power law model, which indicates a community composed of a few highly dominant species next to a long tail of rare species (data not shown; $R \geq 0.91$). Although the dominance of a single bacterial OTU was not observed, the most abundant bacterial OTUs found were those affiliated with unclassified *Actinobacteria* (CL500-29 group; 14%) and *Cyanobacteria* (*Synechococcales*; 15%). Archaeal data sets demonstrated the dominance of a few OTUs affiliated with the uncultured GOM Arc I *Methanosarcinales* group (*Euryarchaeota*) for each sampling site. In Gisenyi, a single OTU represented up to 31% of all archaeal sequences, while 2 OTUs each represented ca. 10% of all archaeal sequences in Ishungu.

Rarefaction analysis, based on OTUs, indicated that most of the bacterial samples may require deeper sequencing to avoid underestimation of microbial diversity present in the samples (8894 OTUs in all samples analysed; Fig. S1A in the Supplement), whereas archaeal rarefaction curves (Fig. S1B in the Supplement) together with archaeal coverage values (up to 100%, Table 2) showed that the sequencing effort captured most of the richness present in Lake Kivu for this domain

with a few exceptions in October 2010 (with a total of 515 OTUs; Fig. S1B, Table 2). When all the bacterial samples were sub-sampled randomly to the same size based on the smallest sample, the number of observed bacterial OTUs per zone (oxic, transition and anoxic zones) ranged from 320 to 836 in Gisenyi and 235 to 587 in Ishungu over the 3 sampling campaigns (Table 2), while observed archaeal OTUs per zone ranged from 4 to 153 in Gisenyi and 1 to 306 in

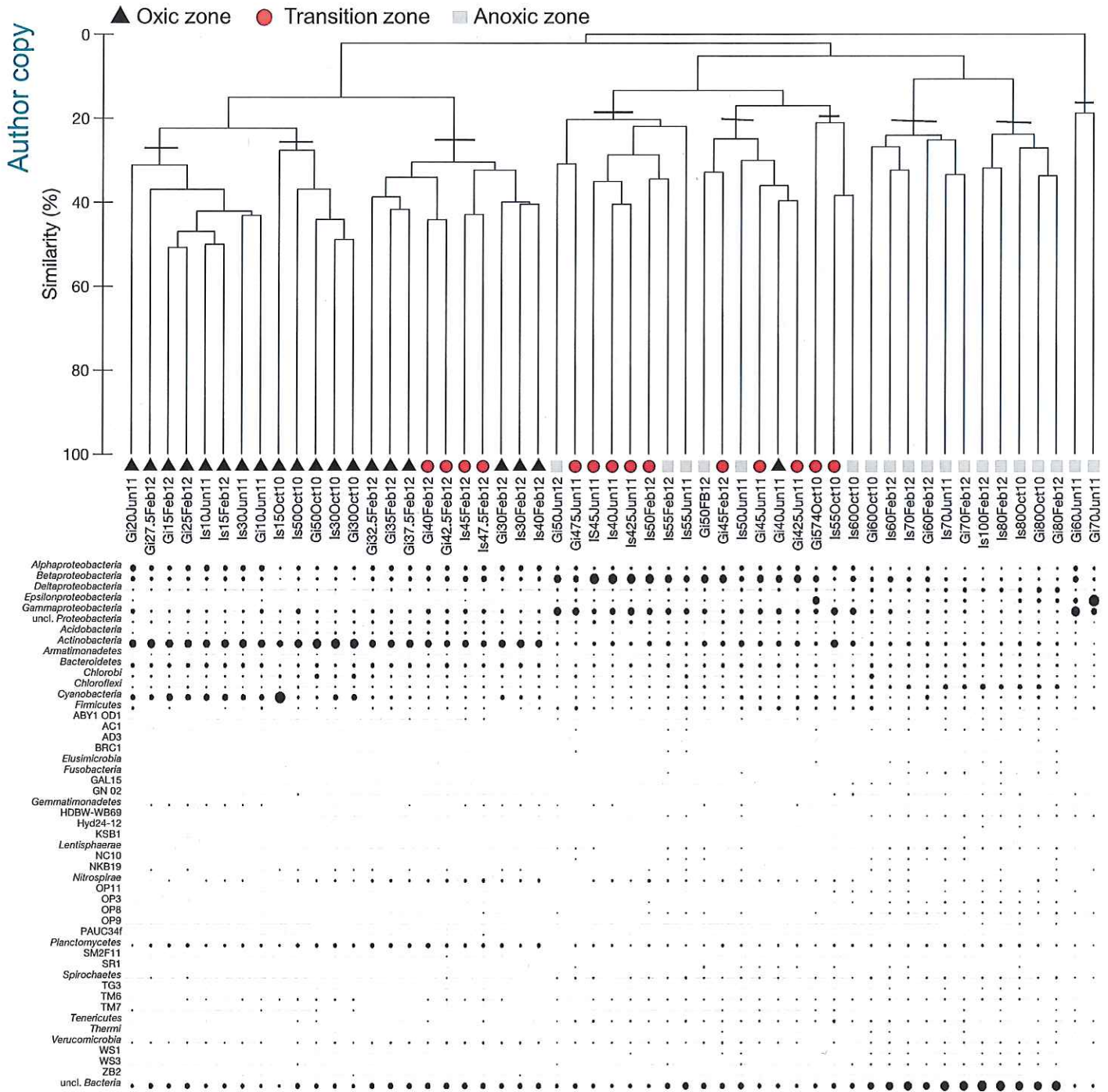


Fig. 3. Dot plot of relative abundance of bacterial taxa along the vertical profile in Gisenyi and Ishungu over the 3 sampling campaigns at the phylum level. Samples are organised according to the similarity of their community composition at the operational taxonomic unit (OTU) level, as revealed by hierarchical clustering of the distribution of taxonomic groups across environmental samples. Zones based on oxygen concentrations are distinguished (oxic >90 µM, transition [1–90 µM], anoxic <1 µM). Oct10: October 2010; Jun11: June 2011; Feb12: February 2012; Is: Ishungu; Gi: Gisenyi; uncl.: unclassified

Ishungu for each of the 3 sampling campaigns (Table 2). Both BCC and ACC revealed a significant increase of richness with depth at both sampling sta-

tions (Table 2, $p < 0.05$). Without sub-sampling to the same sampling size, the highest bacterial richness estimation was also observed in the anoxic zone: for

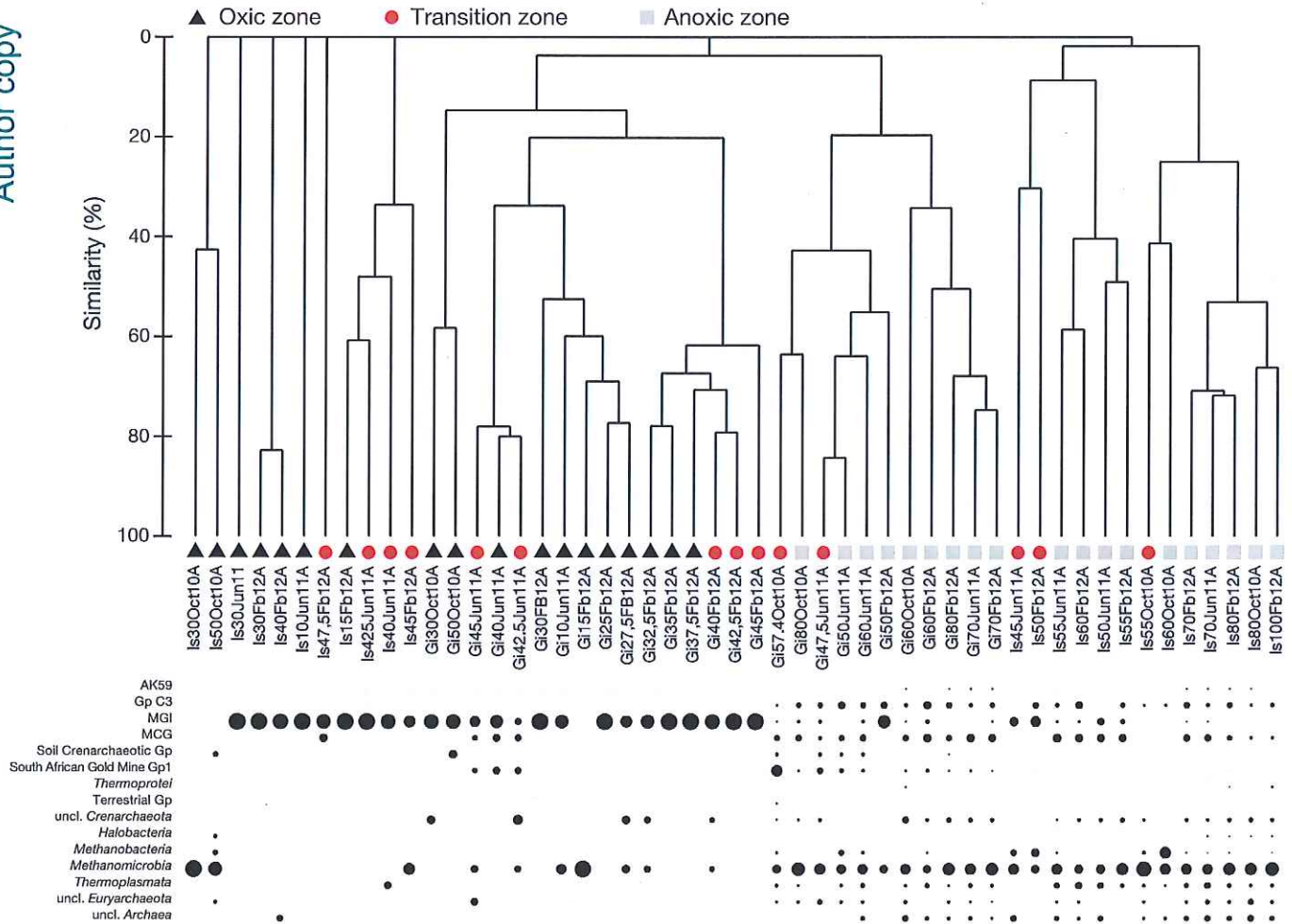


Fig. 4. Dot plot of relative abundance of archaeal taxa along the vertical profile in Gisenyi and Ishungu over the 3 sampling campaigns at the phylum level. Samples are organised according to the similarity of their community composition at the OTU level, as revealed by hierarchical clustering of the distribution of taxonomic groups across environmental samples. See Fig. 3 for other details

instance, 8758 OTUs were detected in the Ishungu anoxic zone in February, while there were only 1732 in the oxidic zone (Table S1 in the Supplement). Furthermore, bacterial OTUs were more evenly distributed in the anoxic water compartment than in the other 2 analysed water compartments. In contrast, archaeal OTUs evidenced a more even distribution in the oxidic and transition water compartments than in the anoxic zone. The lowest coverage values of observed bacterial richness were also observed in the anoxic zone (Table 2).

BCC analysis

All qualified reads could be assigned as *Bacteria*, but 10 to 53% of the analysed sequences per sample could not be assigned to any phylum (Fig. 3). Differ-

ent phyla dominated the different depths analysed. The relative abundance of unclassified bacteria was higher in the anoxic zone (Fig. 3). Altogether, 38 bacterial phyla were recovered from Gisenyi, whereas 41 phyla were recovered from Ishungu. *Actinobacteria*, *Bacteroidetes*, *Chlorobi*, *Chloroflexi* and *Proteobacteria* (*Alpha*-, *Beta*- and *Gammaproteobacteria*) were found in the 3 zones at both stations at all sampling times. Candidate phyla such as BRC1, OP3, OP9, OP10, GAL15 and GN02 were mainly detected in the anoxic zone with a relative abundance below 1%, and *TM6* was mainly detected in the oxidic zone.

At both sampling stations, *Actinobacteria* was the dominant phylum in the oxidic zone (up to 44% of the total bacterial sequences). *Cyanobacteria* (up to 18% and 62% in Gisenyi and Ishungu, respectively) and *Alphaproteobacteria* were also highly represented in the oxidic zone, and their relative abundance decreased

Table 1. Analysis of similarities (ANOSIM) significance values based on operational taxonomic units (OTUs) to evaluate the variation of bacterial and archaeal community composition in Lake Kivu. Significant R values are highlighted in bold. DO: dissolved oxygen

Test for differences between	Bacteria		Archaea	
	R	p	R	p
Water zones based on DO concentrations				
Global test	0.527	0.001	0.287	0.001
Pairwise test				
Oxic–Transition	0.699	0.001	0.075	0.077
Oxic–Anoxic	0.692	0.001	0.466	0.05
Transition–Anoxic	0.550	0.001	0.330	0.1
Sampling time				
Global test	0.437	0.001	0.057	0.1
Pairwise test				
January–October	0.442	0.002	0.074	0.11
January–February	0.476	0.001	0.024	0.24
October–February	0.475	0.002	0.097	0.09
Sampling locations				
Global test	0.061	0.05	0.063	0.001

with depth at both sampling stations; they were replaced by different phyla and members of the proteobacterial class at deeper levels (Fig. 3). Furthermore, the highest relative abundance of *Betaproteobacteria* was detected in the transition zone (up to 28 and 46% in Gisenyi and Ishungu, respectively).

High relative abundance of *Gammaproteobacteria* was detected both in the transition and the anoxic zones at both sampling sites. In turn, *Delta-* and *Epsilonproteobacteria* were mainly detected in the anoxic zone. In contrast to other phyla, higher relative abundances of *Epsilonproteobacteria* were detected in Gisenyi (up to 71%) than in Ishungu anoxic waters. In addition, relative abundance of *Epsilonproteobacteria* was lower in February in Gisenyi, in comparison with the 2 previous sampling campaigns.

ACC analysis

Only 10% of the reads could be assigned to any archaeal phyla. Of all sequences retrieved from Gisenyi and Ishungu, 7.3% and 6.3% were not classified in any archaeal phyla. The highest numbers of non-affiliated sequences were recovered from the deepest depths sampled. All retrieved archaeal amplicons spanned over archaeal lineages covering *Thaumarchaeota*, *Crenarchaeota* and *Euryarchaeota* within both cultured (e.g. Marine Group I *Crenarchaeota* [MGI] or *Methanobacteria*) and uncultured groups (e.g. Miscellaneous Crenarchaeotic Group (MCG) or Deep Sea Hydrothermal Ventic Group 6; Fig. 4).

Table 2. Diversity indices for bacterial and archaeal operational taxonomic units (OTUs) in the water zones analysed defined according to dissolved oxygen concentrations in Lake Kivu. We analysed 1337 bacterial and 3730 archaeal sequences in Gisenyi and 842 bacterial and 4382 archaeal sequences in Ishungu. Sobs: number of observed species; Chao1: Chao1 richness estimate; Shannon: diversity index; Shannoneven: species evenness index; Coverage: non-parametric coverage estimator; nd: not determined

	Bacteria					Archaea				
	Sobs	Chao1	Shannon	Shannoneven	Coverage	Sobs	Chao1	Shannon	Shannoneven	Coverage
Gisenyi										
Oxic–Oct10	320	732	4.58	0.79	0.86	nd	nd	nd	nd	nd
Oxic–Jun11	465	1250	5.26	0.86	0.76	4	4	1.21	0.87	0.75
Oxic–Feb12	538	1351	5.51	0.88	0.73	4	4	1.33	0.96	0.67
Transition–Oct10	357	764	4.78	0.81	0.84	4	6	1.33	0.96	0.4
Transition–Jun11	600	1881	5.74	0.90	0.68	22	43	2.87	0.93	0.59
Transition–Feb12	648	1647	5.9	0.91	0.67	16	19	2.44	0.88	0.87
Anoxic–Oct10	628	1736	5.86	0.91	0.68	153	373	3.34	0.66	0.92
Anoxic–Jun11	680	2431	5.89	0.90	0.62	94	235	3.44	0.76	0.92
Anoxic–Feb12	836	2778	6.43	0.96	0.52	152	225	2.91	0.58	0.96
Ishungu										
Oxic–Oct10	235	550	4.12	0.75	0.82	1	1	0.00	1.00	0.00
Oxic–Jun11	309	748	4.82	0.84	0.75	2	2	0.69	1.00	1.00
Oxic–Feb12	320	913	5.00	0.87	0.74	6	6	1.72	0.96	0.82
Transition–Oct10	380	890	5.33	0.90	0.70	8	10	1.79	0.86	0.79
Transition–June11	401	1159	5.42	0.90	0.66	14	41	2.48	0.94	0.45
Transition–Feb12	425	1217	5.59	0.92	0.64	8	10	1.79	0.86	0.76
Anoxic–Oct10	477	1878	5.73	0.93	0.56	100	157	3.86	0.84	0.90
Anoxic–Jun11	540	2225	5.98	0.95	0.49	110	157	3.67	0.78	0.92
Anoxic–Feb12	587	2479	6.12	0.96	0.43	306	482	4.17	0.73	0.96

Oxic water samples from all sampling sites and dates harboured between 1 and 6 distinct archaeal OTUs, whereas the number of defined OTUs increased in the anoxic water compartment. At the 3 sampling campaigns, oxic waters of both sampling sites were clearly dominated by putatively ammonia-oxidising OTUs belonging to the MGI (56.7% and 51.3% of the analysed sequences in the oxic zone in Gisenyi and Ishungu, respectively; Fig. 4). The transition zone contained a more diverse ACC than the oxic zone, with the presence of *Thaumarchaeota* (13.2% and 6.5% of the analysed sequences in the transition zone at Gisenyi and Ishungu, respectively), *Crenarchaeota* (31.1% and 14.5%) and *Euryarchaeota* (51.9% and 70.3%). In the transition zone, all retrieved *Crenarchaeota* OTUs belonged to as yet uncultured groups, whereas *Euryarchaeota* OTUs were mainly affiliated with *Methanomicrobia* (39.6% and 46.4% of the analysed sequences at Gisenyi and Ishungu, respectively). In turn, anoxic waters were clearly dominated by *Euryarchaeota* (more than 42.6% of the sequences retrieved at these depths from both sites) mainly belonging to the *Methanomicrobia* class (29.3% and 35.3% of all the sequences in the anoxic zone in Gisenyi and Ishungu, respectively), followed by uncultured *Crenarchaeota* and non-affiliated archaea (Fig. 4).

Co-occurrence patterns of *Bacteria* and *Archaea*

The resulting aquatic microbial network of Lake Kivu (Fig. S2 in the Supplement) consisted of 556 highly connected bacterial and archaeal nodes (OTUs), comprising 5.35 edges node⁻¹ on average, structured among densely connected sub-networks (1 major, 11 moderate and 35 small sub-networks). Aside from many unclassified bacterial and archaeal OTUs, co-occurrence of different known taxa was observed. For instance, in the major sub-network (Fig. 5A), the rare taxon *Dehalococcoidetes* showed the highest incidence of co-occurrence and, to a lesser extent, the bacterial lineages *Actinobacteria* and *Bacteroidetes* and the archaeal lineages *Methanoregula* and *Methanospirillum* also showed high co-occurrence values. Other taxa showed more limited co-occurrence patterns, such as sulphate-reducing bacteria (*Desulfobacca*, *Desulfocapsa* and *Desulfobacterium*) and sulphur-oxidising bacteria (*Sulfuricurvum* and *Sulfurimonas*). *Dehalococcoidetes* co-occurred with several uncultivated candidate divisions such as AC1, GN02, OP3 and WS3, but also with taxa like *Actinobacteria* WCHB1-81, *Desul-*

fobacca and *Bacteroidetes* and with archaeal lineages *Methanoregula*, *Methanosaetaceae*. In addition, 2 sub-networks (Fig. 5B) were dominated by different OTUs affiliated with *Methylomonas*. In sub-network 1, *Methylomonas* co-occurred with OTUs affiliated with *Acinetobacter* (*Gammaproteobacteria*), *Rhizobiales* (*Alphaproteobacteria*) and the archaeal taxon *Methanoregula*. In sub-network 2, betaproteobacterial taxa mainly co-occurred with other proteobacterial taxa (*Methylomonas*, *Methyloversatilis*, unclassified *Proteobacteria*, *Rhizobiales*, *Rhodocyclaceae*) and also with *Thaumarchaeota*. There were also 2 other sub-networks mainly composed of uncultured archaea and *Cyanobacteria* (data not shown).

Bacterial abundance classification and overlap estimates

Venn diagrams (Fig. 6; see also Fig. S3 in the Supplement) illustrate the presence of overlapping abundant and rare OTUs between sampling campaigns, as well as OTUs unique to each season in each water zone. Only ca. 10% of the OTUs were found to be abundant in all samples. In turn, 61% in Gisenyi and 68% in Ishungu of the abundant OTUs in the oxic zone were shared between 3 sampling times; 24% and 46% of the abundant taxa were shared in the transition zone in Gisenyi and Ishungu, respectively. Besides, 55% and 40% of the abundant taxa were shared in the anoxic zone from Gisenyi and Ishungu, respectively. In contrast, rare OTUs were found to be specific to sampling time (Figs. 6 & S3). The dynamics of rare bacterial species over time revealed that some of the rare biosphere can become abundant at another sampling time in each water zone. Moreover, Venn diagrams constructed with Gisenyi samples (Fig. S4 in the Supplement) illustrated clear differences between zones at the 3 sampling times. A higher percentage of abundant OTUs was shared among water zones in comparison with rare OTUs. There was a significant positive relationship between

Fig. 5. Network of co-occurring operational taxonomic units (OTUs) based on correlation analysis. A connection represents a strong (Pearson $r > 0.8$) and significant ($p = 0.01$) positive correlation. The size of each node is proportional to the number of connections. (A) major network showing co-occurrence of *Dehalococcoidetes* with *Desulfobacca*, *Sulfurimonas* and *Actinobacteria* and candidate divisions as well as unclassified bacteria (squares) and archaea (circles); (B) sub-networks dominated by *Methylomonas* and their co-occurrence with proteobacterial lineages

A

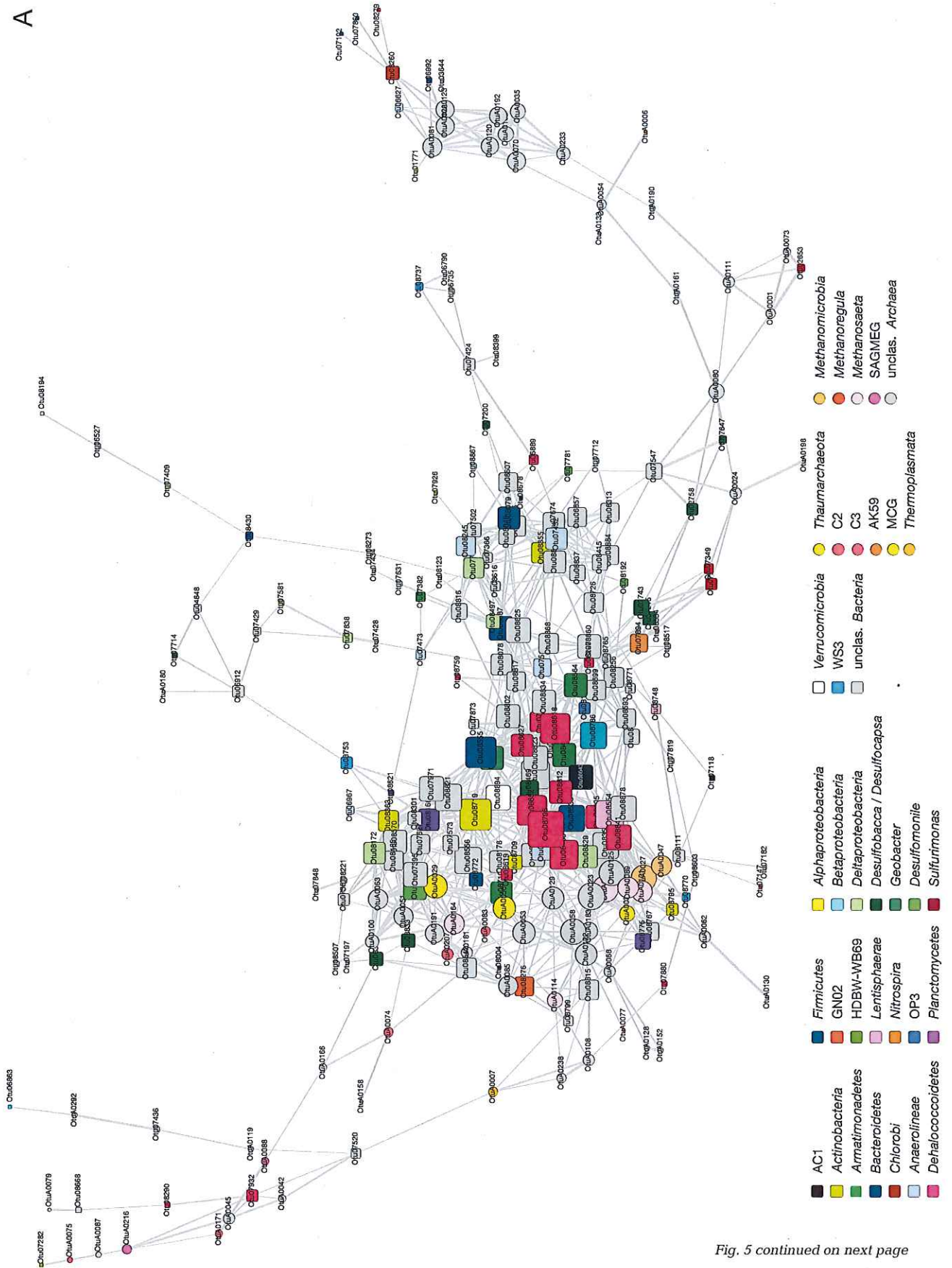


Fig. 5 continued on next page

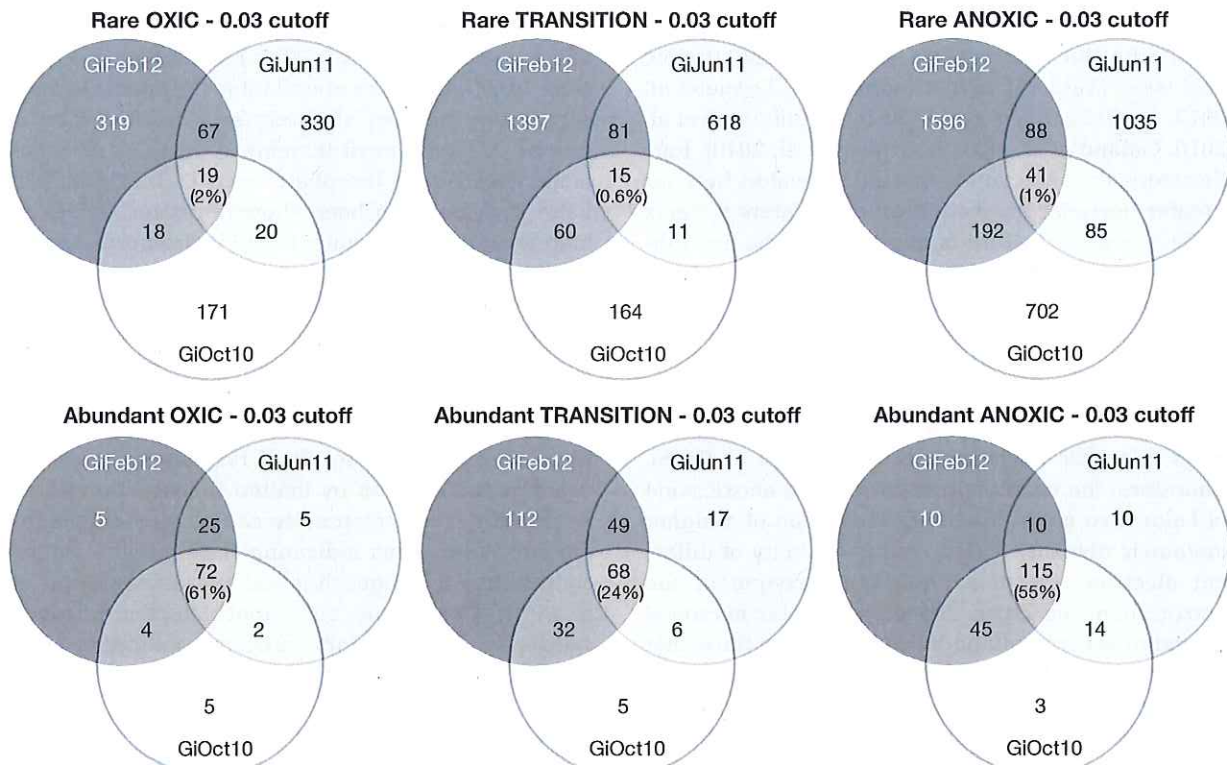


Fig. 6. Distribution of operational taxonomic units (OTUs) among the 3 sampling campaigns over the oxic, transition and anoxic zones in Gisenyi (Gi). Abundant OTUs are defined as taxa represented by more than 6 sequences at each depth, whereas rare OTUs are defined as taxa represented by fewer than 6 sequences

the relative abundance and occupancy of OTUs (Fig. S5 in the Supplement). Further information on generalists and specialists can be found in the Supplement.

DISCUSSION

The present study captures both abundant and rare microbes in a meromictic freshwater African lake, providing information on taxonomic diversity and distribution in relation to environmental gradients. Due to its meromictic nature, vertical variation in the availability of oxygen as well as other electron donors and acceptors plays an overarching role in shaping the distribution and diversity of prokaryotes.

Relative abundance of archaea versus bacteria

As shown by qPCR analyses of microbial communities, 16S rRNA gene copy numbers of archaea were approximately 2 orders of magnitude less abundant than bacteria at each depth along the water column

analysed (Fig. S1 in the Supplement). Although qPCR has drawbacks in performing total cell enumerations (e.g. such as the requirement for careful calibration, the specificity of the primers and the number of gene copies per cell), our data are consistent with previous reports on archaeal relative abundances in Lake Kivu (range: 0.3–4.6% of total prokaryotic abundance) estimated by fluorescent *in situ* hybridisation followed by epifluorescence microscopic enumeration (Llirós et al. 2010). Casamayor & Borrego (2009) also showed that *Archaea* are a minor component of microbial communities in freshwater.

Microbial richness in the water column

Microbial communities in the oxic surface waters were very different from those in the deeper anoxic waters. This microbial stratification can likely be attributed to differences in the availability of electron donors and acceptors as well as the energy sources as a function of depth. Overall, anoxic waters exhibited higher species richness than oxic waters. Richness estimations (up to 1938 OTUs) in the oxic zone of

Lake Kivu were within the range of previously reported values for surface waters of oligotrophic cold lakes (Table S1 in the Supplement; Logue et al. 2012) and for surface marine waters (Andersson et al. 2010, Galand et al. 2010, Kirchman et al. 2010). Furthermore, the observation that anoxic waters harbour greater bacterial diversity than oxic waters appears to be a general feature of extreme aquatic environments (Madrid et al. 2001, Humayoun et al. 2003, Yakimov et al. 2007, Quince et al. 2008, Comeau et al. 2012, Bougouffa et al. 2013). It was previously suggested that anaerobic species with metabolisms less energetically efficient than aerobic respiration might maintain a greater diversity in metabolic pathways in anoxic environments (Lehours et al. 2005). Therefore, the microbial network in the anoxic zone of Lake Kivu might lead to the retention of a higher metabolic diversity. Due to the availability of different electron acceptors other than oxygen in the anoxic zone, conditions that shape aerobic microbial communities are profoundly different from those that regulate anaerobic microbial communities (Humayoun et al. 2003). Notably, a greater proportion of bacterial sequences in the anoxic waters were affiliated with poorly described phyla and uncultured taxa, compared to the oxic waters. This observation may be due to the under-representation of anoxic microbial communities in current databases. This might also reflect the strong potential of deep and anoxic environments to harbour hitherto unknown microbial groups also known as microbial dark matter (Rinke et al. 2013).

Importance of rare taxa

Due largely to methodological limitations, most studies of freshwater microbial ecology to date have focused on abundant species that were thought to mediate biogeochemical processes, while rare species went undetected. In the present work, rank abundance analyses of both archaeal and bacterial sequences revealed a small fraction of highly abundant OTUs and a long tail of less abundant OTUs, suggesting the presence of a so-called rare biosphere (Sogin et al. 2006, Pedrós-Alió 2012). Although incomplete sampling may lead to pseudo-turnover of species, overall most species defined as generalists were abundant, whereas those defined as habitat specialists were for the most part rare (Fig. S5 in the Supplement). Although our grouping was somewhat arbitrary, it was useful to define ecological categories. In the present study, strict habitat specialists

(OTUs that tend to be present in only 1 habitat type and in most samples from that habitat type; Logares et al. 2013) were more abundant in the anoxic waters, supporting the idea of strong selection for specific species in anoxic environments. A complex environment with a rare biosphere such as that found in Lake Kivu has also been shown in other studies in marine anoxic environments and hydrothermal vents (Sogin et al. 2006, Galand et al. 2009).

An evaluation of the effect of sampling time on abundant versus rare species in the 3 different zones of the lake revealed that abundant core members exhibited minimal temporal variability, whereas rare species showed more pronounced fluctuations over seasons (Fig. 6). If rare enough, species can escape detection by limited sequencing efforts. A changing rare community can also mean changing specialists, thus indicating their possible active contribution to biogeochemical processes (Pester et al. 2010). Conversely, consistent detection of given species in a zone might indicate core rather than transient membership in the community.

Possible relationship between microbial community composition and microbial processes

In a higher taxonomical rank (phylum/class), seasonal succession patterns and vertical diversification in microbial communities have also been recently reported in many distinct environments, mostly in fresh water (i.e. Warnecke et al. 2005, Shade et al. 2007), as observed for both archaeal and bacterial assemblages in Lake Kivu. *Actinobacteria*, *Cyanobacteria* and *Thaumarchaeota* dominated the microbial community in the oxic zone, while many other bacterial (distinct *Proteobacteria*, *Bacteroidetes*, *Chlorobi* and *Chloroflexi*, among others) and archaeal (mainly CH_4 -related and uncultured groups) phyla/classes were distributed throughout the water column with significant differences in their relative abundances between transition and fully anoxic waters (Fig. 3). As shown in the current study, *Actinobacteria* were commonly found in epilimnetic water of lakes from all over the world because of their adaptation to the environmental conditions found in this zone: high light intensity (Warnecke et al. 2005) and DO concentration (Allgaier & Grossart 2006, Taipale et al. 2009). *Cyanobacteria*, the second most abundant phylum in the oxic waters in Lake Kivu, were slightly more abundant in the rainy season than in the dry season in concordance with recently published data (Darchambeau et al. 2014)

based on primary production and phytoplankton composition reporting high cyanobacterial abundance during the lake's rainy season. Archaea are also important players in global energy cycles, especially in C and N cycles, in spite of their lower abundance compared to bacteria in lakes (Fig. 2; Casamayor & Borrego 2009). For instance, the oxic zone was dominated by members of the MGI, supporting the presence of archaeal nitrifiers in the water column. Our study is also consistent with data reported by Hu et al. (2011), which showed the importance of light intensity on the vertical distribution of MGI.

In a previous study (Llirós et al. 2012), the transition zone was suggested to be the most active and metabolically diverse water compartment due to the prevailing physico-chemical conditions. The deeper analysis of the microbial diversity present in Lake Kivu performed in this study evidenced the presence of the highest microbial richness in the sampled anoxic zone (Table 2). Even so, important key players such as methylotrophs were identified in the transition zone. Aerobic CH₄ oxidation preferentially occurs in the transition zone of freshwater systems (Segers 1998, Bastviken et al. 2003), where CH₄ and DO are both present. The dominance of *Methylococcales* in the transition zone is consistent with the high rate of bacterial CH₄ oxidation, resulting in low surface water CH₄ concentrations despite the large deep CH₄ reservoir (Borges et al. 2011, Morana et al. 2014).

Furthermore, a connection between 2 OTUs mainly describes their co-occurrence across different samples which might indicate their similar response to a common environmental parameter or their possible direct interactions. For instance, network analysis revealed a clear co-occurrence network within proteobacterial lineages in the transition zone, which might indicate that several members of the *Proteobacteria* are well adapted to the environmental conditions present in the transition zone (Fig. 5B). The presence of archaeal methanogenic lineages at the vicinities of the transition zone might indicate a coupling between the production of CH₄ and its oxidation by microbial processes. Moreover, detection of green sulphur bacteria (*Chlorobium*-related OTUs) and high relative abundance of *Nitrospira*-related sequences in the transition zone might indicate potential oxygenic photoautotrophy and nitrite oxidation, respectively.

Different ecological conditions guiding microbial community composition were reflected in diverse network structures in the 3 water compartments. In

our study, a co-occurrence of *Dehalococcoidetes*, *Actinobacteria* WCHB-81, sulphate-reducing bacteria (SRB), sulphur-oxidising bacteria, acetoclastic methanogenic archaea, as well as candidate bacterial divisions, and uncultured archaea and bacteria was observed in the anoxic zone (Fig. 5A). These microbial connections point towards a potential link between C and S cycles in the pelagic anoxic waters of Lake Kivu. It has been evidenced that a consortium of SRB and methane-oxidising archaea can couple C and S cycles throughout anaerobic oxidation of methane (AOM) with sulphate, manganese or iron as electron acceptors (Hinrichs & Boetius 2002, Beal et al. 2009). Remarkably, the low recovery of sequences affiliated with anaerobic methane oxidisers (the main archaeal group involved in AOM) should not completely rule out AOM, because of the presence of unclassified archaeal groups that could be involved in AOM (e.g. Marine Benthic Group B, C and D, MCG and the recently described AOM-associated archaea; Biddle et al. 2006, 2012, Inagaki et al. 2006, Knittel & Boetius 2009). In contrast, our results indicate the importance of hydrogenotrophic and acetoclastic methanogenesis in the lake, as *Methanomicrobiales* and *Methanosarcinales* were highly abundant in the anoxic zone. As has been shown in Lake Matano (Crowe et al. 2011), the present study supported the direct occurrence of methanogenesis within the water column, even though CH₄ was previously assumed to be solely produced in sediments and diffused in the water column (Pasche et al. 2011). Since water column CH₄ production has been shown to be rare in anoxic water columns (Reeburgh 2007), pelagic methanogenesis should be further studied under persistently anoxic conditions in Lake Kivu. Furthermore, syntrophy or competition between methanogens and SRB in the anoxic sediments must also be considered in the anoxic waters, as previously shown (Kuivila et al. 1990, Holmer & Kristensen 1994, Muyzer & Stams 2008).

Another noteworthy observation in the water column of Lake Kivu was the high relative abundance of *Epsilonproteobacteria* in those water samples in the upper part of the anoxic waters. Previous studies have suggested a chemolithoautotrophic role for some *Epsilonproteobacteria* species like *Sulfuricum* and *Sulfurimonas* using sulphur as electron donors and NO₃⁻ as electron acceptors in oligotrophic and stratified marine environments with sulphidic redox-clines (i.e. the Baltic and Black Seas; Campbell et al. 2006, Grote et al. 2007, Glaubitz et al. 2009). The presence of NO_x traces just below the transition zone of Lake Kivu together with the detection of *Sulfuri-*

curvum-related OTUs point towards putative chemolithoautotrophic processes present in the upper anoxic water compartment.

As presented in the network analysis, a complex interaction between organohalide respiring *Chloroflexi*, *Actinobacteria* WCHB1-81 and SRB could suggest a role in hydrocarbon or refractory organic matter degradation in the anoxic waters as previously evidenced in other environments (Dojka et al. 1998, He et al. 2007, Krzmarzick et al. 2013).

Elevated abundance and diversity of uncultivated candidate divisions were detected in the anoxic zone. Interestingly, only the candidate division TM6 could be detected both in oxic and anoxic conditions in Lake Kivu. Representatives of TM6 have been shown to be facultative anaerobes (McLean et al. 2013). However, candidate divisions such as OP3, OP9 and OP11 were mainly detected in the anoxic zone of Lake Kivu, as previously observed in Lake Pavin and Arctic Lake A (Lehours et al. 2007, Comeau et al. 2012). It has been shown that OP3 bacteria share a high proportion of orthologues with members of the *Deltaproteobacteria*, which might indicate that OP3 evolved metabolic capabilities similar to those of *Deltaproteobacteria* (Glöckner et al. 2010).

CONCLUSIONS

The stratification of microbial communities present in Lake Kivu indicated distinct environmental niches according to the different physico-chemical conditions along the water column with gradual transitions over distinct redox gradients (Canfield & Thamdrup 2009), as has also been reported in other lakes and marine systems (De Wever et al. 2005, Agogue et al. 2011, Peura et al. 2012). The present study evidenced clear differences in BCC and ACC between oxic surface waters and anoxic deep waters in Lake Kivu. Coexistence between key players of the C and S cycles seemed to be evident and need to be further evaluated. In addition, the high relative abundance of un-affiliated bacterial and archaeal OTUs retrieved from anoxic deep waters in the present study highlights the current lack of knowledge on microbial communities in anoxic deep environments, which requires further research. The discovery of yet-to-be-cultured microbial taxa and understanding their potential interactions and the role they play in microbial processes driving biogeochemical cycling are very important from an ecological point of view as well as for possible use of particular species in biotechnology. Deep-

sequencing technologies also provided us with profound information on rare taxa, which might be disproportionately active relative to their abundances (Jones & Lennon 2010, Campbell et al. 2011). To construct a complete picture of the ecological roles of the various microbial communities found at the different depths in this particular environment, RNA-based molecular studies (active community) coupled with measurements of the rates of key microbial processes are of further interest.

Acknowledgements. In addition to the authors of this paper, the Lake Kivu consortium includes the following individuals: S. Bouillon, C. Morana (Katholieke Universiteit Leuven), A.V. Borges, F. Roland (Université de Liège), B. Leporcq, K. de Saedeleer (Université de Namur), A. Anzil (Université Libre de Bruxelles) and M.V. Commarieu (Université de Liège). A.V. Borges is thanked for providing the CH₄ data. We are grateful to the DR Congo local team (G. Alunga, P. Masilya, M. Ishumbisho, B. Kaningini) and to the fishermen Silas and Djoba from DR Congo for their help during the field work. The consortium thanks the Rwanda Energy Company and Michel Halbwachs for free access to their industrial platform off Gisenyi. This work was funded by the Fonds National de la Recherche Scientifique (FNRS) under the MICKI (Microbial diversity and processes in Lake Kivu) project and the Belgian Federal Science Policy Office EAGLES (East African Great Lake Ecosystem Sensitivity to changes, SD/AR/02A) project, and contributes to the European Research Council starting grant project AFRIVAL (African river basins: Catchment-scale carbon fluxes and transformations, 240002). We also thank the 3 anonymous reviewers for their many insightful comments and suggestions that allowed improvement of the manuscript.

LITERATURE CITED

- ▶ Agogue H, Lamy D, Neal PR, Sogin ML, Herndl GJ (2011) Water mass-specificity of bacterial communities in the North Atlantic revealed by massively parallel sequencing. *Mol Ecol* 20:258–274
- ▶ Allgaier M, Grossart HP (2006) Diversity and seasonal dynamics of *Actinobacteria* populations in four lakes in northeastern Germany. *Appl Environ Microbiol* 72: 3489–3497
- ▶ Andersson AF, Riemann L, Bertilsson S (2010) Pyrosequencing reveals contrasting seasonal dynamics of taxa within Baltic Sea bacterioplankton communities. *ISME J* 4: 171–181
- ▶ Bastviken D, Ejlertsson J, Sundh I, Tranvik L (2003) Methane as a source of carbon and energy for lake pelagic food webs. *Ecology* 84:969–981
- ▶ Beal EJ, House CH, Orphan VJ (2009) Manganese- and iron-dependent marine methane oxidation. *Science* 325: 184–187
- ▶ Bhattarai S, Ross KA, Schmid M, Anselmetti FS, Bürgmann H (2012) Local conditions structure unique archaeal communities in the anoxic sediments of meromictic Lake Kivu. *Microb Ecol* 64:291–310
- ▶ Biddle JF, Lipp JS, Lever MA, Lloyd KG and others (2006) Heterotrophic Archaea dominate sedimentary subsur-

- face ecosystems off Peru. *Proc Natl Acad Sci USA* 103: 3846–3851
- ▶ Biddle JF, Cardman Z, Mendlovitz H, Albert DB, Lloyd KG, Boetius A, Teske A (2012) Anaerobic oxidation of methane at different temperature regimes in Guaymas Basin hydrothermal sediments. *ISME J* 6:1018–1031
 - ▶ Borges AV, Abril G, Delille B, Descy JP, Darchambeau F (2011) Diffusive methane emissions to the atmosphere from Lake Kivu (Eastern Africa). *J Geophys Res* 116, G03032, doi:10.1029/2011JG001673
 - ▶ Bougouffa S, Yang JK, Lee OO, Wang Y, Batang Z, Al-Suwailem A, Qian PY (2013) Distinctive microbial community structure in highly stratified deep-sea brine water columns. *Appl Environ Microbiol* 79:3425–3437
 - ▶ Callaway TR, Dowd SE, Edrington TS, Anderson RC and others (2010) Evaluation of bacterial diversity in the rumen and feces of cattle fed different levels of dried distillers grains plus soluble using bacterial tag-encoded FLX amplicon pyrosequencing. *J Anim Sci* 88:3977–3983
 - ▶ Campbell BJ, Engel AS, Porter ML, Takai K (2006) The versatile epsilon-proteobacteria: key players in sulphidic habitats. *Nat Rev Microbiol* 4:458–468
 - ▶ Campbell BJ, Yu L, Heidelberg JF, Kirchman DL (2011) Activity of abundant and rare bacteria in a coastal ocean. *Proc Natl Acad Sci USA* 108:12776–12781
 - ▶ Canfield DE, Thamdrup B (2009) Towards a consistent classification scheme for geochemical environments or why we wish the term 'suboxic' would go away. *Geobiology* 7: 385–392
 - Casamayor EO, Borrego CM (2009) Archaea. In: Likens GE (ed) *Encyclopedia of inland waters*, Vol 3. Elsevier, Oxford, p 167–181
 - Clarke KR, Gorley RN (2006) *PRIMER V6: user manual/tutorial*. PRIMER-E, Plymouth
 - ▶ Cline JD (1969) Spectrophotometric determination of hydrogen sulfide in natural waters. *Limnol Oceanogr* 14: 454–458
 - ▶ Comeau AM, Harding T, Galand PE, Vincent WF, Lovejoy C (2012) Vertical distribution of microbial communities in a perennially stratified Arctic lake with saline anoxic bottom waters. *Sci Rep* 2:604
 - ▶ Coolen MJL, Abbas B, van Bleijswijk J, Hopmans EC, Kuypers MMM, Wakeham SG, Sinninghe-Damste JS (2007) Putative ammonia-oxidizing Crenarchaeota in suboxic waters of the Black Sea: a basinwide ecological study using 16S ribosomal and functional genes and membrane lipids. *Environ Microbiol* 9:1001–1016
 - ▶ Cottrell MT, Kirchman DL (2003) Contribution of major bacterial groups to bacterial biomass production (thymidine and leucine incorporation) in the Delaware estuary. *Limnol Oceanogr* 48:168–178
 - Crowe SA, Katsev S, Leslie K, Sturm A and others (2011) The methane cycle in ferruginous Lake Matano. *Geobiology* 9:61–78
 - ▶ Darchambeau F, Sarmiento H, Descy JP (2014) Primary production in a tropical large lake: the role of phytoplankton composition. *Sci Total Environ* 473-474:178–188
 - ▶ De Wever A, Muylaert K, Pirlot S, Van der Gucht K and others (2005) Bacterial community composition in Lake Tanganyika: vertical and horizontal heterogeneity. *Appl Environ Microbiol* 71:5029–5037
 - ▶ Degens ET, von Herzen RP, Wong HK, Deuser WG, Jannasch HW (1973) Lake Kivu: structure chemistry and biology of an East African Rift Lake. *Geol Rundsch* 62: 245–277
 - ▶ Dojka MA, Hugenholtz P, Haack SK, Pace NR (1998) Microbial diversity in a hydrocarbon- and chlorinated-solvent-contaminated aquifer undergoing intrinsic bioremediation. *Appl Environ Microbiol* 64:3869–3877
 - ▶ Dowd SE, Callaway TR, Wolcott RD, Sun Y, McKeehan T, Hagevoort RG, Edrington TS (2008) Evaluation of the bacterial diversity in the feces of cattle using 16S rDNA bacterial tag-encoded FLX amplicon pyrosequencing bTEFAP. *BMC Microbiol* 8:125
 - ▶ Edgar RC, Haas BJ, Clemente JC, Quince C, Knight R (2011) UCHIME improves sensitivity and speed of chimera detection. *Bioinformatics* 27:2194–2200
 - Faust K, Sathirapongsasuti JF, Izard J, Segata N, Gevers G, Raes J, Huttenhower C (2012). Microbial co-occurrence relationships in the human microbiome. *PLoS Comput Biol* 8:e1002606
 - ▶ Galand PE, Casamayor EO, Kirchman DL, Lovejoy C (2009) Ecology of the rare microbial biosphere of the Arctic Ocean. *Proc Natl Acad Sci USA* 106:22427–22432
 - ▶ Galand PE, Potvin M, Casamayor EO, Lovejoy C (2010) Hydrography shapes bacterial biogeography of the deep Arctic Ocean. *ISME J* 4:564–576
 - ▶ Glaubitz S, Lueders T, Abraham WR, Jost G, Jürgens K, Labrenz M (2009) ¹³C-isotope analyses reveal that chemolithoautotrophic *Gamma*- and *Epsilonproteobacteria* feed a microbial food web in a pelagic redoxcline of the central Baltic Sea. *Environ Microbiol* 11:326–337
 - ▶ Glöckner J, Kube M, Shrestha PM, Weber M, Glöckner FO, Reinhardt R, Liesack W (2010) Phylogenetic diversity and metagenomics of candidate division OP3. *Environ Microbiol* 12:1218–1229
 - ▶ Grote J, Labrenz M, Pfeiffer B, Jost G, Jürgens K (2007) Quantitative distributions of *Epsilonproteobacteria* and a *Sulfurimonas* subgroup in pelagic redoxclines of the central Baltic Sea. *Appl Environ Microbiol* 73:7155–7161
 - ▶ He J, Holmes VF, Lee PKH, Alvarez-Cohen L (2007) Influence of vitamin B12 and cocultures on the growth of *Dehalococcoides* isolates in defined medium. *Appl Environ Microbiol* 73:2847–2853
 - Hinrichs KU, Boetius A (2002) The anaerobic oxidation of methane: new insights in microbial ecology and biochemistry. In: Wefer G, Billett D, Hebbeln D, Jørgensen BB, Schlüter M, Van Weering T (eds) *Ocean margin systems*. Springer-Verlag, Berlin, p 457–477
 - ▶ Holmer M, Kristensen E (1994) Co-existence of sulfate reduction and methane production in an organic-rich sediment. *Mar Ecol Prog Ser* 107:177–184
 - ▶ Hu A, Jiao N, Zhang R, Yang Z (2011) Niche partitioning of Marine Group I *Crenarchaeota* in euphotic and upper mesopelagic zones of the East China Sea. *Appl Environ Microbiol* 77:7469–7478
 - ▶ Humayoun SB, Bano N, Hollibaugh JT (2003) Depth distribution of microbial diversity in Mono Lake, a meromictic Soda Lake in California. *Appl Environ Microbiol* 69: 1030–1042
 - ▶ Inagaki F, Nunoura T, Nakagawa S, Teske A and others (2006) Biogeographical distribution and diversity of microbes in methane hydrate-bearing deep marine sediments on the Pacific Ocean Margin. *Proc Natl Acad Sci USA* 103:2815–2820
 - ▶ Isumbisho M, Sarmiento H, Kaningini B, Micha JC, Descy JP (2006) Zooplankton of Lake Kivu East Africa half a century after the Tanganyika sardine introduction. *J Plankton Res* 28:971–989
 - ▶ Jones SE, Lennon JT (2010) Dormancy contributes to the

- maintenance of microbial diversity. *Proc Natl Acad Sci USA* 107:5881–5886
- Kirchman DL, Cottrell MT, Lovejoy C (2010) The structure of bacterial communities in the western Arctic Ocean as revealed by pyrosequencing of 16S rRNA genes. *Environ Microbiol* 12:1132–1143
- Knittel K, Boetius A (2009) Anaerobic oxidation of methane: progress with an unknown process. *Annu Rev Microbiol* 63:311–334
- Krzmarzick MJ, McNamara PJ, Crary BB, Novak PJ (2013) Abundance and diversity of organohalide-respiring bacteria in lake sediments across a geographical sulfur gradient. *FEMS Microbiol Ecol* 84:248–258
- Kuivila KM, Murray JW, Devol AH (1990) Methane production in the sulfate depleted sediments of two marine basins. *Geochim Cosmochim Acta* 54:403–411
- Lehours AC, Evans P, Bardot C, Joblin K, Gérard F (2007) Phylogenetic diversity of archaea and bacteria in the anoxic zone of a meromictic lake (Lake Pavin, France). *Appl Environ Microbiol* 73:2016–2019
- Lliros M, Gich F, Plasencia A, Auguet JC and others (2010) Vertical distribution of ammonia-oxidizing Crenarchaeota and methanogens in the epipelagic waters of Lake Kivu (Rwanda-Democratic Republic of the Congo). *Appl Environ Microbiol* 76:6853–6863
- Lliros M, Descy JP, Libert X, Morana C and others (2012) Microbial ecology of Lake Kivu. In: Descy JP, Darchambeau F, Schmid M (eds) *Lake Kivu: limnology and biogeochemistry of a tropical great lake*. *Aquat Ecol Ser* 5. Springer, Dordrecht, p 85–105
- Logares R, Lindström ES, Langenheder S, Logue JB and others (2013) Biogeography of bacterial communities exposed to progressive long-term environmental change. *ISME J* 7:937–948
- Logue JB, Langenheder S, Andersson AF, Bertilsson S, Drakare S, Lanzén A, Lindström ES (2012) Freshwater bacterioplankton richness in oligotrophic lakes depends on nutrient availability rather than on species-area relationships. *ISME J* 6:1127–1136
- López-Gutiérrez JC, Henry S, Hallet S, Martin-Laurent F, Catrou G, Philippot L (2004) Quantification of a novel group of nitrate-reducing bacteria in the environment by real-time PCR. *J Microbiol Methods* 57:399–407
- Madrid V, Taylor G, Scranton M, Chistoserdov A (2001) Phylogenetic diversity of bacterial and archaeal communities in the anoxic zone of the Cariaco Basin. *Appl Environ Microbiol* 67:1663–1674
- Magurran AE, Henderson PA (2003) Explaining the excess of rare species in natural species abundance distributions. *Nature* 422:714–716
- McLean JS, Lombardo MJ, Badger JH, Edlund A and others (2013) Candidate phylum TM6 genome recovered from a hospital sink biofilm provides genomic insights into this uncultivated phylum. *Proc Natl Acad Sci USA* 110: E2390–E2399
- Miranda KM, Espey MG, Wink DA (2001) A rapid, simple spectrophotometric method for simultaneous detection of nitrate and nitrite. *Nitric Oxide* 5:62–71
- Morana C, Borges AV, Roland FAE, Darchambeau F, Descy JP, Bouillon S (2014) Methanotrophy within the water column of a large meromictic tropical lake (Lake Kivu, East Africa). *Biogeosci Discuss* 11:15663–15691
- Muyzer G, Stams AJM (2008) The ecology and biotechnology of sulfate-reducing bacteria. *Nat Rev Microbiol* 6: 441–454
- Pasche N, Schmid M, Vasquez F, Schubert CJ and others (2011) Methane sources and sinks in Lake Kivu. *J Geophys Res* 116, G03006, doi:10.1029/2011JG001690
- Pedrós-Alió C (2006) Marine microbial diversity: Can it be determined? *Trends Microbiol* 14:257–263
- Pedrós-Alió C (2012) The rare bacterial biosphere. *Annu Rev Mar Sci* 4:449–466
- Pester M, Bittner N, Deevong P, Wagner M, Loy A (2010) A 'rare biosphere' microorganism contributes to sulfate reduction in a peatland. *ISME J* 4:1591–1602
- Peura S, Eiler A, Bertilsson S, Nykänen H, Tirola M, Jones RI (2012) Distinct and diverse anaerobic bacterial communities in boreal lakes dominated by candidate division OD1. *ISME J* 6:1640–1652
- Quince C, Curtis TP, Sloan WT (2008) The rational exploration of microbial diversity. *ISME J* 2:997–1006
- Reeburgh WS (2007) Oceanic methane biogeochemistry. *Chem Rev* 107:486–513
- Rice EW, Baird RB, Eaton AD, Clesce LS (eds) (2012) *Standard methods for the examination of water and wastewater*, 22nd edn. APHA, Washington, DC
- Rinke C, Schwientek P, Sczyrba A, Ivanova NN and others (2013) Insights into the phylogeny and coding potential of microbial dark matter. *Nature* 499:431–437
- Sarmiento H, Isumbisho M, Descy JP (2006) Phytoplankton ecology of Lake Kivu eastern Africa. *J Plankton Res* 28: 815–829
- SCA (Standing Committee of Analysts) (1981) *Methods for the examination of waters and associated materials Ammonia in waters*. HMSO, London
- Schloss PD, Westcott SL, Ryabin T, Hall JR and others (2009) Introducing mothur: open-source platform-independent community-supported software for describing and comparing microbial communities. *Appl Environ Microbiol* 75:7537–7541
- Schmid M, Wüest A (2012) Stratification mixing and transport processes in Lake Kivu. In: Descy JP, Darchambeau F, Schmid M (eds) *Lake Kivu: limnology and biogeochemistry of a tropical great lake*. *Aquat Ecol Ser* 5. Springer: Dordrecht, p 13–30
- Schmid M, Tietze K, Halb wachs M, Lorke A, McGinnis D, Wüest A (2002) How hazardous is the gas accumulation in Lake Kivu? Arguments for a risk assessment in light of the Nyiragongo volcano eruption. *Acta Vulcanol* 14/15: 115–122
- Schmid M, Halb wachs M, Wehrli B, Wüest A (2005) Weak mixing in Lake Kivu: new insights indicate increasing risk of uncontrolled gas eruption. *Geochim Geophys Geosyst* 6, Q07009, doi:10.1029/2004 GC000892
- Segers R (1998) Methane production and methane consumption: a review of processes underlying wetland methane fluxes. *Biogeochemistry* 41:23–51
- Shade A, Kent AD, Jones SE, Newton RJ, Triplett EW, McMahon KD (2007) Interannual dynamics and phenology of bacterial communities in a eutrophic lake. *Limnol Oceanogr* 52:487–494
- Shannon P, Markiel A, Ozier O, Baliga NS and others (2003) Cytoscape: a software environment for integrated models of biomolecular interaction networks. *Genome Res* 13:2498–2504
- Sogin ML, Morrison HG, Huber JA, Welch DM and others (2006) Microbial diversity in the deep sea and the underexplored 'rare biosphere'. *Proc Natl Acad Sci USA* 103: 12115–12120

- ▶ Taipale S, Jones RI, Tirola M (2009) Vertical diversity of bacteria in an oxygen-stratified humic lake, evaluated using DNA and phospholipid analyses. *Aquat Microb Ecol* 55:1–16
- ▶ Thiery W, Martynov A, Darchambeau F, Descy JP, Plisnier PD, Sushama L, van Lipzig NPM (2014) Understanding the performance of the FLake model over two African Great Lakes. *Geosci Model Dev* 7:317–337
- ▶ Warnecke F, Sommaruga R, Sekar R, Hofer JS, Pernthaler J (2005) Abundances, identity, and growth state of Actinobacteria in mountain lakes of different UV transparency. *Appl Environ Microbiol* 71:5551–5559
- ▶ Werner JJ, Koren O, Hugenholtz P, DeSantis TZ and others (2012) Impact of training sets on classification of high-throughput bacterial 16s rRNA gene surveys. *ISME J* 6: 94–103
- ▶ Wright JJ, Konwar KM, Hallam SJ (2012) Microbial ecology of expanding oxygen minimum zones. *Nat Rev Microbiol* 10:381–394
- ▶ Yakimov MM, La Cono V, Denaro R, D'Auria G and others (2007) Primary producing prokaryotic communities of brine interface and seawater above the halocline of deep anoxic lake L'Atalante Eastern Mediterranean Sea. *ISME J* 1:743–755

*Editorial responsibility: Tom Fenchel,
Helsingør, Denmark*

*Submitted: August 19, 2014; Accepted: November 26, 2014
Proofs received from author(s): March 9, 2015*

Distribution of *Bacteria* and *Archaea* in meromictic tropical Lake Kivu (Africa)

Özgül İnceoğlu¹, Marc Llíros^{2,5}, Tamara García-Armisen¹, Sean A. Crowe³,
Celine Michiels^{1,3}, François Darchambeau⁴, Jean-Pierre Descy², Pierre Servais^{1,*}

¹Ecologie des Systèmes Aquatiques, Campus Plaine, CP 221, Université Libre de Bruxelles, 1050 Brussels, Belgium

²Laboratory of Freshwater Ecology, Université de Namur, 61 rue de Bruxelles, 5000 Namur, Belgium

³Departments of Microbiology and Immunology, and Earth, Ocean and Atmospheric Sciences,
University of British Columbia, V6T 1Z4 Vancouver, Canada

⁴Chemical Oceanography Unit, Université de Liège, 4000 Liège, Belgium

⁵Present address: Department of Genetics and Microbiology, Universitat Autònoma de Barcelona, 08193 Bellesguard, Catalonia, Spain

ABSTRACT: Lake Kivu is a meromictic lake in East Africa with enormous amounts of dissolved methane (CH₄) and carbon dioxide (CO₂) in its deep waters and surprisingly low CH₄ in the surface waters. We applied 454 pyrosequencing of 16S rRNA gene fragments to study the bacterial and archaeal community compositions (BCC and ACC, respectively) to provide insight into the ecology of the microbes in Lake Kivu. The vertical distribution of electron donors and acceptors in the chemically stratified water column may be responsible for the stratified distribution of microbial populations, suggesting well-defined functional specialization. The highest microbial richness was detected in the anoxic zone, which hosted high percentages of bacterial sequences related to uncultured and poorly described phyla. This suggests an under-representation of anoxic environments in current databases and the presence of previously undescribed taxa. Microbial diversity is made up of 2 fractions: abundant species (e.g. Galand et al. 2009) and rare species. Abundant species were more stable than rare species over time. The detection of rare candidate divisions (e.g. OP3, WS3, GN02) co-occurring with sulphur-oxidising *Epsilonproteobacteria*, sulphate-reducing *Deltaproteobacteria*, hydrogen-oxidising *Dehalococcoidetes* and methanogens might indicate interactions in the carbon and sulphur cycles in the anoxic waters.

KEY WORDS: Microbial community · Stratified lake · Diversity · Network · Pyrosequencing · qPCR

Resale or republication not permitted without written consent of the publisher

INTRODUCTION

Meromictic Lake Kivu, located in the volcanic region between Rwanda and the Democratic Republic of the Congo, has a permanent vertical density stratification that separates a seasonally mixed layer (or mixolimnion) with a maximum depth of 65 m from a permanently anoxic zone (or monimolimnion) rich in dissolved salts, carbon dioxide (CO₂) and methane (CH₄). Lake Kivu has garnered attention as a unique ecosystem with one of the largest CH₄ reservoirs in the world (Schmid et al. 2002, 2005). However, the

CH₄ concentrations in the oxic zone are surprisingly low compared to other lakes worldwide (Borges et al. 2011). This might be due to intense bacterial oxidation given that CH₄ diffuses from the depths towards the surface (Borges et al. 2011, Pasche et al. 2011). Furthermore, Lake Kivu has high vertical stability of the water masses and physico-chemical gradients. Variation of the vertical position of the oxic-anoxic interface over time is driven by contrasting precipitation and wind speed regimes between rainy (October–May) and dry (June–September) seasons (Thiery et al. 2014), the latter being characterised by

*Corresponding author: pservais@ulb.ac.be

a deepening of the oxic zone. Several sources of groundwater enter the lake at various depths, which explains the strong gradients observed in the vertical profiles of salinity, temperature and concentrations of dissolved gases (Degens et al. 1973, Schmid et al. 2005, Bhattarai et al. 2012).

Hence, these contrasting conditions might influence the vertical distributions and the level of microbial abundance. However, in contrast to diversity and activity studies of phytoplankton and zooplankton in the mixolimnion of Lake Kivu (Isumbisho et al. 2006, Sarmiento et al. 2006, Darchambeau et al. 2014), very few data are available on the distribution, composition and diversity of the bacterial and archaeal communities present in the lake's water column (Llirós et al. 2010, 2012, Pasche et al. 2011). Moreover, the main focus of these studies was the most abundant members of the microbial communities due to the limitations of the molecular tools used (Llirós et al. 2010, 2012). Although the most abundant species are thought to be the most active and most important in biogeochemical cycles (Cottrell & Kirchman 2003), they account for only a small proportion of microbial diversity. It is now recognised that microbial diversity is made up of 2 fractions: abundant species (e.g. Galand et al. 2009) and rare species (seed bank; Pedrós-Alió 2006, Sogin et al. 2006). Recent advances in high-throughput sequencing technologies (e.g. 454 pyrosequencing) make it possible to describe microbial communities on a scale fine enough to account for rare taxa.

To shed light on patterns and dynamics of microbial diversity in Lake Kivu, the horizontal (2 distinct lake locations) and temporal (3 sampling periods, covering the 2 main seasons) dynamics of the bacterial (BCC) and archaeal (ACC) community composition in 3 water zones of Lake Kivu were studied by means of 16S rRNA gene amplicon 454 pyrosequencing. Network analysis was further used to show the co-occurrence patterns of abundant and rare operational taxonomic units (OTUs) and to reveal their potential roles in microbial processes controlling the main biogeochemical cycles (i.e. C and S) in Lake Kivu.

MATERIALS AND METHODS

The following sections summarise the methods used in this study. More detailed information is provided in the section 'Materials and methods' of the Supplement available at www.int-res.com/articles/suppl/a074p215_supp.pdf.

Sampling sites and chemical analyses

Lake Kivu is located between Rwanda and the Democratic Republic of the Congo at 1463 m above sea level with maximum depth of 485 m in the northern basin. It has a surface area of 2370 km² and a total volume of 580 km³. Further details on the hydrology, physico-chemistry and biology of the lake have been published previously (Isumbisho et al. 2006, Sarmiento et al. 2006, Schmid & Wüest 2012).

To cover the horizontal and vertical heterogeneity of the lake's water column, 2 stations were sampled, 1 in the northern (off Gisenyi; 29.07° E, 1.77° S) and 1 in the southern (Ishungu; 29.12° E, 1.45° S) basins. Water samples were collected on 3 occasions; 2 during the dry season (October 2010 and June 2011) and 1 during the rainy season (February 2012). Vertical depth profiles of temperature, conductivity, pH and dissolved oxygen (DO) were measured *in situ* with a YSI 6600 V2 (Yellow Spring Instruments) multiparametric probe. Up to 20 discrete depths were sampled along a vertical profile between 10 and 100 m to cover the entire gradient of oxygen concentrations, from oxic to anoxic waters; only the upper layer of the anoxic layer was thus sampled. Water samples for chemical and microbiological analyses were collected using a 7.5 l Niskin bottle and stored in 4 l plastic containers for chemical analyses and 2 l Nalgene plastic bottles for biological analyses and kept at 4°C in a portable cooling box until further processing. The concentration of CH₄ was measured using the headspace technique with a gas chromatograph combined with a flame ionisation detector as previously described (Borges et al. 2011). Samples for NO_x (NO₃⁻ and NO₂⁻) and SO₄²⁻ were filtered directly through 0.2 µm pore size cellulose acetate syringe filters and were stored frozen until analysis with no preservative. NH₄⁺ concentrations were determined using the dichloroisocyanurate-salicylate-nitroprusside colorimetric method (SCA 1981). NO₂⁻ concentrations were determined using the sulphanilamide colouration method (Eaton et al. 2012). NO₃⁻ concentrations were determined after vanadium reduction to nitrite and quantified in this form following the nitrite determination procedure (Miranda et al. 2001, Eaton et al. 2012). SO₄²⁻ concentrations were measured using ion chromatography. Samples for H₂S determination were not filtered but preserved in zinc acetate and stored frozen. H₂S concentrations were measured spectrophotometrically (Cline 1969). The detection limits for these methods were 0.5 nM for CH₄ and 0.3, 0.03, 0.1, 2 and 0.5 µM for NH₄⁺, NO₂⁻, NO₃⁻, SO₄²⁻ and H₂S, respectively.

Nucleic acid extraction and quantitative real-time PCR

Water samples (0.5–1.0 l) for nucleic acid extraction were processed as described by Llirós et al. (2010).

The abundance of 16S rRNA bacterial and archaeal genes were determined by quantitative polymerase chain reaction (qPCR) using the primer combinations 341f–534r (López-Gutiérrez et al. 2004) and 519f–915r (Coolen et al. 2007), respectively. qPCR amplifications were performed in triplicate for both standard and unknown templates in a StepOne real-time PCR system (Applied Biosystems). Standard curves were generated from serial dilutions of previously titrated suspensions of conventionally PCR-amplified environmental clones.

16S rRNA bacterial and archaeal pyrosequencing

DNA extractions from each water depth and sampling site were analysed by means of bacterial and archaeal tag-encoded FLX amplicon pyrosequencing (bTEFAP and aTEFAP, respectively) as previously described (Dowd et al. 2008, Callaway et al. 2010). The bTEFAP was based upon the variable regions V1–V3 in the 16S rRNA gene using the 27F (5'-GAG TTT GAT CNT GGC TCA G-3') and 519R (5'-GWN TTA CNG CGG CKG CTG-3') primers, whereas aTEFAP used ARCH 349F (5'-GYG CAS CAG KCG MGA AW-3') and ARCH 806R (5'-GGA CTA CVS GGG TAT CTA AT-3') primers for *Archaea*. Bacterial and archaeal pyrosequencing were done based upon procedures developed by and performed at Research and Testing Laboratory (RTL; Lubbock, TX, USA) based upon RTL protocols.

Pyrosequencing data analyses

All sequences generated in this study can be downloaded from the National Center for Biotechnology Information (NCBI) Short Read Archive, accession number: SRA062980. Pyrosequencing data were processed using Mothur (Schloss et al. 2009). To minimise the effects of random sequencing errors, a denoising algorithm included in the pipeline was used, and low-quality sequences were removed by eliminating those without an exact match to the forward primer, without a recognisable reverse primer, with a length shorter than 200 nucleotides and those containing any ambiguous base calls. We trimmed

the barcodes and primers from the resulting sequences. Chimeras (checked using Uchime software; Edgar et al. 2011) and contaminants (understood as unclassified or misclassified sequences after comparing candidate sequences against the latest SILVA or RDP training set with cutoff values of 80 for both *Bacteria* and *Archaea*, respectively) were removed from sequence collection files. After taxonomic classification of the sequences down to phylum, class and genus level, the relative abundance of a given phylogenetic group was set as the number of sequences affiliated with that group divided by the total number of sequences per sample to normalize the dataset. Due to the advantages of using the largest and most diverse sets available, the latest Greengenes and SILVA were used for classification as bacterial and archaeal 16S rRNA gene sequence databases, respectively, at 80 % confidence threshold with Mothur (Werner et al. 2012). Sequences were clustered into operational taxonomic units (OTUs) by setting a 0.03 distance limit (equivalent to 97 % similarity). Rarefaction curves based on identified OTUs, Shannon diversity index and species richness estimator of Chao1 were generated in Mothur for each sample. To test for differences between water zones and reduce sampling effort influences, all bacterial samples were randomly subsampled to the same size according to the sample with the smallest sampling size (i.e. the smallest number of reads). In turn, no random subsampling was carried out for all archaeal datasets due to the low diversity values within oxic samples and the high observed richness coverage values (see Table 2).

Statistical analyses

Unless otherwise stated, all statistical analyses were performed using PRIMER 6 (Clarke & Gorley 2006). The relative abundance of bacteria and archaea at the phylum, genus and OTU (97 % cut off) levels were square-root transformed, and dissimilarities between samples were computed using the Bray-Curtis similarity coefficient. Dendrograms were generated based on the Bray-Curtis similarity index using complete linkage clustering to visualise the relationships between communities. The effect of time, location and DO conditions on BCC and ACC were tested with 1-way analysis of similarities (ANOSIM). Relative abundances of phyla per sample were visualised as a bubble chart using the bubble.pl.program (www.cmde.science.ubc.ca/hallam/bubble.php).

For network inference, OTUs occurring fewer than 5 times in the whole data set were removed, and Pearson's rank correlations were calculated between remaining OTUs using the CoNet program (Faust et al. 2012), when the coefficient (r) was both above 0.8 and statistically significant (p value 0.01). The results were then translated into an association network using Cytoscape 2.6.3 (Shannon et al. 2003, Faust et al. 2012). Cytoscape depicts taxa as nodes connected by lines that denote the positive correlations between them. In the network, the size of each node is proportional to the number of connections (that is, the degree), and the size of each edge is proportional to the strength of the correlations.

In addition, Venn diagrams were used to show the distribution of OTUs between the 3 sampling campaigns in the oxic, transition and anoxic zones. Abundant OTUs were defined as those taxa containing more than 6 sequences at each depth, whereas rare OTUs were defined as those taxa represented by fewer than 6 sequences at each depth (Magurran & Henderson 2003). In turn, habitat generalists were defined as those OTUs appearing in more than 15 samples (i.e. depths) across the 3 sampling campaigns, and habitat specialists were those OTUs that were locally abundant ($>0.5\%$ of relative abundance) and appeared in fewer than 6 samples (Logares et al. 2013). Additionally, OTUs appearing in 6 to 15 samples were defined as imperfect generalists (able to grow under most environmental conditions and not in others) in the present study.

RESULTS

Environmental parameters along the water column

The water column of Lake Kivu is complex with vertical gradients of temperature, conductivity and DO, as well as CH_4 , NH_4 and H_2S (Fig. 1). The first 100 m of the water column of Lake Kivu were separated into 3 distinct water zones according to DO criteria established previously (Wright et al. 2012), resulting in an oxic surface zone ($\text{DO} > 90 \mu\text{M}$), a transition zone (DO between 1 and $90 \mu\text{M}$) and a deep anoxic zone ($\text{DO} < 1 \mu\text{M}$; Fig. 1). Oxic surface waters were characterised by low nitrogen and CH_4 concentrations, whereas the anoxic deep waters were characterised by high concentrations of NH_4 , and dissolved CO_2 and CH_4 . Oxidised inorganic forms of N (NO_x^-) showed maximum values in the transition zone, whereas high concentrations of H_2S (Fig. 1) and CH_4 were only observed in the anoxic waters. The mixed oxic zone appeared to

be slightly deeper in October 2010 than during the 2 other sampling campaigns (Fig. 1).

Microbial abundance analyses

The numbers of bacterial 16S rRNA gene copies ranged between ca. 10^4 and 10^6 ml^{-1} for the Gisenyi and Ishungu water samples in June 2011 and February 2012. On the other hand, the numbers of archaeal 16S rRNA gene copies ranged between ca. 10^2 and 10^5 ml^{-1} in June 2011 and February 2012 at both sampled stations (Fig. 2). No qPCR analyses were conducted on October 2010 samples due to technical problems. In general, vertical depth profiles for bacterial and archaeal 16S rRNA gene copy numbers showed similar patterns with no or slight differences between each of the 3 water zones defined at each sampling station and time. In contrast to other sampling times, no decrease was observed in the transition zone in Gisenyi in June 2011. Furthermore, 16S rRNA gene copies detected for both bacteria and archaea were fairly constant with depth in oxic and anoxic waters during June and February in Ishungu, whereas 16S rRNA gene copies showed more variation with depth in Gisenyi (Fig. 2).

Bacterial and archaeal diversity analysis

The stratification based on DO concentrations was found as the strongest predictor of the overall BCC structure (Figs. 3 & 4; $R = 0.527$, $p = 0.001$), followed by temporal and then by horizontal variation (Table 1). Clustering analysis of the BCC revealed the presence of 9 sub-clusters, 2 of which were exclusively composed of samples from the oxic zone, and 3 clusters contained only samples from anoxic depths. In turn, those samples from the transition zone occupied transitional sub-clusters containing samples from both oxic and anoxic zones. However, the results were less evident for the ACC, although anoxic water samples clearly clustered apart from oxic samples (Fig. 4). ANOSIM also highlighted the similarity between oxic and transition archaeal communities as well as

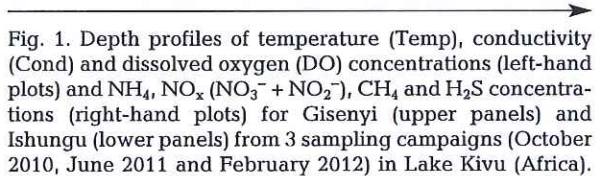


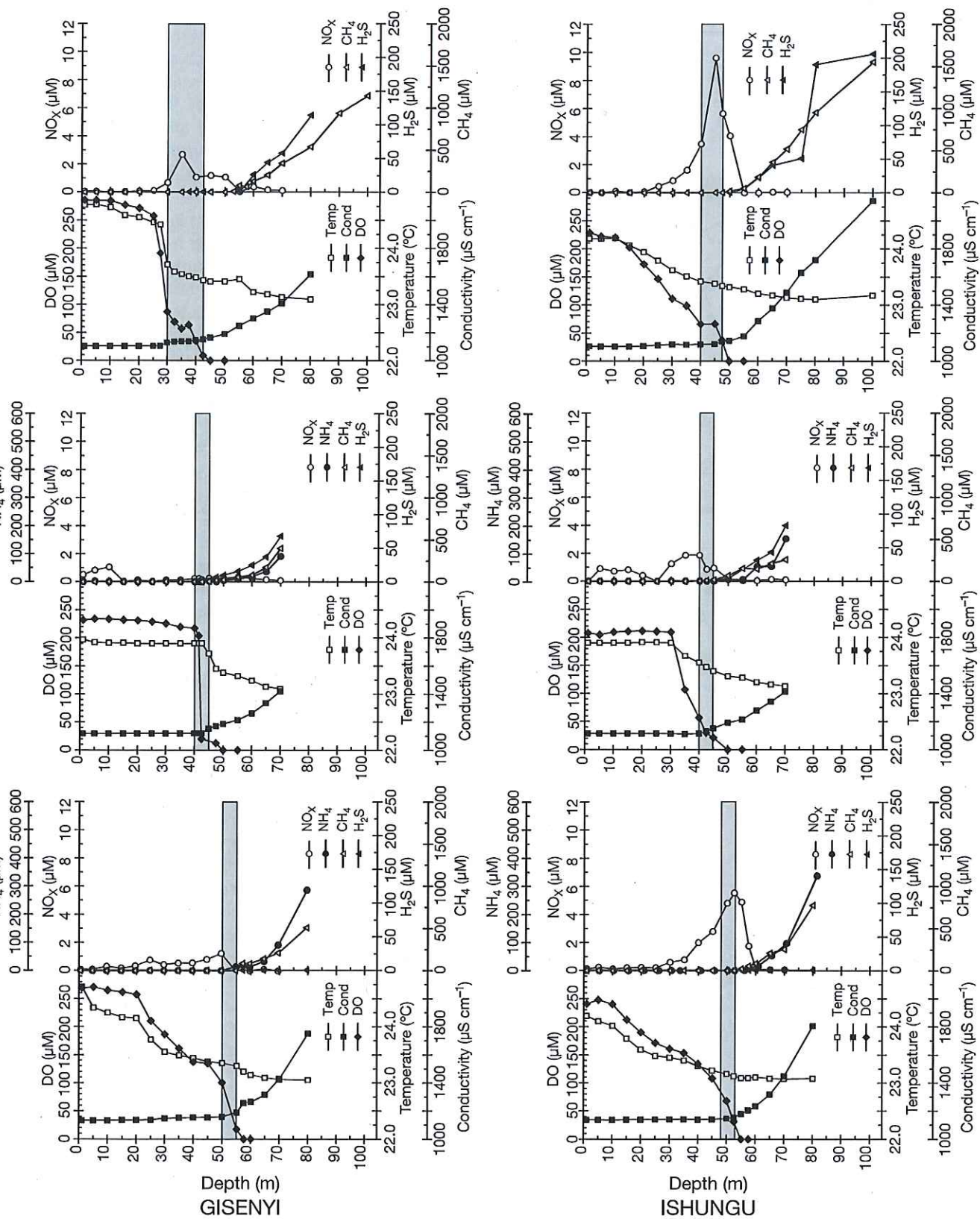
Fig. 1. Depth profiles of temperature (Temp), conductivity (Cond) and dissolved oxygen (DO) concentrations (left-hand plots) and NH_4 , NO_x ($\text{NO}_3^- + \text{NO}_2^-$), CH_4 and H_2S concentrations (right-hand plots) for Gisenyi (upper panels) and Ishungu (lower panels) from 3 sampling campaigns (October 2010, June 2011 and February 2012) in Lake Kivu (Africa).

Grey shading depicts the transition zone

Feb 2012

Jun 2011

Oct 2010



Depth (m)
GISENYI

Depth (m)
ISHUNGU

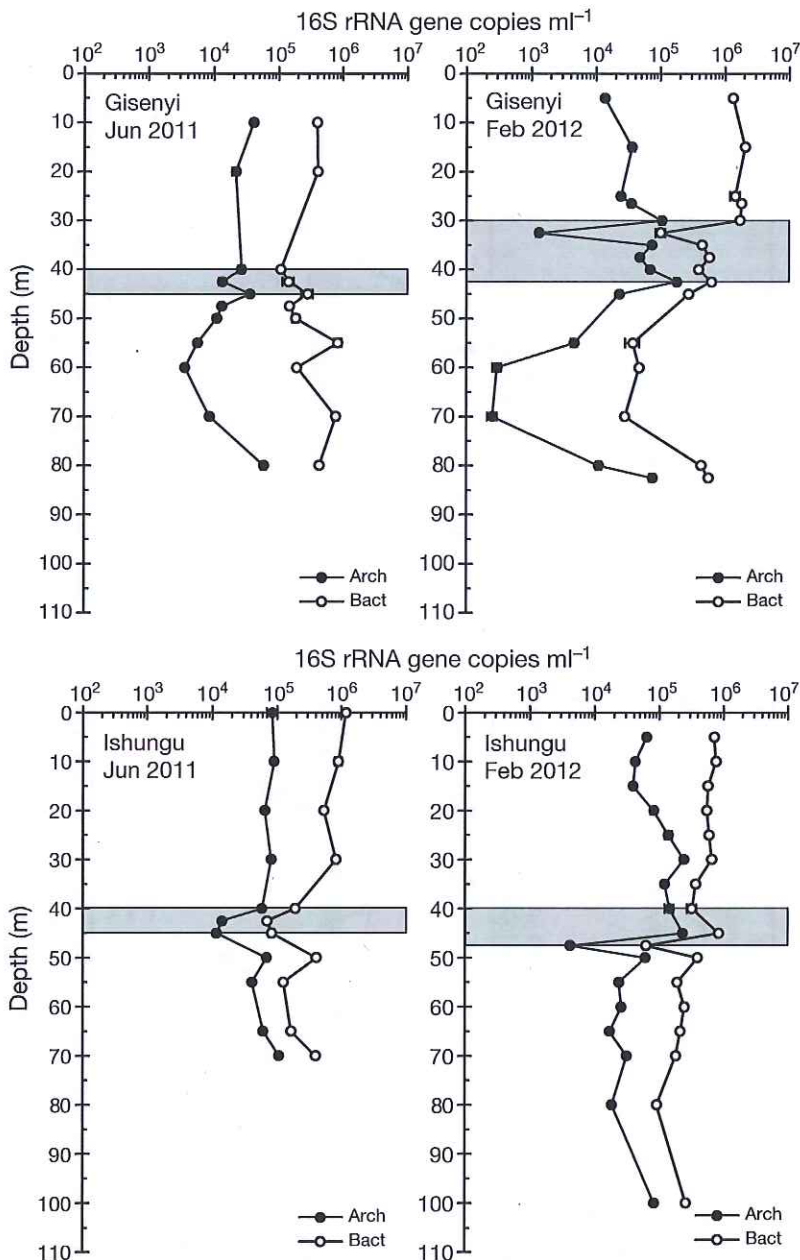


Fig. 2. Bacterial (Bact) and archaeal (Arch) abundances determined by 16S rDNA gene qPCR for 2 sampling campaigns (June 2011 and February 2012) in Lake Kivu. Grey shading depicts the transition zone

significant variations of the ACC between sampling stations, whereas no clear effects between sampling seasons were observed (Table 1).

Richness and diversity estimates

Based upon hierarchical clustering analysis, those samples corresponding to previously defined water

compartments (i.e. oxic, transition and anoxic zones) were pooled for each location and each sampling campaign (18 groups of sequences). We used 44 883 (between 842 and 7513 per group) bacterial and 10 323 (between 1 and 1498 per group) archaeal reads for richness and diversity estimates (Table 2).

Across all samples, rank abundance distributions best fitted the power law model, which indicates a community composed of a few highly dominant species next to a long tail of rare species (data not shown; $R \geq 0.91$). Although the dominance of a single bacterial OTU was not observed, the most abundant bacterial OTUs found were those affiliated with unclassified *Actinobacteria* (CL500-29 group; 14%) and *Cyanobacteria* (*Synechococcaeae*; 15%). Archaeal data sets demonstrated the dominance of a few OTUs affiliated with the uncultured GOM Arc I *Methanosarcinales* group (*Euryarchaeota*) for each sampling site. In Gisenyi, a single OTU represented up to 31% of all archaeal sequences, while 2 OTUs each represented ca. 10% of all archaeal sequences in Ishungu.

Rarefaction analysis, based on OTUs, indicated that most of the bacterial samples may require deeper sequencing to avoid underestimation of microbial diversity present in the samples (8894 OTUs in all samples analysed; Fig. S1A in the Supplement), whereas archaeal rarefaction curves (Fig. S1B in the Supplement) together with archaeal coverage values (up to 100%, Table 2) showed that the sequencing effort captured most of the richness present in Lake Kivu for this domain

with a few exceptions in October 2010 (with a total of 515 OTUs; Fig. S1B, Table 2). When all the bacterial samples were sub-sampled randomly to the same size based on the smallest sample, the number of observed bacterial OTUs per zone (oxic, transition and anoxic zones) ranged from 320 to 836 in Gisenyi and 235 to 587 in Ishungu over the 3 sampling campaigns (Table 2), while observed archaeal OTUs per zone ranged from 4 to 153 in Gisenyi and 1 to 306 in

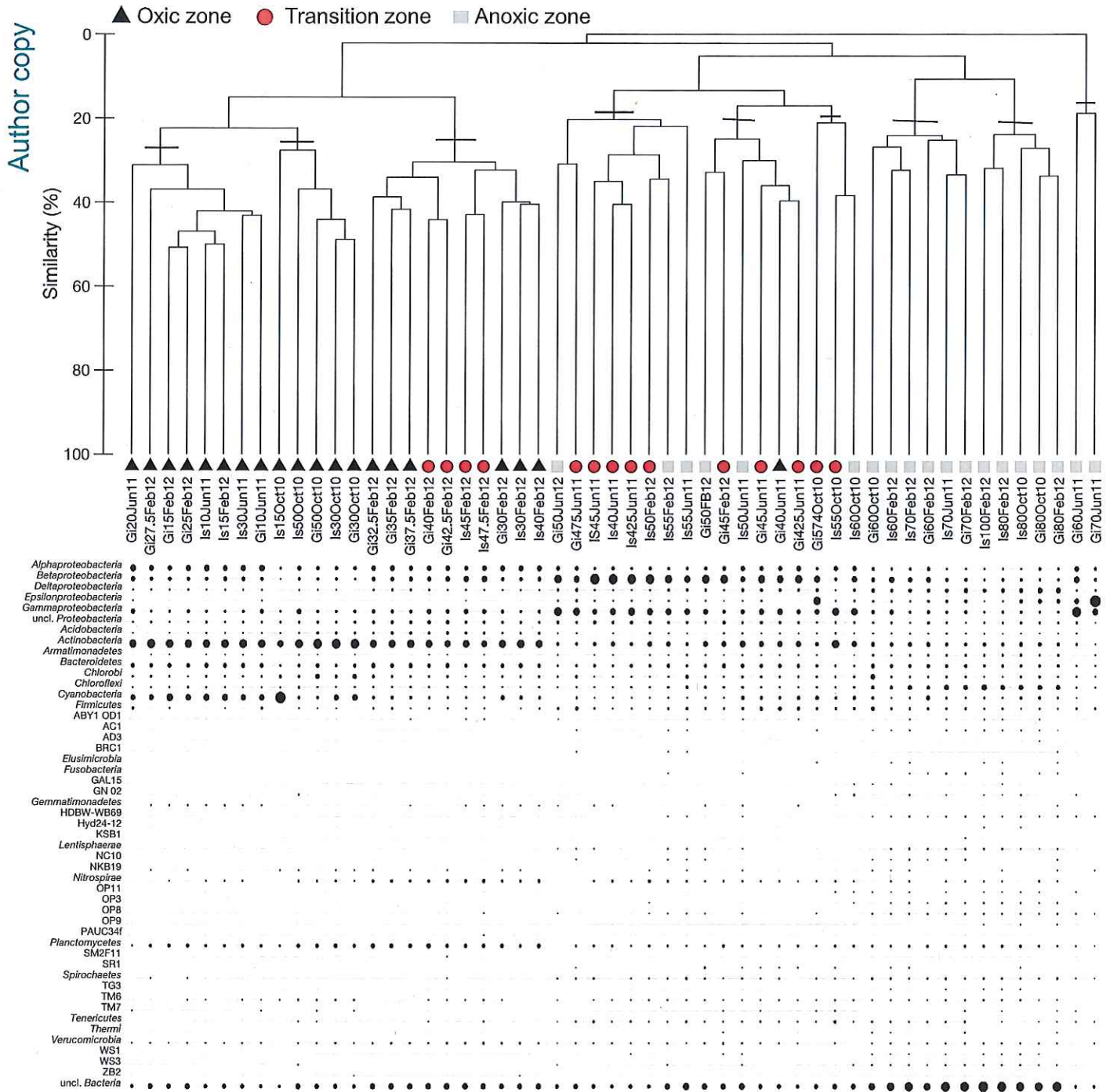


Fig. 3. Dot plot of relative abundance of bacterial taxa along the vertical profile in Gisenyi and Ishungu over the 3 sampling campaigns at the phylum level. Samples are organised according to the similarity of their community composition at the operational taxonomic unit (OTU) level, as revealed by hierarchical clustering of the distribution of taxonomic groups across environmental samples. Zones based on oxygen concentrations are distinguished (oxic [$>90 \mu\text{M}$], transition [$1-90 \mu\text{M}$], anoxic [$<1 \mu\text{M}$]). Oct10: October 2010; Jun11: June 2011; Fb12: February 2012; Is: Ishungu; Gi: Gisenyi; uncl.: unclassified

Ishungu for each of the 3 sampling campaigns (Table 2). Both BCC and ACC revealed a significant increase of richness with depth at both sampling sta-

tions (Table 2, $p < 0.05$). Without sub-sampling to the same sampling size, the highest bacterial richness estimation was also observed in the anoxic zone: for

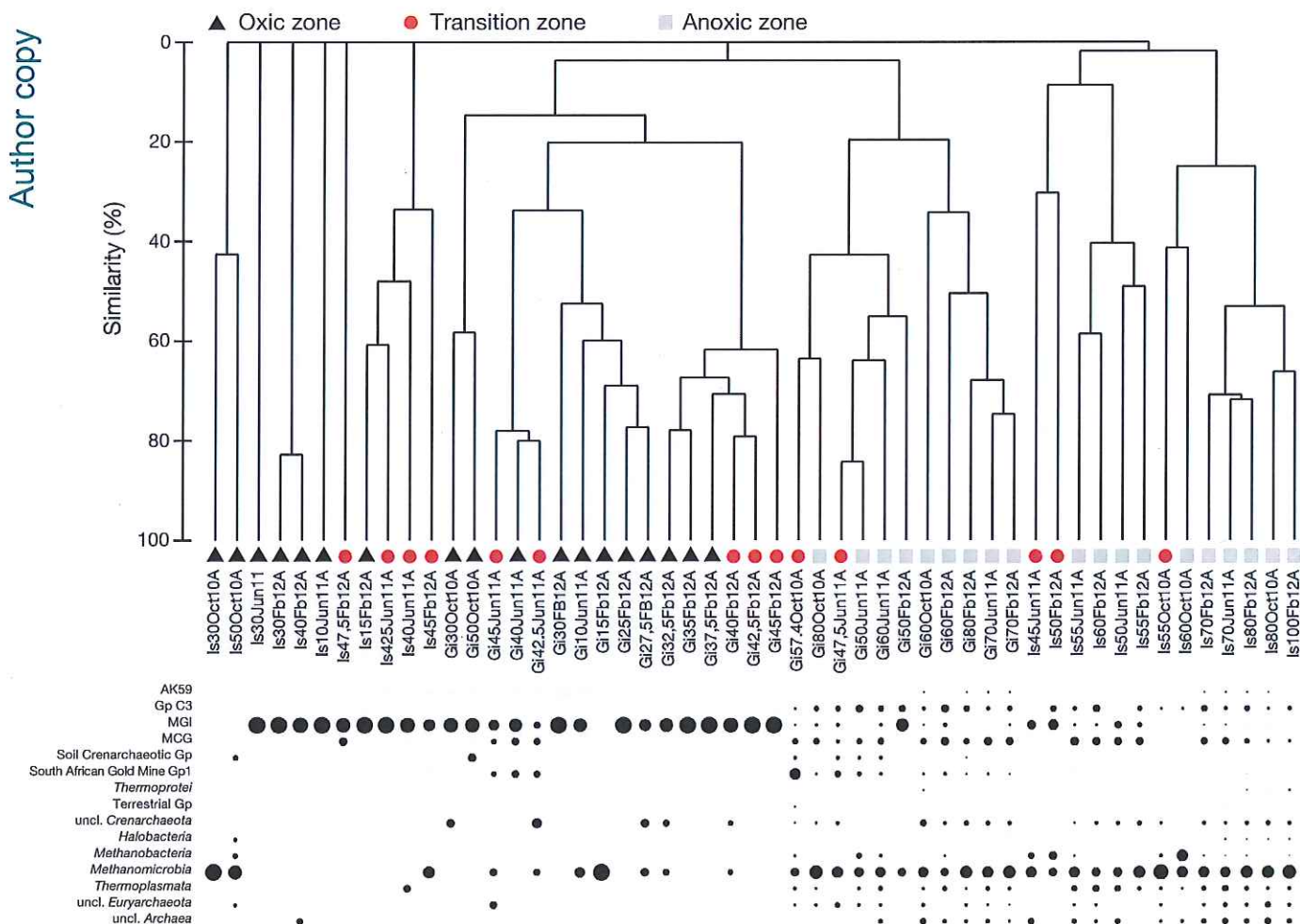


Fig. 4. Dot plot of relative abundance of archaeal taxa along the vertical profile in Gisenyi and Ishungu over the 3 sampling campaigns at the phylum level. Samples are organised according to the similarity of their community composition at the OTU level, as revealed by hierarchical clustering of the distribution of taxonomic groups across environmental samples. See Fig. 3 for other details

instance, 8758 OTUs were detected in the Ishungu anoxic zone in February, while there were only 1732 in the oxidic zone (Table S1 in the Supplement). Furthermore, bacterial OTUs were more evenly distributed in the anoxic water compartment than in the other 2 analysed water compartments. In contrast, archaeal OTUs evidenced a more even distribution in the oxidic and transition water compartments than in the anoxic zone. The lowest coverage values of observed bacterial richness were also observed in the anoxic zone (Table 2).

BCC analysis

All qualified reads could be assigned as *Bacteria*, but 10 to 53 % of the analysed sequences per sample could not be assigned to any phylum (Fig. 3). Differ-

ent phyla dominated the different depths analysed. The relative abundance of unclassified bacteria was higher in the anoxic zone (Fig. 3). Altogether, 38 bacterial phyla were recovered from Gisenyi, whereas 41 phyla were recovered from Ishungu. *Actinobacteria*, *Bacteroidetes*, *Chlorobi*, *Chloroflexi* and *Proteobacteria* (*Alpha*-, *Beta*- and *Gammaproteobacteria*) were found in the 3 zones at both stations at all sampling times. Candidate phyla such as BRC1, OP3, OP9, OP10, GAL15 and GN02 were mainly detected in the anoxic zone with a relative abundance below 1%, and *TM6* was mainly detected in the oxidic zone.

At both sampling stations, *Actinobacteria* was the dominant phylum in the oxidic zone (up to 44 % of the total bacterial sequences). *Cyanobacteria* (up to 18 % and 62 % in Gisenyi and Ishungu, respectively) and *Alphaproteobacteria* were also highly represented in the oxidic zone, and their relative abundance decreased

Table 1. Analysis of similarities (ANOSIM) significance values based on operational taxonomic units (OTUs) to evaluate the variation of bacterial and archaeal community composition in Lake Kivu. Significant R values are highlighted in bold. DO: dissolved oxygen

Test for differences between	Bacteria		Archaea	
	R	p	R	p
Water zones based on DO concentrations				
Global test	0.527	0.001	0.287	0.001
Pairwise test				
Oxic-Transition	0.699	0.001	0.075	0.077
Oxic-Anoxic	0.692	0.001	0.466	0.05
Transition-Anoxic	0.550	0.001	0.330	0.1
Sampling time				
Global test	0.437	0.001	0.057	0.1
Pairwise test				
January-October	0.442	0.002	0.074	0.11
January-February	0.476	0.001	0.024	0.24
October-February	0.475	0.002	0.097	0.09
Sampling locations				
Global test	0.061	0.05	0.063	0.001

with depth at both sampling stations; they were replaced by different phyla and members of the proteobacterial class at deeper levels (Fig. 3). Furthermore, the highest relative abundance of *Betaproteobacteria* was detected in the transition zone (up to 28 and 46% in Gisenyi and Ishungu, respectively).

High relative abundance of *Gammaproteobacteria* was detected both in the transition and the anoxic zones at both sampling sites. In turn, *Delta-* and *Epsilonproteobacteria* were mainly detected in the anoxic zone. In contrast to other phyla, higher relative abundances of *Epsilonproteobacteria* were detected in Gisenyi (up to 71%) than in Ishungu anoxic waters. In addition, relative abundance of *Epsilonproteobacteria* was lower in February in Gisenyi, in comparison with the 2 previous sampling campaigns.

ACC analysis

Only 10% of the reads could be assigned to any archaeal phyla. Of all sequences retrieved from Gisenyi and Ishungu, 7.3% and 6.3% were not classified in any archaeal phyla. The highest numbers of non-affiliated sequences were recovered from the deepest depths sampled. All retrieved archaeal amplicons spanned over archaeal lineages covering *Thaumarchaeota*, *Crenarchaeota* and *Euryarchaeota* within both cultured (e.g. Marine Group I *Crenarchaeota* [MGI] or *Methanobacteria*) and uncultured groups (e.g. Miscellaneous Crenarchaeotic Group (MCG) or Deep Sea Hydrothermal Ventic Group 6; Fig. 4).

Table 2. Diversity indices for bacterial and archaeal operational taxonomic units (OTUs) in the water zones analysed defined according to dissolved oxygen concentrations in Lake Kivu. We analysed 1337 bacterial and 3730 archaeal sequences in Gisenyi and 842 bacterial and 4382 archaeal sequences in Ishungu. Sobs: number of observed species; Chao1: Chao1 richness estimate; Shannon: diversity index; Shannoneven: species evenness index; Coverage: non-parametric coverage estimator; nd: not determined

	Bacteria					Archaea				
	Sobs	Chao1	Shannon	Shannoneven	Coverage	Sobs	Chao1	Shannon	Shannoneven	Coverage
Gisenyi										
Oxic-Oct10	320	732	4.58	0.79	0.86	nd	nd	nd	nd	nd
Oxic-Jun11	465	1250	5.26	0.86	0.76	4	4	1.21	0.87	0.75
Oxic-Feb12	538	1351	5.51	0.88	0.73	4	4	1.33	0.96	0.67
Transition-Oct10	357	764	4.78	0.81	0.84	4	6	1.33	0.96	0.4
Transition-Jun11	600	1881	5.74	0.90	0.68	22	43	2.87	0.93	0.59
Transition-Feb12	648	1647	5.9	0.91	0.67	16	19	2.44	0.88	0.87
Anoxic-Oct10	628	1736	5.86	0.91	0.68	153	373	3.34	0.66	0.92
Anoxic-Jun11	680	2431	5.89	0.90	0.62	94	235	3.44	0.76	0.92
Anoxic-Feb12	836	2778	6.43	0.96	0.52	152	225	2.91	0.58	0.96
Ishungu										
Oxic-Oct10	235	550	4.12	0.75	0.82	1	1	0.00	1.00	0.00
Oxic-Jun11	309	748	4.82	0.84	0.75	2	2	0.69	1.00	1.00
Oxic-Feb12	320	913	5.00	0.87	0.74	6	6	1.72	0.96	0.82
Transition-Oct10	380	890	5.33	0.90	0.70	8	10	1.79	0.86	0.79
Transition-June11	401	1159	5.42	0.90	0.66	14	41	2.48	0.94	0.45
Transition-Feb12	425	1217	5.59	0.92	0.64	8	10	1.79	0.86	0.76
Anoxic-Oct10	477	1878	5.73	0.93	0.56	100	157	3.86	0.84	0.90
Anoxic-Jun11	540	2225	5.98	0.95	0.49	110	157	3.67	0.78	0.92
Anoxic-Feb12	587	2479	6.12	0.96	0.43	306	482	4.17	0.73	0.96

Oxic water samples from all sampling sites and dates harboured between 1 and 6 distinct archaeal OTUs, whereas the number of defined OTUs increased in the anoxic water compartment. At the 3 sampling campaigns, oxic waters of both sampling sites were clearly dominated by putatively ammonia-oxidising OTUs belonging to the MGI (56.7% and 51.3% of the analysed sequences in the oxic zone in Gisenyi and Ishungu, respectively; Fig. 4). The transition zone contained a more diverse ACC than the oxic zone, with the presence of *Thaumarchaeota* (13.2% and 6.5% of the analysed sequences in the transition zone at Gisenyi and Ishungu, respectively), *Crenarchaeota* (31.1% and 14.5%) and *Euryarchaeota* (51.9% and 70.3%). In the transition zone, all retrieved *Crenarchaeota* OTUs belonged to as yet uncultured groups, whereas *Euryarchaeota* OTUs were mainly affiliated with *Methanomicrobia* (39.6% and 46.4% of the analysed sequences at Gisenyi and Ishungu, respectively). In turn, anoxic waters were clearly dominated by *Euryarchaeota* (more than 42.6% of the sequences retrieved at these depths from both sites) mainly belonging to the *Methanomicrobia* class (29.3% and 35.3% of all the sequences in the anoxic zone in Gisenyi and Ishungu, respectively), followed by uncultured *Crenarchaeota* and non-affiliated archaea (Fig. 4).

Co-occurrence patterns of *Bacteria* and *Archaea*

The resulting aquatic microbial network of Lake Kivu (Fig. S2 in the Supplement) consisted of 556 highly connected bacterial and archaeal nodes (OTUs), comprising 5.35 edges node⁻¹ on average, structured among densely connected sub-networks (1 major, 11 moderate and 35 small sub-networks). Aside from many unclassified bacterial and archaeal OTUs, co-occurrence of different known taxa was observed. For instance, in the major sub-network (Fig. 5A), the rare taxon *Dehalococcoidetes* showed the highest incidence of co-occurrence and, to a lesser extent, the bacterial lineages *Actinobacteria* and *Bacteroidetes* and the archaeal lineages *Methanoregula* and *Methanospirillum* also showed high co-occurrence values. Other taxa showed more limited co-occurrence patterns, such as sulphate-reducing bacteria (*Desulfobacca*, *Desulfocapsa* and *Desulfobacterium*) and sulphur-oxidising bacteria (*Sulfuricurvum* and *Sulfurimonas*). *Dehalococcoidetes* co-occurred with several uncultivated candidate divisions such as AC1, GN02, OP3 and WS3, but also with taxa like *Actinobacteria* WCHB1-81, *Desul-*

fobacca and *Bacteroidetes* and with archaeal lineages *Methanoregula*, *Methanosaetaceae*. In addition, 2 sub-networks (Fig. 5B) were dominated by different OTUs affiliated with *Methylomonas*. In sub-network 1, *Methylomonas* co-occurred with OTUs affiliated with *Acinetobacter* (*Gammaproteobacteria*), *Rhizobiales* (*Alphaproteobacteria*) and the archaeal taxon *Methanoregula*. In sub-network 2, betaproteobacterial taxa mainly co-occurred with other proteobacterial taxa (*Methylomonas*, *Methyloversatilis*, unclassified *Proteobacteria*, *Rhizobiales*, *Rhodocyclaceae*) and also with *Thaumarchaeota*. There were also 2 other sub-networks mainly composed of uncultured archaea and *Cyanobacteria* (data not shown).

Bacterial abundance classification and overlap estimates

Venn diagrams (Fig. 6; see also Fig. S3 in the Supplement) illustrate the presence of overlapping abundant and rare OTUs between sampling campaigns, as well as OTUs unique to each season in each water zone. Only ca. 10% of the OTUs were found to be abundant in all samples. In turn, 61% in Gisenyi and 68% in Ishungu of the abundant OTUs in the oxic zone were shared between 3 sampling times; 24% and 46% of the abundant taxa were shared in the transition zone in Gisenyi and Ishungu, respectively. Besides, 55% and 40% of the abundant taxa were shared in the anoxic zone from Gisenyi and Ishungu, respectively. In contrast, rare OTUs were found to be specific to sampling time (Figs. 6 & S3). The dynamics of rare bacterial species over time revealed that some of the rare biosphere can become abundant at another sampling time in each water zone. Moreover, Venn diagrams constructed with Gisenyi samples (Fig. S4 in the Supplement) illustrated clear differences between zones at the 3 sampling times. A higher percentage of abundant OTUs was shared among water zones in comparison with rare OTUs. There was a significant positive relationship between

Fig. 5. Network of co-occurring operational taxonomic units (OTUs) based on correlation analysis. A connection represents a strong (Pearson $r > 0.8$) and significant ($p = 0.01$) positive correlation. The size of each node is proportional to the number of connections. (A) major network showing co-occurrence of *Dehalococcoidetes* with *Desulfobacca*, *Sulfurimonas* and *Actinobacteria* and candidate divisions as well as unclassified bacteria (squares) and archaea (circles); (B) sub-networks dominated by *Methylomonas* and their co-occurrence with proteobacterial lineages

Author copy
A

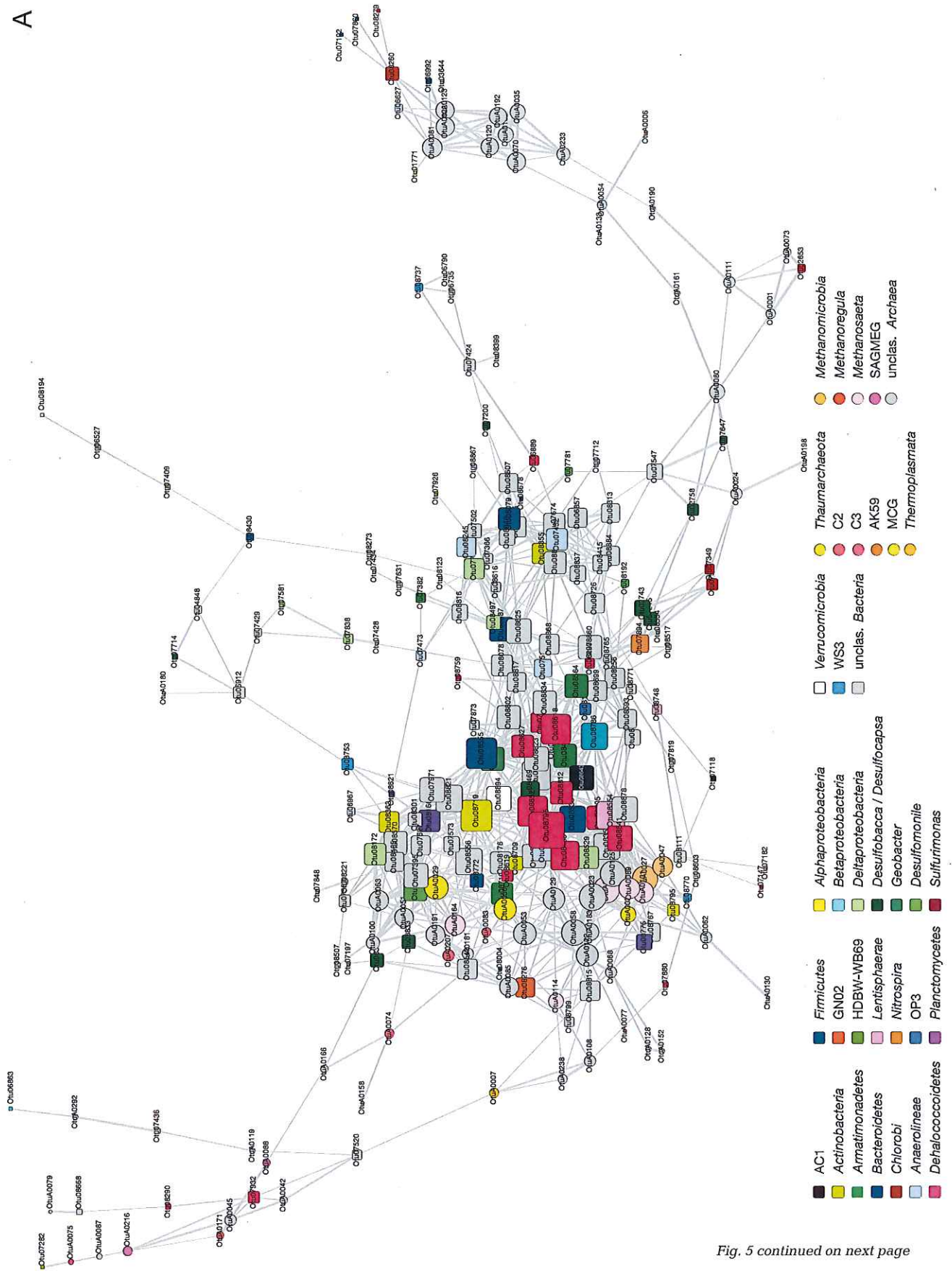


Fig. 5 continued on next page

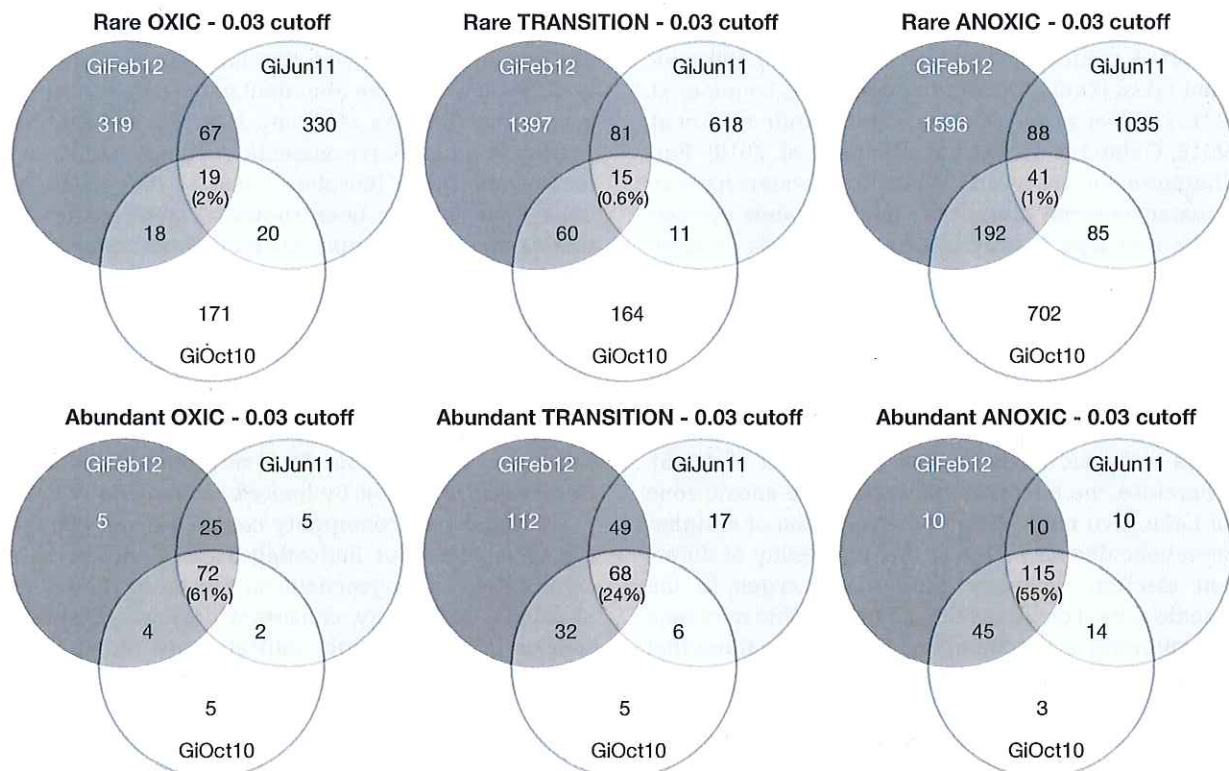


Fig. 6. Distribution of operational taxonomic units (OTUs) among the 3 sampling campaigns over the oxic, transition and anoxic zones in Gisenyi (Gi). Abundant OTUs are defined as taxa represented by more than 6 sequences at each depth, whereas rare OTUs are defined as taxa represented by fewer than 6 sequences

the relative abundance and occupancy of OTUs (Fig. S5 in the Supplement). Further information on generalists and specialists can be found in the Supplement.

DISCUSSION

The present study captures both abundant and rare microbes in a meromictic freshwater African lake, providing information on taxonomic diversity and distribution in relation to environmental gradients. Due to its meromictic nature, vertical variation in the availability of oxygen as well as other electron donors and acceptors plays an overarching role in shaping the distribution and diversity of prokaryotes.

Relative abundance of archaea versus bacteria

As shown by qPCR analyses of microbial communities, 16S rRNA gene copy numbers of archaea were approximately 2 orders of magnitude less abundant than bacteria at each depth along the water column

analysed (Fig. S1 in the Supplement). Although qPCR has drawbacks in performing total cell enumerations (e.g. such as the requirement for careful calibration, the specificity of the primers and the number of gene copies per cell), our data are consistent with previous reports on archaeal relative abundances in Lake Kivu (range: 0.3–4.6% of total prokaryotic abundance) estimated by fluorescent *in situ* hybridisation followed by epifluorescence microscopic enumeration (Llirós et al. 2010). Casamayor & Borrego (2009) also showed that *Archaea* are a minor component of microbial communities in freshwater.

Microbial richness in the water column

Microbial communities in the oxic surface waters were very different from those in the deeper anoxic waters. This microbial stratification can likely be attributed to differences in the availability of electron donors and acceptors as well as the energy sources as a function of depth. Overall, anoxic waters exhibited higher species richness than oxic waters. Richness estimations (up to 1938 OTUs) in the oxic zone of

Lake Kivu were within the range of previously reported values for surface waters of oligotrophic cold lakes (Table S1 in the Supplement; Logue et al. 2012) and for surface marine waters (Andersson et al. 2010, Galand et al. 2010, Kirchman et al. 2010). Furthermore, the observation that anoxic waters harbour greater bacterial diversity than oxic waters appears to be a general feature of extreme aquatic environments (Madrid et al. 2001, Humayoun et al. 2003, Yakimov et al. 2007, Quince et al. 2008, Comeau et al. 2012, Bougouffa et al. 2013). It was previously suggested that anaerobic species with metabolisms less energetically efficient than aerobic respiration might maintain a greater diversity in metabolic pathways in anoxic environments (Lehours et al. 2005). Therefore, the microbial network in the anoxic zone of Lake Kivu might lead to the retention of a higher metabolic diversity. Due to the availability of different electron acceptors other than oxygen in the anoxic zone, conditions that shape aerobic microbial communities are profoundly different from those that regulate anaerobic microbial communities (Humayoun et al. 2003). Notably, a greater proportion of bacterial sequences in the anoxic waters were affiliated with poorly described phyla and uncultured taxa, compared to the oxic waters. This observation may be due to the under-representation of anoxic microbial communities in current databases. This might also reflect the strong potential of deep and anoxic environments to harbour hitherto unknown microbial groups also known as microbial dark matter (Rinke et al. 2013).

Importance of rare taxa

Due largely to methodological limitations, most studies of freshwater microbial ecology to date have focused on abundant species that were thought to mediate biogeochemical processes, while rare species went undetected. In the present work, rank abundance analyses of both archaeal and bacterial sequences revealed a small fraction of highly abundant OTUs and a long tail of less abundant OTUs, suggesting the presence of a so-called rare biosphere (Sogin et al. 2006, Pedrós-Alió 2012). Although incomplete sampling may lead to pseudo-turnover of species, overall most species defined as generalists were abundant, whereas those defined as habitat specialists were for the most part rare (Fig. S5 in the Supplement). Although our grouping was somewhat arbitrary, it was useful to define ecological categories. In the present study, strict habitat specialists

(OTUs that tend to be present in only 1 habitat type and in most samples from that habitat type; Logares et al. 2013) were more abundant in the anoxic waters, supporting the idea of strong selection for specific species in anoxic environments. A complex environment with a rare biosphere such as that found in Lake Kivu has also been shown in other studies in marine anoxic environments and hydrothermal vents (Sogin et al. 2006, Galand et al. 2009).

An evaluation of the effect of sampling time on abundant versus rare species in the 3 different zones of the lake revealed that abundant core members exhibited minimal temporal variability, whereas rare species showed more pronounced fluctuations over seasons (Fig. 6). If rare enough, species can escape detection by limited sequencing efforts. A changing rare community can also mean changing specialists, thus indicating their possible active contribution to biogeochemical processes (Pester et al. 2010). Conversely, consistent detection of given species in a zone might indicate core rather than transient membership in the community.

Possible relationship between microbial community composition and microbial processes

In a higher taxonomical rank (phylum/class), seasonal succession patterns and vertical diversification in microbial communities have also been recently reported in many distinct environments, mostly in fresh water (i.e. Warnecke et al. 2005, Shade et al. 2007), as observed for both archaeal and bacterial assemblages in Lake Kivu. *Actinobacteria*, *Cyanobacteria* and *Thaumarchaeota* dominated the microbial community in the oxic zone, while many other bacterial (distinct *Proteobacteria*, *Bacteroidetes*, *Chlorobi* and *Chloroflexi*, among others) and archaeal (mainly CH₄-related and uncultured groups) phyla/classes were distributed throughout the water column with significant differences in their relative abundances between transition and fully anoxic waters (Fig. 3). As shown in the current study, *Actinobacteria* were commonly found in epilimnetic water of lakes from all over the world because of their adaptation to the environmental conditions found in this zone: high light intensity (Warnecke et al. 2005) and DO concentration (Allgaier & Grossart 2006, Taipale et al. 2009). *Cyanobacteria*, the second most abundant phylum in the oxic waters in Lake Kivu, were slightly more abundant in the rainy season than in the dry season in concordance with recently published data (Darchambeau et al. 2014)

based on primary production and phytoplankton composition reporting high cyanobacterial abundance during the lake's rainy season. Archaea are also important players in global energy cycles, especially in C and N cycles, in spite of their lower abundance compared to bacteria in lakes (Fig. 2; Casamayor & Borrego 2009). For instance, the oxic zone was dominated by members of the MGI, supporting the presence of archaeal nitrifiers in the water column. Our study is also consistent with data reported by Hu et al. (2011), which showed the importance of light intensity on the vertical distribution of MGI.

In a previous study (Llirós et al. 2012), the transition zone was suggested to be the most active and metabolically diverse water compartment due to the prevailing physico-chemical conditions. The deeper analysis of the microbial diversity present in Lake Kivu performed in this study evidenced the presence of the highest microbial richness in the sampled anoxic zone (Table 2). Even so, important key players such as methylotrophs were identified in the transition zone. Aerobic CH_4 oxidation preferentially occurs in the transition zone of freshwater systems (Segers 1998, Bastviken et al. 2003), where CH_4 and DO are both present. The dominance of *Methylococcales* in the transition zone is consistent with the high rate of bacterial CH_4 oxidation, resulting in low surface water CH_4 concentrations despite the large deep CH_4 reservoir (Borges et al. 2011, Morana et al. 2014).

Furthermore, a connection between 2 OTUs mainly describes their co-occurrence across different samples which might indicate their similar response to a common environmental parameter or their possible direct interactions. For instance, network analysis revealed a clear co-occurrence network within proteobacterial lineages in the transition zone, which might indicate that several members of the *Proteobacteria* are well adapted to the environmental conditions present in the transition zone (Fig. 5B). The presence of archaeal methanogenic lineages at the vicinities of the transition zone might indicate a coupling between the production of CH_4 and its oxidation by microbial processes. Moreover, detection of green sulphur bacteria (*Chlorobium*-related OTUs) and high relative abundance of *Nitrospira*-related sequences in the transition zone might indicate potential oxygenic photoautotrophy and nitrite oxidation, respectively.

Different ecological conditions guiding microbial community composition were reflected in diverse network structures in the 3 water compartments. In

our study, a co-occurrence of *Dehalococcoidetes*, *Actinobacteria* WCHB-81, sulphate-reducing bacteria (SRB), sulphur-oxidising bacteria, acetoclastic methanogenic archaea, as well as candidate bacterial divisions, and uncultured archaea and bacteria was observed in the anoxic zone (Fig. 5A). These microbial connections point towards a potential link between C and S cycles in the pelagic anoxic waters of Lake Kivu. It has been evidenced that a consortium of SRB and methane-oxidising archaea can couple C and S cycles throughout anaerobic oxidation of methane (AOM) with sulphate, manganese or iron as electron acceptors (Hinrichs & Boetius 2002, Beal et al. 2009). Remarkably, the low recovery of sequences affiliated with anaerobic methane oxidisers (the main archaeal group involved in AOM) should not completely rule out AOM, because of the presence of unclassified archaeal groups that could be involved in AOM (e.g. Marine Benthic Group B, C and D, MCG and the recently described AOM-associated archaea; Biddle et al. 2006, 2012, Inagaki et al. 2006, Knittel & Boetius 2009). In contrast, our results indicate the importance of hydrogenotrophic and acetoclastic methanogenesis in the lake, as *Methanomicrobiales* and *Methanosarcinales* were highly abundant in the anoxic zone. As has been shown in Lake Matano (Crowe et al. 2011), the present study supported the direct occurrence of methanogenesis within the water column, even though CH_4 was previously assumed to be solely produced in sediments and diffused in the water column (Pasche et al. 2011). Since water column CH_4 production has been shown to be rare in anoxic water columns (Reeburgh 2007), pelagic methanogenesis should be further studied under persistently anoxic conditions in Lake Kivu. Furthermore, syntrophy or competition between methanogens and SRB in the anoxic sediments must also be considered in the anoxic waters, as previously shown (Kuivila et al. 1990, Holmer & Kristensen 1994, Muyzer & Stams 2008).

Another noteworthy observation in the water column of Lake Kivu was the high relative abundance of *Epsilonproteobacteria* in those water samples in the upper part of the anoxic waters. Previous studies have suggested a chemolithoautotrophic role for some *Epsilonproteobacteria* species like *Sulfuricum* and *Sulfurimonas* using sulphur as electron donors and NO_3^- as electron acceptors in oligotrophic and stratified marine environments with sulphidic redoxclines (i.e. the Baltic and Black Seas; Campbell et al. 2006, Grote et al. 2007, Glaubitz et al. 2009). The presence of NO_x traces just below the transition zone of Lake Kivu together with the detection of *Sulfuri-*

curvum-related OTUs point towards putative chemolithoautotrophic processes present in the upper anoxic water compartment.

As presented in the network analysis, a complex interaction between organohalide respiring *Chloroflexi*, *Actinobacteria* WCHB1-81 and SRB could suggest a role in hydrocarbon or refractory organic matter degradation in the anoxic waters as previously evidenced in other environments (Dojka et al. 1998, He et al. 2007, Krzmarzick et al. 2013).

Elevated abundance and diversity of uncultivated candidate divisions were detected in the anoxic zone. Interestingly, only the candidate division TM6 could be detected both in oxic and anoxic conditions in Lake Kivu. Representatives of TM6 have been shown to be facultative anaerobes (McLean et al. 2013). However, candidate divisions such as OP3, OP9 and OP11 were mainly detected in the anoxic zone of Lake Kivu, as previously observed in Lake Pavin and Arctic Lake A (Lehours et al. 2007, Comeau et al. 2012). It has been shown that OP3 bacteria share a high proportion of orthologues with members of the *Deltaproteobacteria*, which might indicate that OP3 evolved metabolic capabilities similar to those of *Deltaproteobacteria* (Glöckner et al. 2010).

CONCLUSIONS

The stratification of microbial communities present in Lake Kivu indicated distinct environmental niches according to the different physico-chemical conditions along the water column with gradual transitions over distinct redox gradients (Canfield & Thamdrup 2009), as has also been reported in other lakes and marine systems (De Wever et al. 2005, Agogué et al. 2011, Peura et al. 2012). The present study evidenced clear differences in BCC and ACC between oxic surface waters and anoxic deep waters in Lake Kivu. Coexistence between key players of the C and S cycles seemed to be evident and need to be further evaluated. In addition, the high relative abundance of un-affiliated bacterial and archaeal OTUs retrieved from anoxic deep waters in the present study highlights the current lack of knowledge on microbial communities in anoxic deep environments, which requires further research. The discovery of yet-to-be-cultured microbial taxa and understanding their potential interactions and the role they play in microbial processes driving biogeochemical cycling are very important from an ecological point of view as well as for possible use of particular species in biotechnology. Deep-

sequencing technologies also provided us with profound information on rare taxa, which might be disproportionately active relative to their abundances (Jones & Lennon 2010, Campbell et al. 2011). To construct a complete picture of the ecological roles of the various microbial communities found at the different depths in this particular environment, RNA-based molecular studies (active community) coupled with measurements of the rates of key microbial processes are of further interest.

Acknowledgements. In addition to the authors of this paper, the Lake Kivu consortium includes the following individuals: S. Bouillon, C. Morana (Katholieke Universiteit Leuven), A.V. Borges, F. Roland (Université de Liège), B. Leporcq, K. de Saedeleer (Université de Namur), A. Anzil (Université Libre de Bruxelles) and M.V. Commarieu (Université de Liège). A.V. Borges is thanked for providing the CH₄ data. We are grateful to the DR Congo local team (G. Alunga, P. Masilya, M. Ishumbisho, B. Kaningini) and to the fishermen Silas and Djoba from DR Congo for their help during the field work. The consortium thanks the Rwanda Energy Company and Michel Halbwachs for free access to their industrial platform off Gisenyi. This work was funded by the Fonds National de la Recherche Scientifique (FNRS) under the MICKI (Microbial diversity and processes in Lake Kivu) project and the Belgian Federal Science Policy Office EAGLES (East African Great Lake Ecosystem Sensitivity to changes, SD/AR/02A) project, and contributes to the European Research Council starting grant project AFRIVAL (African river basins: Catchment-scale carbon fluxes and transformations, 240002). We also thank the 3 anonymous reviewers for their many insightful comments and suggestions that allowed improvement of the manuscript.

LITERATURE CITED

- ▶ Agogué H, Lamy D, Neal PR, Sogin ML, Herndl GJ (2011) Water mass-specificity of bacterial communities in the North Atlantic revealed by massively parallel sequencing. *Mol Ecol* 20:258–274
- ▶ Allgaier M, Grossart HP (2006) Diversity and seasonal dynamics of *Actinobacteria* populations in four lakes in northeastern Germany. *Appl Environ Microbiol* 72: 3489–3497
- ▶ Andersson AF, Riemann L, Bertilsson S (2010) Pyrosequencing reveals contrasting seasonal dynamics of taxa within Baltic Sea bacterioplankton communities. *ISME J* 4: 171–181
- ▶ Bastviken D, Ejlertsson J, Sundh I, Tranvik L (2003) Methane as a source of carbon and energy for lake pelagic food webs. *Ecology* 84:969–981
- ▶ Beal EJ, House CH, Orphan VJ (2009) Manganese- and iron-dependent marine methane oxidation. *Science* 325: 184–187
- ▶ Bhattarai S, Ross KA, Schmid M, Anselmetti FS, Bürgmann H (2012) Local conditions structure unique archaeal communities in the anoxic sediments of meromictic Lake Kivu. *Microb Ecol* 64:291–310
- ▶ Biddle JF, Lipp JS, Lever MA, Lloyd KG and others (2006) Heterotrophic Archaea dominate sedimentary subsur-

- face ecosystems off Peru. *Proc Natl Acad Sci USA* 103: 3846–3851
- ▶ Biddle JF, Cardman Z, Mendlovitz H, Albert DB, Lloyd KG, Boetius A, Teske A (2012) Anaerobic oxidation of methane at different temperature regimes in Guaymas Basin hydrothermal sediments. *ISME J* 6:1018–1031
 - ▶ Borges AV, Abril G, Delille B, Descy JP, Darchambeau F (2011) Diffusive methane emissions to the atmosphere from Lake Kivu (Eastern Africa). *J Geophys Res* 116, G03032, doi:10.1029/2011JG001673
 - ▶ Bougouffa S, Yang JK, Lee OO, Wang Y, Batang Z, Al-Suwailem A, Qian PY (2013) Distinctive microbial community structure in highly stratified deep-sea brine water columns. *Appl Environ Microbiol* 79:3425–3437
 - ▶ Callaway TR, Dowd SE, Edrington TS, Anderson RC and others (2010) Evaluation of bacterial diversity in the rumen and feces of cattle fed different levels of dried distillers grains plus soluble using bacterial tag-encoded FLX amplicon pyrosequencing. *J Anim Sci* 88:3977–3983
 - ▶ Campbell BJ, Engel AS, Porter ML, Takai K (2006) The versatile epsilon-proteobacteria: key players in sulphidic habitats. *Nat Rev Microbiol* 4:458–468
 - ▶ Campbell BJ, Yu L, Heidelberg JF, Kirchman DL (2011) Activity of abundant and rare bacteria in a coastal ocean. *Proc Natl Acad Sci USA* 108:12776–12781
 - ▶ Canfield DE, Thamdrup B (2009) Towards a consistent classification scheme for geochemical environments or why we wish the term 'suboxic' would go away. *Geobiology* 7: 385–392
 - Casamayor EO, Borrego CM (2009) Archaea. In: Likens GE (ed) *Encyclopedia of inland waters*, Vol 3. Elsevier, Oxford, p 167–181
 - Clarke KR, Gorley RN (2006) *PRIMER V6: user manual/tutorial*. PRIMER-E, Plymouth
 - ▶ Cline JD (1969) Spectrophotometric determination of hydrogen sulfide in natural waters. *Limnol Oceanogr* 14: 454–458
 - ▶ Comeau AM, Harding T, Galand PE, Vincent WF, Lovejoy C (2012) Vertical distribution of microbial communities in a perennially stratified Arctic lake with saline anoxic bottom waters. *Sci Rep* 2:604
 - ▶ Coolen MJL, Abbas B, van Bleijswijk J, Hopmans EC, Kuypers MMM, Wakeham SG, Sinninghe-Damste JS (2007) Putative ammonia-oxidizing Crenarchaeota in suboxic waters of the Black Sea: a basinwide ecological study using 16S ribosomal and functional genes and membrane lipids. *Environ Microbiol* 9:1001–1016
 - ▶ Cottrell MT, Kirchman DL (2003) Contribution of major bacterial groups to bacterial biomass production (thymidine and leucine incorporation) in the Delaware estuary. *Limnol Oceanogr* 48:168–178
 - Crowe SA, Katsev S, Leslie K, Sturm A and others (2011) The methane cycle in ferruginous Lake Matano. *Geobiology* 9:61–78
 - ▶ Darchambeau F, Sarmiento H, Descy JP (2014) Primary production in a tropical large lake: the role of phytoplankton composition. *Sci Total Environ* 473-474:178–188
 - ▶ De Wever A, Muylaert K, Pirlot S, Van der Gucht K and others (2005) Bacterial community composition in Lake Tanganyika: vertical and horizontal heterogeneity. *Appl Environ Microbiol* 71:5029–5037
 - ▶ Degens ET, von Herzen RP, Wong HK, Deuser WG, Jannasch HW (1973) Lake Kivu: structure chemistry and biology of an East African Rift Lake. *Geol Rundsch* 62: 245–277
 - ▶ Dojka MA, Hugenholtz P, Haack SK, Pace NR (1998) Microbial diversity in a hydrocarbon- and chlorinated-solvent-contaminated aquifer undergoing intrinsic bioremediation. *Appl Environ Microbiol* 64:3869–3877
 - ▶ Dowd SE, Callaway TR, Wolcott RD, Sun Y, McKeehan T, Hagevoort RG, Edrington TS (2008) Evaluation of the bacterial diversity in the feces of cattle using 16S rDNA bacterial tag-encoded FLX amplicon pyrosequencing bTEFAP. *BMC Microbiol* 8:125
 - ▶ Edgar RC, Haas BJ, Clemente JC, Quince C, Knight R (2011) UCHIME improves sensitivity and speed of chimera detection. *Bioinformatics* 27:2194–2200
 - Faust K, Sathirapongsasuti JF, Izard J, Segata N, Gevers G, Raes J, Huttenhower C (2012). Microbial co-occurrence relationships in the human microbiome. *PLoS Comput Biol* 8:e1002606
 - ▶ Galand PE, Casamayor EO, Kirchman DL, Lovejoy C (2009) Ecology of the rare microbial biosphere of the Arctic Ocean. *Proc Natl Acad Sci USA* 106:22427–22432
 - ▶ Galand PE, Potvin M, Casamayor EO, Lovejoy C (2010) Hydrography shapes bacterial biogeography of the deep Arctic Ocean. *ISME J* 4:564–576
 - ▶ Glaubitz S, Lueders T, Abraham WR, Jost G, Jürgens K, Labrenz M (2009) ¹³C-isotope analyses reveal that chemolithoautotrophic *Gamma*- and *Epsilonproteobacteria* feed a microbial food web in a pelagic redoxcline of the central Baltic Sea. *Environ Microbiol* 11:326–337
 - ▶ Glöckner J, Kube M, Shrestha PM, Weber M, Glöckner FO, Reinhardt R, Liesack W (2010) Phylogenetic diversity and metagenomics of candidate division OP3. *Environ Microbiol* 12:1218–1229
 - ▶ Grote J, Labrenz M, Pfeiffer B, Jost G, Jürgens K (2007) Quantitative distributions of *Epsilonproteobacteria* and a *Sulfurimonas* subgroup in pelagic redoxclines of the central Baltic Sea. *Appl Environ Microbiol* 73:7155–7161
 - ▶ He J, Holmes VF, Lee PKH, Alvarez-Cohen L (2007) Influence of vitamin B12 and cocultures on the growth of *Dehalococcoides* isolates in defined medium. *Appl Environ Microbiol* 73:2847–2853
 - Hinrichs KU, Boetius A (2002) The anaerobic oxidation of methane: new insights in microbial ecology and biochemistry. In: Wefer G, Billett D, Hebbeln D, Jørgensen BB, Schlüter M, Van Weering T (eds) *Ocean margin systems*. Springer-Verlag, Berlin, p 457–477
 - ▶ Holmer M, Kristensen E (1994) Co-existence of sulfate reduction and methane production in an organic-rich sediment. *Mar Ecol Prog Ser* 107:177–184
 - ▶ Hu A, Jiao N, Zhang R, Yang Z (2011) Niche partitioning of Marine Group I *Crenarchaeota* in euphotic and upper mesopelagic zones of the East China Sea. *Appl Environ Microbiol* 77:7469–7478
 - ▶ Humayoun SB, Bano N, Hollibaugh JT (2003) Depth distribution of microbial diversity in Mono Lake, a meromictic Soda Lake in California. *Appl Environ Microbiol* 69: 1030–1042
 - ▶ Inagaki F, Nunoura T, Nakagawa S, Teske A and others (2006) Biogeographical distribution and diversity of microbes in methane hydrate-bearing deep marine sediments on the Pacific Ocean Margin. *Proc Natl Acad Sci USA* 103:2815–2820
 - ▶ Isumbisho M, Sarmiento H, Kaningini B, Micha JC, Descy JP (2006) Zooplankton of Lake Kivu East Africa half a century after the Tanganyika sardine introduction. *J Plankton Res* 28:971–989
 - ▶ Jones SE, Lennon JT (2010) Dormancy contributes to the

- maintenance of microbial diversity. *Proc Natl Acad Sci USA* 107:5881–5886
- Kirchman DL, Cottrell MT, Lovejoy C (2010) The structure of bacterial communities in the western Arctic Ocean as revealed by pyrosequencing of 16S rRNA genes. *Environ Microbiol* 12:1132–1143
- Knittel K, Boetius A (2009) Anaerobic oxidation of methane: progress with an unknown process. *Annu Rev Microbiol* 63:311–334
- Krzmarzick MJ, McNamara PJ, Crary BB, Novak PJ (2013) Abundance and diversity of organohalide-respiring bacteria in lake sediments across a geographical sulfur gradient. *FEMS Microbiol Ecol* 84:248–258
- Kuivila KM, Murray JW, Devol AH (1990) Methane production in the sulfate depleted sediments of two marine basins. *Geochim Cosmochim Acta* 54:403–411
- Lehours AC, Evans P, Bardot C, Joblin K, Gérard F (2007) Phylogenetic diversity of archaea and bacteria in the anoxic zone of a meromictic lake (Lake Pavin, France). *Appl Environ Microbiol* 73:2016–2019
- Lliros M, Gich F, Plasencia A, Auguet JC and others (2010) Vertical distribution of ammonia-oxidizing Crenarchaeota and methanogens in the epipelagic waters of Lake Kivu (Rwanda-Democratic Republic of the Congo). *Appl Environ Microbiol* 76:6853–6863
- Lliros M, Descy JP, Libert X, Morana C and others (2012) Microbial ecology of Lake Kivu. In: Descy JP, Darchambeau F, Schmid M (eds) *Lake Kivu: limnology and biogeochemistry of a tropical great lake*. *Aquat Ecol Ser 5*. Springer, Dordrecht, p 85–105
- Logares R, Lindström ES, Langenheder S, Logue JB and others (2013) Biogeography of bacterial communities exposed to progressive long-term environmental change. *ISME J* 7:937–948
- Logue JB, Langenheder S, Andersson AF, Bertilsson S, Drakare S, Lanzén A, Lindström ES (2012) Freshwater bacterioplankton richness in oligotrophic lakes depends on nutrient availability rather than on species-area relationships. *ISME J* 6:1127–1136
- López-Gutiérrez JC, Henry S, Hallet S, Martin-Laurent F, Catrou G, Philippot L (2004) Quantification of a novel group of nitrate-reducing bacteria in the environment by real-time PCR. *J Microbiol Methods* 57:399–407
- Madrid V, Taylor G, Scranton M, Chistoserdov A (2001) Phylogenetic diversity of bacterial and archaeal communities in the anoxic zone of the Cariaco Basin. *Appl Environ Microbiol* 67:1663–1674
- Magurran AE, Henderson PA (2003) Explaining the excess of rare species in natural species abundance distributions. *Nature* 422:714–716
- McLean JS, Lombardo MJ, Badger JH, Edlund A and others (2013) Candidate phylum TM6 genome recovered from a hospital sink biofilm provides genomic insights into this uncultivated phylum. *Proc Natl Acad Sci USA* 110: E2390–E2399
- Miranda KM, Espey MG, Wink DA (2001) A rapid, simple spectrophotometric method for simultaneous detection of nitrate and nitrite. *Nitric Oxide* 5:62–71
- Morana C, Borges AV, Roland FAE, Darchambeau F, Descy JP, Bouillon S (2014) Methanotrophy within the water column of a large meromictic tropical lake (Lake Kivu, East Africa). *Biogeosci Discuss* 11:15663–15691
- Muyzer G, Stams AJM (2008) The ecology and biotechnology of sulfate-reducing bacteria. *Nat Rev Microbiol* 6: 441–454
- Pasche N, Schmid M, Vasquez F, Schubert CJ and others (2011) Methane sources and sinks in Lake Kivu. *J Geophys Res* 116, G03006, doi:10.1029/2011JG001690
- Pedrós-Alió C (2006) Marine microbial diversity: Can it be determined? *Trends Microbiol* 14:257–263
- Pedrós-Alió C (2012) The rare bacterial biosphere. *Annu Rev Mar Sci* 4:449–466
- Pester M, Bittner N, Deevong P, Wagner M, Loy A (2010) A 'rare biosphere' microorganism contributes to sulfate reduction in a peatland. *ISME J* 4:1591–1602
- Peura S, Eiler A, Bertilsson S, Nykänen H, Tirola M, Jones RI (2012) Distinct and diverse anaerobic bacterial communities in boreal lakes dominated by candidate division OD1. *ISME J* 6:1640–1652
- Quince C, Curtis TP, Sloan WT (2008) The rational exploration of microbial diversity. *ISME J* 2:997–1006
- Reeburgh WS (2007) Oceanic methane biogeochemistry. *Chem Rev* 107:486–513
- Rice EW, Baird RB, Eaton AD, Clesce LS (eds) (2012) *Standard methods for the examination of water and wastewater*, 22nd edn. APHA, Washington, DC
- Rinke C, Schwientek P, Sczyrba A, Ivanova NN and others (2013) Insights into the phylogeny and coding potential of microbial dark matter. *Nature* 499:431–437
- Sarmiento H, Isumbisho M, Descy JP (2006) Phytoplankton ecology of Lake Kivu eastern Africa. *J Plankton Res* 28: 815–829
- SCA (Standing Committee of Analysts) (1981) *Methods for the examination of waters and associated materials Ammonia in waters*. HMSO, London
- Schloss PD, Westcott SL, Ryabin T, Hall JR and others (2009) Introducing mothur: open-source platform-independent community-supported software for describing and comparing microbial communities. *Appl Environ Microbiol* 75:7537–7541
- Schmid M, Wüest A (2012) Stratification mixing and transport processes in Lake Kivu. In: Descy JP, Darchambeau F, Schmid M (eds) *Lake Kivu: limnology and biogeochemistry of a tropical great lake*. *Aquat Ecol Ser 5*. Springer: Dordrecht, p 13–30
- Schmid M, Tietze K, Halbwegs M, Lorke A, McGinnis D, Wüest A (2002) How hazardous is the gas accumulation in Lake Kivu? Arguments for a risk assessment in light of the Nyiragongo volcano eruption. *Acta Vulcanol* 14/15: 115–122
- Schmid M, Halbwegs M, Wehrli B, Wüest A (2005) Weak mixing in Lake Kivu: new insights indicate increasing risk of uncontrolled gas eruption. *Geochim Geophys Geosyst* 6, Q07009, doi:10.1029/2004 GC000892
- Segers R (1998) Methane production and methane consumption: a review of processes underlying wetland methane fluxes. *Biogeochemistry* 41:23–51
- Shade A, Kent AD, Jones SE, Newton RJ, Triplett EW, McMahon KD (2007) Interannual dynamics and phenology of bacterial communities in a eutrophic lake. *Limnol Oceanogr* 52:487–494
- Shannon P, Markiel A, Ozier O, Baliga NS and others (2003) Cytoscape: a software environment for integrated models of biomolecular interaction networks. *Genome Res* 13:2498–2504
- Sogin ML, Morrison HG, Huber JA, Welch DM and others (2006) Microbial diversity in the deep sea and the underexplored 'rare biosphere'. *Proc Natl Acad Sci USA* 103: 12115–12120

- ▶ Taipale S, Jones RI, Tirola M (2009) Vertical diversity of bacteria in an oxygen-stratified humic lake, evaluated using DNA and phospholipid analyses. *Aquat Microb Ecol* 55:1–16
- ▶ Thiery W, Martynov A, Darchambeau F, Descy JP, Plisnier PD, Sushama L, van Lipzig NPM (2014) Understanding the performance of the FLake model over two African Great Lakes. *Geosci Model Dev* 7:317–337
- ▶ Warnecke F, Sommaruga R, Sekar R, Hofer JS, Pernthaler J (2005) Abundances, identity, and growth state of Actinobacteria in mountain lakes of different UV transparency. *Appl Environ Microbiol* 71:5551–5559
- ▶ Werner JJ, Koren O, Hugenholtz P, DeSantis TZ and others (2012) Impact of training sets on classification of high-throughput bacterial 16s rRNA gene surveys. *ISME J* 6: 94–103
- ▶ Wright JJ, Konwar KM, Hallam SJ (2012) Microbial ecology of expanding oxygen minimum zones. *Nat Rev Microbiol* 10:381–394
- ▶ Yakimov MM, La Cono V, Denaro R, D'Auria G and others (2007) Primary producing prokaryotic communities of brine interface and seawater above the halocline of deep anoxic lake L'Atalante Eastern Mediterranean Sea. *ISME J* 1:743–755

*Editorial responsibility: Tom Fenchel,
Helsingør, Denmark*

*Submitted: August 19, 2014; Accepted: November 26, 2014
Proofs received from author(s): March 9, 2015*

Chapter 5

Phytoplankton of Lake Kivu

Hugo Sarmiento, François Darchambeau, and Jean-Pierre Descy

Abstract This chapter reviews taxonomic composition, biomass, production and nutrient limitation of the phytoplankton of Lake Kivu. Present Lake Kivu phytoplankton is dominated by cyanobacteria – mainly *Synechococcus* spp. and thin filaments of *Planktolyngbya limnetica* – and by pennate diatoms, among which *Nitzschia bacata* and *Fragilaria danica* are dominant. Seasonal shifts occur, with cyanobacteria developing more in the rainy season, and the diatoms in the dry season. Other groups present are cryptophytes, chrysophytes, chlorophytes and dinoflagellates. According to a survey conducted in the period 2002–2008, the composition of the phytoplankton assemblage was quasi homogeneous among lake basins. The mean euphotic depth varied between 17 and 20 m, and the increase in the ratio between mixed layer depth and euphotic depth to about 2 in the dry season may have selected for diatoms and cryptophytes, which tended to present their maximal development in this season, when cyanobacteria slightly decreased. Mean chlorophyll *a* concentration was 2.16 mg m⁻³, and the mean daily primary production was 0.62 g C m⁻² day⁻¹ (range, 0.14–1.92), i.e. in the same range as in other large oligotrophic East African Rift lakes. Seston elemental

H. Sarmiento (✉)

Institut de Ciències del Mar – CSIC, Barcelona, Catalunya, Spain
e-mail: hsarmiento@icm.csic.es

F. Darchambeau

Chemical Oceanography Unit, University of Liège, Liège, Belgium
e-mail: francois.darchambeau@ulg.ac.be

J.-P. Descy

Research Unit in Environmental and Evolutionary Biology,
University of Namur, Namur, Belgium
e-mail: jpdescy@fundp.ac.be

ratios indicated a moderate P-deficiency during the dry, mixed season and a severe P limitation during part of the rainy, stratified season; the C:N ratio indicated a moderate N limitation throughout the year. Nutrient addition assays pointed to a direct N-limitation and co-limitation by P during rainy seasons and P or N limitation during dry seasons depending on the year. Thus, phytoplankton ecology in Lake Kivu does not differ from that of other Rift lakes, where seasonal variations result in a trade-off between low light with high nutrient supply and high light with low nutrient supply. Phytoplankton production in Lake Kivu is also similar to that of other Rift lakes, and nutrient limitation of phytoplankton growth may occur as a result of variable availability of N and P, as in Lakes Tanganyika and Malawi, even though the extent of P limitation seems greater in Lake Kivu.

5.1 Introduction

Because of its large size, substantial depth and consequently reduced littoral zone, the ecological functioning of the mixolimnion of Lake Kivu is dominated by pelagic processes, among which phytoplankton photosynthesis supplies the bulk of the organic carbon available for the food web. In this way, the pelagic ecosystem of Lake Kivu is not different from that of the other oligotrophic African Rift lakes, where strong seasonal changes occur, imposing contrasting constraints on phytoplankton growth, resulting in substantial shifts of the composition and biomass of the planktonic assemblages (Hecky and Kling 1987). Since the earlier studies carried out in the first half of the twentieth century, it was suspected that large variations of phytoplankton abundance occurred in Lake Kivu, but, besides taxonomic lists, few data were available (Beadle 1981). Despite the perception of its oligotrophic status by Damas (1937), Lake Kivu was described as more productive than Lake Tanganyika, based on few data on net plankton abundance (Hecky and Kling 1987). Indeed, subsequent studies confirmed that, in recent years, chlorophyll *a* concentration in the pelagic waters of Lake Kivu was two to three times as high as in Lake Tanganyika and Malawi (Sarmiento et al. 2009). But is Lake Kivu “more eutrophic” than Lake Tanganyika (Sarvala et al. 1999)? Is its primary productivity higher than that of the other deep Rift lakes?

Here we review the literature on the autotrophic plankton of Lake Kivu: its taxonomic composition, abundance, production and ecology. Additionally, we summarise the results of the most complete limnological and planktological survey ever realised in Africa, and probably in a tropical lake. The first aim of this review is to establish a well-documented and updated picture of the pelagic phytoplankton of Lake Kivu, which can be used as a reference for the future generations of researchers and naturalists, as well as a baseline for the lake monitoring to evaluate potential effects of the ongoing gas extraction (Chap. 10).

5.2 Light Conditions

Light is an essential factor determining primary productivity and phytoplankton assemblages in aquatic systems (Reynolds 2006). Contrarily to the common sense, light limitation in tropical aquatic systems is relatively common: numerous shallow polymictic lakes receive large amounts of suspended matter due to erosion (e.g. Mukankomeje et al. 1993); in others, like Lake Victoria, phytoplankton is light-limited due to high biomass after eutrophication producing a self-shading effect (Mugidde 1993; Kling et al. 2001). In deep lakes light can equally become a limiting factor as soon as the depth of the upper mixed layer (Z_m) reaches or exceeds the depth of the euphotic zone (Z_{eu}), depth at which the light intensity drops to 1% of the surface incident light. In such periods, the $Z_m:Z_{eu}$ ratio is larger than 1 and light harvesting by primary producers becomes a selective factor shaping phytoplankton composition (Sarmiento et al. 2006).

In Lake Kivu, the $Z_m:Z_{eu}$ ratio is often larger than 1, especially during the deep mixing periods, more frequent in the dry season (Fig. 5.1), when Z_m often exceeds 50 m (typically occurring between June and September). Although water transparency is higher, on average, during the dry season (mean Z_{eu} = 19.8 m) than during the rainy season (17.1 m), it is during that period that phytoplankton experiences the lowest light conditions, and this is reflected in shifts in the phytoplankton composition (discussed below).

The water transparency co-varies seasonally in a similar range in both the main basin and Ishungu basin (Fig. 5.1). However, the dry season winds may disproportionately affect the main basin, which is more exposed to wind than the Ishungu basin, resulting in more intense vertical mixing in the main basin (Fig. 5.1).

5.3 Taxonomic Composition

The first relevant scientific information concerning the plankton of Lake Kivu is from the mid 1930s, when H. Damas carried out an expedition to the “Parc National Albert” (Damas 1935–1936, 1937). The 55 net samples collected from Lake Kivu were studied by several phycologists and the results were published in two issues of the publication of the Institut of National Parks of Belgian Congo devoted to the Mission H. Damas: fasc. 8 “Süsswasser-Diatomeen” by Hustedt (1949) for the diatoms, and fasc. 19 “Algues et Flagellates” by Frémy et al. (1949) for several other groups of algae, namely Cyanobacteria (P. Frémy), Chrysophyta, Pyrrhophyta, Euglenophyta, Volvocales (A. Pascher), Heterokontae, Protococcales, Siphonocladales (W. Conrad). In the samples from Lake Kivu, 157 species and intraspecific taxa of diatoms were found (including benthic and epiphytic samples); 12 were described as new species. The most common diatoms in the main basin were *Nitzschia confinis* Hust., *N. lancettula* O. Müller, *N. tropica* Hust., *N. gracilis* Hantzsch and *Synedra* (now *Fragilaria*) *ulna* (Nitzsch) Ehrenb. Among the

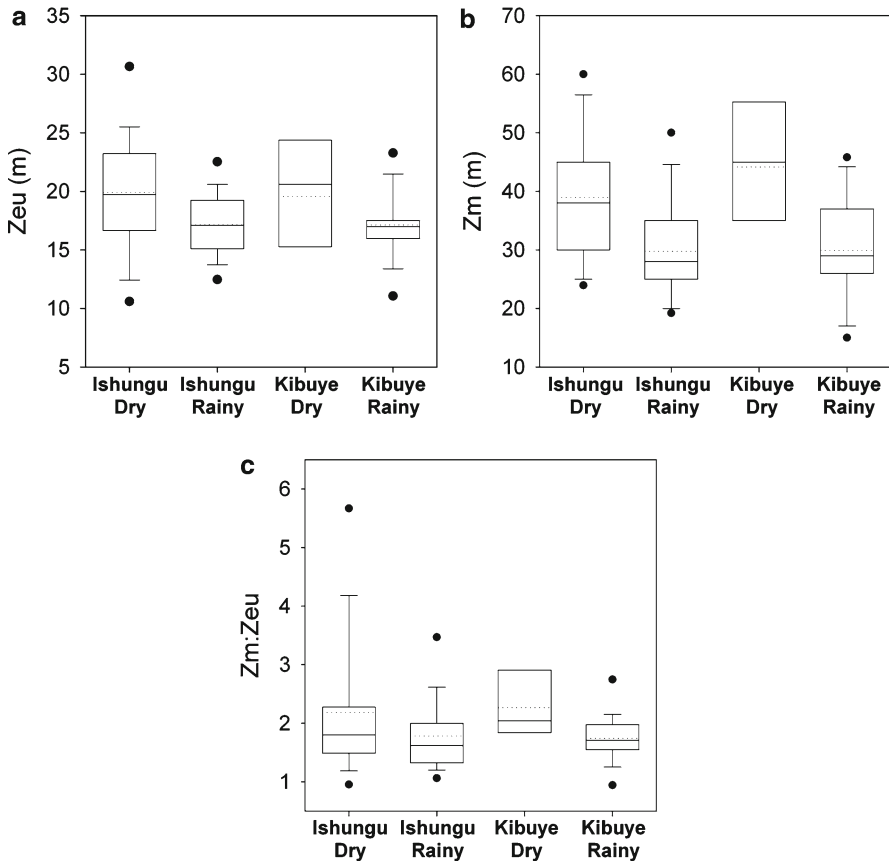


Fig. 5.1 Box plots of (a) the euphotic layer depth (Zeu), (b) the mixed layer depth (Zm) and (c) the Zm:Zeu ratios. Data from two sampling stations (located in Ishungu basin and in the main basin off Kibuye, see Fig. 2.1) and two seasons (rainy vs. dry) are compared. The central full line indicates the median value, the middle dotted line indicates the arithmetic mean values, the box indicates the lower and upper quartiles, the error bars indicate the 10th and 90th percentiles, and the dots correspond to the 5th and 95th percentiles

cyanobacteria, *Microcystis flos-aquae* (Wittrock) Kirchner was the most frequent, together with other *Microcystis* species, such as *M. aeruginosa* (Kütz.) Kütz. and *M. ichthyoblabe* Kütz., and a few planktonic *Lyngbya* (especially *L. circumcreta* West and *L. contorta* Lemm.). Among the other groups, *Botryococcus braunii* Kütz. and *Chlorella vulgaris* Beijerinck were rather abundant, together with several species of *Pediastrum* and *Scenedesmus*. Two new green algae were described from Lake Kivu: *Cosmarium kivuense* Conrad and *Scenedesmus cristatus* Conrad ex Duvigneaud. The data from the Damas' expedition were used by Van Meel (1954) in his book on the phytoplankton of East African great lakes, but without any new addition to the knowledge of the algal flora of Lake Kivu.

Later, in diatom physiology studies, Kilham et al. (1986) and Kilham and Kilham (1990) discussed the *Nitzschia* – *Stephanodiscus* dominance gradient in the

sediments of the lake in the different basins, following a Si:P gradient, and Haberyan and Hecky (1987), in a paleoclimatological study, reported several diatoms and scales of *Paraphysomonas vestita* Stokes (Chrysophyceae) in sediments cores. Drastic changes were recorded around 5,000 years BP in the fauna and flora of the lake, in particular the disappearance of *Stephanodiscus astraeva* var. *minutula* (Kütz.) Grunow (an uncertain taxon, see Spamer and Theriot 1997), and the replacement by several needle-like *Nitzschia*. The authors suggested that the cause of this shift may have been the hydrothermal input of CO₂ into the lake due to high volcanic activity in the region, which would have caused lake turnover and consequent disappearance of the plankton by anoxia, extremely low pH or toxic gases.

In a comparative study of the composition and abundance of phytoplankton from several East African lakes, Hecky and Kling (1987) reported for Lake Kivu an algal assemblage dominated by cyanobacteria and chlorophytes, with higher biomass than in Lake Tanganyika. These authors reported *Lyngbya circumcreta* West, *Cylindrospermopsis*, *Anabaenopsis* and *Raphidiopsis* as the dominant algae found in settled samples collected in March 1972. Among the green algae, *Cosmarium laeve* Rab. was the most common species. In the northern basin, *Peridinium inconspicuum* Lemm., *Gymnodinium pulvisculus* Klebs and *Gymnodinium* sp. were considerably abundant, whereas diatoms *Nitzschia* and *Synedra* (now included in *Fragilaria*) were abundant only in the isolated Kabuno Bay.

The pelagic flora of Lake Kivu was recently updated with new samples from a long term monitoring survey (Sarmiento et al. 2007), in which the most common species (Fig. 5.2) were the pennate diatoms *Nitzschia bacata* Hust. and *Fragilaria danica* (Kütz.) Lange Bert., and the cyanobacteria *Planktolyngbya limnetica* (Lemm.) Komárková-Legnerová and Cronberg. Additionally, the picocyanobacterium *Synechococcus* sp. was shown to constitute a major compartment of the autotrophic plankton in Lake Kivu, with persistently high abundances ($\sim 10^5$ cells mL⁻¹) throughout the year (Sarmiento et al. 2008).

Another important missed (or not reported) aspect in past studies were the high abundances of the centric diatom *Urosolenia* sp. and the cyanobacterium *Microcystis* sp. near the surface under diel stratification conditions (Sarmiento et al. 2007). Typical deep epilimnion/metalimnion populations with species such as *Cryptaulax* sp., *Cryptomonas* sp., *Rhodomonas* sp. and *Merismopedia trolleri* Bach were also described. Vertical stratification at different time scales, from day to season, creates a range of different growing conditions that remain stable long enough to allow the development of these segregated phytoplankton populations in specific layers of the water column. This constitutes an important factor of diversification in Lake Kivu.

5.4 Biomass and Production

Historical data on limnology and planktology parameters of Lake Kivu are scarce, and no long-term surveys had been conducted before the year 2002. Hecky and Kling (1987) reported phytoplankton fresh weight biomass from 550 up to 2,100 mg m⁻³ for March 1972 surface samples. Similar to other East African large

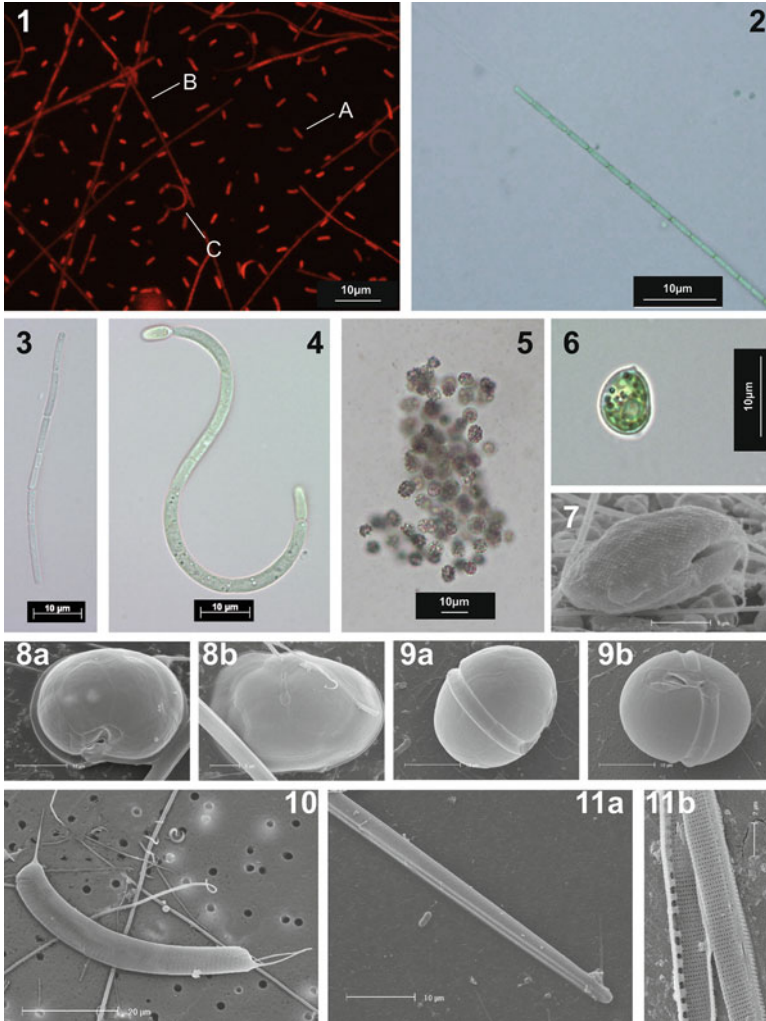


Fig. 5.2 Main phytoplankton taxa present in Lake Kivu. 1. A – *Synechococcus* spp., B – *Planktolyngbya limnetica* (Lemm.) Komárková-Legnerová and Cronberg, C – *Monoraphidium contortum* (Thur.) Kom.-Legn. (epifluorescence microscope); 2. *Planktolyngbya limnetica* (Lemm.) Kom.-Legn. and Cronberg; 3. *Pseudanabaena moniliformis* Kom. and Kling; 4. *Cylandropermopsis* cf. *curvispora* Wat.; 5. *Microcystis* sp.; 6. *Tetraëdron minimum* (A. Braun) Hansg.; 7. *Cryptomonas* sp.; 8a, b. *Peridinium umbonatum* Stein; 9a, b. *Peridinium* sp.; 10. *Urosolenia* sp.; 11a. *Nitzschia bacata* Hust. (11b. detail of fibulae median interruption). Each scale bar is 10 µm

lakes, the planktonic assemblage of Lake Kivu at that time appeared to be dominated to 70–90% by chlorophytes and cyanobacteria, with diatoms at lower abundances (Hecky and Kling 1987). Another trait of Lake Kivu revealed in that study was its higher algal biomass than in the larger Lakes Malawi and Tanganyika, and a slightly

higher primary production: $1.44 \text{ g C m}^{-2} \text{ day}^{-1}$ reported by Beadle (1981), which is an estimate based on few measurements carried out in the 1970s by geochemists (Degens et al. 1973; Jannasch 1975).

In a more complete limnological survey carried out in 2002–2004 (Isumbiso 2006; Isumbiso et al. 2006; Sarmiento 2006; Sarmiento et al. 2006) phytoplankton biomass and composition were assessed combining diverse complementary techniques such as HPLC analysis of marker pigments and CHEMTAX processing, flow cytometry, and epifluorescence and electron microscopy. Annual average chlorophyll *a* (Chl *a*) in the mixed layer was 2.16 mg m^{-3} and the nutrient levels in the euphotic zone were low, placing Lake Kivu clearly in the oligotrophic range. Seasonal variations of algal biomass and composition were related to variability of wind pattern and water column stability. Contrary to earlier reports, diatoms were the dominant group, particularly during the dry season episodes of deep mixing. During the rainy season, the stratified water column, with high light and lower nutrient availability, favoured dominance of filamentous, diazotrophic cyanobacteria and of picocyanobacteria.

Additional data collected in the framework of a cooperation project (ECOSYKI, 2004–2009) extended the record to the year 2008, thus providing a long-term survey (2002–2008) of Lake Kivu phytoplankton (Fig. 5.3). The first striking aspect is the amplitude of the inter-annual variability of phytoplankton biomass peaks. Apparently, phytoplankton usually peaked during the dry season, but not systematically every year. In Ishungu basin, a phytoplankton bloom with a biomass higher than $100 \text{ mg Chl } a \text{ m}^{-2}$ was observed at the end of the dry season (July–August) in 2003, in 2004 and more spectacularly in 2008. A lower dry season peak was observed in 2006 and in 2007, but not in 2002 and in 2005. The variable intensity of the dry season mixing (see Chap. 2) may explain this variation in the phytoplankton biomass peaks.

Grouping the data by station and by season (dry season arbitrarily defined as the period comprised between 1st of June and 30th of September), we can estimate the degree of variance of the total phytoplankton biomass (Chl *a*) and the principal algal groups: diatoms, cyanobacteria and cryptophytes (Fig. 5.4). The dry season Chl *a* values are distributed in a more scattered way than the rainy season values, indicating that extreme and more variable events usually occurred during the dry season. Mean seasonal total biomass was higher during the dry season than during the rainy season in both the main basin and Ishungu basin (Table 5.1, Fig. 5.4). A closer analysis of the phytoplankton community structure indicates a clear seasonal signal: diatoms and cryptophytes were more abundant during the dry season, with a scattered distribution in the box plots, indicating the formation of high biomass peaks during short periods of time, while cyanobacteria showed a more even distribution with slightly lower values during the dry season (Table 5.1, Fig. 5.4). There were no significant differences in the total biomass between the sampling stations, but diatoms and cryptophytes were more abundant in Ishungu basin, while cyanobacteria represented a higher proportion of the biomass in the main basin (Table 5.1, Fig. 5.4).

The vertical distribution of Chl *a* and the major groups of phytoplankton show the typical dominance of cyanobacteria during the stratified conditions of the

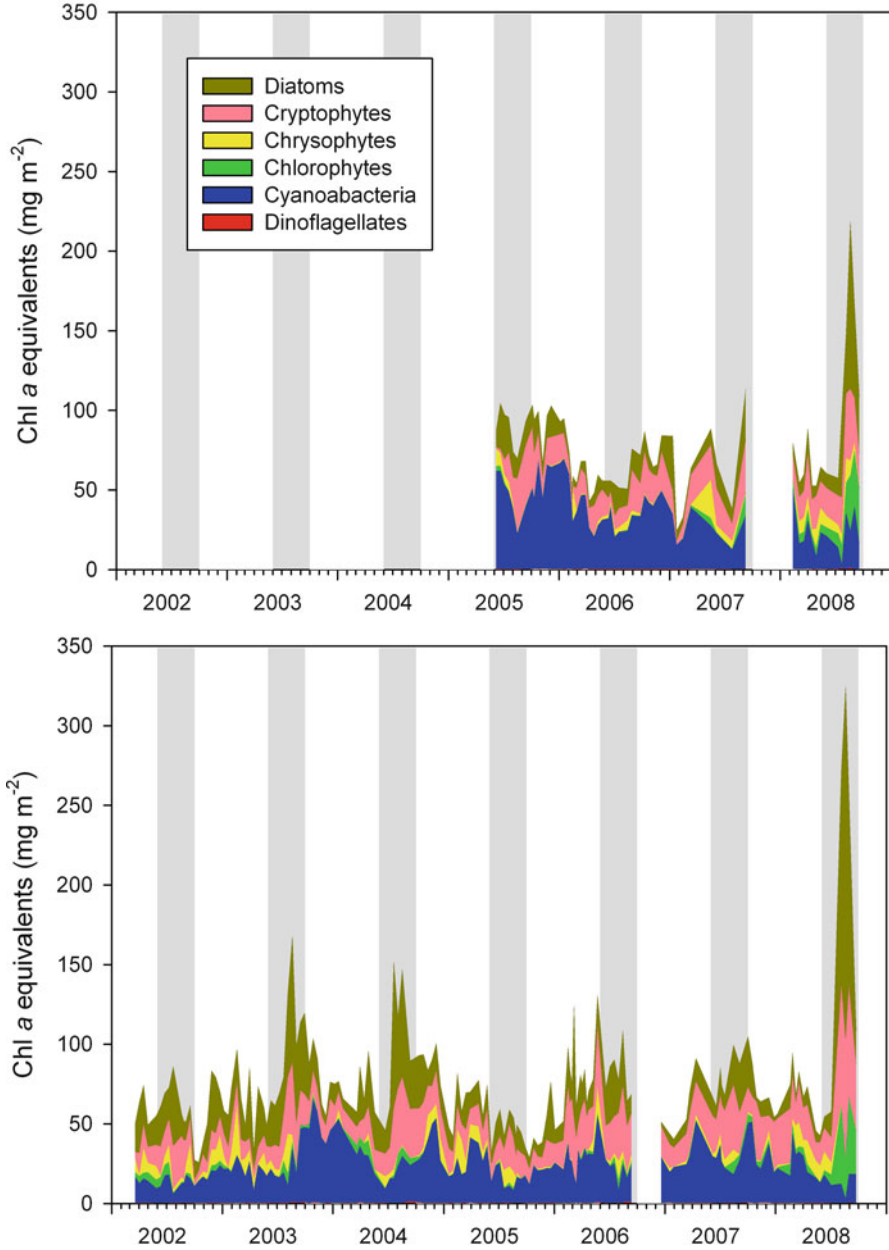


Fig. 5.3 Phytoplankton biomass (chlorophyll *a*, mg m⁻²) and composition from pigment analysis in Lake Kivu integrated in the upper 70 m layer (2002–2008 period in Ishungu basin; 2005–2008 period in the main basin off Kibuye). Grey areas indicate the annual dry season (from June to September)

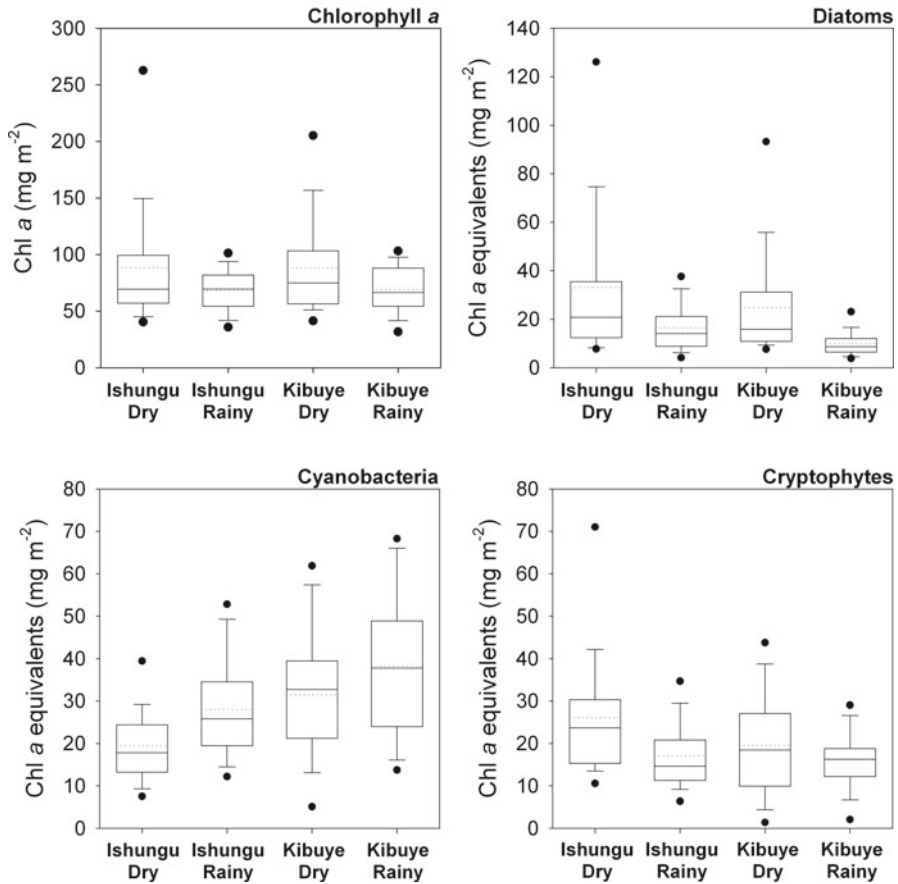


Fig. 5.4 Box plots of the total biomass (chlorophyll *a*, mg m⁻²) and the major groups of phytoplankton in Lake Kivu. Data from two sampling stations (located in Ishungu basin and in the main basin off Kibuye) and two seasons (rainy vs. dry) are compared. The central full line indicates the median value, the middle dotted line indicates the arithmetic mean value, the box indicates the lower and upper quartiles, the error bars indicate the 10th and 90th percentiles, and the dots represent the 5th and 95th percentiles

Table 5.1 Statistical significance (*p* values of full factorial ANOVA tests with log-transformed data) of the comparison between basins (main vs. Ishungu) and seasons (rainy vs. dry) of the biomass (integrated values over the upper 70 m) of the main phytoplankton groups in Lake Kivu estimated from pigments

Effect	Chlorophyll <i>a</i>	Diatoms	Cyanobacteria	Cryptophytes
Basin	0.641	0.003	<0.001	0.006
Season	0.002	<0.001	<0.001	0.008
Basin × Season	0.796	0.192	0.321	0.082

Significant values at the 0.05 confidence level are highlighted

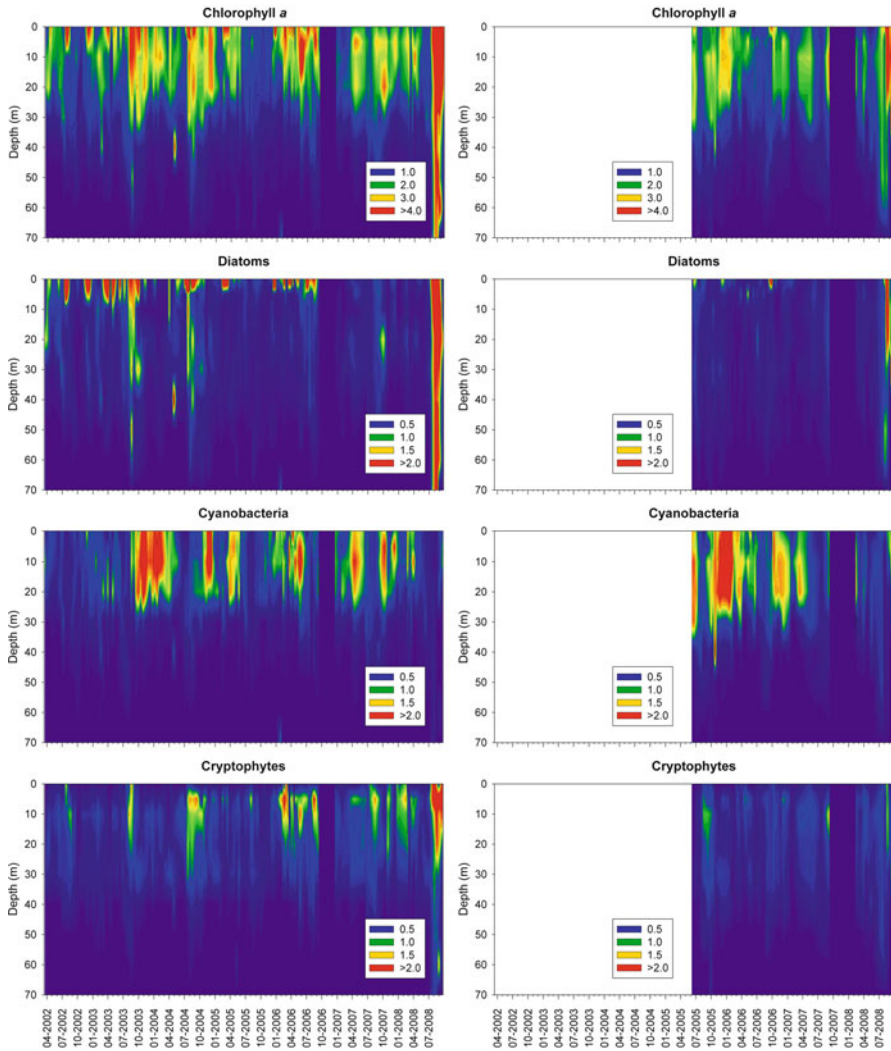


Fig. 5.5 Vertical distribution of the total biomass (chlorophyll *a* , mg m^{-3}) and the major groups of phytoplankton in Ishungu basin during the 2002–2008 period (left column) and the main basin off Kibuye during the 2005–2008 period (right column) in Lake Kivu. Clear areas correspond to missing data

rainy season on the top 20–30 m of the water column (Fig. 5.5). Regularly, during the dry season, lower air temperature (notably night cooling) induced deep mixing, which brought up additional nutrients into the euphotic layer, enhancing phytoplankton and especially diatom growth (Sarmiento et al. 2006). The persistence and intensity of these seasonal mixing events may determine the productivity of

the lake for the whole year, and most likely affect consumer production and ultimately fisheries yield.

The recent analysis of 96 field photosynthesis-irradiance incubations carried out over the 6 year survey allowed a completion of the planktonic primary production data set of Sarmento et al. (2009), and to design a model for prediction of phytoplankton photosynthesis parameters. The irradiance at the onset of light saturation (I_k) ranged between 91 and 752 $\mu\text{E m}^{-2}\text{s}^{-1}$ (mean, 318) and was linearly correlated with the mean irradiance in the mixed layer. The maximum photosynthetic rate (P_{max}) ranged between 1.15 and 7.21 $\text{gC g Chl } a^{-1}\text{h}^{-1}$ (mean, 3.57). The mean observed daily primary production was equal to 0.62 $\text{gC m}^{-2}\text{day}^{-1}$ (range, 0.14–1.92), and annual primary production, calculated using modeled values of photosynthetic parameters, varied between 138 $\text{gC m}^{-2}\text{year}^{-1}$ in 2005 and 258 $\text{gC m}^{-2}\text{year}^{-1}$ in 2003. The mean annual primary production from 2002 to 2008 was 211 $\text{gC m}^{-2}\text{year}^{-1}$. These data clearly show that the inter-annual variation of phytoplankton production in Lake Kivu was important. This large range of variation and the few historic observations, 1.03–1.44 $\text{gC m}^{-2}\text{day}^{-1}$ by Degens et al. (1973), 0.66–1.03 $\text{gC m}^{-2}\text{day}^{-1}$ by Jannasch (1975) and 0.33 $\text{gC m}^{-2}\text{day}^{-1}$ by Descy (1990), preclude to detect any significant changes of planktonic primary production during the last 30 years.

A comparison of phytoplankton production data from East African Great Lakes (Table 5.2) shows that primary production in Lake Kivu is not greater than that in Lakes Tanganyika or Malawi, taking into account the differences in methodologies, as well as spatial heterogeneity as revealed by analysis of satellite images (Bergamino et al. 2010). This contrasts with expectations from Chl *a* concentration: mean Chl *a* in the euphotic zone of Lake Kivu (2.16 mg m^{-3}) is at least twice as high as in Lake Tanganyika – 1.07 mg m^{-3} (2003) – and in Lake Malawi – 0.86 mg m^{-3} (Guildford and Hecky 2000). This observation holds even when taking into account the great inter-annual variation, with a minimum mean annual Chl *a* of 1.59 mg m^{-3} in the least productive year (2005) and a maximum of 2.94 mg m^{-3} in the most productive year (2008).

5.5 Nutrient Limitation

The seston elemental ratios in the mixolimnion of Lake Kivu always remain well above the Redfield ratio and follow a clear seasonal pattern (Fig. 5.6). Significantly lower mean values of C:N, C:P and N:P ratios were observed during the dry season (arbitrarily defined as the period comprised between 1st of June and 30th of September) than during the rainy season ($p < 0.05$). Following elemental thresholds defined by Healey and Hendzel (1980) to estimate nutrient deficiency of phytoplankton in lakes (a C:N ratio between 8.3–14.6 indicates a moderate N-deficiency while a C:N ratio > 14.6 indicates an extreme N-deficiency; a C:P ratio between 129–258 or > 258 indicates, respectively, a moderate or an extreme P-deficiency), the C:P ratios of seston in Lake Kivu indicated a moderate P-deficiency during the dry, mixing season and a severe P limitation during part of

Table 5.2 Chlorophyll *a* concentration (Chl *a*, average in the euphotic zone, standard deviation in parentheses) and mean annual phytoplankton production (PP) in the East African Great Lakes

	Chl <i>a</i> (mg m ⁻³)	Chl <i>a</i> (mg m ⁻²)	PP (g C m ⁻² year ⁻¹)
<i>L. Kivu (Ishungu basin)</i>			
2002	1.78 (0.63)	59 (17)	223
2003	2.32 (0.78)	80 (30)	258
2004	2.54 (0.77)	86 (28)	241
2005	1.67 (0.63)	53 (15)	138
2006	2.58 (0.70)	79 (21)	223
2007	2.05 (0.44)	71 (18)	144
2008	2.95 (2.09)	112 (92)	252
Mean 2002–2008	2.24 (0.99)	75 (39)	211
<i>L. Kivu (main basin)</i>			
2005	2.11 (0.49)	91 (13)	
2006	1.94 (0.42)	63 (16)	
2007	2.03 (1.04)	65 (25)	
2008	2.10 (1.20)	88 (48)	
Mean 2005–2008	2.03 (0.78)	77 (32)	
<i>L. Tanganyika (2002–2003)^a</i>			
Off Kigoma – 2002		23.4	123
Off Kigoma – 2003		25.0	130
Off Mpulungu – 2002		21.7	175
Off Mpulungu – 2003		29.9	205
<i>L. Tanganyika (2003)^b</i>			
Whole-lake, from remote sensing	1.07	42.9	236
<i>L. Malawi (1990s)^c</i>			
Pelagic (south)	0.86 (0.31)	34.4	169
<i>L. Victoria (2001/2002)</i>			
Lake-wide averages ^d			1061
Three inshore bays ^e	49.53	149.1	2333
Pilkington bay ^f	46.7		
Offshore (Bugala)	24.5		

^a Descy et al. (2005), Stenuite et al. (2007)^b Bergamino et al. (2010)^c Guildford et al. (2007)^d Silsbe (2004)^e Recalculated from Silsbe et al. (2006)^f Mugidde (1993)

the rainy, stratified season. The C:N ratios indicated however a moderate N limitation throughout the year, except at some dates during the dry, mixing season where no N-limitation occurred. A comparison of mean values (Table 5.3) from other East African large lakes suggests a stronger nutrient limitation in Lakes Kivu and Malawi than in Lakes Tanganyika and Victoria. The relatively high C:N and C:P ratios point to co-limitation of the phytoplankton community by N and P in Lake Kivu.

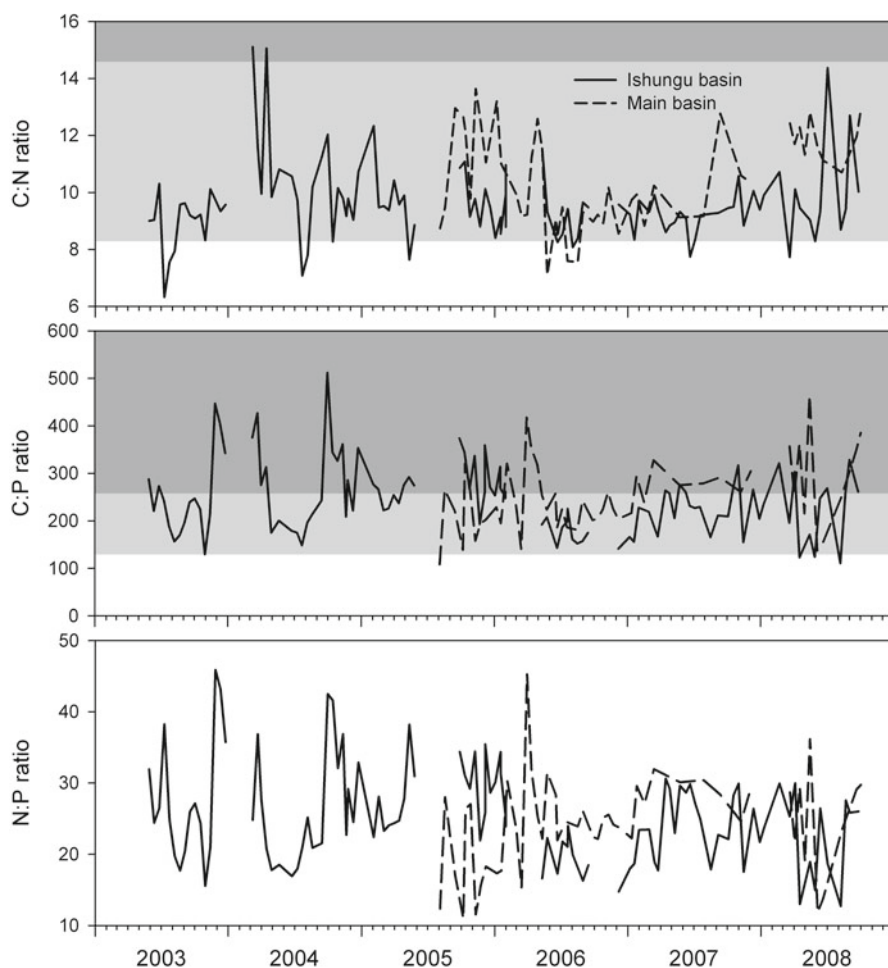


Fig. 5.6 C:N:P elemental ratios (atomic values) of epilimnetic seston in both the main basin and Ishungu basin of Lake Kivu from 2003 to 2008. The light and dark grey areas highlight values indicative of moderate and extreme nutrient limitation, respectively, following Healey and Hendzel (1980)

Table 5.3 C:N:P ratios (elemental values) and chlorophyll *a* (Chl *a*, mg m⁻³) in the East African Great Lakes (average and standard deviation in the euphotic zone)

	C:P	C:N	N:P	Chl <i>a</i> (mg m ⁻³)
L. Kivu (Ishungu basin)	243.8 (±73.6)	9.6 (±1.4)	25.4 (±6.8)	2.24 (±0.99)
L. Kivu (main basin)	251.4 (±75.1)	10.5 (±1.7)	24.3 (±6.7)	2.02 (±0.78)
L. Tanganyika ^a	170.8 (±43.3)	8.1 (±1.1)	21.2 (±5.3)	0.67 (±0.25)
L. Malawi ^b	244.3 (±154.4)	12.5 (±3.6)	19.4 (±8.8)	1.40 (±2.00)
L. Victoria ^b	148.5 (±76.4)	8.2 (±1.7)	18.3 (±7.6)	26.50 (±15.90)

^a Stenuite et al. (2007)

^b Guildford and Hecky (2000)

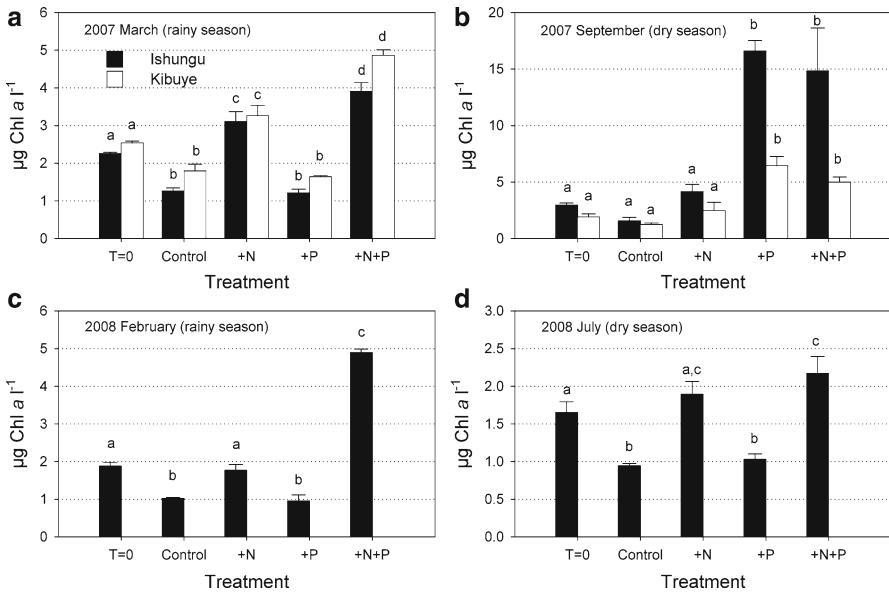


Fig. 5.7 Phytoplankton biomass (chlorophyll *a*, $\mu\text{g Chl } a \text{ l}^{-1}$) after 4–5 days of incubation at lake temperature in six nutrient addition bioassay experiments carried out during rainy (**a** and **c**) and dry (**b** and **d**) seasons in Lake Kivu. The +N treatment received additional $15 \mu\text{M NH}_4\text{Cl}$ (final concentration), the +P treatment received $5 \mu\text{M KH}_2\text{PO}_4$ (final concentration), while both N and P supplements were added in the +N+P treatment. All treatments were performed in triplicates. Note the different biomass scales. Identical small letters indicate treatments with no significant difference between biomass at the 0.05 confidence level (Scheffé test)

Nutrient addition assays carried out during rainy and dry seasons in 2007 and 2008 indicated a direct N-limitation and co-limitation by P during rainy seasons (Fig. 5.7a, c) and P or N limitation during dry seasons depending on the year (Fig. 5.7b, d).

5.6 Conclusions

Present Lake Kivu phytoplankton is dominated by diatoms, cyanobacteria and cryptophytes, with substantial seasonal shifts related to variations in depth of the mixed layer, driving contrasting light exposure, and nutrient availability. In this regard, phytoplankton ecology in Lake Kivu does not differ from that of other Rift lakes, where, despite constant irradiance and temperature of the tropical climate, seasonal variations occur and result in a trade-off between low light with high nutrient supply and high light with low nutrient supply. With regard to phytoplankton production, Lake Kivu is also similar to other Rift lakes, despite its greater mean Chl *a* concentration. Phytoplankton growth can be N or P limited, or co-limited by N and P.

Again, such limitations have been shown in Lakes Tanganyika and Malawi, even though the extent of P limitation seems greater in Lake Kivu, giving some indication of less nutrient recycling in the mixolimnion.

However, some features make Lake Kivu different from the other deep East African lakes: a closer look at the phytoplankton composition reveals a peculiar assemblage, with few chlorophytes, but long and slender *Nitzschia* and *Fragilaria* species, thin filamentous cyanobacteria (e.g., *Planktolyngbya limnetica*), picocyanobacteria, and several cryptophytes. In the surface waters, relatively large biomass of *Urosolenia* sp. can be detected at times, and colonies of *Microcystis* make vertical migration, sometimes becoming visible at the lake surface. Therefore, phytoplankton composition suggests affinities with more productive East African Lakes, such as Lakes Edward and Victoria, from a functional group perspective as discussed in Sarmento et al. (2006). As for the higher chlorophyll *a* concentration in Lake Kivu, it may have resulted from the Tanganyika sardine introduction, through a trophic cascade effect: indeed, metazooplankton abundance decreased by a factor of ~3 after the introduction of *Limnothrissa miodon* (see Chap. 7), likely resulting in a proportional decline of the grazing pressure on phytoplankton. This trophic cascade effect, as well as the interaction of phytoplankton with other organisms of the food web, is discussed in Chap. 11. Finally, a key feature of Lake Kivu is the dry season peak of diatoms and cryptophytes, which may determine the productivity for the whole year. However these peaks may vary by a factor of 2 between years, and this variation may determine the productivity of the lake for the whole year, most likely affecting consumer production and ultimately fisheries yield.

Acknowledgments Hugo Sarmento's work was supported by the Spanish MCyI (Juan de la Cierva Fellowship JCI-2008-2727) and AGLOM project (CGL2010-11556-E). This work was partly funded by the Fonds National de la Recherche Scientifique (FRS-FNRS) under the CAKI (Cycle du carbone et des nutriments au Lac Kivu) project (contract n 2.4.598.07) and contributes to the Belgian Federal Science Policy Office EAGLES (East African Great Lake Ecosystem Sensitivity to changes, SD/AR/02A) project. François Darchambeau was a Postdoctoral Researcher at the FRS-FNRS.

References

- Beadle LC (1981) The inland waters of tropical Africa – an introduction to tropical limnology. Longman, New York
- Bergamino N, Horion S, Stenuite S, Cornet Y, Loiselle S, Plisnier PD, Descy JP (2010) Spatio-temporal dynamics of phytoplankton and primary production in Lake Tanganyika using a MODIS based bio-optical time series. *Remote Sens Environ* 114:772–780. doi:10.1016/j.rse.2009.11.013
- Damas H (1935–1936) Exploration du Parc National Albert. Institut des Parcs Nationaux du Congo Belge, Liège, Belgium
- Damas H (1937) Quelques caractères écologiques de trois lacs équatoriaux: Kivu, Edouard, Ndalaga. *Ann Soc R Zool Belg* 68:121–135
- Degens E, Herzen RP, Wong H-K, Deuser WG, Jannasch HW (1973) Lake Kivu: structure, chemistry and biology of an East African Rift lake. *Geol Rundsch* 62:245–277. doi:10.1007/BF01826830

- Descy J-P (1990) Etude de la production planctonique au lac Kivu – Rapport de mission, Projet PNUD/FAO RWA/87/012. UNECED, Namur
- Descy J-P, Hardy M-A, Stenuite S, Pirlot S, Leporcq B, Kimirei I, Sekadende B, Mwaitega S, Sinyenza D (2005) Phytoplankton pigments and community composition in Lake Tanganyika. *Freshw Biol* 50:668–684. doi:[10.1111/j.1365-2427.2005.01358.x](https://doi.org/10.1111/j.1365-2427.2005.01358.x)
- Frémy P, Pascher A, Conrad W (1949) Exploration du Parc National Albert – Mission H. Damas (1935–1936), Fascicule 19: Algues et Flagellates. Institut des Parcs Nationaux du Congo Belge, Bruxelles, Belgium
- Guildford SJ, Bootsma HA, Taylor WD, Hecky RE (2007) High variability of phytoplankton photosynthesis in response to environmental forcing in oligotrophic Lake Malawi/Nyasa. *J Gt Lakes Res* 33:170–185. doi:[10.3394/0380-1330\(2007\)33\[170:HVOPPI\]2.0.CO;2](https://doi.org/10.3394/0380-1330(2007)33[170:HVOPPI]2.0.CO;2)
- Guildford SJ, Hecky RE (2000) Total nitrogen, total phosphorus, and nutrient limitation in lakes and oceans: Is there a common relationship? *Limnol Oceanogr* 45:1213–1223. doi:[10.4319/lo.2000.45.6.1213](https://doi.org/10.4319/lo.2000.45.6.1213)
- Haberyan KA, Hecky RE (1987) The late pleistocene and holocene stratigraphy and paleolimnology of Lakes Kivu and Tanganyika. *Paleogeogr Paleoclimatol Paleoecol* 61:169–197. doi:[10.1016/0031-0182\(87\)90048-4](https://doi.org/10.1016/0031-0182(87)90048-4)
- Healey FP, Hendzel LL (1980) Physiological indicators of nutrient deficiency in lake phytoplankton. *Can J Fish Aquat Sci* 37:442–453. doi:[10.1139/f80-058](https://doi.org/10.1139/f80-058)
- Hecky RE, Kling HJ (1987) Phytoplankton ecology of the great lakes in the rift valleys of Central Africa. *Arch Hydrobiol Beih Ergeb Limnol* 25:197–228
- Hustedt F (1949) Exploration du Parc National Albert – Mission H. Damas (1935–1936), Fascicule 8: Süßwasser-Diatomeen. Institut des Parcs Nationaux du Congo Belge, Bruxelles, Belgium
- Isumbisho M (2006) Zooplankton ecology of Lake Kivu (eastern Africa). PhD thesis, University of Namur, Belgium
- Isumbisho M, Sarmiento H, Kaningini B, Micha JC, Descy JP (2006) Zooplankton of Lake Kivu, East Africa, half a century after the Tanganyika sardine introduction. *J Plankton Res* 28:971–989. doi:[10.1093/plankt/fbl032](https://doi.org/10.1093/plankt/fbl032)
- Jannasch HW (1975) Methane oxidation in Lake Kivu (central Africa). *Limnol Oceanogr* 20:860–864
- Kilham P, Kilham SS, Hecky RE (1986) Hypothesized resource relationships among African planktonic diatoms. *Limnol Oceanogr* 31:1169–1181
- Kilham SS, Kilham P (1990) Endless summer: internal loading processes dominate nutrient cycling in tropical lakes. *Freshw Biol* 23:379–389. doi:[10.1111/j.1365-2427.1990.tb00280.x](https://doi.org/10.1111/j.1365-2427.1990.tb00280.x)
- Kling H, Mugidde R, Hecky RE (2001) Recent changes in the phytoplankton community of Lake Victoria in response to eutrophication. In: Munawar M, Hecky RE (eds) *The great lakes of the world (GLOW): food-web, health and integrity*. Backhuys Publishers, Leiden, The Netherlands
- Mugidde R (1993) Changes in phytoplankton primary productivity and biomass in Lake Victoria (Uganda). *Verh Int Ver Theor Angew Limnol* 25:846–849
- Mukankomeje R, Plisnier PD, Descy JP, Massaut L (1993) Lake Muzahi, Rwanda – limnological features and phytoplankton production. *Hydrobiologia* 257:107–120. doi:[10.1007/BF00005951](https://doi.org/10.1007/BF00005951)
- Reynolds CS (2006) *The ecology of phytoplankton*. Cambridge University Press, Cambridge
- Sarmiento H (2006) Phytoplankton ecology of Lake Kivu (eastern Africa). PhD thesis, University of Namur, Belgium
- Sarmiento H, Isumbisho M, Descy JP (2006) Phytoplankton ecology of Lake Kivu (eastern Africa). *J Plankton Res* 28:815–829. doi:[10.1093/plankt/fbl017](https://doi.org/10.1093/plankt/fbl017)
- Sarmiento H, Isumbisho M, Stenuite S, Darchambeau F, Leporcq B, Descy JP (2009) Phytoplankton ecology of Lake Kivu (eastern Africa): biomass, production and elemental ratios. *Proc Int Assoc Theor Appl Limnol* 30:709–713
- Sarmiento H, Leitao M, Stoyneva M, Couté A, Compère P, Isumbisho M, Descy JP (2007) Diversity of pelagic algae of Lake Kivu (East Africa). *Cryptogam Algol* 28:245–269

- Sarmento H, Unrein F, Isumbisho M, Stenuite S, Gasol JM, Descy JP (2008) Abundance and distribution of picoplankton in tropical, oligotrophic Lake Kivu, eastern Africa. *Freshw Biol* 53:756–771. doi:[10.1111/j.1365-2427.2007.01939.x](https://doi.org/10.1111/j.1365-2427.2007.01939.x)
- Sarvala J, Salonen K, Jarvinen M, Aro E, Huttula T, Kotilainen P, Kurki H, Langenberg V, Mannini P, Peltonen A, Plisnier PD, Vuorinen I, Molsa H, Lindqvist OV (1999) Trophic structure of Lake Tanganyika: carbon flows in the pelagic food web. *Hydrobiologia* 407:149–173. doi:[10.1023/A:1003753918055](https://doi.org/10.1023/A:1003753918055)
- Silsbe GM (2004) Phytoplankton production in Lake Victoria, East Africa. MSc thesis, Univ. of Waterloo, Canada
- Silsbe GM, Hecky RE, Guildford SJ, Mugidde R (2006) Variability of chlorophyll *a* and photosynthetic parameters in a nutrient-saturated tropical great lake. *Limnol Oceanogr* 51:2052–2063. doi:[10.4319/lo.2006.51.5.2052](https://doi.org/10.4319/lo.2006.51.5.2052)
- Spamer EE, Theriot EC (1997) *Stephanodiscus minutulus*, *S. minutus*, and similar epithets in taxonomic, ecological, and evolutionary studies of modern and fossil diatoms (Bacillariophyceae: Thalassiosiraceae) – a century and a half of uncertain taxonomy and nomenclatural hearsay. *Proc Acad Nat Sci Phila* 148:231–272
- Stenuite S, Pirlot S, Hardy MA, Sarmento H, Tarbe AL, Leporcq B, Descy JP (2007) Phytoplankton production and growth rate in Lake Tanganyika: evidence of a decline in primary productivity in recent decades. *Freshw Biol* 52:2226–2239. doi:[10.1111/j.1365-2427.2007.01829.x](https://doi.org/10.1111/j.1365-2427.2007.01829.x)
- Van Meel L (1954) Le Phytoplancton. Résultats Scientifiques de l'Exploration Hydrobiologique du Lac Tanganyika. Institut Royal des Sciences Naturelles de Belgique, Bruxelles, Belgium

Chapter 7

Zooplankton of Lake Kivu

François Darchambeau, Mwapu Isumbisho, and Jean-Pierre Descy

Abstract The dominant species of the crustacean plankton in Lake Kivu are the cyclopoid copepods *Thermocyclops consimilis* and *Mesocyclops aequatorialis* and the cladoceran *Diaphanosoma excisum*. Mean crustacean biomass over the period 2003–2004 was 0.99 g C m^{-2} . The seasonal dynamics closely followed variations of chlorophyll *a* concentration and responded well to the dry season phytoplankton peak. The mean annual crustacean production rate was $23 \text{ g C m}^{-2} \text{ year}^{-1}$. The mean trophic transfer efficiency between phytoplankton and herbivorous zooplankton was equal to 6.8%, indicating a coupling between both trophic levels similar to that in other East African Great lakes. These observations suggest a predominant bottom-up control of plankton dynamics and biomass in Lake Kivu. Whereas the present biomass of crustacean plankton in Lake Kivu is comparable to that of other African Rift lakes, the zooplankton biomass before *Limnothrissa* introduction was 2.6 g C m^{-2} , based on estimation from available historical data. So, if the sardine introduction in the middle of the last century led to a threefold decrease of zooplankton biomass, it did not affect zooplankton production to a level which would lead to the collapse of the food web and of the fishery.

F. Darchambeau (✉)
Chemical Oceanography Unit, University of Liège, Liège, Belgium
e-mail: francois.darchambeau@ulg.ac.be

M. Isumbisho
Institut Supérieur Pédagogique, Bukavu, D.R. Congo
e-mail: isumbisho@yahoo.fr

J.-P. Descy
Research Unit in Environmental and Evolutionary Biology, University of Namur,
Namur, Belgium
e-mail: jpdescy@fundp.ac.be

7.1 Introduction

In all pelagic systems, metazooplankton is a key link between primary producers and consumers. In this regard, however, Lake Kivu was exceptional, as pelagic fishes were completely missing before the introduction of the “Tanganyika sardine”, *Limnothrissa miodon* (see Chap. 8). In fact, the introduction of the sardine was one of the largest biomanipulations ever, comparable to the introduction of the Nile perch in Lake Victoria. It is hardly surprising that the impact of the sardine introduction has attracted the attention of scientists, who stressed the highly detrimental effect of introducing an efficient predator of zooplankton in a system where there was no zooplanktivorous fish before.

Dumont (1986) described the sardine introduction as an ecological disaster, which caused the disappearance of a major grazer, the cladoceran *Daphnia curvirostris* Eylmann 1887, and a decrease in size and abundance of the remaining crustaceans. However, zooplankton records of Lake Kivu, on which Dumont’s conclusions were based, are somewhat contradictory. In the earliest records of cladocerans of the “Parc National Albert” (Brehm 1939), there is no mention of a *Daphnia* species in the zooplankton of Lake Kivu, but of two *Ceriodaphnia* species, of *Moina dubia*, of three *Alona* species, and of *Chydorus sphaericus*. From samples collected in 1953 by Verbeke (1957), *Daphnia pulex* is mentioned, along with *Moina dubia* and *Ceriodaphnia rigaudi*. But a later re-examination by Reyntjens (1982) of Verbeke’s samples conserved at the Institute of Natural Sciences in Brussels identified the *Daphnia* species as *D. curvirostris*. Monthly samplings in 1953 showed a peak of cladocerans in the dry season (July–August). In the subsequent literature (e.g. Lehman 1996), the crustacean community of Lake Kivu has been reported as comprising three species of cyclopoid copepods, no calanoid, and four species of cladocerans, with *Daphnia* missing. According to Dumont (1986), this large cladoceran vanished from Lake Kivu following the sardine introduction; on the other hand, such large *Daphnia* are so conspicuous that one may question whether it is possible that they were not observed in the samples from the Parc National Albert mission of 1936–1937 (Damas 1937; Brehm 1939). Dumont (1986) also noted an important decrease of copepod mean body size and zooplankton biomass since the introduction of *Limnothrissa* and predicted the collapse of the fishery.

In this chapter, we report the present taxonomic composition of Lake Kivu metazooplankton, its abundance, biomass and production, and how they are influenced by seasonality. Furthermore, we present some data about diel vertical migration of the most important species, and comment about spatial variations at the scale of the whole lake. Diversity and abundance results are from Isumbisho (2006), completed by subsequent new estimates of biomass and productions. We also reanalyze all available historical data in order to reassess the effects of *Limnothrissa* introduction on the zooplankton community.

7.2 Diversity of Lake Kivu Metazooplankton

The three common groups of freshwater metazooplankton are represented in Lake Kivu: copepods, cladocerans and rotifers. The copepod and cladoceran species found in the lake are common in the tropics or with worldwide distribution. By contrast, the presence of rotifers in the plankton of the pelagic zone is rather surprising, as they are totally absent from the pelagic waters of the other oligotrophic Rift lakes, Lake Malawi and Lake Tanganyika. Actually, rotifers are the most diverse metazooplankton group in Lake Kivu, with 12 taxa (among which Bdelloids, with unknown diversity).

7.2.1 Copepods

As in temperate waters, three suborders of copepods inhabit freshwater in the tropics: calanoids, cyclopoids and harpacticoids. The latter comprises exclusively meiobenthic species that are very rarely found in plankton samples (Alekseev 2002). Calanoids are exclusively planktonic and, while they are present in the other oligotrophic Rift lakes, they are absent from Lake Kivu. Therefore, cyclopoids are the sole copepods in the pelagic metazooplankton of Lake Kivu, with only three species: *Mesocyclops aequatorialis* Kiefer 1929, *Thermocyclops consimilis* Kiefer 1934 and *Tropocyclops confinis* (Kiefer 1930).

The genus *Mesocyclops* Sars 1914 occurs worldwide. It is successful in the tropics and subtropics and marginal in temperate and arctic regions (Van de Velde 1984) and is one of the largest genera of the family Cyclopidae. At present, it consists of about 66 species (Ueda and Reid 2003). Distinctive features of *M. aequatorialis* were described in several studies (e.g. Dussart 1967a, b, 1982; Kiefer 1978; Ueda and Reid 2003; Hołyńska et al. 2003) and even revised (e.g. Van de Velde 1984). The most easily recognizable traits during microscopic observations are the following:

- Body slender (Fig. 7.1a–c), female antennule 17-segmented reaching the third thoracic segment;
- Fifth pair of paws (P5) two-segmented, first segment bearing lateral seta, second segment with slender apical and spiniform medial setae, latter seta implanted about mid-length of segment (Fig. 7.1d–e);
- More easily visible is the shape of the furca (Fu): internal median furcal seta of about four times as long as Fu and externally oriented (Fig. 7.1a–c).

With an average body size of about 0.725 mm at adult stage, *M. aequatorialis* is the largest copepod species in Lake Kivu. It is also present in Lake Malawi (Irvine 1995), where it reaches a similar size. Actually it is a common species in the tropics.

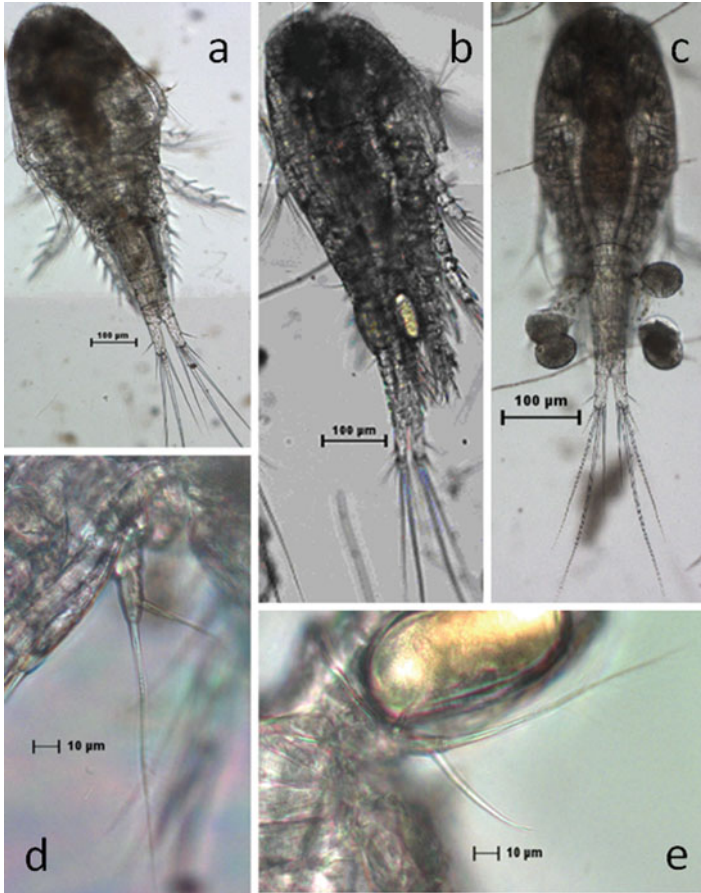


Fig. 7.1 *Mesocyclops aequatorialis*: Adult female without eggs (a), adult male (b), egg-bearing female (c), fifth paw of adult female (d) and male (e). The scale bars indicate 100 μm (a, b, c) and 10 μm (d, e), respectively

The genus *Thermocyclops* Kiefer 1929 is found all over the world and comprises about 50 species and subspecies. It differs from the genus *Mesocyclops* by several characteristics (Fig. 7.2a–c) but the most easily visible are the shape of:

- P5: terminal segment with internal spine and external seta both implanted \pm apical in *Thermocyclops* (Fig. 7.2d) while implanted on a different level in *Mesocyclops*;
- Fu: internal median furcal seta of about two times as long as Fu and internally oriented (Fig. 7.2e).

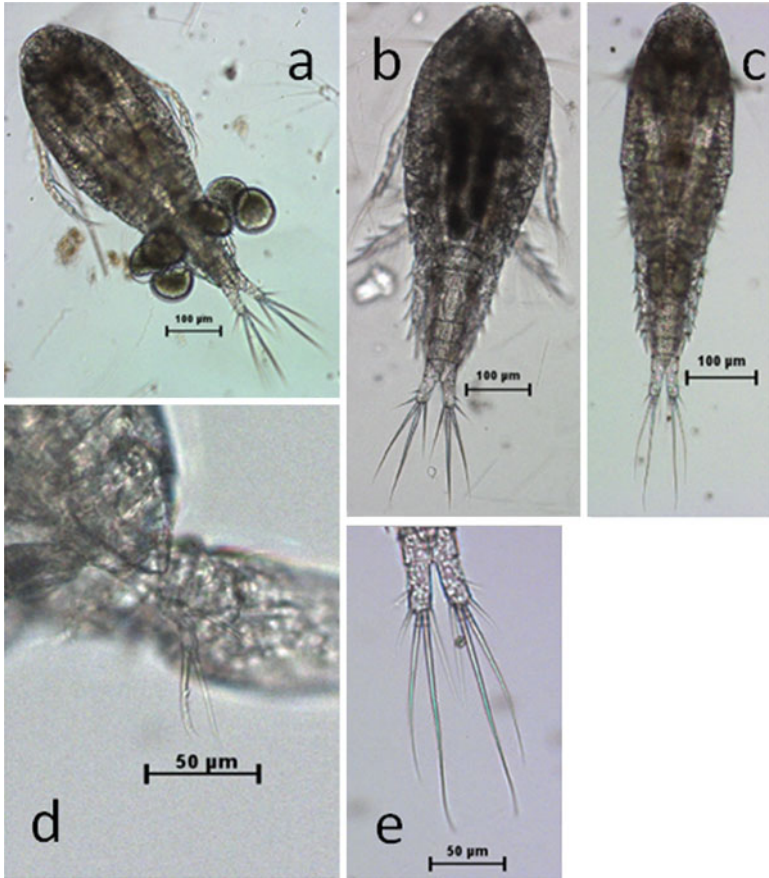


Fig. 7.2 *Thermocyclops consimilis*: egg-bearing female (a), female without eggs (b), adult male (c), fifth paw (d) and the furca (e). The scale bars indicate 100 µm (a, b, c) and 50 µm (d, e), respectively

In Lake Kivu, the genus is represented by *T. consimilis*, a very common species, with an adult average body size of 0.534 mm.

The genus *Tropocyclops* Kiefer 1927 comprises 15 species and 15 subspecies in the tropics (Alekseev 2002) but only *Tropocyclops confinis* occurs in Lake Kivu. It is easily distinguished from both *Thermocyclops* and *Mesocyclops* by:

- Its small size (Fig. 7.3a–b) which is on average 0.417 mm at adult stage;
- The shape of Fu with a very reduced internal furcal seta (Fig. 7.3c).

In addition, the antennules carried by adult females are 12-segmented.

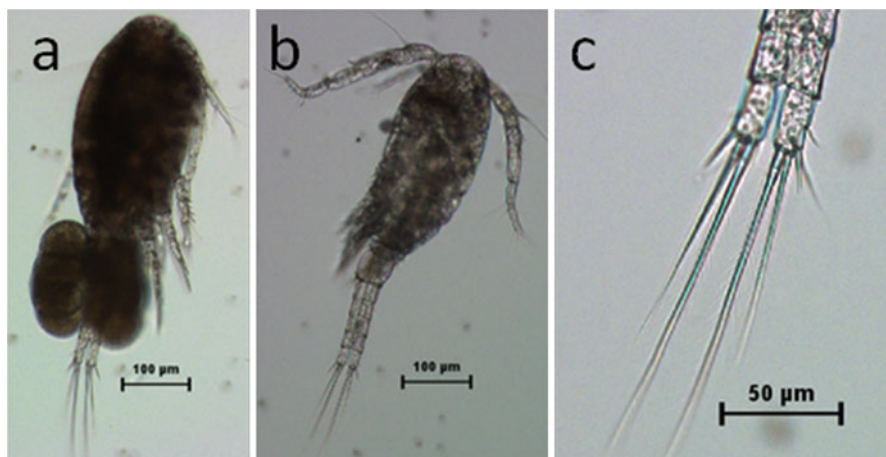


Fig. 7.3 *Tropocyclops confinis*: egg-bearing female (a), adult male (b) and the furca (c). The scale bars indicate 100 µm (a, b) and 50 µm (c), respectively

7.2.2 Cladocera

Cladocera are represented in Lake Kivu by four species belonging to four different families: *Diaphanosoma excisum* Sars 1885 (Sididae), *Moina micrura* Kurz 1875 (Moinidae), *Ceriodaphnia cornuta* Sars 1885 (Daphniidae) and *Coronatella (Alona) rectangula* (Sars 1861) (Chydoridae).

D. excisum (Fig. 7.4a) is one of the most common species of the genus in the tropics and subtropics. It is characterized by a large head, rectangular, with well-developed dorsal part, ventral fold of carapace and two spines near posterior carapace margin (Kořínek 2002). In Lake Kivu samples, it is easily recognized and distinguished from the other cladoceran species by its second biramous antenna with the exopodite presenting two articles. *D. excisum* is a common species in Lake Kivu with a small body size (0.488 mm), smaller than in Lake Malawi (Irvine 1995).

Normally littoral and benthic, *C. rectangula* (Fig. 7.4b) is present also in the pelagic zone of Lake Kivu. With a small body size (0.275 mm), it is recognized and easily distinguished from other cladocerans by the general shape of its body with a visible carapace with two valves.

C. cornuta (Fig. 7.4c) is very rare in Lake Kivu but easily recognized by its small rounded head with small pointed projection. The rostrum is also pointed. In addition, the tip of the caudal side of its carapace is characteristic.

M. micrura (Fig. 7.4d) seems rare in Lake Kivu. Like *D. excisum*, it is recognized by its biramous second antenna but with a four-segmented exopodite. Its average body size in the lake is 0.449 mm. According to Kořínek (2002), *M. micrura* is a species living in all types of water bodies, in pelagic as well as in littoral weedy areas. Originally described in Australia, this species is distributed in the tropics and subtropics of all continents.

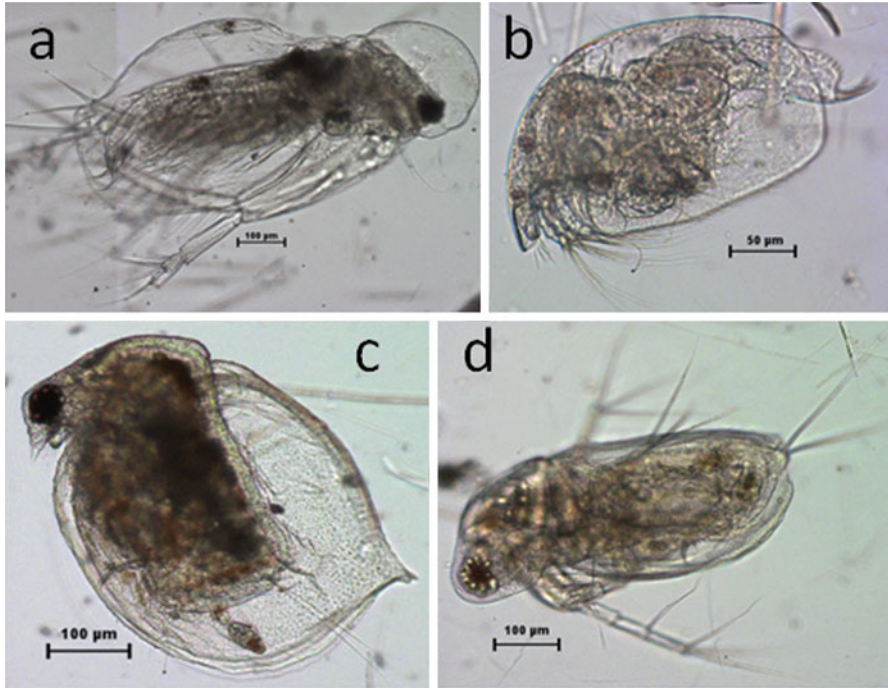


Fig. 7.4 Cladocerans of Lake Kivu: *Diaphanosoma excisum* (a), *Coronatella rectangula* (b), *Ceriodaphnia cornuta* (c) and *Moina micrura* (d). The scale bars indicate 100 μm (a, c, d) and 50 μm (b), respectively

7.2.3 Rotifera

Rotifera (Fig. 7.5) constitute the most diverse group of Lake Kivu pelagic metazooplankton, with 12 taxa: *Anuraeopsis fissa* Gosse 1851, *Brachionus calyciflorus* Pallas 1766, *Brachionus caudatus* Barrois and Daday 1894, *Brachionus falcatus* Zacharias 1898, *Brachionus quadridentatus* Hermann 1783, *Colurella* sp., *Keratella tropica* (Apstein 1907), *Lecane* sp., *Trichocerca* sp., *Polyarthra* sp., *Hexarthra* sp. and unidentified Bdelloids. Among these taxa, the most common are the Bdelloids, *K. tropica*, *Lecane* sp., *Brachionus* spp. and *A. fissa*.

7.3 Abundance, Biomass and Production

Zooplankton was sampled fortnightly in three subsequent years (2003–2005) in the mixolimnion of the Ishungu Basin (see Fig. 2.1), using a 75-cm diameter, 55-μm mesh closing net in three different strata (0–20, 20–40, 40–60 m). The abundance of

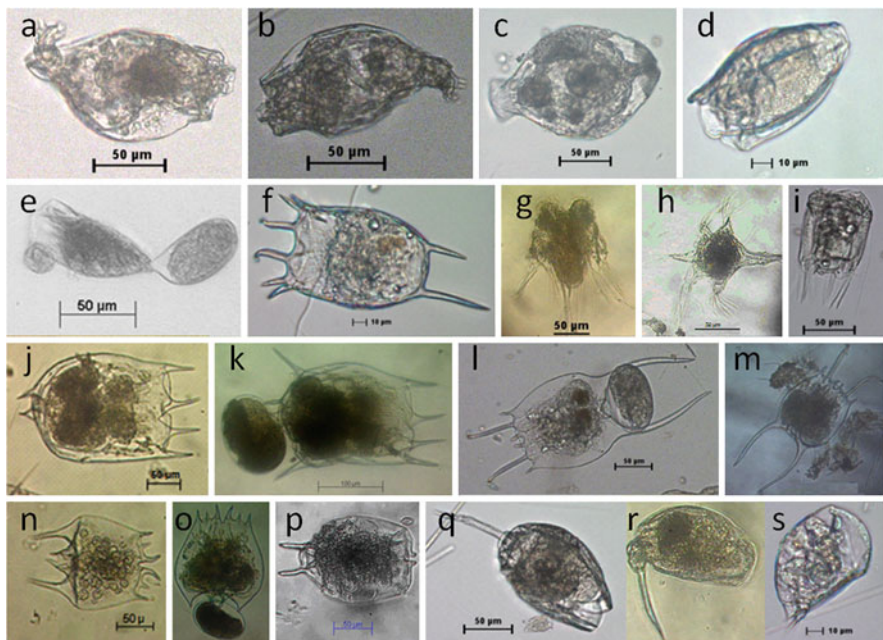


Fig. 7.5 Rotifers of Lake Kivu: Bdelloids (a–c), *Anuraeopsis fissa* (d–e), *Keratella tropica* (f), *Hexarthra* sp. (g–h), *Polyarthra* sp. (i), *Brachionus calyciflorus* (j–k), *Brachionus falcatus* (l–m), *Brachionus quadridentatus* (n–o), *Brachionus caudatus* (p), *Lecane* sp. (q–r), *Colurella* sp. (s). The scale bars indicate 100 µm (k), 50 µm (a, b, c, e, g, h, i, j, l, n, p, q) and 10 µm (d, f, s), respectively

rotifers and crustacean zooplankton was estimated under an inverted microscope. Rotifers, cladocerans and post-naupliar copepods were identified to species, separating copepodids from adults. Nauplii were grouped together. Comparative tests with the 55-µm plankton net and a 20-L Schindler trap mounted with a 37-µm plankton net showed that net hauls systematically underestimated abundance of copepodids and copepods at adult stage by a factor of 1.5, nauplii and rotifers by a factor of 3 and cladocerans by a factor of 1.2 for the 0–20-m layer, and by a factor of 5 and 7, respectively for copepodids and copepods at adult stage, and for nauplii, rotifers and cladocerans, for deeper strata (i.e., 20–40 and 40–60 m). This resulted from rapid net clogging. Consequently, abundance results for each species/stage were multiplied by the respective factor for the considered strata before adding results of each stratum for obtaining areal estimates of abundance.

From each sample, at least 50 individuals, unless rare, of each of the main crustacean species were measured using a calibrated eye-piece graticule. Copepod body length was measured from the top of the head to the base of the furci rami. Cladocerans were measured from the top of the head to the tip of the abdomen excluding spines and projections. Biomass was estimated using length-weight relations from Irvine and Waya (1999) for *D. excisum* and for copepodid and adult stages of *M. aequatorialis* and *Thermocyclops*, from Dumont et al. (1975) for

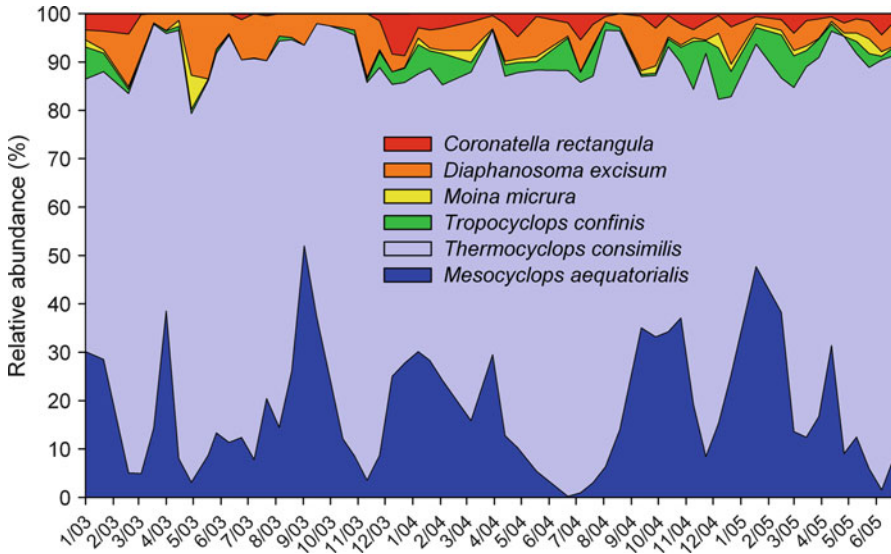


Fig. 7.6 Relative abundance of the six main crustacean species in the mixolimnion of Lake Kivu (Ishungu Basin) from January 2003 to June 2005

nauplii and the other cladoceran species, and using weight data from Sarvala et al. (1999) for *Tropocyclops*. Copepod production was estimated following Irvine and Waya (1999) for production of zooplankton in Lake Malawi. Briefly, we used the Growth Increment Summation Method or the mathematically similar Instantaneous Growth Method which takes into account the development rates of each distinct life-stage or group of life-stages (i.e. nauplii). The production rate of the cyclopoid copepods *M. aequatorialis* and *T. confinis* was calculated assuming linear growth rates within size-classes (Equation 3 in Irvine and Waya 1999) while an exponential growth rate was assumed for *T. consimilis* (Equation 4 in Irvine and Waya 1999). Partitioning of nauplii into the three cyclopoid species was done on the assumption that the proportion of nauplii approximated that of post-naupliar animals. Development times were obtained from Irvine and Waya (1999) for *M. aequatorialis* and from Mavuti (1994) for *Thermocyclops* and *Tropocyclops*.

Production of cladocerans, which generally constituted a low proportion of the zooplankton abundance, was estimated from published production/biomass ratio estimates (Amarasinghe et al. 2008). Production estimates of each crustacean species were calculated for each sampling date. Dry weight biomass and production were converted into C using a C:dry weight ratio of 0.5.

Numerically, copepods dominated other groups (Figs. 7.6 and 7.7), with >90% of crustacean numbers in the dry seasons. They were significantly less abundant in the rainy season, when cladocerans increased up to 20% of total crustacean abundance. Rotifers and cladocerans were always present in lower numbers than copepods with a mean abundance of, respectively for rotifers and cladocerans, 3.6×10^5 ind. m^{-2} and 2.5×10^5 ind. m^{-2} (Fig. 7.7c). Their respective abundance and dynamics were apparently not linked to seasonal events. Rotifers were dominated by Bdelloids,

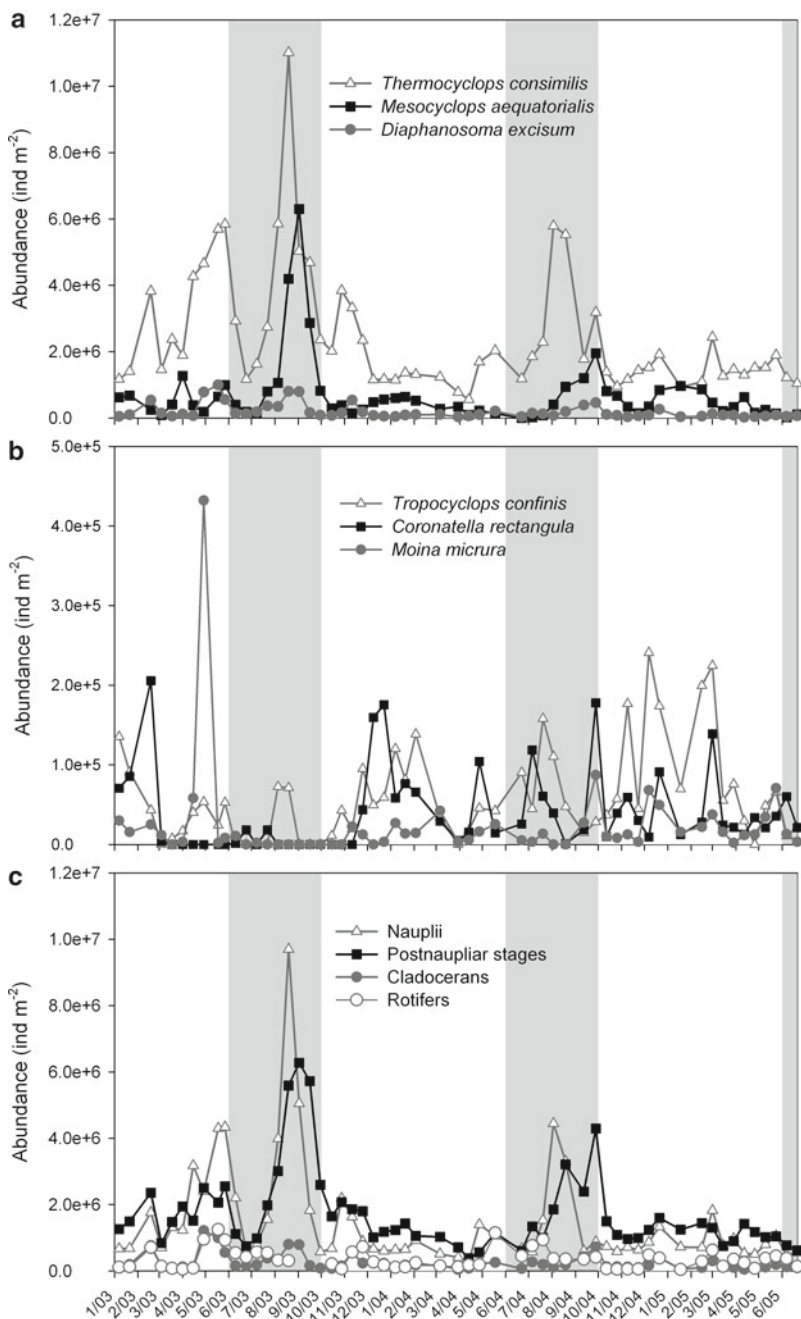


Fig. 7.7 Variation of metazooplankton abundance in the 0–60 m water column of Lake Kivu (Ishungu basin) from January 2003 to June 2005. Note the different scales on the Y-axis for **a**, **b** and **c**. The light grey boxes indicate the dry season periods

with an average of 76% of rotifer individuals, followed in decreasing order by *K. tropica*, *Lecane* sp., *B. calyciflorus*, *B. quadridentatus* and *Anuraeopsis fissa*. Owing to their low number and biomass, rotifers probably play a minor role in the Lake Kivu food web.

The dominant crustacean species were *T. consimilis*, *M. aequatorialis* and *D. excisum*. Total zooplankton abundance may reach 12×10^6 individuals m^{-2} , with conspicuous maxima occurring in the second half of the dry season, around August–September. Contrasting dynamics occurred among species (Fig. 7.7), but the three main taxa showed well-correlated maxima during the dry season (Fig. 7.7a). Nauplii and post-naupliar stages followed the same dynamics, with distinct peaks in the late dry season (Fig. 7.7c). *C. rectangula*, *T. confinis* and *M. micrura* showed a distinct pattern, with higher abundances during the rainy season.

Interannual variability was high, with lower zooplankton numbers but higher diversity in 2004 than in 2003. Seasonal sampling in different lake basins did not show large contrast among lake regions, suggesting homogeneity of zooplankton distribution throughout the lake (Isumbisha et al. 2006).

Crustacean biomass closely followed the abundance pattern. Although maximal metazooplankton biomass could reach up to 3.8 g C m^{-2} , mean biomass over the period 2003–2004 was 0.99 g C m^{-2} . For the whole sampling period (2003–2005), *T. consimilis* contributed about 61% to crustacean biomass, while *M. aequatorialis* and cladocerans accounted for, respectively, 27% and 11% of annual crustacean biomass. Total crustacean biomass was about 14% of phytoplankton biomass (assuming a mass C:chlorophyll *a* ratio of 92.8, according to Isumbisha et al. 2006), and closely followed variations of chlorophyll *a* concentration (Fig. 7.8).

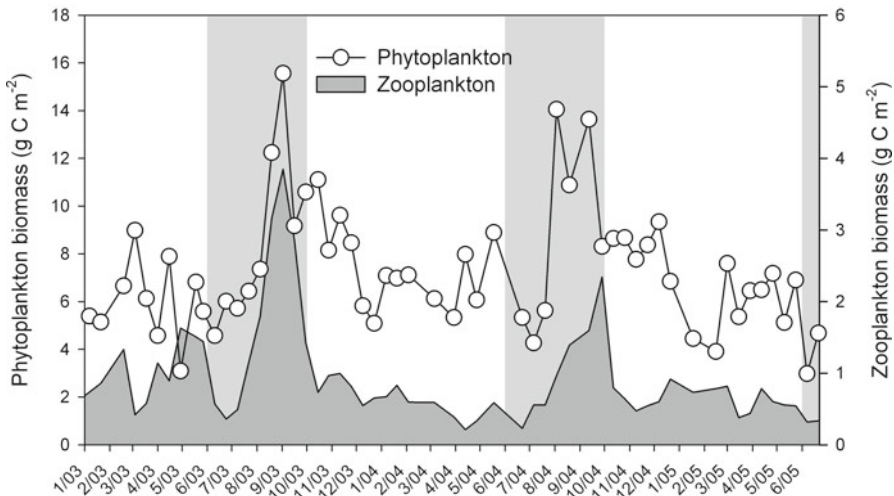


Fig. 7.8 Biomass of phytoplankton and zooplankton integrated in the mixolimnion (0–60 m) from January 2003 to June 2005 in Lake Kivu. Phytoplankton biomass data are from Sarmento et al. (Chap. 5) and converted into C using a C:chlorophyll *a* ratio of 92.8. The light grey boxes indicate the dry season periods

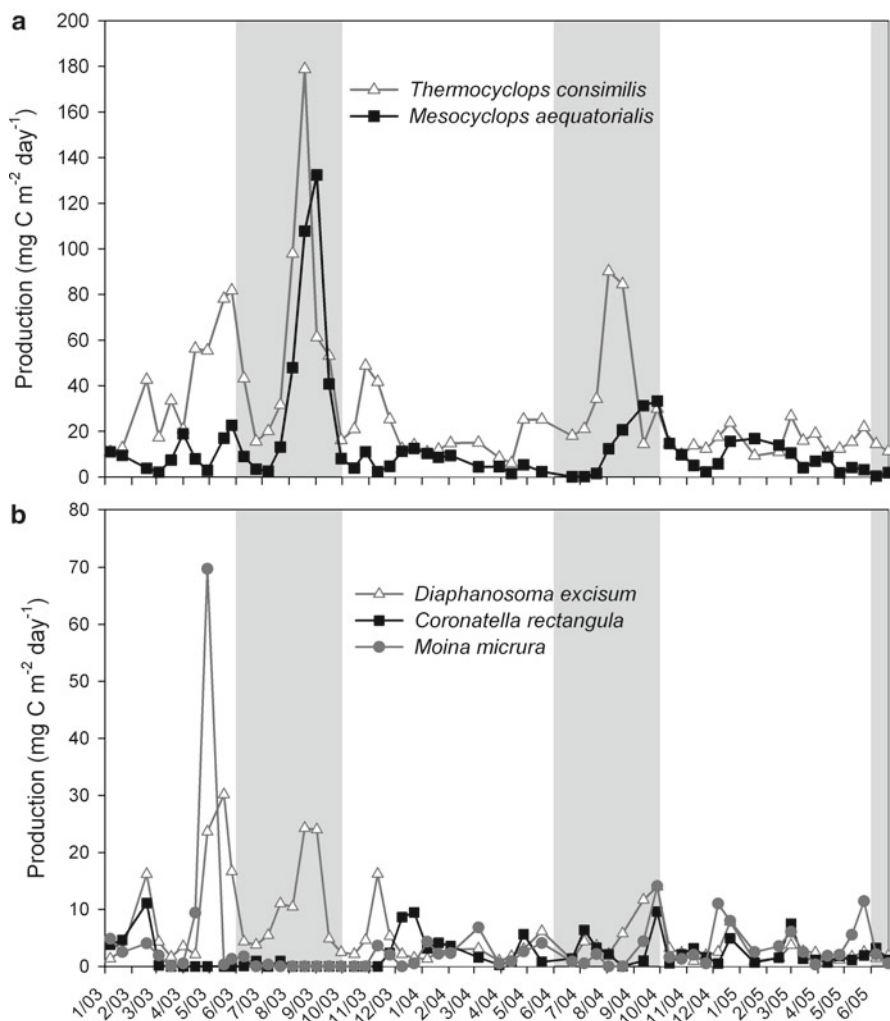


Fig. 7.9 Copepod (a) and cladoceran (b) production of the main crustacean species from January 2003 to June 2005 in Lake Kivu (Ishungu Basin). The light grey boxes indicate the dry season periods

Estimates of production for the five main crustacean species are presented in Fig. 7.9. Copepods accounted on average for 77% of the total crustacean production, with contributions >95% during dry season blooms. *T. consimilis* was the most productive species (on average, 55% of the total crustacean production), followed by *M. aequatorialis* (22%) and *D. excisum* (10%). Maximum total copepod production occurred at the end of the dry season, in August 2003 (~311 mg C m⁻² day⁻¹) and August 2004 (~111 mg C m⁻² day⁻¹), and was generally much lower in the rainy season. Annual crustacean production rates estimated for the 2 years were 29 g C m⁻² year⁻¹ in 2003 and 16 g C m⁻² year⁻¹ in 2004.

Table 7.1 Total and herbivorous plankton crustacean biomass, production, production:biomass (P:B) ratio and trophic transfer efficiency between phytoplankton and herbivorous zooplankton in the East African Rift large lakes

Lake	Total crustacean zooplankton			Herbivorous crustacean zooplankton			Trophic transfer efficiency
	Mean annual biomass (g C m ⁻²)	Mean annual production (g C m ⁻² year ⁻¹)	Mean P:B (year ⁻¹)	Mean annual biomass (g C m ⁻²)	Mean annual production (g C m ⁻² year ⁻¹)	Mean P:B (year ⁻¹)	
Tanganyika ^a	1.00	25.2	25	0.81	23.0	29	3.5–5.4%
Malawi ^b	0.80	29.1	36	0.70	26.4	38	5–8%
Kivu ^c	0.99	22.5	22	0.68	17.0	25	8.3% in 2003 5.2% in 2004

Data from ^aSarvala et al. (1999), ^bIrvine and Waya (1999), ^cThis study

Considering all crustacean species as herbivorous except *M. aequatorialis*, which is raptorial preying mainly on young *T. consimilis*, and based upon a mean annual primary production of 258 and 241 g C m⁻² year⁻¹, respectively, in 2003 and 2004 (Chap. 5), the estimated trophic transfer efficiency between primary producers and herbivorous zooplankton was 8.3% and 5.2%, respectively, in 2003 and 2004 (Table 7.1). These values are in good correspondence with the ones calculated for Lakes Tanganyika and Malawi (Table 7.1). Moreover they are in the middle range of energy transfer efficiencies reported by Pauly and Christensen (1995) for 48 aquatic communities; they indicate a tight coupling between both trophic levels.

7.4 Effects of *Limnothrissa* on Zooplankton Biomass and Body Size

Numerous studies in the limnological literature have documented the effects of a planktivore introduction on lacustrine metazooplankton (e.g. Gliwicz 1985): typical consequences are a shift in zooplankton body size and a decrease of total biomass, as a result of increased predation pressure. Large cladocerans, in particular, are under increased risk of extinction, since they are more visible for a predator than copepods.

The most ancient historical data on zooplankton biomass in Lake Kivu were given by Verbeke (1957) who indicated monthly biovolumes during 1952–1953. For comparison with recent data, Verbeke's biovolumes can be converted to biomass using a density of 1 g fresh weight cm⁻³, a water percentage of 83% and a C:dry mass ratio of 0.5. Results are presented in Fig. 7.10. The mean yearly calculated biomass was 2.6 g C m⁻² which is close to the biomass (3.8 g C m⁻²) calculated from abundance counting and body size measurements of Verbeke's samples made by Reyntjens (1982, in Dumont 1986). Based on three samples collected in July–September 1981 by Reyntjens (1982) and one sample in April 1983, Dumont (1986) observed an important decrease of crustacean biomass, in parallel with the disappearance of the main historical grazer, *D. curvirostris*, and concluded that this dramatic decline would lead to future collapse of the sardine fishery. The more comprehensive survey made by Isumbisho et al. (2006) allows us to calculate in this study a mean annual biomass of 0.99 g C m⁻². While we might not exclude a recovery of the zooplankton community during the last two decades, it appears that the predicted collapse may have been overstated (Fig. 7.10). We estimate that the zooplankton biomass decreased by a factor of 3 after the *Limnothrissa* introduction, reaching at present a level comparable to other great lakes of the East African Rift (Table 7.1).

Effects of *Limnothrissa* on zooplankton may also be investigated from historical data on body size of main zooplankton species. To assess a possible impact of predation by the introduced sardine, the body size of the three dominant zooplankton species was examined. *M. aequatorialis* is the largest zooplankton species in Lake Kivu.

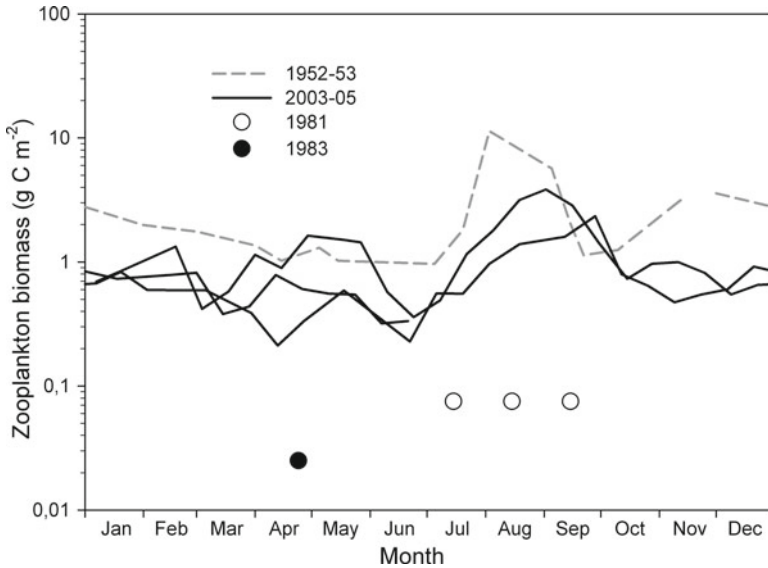


Fig. 7.10 Estimates of zooplankton biomass in Lake Kivu: 1952–1953 data from Verbeke (1957), 1981 data from Reyntjens (1982), 1983 data from Dumont (1986) and 2003–2005 data from the present study. Note the logarithmic Y-scale. See explanations on the calculations in the text

Its adult size was on average 0.725 ± 0.082 mm (mean \pm SD; range 0.54–1.0 mm) throughout 2003 and 0.740 ± 0.09 mm (range 0.51–1.1 mm) in May–June 1990 (Fourniret 1992). The data available from earlier publications are less precise: Dumont (1986) cited an average body length of 0.54 mm and a range of 0.24–0.71 mm, all three copepods species and all stages considered. Dumont (1986) gave a range from Verbeke’s samples (Verbeke 1957) of 0.23–1.05 mm in 1953, again for all copepod species and all stages, and Damas (1937) gave a range of 0.9–1.05 mm for adult *M. aequatorialis*. Given the heterogeneity of the data, no conclusion can be drawn, except for the maximal size of copepods, as *M. aequatorialis* is the largest species found in Lake Kivu. *M. aequatorialis* in the recent zooplankton of Lake Kivu still reached the maximal size recorded before the sardine introduction, suggesting that there was no change in body length of the largest copepod species of the lake.

Isumbisho (2006) mentioned a decreasing trend for the size of the cladoceran *D. excisum*, based on a comparison between his and historical data, but again a closer look shows a large heterogeneity in the data. No or little change in maximal body length of this species occurred since 1981, without available data before the sardine introduction. For the other cladocerans, the data present similar uncertainties, with some differences which might be related to sampling strategy, sample size and consideration of different stages (only adults vs. all stages, including the smallest instars). Therefore, no conclusion can be drawn on a potential decrease of crustacean zooplankton body size as a consequence of the *Limnothrissa* introduction.

7.5 Diel Vertical Migration

The diel vertical migration (DVM) of the three copepod species and of *D. excisum* – the largest prey items among the metazooplankton – was investigated by Isumbisho (2006) in the pelagic zone of Lake Kivu. Vertical migration of zooplankters is generally considered as a predator avoidance behavior, with a trade-off between reducing mortality losses at daytime and the energy costs of moving vertically in a deep water column. According to Gliwicz and Pijanowska (1988), the typical behavior of vertical migration (descent at dawn and ascent at dusk) should only be expected when both following conditions are fulfilled: (1) the risk of mortality due to predation is significantly higher in the upper than in the lower strata during the day, and (2) the gain associated with migration is significantly higher than the energy investment for migration. The first condition is never fulfilled when no visual predator is present; it would also be unfulfilled in the presence of visual predators when predation by invertebrate predators is equally important but restricted to the lower strata. Both conditions for triggering a typical DVM in larger zooplankters are clearly at present fulfilled in the pelagic zone of Lake Kivu, with the presence of an efficient planktivorous fish, without any invertebrate predator.

Isumbisho (2006) calculated the mean residence depth (MRD; Frost and Bollens 1992) from sampling 12 different 5-m deep strata and determining abundance of the following categories: the cladoceran *D. excisum* and several stages (ovigerous females, adult females without eggs, adult males and copepodids) of the three copepod species (*T. consimilis*, *M. aequatorialis* and *T. confinis*). The different species exhibited different survival strategies depending on their feeding habits, life stages and adult body sizes (Fig. 7.11). The relatively small *T. confinis* was permanently present in the euphotic layer while the largest copepod species, *T. consimilis* and *M. aequatorialis*, exhibited a clear DVM behaviour, with some differences among life stages. Egg-bearing females of *T. consimilis* remained permanently in the aphotic zone while *M. aequatorialis* ovigerous females migrated to the top 20 m during the night. *D. excisum* occupied mostly the intermediate layer except at midday.

This suggests that vertical migration at daytime to the aphotic zone may provide the largest copepods with adequate protection against fish predation, and that the cladocerans, which exhibit a smaller range of downward migration, may be more vulnerable.

7.6 Conclusions

The diversity of the Lake Kivu metazooplankton community, with seven species of crustaceans, does not seem that low when compared with other Rift lakes (see e.g. Lehman 1996). Currently, a total of 19 taxa have been identified in samples collected from 2002 to 2009: 3 copepods, 4 cladocerans and 12 rotifers (among which unidentified Bdelloids). Bdelloids were not reported before, whereas

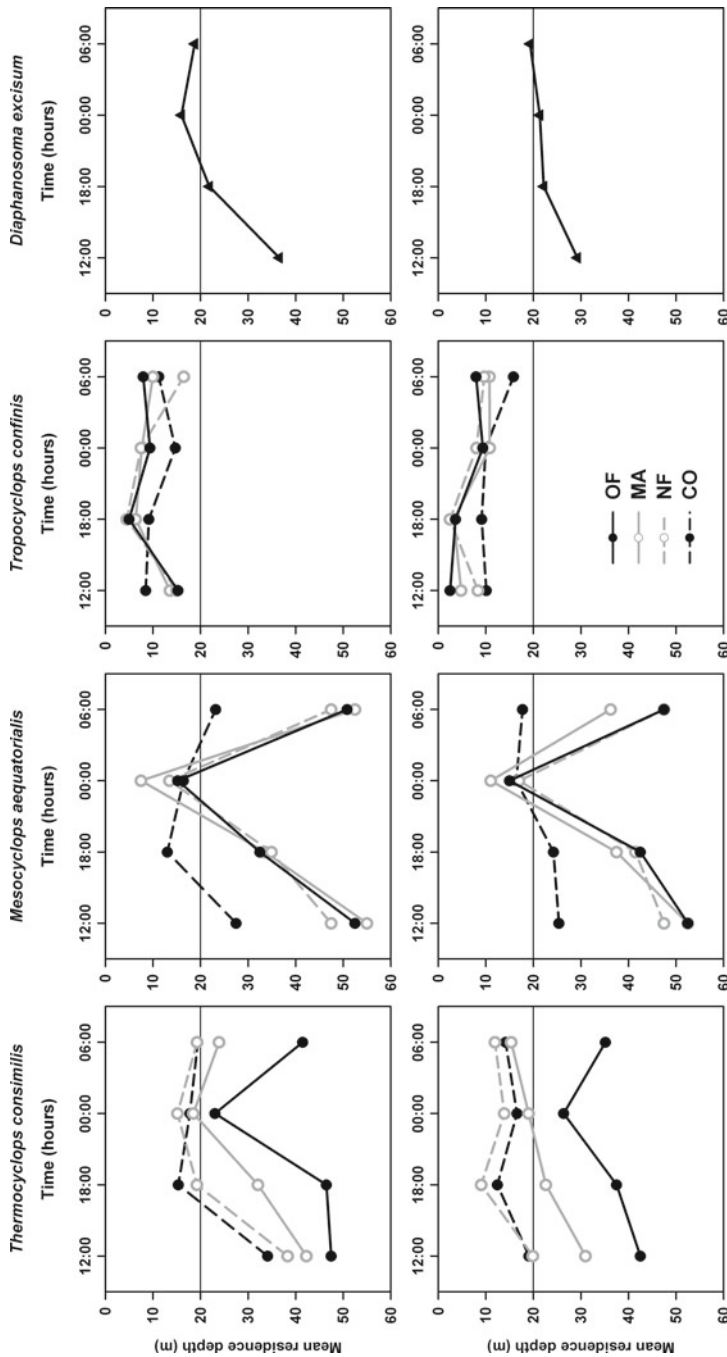


Fig. 7.11 Diel vertical migration of the four main species of crustaceans in Lake Kivu; MRD: mean residence depth; OF: ovigerous females; NF: adult females without eggs; MA: males; CO: copepodids. The horizontal lines indicate the limit of the euphotic zone. Upper panel: 5–6 August 2005, lower panel: 19–20 August 2005 (modified from Isumbicho 2006)

they have a worldwide distribution; in Africa alone, a total of 104 Bdelloid species are known, of which 24 are endemic (Ricci 1987). Also, *Keratella tropica*, another common rotifer in the pelagic Lake Kivu, was not observed before Isumbisho (2006). The reason for the abundance of rotifers in the pelagic waters of Lake Kivu, whereas they are scarce in other oligotrophic Rift lakes, might be the low invertebrate predation, in contrast to other East African great lakes where the dipterans *Chaoborus* (Lake Malawi) or open water shrimps (Lake Tanganyika) are present (Lehman 1996).

The effect of *Limnothrissa miodon* introduction in Lake Kivu, devoid of any pelagic fish in the 1950s, is a key question, but definite, reliable and precise quantitative data are missing to estimate this effect. In particular, the earlier records have many gaps as far as zooplankton abundance and diversity are concerned: even the presence of a *Daphnia* species in the lake before the introduction is not verified according to the earliest plankton record. In the study that directly addressed the effect on metazooplankton, Dumont (1986) based his assessment of the extent of the changes on few samples, collected in a short period of time, whereas the system presents a large seasonal and interannual variability in plankton abundance. Presumably the capture efficiency of his net was also low and abundance data were not corrected. By contrast, estimates based on recent and long-term observations, and comparison with Verbeke's (1957) data, revealed a probable decline of total crustacean biomass by a factor of 3, whereas a change in zooplankton size cannot be asserted on the basis of available data. Yet, the pelagic food web of Lake Kivu when a pelagic planktivorous fish was missing was atypical, with a very large average zooplankton biomass of $\sim 2.6 \text{ g C m}^{-2}$, while comparable Rift lakes have a mean annual biomass of 0.8–1.0 g C m^{-2} (Table 7.1). The appearance of an important top-down control since the *Limnothrissa* introduction reduced the zooplankton biomass and production and the trophic transfer efficiency to levels similar to those of other Rift lakes (Table 7.1). The observed tight coupling between phytoplankton and zooplankton dynamics and the trophic transfer efficiency at the algae-grazer interface suggest that plankton dynamics and biomass in this oligotrophic, large tropical lake are at present predominantly controlled by bottom-up processes, i.e. seasonal mixing and nutrient availability, as already found for Lakes Malawi (Irvine et al. 2000; Guildford et al. 2003) and Tanganyika (Naithani et al. 2007).

Acknowledgments This work was partly funded by the Fonds National de la Recherche Scientifique (FRS-FNRS) under the CAKI (Cycle du carbone et des nutriments au Lac Kivu) project (contract n 2.4.598.07) and contributes to the Belgian Federal Science Policy Office EAGLES (East African Great Lake Ecosystem Sensitivity to changes, SD/AR/02A) project. François Darchambeau was a Postdoctoral Researcher at the FRS-FNRS.

References

Alekseev VR (2002) Copepoda. In: Fernando CH (ed) Tropical freshwater zooplankton: identification, ecology and impact on fisheries. Backhuys Publishers, Leiden, The Netherlands

- Amarasinghe PB, Ariyaratne MG, Chitapalpong T, Vijverberg J (2008) Production, biomass and productivity of copepods and cladocerans in south-east Asian water bodies and the carrying capacity for zooplanktivorous fish. In: Schiemer F, Simon D, Amarasinghe US, Moreau J (eds) Aquatic ecosystems and development: comparative Asian perspectives. Margraf and Backhuys Publishers, Germany, The Netherlands
- Brehm V (1939) Cladocera. In: Exploration du Parc National Albert, Mission H. Damas (1935–1936), fascicule 7. Institut Royal des Sciences Naturelles de Belgique, Bruxelles, Belgium
- Damas H (1937) Quelques caractères écologiques de trois lacs équatoriaux: Kivu, Edouard, Ndalaga. Ann Soc R Zool Belg 68:121–135
- Dumont HJ (1986) The Tanganyika sardine in Lake Kivu: another ecodisaster for Africa? Environ Conserv 13:143–148. doi:[10.1017/S0376892900036742](https://doi.org/10.1017/S0376892900036742)
- Dumont HJ, Van de Velde I, Dumont S (1975) The dry weight estimate of biomass in a selection of cladocera, copepoda and rotifera from the plankton, periphyton and benthos of continental waters. Oecologia 19:75–97. doi:[10.1007/BF00377592](https://doi.org/10.1007/BF00377592)
- Dussart B (1967a) Les copépodes des eaux continentales d'Europe occidentale. I. Calanoïdes et Harpacticoïdes. Boubée and Cie, Paris
- Dussart B (1967b) Les copépodes des eaux continentales d'Europe occidentale. II. Cyclopoïdes et Biologie. Boubée and Cie, Paris
- Dussart B (1982) Crustacés Copépodes des eaux intérieures. In: Faune de Madagascar. ORSTOM-CNRS, Paris
- Fourniret Y (1992) Etude du zooplancton du Lac Kivu et relations avec son prédateur: *Limnothrissa miodon*. Echantillonnage de mai-juin 1990, Unité d'Ecologie des Eaux Douces. University of Namur, Belgium
- Frost BW, Bollens SM (1992) Variability of diel vertical migration in the marine planktonic copepod *Pseudocalanus newmani* in relation to its predators. Can J Fish Aquat Sci 49:1137–1141. doi:[10.1139/f92-126](https://doi.org/10.1139/f92-126)
- Gliwicz ZM (1985) Predation or food limitation: an ultimate reason for extinction of planktonic cladoceran species. Arch Hydrobiol Beih Ergeb Limnol 21:419–430
- Gliwicz ZM, Pijanowska J (1988) Effect of predation and resource depth distribution on vertical migration of zooplankton. Bull Mar Sci 43:695–709
- Guildford SJ, Hecky RE, Taylor WD, Mugidde R, Bootsma HA (2003) Nutrient enrichment experiments in tropical great Lakes Malawi/Nyasa and Victoria. J Great Lakes Res 29(suppl 2): 89–106. doi:[10.1016/S0380-1330\(03\)70541-3](https://doi.org/10.1016/S0380-1330(03)70541-3)
- Hotyńska M, Reid JW, Ueda H (2003) Genus *Mesocyclops* Sars, 1914. In: Ueda H, Reid JW (eds) Copepoda: Cyclopoida: Genera *Mesocyclops* and *Thermocyclops*. Backhuys Publishers, Leiden, The Netherlands
- Irvine K (1995) Standing biomasses, production and spatio-temporal distributions of the crustacean zooplankton. In: Menz A (ed) The fishery potential and productivity of the pelagic zone of Lake Malawi/Niassa. Natural Resources Institute, Chatham, Kent
- Irvine K, Waya R (1999) Spatial and temporal patterns of zooplankton standing biomass and production in Lake Malawi. Hydrobiologia 407:191–205. doi:[10.1023/A:1003711306243](https://doi.org/10.1023/A:1003711306243)
- Irvine K, Patterson G, Allison EH, Thompson AB, Menz A (2000) The pelagic ecosystem of Lake Malawi: trophic structure and current threats. In: Munawar M, Hecky RE (eds) Great Lakes of the World (GLOW): food-web, health and integrity, Ecoinvision World Monograph Series. Backhuys, Leiden, the Netherlands
- Isumbisho M (2006) Zooplankton ecology of Lake Kivu. PhD thesis, University of Namur, Belgium
- Isumbisho M, Sarmiento H, Kaningini B, Micha J-C, Descy J-P (2006) Zooplankton of Lake Kivu, East Africa, half a century after the Tanganyika sardine introduction. J Plankton Res 28:971–989. doi:[10.1093/plankt/fbl032](https://doi.org/10.1093/plankt/fbl032)
- Kiefer F (1978) Freilebende Copepoda. In: Das Zooplankton der Binnengewässer, 2. Teil – Die Binnengewässer, 26, Stuttgart
- Kořínek V (2002) Cladocera. In: Fernando CH (ed) Tropical freshwater zooplankton: identification, ecology and impact on fisheries. Backhuys Publishers, Leiden, The Netherlands
- Lehman JT (1996) Pelagic food webs of the East African Great Lakes. In: Johnson TC, Odada EO (eds) The limnology, climatology and paleoclimatology of the East African Lakes. Gordon & Breach Publishers, Amsterdam

- Mavuti KM (1994) Durations of development and production estimates by two crustacean zooplankton species *Thermocyclops oblongatus* Sars (Copepoda) and *Diaphanosoma excisum* Sars (Cladocera), in Lake Naivasha, Kenya. *Hydrobiologia* 272:185–200. doi:[10.1007/BF00006520](https://doi.org/10.1007/BF00006520)
- Naithani J, Darchambeau F, Deleersnijder E, Descy J-P, Wolanski E (2007) Study of the nutrient and plankton dynamics in Lake Tanganyika using a reduced-gravity model. *Ecol Model* 200:225–233. doi:[10.1016/j.ecolmodel.2006.07.035](https://doi.org/10.1016/j.ecolmodel.2006.07.035)
- Pauly D, Christensen V (1995) Primary production required to sustain global fisheries. *Nature* 374:255–257. doi:[10.1038/374255a0](https://doi.org/10.1038/374255a0)
- Reyntjens D (1982) Bijdrage tot de limnologie van het Kivu-meer. M.Sc. thesis, University of Louvain, Belgium
- Ricci CN (1987) Ecology of bdelloids: how to be successful. *Hydrobiologia* 147:117–127. doi:[10.1007/BF00025734](https://doi.org/10.1007/BF00025734)
- Sarvala J, Salonen K, Järvinen M, Aro E, Huttula T, Kotilainen P, Kurki H, Langenberg V, Mannini P, Peltonen A, Plisnier P-D, Vuorinen I, Mölsä H, Lindqvist OV (1999) Trophic structure of Lake Tanganyika: carbon flows in the pelagic food web. *Hydrobiologia* 407:140–173. doi:[10.1023/A:1003753918055](https://doi.org/10.1023/A:1003753918055)
- Ueda H, Reid JW (2003) Introduction. In: Ueda H, Reid JW (eds) *Copepoda: Cyclopoida: Genera Mesocyclops and Thermocyclops*. Backhuys Publishers, Leiden, The Netherlands
- Van de Velde I (1984) Revision of the African species of the genus *Mesocyclops* Sars, 1914 (Copepoda: Cyclopidae). *Hydrobiologia* 109:3–66. doi:[10.1007/BF00006297](https://doi.org/10.1007/BF00006297)
- Verbeke J (1957) Recherche écologique sur la faune des grands lacs de l'Est du Congo belge. Exploration Hydrobiologique des lacs Kivu, Edouard et Albert (1952–54). *Bull Inst R Sci Nat Belg* 3:1–177

Chapter 8

Fishes in Lake Kivu: Diversity and Fisheries

Jos Snoeks, Boniface Kaningini, Pascal Masilya,
Laetitia Nyina-wamwiza, and Jean Guillard

Abstract This contribution reviews the knowledge on fish diversity and fisheries in Lake Kivu, with an emphasis on the biology and stock assessment of the introduced Tanganyika sardine, *Limnothrissa miodon*. Lake Kivu is famous, compared to the other African great lakes, for its poor fish fauna, with 29 species comprising a.o. 15 endemic haplochromines and a few non-native species. In a first part devoted to diversity and biogeography, all species are briefly described, with some details on their biology and ecology in the lake. A second part of this chapter focuses on the non-native *Limnothrissa miodon*, with a review on its biology, on its past and present abundance, and on available data on the production of the pelagic fishery of this species. The main conclusion is that the fishery yield is relatively low, amounting ~10,000 t year⁻¹. A recent concern is the arrival of a possible competitor, *Lamprichthys tanganicanus*, an endemic fish to Lake Tanganyika. Future studies should be conducted on the food web of the littoral zone, where most endemic cichlids are located. More detailed fisheries surveys are also needed, in order to estimate the pressure on the different species.

J. Snoeks (✉)

Royal Museum for Central Africa, Tervuren, Belgium
e-mail: jos.snoeks@africamuseum.be

B. Kaningini • P. Masilya

Institut Supérieur Pédagogique, Bukavu, D.R. Congo
e-mail: mkaningini@yahoo.com; pascalmasilya@yahoo.fr

L. Nyina-wamwiza

National University of Rwanda, Butare, Rwanda
e-mail: nyinawamwiza@yahoo.fr

J. Guillard

INRA, UMR CARRTEL, Centre Alpin de Recherche sur les Réseaux
Trophiques et Ecosystèmes Limniques, Thonon-les-Bains, France
e-mail: jean.guillard@thonon.inra.fr

To the biologist the main interest of Lake Kivu is the relative poverty of the fauna and its ecological immaturity (Beadle 1981)

8.1 Introduction

With only 29 species of fish described, among which several were introduced, the fish diversity of Lake Kivu is very low compared to its great neighbours. This low diversity is inherently linked to the geological history of the lake. The waters in Lake Kivu area have been at high altitude for maybe as long as the mid-Miocene East African uplifting. This fact in itself might account for part of the poor fish diversity of the current lake. However, the lake also went through some catastrophic events. After the uplifting, the area used to be part of a drainage system encompassing the current Lake Edward region, and a proto-lake even existed, from the mid-Pleistocene (Haberyan and Hecky 1987) or even much longer (Degens et al. 1973), that was connected to Lake Edward, but then got blocked by the Virunga volcanoes. As such, the lake was probably endorheic until it found its current outlet towards the south via the Rusizi river. In the meantime the lake did not escape the large drought that affected the whole area about 18,000–15,000 years ago (Elmer et al. 2009). Though the lake did not dry out completely, most probably it went to one or more stages of higher salinity, affecting the fish fauna. Equally, the lake went through some hydrothermal events that had severe effects on its ecosystem and hence on the fish fauna (Haberyan and Hecky 1987). All of these events must have affected the lake fishes to a certain extent.

Before the introduction of *Limnothrissa miodon* – the “Tanganyika sardine” (called *isambaza* or *sambaza* by the local fishermen, *lumpu* in the Tanganyika region) – the fishery in Lake Kivu was poorly developed (Kaningini et al. 1999). Artisanal fishing took place in the littoral areas and was based on small native cichlids (*Haplochromis* spp.), and on few other species (*Oreochromis niloticus*, two species of *Clarias*), with a maximal annual production of barely 1,500 t. Therefore, several attempts were made for introducing the *Ndakala* (*Stolothrissa tanganyikae*), with the hope of increasing the annual fish production up to 35,000 t (Capart 1959; Collart 1960). The outcome was that *Limnothrissa miodon*, not *Stolothrissa*, colonised Lake Kivu, allowing the progressive development, during the 1970s, of a productive pelagic fishery. The fishery grew rapidly from 1979 to 1991, particularly at the end of this period, due to the promotion of fishing techniques by a PNUD/FAO project, which operated mainly in the Rwandan part of the lake. The fishery grew in parallel in DR Congo, partly thanks to an impulse given by scientists located in Bukavu, who promoted a technique using gill nets (Kaningini et al. 1999), instead of the “trimarans” operating at night with a crew of several fishermen. For most specialists of fisheries, the story of the *sambaza* in Lake Kivu has widely been described as a success (Spliethoff et al. 1983; Roest 1999; Gozlan 2008), with an estimated annual yield of ca. 13,500 t for the whole lake (Spliethoff et al. 1983).

In this chapter we review the most recent results regarding fish diversity, the biology of *Limnothrissa miodon*, fisheries and stock of pelagic fish in Lake Kivu. A recent concern is the appearance in the lake and in the catches of another species introduced from Lake Tanganyika, which may compete with the sardine for the lake's scant planktonic resources.

8.2 Species Diversity

Lake Kivu has traditionally been regarded as a species-poor lake (Snoeks 1994). At present 29 fish species are known from the lake, five of which, however, are introduced (Table 8.1). Of the remaining 24 native species, the majority (16) belongs to one family, the Cichlidae.

Table 8.1 Fish species composition for Lake Kivu

Clupeidae	
<i>Limnothrissa miodon</i> (Boulenger 1906)	Introduced from Lake Tanganyika
Cyprinidae	
<i>Raiamas moorii</i> (Boulenger 1900)	Lake Kivu, Rusizi, Lake Tanganyika, Malagarasi, Lake Rukwa and associated river systems
' <i>Barbus</i> ' <i>kerstenii</i> Peters 1868	Distribution still under discussion. Currently cited from Lakes Victoria, Edward-George and Kivu basins, coastal rivers in Kenya and Tanzania, Okavango, Cunene, Zambezi system, Save, possibly Aswa river in Upper Nile
' <i>Barbus</i> ' <i>pellegrini</i> Poll 1939	Lakes Edward-George, Kivu, Tanganyika and Rukwa drainages, including Rusizi and Malagarasi
' <i>Barbus</i> ' <i>apleurogramma</i> Boulenger 1911	Lakes Victoria, Edward-George, Kivu, Tanganyika and Rukwa basins, including Rusizi and Malagarasi; possibly Lukuga system, coastal rivers in Kenya and Tanzania, possibly Aswa river in Upper Nile system and Aoué in Chad
<i>Labeobarbus altianalis</i> (Boulenger 1900)	Lakes Victoria, Kyoga, Edward-George and Kivu basins, Rusizi and northern part of Lake Tanganyika
Amphiliidae	
<i>Amphilius cf. uranoscopus</i> (Pfeffer 1889)	Distribution still under discussion; coastal rivers in east and south-east Africa, Okavango, Zambezi system, affluents of Lakes Victoria, Kivu and Tanganyika, Upper Zaire system
Clariidae	
<i>Clarias liocephalus</i> Boulenger 1898	Lakes Victoria, Edward-George, Kivu, Tanganyika and their associated river systems including Rusizi and Malagarasi, Bangweulu-Mweru system, Lake Rukwa, Cunene, Okavango, Zambezi system and Lake Malawi catchment

(continued)

Table 8.1 (continued)

<i>Clarias gariepinus</i> (Burchell 1822)	Almost pan-African
Poeciliidae	
<i>Lamprichthys tanganicanus</i> (Boulenger 1898)	Introduced from Lake Tanganyika
Cichlidae	
<i>Oreochromis niloticus</i> (Linnaeus 1758)	Senegal, Gambia, Niger, Benue, Volta, Chad system, Jebel Marra, Nile, Yarkon river (Israel), Lake Turkana system, Lakes Albert, Edward-George, Kivu and Tanganyika basins, Lake Tana, Lake Baringo, Suguta river, Ethiopian rift valley lakes from Lake Zwai to Lake Stefani, Omo system, Awash system [populations from the latter three regarded as <i>O. cancellatus</i> (Nichols 1923) by Seyoum and Kornfield]. The Lake Kivu population is part of the subspecies <i>O. niloticus eduardianus</i>
<i>Oreochromis macrochir</i> (Boulenger 1912)	Introduced (escaped from fish ponds)
<i>Oreochromis leucostictus</i> (Trewavas 1933)	Introduced (escaped from fish ponds?)
<i>Tilapia rendalli</i> (Boulenger 1897)	Introduced (escaped from fish ponds)
<i>Haplochromis</i> spp. (15 species)	All endemic to the lake

For autochthonous species, the currently known natural distribution is indicated (Based on Snoeks et al. 1997; additional data from Snoeks 2004; Muderhwa and Matabaro 2010). Following current taxonomic practice, the genus for the small ‘*Barbus*’ species is put between single quotes

8.2.1 The Non-Cichlid Taxa

Limnothrissa miodon (Fig. 8.1a) is a freshwater clupeid originally endemic to Lake Tanganyika. Confusion about its possible presence in Lake Mweru is due to an erroneous locality record of *Microthrissa stappersii* Poll 1948, a synonym of *L. miodon* (Gourène and Teugels 1993). The species has been introduced in 1959 in a sample of juveniles mixed with *Stolothrissa tanganyicae* Regan 1917, which was the Tanganyika sardine actually targeted for introduction in Lake Kivu (Collart 1960). In addition, *L. miodon* has successfully been introduced in Lake Kariba, from which it invaded Lake Cahora Bassa downstream (Marshall 1991). Both lakes are man-made reservoirs on the Zambezi system. In these areas as well as in Lake Kivu, *L. miodon* has become an important food fish (see Sect. 8.5 on fisheries below).

The family Cyprinidae is represented by five species. *Raiamas moorii* (Fig. 8.1b), a predatory powerful swimmer, may well be the only species that has colonized Lake Kivu from Lake Tanganyika (Robben and Thys van den Audenaerde 1984). Conversely, *Labeobarbus altianalis* (Fig. 8.1f) may have colonized the extreme northern part of Lake Tanganyika by descending the Rusizi from Lake Kivu (Snoeks

et al. 1997). The species is also present in the drainage systems of Lakes Edward and Victoria. While the Kivu population had been allocated in the past to the subspecies *L. altianalis altianalis*, De Vos and Thys van den Audenaerde (1990a) did not find enough evidence to justify the use of subspecies and applied the specific name to all known populations.

Three small '*Barbus*' occur in the lake. '*Barbus*' *kerstenii* (Fig. 8.1c) is the most common in the lake. Most of the confusion surrounding the taxonomy of these species has been clarified by De Vos and Thys van den Audenaerde (1990b) and their distribution has been reviewed by Snoeks et al. (1997). However, some confusion remains within the taxa '*B.*' *kerstenii* and '*B.*' *pellegrini* (Fig. 8.1d). The correct separation of the latter species and '*B.*' *neumayeri* in some Ugandese waters remains problematic (Snoeks pers. obs.).

The catfishes of the Kivu basin are represented by two widespread *Clarias* and one *Amphilius* species. The latter is not living in the lake itself but in its affluent rivers. It has been named *A. cf. uranoscopus* (Fig. 8.2a) by Snoeks et al. 1997 and *A. uranoscopus* by De Vos et al. (2001). *Amphilius uranoscopus* is a widespread species of East and Central Africa (Skelton 1984). Its status in the Kivu drainage system is in need of review.

Recently, a new taxon has been added to the list of Kivu species, i.e. *Lamprichthys tanganicanus* (Fig. 8.2b). This fish is an endemic to Lake Tanganyika. How exactly it arrived in Lake Kivu is unclear. It is excluded that this small Cyprinodontiform species could have migrated up the Rusizi to Lake Kivu. The species is not adapted to the riverine environment and is not capable of mounting the rapids and cascades, an opinion shared by Muderhwa and Matabaro (2010). These authors advanced two hypotheses explaining the presence of *Lamprichthys* in Lake Kivu. The first one implies a recent introduction, probably by an aquarist. While this hypothesis cannot be ruled out, Muderhwa and Matabaro (2010) did not find any indication that such an aquarist has been active in the region. They postulated that juveniles of *Lamprichthys* might have been introduced in 1959 together with those of *Limnothrissa miodon*. Because of its much lower fecundity compared to that of *Limnothrissa* and the possible stronger predation on its fry, it has taken a long time for this species to become abundant (Muderhwa and Matabaro 2010). Assuming the latter scenario, it nevertheless remains strange that it would have taken almost 50 years after its possible introduction before the species was discovered in the lake. Most likely, *Lamprichthys tanganicanus* has been recently introduced in Lake Kivu. It is a pelagic dweller, living in coastal areas and is one of the most abundant fishes in these areas in Lake Tanganyika (Snoeks pers. obs.).

During reproduction, *L. tanganicanus* deposits eggs in cracks and holes between rocks (Wildekamp 2004). While there are abundant rocky areas in Lake Kivu, the abundance of crevices and cracks is much less than in Tanganyika, because of the rocks being "cemented" together by a calcareous precipitate (Beadle 1981). Apparently, since the species is now very abundant, the lack of suitable places is at present no major impediment for its reproduction in Lake Kivu.

Not only is the lake generally species poor; also quite a number of families and genera present in the surrounding areas are lacking. There are no Protopteridae,

Fig. 8.1 (a) *Limnothrissa miodon*; (b) *Raiamas moorii*; (c) 'Barbus' *kerstenii*; (d) 'Barbus' *pellegrini*; (e) 'Barbus' *apleurogramma*; (f) *Labeobarbus altianalis*. (a, b) Unpublished; (c, d, e, f) (From De Vos and Thys van den Audenaerde (1990a, b). Copyright RMCA, Tervuren, Belgium)

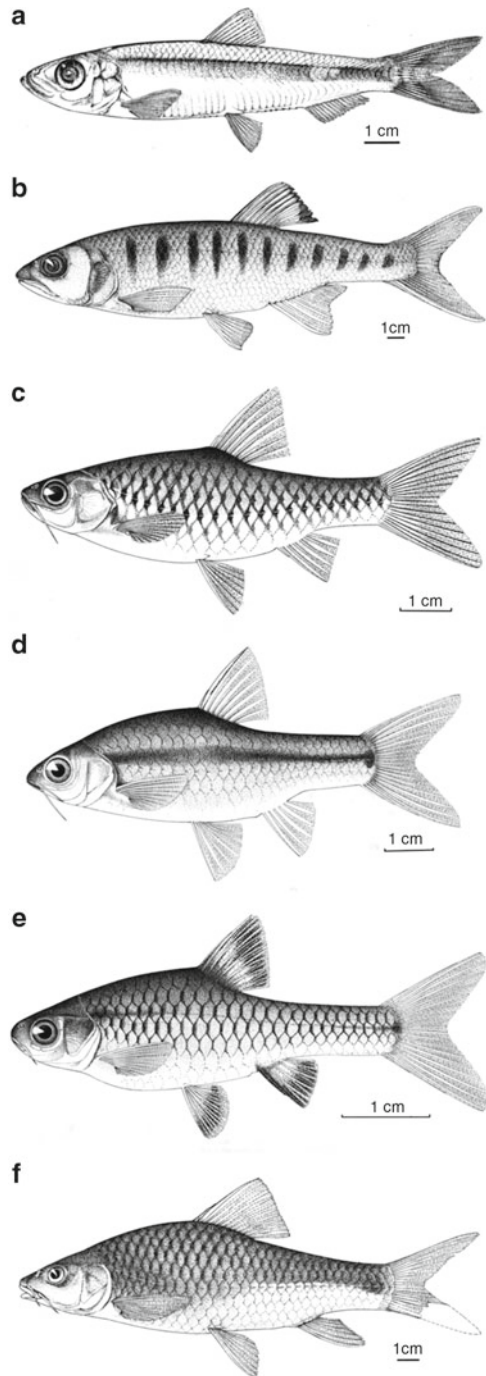
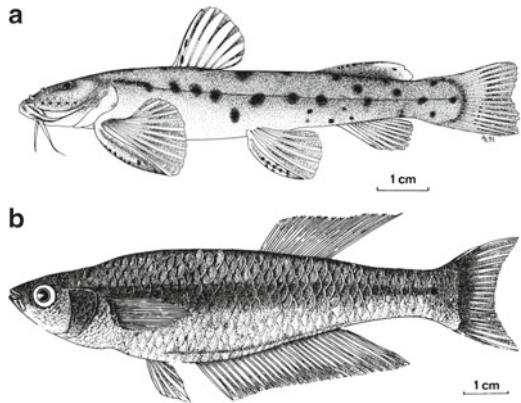


Fig. 8.2 (a) *Amphilius cf. uranoscopus*; (b) *Lamprichthys tanganicus*. Unpublished. Copyright RMCA, Tervuren, Belgium



Mormyridae, Alestidae, Anabantidae or Mastacembelidae present, to name the most obvious ones. Within the Cyprinidae, perhaps most striking is the lack of a species of the genus *Labeo*. Similarly, the obvious missing catfish taxon in Lake Kivu is *Synodontis*. No fossil data are available like for Lake Edward for which families now absent are known to have existed in the past (Greenwood 1983).

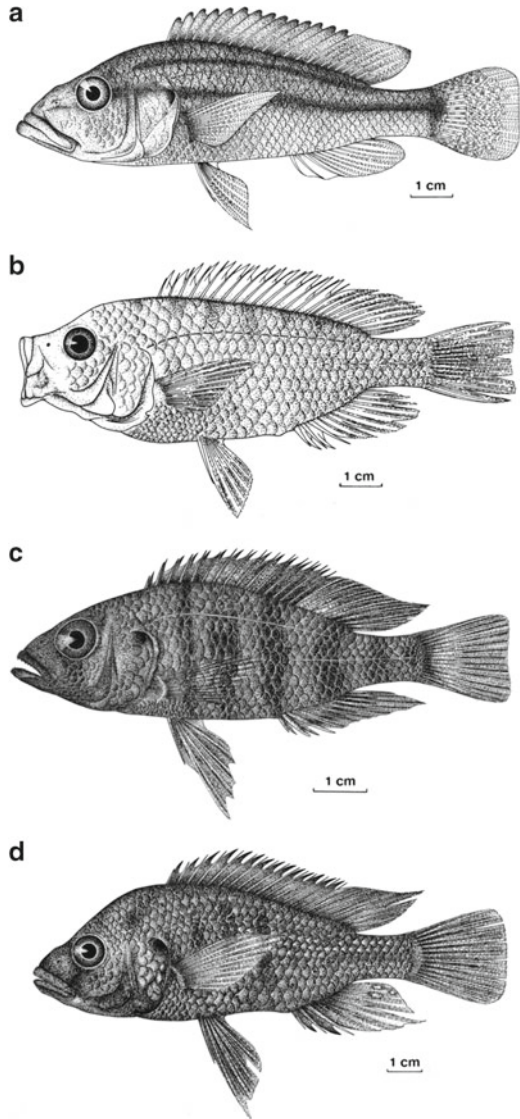
Records of *Gnathonemus petersii* (Günther 1862), *Bryconaethiops microstoma* Günther 1873 and *Hydrocynus vittatus* (Castelnau 1861) from the lake are erroneous (De Vos et al. 2001).

8.2.2 The Cichlids

Currently 19 species of cichlids are known from the lake, four of which are tilapiines and 15 endemic haplochromines (Table 8.1). These tilapiines include three introduced tilapias and the native *Oreochromis niloticus* (De Vos et al. 2001). The Kivu population of the latter species belongs to *O. niloticus eduardianus*, a subspecies also present in the basins of Lakes Albert, Edward-George and Tanganyika.

Lake Kivu haplochromines are notoriously difficult to identify. For most species, a reliable identification can only be done after a check of its most important characteristics under a dissecting microscope. Adult males can have a species-specific colour pattern and can be distinguished by an experienced person, though similar patterns do exist. Except for some species that have a distinctive habitus, the females of most species are very similar and all brown greyish coloured. Because of the large interspecific overlap, a simple dichotomous identification key cannot be compiled. Hence Snoeks (1994) produced a number of identification guidelines that can be used as a first approach, the results of which should be checked against the more elaborate differential diagnoses and species descriptions. Haplochromines are essentially located in the littoral zone of the lake, although some species can be present in the pelagic zone.

Fig. 8.3 (a) *Haplochromis vittatus*; (b) *Haplochromis paucidens*; (c) *Haplochromis gracilior*; (d) *Haplochromis adolphifrederici* (From Snoeks (1994). Copyright RMCA, Tervuren, Belgium)



Haplochromis vittatus (Fig. 8.3a) was the first haplochromine species to be described from the lake. It is the largest species (up to 191.0 mm standard length) and the only large piscivorous predator.

Haplochromis adolphifrederici (Fig. 8.3d) can be distinguished by its molariform pharyngeal dentition. The amount of enlargement of the pharyngeal jaws and the degree of molarization of the teeth is very variable (Snoeks 1986) and the intra-specific variability is larger than in any other known haplochromine species in the region. Such a pharyngeal dentition is typical for mollusc crushers. However, all data currently available indicate that the species is rather entomophagous and only

in a few specimens have mollusc shell fragments been found (Ulyel et al. 1990; Snoeks 1994). This observation was tentatively linked to the rarity of molluscs within the lake.

Haplochromis paucidens (Fig. 8.3b) is a common species with a relatively small mouth with relatively few teeth and thick lips. The species has been described three times, with *H. schoutedeni* (Poll 1932) and *H. wittei* (Poll 1939) as synonyms (Snoeks 1988). Part of this confusion has to do with the species being polymorphic, comprising three morphs with different colour patterns (see below).

In *Haplochromis gracilior* (Fig. 8.3c), almost no vivid colour components are present except for the obvious yellow egg spots in adult males. Territorial males are uniformly dark brown to black while non-territorial males are yellowish-brown. In this species a sexual dimorphism has been discovered in the dentition. The change from bicuspid teeth in the outer rows and from tricuspid teeth in the inner rows towards unicuspid teeth happens at a smaller size in males than in females. This may be linked to a change in feeding behaviour, but no further data are available (Snoeks 1994).

The habitus of *Haplochromis graueri* (Fig. 8.4a), is similar to that of *H. adolphifrederici* and both species have a “heavy head” look. Although the pharyngeal teeth are not enlarged in *H. graueri*, both species have been mixed in the past.

Haplochromis astatodon (Fig. 8.4b) is the only species with a closely-set outer dentition of fine and slender teeth, moveably attached to the jaw and with a large obliquely truncated crown. This type of dentition is typical for epiphytic algae scrapers. However, the species was found to be mainly detritivorous (Ulyel et al. 1990). While most of its capture localities might have been close to submerged or coastal vegetation, the species was captured on rocky habitats as well (Snoeks 1994).

Haplochromis nigroides (Fig. 8.4c) is a problematic species. Described first as a variety of *H. astatodon*, the holotype is clearly different and represents another species. Few of the specimens allocated to *H. nigroides* by subsequent authors actually belong to the species. At this moment, only adult males are included in the re-description of the species (Snoeks 1994). It is very difficult to separate from *H. scheffersi* as all meristics and measurements overlap to a large extent.

Haplochromis kamiranzovu (Fig. 8.4d) is an elongate species. It is the most pelagic-living haplochromine species in Lake Kivu but it has been found near the coast at river mouths as well. It is the most common species in the catches of the local sardine fishermen. *Haplochromis kamiranzovu* has been reported as a microphytophage by Ulyel et al. (1990), though morphologically it is similar to the zooplanktivores from Lake Victoria as described by Witte and van Oijen (1990).

Haplochromis scheffersi (Fig. 8.4e). As for *H. nigroides*, the identification of females of this species remains problematic. Little is known of its ecology though its morphology is quite generalized.

Haplochromis occultidens (Fig. 8.5a) is a rare species, many specimens of which have been identified in the past as *H. paucidens*. Interestingly and in contrast to all other Kivu haplochromines in the lake, the number of teeth in the outer rows of the oral jaws diminishes with size. This is undoubtedly linked to the ecological niche of

Fig. 8.4 (a) *Haplochromis graueri*; (b) *Haplochromis astatodon*; (c) *Haplochromis nigroides*; (d) *Haplochromis kamiranzovu*; (e) *Haplochromis scheffersi* (From Snoeks (1994). Copyright RMCA, Tervuren, Belgium)

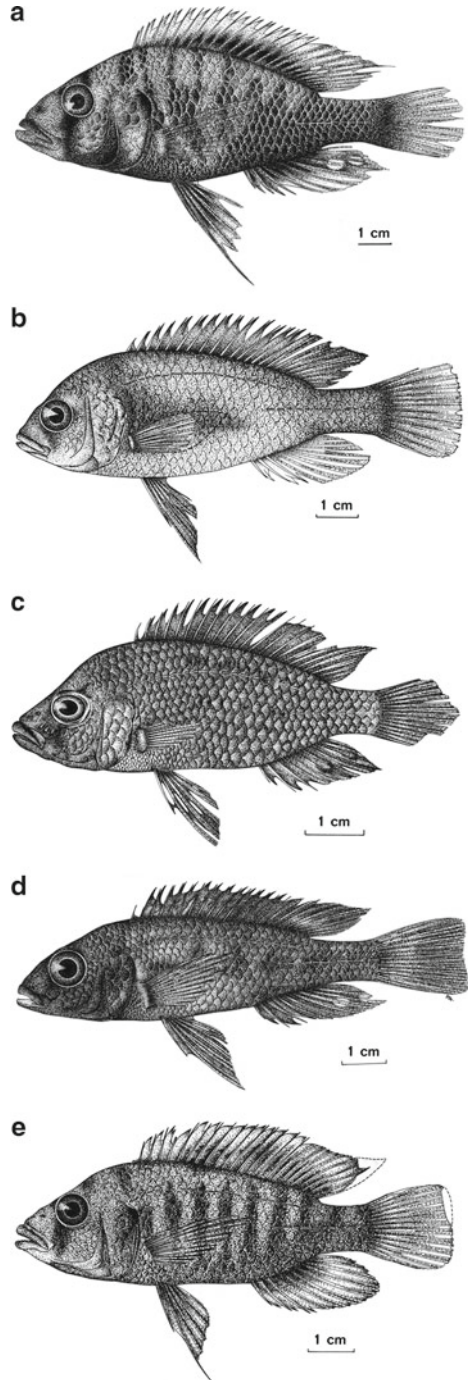
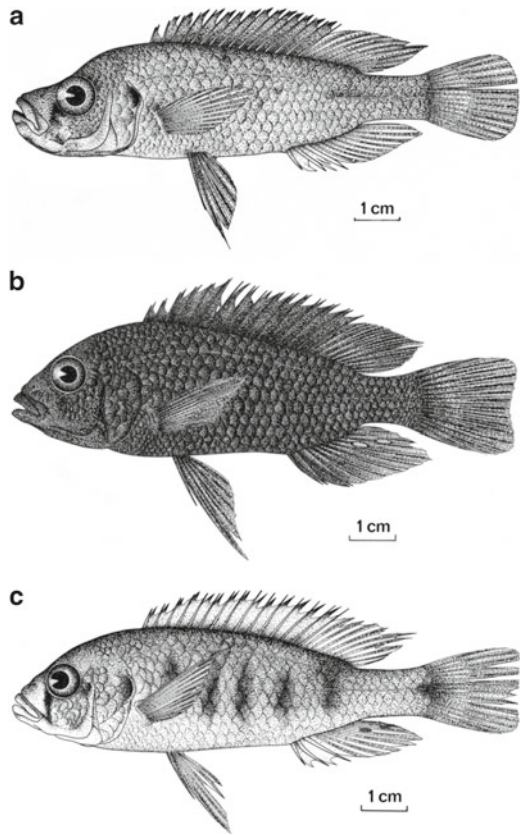


Fig. 8.5 (a) *Haplochromis occultidens*; (b) *Haplochromis olivaceus*; (c) *Haplochromis crebridens* (From Snoeks 1994. Copyright RMCA, Tervuren, Belgium)

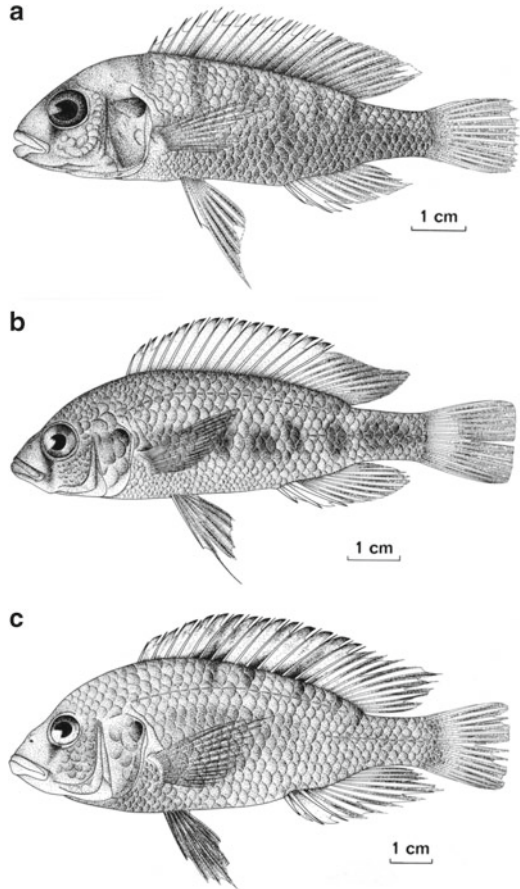


the species. Indeed the diet is composed of young fish and eggs. Its feeding habits have not been observed on live specimens, but it is likely that the species is a paedophage of the snout-engulfing type. The thick oral mucosa with only few teeth hidden, probably forms an effective instrument to engulf the snout of mouth-brooding females (Snoeks 1994).

Haplochromis olivaceus (Fig. 8.5b) and *Haplochromis crebridens* (Fig. 8.5c) form a species pair, at least from a morphological point of view. Again, this represents an example where non-territorial males and females of both species are difficult to distinguish. Both are epilithic algae scrapers, which corresponds well to their dentition with numerous rows of densely set teeth with large cusps (Snoeks et al. 1990). Both species may be ecologically segregated to a certain extent as *H. crebridens* has been found relatively more often in floating gill nets both during the day and at night (Snoeks 1994).

Haplochromis microchrysomelas (Fig. 8.6a) is one of the smaller species in the lake, characterized by a low number of vertical bars on the body. It has relatively few teeth, but more so than *H. occultidens* and *H. paucidens*. Virtually nothing is known about its ecology as the species has been mixed with *H. scheffersi* in the past.

Fig. 8.6 (a) *Haplochromis microchrysomelas*;
 (b) *Haplochromis insidiae*;
 (c) *Haplochromis rubescens*
 (From Snoeks (1994).
 Copyright RMCA, Tervuren,
 Belgium)



Haplochromis insidiae (Fig. 8.6b) represents a combination of morphological characters that puts it midway between *H. astatodon* and *H. kamiranzovu*. Indeed the species is elongated but less so than *H. kamiranzovu* and has protracted teeth but less pronounced than in *H. astatodon*. Most adult males were found in muddy or sandy areas but some non territorial specimens were found amongst the catches of sardines in pelagic waters.

Of *Haplochromis rubescens* (Fig. 8.6c) only seven adult males have been positively identified in the collections. These are characterized by a red colour on the body, which is more pronounced than in *H. graueri*. Nothing is known about its ecology, but its dentition, though less specialized than in *H. crebridens* and *H. olivaceus*, is typical for an epilithic algae grazer.

Some taxonomic issues are not completely solved. There is still a lack of specimens of certain haplochromine species such as *H. nigroides* and *H. rubescens*. Hence it is difficult to delineate these species. Especially, the differential diagnosis between the former and *H. scheffersi* is not well developed.

The endemic haplochromines belong to the superflock of East African haplochromines present in the drainage systems of Lakes Victoria-Kyoga, Edward-George and Albert (Snoeks 1994). The relationships between the taxa have been a matter of discussion for a long time. Greenwood (1979, 1980) did a remarkable attempt to apply a cladistic approach that resulted in the hundreds of species known at that moment, being classified in 25 resurrected or newly described genera whose distributions cut across the boundaries of the various drainage systems (Snoeks 2000; Fryer 2004). Snoeks (1994) tried to apply Greenwood's classification scheme on the Lake Kivu haplochromines, but with moderate success. He preferred using the gender name *Haplochromis*, as was done by the Dutch Hest group for the species from Lake Victoria (e.g. Hoogerhoud 1984; van Oijen 1996; Witte et al. 2009). The use of the generic name *Haplochromis* in a broad geographic context has been supported by recent molecular results (Verheyen et al 2003; Elmer et al. 2009), clearly demonstrating that even when using a fast evolving fragment of mtDNA or a large array of microsatellites, species cannot be distinguished. No signal of genus structuring is present in these results as genetic differentiation for the whole flock is extremely low (Elmer et al. 2009). The global picture as far as relationships are observed is one of Lake Kivu haplochromines mixed with those of the other regions without clear species-specific boundaries except for *H. gracilior* (Verheyen et al. 2003) or Lake Kivu being basal to the remaining parts of the superflock (Elmer et al. 2009). A special feature observed in Lake Kivu haplochromines is the large amount of polychromatism. This is limited to the so-called piebald or bicolor specimens showing an irregular blotched pattern of brown-black pigment on a whitish-yellowish background. Orange blotched specimens (dark blotches on an orange background), such as in some Lake Victoria species (Maan et al. 2008), have never been observed in Lake Kivu. The presence of piebald or bicolor specimens has been observed in four of the fifteen species (*H. vittatus*, *H. occultidens*, *H. adolphifrederici*, *H. paucidens*). In the latter species, a grey, peppered form has been discovered as well, albeit in small numbers and only in females (Snoeks 1994). In *H. adolphifrederici* and *H. paucidens*, for which large samples were available, about half of the females were found to be of the piebald morph. No morphological differences were found between the normal and the piebald specimens (Snoeks 1994). Piebald males are very rare (Snoeks 1995). Another type of polychromatism, found in the normal or plain coloured morph in some Lake Victoria species (Maan et al. 2006) has, up to now, not been found in Lake Kivu. The range of colour variation reported for the latter type of polychromatism is indeed present in Lake Kivu haplochromines, but appears to be confined to intra-individual variability.

8.3 Origin and Ichthyogeography

Lake Kivu currently belongs to the Congo basin through its connection with Lake Tanganyika via the Rusizi. Traditionally, the lake has been included in the Congo region, or if a smaller scale categorization was made, in the same ichthyogeographic

region as Lake Tanganyika (Snoeks et al. 1997). The Rusizi connection is however very recent in geological terms (see above). In 1997, Snoeks et al. discussed the ichthyogeographic position of Lake Kivu and concluded that, with respect to the non-cichlids of the lake, the lake had more affinities with the area to which it was connected before the origin of its current outlet, than with Tanganyika and the Congo basin. After an analysis of the distribution patterns of the fish fauna of the lake, they concluded that, similarly to the classification of Lakes Edward and George into the East Coast province, suggested by Greenwood (1983), the ichthyofauna of Lake Kivu had most affinities with the East Coast province.

This hypothesis, mainly based on non-cichlids, in the opinion of Snoeks et al. (1997) matched the observation that the endemic Kivu haplochromines were part of a larger super species flock comprising the haplochromines from Lakes Victoria, Kyoga, Edward, George, Kivu and affluent river systems. The latter was confirmed by Verheyen et al. (2003), based on a large review of sequencing data of the mitochondrial control region DNA of 290 haplochromine specimens from the region, resulting in 122 different haplotypes. At no level, Kivu, Edward and Victoria haplochromine species could be distinguished from each other. Individual species had multiple haplotypes and haplotypes were shared by different species. One exception proved to be three small specimens identified as *Haplochromis gracilior*, which were found to represent the sister taxon to all other haplochromines of the super species flock. As such, the evolutionary history of the super species flock was traced back to Lake Kivu. These results, but especially the biological refutation of the Lake Victoria desiccation scenario, came as a surprise to those involved in faunal studies of the area and is still a matter of debate (Fryer 2004; Stager and Johnson 2008) with a yet unresolved conflict between the interpretation of geophysical and palaeo-ecological data on the one hand and molecular data on the other hand. However, the scenario outlined was confirmed in a later paper (Elmer et al. 2009) in which 12 nuclear microsatellite loci were analyzed and in which Lake Kivu specimens came out as the ancestral lineage to the Lake Victoria Region haplochromines. Surprisingly, the Kivu haplochromines were found to contain more interspecific genetic differentiation than the more derived and younger, but much larger group of Victoria haplochromines.

In addition, some evolutionary questions are left open. Did the Lake Kivu area also act as the central point of dispersal toward Lakes Edward and Victoria for some of the non-cichlid taxa? Which molecular markers can be used for species recognition in haplochromines?

8.4 The Biology of *Limnothrissa miodon* in Lake Kivu

The growth of *L. miodon* is similar in Lake Tanganyika and Lake Kivu (Kaningini 1995). In both lakes, *L. miodon* grows rapidly, with a mean monthly growth rate of more than 10 mm during its early life (5–6 months), reaching approximately 10 cm after 1 year. Its life expectancy is short, approximately 1 year. In both lakes, *L. miodon* is essentially zooplanktivorous in its early life but becomes omnivorous at the adult stage, feeding on diverse prey: zooplankton, insect larvae and adults,

other small fishes, including their larval and juvenile stages (Isumbisho et al. 2004). However, the habitat preference of *L. miodon* appears to differ between lakes. In Lake Kivu, the larvae of *L. miodon* live along the littoral zone and migrate progressively further offshore during growth (Spliethoff et al. 1983). However, the oldest specimens are found inshore. In contrast, in Lake Tanganyika, *L. miodon* lives essentially in the littoral zone during most of its life; only the oldest specimens migrate offshore, where they live in shoals of *Stolothrissa tanganyicae* (Coulter 1991).

Marshall (1993) noted that, despite considerable differences among the lakes in which *Limnothrissa miodon* became established (Lake Kivu, Lake Kariba and Lake Cahora Bassa), the biology of *Limnothrissa* was similar in many respects in all of them. Similarities included its feeding and breeding biology, whilst its populations fluctuate, on both an annual and a seasonal basis, in relation to environmental changes. The major differences between the lakes concerned the size to which *Limnothrissa* grows. Marshall (1993) observed that the size of *Limnothrissa* in Lake Kivu (up to 169 mm) was similar to that in Lake Tanganyika (up to 200 mm), whereas it had about half the length in the artificial lakes. Marshall explained this by the cannibalistic behaviour of *Limnothrissa* in the two natural lakes and by the fact that *Limnothrissa* can maintain a high biomass and productivity in the face of intense predation. In Lake Kivu, where no piscivorous fish exist in the pelagic zone, predation is replaced by the intense fishing effort.

Limnothrissa was until recently the only species in the pelagic zone of Lake Kivu, with no competitor and no predator, but this has changed since *Lamprichthys* turned up in the lake. Nowadays, *Lamprichthys* has colonized the littoral and the pelagic zone and it is still increasing in the pelagic catches. This recent invader feeds mainly on mesozooplankton offshore, whatever its body size (Fig. 8.7), which results in substantial niche overlap with the sardine. Although the niche overlap appears to be somewhat reduced inshore, the expansion of *Lamprichthys* raises concern about the future of the sardine fishery.

Limnothrissa larvae and juveniles partition their living space: juveniles migrate in an intermediate zone to feed on large zooplankton while larvae remain in the littoral zone and show little or no size selectivity towards copepods (Isumbisho et al. 2004). Adult *Limnothrissa* colonize all the areas of the lake. *Limnothrissa* exhibits this opportunistic foraging in Lake Kivu as well as in other lakes (Poll 1953; Coulter 1991; Mandima 1999, 2000). In Lake Kivu, as in the artificial lakes (Mandima 1999), *Limnothrissa* appears to feed on zooplankton in the middle of the day (Masilya et al. 2005; Masilya 2011), whereas in early morning and late afternoon, it consumes terrestrial insects, small fishes and mesozooplankton in the littoral zone (Masilya 2011).

8.5 Whole-lake Assessment of *Limnothrissa miodon* Abundance

A whole-lake fish stock survey using hydroacoustics was conducted by Lamboeuf (1991), in the framework of the PNUD/FAO/Rwa/87/012 project for the development of the fishery in Lake Kivu. This survey comprised seven hydroacoustics surveys

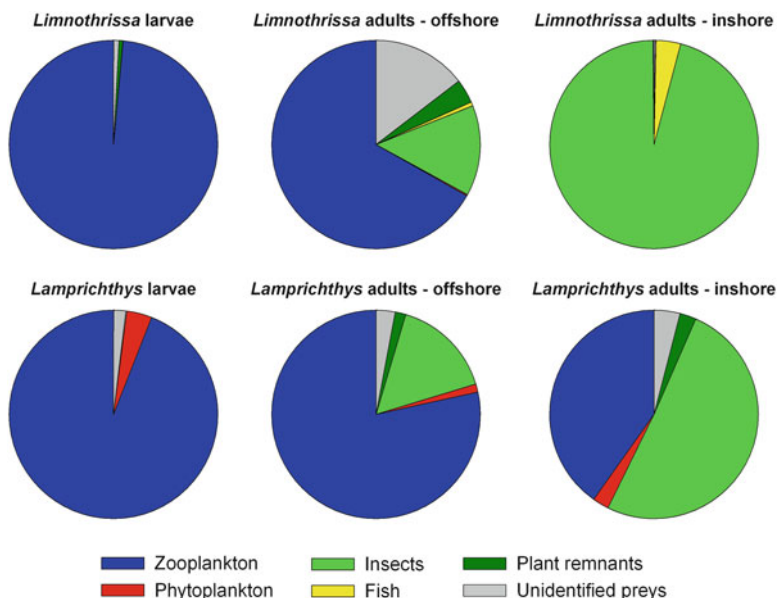


Fig. 8.7 Diet of juveniles and adults (Lauzanne's index expressed as %) of *Limnothrissa miodon* and *Lamprichthys tanganicanus* in Lake Kivu (modified from Masilya et al. 2011)

covering the whole lake, between April 1989 and May 1990. Total abundance of pelagic fish varied little between campaigns and provided a mean stock of 4,460 t. All class sizes were represented in all lake regions, and fishes were distributed down to 50–60 m depth, i.e. all over the mixolimnion, but their vertical distribution was restricted to the oxygenated layers.

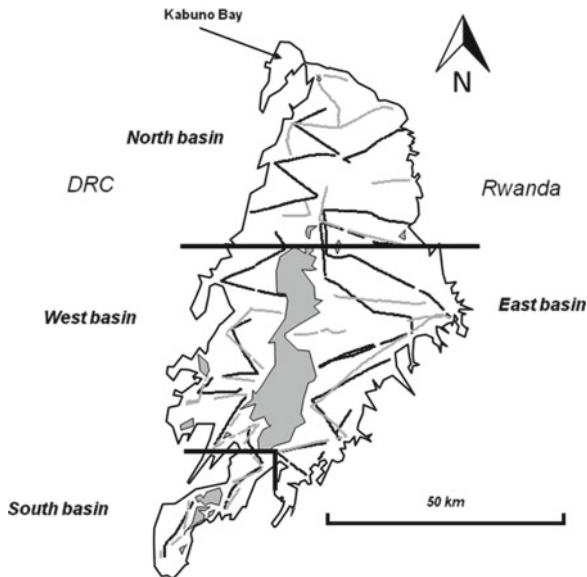
In order to update this fish stock assessment, two new surveys were carried out in 2008 (Guillard et al. 2012), during the rainy season (14–22 February), and in the dry season (1–11 July 2008). The lake was divided into 4 large basins (Table 8.2), and Kabuno Bay was not included in our surveys (Fig. 8.8). The layers were similar to those sampled by Lamboeuf (1991), i.e. from surface to 15 m, 15 to 30 m, 30 to 45 m, and 45 to 60 m, then merged to calculate total biomass. The sampling protocol and all methods for data processing were as close as possible to those of Lamboeuf (1989, 1991).

Daily observations carried out *in situ* showed several types of structure, and the absence of targets in layers lower than 60 m, due to the lack of oxygen; furthermore no fish were detected in layers close to the surface (Fig. 8.9). Very dense schools (Fig. 8.9a) were mainly observed close to the shores, with depths <40–50 m or near areas of shallows in pelagic areas. The night survey (Fig. 8.9c) showed fish dispersion at dusk, in conformity with previous descriptions (Kaningini et al. 1999).

The fish densities (Fig. 8.10) were heterogeneous, according to localizations and seasons. In February, the strongest densities were detected in the south and the east basins, whereas in July the distributions among basins appeared more homogeneous.

Table 8.2 Characteristics of the basins, used for calculations for the hydroacoustic survey

Basin	North	East	West	South	Littoral area depth < 50 m
Surface (km ²)	900 ^a	900 ^a	320	97	50 ^a
Depth max (m)	485	400	225	105	50

^aEstimated**Fig. 8.8** Transects of the hydroacoustic survey carried out in February (grey lines) and July (black lines) 2008 in Lake Kivu

The densities detected inshore were much higher (by a factor 5–7) than those in the pelagic area. The vertical structures were also different according to the season, the fish being more abundant in the upper layers in July. In the deepest layers (45–60 m), average values were always low: furthermore in 80–100% of the Elementary Sampling Distance Units (ESDU) no detection was recorded, except during July in the west and south basins where a few fishes were detected in these deepest layers. When this deepest layer was not taken into account, the percentage of units without fish detections was very low, and over the entire water column there were very few areas without any detection. The fractions in the major size class (>ca. 6 cm, <12–13 cm), were constant in number, around 50%, whatever the season and the basin (Table 8.3). The number of fish per area, and the total tonnage by basin was obtained by multiplying the average areal biomass by the estimated surface area of each basin (Fig. 8.10).

Behaviour such as dispersion at dusk (Fréon et al. 1996) and schooling during day time (Fréon and Misund 1999), described as anti-predatory mechanisms by many authors (Parrish et al. 2002), were observed in Lake Kivu (Fig. 8.9), despite

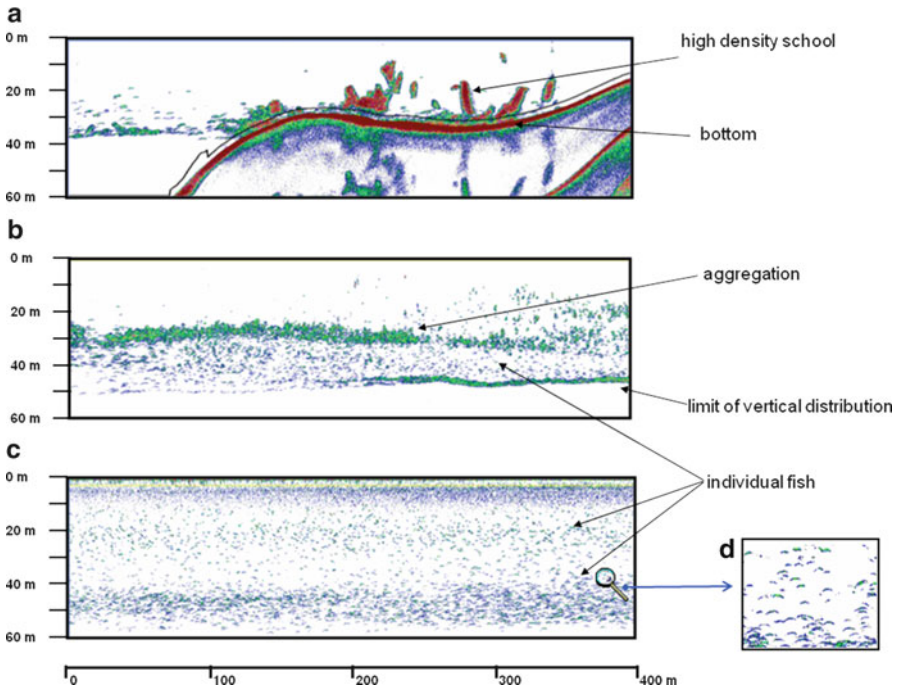


Fig. 8.9 Echograms recorded in Lake Kivu during daylight in the inshore area (a) and in the pelagic area (b), and at night in the pelagic area (c), with a zoom on individual fish (d). The horizontal scale is an approximate of the distance covered

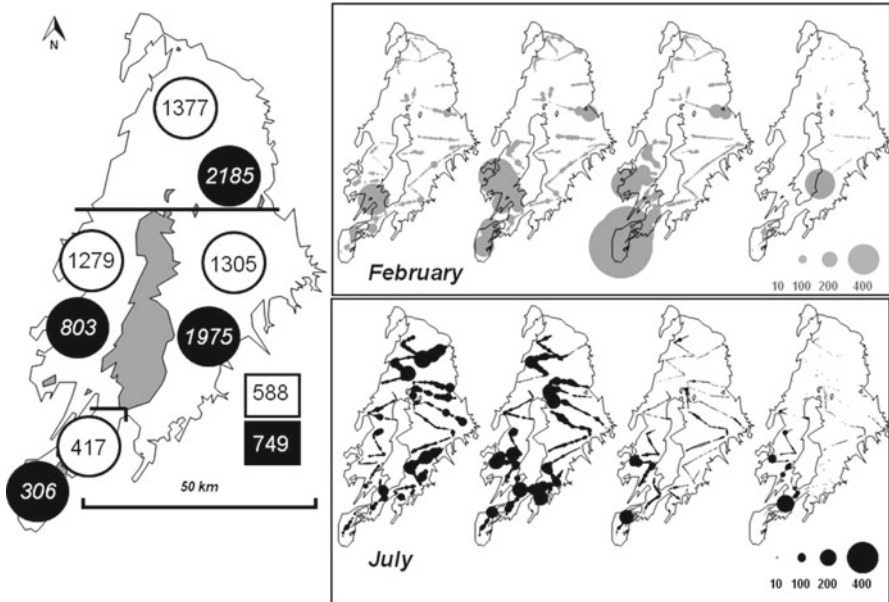


Fig. 8.10 Tonnage by basin for the two surveys (February, white circles; July, black circles) and for littoral areas (February, white square; July, black square). Maps of fish densities for the four layers (3–15, 15–30, 30–45, 45–60 respectively from left to right), during February (grey) and July (black) 2008: the values are in "Sa" ($\text{m}^2 \text{ha}^{-1}$) $\times 100$, i.e. acoustic energy reflected per unit area

Table 8.3 Size classes of fish detected by basin for the two surveys

	North		East		West		South		Littoral depth < 50 m						
	<6 cm	>12-13 cm	<6 cm	>12-13 cm	<6 cm	>12-13 cm	<6 cm	>12-13 cm	<6 cm	>12-13 cm					
<i>February</i>															
%	35	56	9	35	53	12	28	53	18	34	57	10	28	51	21
<i>July</i>															
%	27	49	24	30	51	19	21	62	16	39	46	15	7	70	22

the absence of predators in the pelagic zone. This agrees with previous observations of fish distribution in the lake (Kaniningini et al. 1999). Shallow areas are not well sampled by hydroacoustic surveys, and this affects the whole-lake estimate of fish abundance in most lakes (Brehmer et al. 2006); in Lake Kivu, as the shallow areas make less than 10% of the lake area, this kind of bias is reduced. Furthermore, due to the homogeneous distribution during daytime and the absence of fish close to the surface, which are usually not detected by hydroacoustic, one can be confident that the acoustic surveys were reliable (Simmonds and MacLennan 2005).

Even though high amounts of fish were recorded in the north and east basins in the dry season (July), the densities per unit area were always higher in the west and south basins, whatever the season. The densities in these two basins were higher in the rainy season. In the same way, Marshall (1991) had noted that the catch per unit effort (CPUE) was higher in the south in February and in the north in July, connecting this phenomenon to a south to north migration, related to the morphology of the south basin which presents more coastal zones, favorable to reproduction. The vertical structures were heterogeneous according to areas, but the limit of the vertical distribution was very clear.

The adult fish percentage did not vary according to region and season and was around 50%, the juveniles, greater than ~1–2 cm, accounted for about 30–35% of the total number and the largest fish 15%. The whole-lake sardine stock, from these two recent acoustic surveys, was estimated to 5,000–6,000 t. This estimate is of the same order as for the survey carried out by Lamboeuf (1991) at the end of the 1980s (4,460 t). Average surface densities observed were also similar to those given by Lamboeuf (1991), i.e. 15–40 kg ha⁻¹. Considering a P/B ratio of 1.6 for *Limnothrissa* (Roest 1999), the annual production would be 8,000–9,600 t year⁻¹.

8.6 The Status of the Fishery

The stability of the pelagic fish stock over some 20 years, as shown by the hydroacoustic surveys, offers compelling evidence that, although the fishing effort has probably increased since the end of the 1980s, the *Limnothrissa* population of Lake Kivu has remained remarkably stable.

By contrast, recent direct estimates of the total annual sardine catch have hardly been available, due to the absence of reliable fish statistics from systematic surveys. At the end of the PNUD/FAO project, the estimate of the total number of fishing units over the whole lake (Kaniningini et al. 1999) was 227 fishing units, using 400 m² lift nets, with a mean CPUE of ~50 kg day⁻¹. Catches varied strongly depending on season. Data from Bukavu Bay, where a fishing unit was followed for 1.5 years, provided an average daily catch of ~40 kg, with lowest values (15–20 kg day⁻¹) in the May-July period and highest (50–100 kg day⁻¹) in the November-January period. The total *Limnothrissa* catch around 1990 was ~3,200 t year⁻¹, whereas *Haplochromis* catches amounted to 1,460 t year⁻¹. The use of gill nets, promoted by the EC project

ONG/219/92/Zaire (Kaningini et al. 1999) may have further increased the annual *Limnothrissa* catches by 280 t. A study of population dynamics (Kaningini 1995) demonstrated that natural mortality and mortality from the fishery were nearly equal, suggesting an optimal exploitation rate.

Since then, no update on the fisheries yield in Lake Kivu has been available, with the exception of recent records from the MINAGRI (Ministry of Agriculture of Rwanda, in charge of fisheries and aquaculture), which has recorded data on total catch in the lake. The data available for the years 2007 and 2008 indicate a total fish catch between 5,742 and 6,692 t. Assuming that the sardine represented 85% of the catches (Kaningini et al. 1999), the average sardine catch for the Rwandese waters would be about 5,300 t, which represents ~60% of the annual *Limnothrissa* production. Although no comprehensive catch data are available for the Congolese part of the lake, it may be safe to assume that they were similar to those in the Rwandese waters. This suggests that the total sardine catch in recent years was close to the estimated annual production of ~9,000 t, so that, at lake-wide scale, the *Sambaza* may not have been overexploited since the fishery has developed. However, the fishing pressure is not distributed evenly: some areas may present greater than average sardine production, offer better catches, and hence be subjected to high fishing pressure. This is the case of the Bukavu Bay, where the number of fishing units is greater than elsewhere, resulting in heavy pressure on the sardine stock. In recent years, as the mean fish size was declining, the fishery has been regularly closed for several months in DR Congo (Kaningini pers. comm.). Another concern for the fishery is the catch of sardine larvae and juveniles in the littoral areas, which is a common practice all over the lake shores: the impact of this practice on the pelagic fishery has not been assessed yet, but it remains a serious concern.

8.7 The Food Web Structure

The food web of Lake Kivu was described by Villanueva et al. (2008), using the ECOPATH modeling approach. This model included several fish species and identified phytoplankton and detritus as the major sources of carbon for the food web. However, this study failed to separate the pelagic and the littoral food webs, which are largely uncoupled in Lake Kivu, due to the reduced proportion of the lake area being in the littoral zone. In fact, the pelagic zone is essentially occupied by *Limnothrissa miodon* and by *Lamprichthys tanganicanus*, with only few species of *Haplochromis* (see 8.1) found in the pelagic waters. Moreover, Villanueva et al. (2008), in addition to general assumptions of their modeling approach, used essentially gut content analyses and general knowledge on the biology and the diet of the fish species for describing trophic relationships in the lake. Recent studies based on stable isotopes measurements and on fatty acid analyses may provide a better view of the food web structure of Lake Kivu, although the littoral food web has remained understudied so far. The results of these recent studies (Masilya 2011) showed some separation of pelagic and littoral food webs based on stable isotopes signatures of the organisms (Fig. 8.11).

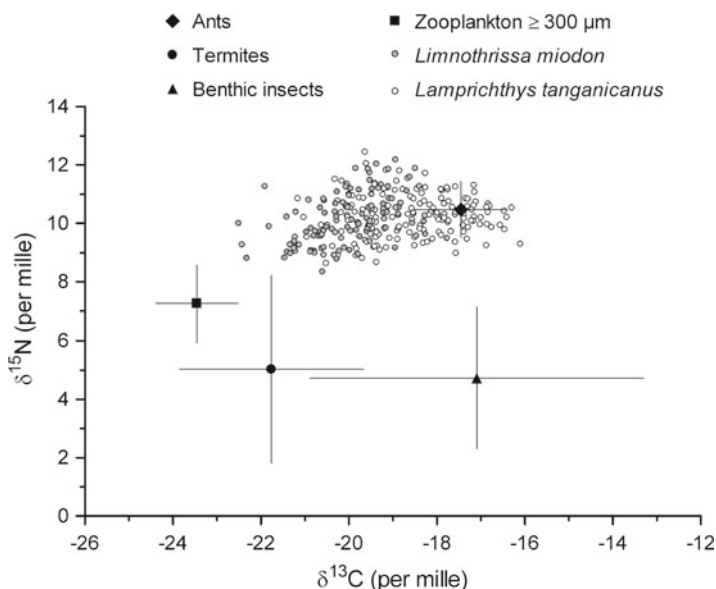


Fig. 8.11 Stable isotopes of C and N in various components of the food web in Lake Kivu (from Masilya 2011)

This analysis (Masilya 2011) shows that *Limnothrissa* and *Lamprichthys* have a similar trophic position, with the sardine being more dependent on the planktonic resources than *Lamprichthys*, which seems to depend also on littoral resources. The study of fatty acids in the seston, the zooplankton and the fishes reveals that the mesozooplankton diet relies on diatoms, cryptophytes and chrysophytes, whereas cyanobacteria are not or less consumed (Masilya 2011). Moreover, bacterial fatty acids found in the picoplankton fraction (seston 0.7–2 μm) were also found in the largest mesozooplankton specimens. This indicates a probable contribution of the microbial loop to the functioning of the pelagic food web in Lake Kivu.

8.8 Conclusion

The ichthyofauna of Lake Kivu is unique because of its fifteen endemic haplochromine species that seem to have played a pivotal role in the evolutionary history of the haplochromine fauna in the region, being in a basal position to the other haplochromines of the Albert-Edward Victoria flock. Identification remains difficult and problems persist in the delineation of certain species such as *H. nigroides* and *H. rubescens*. The non-cichlid fauna is very poor, reflecting the lake's intense geological history. It includes eight native and five introduced species, with some taxonomic confusion remaining in '*Barbus*' *pellegrini* and *Amphilius uranoscopus*

living in the affluent rivers. Major fish families present in other basins in the region are absent from Lake Kivu.

Species diversity is concentrated in the littoral area. However detailed ecological studies on these cichlids and non-cichlids are lacking.

The studies in the field of fish biology and fisheries of the two last decades have been mostly devoted to *Limnothrissa miodon*, and largely used for fisheries management, notably for promoting alternative, size-selective, fishing techniques, aiming at catching the largest size classes of the sardines and allowing the smallest specimens to grow further. The use of hydro-acoustic surveys is particularly adapted to Lake Kivu, where the sole pelagic fish is the sardine, although catches of the recently introduced *Lamprichthys* have been reported by the fishermen. Therefore, in future stock assessment surveys, hydroacoustic records should be complemented by experimental catches, in order to verify the presence of *Lamprichthys* in significant numbers offshore. Indeed, this species, a potential competitor of *Limnothrissa* for zooplankton and other food resources, seems to be preferentially located close to the shore, as in its original habitat. Still, monitoring both species by experimental catches and fisheries statistics remains important to follow the possible expansion of the invader in the fragile pelagic ecosystem of Lake Kivu.

Compared to Lake Tanganyika, the sardine production in Lake Kivu is low. This may be due to several reasons, the most obvious being the low amount and diversity of planktonic resources in the pelagic zone, which is the most extended (>90% of the lake area). Although other preys are found in the adult sardine guts, *Limnothrissa* essentially depends on plankton production, and alternative prey does not compensate for the paucity and variability of zooplankton biomass during most of the year. We may speculate that this dependence on a variable resource may affect the survival of the *Limnothrissa* juveniles, which can only develop to the adult stage when resources are sufficient, i.e. at the end of the dry season. Otherwise, the studies conducted on fatty acids in the seston and in the zooplankton clearly show that the food quality in Lake Kivu is adequate for meeting the planktivore's requirements. Therefore future studies should focus on the survival of *Limnothrissa* juveniles, and explore other less known areas, such as the food web structure and function in the littoral zone, where several endemic and specialized haplochromines are found. There may actually be an issue of species conservation here, as fishing in the littoral zone is commonly practiced, seemingly without regulation. This stresses the need for detailed fishery surveys, which should be conducted in order to be able to assess the pressure on different fish populations, and for a proper management of this lake's resource of vital importance for the local human population.

Acknowledgments This work was partly funded by the Coopération Universitaire au Développement under the ECOSYKI (Study of the functioning of Lake Kivu ecosystem for its sustainable management) project and contributes to the Belgian Federal Science Policy Office EAGLES (East African Great Lake Ecosystem Sensitivity to changes, SD/AR/02A) project.

References

- Beadle LC (1981) The inland waters of tropical Africa, an introduction to tropical limnology, 2nd edn. Longman, London
- Brehmer P, Guillard J, Guennégan Y, Bigot JL, Liorzou B (2006) Evidence of a variable “unsampled” biomass along the shallow water (<20 m) coastline in small pelagic fish stock assessment method. ICES J Mar Sci 63:444–451. doi:10.1016/j.icesjms.2005.10.016
- Capart A (1959) A propos de l'introduction du Ndakala (*Stolothrissa tanganyikae*) dans le Lac Kivu. Bull Agric Congo Belge Ruanda-Urundi 4:1083–1088
- Collart A (1960) L'introduction du *Stolothrissa tanganicae* (Ndagala) au lac Kivu. Bull Agric Congo Belge 51(4):975–985
- Coulter GW (1991) Lake Tanganyika and its life. Oxford University Press, London
- De Vos L, Snoeks J, Thys van den Audenaerde D (2001) An annotated checklist of the fishes of Rwanda (East Central Africa), with historical data on introductions of commercially important species. J East Afr Nat Hist 90:41–68. doi:10.2982/0012-8317(2001)90[41: AACOTF] 2.0.CO;2
- Degens ET, von Herzen RP, Wong H-K, Deuser WG, Jannasch HW (1973) Lake Kivu: structure, chemistry and biology of an East African rift lake. Geol Rundschau 62(1):245–277. doi:10.1007/BF01826830
- De Vos L, Thys van den Audenaerde DFE (1990a) Petits *Barbus* (Pisces, Cyprinidae) du Rwanda. Rev Hydrobiol Trop 23(2):141–159
- De Vos L, Thys van den Audenaerde DFE (1990b) Description de *Barbus claudinae* sp. n. (Cyprinidae) avec synopsis des grandes espèces de *Barbus* du Rwanda. Cybium 14(1):3–25
- Elmer KR, Reggio C, Wirth T, Verheyen E, Salzburger W, Meyer A (2009) Pleistocene desiccation in East Africa bottlenecked but did not extirpate the adaptive radiation of Lake Victoria haplochromine cichlid fishes. Proc Natl Acad Sci USA 106(32):13404–13409. doi:10.1073/pnas.0902299106
- Fréon P, Gerlotto F, Soria M (1996) Diel variability of school structure with special reference to transition. ICES J Mar Sci 53:459–464. doi:10.1006/jmsc.1996.0065
- Fréon P, Misund OA (1999) Dynamics of pelagic fish distribution and behaviour: effects on fisheries and stock assessment. Fishing News Books, Blackwell Science, Oxford
- Fryer G (2004) Speciation rates in lakes and the enigma of Lake Victoria. Hydrobiologia 519: 167–183. doi:10.1023/B:HYDR.0000026503.59198.c5
- Gourène G, Teugels GG (1993) Position taxinomique de *Limnothrissa stappersii*, un clupéidé lacustre d'Afrique centrale. Ichthyol Explor Freshw 4:367–374
- Gozlan RE (2008) Introduction of non-native freshwater fish: is it all bad? Fish Fish 9:106–115. doi:10.1111/j.1467-2979.2007.00267.x
- Greenwood PH (1979) Towards a phyletic classification of the genus *Haplochromis* (Pisces, Cichlidae) and related taxa. Part I. Bull Br Mus Nat Hist (Zool) 35(4):265–322
- Greenwood PH (1980) Towards a phyletic classification of the genus *Haplochromis* (Pisces, Cichlidae) and related taxa. Part II. The species from Lakes Victoria, Nabugabo, Edward, George and Kivu. Bull Br Mus Nat Hist (Zool) 39(1):1–101
- Greenwood PH (1983) The zoogeography of African freshwater fishes: bioaccountancy or biogeography? In: Sims RW, Price JH, Whalley PES (eds) Evolution, time and space: the emergence of the biosphere. Academic Press, London & New York, pp 179–199, Systematics Association, special volume 23
- Guillard J, Darchambeau F, Masilya P, Descy J-P (2012) Is the fishery of the introduced Tanganyika sardine (*Limnothrissa miodon*) in Lake Kivu (East Africa) sustainable? J. Great Lakes Res, in press
- Haberyan KA, Hecky RE (1987) The late Pleistocene and Holocene stratigraphy and paleolimnology of Lakes Kivu and Tanganyika. Palaeogeogr Palaeoclimatol Palaeoecol 61:169–197. doi:10.1016/0031-0182(87)90048-4

- Isumbisho M, Kaningini M, Descy J-P, Baras E (2004) Seasonal and diel variations in diet of the young stages of *Limnothrissa miodon* in Lake Kivu, Eastern Africa. *J Trop Ecol* 20:73–83. doi:10.1017/S0266467403001056
- Kaningini B (1995) Etude de la croissance, de la reproduction et de l'exploitation de *Limnothrissa miodon* au lac Kivu, bassin de Bukavu (Zaïre). PhD thesis, University of Namur, Belgium
- Kaningini B, Micha J-CI, Vandenhoute J, Platteau J-P, Watongoka H, Mélard C, Wilondja MK, Isumbisho M (1999) Pêche du Sambaza au filet maillant dans le lac Kivu. *Presses Universitaires de Namur*, Namur, Belgium
- Lamboeuf M (1989) Estimation de l'abondance du stock d'Isambaza (*Limnothrissa miodon*), résultats de la prospection acoustique de septembre 1989. *RWA/87/012/DOC/TR/20*
- Lamboeuf M (1991) Abondance et répartition du *Limnothrissa miodon* du lac Kivu, résultat des prospections acoustiques d'avril 1989 à juin 1991. *RWA/87/012/DOC/TR/46*
- Maan ME, Eshuis B, Haesler MP, Schneider MV, van Alphen JJM, Seehausen O (2008) Color polymorphism and predation in a Lake Victoria cichlid fish. *Copeia* 2008(3):621–629. doi:10.1643/CE-07-114
- Maan ME, Haesler MP, Seehausen O, van Alphen JJM (2006) Heritability and heterochrony of polychromatism in a Lake Victoria cichlid fish: stepping stones for speciation? *J Exp Zool B Mol Dev Evol* 306B:168–176. doi:10.1002/jez.b.21083
- Mandima JJ (1999) The food and feeding behaviour of *Limnothrissa miodon* (Boulenger, 1906) in Lake Kariba, Zimbabwe. *Hydrobiologia* 407:175–182. doi:10.1023/A:1003752423082
- Mandima JJ (2000) Spatial and temporal variations in the food of the sardine *Limnothrissa miodon* (Boulenger, 1906) in Lake Kariba, Zimbabwe. *Fisheries Research* 48:197–203. doi:10.1016/S0165-7836(00)00161-2
- Marshall E (1991) Impact of the introduced sardine *Limnothrissa miodon* on the ecology of Lake Kariba. *Biol Conserv* 55:151–165. doi:10.1016/0006-3207(91)90054-D
- Marshall BE (1993) Biology of the African clupeid *Limnothrissa miodon* with reference to its small size in artificial lakes. *Rev Fish Biol Fish* 3:17–38. doi:10.1007/BF00043296
- Masilya P, Kaningini B, Isumbisho P, Micha J-C, Ntakimazi G (2005) Food and feeding activity of *Limnothrissa miodon* (Boulenger, 1906) in the southern part of Lake Kivu, Central Africa. In *International Conference Africa's Great Rift: Diversity and Unity*. Royal Academy for Overseas Sciences, Royal Museum for Central Africa, Brussels, 29–30 September, 2005:83–93
- Masilya P (2011) Ecologie alimentaire de *Limnothrissa miodon* au Lac Kivu (Afrique de l'Est). PhD thesis, University of Namur, Belgium
- Masilya MP, Darchambeau F, Isumbisho M, Descy J-P (2011) Diet overlap between the newly introduced *Lamprichthys tanganicanus* and the Tanganyika sardine in Lake Kivu, Eastern Africa. *Hydrobiologia* 675:75–86. doi:10.1007/s10750-011-0797-y
- Muderhwa N, Matabaro L (2010) The introduction of the endemic fish species, *Lamprichthys Tanganicanus* (Poeciliidae), from Lake Tanganyika into Lake Kivu: possible causes and effects. *Aquat Ecosy Health Manag* 13:203–213. doi:10.1080/14634981003800733
- Parrish J, Viscido S, Grünbaum D (2002) Self-organized fish schools: an examination of emergent properties. *Biol Bull* 202:296–305. doi:10.1.1.116.1548
- Robben J, Thys van den Audenaerde D (1984) A preliminary study of the age and growth of the cyprinid fish *Barilius moorii* Blgr. from Lake Kivu. *Hydrobiologia* 108:153–163. doi:10.1007/BF00014875
- Roest FC (1999) Introduction of a pelagic fish into a large natural Lake: Lake Kivu, Central Africa. In: van Densen WLT, MorrisMJ (eds), *Fish and Fisheries of Lakes and Reservoirs in Southeast Asia and Africa*. Westbury Publishing, Otley, pp 327–338
- Simmonds EJ, MacLennan DN (2005) *Fisheries acoustics: theory and practice*. Blackwell Science Ltd., Oxford, p 437
- Skelton PH (1984) A systematic revision of species of the catfish genus *Amphilius* (Siluroidei, Amphiliidae) from east and southern Africa. *Ann Cape Prov Mus (Nat Hist)* 16:41–71
- Snoeks J (1986) Some problems in taxonomic research of the haplochromine taxa from Lake Kivu. In: Crapon de Caprona MD, Fritzsch B (eds), *Proc. Third Eur. Worksh. Cichlid Biol.*, Bielefeld, Germany. *Ann Mus Roy Afr Centr Sc Zool* 251:135–138

- Snoeks J (1988). Redescription d'*Haplochromis paucidens* Regan, 1921 et description d'*Haplochromis occultidens* sp. n. (Pisces, Cichlidae) du lac Kivu en Afrique. *Cybium* 12:203–218
- Snoeks J (1994) The haplochromine fishes (Teleostei, Cichlidae) of Lake Kivu, East Africa: a taxonomic revision with notes on their ecology. *Ann Mus Roy Afr Centr, Sci Zool* 270, Tervuren, 221pp
- Snoeks J (1995) Polychromatism in Lake Kivu haplochromines: two for the price of one? In: Konings A (ed) *The cichlids yearbook*, vol 5. Cichlid Press, Germany, pp 48–53
- Snoeks J (2000). How well known is the ichthyodiversity of the large East African lakes? *Adv Ecol Res* 31:17–38. doi:[10.1016/S0065-2504\(00\)31005-4](https://doi.org/10.1016/S0065-2504(00)31005-4)
- Snoeks J (2004) The non-cichlid fishes of the Lake Malawi/Nyasa/Niassa system. In: Snoeks J (ed) *The cichlid diversity of Lake Malawi/Nyasa/Niassa: identification, distribution and taxonomy*. Cichlid Press, El Paso, USA, pp 20–26
- Snoeks J, Coenen E, De Vos L, Thys van den Audenaerde D (1990) Description de deux nouvelles espèces d'*Haplochromis* (Teleostei, Cichlidae) du lac Kivu (Rwanda). *Cybium* 14:63–76
- Snoeks J, De Vos L, van den Audenaerde DT (1997) The ichthyogeography of Lake Kivu. *South Afr J Sci* 93:579–584
- Spliethoff PC, De Iongh HH, Frank V (1983) Success of the introduction of the freshwater Clupeid *Limnothrissa miodon* (Boulenger) in Lake Kivu. *Fish Manag* 14:17–31. doi:[10.1111/j.1365-2109.1983.tb00050.x](https://doi.org/10.1111/j.1365-2109.1983.tb00050.x)
- Stager JC, Johnson TC (2008) The late Pleistocene desiccation of Lake Victoria and the origin of its endemic biota. *Hydrobiologia* 596:5–16. doi:[10.1007/s10750-007-9158-2](https://doi.org/10.1007/s10750-007-9158-2)
- Ulyel AP, Ollevier F, Ceusters R, Thys van den Audenaerde DFE (1990) Régime alimentaire des *Haplochromis* (Teleostei: Cichlidae) du lac Kivu en Afrique I. Relations trophiques interpécifiques. *Belg J Zool* 120(2):143–155
- van Oijen MJP (1996) The generic classification of the haplochromine cichlids of Lake Victoria, East Africa. *Zool Verh (Leiden)* 302:57–110
- Verheyen E, Salzburger W, Snoeks J, Meyer A (2003) The origin of the superflock of cichlid fishes from Lake Victoria, East Africa. *Science* 300:325–329. doi:[10.1126/science.1080699](https://doi.org/10.1126/science.1080699)
- Villanueva MC, Isumbiso M, Kaningini B, Moreau J, Micha J-C (2008) Modeling trophic interactions in Lake Kivu: what roles do exotics play? *Ecol Model* 30:422–438. doi:[10.1016/j.ecolmodel.2007.10.047](https://doi.org/10.1016/j.ecolmodel.2007.10.047)
- Wildekamp RH (2004) *Atlas of the oviparous Cyprinodontiform fishes of the World*, vol IV. The American Killifish Association, 398pp
- Witte F, van Oijen MJP (1990) Taxonomy, ecology and fishery of Lake Victoria haplochromine trophic groups. *Zool Verh (Leiden)* 262:1–47
- Witte F, van Oijen MJP, Sibbing FA (2009) Fish fauna of the Nile. In: Dumont HJ (ed) *The Nile: origin, environments, limnology and human use*. Springer, The Netherlands, pp 647–675

Chapter 11

Lake Kivu Research: Conclusions and Perspectives

Jean-Pierre Descy, François Darchambeau, and Martin Schmid

Abstract In this chapter the knowledge gained from the interdisciplinary research on Lake Kivu presented in the previous chapters is synthesized. The importance of the sublacustrine springs as a driving force for physical and biogeochemical processes is highlighted, the special properties of the lake's food web structure are discussed, and the consequences and impacts of both the introduction of a new fish species and methane extraction are evaluated. Finally, a list of open research questions illustrates that Lake Kivu has by far not yet revealed all of its secrets.

11.1 Conclusions

11.1.1 The Dynamics of the System: The Importance of the Subaquatic Springs

Observations of vertical profiles of temperature, conductivity and solutes in Lake Kivu show a remarkable horizontal homogeneity and temporal constancy. At first sight, these observations may suggest that Lake Kivu is a relatively simple, near-steady-state

J.-P. Descy (✉)
Research Unit in Environmental and Evolutionary Biology,
University of Namur, Namur, Belgium
e-mail: jpdescy@fundp.ac.be

F. Darchambeau
Chemical Oceanography Unit, University of Liège, Liège, Belgium
e-mail: francois.darchambeau@ulg.ac.be

M. Schmid
Eawag: Swiss Federal Institute of Aquatic Science and Technology,
Kastanienbaum, Switzerland
e-mail: martin.schmid@eawag.ch

system, where no significant changes are expected to occur within time scales of years or even decades. In contrast, biological activity in the surface waters varies strongly from year to year (Chaps. 5 and 7), observations from sediment cores indicate a sudden change that occurred in the 1960s (Chap. 9), and methane concentrations seem to have increased significantly within only a few decades (Chap. 10).

The results presented in this book highlight the relative importance of the subaquatic springs in the lake for governing these processes and their time scales. The subaquatic springs were previously mainly considered as suppliers of the carbon dioxide and minerals dissolved in the deep waters, but not as the driving forces for the vertical structure of density stratification and the nutrient supply to the mixolimnion by upwelling. In fact, the deepest water layers, below the main density gradient, are almost decoupled from the rest of the lake. They are fed by subaquatic springs which are enriched in dissolved salts and carbon dioxide. The discharge of these springs is relatively weak, and residence times of nutrients and gases in the deep zone are on the order of several hundred to one thousand years. At 250 m depth, one or several springs with a much higher discharge introduce less saline, nutrient-poor and cooler water into the lake. These springs create the main density gradient and, together with further springs at shallower depths, are the driving forces for the upwelling of nutrient-rich water towards the lake surface.

The upwelling is the major source for the mixolimnion of the nutrients limiting phytoplankton growth, i.e. nitrogen and phosphorus (Chaps. 3 and 5). However, on short time scales, the access of primary producers to these continuously upwelling nutrients is modified by the mixing dynamics in the surface layer. As a consequence of temporary stratification of the mixolimnion during the rainy season, severe nutrient limitation occurs, both by N and P, which remain trapped in the monimolimnion. This contrasts with the situation in the dry season, when vertical mixing (caused by higher wind velocity and lower surface temperature) increases nutrient supply to the euphotic zone, promoting phytoplankton growth and the subsequent mesozooplankton peak (Chaps. 5 and 7). The fish yield also responds, with some delay, as shown by the increased catches of sardine occurring in the November-January period (Chap. 8).

Because of the dominance of the upwelling and the comparatively low importance of external inputs for nutrient supply to the surface layer, the ecosystem is not expected to react sensitively to increased external nutrient inputs on short time scales (Chap. 3). However, it should be kept in mind that a large fraction of additional external nutrient inputs will be transferred by settling particles to the monimolimnion where they will be mineralized and may accumulate over hundreds of years. The effective and then irreversible impacts of increased external nutrient inputs may thus only become visible after centuries.

The sudden increase in net sedimentation, especially of inorganic carbon, but also of nutrients, observed in sediment cores and dated to the 1960s, must be a result of a sudden change that occurred at this time in the surface layer of the lake (Chap. 9). Whether this was caused by an increased upwelling in connection with higher regional rainfall or by changes in the food web structure due to the introduction of *Limnothrissa miodon*, still remains unclear, as both these changes occurred at almost the same time. However, it seems probable that the same process led to an increase in methane concentrations in the deep water (Chap. 10).

11.1.2 *The Food Web Structure*

The structure of the pelagic food web of Lake Kivu has usually been perceived as rather simple: a linear food chain involving a phytoplankton dominated by few taxa of cyanobacteria, diatoms and cryptophytes, a mesozooplankton with two main copepod species and one cladoceran, and the sardine, *Limnothrissa miodon*, at the top, without a piscivorous predator. A more detailed analysis of the available data reveals that the food web is actually more complex, in particular because it comprises a previously neglected microbial food web, fuelled by autochthonous organic matter provided by phytoplankton DOM (dissolved organic matter) excretion (Chap. 6). The microbial food web of Lake Kivu seems to contribute significantly to consumer productivity: microbes are diverse and abundant in the mixolimnion and the redoxcline, and production of heterotrophic bacteria is high when compared to phytoplankton production (Chap. 6). Still, phytoplankton composition matters, as it determines to a large extent the fate of primary production: the large diatoms dominating in the dry season tend to settle, while cyanobacteria, dominating in the rainy season, seem not to be consumed by mesozooplankton, as revealed by analysis of fatty acid markers (Masilya 2011). Therefore, a substantial part of the primary production contributes to a downward nutrient and carbon flux (Chap. 9) rather than to the pelagic productivity. Moreover, recycling of sedimenting organic matter may be relatively limited due to the shallow oxic layer, which varies seasonally with a maximum depth of 60 m. In contrast, in Lake Tanganyika, most of the sedimenting organic matter is decomposed and recycled in the 120–200 m of oxygenated waters (Descy et al. 2005).

Figure 11.1 presents a synthesis of the available data on production rates and carbon flows between the main ecosystem compartments of the pelagic zone of Lake Kivu. A first look at the annual production rate of producers (phytoplankton) and consumers (mesozooplankton and fish), shows that primary and secondary productions of Lake Kivu are typical of a tropical oligotrophic lake, and compare well with those of Lakes Malawi and Tanganyika, which are also deep and oligotrophic (Chaps. 5 and 7). Worth noting in particular is that mesozooplankton production is remarkably similar to that of those other great lakes, despite the grim predictions made about the consequences of the sardine introduction (Chaps. 7 and 8). It also appears that the trophic transfer efficiency at the phytoplankton/mesozooplankton interface is quite good (up to 8.3% in 2003), and again in a range found in other great lakes of the same trophic status (Chap. 7). However, this estimate can be misleading, as not all the primary production is edible to mesozooplankton: most likely, copepods cannot ingest the large diatoms, and they cannot feed directly on the smallest plankton. Therefore, it is likely that planktonic crustacean production is sustained partly by microzooplankton (unknown rate 9 in Fig. 11.1): thus, grazing by ciliates and flagellates on bacteria (bacterivory, 7) and on photosynthetic picoplankton (herbivory, 8) is just another pathway to channel pelagic photosynthetic production to consumers, as in Lake Tanganyika (Tarbe et al. 2011), where herbivory dominates the microbial food web. Some contribution of autotrophic bacteria and archaea - methanotrophs, Green Sulfur Bacteria and nitrifiers - is also expected, although the C flux involved might be an order of magnitude lower than that transiting through heterotrophic bacteria.

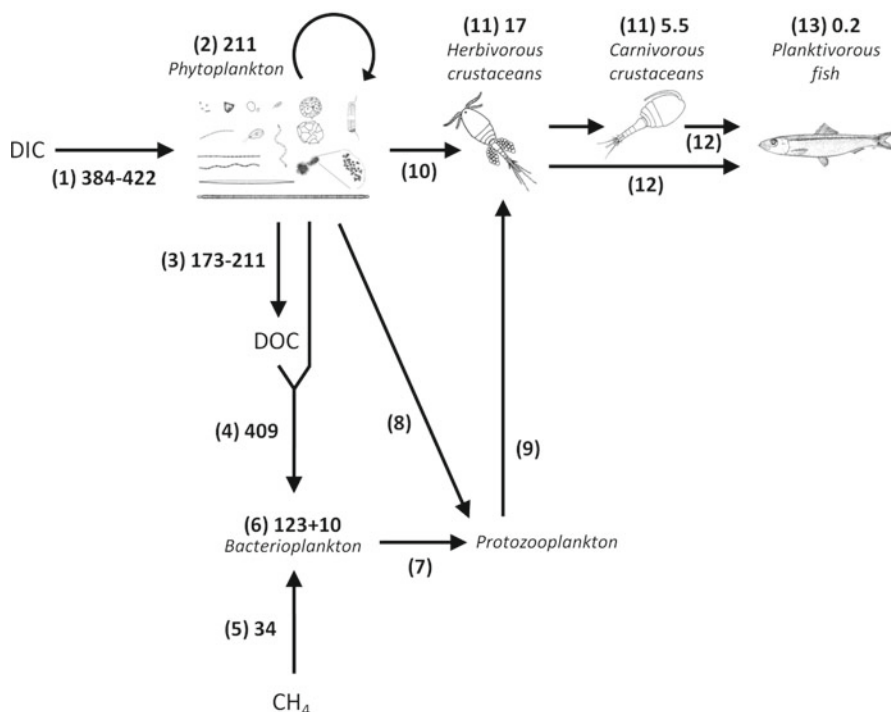


Fig. 11.1 Synthesis of the trophic carbon flows in the pelagic ecosystem of Lake Kivu. Rates are in $\text{g C m}^{-2} \text{ year}^{-1}$. Phytoplankton and zooplankton respiration rates are not taken into account (i.e., rates are net). DIC, dissolved inorganic carbon; DOC, dissolved organic carbon; CH₄, methane. 1: total primary production of phytoplankton (Chap. 6); 2: particulate primary production of phytoplankton (Chap. 5); 3: dissolved primary production of phytoplankton (Chap. 6); 4: bacterioplankton carbon demand (Chap. 6); 5: aerobic and anaerobic methane oxidation by methanotrophs (Pasche et al. 2010); 6: biomass production of heterotrophic (Chap. 6) and methanotrophic bacterioplankton; 7: bacterivory of protozooplankton; 8: herbivory of protozooplankton; 9: mesozooplankton grazing on protozooplankton; 10: crustacean zooplankton grazing on phytoplankton; 11: biomass production of herbivorous and carnivorous crustacean zooplankton (Chap. 7); 12: predation of planktivorous fish on mesozooplankton; 13: planktivorous fish production (Chap. 8)

A second look at the data summarized in Fig. 11.1 allows suspecting that the transfer of crustacean production to fish is lower than the mean trophic transfer efficiency of 10% commonly observed in pelagic food chains (Pauly and Christensen 1995). We recall here that the pelagic fishery yield in Lake Kivu did not meet the historical expectations (Chaps. 1 and 8): *Limnothrissa* production ($\sim 9,000 \text{ t year}^{-1}$ or $\sim 38 \text{ kg ha}^{-1} \text{ year}^{-1}$, Chap. 8) is lower than sardine production in Lake Tanganyika ($\sim 210 \text{ kg ha}^{-1} \text{ year}^{-1}$ considering an estimated mean sardine biomass of 60 kg ha^{-1} , Szcucka 1998, and a conservative production:biomass ratio of 3.5 year^{-1} , Coulter 1981). We believe that this estimate of sardine production in Lake Kivu is robust - other authors have obtained similar figures (Chap. 8). Then, it seems that there is a major bottleneck here, which might have several explanations. As total

phytoplankton and zooplankton productions are comparable in both lakes (Chaps. 5 and 7), productivity effects do not explain the difference in *Limnothrissa* production. Other hypotheses must be considered.

First, the predation rate of *Limnothrissa* on mesozooplankton may greatly depend on zooplankton availability, abundance and size. *Mesocyclops aequatorialis*, the largest copepod species in Lake Kivu, is abundant solely during a few weeks, at the end of the dry season (Chap. 6). During the rest of the year, zooplankton is far less abundant and composed of smaller species (e.g., *Thermocyclops consimilis*, *Tropocyclops confinis*, *Coronatella rectangula*). *Limnothrissa* may therefore suffer from a lack of dietary resources during a major part of the year. This hypothesis is supported by observations of the fish ingestion rate: Masilya (2011) found that *Limnothrissa* ingested daily three times more copepods in the dry season than in the rainy season. In contrast, the mesozooplankton communities of both Lakes Malawi and Tanganyika comprise a large-bodied calanoid copepod, which is an efficient grazer. For instance, in Lake Malawi, the lowest encountered biomass of the calanoid copepod *Tropodiaptomus cunningtoni* during the 1992–1993 surveys was 511 mg dry weight (DW) m⁻² (Irvine and Waya 1999) while in Lake Kivu long periods with biomass of *M. aequatorialis* below 100 mg DW m⁻² have been observed (for example from April to July 2004; Isumbiso 2006). Also, in the other Great Rift lakes, other resources than planktonic crustaceans are available to the planktivorous fish, such as shrimps (Lake Tanganyika) and *Chaoborus* larvae (Lake Malawi).

Another process that can reduce predation efficiency on crustaceans in the rainy season is the copepod vertical migration down to the aphotic layer (Chap. 7). Such a refuge below the euphotic layer is deeper in Lake Tanganyika, where light penetrates to deeper layers (mean euphotic depth = ~35 m, Stenuite et al. 2007) than in Lake Kivu (mean euphotic depth = 20 m, Chap. 5). Sardines, like all zooplanktivorous fish, are visual predators. The predation efficiency should then be reduced by the relatively weak light penetration in Lake Kivu: thus, a shallow oxycline in the wet season and relatively low water transparency may explain why pelagic fish are mostly located in the 0–45 m layer (Chap. 8).

Finally, variations of recruitment and larvae survival play a significant role in clupeid stock fluctuations (Mölsä et al. 2002; Kimirei and Mgaya 2007). In Lake Kivu, the growth of *Limnothrissa* larvae and juveniles takes place in the inshore zone, which is spatially reduced and where fishermen often use inappropriate fishing techniques for catching the young fish. This activity, coupled with the incidence of predation by *Limnothrissa* adults and other fish species in inshore areas (De Iongh et al. 1983; Masilya et al. 2011), might significantly reduce larvae survival. Likewise, little access to benthic resources, which are significant food items for *Limnothrissa* in both Lake Kivu (De Iongh et al. 1983; Masilya 2011; Masilya et al. 2011) and in Lake Tanganyika (Matthes 1968), may not allow feeding the spawning stock and fry during the rainy season, when planktonic resources are low (Chap. 7).

A conclusion ensuing from these reflections is that an increase of the nutrient supply to the mixolimnion would increase primary production, but may not necessarily result in a proportional increase of fish yield (Sect. 11.1.4).

11.1.3 *Consequences of the Sardine Introduction on Biogeochemical Processes and Ecosystem Structure and Function*

As discussed in Chap. 7, the effect of *Limnothrissa miodon* introduction in Lake Kivu, which was devoid of any pelagic fish until the 1950s, is a key issue, primarily because alien species introductions have often produced adverse effects on ecosystems. In the case of Lake Kivu, Dumont (1986), from observations of a decrease of zooplankton abundance, along with the disappearance of a major grazer, predicted that the fishery would collapse.

What we see in Lake Kivu decades later is quite different: it seems that the pelagic fish stock has remained similar to that at the end of the 1980s, the fishery is thriving (even though it doesn't reach the same yield as the sardine fishery of Lake Tanganyika) and zooplankton biomass is remarkably similar to that of other Rift lakes. A comprehensive assessment of changes in ecosystem structure is difficult because of the lack of precise quantitative historic data and the long time series required in order to representatively sample the high seasonal and interannual variability. Nevertheless, a trophic cascade effect can be detected in Lake Kivu. For instance, we were able to estimate that total crustacean biomass has declined by two-third since the 1950s, based on the zooplankton biomass data of Verbeke (1957), as a result of the planktivore introduction (Chap. 7). A substantial release of the grazing pressure on phytoplankton may have resulted from the mesozooplankton decline. As a result, phytoplankton biomass might have increased, reaching values twice as high as in the northern part of Lake Tanganyika where trophic status and primary productivity are similar to those of Lake Kivu (Chap. 5).

However, the change in zooplankton biomass does not completely explain the relatively high chlorophyll *a* concentration in Lake Kivu, as zooplankton biomass is now roughly the same in the two lakes. Part of the explanation may lie in phytoplankton edibility for herbivorous cyclopoids. Indeed, Lake Kivu phytoplankton comprises a large proportion of grazing-resistant forms, such as very long diatoms (*Nitzschia* and *Fragilaria*) or very small cyanobacteria (*Synechococcus*), both out of the typical size range (5–50 μm) of the copepod preys. Accordingly, the mesozooplankton diet consists of diatoms, chrysophytes and cryptophytes, plus some bacterivorous microzooplankton, but almost no cyanobacteria, as indicated by recent data based on fatty acid analysis in components of the pelagic food web (Masilya 2011).

However, these hypotheses involving changes in grazing pressure and in phytoplankton biomass and composition cannot be validated, as we miss data on phytoplankton structure before the sardine introduction: only sediment studies can reveal the changes that occurred in Lake Kivu after the 1950s. First analyses of short sediment cores confirmed that significant changes must have occurred in the lake around 1960 (Chap. 9). The sedimentation flux of carbonates suddenly increased by an order of magnitude, while net sedimentation of organic matter increased by ~50%; both changes may be indicative of increased primary production. In contrast, fluxes of biogenic silica seem to have reduced by 30%, which may have been caused by

a change in the diatom assemblage or a reduced contribution of diatoms to primary production. An evaluation of how exactly these changes observed in the sediments relate to changes in the food web requires more detailed palaeolimnological studies, using different proxies, such as fossil pigments, fossil diatoms and stable isotopes of C, N and Si.

11.1.4 Potential Ecological Impacts of Methane Extraction

Recent studies have provided additional evidence that methane concentrations have indeed been increasing in the past few decades, even though probably at a lower rate than has previously been feared (Pasche et al. 2011; Chap. 10). The enormous potential impact of a gas eruption from the lake and the tectonic and volcanic activity in the region clearly call for the methane being removed from the lake. Nevertheless, this must be done with utmost care, in order not to artificially create a dangerous situation or to irreversibly damage the ecosystem. The possible impacts of different methane exploitation scenarios have been discussed in Chap. 10. The most important consequence of these analyses is that the water from the deep zone must be returned below 200 m depth.

In case of shallower re-injection, the nutrient upward flux would increase, driving higher primary and secondary production. At first sight, this might be beneficial to the fishery as a sardine stock increase would be expected. However, two elements must be taken into account. First, as the rainy season stratification takes place, the lower mixolimnion becomes quickly oxygen-depleted from the decay of particulate and dissolved organic matter. Increased primary production in combination with the additional supply of reduced substances would likely result in more severe and quicker oxygen depletion, reducing the thickness of the water layer accessible to fish (see Chap. 8 for the fish distribution in the mixolimnion). Second, it seems, according to the available productivity estimates at the different trophic levels, that there is a bottleneck at the mesozooplankton-fish interface, so that an increase in planktonic production may not necessarily result in a proportional increase of fish production. Then, the likely consequence of a higher nutrient upward flux would be a degradation of water quality, with negative effects on the fisheries, rather than a benefit.

11.2 Outlook

Many bookshelves would undoubtedly have been filled with scientific publications on Lake Kivu, if it were located in Europe or North America. A search for “Lake Kivu” in scientific publication databases at the time of writing of this book yielded ~100 publications. About the same number were found for a single publication year on each of the North American Great Lakes. The studies presented in this book filled some of the knowledge gaps, but many more questions remain open than have been answered. In the following we outline some of the relevant issues that need to be addressed in future research on Lake Kivu.

The physical and geochemical processes in the lake still need to be investigated further. What is the provenance and the composition of the water that feeds the subaquatic springs? Is there a geogenic source of hydrogen (H_2) that may be used to reduce CO_2 into CH_4 ? And if yes, what is its past and present importance compared to the H_2 produced during the anaerobic degradation of organic matter? Do the springs introduce substances such as sulfate that could be used to oxidise methane and thus affect the methane cycling in the lake? What is the discharge and composition of the subaquatic springs in Kabuno Bay, and how is it hydrologically linked to the main basin?

In order to study the physics of the mixolimnion in more detail, it would be important to collect meteorological data on the lake. Because of the steep shores, stations located on the shore cannot be expected to be representative for the conditions on the lake. This is especially true for wind speed, precipitation and radiation. Data from the lake itself could help to better constrain the water balance and could be used to drive models of the mixing processes in the surface layer.

The sediments of Lake Kivu certainly contain much more information than what we have learnt from them up to now. Can the history of the lake be reconstructed in more detail and with more confidence? Can we gain information on the past nutrient cycle, phytoplankton, zooplankton and fish communities? Is there a way to confirm or reject the hypothesis that gas eruptions from the lake did occur in the past? Can we derive more information on past fluctuations in lake levels, salinity or temperature? Model predictions for the impacts of methane extraction currently assume near steady-state of the hydrological conditions (Chap. 10). A better knowledge of the lake history would be important to understand how its present state evolved and to derive scenarios for its future development.

The microbiology of the lake has hardly been touched. Microbially-mediated processes are of utmost importance for the biogeochemistry of the lake. The water column of Lake Kivu provides a huge natural laboratory with a sequence of different redox conditions, and large volumes of water with nearly constant properties over long time scales, where all kinds of microbially-mediated processes could be studied. We currently do not know which organisms are supporting which processes in this system, and even less do we know about their physiological constraints. The subaquatic springs could also be hot spots for microbial diversity and activity.

During the last decade, a continuous set of limnological and phytoplankton data has been collected in Lake Kivu. This dataset is unique for an African lake. It highlights important inter-annual variations of the duration and the magnitude of the seasonal mixing and the phytoplankton bloom. What are the main climatic drivers of this mixing? And how may these inter-annual variations be explained? Connections with climate fluctuations at regional and global scales must be investigated. Another key issue is to examine the link between annual phytoplankton and fish productivity. Are the years with high phytoplankton blooms characterized with high *Limnothrissa* production? If so, can we predict the annual fish yield based upon some regional or global climate indexes? These issues are of great importance for local populations which depend on fish resources.

Despite the low fish biodiversity, much knowledge still needs to be acquired, in particular on the ecology of the fish species. For instance, the endemic cichlids inhabiting the littoral zone have been exploited by local fishermen for a long time and very little is known about their biology and ecology. The same is true for the littoral food web, which plays a role in the maintenance of the pelagic *Sambaza* population: it is there that the *Limnothrissa* larvae grow, but what are the respective contributions of allochthonous, littoral and pelagic prey to *Limnothrissa* growth, maintenance, and reproduction at their different life stages? Abundance and production of benthic resources (algae, macrophytes and invertebrates) have never been investigated in Lake Kivu. Are they different from those in Lakes Tanganyika and Malawi? We may suspect that the important calcareous incrustations of submerged substrates in Lake Kivu reduce significantly habitat diversity, but does it influence invertebrate abundance and production? Harvesting *Sambaza* larvae with mosquito nets is a common practice in some parts of the lake, and has always been a concern for fish biologists. The larvae are also submitted to predation by the adult *Limnothrissa*, and the impact of cannibalism has never been assessed: is it harmful or beneficial for the *Sambaza* population? A recent cause for concern is the arrival of *Lamprichthys tanganicanus*: does this invader add to the lake biodiversity, increasing fish productivity? What is its impact on littoral and pelagic species? These issues have only been partially addressed so far, revealing the possibility of interspecific competition between *Limnothrissa* and *Lamprichthys* from exploitation of the same planktonic and benthic preys (Masilya 2011; Masilya et al. 2011), calling for monitoring of the recent invader.

Concerning the hazard assessment, no thorough studies have been performed up to now. We know that lava inflows at the lake surface of the size of those during the Nyiragongo eruption in 2002 are harmless (Lorke et al. 2004). But what if there would be a magmatic eruption inside the lake? What is the probability of such an event? How much magma could be released, and would it be sufficient to trigger a gas eruption? And what about an internal tsunami caused by the failure of an unstable slope? How much sediment has accumulated in delta areas? Is there a significant risk of large slope failures? What would be the size of the resulting internal waves? And could such an event be sufficient to trigger a gas eruption?

Finally, the impacts of the upcoming industrial methane exploitation need to be carefully investigated. Because of the long time scales involved, wrong decisions made today may affect the lake irreversibly for several centuries. In order to be able to early identify potentially harmful alterations, it will be important to monitor the development of the lake stratification, but also geochemical processes as well as the biology in the lake with great accuracy. Observations need to be compared with model predictions, and in case of significant discrepancies, the predictive models need to be improved. This will require high-level monitoring efforts, and an open-minded and critical scientific attitude to gain a further understanding of the relevant processes. Although this book has summarized our current knowledge on Lake Kivu, it is clear that there is still a lot to be learned from this fascinating lake.

References

- Coulter GW (1981) Biomass, production, and potential yield of the Lake Tanganyika pelagic fish community. *Trans Am Fish Soc* 110:325–335. doi:[10.1577/1548-8659\(1981\)110<325:BPAPYO>2.0.CO;2](https://doi.org/10.1577/1548-8659(1981)110<325:BPAPYO>2.0.CO;2)
- de Jongh HH, Spliethoff PC, Frank VG (1983) Feeding habits of the clupeid *Limnothrissa miodon* (Boulenger), in Lake Kivu. *Hydrobiologia* 102:113–122. doi:[10.1007/BF00006074](https://doi.org/10.1007/BF00006074)
- Descy J-P, Hardy M-A, Sténuite S, Pirlot S, Leporcq B, Kimirei I, Sekadende B, Mwaitega SR, Sinyenza D (2005) Phytoplankton pigments and community composition in Lake Tanganyika. *Freshw Biol* 50:668–684. doi:[10.1111/j.1365-2427.2005.01358.x](https://doi.org/10.1111/j.1365-2427.2005.01358.x)
- Dumont HJ (1986) The Tanganyika sardine in Lake Kivu: another ecodisaster for Africa? *Environ Conserv* 13:143–148. doi:[10.1017/S0376892900036742](https://doi.org/10.1017/S0376892900036742)
- Irvine K, Waya R (1999) Spatial and temporal patterns of zooplankton standing biomass and production in Lake Malawi. *Hydrobiologia* 407:191–205. doi:[10.1023/A:1003711306243](https://doi.org/10.1023/A:1003711306243)
- Isumbisho M (2006) Zooplankton ecology of Lake Kivu (East Africa). PhD thesis, University of Namur, Belgium
- Kimirei IA, Mgaya YD (2007) Influence of environmental factors on seasonal changes in clupeid catches in the Kigoma area of Lake Tanganyika. *Afric J Aquat Sci* 32:291–298. doi:[10.2989/AJAS.2007.32.3.9.308](https://doi.org/10.2989/AJAS.2007.32.3.9.308)
- Lorke A, Tietze K, Halbwachs M, Wüest A (2004) Response of Lake Kivu stratification to lava inflow and climate warming. *Limnol Oceanogr* 49:778–783. doi:[10.4319/lo.2004.49.3.0778](https://doi.org/10.4319/lo.2004.49.3.0778)
- Masilya P (2011) Ecologie alimentaire comparée de *Limnothrissa miodon* et de *Lamprichthys tanganicus* au lac Kivu (Afrique de l'Est). PhD thesis, University of Namur, Belgium
- Masilya MP, Darchambeau F, Isumbisho M, Descy J-P (2011) Diet overlap between the newly introduced *Lamprichthys tanganicus* and the Tanganyika sardine in Lake Kivu, Eastern Africa. *Hydrobiologia* 675:75–86. doi:[10.1007/s10750-011-0797-y](https://doi.org/10.1007/s10750-011-0797-y)
- Matthes H (1968) Preliminary investigations into the biology of the Lake Tanganyika clupeidae. *Fish Res Bull Zambia* 4:39–46
- Mölsä H, Sarvala J, Badende S, Chitamwebwa D, Kanyaru R, Mulimbwa N, Mwape L (2002) Ecosystem monitoring in the development of sustainable fisheries in Lake Tanganyika. *Aquat Ecosys Health Manag* 5:267–281
- Pasche N, Alunga G, Mills K, Muvundja F, Ryves DB, Schurter M, Wehrli B, Schmid M (2010) Abrupt onset of carbonate deposition in Lake Kivu during the 1960s: response to recent environmental changes. *J Paleolimnol* 44:931–946. doi:[10.1007/s10933-010-9465-x](https://doi.org/10.1007/s10933-010-9465-x)
- Pasche N, Schmid M, Vazquez F, Schubert CJ, Wüest A, Kessler J, Pack MA, Reeburgh WS, Bürgmann H (2011) Methane sources and sinks in Lake Kivu. *J Geophys Res Biogeosci* 116:G03006. doi:[10.1029/2011JG001690](https://doi.org/10.1029/2011JG001690)
- Pauly D, Christensen V (1995) Primary production required to sustain global fisheries. *Nature* 374:255–257. doi:[10.1038/374255a0](https://doi.org/10.1038/374255a0)
- Stenuite S, Pirlot S, Hardy M-A, Sarmento H, Tarbe A-L, Leporcq B, Descy J-P (2007) Phytoplankton production and growth rate in Lake Tanganyika: evidence of a decline in primary productivity in recent decades. *Freshw Biol* 52:2226–2239. doi:[10.1111/j.1365-2427.2007.01829.x](https://doi.org/10.1111/j.1365-2427.2007.01829.x)
- Szczucka J (1998) Acoustical estimation of fish abundance and their spatial distributions in Lake Tanganyika. FAO/FINNIDA research for the management of the fisheries of Lake Tanganyika. GCP/RAF/271/FIN-TD/84, 64pp
- Tarbe A-L, Unrein F, Stenuite S, Pirlot S, Sarmento H, Sinyenza D, Descy J-P (2011) Protist herbivory: a key pathway in the pelagic food web of Lake Tanganyika. *Microb Ecol* 62:314–323. doi:[10.1007/s00248-011-9817-8](https://doi.org/10.1007/s00248-011-9817-8)
- Verbeke J (1957) Recherche écologique sur la faune des grands lacs de l'Est du Congo belge. Exploration hydrobiologique des lacs Kivu, Edouard et Albert (1952–54). *Bull Inst R Sci Nat Belg* 3:1–177

SCIENTIFIC REPORTS



OPEN

Pelagic photoferrotrophy and iron cycling in a modern ferruginous basin

Received: 18 June 2015
Accepted: 05 August 2015
Published: 08 September 2015

Marc Llorós^{1,2,†}, Tamara García–Armisen³, François Darchambeau⁴, Cédric Morana⁵, Xavier Triadó–Margarit^{6,7}, Özgül Inceoğlu³, Carles M. Borrego^{7,8}, Steven Bouillon⁵, Pierre Servais³, Alberto V. Borges⁴, Jean–Pierre Descy¹, Don E. Canfield⁹ & Sean A. Crowe^{9,10}

Iron-rich (ferruginous) ocean chemistry prevailed throughout most of Earth's early history. Before the evolution and proliferation of oxygenic photosynthesis, biological production in the ferruginous oceans was likely driven by photoferrotrophic bacteria that oxidize ferrous iron {Fe(II)} to harness energy from sunlight, and fix inorganic carbon into biomass. Photoferrotrophs may thus have fuelled Earth's early biosphere providing energy to drive microbial growth and evolution over billions of years. Yet, photoferrotrophic activity has remained largely elusive on the modern Earth, leaving models for early biological production untested and imperative ecological context for the evolution of life missing. Here, we show that an active community of pelagic photoferrotrophs comprises up to 30% of the total microbial community in illuminated ferruginous waters of Kabuno Bay (KB), East Africa (DR Congo). These photoferrotrophs produce oxidized iron {Fe(III)} and biomass, and support a diverse pelagic microbial community including heterotrophic Fe(III)-reducers, sulfate reducers, fermenters and methanogens. At modest light levels, rates of photoferrotrophy in KB exceed those predicted for early Earth primary production, and are sufficient to generate Earth's largest sedimentary iron ore deposits. Fe cycling, however, is efficient, and complex microbial community interactions likely regulate Fe(III) and organic matter export from the photic zone.

Ferruginous water bodies are rare on the modern Earth, yet they are invaluable natural laboratories for exploring the ecology and biogeochemistry of Fe-rich waters extensible to the ferruginous oceans of the Precambrian Eons^{1–4}. One modern ferruginous system, Lake Matano (Indonesia) hosts large populations of anoxygenic phototrophic bacteria implicated in photoferrotrophy due to the scarcity of sulfur substrates⁴. Low light levels and extremely slow growth rates, however, have precluded the direct measurement of photoferrotrophy in its water column⁵. In contrast, recent measurements of Fe-dependent

¹Laboratory of Freshwater Ecology, Research Unit in Environmental and Evolutionary Biology, University of Namur, B-5000 Namur, Belgium. ²Department of Genetics and Microbiology, Universitat Autònoma de Barcelona, E-08913 Bellaterra, Catalonia, Spain. ³Ecologie des Systèmes Aquatiques, Université Libre de Bruxelles, B-1050 Brussels, Belgium. ⁴Chemical Oceanography Unit, University of Liège, B-4000 Liège, Belgium. ⁵Department of Earth and Environmental Sciences, Katholieke Universiteit Leuven, B-3001 Leuven, Belgium. ⁶Integrative Freshwater Ecology Group, Center for Advanced Studies of Blanes – Spanish Research Council, E-17300 Blanes, Spain. ⁷Group of Molecular Microbial Ecology, Institute of Aquatic Ecology, University of Girona, E-17071 Girona, Catalonia, Spain. ⁸Water Quality and Microbial Diversity, Catalan Institute for Water Research, E-17003, Girona, Catalonia, Spain. ⁹Institute of Biology, Nordic Center for Earth Evolution, University of Southern Denmark, 5230 Odense, Denmark. ¹⁰Departments of Microbiology and Immunology and Earth, Ocean, and Atmospheric Sciences, University of British Columbia, V6T 1Z3 Vancouver, Canada. [†]Present address: Institute des Sciences de la Vie, Université Catholique de Louvain, Place Croix du Sud 4/5, B-1348 Louvain-La-Neuve, Belgium. Correspondence and requests for materials should be addressed to M.L.L. (email: marc.lloirosdupre@uclouvain.be) or S.A.C. (email: sean.crowe@ubc.ca)

carbon fixation reveal photoferrotrophy in Lake La Cruz (Spain) where photoferrotrophs have been enriched from the water column, but represent a minor fraction of the natural microbial community⁶. Inspired by the emerging evidence for photoferrotrophy in modern environments, we sought a photoferrotroph-dominated ecosystem that could be used to place constraints on the ecology of ancient ferruginous environments.

Kabuno Bay (KB) is a ferruginous sub-basin of Lake Kivu, situated in the heart of East Africa on the border of the Democratic Republic of Congo (DRC) and Rwanda (Supplementary Fig. S1). Lake Kivu is of tectonic origin and is fed by deep-water inflows containing high concentrations of dissolved salts and geogenic gases⁷. KB is separated from the main basin of Lake Kivu by a shallow volcanic sill that restricts water exchange between the basins⁷. KB has a strongly stratified water column with oxic surface waters giving way to anoxic waters below about 10 m (Fig. 1a,b,e,f; Supplementary Fig. S2a,e)⁷. The deep anoxic waters of KB are iron-rich (Fe(II), 0.5M HCl extractable), containing up to 1.2 mM ferrous Fe {Fe(II)}, unlike the deep waters of Lake Kivu's main basin, which contain abundant hydrogen sulfide (ca. 0.3 mM in deep waters)⁸. Fe(II)-rich hydrothermal springs with chemistry matching deep waters of KB are observed within the catchment basin⁹ (Supplementary Table S1), implicating hydrothermal Fe inputs to KB. Oxidation of upward diffusing Fe(II) generates both sharp gradients in dissolved Fe(II) concentration and an accumulation of mixed-valence Fe particles around the oxic-anoxic boundary (i.e., chemocline; Fig. 1b,c,f,g). Reduction of the settling particulate ferric Fe {Fe(III)} to Fe(II) partly closes the Fe-cycle (Fig. 1c,g).

The physical and chemical stratification of the water column is also reflected in microbial community composition. In the oxic sunlit waters (between surface and 10.0 m depth), cyanobacteria (ca. 10% of total cell counts by flow cytometry), algae, and heterotrophic bacteria typical of freshwater environments¹⁰ dominate (Fig. 1d,h; Fig. 2a; Supplementary Table S2). Light, however, penetrates well below these surface waters illuminating the Fe(II)-rich anoxic waters below (Fig. 1d,h). Here, we find a very different microbial community (Fig. 2a; Supplementary Fig. S2b,c,f,g). Anoxygenic photosynthetic green-sulfur bacteria (GSB) dominate in the chemocline where they comprise up to 30% of the total microbial community (Fig. 2b). Concentrations of Bacteriochlorophyll (BChl) *e*, a photosynthetic pigment utilized by brown-coloured, low light adapted GSB^{11,12} reach up to ca. 235 $\mu\text{g l}^{-1}$ (Fig. 1d,h) and clearly delineate the distribution of GSB in the chemocline waters. Depth-integrated BChl *e* concentrations (130 mg m^{-2}) are 10-fold higher than Chlorophyll (Chl) *a* (13 mg m^{-2}) concentrations in the upper waters. Analysis of the 16S small subunit rRNA gene reveals that the GSB present in KB are closely related to *Chlorobium* (*Chl.*) *ferrooxidans* strain KoFox (Fig. 2c and Supplementary Fig. S3 and S4). To date, str. KoFox is the sole member of the GSB known to conduct photoferrotrophy¹³ using Fe(II) as electron donor, and lacking the capacity to grow with reduced sulfur species¹³. Such physiology is consistent with the sub- μM concentrations (0–0.6 μM , maximum at 10.5 m; Fig. 1b,f) of reduced sulfur species observed in the illuminated waters of KB.

To directly test for photoferrotrophic activity in KB, we conducted a suite of incubation experiments in which rates of Fe(II) oxidation were measured over time. In the first set of experiments, we incubated water samples between 10.5 and 11.3 m by suspending triplicate glass incubation vessels directly in the water column so that the microbial community would experience near *in situ* light conditions with an average diel illumination of 0.6 $\mu\text{E m}^{-2} \text{ s}^{-1}$ and a mid-day maximum of 3.2 $\mu\text{E m}^{-2} \text{ s}^{-1}$. We measured light-dependant Fe(II) oxidation rates up to 100 $\mu\text{mol Fe l}^{-1} \text{ d}^{-1}$, demonstrating active photoferrotrophic activity in the KB chemocline (Fig. 3a). At 8×10^7 GSB cells l^{-1} , cell specific Fe oxidation rates are up to 1.25 $\text{pmol cell}^{-1} \text{ d}^{-1}$. Depth-integrated Fe(II) oxidation rates of 36.8 $\text{mmol Fe m}^{-2} \text{ d}^{-1}$ were computed by taking the mean of the measured rates between 10.5 and 11.3 m, and multiplying by the 0.8 m interval. This Fe(II) oxidation could drive carbon (C) fixation at rates of 9.2 $\text{mmol C m}^{-2} \text{ d}^{-1}$ based on the expected (4:1) relationship between Fe oxidation to C-fixation during photoferrotrophy¹⁴; nearly the same rate (9 $\text{mmol C m}^{-2} \text{ d}^{-1}$) as measured directly by ¹³C labelling experiments. Rates of photosynthetic C fixation in the chemocline were up to 28% of the production in the oxic surface waters (32 $\text{mmol C m}^{-2} \text{ d}^{-1}$). While cyanobacteria and GSB co-occur in the chemocline, low average Chl *a* concentrations (ca. 1.1 $\mu\text{g l}^{-1}$) and BChl *e*:Chl *a* ratios of more than about 100 highlight the dominance of GSB in the ferruginous waters. The importance of photoferrotrophy in the chemocline of KB is underscored by mass balance on the stable C isotope composition of particulate organic matter. Using a simple isotope-mixing model (Supplementary Information) we estimated that $74\% \pm 13\%$ of the particulate organic carbon pool in the chemocline is derived through anoxygenic photosynthesis by GSB, with a maximum (89%) at 11.25 m. This mass balance reveals that GSB constituted 208 mmol m^{-2} biomass, which together with the light-dependent C fixation rates translates to a GSB biomass turnover time of 23 d.

Fe(III) reduction rates measured in glass vessels kept dark and incubated alongside the light vessels are nearly equivalent (48 $\text{mmol m}^{-2} \text{ d}^{-1}$) to Fe(II) oxidation rates, suggesting a tightly coupled, pelagic Fe-cycle driven by photoferrotrophy, with comparably little net Fe oxidation. Sulfate reduction and potential sulfide oxidation also occurred, but these S-based metabolisms proceed at rates much lower than Fe-reduction and oxidation, respectively (Fig. 3a). This implies that sulfide produced during sulfate reduction plays a small role in reduction of Fe, and most Fe reduction is likely heterotrophic. Fe reduction driven by GSB biomass breakdown is likely reflected by bacterial production rates, which were highest in the illuminated ferruginous waters of the chemocline (Supplementary Fig. S2d). Photoferrotrophy therefore appears to support much of the biogeochemical cycling in the KB chemocline, with primary

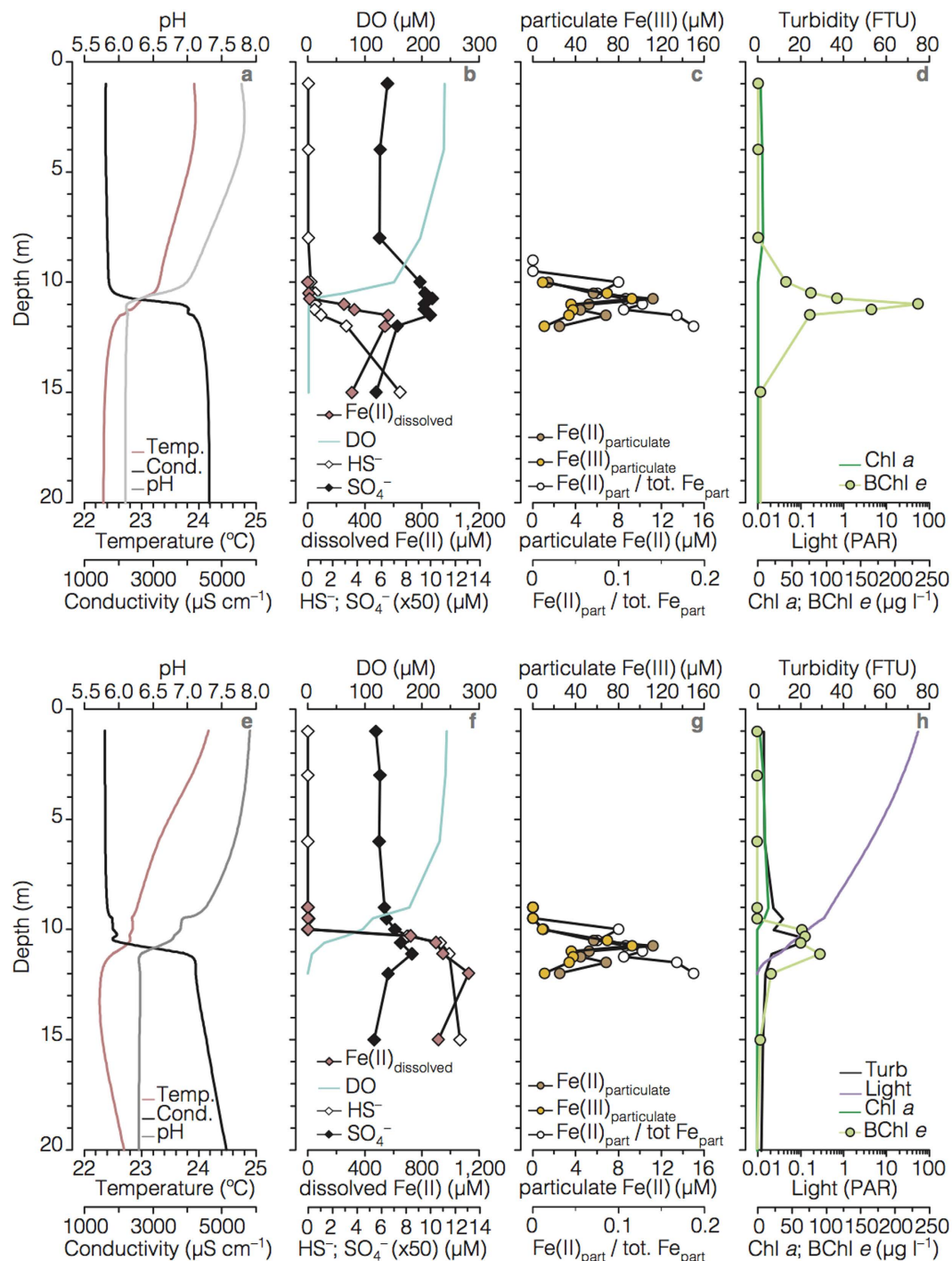


Figure 1. Physical and chemical depth profiles from Kabuno Bay. Data in the upper panels are from the rainy season (RS; February 2012) and lower panels from the dry season (DS; October 2012). (**a,e**) temperature ($^{\circ}\text{C}$), conductivity ($\mu\text{S cm}^{-1}$), and pH; (**b,f**) dissolved oxygen (DO, μM), sulfide (HS^{-} , μM), sulfate (SO_4^{-} , μM), and dissolved ferrous Fe (μM); (**c,g**) particulate ferrous Fe {Fe(II)} and ferric Fe {Fe(III)} (μM), and ratio of particulate Fe(II) with respect to total particulate Fe (*i.e.*, particulate Fe(II)/[particulate Fe(II) + particulate Fe(III)]); (**d,h**) light (% PAR) and turbidity (FTU) profiles, and Chl *a* ($\mu\text{g l}^{-1}$) and intercalibrated BChl *e* concentration ($\mu\text{g l}^{-1}$) measured with multiparametric probes.

production of organic matter driving heterotrophic microbial Fe(III) reduction. The rapid GSB turnover rates estimated through our stable isotope mass balance also indicate the effective breakdown of GSB biomass implying that fermentation of this biomass provides substrates (*e.g.*, $\text{CH}_3\text{COO}^{-}$, H_2) to fuel Fe reduction, and possible pelagic heterotrophy with other electron acceptors such as sulfate, or methanogenesis. Both $\text{CH}_3\text{COO}^{-}$ and H_2 can be detected in the KB water column (Fig. S2e).

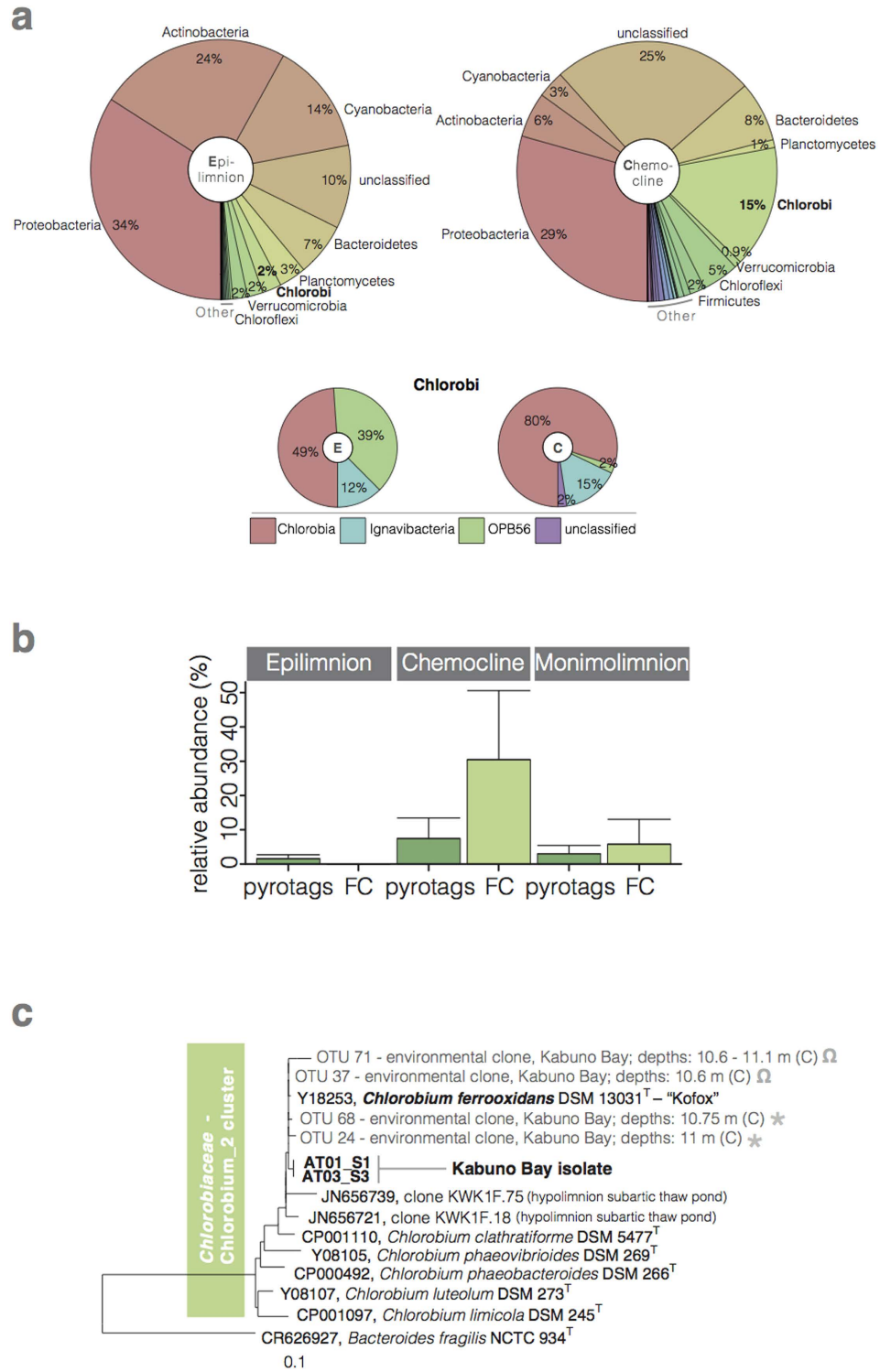


Figure 2. Microbial diversity in Kabuno Bay. (a) Pie charts showing relative sequence abundances of retrieved bacterial phyla, with detailed hierarchy for the *Chlorobi* phylum, detected in epilimnetic (left, E), and chemocline (right, C) waters of KB. (b) Relative abundances of *Chlorobi* sequences (dark green) retrieved by pyrosequencing (pyrotags) and cell abundances (light green) determined by flow cytometry (FC) from KB water samples. (c) 16S rRNA gene phylogenetic tree of the *Chlorobiaceae* including representative OTUs (0.03 cut-off) from those depths with maximum relative abundances of GSB from both the rainy (RS; asterisk) and dry (DS; omega) season water samples, as well as full 16S rRNA gene sequences from the KB isolate. The identifier code for each OTU and the metadata describing the depths and the layers (E for epilimnion, C for chemocline, and M for monimolimnion) where sequences were recovered are also indicated.

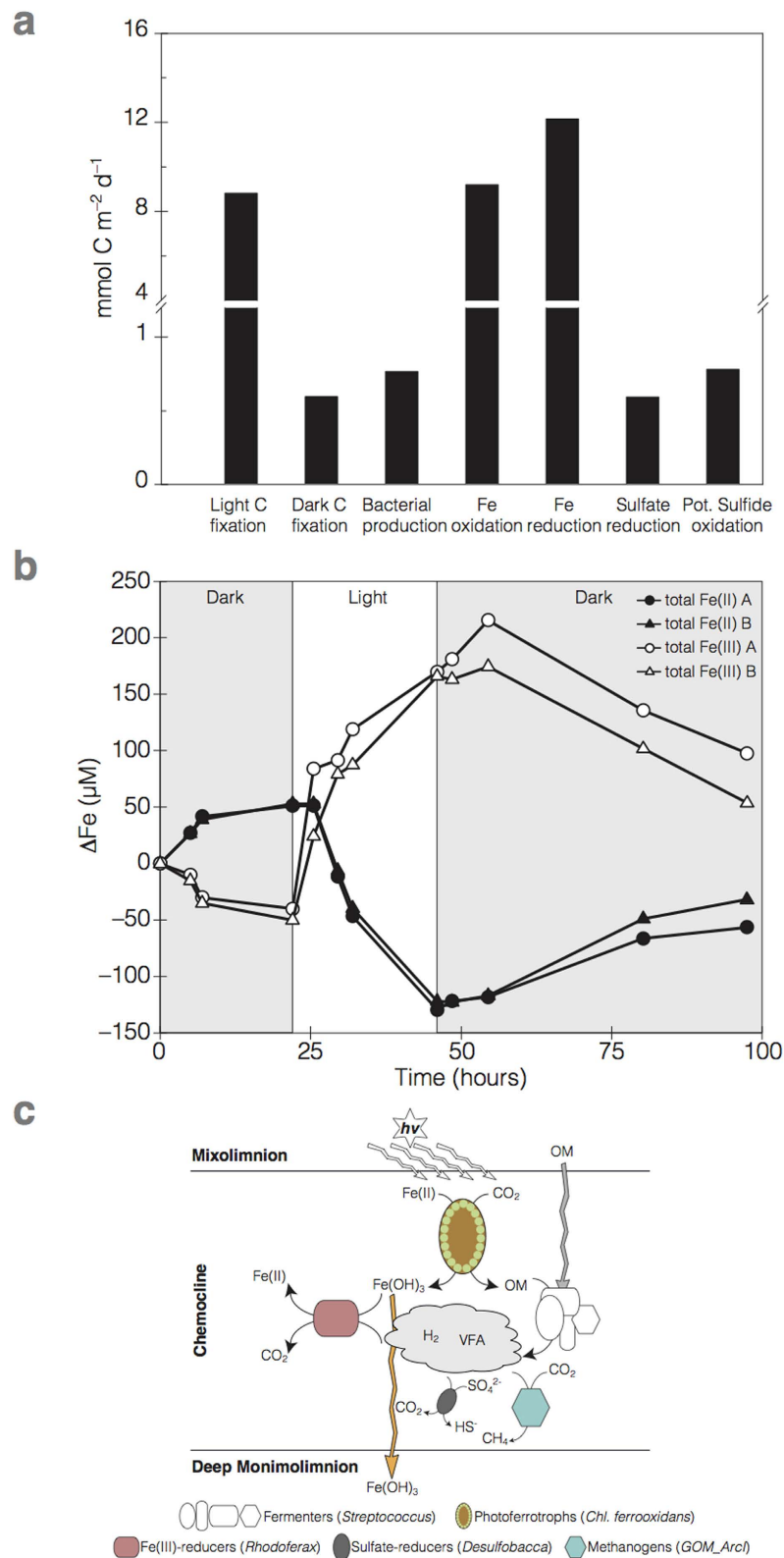


Figure 3. Process rates in Kabuno Bay chemocline. (a) depth integrated rates (Carbon normalized; mmol C m⁻² d⁻¹) of: light and dark C fixation; bacterial production (as ³H-Thymidine incorporation); Fe oxidation and reduction; sulfate reduction; and potential sulfide oxidation from *in situ* measurements conducted in KB. (b) total Fe(II) (black) and total Fe(III) (white) concentrations over time from duplicate vessels incubated *ex situ* through a light (white background) and dark (light grey background) cycle. (c) proposed metabolic model for Fe and C cycling in ferruginous waters; legend: *hν*, sunlight; VFA, volatile fatty acids; OM, organic matter.

To more directly test the potential for pelagic Fe cycling, the microbial community was also subjected to alternating light and dark conditions in a second incubation experiment conducted *ex situ* with an inhibitor of oxygenic photosynthesis¹⁵ (3-(3,4-dichlorophenyl)-1,1-dimethylurea; DCMU; 0.55 mg l⁻¹; Fig. 3b) and at light intensities known to support maximum Fe oxidation rates by *Chl. ferrooxidans* str. KoFox (15 μE m⁻² s⁻¹). These *ex situ* Fe(II) oxidation rates are similar to *in situ* rates (115 μmol l⁻¹ d⁻¹; Fig. 3b), and at 9 × 10⁷ GSB cells l⁻¹ in this experiment translate to 1.3 pmol cell⁻¹ d⁻¹. Fe(III) reduction rates, in contrast, are much lower (44 μmol l⁻¹ d⁻¹; Fig. 3b), allowing net Fe(II) oxidation of 71 μmol l⁻¹ d⁻¹ and Fe(III) accumulation (Fig. 3b). These measurements demonstrate that Fe(II) oxidation can outpace the reactions, like fermentation, that degrade GSB biomass and ultimately lead to Fe(III) reduction.

We also isolated the dominant GSB from the water column into axenic culture. Analyses of the small subunit 16S rRNA gene sequence from the axenic culture reveal that the KB GSB isolate is closely related (98.7% of sequence similarity) to *Chl. ferrooxidans* str. KoFox (Fig. 2c and Supplementary Fig. S4) and clusters with the dominant *Chlorobii* 16S rRNA gene sequences recovered from the KB water column. Unlike str. KoFox though, which only grows in co-culture¹³, the KB strain grows in a pure culture. Str. KB is clearly adapted to pelagic growth under low light conditions synthesizing BChl *e* pigments rather than BChl *c* as does str. KoFox¹³, which was isolated from the surface of shallow creek sediments¹³. Detailed pigment analyses show low-light adaptations in KB strain's light harvesting apparatus, including high abundances of higher alkylated BChl *e* homologs and a lack of the first BChl *e* homolog (Supplementary Fig. S5). These adaptations may be essential for photoferrotohy under the low light conditions (Fig. 1h) encountered in ferruginous water columns^{11,16}. Incubation experiments with the KB isolate also demonstrate its capacity to grow photoferrotohy under low light conditions (*i.e.*, 0.64 μE m⁻² s⁻¹) oxidizing Fe at a rate of 1.4 mmol l⁻¹ d⁻¹ (Supplementary Fig. S6).

As primary producers in the KB chemocline, photoferrotohy GSB play a key role supporting and shaping the resident microbial community. This community is taxonomically and functionally diverse with common diversity metrics indicating nearly 3,000 estimated species (Supplementary Table S3), which is comparable to typical modern coastal marine waters or oxygen-minimum zones^{17,18}. This community is comprised of known heterotrophic Fe(III)-reducers¹⁹ with members of the *Rhodofera* genera making up 8% of the OTUs (operational taxonomic units) retrieved. Other community members include micro-aerophilic Fe(II)-oxidizers, sulfate reducers (*e.g.*, *Desulfobacca*, *Desulfomonile*), fermenters (*e.g.*, *Streptococcus*), methanotrophs (*e.g.*, *Methylobacterium*), and methanogens (*e.g.*, *Methanosaeta*, *GOM_ArcI*), as well as an appreciable fraction (>13%) of taxa belonging to phyla lacking cultured representatives (Supplementary Table S2 and Fig. 2a). Anoxygenic phototrophs in addition to the 15% GSB, include purple sulfur bacteria and *Chloroflexi*, but these combined never exceed 9% of the OTUs retrieved (Fig. 2a). The archaeal community is dominated by methanogens suggesting pelagic methanogenic activity in these ferruginous waters (Supplementary Fig. S2c,g). Overall, the most abundant taxa in the chemocline are involved in C cycling linked to the oxidation and reduction of Fe, but other members almost certainly play key roles in microbial community metabolism and biogeochemical cycling. For example, the presence of sulfate reducers and methanogens directly in the KB water column implies that some organic matter degradation is channelled through sulfate reduction and methanogenesis, thereby escaping remineralization through Fe reduction. By extension, this also requires that some Fe(III) escapes reduction, perhaps through aging and recrystallization to forms less available towards Fe reduction²⁰, for subsequent export to underlying sediments. Mixed valence Fe particles at the base of the chemocline indeed are comprised of 20% Fe(II) and 80% Fe(III) (mean redox state of 2.8, Fig. 1c), demonstrating the export of ferric iron from the photic zone.

Our observations from KB provide possible insight into the structure and functioning of ancient photoferrotohy microbial communities thought to have sustained the global C-cycle prior to the evolution and proliferation of oxygenic phototrophs. Rates of photoferrotohy in the KB water column (3.4 mol C m⁻² yr⁻¹) are within the range of those modelled for global photoferrotohy production in Earth's early ferruginous oceans (1.4 mol m⁻² yr⁻¹ based on 5 × 10¹⁴ mol C yr⁻¹ and an ocean area of 3.6 × 10¹⁴ m²)²¹. Previous computations also suggest Fe deposition rates of up to 45 mol m⁻² yr⁻¹ were needed to deposit the largest Precambrian banded iron formations (BIFs)²². Net Fe oxidation rates of 0.8 pmol cell⁻¹ d⁻¹ in KB show that for a photic zone depth of 100 m, photoferrotohy GSB at low cell densities of 1.7 × 10³ cells ml⁻¹ could produce up to 50 mol m⁻² yr⁻¹ Fe(III) under modest light conditions, enough to deposit even the largest BIF (*i.e.*, Hammersley Basin; Australia)²². Notably, the mean redox state of 2.8 for mixed valence Fe particles exported from the KB photic zone is sufficiently oxidized to explain the Fe(III) component in many BIFs, which have an average Fe redox state of 2.4²³. In KB, pelagic Fe(III) reduction results from microbial community metabolism illustrating the importance of considering net Fe(II) oxidation rates in photoferrotohy models of BIF deposition. Photoferrotohy deposition of BIF then likely requires that rates of Fe(II) oxidation outpace processes like fermentation that ultimately lead to pelagic Fe(III) reduction. Our observations implicate complex interactions between microbial community metabolism and physical and chemical dynamics in the regulation of C and Fe export from ferruginous euphotic zones, but the quantitative nature of these interactions remains uncertain for now. Future work at KB and in other ferruginous water bodies will help tease apart these interactions, and elucidate the microbial controls on biogeochemical cycling in modern and ancient ferruginous waters.

Methods Summary

Water samples from the water column of Kabuno Bay (1.58°–1.70° S, 29.01°–29.09° E; DR Congo) were collected in February (rainy season, RS) and October (dry season, DS) 2012 and processed for physico-chemical characteristics, microbial abundance, diversity, activity, and cultivation of green sulfur bacteria. Vertical CTD (conductivity, temperature, depth) profiles were measured *in situ* with two multiparametric probes (Hydrolab DS5, OTT Hydromet, Germany; and Sea & Sun CTD90, Sea and Sun Technology, Germany). Photosynthetically Active Radiation (PAR) was measured using a submersible Li-Cor LI-193SA spherical quantum sensor (Lincoln, NE, USA). pH, CH₄ (methane) concentrations, and stable C isotopic composition ($\delta^{13}\text{C}$) of particulate organic carbon (POC; $\delta^{13}\text{C}$ -POC) were measured as previously described^{24,25}. Bacterial production was estimated from tritiated thymidine (³H-Thymidine) incorporation rates^{25,26}. Bulk light and dark inorganic C fixation was measured by NaH¹³CO₃ incorporation (see supplementary methods for description). Fe speciation was measured using the ferrozine method²⁷, while Fe oxidation and reduction rates were determined following changes in Fe speciation over time. Sulfate reduction rates were determined by using the ³⁵S radiotracer method²⁸. Photosynthetic pigments were analysed by High Performance Liquid Chromatography according to^{29,30}. Genomic DNA was extracted as previously described³¹ and further subjected to pyrosequencing³². *Chlorobi* enrichment cultures were generated by supplementing water with nutrients and Fe. Isolates were obtained through multiple serial dilutions in a defined mineral media³³. Small aliquots from the isolates were subjected to polymerase chain reaction (PCR) amplification of the 16S rRNA gene, and PCR products sequenced. All *Chlorobi*-retrieved 16S rRNA gene sequences were analysed by means of ARB³⁴ loaded with a SILVA 16S rRNA compatible database.

References

- Poulton, S. W. & Canfield, D. E. Ferruginous conditions: a dominant feature of the ocean through Earth's History. *Elements* **7**, 107–112 (2011).
- Planavsky, N. J. *et al.* Widespread iron-rich conditions in the mid-Proterozoic ocean. *Nature* **477**, 448–451 (2011).
- Holland, H. D. in *Treatise on Geochemistry* (eds. Holland, H. D. & Turekian, K. K.) **6**, 583–625 (Elsevier, 2004).
- Crowe, S. A. *et al.* Photoferrotrophs thrive in an Archean Ocean analogue. *Proc. Natl. Acad. Sci. USA* **105**, 15938–15943 (2008).
- Crowe, S. A. *et al.* Deep-water anoxygenic photosynthesis in a ferruginous chemocline. *Geobiology* **12**, 322–339 (2014).
- Walter, X. A. *et al.* Phototrophic Fe(II)-oxidation in the chemocline of a ferruginous meromictic lake. *Front. Microbiol.* **5**, 1–9 (2014).
- Degens, E. T. & Kulbicki, G. Hydrothermal origin of metals in some East African rift lakes. *Mineral Deposita* **8**, 388–404 (1973).
- Pasche, N., Dinkel, C., Müller, B., Schmid, M. & Wehrli, B. Physical and biogeochemical limits to internal nutrient loading of meromictic Lake Kivu. *Limnol. Oceanogr.* **54**, 1863–1873 (2009).
- Tassi, F. *et al.* Water and gas chemistry at Lake Kivu (DRC): Geochemical evidence of vertical and horizontal heterogeneities in a multibasin structure. *Geochem Geophys Geosyst* **10**, 1–22 (2009).
- Newton, R. J., Jones, S. E., Eiler, A., McMahon, K. D. & Bertilsson, S. A guide to the natural history of freshwater lake bacteria. *Microbiol. Mol. Biol. Rev.* **75**, 14–49 (2011).
- Borrego, C. M. & Garcia-Gil, L. J. Rearrangement of light harvesting bacteriochlorophyll homologues as a response of green sulfur bacteria to low light intensity. *Photosynth. Res.* **45**, 21–30 (1995).
- Borrego, C. M. *et al.* Distribution of bacteriochlorophyll homologs in natural populations of brown-colored phototrophic sulfur bacteria. **24**, 301–309 (1997).
- Heising, S., Richter, L., Ludwig, W. & Schink, B. *Chlorobium ferrooxidans* sp. nov., a phototrophic green sulfur bacterium that oxidizes ferrous iron in coculture with a 'Geospirillum' sp. strain. *Arch. Microbiol.* **172**, 116–124 (1999).
- Widdel, F., Schnell, S., Heising, S. & Ehrenreich, A. Ferrous iron oxidation by anoxygenic phototrophic bacteria. *Nature* **362**, 834–836 (1993).
- Jørgensen, B. B., Kuenen, J. G. & Cohen, Y. Microbial transformations of sulfur compounds in a stratified lake (Solar Lake, Sinai). *Limnol. Oceanogr.* **24**, 799–822 (1979).
- Kappler, A., Pasquero, C., Konhauser, K. O. & Newman, D. K. Deposition of banded iron formations by anoxygenic phototrophic Fe(II)-oxidizing bacteria. *Geology* **33**, 865–868 (2005).
- Stewart, F. J., Ulloa, O. & DeLong, E. F. Microbial metatranscriptomics in a permanent marine oxygen minimum zone. *Environ. Microbiol.* **14**, 23–40 (2012).
- Ulloa, O., Wright, J. J., Belmar, L. & Hallam, S. J. in *The Prokaryotes* (eds. Rosenberg, E., DeLong, E. F., Lory, S., Stackebrandt, E. & Thompson, F.) 113–122 (Springer Berlin Heidelberg, 2013).
- Finneran, K. T., Johnsen, C. V. & Lovley, D. R. *Rhodospirillum rubrum* sp. nov., a psychrotolerant, facultatively anaerobic bacterium that oxidizes acetate with the reduction of Fe(III). *Int. J. Syst. Evol. Microbiol.* **53**, 669–673 (2003).
- Roden, E. E. Fe(III) oxide reactivity toward biological versus chemical reduction. *Environ. Sci. Technol.* **37**, 1319–1324 (2003).
- Canfield, D. E., Rosing, M. T. & Bjerrum, C. Early anaerobic metabolisms. *Philos T Roy Soc B* **361**, 1819–1836 (2006).
- Konhauser, K. O. *et al.* Could bacteria have formed the Precambrian banded iron formations? *Geology* **30**, 1079–1082 (2002).
- Klein, C. & Beukes, N. J. in *The Proterozoic Biosphere* (eds. Schopf, J. W. & Klein, C.) 139–146 (1992).
- Borges, A. V., Abril, G., Delille, B., Descy, J.-P. & Darchambeau, F. Diffusive methane emissions to the atmosphere from Lake Kivu (Eastern Africa). *J. Geophys. Res.* 1–15 (2011).
- Borges, A. V. *et al.* Carbon cycling of Lake Kivu (East Africa): net autotrophy in the epilimnion and emission of CO₂ to the atmosphere sustained by geogenic inputs. *PLoS ONE* **9**, e109500 (2014).
- Fuhrman, J. A. & Azam, F. Thymidine incorporation as a measure of heterotrophic bacterioplankton production in marine surface waters: Evaluation and field results. *Mar. Biol.* **66**, 109–120 (1982).
- Viollier, E., Inglett, P. W., Hunter, K., Roychoudhury, A. N. & Van Cappellen, P. The ferrozine method revisited: Fe(II)/Fe(III) determination in natural waters. *Appl. Geochem.* **15**, 785–790 (2000).
- Fossing, H. & Jørgensen, B. B. Measurement of bacterial sulfate reduction in sediments – Evaluation of a single-step Chromium reduction method. *Biogeochemistry* **8**, 205–222 (1989).
- Descy, J.-P., Higgins, H. W., Mackey, D. J., Hurley, J. P. & Frost, T. M. Pigment ratios and phytoplankton assessment in northern Wisconsin lakes. *J. Phycol.* **36**, 274–286 (2000).
- Borrego, C. M. & Garcia-Gil, L. J. Separation of bacteriochlorophyll homologues from green photosynthetic sulfur bacteria by reversed-phase HPLC. *Photosynth. Res.* **41**, 157–164 (1994).

31. Llíros, M., Casamayor, E. O. & Borrego, C. M. High archaeal richness in the water column of a freshwater sulfurous karstic lake along an interannual study. *66*, 331–342 (2008).
32. Shah, V. *et al.* Bacterial and archaea community present in the Pine Barrens Forest of Long Island, NY: unusually high percentage of ammonia oxidizing bacteria. *PLoS ONE* **6**, e26263 (2011).
33. Hegler, F., Posth, N. R., Jiang, J. & Kappler, A. Physiology of phototrophic iron(II)-oxidizing bacteria: implications for modern and ancient environments. *66*, 250–260 (2008).
34. Ludwig, W. *et al.* ARB: a software environment for sequence data. *Nucleic Acids Res.* **32**, 1363–1371 (2004).

Acknowledgements

The authors thank Georges Alunga, Pascal Masilya, Pascal Mwapu Ishumbisho, Boniface Kaningini, Charles Balagizi, Katcho Karume, Mathieu Yalire, Djoba, Silas, Laetitia Nyinawamwiza, Bruno Leporcq, Adriana Anzil, Marc-Vincent Commarieu, Fleur A E Roland, Laetitia Montante, Alexander Treusch and Niko Finke for help with laboratory and field work. This work was partially supported by Belgian (FNRS 2.4.515.11 and BELSPO SD/AR/02A contracts), Danish (grant no. DNRF53 to DEC), and European (grant no. ERC-StG 240002, for stable isotope measurements) funds. AVB is a senior research associate at the FRS-FNRS. SAC was supported by the Agouron institute.

Author Contributions

S.A.C., A.V.B., F.D. and M.L.I. conceived research; M.L., A.V.B., S.A.C., F.D., J.-P.D., T.G.-A., Ö.I. and C.M. collected and analyzed samples; M.L., T.G.-A., Ö.I. and X.T.-M. conducted gene sequence analyses; S.A.C. isolated the Kabuno Bay strain and conducted Fe oxidation and reduction rate measurements; C.M. and F.D. conducted C-fixation rate measurements; M.L., S.A.C., F.D., C.M., A.V.B., X.T.-M., C.M.B., S.B., T.G.-A., Ö.I., P.S. and D.E.C. analyzed the data; M.L. and S.A.C. wrote the manuscript with input from all authors.

Additional Information

Supplementary information accompanies this paper at <http://www.nature.com/srep>

Competing financial interests: The authors declare no competing financial interests.

How to cite this article: Llíros, M. *et al.* Pelagic photoferrotrophy iron cycling in a modern ferruginous basin. *Sci. Rep.* **5**, 13803; doi: 10.1038/srep13803 (2015).



This work is licensed under a Creative Commons Attribution 4.0 International License. The images or other third party material in this article are included in the article's Creative Commons license, unless indicated otherwise in the credit line; if the material is not included under the Creative Commons license, users will need to obtain permission from the license holder to reproduce the material. To view a copy of this license, visit <http://creativecommons.org/licenses/by/4.0/>



Decadal Trends and Common Dynamics of the Bio-Optical and Thermal Characteristics of the African Great Lakes

Steven Loiselle^{1*}, Andrés Cózar², Enyew Adgo³, Thomas Ballatore⁴, Geoffrey Chavula⁵, Jean Pierre Descy⁶, David M. Harper⁷, Frank Kansime⁸, Ismael Kimirei⁹, Victor Langenberg¹⁰, Ronghua Ma¹¹, Hugo Sarmento¹², Eric Odada¹³

1 Dipartimento di Biotecnologia, Chimica e Farmacia, Consorzio per lo Sviluppo dei Sistemi a Grande Interfase, Università degli Studi di Siena, Siena, Italy, **2** Departamento de Biología, Universidad de Cádiz, Puerto Real, Spain, **3** College of Agriculture and Environmental Science, Bahir Dar University, Bahir Dar, Ethiopia, **4** Lake Basin Action Network, Moriyo, Japan, **5** Department of Civil Engineering, University of Malawi - The Polytechnic, Blantyre, Malawi, **6** Department of Biology, University of Namur, Namur, Belgium, **7** Department of Biology, University of Leicester, Leicester, United Kingdom, **8** Department of Environmental Management, Makerere University, Kampala, Uganda, **9** Kigoma Research Centre, Tanzanian Fisheries Research Institute, Kigoma, Tanzania, **10** DELTARES, Delft, The Netherlands, **11** Nanjing Institute of Geography and Limnology, Chinese Academy of Sciences, Nanjing, China, **12** Federal University of Sao Carlos, Department of Hydrobiology, São Carlos, Brazil, **13** Geology Department, University of Nairobi, Nairobi, Kenya

Abstract

The Great Lakes of East Africa are among the world's most important freshwater ecosystems. Despite their importance in providing vital resources and ecosystem services, the impact of regional and global environmental drivers on this lacustrine system remains only partially understood. We make a systematic comparison of the dynamics of the bio-optical and thermal properties of thirteen of the largest African lakes between 2002 and 2011. Lake surface temperatures had a positive trend in all Great Lakes outside the latitude of 0° to 8° south, while the dynamics of those lakes within this latitude range were highly sensitive to global inter-annual climate drivers (i.e. El Niño Southern Oscillation). Lake surface temperature dynamics in nearly all lakes were found to be sensitive to the latitudinal position of the Inter Tropical Convergence Zone. Phytoplankton dynamics varied considerably between lakes, with increasing and decreasing trends. Intra-lake differences in both surface temperature and phytoplankton dynamics occurred for many of the larger lakes. This inter-comparison of bio-optical and thermal dynamics provides new insights into the response of these ecosystems to global and regional drivers.

Citation: Loiselle S, Cózar A, Adgo E, Ballatore T, Chavula G, et al. (2014) Decadal Trends and Common Dynamics of the Bio-Optical and Thermal Characteristics of the African Great Lakes. PLOS ONE 9(4): e93656. doi:10.1371/journal.pone.0093656

Editor: Moncho Gomez-Gesteira, University of Vigo, Spain

Received: October 13, 2013; **Accepted:** March 5, 2014; **Published:** April 3, 2014

Copyright: © 2014 Loiselle et al. This is an open-access article distributed under the terms of the Creative Commons Attribution License, which permits unrestricted use, distribution, and reproduction in any medium, provided the original author and source are credited.

Funding: This research was supported by the NERC ESPA grant (NE/1003266/1) AND THE AGLOM project (CGL2010-11556-E). The funders had no role in study design, data collection and analysis, decision to publish, or preparation of the manuscript.

Competing Interests: The authors have declared that no competing interests exist.

* E-mail: loiselle@unisi.it

Introduction

The Great Lakes of East Africa are among the world's most important aquatic ecosystems from the point of view of ecosystem services, biodiversity and carbon cycling [1]. They are highly heterogeneous, presenting an array of hydrological and biological characteristics, ranging from shallow eutrophic water bodies (e.g. Lake Victoria) to deep oligotrophic lakes (e.g. Lake Tanganyika). Recent studies have demonstrated linkages between climate variability and productivity of several African lakes [2,3,4]. This is partially due to the importance of direct rainfall and evaporation in the water balances in the larger lakes (e.g. Lakes Tanganyika, Malawi and Victoria) and river flow in the smaller lakes (e.g. Lake Turkana) as well as climate driven lake stratification cycles [5,6,7]. Inter-annual variations in regional and global climate patterns have a strong influence on monsoon dynamics, in particular the Inter Tropical Convergence Zone (ITCZ) [8]. Local and regional impacts also play an important role on the chemical and biological dynamics of many of these lakes [9,10,11]. Remote measurements have been used to explore the spatio-temporal variability of the

temperature and bio-optical properties in several of these lakes [12,13,14]. However, a systematic inter-lake comparison using a common methodology has yet to be performed. There are multiple reasons for this, geographical (e.g. altitude) and seasonal differences in atmospheric optical conditions and seasonal differences in aquatic optical properties. Most importantly, there are limited data for lake specific algorithm development and validation while standard bio-optical algorithms have been predominately developed for phytoplankton dominated water bodies found at sea level [15]. In the present study, we make a comparative analysis of the thermal and bio-optical dynamics of thirteen lakes lying in or between the two branches of the Great Rift in Eastern-Central Africa; Lakes Albert, Chilwa, Edward, Kivu, Kyoga, Malawi, Mweru, Naivasha, Rukwa, Tana, Tanganyika, Turkana and Victoria (Figure 1). Using site-specific seasonal smoothing of the time series, we examine their decadal trends. These trends are also compared to interannual climate drivers, allowing us to explore commonalities between lakes and potential drivers of change.

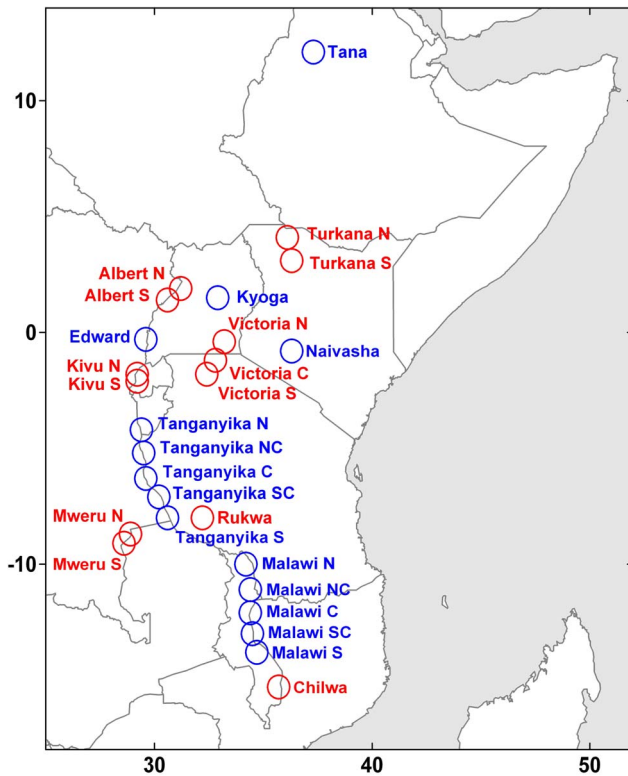


Figure 1. Lakes and lake sections included in the present analysis of the African Great Lakes.
doi:10.1371/journal.pone.0093656.g001

Materials and Methods

Monthly estimates of chlorophyll-a concentrations and lake surface temperatures (night) were obtained as Level 3 data from the MODIS AQUA mission dataset from the Goddard Earth Sciences Data and Information Services Centre (<http://disc.sci.gsfc.nasa.gov/giovanni>, Ocean Color Radiometry Online Visualization and Analysis Monthly Data), following Reprocessing 1.1 [16] and covering the period from July 2002 to July 2011.

Lake sections (64 km^2 – 128 km^2) were delineated using MODIS AQUA data at 4 km spatial resolution for the bio-optical estimates (MAMO_CHLO_4 km). Surface temperature estimates of the same lake section were obtained using MODIS AQUA data at 9 km spatial resolution (MAMO_NSST_9 km). Larger lakes were divided into separate lake sections based on the large scale patterns identified in previous studies or where lake dimension suggested such patterns could be possible [17,14]. Possible influences of coastal waters and edge effects were minimized in the large lakes by selecting lake sections at least 10 km from the lake border.

To avoid errors due to geographical differences between the optical conditions (atmospheric and aquatic) of the African lakes and those of standard MODIS processing, each record category was converted to a vector of anomalies by subtracting the lake wide average and dividing by the lake wide standard deviation. In such a manner, consistent spatial differences in optical conditions between lake sections would not influence the analysis of lake dynamics [17].

To remove the influence of seasonal variability in optical conditions (atmospheric and aquatic) between lakes and lake sections, each vector underwent a seasonal smoothing by using a yearly centred moving average with a length of 12 (months). The

resulting trend vector for each parameter was then subtracted from the original data and the differences were averaged across all contemporary (monthly) observations to produce a seasonal index. The trend vector and seasonal indices were subtracted from the data to give a residual component which was checked for normal distribution.

The resulting trend vectors (SST for the trend vector of lake surface temperature anomalies, CHLa for the trend vector of chlorophyll a anomalies) were independent of seasonal and intra-lake spatial variations in optical conditions (atmospheric and aquatic). These vectors of seasonally smoothed data anomalies were then used to compare dynamics between lakes and lake sections to determine commonalities in inter-annual trends.

Seasonally smoothed trend vectors of meridional wind speed anomalies (WIND) and precipitation rate anomalies (RAIN) for each lake section were constructed using NCEP/NCAR data [18,19] (<http://www.esrl.noaa.gov/psd/data/gridded/data.ncep.reanalysis.html>). Likewise, a trend vector of the Multivariate El-Niño Southern Oscillation Index (MEI) was also constructed [20] (<http://www.esrl.noaa.gov/psd/enso/mei/>). To examine the role of the ITCZ, we used historical dekadal (10-day) data for the African position of the ITCZ from April 2003 to July 2011 provided by the NOAA CPC Africa Desk/International Desk's Team (www.cpc.ncep.noaa.gov/products/fews/ITCZ/itcz) [21]. Monthly averages of dekadal positional data for longitudes of 30 and 35 were averaged and compared to SST and CHLa anomalies.

Factor analysis was utilised to identify common temporal co-variation between lake sections. This analysis was based on a linear combination of variables which contained the maximum variance. The reduced numbers of factors (eigenfunctions) is orthogonal (uncorrelated) while the eigenvalue of each factor was used to determine the fraction of the variability explained. In this manner, the temporal dynamics of the 27 lake sections was reduced to a smaller number of dominant factors. Common temporal modes were identified by determining the correlation between each lake section and the dominant factors for each variable. Lake sections with similar temporal dynamics were correlated to the same factor. It should be noted that this approach assumes that the temporal variability of each variable dataset is due to common forcing agents.

Decadal trends and correlations between drivers and anomaly vectors were determined by using linear model with a monthly time scale where direct correlations (increasing) had positive Pearson correlation coefficients (r) and indirect correlations (decreasing) had negative coefficients.

Results

The SST trend vectors of each lake section (27), analyzed by factor analysis, had five significant temporal modes which accounted for 92.5% of the total variability of the dataset (60.2%, 14.0%, 9.0%, 5.6%, 3.8% respectively). Sections of the same lake most often followed the same temporal mode (Table 1).

The SST trend vector for each lake section from 2002–2011, examined using a linear model and decadal trends, was identified as either positive (increasing), negative (decreasing) or not significant at $p > 0.01$ (Table 1, Figure S1 in File S1). The decadal trend for the SST vector was positive for Lakes Albert, Chilwa, Edward, Kyoga, Malawi (all sections), Mweru (both sections), Rukwa, Tanganyika (south and southcentre), and Turkana (both sections), indicating an overall warming of the lake surface waters. A negative trend was observed for Lake Tana. The highest inter-

Table 1. Dominant factors, decadal (2002–2011) trends and correlations between bio-optical, thermal and climate trends in 27 lakes sections of the African Great Lakes (n = 100 for SST, CHLa and MEI, n = 60 for ITCZ).

Lake section	Dominant factors				Trends (r)				Correlation between parameters (r)			
	CHLa	SST	WIND	RAIN	CHLa	SST	CHLa MEI	SST MEI	CHLa SST	SST ITCZ	CHLa ITCZ	
L. Tana		2	3	4		-0.61		0.03		0.08		
L. Turkana north	3	3	2	1	-0.61	0.25	0.54	0.00	0.28	-0.27	-0.22	
L. Turkana south	3	3	2	1	-0.53	0.27	0.56	-0.05	0.18	-0.41	-0.11	
L. Albert north	1	2	3	4	0.67	0.58	-0.55	0.11	0.23	-0.73	0.06	
L. Albert south	1	2	3	4	0.61	0.49	-0.22	0.19	0.13	-0.78	0.10	
L. Kyoga	4	4	3	4	-0.44	0.56	0.00	-0.24	-0.08	-0.75	0.07	
L. Edward	5	4	3	4	0.61	0.35	0.03	-0.06	0.40	-0.71	0.21	
L. Naivasha		1	1	1		0.25		0.22		-0.64		
L. Victoria north	4	1	1	1	0.11	-0.02	-0.06	0.39	-0.28	-0.80	0.58	
L. Victoria centre	3	1	1	1	0.35	-0.17	-0.20	0.31	0.08	-0.59	0.56	
L. Victoria south	2	1	1	1	0.22	-0.17	-0.03	0.33	0.16	-0.73	0.35	
L. Kivu north	5	1	1	3	0.09	0.05	-0.03	0.29	-0.17	-0.73	0.46	
L. Kivu south	5	1	1	3	-0.11	-0.11	-0.19	0.26	-0.32	-0.66	0.37	
L. Tanganyika north	5	1	1	3	-0.73	-0.05	0.36	0.44	-0.12	-0.75	0.44	
L. Tanganyika northcentre	5	1	1	3	-0.37	-0.06	0.06	0.31	-0.11	-0.77	0.27	
L. Tanganyika centre	4	1	1	3	0.02	0.18	0.07	0.28	-0.38	-0.85	0.33	
L. Tanganyika southcentre	4	1	1	3	0.05	0.29	-0.35	0.19	-0.51	-0.88	0.41	
L. Tanganyika south	4	2	1	3	0.13	0.42	-0.16	0.10	-0.48	-0.86	0.37	
L. Rukwa		4	2	2		0.47		0.01		-0.90		
L. Mweru north	1	2	2	4	0.72	0.45	-0.10	0.12	0.28	-0.84	0.51	
L. Mweru south	1	2	2	4	0.62	0.26	0.03	0.28	0.20	-0.82	0.59	
L. Malawi north	2	2	2	2	0.37	0.45	-0.12	0.11	0.37	-0.93	0.00	
L. Malawi northcentre	2	2	2	2	0.33	0.53	-0.10	0.02	0.42	-0.93	0.19	
L. Malawi centre	2	2	2	2	0.4	0.55	-0.10	-0.01	0.25	-0.93	0.59	
L. Malawi southcentre	2	2	2	2	0.58	0.56	-0.09	-0.19	0.16	-0.92	0.30	
L. Malawi south	1	2	2	2	0.61	0.67	-0.20	-0.12	0.24	-0.89	0.15	
L. Chilwa		5	2	2		0.40		-0.31		-0.78		

Significant correlations (p<0.01) are presented in bold.
doi:10.1371/journal.pone.0093656.t001

annual variability (lowest r) was found in those lakes south of the equator (Lakes Victoria, Kivu, Tanganyika (north)).

Using the CHLa trend vectors, factor analysis identified five significant temporal modes that accounted for 80.8% of the variability of the dataset (27.0%, 24.8%, 13.5%, 8.6%, and 6.9%, respectively). Differences in the inter-annual trend between sections of the same lake were evident in Lakes Tanganyika and Victoria. Positive trends ($p < 0.01$) in CHLa occurred in Lakes Albert, Edward, Malawi (all sections), Mweru (both sections) and Victoria (centre) (Table 1, Figure S1 in File S1). Negative trends were evident in Lakes Kyoga, Tanganyika (north and north centre) and Turkana. The highest inter-annual variability was in the smaller lakes as well as the south section of Lakes Tanganyika and Malawi.

Factor analysis of WIND and RAIN identified three and four dominant modes that accounted for 89.9% and 95.2% of the variability of each dataset. Negative trends in WIND were observed in most lakes at or above the equator, while positive trends occurred in lakes below the equator. Positive trends in RAIN were observed in all lakes except Lakes Malawi and Mweru (negative) and Lake Tanganyika (not significant).

The multivariate ENSO index (MEI), used to compare inter-annual global climate variations with the SST and CHLa dynamics in each lake section (Table 1, Figure S2 in File S1), showed a significant positive correlation between MEI and SST ($p < 0.01$) in sections of Lakes Victoria, Tanganyika, Kivu and Mweru, while a negative correlation for Lake Chilwa. Correlations between CHLa trends and MEI were both positive and negative (Table 1) with intra-lake differences. The decadal trend of MEI during the study period was negative and included the 2007–2009 and 2010–2011 La Niña events and the 2009–2010 El Niño events. WIND was positively correlated to MEI in most lakes while RAIN was negatively correlated.

The comparison of SST anomalies to ITCZ positional data (Table 1) showed a significant negative correlation between ITCZ and SST ($p < 0.01$) in all lake sections with the exception of Lakes Tana and Turkana (north). The correlation increased at lakes with latitudes below the equator. Correlations between CHLa anomalies and ITCZ positional data were positive in several lakes, most significantly in Lakes Victoria and Mweru (Figure S2 in File S1).

Discussion

The decadal warming observed in both large and small lakes results from inter-annual variability in radiative balances and latent heat exchange, as well as indirectly from changes in lake mixing and lake water balances. Interestingly, significant warming trends were limited to those lakes which displayed the lowest correlation with MEI. SST trends in Lakes Victoria, Tanganyika (north, north centre and centre) and Kivu (both sections) showed a clear sensitivity to MEI, which led to higher inter-annual fluctuations but no significant decadal trend. The spatial pattern of the MEI-SST relationship confirms that the lakes between 0° to 8° south are most sensitive to El-Niño effect on the ITCZ and the related weakening of the monsoon wind flow over East Africa [23]. Our observations suggest that the effect of El-Niño phenomenon on surface heat balances can be recurrent and significant for many lakes in Tropical East Africa [14]. The high correlation between the SST dynamics and the latitudinal movement of the ITCZ (Table 1) confirms the influence of climate drivers on the dynamics of the African lakes [21,22].

Trends in CHLa are influenced by inter-annual variability in nutrient availability and optical conditions related to light limitation. Both factors are related to long term trends in local

and regional conditions, as well as climate. The Lake Albert CHLa trend had a high negative correlation with MEI while Lake Turkana CHLa (north and south) was positively correlated. Opposing correlations between CHLa trends and MEI in the north and south of Lake Tanganyika were found. The influence of the latitudinal movement of the ITCZ was evident in several lakes (Lakes Kivu, Mweru and Victoria) and individual sections of Lakes Malawi and Tanganyika.

Decadal trends in CHLa in Lake Tanganyika also showed latitudinal differences, while all sections of Lake Malawi demonstrated a positive trend in CHLa over the study period, indicating a general increase in phytoplankton biomass. The centre section of Lake Victoria showed a significant positive trend, while the south section showed a similarly positive but less significant ($p = 0.025$) decadal trend.

CHLa dynamics are influenced by lake hydrodynamics through variations in seasonal cycles in mixing depth and nutrient upwelling. While SST dynamics are based on thermal emission from surface waters, surface temperature anomalies have been used to track changes in lake hydrodynamics [12,14]. Lake Tanganyika CHLa (south, southcentre and centre) was negatively correlated to SST. Such a negative relationship would indicate that upwelling nutrient rich waters have a positive impact on phytoplankton productivity [12]. A similar negative relationship was found for the south section of Lakes Kivu. Lake Victoria behaved in an opposite manner, as CHLa and SST were negatively correlated in the north section only, with a weak, but positive relationship in the south. A positive relationship between CHLa and SST could indicate a positive effect of lake stratification on phytoplankton growth (e.g. due to light limited growth). The CHLa trend in the north and centre sections of Lake Malawi showed a positive correlation to SST, as did correlations between SST and CHLa in Lakes Edward, Mweru (north) and Turkana (north).

Intra-lake Variability in Trend Vectors

In the present dataset, intra-lake differences in trend vectors of SST (Table 1) were significant in Lakes Malawi, Tanganyika, Victoria and Albert ($p < 0.001$) and to a lesser degree in Lakes Mweru ($p = 0.01$). In Lakes Victoria, Malawi and Mweru, the northern SST trend vectors were continuously higher than the southern lake sections, indicating a stable latitudinal SST difference in each lake. Lake Albert SST trend vectors were highest in the south section. It should be noted that seasonal latitudinal switches in SST may also be present but could remain undetected using anomaly trend vectors. Large scale latitudinal differences in surface temperature have been associated to differences in the exposure to the monsoon winds and the duration of the windy season (e.g. Lake Victoria [14]). On the other hand, the highest SST trend vectors in Lake Tanganyika were found in the north and south sections while the lowest SST vector occurred in the centre section. Large scale latitudinal circulation has been reported in Lake Tanganyika [24,25].

Intra-lake differences in CHLa trends were significant in most lakes. In Lakes Tanganyika and Malawi, the CHLa trend vectors in the south were significantly higher than those of the northern sections. In Lake Tanganyika, latitudinal differences in chlorophyll a concentration have been confirmed in several studies [26,27,28,29]. Similarly, the south sections of Lake Malawi had been reported to have the highest productivity for most of the year [30,31]. In Lakes Albert and Mweru (Figure 2), the north section CHLa trend vectors were consistently higher than those of the south. Lake Kivu's CHLa dynamics showed less clear latitudinal differences, even though differences in phytoplankton composition

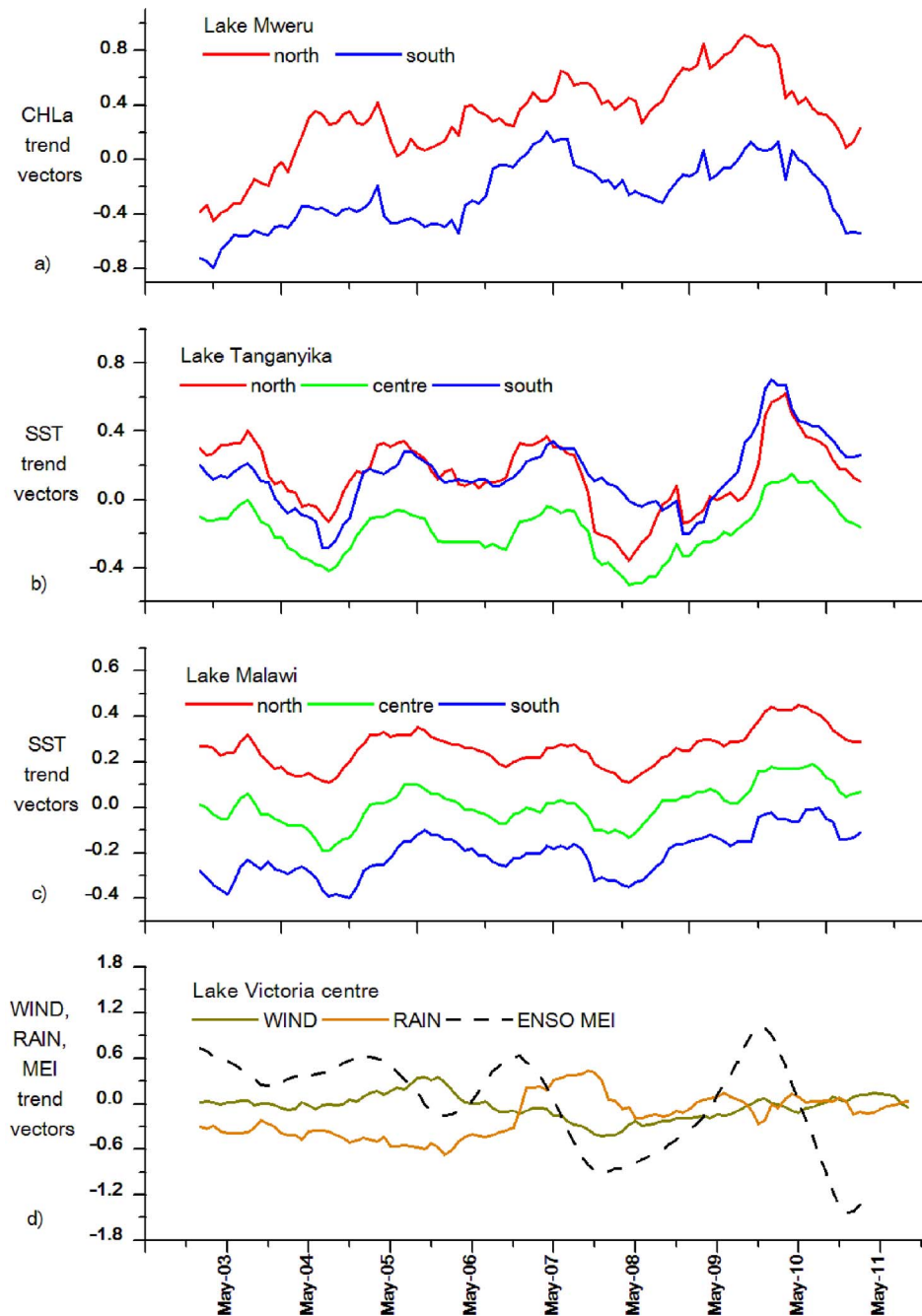


Figure 2. Trend vectors of A) CHLa for north and south sections of Lake Mweru, B) SST for north, centre and south sections of Lake Tanganyika, C) SST for north, centre and south sections of Lake Malawi, and D) WIND and RAIN for Lake Victoria centre section and ENSO MEI.

doi:10.1371/journal.pone.0093656.g002

have been reported, with cyanobacteria more abundant in the north section while diatoms and cryptophytes being a higher proportion of total phytoplankton biomass in the south [32].

Conclusions

The anomaly trend vectors of SST indicated that a decadal warming has occurred in all of the Great Lakes outside the latitude range of 0° to 8° south. Those lakes unaffected by the decadal warming trend were found to be more sensitive to inter-annual climate fluctuations related to the El Niño phenomena. It should

be noted that the warming trends are limited to the study period, but the increased sensitivity of lakes in the latitudinal band of 0° – 8° south to El Niño was clear. On the other hand, the sensitivity to the latitudinal position of the ITCZ was elevated in nearly all lakes south of the equator.

The relative response of CHLa to changes in SST, MEI and ITCZ varied between lakes and between sections of the same lake. There was no clear regional trend towards eutrophication, as some lakes showed a negative decadal trend in CHLa, including sections of Lakes Tanganyika, Kyoga and Turkana. Lake Malawi presents

a positive decadal trend in CHLa and a positive relationship between SST and CHLa, indicating that this lake is moving to a higher trophic status, with a marked sensitivity to hydrodynamics.

The regional and seasonal differences in the atmospheric and aquatic optical properties of the East African Great lakes, combined with limited field data have hampered a regional analysis. The present approach does not replace the need for extensive field data or for the development of lake specific algorithms to estimate aquatic and atmospheric parameters. However, the use of anomaly trend vectors allows for the identification of common lake trends and possible links between potential drivers and lake responses.

Supporting Information

File S1 Figure S1. Decadal trends (2002–2011) in anomaly vectors of A) SST and B) CHLa in the African Great Lakes, blue circles for a positive trends, red circles for a negative trends, open circles for no significant trend ($p > 0.01$). Figure S2. Correlations

References

- Ogutu-Ohwayo R, Hecky RE, Cohen AS, Kaufman L (1997) Human impacts on the African Great Lakes. *Env. Biol. Fish.* 50: 117–131.
- Stager JC, Cocquyt C, Bonnefille R, Weyhenmeyer C, Bowerman N (2009) A late Holocene paleoclimatic history of Lake Tanganyika, East Africa. *Quaternary Res.* 72: 47–56.
- Tierney JE, Mayes MT, Meyer N, Johnson C, Swarzenski P, et al. (2010) Late-twentieth-century warming in Lake Tanganyika unprecedented since AD 500. *Nat. Geosci.* 3: 422–425.
- Wolff C, Haug GH, Timmermann A, Sinninghe Damsté JS, Brauer A, et al. (2011) Reduced inter-annual rainfall variability in East Africa during the last ice age. *Science* 333: 743–747.
- Talling JF, Lemoalle J (1998) *Ecological Dynamics of tropical inland waters*. United Kingdom: Cambridge University Press.
- Hulme M, Doherty R, Ngara T, New M, Lister D (2001) African climate change: 1900–2100. *Clim. Res.* 17: 145–168.
- Olaka L, Odada E, Trauth M, Olago D (2010) The sensitivity of Eastern African rift lakes to climate fluctuations. *J. Paleolimnol.* 44: 629–644.
- Nicholson SE (2000) The nature of rainfall variability over Africa on time scales of decades to millennia. *Global and Planet Change* 26: 137–158.
- Verburg P, Hecky RE, Kling HJ (2006) Climate warming decreased primary productivity in Lake Tanganyika, inferred from accumulation of dissolved silica and increased transparency. Comment to Sarvala et al. (2006) (*Verh. Internat. Verein. Limnol.* 29, p. 1182–1188). *Verh. Internat. Verein. Limnol.* 29: 2335–2338.
- Pasche N, Wehrli B, Alunga G, Muvundja F, Schurter M, et al. (2010) Abrupt onset of carbonate deposition in Lake Kivu during the 1960s: response to recent environmental changes. *J. Paleolimnol.* 44: 931–946.
- Hecky RE, Mugidde R, Ramlal PS, Talbot MR, Kling GW (2010) Multiple stressors cause rapid ecosystem change in Lake Victoria. *Freshwater Biol.* 55: 19–42.
- Bergamino N, Horion S, Stenuite S, Cornet Y, Loiseau SA, et al. (2010) Spatio-temporal dynamics of phytoplankton and primary production in Lake Tanganyika using a MODIS based bio-optical time series. *Remote. Sens. Environ.* 114: 772–780.
- Sørensen K, Folkestad A, Stelzer K, Brockmann C, Doerffer R, et al. (2008) Performance of Meris Products in Lake Victoria ESA SP-666 Proceedings from MERIS-(A)TSR Workshop.
- Cózar A, Bruno M, Bergamino N, Úbeda B, Bracchini L, et al. (2012) Basin-scale Control on the Phytoplankton Biomass in Lake Victoria, Africa. *Plos One* 7(1): e29962 (doi:10.1371/journal.pone.0029962).
- Horion S, Bergamino N, Stenuite S, Descy JP, Plisnier PD, et al. (2010) Optimized extraction of daily bio-optical time series derived from MODIS/Aqua imagery for Lake Tanganyika, Africa. *Remote Sens. Environ.* 114: 781–791.
- Acker J, Leptoukh G (2007) Online analysis enhances use of NASA Earth science data. *Trans. Amer. Geophysical Union* 88: 14.
- Bergamino N, Loiseau SA, Cózar A, Dattilo AM, Bracchini L, et al. (2007) Examining the dynamics of phytoplankton biomass in Lake Tanganyika using Empirical Orthogonal Functions. *Ecol. Model.* 204: 155–162.
- Kalnay E, Kanamitsu M, Kistler R, Collins W, Deaven D, et al. (1996) The NCEP/NCAR Reanalysis 40-year Project. *Bull. Amer. Meteor. Soc.* 77: 437–471.
- Bosilovich MG, Chen J, Robertson FR, Adler RF (2008) Evaluation of Global Precipitation in Reanalyses. *J. Appl. Meteor. Climatol.* 47: 2279–2299.
- Wolter K, Timlin MS (2011) El Niño/Southern Oscillation behaviour since 1871 as diagnosed in an extended multivariate ENSO index (MEI.ext). *Int. J. Climatology* 31: 1074–1087.
- Lélé MI, Lamb PJ (2010) Variability of the Intertropical Front (ITF) and Rainfall over the West African Sudan–Sahel Zone. *J. Climate* 23: 3984–4004.
- Stager JC, Ruzmaikin A, Conway D, Verburg P, Mason PJ (2007) Sunspots, El Niño, and the levels of Lake Victoria, East Africa. *J. Geophys. Res.-Atmos.* 112 D15106.22.
- Tierney JE, Lewis SC, Cook BI, LeGrande AN, Schmidt GA (2011) Model, proxy and isotopic perspectives on the East African Humid Period. *Earth Planet. Sci. Lett.* 307: 103–112.
- Plisnier PD, Chitamwebwa D, Mwape L, Tshibangu K, Langenberg V, et al. (1999) Limnological annual cycle inferred from physical-chemical fluctuations at three stations of lake Tanganyika. *Hydrobiologia* 407: 45–58.
- Verburg P, Antenucci JP, Hecky RE (2011) Differential cooling drives large-scale convective circulation in Lake Tanganyika. *Limnol. Oceanogr.* 56: 910–926.
- Sarvala J, Langenberg VT, Salonen K, Chitamwebwa D, Coulter GW, et al. (2006) Changes in dissolved silica and transparency are not sufficient evidence for decreased primary productivity due to climate warming in Lake Tanganyika. *Verh. Internat. Verein. Limnol.* 29 (2006): 2339–2342.
- Coulter GW, Spiegel RH (1991) *Hydrodynamics*. Chapter 3 In Coulter GW (ed.) *Lake Tanganyika and its Life*. Oxford Univ. Press: 49–75.
- O'Reilly CM, Alin SR, Plisnier PD, Cohen AS, McKee BA (2003) Climate change decreases aquatic ecosystem productivity of Lake Tanganyika, Africa. *Nature* 424: 766–768.
- Descy JP, Tarbe AL, Stenuite S, Pirlot S, Stimart J, et al. (2010) Drivers of phytoplankton diversity in Lake Tanganyika. *Hydrobiologia* 653: 29–44.
- Patterson G, Kachinjika O (1995) Limnology and phytoplankton ecology, p. 1–67. In A. Menz [ed.], *The fishery potential and productivity of the pelagic zone of lake Malawi/Niassa - Scientific report of the UK/SADC pelagic fish resource assessment project*. Natural Resources Institute, Overseas Development Administration.
- Hecky RE, Kling HJ (1987) Phytoplankton ecology of the great lakes in the rift valleys of Central Africa. *Arch. Hydrobiologia* 25: 197–228.
- Sarmiento H, Isumbisho P, Descy JP (2012) Phytoplankton. In Descy, J P, F Darchambeau & M Schmid (eds) *Lake Kivu: Limnology and geochemistry of a unique tropical great lake*. Aquatic Ecology Series, vol 5. Springer Dordrecht, Heidelberg, New York, London, 67–83.

Diet overlap between the newly introduced *Lamprichthys tanganicus* and the Tanganyika sardine in Lake Kivu, Eastern Africa

M. P. Masilya · F. Darchambeau · M. Isumbisho · J.-P. Descy

Received: 16 February 2011 / Revised: 28 May 2011 / Accepted: 13 June 2011 / Published online: 1 July 2011
© Springer Science+Business Media B.V. 2011

Abstract This study evaluates the possible competition for food between *Lamprichthys tanganicus*, recently introduced in Lake Kivu, and *Limnothrissa miodon*, which has been the basis of the pelagic fishery in this lake for several decades. Since 2006, *L. tanganicus* has expanded in the lake and its numbers have increased in the captures, raising concern for the sardine fishery. We carried out a 2-year monthly survey, based on experimental captures in littoral and pelagic stations, which demonstrated the invasive dispersal of *L. tanganicus* in littoral and pelagic waters. The diet of both species was determined on the basis of gut content analyses, taking into account the influence of site and season, and a diet overlap index was calculated. In the pelagic zone, where almost all size classes of both

species were present and essentially fed upon mesozooplankton, the diet overlap was high. This situation stems from the fact that *L. tanganicus* has colonized the pelagic zone in Lake Kivu, likely in search for more abundant mesozooplankton. Inshore, the diet overlap between the two species was lower, as *L. tanganicus* consumed a broad range of food, whereas *L. miodon* strongly selected insects and, chiefly for the largest specimens, fishes. These results suggest a likelihood of interspecific competition, particularly offshore, where mesozooplankton is the main available food type, and call for further monitoring of the sardine fishery, to assess a possible impact of the invader.

Keywords Exotic species · Resource competition · Large African lake · Fisheries

Handling editor: M. Power

M. P. Masilya (✉) · F. Darchambeau · J.-P. Descy
Laboratory of Freshwater Ecology, URBE, Department of
Biology, University of Namur, 5000 Namur, Belgium
e-mail: pascalmasilya@yahoo.fr;
pascal.masilyamulungula@fundp.ac.be

M. P. Masilya · M. Isumbisho
Unité d'Enseignement et de Recherche en Hydrobiologie
Appliquée (UERHA), ISP/Bukavu, B.P. 854, Bukavu,
Democratic Republic of Congo

F. Darchambeau
Chemical Oceanography Unit, Université de Liège,
4000 Liège, Belgium

Introduction

Accidental and/or deliberate introduction of exogenous species into ecosystems has been a frequent phenomenon (Lodge et al., 1998). In the aquatic ecosystems, direct competition between exotic and native fish species (Lévêque, 1997; Ogutu-Ohwayo et al., 1997; Pardo et al., 2009) may eventually lead to modified fisheries activities (Lévêque, 1997; Ogutu-Ohwayo et al., 1997; Preikshot et al., 1998). Moreover, Gozlan (2008) notes that these introductions will have inevitable implications in the future on the

distribution of native freshwater fish species; so the need to rely on non-native fish may become a growing reality.

Lake Kivu has a very poor fish fauna compared to other large lakes of East-African rift valley (Beadle, 1981). Only 29 species have been described, among which four species were accidentally or voluntarily introduced (Snoeks et al., 1997): 3 cichlids (*Oreochromis macrochir* (Boulenger, 1912); *Oreochromis leucostictus* (Trewavas, 1933) and *Tilapia rendalli* (Boulenger, 1896)) and 1 clupeid (*Limnothrissa miodon* Boulenger, 1906). Among those introduced species, the most famous is the “Tanganyika sardine”, *L. miodon* which was voluntarily introduced in 1959 (Collart, 1960) into Lake Kivu, where no planktivorous fish existed in the pelagic waters. Though this introduction maybe seen as a major disturbance of the pelagic ecosystem (Dumont, 1986; Isumbisho et al., 2006a), it permitted the development of an important fishery with an exploitable stock evaluated at about 6,000 tons (Lamboeuf, 1989, 1991). Despite pessimistic predictions of the future harvestable stock based on observed changes in the mesozooplankton composition and biomass (Dumont, 1986), the stock of *L. miodon* seems to have maintained itself over the years (Guillard, 2009).

In 2006, *Lamprichthys tanganicus* (Boulenger, 1898), an omnivorous Poeciliidae, also endemic to Lake Tanganyika (Coulter, 1991), began to appear in the commercial catches of fishermen from several sites of Lake Kivu (Muderhwa & Matabaro, 2010). Few data exist on the biology and ecology of *L. tanganicus* in its natural ecosystem. The species lives mainly among rocks along the littoral zone and rarely offshore (Coulter, 1991). It feeds upon small zooplankton and insects (adults and larvae). Sometimes fishes’ scales were also found in gut contents (Lushombo & Nshombo, 2008). Nothing is known about the biology and the ecology of this fish in Lake Kivu. However, some characteristics of Lake Kivu raise the concern that food competition may develop between *L. tanganicus* and *L. miodon*. Lake Kivu has an extremely reduced littoral zone—the pelagic zone extends up to >90% of the surface area of the lake (Beadle, 1981)—consisting of submerged rocks covered with calcareous precipitates and dense mats of the filamentous green alga *Cladophora* (Verbeke, 1957). In addition, in Lake Kivu, *L. miodon* is

essentially zooplanktivorous in its early life but becomes omnivorous at the adult stage, feeding on diverse preys: zooplankton, insect larvae and adults, other small fishes and their own young stages (de Jongh et al., 1983; Isumbisho et al., 2004; Masilya et al., 2005). So, at first sight, the diet of the two species is rather similar, and their coexistence in a lake where resources are scarce may lead to severe interspecific competition.

This article presents a study of the diet of *L. tanganicus* and *L. miodon* in the pelagic and in the littoral zone of Lake Kivu, based on stomach content analyses. We attempted to evaluate a possible niche overlap between the two species, which would point to potential competition for resources. In addition, we analyzed the ability of invasive dispersal of *L. tanganicus* through experimental catches.

Materials and methods

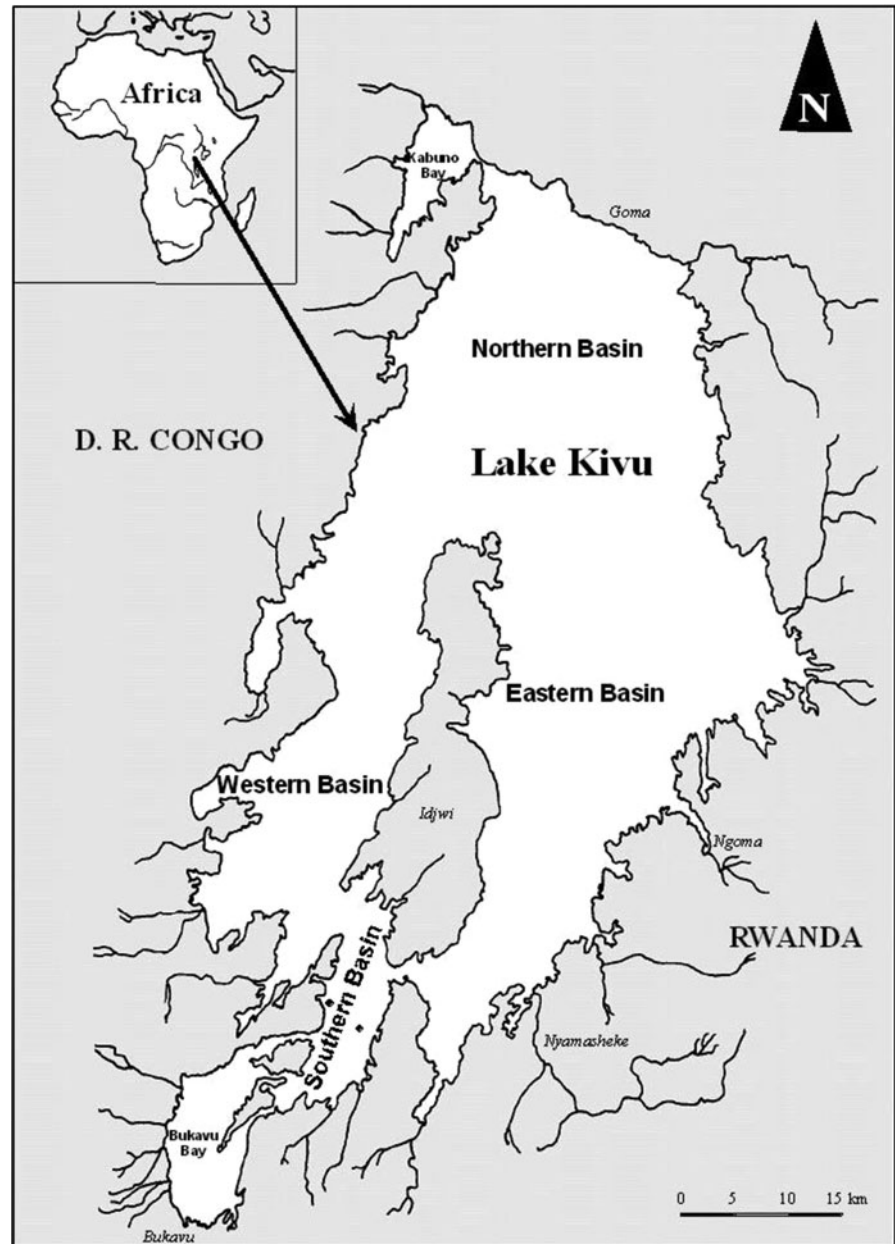
Study area

Lake Kivu is a large (surface area 2,370 km²), deep (max. depth 489 m), oligotrophic lake with a reduced littoral zone (<10% of the lake surface area; Beadle, 1981). The lake is meromictic, with oxygenated waters limited to the upper 60 m and permanently separated from the deep waters by several steep salinity gradients (Degens et al., 1973). The study site is located in the southern (Ishungu) basin (Fig. 1). Two stations were sampled, one located in the pelagic area (02.3394°S, 28.9765°E), where the lake is ~120 m deep, and one located in the littoral zone along the shoreline (02.1969°S, 28.5794°E). The littoral station was ~10 m deep and the substrate mainly constituted of submerged rocks, macrophytes, and sand. Most native fish species in Lake Kivu are confined to the littoral zone (Snoeks et al., 1997) where zooplankton density is 15–50 times lower than in the pelagic zone (Isumbisho et al., 2004, 2006a).

Fish sampling

Diurnal fishing was carried out monthly at both stations from September 2007 to September 2009. At each station, fishes were passively captured using a 10-mm mesh—size fish net (length: 200 m; height: 9 m), left floating vertically from the water surface

Fig. 1 Lake Kivu geographic situation and sampling sites location (black dots)



for 1 h around noon. In addition, larvae and juveniles of *L. tanganicanus* and *L. miodon* were actively captured in the littoral station using a small seine net (3.5 m × 1.3 m; 300- μ m mesh size).

In the field, fishes were sorted by species, counted, and measured (nearest 1-mm length, total length, TL) using a graduated board. Fishes were dissected and their sex was noted after observation of their gonads. Their digestive tracts were extracted and preserved in 5% buffered formalin.

Fish diet analysis (gut contents)

In the laboratory, the content of digestive tracts was removed, weighed (nearest 0.01 mg), and examined under a dissecting microscope. For *L. miodon*, only the stomach content was examined, while for *L. tanganicanus*, which does not have a true pylorus between stomach and intestine (personal observation), the contents of stomach and anterior intestine were examined. For the young stages of *L. tanganicanus*

and *L. miodon* which did not have a developed stomach, all the digestive tract (from esophagus to lower intestine) was examined. All items present in the digestive tracts were counted and identified to the lowest possible taxonomic level, using Tachet et al. (1980) for macroinvertebrates, Sarmiento et al. (2007) for phytoplankton, and Isumbisho et al. (2006b) for mesozooplankton.

The fishes' diet was described using three common dietary indices (Hyslop, 1980): the occurrence (%FO), the abundance (%N), and the volume (%V) of each prey category. For volume, as *L. miodon* and *L. tanganicanus* have a small stomach and their preys are small, we employed the point method as recommended by Hyslop (1980): each food category is awarded points proportional to its estimated contribution to stomach volume. The points allocated to a food category were summed up and expressed as a percentage of the total points awarded. Empty guts were not taken into account in abundance and volume calculations.

In order to characterize and compare diets, the contribution of each food category (*i*) to the diet was estimated using the percentage of Lauzanne's index (%IA_{*i*}) (Lauzanne, 1976):

$$\%IA_i = \frac{IA_i}{\sum_{i=1}^n IA_i} * 100$$

where IA_{*i*} (Lauzanne's index) = (%FO_{*i*} * %V_{*i*})/100, and *n* is the number of the different food categories. Compared to other compound indices used in the study of fish feeding (Rosecchi & Nouazé, 1987), Lauzanne's index allows considering countable and uncountable food type, which is a real advantage when the diets of omnivorous or opportunistic fishes must be compared.

Diet overlap

Similarity between diets and dietary overlap between two species indicates their potential for trophic interactions (Qin et al., 2007; Bănaru & Harmelin-Vivien, 2009). In the present study, we calculated the Pianka's index (*O*) (Pianka, 1974):

$$O = \frac{\sum \%V_{iA} \%V_{iB}}{\sqrt{\sum \%V_{iA}^2 \sum \%V_{iB}^2}}$$

where %V_{*iA*} is the percentage by volume of food category *i* in the diet of the species A, and %V_{*iB*} is the

percentage by volume of the same food category in the diet of the species B. Only the food categories that were identified were considered in this calculation, using the lowest possible taxonomic level: fragments of zooplankters, insects, and fishes were not considered.

Pianka's index varies from 0 (no overlap) to 1 (complete overlap); an overlap was considered significant in several studies (Dolbeth et al., 2008; Corrêa et al., 2009) when values exceeded 0.6.

Data analyses

Effects of species, station, and season (the dry season from June to August and the rainy season from September to May) on captures were evaluated using generalized linear models with a quasi-Poisson error distribution (log-linear models). Models were compared using *F* test and the most parsimonious model was retained. All statistical tests were carried out in the R environment (R Development Core Team, 2005).

Results

In total, from September 2007 to September 2009, 542 *L. tanganicanus* and 208 *L. miodon* adults were caught in our experimental catches. *L. tanganicanus* represented 52% of the catch in the pelagic station and 81% in the littoral station while *L. miodon* represented 48 and 17% of the catch respectively in the pelagic and the littoral stations. Some *Haplochromis* spp. were also caught with *L. miodon* and *L. tanganicanus* but only in the littoral station where they represented 2% of the total catch. For the littoral station, the mean monthly catch was 3.8 (range 0–25) for *L. miodon* and 16.3 (0–60) for *L. tanganicanus*, while the mean monthly catch was 4.2 (0–23) for *L. miodon* and 4.6 (0–35) for *L. tanganicanus*, in the pelagic station. The simplest generalized linear model of captures is presented in Table 1. It was not significantly different from the full model ($F_{96,97} = 0.126$, $P = 0.723$). There was no effect of season on captures, but there were significant main and interactive effects of species and stations on captures. In other words, *L. tanganicanus* dominated in all captures, especially in the littoral zone.

Table 1 Results of the most simplified but significant generalized linear model of captures with a quasi-Poisson error distribution

Effects	SS	df	F	P (>F)
Species	154.10	1	10.903	0.001
Station	116.75	1	8.260	0.005
Season	19.70	1	1.394	0.241
Species * station	62.80	1	4.444	0.038
Species * season	10.64	1	0.753	0.388
Station * season	0.19	1	0.013	0.909
Residuals	1370.95	97		

Significant effects at 0.05 level are highlighted (*bold* values in the table)

Food composition in the gut contents

Six main food categories were identified in the gut contents of both species: terrestrial plant remains, benthic algae (*Cladophora* sp.), phytoplankton, zooplankton, insects, and fishes (Table 2). Fishes were more frequently observed in *L. miodon* stomachs than in *L. tanganicanus*.

Numerically, zooplankton (mainly *Thermocyclops consimilis* Kiefer, 1934; *Diaphanosoma excisum* Sars, 1885; and Bdelloids) was the most abundant food type in the diet of both species. By volume, insects (mainly Formicidae and Culicidae) were the dominant food type in *L. miodon* adults while zooplankton and insects (mainly Formicidae) contributed volumetrically in similar proportions (46.8% vs. 39.3%) to the diet of *L. tanganicanus* adults. The diet of young stages of *L. tanganicanus* and *L. miodon* was, in terms of occurrence and volume, dominated by zooplankton (Table 2).

Variability in fish diet

The importance of the different food items in the diet of both species varied depending on size and habitat (littoral vs. pelagic) (Figs. 2 and 3). Insects were the dominant food type for *L. miodon* adults caught in the littoral zone but in the biggest *L. miodon*, fishes were most frequently observed (Fig. 2). In the pelagic area, some differences were observed in function of size: fish smaller than 110 mm fed preferentially upon zooplankton, while larger fish fed mainly upon insects (especially ants and mosquito larvae) and fishes (Fig. 2). In comparison, *L. tanganicanus* from the pelagic area fed mainly upon zooplankton, whatever the size (Fig. 3). In contrast, in the littoral area, *L. tanganicanus* shifted their diet to insects (mainly ants) as their size increased (Fig. 3). There

was no clear seasonal variation in the diet of both species. Young stages of both *L. miodon* and *L. tanganicanus* were mainly zooplanktivorous (Fig. 4).

Diet overlap

Diet overlap estimated by the Pianka's index varied according to habitat and season. It was relatively high (>0.6) between both fish species at the pelagic station but was lower in the littoral zone (≤ 0.6). Diet overlap varied between seasons: the index reached 0.73 offshore and 0.54 inshore during the dry season, whereas, in the rainy season, it tended to decrease in both sites (0.68 offshore and 0.37 inshore). Concerning the larvae, their diet overlap was extremely high whatever the season. Their diet overlap index was equal to 0.99 and 0.98 in rainy and dry season respectively.

Discussion

The present study investigated the invasive dispersal and the feeding ecology of *L. tanganicanus*, an endemic species of Lake Tanganyika recently introduced in Lake Kivu.

The first scientific observation of *L. tanganicanus* presence in Lake Kivu was made in December 2006 (Muderhwa & Matabaro, 2010). The time of its arrival into Lake Kivu is not well established but some evidence points to a recent, likely accidental, introduction, contrary to the opinion that this species was accidentally introduced with *L. miodon* in 1959 (Muderhwa & Matabaro, 2010). Indeed, if the new species had been introduced at the end of the 1950s, it would have been noticed by the fishermen before, since this species is easily distinguished from

Table 2 Importance of food types (%FO, occurrence in %; %N, abundance in %; %V, volume in %) in gut contents of *Limnothrissa miodon* and *Lamprichthys tangaicanus* from Lake Kivu

Size range (TL, mm): Food types/indices	<i>Lamprichthys tangaicanus</i>						<i>Limnothrissa miodon</i>									
	Young			Adult			Young			Adult						
	9–36	%FO	%N	%V	72–129	%FO	%N	%V	11–42	%FO	%N	%V	85–164	%FO	%N	%V
Plant remnants	8.3	–	–	0.7	36.6	–	–	2.8	1.0	–	–	0.7	21.1	–	–	2.4
<i>Cladophora</i> sp.	–	–	–	–	2.7	–	–	0.1	–	–	–	–	–	–	–	–
Phytoplankton	75.8	29.1	4.9	–	44.4	4.8	3.1	–	0.1	0.1	0.1	<0.1	4.7	<0.1	–	0.5
Cyanobacteria (<i>Microcystis</i> sp.)	–	–	–	–	41.3	–	–	2.5	0.1	0.1	0.1	<0.1	4.7	–	–	0.5
Diatom (<i>Nitzschia</i> sp.)	–	–	–	–	7.6	4.8	0.6	–	0.1	0.1	0.1	<0.1	0.6	<0.1	–	<0.1
Zooplankton	99.2	70.9	89.9	–	68.4	92.0	46.8	–	92.8	99.0	99.0	91.0	34.5	94.8	–	23.2
Copepods	98.0	67.2	85.3	–	53.3	42.7	6.9	–	86.9	89.0	89.0	82.8	28.1	15.4	–	2.9
<i>Mesocyclops aequatorialis</i>	–	–	–	–	6.9	0.3	0.2	–	–	–	–	–	2.3	0.1	–	0.1
<i>Thermocyclops consimilis</i>	–	–	–	–	52.8	42.3	6.7	–	–	–	–	–	28.1	15.3	–	2.9
<i>Tropocyclops confinis</i>	–	–	–	–	0.2	0.1	<0.1	–	–	–	–	–	–	–	–	–
Nauplii larvae	–	–	–	–	–	–	–	–	–	–	–	–	0.6	<0.1	–	<0.1
Cladoceran	51.2	0.8	2.1	–	43.2	36.8	6.6	–	10.4	9.9	9.9	6.9	17.5	15.9	–	2.3
<i>Alona rectangula</i>	–	–	–	–	6.9	0.1	0.1	–	–	–	–	–	5.3	0.1	–	<0.1
<i>Ceriodaphnia cornuta</i>	–	–	–	–	4.4	0.1	0.1	–	–	–	–	–	0.6	<0.1	–	<0.1
<i>Diaphanosoma excisum</i>	–	–	–	–	39.8	35.5	6.1	–	–	–	–	–	14.6	15.7	–	2.3
<i>Moina micrura</i>	–	–	–	–	6.5	1.1	0.4	–	–	–	–	–	0.6	<0.1	–	<0.1
Rotifera	84.9	2.9	2.6	–	44.4	12.6	1.5	–	–	–	–	–	30.4	63.5	–	2.4
Unidentified Bdelloids	–	–	–	–	43.6	12.5	1.5	–	–	–	–	–	30.4	63.5	–	2.4
<i>Brachionus calyciflorus</i>	–	–	–	–	0.2	<0.1	<0.1	–	–	–	–	–	–	–	–	–
<i>Lecane</i> sp.	–	–	–	–	1.5	<0.1	<0.1	–	–	–	–	–	–	–	–	–
Zooplankton fragment	–	–	–	–	66.9	–	31.8	–	2.1	–	–	1.3	34.5	–	–	15.5
Insects	6.7	–	0.9	–	67.6	3.2	39.3	–	1.1	0.5	0.5	0.5	65.5	4.9	–	53.4
Imago	–	–	–	–	26.3	0.8	15.2	–	–	–	–	–	31.6	2.0	–	18.7
<i>Apidae</i>	–	–	–	–	1.1	<0.1	0.1	–	–	–	–	–	0.6	<0.1	–	<0.1
<i>Coccinellidae</i>	–	–	–	–	0.8	<0.1	<0.1	–	–	–	–	–	1.8	0.1	–	0.3
<i>Corixidae</i>	–	–	–	–	–	–	–	–	–	–	–	–	1.2	<0.1	–	0.4
<i>Formicidae</i>	–	–	–	–	22.7	0.6	13.5	–	–	–	–	–	29.2	1.5	–	16.6
<i>Muscidae</i>	–	–	–	–	–	–	–	–	–	–	–	–	1.8	<0.1	–	<0.1

Table 2 continued

	<i>Lamprichthys tanganicanus</i>				<i>Limnothrissa miodon</i>							
	Young		Adult		Young		Adult					
	%FO	%N	%V	%FO	%N	%V	%FO	%N	%V			
Size range (TL, mm):	9–36			72–129			11–42			85–164		
Food types/indices	%FO	%N	%V	%FO	%N	%V	%FO	%N	%V	%FO	%N	%V
<i>Termitidae</i>	–	–	–	3.8	0.2	1.5	–	–	–	3.5	0.4	1.3
Larvae	–	–	–	0.4	1.6	<0.1	1.1	0.5	0.5	28.7	2.3	14.1
<i>Chironomidae</i>	–	–	–	0.2	1.6	<0.1	1.1	0.5	0.5	0.6	<0.1	<0.1
<i>Culicidae</i>	–	–	–	0.2	<0.1	<0.1	–	–	–	26.9	2.0	12.7
<i>Leuctridae</i>	–	–	–	–	–	–	–	–	–	7.6	0.3	1.4
Nymph	–	–	–	12.6	0.8	0.6	–	–	–	8.8	0.6	0.8
Insects fragment	6.7	–	0.9	52.8	–	23.5	–	–	–	37.4	–	19.9
Fish	–	–	–	0.6	<0.1	0.1	–	–	–	13.5	0.3	10.8
<i>Limnothrissa miodon</i>	–	–	–	–	–	–	–	–	–	8.2	0.3	5.9
Larvae	–	–	–	–	–	–	–	–	–	5.8	0.3	4.1
Juvenile	–	–	–	–	–	–	–	–	–	2.3	<0.1	1.8
<i>Lamprichthys tanganicanus</i>	–	–	–	0.2	<0.1	0.1	–	–	–	–	–	–
Juvenile	–	–	–	0.2	<0.1	0.1	–	–	–	–	–	–
<i>Haplochromis</i> spp.	–	–	–	–	–	–	–	–	–	1.8	<0.1	1.3
Juvenile	–	–	–	–	–	–	–	–	–	1.8	<0.1	1.3
Fish fragments	–	–	–	0.6	–	<0.1	–	–	–	8.2	–	3.6
Unidentified prey	51.6	–	3.5	39.8	<0.1	7.7	9.3	0.5	7.8	22.2	<0.1	9.6
Number of non empty stomach analyzed	252			475			962			171		
Number of stomach analyzed	252			542			962			208		

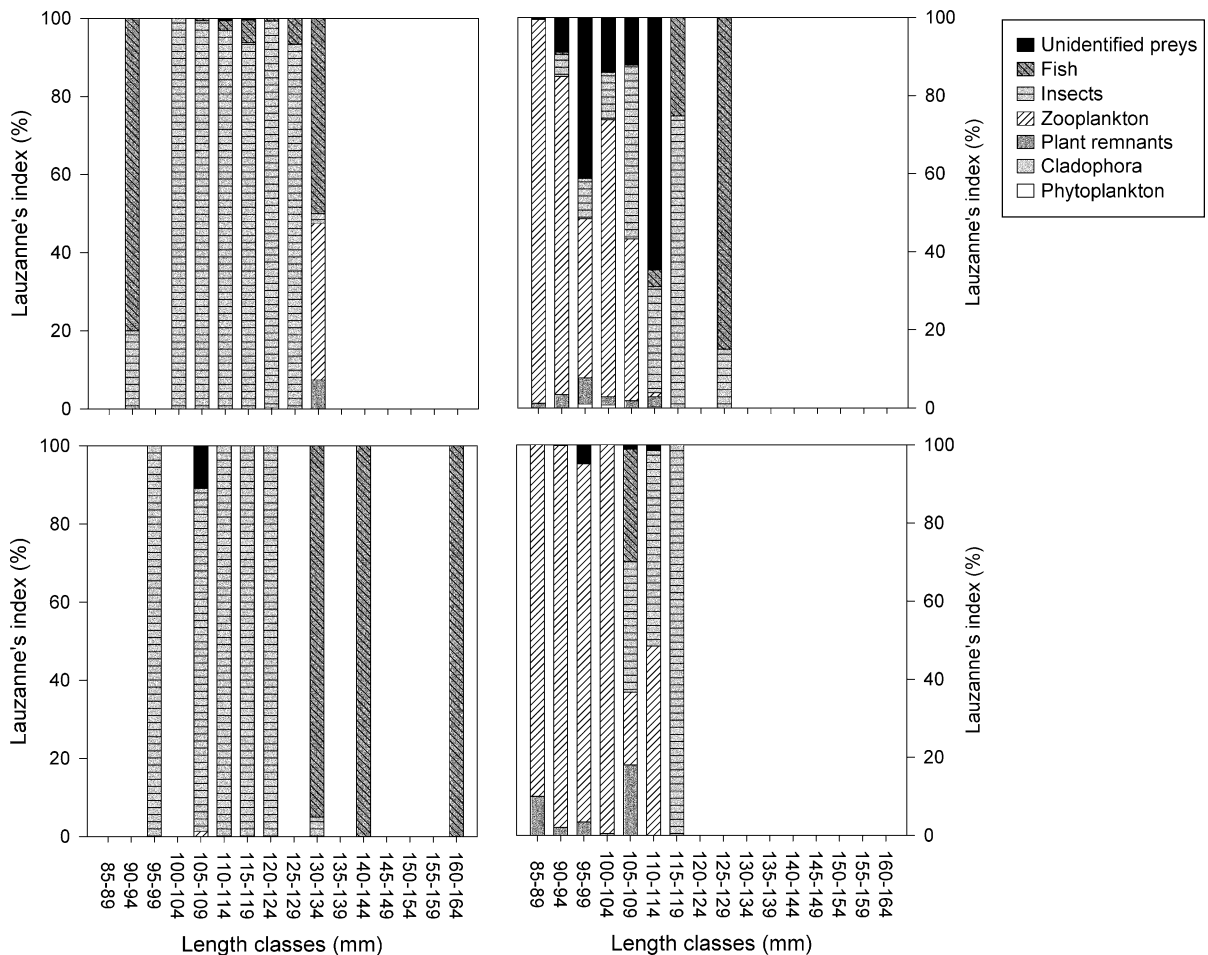


Fig. 2 Percentage of Lauzanne's index of broad taxonomic groups for different length classes of adults *Limnothrissa miodon* from the littoral (left panels) and pelagic (right panels) stations of Lake Kivu during rainy (upper panels) and dry season (lower panels)

L. miodon. Moreover, several scientific studies on *L. miodon* were conducted in the past decades (e.g., Lamboeuf, 1989, 1991; Kaningini, 1995) and none ever mentioned the presence of *L. tanganicus*. Presently, as shown by our experimental captures, the species, which retains its original preference for the littoral areas, has invaded the pelagic zone of Lake Kivu.

The occupation of pelagic waters by *L. tanganicus* in Lake Kivu is a behavior not observed in Lake Tanganyika, where the species is mainly present in the rocky shore but rarely in the pelagic area (Coulter, 1991). The occupation of the pelagic niche in Lake Tanganyika is probably prevented by biotic interactions, i.e., competition and/or predation, with native species. The recent Lake Kivu dates from Late

Pleistocene (25,000–20,000 years BP according to Beadle, 1981; 14,000–11,000 years BP according to Pouclet, 1978) while Lake Tanganyika communities have evolved for at least 9–12 million years (Cohen et al., 1993). In Lake Tanganyika, pelagic piscivorous fishes (e.g., *Lates stappersii* (Boulenger, 1914); *Lates microlepis* Boulenger, 1898) are present and feed upon *L. miodon* and *Stolothrissa tanganicae* Regan, 1917 shoals (Coulter, 1991). The absence of large predators in Lake Kivu most probably allowed *L. tanganicus* to successfully colonize new habitats, including the pelagic area where it found fewer competitors (most of native fish in Lake Kivu are confined to the littoral zone; Snoeks et al., 1997) and more abundant mesozooplankton (Isumbusho et al., 2004; Isumbusho et al., 2006a).

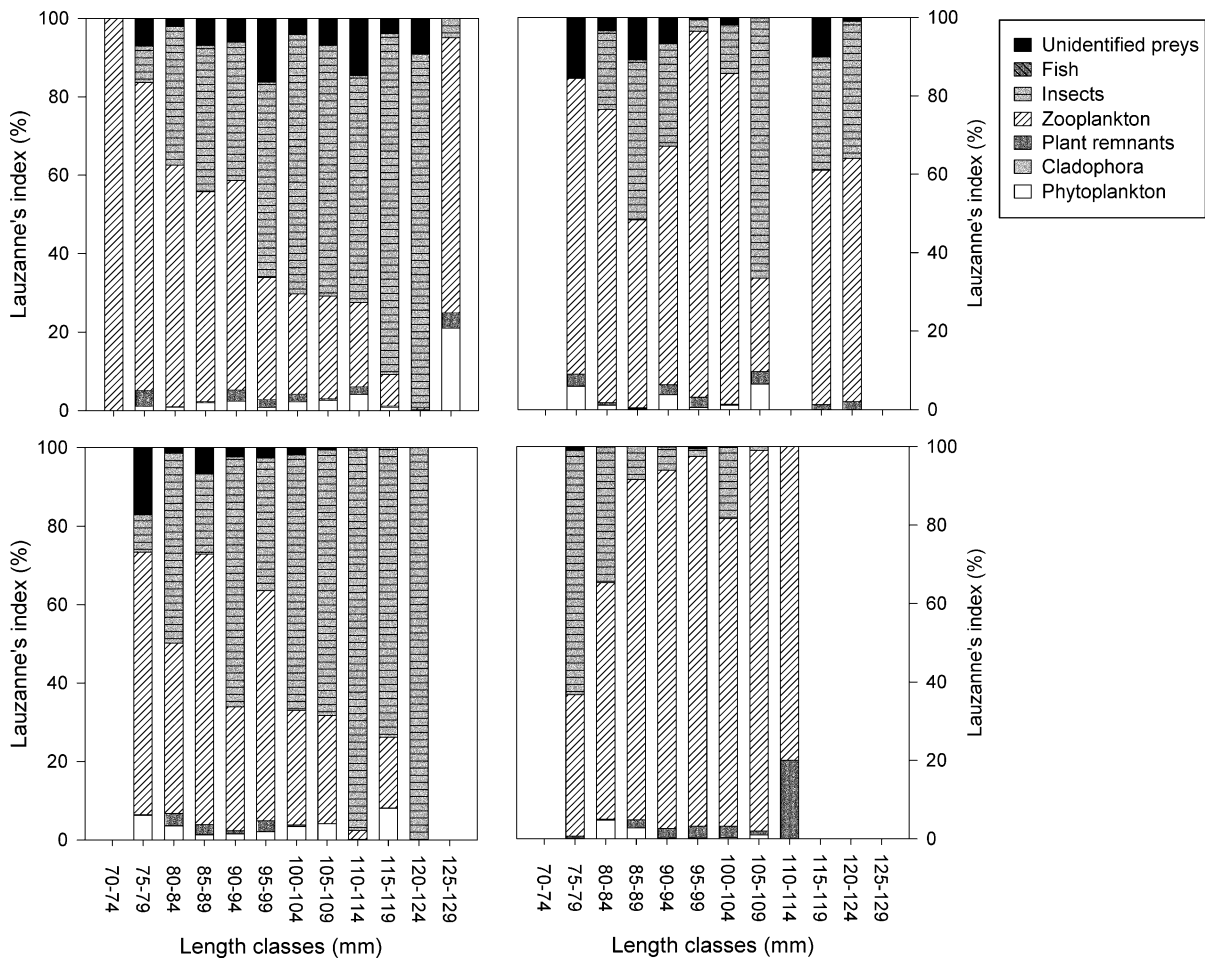


Fig. 3 Percentage of Lauzanne’s index of broad taxonomic groups for different length classes of adults *Lamprichthys tanganicanus* from the littoral (left panels) and pelagic (right

panels) stations of Lake Kivu during rainy (upper panels) and dry season (lower panels)

Our results show that *L. miodon*, despite being primarily a zooplanktivore, feeds on diverse prey in Lake Kivu, including phytoplankton, insects, and fishes, as previously reported by other authors (de Iongh et al., 1983; Isumbisho et al., 2004; Masilya et al., 2005). This ability to feed on various resources was already mentioned by those who studied *L. miodon* in the other lakes where the species was also introduced, i.e., lakes Kariba and Cahora Bassa (Mandima, 1999, 2000). The diet of *L. miodon* varies with habitat and size (de Iongh et al., 1983; Mandima, 2000): small fish essentially present in pelagic waters ingest mainly zooplankton, while larger fish tend to move inshore, where the contribution of floating insects increases in their diet. By contrast, most size classes of *L. tanganicanus* consumed mesozooplankton, even though for

littoral specimens the share of mesozooplankton in the guts decreased with size and was replaced by insects. The presence of copepods in the gut contents of *L. tanganicanus* from Lake Kivu were reported also by Lushombo & Nshombo (2008). Its important to note that food types as terrestrial plant remnants and benthic algae seemed to have been incidentally ingested.

The analysis of gut contents from both species suggests their opportunistic feeding in Lake Kivu. This behavior may be related to the scarce resources in the lake (Isumbisho et al., 2006a; Sarmiento et al., 2009). Evidence of opportunistic feeding in both species is provided by the high contribution of insects, when they are present, in the diet of the largest specimen along the littoral zone (see Figs. 2 and 3) as well as by the high diet overlap index in dry

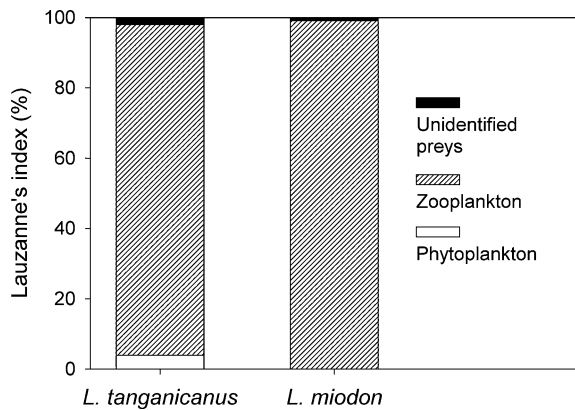


Fig. 4 Percentage of Lauzanne's index of broad taxonomic groups for larvae of *Limnothrissa miodon* and *Lamprichthys tanganicanus* of Lake Kivu

season when bigger zooplankton are abundant and zooplankton biomass high than in rainy season (Isumbisho et al., 2006a). Opportunistic feeding on large prey is a common behavior in freshwater fishes (Lazzaro, 1987) and is explained by the optimal foraging theory (Persson, 1985; Lazzaro et al., 2009).

The high diet overlap observed at all times in the pelagic zone suggests a significant niche overlap between *L. miodon* and *L. tanganicanus*. Several authors used Pianka's index or other indexes for estimating diet overlap between fish species (Qin et al., 2007; Corrêa et al., 2009), with contrasting conclusions in terms of interspecific competition. In theory, we may expect low or absence of food competition, whatever the degree of diet overlap observed, between species which have coexisted in the same environment for a long time (Sale, 1974; Genner et al., 1999) or which live in productive systems where resources are abundant (Dolbeth et al., 2008; Macneale et al., 2010). Pianka as well as Sale discussed this point, insisting that high diet overlap between two species may indicate competition only where and when available food resources are limited (Pianka, 1974; Sale, 1974). Accordingly, Sampson et al. (2009) and Museth et al. (2010) concluded from their studies of interactions between introduced fish species in various systems that high diet overlap did not necessarily point to effective competition. Moreover, resource use and habitat occupation by an introduced species may change with time (e.g., Museth et al., 2010), depending on the interactions with the species already present in the system. The

same situation can also be observed with a native species after an introduction of an exotic species (Qin et al., 2007).

Lake Kivu is a low-productivity lake, as a result of low nutrient concentration, limiting primary production (Sarmiento et al., 2009). Moreover, a large fraction of the phytoplankton biomass is lost by sedimentation to the anoxic deep waters (Pasche, 2009). Another significant fraction is composed of picoplankton (Sarmiento et al., 2008), on which mesozooplankton cannot feed directly (Hansen et al., 1994). The mesozooplankton diversity is low, with four main crustacean species which present large variations over an annual cycle, and an efficient grazer is missing (Isumbisho et al., 2006a). Actually, the pelagic zone of Lake Kivu harbors a low zooplankton biomass most of the time, except for the relatively short-lived increase of primary production of the dry season (June–August), on which mesozooplankton and fish production heavily depend (Isumbisho et al., 2006a). In this context, it is very likely that competition for food resources between *L. tanganicanus* and *L. miodon* is strong in the pelagic zone of Lake Kivu, where both species consume essentially mesozooplankton. This likely food competition for resources must still be higher in the littoral zone between the young stages of these species, exclusively zooplanktivorous, as in this zone of lake, zooplankton is less abundant than in pelagic zone (Isumbisho et al., 2004, 2006a). If so, we assume that this could have a negative effect on the survival rates of the young stages of these species and consequently on the future of their populations.

The outcome of interspecific competition is theoretically competitive exclusion of the less efficient species (e.g., Qin et al., 2007), but prediction at this stage remains risky. However, a likely outcome in the years to come is that the pelagic fishery yield, which is relatively low in Lake Kivu (Roest, 1999), is going to be negatively affected by the introduction and the consecutive expansion of *L. tanganicanus*. Therefore, continued monitoring of the stock of the two species is needed, as well as the study of their interactions.

Acknowledgments This study was financed by the Commission Universitaire pour le Développement de la Communauté française de Belgique through the ECOSYKI Project and by the University of Namur through the Ph.D. scholarship to Pascal Masilya. François Darchambeau is a Postdoctoral researcher of the Belgian National Fund for

Scientific Research. The authors are grateful to Mrs Georges Alunga Lufungula, Pitchou Munini M'Mende, and Kisekelwa Tchalondawa for field and laboratory assistance. Thanks to two anonymous reviewers for their many useful suggestions and comments to improve this article.

References

- Bănar, D. & M. Harmelin-Vivien, 2009. Feeding behaviour of Black Sea bottom fishes: did it change over time? *Acta Oecologica* 35: 769–777.
- Beadle, L. C., 1981. *The Inland Waters of Tropical Africa, an Introduction to Tropical Limnology*, 2nd ed. Longman, London.
- Cohen, A. S., M. J. Soreghan & C. A. Scholz, 1993. Estimating the age of formation of lakes – an example from Lake Tanganyika, East-African rift system. *Geology* 21: 511–514.
- Collart, A., 1960. L'introduction du *Stolothrissa tanganyicae* (Ndagala) au lac Kivu. *Bulletin Agricole du Congo LI*: 975–986.
- Corrêa, C. A., N. S. Hahn & R. L. Delariva, 2009. Extreme trophic segregation between sympatric fish species: the case of small sized body *Aphyocharax* in the Brazilian Pantanal. *Hydrobiologia* 635: 57–65.
- Coulter, G. W., 1991. Pelagic and the benthic fish community. In Coulter, G. W. (ed.), *Lake Tanganyika and Its Life*. Natural History Museum Publications/Oxford University Press, London: 111–138, 151–199.
- de Jongh, H. H., P. C. Spliethoff & V. G. Frank, 1983. Feeding habits of the clupeid *Limnothrissa miodon* (Boulenger), in Lake Kivu. *Hydrobiologia* 102: 113–122.
- Degens, E., R. P. Herzen, H.-K. Wong, W. G. Deuser & H. W. Jannasch, 1973. Lake Kivu: structure, chemistry and biology of an East African rift lake. *Geologische Rundschau* 62: 245–277.
- Dolbeth, M., F. Martinho, R. Leitao, H. Cabral & M. A. Pardal, 2008. Feeding patterns of the dominant benthic and demersal fish community in a temperate estuary. *Journal of Fish Biology* 72: 2500–2517.
- Dumont, H. J., 1986. The Tanganyika sardine in Lake Kivu: another ecodisaster for Africa? *Environmental Conservation* 13: 143–148.
- Genner, M. J., G. F. Turner & S. J. Hawkins, 1999. Foraging of rocky habitat cichlid fishes in Lake Malawi: coexistence through niche partitioning? *Oecologia* 121: 283–292.
- Gozlan, R. E., 2008. Introduction of non-native freshwater fish: is it all bad? *Fish and Fisheries* 9: 106–115.
- Guillard, J., 2009. Estimation de l'abondance du stock de *Limnothrissa miodon* dans le lac Kivu au cours de deux campagnes : février et juillet 2008. Rapport ECOSYKI, Commission Universitaire pour le Développement, Communauté Française de Belgique.
- Hansen, B., P. K. Bjørnsen & P. J. Hansen, 1994. The size ratio between planktonic predators and their prey. *Limnology and Oceanography* 39: 395–403.
- Hyslop, E. J., 1980. Stomach contents analysis – a review of methods and their application. *Journal of Fish Biology* 17: 411–429.
- Isumbisha, M., M. Kaningini, J.-P. Descy & E. Baras, 2004. Seasonal and diel variations in diet of the young stages of *Limnothrissa miodon* in Lake Kivu, Eastern Africa. *Journal of Tropical Ecology* 20: 73–83.
- Isumbisha, M., H. Sarmento, B. Kaningini, J.-C. Micha & J.-P. Descy, 2006a. Zooplankton of Lake Kivu, East Africa, half a century after the Tanganyika sardine introduction. *Journal of Plankton Research* 28: 971–989.
- Isumbisha, M., H. Sarmento & J.-P. Descy, 2006b. Qualitative composition of the pelagic mesozooplankton in Lake Kivu, eastern Africa: impact of *Limnothrissa miodon* introduction. In Isumbisha, M. (ed.), *Zooplankton Ecology of Lake Kivu (Eastern Africa)*. PhD thesis, Presses Universitaires de Namur, Belgium: 39–55.
- Kaningini, M., 1995. Etude de la croissance, de la reproduction et de l'exploitation de *Limnothrissa miodon* au lac Kivu, bassin de Bukavu (Zaïre). Faculté de Sciences, Thèse, Facultés Universitaires Notre Dame de la Paix, Namur, Belgique.
- Lamboeuf, M., 1989. Estimation de l'abondance du stock d'Isambaza (*Limnothrissa miodon*), résultats de la prospection acoustique de septembre 1989. *Projet/RWA/87/012*: 13 pp.
- Lamboeuf, M., 1991. Abondance et répartition du *Limnothrissa miodon* du lac Kivu, résultat des prospections acoustiques d'avril 1989 à juin 1991. *DOC/TR NO. RWA/87/012/DOC/TR/46 (Fr)*. FAO.
- Lauzanne, L., 1976. Régimes alimentaires et relations trophiques des poissons du lac Tchad. *Cahiers Orstom, Série Hydrobiologie* 10: 267–310.
- Lazzaro, X., 1987. A review of planktivorous fishes: their evolution, feeding behaviours, selectivities, and impacts. *Hydrobiologia* 146: 97–167.
- Lazzaro, X., G. Lacroix, B. Gauzens, J. Gignoux & S. Legendre, 2009. Predator foraging behaviour drives food-web topological structure. *Journal of Animal Ecology* 78: 1307–1317.
- Lévêque, C., 1997. Introductions de nouvelles espèces de poissons dans les eaux douces tropicales : objectifs et conséquences. *Bulletin Française de Pêche et de Pisciculture* 344(345): 79–91.
- Lodge, D. M., R. A. Stein, K. M. Brown, A. R. Covich, C. Brönmark, J. E. Garvey & S. P. Klosiewski, 1998. Predicting impact of freshwater exotic species on native biodiversity: challenges in spatial scaling. *Australian Journal of Ecology* 23: 53–67.
- Lushombo, M. & M. Nshombo, 2008. Apparition au lac Kivu du poisson *Lamprichthys tanganyicanus* (Poeciliidae), espèce endémique du lac Tanganyika. *Annales des Sciences de l'Université Officielle de Bukavu* 1: 1–5.
- Macneale, K. H., B. L. Sanderson, J.-Y. P. Courbois & P. M. Kiffney, 2010. Effects of non-native brook trout (*Salvelinus fontinalis*) on threatened juvenile Chinook salmon (*Oncorhynchus tshawytscha*) in an Idaho stream. *Ecology of Freshwater Fish* 19: 139–152.
- Mandima, J. J., 1999. The food and feeding behaviour of *Limnothrissa miodon* (Boulenger, 1906) in Lake Kariba, Zimbabwe. *Hydrobiologia* 407: 175–182.
- Mandima, J. J., 2000. Spatial and temporal variations in the food of the sardine *Limnothrissa miodon* (Boulenger,

- 1906) in Lake Kariba, Zimbabwe. Fisheries Research 48: 197–203.
- Masilya, P., B. Kaningini, P. Isumbisho, J.-C. Micha & G. Ntakimazi, 2005. Food and feeding activity of *Limnothrissa miodon* (Boulenger, 1906) in the southern part of Lake Kivu, Central Africa. In International Conference Africa's Great Rift: Diversity and Unity. Royal Academy for Overseas Sciences Royal Museum for Central Africa, Brussels, 29–30 September, 2005: 83–93.
- Muderhwa, N. & L. Matabaro, 2010. The introduction of the endemic fish species, *Lamprichthys tanganicanus* (Poeciliidae), from Lake Tanganyika into Lake Kivu: possible causes and effects. Aquatic Ecosystem Health and Management 13: 203–213.
- Museth, J., R. Borgström & J. E. Brittain, 2010. Diet overlap between introduced European minnow (*Phoxinus phoxinus*) and young brown trout (*Salmo trutta*) in the lake, Øvre Heimdalsvatn: a result of abundant resources or forced niche overlap? Hydrobiologia 642: 93–100.
- Ogutu-Ohwayo, R., R. E. Hecky, A. S. Cohen & L. Kaufman, 1997. Human impacts on the African Great Lakes. Environmental Biology of Fishes 50: 117–131.
- Pardo, R., I. Vila & J. J. Capella, 2009. Competitive interaction between introduced rainbow trout and native silverside in a Chilean stream. Environmental Biology of Fishes 86: 353–359.
- Pasche, N., 2009. Nutrient Cycling and Methane Production in Lake Kivu. Thèse de Doctorat, Swiss Federal Institute of Technology, Zurich.
- Persson, L., 1985. Optimal foraging: the difficulty of exploiting different feeding strategies simultaneously. Oecologia (Berlin) 67: 338–341.
- Pianka, E. R., 1974. Niche overlap and diffuse competition. Proceedings of the National Academy of Sciences 71: 2141–2145.
- Poucllet, A., 1978. Les communications entre les grands lacs de l'Afrique centrale. Implications sur la structure du rift occidental. Musée royal d'Afrique centrale, Département de Géologie et Minéralogie. Rapport annuel 1977: 145–155.
- Preikshot, D., E. Nsiku, T. Pitcher & D. Pauly, 1998. An interdisciplinary evaluation of the status and health of African lake fisheries using a rapid appraisal technique. Journal of Fish Biology 53: 381–393.
- Qin, J., J. Xu & P. Xie, 2007. Diet overlap between the endemic fish *Anabarilius grahami* (Cyprinidae) and the exotic noodlefish *Neosalanx taihuensis* (Salangidae) in Lake Fuxian, China. Journal of Freshwater Ecology 22: 365–370.
- R Development Core Team, 2005. R: A Language and Environment for Statistical Computing, Reference Index Version 2.2.1. R Foundation for Statistical Computing, Vienna, Australia. ISBN 3-900051-07-0. <http://www.R-project.org>.
- Roest, F. C., 1999. Introduction of a pelagic fish into a large natural Lake: Lake Kivu, Central Africa. In van Densen, W. L. T. & M. J. Morris (eds), Fish and Fisheries of Lakes and Reservoirs in Southeast Asia and Africa. Westbury Publishing, Otley: 327–338.
- Rosecchi, E. & Y. Nouazé, 1987. Comparaison de cinq indices alimentaires utilisés dans l'analyse des contenus stomacaux. Revue des Travaux de l'Institut des Pêches Maritimes 49: 111–123.
- Sale, F. P., 1974. Overlap in resource use, and interspecific competition. Oecologia (Berlin) 17: 245–256.
- Sampson, S. J., J. H. Chick & M. A. Pegg, 2009. Diet overlap among two Asian carp and three native fishes in backwater lakes on the Illinois and Mississippi rivers. Biological Invasions 11: 483–496.
- Sarmiento, H., M. Leitao, M. Stoyneva, P. Compère, A. Couté, M. Isumbisho & J.-P. Descy, 2007. Species diversity of pelagic algae in Lake Kivu (East Africa). Cryptogamie and Algologie 28: 245–269.
- Sarmiento, H., F. Unrein, I. Mwapu, S. Sténuite, J. M. Gasol & J.-P. Descy, 2008. Abundance and distribution of picoplankton in tropical, oligotrophic Lake Kivu, eastern Africa. Freshwater Biology 53: 756–771.
- Sarmiento, H., M. Isumbisho, S. Sténuite, F. Darchambeau, B. Leporcq & J.-P. Descy, 2009. Phytoplankton ecology of Lake Kivu (eastern Africa): biomass, production and elemental ratios. Verhandlungen des Internationalen Verein Limnologie 30: 709–713.
- Snoeks, J., L. De Vos & D. Thys van den Audenaerde, 1997. The ichthyogeography of Lake Kivu. South African Journal of Science 93: 579–584.
- Tachet, H., M. Bournaud & P. Richoux, 1980. Introduction à l'étude des macroinvertébrés des eaux douces (Systématique élémentaire et aperçu écologique). Association Française de Limnologie, Lyon, France.
- Verbeke, J., 1957. Exploration hydrobiologique des lacs Kivu, Edouard et Albert. Recherches Ecologiques sur la faune des Grands Lacs de l'est du Congo Belge, Vol. III. Institut Royal des Sciences Naturelles de Belgique, Bruxelles.



Biogeochemistry of a large and deep tropical lake (Lake Kivu, East Africa: insights from a stable isotope study covering an annual cycle

C. Morana¹, F. Darchambeau², F. A. E. Roland², A. V. Borges², F. Muvundja^{3,4}, Z. Kelemen¹, P. Masilya⁴, J.-P. Descy³, and S. Bouillon¹

¹Department of Earth and Environmental Sciences, Katholieke Universiteit Leuven, Leuven, Belgium

²Chemical Oceanography Unit, Université de Liège, Liège, Belgium

³Research Unit in Environmental and Evolutionary Biology, Université de Namur, Namur, Belgium

⁴Unité d'Enseignement et de Recherche en Hydrobiologie Appliquée, ISP-Bukavu, Bukavu, Democratic Republic of the Congo

Correspondence to: C. Morana (cedric.morana@ees.kuleuven.be)

Received: 14 October 2014 – Published in Biogeosciences Discuss.: 11 December 2014

Revised: 23 July 2015 – Accepted: 9 August 2015 – Published: 19 August 2015

Abstract. During this study, we investigated the seasonal variability of the concentration and the stable isotope composition of several inorganic and organic matter (OM) reservoirs in the large, oligotrophic and deep tropical Lake Kivu (East Africa). Data were acquired over 1 year at a fortnightly temporal resolution. The $\delta^{13}\text{C}$ signature of the dissolved inorganic carbon (DIC) increased linearly with time during the rainy season, then suddenly decreased during the dry season due to vertical mixing with ^{13}C -depleted DIC waters. The $\delta^{13}\text{C}$ signature of the particulate organic carbon pool (POC) revealed the presence of a consistently abundant methanotrophic biomass in the oxycline throughout the year. We also noticed a seasonal shift during the dry season toward higher values in the $\delta^{15}\text{N}$ of particulate nitrogen (PN) in the mixed layer and $\delta^{15}\text{N}$ -PN was significantly related to the contribution of cyanobacteria to the phytoplankton assemblage, suggesting that rainy season conditions could be more favourable to atmospheric nitrogen-fixing cyanobacteria. Finally, zooplankton were slightly enriched in ^{13}C compared to the autochthonous POC pool, and the $\delta^{15}\text{N}$ signature of zooplankton followed well the seasonal variability in $\delta^{15}\text{N}$ -PN, consistently 3.0 ± 1.1 ‰ heavier than the PN pool. Together, $\delta^{13}\text{C}$ and $\delta^{15}\text{N}$ analysis suggests that zooplankton directly incorporate algal-derived OM in their biomass, and that they rely almost exclusively on this source of OM throughout the

year in general agreement with the very low allochthonous OM inputs from rivers in Lake Kivu.

1 Introduction

Stable carbon (C) and nitrogen (N) isotope analyses of diverse inorganic and organic components have been successfully used to assess the origin of organic matter (OM) and better understand its cycling in aquatic systems (Lehmann et al., 2004). For instance, an extensive sampling of diverse C and N pools over an annual cycle in the Loch Ness showed important seasonal variation of the $^{13}\text{C}/^{12}\text{C}$ and $^{15}\text{N}/^{14}\text{N}$ ratios in the crustacean zooplankton biomass, reflecting a diet switch from allochthonous to autochthonous OM sources (Grey et al., 2001). In small humic boreal lakes with permanently anoxic waters, stable C isotope analyses demonstrated that methanotrophic bacteria could be an important food source for crustacean zooplankton, and hence methane-derived C contributed to a large fraction of the lake food web (Kankaala et al., 2006). Analyses of the stable C isotope composition of carbonates and OM in sedimentary records of stratified lakes can also provide reliable information about past land use of the catchment (Castañeda et al., 2009), or be used to infer changes in lake productivity and climate (Schelske and Hodell, 1991). However, a detailed un-

derstanding of the stable isotope dynamics in the water column is a prerequisite for a good interpretation of isotope data from sedimentary archives (Lehmann et al., 2004).

A new paradigm has progressively emerged over the last decade, proposing that freshwaters ecosystems are predominantly net heterotrophic, as respiration of OM exceeds autochthonous photosynthetic production (Del Giorgio et al., 1997; Cole, 1999; Duarte and Prairie, 2005). This concept seems to hold especially true for oligotrophic unproductive ecosystems (Del Giorgio et al., 1997), that are subsidised by substantial inputs of allochthonous OM of terrestrial origin, which support the production of heterotrophic organisms. Net heterotrophy has been recognised as one of the main cause for the net emission of carbon dioxide (CO₂) from freshwater ecosystems to the atmosphere (Prairie et al., 2002), although there is growing evidence of the contribution from external hydrological CO₂ inputs from the catchment (Stets et al., 2009; Finlay et al., 2010; Borges et al., 2014; Marcé et al., 2015). However, the current understanding of the role of inland waters on CO₂ emissions could be biased because most observations were obtained in temperate and boreal systems, and mostly in medium-to-small lakes, during open-water (ice-free) periods, but tropical and temperate lakes differed in some fundamental characteristics. Among them, the constantly high temperature and irradiance have strong effects on water column stratification and biological processes (Sarmiento, 2012). For instance, primary production in tropical lakes has been recognised to be 2 times higher than in temperate lakes on a given nutrient base (Lewis, 1996). Also, the contribution of dissolved primary production in oligotrophic tropical lakes has been found to be substantially more important than in their temperate counterparts (Morana et al., 2014).

East Africa harbours the densest aggregation of large tropical lakes (Bootsma and Hecky, 2003). Some of them are among the largest (lakes Victoria, Tanganyika, Malawi), and deepest lakes in the world (lakes Tanganyika, Malawi, Kivu) and consequently remain stratified all year round. Due to the size and the morphometric traits of the East African Great Lakes, pelagic processes are predominant in these systems, with the microbial food web playing a particularly essential role in OM transfer between primary producers and higher levels of the food web, and in nutrient cycling (Descy and Sarmiento, 2008). Most of them are also characterized by highly productive fisheries that provide an affordable food source to local populations (Descy and Sarmiento, 2008). However, while these lakes are potentially important components of biogeochemical cycles at the regional scale (Borges et al., 2011), and significant for local populations from an economic perspective (Kaningini, 1995), the East African Great Lakes are relatively poorly studied, most probably because of their remote location combined with frequent political unrest.

In this study, we present a comprehensive data set covering a full annual cycle, including hydrochemical data and mea-

surements of the concentration of dissolved methane (CH₄) and the concentrations and stable isotope compositions of dissolved inorganic carbon (DIC), dissolved and particulate organic carbon (DOC and POC), particulate nitrogen (PN), and zooplankton. Data were acquired over one full year at a fortnightly/monthly temporal resolution. We aimed to assess the net metabolic status of Lake Kivu, the seasonal and depth variability of sources of OM within the water column, and the relative contribution of autochthonous or allochthonous OM to the zooplankton. To our best knowledge, this is the first detailed study to assess the seasonal dynamics of different OM reservoirs by means of their stable isotope composition in any of the East African Great Lakes. The detailed analysis of the stable isotope composition of diverse organic and inorganic components carried out during this study allowed one to trace the OM dynamics in Lake Kivu over a seasonal cycle, and might be useful to improve the interpretation of sedimentary archives of this large and deep tropical lake.

2 Material and methods

Lake Kivu (East Africa) is a large (2370 km²) and deep (maximum depth of 485 m) meromictic lake located at the border between the Democratic Republic of the Congo and Rwanda. Its vertical structure consists of an oxic and nutrient-poor mixed layer down to a maximum depth of 70 m, and a permanently anoxic monimolimnion rich in dissolved gases (CH₄, and CO₂) and inorganic nutrients. Seasonal variation of the vertical position of the oxic–anoxic transition is driven by contrasting air humidity and incoming long-wave radiation between rainy (October–May) and dry (June–September) seasons (Thiery et al., 2014). The euphotic zone, defined at the depth at which light is 1% of surface irradiance, is relatively shallow (annual average: 18 m, Darchambeau et al., 2014).

Sampling was carried out in the southern basin (02°20' S, 28°58' E) of Lake Kivu between January 2012 and May 2013 at a monthly or fortnightly time interval. Vertical oxygen (O₂), temperature and conductivity profiles were obtained with a Hydrolab DS5 multiprobe. The conductivity cell was calibrated with a 1000 μS cm⁻¹ (25 °C) Merck standard and the O₂ membrane probe was calibrated with humidity saturated ambient air. Water was collected with a 7 L Niskin bottle (Hydro-Bios) at a depth interval of 5 m from the lake surface to the bottom of the mixolimnion, at 70 m. Additionally, zooplankton was sampled with a 75 cm diameter, 55 μm mesh plankton net hauled along the whole mixolimnion (0–70 m).

Samples for CH₄ concentrations were collected in 50 mL glass serum bottles from the Niskin bottle with a tube, left to overflow, poisoned with 100 μL of saturated HgCl₂ and sealed with butyl stoppers and aluminium caps. Concentrations of CH₄ were measured by headspace technique using gas chromatography (Weiss, 1981) with flame ionisation de-

tection (SRI 8610C), after creating a 20 mL headspace with N₂ in the glass serum bottles, and then analysed as described by Borges et al. (2011).

Samples for stable C isotopic composition of dissolved inorganic carbon ($\delta^{13}\text{C-DIC}$) were collected by filling water directly from the Niskin bottle 12 mL headspace vials (Labco Exetainer) without bubbles. Samples were preserved with the addition of 20 μL of a saturated HgCl₂ solution. Prior to the analysis of $\delta^{13}\text{C-DIC}$, a 2 mL helium headspace was created, and 100 μL of phosphoric acid (H₃PO₄, 99 %) was added in the vial in order to convert all inorganic C species to CO₂. After overnight equilibration, 200 μL of gas was injected with a gastight syringe into a elemental analyser – isotopic ratio mass spectrometer (EA-IRMS; Thermo FlashHT with Thermo DeltaV Advantage). The obtained data were corrected for isotopic equilibration between dissolved and gaseous CO₂ as described in Gillikin and Bouillon (2007). Calibration of $\delta^{13}\text{C-DIC}$ measurement was performed with the international certified standards IAEA-CO1 and LSVEC. The reproducibility of $\delta^{13}\text{C-DIC}$ measurement was typically better than $\pm 0.2\%$. Measurements of total alkalinity (TA) were carried out by open-cell titration with HCl 0.1 mol L⁻¹ according to Gran (1952) on 50 mL water samples, and data were quality checked with certified reference material obtained from Andrew Dickinson (Scripps Institution of Oceanography, University of California, San Diego, USA). Typical reproducibility of TA measurements was better than $\pm 3\ \mu\text{mol L}^{-1}$. DIC concentration was computed from pH and TA measurements using the carbonic acid dissociation constants of Millero et al. (2006).

Samples for DOC concentration and stable C isotopic composition ($\delta^{13}\text{C-DOC}$) were filtered through pre-flushed 0.2 μm syringe filters, kept in 40 mL borosilicate vials with Teflon-coated screw caps and preserved with 100 μL of H₃PO₄ (50 %). Sample analysis was carried out with a IO Analytical Aurora 1030W coupled to an IRMS (Thermo delta V Advantage). Quantification and calibration of DOC and $\delta^{13}\text{C-DOC}$ was performed with IAEA-C6 and an internal sucrose standard ($\delta^{13}\text{C} = -26.99 \pm 0.04\%$) calibrated against international reference materials.

Samples for POC and particulate nitrogen (PN) concentration and stable carbon and nitrogen isotope composition ($\delta^{13}\text{C-POC}$; $\delta^{15}\text{N-PN}$) were obtained by filtering a known volume of water on pre-combusted (overnight at 450 °C) 25 mm glass fiber filters (Advantec GF-75; 0.3 μm), kept frozen until subsequent processing. The filters were later decarbonated with HCl fumes for 4 h, dried and packed in silver cups prior to analysis on a EA-IRMS (Thermo FlashHT with Thermo DeltaV Advantage). Calibration of $\delta^{13}\text{C-POC}$, $\delta^{15}\text{N-PN}$, POC and PN measurements was performed with acetanilide ($\delta^{13}\text{C} = -27.65 \pm 0.05$; $\delta^{15}\text{N} = 1.34 \pm 0.04$) and leucine ($\delta^{13}\text{C} = -13.47 \pm 0.07$; $\delta^{15}\text{N} = 0.92 \pm 0.06$) as standards. All standards were internally calibrated against the international standard IAEA-C6 and IAEA-N1. Reproducibility of $\delta^{13}\text{C-POC}$ and $\delta^{15}\text{N-PN}$

measurement was typically better than $\pm 0.2\%$ and relative standard deviation for POC and PN measurement were always below 5 %. Samples for $\delta^{13}\text{C}$ and $\delta^{15}\text{N}$ of zooplankton were collected on precombusted 25 mm glass fiber filters (Advantec GF-75; 0.3 μm), and dried. Subsequent preparation of the samples and analysis on the EA-IRMS were performed similarly as described for the $\delta^{13}\text{C-POC}$ and $\delta^{15}\text{N-PN}$ samples.

Pigment concentrations were determined by high performance liquid chromatography (HPLC). 2–4 L of water were filtered through Macherey-Nägel GF-5 filter (average retention of 0.7 μm). Pigment extraction was carried out in 10 mL of 90 % HPLC grade acetone. After two sonication steps of 15 min separated by an overnight period at 4 °C, the pigments extracts were stored in 2 mL amber vials at -25 °C. HPLC analysis was performed following the gradient elution method described in Wright et al. (1991), with a Waters system comprising photodiode array and fluorescence detectors. Calibration was made using commercial external standards (DHI Lab Products, Denmark). Reproducibility for pigment concentration measurement was better than 7 %. Pigment concentrations were processed with the CHEMTAX software (CSIRO Marine Laboratories) using input ratio matrices adapted for freshwater phytoplankton (Descy et al., 2000). Data processing followed a procedure similar to that of Sarmiento et al. (2006) in Lake Kivu that allows one to estimate chlorophyll *a* (Chl *a*) biomass of cyanobacteria, taking into account variation of pigment ratios with season and depth.

3 Results

Analysis of the vertical and seasonal variability of temperature and dissolved O₂ concentrations for 18 months allow us to divide the annual cycle into two distinct limnological periods. Rainy season conditions resulted in a thermal stratification within the mixolimnion (October–June) while the dry season was characterized by deeper vertical mixing of the water column down to the upper part of the permanent chemocline at 65 m (July–September) (Fig. 1a). The vertical position of the oxycline varied seasonally: the oxic–anoxic transition reached its deepest point (65 m) during the dry season, then became gradually shallower after the re-establishment of the thermal stratification within the mixolimnion at the start of the following rainy season to finally stabilise at approximately 35 m, corresponding to the bottom of the mixed layer during the rainy season (Fig. 1b). The temporal variability of the vertical distribution of CH₄ corresponded well with the seasonal variation of the oxycline. The CH₄ concentrations were very high in the monimolimnion throughout the year (average at 70 m: $356 \pm 69\ \mu\text{mol L}^{-1}$, $n = 24$) but sharply decreased at the oxic–anoxic transition, and were 4 orders of mag-

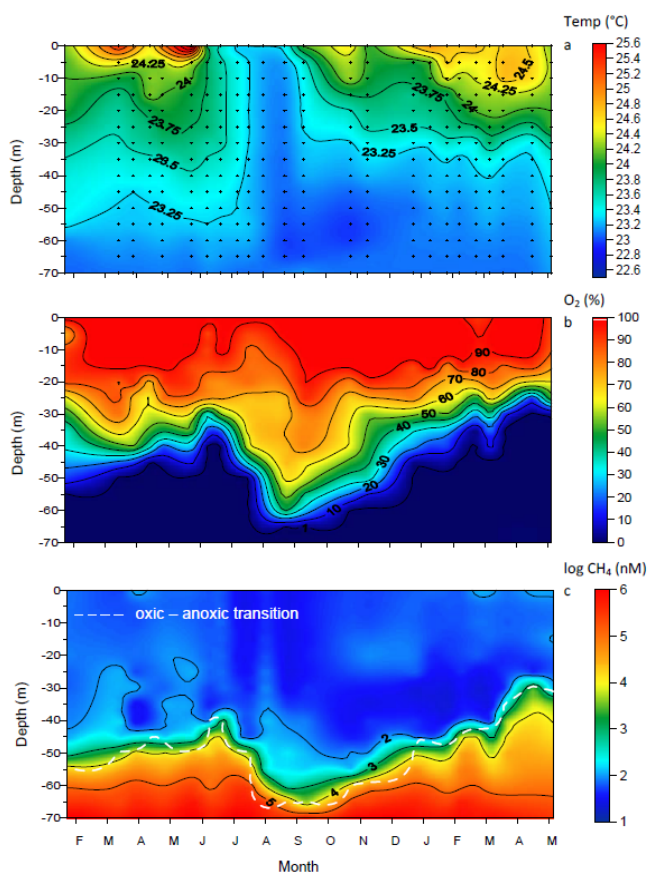


Figure 1. Temporal variability of (a) temperature ($^{\circ}\text{C}$), (b) oxygen saturation (in percentage), and (c) the log-transformed CH_4 concentration (nmol L^{-1}) in the mixolimnion of Lake Kivu, between February 2012 and May 2013. Small crosses in the figure (a) represent each sampling points. The white dashed line represents the vertical position of the oxic–anoxic transition.

nitude lower in surface waters (annual average at 10 m: $0.062 \pm 0.016 \mu\text{mol L}^{-1}$, $n = 24$) (Fig. 1c).

DIC concentrations in the mixed layer were very high (annual average at 10 m: $11.9 \pm 0.2 \text{ mmol L}^{-1}$, $n = 24$) and did not show any consistent seasonal pattern (not shown). The $\delta^{13}\text{C-DIC}$ values were vertically homogeneous in the mixed layer but gradually decreased in the oxycline to reach minimal values at 70 m (Fig. 2a). $\delta^{13}\text{C-DIC}$ values in the mixed layer increased linearly with time during the rainy season ($r^2 = 0.79$, $n = 12$), then suddenly decreased at the start of the dry season due to the vertical mixing with ^{13}C -depleted DIC from deeper waters (Fig. 2b). Taking into account the analytical precision of $\delta^{13}\text{C-DIC}$ measurement (better than $\pm 0.2\text{‰}$), this small but linear ^{13}C enrichment with time was significant. The DOC concentration ($142 \pm 20 \mu\text{mol CL}^{-1}$, $n = 304$) and $\delta^{13}\text{C-DOC}$ signature ($-23.2 \pm 0.4\text{‰}$, $n = 304$) did not show any consistent variations with depth or time in the mixolimnion over the entire sampling period. A vertical profile performed down

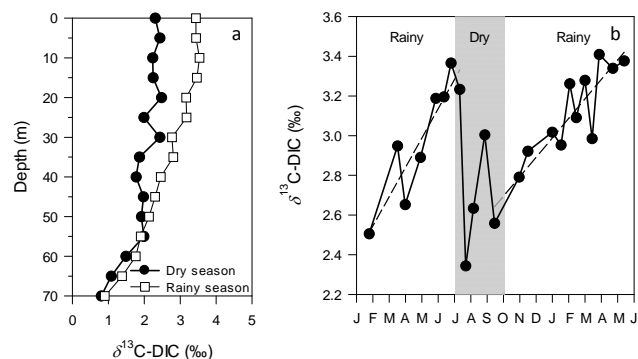


Figure 2. Depth profile of the $\delta^{13}\text{C}$ of the dissolved inorganic carbon (DIC) pool in the mixolimnion during the dry (18 July 2012) and the rainy (20 March 2013) season and (b) temporal variation of the $\delta^{13}\text{C-DIC}$ in the mixed layer of Lake Kivu between January 2012 and June 2013.

to the lake floor revealed that the $\delta^{13}\text{C-DOC}$ did not vary significantly in the monimolimnion (vertical profile average: $-23.0\text{‰} \pm 0.2$, $n = 18$, Fig. 3); however, an important increase in DOC concentrations was observed starting at 260 m (Fig. 3), to reach a maximum near the lake floor (350 m , $301 \mu\text{mol CL}^{-1}$).

Chlorophyll *a* concentrations exhibited little variation during the rainy season (average $74 \pm 15 \text{ mg Chl } a \text{ m}^{-2}$, $n = 16$) but increased significantly during the dry season to reach a maximal value ($190 \text{ mg Chl } a \text{ m}^{-2}$) in September 2012 (Fig. 5b). This increase corresponded with a change in phytoplankton community composition. The relative contribution of cyanobacteria to the phytoplankton assemblage, as assessed from the concentration of marker pigments, was smaller during the dry season than in the preceding (t test; $p < 0.01$, $\text{mean}_{\text{jan-jun}} = 23.4 \pm 5.5\%$, $\text{mean}_{\text{jul-sep}} = 9.4 \pm 1.3\%$) and the following (t test; $p < 0.05$, $\text{mean}_{\text{oct-may}} = 14.6 \pm 3.8\%$, $\text{mean}_{\text{jul-sep}} = 9.4 \pm 1.3\%$) rainy seasons (Fig. 5b).

4 Discussion

Stable isotope analysis of DIC is a useful tool for understanding the fate of C in aquatic ecosystems and could provide information on the lake metabolism, defined as the balance between gross primary production and community respiration of OM. Primary producers preferentially incorporate the lighter isotope (^{12}C) into the biomass with the consequence that the heavier isotope (^{13}C) accumulates into the DIC pool, whereas mineralisation releases ^{13}C -depleted CO_2 from the OM being respired into the DIC pool. Therefore, increasing primary production leads to higher $\delta^{13}\text{C-DIC}$ but increasing respiration should tend to decrease $\delta^{13}\text{C-DIC}$ (Bade et al., 2004). For instance, several studies conducted in temperate lakes have reported a significant increase in $\delta^{13}\text{C-DIC}$ during summer, resulting from primary production (Herczeg,

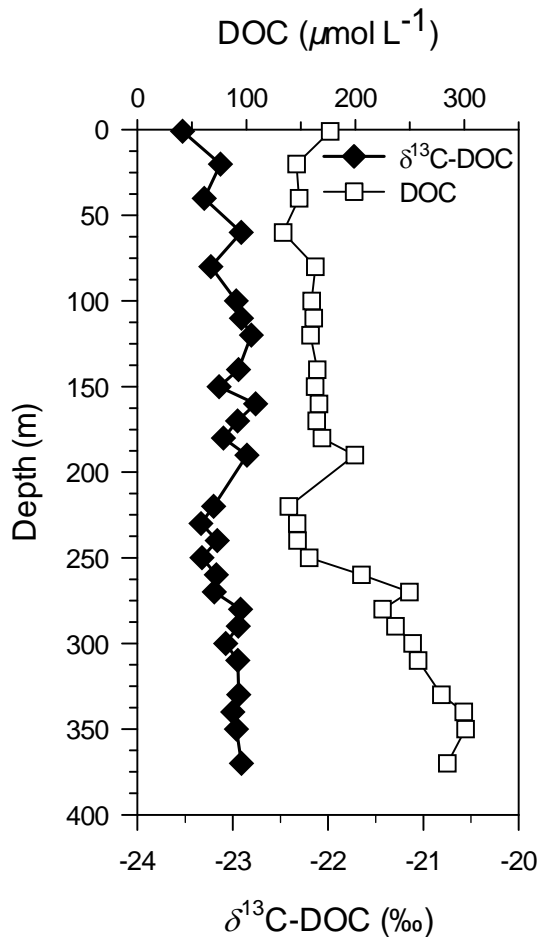


Figure 3. Depth profile from the lake surface to the lake floor of the dissolved organic carbon (DOC) concentration ($\mu\text{mol L}^{-1}$) and the $\delta^{13}\text{C}$ signature of the DOC pool, in September 2012. The white dashed line represents the vertical position of the oxic–anoxic transition.

1987; Hollander and McKenzie, 1991). In Lake Kivu, the $\delta^{13}\text{C}$ -DIC increased linearly with time during the stratified rainy season, deviating gradually from the $\delta^{13}\text{C}$ -DIC value expected if the DIC pool was at equilibrium with the atmospheric CO_2 ($\sim 0.49\text{‰}$). It appears unlikely that this linear isotopic enrichment of the DIC pool is due to physical processes: the $\delta^{13}\text{C}$ -DIC signature of the DIC input from the inflowing rivers (Borges et al., 2014) and deep waters (Fig. 3a) was indeed lower than the measured $\delta^{13}\text{C}$ -DIC in the mixed layer. Therefore, biological processes (i.e. photosynthetic CO_2 uptake) are likely responsible of the isotopic enrichment of the DIC pool observed during the stratified rainy season. Nevertheless, a small decrease in $\delta^{13}\text{C}$ -DIC was recorded at the beginning of the dry season (early in July 2012), but was concomitant with the characteristic deepening of the mixed layer observed during the dry season. As the depth profile of $\delta^{13}\text{C}$ -DIC revealed that the DIC pool was isotopically lighter in the bottom of the mixolimnion,

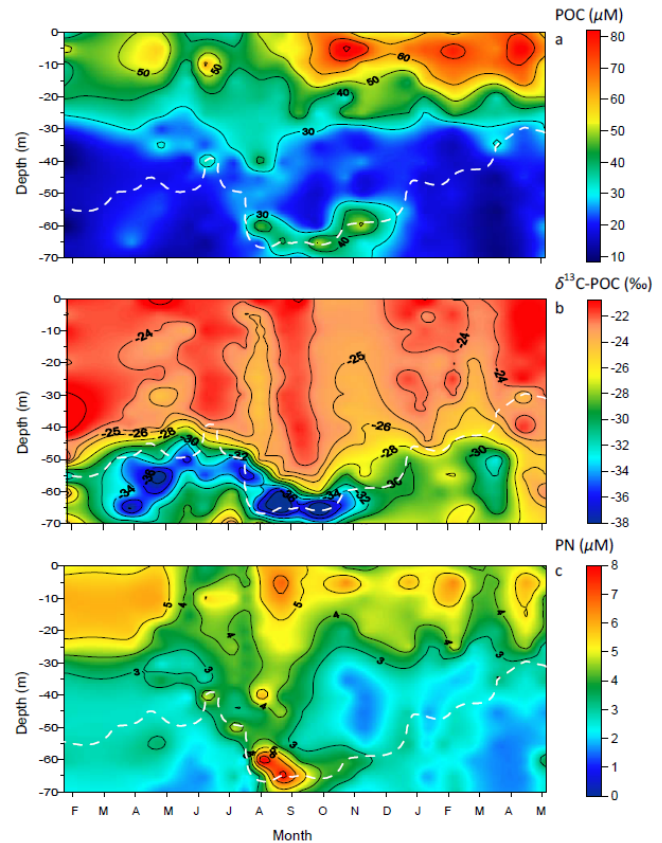


Figure 4. Temporal variability of (a) the particulate organic carbon (POC) concentration ($\mu\text{mol L}^{-1}$), (b) the $\delta^{13}\text{C}$ signature of the POC pool, and (c) the particulate nitrogen (PN) concentration ($\mu\text{mol L}^{-1}$) in the mixolimnion of Lake Kivu, between February 2012 and May 2013.

the measurement of lower $\delta^{13}\text{C}$ -DIC values during the dry season could have resulted from the seasonal vertical mixing of surface waters with bottom waters containing relatively ^{13}C -depleted DIC.

Overall, the data suggest that the input of DIC originating from the monimolimnion during the dry season had a strong influence on $\delta^{13}\text{C}$ -DIC in the mixolimnion, but the seasonal variability of $\delta^{13}\text{C}$ -DIC observed in the mixed layer holds information on biological processes. The gradual increase with time of the $\delta^{13}\text{C}$ -DIC in the mixed layer supports the conclusions of other studies carried out in Lake Kivu (Morana et al., 2014; Borges et al., 2014) which showed, based on a detailed DIC and DI^{13}C mass balance approach and several microbial processes measurements, that photosynthetic CO_2 fixation should exceed the respiration of OM. Indeed, in Lake Kivu, riverine inputs of allochthonous OM from the catchment ($0.7\text{--}3.3\text{ mmol m}^{-2}\text{ d}^{-1}$, Borges et al., 2014) are minimal compared to primary production ($49\text{ mmol m}^{-2}\text{ d}^{-1}$; Darchambeau et al., 2014) and the export of organic carbon to the monimolimnion ($9.4\text{ mmol m}^{-2}\text{ d}^{-1}$) reported by Pasche et al. (2010). The outflow of organic carbon through

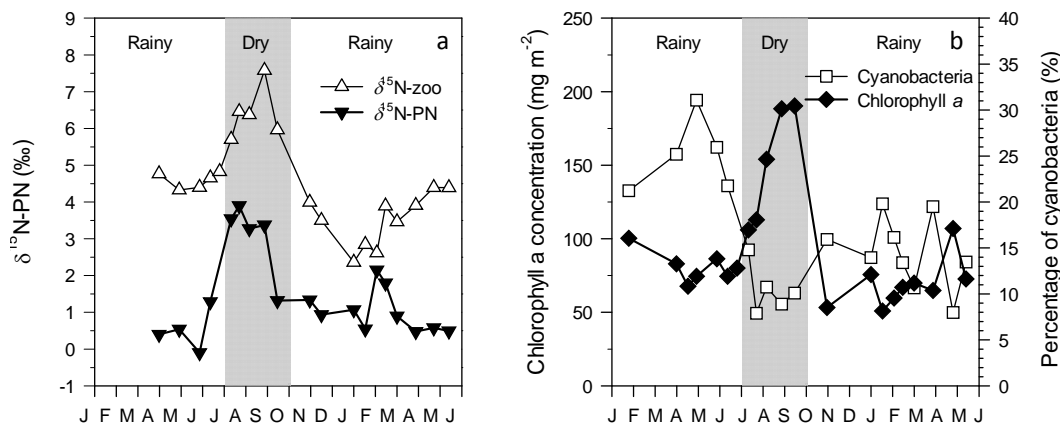


Figure 5. Temporal variability of (a) the $\delta^{15}\text{N}$ signature of the particulate nitrogen (PN) pool and zooplankton in the mixed layer, and (b) the chlorophyll *a* concentration (mg m^{-2}) and the relative contribution of cyanobacteria to the phytoplankton assemblage (percentage of biomass) in the mixolimnion, assessed from pigment analyses, between February 2012 and May 2013.

the Ruzizi River is also relatively low and was computed to be $0.6 \text{ mmol m}^{-2} \text{ d}^{-1}$ (this study) based on the long-term discharge average of Ruzizi ($83.2 \text{ m}^3 \text{ s}^{-1}$, Borges et al., 2014), the average POC and DOC in surface waters (0.052 and $0.142 \text{ mmol L}^{-1}$, this study). It implies that the outputs of OM ($9.4 + 0.7 = 10.1 \text{ mmol m}^{-2} \text{ d}^{-1}$) are higher than the inputs of OM from the catchment ($0.7\text{--}3.3 \text{ mmol m}^{-2} \text{ d}^{-1}$) suggesting a net autotrophic status of Lake Kivu.

However, these results contradict the commonly held view that oligotrophic lacustrine and marine systems tend to be net heterotrophic (Del Giorgio et al., 1997; Cole, 1999). Net heterotrophy implies that heterotrophic prokaryotes rely on a substantial amount of allochthonous OM; however, in Lake Kivu, riverine inputs of allochthonous OM from the catchment ($0.7\text{--}3.3 \text{ mmol m}^{-2} \text{ d}^{-1}$, Borges et al., 2014) are minimal. Indeed, the magnitude of allochthonous OM inputs relative to phytoplankton production depends strongly on the catchment to surface area ratio (Urban et al., 2005), that is particularly low (2.2) in Lake Kivu. Therefore, Lake Kivu is relatively poor in organic C, with DOC concentrations of $\sim 0.15 \text{ mmol L}^{-1}$ in contrast to smaller boreal humic lakes which show DOC concentrations of on average $\sim 1 \text{ mmol L}^{-1}$ (Sobek et al., 2007), and with values up to $\sim 4.5 \text{ mmol L}^{-1}$ (Weyhenmeyer and Karlsson, 2009). Humic substances are usually low-quality substrates for bacterial growth (Castillo et al., 2003), but limit primary production by absorbing incoming light. Hence, heterotrophic production in the photic zone of humic lakes usually exceeds phytoplankton production and DOC concentrations, despite the low substrate quality of humic substances, have been found to be a good predictor of the metabolic status of lakes in the boreal region, with a prevalence of net heterotrophy in organic-rich lakes (Jansson et al., 2000). However, low allochthonous OM inputs and low DOC concentration do not necessarily cause a system to be net autotrophic. For instance, Lake Superior, subsidised by a simi-

lar amount of allochthonous OM ($\sim 3 \text{ mmol m}^{-2} \text{ d}^{-1}$), has a lower catchment-to-surface area ratio (1.6), and its water has a DOC concentration even lower than in Lake Kivu ($\sim 0.1 \text{ mmol L}^{-1}$). However, it has been found to be net heterotrophic despite the limited allochthonous OM inputs (Urban et al., 2005). Lake Superior, as the majority of the lakes of the world, is holomictic, meaning that the mixing of its water column can seasonally reach the lake floor, and a substantial amount of sediments, including OM, could then be resuspended during these mixing events and hence re-exposed to microbial mineralisation in well-oxygenated waters (Meyers and Eadie, 1993; Cotner, 2000; Urban et al., 2005). The resuspension of bottom sediments could be important in the ecological functioning of these systems. In contrast, Lake Kivu, as other East African Great Lakes such as Tanganyika and Malawi, are particularly deep meromictic lakes, so that their water column is characterized by an almost complete decoupling between the surface and deep waters, preventing any resuspended bottom sediment to reach the surface waters in this system. In consequence, the coupling between the phytoplankton production of DOC and its heterotrophic consumption by prokaryotes in the clear, nutrient-depleted waters of Lake Kivu was found to be high throughout the year (Morana et al., 2014).

Besides morphometrical features, the net autotrophic status of Lake Kivu might also be related to general latitudinal and climatic patterns. Due to the warmer temperature in the tropics, phytoplankton production is comparatively higher in the East African Great Lakes compared with the Laurentian Great Lakes, despite similar phytoplankton abundance (Bootsma and Hecky, 2003). Alin and Johnson (2007) examined phytoplankton primary production and CO_2 emissions to the atmosphere fluxes in large lakes of world ($> 500 \text{ km}^2$). At the global scale, they found a statistically significant increase of the areal phytoplankton production in large lakes with the mean annual water temperature and the insolation;

as a consequence, a significant decrease of phytoplankton production with latitude. Also, they report a significant decrease of the CO₂ emissions to the atmosphere with the mean annual water temperature and therefore an increase of the CO₂ emission with the latitude. According to their estimations, less than 20 % of the phytoplankton primary production is sufficient to balance the carbon loss through CO₂ evasion and OM burial in sediments in large lakes located between the equator and the latitude 30°, but the CO₂ emission and OM accumulation in sediments exceed the phytoplankton primary production in systems located at latitude higher than 40° (Alin and Johnson, 2007). Overall, in morphometrically comparable systems, this global analysis suggests a trend from autotrophic to increasingly heterotrophic conditions with increasing latitude and decreasing mean annual water temperature and insolation (Alin and Johnson, 2007). Therefore, our study supports the view that paradigms established with data gathered in comparatively small temperate and boreal lakes may not directly apply to larger, tropical lakes (Bootsma and Hecky, 2003). It also highlights the need to consider the unique limnological characteristics of a vast region of the world that harbours 16 % of the total surface of lakes (Lehner and Döll, 2004), and account for 50 % of the global inputs of OM from continental waters to the oceans (Ludwig et al., 1996).

The $\delta^{13}\text{C}$ data indicate a difference in the origins of the POC and DOC pools in the mixed layer. Indeed, the $\delta^{13}\text{C}$ -DOC showed very little variation and appeared to be vertically and temporally uncoupled from the POC pool in the mixed layer (Fig. 6). A recent study (Morana et al., 2014) demonstrated that phytoplankton extracellular release of DOC is relatively high in Lake Kivu, and the fresh and labile autochthonous DOC produced by cell lysis, grazing or phytoplankton excretion, which reflects the $\delta^{13}\text{C}$ signature of POC, is quickly mineralised by heterotrophic bacteria. Therefore, it appears that the freshly produced autochthonous DOC contributes less than 1 % of the total DOC pool (Morana et al., 2014), and as the standing stock of phytoplankton-derived DOC seems very small, it can be hypothesised that the bulk DOC pool is mainly composed of older, more refractory compounds that reach the mixed layer through vertical advective and diffusive fluxes. Indeed, the $\delta^{13}\text{C}$ signature of the DOC in the monimolimnion (80–370 m, $-23.0 \pm 0.2\text{‰}$, $n = 24$) did not differ from the $\delta^{13}\text{C}$ -DOC in the mixolimnion (0–70 m, $-23.2 \pm 0.2\text{‰}$, $n = 5$), suggesting that they share the same origin (Fig. 4).

The concentration of the POC pool varied largely with depth, being the highest in the 0–20 m layer, i.e. roughly the euphotic zone. However, during the dry season, POC concentrations were almost as high in the oxycline than in surface waters. High POC concentrations in deep waters have frequently been observed in lakes, usually as a result of the resuspension of bottom sediments near the lake floor or the accumulation of sedimenting material in density gradients (Hawley and Lee, 1999). However, in the deep Lake Kivu,

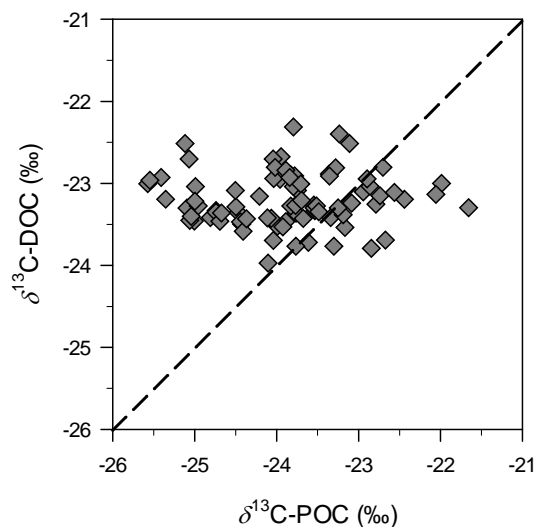


Figure 6. Relationship between the $\delta^{13}\text{C}$ signature of the particulate and dissolved organic carbon pool (POC and DOC, respectively) in the mixed layer.

this maximum POC zone is located approximately 300 m above the lake floor and is characterized by a strong depletion in ^{13}C of the POC pool. While DIC is probably the major C source of the POC pool in the mixed layer, the important decrease of $\delta^{13}\text{C}$ -POC values observed in the oxycline suggests that another ^{13}C -depleted C source was actively incorporated into the biomass at the bottom of the mixolimnion. Slight depletion in ^{13}C of the POC pool in oxyclines, such as in the Black Sea, has sometimes been interpreted as a result of the heterotrophic mineralisation of the sedimenting OM (Çoban-Yıldız et al., 2006), but it seems unlikely that, in Lake Kivu, heterotrophic processes could have caused an abrupt excursion of $\delta^{13}\text{C}$ -POC to values as low as -41.6‰ (65 m, 22 August 2012). Such large isotopic depletion of the POC pool in the water column has been reported by Blee et al. (2014), who measured $\delta^{13}\text{C}$ -POC as low as -49‰ in Lake Lugano, and it was related to high methanotrophic activity. In Lake Kivu, CH₄ concentrations were found to decrease sharply with decreasing depth at the oxic–anoxic transition (Borges et al., 2011), and the dissolved CH₄ that reached the oxycline via turbulent diffusivity and vertical advection (Schmid et al., 2005) is known to be isotopically light, with a $\delta^{13}\text{C}$ signature of approximately -60‰ (Pasche et al., 2011; Morana et al., 2015). Therefore, the vertical patterns in CH₄ concentrations and $\delta^{13}\text{C}$ -POC values observed during this study suggest that a substantial part of CH₄ was consumed and incorporated into the microbial biomass in the oxycline. Indeed, experiments carried out in Lake Kivu in February 2012 and September 2012 showed that microbial CH₄ oxidation was significant in the oxycline, and phospholipid fatty acid analysis revealed high abundance of methanotrophic bacteria of type I at the same depths (Morana et al., 2015). With es-

imates of the isotope fractionation factor during microbial CH_4 oxidation (1.016, Morana et al., 2015), and of the $\delta^{13}\text{C}$ - CH_4 at each sampling point, it is possible to estimate the theoretical $\delta^{13}\text{C}$ signature of methanotrophic organisms at each depth. Note that the $\delta^{13}\text{C}$ - CH_4 was not directly measured during this study but a very strong linear correlation between the log-transformed CH_4 concentrations and $\delta^{13}\text{C}$ - CH_4 was found along vertical profiles performed in February and September 2012 in Lake Kivu ($\delta^{13}\text{C}$ - $\text{CH}_4 = -7.911 \log(\text{CH}_4) - 13.027$; $r^2 = 0.87$, $n = 34$; Morana et al., 2015). Hence the $\delta^{13}\text{C}$ - CH_4 at each sampling point between January 2012 and May 2013 can be approximated from the measured CH_4 concentrations using this empirical relationship. Then, a simple isotope mixing model with the calculated $\delta^{13}\text{C}$ signature of methanotrophs and the average $\delta^{13}\text{C}$ -POC in the mixed layer as end-members allows us to determine the contribution of CH_4 -derived C to POC at each sampling depth. It appears that $4.4 \pm 1.9\%$ ($n = 13$) and $6.4 \pm 1.6\%$ ($n = 5$) of the depth-integrated POC pool in the mixolimnion was derived from CH_4 incorporation into the biomass during the rainy and dry season, respectively, and these percentages did not significantly differ between seasons (two-tailed t test, $p = 0.055$). Nevertheless, the low $\delta^{13}\text{C}$ signatures measured locally in the oxycline indicate that the contribution of CH_4 -derived C could be episodically as high as 50% (65 m, 22 August 2012). We hypothesise that microbial CH_4 oxidation could play an important role in the ecological functioning of Lake Kivu. Along with heterotrophic mineralisation of the sinking OM, and presumably other chemoautotrophic processes occurring in the oxycline such as nitrification (Llirós et al., 2010), CH_4 oxidation contributed substantially to O_2 consumption in the water column and was partly responsible for the seasonal uplift of the oxycline observed after the re-establishment of the thermal stratification during the rainy season. Furthermore, the methanotrophs in the oxycline actively participated in the uptake of dissolved inorganic phosphorus (DIP), and hence exerted an indirect control on phytoplankton by constantly limiting the vertical DIP flux to the illuminated surface waters (Haberyan and Hecky, 1987). Indeed, phytoplankton in Lake Kivu suffer from a severe P limitation throughout the year as pointed out by the relatively high sestonic C:P ratio (256 ± 75 ; Sarmento et al., 2009; Darchambeau et al., 2014).

The $\delta^{15}\text{N}$ signature of the autochthonous OM in the mixed layer of Lake Kivu oscillated around 0‰ during the rainy season in Lake Kivu but was significantly higher during the dry season (3–4‰). Also, the $\delta^{15}\text{N}$ -PN in the mixed layer correlated negatively with the proportion of cyanobacteria in waters (Fig. 7, Pearson's r : -0.65 , $p = 0.004$, $n = 17$). This pattern may highlight the seasonal importance of N_2 -fixing cyanobacteria in Lake Kivu during the rainy season. Indeed, the $\delta^{15}\text{N}$ signature of atmospheric N_2 is close to 0‰, and isotope fractionation during cyanobacterial N_2 -fixation is known to be small (Fogel and Cifuentes, 1993). Several studies carried out in marine (Pacific Ocean and Gulf of

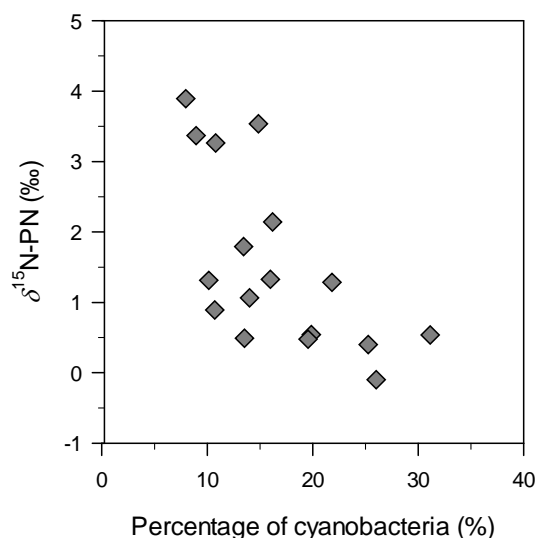


Figure 7. Relationship between the relative contribution of cyanobacteria to the phytoplankton assemblage (percentage of biomass) and the $\delta^{15}\text{N}$ signature of the particulate nitrogen pool in the mixed layer.

Mexico) and lacustrine (Lake Lugano) systems have shown that $\delta^{15}\text{N}$ -PN varied between -2 and $+1$ ‰ when N_2 -fixing cyanobacteria were dominating the phytoplankton assemblage (Wada and Hattori, 1976; Macko et al., 1987; Lehmann et al., 2004). Moreover, a good relationship between the $\delta^{15}\text{N}$ -PN and the abundance of N_2 -fixing cyanobacteria has already been reported for others systems, such as coastal lagoons (Lesutienė et al., 2014). In Lake Victoria, biological N_2 fixation has been identified as having the largest input of N, exceeding atmospheric deposition and river inputs, and N_2 fixation has been found to increase with light availability (Mugidde et al., 2003). This suggests that during the rainy season, when thermal stratification of the mixolimnion leads to reduced nitrogen supply combined with exposure to high light levels, N_2 -fixing cyanobacteria have a competitive advantage which may explain their seasonally higher contribution to the autochthonous OM pool (Sarmento et al., 2006). Indeed, the significantly higher molar C:N ratio during the rainy season than the dry season indicates that N limitation in the mixed layer was stronger during the rainy season (this study, Sarmento et al., 2009). By contrast, the deepening of the mixed layer during the dry season leads to increased nutrient input and reduced light availability that favours alternative phytoplankton strategies (Hecky and Kling, 1987, 2006; Sarmento et al., 2006; Darchambeau et al., 2014), and consequently the proportion N_2 -fixing cyanobacteria decreases. A similar seasonal pattern of N_2 fixation was reported in Lake Victoria by Mugidde et al. (2003). In contrast with the rather constant $\delta^{13}\text{C}$ signature of zooplankton (-22.9 ± 0.8 ‰), the $\delta^{15}\text{N}$ analysis revealed that the $\delta^{15}\text{N}$ of zooplankton varied significantly, following well the sea-

sonal change in $\delta^{15}\text{N}$ -PN in the mixed layer. The difference between $\delta^{15}\text{N}$ -zooplankton and $\delta^{15}\text{N}$ -PN ($\Delta^{15}\text{N}_{\text{Zoo-PN}}$) was on average $3.2 \pm 1.0\text{‰}$ throughout the year while it was on average enriched in ^{13}C ($\Delta^{13}\text{C}_{\text{Zoo-POC}}$) by $0.9 \pm 0.8\text{‰}$. In nature, comparison of the $\delta^{15}\text{N}$ signature of consumers and their diet indicates that the $\delta^{15}\text{N}$ value increases consistently with the trophic level, because of the preferential excretion of the isotopically lighter ^{14}N (Montoya et al., 2002). However, the C isotope fractionation between consumers and diet is usually considered to be less than 1‰ (Sirevåg et al., 1977). The constant $\Delta^{15}\text{N}_{\text{Zoo-PN}}$ value found in Lake Kivu is within the range of trophic level enrichment between algae and *Daphnia magna* (~ 2 to 5‰) estimated in laboratory experiment (Adams and Sterner, 2000), and very close to the cross-system trophic enrichment value ($3.4 \pm 1.0\text{‰}$) proposed by Post (2002). Together with the slight enrichment in ^{13}C compared with the autochthonous POC pool, $\delta^{13}\text{C}$ and $\delta^{15}\text{N}$ analysis suggests that zooplankton directly incorporate phytoplankton-derived OM in their biomass (Masilya, 2011), and they rely almost exclusively on this source of OM throughout the year. This is in general agreement with the very low allochthonous OM inputs from rivers in Lake Kivu (Borges et al., 2014).

In conclusion, stable isotope data revealed large seasonal variability in the $\delta^{15}\text{N}$ signature of the PN pool, most likely related to changes in the phytoplankton assemblage and to N_2 -fixation. Contradicting the common observation that oligotrophic aquatic ecosystems tend to be net heterotrophic, the seasonality of $\delta^{13}\text{C}$ -DIC supports the view that the mixed layer of Lake Kivu is net autotrophic, as demonstrated by Borges et al. (2014) based on DIC and DI^{13}C mass balance considerations. The $\delta^{13}\text{C}$ -POC showed an important variation with depth due to the abundance of methanotrophic bacteria in the oxycline that fixed the lighter CH_4 -derived C into their biomass. The $\delta^{13}\text{C}$ -POC and $\delta^{13}\text{C}$ -DOC appeared to be uncoupled vertically and temporally, which could indicate that most of the DOC pool was composed of relatively refractory compounds. Finally, the $\delta^{13}\text{C}$ of zooplankton mirrored the $\delta^{13}\text{C}$ signature of the autochthonous POC pool, and its $\delta^{15}\text{N}$ signature followed the seasonal variability of the $\delta^{15}\text{N}$ -PN pool in good agreement with the expected consumer–diet isotope fractionation. This suggests that zooplankton rely throughout the year on phytoplankton-derived biomass as a organic C source.

Acknowledgements. We are grateful to Boniface Kaningini, Pascal Isumbisho (Institut Supérieur Pédagogique, Bukavu, DRC) for logistical support during the cruises, to Georges Alunga and the staff of the Unité d'Enseignement et de Recherche en Hydrobiologie Appliquée (UERHA – ISP Bukavu), who carried out the field sampling in DRC. We are also grateful to Marc-Vincent Commarieu, who carried out the TA measurements in the University of Liège, to Stephan Hoornaert, who carried out part of the CH_4 measurements and to Bruno Leporcq, who carried out the pigment analysis in the University of Namur. We thank

the two anonymous reviewers and the editor S. W. A. Naqvi for their comments and suggestions, which significantly contributed to improving the manuscript. This work was funded by the EAGLES (East African Great Lake Ecosystem Sensitivity to Changes, SD/AR/02A) project from the Belgian Federal Science Policy Office (BELSPO, Belgium) and contributes to the European Research Council (ERC) starting grant project AFRIVAL (African river basins: Catchment-scale carbon fluxes and transformations, 240002). Alberto V. Borges is a senior research associate at the FNRS (Belgium).

Edited by: S. W. A. Naqvi

References

- Adams, T. S. and Sterner, R. W.: The effect of dietary nitrogen content on trophic level ^{15}N enrichment, *Limnol. Oceanogr.*, 45, 601–607, 2000.
- Alin, S. R. and Johnson, T. C.: Carbon cycling in large lakes of the world: A synthesis of production, burial, and lake-atmosphere exchange estimates, *Global Biogeochem. Cy.*, 21, GB3002, doi:10.1029/2006GB002881, 2007.
- Bade, D. L., Carpenter, S. R., Cole, J. J., Hanson, P. C., and Hesslein, R. H.: Controls of $\delta^{13}\text{C}$ -DIC in lakes: Geochemistry, lake metabolism, and morphometry, *Limnol. Oceanogr.*, 49, 1160–1172, 2004.
- Blees, J., Niemann, H., Wenk, C. B., Zopfi, J., Schubert, C. J., Kirf, M. K., Veronesi, M. L., Hitz, C., and Lehmann, M. F.: Micro-aerobic bacterial methane oxidation in the chemocline and anoxic water column of deep south-Alpine Lake Lugano (Switzerland), *Limnol. Oceanogr.*, 59, 311–324, 2014.
- Bootsma, H. A. and Hecky, R. E.: A comparative introduction to the biology and limnology of the African Great Lakes, *J. Great Lakes Res.*, 29, 3–18, 2003.
- Borges, A. V., Abril, G., Delille, B., Descy, J. P., and Darchambeau, F.: Diffusive methane emissions to the atmosphere from Lake Kivu (Eastern Africa), *J. Geophys. Res.*, 116, G03032, doi:10.1029/2011JG001673, 2011.
- Borges, A. V., Morana, C., Bouillon, S., Servais, P., Descy, J.-P., and Darchambeau, F.: Carbon cycling of Lake Kivu (East Africa) : Net autotrophy in the epilimnion and emission of CO_2 to the atmosphere sustained by geogenic inputs, *PLoS ONE*, 9, e109500, doi:10.1371/journal.pone.0109500, 2014.
- Castañeda, I. S., Werne, J. P., Johnson, T. C., and Filley, T. R.: Late Quaternary vegetation history of southeast Africa: the molecular isotopic record from Lake Malawi. *Palaeogeography, Palaeoclimatology, Palaeoecology*, 275, 100–112, 2009.
- Castillo, M. M., Kling, G. W., and Allan, J. D.: Bottom-up controls on bacterial production in tropical lowland rivers, *Limnol. Oceanogr.*, 48, 1466–1475, 2003.
- Çoban-Yıldız, Y., Altabet, M. A., Yılmaz, A., and Tuğrul, S.: Carbon and nitrogen isotopic ratios of suspended particulate organic matter (SPOM) in the Black Sea water column, *Deep-Sea Res. Pt. II*, 53, 1875–1892, 2006.
- Cole, J. J.: Aquatic microbiology for ecosystem scientists: new and recycled paradigms in ecological microbiology, *Ecosystems*, 2, 215–225, 1999.

- Cotner, J. B., Johengen, T. H., and Biddanda, B. A.: Intense winter heterotrophic production stimulated by benthic resuspension, *Limnol. Oceanogr.*, 45, 1672–1676, 2000.
- Darchambeau, F., Sarmiento, H., and Descy, J.-P.: Primary production in a tropical large lake: The role of phytoplankton composition, *Sci. Total Environ.*, 473, 178–188, 2014.
- Del Giorgio, P. A., Cole, J. J., and Cimbleris, A.: Respiration rates in bacteria exceed phytoplankton production in unproductive aquatic systems, *Nature*, 385, 148–151, 1997.
- Descy, J.-P. and Sarmiento, H.: Microorganisms of the East African Great Lakes and their response to environmental changes, *Freshwater Reviews*, 1, 59–73, 2008.
- Descy, J.-P., Higgins, H. W., Mackey, D. J., Hurley, J. P., and Frost, T. M.: Pigment ratios and phytoplankton assessment in northern Wisconsin lakes, *J. Phycol.*, 36, 274–286, 2000.
- Duarte, C. M. and Prairie, Y. T.: Prevalence of heterotrophy and atmospheric CO₂ emissions from aquatic ecosystems, *Ecosystems*, 8, 862–870, 2005.
- Finlay, K., Leavitt, P. R., Patoine, A., and Wissel, B.: Magnitudes and controls of organic and inorganic carbon flux through a chain of hardwater lakes on the northern Great Plains, *Limnol. Oceanogr.*, 55, 1551–1564, 2010.
- Fogel, M. L. and Cifuentes, L. A.: Isotope fractionation during primary production, 73–98, in: *Organic geochemistry*, edited by: Engel, M. H. and Macko, S. A., Plenum Press, New York, 1993.
- Gillikin, D. P. and Bouillon, S.: Determination of $\delta^{18}\text{O}$ of water and $\delta^{13}\text{C}$ of dissolved inorganic carbon using a simple modification of an elemental analyser-isotope ratio mass spectrometer: an evaluation, *Rapid Commun. Mass Sp.*, 21, 1475–1478, 2007.
- Gran, G.: Determination of the equivalence point in potentiometric titrations. Part II, *Analysis*, 77, 661–671, 1952.
- Grey, J., Jones, R. I., and Sleep, D.: Seasonal changes in the importance of the source of organic matter to the diet of zooplankton in Loch Ness, as indicated by stable isotope analysis, *Limnol. Oceanogr.*, 46, 505–513, 2001.
- Haberyan, K. A. and Hecky, R. E.: The late Pleistocene and Holocene stratigraphy and paleolimnology of Lakes Kivu and Tanganyika, *Palaeogeogr. Palaeoclimatol.*, 61, 169–197, 1987.
- Hawley, N. and Lee, C. H.: Sediment resuspension and transport in Lake Michigan during the unstratified period, *Sedimentology*, 46, 791–805, 1999.
- Hecky, R. E. and Kling, H. J.: Phytoplankton ecology of the great lakes in the rift valleys of Central Africa, *Arch. Hydrobiol.-Beiheft Ergebnisse der Limnologie*, 25, 197–228, 1987.
- Herczeg, A. L.: A stable carbon isotope study of dissolved inorganic carbon cycling in a softwater lake, *Biogeochemistry*, 4, 231–263, 1987.
- Hollander, D. J. and McKenzie, J. A.: CO₂ control on carbon-isotope fractionation during aqueous photosynthesis: A paleo-pCO₂ barometer, *Geology*, 19, 929–932, 1991.
- Jansson, M., Bergström, A. K., Blomqvist, P., and Drakare, S.: Allochthonous organic carbon and phytoplankton/bacterioplankton production relationships in lakes, *Ecology*, 81, 3250–3255, 2000.
- Kaningini, M.: Etude de la croissance, de la reproduction et de l'exploitation de *Limnothrissa miodon* au lac Kivu, bassin de Bukavu (Zaire), PhD thesis, Facultés Universitaires Notre Dame de la Paix, Namur, Belgium, 1995.
- Kankaala, P., Taipale, S., Grey, J., Sonninen, E., Arvola, L., and Jones, R. I.: Experimental $\delta^{13}\text{C}$ evidence for a contribution of methane to pelagic food webs in lakes, *Limnol. Oceanogr.*, 51, 2821–2827, 2006.
- Lehmann, M. F., Bernasconi, S. M., McKenzie, J. A., Barbieri, A., Simona, M., and Veronesi, M.: Seasonal variation of the $\delta^{13}\text{C}$ and $\delta^{15}\text{N}$ of particulate and dissolved carbon and nitrogen in Lake Lugano: Constraints on biogeochemical cycling in a eutrophic lake, *Limnol. Oceanogr.*, 49, 415–429, 2004.
- Lehner, B. and Döll, P.: Development and validation of a global database of lakes, reservoirs and wetlands, *J. Hydrol.*, 296, 1–22, 2004.
- Lesutienė, J., Bukaveckas, P. A., Gasiūnaitė, Z. R., Pilkaitytė, R., and Razinkovas-Baziukas, A.: Tracing the isotopic signal of a cyanobacteria bloom through the food web of a Baltic Sea coastal lagoon, *Estuar. Coast. Shelf Sci.*, 138, 47–56, 2014.
- Lewis, W. M. J.: Tropical lakes: how latitude makes a difference, in: *Perspectives Tropical Limnology*, edited by: F. Schiemer and Boland, K. T., SPB Academic Publishing, Amsterdam, 43–64, 1996.
- Llirós, M., Gich, F., Plasencia, A., Auguet, J. C., Darchambeau, F., Casamayor, E. O., Descy, J.-P., and Borrego, C.: Vertical distribution of ammonia-oxidizing crenarchaeota and methanogens in the epipelagic waters of Lake Kivu (Rwanda-Democratic Republic of the Congo), *Appl. Environ. Microb.*, 76, 6853–6863, 2010.
- Ludwig, W., Probst, J. L., and Kempe, S.: Predicting the oceanic input of organic carbon by continental erosion, *Global Biogeochem. Cy.*, 10, 23–41, 1996.
- Macko, S. A., Fogel, M. L., Hare, P. E., and Hoering, T. C.: Isotopic fractionation of nitrogen and carbon in the synthesis of amino acids by microorganisms, *Chem. Geol.*, 65, 79–92, 1987.
- Marcé, R., Obrador, B., Morguá, J.-A., Lluís Riera, J., López, P., and Armengol, J.: Carbonate weathering as a driver of CO₂ supersaturation in lakes, *Nature Geosci.*, 8, 107–111, 2015.
- Masilya, P.: Ecologie alimentaire compare de *Limnothrissa miodon* et de *Lamprichthys tanganicus* au lac Kivu (Afrique de l'Est), PhD thesis, Facultés Universitaires Notre Dame de la Paix, Namur, Belgium, 2011.
- Meyers, P. A. and Eadie, B. J.: Sources, degradation and recycling of organic matter associated with sinking particles in Lake Michigan, *Org. Geochem.*, 20, 47–56, 1993.
- Millero, F. J., Graham, T. B., Huang, F., Bustos-Serrano, H., and Pierrot, D.: Dissociation constants of carbonic acid in sea water as a function of salinity and temperature, *Mar. Chem.*, 100, 80–94, 2006.
- Montoya, J. P., Carpenter, E. J., and Capone, D. G.: Nitrogen fixation and nitrogen isotope abundances in zooplankton of the oligotrophic North Atlantic, *Limnol. Oceanogr.*, 47, 1617–1628, 2002.
- Morana, C., Sarmiento, H., Descy, J.-P., Gasol, J. M., Borges, A. V., Bouillon, S., and Darchambeau, F.: Production of dissolved organic matter by phytoplankton and its uptake by heterotrophic prokaryotes in large tropical lakes, *Limnol. Oceanogr.*, 59, 1364–1375, 2014.
- Morana, C., Borges, A. V., Roland, F. A. E., Darchambeau, F., Descy, J.-P., and Bouillon, S.: Methanotrophy within the water column of a large meromictic tropical lake (Lake Kivu, East Africa), *Biogeosciences*, 12, 2077–2088, doi:10.5194/bg-12-2077-2015, 2015.

- Mugidde, R., Hecky, R. E., Hendzel, L. L., and Taylor, W. D.: Pelagic nitrogen fixation in Lake Victoria (East Africa), *J. Great Lakes Res.*, 29, 76–88, 2003.
- Pasche, N., Alunga, G., Mills, K., Muvundja, F., Ryves, D. B., Schurter, M., Wehrli, B., and Schmid, M.: Abrupt onset of carbonate deposition in Lake Kivu during the 1960s: response to recent environmental changes, *J. Paleolimnol.*, 44, 931–946, 2010.
- Pasche, N., Schmid, M., Vazquez, F., Schubert, C. J., Wüest, A., Kessler, J. D., Pack, M. A., Reeburgh, W. S., and Bürgmann, H.: Methane sources and sinks in Lake Kivu, *J. Geophys. Res.*, 116, G03006, doi:10.1029/2011JG001690, 2011.
- Post, D. M.: Using stable isotopes to estimate trophic position: models, methods, and assumptions, *Ecology*, 83, 703–718, 2002.
- Prairie, Y. T., Bird, D. F., and Cole, J. J.: The summer metabolic balance in the epilimnion of southeastern Quebec lakes, *Limnol. Oceanogr.*, 47, 316–321, 2002.
- Sarmiento, H.: New paradigms in tropical limnology: the importance of the microbial food web, *Hydrobiologia*, 686, 1–14, 2012.
- Sarmiento, H., Isumbusho, M., and Descy, J.-P.: Phytoplankton ecology of Lake Kivu (eastern Africa), *J. Plankton Res.*, 28, 815–829, 2006.
- Sarmiento, H., Isumbusho, M., Stenuite, S., Darchambeau, F., Leporcq, B., and Descy, J.-P.: Phytoplankton ecology of Lake Kivu (eastern Africa): biomass, production and elemental ratios, *Int. Ver. Theor. Angew.*, 30, 709–713, 2009.
- Schelske, C. L. and Hodell, D. A.: Recent changes in productivity and climate of Lake Ontario detected by isotopic analysis of sediments, *Limnol. Oceanogr.*, 36, 961–975, 1991.
- Schmid, M., Halbwachs, M., Wehrli, B., and Wüest, A.: Weak mixing in Lake Kivu: new insights indicate increasing risk of uncontrolled gas eruption, *Geochem. Geophys. Geosy.*, 6, Q07009, doi:10.1029/2004GC000892, 2005.
- Sirevåg, R., Buchanan, B. B., Berry, J. A., and Troughton, J. H.: Mechanisms of CO₂ fixation in bacterial photosynthesis studied by the carbon isotope fractionation technique, *Arch. Microbiol.*, 112, 35–38, 1977.
- Sobek, S., Tranvik, L. J., Prairie, Y. T., Kortelainen, P., and Cole, J. J.: Patterns and regulation of dissolved organic carbon: An analysis of 7,500 widely distributed lakes, *Limnol. Oceanogr.*, 52, 1208–1219, 2007.
- Stets, E. G., Striegl, R. G., Aiken, G. R., Rosenberry, D. O., and Winter, T. C.: Hydrologic support of carbon dioxide flux revealed by whole-lake carbon budgets, *J. Geophys. Res.*, 114, G01008, doi:10.1029/2008JG000783, 2009.
- Thiery, W., Martynov, A., Darchambeau, F., Descy, J.-P., Plisnier, P.-D., Sushama, L., and van Lipzig, N. P. M.: Understanding the performance of the FLake model over two African Great Lakes, *Geosci. Model Dev.*, 7, 317–337, doi:10.5194/gmd-7-317-2014, 2014.
- Urban, N. R., Auer, M. T., Green, S. A., Lu, X., Apul, D. S., Powell, K. D., and Bub, L.: Carbon cycling in Lake Superior, *J. Geophys. Res.-Oceans*, 110, C06S90, doi:10.1029/2003JC002230, 2005.
- Wada, E. and Hattori, A.: Natural abundance of ¹⁵N in particulate organic matter in the North Pacific Ocean, *Geochim. Cosmochim. Ac.*, 40, 249–251, 1976.
- Weiss, R. F.: Determinations of carbon dioxide and methane by dual catalyst flame ionization chromatography and nitrous oxide by electron capture chromatography, *J. Chromatogr. Sci.*, 19, 611–616, 1981.
- Weyhenmeyer, G. A. and Karlsson, J.: Nonlinear response of dissolved organic carbon concentrations in boreal lakes to increasing temperatures, *Limnol. Oceanogr.*, 54, 2513–2519, 2009.
- Wright, S. W., Jeffrey, S. W., Mantoura, R. F. C., Llewellyn, C. A., Bjornland, T., Repeta, D., and Welschmeyer, N.: Improved HPLC method for the analysis of chlorophylls and carotenoids from marine phytoplankton, *Mar. Ecol.-Prog. Ser.*, 77, 183–196, 1991.



Biogeochemistry of a large and deep tropical lake (Lake Kivu, East Africa: insights from a stable isotope study covering an annual cycle

C. Morana¹, F. Darchambeau², F. A. E. Roland², A. V. Borges², F. Muvundja^{3,4}, Z. Kelemen¹, P. Masilya⁴, J.-P. Descy³, and S. Bouillon¹

¹Department of Earth and Environmental Sciences, Katholieke Universiteit Leuven, Leuven, Belgium

²Chemical Oceanography Unit, Université de Liège, Liège, Belgium

³Research Unit in Environmental and Evolutionary Biology, Université de Namur, Namur, Belgium

⁴Unité d'Enseignement et de Recherche en Hydrobiologie Appliquée, ISP-Bukavu, Bukavu, Democratic Republic of the Congo

Correspondence to: C. Morana (cedric.morana@ees.kuleuven.be)

Received: 14 October 2014 – Published in Biogeosciences Discuss.: 11 December 2014

Revised: 23 July 2015 – Accepted: 9 August 2015 – Published: 19 August 2015

Abstract. During this study, we investigated the seasonal variability of the concentration and the stable isotope composition of several inorganic and organic matter (OM) reservoirs in the large, oligotrophic and deep tropical Lake Kivu (East Africa). Data were acquired over 1 year at a fortnightly temporal resolution. The $\delta^{13}\text{C}$ signature of the dissolved inorganic carbon (DIC) increased linearly with time during the rainy season, then suddenly decreased during the dry season due to vertical mixing with ^{13}C -depleted DIC waters. The $\delta^{13}\text{C}$ signature of the particulate organic carbon pool (POC) revealed the presence of a consistently abundant methanotrophic biomass in the oxycline throughout the year. We also noticed a seasonal shift during the dry season toward higher values in the $\delta^{15}\text{N}$ of particulate nitrogen (PN) in the mixed layer and $\delta^{15}\text{N}$ -PN was significantly related to the contribution of cyanobacteria to the phytoplankton assemblage, suggesting that rainy season conditions could be more favourable to atmospheric nitrogen-fixing cyanobacteria. Finally, zooplankton were slightly enriched in ^{13}C compared to the autochthonous POC pool, and the $\delta^{15}\text{N}$ signature of zooplankton followed well the seasonal variability in $\delta^{15}\text{N}$ -PN, consistently 3.0 ± 1.1 ‰ heavier than the PN pool. Together, $\delta^{13}\text{C}$ and $\delta^{15}\text{N}$ analysis suggests that zooplankton directly incorporate algal-derived OM in their biomass, and that they rely almost exclusively on this source of OM throughout the

year in general agreement with the very low allochthonous OM inputs from rivers in Lake Kivu.

1 Introduction

Stable carbon (C) and nitrogen (N) isotope analyses of diverse inorganic and organic components have been successfully used to assess the origin of organic matter (OM) and better understand its cycling in aquatic systems (Lehmann et al., 2004). For instance, an extensive sampling of diverse C and N pools over an annual cycle in the Loch Ness showed important seasonal variation of the $^{13}\text{C}/^{12}\text{C}$ and $^{15}\text{N}/^{14}\text{N}$ ratios in the crustacean zooplankton biomass, reflecting a diet switch from allochthonous to autochthonous OM sources (Grey et al., 2001). In small humic boreal lakes with permanently anoxic waters, stable C isotope analyses demonstrated that methanotrophic bacteria could be an important food source for crustacean zooplankton, and hence methane-derived C contributed to a large fraction of the lake food web (Kankaala et al., 2006). Analyses of the stable C isotope composition of carbonates and OM in sedimentary records of stratified lakes can also provide reliable information about past land use of the catchment (Castañeda et al., 2009), or be used to infer changes in lake productivity and climate (Schelske and Hodell, 1991). However, a detailed un-

derstanding of the stable isotope dynamics in the water column is a prerequisite for a good interpretation of isotope data from sedimentary archives (Lehmann et al., 2004).

A new paradigm has progressively emerged over the last decade, proposing that freshwaters ecosystems are predominantly net heterotrophic, as respiration of OM exceeds autochthonous photosynthetic production (Del Giorgio et al., 1997; Cole, 1999; Duarte and Prairie, 2005). This concept seems to hold especially true for oligotrophic unproductive ecosystems (Del Giorgio et al., 1997), that are subsidised by substantial inputs of allochthonous OM of terrestrial origin, which support the production of heterotrophic organisms. Net heterotrophy has been recognised as one of the main cause for the net emission of carbon dioxide (CO₂) from freshwater ecosystems to the atmosphere (Prairie et al., 2002), although there is growing evidence of the contribution from external hydrological CO₂ inputs from the catchment (Stets et al., 2009; Finlay et al., 2010; Borges et al., 2014; Marcé et al., 2015). However, the current understanding of the role of inland waters on CO₂ emissions could be biased because most observations were obtained in temperate and boreal systems, and mostly in medium-to-small lakes, during open-water (ice-free) periods, but tropical and temperate lakes differed in some fundamental characteristics. Among them, the constantly high temperature and irradiance have strong effects on water column stratification and biological processes (Sarmiento, 2012). For instance, primary production in tropical lakes has been recognised to be 2 times higher than in temperate lakes on a given nutrient base (Lewis, 1996). Also, the contribution of dissolved primary production in oligotrophic tropical lakes has been found to be substantially more important than in their temperate counterparts (Morana et al., 2014).

East Africa harbours the densest aggregation of large tropical lakes (Bootsma and Hecky, 2003). Some of them are among the largest (lakes Victoria, Tanganyika, Malawi), and deepest lakes in the world (lakes Tanganyika, Malawi, Kivu) and consequently remain stratified all year round. Due to the size and the morphometric traits of the East African Great Lakes, pelagic processes are predominant in these systems, with the microbial food web playing a particularly essential role in OM transfer between primary producers and higher levels of the food web, and in nutrient cycling (Descy and Sarmiento, 2008). Most of them are also characterized by highly productive fisheries that provide an affordable food source to local populations (Descy and Sarmiento, 2008). However, while these lakes are potentially important components of biogeochemical cycles at the regional scale (Borges et al., 2011), and significant for local populations from an economic perspective (Kaningini, 1995), the East African Great Lakes are relatively poorly studied, most probably because of their remote location combined with frequent political unrest.

In this study, we present a comprehensive data set covering a full annual cycle, including hydrochemical data and mea-

surements of the concentration of dissolved methane (CH₄) and the concentrations and stable isotope compositions of dissolved inorganic carbon (DIC), dissolved and particulate organic carbon (DOC and POC), particulate nitrogen (PN), and zooplankton. Data were acquired over one full year at a fortnightly/monthly temporal resolution. We aimed to assess the net metabolic status of Lake Kivu, the seasonal and depth variability of sources of OM within the water column, and the relative contribution of autochthonous or allochthonous OM to the zooplankton. To our best knowledge, this is the first detailed study to assess the seasonal dynamics of different OM reservoirs by means of their stable isotope composition in any of the East African Great Lakes. The detailed analysis of the stable isotope composition of diverse organic and inorganic components carried out during this study allowed one to trace the OM dynamics in Lake Kivu over a seasonal cycle, and might be useful to improve the interpretation of sedimentary archives of this large and deep tropical lake.

2 Material and methods

Lake Kivu (East Africa) is a large (2370 km²) and deep (maximum depth of 485 m) meromictic lake located at the border between the Democratic Republic of the Congo and Rwanda. Its vertical structure consists of an oxic and nutrient-poor mixed layer down to a maximum depth of 70 m, and a permanently anoxic monimolimnion rich in dissolved gases (CH₄, and CO₂) and inorganic nutrients. Seasonal variation of the vertical position of the oxic–anoxic transition is driven by contrasting air humidity and incoming long-wave radiation between rainy (October–May) and dry (June–September) seasons (Thiery et al., 2014). The euphotic zone, defined at the depth at which light is 1% of surface irradiance, is relatively shallow (annual average: 18 m, Darchambeau et al., 2014).

Sampling was carried out in the southern basin (02°20' S, 28°58' E) of Lake Kivu between January 2012 and May 2013 at a monthly or fortnightly time interval. Vertical oxygen (O₂), temperature and conductivity profiles were obtained with a Hydrolab DS5 multiprobe. The conductivity cell was calibrated with a 1000 μS cm⁻¹ (25 °C) Merck standard and the O₂ membrane probe was calibrated with humidity saturated ambient air. Water was collected with a 7 L Niskin bottle (Hydro-Bios) at a depth interval of 5 m from the lake surface to the bottom of the mixolimnion, at 70 m. Additionally, zooplankton was sampled with a 75 cm diameter, 55 μm mesh plankton net hauled along the whole mixolimnion (0–70 m).

Samples for CH₄ concentrations were collected in 50 mL glass serum bottles from the Niskin bottle with a tube, left to overflow, poisoned with 100 μL of saturated HgCl₂ and sealed with butyl stoppers and aluminium caps. Concentrations of CH₄ were measured by headspace technique using gas chromatography (Weiss, 1981) with flame ionisation de-

tection (SRI 8610C), after creating a 20 mL headspace with N₂ in the glass serum bottles, and then analysed as described by Borges et al. (2011).

Samples for stable C isotopic composition of dissolved inorganic carbon ($\delta^{13}\text{C-DIC}$) were collected by filling water directly from the Niskin bottle 12 mL headspace vials (Labco Exetainer) without bubbles. Samples were preserved with the addition of 20 μL of a saturated HgCl₂ solution. Prior to the analysis of $\delta^{13}\text{C-DIC}$, a 2 mL helium headspace was created, and 100 μL of phosphoric acid (H₃PO₄, 99 %) was added in the vial in order to convert all inorganic C species to CO₂. After overnight equilibration, 200 μL of gas was injected with a gastight syringe into a elemental analyser – isotopic ratio mass spectrometer (EA-IRMS; Thermo FlashHT with Thermo DeltaV Advantage). The obtained data were corrected for isotopic equilibration between dissolved and gaseous CO₂ as described in Gillikin and Bouillon (2007). Calibration of $\delta^{13}\text{C-DIC}$ measurement was performed with the international certified standards IAEA-CO1 and LSVEC. The reproducibility of $\delta^{13}\text{C-DIC}$ measurement was typically better than $\pm 0.2\%$. Measurements of total alkalinity (TA) were carried out by open-cell titration with HCl 0.1 mol L⁻¹ according to Gran (1952) on 50 mL water samples, and data were quality checked with certified reference material obtained from Andrew Dickinson (Scripps Institution of Oceanography, University of California, San Diego, USA). Typical reproducibility of TA measurements was better than $\pm 3 \mu\text{mol L}^{-1}$. DIC concentration was computed from pH and TA measurements using the carbonic acid dissociation constants of Millero et al. (2006).

Samples for DOC concentration and stable C isotopic composition ($\delta^{13}\text{C-DOC}$) were filtered through pre-flushed 0.2 μm syringe filters, kept in 40 mL borosilicate vials with Teflon-coated screw caps and preserved with 100 μL of H₃PO₄ (50 %). Sample analysis was carried out with a IO Analytical Aurora 1030W coupled to an IRMS (Thermo delta V Advantage). Quantification and calibration of DOC and $\delta^{13}\text{C-DOC}$ was performed with IAEA-C6 and an internal sucrose standard ($\delta^{13}\text{C} = -26.99 \pm 0.04\%$) calibrated against international reference materials.

Samples for POC and particulate nitrogen (PN) concentration and stable carbon and nitrogen isotope composition ($\delta^{13}\text{C-POC}$; $\delta^{15}\text{N-PN}$) were obtained by filtering a known volume of water on pre-combusted (overnight at 450 °C) 25 mm glass fiber filters (Advantec GF-75; 0.3 μm), kept frozen until subsequent processing. The filters were later decarbonated with HCl fumes for 4 h, dried and packed in silver cups prior to analysis on a EA-IRMS (Thermo FlashHT with Thermo DeltaV Advantage). Calibration of $\delta^{13}\text{C-POC}$, $\delta^{15}\text{N-PN}$, POC and PN measurements was performed with acetanilide ($\delta^{13}\text{C} = -27.65 \pm 0.05$; $\delta^{15}\text{N} = 1.34 \pm 0.04$) and leucine ($\delta^{13}\text{C} = -13.47 \pm 0.07$; $\delta^{15}\text{N} = 0.92 \pm 0.06$) as standards. All standards were internally calibrated against the international standard IAEA-C6 and IAEA-N1. Reproducibility of $\delta^{13}\text{C-POC}$ and $\delta^{15}\text{N-PN}$

measurement was typically better than $\pm 0.2\%$ and relative standard deviation for POC and PN measurement were always below 5 %. Samples for $\delta^{13}\text{C}$ and $\delta^{15}\text{N}$ of zooplankton were collected on precombusted 25 mm glass fiber filters (Advantec GF-75; 0.3 μm), and dried. Subsequent preparation of the samples and analysis on the EA-IRMS were performed similarly as described for the $\delta^{13}\text{C-POC}$ and $\delta^{15}\text{N-PN}$ samples.

Pigment concentrations were determined by high performance liquid chromatography (HPLC). 2–4 L of water were filtered through Macherey-Nägél GF-5 filter (average retention of 0.7 μm). Pigment extraction was carried out in 10 mL of 90 % HPLC grade acetone. After two sonication steps of 15 min separated by an overnight period at 4 °C, the pigments extracts were stored in 2 mL amber vials at -25 °C. HPLC analysis was performed following the gradient elution method described in Wright et al. (1991), with a Waters system comprising photodiode array and fluorescence detectors. Calibration was made using commercial external standards (DHI Lab Products, Denmark). Reproducibility for pigment concentration measurement was better than 7 %. Pigment concentrations were processed with the CHEMTAX software (CSIRO Marine Laboratories) using input ratio matrices adapted for freshwater phytoplankton (Descy et al., 2000). Data processing followed a procedure similar to that of Sarmiento et al. (2006) in Lake Kivu that allows one to estimate chlorophyll *a* (Chl *a*) biomass of cyanobacteria, taking into account variation of pigment ratios with season and depth.

3 Results

Analysis of the vertical and seasonal variability of temperature and dissolved O₂ concentrations for 18 months allow us to divide the annual cycle into two distinct limnological periods. Rainy season conditions resulted in a thermal stratification within the mixolimnion (October–June) while the dry season was characterized by deeper vertical mixing of the water column down to the upper part of the permanent chemocline at 65 m (July–September) (Fig. 1a). The vertical position of the oxycline varied seasonally: the oxic–anoxic transition reached its deepest point (65 m) during the dry season, then became gradually shallower after the re-establishment of the thermal stratification within the mixolimnion at the start of the following rainy season to finally stabilise at approximately 35 m, corresponding to the bottom of the mixed layer during the rainy season (Fig. 1b). The temporal variability of the vertical distribution of CH₄ corresponded well with the seasonal variation of the oxycline. The CH₄ concentrations were very high in the monimolimnion throughout the year (average at 70 m: $356 \pm 69 \mu\text{mol L}^{-1}$, $n = 24$) but sharply decreased at the oxic–anoxic transition, and were 4 orders of mag-

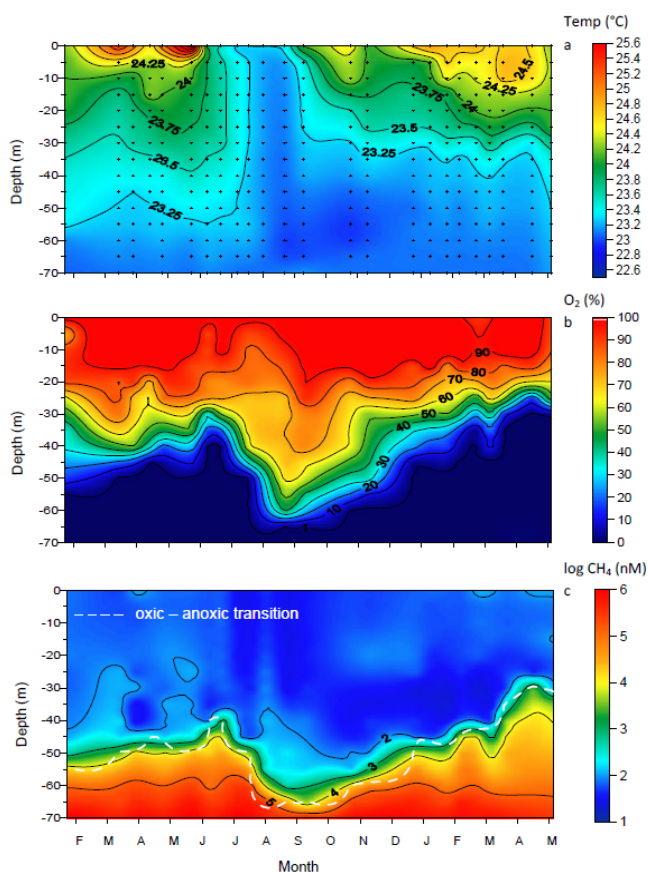


Figure 1. Temporal variability of (a) temperature ($^{\circ}\text{C}$), (b) oxygen saturation (in percentage), and (c) the log-transformed CH_4 concentration (nmol L^{-1}) in the mixolimnion of Lake Kivu, between February 2012 and May 2013. Small crosses in the figure (a) represent each sampling points. The white dashed line represents the vertical position of the oxic–anoxic transition.

nitude lower in surface waters (annual average at 10 m: $0.062 \pm 0.016 \mu\text{mol L}^{-1}$, $n = 24$) (Fig. 1c).

DIC concentrations in the mixed layer were very high (annual average at 10 m: $11.9 \pm 0.2 \text{ mmol L}^{-1}$, $n = 24$) and did not show any consistent seasonal pattern (not shown). The $\delta^{13}\text{C-DIC}$ values were vertically homogeneous in the mixed layer but gradually decreased in the oxycline to reach minimal values at 70 m (Fig. 2a). $\delta^{13}\text{C-DIC}$ values in the mixed layer increased linearly with time during the rainy season ($r^2 = 0.79$, $n = 12$), then suddenly decreased at the start of the dry season due to the vertical mixing with ^{13}C -depleted DIC from deeper waters (Fig. 2b). Taking into account the analytical precision of $\delta^{13}\text{C-DIC}$ measurement (better than $\pm 0.2\text{‰}$), this small but linear ^{13}C enrichment with time was significant. The DOC concentration ($142 \pm 20 \mu\text{mol CL}^{-1}$, $n = 304$) and $\delta^{13}\text{C-DOC}$ signature ($-23.2 \pm 0.4\text{‰}$, $n = 304$) did not show any consistent variations with depth or time in the mixolimnion over the entire sampling period. A vertical profile performed down

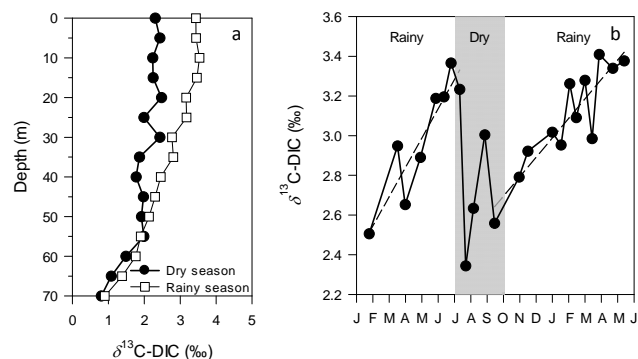


Figure 2. Depth profile of the $\delta^{13}\text{C}$ of the dissolved inorganic carbon (DIC) pool in the mixolimnion during the dry (18 July 2012) and the rainy (20 March 2013) season and (b) temporal variation of the $\delta^{13}\text{C-DIC}$ in the mixed layer of Lake Kivu between January 2012 and June 2013.

to the lake floor revealed that the $\delta^{13}\text{C-DOC}$ did not vary significantly in the monimolimnion (vertical profile average: $-23.0\text{‰} \pm 0.2$, $n = 18$, Fig. 3); however, an important increase in DOC concentrations was observed starting at 260 m (Fig. 3), to reach a maximum near the lake floor (350 m , $301 \mu\text{mol CL}^{-1}$).

Chlorophyll *a* concentrations exhibited little variation during the rainy season (average $74 \pm 15 \text{ mg Chl } a \text{ m}^{-2}$, $n = 16$) but increased significantly during the dry season to reach a maximal value ($190 \text{ mg Chl } a \text{ m}^{-2}$) in September 2012 (Fig. 5b). This increase corresponded with a change in phytoplankton community composition. The relative contribution of cyanobacteria to the phytoplankton assemblage, as assessed from the concentration of marker pigments, was smaller during the dry season than in the preceding (t test; $p < 0.01$, $\text{mean}_{\text{jan-jun}} = 23.4 \pm 5.5\%$, $\text{mean}_{\text{jul-sep}} = 9.4 \pm 1.3\%$) and the following (t test; $p < 0.05$, $\text{mean}_{\text{oct-may}} = 14.6 \pm 3.8\%$, $\text{mean}_{\text{jul-sep}} = 9.4 \pm 1.3\%$) rainy seasons (Fig. 5b).

4 Discussion

Stable isotope analysis of DIC is a useful tool for understanding the fate of C in aquatic ecosystems and could provide information on the lake metabolism, defined as the balance between gross primary production and community respiration of OM. Primary producers preferentially incorporate the lighter isotope (^{12}C) into the biomass with the consequence that the heavier isotope (^{13}C) accumulates into the DIC pool, whereas mineralisation releases ^{13}C -depleted CO_2 from the OM being respired into the DIC pool. Therefore, increasing primary production leads to higher $\delta^{13}\text{C-DIC}$ but increasing respiration should tend to decrease $\delta^{13}\text{C-DIC}$ (Bade et al., 2004). For instance, several studies conducted in temperate lakes have reported a significant increase in $\delta^{13}\text{C-DIC}$ during summer, resulting from primary production (Herczeg,

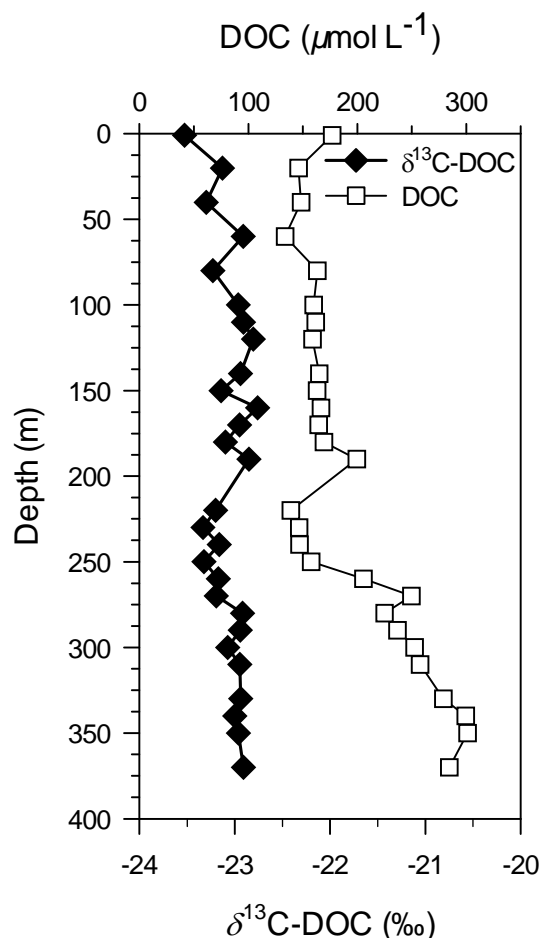


Figure 3. Depth profile from the lake surface to the lake floor of the dissolved organic carbon (DOC) concentration ($\mu\text{mol L}^{-1}$) and the $\delta^{13}\text{C}$ signature of the DOC pool, in September 2012. The white dashed line represents the vertical position of the oxic–anoxic transition.

1987; Hollander and McKenzie, 1991). In Lake Kivu, the $\delta^{13}\text{C}$ -DIC increased linearly with time during the stratified rainy season, deviating gradually from the $\delta^{13}\text{C}$ -DIC value expected if the DIC pool was at equilibrium with the atmospheric CO_2 ($\sim 0.49\text{‰}$). It appears unlikely that this linear isotopic enrichment of the DIC pool is due to physical processes: the $\delta^{13}\text{C}$ -DIC signature of the DIC input from the inflowing rivers (Borges et al., 2014) and deep waters (Fig. 3a) was indeed lower than the measured $\delta^{13}\text{C}$ -DIC in the mixed layer. Therefore, biological processes (i.e. photosynthetic CO_2 uptake) are likely responsible of the isotopic enrichment of the DIC pool observed during the stratified rainy season. Nevertheless, a small decrease in $\delta^{13}\text{C}$ -DIC was recorded at the beginning of the dry season (early in July 2012), but was concomitant with the characteristic deepening of the mixed layer observed during the dry season. As the depth profile of $\delta^{13}\text{C}$ -DIC revealed that the DIC pool was isotopically lighter in the bottom of the mixolimnion,

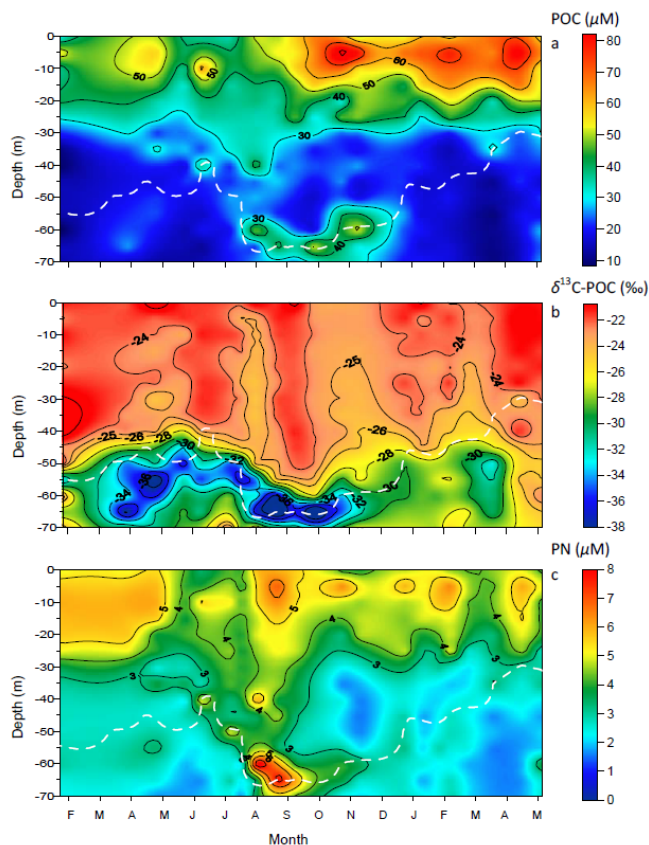


Figure 4. Temporal variability of (a) the particulate organic carbon (POC) concentration ($\mu\text{mol L}^{-1}$), (b) the $\delta^{13}\text{C}$ signature of the POC pool, and (c) the particulate nitrogen (PN) concentration ($\mu\text{mol L}^{-1}$) in the mixolimnion of Lake Kivu, between February 2012 and May 2013.

the measurement of lower $\delta^{13}\text{C}$ -DIC values during the dry season could have resulted from the seasonal vertical mixing of surface waters with bottom waters containing relatively ^{13}C -depleted DIC.

Overall, the data suggest that the input of DIC originating from the monimolimnion during the dry season had a strong influence on $\delta^{13}\text{C}$ -DIC in the mixolimnion, but the seasonal variability of $\delta^{13}\text{C}$ -DIC observed in the mixed layer holds information on biological processes. The gradual increase with time of the $\delta^{13}\text{C}$ -DIC in the mixed layer supports the conclusions of other studies carried out in Lake Kivu (Morana et al., 2014; Borges et al., 2014) which showed, based on a detailed DIC and DI^{13}C mass balance approach and several microbial processes measurements, that photosynthetic CO_2 fixation should exceed the respiration of OM. Indeed, in Lake Kivu, riverine inputs of allochthonous OM from the catchment ($0.7\text{--}3.3\text{ mmol m}^{-2}\text{ d}^{-1}$, Borges et al., 2014) are minimal compared to primary production ($49\text{ mmol m}^{-2}\text{ d}^{-1}$; Darchambeau et al., 2014) and the export of organic carbon to the monimolimnion ($9.4\text{ mmol m}^{-2}\text{ d}^{-1}$) reported by Pasche et al. (2010). The outflow of organic carbon through

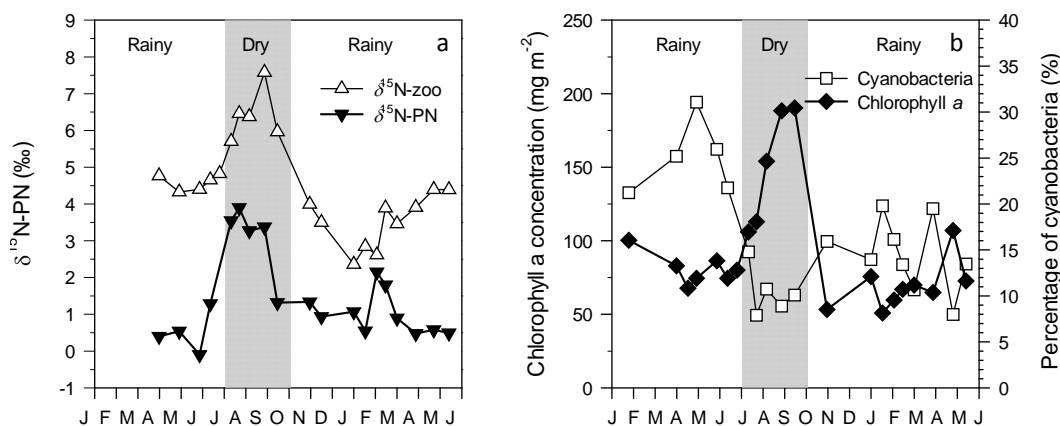


Figure 5. Temporal variability of (a) the $\delta^{15}\text{N}$ signature of the particulate nitrogen (PN) pool and zooplankton in the mixed layer, and (b) the chlorophyll *a* concentration (mg m^{-2}) and the relative contribution of cyanobacteria to the phytoplankton assemblage (percentage of biomass) in the mixolimnion, assessed from pigment analyses, between February 2012 and May 2013.

the Ruzizi River is also relatively low and was computed to be $0.6 \text{ mmol m}^{-2} \text{ d}^{-1}$ (this study) based on the long-term discharge average of Ruzizi ($83.2 \text{ m}^3 \text{ s}^{-1}$, Borges et al., 2014), the average POC and DOC in surface waters (0.052 and $0.142 \text{ mmol L}^{-1}$, this study). It implies that the outputs of OM ($9.4 + 0.7 = 10.1 \text{ mmol m}^{-2} \text{ d}^{-1}$) are higher than the inputs of OM from the catchment ($0.7\text{--}3.3 \text{ mmol m}^{-2} \text{ d}^{-1}$) suggesting a net autotrophic status of Lake Kivu.

However, these results contradict the commonly held view that oligotrophic lacustrine and marine systems tend to be net heterotrophic (Del Giorgio et al., 1997; Cole, 1999). Net heterotrophy implies that heterotrophic prokaryotes rely on a substantial amount of allochthonous OM; however, in Lake Kivu, riverine inputs of allochthonous OM from the catchment ($0.7\text{--}3.3 \text{ mmol m}^{-2} \text{ d}^{-1}$, Borges et al., 2014) are minimal. Indeed, the magnitude of allochthonous OM inputs relative to phytoplankton production depends strongly on the catchment to surface area ratio (Urban et al., 2005), that is particularly low (2.2) in Lake Kivu. Therefore, Lake Kivu is relatively poor in organic C, with DOC concentrations of $\sim 0.15 \text{ mmol L}^{-1}$ in contrast to smaller boreal humic lakes which show DOC concentrations of on average $\sim 1 \text{ mmol L}^{-1}$ (Sobek et al., 2007), and with values up to $\sim 4.5 \text{ mmol L}^{-1}$ (Weyhenmeyer and Karlsson, 2009). Humic substances are usually low-quality substrates for bacterial growth (Castillo et al., 2003), but limit primary production by absorbing incoming light. Hence, heterotrophic production in the photic zone of humic lakes usually exceeds phytoplankton production and DOC concentrations, despite the low substrate quality of humic substances, have been found to be a good predictor of the metabolic status of lakes in the boreal region, with a prevalence of net heterotrophy in organic-rich lakes (Jansson et al., 2000). However, low allochthonous OM inputs and low DOC concentration do not necessarily cause a system to be net autotrophic. For instance, Lake Superior, subsidised by a simi-

lar amount of allochthonous OM ($\sim 3 \text{ mmol m}^{-2} \text{ d}^{-1}$), has a lower catchment-to-surface area ratio (1.6), and its water has a DOC concentration even lower than in Lake Kivu ($\sim 0.1 \text{ mmol L}^{-1}$). However, it has been found to be net heterotrophic despite the limited allochthonous OM inputs (Urban et al., 2005). Lake Superior, as the majority of the lakes of the world, is holomictic, meaning that the mixing of its water column can seasonally reach the lake floor, and a substantial amount of sediments, including OM, could then be resuspended during these mixing events and hence re-exposed to microbial mineralisation in well-oxygenated waters (Meyers and Eadie, 1993; Cotner, 2000; Urban et al., 2005). The resuspension of bottom sediments could be important in the ecological functioning of these systems. In contrast, Lake Kivu, as other East African Great Lakes such as Tanganyika and Malawi, are particularly deep meromictic lakes, so that their water column is characterized by an almost complete decoupling between the surface and deep waters, preventing any resuspended bottom sediment to reach the surface waters in this system. In consequence, the coupling between the phytoplankton production of DOC and its heterotrophic consumption by prokaryotes in the clear, nutrient-depleted waters of Lake Kivu was found to be high throughout the year (Morana et al., 2014).

Besides morphometrical features, the net autotrophic status of Lake Kivu might also be related to general latitudinal and climatic patterns. Due to the warmer temperature in the tropics, phytoplankton production is comparatively higher in the East African Great Lakes compared with the Laurentian Great Lakes, despite similar phytoplankton abundance (Bootsma and Hecky, 2003). Alin and Johnson (2007) examined phytoplankton primary production and CO_2 emissions to the atmosphere fluxes in large lakes of world ($> 500 \text{ km}^2$). At the global scale, they found a statistically significant increase of the areal phytoplankton production in large lakes with the mean annual water temperature and the insolation;

as a consequence, a significant decrease of phytoplankton production with latitude. Also, they report a significant decrease of the CO₂ emissions to the atmosphere with the mean annual water temperature and therefore an increase of the CO₂ emission with the latitude. According to their estimations, less than 20 % of the phytoplankton primary production is sufficient to balance the carbon loss through CO₂ evasion and OM burial in sediments in large lakes located between the equator and the latitude 30°, but the CO₂ emission and OM accumulation in sediments exceed the phytoplankton primary production in systems located at latitude higher than 40° (Alin and Johnson, 2007). Overall, in morphometrically comparable systems, this global analysis suggests a trend from autotrophic to increasingly heterotrophic conditions with increasing latitude and decreasing mean annual water temperature and insolation (Alin and Johnson, 2007). Therefore, our study supports the view that paradigms established with data gathered in comparatively small temperate and boreal lakes may not directly apply to larger, tropical lakes (Bootsma and Hecky, 2003). It also highlights the need to consider the unique limnological characteristics of a vast region of the world that harbours 16 % of the total surface of lakes (Lehner and Döll, 2004), and account for 50 % of the global inputs of OM from continental waters to the oceans (Ludwig et al., 1996).

The $\delta^{13}\text{C}$ data indicate a difference in the origins of the POC and DOC pools in the mixed layer. Indeed, the $\delta^{13}\text{C}$ -DOC showed very little variation and appeared to be vertically and temporally uncoupled from the POC pool in the mixed layer (Fig. 6). A recent study (Morana et al., 2014) demonstrated that phytoplankton extracellular release of DOC is relatively high in Lake Kivu, and the fresh and labile autochthonous DOC produced by cell lysis, grazing or phytoplankton excretion, which reflects the $\delta^{13}\text{C}$ signature of POC, is quickly mineralised by heterotrophic bacteria. Therefore, it appears that the freshly produced autochthonous DOC contributes less than 1 % of the total DOC pool (Morana et al., 2014), and as the standing stock of phytoplankton-derived DOC seems very small, it can be hypothesised that the bulk DOC pool is mainly composed of older, more refractory compounds that reach the mixed layer through vertical advective and diffusive fluxes. Indeed, the $\delta^{13}\text{C}$ signature of the DOC in the monimolimnion (80–370 m, $-23.0 \pm 0.2\text{‰}$, $n = 24$) did not differ from the $\delta^{13}\text{C}$ -DOC in the mixolimnion (0–70 m, $-23.2 \pm 0.2\text{‰}$, $n = 5$), suggesting that they share the same origin (Fig. 4).

The concentration of the POC pool varied largely with depth, being the highest in the 0–20 m layer, i.e. roughly the euphotic zone. However, during the dry season, POC concentrations were almost as high in the oxycline than in surface waters. High POC concentrations in deep waters have frequently been observed in lakes, usually as a result of the resuspension of bottom sediments near the lake floor or the accumulation of sedimenting material in density gradients (Hawley and Lee, 1999). However, in the deep Lake Kivu,

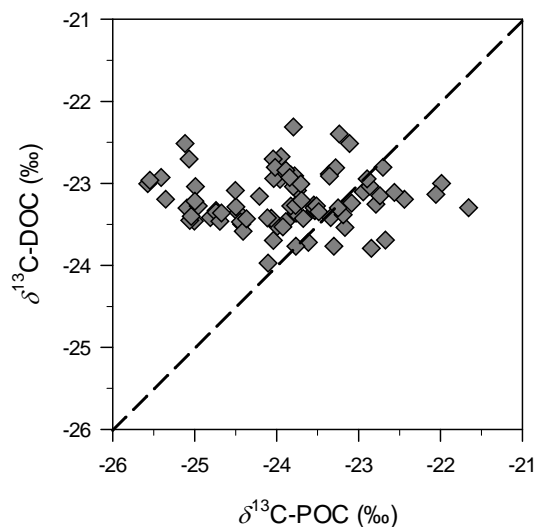


Figure 6. Relationship between the $\delta^{13}\text{C}$ signature of the particulate and dissolved organic carbon pool (POC and DOC, respectively) in the mixed layer.

this maximum POC zone is located approximately 300 m above the lake floor and is characterized by a strong depletion in ^{13}C of the POC pool. While DIC is probably the major C source of the POC pool in the mixed layer, the important decrease of $\delta^{13}\text{C}$ -POC values observed in the oxycline suggests that another ^{13}C -depleted C source was actively incorporated into the biomass at the bottom of the mixolimnion. Slight depletion in ^{13}C of the POC pool in oxyclines, such as in the Black Sea, has sometimes been interpreted as a result of the heterotrophic mineralisation of the sedimenting OM (Çoban-Yıldız et al., 2006), but it seems unlikely that, in Lake Kivu, heterotrophic processes could have caused an abrupt excursion of $\delta^{13}\text{C}$ -POC to values as low as -41.6‰ (65 m, 22 August 2012). Such large isotopic depletion of the POC pool in the water column has been reported by Blee et al. (2014), who measured $\delta^{13}\text{C}$ -POC as low as -49‰ in Lake Lugano, and it was related to high methanotrophic activity. In Lake Kivu, CH₄ concentrations were found to decrease sharply with decreasing depth at the oxic–anoxic transition (Borges et al., 2011), and the dissolved CH₄ that reached the oxycline via turbulent diffusivity and vertical advection (Schmid et al., 2005) is known to be isotopically light, with a $\delta^{13}\text{C}$ signature of approximately -60‰ (Pasche et al., 2011; Morana et al., 2015). Therefore, the vertical patterns in CH₄ concentrations and $\delta^{13}\text{C}$ -POC values observed during this study suggest that a substantial part of CH₄ was consumed and incorporated into the microbial biomass in the oxycline. Indeed, experiments carried out in Lake Kivu in February 2012 and September 2012 showed that microbial CH₄ oxidation was significant in the oxycline, and phospholipid fatty acid analysis revealed high abundance of methanotrophic bacteria of type I at the same depths (Morana et al., 2015). With es-

imates of the isotope fractionation factor during microbial CH_4 oxidation (1.016, Morana et al., 2015), and of the $\delta^{13}\text{C}$ - CH_4 at each sampling point, it is possible to estimate the theoretical $\delta^{13}\text{C}$ signature of methanotrophic organisms at each depth. Note that the $\delta^{13}\text{C}$ - CH_4 was not directly measured during this study but a very strong linear correlation between the log-transformed CH_4 concentrations and $\delta^{13}\text{C}$ - CH_4 was found along vertical profiles performed in February and September 2012 in Lake Kivu ($\delta^{13}\text{C}$ - $\text{CH}_4 = -7.911 \log(\text{CH}_4) - 13.027$; $r^2 = 0.87$, $n = 34$; Morana et al., 2015). Hence the $\delta^{13}\text{C}$ - CH_4 at each sampling point between January 2012 and May 2013 can be approximated from the measured CH_4 concentrations using this empirical relationship. Then, a simple isotope mixing model with the calculated $\delta^{13}\text{C}$ signature of methanotrophs and the average $\delta^{13}\text{C}$ -POC in the mixed layer as end-members allows us to determine the contribution of CH_4 -derived C to POC at each sampling depth. It appears that $4.4 \pm 1.9\%$ ($n = 13$) and $6.4 \pm 1.6\%$ ($n = 5$) of the depth-integrated POC pool in the mixolimnion was derived from CH_4 incorporation into the biomass during the rainy and dry season, respectively, and these percentages did not significantly differ between seasons (two-tailed t test, $p = 0.055$). Nevertheless, the low $\delta^{13}\text{C}$ signatures measured locally in the oxycline indicate that the contribution of CH_4 -derived C could be episodically as high as 50% (65 m, 22 August 2012). We hypothesise that microbial CH_4 oxidation could play an important role in the ecological functioning of Lake Kivu. Along with heterotrophic mineralisation of the sinking OM, and presumably other chemoautotrophic processes occurring in the oxycline such as nitrification (Llirós et al., 2010), CH_4 oxidation contributed substantially to O_2 consumption in the water column and was partly responsible for the seasonal uplift of the oxycline observed after the re-establishment of the thermal stratification during the rainy season. Furthermore, the methanotrophs in the oxycline actively participated in the uptake of dissolved inorganic phosphorus (DIP), and hence exerted an indirect control on phytoplankton by constantly limiting the vertical DIP flux to the illuminated surface waters (Haberyan and Hecky, 1987). Indeed, phytoplankton in Lake Kivu suffer from a severe P limitation throughout the year as pointed out by the relatively high sestonic C:P ratio (256 ± 75 ; Sarmiento et al., 2009; Darchambeau et al., 2014).

The $\delta^{15}\text{N}$ signature of the autochthonous OM in the mixed layer of Lake Kivu oscillated around 0‰ during the rainy season in Lake Kivu but was significantly higher during the dry season (3–4‰). Also, the $\delta^{15}\text{N}$ -PN in the mixed layer correlated negatively with the proportion of cyanobacteria in waters (Fig. 7, Pearson's r : -0.65 , $p = 0.004$, $n = 17$). This pattern may highlight the seasonal importance of N_2 -fixing cyanobacteria in Lake Kivu during the rainy season. Indeed, the $\delta^{15}\text{N}$ signature of atmospheric N_2 is close to 0‰, and isotope fractionation during cyanobacterial N_2 -fixation is known to be small (Fogel and Cifuentes, 1993). Several studies carried out in marine (Pacific Ocean and Gulf of

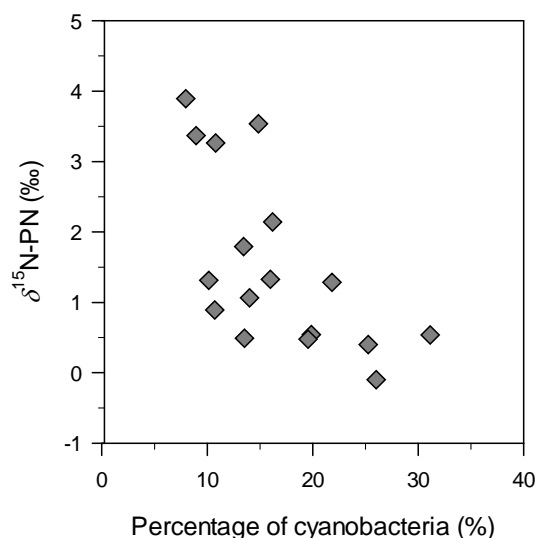


Figure 7. Relationship between the relative contribution of cyanobacteria to the phytoplankton assemblage (percentage of biomass) and the $\delta^{15}\text{N}$ signature of the particulate nitrogen pool in the mixed layer.

Mexico) and lacustrine (Lake Lugano) systems have shown that $\delta^{15}\text{N}$ -PN varied between -2 and $+1$ ‰ when N_2 -fixing cyanobacteria were dominating the phytoplankton assemblage (Wada and Hattori, 1976; Macko et al., 1987; Lehmann et al., 2004). Moreover, a good relationship between the $\delta^{15}\text{N}$ -PN and the abundance of N_2 -fixing cyanobacteria has already been reported for others systems, such as coastal lagoons (Lesutienė et al., 2014). In Lake Victoria, biological N_2 fixation has been identified as having the largest input of N, exceeding atmospheric deposition and river inputs, and N_2 fixation has been found to increase with light availability (Mugidde et al., 2003). This suggests that during the rainy season, when thermal stratification of the mixolimnion leads to reduced nitrogen supply combined with exposure to high light levels, N_2 -fixing cyanobacteria have a competitive advantage which may explain their seasonally higher contribution to the autochthonous OM pool (Sarmiento et al., 2006). Indeed, the significantly higher molar C:N ratio during the rainy season than the dry season indicates that N limitation in the mixed layer was stronger during the rainy season (this study, Sarmiento et al., 2009). By contrast, the deepening of the mixed layer during the dry season leads to increased nutrient input and reduced light availability that favours alternative phytoplankton strategies (Hecky and Kling, 1987, 2006; Sarmiento et al., 2006; Darchambeau et al., 2014), and consequently the proportion N_2 -fixing cyanobacteria decreases. A similar seasonal pattern of N_2 fixation was reported in Lake Victoria by Mugidde et al. (2003). In contrast with the rather constant $\delta^{13}\text{C}$ signature of zooplankton (-22.9 ± 0.8 ‰), the $\delta^{15}\text{N}$ analysis revealed that the $\delta^{15}\text{N}$ of zooplankton varied significantly, following well the sea-

sonal change in $\delta^{15}\text{N}$ -PN in the mixed layer. The difference between $\delta^{15}\text{N}$ -zooplankton and $\delta^{15}\text{N}$ -PN ($\Delta^{15}\text{N}_{\text{Zoo-PN}}$) was on average $3.2 \pm 1.0\text{‰}$ throughout the year while it was on average enriched in ^{13}C ($\Delta^{13}\text{C}_{\text{Zoo-POC}}$) by $0.9 \pm 0.8\text{‰}$. In nature, comparison of the $\delta^{15}\text{N}$ signature of consumers and their diet indicates that the $\delta^{15}\text{N}$ value increases consistently with the trophic level, because of the preferential excretion of the isotopically lighter ^{14}N (Montoya et al., 2002). However, the C isotope fractionation between consumers and diet is usually considered to be less than 1‰ (Sirevåg et al., 1977). The constant $\Delta^{15}\text{N}_{\text{Zoo-PN}}$ value found in Lake Kivu is within the range of trophic level enrichment between algae and *Daphnia magna* (~ 2 to 5‰) estimated in laboratory experiment (Adams and Sterner, 2000), and very close to the cross-system trophic enrichment value ($3.4 \pm 1.0\text{‰}$) proposed by Post (2002). Together with the slight enrichment in ^{13}C compared with the autochthonous POC pool, $\delta^{13}\text{C}$ and $\delta^{15}\text{N}$ analysis suggests that zooplankton directly incorporate phytoplankton-derived OM in their biomass (Masilya, 2011), and they rely almost exclusively on this source of OM throughout the year. This is in general agreement with the very low allochthonous OM inputs from rivers in Lake Kivu (Borges et al., 2014).

In conclusion, stable isotope data revealed large seasonal variability in the $\delta^{15}\text{N}$ signature of the PN pool, most likely related to changes in the phytoplankton assemblage and to N_2 -fixation. Contradicting the common observation that oligotrophic aquatic ecosystems tend to be net heterotrophic, the seasonality of $\delta^{13}\text{C}$ -DIC supports the view that the mixed layer of Lake Kivu is net autotrophic, as demonstrated by Borges et al. (2014) based on DIC and DI^{13}C mass balance considerations. The $\delta^{13}\text{C}$ -POC showed an important variation with depth due to the abundance of methanotrophic bacteria in the oxycline that fixed the lighter CH_4 -derived C into their biomass. The $\delta^{13}\text{C}$ -POC and $\delta^{13}\text{C}$ -DOC appeared to be uncoupled vertically and temporally, which could indicate that most of the DOC pool was composed of relatively refractory compounds. Finally, the $\delta^{13}\text{C}$ of zooplankton mirrored the $\delta^{13}\text{C}$ signature of the autochthonous POC pool, and its $\delta^{15}\text{N}$ signature followed the seasonal variability of the $\delta^{15}\text{N}$ -PN pool in good agreement with the expected consumer–diet isotope fractionation. This suggests that zooplankton rely throughout the year on phytoplankton-derived biomass as a organic C source.

Acknowledgements. We are grateful to Boniface Kaningini, Pascal Isumbisho (Institut Supérieur Pédagogique, Bukavu, DRC) for logistical support during the cruises, to Georges Alunga and the staff of the Unité d'Enseignement et de Recherche en Hydrobiologie Appliquée (UERHA – ISP Bukavu), who carried out the field sampling in DRC. We are also grateful to Marc-Vincent Commarieu, who carried out the TA measurements in the University of Liège, to Stephan Hoornaert, who carried out part of the CH_4 measurements and to Bruno Leporcq, who carried out the pigment analysis in the University of Namur. We thank

the two anonymous reviewers and the editor S. W. A. Naqvi for their comments and suggestions, which significantly contributed to improving the manuscript. This work was funded by the EAGLES (East African Great Lake Ecosystem Sensitivity to Changes, SD/AR/02A) project from the Belgian Federal Science Policy Office (BELSPO, Belgium) and contributes to the European Research Council (ERC) starting grant project AFRIVAL (African river basins: Catchment-scale carbon fluxes and transformations, 240002). Alberto V. Borges is a senior research associate at the FNRS (Belgium).

Edited by: S. W. A. Naqvi

References

- Adams, T. S. and Sterner, R. W.: The effect of dietary nitrogen content on trophic level ^{15}N enrichment, *Limnol. Oceanogr.*, 45, 601–607, 2000.
- Alin, S. R. and Johnson, T. C.: Carbon cycling in large lakes of the world: A synthesis of production, burial, and lake-atmosphere exchange estimates, *Global Biogeochem. Cy.*, 21, GB3002, doi:10.1029/2006GB002881, 2007.
- Bade, D. L., Carpenter, S. R., Cole, J. J., Hanson, P. C., and Hesslein, R. H.: Controls of $\delta^{13}\text{C}$ -DIC in lakes: Geochemistry, lake metabolism, and morphometry, *Limnol. Oceanogr.*, 49, 1160–1172, 2004.
- Blees, J., Niemann, H., Wenk, C. B., Zopfi, J., Schubert, C. J., Kirf, M. K., Veronesi, M. L., Hitz, C., and Lehmann, M. F.: Micro-aerobic bacterial methane oxidation in the chemocline and anoxic water column of deep south-Alpine Lake Lugano (Switzerland), *Limnol. Oceanogr.*, 59, 311–324, 2014.
- Bootsma, H. A. and Hecky, R. E.: A comparative introduction to the biology and limnology of the African Great Lakes, *J. Great Lakes Res.*, 29, 3–18, 2003.
- Borges, A. V., Abril, G., Delille, B., Descy, J. P., and Darchambeau, F.: Diffusive methane emissions to the atmosphere from Lake Kivu (Eastern Africa), *J. Geophys. Res.*, 116, G03032, doi:10.1029/2011JG001673, 2011.
- Borges, A. V., Morana, C., Bouillon, S., Servais, P., Descy, J.-P., and Darchambeau, F.: Carbon cycling of Lake Kivu (East Africa) : Net autotrophy in the epilimnion and emission of CO_2 to the atmosphere sustained by geogenic inputs, *PLoS ONE*, 9, e109500, doi:10.1371/journal.pone.0109500, 2014.
- Castañeda, I. S., Werne, J. P., Johnson, T. C., and Filley, T. R.: Late Quaternary vegetation history of southeast Africa: the molecular isotopic record from Lake Malawi. *Palaeogeography, Palaeoclimatology, Palaeoecology*, 275, 100–112, 2009.
- Castillo, M. M., Kling, G. W., and Allan, J. D.: Bottom-up controls on bacterial production in tropical lowland rivers, *Limnol. Oceanogr.*, 48, 1466–1475, 2003.
- Çoban-Yıldız, Y., Altabet, M. A., Yılmaz, A., and Tuğrul, S.: Carbon and nitrogen isotopic ratios of suspended particulate organic matter (SPOM) in the Black Sea water column, *Deep-Sea Res. Pt. II*, 53, 1875–1892, 2006.
- Cole, J. J.: Aquatic microbiology for ecosystem scientists: new and recycled paradigms in ecological microbiology, *Ecosystems*, 2, 215–225, 1999.

- Cotner, J. B., Johengen, T. H., and Biddanda, B. A.: Intense winter heterotrophic production stimulated by benthic resuspension, *Limnol. Oceanogr.*, 45, 1672–1676, 2000.
- Darchambeau, F., Sarmiento, H., and Descy, J.-P.: Primary production in a tropical large lake: The role of phytoplankton composition, *Sci. Total Environ.*, 473, 178–188, 2014.
- Del Giorgio, P. A., Cole, J. J., and Cimbleris, A.: Respiration rates in bacteria exceed phytoplankton production in unproductive aquatic systems, *Nature*, 385, 148–151, 1997.
- Descy, J.-P. and Sarmiento, H.: Microorganisms of the East African Great Lakes and their response to environmental changes, *Freshwater Reviews*, 1, 59–73, 2008.
- Descy, J.-P., Higgins, H. W., Mackey, D. J., Hurley, J. P., and Frost, T. M.: Pigment ratios and phytoplankton assessment in northern Wisconsin lakes, *J. Phycol.*, 36, 274–286, 2000.
- Duarte, C. M. and Prairie, Y. T.: Prevalence of heterotrophy and atmospheric CO₂ emissions from aquatic ecosystems, *Ecosystems*, 8, 862–870, 2005.
- Finlay, K., Leavitt, P. R., Patoine, A., and Wissel, B.: Magnitudes and controls of organic and inorganic carbon flux through a chain of hardwater lakes on the northern Great Plains, *Limnol. Oceanogr.*, 55, 1551–1564, 2010.
- Fogel, M. L. and Cifuentes, L. A.: Isotope fractionation during primary production, 73–98, in: *Organic geochemistry*, edited by: Engel, M. H. and Macko, S. A., Plenum Press, New York, 1993.
- Gillikin, D. P. and Bouillon, S.: Determination of $\delta^{18}\text{O}$ of water and $\delta^{13}\text{C}$ of dissolved inorganic carbon using a simple modification of an elemental analyser-isotope ratio mass spectrometer: an evaluation, *Rapid Commun. Mass Sp.*, 21, 1475–1478, 2007.
- Gran, G.: Determination of the equivalence point in potentiometric titrations. Part II, *Analysis*, 77, 661–671, 1952.
- Grey, J., Jones, R. I., and Sleep, D.: Seasonal changes in the importance of the source of organic matter to the diet of zooplankton in Loch Ness, as indicated by stable isotope analysis, *Limnol. Oceanogr.*, 46, 505–513, 2001.
- Haberyan, K. A. and Hecky, R. E.: The late Pleistocene and Holocene stratigraphy and paleolimnology of Lakes Kivu and Tanganyika, *Palaeogeogr. Palaeoclimatol.*, 61, 169–197, 1987.
- Hawley, N. and Lee, C. H.: Sediment resuspension and transport in Lake Michigan during the unstratified period, *Sedimentology*, 46, 791–805, 1999.
- Hecky, R. E. and Kling, H. J.: Phytoplankton ecology of the great lakes in the rift valleys of Central Africa, *Arch. Hydrobiol.-Beiheft Ergebnisse der Limnologie*, 25, 197–228, 1987.
- Herczeg, A. L.: A stable carbon isotope study of dissolved inorganic carbon cycling in a softwater lake, *Biogeochemistry*, 4, 231–263, 1987.
- Hollander, D. J. and McKenzie, J. A.: CO₂ control on carbon-isotope fractionation during aqueous photosynthesis: A paleo-pCO₂ barometer, *Geology*, 19, 929–932, 1991.
- Jansson, M., Bergström, A. K., Blomqvist, P., and Drakare, S.: Allochthonous organic carbon and phytoplankton/bacterioplankton production relationships in lakes, *Ecology*, 81, 3250–3255, 2000.
- Kaningini, M.: Etude de la croissance, de la reproduction et de l'exploitation de *Limnothrix miodon* au lac Kivu, bassin de Bukavu (Zaire), PhD thesis, Facultés Universitaires Notre Dame de la Paix, Namur, Belgium, 1995.
- Kankaala, P., Taipale, S., Grey, J., Sonninen, E., Arvola, L., and Jones, R. I.: Experimental $\delta^{13}\text{C}$ evidence for a contribution of methane to pelagic food webs in lakes, *Limnol. Oceanogr.*, 51, 2821–2827, 2006.
- Lehmann, M. F., Bernasconi, S. M., McKenzie, J. A., Barbieri, A., Simona, M., and Veronesi, M.: Seasonal variation of the $\delta^{13}\text{C}$ and $\delta^{15}\text{N}$ of particulate and dissolved carbon and nitrogen in Lake Lugano: Constraints on biogeochemical cycling in a eutrophic lake, *Limnol. Oceanogr.*, 49, 415–429, 2004.
- Lehner, B. and Döll, P.: Development and validation of a global database of lakes, reservoirs and wetlands, *J. Hydrol.*, 296, 1–22, 2004.
- Lesutienė, J., Bukaveckas, P. A., Gasiūnaitė, Z. R., Pilkaitytė, R., and Razinkovas-Baziukas, A.: Tracing the isotopic signal of a cyanobacteria bloom through the food web of a Baltic Sea coastal lagoon, *Estuar. Coast. Shelf Sci.*, 138, 47–56, 2014.
- Lewis, W. M. J.: Tropical lakes: how latitude makes a difference, in: *Perspectives Tropical Limnology*, edited by: F. Schiemer and Boland, K. T., SPB Academic Publishing, Amsterdam, 43–64, 1996.
- Llirós, M., Gich, F., Plasencia, A., Auguet, J. C., Darchambeau, F., Casamayor, E. O., Descy, J.-P., and Borrego, C.: Vertical distribution of ammonia-oxidizing crenarchaeota and methanogens in the epipelagic waters of Lake Kivu (Rwanda-Democratic Republic of the Congo), *Appl. Environ. Microb.*, 76, 6853–6863, 2010.
- Ludwig, W., Probst, J. L., and Kempe, S.: Predicting the oceanic input of organic carbon by continental erosion, *Global Biogeochem. Cy.*, 10, 23–41, 1996.
- Macko, S. A., Fogel, M. L., Hare, P. E., and Hoering, T. C.: Isotopic fractionation of nitrogen and carbon in the synthesis of amino acids by microorganisms, *Chem. Geol.*, 65, 79–92, 1987.
- Marcé, R., Obrador, B., Morguá, J.-A., Lluís Riera, J., López, P., and Armengol, J.: Carbonate weathering as a driver of CO₂ supersaturation in lakes, *Nature Geosci.*, 8, 107–111, 2015.
- Masilya, P.: Ecologie alimentaire compare de *Limnothrix miodon* et de *Lamprichthys tanganicanus* au lac Kivu (Afrique de l'Est), PhD thesis, Facultés Universitaires Notre Dame de la Paix, Namur, Belgium, 2011.
- Meyers, P. A. and Eadie, B. J.: Sources, degradation and recycling of organic matter associated with sinking particles in Lake Michigan, *Org. Geochem.*, 20, 47–56, 1993.
- Millero, F. J., Graham, T. B., Huang, F., Bustos-Serrano, H., and Pierrot, D.: Dissociation constants of carbonic acid in sea water as a function of salinity and temperature, *Mar. Chem.*, 100, 80–94, 2006.
- Montoya, J. P., Carpenter, E. J., and Capone, D. G.: Nitrogen fixation and nitrogen isotope abundances in zooplankton of the oligotrophic North Atlantic, *Limnol. Oceanogr.*, 47, 1617–1628, 2002.
- Morana, C., Sarmiento, H., Descy, J.-P., Gasol, J. M., Borges, A. V., Bouillon, S., and Darchambeau, F.: Production of dissolved organic matter by phytoplankton and its uptake by heterotrophic prokaryotes in large tropical lakes, *Limnol. Oceanogr.*, 59, 1364–1375, 2014.
- Morana, C., Borges, A. V., Roland, F. A. E., Darchambeau, F., Descy, J.-P., and Bouillon, S.: Methanotrophy within the water column of a large meromictic tropical lake (Lake Kivu, East Africa), *Biogeosciences*, 12, 2077–2088, doi:10.5194/bg-12-2077-2015, 2015.

- Mugidde, R., Hecky, R. E., Hendzel, L. L., and Taylor, W. D.: Pelagic nitrogen fixation in Lake Victoria (East Africa), *J. Great Lakes Res.*, 29, 76–88, 2003.
- Pasche, N., Alunga, G., Mills, K., Muvundja, F., Ryves, D. B., Schurter, M., Wehrli, B., and Schmid, M.: Abrupt onset of carbonate deposition in Lake Kivu during the 1960s: response to recent environmental changes, *J. Paleolimnol.*, 44, 931–946, 2010.
- Pasche, N., Schmid, M., Vazquez, F., Schubert, C. J., Wüest, A., Kessler, J. D., Pack, M. A., Reeburgh, W. S., and Bürgmann, H.: Methane sources and sinks in Lake Kivu, *J. Geophys. Res.*, 116, G03006, doi:10.1029/2011JG001690, 2011.
- Post, D. M.: Using stable isotopes to estimate trophic position: models, methods, and assumptions, *Ecology*, 83, 703–718, 2002.
- Prairie, Y. T., Bird, D. F., and Cole, J. J.: The summer metabolic balance in the epilimnion of southeastern Quebec lakes, *Limnol. Oceanogr.*, 47, 316–321, 2002.
- Sarmiento, H.: New paradigms in tropical limnology: the importance of the microbial food web, *Hydrobiologia*, 686, 1–14, 2012.
- Sarmiento, H., Isumbisho, M., and Descy, J.-P.: Phytoplankton ecology of Lake Kivu (eastern Africa), *J. Plankton Res.*, 28, 815–829, 2006.
- Sarmiento, H., Isumbisho, M., Stenuite, S., Darchambeau, F., Leporcq, B., and Descy, J.-P.: Phytoplankton ecology of Lake Kivu (eastern Africa): biomass, production and elemental ratios, *Int. Ver. Theor. Angew.*, 30, 709–713, 2009.
- Schelske, C. L. and Hodell, D. A.: Recent changes in productivity and climate of Lake Ontario detected by isotopic analysis of sediments, *Limnol. Oceanogr.*, 36, 961–975, 1991.
- Schmid, M., Halbwachs, M., Wehrli, B., and Wüest, A.: Weak mixing in Lake Kivu: new insights indicate increasing risk of uncontrolled gas eruption, *Geochem. Geophys. Geosy.*, 6, Q07009, doi:10.1029/2004GC000892, 2005.
- Sirevåg, R., Buchanan, B. B., Berry, J. A., and Troughton, J. H.: Mechanisms of CO₂ fixation in bacterial photosynthesis studied by the carbon isotope fractionation technique, *Arch. Microbiol.*, 112, 35–38, 1977.
- Sobek, S., Tranvik, L. J., Prairie, Y. T., Kortelainen, P., and Cole, J. J.: Patterns and regulation of dissolved organic carbon: An analysis of 7,500 widely distributed lakes, *Limnol. Oceanogr.*, 52, 1208–1219, 2007.
- Stets, E. G., Striegl, R. G., Aiken, G. R., Rosenberry, D. O., and Winter, T. C.: Hydrologic support of carbon dioxide flux revealed by whole-lake carbon budgets, *J. Geophys. Res.*, 114, G01008, doi:10.1029/2008JG000783, 2009.
- Thiery, W., Martynov, A., Darchambeau, F., Descy, J.-P., Plisnier, P.-D., Sushama, L., and van Lipzig, N. P. M.: Understanding the performance of the FLake model over two African Great Lakes, *Geosci. Model Dev.*, 7, 317–337, doi:10.5194/gmd-7-317-2014, 2014.
- Urban, N. R., Auer, M. T., Green, S. A., Lu, X., Apul, D. S., Powell, K. D., and Bub, L.: Carbon cycling in Lake Superior, *J. Geophys. Res.-Oceans*, 110, C06S90, doi:10.1029/2003JC002230, 2005.
- Wada, E. and Hattori, A.: Natural abundance of ¹⁵N in particulate organic matter in the North Pacific Ocean, *Geochim. Cosmochim. Ac.*, 40, 249–251, 1976.
- Weiss, R. F.: Determinations of carbon dioxide and methane by dual catalyst flame ionization chromatography and nitrous oxide by electron capture chromatography, *J. Chromatogr. Sci.*, 19, 611–616, 1981.
- Weyhenmeyer, G. A. and Karlsson, J.: Nonlinear response of dissolved organic carbon concentrations in boreal lakes to increasing temperatures, *Limnol. Oceanogr.*, 54, 2513–2519, 2009.
- Wright, S. W., Jeffrey, S. W., Mantoura, R. F. C., Llewellyn, C. A., Bjornland, T., Repeta, D., and Welschmeyer, N.: Improved HPLC method for the analysis of chlorophylls and carotenoids from marine phytoplankton, *Mar. Ecol.-Prog. Ser.*, 77, 183–196, 1991.

Production of dissolved organic matter by phytoplankton and its uptake by heterotrophic prokaryotes in large tropical lakes

Cedric Morana,^{1,*} Hugo Sarmiento,^{2,3} Jean-Pierre Descy,⁴ Josep M. Gasol,³ Alberto V. Borges,⁵ Steven Bouillon,¹ and François Darchambeau⁵

¹Katholieke Universiteit Leuven (KU Leuven), Department of Earth and Environmental Sciences, Leuven, Belgium

²Federal University of São Carlos (UFSCar), Department of Hydrobiology (DHb), São Carlos, Brazil

³Institut de Ciències del Mar–Consejo Superior de Investigaciones Científicas (CSIC), Barcelona, Catalunya, Spain

⁴Université de Namur, Research Unit in Environmental and Evolutionary Biology, Namur, Belgium

⁵Université de Liège, Chemical Oceanography Unit, Liège, Belgium

Abstract

In pelagic ecosystems, phytoplankton extracellular release can extensively subsidize the heterotrophic prokaryotic carbon demand. Time-course experiments were carried out to quantify primary production, phytoplankton excretion, and the microbial uptake of freshly released dissolved organic carbon (DOC) derived from phytoplankton extracellular release (DOC_p) in four large tropical lakes distributed along a productivity gradient: Kivu, Edward, Albert, and Victoria. The contributions of the major heterotrophic bacterial groups to the uptake of DOC_p was also analyzed in Lake Kivu, using microautoradiography coupled to catalyzed reporter deposition fluorescent in situ hybridization. The percentage of extracellular release (PER) varied across the productivity gradient, with higher values at low productivity. Furthermore, PER was significantly related to high light and low phosphate concentrations in the mixed layer and was comparatively higher in oligotrophic tropical lakes than in their temperate counterparts. Both observations suggest that environmental factors play a key role in the control of phytoplankton excretion. Standing stocks of DOC_p were small and generally contributed less than 1% to the total DOC because it was rapidly assimilated by prokaryotes. In other words, there was a tight coupling between the production and the heterotrophic consumption of DOC_p. None of the major phylogenetic bacterial groups that were investigated differed in their ability to take up DOC_p, in contrast with earlier results reported for standard labeled single-molecule substrates (leucine, glucose, adenosine triphosphate). It supports the idea that the metabolic ability to use DOC_p is widespread among heterotrophic prokaryotes. Overall, these results highlight the importance of carbon transfer between phytoplankton and bacterioplankton in large African lakes.

In aquatic systems, the dissolved organic carbon (DOC) pool is a mixture of molecules in a continuum of biological lability, with components from different origins: allochthonous, in freshwaters mainly deriving from the watershed runoff, and autochthonous material produced in situ, such as DOC derived from phytoplankton extracellular release (DOC_p) or cell lysis (Myklestad 2000). Both carbon (C) sources can be important to sustain the growth of heterotrophic prokaryotes, but bacteria are highly selective toward the substrate they use (Sarmiento and Gasol 2012). In most aquatic systems, heterotrophic bacteria preferentially use labile freshly produced DOC_p over more recalcitrant allochthonous compounds (Pérez and Sommaruga 2006). Positive correlations between particulate primary production (pPP) and bacterial production (BP) have been reported for many aquatic systems (Cole et al. 1988; Fouilland and Mostajir 2010). These observations have been used to demonstrate the dependence of heterotrophic bacteria on phytoplankton activity mediated by the release of DOC_p. But both phytoplankton and bacterial populations might also be regulated by the same environmental factors, such as inorganic nutrient availability, and then might co-vary with no major interaction (Fouilland and Mostajir 2010). One way to test the interaction strength between primary producers and

bacteria is to measure the phytoplankton production of DOC_p (dissolved primary production; dPP) and the kinetics of its uptake by heterotrophic prokaryotes (Morán et al. 2001; Sarmiento and Gasol 2012).

Despite its relevance in ecosystem studies, measurements of dPP are scarce, especially in freshwater ecosystems. Based on a literature review, Baines and Pace (1991) proposed an average cross-system percentage of extracellular release (PER) of 13% of total C fixation. However, when comparing freshwater and marine data, it was observed that PER in marine systems was constant across the productivity gradient; whereas, in temperate freshwaters, PER was inversely related to productivity (Baines and Pace 1991). A similar inverse relation in temperate freshwater was found in the recent literature review by Fouilland and Mostajir (2010). There is an ongoing debate about whether DOC_p release is an overflow mechanism, whereby DOC_p is actively released by healthy phytoplankton cells and is, therefore, constrained by the availability of photosynthates (Fogg 1983; Baines and Pace 1991; Morán and Estrada 2002), or whether DOC_p release is a purely passive physiological mechanism, directly proportional to phytoplankton biomass (Bjørnsen 1988; Marañón et al. 2004). Several environmental factors affect PER rates, such as nutrient availability (Obernosterer and Herndl 1995), light conditions (Fogg 1983), and temperature (Zlotnik and Dubinsky 1989); but no consensus has been achieved so far

* Corresponding author: cedric.morana@ees.kuleuven.be

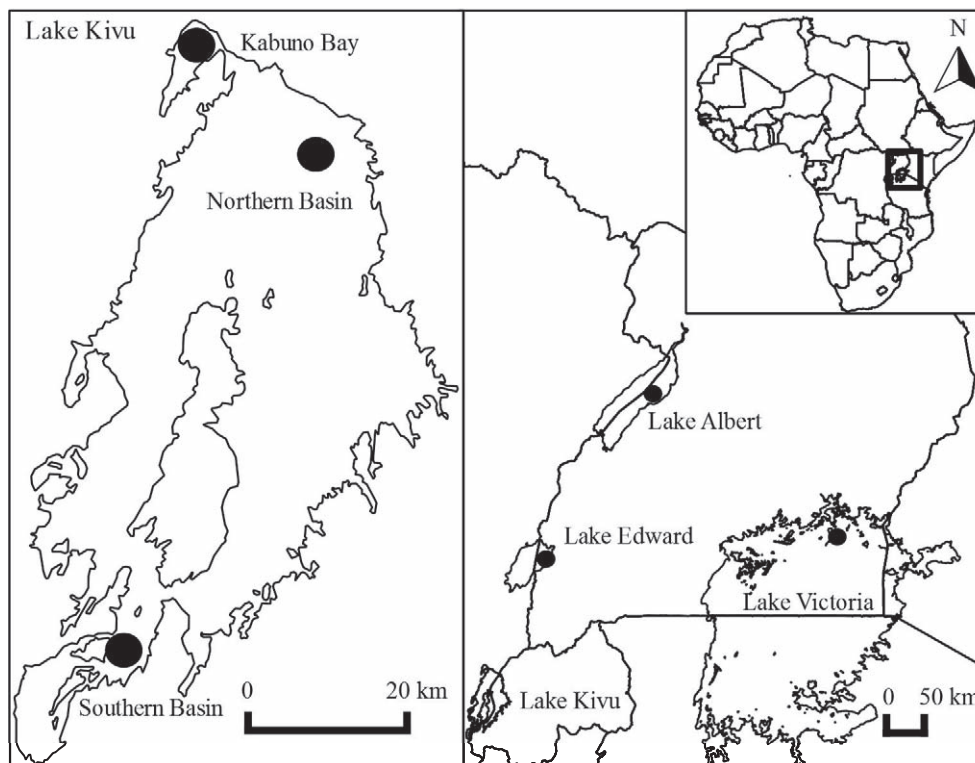


Fig. 1. Map of lakes Kivu, Albert, Edward, and Victoria, showing the location of the sampling sites (black circle) in April 2009, October 2010, and June 2011 in Lake Kivu, and in May 2012 in lakes Edward, Albert, and Victoria.

on the key environmental factors that determine the importance of PER and on how PER varies in the function of each one of these factors.

The aims of this study were to quantify dPP and the subsequent microbial uptake of DOCp in several large tropical lakes and to elucidate whether the PER was constant, or not, across a range of productivity. Due to the constant exposure to low-nutrient and high-light conditions over long periods of time in oligotrophic tropical lakes, we expected a strong coupling between phytoplankton and heterotrophic prokaryotes through high DOCp release. We performed several time-course experiments of radiocarbon incorporation into dissolved and particulate organic pools, which allowed for correction for heterotrophic uptake of DOCp during the experiments. Furthermore, in one of our study sites (Lake Kivu), we applied the microautoradiography coupled with catalyzed reporter deposition fluorescence in situ hybridization (MAR-FISH) technique to assess the extent to which different groups of heterotrophic prokaryotes were active in the uptake of DO^{14}Cp released by the natural phytoplankton communities and of ^3H -leucine, a widely used tracer for BP measurements (Kirchman et al. 1985).

Methods

Study site and water sampling—Data were obtained in large East African lakes Kivu, Edward, Albert, and Victoria (Fig. 1). Sampling in Lake Kivu was conducted

in the main lake (northern basin $01^{\circ}43'S$, $29^{\circ}14'E$; southern basin $02^{\circ}20'S$, $28^{\circ}58'E$) and in Kabuno Bay ($01^{\circ}37'S$, $29^{\circ}02'E$) in April 2009 (late rainy season), October 2010 (rainy season), and June 2011 (dry season; Fig. 1). Both systems are meromictic but differ in terms of morphometry, with a shallower permanent chemocline in Kabuno Bay compared to the main lake (Borges et al. 2011). Lakes Edward ($00^{\circ}12'N$, $29^{\circ}49'E$), Albert ($01^{\circ}48'N$, $31^{\circ}16'E$), and Victoria ($00^{\circ}33'N$, $33^{\circ}16'E$) were sampled in May 2012. They are shallower than Lake Kivu and are holomictic; consequently, chlorophyll *a* (Chl *a*) concentrations are usually higher in their mixed layer. General limnological characteristics of the four lakes are provided in Table 1.

Sampling procedure—The mixed-layer depth was determined at each occasion, based on in situ observed vertical profiles of temperature and oxygen obtained with a Yellow Springs Instruments 6600 v2 multiparameter probe. Water was collected with a 7 liter Niskin bottle (Hydro-Bios) at a depth interval of 5 m from the surface to the bottom of the mixed layer and was then pooled to obtain a representative sample of the mixed layer. The vertical light attenuation coefficient, K (m^{-1}), was calculated from simultaneous measurements of surface irradiance with a Li-Cor LI-190 quantum sensor and underwater photosynthetically active radiation (PAR) measurements with a submersible Li-Cor LI-193SA spherical quantum sensor. K was derived from the slope of the semi-logarithmic regression between relative

Table 1. General limnological characteristics of the lakes investigated.

	Lake Kivu (main lake)	Lake Kivu (Kabuno Bay)	Lake Edward	Lake Albert	Lake Victoria
Lake area (km ²)	2322	48	2325	5300	68800
Catchment area (km ²)	4613	3	15840	17000	195000
Maximum depth (m)	485	120	117	58	79
Mean depth (m)	245	65	40	25	40
Mixing regime	Meromictic	Meromictic	Holomictic	Holomictic	Holomictic
Mixed layer temperature (°C)	23.0–24.5*	22.5–24.5*	25.2–27.2†	27.4–29.0†	25.2–27.7‡
Mean Chl <i>a</i> (mg m ⁻³)	2.2§	2.6*	5–10	13–60‡	26.5¶
Mean TP concentration (μmol L ⁻¹)	0.6*	1.0*	1.4	2.5	2.5¶
Mean euphotic depth 1% (m)	18§	10*	13	6–12‡	9‡

* This study.

† Verbeke 1957.

‡ R. Mugidde unpubl.

§ Darchambeau et al. 2014.

| Lehman et al. 1998.

¶ Guildford and Hecky 2000.

quantum irradiance and depth. The mean irradiance in the mixed layer (I_{Z_m}) was calculated following Riley (1957):

$$I_{Z_m} = I_0 \times (1 - e^{-K \times Z_m}) / (K \times Z_m)$$

where I_0 is the incident irradiance at the surface ($\mu\text{mol photon m}^{-2} \text{ s}^{-1}$), K (m^{-1}) is the vertical light attenuation coefficient, and Z_m (m) is the mixed-layer depth.

Chemical analyses—Phosphate (PO_4^{3-}) concentrations were quantified spectrophotometrically following standard procedures (American Public Health Association 1998). Measurements of pH were carried out with a Metrohm (6.0253.100) combined electrode calibrated with U.S. National Bureau of Standards buffers of pH 4.002 (25°C) and pH 6.881 (25°C), prepared according to Frankignoulle and Borges (2001). Measurements of total alkalinity (TA) were carried out by open-cell titration with HCl 0.1 mol L⁻¹ on 50 mL water samples, and data were quality checked with Certified Reference Material acquired from Andrew Dickson (Scripps Institution of Oceanography, University of California, San Diego). Typical precision for TA measurements was better than $\pm 3 \mu\text{mol L}^{-1}$. Dissolved inorganic carbon (DIC) was computed from pH and TA measurements, using the carbonic acid dissociation constants of Millero et al. (2006). Water samples for DOC concentrations were filtered through preflushed 0.2 μm syringe filters in 40 mL borosilicate vials with Teflon-coated screw caps and were preserved with 0.1 mL of H₃PO₄ (50%). DOC concentrations were measured with a customized Thermo Hipertoc coupled to a Delta+XL isotope ratio mass spectrometer, whereby complete oxidation of the sample is ensured by a combination of sodium persulfate addition, heating, and ultraviolet radiation. Quantification and calibration was performed with a standard solution of sucrose purchased from the International Atomic Energy Agency (IAEA-C6). Typical reproducibility for DOC analyses was on the order of < 5%.

Chl *a* concentration—Chl *a* concentrations were determined by high-performance liquid chromatography

(HPLC). At each sampling site, 3 liters of water from the mixed layer pool was filtered on a Macherey-Nägel GF-5 filter (nominal porosity of 0.4 μm). Pigment extraction was carried out in 10 mL of 90% HPLC grade acetone. After two sonication steps of 15 min separated by an overnight period at 4°C, the extracts were stored in 2 mL amber vials at -25°C. HPLC analysis was performed following the method described in Sarmiento et al. (2008), with a Waters system comprising a photodiode array and fluorescence detectors. Calibration was made using commercial external standards (DHI Lab Products). Precision for Chl *a* measurement was better than $\pm 7\%$.

pPP and dPP and heterotrophic uptake of freshly excreted compounds—pPP and microbial uptake are usually estimated by tracing the incorporation of a radioactive tracer (¹⁴C) into two different size fractions representing phytoplankton (> 2 μm) and heterotrophic prokaryotes (< 2 μm ; Cole et al. 1982). However, the important contribution of picophytoplankton (< 2 μm) to total phytoplankton biomass in some African lakes (21% in Lake Kivu; Sarmiento et al. 2008) complicates the physical separation of the primary producers from heterotrophic prokaryotes by such a size-selective filtration. This problem may be overcome by measurement of the time-course incorporation of ¹⁴C into the dissolved (< 0.2 μm) and particulate (> 0.2 μm) phase, the latter including both heterotrophic prokaryotes and phytoplankton (Morán et al. 2001; Morán and Estrada 2002). Results are then modeled by a compartmental organic C exchange model, extensively described by Morán and Estrada (2002), and are briefly summarized in the next section. Due to the importance of picophytoplankton in some lakes studied, this approach was preferred for this study.

In the field, aliquots of 40 mL of water from the mixed-layer pool were introduced in transparent 70 mL sterile polycarbonate cell culture flasks. Each bottle was spiked with 62.5 μCi of NaH¹⁴CO₃ (specific activity of 40–60 mCi mmol⁻¹; Perkin Elmer) and then was incubated at in situ temperature under a constant PAR of 200 $\mu\text{mol photon m}^{-2} \text{ s}^{-1}$ provided by a Philips fluorescent lamp (PL

Table 2. Mixed-layer depth (Z_m ; m), mean daylight irradiance in the mixed layer (I_{Z_m} ; $\mu\text{mol photon m}^{-2} \text{s}^{-1}$), particulate and dissolved primary production (pPP and dPP; $\text{mg C m}^{-3} \text{h}^{-1}$), percentage of extracellular release (PER; %), concentrations of Chl *a* (mg m^{-3}), dissolved organic carbon (DOC; mg C m^{-3}), freshly excreted dissolved organic carbon (DOCp; mg C m^{-3}), and DOCp turnover times (h) in lakes Kivu (Southern bay, Northern bay, Kabuno Bay), Edward, Albert, and Victoria.

Station	Year	Z_m	I_{Z_m}	pPP	dPP	PER	Chl <i>a</i>	DOC	DOCp	Turnover DOCp
Southern bay	2009	20	220	0.8	1.1	57	1.9	1967	1.7	1.5
Southern bay	2010	12.5	381	2.8	2.8	50	2.1	1924	3.6	1.3
Southern bay	2011	30	186	1.7	3.0	64	2.1	1757	3.9	1.3
Northern bay	2009	22.5	249	1.6	2.6	62	1.2	1911	6.4	2.1
Northern bay	2010	22.5	243	4.0	3.9	49	2.3	1872	2.3	0.6
Northern bay	2011	42.5	76	2.9	2.7	48	2.0	1709	3.6	1.3
Kabuno Bay	2009	10	162	3.9	3.9	50	2.4	2341	8.3	2.5
Kabuno Bay	2011	5	265	5.1	3.7	42	2.6	1779	13.2	3.6
Lake Edward	2012	7.5	145	26.8	6.5	20	9.9	4757	5.5	0.8
Lake Albert	2012	20	95	27.4	5.9	18	5.4	4383	3.6	0.6
Lake Victoria	2012	15	108	172.7	9.4	5	5.1	1807	102.3	10.9

55W Daylight DeLuxe). This light intensity was close to the mean I_{Z_m} of the investigated lakes at the time of the experiments (Table 2) and to the saturation irradiance value (I_k) reported for Lake Kivu ($318 \mu\text{mol photon m}^{-2} \text{s}^{-1}$; Darchambeau et al. 2014). The incubations lasted for 5–6 h, and, at 30 or 60 min intervals, biological activity was stopped by adding neutral formaldehyde (0.02% final concentration) into two transparent flasks. Two additional flasks covered with aluminum foil were processed in the same manner immediately at the beginning and at the end of the experiment, providing a dark incorporation control. The bottles were then kept overnight at 4°C before subsequent processing. From each flask, a 20 mL subsample was filtered under low-pressure vacuum on membrane filters (Millipore GSWP; $0.22 \mu\text{m}$ nominal porosity) to separate the particulate from the dissolved fraction. In order to remove the labeled inorganic C (DI^{14}C), liquid samples (DO^{14}C) were acidified with 1 mL of HCl (6 mol L^{-1}) and were left open overnight in an orbital shaker, and filters (PO^{14}C) were fumed overnight with

concentrated HCl. Radioactivity of the filters and liquid samples was measured using a Packard Tri-Carb Liquid Scintillation Counter with Ultima Gold (Perkin Elmer) as scintillation cocktail and the external standard method for quench correction. T_0 values were subtracted from values of subsequent samples in order to correct for the abiotic radiocarbon incorporation. The radioactivity values in dark incorporation control bottles at the end of every experiment were never significantly different than values in the respective T_0 -bottles; therefore, they were not subtracted.

Organic C exchange model—Assuming steady state, the experimental results were fitted with a three-compartment model of organic C exchange, extensively described in Morán et al. (2001) and Morán and Estrada (2002). The rate of change of the radiocarbon content in the three different compartments is described by the following equations (Fig. 2):

$$dC_1/dt = -k_{(2,1)} \times C_1 + k_{(1,2)} \times C_2 - k_{(3,1)} \times C_1 \quad (1)$$

$$dC_2/dt = k_{(2,1)} \times C_1 - k_{(1,2)} \times C_2 + k_{(2,3)} \times C_3 \quad (2)$$

$$dC_3/dt = k_{(3,1)} \times C_1 - k_{(2,3)} \times C_3 \quad (3)$$

where C_1 is the radiocarbon concentration in the DIC pool, C_2 is the radiocarbon concentration in the particulate organic carbon (POC) pool, and C_3 is the radiocarbon concentration in the DOC pool; $k_{(i,j)}$ is the rate constant of C flux from pool *j* to pool *i* (in h^{-1}). Hence, $k_{(2,1)}$ is the rate constant of pPP, $k_{(1,2)}$ is the rate constant of respiration of synthesized POC, inferred from its influence on the PO^{14}C kinetics, $k_{(3,1)}$ is the rate constant of phytoplankton excretion or dPP, and $k_{(2,3)}$ is the rate constant of heterotrophic uptake of freshly produced DOCp.

A striking particularity of the model lies in the origin of the DOCp production flux. Although it is obvious that DOCp should first be incorporated by phytoplankton before its excretion, the model considers the DOCp to be directly produced from a subcompartment integrated into the DIC pool, the organic C fated for release (OCR) pool. This subcompartment is defined as an intracellular

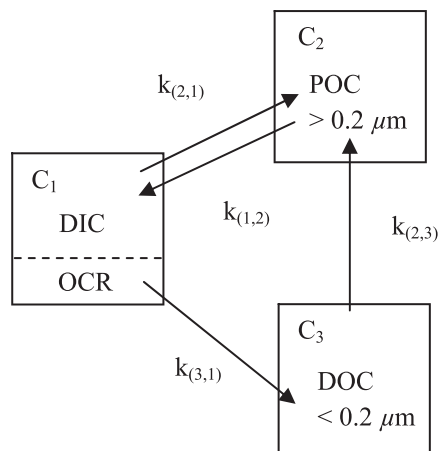


Fig. 2. Schematic representation of the three-compartment model applied on the experimental data. DIC = dissolved inorganic carbon, DOC = dissolved organic carbon, POC = particulate organic carbon, OCR = intracellular pool of organic carbon fated for release pool; see text and Morán et al. (2001) for further details.

phytoplankton C pool of organic compounds and is assumed to be quasi-instantaneously in isotopic equilibrium with the DIC pool (Morán et al. 2001; Morán and Estrada 2002). This assumption was confirmed experimentally, for example, by the absence of any lag phase in DO¹⁴C kinetic curve when phytoplankton incorporates labeled-DIC (Wiebe and Smith 1977; our own results below).

Least-squares nonlinear fitting of the model to dissolved (DO¹⁴C) and particulate (PO¹⁴C) radioactivity measurement was performed using Saam II software (Epsilon Group). Data were weighted by the inverse of the standard deviation of duplicates. The pPP and dPP rates were respectively calculated from $k_{(2,1)}$ and $k_{(3,1)}$ multiplied by the DIC concentration. PER (%) was calculated as:

$$\text{PER} = \text{dPP}/(\text{pPP} + \text{dPP}) \times 100 \quad (4)$$

MAR-FISH—MAR-FISH allows tracking at the single-cell level of substrate uptake by heterotrophic organisms. We investigated the heterotrophic uptake of two types of substrate: ³H-leucine, a widely used tracer for bulk BP measurements (Kirchman et al. 1985), and an uncharacterized mixture of DO¹⁴Cp produced by natural lake water phytoplankton assemblages during the experiment. In 2011, in parallel to the dPP experiments carried out in Kabuno Bay and in the southern basin of Lake Kivu, four supplementary culture flasks were filled with 20 mL of water from the mixed layer pool and were spiked with 62.5 μCi of NaH¹⁴CO₃. Two of these flasks were incubated for 5 h under a constant PAR as described above, whereas the two others were covered with aluminum foil and were incubated in the dark, in order to correct for bacterial DI¹⁴C uptake. The isotopic equilibrium between the DIC and DOCp pool was reached before the end of the 5 h incubations, and the specific activity of the DO¹⁴Cp was 258 $\mu\text{Ci mmol}^{-1}$. Finally, two additional culture flasks were spiked with ³H-leucine (0.5 nmol L⁻¹ final concentration; specific activity 162 Ci mmol⁻¹) and were kept in the dark for 5 h. Incubations were stopped by adding neutral formaldehyde (1.8% final concentration), and the samples were stored overnight at 4°C, followed by gentle filtration of 5 mL on a 0.2 μm isopore membrane polycarbonate filter (Millipore). Filters were then stored at -20°C until further processing.

Catalyzed reporter fluorescent in situ hybridization (CARD-FISH) analyses were carried out as follows. The cells were permeabilized with lysozyme and achromopeptidase prior to the hybridization. Several horseradish peroxidase (HRP)-probes were used to characterize the composition of the bacterial community in the water samples, using the procedure described by Alonso-Sáez and Gasol (2007). The HRP-labeled probes used were EUB338-II -III (targets most Eubacteria), GAM42a (targets most Gammaproteobacteria), BET42a (targets most Betaproteobacteria), ALF968 (targets most Alphaproteobacteria), and CF319 (targets many groups belonging to Bacteroidetes). The unlabeled competitors BET42a for GAM42a and GAM42a for BET42a were used. Specific hybridization conditions were established by adding formamide to the hybridization

buffer (45% formamide for ALF968, 55% for the other probes). All probes were purchased from Biomers. Counterstaining of CARD-FISH preparations was done with 4,6 diamidino-2-phenylindole (DAPI; final concentration 1 $\mu\text{g mL}^{-1}$). Between 500 and 1000 DAPI-positive cells were counted with an Olympus BX61 epifluorescence microscope in a minimum of 10 fields.

MAR-FISH analyses were performed after hybridization following the CARD-FISH protocol. The filters were glued onto glass slides with an epoxy adhesive (Uhu plus). The slides were embedded in 46°C tempered photographic emulsion (Kodak NTB-2) containing 0.1% agarose (gel strength 1%, > 1 kg cm⁻²) and were placed in a dark room on an ice-cold metal bar for about 5 min to allow the emulsion to solidify. They were subsequently placed inside black boxes at 4°C until development. Based on preliminary trials, we used an optimal exposure time of 7 d for samples incubated with ³H-leucine and 10 d for samples incubated with DO¹⁴Cp. For development, exposed slides were submerged for 3 min in a developer (Kodak D-19), rinsed 30 s with distilled water, and then placed for 3 min in a fixer (Kodak T-max), followed by 5 min of washing with tap water. The slides were then dried in a dessicator overnight, stained with DAPI (1 $\mu\text{g mL}^{-1}$), and inspected under an Olympus BX61 epifluorescence microscope. CARD-FISH positive cells (hybridized with the specific probe) appear in bright green under blue light excitation. Additionally, MAR-FISH positive cells contain dark silver grains accumulated above the bacterial cells on the radiographic emulsion, resulting from radioactive decay of labeled substrates.

Results

dPP and pPP and bacterial uptake of DOCp—The kinetics of incorporation of labeled substrate in the POC and DOC pools followed two distinct patterns (Fig. 3a,b). In all experiments, the radioactivity increased in the POC pool almost linearly with time, whereas the increase of radioactivity in the DOC pool was initially linear but rapidly leveled off at a maximum value after 2–4 h.

The measured pPP rates in Lake Kivu ranged from 0.8 mg C m⁻³ h⁻¹ to 5.1 mg C m⁻³ h⁻¹, and the dPP rates from 1.1 mg C m⁻³ h⁻¹ to 3.9 mg C m⁻³ h⁻¹ (Table 2). Normalized to Chl *a*, the total primary production (dPP + pPP) in Lake Kivu averaged 2.8 ± 0.8 mg C mg Chl *a*⁻¹ h⁻¹. PER values ranged between 42% and 64%, with an average of 53%. Higher rates of pPP and dPP, but lower PER values, were found in lakes Edward, Albert, and Victoria (Table 2). Volumetric rates of pPP and dPP were positively correlated with Chl *a* concentration (Table 3; Fig. 4a,b). Furthermore, dPP was positively correlated to pPP, and the slopes of the model I and model II linear regressions were both significantly lower than 1 (Table 3; Fig. 5), implying that PER decreased with increasing primary production rates.

The turnover time of the DOCp in surface waters, calculated as the inverse of the $k_{(2,3)}$ constant rate, ranged between 0.6 h and 3.6 h, with an average of 1.8 ± 0.9 h in Lake Kivu. The turnover time of DOCp was in the same

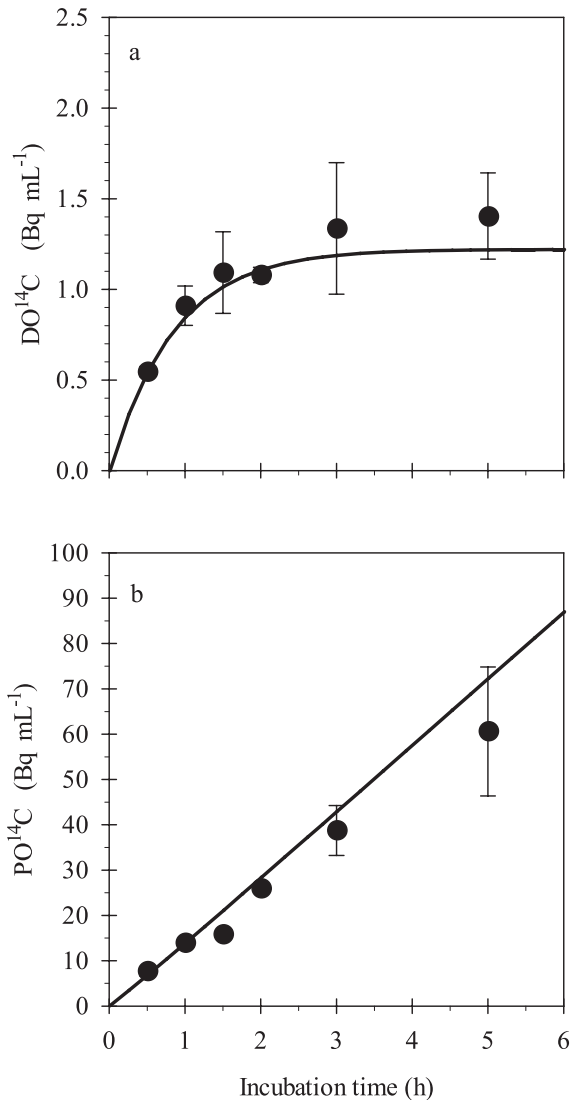


Fig. 3. Example of the kinetics of phytoplankton production of (a) $DO^{14}C$ and (b) $PO^{14}C$ during 5 h of incubation in Lake Edward. The fitted curves are derived from the three-compartment model presented in Fig. 2. Symbols are mean of duplicate measurements, and error bars are maximum and minimum values.

range in lakes Edward (0.8 h) and Albert (0.6 h) but was clearly higher in the eutrophic Lake Victoria (10.9 h; Table 2). The size of the DOC_p pool, calculated as the dPP rate multiplied by the turnover time of DOC_p , ranged between 1.7 mg C m^{-3} and 13.2 mg C m^{-3} (but with a higher value of $102.3 \text{ mg C m}^{-3}$ for Lake Victoria), and contributed less than 1% to the DOC pool in lakes Kivu,

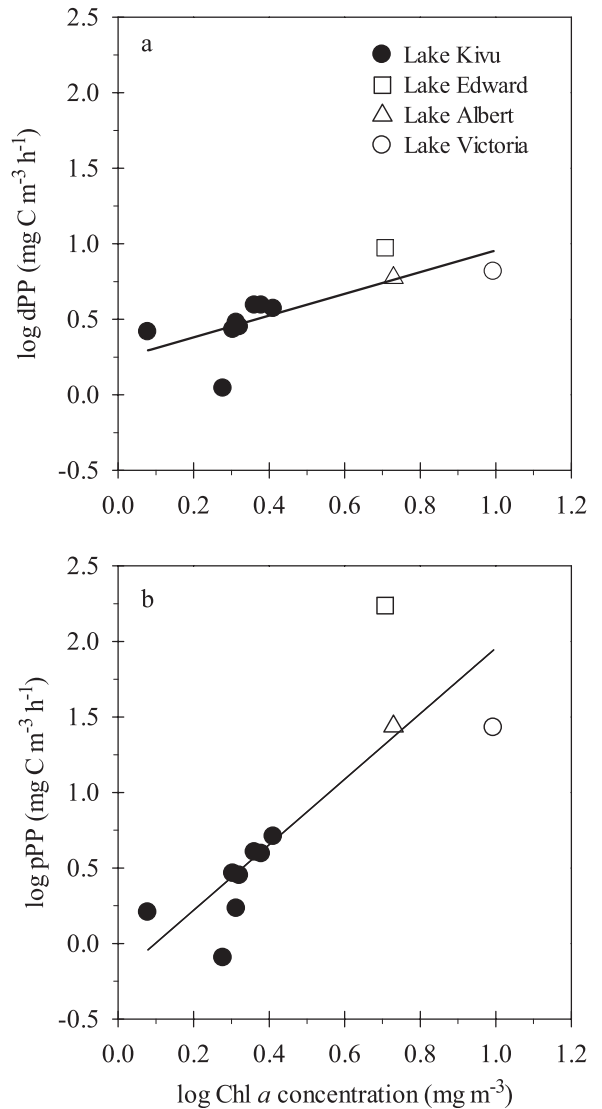


Fig. 4. Relationships between $\log(\text{Chl } a)$ and (a) $\log(dPP)$ or (b) $\log(pPP)$ in lakes Kivu, Edward, Albert, and Victoria. Continuous lines illustrate model I linear regression lines.

Edward, and Albert, and approximately 5% in Lake Victoria (Table 2).

³H-leucine and $DO^{14}C_p$ uptake by different bacterial phylogenetic groups—The bacterial community structure and the percentage of active cells taking up 3H -leucine and $DO^{14}C_p$ were investigated in 2011 in the southern basin of Lake Kivu and in Kabuno Bay, where, respectively, 75%

Table 3. Summary of model I and model II log-log linear regressions between particulate and dissolved primary production (respectively, pPP and dPP) and between pPP and $\text{Chl } a$. In parentheses, 95% confidence interval.

y	x	n	Model I regression				Model II regression
			Slope	Intercept	R^2	p	Slope
$\log(pPP)$	$\log(\text{Chl } a)$	11	2.16 (1.05, 3.27)	-0.21 (-0.77, 0.35)	0.68	<0.05	2.10 (1.79, 2.41)
$\log(dPP)$	$\log(\text{Chl } a)$	11	0.07 (0.01, 0.12)	0.37 (0.11, 0.56)	0.46	<0.05	0.60 (0.38, 0.83)
$\log(dPP)$	$\log(pPP)$	11	0.33 (0.23, 0.44)	0.31 (0.23, 0.44)	0.85	<0.0001	0.33 (0.25, 0.40)

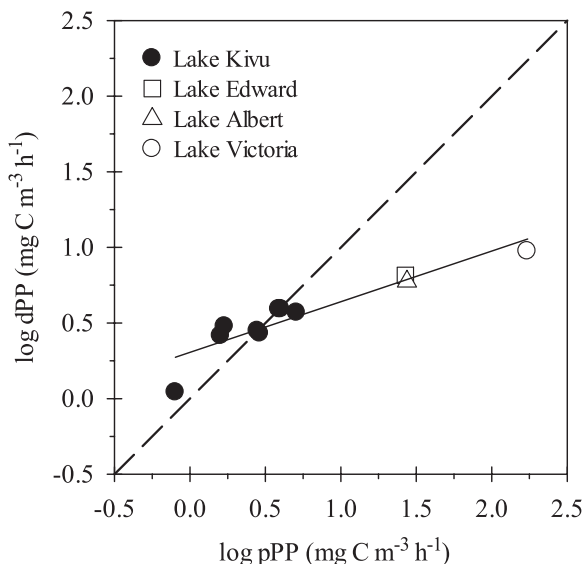


Fig. 5. Relationship between $\log(\text{pPP})$ and $\log(\text{dPP})$ in lakes Kivu, Edward, Albert, and Victoria. Continuous line illustrates model I linear regression line; dashed line is the 1:1 line.

and 83% of total cells counts were hybridized with EUB338-II-III probe (EUB, Eubacteria cells; Fig. 6). Members of Alphaproteobacteria, Betaproteobacteria, Gammaproteobacteria, and Bacteroidetes jointly comprised 49% and 50% of the total cell count and covered 65% and 60% of the bacterial domain in the southern basin and Kabuno Bay, respectively. Bacterial community structure, at the large group level targeted by CARD-FISH probes, was fairly similar between the two sites (Fig. 6). After 5 h of incubation in the dark with ^3H -leucine, 21% and 17% of the Eubacteria cells were found to take up ^3H -leucine in the southern basin and Kabuno Bay, respectively. Of the Eubacteria cells, 12% and 11% were labeled at the end of the incubation when considering DO^{14}Cp uptake. In the two stations, we found that less than 1% of the EUB338 cells were labeled by DI^{14}C ; therefore, bacterial DIC fixation via chemoautotrophic or anapleurotic pathways seemed to have been insignificant in the surface waters of Lake Kivu during these short-term incubations.

By comparing the relative contribution of each bacterial group in substrate uptake with its relative abundance (Fig. 7a,b), we can examine whether these broad bacterial groups participated in the DO^{14}Cp and ^3H -leucine uptake proportionally to their contribution to community structure. The ^3H -leucine uptake pattern was roughly similar between the two stations. In the southern basin and at Kabuno Bay station, we found that 85% and 75% of all the bacteria taking up ^3H -leucine belonged to two groups: Betaproteobacteria and Alphaproteobacteria. Accounting together for 42% and 41% of the bacterial community abundance, the contribution of these two groups to ^3H -leucine uptake was clearly higher than expected from their relative abundance. By contrast, the Bacteroidetes, the Gammaproteobacteria, and the bacterial cells unrelated to any of the bacterial groups investigated in this study

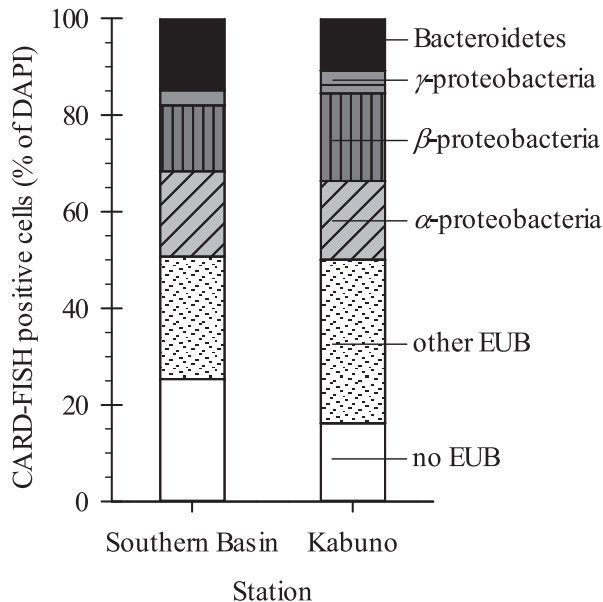


Fig. 6. Relative abundances of heterotrophic prokaryotes analyzed by CARD-FISH and scaled to total DAPI counts in Lake Kivu, in June 2011. “Other EUB” stands for cells identified with the probe mix EUB338-II-III but not detected with any of the probes used, targeting the large phylogenetic groups of Eubacteria: Alpha, Beta, Gammaproteobacteria, and Bacteroidetes. “No EUB” stands for cells counted with DAPI but not identified with the probe mix EUB338-II-III.

(other EUB), were underrepresented in ^3H -leucine uptake (Fig. 7a). The pattern of DO^{14}Cp uptake was different compared to that of ^3H -leucine. All the data points were closer to the 1:1 line, indicating that the bacterial groups were participating in DO^{14}Cp uptake proportionally to their relative contribution to the bacterial community. For instance, Betaproteobacteria and Alphaproteobacteria, the two dominant and overrepresented groups in the portion of the assemblage consuming ^3H -leucine, accounted for only 47% and 41% of cells taking up DO^{14}Cp in the southern basin and Kabuno Bay, respectively. Because they contributed 42% and 41% to the bacterial community structure, their share in DO^{14}Cp consumption was proportional to their in situ abundance.

Discussion

In this study, we gathered a first consistent set of concurrent measurements of pPP and dPP rates in tropical African lakes. The methodology to measure dPP differs largely among different studies available in the literature, and only a few of them account for the heterotrophic uptake of labeled DOCp during the course of the experiment, which can lead to an underestimation of PER. A way to overcome this bias is to observe the kinetics of labeling in the DOC and POC pools and to fit the data with a compartmental organic C exchange model (Morán et al. 2001; Morán and Estrada 2002).

It has recently been proposed that high DOC release rates, especially in oligotrophic systems, are not sustained by active excretion of healthy phytoplankton, but rather by

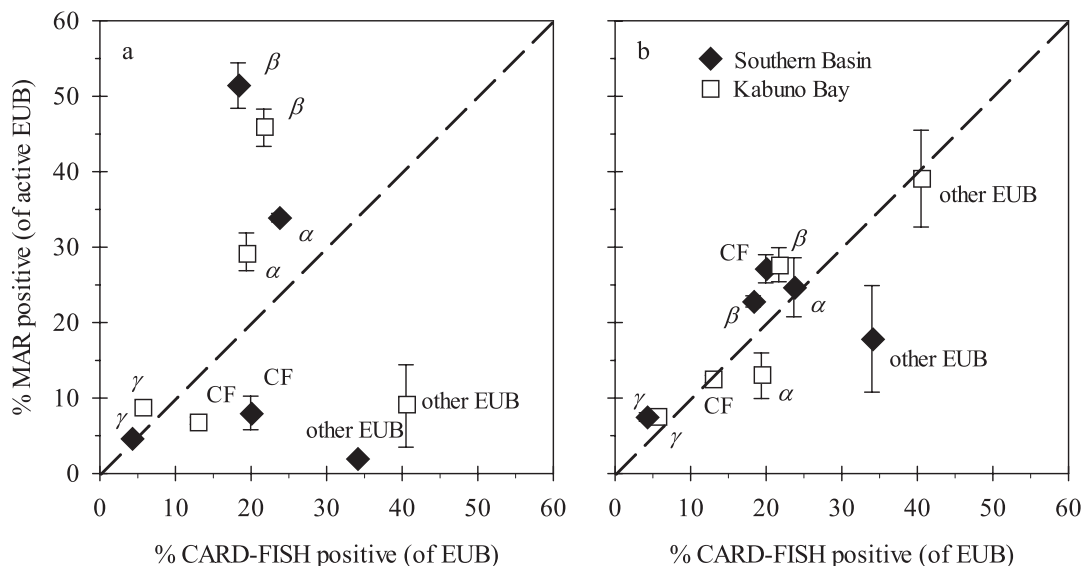


Fig. 7. Relative contribution of each phylogenetic group to the Eubacteria (EUB) community (CARD-FISH positive) against their relative contribution to the (a) ^3H -leucine or (b) DO^{14}Cp uptake (MAR positive) in Lake Kivu, in June 2011. Symbols are mean of duplicate measurements, and error bars are the maximum and minimum values. The dashed line is the 1 : 1 line. α = Alphaproteobacteria, β = Betaproteobacteria, γ = Gammaproteobacteria, CF = Bacteroidetes, other EUB = cells identified with the probe mix EUB338-II-III but not detected with any of the other probes used.

the lysis of dying cells (Agustí and Duarte 2013). During our short-term experiments, a significant amount of labeled DOCp was released after only 30 min of incubation, and no lag phase was observed in the appearance of radioactivity in the DOC pool. According to Lancelot (1979), such a lag phase is expected when the specific activity of the intracellular pool of molecules that can be exchanged with the external medium does not immediately reach a stable value. Therefore, the absence of lag phase (Fig. 3a) implies that the excreted compounds originate from a small intracellular pool that has a relatively high turnover rate (Marañón et al. 2004). Based on this observation, it appears unlikely that cell lysis or trophic processes such as zooplankton grazing were the main mechanisms of DOCp release, because then a large amount of non-recent, presumably unlabeled metabolites would have been part of the intracellular pool of molecules fated for release, considerably increasing its size. Instead, it seems to be driven by a purely physiological mechanism of phytoplankton excretion of freshly produced photosynthates (Marañón et al. 2004).

Why do phytoplankton cells actively release photosynthates? Previous studies have shown that high irradiance (Zlotnik and Dubinsky 1989) and nutrient limitation enhance phytoplankton excretion, particularly in P-limited situations (Obernosterer and Herndl 1995; Mykkestad 2000). Under high-light conditions, such as in the tropics, photorespiration, the fixation of O_2 on ribulose-1,5-phosphate catalyzed by ribulose-1,5-bisphosphate carboxylase oxygenase (RubisCO) with glycolate as a byproduct, is an effective protection mechanism against photoinhibition. It keeps the consumption of nicotinamide adenine dinucleotide phosphate and adenosine triphosphate (ATP) at high levels and lowers the saturation of the electron transport chain, preventing the production of reactive

oxygen species. An important fraction of this glycolate can be actively excreted by phytoplankton cells to the water (Fogg 1983), where it can be rapidly consumed by heterotrophic prokaryotes (Lau et al. 2007). Besides photorespiration, the active release of photosynthate by phytoplankton cells can be viewed as a mechanism occurring under nutrient limitation, when the synthesis of molecules containing N or P is not possible (Wood and Van Valen 1990; Morán et al. 2002). Because of the nutrient limitation, a fraction of the freshly fixed C is a surplus and is, therefore, excreted. It has also been proposed that DOCp release could be a purely passive diffusion process of molecules across the membrane due to a concentration gradient and, thus, directly proportional to phytoplankton biomass (Björnsen 1988; Marañón et al. 2004).

The PER value measured in Lake Kivu (42–64%) was much higher than the cross-system average of 13% proposed by Baines and Pace (1991) but was within the large range of values reported for lakes (3–82%). PER decreased with increasing pPP, the highest value being observed in the oligotrophic Lake Kivu and the lowest in the eutrophic Lake Victoria (Fig. 8). The use of a multiple linear regression model combining log-transformed I_{Z_m} and PO_4^{3-} to predict PER explained a high amount of the variance (adjusted $r^2 = 0.51$) and shows that both independent variables had a significant effect on PER ($\text{PER} = -92.13 + 49.99 \times \log I_{Z_m} - 27.16 \times \log \text{PO}_4^{3-}$; $p = 0.030$ for $\log I_{Z_m}$; $p = 0.036$ for $\log \text{PO}_4^{3-}$; $n = 11$). No significant correlations were found when using a univariate linear model ($p > 0.05$) to predict PER. Hence, high I_{Z_m} and low PO_4^{3-} concentration in the mixed layer had a significant combined positive effect on phytoplankton excretion. Overall, these results support the view that environmental factors play an important role in the control of PER in large African lakes. Furthermore, the relationship

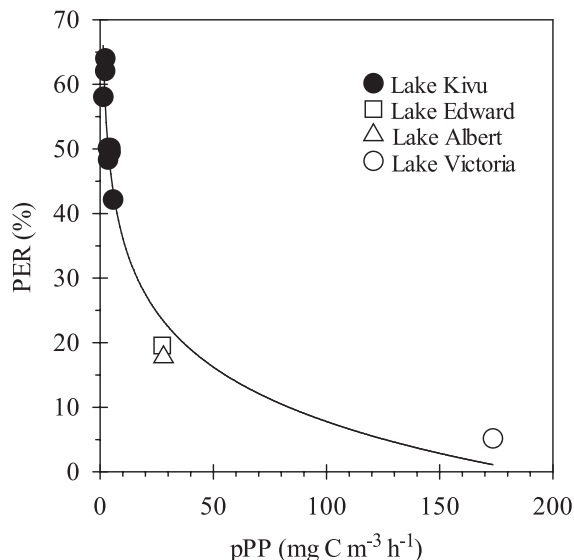


Fig. 8. Relationship between the percentage of extracellular release (PER) and particulate primary production (pPP) in the four lakes studied.

between PER and pPP was nonlinear, because PER tended to level off at a minimum value in the most productive waters. Because the debate around the physiological mechanisms driving phytoplankton excretion remains unresolved (Fogg 1983; Bjørnsen 1988), we hypothesize that the passive diffusion and the transport-mediated mechanisms are not mutually exclusive, but that the dominance of one on the other may change. For instance, we would suggest that passive DOC_p leakage across the membrane would be relatively constant, whereas active loss by a transport-mediated mechanism would be related to environmental conditions, such as nutrient and light availability. Hence, in tropical oligotrophic waters, under high-light and low-nutrient conditions, the transport-mediated mechanism could be the main process responsible for extracellular excretion, but its dominance over the passive diffusion mechanism would decrease along the productivity gradient.

In a review of published dPP values corrected for heterotrophic uptake, Fouilland and Mostajir (2010) found a similar nonlinear inverse relationship between PER and primary production in freshwater temperate lakes (Fig. 9), but the slope of the log–log relationship between dPP and pPP in the African tropical lakes (0.23–0.44, 95% confidence interval) is significantly lower than the one for temperate lakes (0.48–0.65, 95% confidence interval; ANCOVA, $f_{1,81} = 8.047$; $p < 0.01$). This difference indicates that, in unproductive waters, PER is higher in tropical lakes than in their temperate counterparts, consistent with the higher and relatively constant irradiance distinctive of tropical environments. We predict, therefore, that high PER values should be expected in other large oligotrophic tropical lakes, such as Lake Malawi and Lake Tanganyika.

The mean annual BP in the mixed layer of Lake Kivu was $336 \text{ mg C m}^{-2} \text{ d}^{-1}$ ($n = 10$ sampling dates in 2008; Llirós et al. 2012). Bacterial respiration has not been directly measured in Lake Kivu; but, using a range of

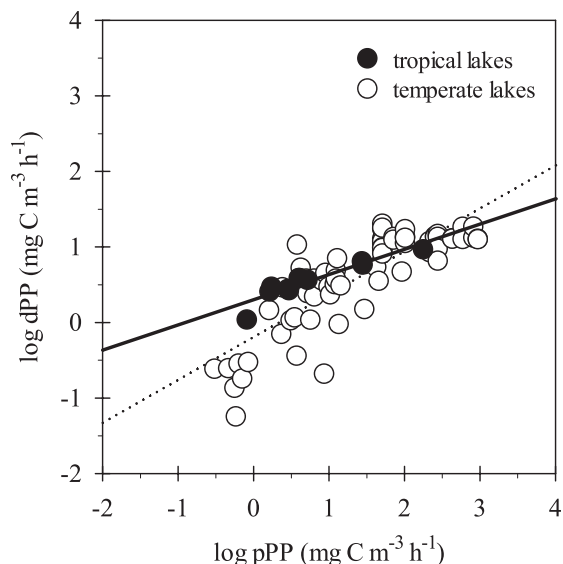


Fig. 9. Relationship between $\log(\text{pPP})$ and $\log(\text{dPP})$ in several African large tropical lakes (solid line, model I regression, our dataset) and several temperate lakes (dotted line, model I regression, data from Fouilland and Mostajir 2010). The tropical lakes regression is described in Table 3, and the temperate lakes regression is $\log(\text{dPP}) = -0.57 \log(\text{pPP}) - 0.19$; $R^2 = 0.71$, $p < 0.0001$; $n = 73$.

bacterial growth efficiency (BGE) values expected in tropical systems (10–20%), the bacterial C demand (BCD; $\text{BCD} = \text{BP}/\text{BGE}$) would range between $1680 \text{ mg C m}^{-2} \text{ d}^{-1}$ and $3360 \text{ mg C m}^{-2} \text{ d}^{-1}$. The mean phytoplankton pPP in Lake Kivu ($620 \text{ mg C m}^{-2} \text{ d}^{-1}$; Darchambeau et al. 2014) is clearly unable to support the BCD by itself, but the high PER values (42–64%) reported in this study would allow total phytoplankton production to meet 32–103% of the BCD in Lake Kivu. This reasoning can be extended to Lake Tanganyika, where total primary production would sustain 36–117% of BCD (Table 4). The range of BCD estimates that can be sustained by total phytoplankton production is wide, but it strongly depends on the choice of BGE values. In addition, other processes that were not measured during this study, such as grazing by zooplankton or cell lysis, can significantly contribute to the release of autochthonous DOC.

DOC_p is a highly complex pool of diverse molecules whose exact chemical natures are unknown. Carbohydrates of various sizes should be predominant in the excreted products (Myklestad 2000). It has recently been shown that the nature of the DOC_p depends on phytoplankton community composition (Sarmiento et al. 2013). In the large African lakes investigated, the DOC_p standing stock was relatively small compared to the high dPP rates observed, and the turnover times of the DOC_p were, therefore, short (Table 2). In other words, the consumption of DOC_p was tightly coupled to its production, and only a small amount of DOC_p accumulated in the water. This suggests that the DOC_p pool was mainly composed of labile molecules that were preferentially assimilated by heterotrophic prokaryotes over other organic C sources. These observations highlight the importance of a direct

Table 4. Estimates of bacterial carbon demand (BCD) using a range of bacterial growth efficiencies (BGE) and bacterial production (BP) data obtained from the literature. Estimates of the fraction of the BCD met by phytoplankton production (PP = dPP + pPP) using the range of PER measured in Lake Kivu during this study.

Variable	Lake Kivu	Lake Tanganyika
BCD (mg C m ⁻² d ⁻¹)	1680–3360	1550–3100
BGE (%)	10–20	10–20
BP (mg C m ⁻² d ⁻¹)	336*	310†
pPP (mg C m ⁻² d ⁻¹)	620‡	654†
PER (%)	42–64§	
PP/BCD	0.32–1.03	0.36–1.17

* Llíros et al. 2012.

† Sténuite et al. 2009.

‡ Darchambeau et al. 2014.

§ This study.

transfer of organic matter from phytoplankton to bacterioplankton in Lake Kivu.

The fraction of cells active in the uptake of leucine after 5 h of incubation (average 19%) was close to the range of values of metabolically active cells reported in the literature (20–40%, del Giorgio and Gasol 2008), but the fraction of active cells in DOCp uptake (average 11.5%) was low compared to this range. However, these studies used low-molecular-weight, very labile molecules as tracers, but the DOCp pool presumably comprises higher-molecular-weight substrates that require more complex enzymatic pathways and that are, therefore, harder to assimilate in short incubations. Additionally, the activity of some light-sensitive heterotrophic prokaryotes might have been inhibited by the high light irradiance during our incubations. Also, the labeled DO¹⁴Cp was diluted with nonlabeled and equally labile compounds, which decreased the sensitivity of the technique at this range of incubation times.

In contrast to earlier studies that used standard labeled molecules, such as leucine, ATP, or glucose (Alonso-Sáez and Gasol 2007), our MAR-FISH results show that all different phylogenetic groups of heterotrophic prokaryotes were involved in the uptake of molecules belonging to the uncharacterized pool of DO¹⁴Cp. The high abundance and activity of members of the Betaproteobacteria group is not surprising; their abundance has been found to be positively related with the amount of algal-derived substrates (Simek et al. 2008; Paver et al. 2012), and they are usually ubiquitous in freshwaters. The relatively high abundance of Alphaproteobacteria and Bacteroidetes members is more difficult to interpret. Members of these groups are generally not abundant in freshwaters but seem to be effectively resistant to eukaryote predation (Newton et al. 2011); however, bacterivory pressure has never been estimated in Lake Kivu. Overall, our observations support the idea that the metabolic ability to process labile algal-derived dissolved organic matter is widespread among broad prokaryote groups (Landa et al. 2013). Furthermore, it is possible that the diversity of molecules excreted by the phytoplankton community present in Lake Kivu can support a variety of ecological niches for heterotrophic prokaryotes, thereby allowing them to avoid direct

resource competition. It was, indeed, recently shown that the composition of the extracellular release of dissolved free amino acids by phytoplankton was species dependent (Sarmiento et al. 2013).

³H-leucine is a widely used tracer for BP measurements (Kirchman et al. 1985). This method requires a parallel estimate of the leucine-to-C conversion factor, defined as the yield of bacterial biomass per unit of leucine incorporated. Nevertheless, a difference in ability to take up leucine among different phylogenetic groups of prokaryotes has been reported (Pérez et al. 2010), and community composition could affect leucine-to-C conversion factor estimates (Alonso-Sáez et al. 2010). To our best knowledge, our study is the first to compare the uptake pattern of ³H-leucine to the uptake pattern of DO¹⁴Cp produced by a natural phytoplankton community. In Lake Kivu, members of Alphaproteobacteria, Betaproteobacteria, and Bacteroidetes were involved in DO¹⁴Cp uptake proportionally to their abundance, but they differed strongly in their ability to take up ³H-leucine. This discrepancy suggests that leucine may not be a good representative of other naturally occurring, but more complex, organic C sources, such as DOCp.

Acknowledgments

We thank Boniface Kaningini, Pascal Isumbisho, and Pascal Masilya (Institut Supérieur Pédagogique, Bukavu, Democratic Republic of Congo), Laetitia Nyinawamwiza (National University of Rwanda, Rwanda), William Okello (National Fisheries Resources Research Institute, Jinja, Uganda), and their respective teams for logistic support during the cruises; Bruno Leporcq, Marc-Vincent Commarieu, and Irene Forn for laboratory assistance; and Sébastien Knops, Xavier Libert, and Mélodie Schmitz for help during fieldwork. We also thank Eric Fouilland for providing his dataset, and the associate editor (J. Melack) and four anonymous referees for constructive comments on this manuscript. This work was funded by the “East African Great Lake Ecosystem Sensitivity to Changes” (EAGLES, SD/AR/02A) project from the Belgian Federal Science Policy Office (BELSPO, Belgium), the “Cycle du Carbone et des Nutriments au Lac Kivu” (CAKI, contract 2.4.598.07), and “Microbial Diversity and Processes in Lake Kivu” (MICKI, contract 2.4.515.11) projects from the “Fonds National de la Recherche Scientifique” (FNRS, Belgium), and project (CGL2010-11556-E) from the Spanish Ministry for Science and Technology. This publication contributes to the European Research Council (ERC) starting grant project “African river basins: Catchment-scale carbon fluxes and transformations” (AFRIVAL, 240002). H.S. benefited from fellowships from the Spanish “Ministerio de Educación y Ciencia” (JCI-2008-2727) and the Brazilian National Council for Scientific and Technological Development (CNPq) and Foundation for Research Support of the State of São Paulo (FAPESP).

References

- AGUSTÍ, S., AND C. M. DUARTE. 2013. Phytoplankton lysis predicts dissolved organic carbon release in marine plankton communities. *Biogeosciences* **10**: 1259–1264, doi:10.5194/bg-10-1259-2013
- ALONSO-SÁEZ, L., AND J. M. GASOL. 2007. Seasonal variations in the contributions of different bacterial groups to the uptake of low-molecular-weight compounds in northwestern Mediterranean coastal waters. *Appl. Environ. Microbiol.* **73**: 3528–3535, doi:10.1128/AEM.02627-06

- , J. PINHASSI, J. PERNTHALER, AND J. M. GASOL. 2010. Leucine-to-carbon empirical conversion factor experiments: Does bacterial community structure have an influence? *Environ. Microbiol.* **12**: 2988–2997, doi:10.1111/j.1462-2920.2010.02276.x
- AMERICAN PUBLIC HEALTH ASSOCIATION. 1998. Standard methods for the examination of water and wastewater, 20th ed. APHA.
- BAINES, S. B., AND M. L. PACE. 1991. The production of dissolved organic matter by phytoplankton and its importance to bacteria: Patterns across marine and freshwater systems. *Limnol. Oceanogr.* **36**: 1078–1090, doi:10.4319/lo.1991.36.6.1078
- BJØRNSEN, P. K. 1988. Phytoplankton exudation of organic matter: Why do healthy cells do it? *Limnol. Oceanogr.* **33**: 151–154, doi:10.4319/lo.1988.33.1.0151
- BORGES, A. V., G. ABRIL, B. DELILLE, J.-P. DESCY, AND F. DARCHAMBEAU. 2011. Diffusive methane emissions to the atmosphere from Lake Kivu (Eastern Africa). *J. Geophys. Res.* **116**: G03032, doi:10.1029/2011JG001673
- COLE, J. J., S. FINDLAY, AND M. L. PACE. 1988. Bacterial production in fresh and saltwater ecosystems: A cross-system overview. *Mar. Ecol. Prog. Ser.* **43**: 1–10, doi:10.3354/meps043001
- , G. E. LIKENS, AND D. L. STRAYER. 1982. Photosynthetically produced dissolved organic carbon: An important carbon source for planktonic bacteria (Mirror Lake, New Hampshire, algae). *Limnol. Oceanogr.* **27**: 1080–1090, doi:10.4319/lo.1982.27.6.1080
- DARCHAMBEAU, F., H. SARMENTO, AND J.-P. DESCY. 2014. Primary production in a tropical large lake: The role of phytoplankton composition. *Sci. Total Environ.* **473**: 178–188, doi:10.1016/j.scitotenv.2013.12.036
- DEL GIORGIO, P. A., AND J. M. GASOL. 2008. Physiological structure and single-cell activity in marine bacterioplankton, p. 243–298. *In* D. L. Kirchman [ed.], *Microbial ecology of the oceans*, 2nd ed. John Wiley and Sons.
- FOGG, G. E. 1983. The ecological significance of extracellular products of phytoplankton photosynthesis. *Botanica Marina* **26**: 3–14, doi:10.1515/botm.1983.26.1.3
- FOUILLAND, E., AND B. MOSTAJIR. 2010. Revisited phytoplanktonic carbon dependency of heterotrophic bacteria in freshwaters, transitional, coastal and oceanic waters. *FEMS Microbiol. Ecol.* **73**: 419–429, doi:10.1111/j.1574-6941.2010.00896.x
- FRANKIGNOULLE, M., AND A. V. BORGES. 2001. Direct and indirect pCO₂ measurements in a wide range of pCO₂ and salinity values (the Scheldt estuary). *Aquat. Geochem.* **7**: 267–273, doi:10.1023/A:1015251010481
- GUILDFORD, S. J., AND R. E. HECKY. 2000. Total nitrogen, total phosphorus, and nutrient limitation in lakes and oceans: Is there a common relationship? *Limnol. Oceanogr.* **45**: 1213–1223, doi:10.4319/lo.2000.45.6.1213
- KIRCHMAN, D., E. K'NEES, AND R. HODSON. 1985. Leucine incorporation and its potential as a measure of protein synthesis by bacteria in natural aquatic systems. *Appl. Environ. Microbiol.* **49**: 599–607.
- LANCELOT, C. 1979. Gross excretion rates of natural marine phytoplankton and heterotrophic uptake of excreted products in the southern North Sea, as determined by short-term kinetics. *Mar. Ecol. Prog. Ser.* **1**: 179–186, doi:10.3354/meps001179
- LANDA, M., AND OTHERS. 2013. Phylogenetic and structure response of heterotrophic bacteria to dissolved organic matter of different chemical composition in a continuous culture study. *Environ. Microbiol.*, doi:10.1111/1462-2920.12242
- LAU, W. W., R. G. KEIL, AND E. V. ARMBRUST. 2007. Succession and diel transcriptional response of the glycolate-utilizing component of the bacterial community during a spring phytoplankton bloom. *Appl. Environ. Microbiol.* **73**: 2440–2450, doi:10.1128/AEM.01965-06
- LEHMAN, J. T., A. H. LITT, R. MUGIDDE, AND D. A. LEHMAN. 1998. Nutrients and plankton biomass in the rift lake sources of the White Nile: Lakes Albert and Edward, p. 157–172. *In* J. T. Lehman [ed.], *Environmental change and response in East African lakes*. Kluwer Academic Publishers.
- LLIRÓS, M., AND OTHERS. 2012. Microbial ecology of Lake Kivu, p. 85–105. *In* J.-P. Descy, F. Darchambeau, and M. Schmid [eds.], *Lake Kivu: Limnology and biogeochemistry of a tropical great lake*. Springer.
- MARAÑÓN, E., P. CERMENO, E. FERNÁNDEZ, J. RODRIGUEZ, AND L. ZABALA. 2004. Significance and mechanisms of photosynthetic production of dissolved organic carbon in a coastal eutrophic ecosystem. *Limnol. Oceanogr.* **49**: 1652–1666, doi:10.4319/lo.2004.49.5.1652
- MILLERO, F. J., T. B. GRAHAM, F. HUANG, H. BUSTOS-SERRANO, AND D. PIERROT. 2006. Dissociation constants of carbonic acid in sea water as a function of salinity and temperature. *Mar. Chem.* **100**: 80–94, doi:10.1016/j.marchem.2005.12.001
- MORÁN, X. A. G., AND M. ESTRADA. 2002. Phytoplanktonic DOC and POC production in the Bransfield and Gerlache Straits as derived from kinetic experiments of ¹⁴C incorporation. *Deep Sea Res. II* **49**: 769–786, doi:10.1016/S0967-0645(01)00123-0
- , J. M. GASOL, C. PEDRÓS-ALÍO, AND M. ESTRADA. 2001. Dissolved and particulate primary production and bacterial production in offshore Antarctic waters during austral summer: Coupled or uncoupled? *Mar. Ecol. Prog. Ser.* **222**: 25–39, doi:10.3354/meps222025
- MYKLESTAD, S. M. 2000. Dissolved organic carbon from phytoplankton, p. 111–148. *In* P. Wangersky [ed.], *Marine chemistry*. Springer.
- NEWTON, R. J., S. E. JONES, A. EILER, K. D. MCMAHON, AND S. BERTILSSON. 2011. A guide to the natural history of freshwater lake bacteria. *Microbiol. Mol. Biol. Rev.* **75**: 14–49, doi:10.1128/MMBR.00028-10
- OBERNOSTERER, I., AND G. J. HERNDL. 1995. Phytoplankton extracellular release and bacterial growth: Dependence on the inorganic N:P ratio. *Mar. Ecol. Prog. Ser.* **116**: 247–257, doi:10.3354/meps116247
- PAVER, S. F., C. E. NELSON, AND A. D. KENT. 2012. Temporal succession of putative glycolate-utilizing bacterioplankton tracks changes in dissolved organic matter in a high-elevation lake. *FEMS Microbiol. Ecol.* **83**: 541–551, doi:10.1111/1574-6941.12012
- PÉREZ, M. T., P. HÖRTNAGL, AND R. SOMMARUGA. 2010. Contrasting ability to take up leucine and thymidine among freshwater bacterial groups: Implications for bacterial production measurements. *Environ. Microbiol.* **12**: 74–82, doi:10.1111/j.1462-2920.2009.02043.x
- , AND R. SOMMARUGA. 2006. Differential effect of algal- and soil-derived dissolved organic matter on alpine lake bacterial community composition and activity. *Limnol. Oceanogr.* **51**: 2527–2537, doi:10.4319/lo.2006.51.6.2527
- RILEY, G. A. 1957. Phytoplankton of the north central Sargasso Sea, 1950–52. *Limnol. Oceanogr.* **2**: 252–270.
- SARMENTO, H., AND J. M. GASOL. 2012. Use of phytoplankton-derived dissolved organic carbon by different types of bacterioplankton. *Environ. Microbiol.* **14**: 2348–2360, doi:10.1111/j.1462-2920.2012.02787.x
- , F. UNREIN, M. ISUMBISHO, S. STENUITE, J. M. GASOL, AND J.-P. DESCY. 2008. Abundance and distribution of picoplankton in tropical, oligotrophic Lake Kivu, eastern Africa. *Freshw. Biol.* **53**: 756–771, doi:10.1111/j.1365-2427.2007.01939.x
- , AND OTHERS. 2013. Selective influences of dissolved free amino acid release by phytoplankton on bacterioplankton communities. *Limnol. Oceanogr.* **58**: 1123–1135, doi:10.4319/lo.2013.58.3.1123

- SIMEK, K., K. HORNAK, J. JEZBERA, J. NEDOMA, P. ZNACHOR, J. HEJZLAR, AND J. SED'A. 2008. Spatio-temporal patterns of bacterioplankton production and community composition related to phytoplankton composition and protistan bacterivory in a dam reservoir. *Aquat. Microb. Ecol.* **51**: 249–262, doi:10.3354/ame01193
- STÉNUITE, S., AND OTHERS. 2009. Abundance and production of bacteria, and relationship to phytoplankton production, in a large tropical lake (Lake Tanganyika). *Freshw. Biol.* **54**: 1300–1311, doi:10.1111/j.1365-2427.2009.02177.x
- VERBEKE, J. 1957. Exploration hydrobiologique des lacs Kivu, Edouard et Albert (1952–1954). Resultats Scientifiques. V. III, Fascicule 1: Recherche écologique sur la faune des grands lacs de l'est du Congo Belge. Royal Institute of Natural Sciences of Belgium, Brussels. [Hydrobiological exploration of Lakes Kivu, Edward and Albert (1952–1954). Scientific Results. V. III, Part 1: Research about the ecology of the fauna in the large lakes in the East Belgian Congo.]
- WIEBE, W. J., AND D. F. SMITH. 1977. Direct measurement of dissolved organic carbon release by phytoplankton and incorporation by microheterotrophs. *Mar. Biol.* **42**: 213–223, doi:10.1007/BF00397745
- WOOD, A., AND L. M. VAN VALEN. 1990. Paradox lost? On the release of energy-rich compounds by phytoplankton. *Mar. Microb. Food Webs* **4**: 103–116.
- ZLOTNIK, I., AND Z. DUBINSKY. 1989. The effect of light and temperature on DOC excretion by phytoplankton. *Limnol. Oceanogr.* **34**: 831–839, doi:10.4319/lo.1989.34.5.0831

Associate editor: John M. Melack

Received: 16 December 2013

Accepted: 16 April 2014

Amended: 21 April 2014

**Methanotrophy in
Lake Kivu**

C. Morana et al.

Methanotrophy within the water column of a large meromictic tropical lake (Lake Kivu, East Africa)

C. Morana¹, A. V. Borges², F. A. E. Roland², F. Darchambeau², J.-P. Descy³, and S. Bouillon¹

¹Department of Earth and Environmental Sciences, KU Leuven, Leuven, Belgium

²Chemical Oceanography Unit, Université de Liège, Liège, Belgium

³Research Unit in Environmental and Evolutionary Biology, UNamur, Namur, Belgium

Received: 9 October 2014 – Accepted: 17 October 2014 – Published: 7 November 2014

Correspondence to: C. Morana (cedric.morana@ees.kuleuven.be)

Published by Copernicus Publications on behalf of the European Geosciences Union.

Title Page

Abstract

Introduction

Conclusions

References

Tables

Figures



Back

Close

Full Screen / Esc

Printer-friendly Version

Interactive Discussion



Abstract

The permanently stratified Lake Kivu is one of the largest freshwater reservoirs of dissolved methane (CH_4) on Earth. Yet CH_4 emissions from its surface to the atmosphere has been estimated to be 2 orders of magnitude lower than the CH_4 upward flux to the mixed layer, showing that microbial CH_4 oxidation is an important process within the water column. A combination of natural abundance carbon stable isotope analysis ($\delta^{13}\text{C}$) of several inorganic and organic carbon pools and $^{13}\text{CH}_4$ -labelling experiments was carried out during rainy and dry season to quantify (i) the contribution of CH_4 -derived carbon to the biomass, (ii) methanotrophic bacterial production (MBP), and (iii) methanotrophic bacterial growth efficiency (MBGE), defined as the ratio between MBP and gross CH_4 oxidation. We also investigated the distribution and the $\delta^{13}\text{C}$ of specific phospholipid fatty acids (PLFA), used as biomarkers for aerobic methanotrophs. Data revealed that methanotrophic organisms oxidized within the water column most of the upward flux of CH_4 to the mixed layer and a significant amount of CH_4 -derived carbon was incorporated into the microbial biomass in the oxycline. Maximal MBP rates were measured in the oxycline, suggesting that CH_4 oxidation was mainly driven by oxic processes. The MBGE was variable (2–50%) and negatively related to $\text{CH}_4:\text{O}_2$ molar ratios. Thus, a comparatively smaller fraction of CH_4 -derived carbon was incorporated into the cellular biomass in deeper waters, at the bottom of the oxycline where oxygen was scarce. The aerobic methanotrophic community was clearly dominated by type I methanotrophs and no evidence was found for an active involvement of type II methanotrophs in CH_4 oxidation in Lake Kivu. Vertically integrated over the water column, the MBP was equivalent to 16–58% of the average phytoplankton primary production. This relatively high magnitude of MBP, and the substantial contribution of CH_4 -derived carbon to the overall biomass in the oxycline, suggest that methanotrophic bacteria could potentially sustain a significant fraction of the pelagic food-web in the deep oligotrophic Lake Kivu.

Methanotrophy in Lake Kivu

C. Morana et al.

Title Page

Abstract

Introduction

Conclusions

References

Tables

Figures



Back

Close

Full Screen / Esc

Printer-friendly Version

Interactive Discussion



1 Introduction

Although the atmospheric methane (CH₄) concentration is low compared to carbon dioxide (CO₂), CH₄ contributes significantly to the anthropogenic radiative forcing (18%) because of its 25 times higher global warming potential than CO₂ (Forster et al., 2007). CH₄ has several natural and anthropogenic sources and sinks, whereby natural and artificial wetlands are recognized as major CH₄ sources to the atmosphere (e.g. Kirschke et al., 2012). Bastviken et al. (2011) estimated that CH₄ emissions to the atmosphere from freshwater ecosystems (0.65 Pg C yr⁻¹ as CO₂ equivalent) would correspond to 25% of the global land carbon (C) sink (2.6 ± 1.7 Pg C yr⁻¹, Denman et al., 2007). Tropical regions are responsible for approximately half of the estimated CH₄ emissions from freshwater ecosystems to the atmosphere, although they have been consistently undersampled (Bastviken et al., 2011). Thus, more information on both the magnitude and controlling factors of CH₄ emissions from tropical inland waters are warranted. CH₄ is produced mainly in anoxic sediments by methanogenic archaea following two different pathways: acetoclastic methanogenesis (Reaction 1), using acetate produced from organic matter degradation, or CO₂ reduction (Reaction 2).



Although both methanogenic pathways may co-occur, CO₂ reduction is dominant in marine sediments, while acetate fermentation is the major pathway in freshwater sediments (Whiticar et al., 1986). CH₄ production rates are typically higher than CH₄ emission fluxes to the atmosphere, since aerobic and anaerobic microbial CH₄ oxidation within lacustrine sediments or in water columns are effective processes that limit the amount of CH₄ reaching the atmosphere, in particular when vertical CH₄ transport occurs mainly through diffusive transport, rather than through ebullition. A wide variety of electron acceptors can be used during microbial CH₄ oxidation, including but not limited to oxygen (O₂, Rudd et al., 1974) and sulphate (SO₄²⁻, Boetius

BGD

11, 15663–15691, 2014

Methanotrophy in Lake Kivu

C. Morana et al.

Title Page

Abstract

Introduction

Conclusions

References

Tables

Figures

◀

▶

◀

▶

Back

Close

Full Screen / Esc

Printer-friendly Version

Interactive Discussion



et al., 2000). Micro-organisms performing aerobic CH₄ oxidation (Reaction 3) belong to the Proteobacteria phylum and anaerobic CH₄ oxidation coupled with SO₄²⁻ reduction (Reaction 4) is carried out by a syntrophic consortium of CH₄-oxidizing archaea and sulphate-reducing bacteria (Boetius et al., 2000), although up to now this process has not been frequently reported in freshwater ecosystems.



Methanotrophic organisms not only use CH₄ as electron donors but they are also able to incorporate a fraction of the CH₄-derived C into their biomass, and could therefore contribute to fuel the pelagic food web (Bastviken et al., 2003; Jones and Grey, 2011; Sanseverino et al., 2012). A recent study carried out in small boreal lakes (surface area < 0.01 km²) demonstrated that methanotrophic bacterial production (MBP) contributed to 13–52 % of the autochthonous primary production in the water column (Kankaala et al., 2013). But in spite of the potential importance of this alternative C source in aquatic ecosystems, direct measurements of MBP in lakes are still scarce. Also, the methanotrophic bacterial growth efficiency (MBGE), defined as the amount of biomass synthesized from CH₄ per unit of CH₄ oxidized, was found to vary widely in aquatic environments (15–80 % according to King, 1992; 6–77 % according to Bastviken et al., 2003), and moreover, little is known about the factors driving its variability.

Lake Kivu, located in a volcanic area, is one of the largest freshwater CH₄ reservoirs, with approximately 60 km³ (at standard temperature and pressure) dissolved in its permanently stratified water (Schmid et al., 2005). One third of the CH₄ accumulated in its deep waters is estimated to be produced via the acetoclastic pathway and two thirds by reduction of geogenic CO₂ (Schoell et al., 1988). Based on a modelling approach, Schmid et al. (2005) estimated that CH₄ production recently increased by threefold since the 1970s for a still unknown reason. However, the emission of CH₄ from surface waters to the atmosphere (0.038 mmol m⁻² d⁻¹, Borges et al., 2011) is several orders of magnitude lower than the upward flux of CH₄ to the mixed layer (9.38 mmol m⁻² d⁻¹,

Methanotrophy in Lake Kivu

C. Morana et al.

Title Page

Abstract

Introduction

Conclusions

References

Tables

Figures

◀

▶

◀

▶

Back

Close

Full Screen / Esc

Printer-friendly Version

Interactive Discussion



Pasche et al., 2009), showing that CH₄ oxidation prevents most of CH₄ to reach the lake surface waters.

Due to its inherent characteristics, the meromictic Lake Kivu offers an ideal natural laboratory to investigate the role of methanotrophy in large tropical lakes. In this study, we used the difference in C stable isotope abundance ($\delta^{13}\text{C}$) of different C sources to estimate the fraction of CH₄ inputs to the mixed layer from deep waters that is microbially oxidized within the water column, and to quantify the relative contribution of CH₄-derived C to the particulate biomass. Additionally, phospholipid fatty acids (PLFA) and their $\delta^{13}\text{C}$ signatures were analyzed to characterize the populations of methanotrophic bacteria present in the water column. We also carried out ¹³CH₄-labelling experiments to trace the incorporation of CH₄-derived C into the biomass (to quantify methanotrophic bacterial production) and its conversion to CO₂ (to quantify methanotrophic bacterial growth efficiency). Finally, stable isotope probing (SIP) of specific PLFA (SIP-PLFA) after ¹³C-CH₄ labelling allowed to characterize the bacterial populations active in methanotrophy.

2 Material and methods

2.1 Study site description and sampling

Lake Kivu (East Africa) is a large (2370 km²) and deep (maximum depth of 485 m) meromictic lake. Its vertical structure consists of an oxic and nutrient-poor mixed layer (seasonally variable depth, up to 70 m), and a permanently anoxic monimolimnion rich in dissolved gases (CH₄, CO₂) and inorganic nutrients (Damas, 1937; Degens et al., 1973; Schmid et al., 2005). Seasonal variations of the vertical position of the oxic–anoxic transition are driven by contrasting hygrometry and long wave radiation between rainy (October–May) and dry (June–September) seasons (Thiery et al., 2014), the latter being characterized by a deepening of the oxic zone, and an increased input of dissolved gases and inorganic nutrients into the mixed layer (Sarmiento et al., 2006;

BGD

11, 15663–15691, 2014

Methanotrophy in Lake Kivu

C. Morana et al.

Title Page

Abstract

Introduction

Conclusions

References

Tables

Figures

◀

▶

◀

▶

Back

Close

Full Screen / Esc

Printer-friendly Version

Interactive Discussion



Borges et al., 2011). Sampling was carried out in the Northern Basin (1.72° S, 29.23° E) in February 2012 (rainy season), and in the Northern Basin and Southern Basin (2.34° S, 28.98° E) in September 2012 (dry season).

O₂ concentration was measured with a YSI-proODO probe with a optical O₂ sensor (detection limit is 3 μmolL⁻¹), calibrated using air saturated water. Hereafter, “low-oxygen waters” stands for waters with concentration < 3 μmolL⁻¹. Lake water was collected with a 7 L Niskin bottle (Hydro-Bios) at a depth interval of 5 m from the lake surface to the top of the monimolimnion, at 80 m.

2.2 Chemical analyses

Samples for CH₄ concentrations were collected in 50 mL glass serum bottles from the Niskin bottle with a tube, left to overflow, poisoned with 100 μL of saturated HgCl₂ and sealed with butyl stoppers and aluminium caps. Concentrations of CH₄ were measured by headspace technique (Weiss, 1981) using gas chromatography with flame ionization detection (GC-FID, SRI 8610C), after creating a 20 mL headspace with N₂ in the glass serum bottles, and then analyzed following the method described by Borges et al. (2011). Samples for the determination of the δ¹³C signature of CH₄ (δ¹³C-CH₄) were collected in 250 mL glass serum bottles similarly to CH₄ concentration samples. δ¹³C-CH₄ was determined by a custom developed technique, whereby a helium headspace was first created, and CH₄ was flushed out through a double-hole needle, CO₂ was removed with a CO₂ trap (soda lime), and the CH₄ was converted to CO₂ in an online combustion column similar to that in an Elemental Analyzer (EA). The resulting CO₂ was subsequently preconcentrated by immersion of a stainless steel loop in liquid nitrogen in a custom-built cryofocussing device, passed through a micropacked GC column (HayeSep Q 2m, 0.75 mm ID ; Restek), and finally measured on a Thermo DeltaV Advantage isotope ratio mass spectrometer (IRMS). Certified reference standards (IAEA-CO1 and LSVEC) were used to calibrate δ¹³C-CH₄ data.

**Methanotrophy in
Lake Kivu**

C. Morana et al.

[Title Page](#)[Abstract](#)[Introduction](#)[Conclusions](#)[References](#)[Tables](#)[Figures](#)[I ◀](#)[▶ I](#)[◀](#)[▶](#)[Back](#)[Close](#)[Full Screen / Esc](#)[Printer-friendly Version](#)[Interactive Discussion](#)

Samples for the determination of $\delta^{13}\text{C}$ signatures of dissolved inorganic carbon (DIC) were collected by gently overfilling 12 mL glass vial (Labco Exetainer), preserved with 20 μL of HgCl_2 saturated. For the analysis of $\delta^{13}\text{C}$ -DIC, a 2 mL helium headspace was created and 100 μL of H_3PO_4 (99%) was added into each vial to convert all DIC species into CO_2 . After overnight equilibration, a variable volume of the headspace was injected into an EA coupled to an isotope ratio mass spectrometer (EA-IRMS; Thermo FlashHT with Thermo DeltaV Advantage). Calibration of $\delta^{13}\text{C}$ -DIC measurements was performed with certified reference materials (LSVEC and either NBS-19 or IAEA-CO-1).

Samples for particulate organic carbon (POC) concentrations and its stable C isotope signature ($\delta^{13}\text{C}$ -POC) were filtered on pre-combusted (overnight at 450°C) 25 mm glass fiber filters (Advantec GF-75; 0.3 μm), and dried. These filters were later decarbonated with HCl fumes for 4 h, dried and packed in silver cups. POC and $\delta^{13}\text{C}$ -POC were determined on an EA-IRMS (Thermo FlashHT with Thermo DeltaV Advantage). Calibration of POC and $\delta^{13}\text{C}$ -POC was performed with IAEA-C6 and acetanilide, and reproducibility of $\delta^{13}\text{C}$ -POC measurements was typically better than 0.2‰.

Samples ($\sim 2\text{ L}$) for measurements of phospholipid fatty acid concentrations (PLFA) and their $\delta^{13}\text{C}$ signature were filtered on pre-combusted 47 mm glass fiber filters (Advantec GF-75; 0.3 μm), and kept frozen until further processing. Extraction and derivatisation of PLFA was performed following a modified Bligh and Dyer extraction, silica column partitioning, and mild alkaline transmethylation as described by Boschker et al. (2004). Analyses were made on a Isolink GC-c-IRMS coupled to a Thermo DeltaV Advantage. All samples were analyzed in splitless mode, using an apolar GC column (Agilent DB-5) with a flow rate of 2 mL min^{-1} of helium as carrier gas. Initial oven temperature was set at 60°C for 1 min, then increased to 130°C at 40°C min^{-1} , and subsequently reached 250°C at a rate of 3°C min^{-1} . $\delta^{13}\text{C}$ -PLFA were corrected for the addition of the methyl group by a simple mass balance calculation, and were calibrated using internal (C19:0) and external (mixture of C14:0, C16:0, C18:0, C20:0, C22:0)

fatty acid methyl ester (FAME) standards. Reproducibility was estimated to be $\pm 0.6\%$ or better for natural abundance samples.

2.3 Determination of the isotope fractionation factor

In September 2012, the isotope fractionation factor (ϵ) was estimated by monitoring the changes in CH_4 concentration and $\delta^{13}\text{C}\text{-CH}_4$ over time in microcosms at several depths across the oxycline. Six glass serum bottles (60 mL) were gently overfilled at each depth and tightly capped with a butyl rubber stopper and an aluminium cap. They were then incubated in the dark at the lake temperature during 0, 24, 48, 72, 96 or 120 h. The incubation was stopped by poisoning the bottles with 100 μL of saturated HgCl_2 . The measurement of the concentration of CH_4 and the $\delta^{13}\text{C}\text{-CH}_4$ in every bottle was performed as described before. The isotope fractionation factor was calculated according to Coleman et al. (1981).

2.4 Methanotrophic bacterial production and growth efficiency measurement

At several depths throughout the water column, the methanotrophic bacterial production and methanotrophic bacterial growth efficiency were estimated by quantifying the incorporation of ^{13}C -labelled CH_4 ($^{13}\text{C}\text{-CH}_4$, 99.9%, Eurisotop) into the POC and DIC pool. Water from each sampling depth was transferred with a tube into 12 serum bottles (60 mL), capped with butyl stoppers and sealed with aluminium caps. Thereafter, 4 different volumes (50, 100, 150, or 200 μL) of a $^{13}\text{C}\text{-CH}_4$ gas mixture (1 : 10 in He) were injected in triplicate and 100 μL of saturated HgCl_2 was immediately added to one bottle per gas concentration treatment, serving as control bottle without biological activity. After vigorous shaking, the bottles were incubated in the dark during 24 h at the lake temperature. The incubation was stopped by filtration of a 40 mL subsample on 25 mm glass fiber filters (Advantec GF-75; 0.3 μm) to measure the ^{13}C -POC enrichment, and a 12 mL Exetainer was filled and poisoned with the addition of HgCl_2 in order to measure the ^{13}C -DIC enrichment. The exact amount of $^{13}\text{C}\text{-CH}_4$

Methanotrophy in Lake Kivu

C. Morana et al.

Title Page

Abstract

Introduction

Conclusions

References

Tables

Figures

◀

▶

◀

▶

Back

Close

Full Screen / Esc

Printer-friendly Version

Interactive Discussion



added in the bottles was determined from the bottles poisoned at the beginning of the experiment. The measurements of the concentration of POC, the $\delta^{13}\text{C}$ -POC, the $\delta^{13}\text{C}$ -DIC and the $\delta^{13}\text{C}$ -CH₄ were performed as described above. Methanotrophic bacterial production (MBP, $\mu\text{molL}^{-1}\text{d}^{-1}$) rates were calculated according to Hama et al. (1983):

$$\text{MBP} = \text{POC}_f \cdot \left(\%^{13}\text{C}\text{-POC}_f - \%^{13}\text{C}\text{-POC}_i \right) / \left(t \cdot \left(\%^{13}\text{C}\text{-CH}_4 - \%^{13}\text{C}\text{-POC}_i \right) \right) \quad (1)$$

where POC_f is the concentration of POC at the end of incubation (μmolL^{-1}), $\%^{13}\text{C}\text{-POC}_f$ and $\%^{13}\text{C}\text{-POC}_i$ are the percentage of ¹³C in the POC and the end and the beginning of incubation, *t* is the incubation time (d^{-1}) and $\%^{13}\text{C}\text{-CH}_4$ is the percentage of ¹³C in CH₄ directly after the inoculation of the bottles with the ¹³C tracer.

The methanotrophic bacterial respiration rates (MBR, $\mu\text{molL}^{-1}\text{d}^{-1}$) were calculated according to:

$$\text{MBR} = \text{DIC}_f \cdot \left(\%^{13}\text{C}\text{-DIC}_f - \%^{13}\text{C}\text{-DIC}_i \right) / \left(t \cdot \left(\%^{13}\text{C}\text{-CH}_4 - \%^{13}\text{C}\text{-DIC}_i \right) \right) \quad (2)$$

where DIC_f is the concentration of DIC after the incubation (μmolL^{-1}), $\%^{13}\text{C}\text{-DIC}_f$ and $\%^{13}\text{C}\text{-DIC}_i$ are the final and initial percentage of ¹³C in DIC. Finally, the methanotrophic bacterial growth efficiency (MBGE, %) was calculated according to:

$$\text{MBGE} = \text{MBP} / (\text{MBP} + \text{MBR}) \cdot 100 \quad (3)$$

The CH₄ concentration in the bottles sometimes increased drastically because of the ¹³C-CH₄ addition, which could have induced a bias in the estimation of MBP and MBR in case of CH₄-limitation of the methanotrophic bacteria community. However, performing incubation along a gradient of CH₄ concentrations allowed us to assess if the measured MBP and MBR were positively related to the amount of tracer inoculated in the bottles. In case of such an effect (only at 50m in the Northern Basin in February 2012 and at 60m in the Southern Basin in September 2012) we applied a linear regression model ($r^2 > 0.90$) to estimate the intercept with the *y* axis, which was assumed to correspond to the MBP or MBR rates at in-situ CH₄ concentration.

**Methanotrophy in
Lake Kivu**

C. Morana et al.

Title Page

Abstract

Introduction

Conclusions

References

Tables

Figures

⏪

⏩

◀

▶

Back

Close

Full Screen / Esc

Printer-friendly Version

Interactive Discussion



2.5 Stable isotope probing of PLFA (SIP-PLFA) with $^{13}\text{C-CH}_4$

At each sampling depth and in parallel with the MBP measurement, 4 serum bottles (250 mL) were filled with water, overflowed and sealed with butyl stopper and aluminium caps. Bottles were spiked with 500 μL of $^{13}\text{C-CH}_4$ (99.9%). After 24 h of incubation in the dark at lake temperature, the water from the 4 bottles was combined and filtered on a single pre-combusted 47 mm glass fiber filter (Advantec GF-75; 0.3 μm) to quantify the incorporation of the tracer in bacterial PLFA. The filters were kept frozen until further processing. The extraction, derivatisation and analysis by GC-c-IRMS were carried out as described above.

3 Results

3.1 Physico-chemical parameters

In September 2012, the water column in the Southern Basin was oxic ($> 3 \mu\text{mol L}^{-1}$) from the surface to 65 m (Fig. 1a). CH_4 was abundant in deep waters, with a maximum concentration of 899 $\mu\text{mol L}^{-1}$ at 80 m, however CH_4 decreased abruptly in the oxycline (50–65 m), being 4 orders of magnitude lower in surface waters (Fig. 1a). Consistent with its biogenic origin, the upcoming CH_4 was depleted in ^{13}C in deep waters ($\delta^{13}\text{C-CH}_4$: -55.0‰) but became abruptly enriched in ^{13}C at the oxic–anoxic transition, where CH_4 concentrations sharply decreased, to reach a maximal value of -39.0‰ at 62.5 m depth (Fig. 1a). The $\delta^{13}\text{C-POC}$ values mirrored the pattern of $\delta^{13}\text{C-CH}_4$: they were almost constant from the surface to 55 m ($-24.4 \pm 0.3\text{‰}$), then showed an abrupt excursion towards more negative values at the bottom of the oxycline, with a minimum value (-42.8‰) at 65 m depth (Fig. 1a). Similar results were found in September 2012 in the Northern Basin, where the water was oxic ($> 3 \mu\text{mol L}^{-1}$) down to 55 m (Fig. 1b). At the oxic–anoxic transition, an abrupt isotopic enrichment of the

Title Page

Abstract

Introduction

Conclusions

References

Tables

Figures

◀

▶

◀

▶

Back

Close

Full Screen / Esc

Printer-friendly Version

Interactive Discussion



CH₄ was also observed and the $\delta^{13}\text{C}$ -POC was relatively depleted in ^{13}C , similarly as in the Southern Basin (Fig. 1b).

In February 2012 in the Northern Basin, the water was oxic until 45 m depth (> 3 μmolL^{-1}) but the O₂ concentrations were below the limit of detection deeper in the water column (Fig. 1c). The gradual decrease in the CH₄ concentration between 60 and 45 m (from 110 to 3 μmolL^{-1}) was accompanied by a parallel increase of the $\delta^{13}\text{C}$ -CH₄ signature in the same depth interval (from -55.9 to -41.7‰), the residual CH₄ becoming isotopically enriched as CH₄ concentration decreased (Fig. 1c). $\delta^{13}\text{C}$ -POC values were also slightly lower below the oxic zone, with a minimum at 50 m (-26.9‰) (Fig. 1c).

3.2 Phospholipid fatty acid concentration and stable isotopic composition

Figure 2 shows profiles of the relative concentration and the $\delta^{13}\text{C}$ signature of specific PLFA in September 2012 (Fig. 2a and b; Southern basin) and February 2012 (Fig. 2c and d; Northern Basin). Irrespective of station, season and depth, the C16:0 saturated PLFA was always the most abundant PLFA (18–35% of all PLFA). The relative abundance of the C16 monounsaturated fatty acids (C16 MUFA) significantly increased at the bottom of the oxycline in February and September 2012. The $\delta^{13}\text{C}$ signature of the C16 MUFA was comparable to the $\delta^{13}\text{C}$ signature of the C16:0 in oxic waters, oscillating around -27 or -29‰ in February and September 2012, respectively. However, C16 MUFA were largely depleted in ^{13}C in the oxycline, with minimal $\delta^{13}\text{C}$ values as low as -55.3‰ at the oxic–anoxic transition in September 2012, and -49.5‰ in February 2012. This very strong depletion in $\delta^{13}\text{C}$ was only observed for this particular type of PLFA (C16 MUFA). The C18 MUFA were slightly more abundant in oxic waters (on average 9%) than in deeper waters (1–4%). Their isotopic composition varied with depth following the same vertical pattern than C16 MUFA, but with a lower amplitude. C18 MUFA minima in $\delta^{13}\text{C}$ were observed in low-oxygen waters in February 2012 (55 m, -35.1‰) and September 2012 (70 m, -30.5‰). The

BGD

11, 15663–15691, 2014

Methanotrophy in Lake Kivu

C. Morana et al.

Title Page

Abstract

Introduction

Conclusions

References

Tables

Figures

◀

▶

◀

▶

Back

Close

Full Screen / Esc

Printer-friendly Version

Interactive Discussion



relative abundance of iso- and anteiso-branched C15:0 PLFA was systematically low (1–5%) and did not follow any depth pattern. Their isotopic signature was however slightly lower in oxygen-depleted waters than in oxic waters.

3.3 Isotope fractionation factor determination

5 During the isotope fractionation factor experiment, a significant decrease of the CH₄ concentration over time and a parallel enrichment of the residual CH₄ (Fig. 3) were monitored in every bottle incubated under oxic conditions. However, no consumption of CH₄ was measured in low-oxygen conditions. The isotope fractionation factor measured at several depths across the oxycline ranged between 1.008 and 1.024, and averaged 1.016 ± 0.007 (*n* = 5).

3.4 Methanotrophic bacterial production

MBP rates within the oxycline were variable (from 0 to 7.0 μmol C L⁻¹ d⁻¹). Maximum values were always observed near the oxic–anoxic transition (Fig. 1d–f), however substantial MBP (up to 2.2 μmol L⁻¹ d⁻¹) were also recorded under low-oxygen conditions (< 3 μmol L⁻¹) in February 2012 (Fig. 1f). Vertically integrated over the water column, MBP rates were estimated at 28.6 and 8.2 mmol m⁻² d⁻¹ in September 2012 in the Southern and Northern Basin, respectively, and 12.2 mmol m⁻² d⁻¹ in February 2012 in the Northern Basin. MBGE was found to be highly variable in the water column ranging between 50% at 52.5 m in the Northern Basin (September 2012) and 2% at 67.5 m in the Southern Basin (September 2012). Computed from depth-integrated MBP and MBR rates, the water column mean MBGE were 23% in September 2012 in the Southern and Northern Basins, and 42% in February 2012 in the Northern Basin.

Specific CH₄-derived C incorporation rates in PLFA (d⁻¹; incorporation rates normalized on PLFA concentration) show that bacteria containing C16 MUFA and C14:0 were particularly active in CH₄-derived C fixation in the oxycline in February

BGD

11, 15663–15691, 2014

Methanotrophy in Lake Kivu

C. Morana et al.

Title Page

Abstract

Introduction

Conclusions

References

Tables

Figures

◀

▶

◀

▶

Back

Close

Full Screen / Esc

Printer-friendly Version

Interactive Discussion



and September 2012 (Fig. 4a and b). In contrast, the specific incorporation pattern was dominated by C17 MUFA, and to a lesser extent 10Me16:0 and C16 MUFA in low-oxygen waters in February 2012 (Fig. 4b).

4 Discussion

The sharp decrease of CH₄ concentration and the isotopic enrichment of the residual CH₄ in the oxycline, mirrored by the isotopic depletion of the POC pool at these depths indicated that microbial CH₄ oxidation is a strong CH₄ sink within the water column of Lake Kivu. Similar patterns characterized by a strong isotopic depletion of the POC pool in the oxycline were reported in other systems, such as the meromictic Northern Basin of Lake Lugano (Lehmann et al., 2004; Blees et al., 2014).

The fraction of the upward CH₄ flux oxidized within a depth interval can be estimated from a model of isotope fractionation for open systems at steady-state described by the following Rayleigh equation (Eq. 4; Bastviken et al., 2002):

$$f = \left(\delta^{13}\text{CH}_{4b} - \delta^{13}\text{CH}_{4t} \right) / \left(\left(\delta^{13}\text{CH}_{4t} + 1000 \right) \cdot \left((1/\alpha) - 1 \right) \right) \quad (4)$$

where f is the fraction of CH₄ oxidized within the depth interval, $\delta^{13}\text{CH}_{4b}$ and $\delta^{13}\text{CH}_{4t}$ are the $\delta^{13}\text{C}$ values of CH₄ at the bottom and the top of the depth interval, respectively, and α is the isotope fractionation factor for CH₄ oxidation estimated in Lake Kivu in September 2012 ($\alpha = 1.016 \pm 0.007$). Based on this equation and using a range of isotope fractionation factors (from 1.009 to 1.023), we can estimate that 57–105 % of the upward flux of CH₄ was microbially oxidized within a 10 m depth interval in the oxycline (60–70 m) in the Southern Basin during the dry season (September 2012). Similarly, 67–142 % of the CH₄ flux was oxidized between 50 and 55 m in the Northern Basin during the dry season, and 55–93 % of the CH₄ flux was oxidized within a wider depth interval (45–70 m) during the rainy season (February 2012). The relatively wide range of the estimated percentage of CH₄ flux oxidized is due to the uncertainty

on the isotope fractionation factor. Nevertheless, these calculations illustrate clearly the importance of microbial CH₄ oxidation processes in preventing CH₄ to reach the surface waters of the lake.

The theoretical δ¹³C signature of methanotrophs can be estimated at each depth from δ¹³C-CH₄ values and the experimental isotope fractionation factor (α, ranged between 1.009–1023). Then, applying a simple isotope mixing model with the δ¹³C signature of methanotrophs as an end-member and the δ¹³C-POC in surface as a sedimenting organic matter end-member, it is possible to estimate the contribution of CH₄-derived C to the POC pool. Indeed, the contribution of CH₄-derived C appeared to be substantial at the bottom of the mixolimnion. In September 2012 in the Southern Basin, 32–44 % of the depth-integrated POC pool in the oxycline (between 60 and 70 m) originated from CH₄ incorporation, with a local maximum at the oxic–anoxic transition (65 m, 44–54 %). In the Northern Basin, 13–16 % of the POC in the oxycline (between 50 and 60 m) derived from CH₄. However, the contribution of CH₄ to the POC pool was relatively lower during the rainy season, as only 4–6 % of the POC in the 50–70 m depth interval, below the oxycline, had been fixed by methanotrophic organisms in the Northern Basin in February 2012 (local maximum slightly below the oxycline at 50 m, 8–10 %).

¹³CH₄ tracer experiments allowed to estimate the net MBP and the MBGE. Whatever the season, the highest MBP (0.8–7.2 μmol C L⁻¹ d⁻¹) rates were found in the oxycline. Hence, CH₄ oxidation in Lake Kivu seems to be mainly driven by oxic processes. Furthermore, maximal MBP rates were observed where the in situ CH₄ : O₂ ratio ranged between 0.1 and 10 (molar units, Fig. 5a), encompassing the stoichiometric CH₄ : O₂ ratio for aerobic microbial CH₄ oxidation (0.5) and the optimal ratio estimated in culture experiment (0.9, Amaral and Knowles, 1995). This relationship highlights the importance of the regulation of aerobic methanotrophic production by both CH₄ and O₂ availability. Vertically integrated over the water column, the MBP was estimated at 12.2 mmol m⁻² d⁻¹ during rainy season in the Northern Basin, and 28.6 and 8.2 mmol m⁻² d⁻¹ during dry season in the Southern Basin and the Northern Basin,

Methanotrophy in Lake Kivu

C. Morana et al.

Title Page

Abstract

Introduction

Conclusions

References

Tables

Figures

◀

▶

◀

▶

Back

Close

Full Screen / Esc

Printer-friendly Version

Interactive Discussion



respectively. These rates are comparable to the gross CH₄ oxidation rate reported earlier by Jannasch (1975) in Lake Kivu (7.2 mmol m⁻² d⁻¹) and the upward CH₄ flux recently estimated (9.38 mmol m⁻² d⁻¹) by Pasche et al. (2009). Areal MBP in Lake Kivu are equivalent to 16–58 % of the mean annual phytoplankton primary production (49 mmol m⁻² d⁻¹, Darchambeau et al., 2014), suggesting that biomass production by methanotrophs has the potential to sustain a significant fraction of the pelagic food-web. For example, it has been shown that cyclopoid copepods (mesozooplankton) of Lake Kivu escape visual predators by migrating below the euphotic zone, sometimes down to low-oxygen waters (Isumbisho et al., 2006), where they might feed on CH₄-derived C sources.

The relative contribution of MBP to the autochthonous production in Lake Kivu was distinctly higher than those reported in 3 Swedish lakes during summer, where MBP was equivalent to 0.3 and 7.0 % of the phytoplankton production (Bastviken et al., 2003). This was unrelated to the phytoplankton production rates in the Swedish lakes that ranged between 7 and 83 mmol m⁻² d⁻¹ and encompassed the average phytoplankton production value in Lake Kivu (49 mmol m⁻² d⁻¹). The MBP rates in the Swedish lakes (based on ¹⁴C incubations) were, however, distinctly lower than in Lake Kivu, ranging between 0.3 and 1.8 mmol m⁻² d⁻¹. This difference is probably related to the high CH₄ concentrations at the oxic–anoxic transition zone in Lake Kivu, as MBP peaked in the Swedish lakes at CH₄ concentrations < 100 μmol L⁻¹, while MBP peaked in Lake Kivu at CH₄ concentrations one to two orders of magnitude higher. Kankaala et al. (2013) reported seasonally resolved (for the ice-free period) MBP in five small (0.004–13.4 km²) boreal humic lakes (with dissolved organic C concentrations ranging between 7 and 24 mg CL⁻¹) in southern Finland. In these lakes phytoplankton production and MBP were highly variable, ranging between 5 and 50 mmol m⁻² d⁻¹ and < 0.2 mmol C m⁻² d⁻¹ and 41 mmol m⁻² d⁻¹, respectively. MBP was significantly higher in the two smallest lakes (0.004–0.008 km²), characterized by high CH₄ concentrations (< 750 μmol L⁻¹) and permanent anoxia throughout the year in bottom waters. Considering a MBGE of 25 %, their MBP estimates corresponded to a highly

Methanotrophy in Lake Kivu

C. Morana et al.

Title Page

Abstract

Introduction

Conclusions

References

Tables

Figures

◀

▶

◀

▶

Back

Close

Full Screen / Esc

Printer-friendly Version

Interactive Discussion



**Methanotrophy in
Lake Kivu**

C. Morana et al.

[Title Page](#)[Abstract](#)[Introduction](#)[Conclusions](#)[References](#)[Tables](#)[Figures](#)[I ◀](#)[▶ I](#)[◀](#)[▶](#)[Back](#)[Close](#)[Full Screen / Esc](#)[Printer-friendly Version](#)[Interactive Discussion](#)

variable percentage of phytoplankton production, between 35 and 100% in the two smallest lakes, and between 0.4 and 5.0% in the three larger lakes (0.04–13.4 km²), and therefore they proposed that the relative contribution of methanotrophic bacteria to the total autotrophic production in a lake is related to its size (Kankaala et al., 2013).

5 However, the results reported for the large (2370 km²) Lake Kivu do not fit with this general pattern, probably because of the permanent and strong stratification of its water column that on one hand promotes a long residence time of deep waters and the accumulation of CH₄, and on the other hand leads to very slow upward diffusion of solutes, promoting the removal of CH₄ by bacterial oxidation as it diffuses to the
10 surface.

The MBGE found during this study was variable (2–50%), but within the range of reported values in fresh waters (15–80%, King, 1992; 6–72%, Bastviken et al., 2003). MBGE was negatively related to the CH₄:O₂ ratio (Fig. 5b), i.e., a smaller fraction of the oxidized CH₄ was incorporated into the biomass at the bottom of the
15 oxycline, where O₂ availability was relatively limited compared to CH₄. It has been recently suggested that under O₂-limiting conditions, methanotrophic bacteria are able to generate energy (adenosine triphosphate) by fermentation of formaldehyde (Kalyuzhnaya et al., 2013), the key intermediate in the oxidation of CH₄. This CH₄-based fermentation pathway would lead to the production of excreted organic acids (lactate, formate, ...) from CH₄-derived C instead of converting CH₄ into cellular
20 biomass. If the metabolic abilities for this process are ubiquitous in methanotrophic organisms, it may potentially occur within the water column of Lake Kivu, at the bottom of the oxycline or in micro-oxic zone, as suggested by the low MBGE values found at high CH₄:O₂ molar ratio.

25 Almost all known aerobic methanotrophic bacteria are phylogenetically affiliated to Proteobacteria, belonging either to the *Alphaproteobacteria* (also referred to type I methanotrophs) or *Gammaproteobacteria* (type II methanotrophs) classes (Hanson and Hanson, 1996). The two distinct groups differ in some important physiological characteristics. Notably, they use different C fixation pathway (ribulose monophosphate

**Methanotrophy in
Lake Kivu**

C. Morana et al.

[Title Page](#)[Abstract](#)[Introduction](#)[Conclusions](#)[References](#)[Tables](#)[Figures](#)[I◀](#)[▶I](#)[◀](#)[▶](#)[Back](#)[Close](#)[Full Screen / Esc](#)[Printer-friendly Version](#)[Interactive Discussion](#)

for type I; the serine pathway for type II) and possess different patterns of PLFA. C16 MUFA are especially abundant in the type I methanotrophs while the type II methanotrophs contain mainly C18 MUFA (Le Bodelier et al., 2009). Therefore, the larger amount of ^{13}C -depleted C16 MUFA found in the oxycline and the strong labelling of C16 MUFA during the incubation with ^{13}C - CH_4 indicate that the aerobic methanotrophic community was dominated by type I methanotrophs in the water column during this study. In contrast, Type II methanotrophs did not appear to contribute much to the CH_4 oxidation in Lake Kivu, in good agreement with the results of Pasche et al. (2011). The dominance of type I over type II methanotrophs has been frequently reported in various stratified freshwater (Sundh et al., 1995; Brees et al., 2014) or marine environments (Schubert et al., 2006; Schmale et al., 2012), but this recurrent observation is still difficult to explain. In a recent review, Ho et al. (2013) attempted to classify several genus of methanotrophs according to their life strategies, using the competitor/stress tolerator/ruderal functional classification framework (Grime, 1977). Since type I methanotrophs dominate the active community in many environments and are known to respond rapidly to substrate availability, they classified them as competitors, or competitors-ruderals. In contrast, they proposed that type II members would be able to persist in the environment in a reversible state of reduced metabolic activity under non-favourable conditions, and thus classified them as stress tolerator, or stress tolerator-ruderal. Relatively large availability of CH_4 and O_2 (Figs. 1 and 5) at the oxic–anoxic transition of Lake Kivu is a favourable environment for the competitor-ruderal bacterial communities that could explain the dominance of type I methanotrophs over type II methanotrophs in this lake.

Also, a significant MBP rate ($1.3\ \mu\text{mol L}^{-1}\text{d}^{-1}$) was measured under low-oxygen conditions ($< 3\ \mu\text{mol L}^{-1}$) at 60 m during the rainy season (February 2012). Moreover, the PLFA labelling pattern was drastically different, with a more important specific ^{13}C incorporation into 10Me16:0 and C17 MUFA instead of the C16 MUFA, relative to their concentrations. This different labelling pattern suggests that a different population of methanotrophs was active in CH_4 oxidation deeper in the water column. Archaea

lack ester-linked fatty acids in their membrane and are therefore undetectable in PLFA analysis. However 10Me16:0 and C17 MUFA are known to be especially abundant in sulphate-reducing bacteria (Macalady et al., 2000), the syntrophic partner of anaerobic CH₄ oxidizing archaea (Boetius et al., 2000). Hence, the specific labelling of 10Me16:0 and C17 MUFA under low-oxygen conditions could indicate that a fraction of the upward flux of CH₄ was oxidized syntrophically with SO₄²⁻ reduction during the rainy season, and might support the hypothesis that SO₄²⁻-reducing bacteria grow on CH₄-derived carbon source supplied by anaerobic methane oxidizers within the archaea/SO₄²⁻-reducers consortium, as already suggested by the results of an in vitro labelling (¹³CH₄) study (Blumenberg et al., 2005).

5 Conclusions

Lake Kivu ranks globally among the lakes with the lowest CH₄ emissions to the atmosphere (Borges et al., 2011), although the deep layers of the lake contain a huge amount of dissolved CH₄. This apparent paradox is linked to its strong meromictic nature that on one hand promotes a long residence time of deep waters and the accumulation of CH₄, and on the other hand leads to very slow upward diffusion of solutes, promoting the removal of CH₄ by bacterial oxidation as it diffuses to the surface. Our knowledge on bacterial CH₄ oxidation in Lake Kivu has been so far based on circumstantial evidence such as mass balance considerations (Borges et al., 2011; Pasche et al., 2011) and a few incubations carried out almost 40 years ago (Jannasch, 1975). Here, we provide conclusive evidences on the occurrence of CH₄ oxidation in the oxycline of Lake Kivu using stable isotopic characterisation of a suite of carbon pools (CH₄, POC, PLFA) as well as rate measurements (MBP). Vertically integrated MBP ranged between 8 and 29 mmol m⁻² d⁻¹, and was higher than previously reported in other lakes (Bastvinken et al., 2003; Kankaala et al., 2013). MBP was equivalent to 16–58% of the average annual phytoplankton primary production, a fraction distinctly

BGD

11, 15663–15691, 2014

Methanotrophy in Lake Kivu

C. Morana et al.

Title Page

Abstract

Introduction

Conclusions

References

Tables

Figures

◀

▶

◀

▶

Back

Close

Full Screen / Esc

Printer-friendly Version

Interactive Discussion



higher than previously reported in other lakes, usually < 10 % (Bastvinken et al., 2003; Kankaala et al., 2006). Hence, methanotrophic bacteria could potentially sustain a significant fraction of the pelagic food-web in this oligotrophic CH₄-rich lake.

Acknowledgements. We are grateful to Boniface Kaningini, Pascal Isumbisho and Pascal Masilya (Institut Supérieur Pédagogique, Bukavu, DRC), Laetitia Nyinawamwiza (National University of Rwanda, Rwanda), for logistic support during the cruises, to Laetitia Montante and to Stephan Hoornaert for help during fieldwork and during laboratory analysis. This work was funded by the EAGLES (East African Great lake Ecosystem Sensitivity to Changes, SD/AR/02A) project from the Belgian Federal Science Policy Office (BELSPO, Belgium), the CAKI (Cycle du carbone et des nutriments au Lac Kivu, contract 2.4.598.07) and MICKI (Microbial diversity and processes in Lake Kivu, contract 2.4.515.11) projects from the Fonds National de la Recherche Scientifique (FNRS, Belgium), and contributes to the European Research Council (ERC) starting grant project AFRIVAL (African river basins: Catchment-scale carbon fluxes and transformations, 240002). AVB is a senior research associate at the FNRS.

References

- Amaral, J. A. and Knowles, R.: Growth of methanotrophs in methane and oxygen counter gradients, *FEMS Microbiol. Lett.*, 126, 215–220, 1995.
- Bastviken, D., Ejlertsson, J., and Tranvik, L.: Measurement of methane oxidation in lakes: a comparison of methods, *Environ. Sci. Technol.*, 36, 3354–3361, 2002.
- Bastviken, D., Ejlertsson, J., Sundh, I., and Tranvik, L.: Methane as a source of carbon and energy for Lake Pelagic food webs, *Ecology*, 84, 969–981, 2003.
- Bastviken, D., Tranvik, L. J., Downing, J. A., Crill, P. M., and Enrich-Prast, A.: Freshwater methane emissions offset the continental carbon sink, *Science*, 331, 50–50, 2011.
- Blees, J., Niemann, H., Wenk, C. B., Zopfi, J., Schubert, C. J., Kirf, M. K., Veronesi, M. L., Hitz, C., and Lehmann, M. F.: Micro-aerobic bacterial methane oxidation in the chemocline and anoxic water column of deep south-Alpine Lake Lugano (Switzerland), *Limnol. Oceanogr.*, 59, 311–324, 2014.
- Blumenberg, M., Seifert, R., Nauhaus, K., Pape, T., and Michaelis, W.: In vitro study of lipid biosynthesis in an anaerobically methane-oxidizing microbial mat, *Appl. Environ. Microb.*, 71, 4345–4351, 2005.

Methanotrophy in Lake Kivu

C. Morana et al.

Title Page

Abstract

Introduction

Conclusions

References

Tables

Figures

◀

▶

◀

▶

Back

Close

Full Screen / Esc

Printer-friendly Version

Interactive Discussion



Methanotrophy in
Lake Kivu

C. Morana et al.

Title Page

Abstract

Introduction

Conclusions

References

Tables

Figures

I ◀

▶ I

◀

▶

Back

Close

Full Screen / Esc

Printer-friendly Version

Interactive Discussion



- Boetius, A., Ravenschlag, K., Schubert, C. J., Rickert, D., Widdel, F., Gieseke, A., Amann, R., Jørgensen, B. B., Witte, U., and Pfannkuche, O.: A marine microbial consortium apparently mediating anaerobic oxidation of methane, *Nature*, 407, 623–626, 2000.
- Borges, A. V., Abril, G., Delille, B., Descy, J. P., and Darchambeau, F.: Diffusive methane emissions to the atmosphere from Lake Kivu (Eastern Africa), *J. Geophys. Res.*, 116, G03032, doi:10.1029/2011JG001673, 2011.
- Boschker, H. T. S.: Linking microbial community structure and functioning: stable isotope (^{13}C) labeling in combination with PLFA analysis, in: *Molecular Microbial Ecology Manual II*, edited by: Kowalchuk, G. A., de Bruijn, F. J., Head, I. M., Akkermans, A. D., and van Elsas, J. D., Kluwer Academic Publishers, The Netherlands, 1673–1688, 2004.
- Coleman, D. D., Risatti, J. B., and Schoell, M.: Fractionation of carbon and hydrogen by methane-oxidizing bacteria, *Geochim. Cosmochim. Ac.*, 45, 1033–1037, 1981.
- Damas, H.: La stratification thermique et chimique des lacs Kivu, Edouard et Ndalaga (Congo Belge), *Verhandlungen der Internationalen Vereinigung für Theoretische und Angewandte Limnologie*, Schweizerbart Science Publishers, Stuttgart, 8, 51–68, 1937.
- Darchambeau, F., Sarmento, H., and Descy, J. P.: Primary production in a tropical large lake: the role of phytoplankton composition, *Sci. Total Environ.*, 473, 178–188, 2014.
- Degens, E. T., vos Herzes, R. P., Wosq, H.-K., Deuser, W. G., and Jannasch, H. W.: Lake Kivu: structure, chemistry and biology of an East African rift lake, *Geol. Rundsch.*, 62, 245–277, 1973.
- Denman, K. L., Brasseur, G., Chidthaisong, A., Ciais, P., Cox, P. M., Dickinson, R. E., Hauglustaine, D., Heinze, C., Holland, E., Jacob, D., Lohmann, U., Ramachandran, S., da Silva Dias, P. L., Wofsy, S. C., and Zhang, X.: Couplings between changes in the climate system and biogeochemistry, in: *Climate Change 2007: the Physical Science Basis*, contribution of Working Group I to the Fourth Assessment Report of the Intergovernmental Panel on Climate Change, edited by: Solomon, S., Qin, D., Manning, M., Chen, Z., Marquis, M., Averyt, K. B., Tignor, M., and Miller, H. L., Cambridge University Press, Cambridge, UK and New York, NY, USA, 499–587, 2007.
- Forster, P., Ramaswamy, V., Artaxo, P., Berntsen, T., Betts, R., Fahey, D. W., Haywood, J., Lean, J., Lowe, D. C., Myhre, G., Nganga, J., Prinn, R., Raga, G., Schulz, M., and Van Dorland, R.: Changes in atmospheric constituents and in radiative forcing, in: *Climate Change 2007: the Physical Science Basis*, contribution of Working Group I to the Fourth Assessment Report of the Intergovernmental Panel on Climate Change, edited by:

**Methanotrophy in
Lake Kivu**

C. Morana et al.

Title Page

Abstract

Introduction

Conclusions

References

Tables

Figures

I ◀

▶ I

◀

▶

Back

Close

Full Screen / Esc

Printer-friendly Version

Interactive Discussion



Solomon, S., Qin, D., Manning, M., Chen, Z., Marquis, M., Averyt, K. B., Tignor, M., and Miller, H. L., Cambridge University Press, Cambridge, UK and New York, NY, USA, 129–234, 2007.

Grime, J. P.: Evidence for the existence of three primary strategies in plants and its relevance to ecological and evolutionary theory, *Am. Nat.*, 111, 1169–1194, 1977.

Hama, T., Miyazaki, T., Ogawa, Y., Iwakuma, T., Takahashi, M., Otsuki, A., and Ichimura, S.: Measurement of photosynthetic production of a marine phytoplankton population using a stable ^{13}C isotope, *Mar. Biol.*, 73, 31–36, 1983.

Hanson, R. S. and Hanson, T. E.: Methanotrophic bacteria, *Microbiol. Rev.*, 60, 439–471, 1996.

Ho, A., Kerckhof, F. M., Luke, C., Reim, A., Krause, S., Boon, N., and Le Bodelier, P. L.: Conceptualizing functional traits and ecological characteristics of methane-oxidizing bacteria as life strategies, *Environ. Microbiol. Reports*, 5, 335–345, 2013.

Isumbisho, M., Sarmiento, H., Kaningini, B., Micha, J. C., and Descy, J.-P.: Zooplankton of Lake Kivu, East Africa, half a century after the Tanganyika sardine introduction, *J. Plankton Res.*, 28, 971–989, 2006.

Jannasch, H. W.: Methane oxidation in Lake Kivu (central Africa), *Limnol. Oceanogr.*, 20, 860–864, 1975.

Jones, R. I. and Grey, J.: Biogenic methane in freshwater food webs, *Freshwater Biol.*, 56, 213–229, 2011.

Kalyuzhnaya, M. G., Yang, S., Rozova, O. N., Smalley, N. E., Clubb, J., Lamb, A., Nagana, G. A., Gowda, D., Rafferty, D., Fu, Y., Bringel, F., Vuilleumier, S., Beck, D. A. C., Trosenko, Y. A., Khmelenina, V. N., and Lidstrom, M. E.: Highly efficient methane biocatalysis revealed in a methanotrophic bacterium, *Nature Communications*, 4, 2785, doi:10.1038/ncomms3785, 2013.

Kankaala, P., Bellido, J. L., Ojala, A., Tulonen, T., and Jones, R. I.: Variable production by different pelagic energy mobilizers in boreal lakes, *Ecosystems*, 16, 1152–1164, 2013.

King, G. M.: Ecological aspects of methane oxidation, a key determinant of global methane dynamics, in: *Advances in Microbial Ecology*, edited by: Marshall, K. C., Plenum Press, New York, NY, USA, 431–468, 1992.

Kirschke, S., Bousquet, P., Ciais, P., et al.: Three decades of global methane sources and sinks, *Nat. Geosci.*, 6, 813–823, doi:10.1038/NGEO1955, 2013.

**Methanotrophy in
Lake Kivu**

C. Morana et al.

[Title Page](#)[Abstract](#)[Introduction](#)[Conclusions](#)[References](#)[Tables](#)[Figures](#)[I ◀](#)[▶ I](#)[◀](#)[▶](#)[Back](#)[Close](#)[Full Screen / Esc](#)[Printer-friendly Version](#)[Interactive Discussion](#)

- Le Bodelier, P. L., Gillisen, M. J. B., Hordijk, K., Damsté, J. S. S., Rijpstra, W. I. C., Geenevasen, J. A., and Dunfield, P. F.: A reanalysis of phospholipid fatty acids as ecological biomarkers for methanotrophic bacteria, *ISME J.*, 3, 606–617, 2009.
- Lehmann, M. F., Bernasconi, S. M., McKenzie, J. A., Barbieri, A., Simona, M., and Veronesi, M.: Seasonal variation of the $\delta^{13}\text{C}$ and $\delta^{15}\text{N}$ of particulate and dissolved carbon and nitrogen in Lake Lugano: constraints on biogeochemical cycling in a eutrophic lake, *Limnol. Oceanogr.*, 49, 415–429, 2004.
- Macalady, J. L., Mack, E. E., Nelson, D. C., and Scow, K. M.: Sediment microbial community structure and mercury methylation in mercury-polluted Clear Lake, California, *Appl. Environ. Microb.*, 66, 1479–1488, 2000.
- Pasche, N., Dinkel, C., Müller, B., Schmid, M., Wüest, A., and Wehrli, B.: Physical and biogeochemical limits to internal nutrient loading of meromictic Lake Kivu, *Limnol. Oceanogr.*, 54, 1863–1873, 2009.
- Pasche, N., Schmid, M., Vazquez, F., Schubert, C. J., Wüest, A., Kessler, J. D., Pack, M. A., Reeburgh, W. S., and Bürgmann, H.: Methane sources and sinks in Lake Kivu, *J. Geophys. Res.*, 116, G03006, doi:10.1029/2011JG001690, 2011.
- Rudd, J. W., Hamilton, R. D., and Campbell, N. E. R.: Measurement of microbial oxidation of methane in lake water, *Limnol. Oceanogr.*, 19, 519–524, 1974.
- Sanseverino, A. M., Bastviken, D., Sundh, I., Pickova, J., and Enrich-Prast, A.: Methane carbon supports aquatic food webs to the fish level, *PLoS ONE*, 7, e42723, doi:10.1371/journal.pone.0042723, 2012.
- Sarmiento, H., Isumbisho, M., and Descy, J.-P.: Phytoplankton ecology of Lake Kivu (Eastern Africa), *J. Plankton Res.*, 28, 815–829, 2006.
- Schmale, O., Blumenberg, M., Kiebllich, K., Jakobs, G., Berndmeyer, C., Labrenz, M., Thiel, V., and Rehder, G.: Aerobic methanotrophy within the pelagic redox-zone of the Gotland Deep (central Baltic Sea), *Biogeosciences*, 9, 4969–4977, doi:10.5194/bg-9-4969-2012, 2012.
- Schmid, M., Halbwachs, M., Wehrli, B., and Wüest, A.: Weak mixing in Lake Kivu: new insights indicate increasing risk of uncontrolled gas eruption, *Geochem. Geophys. Geosy.*, 6, Q07009, doi:10.1029/2004GC000892, 2005.
- Schoell, M., Tietze, K., and Schoberth, S. M.: Origin of methane in Lake Kivu (east-central Africa), *Chem. Geol.*, 71, 257–265, 1988.
- Schubert, C. J., Coolen, M. J., Neretin, L. N., Schippers, A., Abbas, B., Durisch-Kaiser, E., Wehrli, B., Hopmans, E. C., Sinninghe Damsté, J. S., Wakeham, S., and Kuypers, M. M.:

Aerobic and anaerobic methanotrophs in the Black Sea water column, *Environ. Microbiol.*, 8, 1844–1856, 2006.

Sundh, I., Bastviken, D., and Tranvik, L. J.: Abundance, activity, and community structure of pelagic methane-oxidizing bacteria in temperate lakes, *Appl. Environ. Microb.*, 71, 6746–6752, 2005.

Thiery, W., Martynov, A., Darchambeau, F., Descy, J.-P., Plisnier, P.-D., Sushama, L., and van Lipzig, N. P. M.: Understanding the performance of the FLake model over two African Great Lakes, *Geosci. Model Dev.*, 7, 317–337, doi:10.5194/gmd-7-317-2014, 2014.

Weiss, R. F.: Determinations of carbon dioxide and methane by dual catalyst flame ionization chromatography and nitrous oxide by electron capture chromatography, *J. Chromatogr. Sci.*, 19, 611–616, 1981.

Whiticar, M. J., Faber, E., and Schoell, M.: Biogenic methane formation in marine and freshwater environments: CO₂ reduction vs. acetate fermentation – isotope evidence, *Geochim. Cosmochim. Ac.*, 50, 693–709, 1986.

BGD

11, 15663–15691, 2014

Methanotrophy in Lake Kivu

C. Morana et al.

Title Page

Abstract

Introduction

Conclusions

References

Tables

Figures

⏪

⏩

◀

▶

Back

Close

Full Screen / Esc

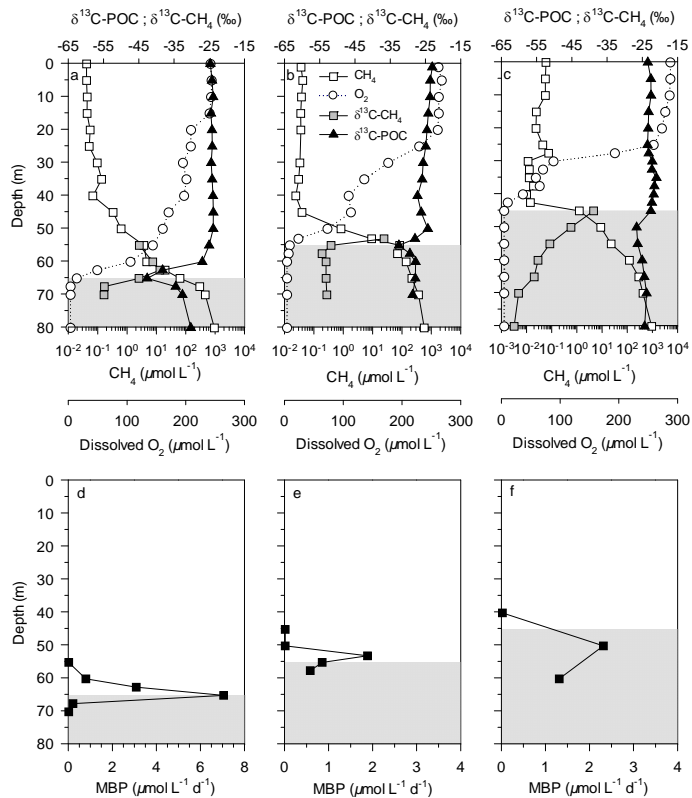
Printer-friendly Version

Interactive Discussion



Methanotrophy in
Lake Kivu

C. Morana et al.



Title Page

Abstract

Introduction

Conclusions

References

Tables

Figures



Back

Close

Full Screen / Esc

Printer-friendly Version

Interactive Discussion



Figure 1. Vertical profiles of dissolved O₂ concentration (μmolL⁻¹), CH₄ concentration (μmolL⁻¹), δ¹³C-CH₄ (‰) and δ¹³C-POC (‰) in Lake Kivu, in September 2012 (dry season) in the Southern Basin **(a)** and Northern Basin **(b)**, and in February 2012 (rainy season) in the Northern Basin **(c)**. Methanotrophic bacterial production rates (MBP, μmolL⁻¹d⁻¹) in September 2012 in the Southern Basin **(d)** and Northern Basin **(e)** and in February 2012 in the Northern Basin **(f)**. The grey zone corresponds to waters with dissolved O₂ concentration < 3 μmolL⁻¹.

Methanotrophy in Lake Kivu

C. Morana et al.

Title Page

Abstract

Introduction

Conclusions

References

Tables

Figures

⏪

⏩

◀

▶

Back

Close

Full Screen / Esc

Printer-friendly Version

Interactive Discussion



Methanotrophy in
Lake Kivu

C. Morana et al.

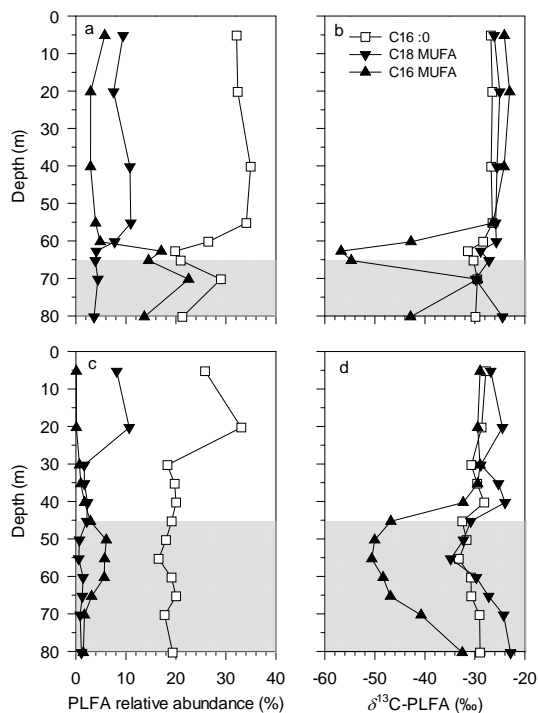


Figure 2. Vertical profiles of the relative abundance of phospholipid fatty acids (PLFA, %) and their respective carbon isotopic signature ($\delta^{13}\text{C}\text{-PLFA}$, ‰) in **(a, b)** the Southern Basin in September 2012 (dry season) and **(c, d)** in the Northern Basin in February 2012. The grey zone corresponds to waters with dissolved O₂ concentration < 3 μmol L⁻¹.

Title Page

Abstract

Introduction

Conclusions

References

Tables

Figures

◀

▶

◀

▶

Back

Close

Full Screen / Esc

Printer-friendly Version

Interactive Discussion



Methanotrophy in Lake Kivu

C. Morana et al.

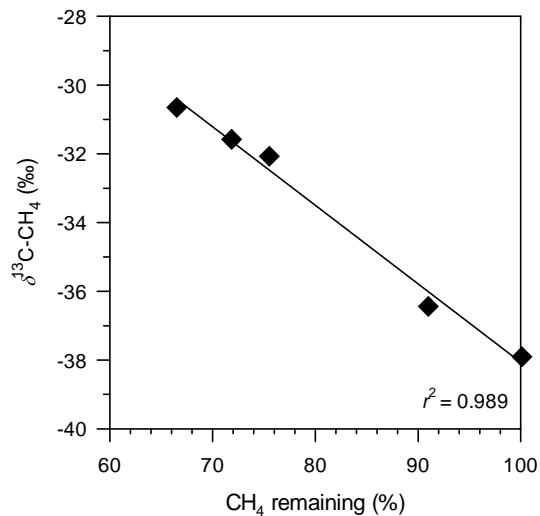


Figure 3. Example (62.5 m) of relationship between the $\delta^{13}\text{C-CH}_4$ and the fraction of CH_4 remaining in the bottles during the incubation to determine the isotope fractionation factor (%) carried out in September 2012 in the Southern Basin.

[Title Page](#)[Abstract](#)[Introduction](#)[Conclusions](#)[References](#)[Tables](#)[Figures](#)[◀](#)[▶](#)[◀](#)[▶](#)[Back](#)[Close](#)[Full Screen / Esc](#)[Printer-friendly Version](#)[Interactive Discussion](#)

Methanotrophy in
Lake Kivu

C. Morana et al.

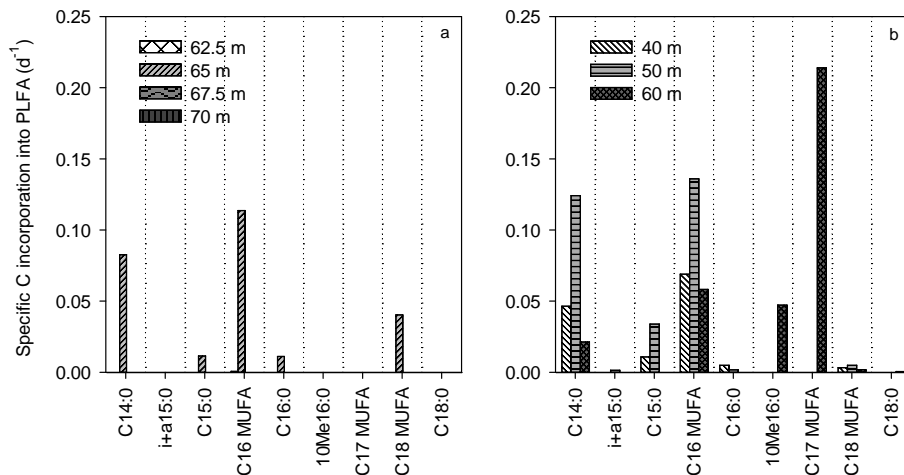


Figure 4. Specific CH_4 -derived C incorporation pattern into phospholipid fatty acids (PLFA) (incorporation rates of C into PLFA normalized on PLFA concentration, d^{-1}) in **(a)** September 2012 (dry season) in the Southern Basin and **(b)** in February 2012 (rainy season) in the Northern Basin.

Title Page

Abstract

Introduction

Conclusions

References

Tables

Figures

◀

▶

◀

▶

Back

Close

Full Screen / Esc

Printer-friendly Version

Interactive Discussion



Methanotrophy in
Lake Kivu

C. Morana et al.

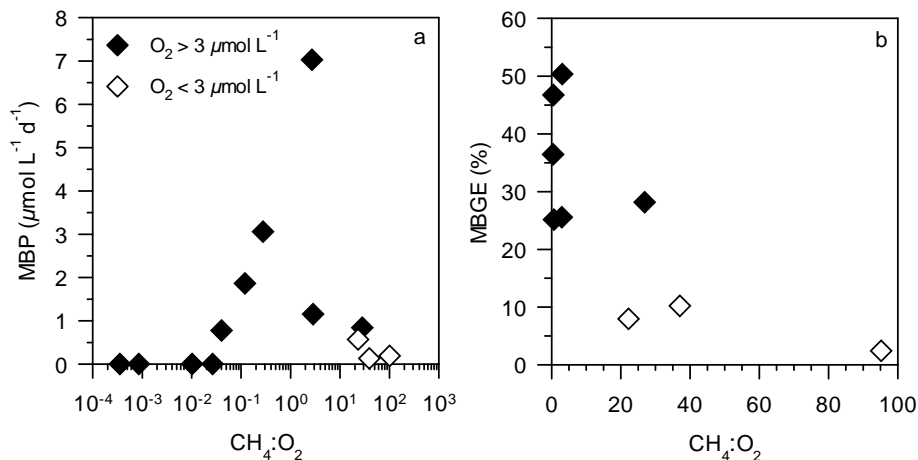


Figure 5. In Lake Kivu, **(a)** relationship between the methanotrophic bacterial production rates (MBP, $\mu\text{mol C L}^{-1} \text{d}^{-1}$) and the in situ $\text{CH}_4:\text{O}_2$ molar ratio and **(b)** relationship between the methanotrophic bacterial growth efficiency and the the in situ $\text{CH}_4:\text{O}_2$ molar ratio. The ratio was calculated with an O_2 concentration value of $3 \mu\text{mol L}^{-1}$ when observed in situ values were below the detection limit of the probe ($3 \mu\text{mol L}^{-1}$).

Climate change in tropical fresh waters (comment on the paper 'Plankton dynamics under different climatic conditions in space and time' by de Senerpont Domis *et al.*, 2013)

HUGO SARMENTO*, ANDRÉ M. AMADO* AND JEAN-PIERRE DESCY†

*Department of Oceanography and Limnology, 'Pós-Graduação em Ecologia', Federal University of Rio Grande do Norte, Natal, Brazil

†Department of Biology, Laboratory of Freshwater Ecology, URBE, University of Namur, Namur, Belgium

SUMMARY

1. de Senerpont Domis *et al.* (2013, *Freshwater Biology*, **58**, 463–482) forecasted changes in plankton dynamics in temperate, polar and tropical regions resulting from climate change. For tropical regions, they predicted an increase in precipitation intensity that would increase nutrient loading, increasing phytoplankton biomass and select for plankton adapted to flushing.
2. We do not agree with these predictions, as regional projections from the IPCC did not forecast a major increase in precipitation in tropical regions. The only regions where a slight increase in precipitation was projected were eastern Africa and South-East Asia. In eastern Africa, the major freshwater bodies are large, deep lakes that have very long residence times and are unlikely to be affected by flushing. Moreover, nutrient inputs from their catchment represent a small fraction of their total nutrient loading.
3. Several independent studies carried out in this region have provided evidence of a decrease in primary productivity in some of these large tropical lakes due to climate change. The major process providing nutrients to the euphotic layer is internal loading, which has been reduced as warming of the surface waters has increased the temperature gradient and the water column stability. Moreover, reduced velocity of trade winds during the dry season has affected the mixed layer depth and decreased internal nutrient fluxes. Therefore, the trend for large tropical lakes in a warming climate is oligotrophication, not eutrophication.
4. In tropical South America, the rainfall increase is not the dominant scenario; thus, the predicted changes in plankton dynamics do not stand.
5. Therefore, we believe that the predictions presented in the paper for tropical systems under a changing climate are invalid for most tropical systems.

Keywords: climate change, phytoplankton, Plankton Ecology Group model, tropical limnology, zooplankton

In their paper, de Senerpont Domis *et al.* (2013) discussed possible changes in plankton dynamics in temperate, polar and tropical regions resulting from climate change. According to the authors, this paper is an extension of the model designed by the Plankton Ecology Group (Sommer *et al.*, 1986), initially developed in temperate regions, to other latitudes, polar and tropical.

Most of the argumentation regarding the effect of climate change is based on changes in temperature and

precipitation. Changes in temperature are not questionable, as the IPCC projections point towards a general temperature increase in all latitudes. However, the forecast for precipitation in tropical regions is not as straightforward as it may appear from this paper due to the fact that local or regional features might be stronger constraints than global climate to biological activity. Regional projections from the IPCC (Meehl *et al.*, 2007) for tropical regions (between 23°N and 23°S) did not

forecast major changes in precipitation, as it might seem in fig. 2 in the paper by de Senerpont Domis *et al.*

The expected changes in precipitation in tropical regions are practically insignificant compared with higher latitudes and restricted to some specific areas. In the tropics, the only regions where precipitation is projected to increase are eastern Africa, South-East Asia (Table 1) and possibly the extreme north-west of South America, in the coast of Peru and Ecuador (Marengo *et al.*, 2010). Regional climate models for South America predict that rather than higher precipitation, most areas will experience higher frequency of extreme rainfall (storm) events but also longer periods of drought (Marengo *et al.*, 2010). These changes would decrease even more the predictabil-

ity of seasonal rainfall and associated processes, when relevant (e.g. floodplain ecosystems), and thus, the ecological consequences should be studied in shorter-scale approaches (Roland *et al.*, 2012).

The generalised seasonal development of current and future phytoplankton and zooplankton biomass presented in fig. 3 in the paper by de Senerpont Domis *et al.* does not reflect a general pattern for tropical lakes, but may only be valid for lowland, shallow, floodplain lakes usually observed in large tropical river basins. None of the 21 models of the IPCC predict an increase in precipitation in the Amazon and very little in the Congo basin, where these lowland floodplain lakes are most common. Thus, the prediction of phytoplankton dynamics changes as a result of higher rainfall may be incorrect.

In eastern Africa, which is the only region where precipitation would actually increase according to the IPCC (Table 1), most lakes are large and deep. Given their size, long retention time and small catchments, these large lakes will not be affected by flushing, as suggested by de Senerpont Domis *et al.* (2013). On the contrary, it has been well accepted for decades that internal loading is the major process affecting nutrient availability in large tropical lakes (Kilham & Kilham, 1990). The major effect of global and regional warming on these lakes has been an increase in temperature-driven density gradients due to warmer surface temperature with a subsequent increase in water column stability. At the same time, reduced wind speed has decreased vertical mixing and nutrient fluxes from internal loading (affecting mainly P inputs), resulting in reduced primary production. This has been evidenced in several studies on Lake Tanganyika, East Africa, based on recent data (Verburg, Hecky & Kling, 2003, 2006; Stenuite *et al.*, 2007) as well as palaeolimnological records (e.g. O'Reilly *et al.*, 2003; O'Reilly, Dettman & Cohen, 2005; Cohen *et al.*, 2006; Tierney *et al.*, 2010). Thus, despite the slight increase in precipitation that might occur, the effect of climate change alone on eastern African great lakes is oligotrophication, rather than an increase in planktonic productivity. However, this reasoning holds for large, deep lakes with a permanent hypolimnion, whereas shallower lakes may respond to climate change in a different way. It is also obvious that other anthropogenic impacts may override the effects of climate change and totally invalidate predictions based solely on climate. For instance, eutrophication of Lake Victoria resulted from multiple stresses including population growth, increased land use, exotic species introduction and meteorological variability (Hecky *et al.*, 2010).

Table 1 Regional averages of precipitation projections from a set of 21 global models in the MMD for the A1B scenario, adapted from the 2007 IPCC Report (Meehl *et al.*, 2007)

	Months	Precipitation Response (%)				
		Min	25	50	75	Max
West Africa 12S,20W to 22N,18E	DJF	-16	-2	6	13	23
	MAM	-11	-7	-3	5	11
	JJA	-18	-2	2	7	16
	SON	-12	0	1	10	15
	Annual	-9	-2	2	7	13
East Africa 12S,22E to 18N,52E	DJF	-3	6	13	16	33
	MAM	-9	2	6	9	20
	JJA	-18	-2	4	7	16
	SON	-10	3	7	13	38
	Annual	-3	2	7*	11	25
South-East Asia 11S,95E to 20N,115E	DJF	-4	3	6	10	12
	MAM	-4	2	7	9	17
	JJA	-3	3	7	9	17
	SON	-2	2	6	10	21
	Annual	-2	3	7*	8	15
Central America 10N,116W to 30N,83W	DJF	-57	-18	-14	-9	0
	MAM	-46	-25	-16	-10	15
	JJA	-44	-25	-9	-4	12
	SON	-45	-10	-4	7	24
	Annual	-48	-16	-9*	-5	9
Amazon 20S,82W to 12N,34W	DJF	-13	0	4	11	17
	MAM	-13	-1	1	4	14
	JJA	-38	-10	-3	2	13
	SON	-35	-12	-2	8	21
	Annual	-21	-3	0	6	14

The mean precipitation responses are first averaged for each model over all available realisations of the 1980–1999 period from the 20th Century Climate in Coupled Models (20C3M) simulations and the 2080–2099 period of A1B. Computing the difference between these two periods, the table shows the minimum, maximum, median (50%) and 25 and 75% quartile values among the 21 models, for precipitation (%) change. A value of 5% indicates no change, as this is the nominal value for the control period by construction (significant median annual values are marked with an asterisk).

In South America, there are three distinct climate change scenarios, with respect to precipitation patterns, that could affect ecosystem functioning (Roland *et al.*, 2012): zone 1, western Amazon and sub-tropical region with a slight increase in precipitation; zone 2, east Amazon and north-east (semi-arid region) with lower precipitation; and zone 3, south-east and coastline with similar precipitation amounts but increased frequency of storms. The aquatic ecosystems present in these three areas differ in several ways (e.g. with regard to frequency of connection of river to the ocean, to their humic content, and food-web structure), so that the interactions of the predicted changes with climate would be certainly different. The only zone that might follow the changes predicted by de Senerpont Domis *et al.* is zone 1 (i.e. western Amazon) which is dominated by rivers and oxbow lakes. Thus, lake type and regional characteristics should be taken into account for more precise predictions of changes in ecosystem function as a consequence of climate change.

Overall, the discussion throughout the paper concerning the tropical regions might be biased. The authors did not take into account the specificity of tropical systems, and some of the studies extensively cited by de Senerpont Domis *et al.* (e.g. studies comparing subtropical versus temperate systems, or long-term warming experiments in mesocosms conducted in northern Europe) are not the most relevant to describe and even less to predict plankton dynamics in tropical regions. We believe that more studies in tropical lakes, both large and small, in different regions, are still necessary to infer the impact of climate change on these ecosystems.

References

- Cohen A.S., Lezzar K.E., Cole J., Dettman D., Ellis G.S., Gonnea M.E. *et al.* (2006) Late Holocene linkages between decade-century scale climate variability and productivity at Lake Tanganyika, Africa. *Journal of Paleolimnology*, **36**, 189–209.
- Hecky R.E., Mugidde R., Ramlal P.S., Talbot M.R. & Kling G.W. (2010) Multiple stressors cause rapid ecosystem change in Lake Victoria. *Freshwater Biology*, **55**, 19–42.
- Kilham S.S. & Kilham P. (1990) Endless summer: internal loading processes dominate nutrient cycling in tropical lakes. *Freshwater Biology*, **23**, 379–389.
- Marengo J., Ambrizzi T., Da Rocha R., Alves L., Cuadra S., Valverde M. *et al.* (2010) Future change of climate in South America in the late twenty-first century: intercomparison of scenarios from three regional climate models. *Climate Dynamics*, **35**, 1073–1097.
- Meehl G.A., Stocker T.F., Collins W.D., Friedlingstein P., Gaye A.T., Gregory J.M. *et al.* (2007) Global climate projections. In: *Climate Change 2007: The Physical Science Basis. Contribution of Working Group I to the Fourth Assessment Report of the Intergovernmental Panel on Climate Change.* (Eds S. Solomon, D. Qin, M. Manning, Z. Chen, M. Marquis, K.B. Averyt, M. Tignor & H.L. Miller), pp. 747–845. Cambridge University Press, Cambridge, U.K.
- O'Reilly C., Dettman D. & Cohen A. (2005) Paleolimnological investigations of anthropogenic environmental change in Lake Tanganyika: VI. Geochemical indicators. *Journal of Paleolimnology*, **34**, 85–91.
- O'Reilly C.M., Alin S.R., Plisnier P.-D., Cohen A.S. & McKee B.A. (2003) Climate change decreases aquatic ecosystem productivity in Lake Tanganyika, Africa. *Nature*, **424**, 766–768.
- Roland F., Huszar V., Farjalla V., Enrich-Prast A., Amado A. & Ometto J. (2012) Climate change in Brazil: perspective on the biogeochemistry of inland waters. *Brazilian Journal of Biology*, **72**, 709–722.
- de Senerpont Domis L.N., Elser J.J., Gsell A.S., Huszar V.L.M., Ibelings B.W., Jeppesen E. *et al.* (2013) Plankton dynamics under different climatic conditions in space and time. *Freshwater Biology*, **58**, 463–482.
- Sommer U., Gliwicz Z.M., Lampert W. & Duncan A. (1986) The PEG-Model of seasonal succession of planktonic events in fresh waters. *Archiv Fur Hydrobiologie*, **106**, 433–471.
- Stenuite S., Pirlot S., Hardy M.A., Sarmiento H., Tarbe A.L., Leporcq B. *et al.* (2007) Phytoplankton production and growth rate in Lake Tanganyika: evidence of a decline in primary productivity in recent decades. *Freshwater Biology*, **52**, 2226–2239.
- Tierney J.E., Mayes M.T., Meyer N., Johnson C., Swarzenski P.W., Cohen A.S. *et al.* (2010) Late-twentieth-century warming in Lake Tanganyika unprecedented since AD 500. *Nature Geoscience*, **3**, 422–425.
- Verburg P., Hecky R.E. & Kling H. (2003) Ecological consequences of a century of warming in Lake Tanganyika. *Science*, **301**, 505–507.
- Verburg P., Hecky R.E. & Kling H.J. (2006) Climate warming decreased primary productivity in Lake Tanganyika, inferred from accumulation of dissolved silica and increased transparency — Comment to Sarvala *et al.* 2006 (Verh. Internat. Verein. Limnol. 29, p. 1182–1188). *International Association of Theoretical and Applied Limnology*, **29**, 2335–2338.

(Manuscript accepted 15 March 2013)

The queer *Tetraëdron minimum* from Lake Kivu (Eastern Africa): is it a result of a human impact?

Maya P. Stoyneva · Jean-Pierre Descy ·
Vanessa Balagué · Pierre Compère ·
Maria Leitao · Hugo Sarmiento

Received: 14 November 2011 / Accepted: 17 March 2012
© Springer Science+Business Media B.V. 2012

Abstract The coccal unicellular green algal genus *Tetraëdron* Kütz. ex Korshikov, which can be easily identified by its typical polygonal shape, is a common member of freshwater plankton and metaphyton, frequently observed in lowland temperate and tropical waters. During the analysis of samples from tropical Lake Kivu (Eastern Africa), we found an interesting “lemon-shaped” alga, which, after observations in

light microscope and scanning electron microscope, had been listed as *Tetraëdron* sp. Isolation in pure culture allowed a deeper study on morphology at different stages of the life cycle and the partial sequencing of the 18S rDNA. The results from the different combined approaches confirmed that it belongs to the species *Tetraëdron minimum* (A. Braun) Hansg. The unusual “lemon-shaped” forms predominant in Lake Kivu are young stages of the life cycle. This study contributes to the knowledge of the morphological variability, reproduction, and resting stages of *T. minimum* and discusses the reasons for the dominance of such unusual shape found in Lake Kivu, a lake strongly impacted by human activities as resulted by the large-scale biomanipulation following the introduction of the “Tanganyika sardine,” *Limnithrissa miodon* (Boulenger, 1906), at the end of the 1950s.

Guest editors: N. Salmaso, L. Naselli-Flores, L. Cerasino, G. Flaim, M. Tolotti & J. Padisák / Phytoplankton responses to human impacts at different scales: 16th workshop of the International Association of Phytoplankton Taxonomy and Ecology (IAP)

M. P. Stoyneva (✉)
Department of Botany, Faculty of Biology, Sofia
University “St Kl. Ohridski”, 8 Bld. Dragan Zankov,
1164 Sofia, Bulgaria
e-mail: mstoyneva@abv.bg

J.-P. Descy
Laboratory of Freshwater Ecology, URBO, Department of
Biology, University of Namur, 5000 Namur, Belgium

V. Balagué · H. Sarmiento
Institut de Ciències del Mar (CSIC), Pg Marítim de la
Barceloneta 37-49, 08003 Barcelona, Spain

P. Compère
Jardin Botanique National de Belgique, 1860 Meise,
Belgium

M. Leitao
Bi-Eau, 4900 Angers, France

Keywords Green algae · Phytoplankton ·
Zooplankton · Grazing · Tropical lake · Akinetes

Introduction

“Although, from one point of view, *Homo sapiens* is just one more species among the millions, it is unique in its power to influence the environment of all the others” (Reynolds, 1997, p. 295). From this sentence, it is possible to turn to a special problem of a great concern—the human impact on the phytoplankton.

This peculiar community consists of organisms, and the distribution and success of each of them is a function of abiotic constraints and biotic processes with a hierarchical importance of different factors (Brönmark & Hansson, 2005). The abiotic environment of a water body often is altered by human-induced disturbances (Brönmark & Hansson, 2005), and the effects which some of them cause to the phytoplankton are generally well known. Among them are the consequences of eutrophication, acidification, and biomanipulation. However, in spite of the increasing number of reports on exotic species introductions and to the influence of invasive alien species on biological diversity and ecosystem integrity, it is possible to stand that the consequences of such introductions at the level of morphological variation of a given species, belonging to a different trophic level from that of the allochthonous species, are practically unknown.

This article shows the probability for the occurrence of unusual small-shaped cells of *Tetraëdron minimum* due to changes in the grazing pressure in tropical Lake Kivu, ca. 50 years after the introduction of the planktivorous endemic sardine *Limnothrissa miodon* from the lake Tanganyika in order to “improve” the food web and to become the basis of fisheries activities (Collart, 1960; Simberloff, 1995). With this article, based on microscopic observations on field and cultured material in combination with molecular methods, we would like to contribute also to the knowledge on the cytology, reproduction, and resting stages of *T. minimum*.

Materials and methods

Study site and sampling procedures

Lake Kivu, located between Rwanda and the Democratic Republic of the Congo (Kivu Province), is one of the Great Lakes of the East African Rift Valley and is formed by four main basins (Fig. 1). It is a deep (max. 489 m), meromictic lake, with an oxygenated epilimnion of about 70 m and a deep hypolimnion rich in dissolved gases (CO₂, methane). With an annual average of chlorophyll *a* in the mixed layer of 2.2 mg m⁻³ and primary production of 0.71 g C m⁻² day⁻¹ (~260 g C m⁻² year⁻¹), the lake is clearly oligotrophic (Sarmiento et al., 2006, 2009).

Phytoplankton samples were collected regularly from September 2002 till February 2004 twice a month in the southern basin, while northern, eastern, and western basins were visited twice a year (once in the dry season and once in the rainy season). The qualitative samples were collected by vertical plankton net (10 µm mesh size) in the 0–60-m layer, and the quantitative samples were collected with a Van Dorn bottle at different depths (surface, 5, 10, 20, 30, 40, 50, and 60 m). The samples were preserved immediately after collection with neutral formaldehyde (2–4% final concentration) and Lugol solution. Before observation, the samples were concentrated by settling. For scanning electron microscopy (SEM), samples were fixed with glutaraldehyde at 1–2% final concentration. More details on sampling sites and procedures can be found in Sarmiento et al. (2007).

Strain isolation and cultivation

In September 2008, half a liter of subsurface water from Lake Kivu was shipped to the Institut de Ciències del Mar (CSIC) in Barcelona (Spain), within 48 h and then enriched with an equivalent volume of BG-11 culture medium. In sterile conditions, serial dilutions of the mixture were carried out in 12-well polystyrene plates. The plates were sealed with parafilm and incubated at 23°C under artificial photosynthetic active radiation (PAR) of 100 µmol photon m⁻² s⁻¹, in a 16:8-h light:dark cycle for several weeks. Microbial growth was regularly checked directly on the plates without opening it, under an inverted microscope at 40× magnification. The wells in which the specimen of interest was found in large abundance were transferred to BG-11 culture medium agar plates for strain isolation. Individual dark green colonies were re-grown in fresh BG-11 liquid culture medium and filtered through a 0.2-µm filter (Durapore 47 mm), preserved in 750 µl of lysis buffer (40 mM EDTA, 50 mM Tris-HCl, 0.75 M sucrose) and stored at –80°C until nucleic acid extraction (Fig. 2).

In December 2008, a part of the material was transported to the Algal Collection of Sofia University (ACUS). There, the material was analyzed immediately by means of light microscopy (LM) and then transferred on new agar plates, enriched by Bold Basal medium (BBM). The transfer followed standard techniques (Ettl & Gärtner, 1995; Andersen, 2005). In an attempt to observe zoospore production, BBM

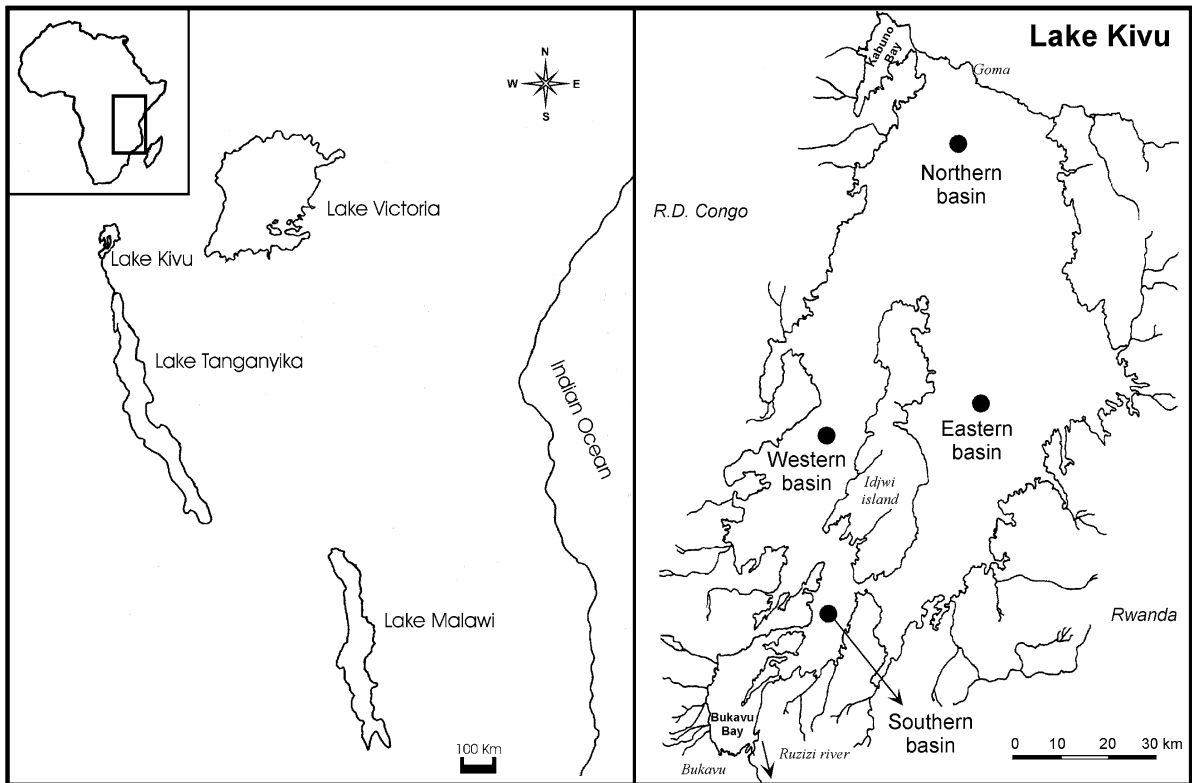


Fig. 1 Geographic situation of Lake Kivu with indication of its four major basins

liquid cultures were regrown several times, from the agar cultures. They were kept in darkness for ca. 16 h and then checked for zoospores.

LM and SEM processing with photo documentation of field and culture material

Light microscopic (LM) investigations were done on Olympus BX-50 (field material) and Motic BA 400 (culture material) microscopes with objectives 40 \times and 100 \times (oil immersion), both equipped with phase contrast. SEM study was done on Philips XL-microscope. Cell walls were stained with Gentian violet and Methylene Blue, and starch was colored with Lugol's solution (Ettl & Gärtner, 1995). Photomicrographs were taken with an Olympus Camedia digital camera (field material) and Moti-cam 2000 camera attached to the Motic BA 400 microscope with special adaptors (culture material). For processing of the photos, the computer software "Motic Images Plus 2.0" was used.

Nucleic acid extraction, amplification and sequencing

Nucleic acids were extracted by adding lysozyme (1 mg ml⁻¹) to the filter unit and incubating at 37°C for 45 min. Subsequently, proteinase K (0.2 mg ml⁻¹) and sodium dodecyl sulfate (SDS, 1%) were added, and the filter was incubated at 55°C for 1 h. The lysate was then extracted twice with an equal amount of phenol–chloroform–isoamyl alcohol (25:24:1, pH 8) and once with an equal amount of chloroform–isoamyl alcohol (24:1). The aqueous phase was spun down in a microconcentrator (Amicon-100, Millipore), washed with 2 ml of sterile MilliQ water three times, and reduced to a volume of 100 μ l. The recovered DNA was quantified using Nanodrop (Thermo Scientific). Nucleic acid extract was stored at -80°C.

One nanogram of DNA was used as template for PCR amplification of eukaryotic 18S rDNA. The reaction (50- μ l volume) contained 200 μ M of each of the deoxynucleoside triphosphates, 0.5 μ M of each of the primers, 1.5 mM MgCl₂, 1 \times PCR-buffer and 1.25

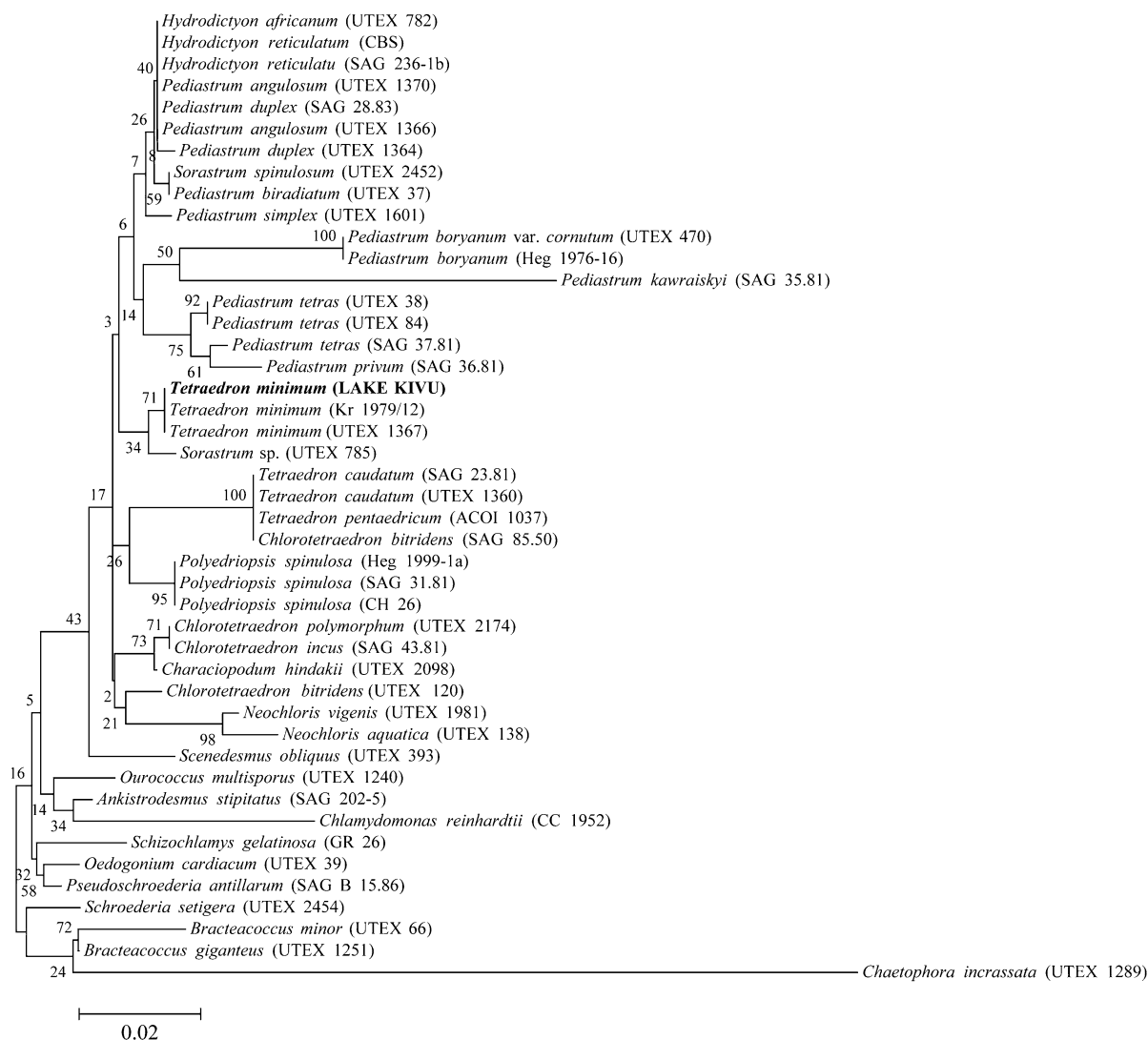


Fig. 2 Molecular phylogenetic analysis by maximum likelihood method. The evolutionary history was inferred using the maximum likelihood method based on the data specific model (Nei & Kumar, 2000). The bootstrap consensus tree inferred from 1,000 replicates is taken to represent the evolutionary history of the taxa analyzed (Felsenstein, 1985). Branches corresponding to partitions reproduced in less than 50% bootstrap replicates are collapsed. The percentage of replicate trees in which the associated taxa clustered together in the

bootstrap test (1,000 replicates) is shown next to the branches (Felsenstein, 1985). The rate variation model allowed for some sites to be evolutionarily invariable ([+I], 64.2418% sites). The tree is drawn to scale, with branch lengths measured in the number of substitutions per site. All positions containing gaps and missing data were eliminated. There were a total of 345 positions in the final dataset. Evolutionary analyses were conducted in MEGA5 (Tamura et al., 2011)

Units of Taq DNA Polymerase (Invitrogen). We used the eukaryotic specific primers EUK1F (5'-AAC CTG GTT GAT CCT GCC AGT-3') and 516r (5'-ACC AGA CTT GCC CTC C-3'). The PCR was performed with a thermal cycler (Bio-Rad) using the following program: initial denaturation at 94°C for 2 min 10 s; 30 cycles of denaturation (at 94°C for 30 s), annealing

(at 56 for 45 s) and extension (at 72°C for 2 min 10 s); and a final extension at 72°C for 10 min. PCR products were verified and quantified by agarose gel electrophoresis with a standard in the gel (Low DNA Mass Ladder, Invitrogen).

Positive PCR products were purified and sequenced by Macrogen Sequencing Service (South Korea). The

nucleotide sequence was deposited in GenBank under accession number BankIt1523118 LKO1 JQ797441. The sequence obtained was aligned with the software MEGA 5.05 (Tamura et al., 2011) and compared with DNA sequences from algal culture collections used by Buchheim et al. (2005). Evolutionary analyses were conducted in MEGA5.05 (Tamura et al., 2011).

Results

By means of LM in almost all phytoplankton samples from Lake Kivu, a free-floating alga with peculiar cell outline was found. The cells were solitary, ovoid, asymmetric to pyriform when seen in side view, and triangular (very rarely quadrangular) in front view, (5)–7–12–(14) μm in diameter. Each cell bears one or two, very rarely three or four, short-thickened polar protuberances, which were important for the “lemon-shaped” outline of the cell (Figs. 3–9, 20b). On higher magnifications, the rough character of the cell wall was visible, and by SEM, its scrobiculated character was confirmed (Figs. 14–17). Each cell contained a parietal, massive chloroplast, with a single pyrenoid (Figs. 5, 7–9) and oil droplets (Fig. 4). The pyrenoid bears a starch sheath, clearly visible after staining by iodine (Figs. 5, 8), thus confirming the disposition of the alga in the green lineage. The reproduction stages were rarely observed in the field material. They were represented by more or less developed autosporangia with 4 (8) autospores. Their release was preceded by cell wall rupture and its division in two parts. In the field material, the autospores have the peculiar “lemon-shape” of the free-floating cells, while some of the autosporangia showed a tetrahedral character. This was the first clear feature, which inspired the idea that the alga under investigation belonged to the genus *Tetraëdron*.

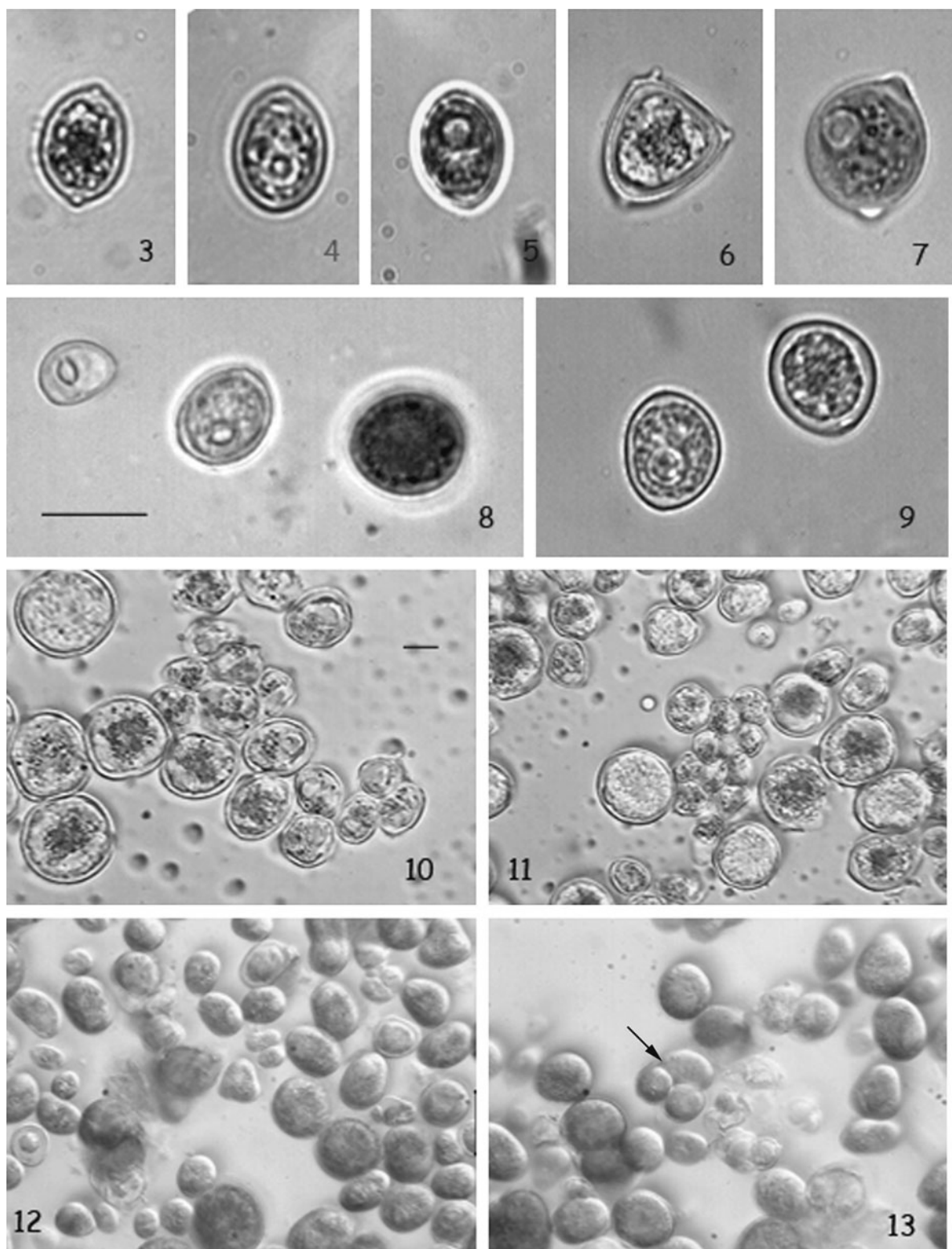
The next step—species identification—was more complicated. Finally, on the slides from the field material, we came to the conclusion that features observed overlap partially with the descriptions of two species, known for their polymorphism—*Tetraëdron regulare* Kütz. auct. post. (incl. var. *ornatum* Lemmerm.) and *T. minimum* (incl. var. *scrobiculatum* Lagerh.)—Sarmiento et al. (2007). At the same time, we had to take into account that in less than 10% of the samples, in small amount, typical, and well-developed tetrahedral cells with pronounced protuberances of *T. regulare* were observed (Fig. 16 in Sarmiento et al.,

2007). In this case, the only possible correct solution was to postpone the final identification decision and to list the material as *Tetraëdron* sp. (Sarmiento et al., 2007, Figs. 16, 47–50, 66) until we study it in pure cultures.

After the isolation of a clonal culture (in 2008), a part of the material was transferred for long-term cultivation on agar, and a small amount was immediately controlled for eventual zoospore production. However, zoospores were not observed. The first observations by LM of the material on agar plates did not reveal new features or significant morphological deviations compared with the data obtained from field material, except more abundant autosporangial and autospore production. In April 2009, on the original plate, sent to ACUS, a drying of the agar was detected, attended by the change in the color of algal stripes from green to yellowish-green. This was due to the abundant presence of akinetes—large (up to 25–30 μm in diameter) spherical cells with thick cell walls, which probably contained haematochrome (Figs. 10, 11). Some of them were in stage of division in two. The akinetes were immediately transferred to new agar plates.

In May 2010, PCR amplification and sequencing of the 18S rDNA of the material previously conserved from the first clonal cultures revealed the phylogenetic affiliation of the Kivu alga to *T. minimum* (Fig. 2). The partial sequence obtained was 100% similar to those of two *T. minimum* strains from other culture collections (Kr 1979/12 and UTEX 1367).

The culture material was studied again by LM from September 2010 to April 2011, after the algae in the new cultures, obtained from the akinetes, were developed more abundantly (Figs. 12, 13). Then an alteration in the abundance of the well-developed vegetative cells (some with typical for *T. regulare* shape) and autosporangia (Figs. 13, 18–28), and the smaller “lemon-shaped” cells was observed: the last ones dominated in February 2011 and then again in April 2011. All of the well-developed single vegetative cells were of bright green color and contained very large pyrenoids. Their starch sheath was clearly visible even without iodine staining (Fig. 7) and generally shows a bipartite character (Figs. 5, 8, 9). Again, a part of the material was transferred in BBM liquid and afterward checked by LM for zoospore formation. However, only autosporangia together with small “lemon-shaped” cells were recorded.



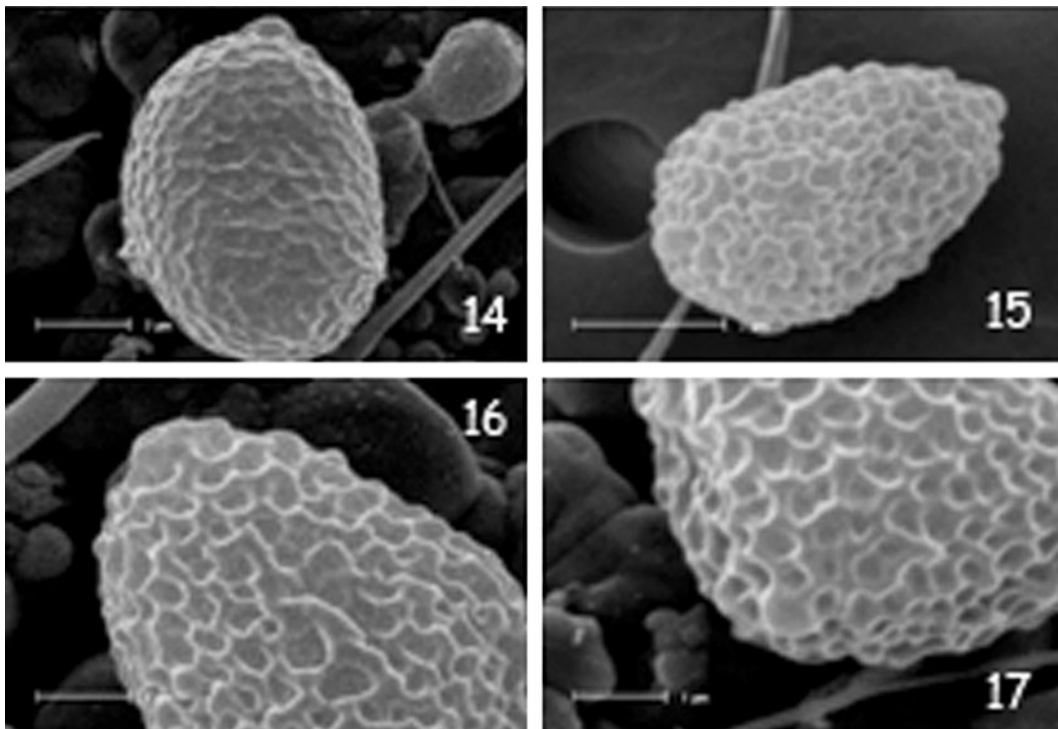
◀ **Figs. 3–13** *Tetraëdron minimum* in LM: 3–7, 9—single cells of the species; 8—single cells and initial autosporangium; 10, 11—akinetes with large *spots* or total content with resemblance to haematachromes and single cells in a drying culture; 12, 13—general view on a culture, developed from akinetes with new well developed vegetative single cells (some of them with typical triangular outfit like the cell in the centre of the photo, some more ovoid or spherical; among them smaller “lemon-shaped” cells could be seen), new young autosporangia and autosporangium with consecutive formation of autospores (arrow). Scale bar for Figs. 3–9—5 µm, for Figs. 10–13—10 µm

Discussion

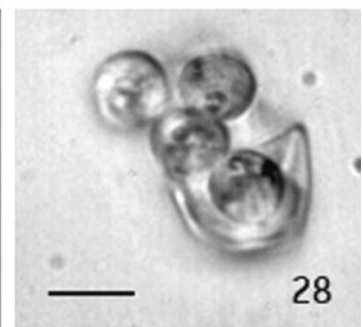
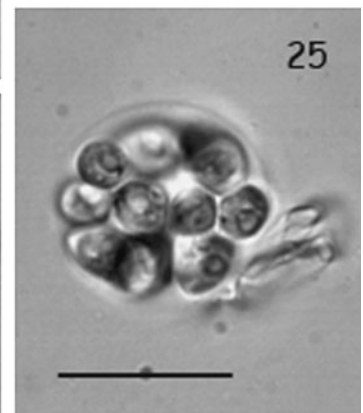
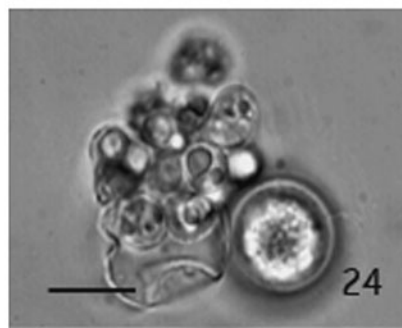
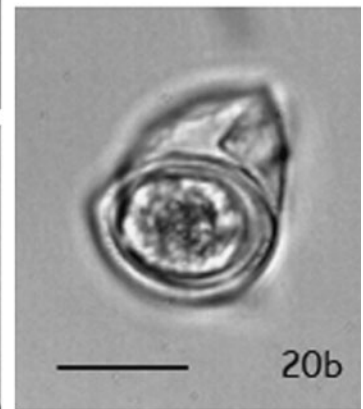
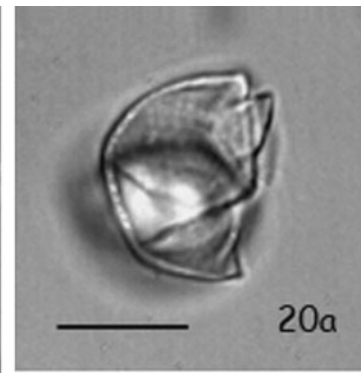
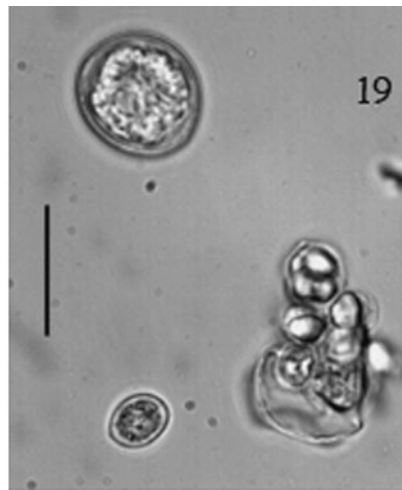
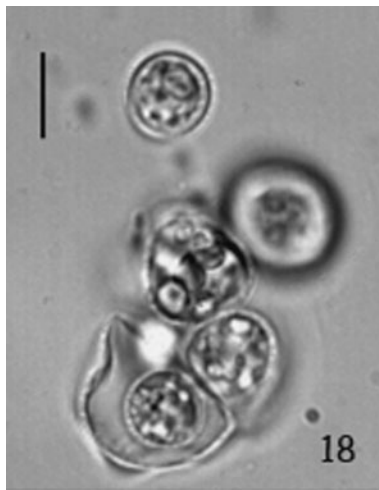
The observations on the morphology and reproduction show that the peculiar alga, found in the Lake Kivu, belongs to the genus *Tetraëdron* and is able of asexual reproduction by autospores and, additionally, of akinete formation. Until recently, production of akinetes as a process of enlargement of cells under harsh conditions supplied by increase of dimensions and changes of the shape and coloration (from green to yellow or red) in *Tetraëdron* was described only by Troitzkaja (1933) for *T. minimum* and for *T. regulare*,

and later by Korshikov (1953) for *T. incus* (Teiling) G. M. Sm. and by Davis (1966) for *T. bitridens* Beck-Managetta. All of the aforementioned authors noted their role as resting stages, but only Troitzkaja (1933) used the term “cysts” instead of “akinetes.” Both terms could be applied to the “giant” cells, observed in our cultures, because they were formed in asexual way from vegetative cells through enlargement, supplied by cell wall thickening and change in cell protoplast toward production of reddish content (possibly haematochrome). Due to this asexual (vegetative) way of forming, which is not always clear when term “cyst” is used (Ettl, 1980) we prefer to refer the stages found as “akinetes.” The vegetative division of akinetes, observed by us, is rarely reported in the physiological literature, but is a known process (Ettl, 1980).

The main cytological features observed in the vegetative cells (e.g., parietal chloroplast, single distinct pyrenoid with starch sheath, oil droplets) are on conformity with all former observations (see Kováčik, 1975 for details). Our records clarify the general bipartite character of the starch sheath around



Figs. 14–17 *Tetraëdron minimum* in SEM: 14, 15—general view on total cells; 16, 17—parts of cell surface with scrobiculated cell wall



◀ **Figs. 18–28** Autospores and autosporangia of *Tetraëdron minimum* in LM: 18, 22, 26, 28—autosporangia with four autospores (18 and 28—the release of the autospores after rupture of the autosporangium wall in two parts is seen; 22—autosporangium with one large and two smaller cells, showing the consecutive formation of autospores); 19, 24, and 27—autosporangia with more than four autospores; 20, 21, and 23—autosporangia with two autospores and ruptured autosporangium wall; 25—released autospores in a mucilage vesicle with remnants of the autosporangium wall beneath them. Scale bar for Figs. 18, 20–23, 26, and 28—5 µm, for Figs. 19, 24, 25, and 27—10 µm

the pyrenoid. The two parts of the sheath are distinct on the first photo from Plate 4 in the paper of Pickett-Heaps (1972) and on one drawing provided by Kováčik (1975, p. 365, plate 3c), but were not described or discussed by the authors. It could be supposed that the bipartite character of the pyrenoid sheath is typical for the genus. The cell wall surface in its outline by LM and its vision in SEM coincide with the data of Kováčik & Kalina (1975) on cell wall surface of *T. minimum*. The cell dimensions and mode of asexual reproduction by autospores only, as well as the data from molecular analyses, are on conformity with the same species.

The more frequent appearance of tetrahedral cells, resembling in outline *T. regulare*, than of more flat, quadrangular cells, widely known as typical of *T. minimum*, is on conformity with the data of Troitzkaja (1933), who underlined the simultaneous appearance of both types of cells in clonal cultures of *T. minimum*. However, the predominance of the peculiar “lemon-shaped” outline (with one or two small protuberances) of most of the cells found in the field and in some of the cultures provokes the question about the reasons which trigger the alga to appear in this form instead of its typical, widespread polygonal shape?

The change of the ratio of polyhedral and non-polyhedral cells in cultures of different age and observations of autosporangia and their development lead us to the idea that the “lemon-shaped” cells are just juvenile stages in the development of normal vegetative cells. This hypothesis finds support in the published details and illustrations on the development of different *Tetraëdron* species (e.g., Troitzkaja, 1933; Starr, 1954). After prolonged observations in cultures of *T. bitridens*, Starr (1954, p. 19) wrote that generally “each autospore is an exact replica of a mature vegetative cell, although, in some instances, where the

spores are retained within a sporangial wall for a long time, the autospores may have less pronounced angular processes.” Troitzkaja (1933) showed that in *T. minimum* the enlargement of the cell and increase in volume sometimes did not start from the central region (when a classical tetrahedral shape is formed), but from one of the sides, bringing to irregular, asymmetrical outline of the whole cell.

The data and conclusions of Kováčik & Kalina (1975) on cell wall surface, observed by SEM, are also on conformity with the idea that “lemon-shaped” cells found in Kivu waters and are young stages of *T. minimum*. The authors postulated that the network character of *Tetraëdron* cell wall surface, found by them in *T. caudatum* (Corda) Hansg. and *T. minimum*, is typical for the genus and the superficial undulation represents corrugation of two surface layers of the cell wall. Detailed analysis showed ontogenetical differences in the thickness and folding of the layers: in young cells the periphery of the middle layer is abundantly folded and the network is very dense, whereas in older cells the corrugated surface of outer layers evens out, the network thins out, and is composed of larger, often interlocked meshes. In old, large, rounded cells, the network is reduced or the cell surface is completely smooth (op. cit.). The photos of Kivu material, obtained by means of SEM, clearly show a well-developed mesh-network of the cell surface with deep folds (Figs. 14–17), which confirms that the “lemon-shaped” cells are young stages in development phase.

Alone, this result cannot explain the predominant occurrence of the immature stages of *T. minimum* in the oligotrophic Kivu waters. Lake Kivu phytoplankton composition is peculiar when compared to that of the other Rift Lakes (Sarmiento et al., 2007): it is dominated by diatoms, cyanoprokaryotes (cyanobacteria/blue-green algae), and cryptophytes. Green algae, which, for example, in Lake Tanganyika are a dominant group, have here a secondary role in terms of abundance and biomass (Sarmiento et al., 2006, 2008). Their diversity is also low, and the few taxa found are mainly colonial coccal green algae and desmids; unicellular forms are comparatively rare. This suggests that most green algae of Lake Kivu are grazing-resistant forms, as Stoyneva et al. (2007) supposed for a new *Eremosphaera* taxon in Lake Tanganyika.

Grazers in Lake Kivu are essentially three species: two cyclopoid copepods and one cladoceran (Isumbisho

et al., 2006). Although their grazing rates on algae are not known, their diet was studied using fatty acids (FA) as biomarkers: Masilya (2011) measured FA in several zooplankton size classes and found that small zooplankton (i.e., the 50–100 μm size class, comprising rotifers and copepod nauplii) fed essentially upon cryptophytes and diatoms. Copepods in the 100–300- μm size fractions also consumed chrysophytes, while the larger copepods (>300 μm) fed on cryptophytes, chrysophytes, and cyanoprokaryotes. FA from green algae were not found in zooplankton fractions, although they were present in the seston fractions. This indicates that green algae were either not ingested by zooplankters or that they were ingested but not assimilated.

Regarding *T. minimum* autospores, they are in the lower range of edible size for copepods (see, e.g., Sterner, 1989), and this could be a refuge strategy from grazing by the most abundant zooplankters in Lake Kivu. Small algae are more readily grazed by rotifers and by herbivorous protists. Rotifers are abundant in Lake Kivu, in contrast with the other oligotrophic Rift lakes (Isumbisho et al., 2006), and large ciliates are also present, although data on their abundance are lacking. Therefore, small algae, in order to survive in environments where grazing pressure is high and permanent, need to have traits that provide adequate refuge from grazers. In the case of *T. minimum*, fast reproduction rates with mass formation of autospores are a clear advantage for compensating grazing losses. Another trait which could be seen as a defense mechanism is the hard cell wall of *Tetraëdron* with high algaenans content, where the biopolymers are composed of long-chain even-carbon-numbered ω^9 -unsaturated ω -hydroxy FA monomers varying in chain length from 30 to 34 carbon atoms (Blokker et al., 1998). This renders the cells and autospores resistant to digestive enzymes: several authors have reported that ingested phytoplankton cells may transit through zooplankton guts and be egested undamaged and able to grow (see a review of defense mechanisms in Van Donk et al., 2011).

Thus, grazing pressure in this tropical great lake may explain why these peculiar stages of *T. minimum* are so abundant and make the bulk of the population of this alga. In Lake Tanganyika, another green alga, *Eremosphaera tanganyikae* Stoyneva, Cocquyt, Gärtner, and Vyverman, efficiently escapes grazing thanks to large cell size (Stoyneva et al., 2007): this is a similar “strategy,” at the other extreme of the size spectrum of the main grazers. A similar process was

described for planktonic bacterial communities, who under high grazing pressure show a higher proportion of extremely small coccoid shapes or large filaments, out of the edible range for predators (Jürgens & Güde, 1994). The role of grazing in molding the size and shape of phytoplankters was recently summarized by Naselli-Flores & Barone (2011), who showed that inducible defenses in prey traits in response to predation risk are particularly common in natural systems and that these low energetic cost adaption reduces phytoplankton mortality due to herbivory.

As for the “human impact” issue, it may be indirectly involved in these morphological defenses of *T. minimum*. Indeed, Lake Kivu is an example of large-scale biomanipulation, which consisted in the introduction of the “Tanganyika sardine,” *L. miodon*, at the end of the 1950s (Collart, 1960). This planktivorous fish induced important changes in the zooplankton structure, affecting both composition and abundance (Dumont, 1986). Thus, present zooplankton of Lake Kivu, different from that of the other Rift lakes in several respects, and the related grazing pressure, are the result of a major anthropogenic change. Due to the lack of detail in the knowledge of phytoplankton structure and composition before the sardine was introduced, the extent of the changes affecting the whole plankton is not easily evaluated. However, Sarmiento et al. (2012) estimated that crustacean abundance may have declined by a factor of three as a result of the introduction; also, a major grazer, a large cladoceran has disappeared (Dumont, 1986). It is likely that a reduction in zooplankton body size distribution occurred from predation on large zooplankton (Brooks & Dodson, 1965), and that small zooplankton (small crustaceans, rotifers and protists) became more abundant, thereby resulting in an increased grazing pressure on small phytoplankton. In this context, phytoplankton taxa exhibiting traits providing efficient defense against grazing may have had an advantage, and this may explain the peculiar morphology of *T. minimum* in Lake Kivu as a device for reducing grazing losses, exploited consequently after the human impact on the food web of the lake.

Acknowledgments We thank Mwapu Isumbisho, Pascal Masilya, and François Darchambeau for their assistance in fieldwork and organizing the sampling cruises. Hugo Sarmiento’s work was supported by the Spanish MCyI (Juan de la Cierva Fellowship JCI-2008-2727) and AGLOM project (CGL2010-11556-E). This study was also carried out in the

framework of the ECOSYKI Project, supported by the CUD (Commission Universitaire pour le Développement de la Communauté française de Belgique). Part of the work of Maya Stoyneva and her participation at the 16th IAP meeting was supported by CEBDER project of the National Science Fund of the Ministry of Education of Bulgaria (D002-15/17.2.2009). The authors are thankful to the anonymous reviewer and to the editor Luigi Naselli-Flores for the helpful comments on the article.

References

- Andersen, R. (ed.), 2005. Algal Culturing Techniques. Elsevier Academic Press, Phycological Society of America, London.
- Blokker, P., S. Schouten, H. van den Ende, J. W. de Leeuw, P. G. Hatcher & J. S. S. Damsté, 1998. Chemical structure of algaenans from the fresh water algae *Tetraedron minimum*, *Scenedesmus communis* and *Pediastrum boryanum*. *Organic Geochemistry* 29: 1453–1468.
- Brönmark, C. & L.-A. Hansson, 2005. The Biology of Lakes and Ponds. Oxford University Press, Oxford.
- Brooks, J. L. & S. I. Dodson, 1965. Predation, body size, and composition of plankton. *Science* 150: 28–35.
- Buchheim, M., J. Buchheim, T. Carlson, A. Braband, D. Hepperle, L. Krienitz, M. Wolf & E. Hegewald, 2005. Phylogeny of the Hydrodictyaceae (Chlorophyceae) inferences from rDNA data. *Journal of Phycology* 41: 1039–1054.
- Collart, A., 1954. La pêche au Ndagala au lac Tanganyika. *Bulletin Agricole Congo Belge* 45: 3–49.
- Collart, A., 1960. L'introduction du *Stolothrissa tanganicae* (Ndagala) au lac Kivu. *Bull Agric Congo Belg* 51:975–985
- Davis, J. S., 1966. Akinetes of *Tetraedron*. *Transactions of the American Microscopical Society* 85: 573–575.
- Dumont, H. J., 1986. The Tanganyika sardine in Lake Kivu: Another ecodisaster for Africa? *Environmental Conservation* 13: 143–148.
- Ettl, H., 1980. *Grundriß der allgemeinen Algologie*. Gustav Fischer Verlag, Stuttgart.
- Ettl, H. & G. Gärtner, 1995. *Syllabus der Boden-, Luft- und Flechtalgen*. Gustav Fischer, Stuttgart, Jena, New York.
- Felsenstein, J., 1985. Confidence limits on phylogenies: an approach using the bootstrap. *Evolution* 39: 783–791.
- Isumbisha, M., H. Sarmiento, B. Kaningini, J.-C. Micha & J.-P. Descy, 2006. Zooplankton of Lake Kivu, East Africa, half a century after a Tanganyika sardine introduction. *Journal of Plankton Research* 28: 1–10.
- Jürgens, K. & H. Güde, 1994. The potential importance of grazing-resistant bacteria in planktonic systems. *Marine Ecology-Progress Series* 112: 169–188.
- Korshikov, O. A., 1953. *Viznachnik prsnovodnih vodorostey Ukrainskoy RSR*. V. Protococcineae. *Naukova dumka, Kiiiv* (in Ukrainian).
- Kováčik, L., 1975. Taxonomic review of the genus *Tetraedron* (Chlorococcales). *Archiv für Hydrobiologie, Supplement* 46, *Algological Studies* 13: 354–391.
- Kováčik, L. & T. Kalina, 1975. Ultrastructure of the cell wall of some species in the genus *Tetraedron* (Chlorococcales). *Archiv für Hydrobiologie, Supplement* 46, *Algological Studies* 13: 433–444.
- Masilya, P., 2011. *Ecologie alimentaire comparée de Limnotherissa miodon et de Lamprichthys tanganicanus au lac Kivu (Afrique de l'Est)*. PhD thesis, Faculty of Sciences, Department of Biology, University of Namur, Namur, Belgium.
- Naselli-Flores, L. & R. Barone, 2011. Fight on plankton! Or, phytoplankton shape and size as adaptive tools to get ahead in the struggle for life. *Cryptogamie, Algologie* 32: 157–204.
- Nei, M. & S. Kumar, 2000. *Molecular Evolution and Phylogenetics*. Oxford University Press, New York.
- Pickett-Heaps, J., 1972. Cell division in *Tetraedron*. *Annals of Botany* 36: 693–701.
- Reynolds, C. S., 1997. *Vegetation Process in the Pelagic: A Model for Ecosystem Theory*. Ecology Institute, Oldendorf/Luhe, Germany.
- Sarmiento, H., M. Isumbisha & J.-P. Descy, 2006. Phytoplankton ecology of Lake Kivu (eastern Africa). *Journal of Plankton Research* 28: 815–829.
- Sarmiento, H., M. Leitao, M. Stoyneva, A. Couté, P. Compère, M. Isumbisha & J.-P. Descy, 2007. Species diversity of pelagic algae in Lake Kivu (East Africa). *Cryptogamie, Algologie* 28: 245–269.
- Sarmiento, H., F. Unrein, M. Isumbisha, S. Stenuite, J. M. Gasol & J.-P. Descy, 2008. Abundance and distribution of picoplankton in tropical, oligotrophic Lake Kivu, eastern Africa. *Freshwater Biology* 53: 756–771.
- Sarmiento, H., M. Isumbisha, S. Stenuite, F. Darchambeau, B. Leporcq & J.-P. Descy, 2009. Phytoplankton ecology of Lake Kivu (eastern Africa): biomass, production and elemental ratios. *Verhandlungen des Internationalen Verein Limnologie* 30: 709–713.
- Sarmiento, H., F. Darchambeau & J.-P. Descy, 2012. Phytoplankton of Lake Kivu. In Descy J.-P., F. Darchambeau, M. Schmid (eds.), *Lake Kivu: Limnology and biogeochemistry of a tropical great lake*, *Aquatic Ecology Series* 5, Springer. doi:10.1007/978-94-007-4243-7_5.
- Simberloff, D., 1995. Why do introduced species appear to devastate islands more than mainland areas? *Pacific Science* 49: 87–97.
- Starr, R. C., 1954. Reproduction by zoospores in *Tetraedron bitridens*. *American Journal of Botany* 41: 17–21.
- Sterner, R. W., 1989. The role of grazers in phytoplankton succession. In Sommer, U. (ed.), *Plankton Ecology. Succession in Plankton Communities*. Springer-Verlag, Berlin: 107–170.
- Stoyneva, M. P., J.-P. Descy & W. Vyverman, 2007. Green algae in Lake Tanganyika: is morphological variation a response to seasonal changes? *Hydrobiologia* 578: 7–16.
- Tamura, K., D. Peterson, N. Peterson, G. Stecher, M. Nei & S. Kumar, 2011. MEGA5: molecular evolutionary genetics analysis using maximum likelihood, evolutionary distance, and maximum parsimony methods. *Molecular Biology and Evolution* 28: 2731–2739.
- Troitzkaja, O. W., 1933. Über die Morphologische Variabilität bei den Protococcales. *Acta Instituti Botanici Academiae Scientiarum USSR, Series II*, 1: 115–224 (in Russian, German summ.).
- Van Donk, E., A. Ianora & M. Vos, 2011. Induced defenses in marine and freshwater phytoplankton: a review. *Hydrobiologia* 668: 3–19.



Understanding the performance of the FLake model over two African Great Lakes

W. Thiery¹, A. Martynov^{2,3}, F. Darchambeau⁴, J.-P. Descy⁵, P.-D. Plisnier⁶, L. Sushama², and N. P. M. van Lipzig¹

¹Department of Earth and Environmental Sciences, University of Leuven, Leuven, Belgium

²Centre pour l'Étude et la Simulation du Climat à l'Échelle Régionale (ESCER), Université du Québec à Montréal, Montréal, Canada

³Institute of Geography and Oeschger Centre for Climate Change Research, University of Bern, Bern, Switzerland

⁴Unité d'Océanographie Chimique, Université de Liège, Liège, Belgium

⁵Laboratoire d'écologie des Eaux Douces, University of Namur, Namur, Belgium

⁶Royal Museum for Central Africa, Tervuren, Belgium

Correspondence to: W. Thiery (wim.thiery@ees.kuleuven.be)

Received: 25 July 2013 – Published in Geosci. Model Dev. Discuss.: 2 October 2013

Revised: 14 January 2014 – Accepted: 15 January 2014 – Published: 18 February 2014

Abstract. The ability of the one-dimensional lake model FLake to represent the mixolimnion temperatures for tropical conditions was tested for three locations in East Africa: Lake Kivu and Lake Tanganyika's northern and southern basins. Meteorological observations from surrounding automatic weather stations were corrected and used to drive FLake, whereas a comprehensive set of water temperature profiles served to evaluate the model at each site. Careful forcing data correction and model configuration made it possible to reproduce the observed mixed layer seasonality at Lake Kivu and Lake Tanganyika (northern and southern basins), with correct representation of both the mixed layer depth and water temperatures. At Lake Kivu, mixolimnion temperatures predicted by FLake were found to be sensitive both to minimal variations in the external parameters and to small changes in the meteorological driving data, in particular wind velocity. In each case, small modifications may lead to a regime switch, from the correctly represented seasonal mixed layer deepening to either completely mixed or permanently stratified conditions from ~ 10 m downwards. In contrast, model temperatures were found to be robust close to the surface, with acceptable predictions of near-surface water temperatures even when the seasonal mixing regime is not reproduced. FLake can thus be a suitable tool to parameterise tropical lake water surface temperatures within atmospheric prediction models. Finally, FLake was used to attribute the seasonal mixing cycle at Lake Kivu to variations

in the near-surface meteorological conditions. It was found that the annual mixing down to 60 m during the main dry season is primarily due to enhanced lake evaporation and secondarily to the decreased incoming long wave radiation, both causing a significant heat loss from the lake surface and associated mixolimnion cooling.

1 Introduction

Owing to the strong contrast in albedo, roughness and heat capacity between land and water, lakes significantly influence the surface-atmosphere exchange of moisture, heat and momentum (Bonan, 1995; Mironov et al., 2010). Some effects of this modified exchange are (i) the dampening of the diurnal temperature cycle and lagged temperature response over lakes compared to adjacent land, (ii) enhanced winds due to the lower surface roughness, (iii) higher moisture input into the atmosphere as lakes evaporate at the potential evaporation rate, and (iv) the formation of local winds, such as the lake/land breezes (Savijärvi and Järvenoja 2000; Samuelsson et al., 2010; Lauwaet et al., 2011).

One such region where lakes are a key component of the climate system is the African Great Lakes region. During last decades, the African Great Lakes experienced fast changes in ecosystem structure and functioning, and their future evolution is a major concern (O'Reilly et al., 2003; Verburg et

al., 2003; Verburg and Hecky, 2009). To better understand the present lake hydrodynamics and their relation to aquatic chemistry and biology, several comprehensive one-, two- or three-dimensional hydrodynamic models have been developed and applied in standalone mode to lakes in this region (Schmid et al., 2005; Naithani et al., 2007; Gourgue et al., 2011; Verburg et al., 2011). However, to investigate the two-way interactions between climate and lake processes over East Africa, a correct representation of lakes within regional climate models (RCMs) and general circulation models (GCMs) is essential (Stepanenko et al., 2013; see Appendix for a list of all acronyms, variables and simulation names). For now, the high computational expense of complex hydrodynamic lake models limits the applicability of coupled lake–atmosphere model systems to process studies (Anyah et al., 2006; Thiery et al., 2014). To overcome this issue, the Freshwater Lake model (FLake) was recently developed (Mironov, 2008; Mironov et al., 2010). It offers a very good compromise between physical realism and computational efficiency.

As a one-dimensional lake parameterisation scheme, FLake has already been coupled to a large number of numerical weather prediction (NWP) systems, RCMs and GCMs (Kourzeneva et al., 2008; Dutra et al., 2010; Mironov et al., 2010; Salgado and Le Moigne, 2010; Samuelsson et al., 2010; Martynov et al., 2012). However, even though it has become a landmark in this respect, FLake has never been thoroughly tested for tropical conditions. Moreover, as several joint efforts to provide society with climate change information, such as the COordinated Regional climate Downscaling EXperiment (CORDEX), explicitly focus on the African continent (Giorgi et al., 2009), a correct representation of the African Great Lakes within NWP, RCMs and GCMs becomes of particular importance.

Hence, the main goal of this study is to test – for the first time – the ability of FLake to reproduce the temperature regimes of two tropical lakes in East Africa. Lake Kivu and Lake Tanganyika are selected, as they are the only rift lakes for which both local weather conditions and lake water temperatures have been monitored for several years. Lake Kivu (Fig. 1b), is a deep meromictic lake, with an oxic mixolimnion seasonally extending down to 60–70 m, below which the monimolimnion is found rich in nutrients and dissolved gases, in particular carbon dioxide and methane (Fig. 2; Degens et al., 1973; Borgès et al., 2011; Descy et al., 2012). Due to the input of heat and salts from deep geothermal springs, temperature and salinity in the monimolimnion increase with depth (Degens et al., 1973; Spigel and Coulter, 1996; Schmid et al., 2005). Moreover, in the deeper layers, vertical diffusive transport is dominated by double diffusive convection (Schmid et al., 2010). Lake Tanganyika (Fig. 1c), the first Albertine rift lake south of Lake Kivu, stretches 670 km southwards and, with its 60 km mean width and maximum depth of 1470 m, represents the second largest surface freshwater reservoir on earth (18 880 km³; Savijärvi,

1997; Alleman et al., 2005; Verburg and Hecky, 2009). Lake Tanganyika is also meromictic (Naithani et al., 2007), but its salt content is lower compared to Lake Kivu (Spigel and Coulter, 1996). Lake Kivu and Lake Tanganyika are both characterised by long lake water retention times (~ 100 yr and ~ 800 yr, respectively; Schmid and Wüest, 2012; Coulter, 1991), hence the impact of riverine in- and outflow is of little importance to the circulation within these lakes.

In this study, lake temperatures were calculated for three sites, one at Lake Kivu and two at Lake Tanganyika, by forcing FLake with observations from surrounding automatic weather stations (AWSs) and subsequently comparing them to observed time series. Besides integrating them with the raw meteorological observations, wind speed measurements and water transparency were also refined within their uncertainty range to yield a control simulation representing the correct mixing regime. At each location, FLake was also driven by the re-analysis product ERA-Interim (Simmons et al., 2007). Furthermore, a systematic analysis of FLake's sensitivity to variations in external parameters, meteorological forcing data, and temperature initialisation was conducted. Finally, a study of the surface energy balance allowed attributing the mixing regime at Lake Kivu to changes in near-surface meteorological conditions.

2 Data and methods

2.1 AWS data

The Lake Kivu region is characterised by a long dry season extending from June to September, and a wet season from October to May, interrupted by a short dry season around January (Beadle, 1981). Further south in Lake Tanganyika, the dry season sets in one month earlier (Spigel and Coulter, 1996; Verburg and Hecky, 2003). Over both lakes, predominantly southeasterly winds reach a maximum during the dry season (Nicholson, 1996; Verburg and Hecky, 2003; Sarmiento et al., 2006).

AWS 1 is located on the roof of the Institut Supérieur Pédagogique in Bukavu, Democratic Republic of the Congo, approximately 1 km from the southern border of Lake Kivu and 27 km southwest from the monitoring site in the Ishungu Basin (Fig. 1b). For this study, meteorological observations covering a period of 9 yr (2003–2011) were used. AWS 2 is situated at the Tanzania Fisheries Research Institute in Kigoma, Tanzania, 50 m from the lake shore and 4 km southeast from the evaluation site in Kigoma (Fig. 1c). As such, this station recorded meteorological conditions representative for the northern Tanganyika Basin from 2002 to 2006. Finally, considered as representative for the southern Tanganyika Basin, AWS 3 is located at Mpulungu Department of Fisheries, on the lake shore and 8.5 km south of the monitoring site of Mpulungu (Fig. 1c). Unfortunately, for this station only 13 months of data (February 2002–April 2003) were

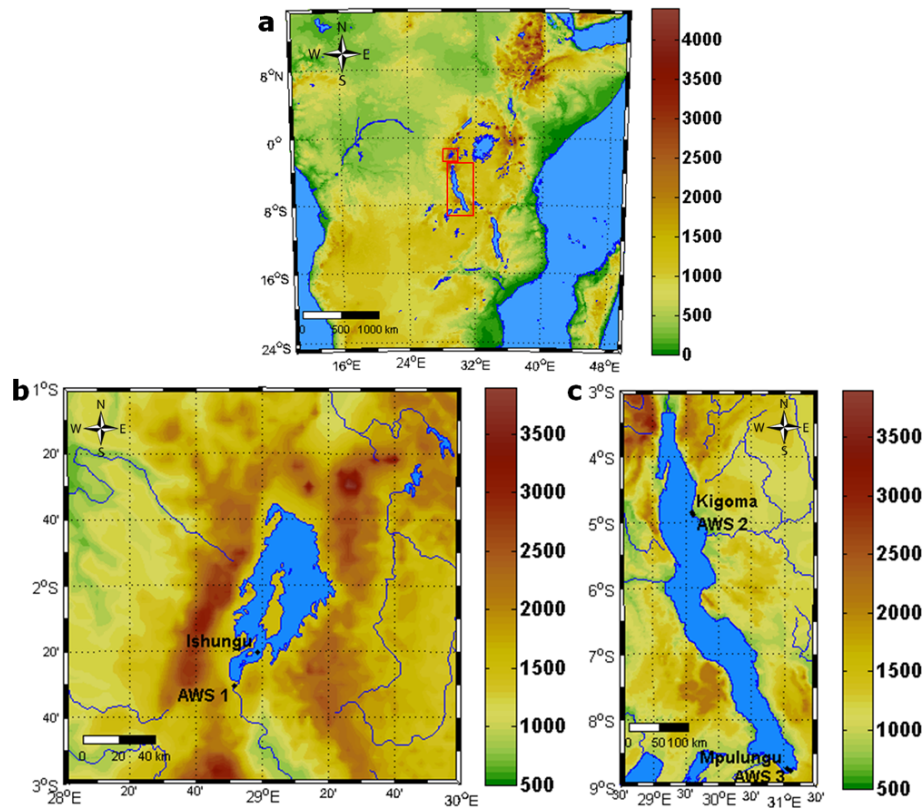


Fig. 1. (a) overview of East Africa with rectangles around Lake Kivu (upper) and Lake Tanganyika (lower), (b) Lake Kivu, (c) Lake Tanganyika. Surface altitude is shown in m.a.s.l.

available. With all three AWSs located on land, one can expect some differences between the measured values and actual meteorological conditions at the sites they aim to represent. However, given the lack of meteorological observations at these locations, it is difficult to assess the degree to which these stations represent their respective evaluation site, except probably for wind speed measurements (Sect. 2.4). Possibly AWS 3, the most exposed station and located on the lake shore, succeeds best at representing the meteorological conditions of the evaluation site. AWS topographic characteristics and meteorological averages are listed in Table 1.

Each AWS records air temperature (T), pressure (p), wind speed (ff) and direction (dd), relative humidity (RH) and downward short-wave radiation (SW_{in}) at a single level above the surface, and at an estimated accuracy of $\pm 0.5^\circ\text{C}$, $\pm 1\text{ hPa}$, $\pm 5\%$, $\pm 3^\circ$, $\pm 3\%$ and $\pm 5\%$, respectively. The measurement frequency is 30 min at AWS 1 and 15 min at AWS 2 and 3, but for the integrations only hourly instantaneous values were retained. Three problems needed to be overcome to prepare the forcing data for the FLake simulations. First, all stations experience frequent data gaps (50%, 23% and 37% of the time at AWS 1, 2 and 3, respectively), and gaps are too long to be filled using simple interpolation techniques. This issue was solved by calculating for each hour of the year the climatological average from

available observations and subsequently filling all data gaps with the corresponding climatological value. When no climatological value is available for SW_{in} , the value of the previous day was used. At AWS 3, where the time series is too short to obtain climatological values, data gaps were instead filled by the average daily cycle. Second, time series of downward long-wave radiation (LW_{in}), a necessary forcing variable to FLake, are not measured by the AWSs. Hence, they were retrieved from the ERA-Interim grid point closest to the evaluation site and subsequently converted from 6-hourly accumulated values to hourly instantaneous value.

2.2 FLake model

The one-dimensional FLake model is designed to represent the evolution of a lake column temperature profile and the integral energy budgets of its different layers (Mironov, 2008; Mironov et al., 2010). In particular, the model consists of two vertical water layers: a mixed layer, which is assumed to have a uniform temperature (T_{ML}), and an underlying thermocline, extending down to the lake bottom (Fig. 2). The temperature-depth curve in the thermocline is parameterised through the concept of self-similarity, or assumed-shape (Kitaigorodskii and Miropolskii, 1970), meaning that the characteristic shape of the temperature profile is conserved

Table 1. Automatic Weather Station (AWS) topographic and meteorological characteristics.

	AWS 1	AWS 2	AWS 3
Location			
Corresponding evaluation site	Ishungu	Kigoma	Mpulungu
Latitude	2°30'27" S	4°53'15" S	8°45'59"
Longitude	28°51'27" E	29°37'11" E	31°6'25"
Altitude (m a.s.l.)	1570	777	782
Set-up of this study			
Start of observation	1 Jan 2003	1 Jan 2002	2 Feb 2002
End of observation	31 Dec 2011	31 Dec 2006	4 Apr 2003
Meteorological averages, after corrections			
T (°C)	19.4	24.5	24.1
RH (%)	76	70	58
\overline{w} (m s ⁻¹)	1.9	0.3	2.6

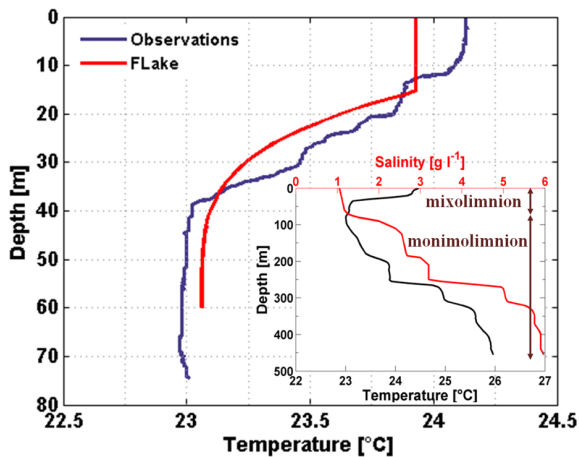


Fig. 2. Water temperature recorded at Ishungu on 21 April 2009 and corresponding FLake midday temperature profile, the latter with its distinct two-layer structure (mixed layer and thermocline). Inset: temperature (black) and salinity (red) profile representative for the main basin during February 2004, as reported by Schmid et al. (2005). For Lake Kivu, the artificial lake depth set in FLake corresponds to the mixolimnion depth, hence the monimolimnion has no counterpart in FLake. Note the strong increase in salinity from 60–70 m downwards, i.e. below the mixolimnion.

irrespective of the depth of this layer (Munk and Anderson, 1948). Hence, within the thermocline, temperature at a relative (dimensionless) depth within the thermocline depends only on the shape of the thermocline curve. In turn, this shape is determined only by the temperature at the top and bottom of the thermocline and by a shape factor, describing the curve through a fourth-order polynomial (Mironov, 2008). Additionally, FLake includes the representation of the thermal structure of lake ice and snow cover and (optionally) also of the temperature of two layers in the bottom

sediments, all using the concept of self-similarity. Without considering ice/snow cover and bottom sediments, the prognostic variables computed by the model reduce to: the mixed layer depth (h_{ML}), the bottom temperature (T_{BOT}), the water column average temperature (T_{MW}) and the shape factor with respect to the temperature profile in the thermocline (C_T). The mixed layer depth is calculated including effects of both convective and mechanical mixing, while volumetric heating is accounted for through the net short-wave radiation penetrating the water and becoming absorbed according to the Beer–Lambert law (Mironov, 2008; Mironov et al., 2010). Finally, along with the standalone FLake model comes a set of surface flux subroutines originating from the limited-area atmospheric model COSMO (Consortium for Small-scale Modeling; Doms and Schättler, 2002), hence the components of the surface energy balance are computed following the method described by Raschendorfer (2001; see also Doms et al., 2011; Akkermans et al., 2012).

The approach adopted in this study is to test FLake version 1 as close as possible to its native configuration, i.e. how it is operationally used as a lake parameterisation scheme within most atmospheric prediction models. Consequently, modifications in the source code from which the predictions would potentially benefit, such as including time-dependent water transparency, making the distinction between the visible and near-infrared fractions of SW_{in} (each with their own absorption characteristics), improving the parameterisation of the thermocline's shape factor, defining a geothermal heat flux, accounting for the effect of bottom sediments, and including an abyssal layer or diurnal stratification, were not taken into account in this study. Conversely, some of these effects were considered during the lake model intercomparison experiment for Lake Kivu (Thiery et al., 2014).

2.3 Water transparency and temperature profiles

In oligotrophic environments such as Lake Tanganyika and Kivu, water transparency is predominantly related to phytoplankton development, which is usually confirmed by a good correlation between the chlorophyll *a* concentrations and the downward light attenuation coefficient k (m^{-1}) or related quantity (Naithani et al., 2007; Darchambeau et al., 2014). In FLake, however, k has to be ascribed a constant value. A large measurement set of disappearance depths of the Secchi disk z_{sd} (m) are available for each site (Table 2). z_{sd} were converted to k using the relationship

$$k = \frac{-\ln(0.25)}{z_{\text{sd}}}, \quad (1)$$

where 0.25 refers to the fraction of incident radiation penetrating to the depth at which the Secchi disk is no longer visible. This fraction, differing from one Secchi disk to another, was retrieved at Lake Kivu by means of 15 simultaneous measurements of z_{sd} and the vertical profile of light conditions using a LI-193SA Spherical Quantum Sensor, from which k was estimated. For each data set of k , a gamma probability density function was fitted (Fig. 3), from which subsequently average \bar{k} and standard deviation σ_k were calculated (Table 2). The higher \bar{k} observed at Ishungu relative to Kigoma and Mpulungu is caused by the higher phytoplankton biomass (represented by chlorophyll *a* concentrations) in Lake Kivu ($2.02 \pm 0.78 \text{ mg m}^{-3}$; Sarmiento et al., 2012) compared to Lake Tanganyika ($0.67 \pm 0.25 \text{ mg m}^{-3}$; Stenuite et al., 2007). Note that, since an uncertainty remains associated with the exact value of k , its value was allowed to vary within given bounds in the different simulations (see Sect. 2.4).

The evaluation of the FLake simulations was made by the use of 419 conductivity-temperature-depth (CTD) casts collected at Ishungu (Lake Kivu), Kigoma (Lake Tanganyika's northern basin) and Mpulungu (Lake Tanganyika's southern basin; Table 2). At each of these locations, they provide a clear image of the surface lake's thermal structure and hence mixing regime. While it can be argued that temperature recordings at Ishungu are representative for the whole of Lake Kivu, except Bukavu Bay and Kabuno Bay (Thiery et al., 2014), the same cannot be claimed for Lake Tanganyika, where seasonal variations in wind velocity and internal wave motions cause spatially variant mixing dynamics (Plisnier et al., 1999). This is also apparent from the comparison of the CTD casts of Kigoma and Mpulungu (Sects. 3.2 and 3.3). Consequently, the results of the FLake simulations for Ishungu can be used to study the mixing physics of Lake Kivu (Sect. 3.6), whereas the mixing processes within the whole of Lake Tanganyika cannot be captured by single-column simulations at two sites only.

To ease the intercomparison of the different CTD casts, first, each temperature profile was spatially interpolated to a regular vertical grid with increment 0.1 m using the piecewise cubic Hermite interpolation technique (De Boor, 1978).

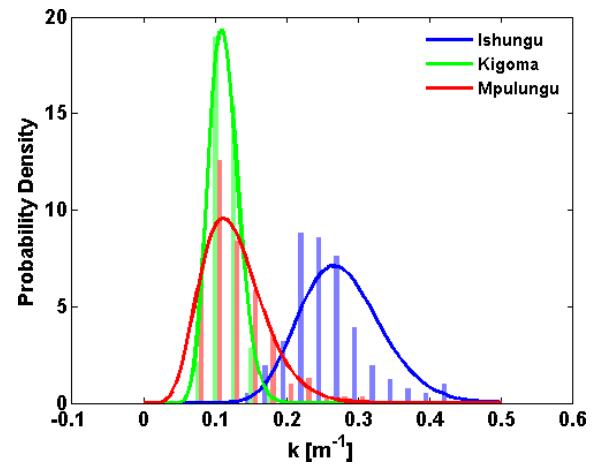


Fig. 3. Comparative histogram of the downward light attenuation coefficient k (m^{-1}) as observed at Ishungu Basin (Lake Kivu) and Kigoma and Mpulungu stations (Lake Tanganyika). Gamma distribution probability density functions are plotted to the data ($R^2 = 0.82, 0.99$ and 0.93 for Ishungu, Kigoma and Mpulungu, respectively).

Subsequently, the depth of the mixed layer was determined for each cast as the depth with the maximum downward temperature change per metre lower than a predefined threshold ($-0.03 \text{ }^\circ\text{C m}^{-1}$). Whenever the thermal gradient did not exceed this threshold, the lake was assumed to be mixed down to the artificial model depth (see Sect. 2.4). Finally, both temperature profiles and mixed layer depths were also temporally interpolated to a grid with increment of one day using the same spline interpolation.

2.4 Model configuration, evaluation and sensitivity

Both in situ meteorological measurements and ERA-Interim data from the nearest grid cell were used to drive FLake in standalone mode (decoupled from an atmospheric model) for three different locations: Ishungu, Kigoma and Mpulungu (Fig. 1). One of FLake's main external parameters is the lake depth (Mironov, 2008; Kourzeneva et al., 2012b). However, for most of the deep African Great Lakes, their actual lake depth cannot be used, since FLake only describes the mixed layer and thermocline, whereas in reality a monimolimnion is found below the thermocline of these meromictic lakes. Consequently, an artificial model lake depth was defined at the maximum depth for which the observed temperature range exceeds $1 \text{ }^\circ\text{C}$ during the measurement period. When applying this criterion to the vertically interpolated temperature profiles, it was found that 60 m is an appropriate artificial depth for Lake Kivu, while for both basins of Lake Tanganyika the seasonal temperature cycle penetrates down to a depth of 100 m. Note that for Lake Kivu, this depth coincides with the onset of the salinity increase, which inhibits deeper mixing (Fig. 2). As a consequence of using an artificial lake depth,

Table 2. Characteristics of the model evaluation sites. Water transparency characteristics are the downward light attenuation coefficient k (m^{-1}) and its standard deviation σ_k (m^{-1}). Control run scores are standard deviation σ_T ($^{\circ}\text{C}$), centred root mean square error (RMSE_c) ($^{\circ}\text{C}$), Pearson correlation coefficient r and Brier Skill Score (BSS).

	Ishungu	Kigoma	Mpulungu
General characteristics			
Lake	Kivu	Tanganyika (northern basin)	Tanganyika (southern basin)
Latitude	2°20′25″ S	4°51′16″ S	8°43′59″ S
Longitude	28°58′36″ E	29°35′32″ E	31°2′26″ E
Altitude (m a.s.l.)	1463	768	768
Depth (m)	120	600	120
Number of CTD casts	174	119	126
Water transparency			
Number of Secchi depths	163	114	124
Average k (m^{-1})	0.28	0.11	0.13
σ_k (m^{-1})	0.06	0.02	0.05
Minimum k (m^{-1})	0.15	0.07	0.06
Maximum k (m^{-1})	0.46	0.17	0.31
Vertically averaged scores for control run			
σ_T ($^{\circ}\text{C}$)	0.30	0.70	0.67
(relative to $\sigma_{T,\text{obs}}$ ($^{\circ}\text{C}$))	0.32	0.49	0.65
RMSE_c ($^{\circ}\text{C}$)	0.22	0.59	0.89
r	0.71	0.51	0.05
BSS	-0.13	-9.63	-1.81

the bottom sediments module was switched off in all simulations. Therewith, a zero heat flux assumption was adopted at the bottom boundary.

At each location, three simulations were conducted. First, FLake was integrated with observed meteorological values and using the average observed value for k (hereafter referred to as “raw”). However, due to the location of AWS 1 and 2 – both surrounded by several buildings and large trees – especially the wind speed values are expected to be underestimated by these stations. Moreover, as the data gap-filling technique averaged out high values for \overline{ff} , unrecorded high wind speed events were not recreated. Consequently, wind speed recordings at these stations can be considered as a lower bound for the actual \overline{ff} at the respective evaluation sites. As a supplementary evidence, wind velocity measurements from a state-of-the-art AWS, newly installed over the lake surface on a floating platform in the main basin and 2 km off the shoreline (AWS Kivu: 1°43′30″ S, 29°14′15″ E), showed that wind speeds at AWS Kivu were on average 2.0 m s^{-1} higher compared to AWS 1 (from October to November 2012, $n = 892$, root mean square error $\text{RMSE} = 2.7 \text{ m s}^{-1}$). By applying a constant increase of 2.0 m s^{-1} to the wind velocities observed at AWS 1, the RMSE between wind velocities from both AWSs reduced to 1.8 m s^{-1} . Since the location of AWS Kivu is much more exposed than the Ishungu Basin – especially given the predominance of southeasterlies over the lake – wind velocities

measured by AWS Kivu provide a definite upper bound for wind velocities in the Ishungu Basin. Hence, a second AWS-driven simulation was conducted wherein wind velocities were allowed to vary within specific upper (from AWS Kivu) and lower (from AWS 1) bounds until the observed mixing regime is reproduced (0.1 m s^{-1} increment; see Sect. 3.5.2 for another important argument in support of this operation). It was found that at Ishungu, increasing all \overline{ff} by 1.0 m s^{-1} resulted in a correct representation of the mixing regime (Sect. 3.1), whereas at Kigoma, \overline{ff} had to be increased by 2.0 m s^{-1} (Sect. 3.2). At Mpulungu, where the driving AWS is located close by the evaluation site and on the lake shore, the correct mixing regime is already reproduced by the raw integration, and hence no wind speed correction needed to be applied (Sect. 3.3). After correcting for the wind speed, k was varied iteratively between bounds $\bar{k} - \sigma_k$ and $\bar{k} + \sigma_k$ until the best values for the set of model efficiency scores were obtained (see below; hereafter referred to as “control”). This operation led to values of 0.32 m^{-1} , 0.10 m^{-1} and 0.09 m^{-1} for k at Ishungu, Kigoma and Mpulungu, respectively. Note however that this second correction, restricted by σ_k (Table 2), had little to no impact upon the final model outcome (At Ishungu, for instance, mean mixed layer and water column temperatures differ less than $0.001 \text{ }^{\circ}\text{C}$ and $0.04 \text{ }^{\circ}\text{C}$, respectively, after this second correction).

Finally, FLake was integrated using ERA-Interim data from the nearest grid cell as forcing. ERA-Interim is a global reanalysis product produced by the European Centre for Medium-Range Weather Forecasts (ECMWF; Simmons et al., 2007). It consists of a long-term atmospheric model simulation in which historical meteorological observations are consistently assimilated. Note however that the horizontal resolution of this product is T255 (0.703125° or about 80 km), hence a large fraction of each nearest pixel represents land instead of lake. Moreover, only few observations are assimilated into ERA-Interim over tropical Africa, adding to the uncertainty of this product as a source of meteorological input to FLake. At Mpulungu, the only site where this integration led to a correct representation of the mixing regime (Sect. 3.3), k was again allowed to vary within bounds $\bar{k} - \sigma_k < k < \bar{k} + \sigma_k$, with $k = 0.09 \text{ m}^{-1}$ retained.

In each simulation, lake water temperatures were initialised by the average T_{ML} , T_{WM} and T_{BOT} calculated from the linearly interpolated observed January temperature profiles ($n = 14, 8$ and 10 at Ishungu, Kigoma and Mpulungu, respectively). Then, for each location the spin-up time was determined by repeatedly forcing the model with the atmospheric time series until the initial T_{BOT} remained constant. This approach was found to be preferable above a spin-up with a constant forcing or with a climatological year (Mironov et al., 2010), as the averaging of the wind speed observations removes extremes which may trigger the deep mixing in these lakes. It was found that, depending on the location and for the control model configuration, a spin-up time from 9 to 330 yr is needed before convergence is reached.

The ability of FLake to reproduce the observed temperature structure was tested by comparing FLake’s near-surface and bottom temperature to the corresponding observed values at each location. Note that a depth of 5 m was chosen representative for the surface waters, since (i) CTD casts were generally collected around noon and temperatures in the first metres are therefore positively biased relative to the daily averages, and (ii) FLake does not fully account for the daytime surface stratification because the mixed layer has a uniform temperature. Furthermore, a set of four model efficiency scores was computed: the standard deviation σ_T (°C), the centred root mean square error RMSE_c (°C), the Pearson correlation coefficient r and the Brier Skill Score BSS (Nash and Sutcliffe, 1970; Taylor, 2001; Wilks, 2005). The former three calculated scores are visualised together in a Taylor diagram (Taylor, 2001), enabling the performance assessment of FLake. The RMSE_c is given by

$$\text{RMSE}_c = \sqrt{\frac{1}{N} \sum_{i=1}^n ((m_i - \bar{m}) - (o_i - \bar{o}))^2}, \quad (2)$$

while the BSS is computed according to

$$\text{BSS} = 1 - \frac{\sum_{i=1}^n (o_i - m_i)^2}{\sum_{i=1}^n (o_i - \bar{o})^2}, \quad (3)$$

with o_i the observed (interpolated) water temperature, \bar{o} the average observed water temperature, and m_i and \bar{m} the corresponding modelled values at time i . Values for BSS range from $-\infty$ (no relation between observed and predicted value) to $+1$ (perfect prediction). Note that, compared to the variables displayed in a Taylor diagram, the BSS has the advantage of accounting for the model bias.

The sensitivity of the model was evaluated by conducting a number of simulations, each with an alternative configuration. In particular, the effects of variations in the external parameter values, the driving data and the initial conditions were investigated in this sensitivity study. Depending on the nature of each sensitivity experiment, different scores are applied to quantify the effect of a specific modification. Details of the different experiments are outlined in Sect. 3.5.

3 Results

3.1 Ishungu

Comparing modelled and observed water temperatures of Lake Kivu near the surface (5 m) shows that the timing of the near-surface seasonal cycle is well represented by the raw, control and ERA-Interim simulations (Fig. 4a). However, whereas it shows a small negative bias compared to the observations, only the control integration grasps the correct magnitude of the seasonal temperature range. The overestimation of the temperature seasonality in the raw and ERA-Interim simulations is reflected by 5 m BSS of -0.36 and -2.13 , respectively, compared to only -0.26 for the control case. At a depth of 60 m, both the raw and ERA-Interim integration predict a year-round constant temperature of $3.98 \text{ }^\circ\text{C}$, the temperature of maximum density, resulting in a cold bias of about $19 \text{ }^\circ\text{C}$. At the bottom, the lake’s thermal structure is reproduced only by the control simulation (BSS = -0.17 ; Fig. 4b).

Once a year, during the dry season (from June to August), the mixed layer depth at Ishungu extends down to approximately 60 m. At this depth, the upwelling of deep, saline waters (0.5 yr^{-1} ; Schmid and Wüest, 2012) equilibrates with mixing forces. The result is a strong salinity gradient from 60 m downwards (Fig. 2). During the remainder of the year, stratified conditions dominate, with the mixed layer depth varying between 10 and 30 m (Fig. 5a). The raw simulation does not reproduce this mixing seasonality, but instead predicts permanently stratified conditions and a complete cooling down to $3.98 \text{ }^\circ\text{C}$ from 30 m downwards. On the other hand, with f corrected for the land effect and k tuned to

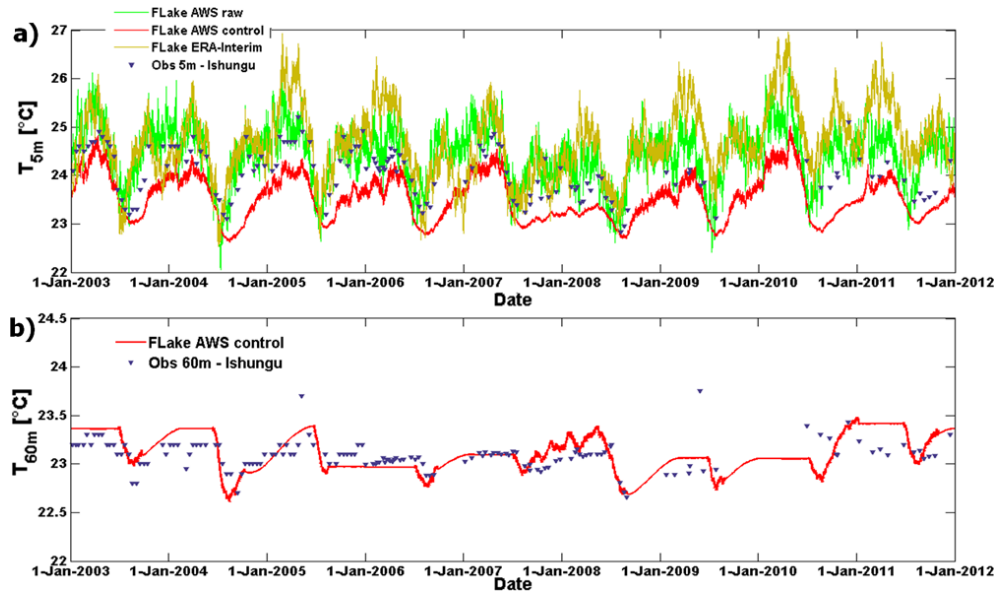


Fig. 4. Modelled and observed temperature evolution at Ishungu (Lake Kivu) at (a) 5 m, and (b) 60 m depth. FLake temperatures at 60 m predicted by the raw and ERA-Interim integration are omitted as they are constant at 3.98 °C.

0.32 m^{-1} , the control simulation closely reproduces the mixing regime at Ishungu (Fig. 5b; Table 2). In this case, also the lower stability, indicated by the observations near the end of 2006 and during 2008 and 2009, is captured by this control simulation, although it is somewhat overestimated in 2008 with a predicted year-round mixing down to $\sim 55 \text{ m}$. Note however that, due to the lower stability during these years, the effect on the near-surface water temperatures is limited. Furthermore, also the late onset of the stratification in early 2007 is represented by the model.

Finally, feeding FLake with ERA-Interim-derived near-surface meteorology does not succeed in reproducing the mixing regime. Instead, this simulation predicts permanently stratified conditions and a complete cooling down to 3.98 °C, the temperature of maximum density, from 30 m downwards (Fig. 5c). The low and constant mixed layer depth generates near-surface temperature fluctuations found too strong on seasonal timescales (Fig. 4a). Similar to the raw integration, the inability of the ERA-Interim integration to produce deep mixing is primarily due to the predicted values for the wind velocity, which are 33 % lower compared to the control run average wind velocity and 49 % lower compared to wind speeds from AWS Kivu (measured over the lake surface during 59 days from October to November 2012). Underlying reasons for this deviation are (i) the fact that the lake surface covers only a fraction of the selected ERA-Interim grid box, and (ii) the higher uncertainty of this product in central Africa owing to the sparse observational data coverage in this region (Dee et al., 2011).

3.2 Kigoma

At Kigoma, the raw and ERA-Interim integrations both predict too high temperature seasonality in the near-surface water (Fig. 6a). On the other hand, the control experiment clearly displays improved skill at 5 m, especially during 2004 and 2005. At depth, both the raw and ERA-Interim integrations obtain a constant 3.98 °C and therewith strongly deviate from the observations (Fig. 6b). In return, the control simulation again captures the actual conditions much better, even though it slightly underestimates the seasonal temperature range and retains a positive bias between 0 and 2 °C.

Contrary to Lake Kivu, in Lake Tanganyika salinity-induced stratification below 60 m is negligible and seasonal variations in near-surface meteorology are more pronounced (Sect. 3.4). Consequently, the seasonal mixed layer extends further down both during the dry and wet season (Fig. 7a), with mixing recorded down to even 150 m (Verburg and Hecky, 2003) and 300 m (Plisnier et al., 1999). Similar to Ishungu, also at Kigoma the raw simulation does not result in a correct representation of the mixing regime, but predicts permanent stratified conditions and a complete cooling along the thermocline. Again, upward correction of \overline{ff} by 2 m s^{-1} and reducing k to a value of 0.09 m^{-1} brings the model to the correct mixing regime at Kigoma (Fig. 7b; Table 2). The ERA-Interim simulation predicts permanent stratification due to too low wind velocities (Fig. 7c). Note that in both the ERA-Interim and the raw simulations, decreasing k from 0.11 m^{-1} to 0.09 m^{-1} leads to a regime switch from permanent stratification directly to fully mixed conditions (down to the model lake depth), the latter associated with a strong positive temperature bias both near the surface and at depth.

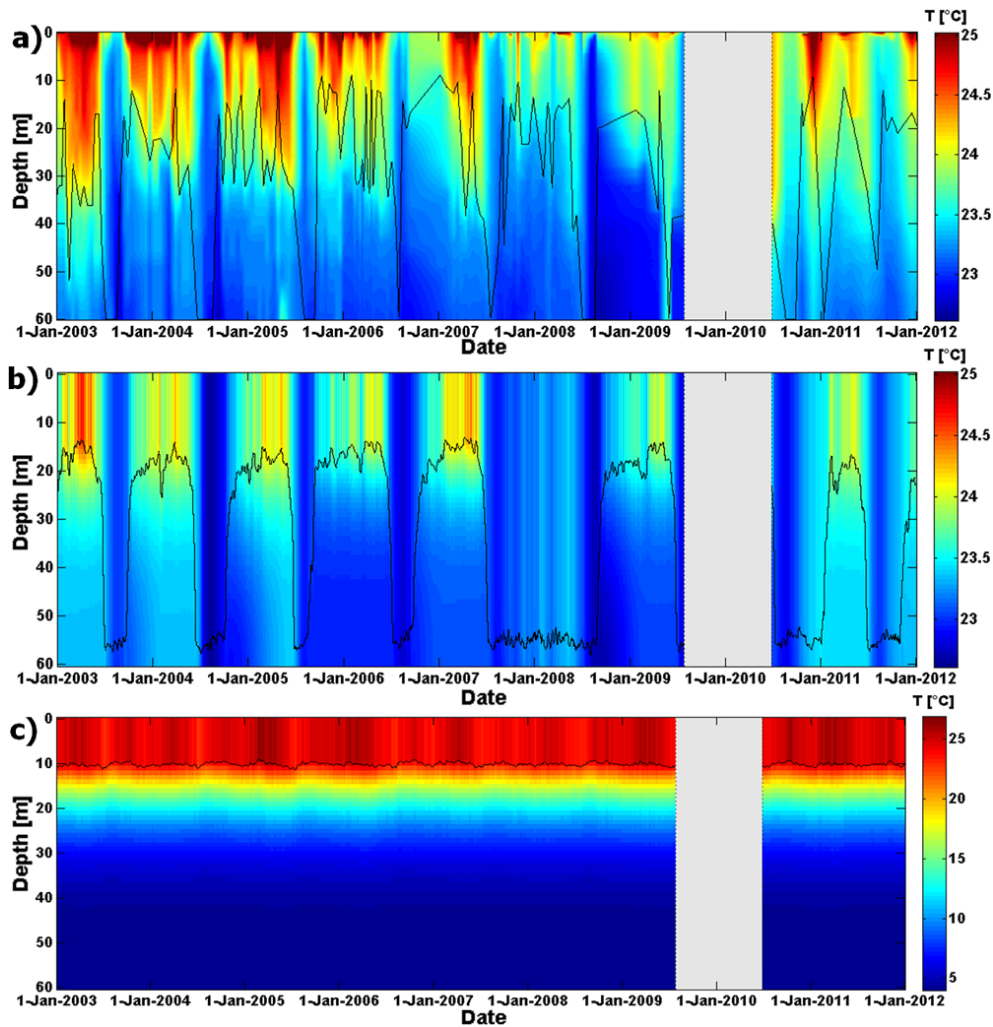


Fig. 5. Lake water temperatures (°C) at Ishungu (Lake Kivu) (a) from observations, (b) as predicted by the AWS-driven FLake-control, and (c) as predicted by FLake-ERA-Interim. The black line depicts the mixed layer depth (Sect. 2.3; weekly mean for the simulations). Note the different colour scaling in (c). The lake water temperatures for the raw simulation are not shown as they strongly resemble the predictions of the ERA-Interim simulation.

3.3 Mpulungu

At Mpulungu, all three experiments capture the magnitude of the seasonal cycle in near-surface temperature and show little to no bias compared to the observations (Fig. 8a). However, also in each simulation the onset of complete mixing lags by around one month and lasts too long compared to observations (Fig. 8a). At 60 m, a similar lag is found (Fig. 8b). Furthermore at this depth, the enhanced temperature seasonality of the control integration compared to the raw integration depicts its improved skill.

Although the FLake-AWS simulation at Mpulungu spans only 13 months, during this period two stratified periods and one fully mixed season are predicted by the model in both the raw ($k = 0.13 \text{ m}^{-1}$) and control ($k = 0.09 \text{ m}^{-1}$) set-up, in agreement with observations (Fig. 9a and b; Table 2). With

AWS 3 located on the lake shore (exposed) and relatively close to the evaluation site, no correction of \overline{ff} was necessary, and the mixing regime is correctly represented within the range $0.09 \text{ m}^{-1} < k < 0.22 \text{ m}^{-1}$. Furthermore, also driving FLake with ERA-Interim at Mpulungu leads to a correct representation of the mixing regime (Fig. 9c).

From May to September, persistent southeasterly winds over Lake Tanganyika cause a tilting (downwards towards the north) of the mixolimnion-monimolimnion interface, and therewith generate the upwelling of deep, cold waters at the southern end of the lake (Plisnier et al., 1999). The resulting breakdown of the stratification appears through the absence of the thermocline at Mpulungu during the dry season (Fig. 9a), whereas at Kigoma, even during this period a weak thermocline remains present (Fig. 7a). Due to its self-similar, one-dimensional nature, FLake does not account for complex

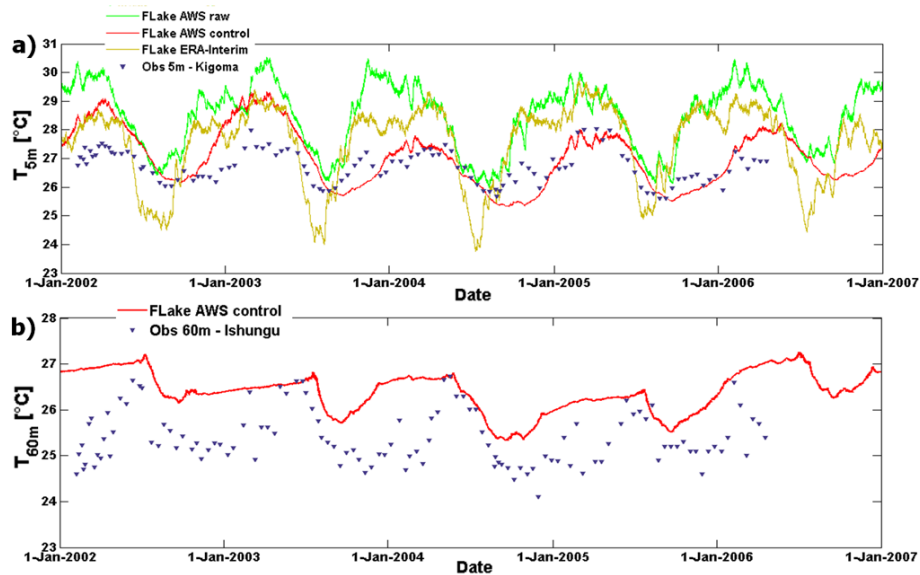


Fig. 6. Modelled and observed temperature evolution at Kigoma (northern basin of Lake Tanganyika) at (a) 5 m, and (b) 60 m depth. FLake temperatures at 60 m predicted by the raw and ERA-Interim integration are omitted as they are constant at 3.98 °C.

hydrodynamic phenomena such as local upwelling and associated internal wave phenomena (Naithani et al., 2003), and therefore does not capture this difference between both sites (Figs. 7 and 9). It is likely that this phenomenon may also explain the time lag noticed in all Mpulungu simulations. The hydrodynamic response to the wind stress reinforces the seasonal cycle induced by lake–atmosphere interactions (Sect. 3.6): while the onset of the upwelling accelerates the cooling at the start of the dry season, a cessation of southeasterly winds in September generates the fast advection of warm mixolimnion waters from the north back towards Mpulungu, inducing a faster restoration of stratification than can be predicted by FLake from lake–atmosphere interactions alone.

3.4 Comparison between sites

A number of differences can be noted between the three locations. First, the average observed 5 m temperature is 2.6 °C and 2.4 °C lower in Ishungu (altitude 1463 m a.s.l.) compared to Kigoma and Mpulungu (altitude 768 m a.s.l.), respectively. Second, it can be observed that the water temperature seasonality increases with distance from the equator: at 5 m, the maximal observed temperature ranges are 2.4 °C, 2.5 °C and 5.4 °C in Ishungu, Kigoma and Mpulungu, respectively. This is related to differences in near-surface meteorology, since in the Southern Hemisphere at tropical latitudes, a higher distance from the equator coincides with a higher distance from the Intertropical Convergence Zone (ITCZ) during austral winter and thus creates a larger contrast between dry and wet season (Akkermans et al., 2014).

Third, although the average latent heat flux (LHF) is very similar at Ishungu (88 W m^{-2}) and Kigoma (86 W m^{-2}), it increases by 56 % at Mpulungu (134 W m^{-2}) during the respective measurement periods. Extrapolating the average LHF at Ishungu to the entire Lake Kivu surface (estimated by the control simulation and using a surface area of 2370 km^2 ; Schmid and Wüest, 2012) leads to a preliminary estimate of the total annual evaporative flux of $2.6 \text{ km}^3 \text{ yr}^{-1}$ for the period 2003–2011. Note that, based on calculations from Bulot (1971), Schmid and Wüest (2012) estimate a total annual evaporation of $3.0\text{--}4.0 \text{ km}^3 \text{ yr}^{-1}$ for Lake Kivu. Analogously, extrapolating the average LHF computed for Kigoma to the northern Tanganyika Basin ($17\,572 \text{ km}^2$; Plisnier et al., 2007) leads to a preliminary estimate of $18.8 \text{ km}^3 \text{ yr}^{-1}$ for the total annual evaporation from the northern basin. At Mpulungu, where the control simulation predicts an average LHF of 133 W m^{-2} for the measurement period, extrapolation yields a total annual evaporation of $23.8 \text{ km}^3 \text{ yr}^{-1}$ from the southern basin ($14\,173 \text{ km}^2$; Plisnier et al., 2007). For the ERA-Interim simulations, the average LHF amounts up to 114 W m^{-2} ($25.3 \text{ km}^3 \text{ yr}^{-1}$) at Kigoma and 138 W m^{-2} ($24.7 \text{ km}^3 \text{ yr}^{-1}$) at Mpulungu. Note that Verburg and Antenucci (2010) computed a lake-wide evaporation amounting up to $63 \text{ km}^3 \text{ yr}^{-1}$, when assuming a total surface area of $31\,745 \text{ km}^2$ for Lake Tanganyika. The annual lake-wide evaporation estimates from the control and ERA-Interim simulations are only 65 % (42.6 km^3) and 80 % (50.1 km^3) of this value, respectively. Possible explanations for this discrepancy are (i) the different method used to compute the latent heat flux, (ii) differences in the quality and length of the meteorological time series, and (iii) the period of observation (1994–1996 versus 2002–2003 and 2002–2006,

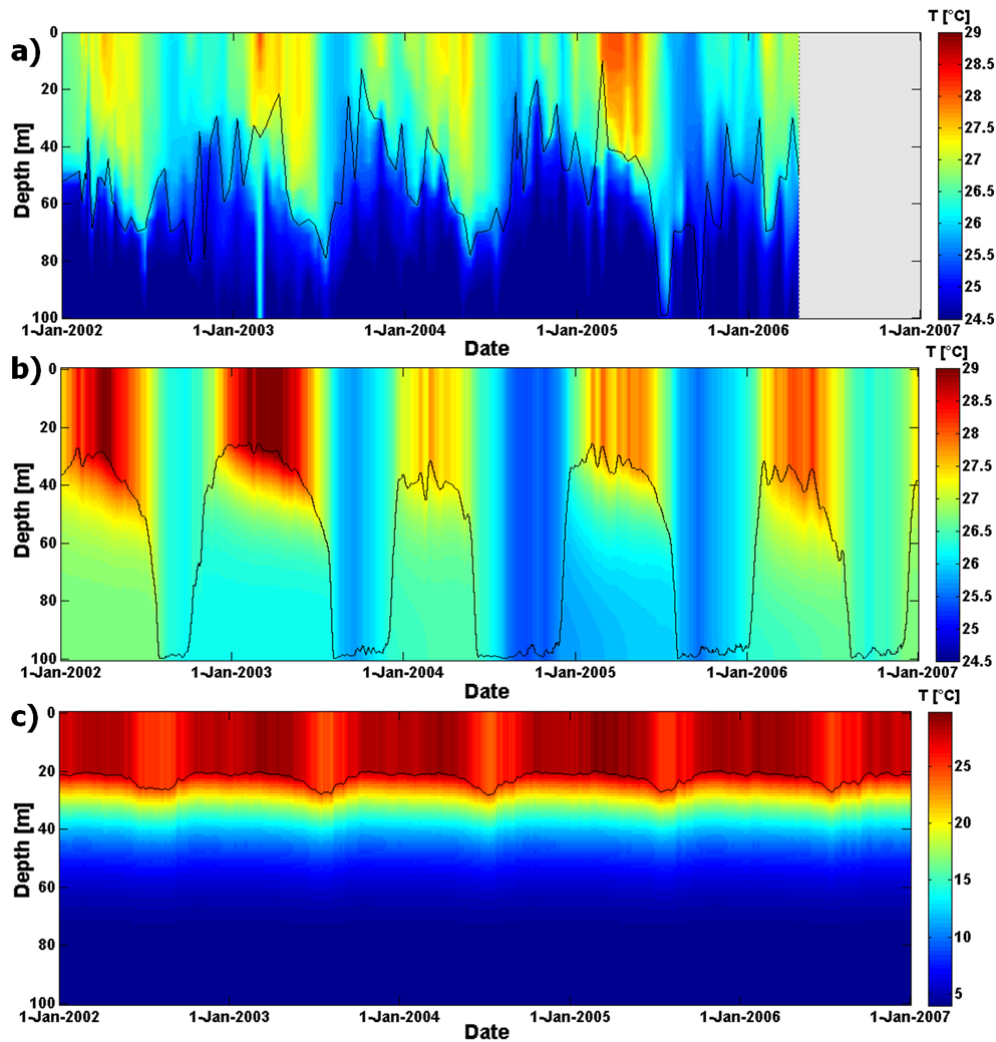


Fig. 7. Lake water temperatures ($^{\circ}\text{C}$) at Kigoma (northern basin of Lake Tanganyika) (a) from observations, (b) as predicted by the AWS-driven FLake-control, and (c) as predicted by FLake-ERA-Interim. The black line depicts the mixed layer depth (Sect. 2.3; weekly mean for the simulations). Note the different colour scaling in (c).

respectively). Especially the latter effect is potentially relevant, given the influence of large-scale climate oscillations such as the El Niño–Southern Oscillation (ENSO) on the regional climate (Plisnier et al., 2000) and the contrasting ENSO indices found for both periods (La Niña years versus El Niño years). Further research will aim at quantifying uncertainties associated with lake-wide evaporation estimates for tropical lakes.

Results from the AWS control simulations show that FLake successfully incorporates these differences between the sites, since the model, through the differences in forcing and configuration, successfully represents the thermal structure of both Lake Kivu and Lake Tanganyika and discerns the differences between the two basins within Lake Tanganyika.

3.5 Sensitivity study

Originally designed for implementation within NWP systems or climate models, FLake requires information on lake depth and water transparency (downward light attenuation coefficient) for each lake within its domain. But despite recent efforts to gather and map lake depth on a global scale (Kourzeneva, 2010; Kourzeneva et al., 2012a), in East Africa information on lake depth and water transparency is only available for the largest lakes, adding uncertainty to FLake's outcome when it is applied to the entire region. Furthermore, the effect of the forcing data source – e.g. originating from an AWS, a reanalysis product or RCM output – and its associated quality might significantly affect the outcome of a simulation. As RCMs and standalone lake models are being applied to increasingly remote lakes, the need to consider this data quality issue grows (Martynov et al., 2010). Finally, in

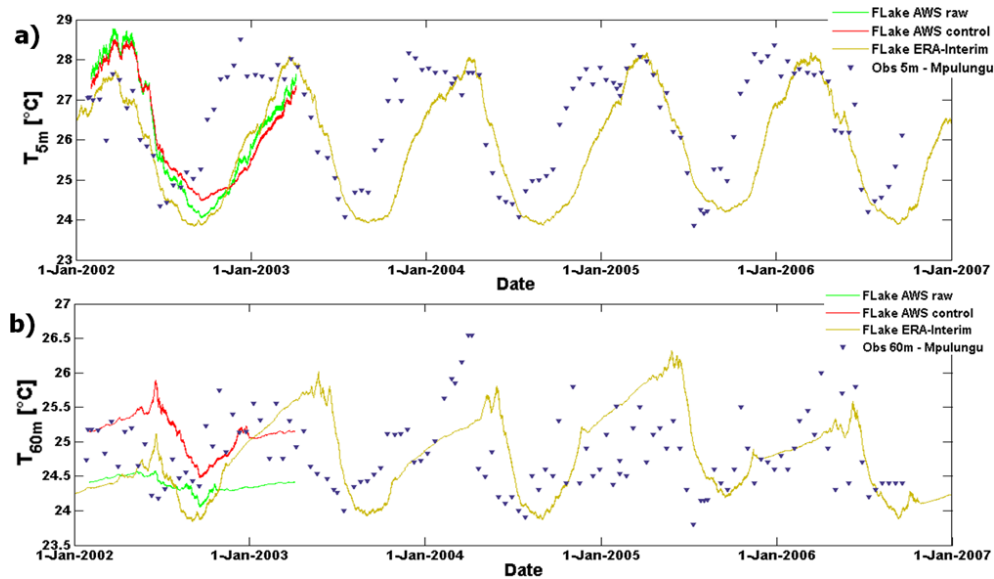


Fig. 8. Modelled and observed temperature evolution at Mpulungu (southern basin of Lake Tanganyika) at (a) 5 m, and (b) 60 m depth.

the absence of initialisation data, several approaches to lake temperature initialisation and spin-up have been applied in the past (Kourzeneva et al., 2008; Mironov et al., 2010; Balsamo et al., 2012; Hernández-Díaz et al., 2012; Rontu et al., 2012). Hence, a systematic study of the sensitivity of the model to different sources of error is appropriate. Hereafter, results of FLake’s sensitivity to variations in (i) external parameters, (ii) meteorological forcing data, and (iii) temperature initialisation are presented. Note that each set of the following tests was conducted starting from the Lake Kivu control simulation (Sect. 3.1). However, the same experiments have been conducted for Kigoma and Mpulungu as well, and revealed very similar responses to the imposed changes.

3.5.1 External parameters

The first set of model sensitivity tests was conducted to investigate FLake’s sensitivity to changes in the model’s external parameters. Using a set of four model efficiency scores (Sect. 2.4), the impact of setting the model lake depth to a relatively shallow 30 m (SHA) or a relatively deep 120 m (DEE), and setting k to the highest (KHI) or lowest (KLO) observed value at Ishungu (Table 2) was quantified. σ_T , $RMSE_c$ and r calculated at three depths (5 m, 30 m and 60 m, respectively) are visualised in Taylor diagrams (Fig. 10). Furthermore, note that we also investigated the sensitivity of FLake to changes in the fetch, by conducting a set of simulations with the fetch varying between 1 and 100 km, respectively (the value in all other simulations is 10 km). It was found, however, that for Lake Kivu, FLake exhibits only little sensitivity to modifications in this parameter.

At 5 m depth, the different sensitivity experiments produce similar values for $RMSE_c$, r , and BSS (not shown). The only score for which the control simulation outcompetes the other members is σ_T , suggesting that in this case seasonal temperature variability is closest to reality. At 30 m, some changes to this pattern can already be noticed (Fig. 10b). Most notably, for the SHA test case predictive skill significantly decreases. For this test, FLake predicts fully mixed conditions down to 30 m most of the time, except during the 2005, 2007 and 2009 rainy seasons, when mixing down to 10 m is predicted. However, only at 60 m do the differences fully emerge, with a clear reduction in predictive skill for the simulations with k decreased (increased) to the lowest (highest) observed values at Ishungu. Higher water transparency leads to deeper mixing, as solar radiation penetrates down to the interface between mixed layer and thermocline and therewith enhances h_{ML} . Note that for the more transparent Lake Tanganyika, FLake’s sensitivity to changes in k is even more important. There, a change of less than 1σ away from the average observed k already led to a switch from permanently mixed conditions to a continuously stratified regime.

3.5.2 Forcing data

In a second set of experiments, FLake’s sensitivity to changes in forcing variables was investigated. Starting from the control simulation at Ishungu, values for T , RH, \overline{ff} and LW_{in} were varied in pairs between bounds $o_i - 2\sigma$ to $o_i + 2\sigma$, with o_i the actual observed value at time step i , and σ the standard deviation of a given variable (see also Thiery et al., 2012). Standard deviations for T , RH, \overline{ff} and LW_{in} are 2.4°C , 14 %, 1.7 m s^{-1} and 18 W m^{-2} , respectively. The perturbation increment was $0.4 \times \sigma$ in each experiment. The

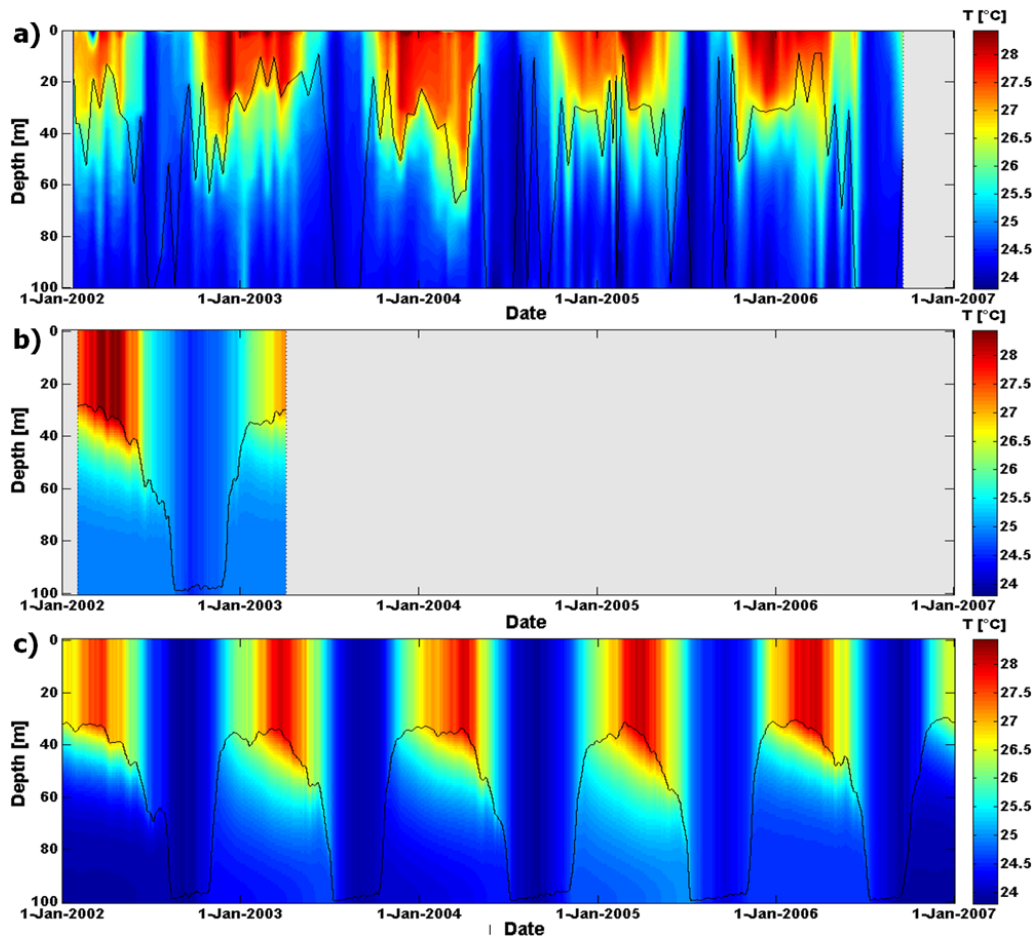


Fig. 9. Lake water temperatures (°C) at Mpulungu (southern basin of Lake Tanganyika) (a) from observations, (b) as predicted by the AWS-driven FLake-control, and (c) as predicted by FLake-ERA-Interim. The black line depicts the mixed layer depth (Sect. 2.3; weekly mean for the simulations). Results in (c) were obtained with $k = 0.09 \text{ m}^{-1}$.

vertically averaged BSS for water temperature calculated per metre depth for 2003–2011 after this pairwise perturbation (Fig. 11) allowed for the selection of the main environmental variables controlling h_{ML} in tropical conditions. Sensitivity experiments for p and SW_{in} are not shown, the former since FLake was found to be not sensitive to this variable, the latter since its high standard deviation (252 W m^{-2}) led to unrealistic perturbations. To overcome this issue, an additional experiment was conducted wherein the SW_{in} and LW_{in} time series were perturbed by the respective standard deviations of their daily means (σ_{dm} , with values of 35 W m^{-2} and 12 W m^{-2} , respectively; Fig. 12).

For Lake Kivu, FLake results reveal a marked sensitivity to variations in wind speed (Fig. 11a and b). Generally, when wind velocities increase (decrease), mechanical mixing reaches deeper (less deep) into the lake, causing a cooling (warming) of the mixed layer for the same energy budget. For Lake Kivu, however, at some point the increased wind velocity provokes a regime switch from seasonally mixed conditions to (almost) permanently mixed conditions. This switch,

illustrated by the sharp decrease in BSS in Fig. 11a, b along the ff axis, is already reached before ff is enhanced by 0.4σ . Similarly, only slightly decreasing ff already leads to a sharp switch to the permanently stratified regime. Increasing (decreasing) T and RH by their respective σ equally contributes to higher (lower) mixed layer temperatures, which in turn enhances (reduces) stratification (Fig. 11c). Again, the vertically averaged BSS depicts the switch to both other regimes: a sharp transition to permanent stratification for increased T and RH and a gradual transition to fully mixed conditions for lower T and RH. A similar sensitivity is found when testing for LW_{in} , although FLake seems less sensitive to variations in this variable (Fig. 11d). When comparing SW_{in} and LW_{in} for perturbations of the order of their respective σ_{dm} (Fig. 12), it can be noted that fairly large perturbations are needed to provoke a regime switch, and that such a switch is provoked more easily by modifying SW_{in} than LW_{in} by their respective σ_{dm} . Note that when combined in pairs, errors may compensate each other and still generate adequate model predictions, as is the case when, e.g. simultaneously reducing ff and T by

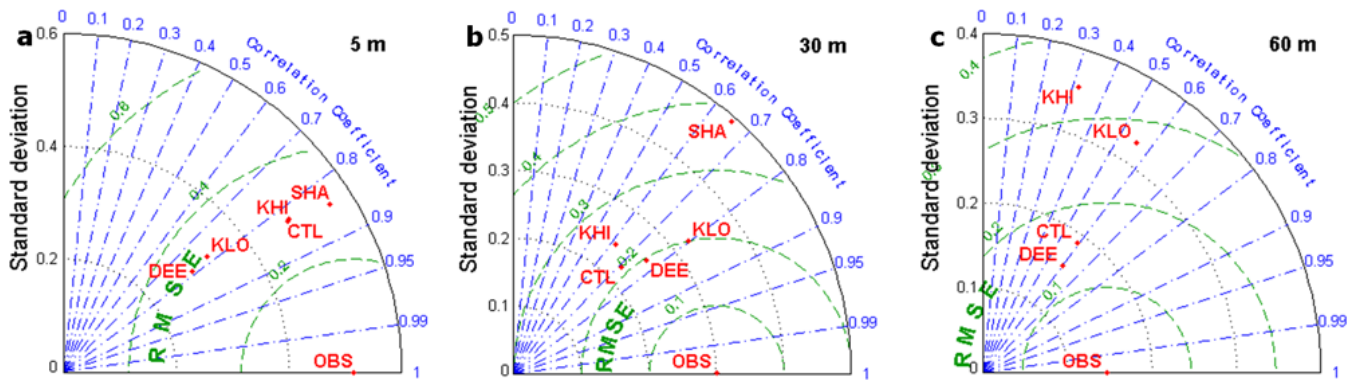


Fig. 10. Taylor diagram indicating model performance for water temperature at (a) 5 m, (b) 30 m and (c) 60 m depths for different external parameter values at Ishungu (January 2003–December 2011). Standard deviation σ_T ($^{\circ}\text{C}$; radial distance), centred root mean square error RMSE_c ($^{\circ}\text{C}$; distance apart) and Pearson correlation coefficient r (azimuthal position of the simulation field) were calculated from the observed T-profile interpolated to a regular grid (1 m increment) and corresponding midday FLake profile. OBS: observations, CTL: control, SHA (DEE): model lake depth set to and 30 m (120 m), KHI (KLO): downward light attenuation coefficient k set to the highest (lowest) observed value at Ishungu. Note that model performance indicators at 60 m cannot be calculated for the SHA integration.

one respective σ , or increasing LW_{in} while decreasing RH by one respective σ .

Finally, for each variable in this experiment, one can also derive an uncertainty range for which FLake predicts the correct mixing regime. With a vertically averaged BSS threshold set to -20 , the range width of wind velocities for which a correct mixing regime is predicted is 0.7 m s^{-1} around the actual observed values of the control run (Fig. 11a). For RH, T , LW_{in} and SW_{in} , this range is 17 %, 2.0°C , 50 W m^{-2} and 42 W m^{-2} , respectively. While for the latter four variables, collecting in situ measurements within these uncertainty bounds is feasible, clearly, the room for manoeuvre in case of wind velocity measurements is very small. Consequently, the need for reliable wind velocities is critical to have FLake predicting the right mixing conditions over deep tropical lakes. Note that this is also the reason why wind speed was selected as the forcing variable to correct (Sect. 2.4). In return, when the same computation is conducted for the 5 m BSS instead of the vertically averaged BSS, the narrow band widens to 3.4 m s^{-1} (even with a 5 m BSS threshold set to only -2 , the acceptable uncertainty range is still 2.0 m s^{-1}). Thus, in cases where the primary interest of the FLake application is the correct representation of near-surface water temperatures, the need for very high accuracy wind velocity measurements becomes less pressing.

This has implications for the applicability of FLake to the study of tropical lake–climate interactions. When FLake is interactively coupled to an atmospheric model, it may very well be that, e.g. the near-surface wind velocities serving as input to FLake will not fall within the narrow range for which it predicts a correct mixing regime. However, the only FLake variable which directly influences the atmospheric boundary layer is T_{ML} , the variable from which the exchange of water and energy between the lake and the atmosphere

are computed. In this study, T_{ML} predictions were found to be robust, even when modelled T_{BOT} values are biased. We may therefore suppose that for tropical conditions, a coupled model system will not be much affected by the strong sensitivity of FLake’s deepwater temperatures to, for instance, wind speed values.

3.5.3 Initial conditions

The third set of experiments at Lake Kivu was designed to test the model to different initial conditions. In the control simulation, FLake was initialised with the average mixed layer, total water column and bottom temperatures calculated from the January CTD profiles ($n = 14$), after which spin-up cycles were repeated until convergence is reached. Sensitivity experiments encompassed a simulation with the same initialisation but excluding spin-up (CES), a fully mixed (i.e. down to 60 m depth) water column initialisation including (MIS) or excluding spin-up (MES), and a stratified water column excluding spin-up (SES). By setting the initial mixed layer depth to 60 m and the lake water temperature to 28°C , full mixing was imposed, whereas permanently stratified conditions were obtained by setting the initial mixed layer depth to 8 m, T_{ML} to 23.5°C and T_{bot} to 4°C (comparable to Hernández-Díaz et al., 2012; Martynov et al., 2012). Note that a stratified initialisation including spin-up is omitted, since downward heat transport within the thermocline can only occur through molecular diffusion in this case, and hence would require millennia-scale spin-up time. Again, σ_T , RMSE_c , and r were calculated and visualised for three depths (Fig. 13).

First, it can be noted that omitting spin-up in the optimal simulation (CES) has only limited, though negative, influence on the predictive skill. This shows that when a reliable initial CTD profile is available, spin-up has some, but

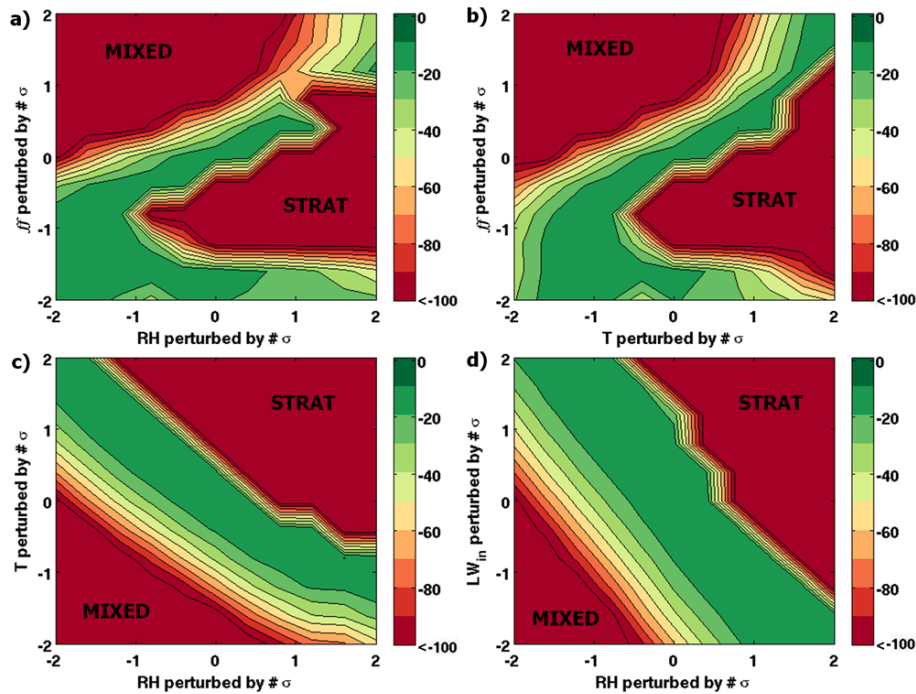


Fig. 11. Vertically averaged Brier Skill Scores (BSS) of water temperature profiles (0–60 m; 1 m vertical increment) at Ishungu from 4 sensitivity experiments, wherein pairs of forcing variables recorded at AWS 1 were perturbed by proportions of their respective standard deviations σ . Perturbed forcing variables are wind velocity (ff), Relative humidity (RH), air temperature (T) and incoming long-wave radiation (LW_{in}). Generally, values for BSS range from +1 (perfect prediction) to $-\infty$ (no relation between observation and prediction). Here, BSS below -100 are set to -100 . Permanently stratified (STRAT) and fully mixed conditions down to 60 m (MIXED) are indicated.

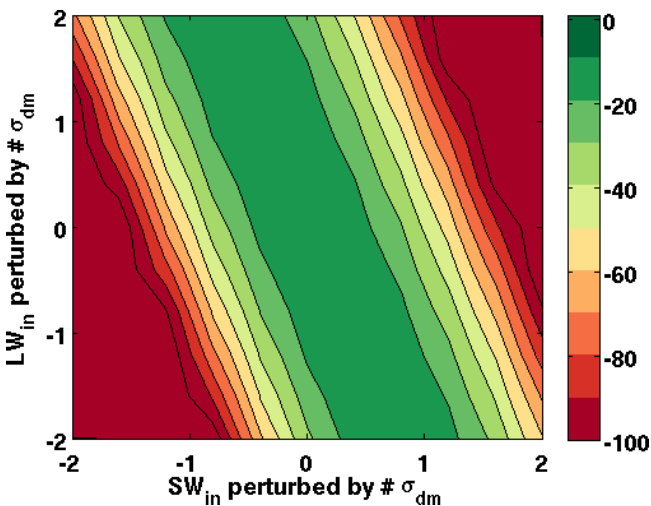


Fig. 12. Vertically averaged Brier Skill Scores (BSS) of water temperature profiles (0–60 m; 1 m vertical increment) at Ishungu from a set of simulations with SW_{in} and LW_{in} perturbed by proportions of their respective standard deviations of daily mean values (σ_{dm}).

only little added value. More interestingly, however, is the fact that a fully mixed and artificially warm initialisation with spin-up (MIS) succeeds very well in reproducing the thermal structure of Lake Kivu. Within 9 spin-up years, the

complete mixing allows for an efficient heat release until the regime switches to the expected pattern. Since the model is allowed to spin-up until convergence is reached, the selection of the initial water column temperature does not influence the model performance, as long as it is chosen artificially warm. However, without spin-up (MES), this advantage vanishes and results have limited skill, since the lake has been initialised too warm. Alternatively, when offline spin-up of lake temperatures is not feasible within the coupled model system, imposing permanently stratified conditions by means of a 4 °C lake bottom (SES) becomes an option, given the acceptable results near the lake surface even though the thermal structure is not reproduced. Note that this was the approach adopted for the CORDEX-Africa simulations conducted with the Canadian Regional Climate Model version 5 (Hernández-Díaz et al., 2012; Martynov et al., 2012). Hence, for coupled FLake-atmosphere simulations over regions with no initialisation information available, a fully mixed, artificially warm initialisation appears to be the best option, but only if offline lake temperature spin-up is applied; otherwise an imposed, permanently stratified regime is to be preferred.

3.6 Mixing physics at Lake Kivu

Studying the seasonal variations in the near-surface meteorological conditions and in the surface energy balance of

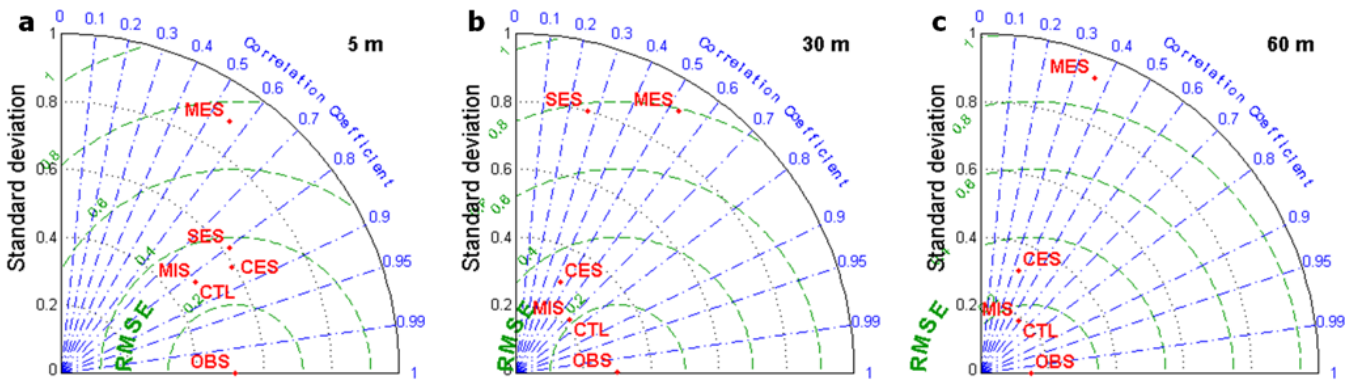


Fig. 13. Taylor diagram indicating model performance for water temperature at (a) 5 m, (b) 30 m and (c) 60 m depths for different initial conditions at Ishungu (January 2003–December 2011). OBS: observations, CTL: control, CES: control excluding spin-up, SES: stratified excluding spin-up, MIS (MES): mixed warm initialisation including (excluding) spin-up. Note that SES is omitted at 60 m given its strong deviation from observations there.

the Ishungu control experiment allows us to attribute the seasonal mixing cycle for Lake Kivu. On the one hand, even though ff depicts some seasonality (Fig. 14a), neither ff nor T influence the seasonality of the mixed layer depth at Ishungu. First, a comparative histogram of corrected ff binned per month (1 m s^{-1} bin width; not shown) reveals that the probability of occurrence of stronger winds ($ff > 5 \text{ m s}^{-1}$) is lower from April to July, adding to the hypothesis that higher wind velocities are not responsible for the deepening mixed layer depth during the dry season. This is confirmed by FLake, who attributes the mixed layer deepening at the start of the dry season to convection rather than wind-driven mixing. Moreover, when conducting the Ishungu control simulation with the seasonality removed from ff , the predicted water temperatures are almost identical to the control simulation. This indicates that the ff seasonality also has no major influence on the convective-driven mixing.

On the other hand, in contrast to ff and T , RH and LW_{in} both show a clear seasonality, with 3-monthly averages 13 % and 11 W m^{-2} , respectively, lower for the June–August period compared to December–February period. Their monthly average values show that the seasonal RH cycle lags the LW_{in} cycle by about one month, but they confirm the strong drop during the main dry season (Fig. 14b). Here, two effects enforce each other to reduce the amount of energy available to stratify the lake surface. First, as a consequence of reduced cloudiness during the dry season, less thermal radiation reaches the surface. This, in turn, causes a higher upward net long-wave radiation flux (LW_{net}) from May to July (Fig. 15). Second, more importantly, while a moisture climate close to saturation inhibits significant evaporation throughout most of the year, the RH drop during the dry season opens a larger potential to evaporation. This effect can be noted in the monthly average anomalies of the surface energy balance components, wherein the LHF shows a marked positive anomaly in months with low RH (Fig. 15). The energy

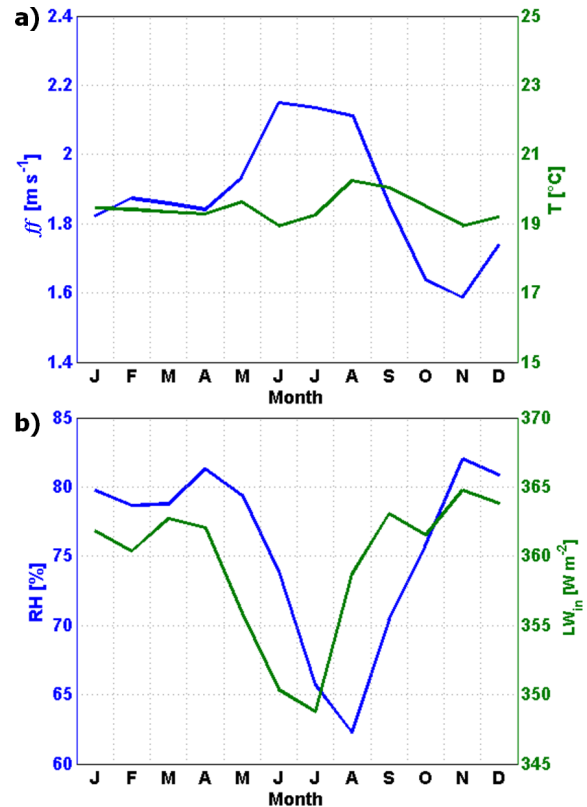


Fig. 14. Monthly averages for 2003–2011 of (a) wind velocity ff (m s^{-1}) and air temperature T ($^{\circ}\text{C}$); (b) relative humidity RH (%) recorded at Automatic Weather Station (AWS) 1 and incoming long-wave radiation LW_{in} (W m^{-2}) from ERA-Interim. Note the different y axes increments.

consumed for evaporating is no longer available to heat the water surface. Thus, lower thermal radiation input and especially enhanced evaporation cause a significant reduction in the amount of energy available to heat near-surface waters.

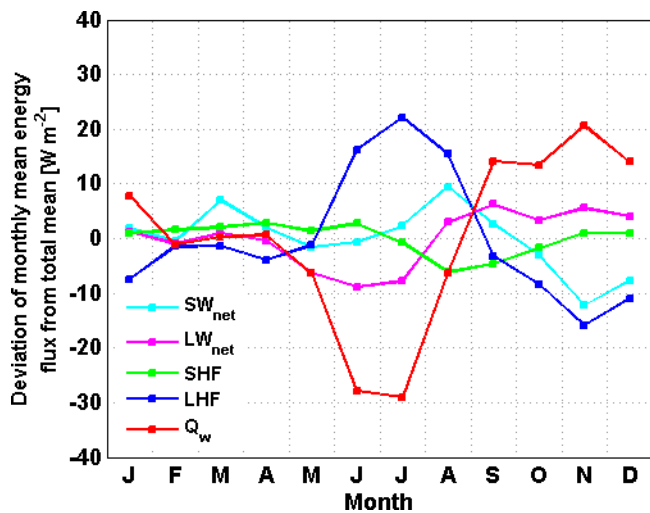


Fig. 15. Deviation of the monthly average of the surface energy balance components from its long-term mean (W m^{-2}) at Ishungu, 2003–2011, calculated by FLake's surface flux routines. Components are net short-wave radiation (SW_{net}), net long-wave radiation (LW_{net}), sensible heat flux (SHF), latent heat flux (LHF) and sub-surface conductive heat flux (Q_w).

To compensate for this surface heat deficit, the upward sub-surface conductive heat flux enhances, in turn generating a drop in the mixed layer temperature.

From mid-June onwards, near-surface water temperatures become low enough for the deep mixing to set in. Near the end of the dry season, from mid-August onwards, evaporation rates dramatically drop, causing the warming of surface waters from mid-September forward. Note that whereas enhanced solar radiation penetration into the lake is absent during the first phase of the dry season, near the end it slightly contributes to the restoration of surface stratification (Fig. 15). Overall, monthly variations in downward short-wave radiation (SW_{in}) seem to have only little effect on the mixed layer seasonality. Possibly, the interplay of astronomic short-wave radiation variability (with less short-wave radiation reaching the top of the atmosphere during the dry seasons) and seasonally varying cloud properties (Capart, 1952) balances out the amount of short-wave radiation reaching the surface on monthly timescales.

4 Discussion and conclusions

In general, this study shows that the thermal structure of the mixed layer and thermocline of two African Great Lakes can be reproduced by the FLake model. In particular, the seasonality of the near-surface water temperatures of Lake Kivu and Lake Tanganyika is well captured by the AWS-driven simulations when choosing appropriate values for the wind speed correction factor and k within their uncertainty range. Moreover, FLake was found capable of reproducing

the observed interannual variability, as well as the observed differences between the three sites. The spatial variability is accounted for through varying lake characteristics and meteorological conditions associated with different surface altitude and distance from the equator. At Ishungu, a study of the near-surface meteorology and surface heat balance was used to attribute seasonal mixing cycle of Lake Kivu. Rather than seasonal variations in wind velocity or air temperature, the marked dry season decrease of the incoming long-wave radiation and, especially, relative humidity with an associated evaporation peak, reduce the amount of energy available to induce surface stratification.

The near-surface water temperatures were found to be quite robust to changes in the model configuration. If the observed mixing regime is not reproduced, 5 m temperature predictions deteriorate compared to the control integration, but are relatively little affected. Hence, FLake can be considered an appropriate tool to study the climatic impact of lakes in the region of the African Great Lakes. In contrast, an accurate representation of the thermal structure of the mixed layer and thermocline depends strongly on the reliability of meteorological forcing data and a correct choice of model lake depth and water transparency. Slight differences in external parameters, and uncertainties associated with the meteorological forcing data (for instance related to measurement or atmospheric model uncertainty, or to the representativity of the data for over-lake conditions) may already lead to a switch from the observed regime of seasonal mixed layer deepening to either the permanently stratified or the fully mixed regime.

One important reason for this delicate balance found at Lake Kivu is the absence of an abyssal layer in FLake. In reality, the abyssal layer acts as a heat reservoir which buffers potential changes in bottom temperature. FLake, on the contrary, assumes a zero heat flux at the water–sediment interface (sediment routine switched off) or at the lower bound of the active sediment layer (sediment routine switched on). In cases where an artificial lake depth is set, this assumption can lead to unrealistic temperature fluctuations near the bottom. Hence, a future development could be to include an abyssal layer in FLake (Mironov et al., 2010).

A second issue is the reliability of water transparency values. Even in more studied areas, information on the spatial and temporal variability of water transparency is mostly lacking (Kirillin, 2010; Kourzeneva et al., 2012b; Rontu et al., 2012). Therefore, the first need is to collect more observations of k and to gain more insight into the relationship between water transparency and seasonal mixing cycles in deep tropical lakes. In the future, FLake could then also be adapted to account for these seasonal fluctuations in k .

When applying FLake over regions containing warm deep lakes, values for the external parameters thus need to be considered carefully. This is especially true when FLake is coupled to NWP, RCM or GCM models, since the meteorological forcing data are potentially biased in that case.

When setting up a climate or NWP simulation with interactive lakes, moreover, no information on the lake's initial conditions is available. In that respect, this study clearly shows that it is advisable to initialise all lakes with an artificially warm, uniform temperature and to allow for a considerable offline spin-up of the lake module. When such an offline lake spin-up is not feasible, initialising FLake with stratified conditions and an artificially low bottom temperature of 4 °C is to be preferred.

To conclude, the goal of this study was to assess the quality of lake temperature predictions by FLake when applied to tropical lakes. This was done through a number of simulations for three locations in the African Great lakes region: Ishungu (Lake Kivu), Kigoma (northern basin of Lake Tanganyika) and Mpulungu (southern basin of Lake Tanganyika). Results show that FLake is able to well represent the mixing regime at these different locations, however only when the model was carefully configured and allowed to spin-up over a considerable period. When input data quality is an issue, or the model is poorly configured, model results tend to deviate from observations towards the deep in large tropical lakes.

Code availability

FLake is freely available under the terms of the GNU Lesser General Public License (<http://www.gnu.org/licenses/lgpl.html>). The model source code, external parameter data sets and a comprehensive model description can be obtained from the official FLake website (<http://www.lakemodel.net>), along with pre-processed meteorological forcing for several test cases.

Appendix A

Table A1. Acronyms and variable names

AWS	Automatic Weather Station
BSS	Brier Skill Score []
CORDEX	Coordinated Regional climate Downscaling Experiment
COSMO	Consortium for Small-scale Modeling
control	FLake simulation with ff and k corrected
C_T	Shape factor with respect to the temperature profile in the thermocline []
CES	Same as control, but excluding spin-up
CTD	Conductivity-Temperature-Depth cast
dd	Wind direction [°]
DEE	Same as control, but with lake depth set to 120 m
ENSO	El Niño–Southern Oscillation

ERA-Interim	Reanalysis product from January 1979 onward, produced by the European Centre for Medium-Range Weather Forecasts
ff	Wind velocity [m s^{-1}]
FLake	Freshwater Lake model
GCM	General Circulation Model
h_{ML}	Mixed layer depth [m]
ITCZ	Intertropical Convergence Zone
k	Downward light attenuation coefficient [m^{-1}]
KHI	Same as control, but with k set to 0.46 m^{-1}
KLO	Same as control, but with k set to 0.15 m^{-1}
LHF	Latent heat flux [W m^{-2}]
LW_{in}	Downward long-wave radiation [W m^{-2}]
LW_{net}	Net long-wave radiation [W m^{-2}]
MES	Same as control, but initially fully mixed and excluding spin-up
MIS	Same as control, but initially fully mixed
n	Number of observations []
NWP	Numerical Weather Prediction
p	Air pressure [Pa]
r	Pearson correlation coefficient []
raw	FLake simulation with observed meteorology and k
RCM	Regional Climate Model
RH	Relative humidity [%]
RMSE	root mean square error [respective unit]
RMSE _c	Centred root mean square error [respective unit]
σ	Standard deviation [respective unit]
SES	Same as control, but initially strongly stratified and excluding spin-up
SHA	Same as control, but with lake depth set to 30 m
SW_{in}	Downward short-wave radiation [W m^{-2}]
T	Air temperature [°C]
T_{BOT}	Bottom temperature [°C]
T_{ML}	Mixed layer temperature [°C]
T_{MW}	Water column average temperature [°C]
z_{sd}	Disappearance depths of the Secchi disk [m]

Acknowledgements. We would like to thank Dmitrii Mironov for the helpful discussions on the modelling of tropical lakes and the Institut Supérieur Pédagogique in Bukavu for supplying data of AWS 1. We also sincerely thank the Editor and the two anonymous reviewers for their constructive remarks. This work was financially and logistically supported by the Research Foundation – Flanders (FWO) and the Belgian Science Policy Office (BELSPO), the latter through the research projects EAGLES and CHOLTIC.

Edited by: J. Neal

References

- Akkermans, T., Lauwaet, D., Demuzere, M., Vogel, G., Nouvellon, Y., Ardö, J., Caquet, B., De Grandcourt, A., Merbold, L., Kutsch, W., and van Lipzig, N.: Validation and comparison of two soil-vegetation-atmosphere transfer models for tropical Africa, *J. Geophys. Res.*, 117, G02013, doi:10.1029/2011JG001802, 2012.
- Akkermans, T., Thiery, W., and van Lipzig, N.: The regional climate impact of a realistic future deforestation scenario in the Congo Basin, *J. Climate*, doi:10.1175/JCLI-D-13-00361.1, 2014.
- Alleman, L. Y., Cardinal, D., Cocquyt, C., Plisnier, P.-D., Descy, J.-P., Kimirei, I., Sinyinza, D., and André, L.: Silicon Isotopic Fractionation in Lake Tanganyika and Its Main Tributaries, *J. Great Lakes Res.*, 31, 509–519, 2005.
- Anyah, R. O., Semazzi, F. H. M., and Xie, L.: Simulated Physical Mechanisms Associated with Climate Variability over Lake Victoria Basin in East Africa, *Mon. Weather Rev.*, 134, 3588–3609, 2006.
- Balsamo, G., Salgado, R., Dutra, E., Boussetta, S., and Stockdale, T.: On the contribution of lakes in predicting near-surface temperature in a global weather forecasting model, *Tellus A*, 64, 15829, doi:10.3402/tellusa.v64i0.15829, 2012.
- Beadle, L. C.: The inland waters of Tropical Africa, An introduction to tropical limnology, Longman, London, United Kingdom, 475 pp., 1981.
- Bonan, G. B.: Sensitivity of a GCM Simulation to Inclusion of Inland Water Surfaces, *J. Climate*, 8, 2691–2703, 1995.
- Borgès, A. V., Abril, G., Delille, B., Descy, J.-P., and Darchambeau, F.: Diffusive methane emissions to the atmosphere from Lake Kivu (Eastern Africa), *J. Geophys. Res.*, 116, G03032, doi:10.1029/2011JG001673, 2011.
- Bultot, F.: Atlas climatique du bassin Congolais, vol 2: Les composantes du bilan d'eau, Publications de l'Institut National pour l'Étude Agronomique du Congo, Brussels, Belgium, 1971.
- Capart, A.: Le milieu géographique et géophysique, Résultats scientifiques de l'exploration hydrobiologique du Lac Tanganyika (1946–1947), Royal Belgian Institute of Natural Sciences, Brussels, Belgium, 27 pp., 1952.
- Coulter, G. W. (Ed.): Lake Tanganyika and its life, Oxford University Press, London, United Kingdom, 354 pp., 1991.
- Darchambeau, F., Sarmento, H., and Descy, J.-P.: Primary production in a tropical large lake: The role of phytoplankton composition, *Sci. Total Environ.*, 473, 178–188, 2014.
- De Boor, C.: A Practical Guide to Splines, Applied Mathematical Sciences series, 27, Springer-Verlag, New York, 346 pp., 1978.
- Dee, D. P., Uppala, S. M., Simmons, A. J., Berrisford, P., Poli, P., Kobayashi, S., Andrae, U., Balmaseda, M. A., Balsamo, G., Bauer, P., Bechtold, P., Beljaars, A. C. M., van de Berg, L., Bidlot, J., Bormann, N., Delsol, C., Dragani, R., Fuentes, M., Geer, A. J., Haimberger, L., Healy, S. B., Hersbach, H., Hólm, E. V., Isaksen, L., Källberg, P., Köhler, M., Matricardi, M., McNally, A. P., Monge-Sanz, B. M., Morcrette, J.-J., Park, B.-K., Peubey, C., de Rosnay, P., Tavolato, C., Thépaut, J.-N., and Vitart, F.: The ERA-Interim reanalysis: Configuration and performance of the data assimilation system, *Q. J. Roy. Meteor. Soc.*, 137, 553–597, 2011.
- Degens, E. T., von Herzen, R. P., Wong, H.-K., Deuser, W. G., and Jannash, H. W.: Lake Kivu: Structure, Chemistry and Biology of an East African Rift Lake, *Geol. Rundsch.*, 62, 245–277, doi:10.1007/BF01826830, 1973.
- Doms, G. and Schättler, U.: A Description of the Nonhydrostatic Regional Model LM. Part 1: Dynamics and Numerics, German Weather Service, Offenbach am Main, Germany, 140 pp., 2002.
- Doms, G., Förstner, J., Heise, E., Herzog, H.-J., Mironov, D., Raschendorfer, M., Reinhardt, T., Ritter, B., Schrodin, R., Schulz, J.-P., and Vogel, G.: A Description of the Nonhydrostatic Regional COSMO Model. Part 2: Physical Parameterization, German Weather Service, Offenbach am Main, Germany, 161 pp., 2011.
- Dutra, E., Stepanenko, V. M., Balsamo, G., Viterbo, P., Miranda, P. M. A., Mironov, D., and Schär, C.: An offline study of the impact of lakes on the performance of the ECMWF surface scheme, *Boreal Environ. Res.*, 15, 100–112, 2010.
- Giorgi, F., Jones, C., and Asrar, G. R.: Addressing climate information needs at the regional level: the CORDEX framework, *WMO Bull.*, 58, 175–183, 2009.
- Gourgue, O., Deleersnijder, E., Legat, V., Marchal, E., and White, L.: Free and forced thermocline oscillations in Lake Tanganyika, in: Factor separation in the atmosphere: applications and future prospects, edited by: Alpert, P. and Sholokhman, T., Cambridge University Press, Cambridge, United Kingdom, 146–162, 2011.
- Hernández-Díaz, L., Laprise, R., Sushama, L., Martynov, A., Winger, K., and Dugas, B.: Climate simulation over CORDEX Africa domain using the fifth-generation Canadian Regional Climate Model (CRCM5), *Clim. Dynam.*, 40, 1415–1433, doi:10.1007/s00382-012-1387-z, 2012.
- Kirillin, G.: Modelling the impact of global warming on water temperature and seasonal mixing regimes in small temperature lakes, *Boreal Environ. Res.*, 15, 279–293, 2010.
- Kitaigorodskii, S. A. and Miropolskii, Yu. Z.: On the theory of the open ocean active layer, *Izv. Atmos. Oceanic Phys.*, 6, 97–102, 1970.
- Kourzeneva, E. V.: External data for lake parameterization in Numerical Weather Prediction and climate modelling, *Boreal Environ. Res.*, 15, 165–177, 2010.
- Kourzeneva, E. V., Samuelsson, P., Ganbat, G., and Mironov, D.: Implementation of Lake Model FLake in HIRLAM, HIRLAM Newsletter no 54, 54–61, 2008.
- Kourzeneva, E. V., Asensio, H., Martin, E., and Faroux, S.: Global gridded dataset of lake coverage and lake depth for use in numerical weather prediction and climate modelling, *Tellus A*, 64, 15640, doi:10.3402/tellusa.v64i0.15640, 2012a.
- Kourzeneva, E. V., Martin, E., Batrak, Y., and Le Moigne, P.: Climate data for parameterisation of lakes in Numerical Weather Prediction models, *Tellus A*, 64, 17226, doi:10.3402/tellusa.v64i0.17226, 2012b.
- Lauwaet, D., van Lipzig, N. P. M., Van Weverberg, K., De Ridder, K., Goyens, C.: The precipitation response to the desiccation of Lake Chad, *Q. J. Roy. Meteor. Soc.*, 138, 707–719, doi:10.1002/qj.942, 2011.
- Martynov, A., Sushama, L., and Laprise, R.: Simulation of temperate freezing lakes by one-dimensional lake models: performance assessment for interactive coupling with regional climate models, *Boreal Environ. Res.*, 15, 143–164, 2010.
- Martynov, A., Sushama, L., Laprise, R., Winger, K., and Dugas, B.: Interactive Lakes in the Canadian Regional Climate Model, version 5: The Role of Lakes in the Regional Climate of North America, *Tellus A*, 64, 16226, doi:10.3402/tellusa.v64i0.16226, 2012.

- Mironov, D.: Parameterization of Lakes in Numerical Weather Prediction. Description of a Lake Model, COSMO Technical Report No. 11, German Weather Service, Offenbach am Main, Germany, 44 pp., 2008.
- Mironov, D., Heise, E., Kourzeneva, E., Ritter, B., Schneider, N., and Terzhevik, A.: Implementation of the lake parameterisation scheme FLake into the numerical weather prediction model COSMO, *Boreal Environ. Res.*, 15, 218–230, 2010.
- Munk, W. H. and Anderson, E. R.: Notes on a theory of the thermocline, *J. Marine Res.*, 7, 276–295, 1948.
- Naithani, J., Deleersnijder, E., and Plisnier, P.-D.: Analysis of Wind-Induced Thermocline Oscillations of Lake Tanganyika, *Environ. Fluid Mech.*, 3, 23–39, 2003.
- Naithani, J., Darchambeau, F., Deleersnijder, E., Descy, J. P., and Wolanski, E.: Study of the nutrient and plankton dynamics in lake Tanganyika using a reduced-gravity model, *Ecol. Model.*, 200, 225–233, 2007.
- Nash, J. E. and Sutcliffe, J. V.: River flow forecasting through conceptual models part I – A discussion of principles, *J. Hydrol.*, 10, 282–290, 1970.
- Nicholson, S. E.: A review of climate dynamics and climate variability in eastern Africa, in: *The Limnology, Climatology and Paleoclimatology of the East African Lakes*, edited by: Johnson, T. C. and Odada, E., Gordon & Breach, Amsterdam, 25–56, 1996.
- O'Reilly, C. M., Alin, S. R., Plisnier, P., Cohen, A. S., and McKee, B. A.: Climate change decreases aquatic ecosystem productivity of lake Tanganyika, *Africa, Nature*, 424, 766–768, 2003.
- Plisnier, P.-D., Chitamwebwa, D., Mwape, L., Tshibangu, K., Langenberg, V., and Coenen, E.: Limnological annual cycle inferred from physical-chemical fluctuations at three stations of Lake Tanganyika, *Hydrobiologia*, 407, 45–58, 1999.
- Plisnier, P.-D., Serneels, S., and Lambin, E. F.: Impact of ENSO on East African ecosystems: a multivariate analysis based on climate and remote sensing data, *Global Ecol. Biogeogr.*, 9, 481–497, 2000.
- Plisnier, P.-D., Cornet, Y., Naithani, J., Deleersnijder, E., and Descy, J.-P.: Climate change impact on the sustainable use of Lake Tanganyika fisheries (CLIMFISH), Royal Museum for Central Africa, Tervuren, Belgium, BELSPO final report, 155 pp., 2007.
- Raschendorfer, M.: The new turbulence parameterization of LM, German Weather Service, Offenbach am Main, Germany, COSMO Newsletter No. 1, 89–97, 2001.
- Rontu, L., Eerola, K., Kourzeneva, E., and Vehviläinen, B.: Data assimilation and parametrisation of lakes in HIRLAM, *Tellus A*, 64, 17611, doi:10.3402/tellusa.v64i0.17611, 2012.
- Salgado, R. and Le Moigne, P.: Coupling of the FLake model to the Surfex externalized surface model, *Boreal Environ. Res.*, 15, 231–244, 2010.
- Samuelsson, P., Kourzeneva, E., and Mironov, D.: The impact of lakes on the European climate as simulated by a regional climate model, *Boreal Environ. Res.*, 15, 113–129, 2010.
- Sarmiento, H., Isumbishu, M., and Descy, J.-P.: Phytoplankton ecology of Lake Kivu (eastern Africa), *J. Plankton Res.*, 28, 815–829, doi:10.1029/2004GC000892, 2006.
- Sarmiento, H., Darchambeau, F., and Descy, J.-P.: Phytoplankton of Lake Kivu, in: *Lake Kivu: Limnology and biogeochemistry of a tropical great lake*, edited by: Descy, J.-P., Darchambeau, F., and Schmid, M., Springer, Dordrecht, 67–83, 2012.
- Savijärvi, H.: Diurnal winds around Lake Tanganyika, *Q. J. Roy. Meteor. Soc.*, 123, 901–918, 1997.
- Savijärvi, H. and Järvenoja, S.: Aspects of Fine-Scale Climatology Over Lake Tanganyika as Resolved by a Mesoscale Model, *Meteorol. Atmos. Phys.*, 73, 77–88, 2000.
- Schmid, A. and Wüest, A.: Stratification, Mixing and Transport Processes in Lake Kivu, in: *Lake Kivu: Limnology and biogeochemistry of a tropical great lake*, edited by: Descy, J.-P., Darchambeau, F., and Schmid, M., Springer, Dordrecht, 13–29, 2012.
- Schmid, M., Halbwegs, M., Wehrli, B., and Wüest, A.: Weak mixing in Lake Kivu: New insights indicate increasing risk of uncontrolled gas eruption, *Geochim. Geophys. Geosci.*, 6, Q07009, doi:10.1029/2004GC000892, 2005.
- Schmid, M., Busbridge, M., and Wüest, A.: Double-diffusive convection in Lake Kivu, *Limnol. Oceanogr.*, 55, 225–238, 2010.
- Simmons, A., Uppala, S., Dee, D., and Kobayashi, S.: ERA-Interim: New ECMWF reanalysis products from 1989 onwards, European Centre for Medium-Range Weather Forecasts, Reading, UK, ECMWF Newsletter No. 110, 25–35, 2007.
- Spigel, R. H. and Coulter, G. W.: Comparison of hydrology and physical limnology of the East African Great Lakes: Tanganyika, Malawi, Victoria, Kivu and Turkana (with references to some North American Great Lakes), in: *The Limnology, Climatology and Paleoclimatology of the East African lakes*, edited by: Johnson, T. C. and Odada, E., Gordon and Breach Publishers, Amsterdam, The Netherlands, 103–140, 1996.
- Stenuite, S., Pirlot, S., Hardy, M. A., Sarmiento, H., Tarbe, A. L., Leporcq, B., and Descy, J.-P.: Phytoplankton production and growth rate in Lake Tanganyika: evidence of a decline in primary productivity in recent decades, *Freshwater Biol.*, 52, 2226–2239, doi:10.1111/j.1365-2427.2007.01829.x, 2007.
- Stepanenko, V. M., Martynov, A., Jöhnk, K. D., Subin, Z. M., Perroud, M., Fang, X., Beyrich, F., Mironov, D., and Goyette, S.: A one-dimensional model intercomparison study of thermal regime of a shallow, turbid midlatitude lake, *Geosci. Model Dev.*, 6, 1337–1352, doi:10.5194/gmd-6-1337-2013, 2013.
- Taylor, K. E.: Summarizing multiple aspects of model performance in a single diagram, *J. Geophys. Res.*, 106, 7183–7192, 2001.
- Thiery, W., Gorodetskaya, I. V., Bintanja, R., Van Lipzig, N. P. M., Van den Broeke, M. R., Reijmer, C. H., and Kuipers Munneke, P.: Surface and snowdrift sublimation at Princess Elisabeth station, East Antarctica, *The Cryosphere*, 6, 841–857, doi:10.5194/tc-6-841-2012, 2012.
- Thiery, W., Stepanenko, V. M., Fang, X., Jöhnk, K. D., Li, Z., Martynov, A., Perroud, M., Subin, Z. M., Darchambeau, F., Mironov, D., and van Lipzig, N. P. M.: LakeMIP Kivu: Evaluating the representation of a large, deep tropical lake by a set of one-dimensional lake models, *Tellus, Ser. A*, 66, 21390, doi:10.3402/tellusa.v66.21390, 2014.
- Verburg, P. and Antenucci, J. P.: Persistent unstable atmospheric boundary layer enhances sensible and latent heat loss in a tropical great lake: Lake Tanganyika, *J. Geophys. Res.*, 115, D11109, doi:10.1029/2009JD012839, 2010.
- Verburg, P. and Hecky, R. E.: Wind patterns, Evaporation and Related Physical Variables in Lake Tanganyika, East-Africa, *J. Great Lakes Res.*, 29, 48–61, 2003.
- Verburg, P. and Hecky, R. E.: The physics of warming of lake Tanganyika by climate change, *Limnol. Oceanogr.*, 54, 2418–2430, 2009.

Verburg, P., Hecky, R. E., and Kling, H.: Ecological Consequences of a Century of Warming in Lake Tanganyika, *Science*, 301, 505–507, 2003.

Verburg, P., Antenucci, J. P., and Hecky, R. E.: Differential cooling drives large-scale convective circulation in Lake Tanganyika, *Limnol. Oceanogr.*, 56, 910–926, doi:10.4319/lo.2011.56.3.0910, 2011.

Wilks, D. S.: Statistical methods in atmospheric sciences, *International Geophysics Series*, 100, Academic Press, Oxford, United Kingdom, 676 pp., 2005.

The Impact of the African Great Lakes on the Regional Climate

WIM THIERY

Department of Earth and Environmental Sciences, KU Leuven, Leuven, Belgium

EDOUARD L. DAVIN

Institute for Atmospheric and Climate Science, ETH Zürich, Zürich, Switzerland

HANS-JÜRGEN PANITZ

Institute for Meteorology and Climate Research, Karlsruhe Institute of Technology, Karlsruhe, Germany

MATTHIAS DEMUZERE, STEF LHERMITTE, AND NICOLE VAN LIPZIG

Department of Earth and Environmental Sciences, KU Leuven, Leuven, Belgium

(Manuscript received 21 July 2014, in final form 2 February 2015)

ABSTRACT

Although the African Great Lakes are important regulators for the East African climate, their influence on atmospheric dynamics and the regional hydrological cycle remains poorly understood. This study aims to assess this impact by comparing a regional climate model simulation that resolves individual lakes and explicitly computes lake temperatures to a simulation without lakes. The Consortium for Small-Scale Modelling model in climate mode (COSMO-CLM) coupled to the Freshwater Lake model (FLake) and Community Land Model (CLM) is used to dynamically downscale a simulation from the African Coordinated Regional Downscaling Experiment (CORDEX-Africa) to 7-km grid spacing for the period of 1999–2008. Evaluation of the model reveals good performance compared to both in situ and satellite observations, especially for spatiotemporal variability of lake surface temperatures (0.68-K bias), and precipitation (-116 mm yr^{-1} or 8% bias). Model integrations indicate that the four major African Great Lakes almost double the annual precipitation amounts over their surface but hardly exert any influence on precipitation beyond their shores. Except for Lake Kivu, the largest lakes also cool the annual near-surface air by -0.6 to -0.9 K on average, this time with pronounced downwind influence. The lake-induced cooling happens during daytime, when the lakes absorb incoming solar radiation and inhibit upward turbulent heat transport. At night, when this heat is released, the lakes warm the near-surface air. Furthermore, Lake Victoria has a profound influence on atmospheric dynamics and stability, as it induces circular airflow with over-lake convective inhibition during daytime and the reversed pattern at night. Overall, this study shows the added value of resolving individual lakes and realistically representing lake surface temperatures for climate studies in this region.

1. Introduction

The African Great Lakes (AGL) represent the largest reservoir of freshwater lakes in the tropics, including the second largest freshwater lake on earth in terms of surface area (Lake Victoria, $68\,800 \text{ km}^2$) and the second largest in terms of volumetric water storage (Lake Tanganyika,

$17\,800 \text{ km}^3$). The AGL provide numerous ecosystem services to local communities, such as fishing resources, drinking water, and electrical power. Lake Victoria alone directly supports 200 000 fishermen operating from its shores and sustains the livelihood of more than 30 million people living at its coasts (Semazzi 2011).

Lakes also influence regional climate conditions, in particular in regions where they are abundant. Mediated by the fluxes of energy, moisture, and momentum, they significantly alter the surface energy and water balance in a particular region and therefore its climate. Such reciprocal relations are often studied using numerical

Corresponding author address: Wim Thiery, Department of Earth and Environmental Sciences, KU Leuven, Celestijnenlaan 200E, 3001 Leuven, Belgium.
E-mail: wim.thiery@ees.kuleuven.be

models. At the global scale, general circulation model (GCM) studies demonstrate an average annual cooling effect of lakes but also highlight important seasonal and regional effects (Bonan 1995; Subin et al. 2012; Rooney and Bornemann 2013). Numerous studies also mention the increase in annual precipitation due to the presence of lakes (e.g., Coe and Bonan 1997). Regional climate model (RCM) studies have been performed at higher horizontal resolution (e.g., 50 km), thereby better emphasizing the lake–atmosphere interplay at the local scale (e.g., Hostetler et al. 1994; Hostetler and Giorgi 1995; Bates et al. 1995; Goyette et al. 2000; Anyah et al. 2006; Samuelsson et al. 2010; Gula and Peltier 2012; Lauwaet et al. 2012; Martynov et al. 2012; Gu et al. 2015; Notaro et al. 2013; Bennington et al. 2014; Williams et al. 2015).

Although the AGL are widely recognized as an important driver of the East African regional climate system, their impact on atmospheric dynamics and the regional hydrological cycle remains poorly understood. Studies on the interplay between climate and the AGL are therefore necessary to identify, among other information, the patterns of evaporation and precipitation induced by lake presence and the reasons behind their observed spatiotemporal variability. The need to enhance the understanding is urgent, as every year, possibly more than 5000 fishermen lose their lives over Lake Victoria alone, mostly due to hazardous weather conditions and associated water currents (Semazzi 2011).

The poor understanding of African lake–climate interactions is related to a number of challenges when applying a regional climate model to the AGL region: (i) First, a model should be applicable to tropical conditions. Among other requirements, such a setup must be able to reproduce tropical features, such as deep convection or mesoscale convective systems [and associated precipitation extremes; Lauwaet et al. (2009); Goyens et al. (2012)] and must include a land surface model (LSM) capable of simulating tropical vegetation. In recent climate model studies over tropical Africa, these challenges have received particular attention (e.g., Vizi and Cook 2012; Saeed et al. 2013; Cr  tat et al. 2014; Panitz et al. 2014; Dosio et al. 2015). (ii) Second, the horizontal model grid resolution should be sufficiently high to resolve individual lakes and strong orography of the region. Combined with the long integration period and high vertical extent necessary to model tropical climatic conditions, the need for computational resources rises. (iii) Third, a correct representation of lake surface temperatures within the atmospheric model is essential to investigate the two-way interactions between climate and lake processes over East Africa (Stepanenko et al. 2013). This can be particularly

challenging for large, deep lakes given the role of vertical heat transport and three-dimensional water circulation within these lakes (Gu et al. 2015; Bennington et al. 2014). (iv) Last, the limited number of observational datasets available and issues regarding the quality of available products over highly mountainous, tropical domains (e.g., Dinku et al. 2008) complicate a comprehensive model evaluation over this region. Consequently, up to now only a few RCM studies explicitly examine aspects of lake–atmosphere interactions over a specific African Great Lake (Savij  rvi and J  rvenoja 2000; Song et al. 2004; Anyah and Semazzi 2004; Anyah et al. 2006; Argent et al. 2015; Sun et al. 2014a,b; Williams et al. 2015), while none investigates these interactions for the whole region.

Hence, the main goals of this study are to assess the regional climate impact of the AGL and understand the physical mechanisms underlying these impacts. This is achieved by addressing the aforementioned challenges in the following ways: (i) The regional Consortium for Small-Scale Modelling model in climate mode (COSMO-CLM; Rockel et al. 2008) is applied in its tropical setup [configuration following Panitz et al. (2014)]. In their comprehensive evaluation of the COSMO-CLM evaluation simulation conducted in the framework of the African Coordinated Regional Downscaling Experiment (CORDEX-Africa; Giorgi et al. 2009), Panitz et al. (2014) demonstrate the ability of COSMO-CLM to reproduce the overall features of the African climate (when downscaling ERA-Interim) and show that, relative to several gridded observational products, it even outperforms ERA-Interim in terms of the mean annual precipitation cycles and interannual variability over major parts of the domain. Among the considered regional biases, the authors point to an underestimation of the precipitation intensity by 2 mm day^{-1} in East Africa, which is ascribed to an underestimation of the latent heat flux and overestimation of the sensible heat flux. To address this issue, here we employ COSMO-CLM coupled to a state-of-the-art LSM, the Community Land Model, version 3.5 (CLM3.5; Davin and Seneviratne 2012). For various applications, this version already showed improved skills compared to the standard version (see section 2a). (ii) Model integrations are performed for a period of 13 years on a horizontal resolution high enough for large to medium-sized lakes to become resolved features (0.0625° ; $\sim 7 \text{ km}$). (iii) The one-dimensional Freshwater Lake model (FLake), recently coupled to COSMO-CLM (Mironov et al. 2010), is used to compute lake water surface temperatures. (iv) Special attention is paid to model evaluation, in particular by using remote sensing products and comprehensive in situ observational datasets to assess the model's ability to reproduce

observed spatial and temporal lake surface temperature variability, turbulent fluxes, and precipitation. Adopting one or more of the above challenges may improve the representation of the regional climate, as demonstrated in many recent studies (e.g., Mironov et al. 2010; Nikulin et al. 2012; Akkermans 2013; Laprise et al. 2013; Akkermans et al. 2014; Cr  tat et al. 2014; Dosio et al. 2015; Williams et al. 2015).

Within this paper, the results of the RCM control simulation are extensively evaluated. This simulation is subsequently compared to a no-lake simulation, where the lakes are replaced by representative land pixels. This approach makes it possible to quantify the impact on the regional climate, in particular on near-surface temperature and precipitation. The impact of the lakes is then investigated in more detail by applying a surface energy balance decomposition technique and studying the dynamical changes induced by the lakes.

2. Model, data, and methodology

a. COSMO-CLM²

To investigate the influence of the AGL on the climate, we use the three-dimensional, nonhydrostatic regional climate model, COSMO-CLM (Rockel et al. 2008), version 4.8. The model development is a joint effort of the Consortium for Small-Scale Modelling and the Climate Limited-Area Modelling Community (CLM-Community). Its dynamical core solves the fully compressible hydrothermodynamical equations for three-dimensional Cartesian wind components; pressure perturbation; temperature; specific humidity; cloud water content and optionally cloud ice content; turbulent kinetic energy; and rain, snow, and graupel specific water content (Doms 2011). Physical parameterizations include a description of subgrid-scale turbulence (Raschendorfer 2001), grid-scale clouds and precipitation (Doms et al. 2011), shallow and moist convection (Tiedtke 1989), and δ -two-stream radiative transfer (Ritter and Geleyn 1992). A detailed description of the model system dynamics, numeric, and physical parameterizations can be found in the model documentation (e.g., Doms 2011; Doms et al. 2011; <http://www.cosmo-model.org>).

Additionally, the native COSMO-CLM Multi-Layered land surface model (TERRA-ML; Grasselt et al. 2008) is replaced by the more comprehensive Community Land Model (CLM; Oleson et al. 2004, 2008), version 3.5. CLM3.5 is maintained at the National Center for Atmospheric Research (NCAR), and given its explicit treatment of the photosynthetic process and its control on the stomatal conductance (big-leaf approach), it can be considered a third-generation LSM (Sellers et al. 1997).

Moreover, an individual land pixel can be composed of multiple land units due to the nested tile approach, which allows representation of multiple soil columns and represents biomes as a combination of different plant functional types. An extensive description and evaluation of CLM3.5 in offline mode is presented in Oleson et al. (2004, 2008) and St  ckli et al. (2008).

The model system COSMO-CLM coupled to CLM3.5 (hereinafter referred to as COSMO-CLM²) is described in detail by Davin and Seneviratne (2012) and references therein. The added value of COSMO-CLM², relative to the standard setup, was recently demonstrated over Europe (Davin et al. 2011; Davin and Seneviratne 2012; Lorenz et al. 2012) and central Africa (Akkermans 2013). A better partitioning of the turbulent fluxes and associated improvement of climate characteristics, such as near-surface temperature, precipitation, and cloud cover, were found in all cases, supporting the usage of this model for studying biogeophysical impacts of altered land surface characteristics (e.g., Davin et al. 2014; Lejeune et al. 2015; Jacobs et al. 2015; Vanden Broucke et al. 2015). Based on an offline comparison of both LSMs at four central African flux tower sites, Akkermans et al. (2012) attributed this enhanced skill mainly to a more realistic representation of the leaf area index, surface albedo, and root depth in CLM3.5 compared to TERRA-ML. Furthermore, Akkermans et al. (2014) extensively evaluated COSMO-CLM² over the larger central African domain and found a close correspondence between the observed and modeled near-surface temperature, column precipitable water, and surface net longwave radiation. For precipitation, cloud cover, top of the atmosphere outgoing longwave radiation, and various solar radiation quantities, the model adequately reproduced observed values, with some notable differences potentially ascribed to an underestimation of the optical thickness of convective clouds by COSMO-CLM².

b. FLake

As a one-dimensional lake model embedded in COSMO-CLM², FLake computes the evolution of a lake column temperature profile and the integral energy budgets of its different layers (Mironov et al. 2010). The model considers two layers in the water column: a mixed layer at the top and a thermocline down to the lake bottom. While the mixed layer is assumed to have a uniform temperature (T_{ML}), the temperature-depth curve in the thermocline is parameterized through the concept of self-similarity or assumed shape (Kitaigorodskii and Miropolskii 1970). This shape is only dependent on the temperature at its extremities and a shape factor, which describes the curve through a fourth-order polynomial (Mironov 2008). In the absence of snow and ice cover and

when neglecting bottom sediments, the prognostic variables are the mixed layer depth (h_{ML}), the bottom and water column average temperatures (T_{BOT} and T_{MW} , respectively), and the shape factor with respect to the temperature profile in the thermocline (C_T). Given their control on turbulence in the surface mixed layer (Read et al. 2012), h_{ML} is predicted taking convective and mechanical mixing into account, whereas volumetric heating is computed from the net shortwave radiation penetration through the lake surface and absorption at depth according to the Beer–Lambert law. To this end, the default downward light attenuation coefficient of 3 m^{-1} is employed. A recent global bathymetry dataset (Kourzeneva 2010; Kourzeneva et al. 2012) is used to specify lake depth of each lake pixel, thereby assuming a maximum lake depth of 50 m. A detailed description of FLake is provided in Mironov (2008) and Mironov et al. (2010).

Although FLake is a relatively simple model, its skill proves comparable to other, more comprehensive one-dimensional lake models for various lake types and climatic conditions (e.g., Perroud and Goyette 2009; Stepanenko et al. 2010, 2013, 2014). Moreover, FLake was extensively tested in offline mode over several AGL and judged an adequate tool to compute lake surface temperatures in comparison to other one-dimensional lake models, even though lake bottom temperatures may be sensitive to changes in certain external parameters and driving variables, such as wind speed (Thiery et al. 2014a,b). This is the first study to consider lake–atmosphere interactions over the AGL using FLake interactively coupled to an RCM. Previous RCM studies focusing on Lake Victoria either used prescribed lake surface temperatures (e.g., Anyah and Semazzi 2004; Argent et al. 2015; Sun et al. 2014a; Williams et al. 2015), the Hostetler lake model (e.g., Song et al. 2004), or the Princeton Ocean Model (POM; e.g., Song et al. 2004; Anyah and Semazzi 2006; Sun et al. 2014b).

c. Model setup

To obtain information on small-scale variability, RCMs dynamically downscale lateral boundary conditions at a coarser resolution to a regional finer-scale model grid (Laprise et al. 2008). Here, we use the COSMO-CLM CORDEX-Africa evaluation simulation (Panitz et al. 2014) as lateral boundary conditions. The CORDEX-Africa evaluation simulation represents a dynamical downscaling to a 50-km (0.44°) horizontal grid spacing of the ERA-Interim, made available by the European Center for Medium-Range Weather Forecast (ECMWF; Dee et al. 2011) for 1979–2014 at 79-km (T255) resolution. Given the large difference in resolution between the latter and the target configuration, a direct downscaling of ERA-Interim is not advisable in this case.

The COSMO-CLM² model system is used to generate two climate simulations. First, a control simulation (CTL) is conducted where the lakes are included in the model integration. For this purpose, FLake is employed to compute the water temperatures for the AGL. The second simulation [the no-lake simulation (NOL)] is identical to the control experiment, but each lake pixel is replaced by a representative land pixel selected from all land pixels within a distance of 50 km. The external parameters and initial conditions of replaced land pixels consequently show similar values and spatial patterns as the surrounding land; for instance, the area change of various plant functional types (PFTs) within the domain is 0.35% on average and less than 3% for each individual PFT.

Both experiments are conducted at a horizontal resolution of 0.0625° (~ 7 km), which is finer than previous multiyear RCM experiments over this region (e.g., Sun et al. 1999; Song et al. 2004; Anyah and Semazzi 2004; Anyah et al. 2006; Williams et al. 2015; with resolutions ranging from 20 to 60 km), using 50 vertical levels and a time step of 60 s. The model domain encompasses the central part of the East African rift (Fig. 1) and, therewith, includes most of the AGL. Since enlarging the model domain by 50 grid points (3.125°) in each direction reduced the predictive skill of a 1-yr test simulation and more than doubled the total computation time, this option was not considered. The simulations cover the period 1996–2008 (13 yr), of which the first three years are considered as spin-up time and excluded from the analysis. Inspection of predicted lake water surface temperatures shows that three years is enough to spin up the model: lake water surface temperatures evolve to normal climatological values within the first year already. Finally, on each side, 10 grid points were excluded from the analysis. Computation of the Davies relaxation function (Davies 1983) in the east–west direction showed that direct influence of lateral boundary conditions vanishes beyond this zone. The presence of two north–south oriented mountain ranges within the model domain are expected to further reduce the imprint of the parent model on the COSMO-CLM² predictions.

The configuration used in this study is based on the tropical setup of COSMO-CLM described by Panitz et al. (2014) and used for the CORDEX-Africa simulations (Panitz et al. 2014; Dosio et al. 2015). In the tropical configuration, the model top is set to 30 km, and the lower height of the damping layer is increased from 11 to 18 km. In addition, we introduced the following modifications: (i) First, CLM3.5 replaces the default LSM in COSMO-CLM. (ii) Second, FLake is used instead of the Hostetler-based lake model embedded within CLM3.5 (Bonan et al. 2002), as the latter

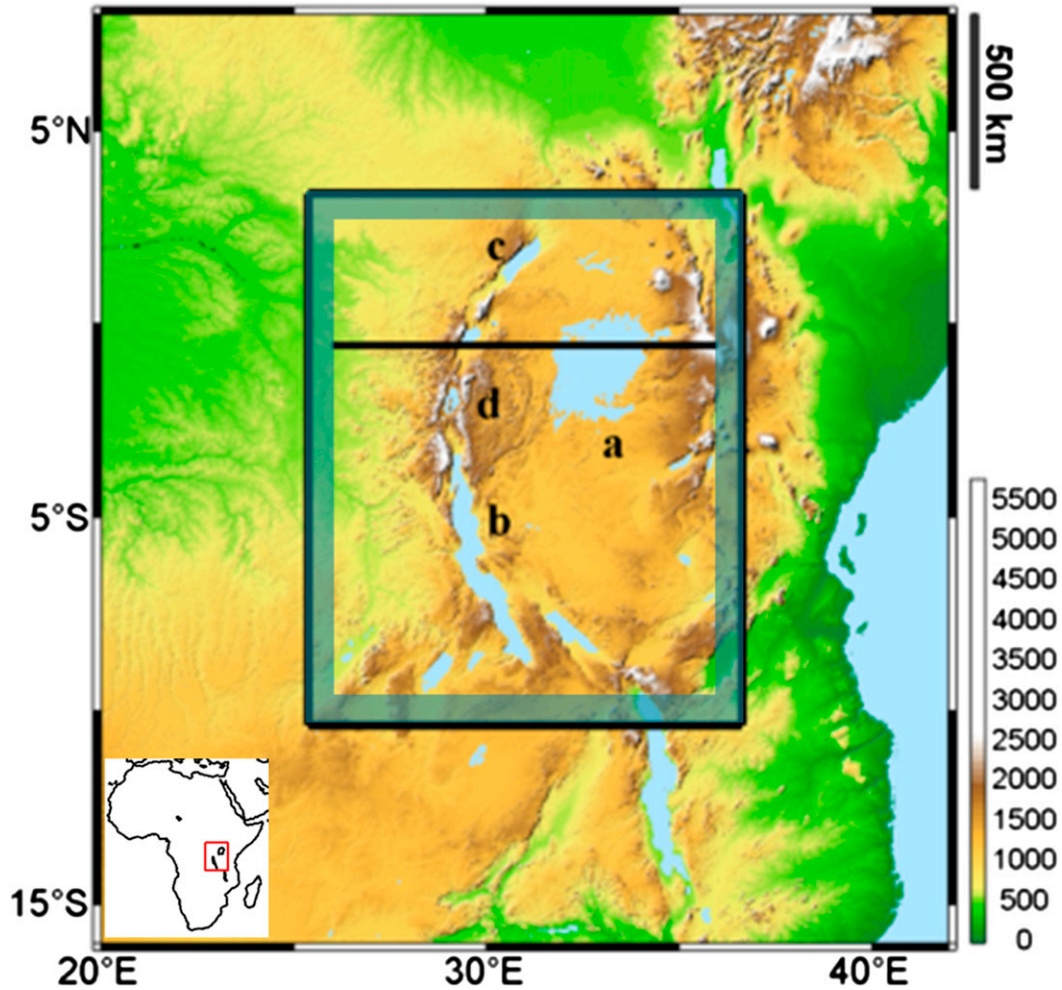


FIG. 1. Shuttle Radar Topography Mission (SRTM) surface height (m) over the African Great Lakes region. The model domain used in this study is denoted by the black rectangle (10.375°S – 3.375°N , 25.375°E – 36.625°E ; center at 3.5°S , 31°E) and a 10-gridpoint-wide zone excluded from the analysis by the blue band. The transect (26° – 36°E , 0.55°S) used for the vertical cross section in Figs. 13 and 14 is shown by the black line. The four largest African Great Lakes within the model domain are (a) Lake Victoria, (b) Lake Tanganyika, (c) Lake Albert, and (d) Lake Kivu.

exhibits a cold lake temperature bias over the AGL (Thiery et al. 2014b). As recommended by Thiery et al. (2014a), the lake temperature profile is initialized with stratified conditions, an approach also adopted by Hernández-Díaz et al. (2013). (iii) Last, certain model settings (e.g., time step, number of vertical layers, and width of the relaxation layer) were adapted to be consistent with the higher horizontal grid resolution.

d. Evaluation datasets

The performance of the CTL simulation is assessed by comparing model output to observational products for various quantities (see Table 1 for their technical specifications). For precipitation, we use gridded datasets from the following sources: the Global Precipitation

Climatology Project (GPCP; Huffman et al. 2001), the Global Precipitation Climatology Centre (GPCC; Rudolf et al. 2011), the University of Delaware (UDEL; Legates and Willmott 1990), the Climate Prediction Center Morphing Technique (CMORPH; Joyce et al. 2004), and satellite-derived precipitation rates from the Tropical Rainfall Measurement Mission (TRMM) products 3B42 and 2B31 (Kummerow et al. 2000). The TRMM 2B31 product is a combined rainfall-profile product derived from the Precipitation Radar and TRMM Microwave Imager (Bookhagen and Strecker 2008). Since the standard TRMM precipitation product (3B42) and CMORPH demonstrate poor performance over complex African terrain (Dinku et al. 2008), the TRMM 2B31 product is preferred over 3B42, given the

TABLE 1. Data products used for model evaluation (SRes.: spatial resolution; TRes.: temporal resolution).

Variable, symbol (units)	Dataset	Version	Source	SRes.	TRes.	Years	References
Precipitation, P (mm month ⁻¹)	TRMM	3B42	Mixed	0.25°	Monthly	1999–2008	Kummerow et al. (2000)
—	TRMM	2B31	Satellite	~0.04°	~1.5-hourly	1999–2008	Kummerow et al. (2000)
—	GPCP	IDD	Mixed	1.00°	Daily	1999–2008	Huffman et al. (2001)
—	GPCC	v6	Stations	0.50°	Monthly	1999–2008	Rudolf et al. (2011); Schneider et al. (2014)
—	UDEL	v3.01	Stations	0.50°	Monthly	1999–2008	Legates and Willmott (1990)
—	CMORPH	ds502.0	Mixed	0.25°	3-hourly	2003–08	Joyce et al. (2004); Climate Prediction Center (2011)
—	in situ	—	Stations	—	Daily	1999–2008	Nyeko-Ogramoi et al. (2010, 2013)
Near-surface temperature, T_{2m} (K)	in situ	—	Stations	—	Daily	1999–2008	Plisnier et al. (2000)
Lake surface temperature, T_S (K)	ARC-Lake	v1.1.2	Satellite	0.05°	Variable	1999–2008	MacCallum and Merchant (2012)
Lake water temperature, $T_{0.5m}$ (°C)	in situ	—	Stations	—	Bimonthly	1999–2008	Plisnier et al. (2009); Darchambeau et al. (2014)
Surface net shortwave radiation, SW_{net} (W m ⁻²)	GEWEX-SRB	REL3.0	Satellite	1.0°	Monthly	1999–2007	Stackhouse et al. (2011)
Surface net longwave radiation, LW_{net} (W m ⁻²)	GEWEX-SRB	REL3.1	Satellite	1.0°	Monthly	1999–2007	Stackhouse et al. (2011)
Latent heat flux, LHF (W m ⁻²)	LandFlux-EVAL	—	Mixed	1.0°	Monthly	1999–2005	Mueller et al. (2013)
Sensible heat flux, SHF (W m ⁻²)	FLUXNET-MTE	—	Stations	0.50°	Monthly	1999–2008	Jung et al. (2010)
Cloud cover fraction, CCF (%)	ISCCP	D2	Satellite	2.5°	Monthly	1999–2008	Rosow and Schiffer (1999)

higher spatial resolution and ability to reproduce orographically induced precipitation patterns over complex terrain (Bookhagen and Burbank 2006; Bookhagen and Strecker 2008; Burbank et al. 2012). The high-spatial-resolution TRMM 2B31 1999–2008 data were reprojected from their original 4.3–5-km resolution to the 0.0625° grid using a bilinear interpolation algorithm to account for projection and resolution inhomogeneities (Bookhagen and Strecker 2008). The precipitation rates (mm h⁻¹) from each satellite overpass (~16 day⁻¹) were subsequently rescaled to monthly mean precipitation values using the number of measurements within each grid cell, after which a convolution filter with a 5 × 5 equal weights window was applied. Note that no further calibration of the data was performed. Finally, a dataset of in situ daily accumulated precipitation measurements was compiled. A similar approach was followed for observed monthly and daily mean near-surface temperature observations; however, measurements of this type are very sparse in the region.

Particular attention is paid to the model's ability to reproduce observed lake surface water temperatures (LSWT), using both in situ and satellite measurements as a reference. To this end, the Along-Track Scanning Radiometers (ATSR) Reprocessing for Climate: LSWT and ice cover (ARC-Lake) project provides high-resolution, spatially explicit global LSWT observations (MacCallum and Merchant 2012). The lake temperature evaluation is complemented using 419 conductivity–temperature–depth (CTD) casts collected during daytime at three multiyear monitoring sites: Ishungu (Lake Kivu), Kigoma (Lake Tanganyika's northern basin) and Mpulungu (Lake Tanganyika's southern basin) (Plisnier et al. 2009; Darchambeau et al. 2014). Vertical piecewise cubic Hermite interpolation (increment 0.1 m; De Boor 1978) was applied to each cast, after which the near-surface water temperature (0.5 m) was extracted and used as a reference. This depth is assumed to be the depth closest to the surface with a reliable measurement from the CTD cast.

The net surface shortwave (SW_{net}) and longwave (LW_{net}) radiation, latent heat flux (LHF), and sensible heat flux (SHF) were compared to satellite-derived values available from the Global Energy and Water Cycle Experiment Surface Radiation Budget (GEWEX-SRB; Stackhouse et al. 2011), the benchmark synthesis of available diagnostic evapotranspiration estimates (LandFlux-EVAL; Mueller et al. 2013), and the global upscaling of observations from eddy-covariance flux towers using the Flux Network Multi-Tree Ensembles (FLUXNET-MTE; Jung et al. 2010), respectively. The MTE approach represents a machine learning algorithm integrating in situ flux measurements with satellite

observations and surface meteorological data to produce global gridded evapotranspiration estimates and associated uncertainties (Jung et al. 2009). Finally, the cloud cover fraction (CCF) is evaluated using the International Satellite Cloud Climatology Project (ISCCP) D2 dataset (Rossow and Schiffer 1999).

All gridded datasets used are available for the entire analysis period, except for CMORPH (2003–08), LandFlux-EVAL (1999–2005), and GEWEX-SRB (1999–2007). Aside from ARC-Lake, their horizontal resolution is usually much coarser than the CTL simulation (Table 1). No height correction, gap filling, or other modifications were applied to the various datasets. The COSMO-CLM² rotated model grid is considered as the reference grid to which all other gridded products are remapped using bilinear interpolation. Evaluation with in situ data is performed by comparing the observed time series to the model grid box encompassing the measurement site.

e. Surface energy balance decomposition

The energy balance at the surface–atmosphere interface is given by

$$\epsilon\sigma T_s^4 = (1 - \alpha)SW_{in} + LW_{in} - LHF - SHF - G, \quad (1)$$

where ϵ is the surface emissivity, σ is the Stefan–Boltzmann constant ($5.67 \times 10^{-8} \text{ W m}^{-2} \text{ K}^{-4}$), T_s is the surface temperature, α is the surface albedo with respect to shortwave radiation, SW_{in} is the incoming shortwave radiation, LW_{in} is the incoming longwave radiation, LHF and SHF are the turbulent fluxes of latent heat and sensible heat, and G is the combined subsurface storage and conductive heat fluxes.

The causes for the surface temperature response to the presence of lakes are investigated using a surface energy balance decomposition method developed by Juang et al. (2007) and further modified by Luyssaert et al. (2014) and Akkermans et al. (2014). The net impact of the AGL on surface temperature is decomposed a posteriori and attributed to direct contributions of modified biogeophysical processes (such as surface reflection and evapotranspiration) and indirect contributions due to atmospheric feedbacks (such as cloud radiative feedbacks or surface layer stability changes).

The net change in outgoing longwave radiation is given by $4\epsilon\sigma T_s^3 \delta T_s$; that is, the first-order derivative of the left hand side in Eq. (1) with respect to T_s . Note that here, the term surface temperature (T_s) denotes the surface radiative temperature at which the soil–vegetation–lake complex emits longwave radiation to the atmosphere. From this, δT_s can be derived by solving the total derivative of the Eq. (1) and solving for δT_s :

$$\delta T_s = \frac{1}{4\epsilon\sigma T_s^3} [-SW_{in}\delta\alpha + (1 - \alpha)\delta SW_{in} + \delta LW_{in} - \delta LHF + \delta SHF - \delta G - \sigma T_s^4 \delta\epsilon], \quad (2)$$

with δSHF encompassing the SHF changes induced by the modified aerodynamic resistance and the modified temperature gradient. Most terms in Eq. (2) can be calculated from the difference between mean quantities in the control and no-lake simulation (CTL minus NOL), except for $\delta\epsilon$, which is recomputed from the model equations.

3. Results

a. Model evaluation

1) PRECIPITATION AND AIR TEMPERATURE

Observed precipitation patterns are reasonably reproduced by COSMO-CLM², in terms of spatial patterns (Fig. 2) as well as the amplitude and phase of the annual cycle (Fig. 3). The model captures the enhanced precipitation in the northwestern part of the domain, associated with strong orographically induced convection in a region where tropical rainforest is the dominant land cover type (Figs. 2a–g). However, the disagreement between the various observational products regarding the magnitude of precipitation over this part of the domain is large (with differences locally exceeding 3900 mm yr^{-1} ; Fig. 2h), and the bias is either positive or negative, depending on the benchmark product considered. Generally, the limited number of rain gauges within the model domain and the numerous data gaps in the available time series call for cautious use of gridded precipitation datasets based on in situ measurements, but also satellite-based or mixed-source products contain important uncertainties over the mountainous regions of tropical Africa (e.g., Dinku et al. 2008; Nikulin et al. 2012; Endris et al. 2013; Sylla et al. 2013). Furthermore, COSMO-CLM² is able to reproduce the higher precipitation observed by TRMM 3B42 and TRMM 2B31 over some AGL, especially during the wet seasons [March–May (MAM) and October–December (OND), see below]. In particular, the strong precipitation signal over Lake Kivu is reproduced, while the spatial pattern of precipitation over Lake Victoria is reproduced but underestimated relative to both TRMM products. The dry bias over Lake Victoria relative to TRMM 3B42 and 2B31 amounts to -493 mm yr^{-1} (-24%) and -691 mm yr^{-1} (-30%), respectively, and is centered over the western half of the lake, as the modeled precipitation maximum is shifted towards the northeast. Relative to GPCP and CMORPH, in contrast, COSMO-CLM² overestimates precipitation over Lake Victoria by 217 mm yr^{-1} (16%) and 250 mm yr^{-1}

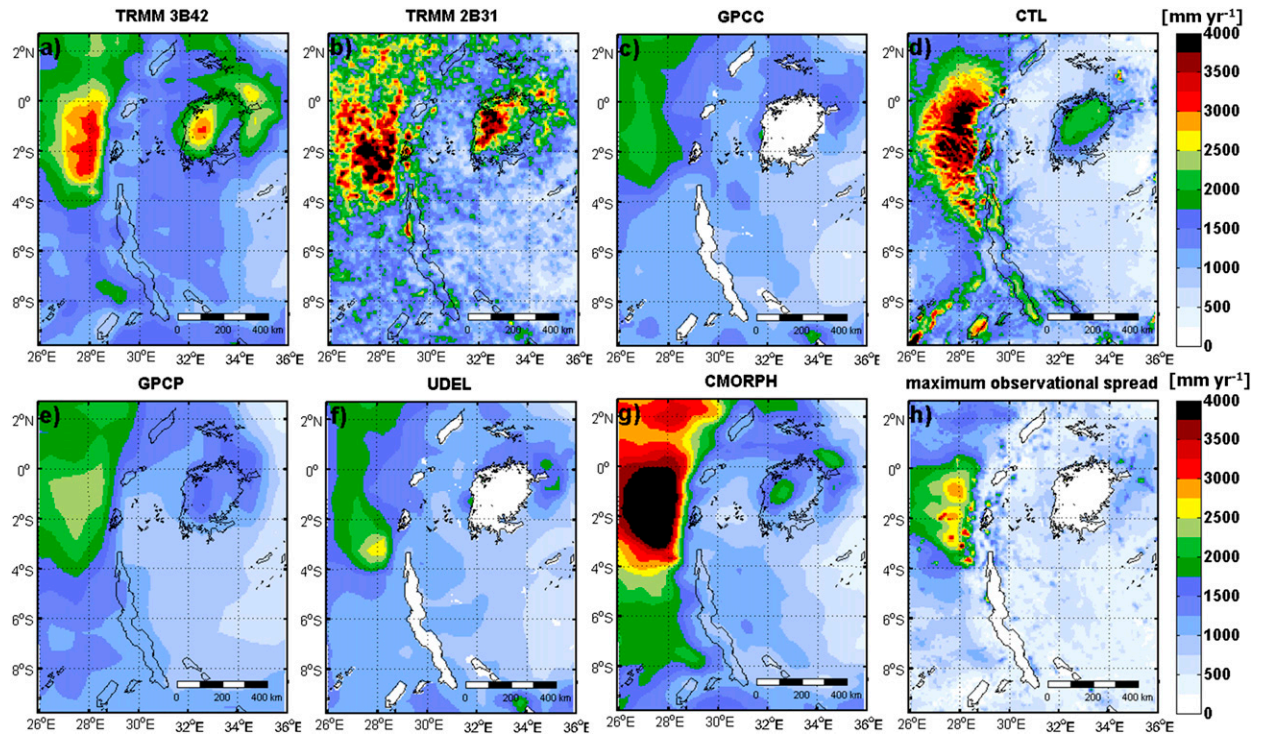


FIG. 2. Observed annual mean precipitation P (mm yr^{-1}) from the datasets described in Table 1—(a) TRMM 3B42, (b) TRMM 2B31, (c) GPCC, (e) GPCP, (f) UDEL, and (g) CMORPH—averaged over the period 1999–2008 (CMORPH data is averaged over 2003–08). (d) The 1999–2008 modeled P (CTL). (h) Maximum difference among observational products, considering only land pixels. The observational products GPCC and UDEL are masked out over the lakes, as they are based solely on land station data.

(19%), respectively. Again, the maximum difference between the gridded observational products is large (1131 mm yr^{-1} averaged over Lake Victoria; Fig. 2h), and largely exceeds the biases between COSMO-CLM² and individual products. Such a large spread calls for further research to quantify the uncertainties of observed precipitation in the region. Furthermore, over the central plateau, where the observational products agree fairly well, a dry bias is apparent. This is confirmed by the comparison to in situ precipitation records, located mostly on the central plateau (Figs. 4a,b). Over 75% of the domain, the absolute precipitation bias against individual products remains below 185 mm yr^{-1} , corresponding to 13% of the average precipitation observed over the region (observational ensemble mean).

Seasonal precipitation variability in the AGL region is primarily governed by the north–south migration of the intertropical convergence zone (ITCZ) across the region (Nicholson 1996; Williams et al. 2015). Monthly mean precipitation subsequently indicates a bimodal distribution with a distinct dry season during June–August (JJA) and two wet seasons: MAM (long rains; northward ITCZ migration) and OND (short rains; southward ITCZ migration), separated by the slight

decrease in rainfall during January–February (JF) (little dry season; Fig. 3). The annual cycle of precipitation is reasonably captured by COSMO-CLM²; averaged over the entire domain, fair correspondence exists between

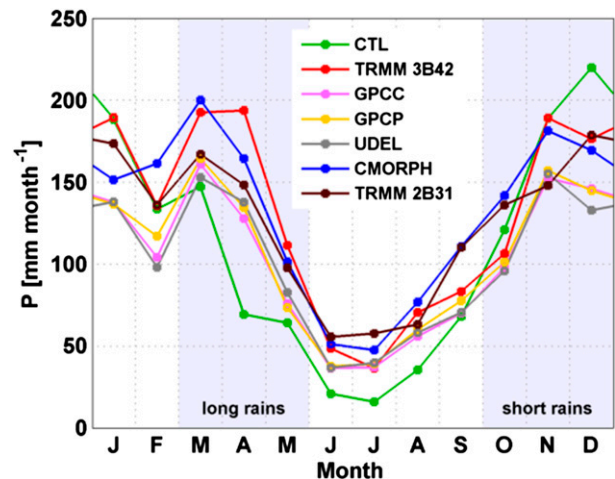


FIG. 3. Observed and modeled domain-averaged seasonal precipitation cycles (mm month^{-1}) over the period 1999–2008 (CMORPH data is averaged over 2003–08).

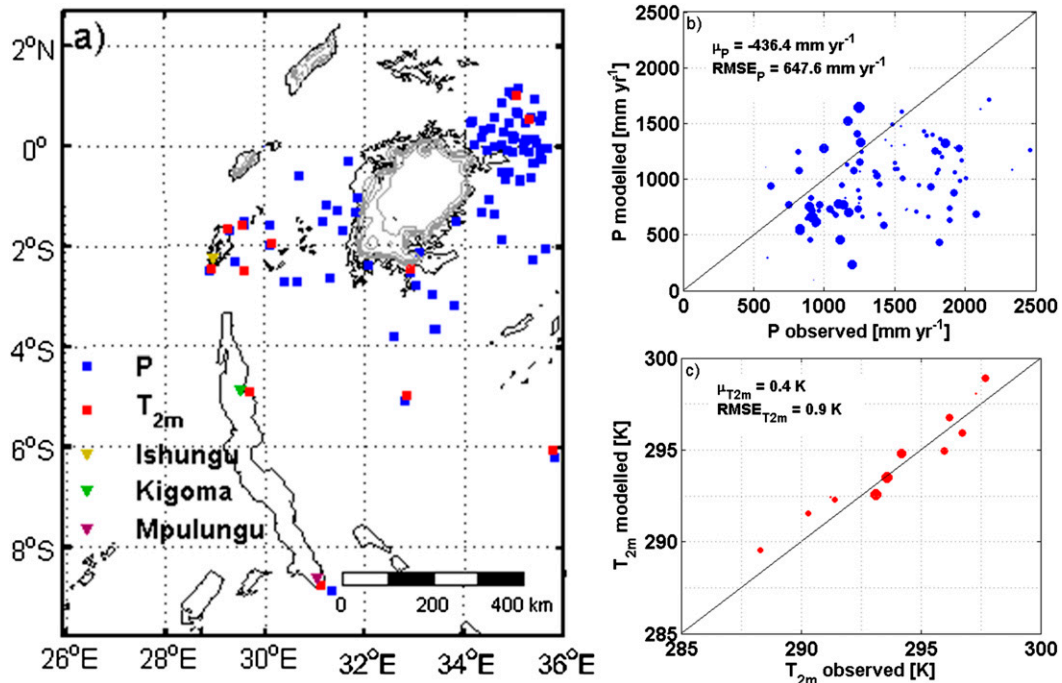


FIG. 4. (a) Map of in situ measurement locations of near-surface temperature T_{2m} (red squares) and precipitation P (blue squares), as well as three lake water temperature monitoring sites (colored triangles; see Fig. 6). Grey lines represent the bathymetry data (Kourzeneva et al. 2012) employed for the COSMO-CLM² CTL simulation (10-m equidistance and lake depths capped at 50 m, resulting in the absence of contours for several deep lakes). Scatter plots of modeled vs observed mean (b) P (mm yr^{-1}) and (c) T_{2m} (K). The variable μ presents the mean difference and RMSE of modeled vs observed P and T_{2m} , respectively. Data gaps in the observations were removed from the corresponding modelled time series. The size of the individual points reflects the availability of data during the analysis period (1999–2008) (the larger, the more data).

the observations and CTL, although precipitation is underestimated in April and during the main dry season. Multiyear monthly accumulated, domain-averaged precipitation biases against individual observational products are smaller than 90 mm month^{-1} during 90% of all months. Furthermore, monthly mean, domain-averaged modelled precipitation values are positively correlated with corresponding observations [significant ($p < 0.001$) Spearman rank correlation of 0.72, 0.85, 0.84, 0.80, and 0.84 with respect to TRMM 3B42, GPCP, GPCP, UDEL, and CMORPH, respectively].

Although very sparse, aggregated daily and monthly mean near-surface temperature observations in the region (T_{2m}) suggest the ability of COSMO-CLM² to reproduce spatial differences in T_{2m} (Fig. 4c). In addition, their annual cycle is well captured by COSMO-CLM², but the magnitude of the seasonality is slightly exaggerated by the model (not shown).

2) LAKE TEMPERATURE

COSMO-CLM² succeeds in reproducing the observed differences in LSWT among four major AGL but

demonstrates a slight warm bias for each of them (0.68 K on average; Figs. 5a–h; Table 2) and overestimates the amplitude of the seasonal LSWT cycle (Figs. 5i–l). Spatial LSWT patterns correspond to observations especially over Lake Victoria and Lake Tanganyika, with statistically significant spatial rank correlations of 0.68 and 0.61, respectively, and to a lesser extent over the other AGL. Over Lake Victoria, COSMO-CLM² suggests a positive temperature gradient from southwest to northeast, with a maximum temperature difference of 1 K. Although this modeled pattern is in contradiction with previous studies (e.g., Song et al. 2004; Anyah et al. 2006; Sun et al. 2014b,a), it matches with the spatial pattern derived from remote sensing (Figs. 5a,e), as well as with recent observations based on water temperature measurements at 48 locations during two cruises in February and August 2000 (MacIntyre et al. 2014). Unlike the observations, COSMO-CLM² furthermore predicts slightly higher lake surface temperatures in coastal zones and embayments as a result of the lower lake depths in these sectors.

The model's ability to reproduce lake surface temperatures is also apparent from the comparison between

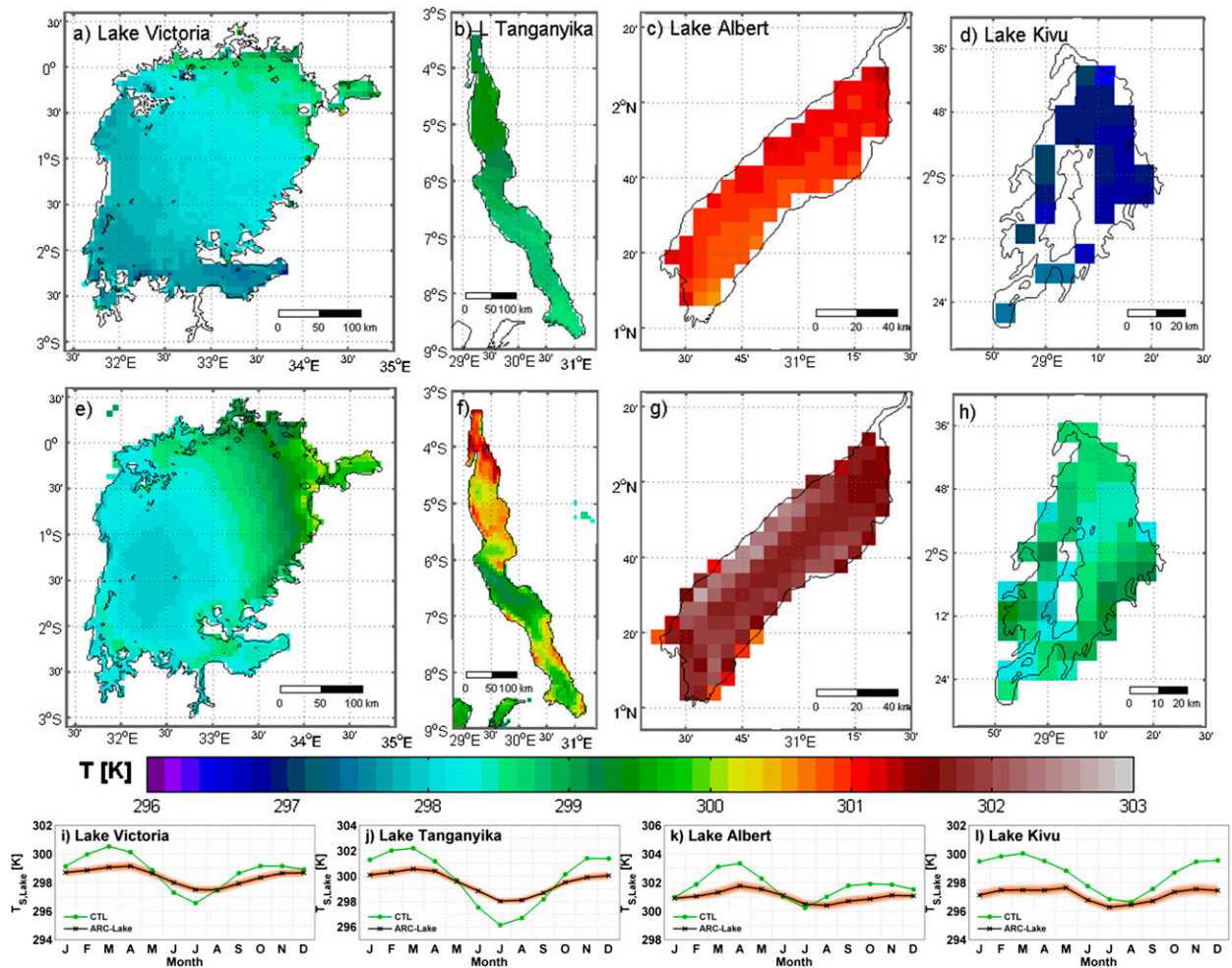


FIG. 5. The 1999–2008 (top) observed LSWT (K) from the ARC-Lake dataset and (middle) modeled LSWT from the COSMO-CLM²CTL simulation for (a),(e) Lake Victoria; (b),(f) Lake Tanganyika; (c),(g) Lake Kivu; and (d),(h) Lake Albert. (i)–(l) Lake-averaged observed (black line) and modeled (green line) monthly mean LSWT, including observational error estimate as provided with the product (red shading).

modeled and observed lake water temperatures at 0.5 m for three multiyear monitoring sites in Lake Kivu and Lake Tanganyika (Fig. 6). FLake reasonably predicts the annual mean 0.5-m lake temperature (with a warm bias of 1.23°, 0.71°, and 0.60°C at Ishungu, Kigoma, and Mpulungu, respectively) and reproduces the phase of the annual cycle but again exaggerates the amplitude of the seasonal temperature variations. Despite this overestimation, FLake captures the increasing seasonal cycle's amplitude with distance from the equator (Fig. 6). As this distance grows, the dry season becomes more pronounced, leading to a stronger evaporative-driven cooling of the lakes' mixed layer (Thiery et al. 2014a). Furthermore, interannual (near) surface lake temperature variability is present but can be considered small compared to the seasonal cycle. Observed anomalies

include the high temperatures during the 2005 long rains at Kigoma relative to the preceding months and the low temperatures during the 2007/08 stratified season at Ishungu (Figs. 6a,b). While the model reproduces the former warm anomaly at Kigoma, it does not predict the cold anomaly at Ishungu.

The overestimation of the annual LSWT cycle is primarily due to the underestimation of the mixed layer depth when stratified conditions are imposed in FLake (Thiery et al. 2014a). For a relatively shallow mixed layer, heat is concentrated in the top of the water column rather than being distributed over a larger volume. This, in turn, causes a stronger temperature response to seasonal changes in the lake's heat content and hence an overestimation of the annual LSWT cycle (Figs. 5i–l). Another potential cause for the remaining biases might

TABLE 2. Bias and spatial RMSE of COSMO-CLM², ERA-Interim, and the CORDEX parent simulation (section 2c) vs various observational products (see Table 1 for an overview).

Physical quantity (units)	COSMO-CLM ²		ERA-Interim		CORDEX	
	Bias	RMSE	Bias	RMSE	Bias	RMSE
TRMM 3B42 precipitation (mm yr ⁻¹)	-261	683	612	881	-717	838
GPCP precipitation (mm yr ⁻¹)	68	631	941	1160	-389	508
GPCP precipitation (mm yr ⁻¹)	30	554	903	1069	-427	519
UDEL precipitation (mm yr ⁻¹)	84	604	957	1167	-373	478
CMORPH precipitation (mm yr ⁻¹)	-330	712	739	907	-771	973
TRMM 2B31 precipitation (mm yr ⁻¹)	-273	678	599	873	-730	927
Ensemble precipitation* (mm yr ⁻¹)	-116	554	757	932	-573	669
GEWEX-SRB SW _{net} (W m ⁻²)	-12	22	39	42	-26	33
GEWEX-SRB LW _{net} (W m ⁻²)	-5	8	-21	24	1	7
LandFlux-EVAL LHF (W m ⁻²)	-22	34	32	35	-27	31
FLUXNET-MTE SHF (W m ⁻²)	10	22	-2	15	6	23
ISCCP CCF (%)	4	7	-1	6	3	6
ARC-Lake LSWT Victoria (K)	0.40	0.53	-4.16**	4.52**	-2.70	2.81
ARC-Lake LSWT Tanganyika (K)	1.09	1.16	-7.58**	7.82**	-3.07	3.35
ARC-Lake LSWT Albert (K)	0.90	0.94	—	—	-5.90	5.94
ARC-Lake LSWT Kivu (K)	1.80	1.83	—	—	-4.19	4.19

* Average of the six gridded precipitation products.

** Given the coarse resolution of this product and associated limited number of lake pixels, nearest neighbour interpolation was used in this case instead of bilinear interpolation.

be the role of three-dimensional water circulation within the larger lakes. For the relatively shallow Lake Victoria, Song et al. (2004) argue that an RCM coupled to a one-dimensional lake model reproduces first-order spatial lake surface temperature patterns but that only a three-dimensional lake model predicts a southwest–northeast heat transport within the lake. In the deep Lake Tanganyika, actual lake

hydrodynamics are still debated (e.g., Naithani et al. 2003; Verburg et al. 2011), but here variable wind forcing (Naithani et al. 2002), differential cooling (Verburg and Antenucci 2010; Verburg et al. 2011), water exchange across the thermocline (Gourgue et al. 2007), and internal Kelvin waves (Naithani and Deleersnijder 2004) may also eventually influence LSWT patterns. Further research could help to

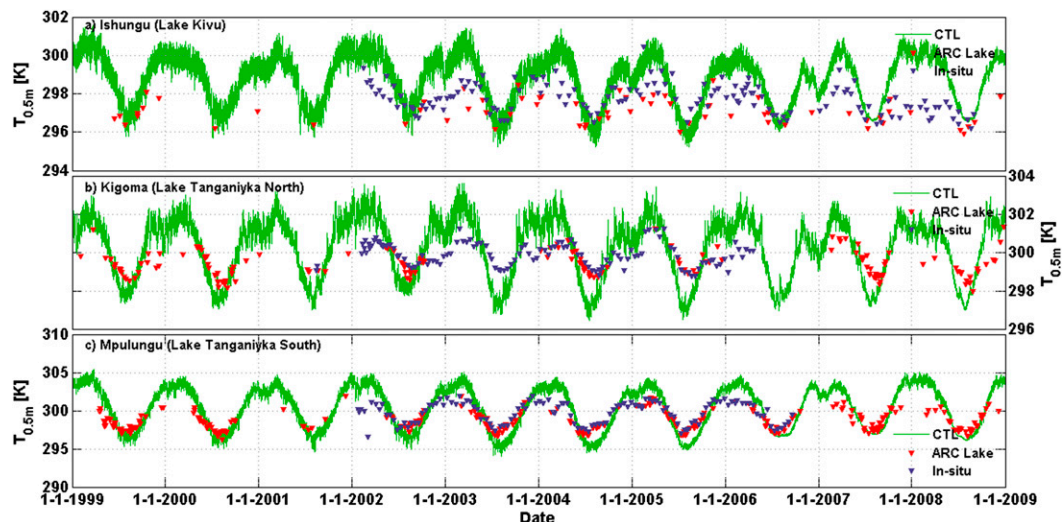


FIG. 6. Modeled (green lines), remotely sensed (ARC-Lake; red triangles) and bimonthly, in situ observed (blue triangles) lake temperatures (K) at (a) Ishungu (Lake Kivu; 2.34°S, 28.98°E), (b) Kigoma (Lake Tanganyika's northern basin; 4.85°S, 29.59°E), and (c) Mpulungu (Lake Tanganyika's southern basin; 8.73°S, 31.04°E) at a depth of 0.5 m (lake surface water temperatures in case of ARC-Lake).

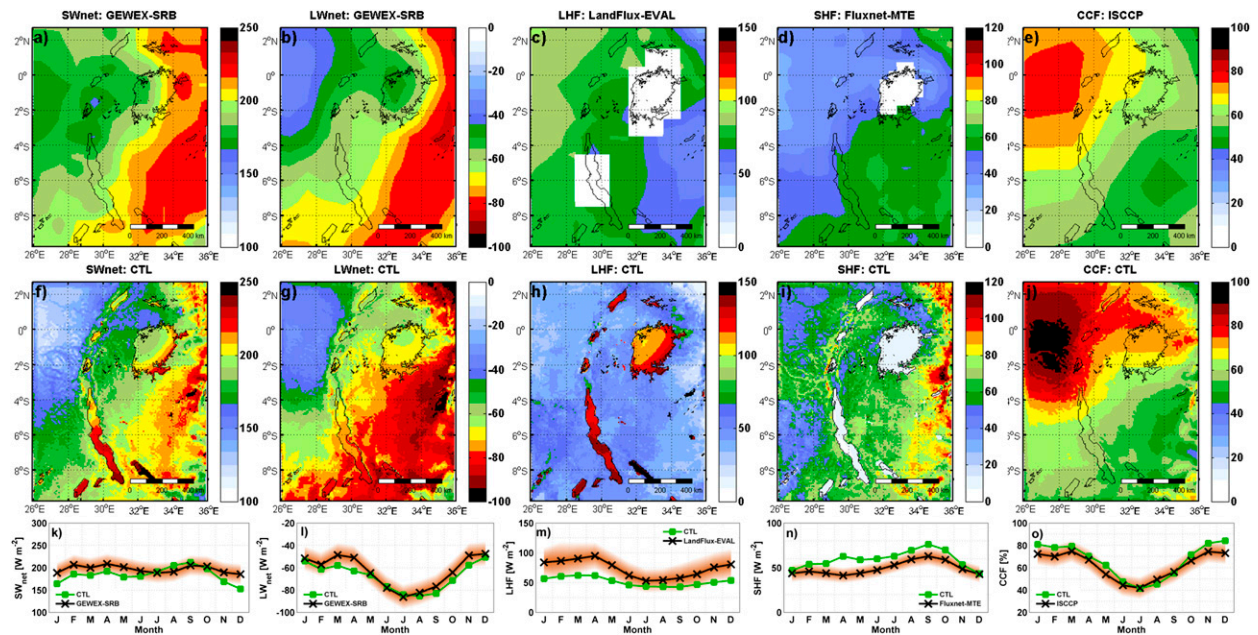


FIG. 7. (top) Observed and (middle) modeled annual mean maps and (bottom) domain-averaged seasonal cycles for (a),(f),(k) SW_{net} ($W m^{-2}$); (b),(g),(l) LW_{net} ($W m^{-2}$); (c),(h),(m) LHF ($W m^{-2}$); (d),(i),(n) SHF ($W m^{-2}$); and (e),(j),(o) CCF (%). The various observational products are described in Table 1, and both observational products and model output are shown for the respective measurement periods [(a),(e) 1999–2008; (b),(c) 1999–2007; and (d) 1999–2005]. For the white areas in (c) and (d), no data is available. The red shading around the observed annual cycle (black line) indicates the observational uncertainty as provided with the products.

discriminate the influence of lake hydrodynamics on lake–atmosphere exchanges for this region.

3) SURFACE ENERGY BALANCE AND CLOUDS

The ability of COSMO-CLM² to represent the surface climate is investigated by evaluating the surface energy fluxes. Good agreement is noted for the surface radiative fluxes, SW_{net} and LW_{net} , both in terms of spatial patterns and the domain-averaged annual cycle, indicating, among other things, the skill of CLM3.5 to simulate spatial and temporal albedo patterns over land (Figs. 7a,b,f,g,k,l). Modeled over-lake variations in SW_{net} (Fig. 7f) are due to spatial cloud cover variability, given the constant water surface albedo employed in FLake (0.07). Furthermore, very good agreement exists between the model and observations for cloud cover fraction (+4% bias; Figs. 7e,j,o; Table 2). The seasonal cycles of LW_{net} and CCF are strongly linked to each other and indicate more longwave radiative energy loss during the main dry season, when lower cloud cover fraction reduces the amount of incoming longwave radiation. During the short rains and the little dry season, a slight overestimation of CCF by $\sim 8\%$ induces a negative LW_{net} bias of $-5 W m^{-2}$ during these months. Lower performance is noted for the turbulent fluxes, LHF and SHF ($-22 W m^{-2}$ and $+10 W m^{-2}$ bias, respectively; Figs. 7c,d,h,i,m,n; Table 2), with generally an

underestimation of LHF and an overestimation of SHF. Possibly, this overestimation of the Bowen ratio is caused by limited soil moisture availability, but given the lack of observational evidence, this is impossible to verify. Overall, domain-averaged monthly mean values for SW_{net} , LW_{net} , LHF, SHF, and CCF are within the observational uncertainty range during 10, 11, 7, 4, and 11 months of the year, respectively.

4) COMPARISON TO ERA-INTERIM AND CORDEX

To put the performance of the COSMO-CLM² CTL simulation into perspective, the same evaluation procedure was repeated for ERA-Interim and the COSMO-CLM CORDEX-Africa evaluation simulation (herein referred to as CORDEX; Panitz et al. 2014), each, respectively, representative of a state-of-the-art global reanalysis product and a continental-scale RCM simulation. Results indicate that COSMO-CLM² largely outperforms ERA-Interim for all considered variables, except for SHF and CCF, where both products depict similar skill (Table 2), and with the seasonal cycles of CCF mostly within the margins of observation uncertainty. Especially for precipitation and lake surface temperatures, COSMO-CLM² demonstrates remarkably lower biases and spatial root-mean-square errors (RMSE) compared to ERA-Interim. Relative to

the CORDEX simulation, the enhanced skill of COSMO-CLM² is also evident for P , SW_{net} , and $LSWT$, whereas LW_{net} , LHF , SHF , and CCF predictions demonstrate similar skill. Several effects are responsible for this enhanced skill. First, relatively few observations are assimilated into ERA-Interim over central Africa, leaving the model to run more freely over this region compared to other parts of the globe. Second, the use of a lake model clearly improves model performance relative to other common techniques, such as the sea surface temperature interpolation employed in ERA-Interim and CORDEX (Balsamo et al. 2012), for instance by reducing the absolute $LSWT$ error over Lake Tanganyika by 86% and 65% relative to ERA-Interim and CORDEX, respectively (Table 2). Third, COSMO-CLM² benefits from the higher resolution relative to ERA-Interim and CORDEX (7 vs 79 and 50 km, respectively), allowing for more finescale circulation and associated precipitation patterns to develop over this complex terrain. Finally, the use of the Community Land Model improves the representation of the land surface albedo and other land surface characteristics relative to the default LSM of COSMO-CLM (Akkermans 2013).

In addition, the evaluation procedure was repeated for the NOL simulation, wherein lakes have been replaced by representative land pixels (see section 2c). The added value of the CTL simulation relative to NOL is apparent especially for precipitation and (lake) surface temperature (not shown). For precipitation, the enhanced skill of CTL can be attributed to the underestimation of the moisture input into the atmosphere in NOL (in the absence of lake evaporation), whereas an underestimation of surface thermal inertia deteriorates surface temperature variability in NOL.

In general, the evaluation results demonstrate that the near-surface climate is well represented by COSMO-CLM², the resolution is sufficient to capture effects of lakes and local orography on precipitation and other atmospheric variables, and the spatial and temporal patterns of the lake surface temperatures as well as differences between individual lakes are well represented by FLake. We therefore conclude that COSMO-CLM² is an appropriate tool to investigate the impact of the AGL on the regional climate.

b. Impact of the African Great Lakes on the regional climate

1) TEMPERATURE

Generally, the AGL clearly cool over-lake near-surface air (Table 3; Fig. 8), with average values of -0.67 , -0.58 , and -0.86 K for Lake Victoria, Lake Tanganyika and Lake Albert, respectively. Locally, the

TABLE 3. Impact of the African Great Lakes on different climatological values (CTL – NOL). ABS and REL denote the absolute and percentage change, respectively, of each given quantity, and * denotes the changes significant at the 5% significance level (two-tailed t test).

Physical quantity [Units]	All pixels		Lake pixels	
	ABS	REL	ABS	REL
Temperature at 2 m (K)	-0.17	-1	-0.57*	-2
Precipitation (mm yr ⁻¹)	59.10	5	712.77*	79
Surface temperature (K)	0.26	1	3.02*	13
Net SW radiation, surface (W m ⁻²)	3.28*	2	30.63*	17
Net LW radiation, surface (W m ⁻²)	-0.23	0	-4.95*	7
Latent heat flux (W m ⁻²)	6.97	15	73.56*	142
Sensible heat flux (W m ⁻²)	-4.34	-7	-52.36*	-85
Sea level pressure (hPa)	0.15	0	0.43*	0
Cloud cover fraction (%)	-0.05	0	-0.94	-1
evaporation (mm yr ⁻¹)	87.96	15	927.9*	142

cooling exceeds -1.5 K over each of these lakes, and -2 K over Lake Victoria. An interesting exception to this general pattern is Lake Kivu, where the lake presence induces an average warming of over-lake T_{2m} by $+0.75$ K relative to the NOL simulation. In section 3c, we further investigate causes of the temperature impact induced by the AGL.

Besides cooling the over-lake surfaces, the AGL also have a pronounced downwind influence on T_{2m} , as the cooler temperatures are advected by the daytime lake breeze into the adjacent land. This is especially visible north of Lake Victoria and around Lake Tanganyika and results in a domain-averaged cooling of -0.17 K. In contrast, the central part of the Albertine Rift mountains [e.g., Rwenzori (0.0° – 0.8° N, 29.7° – 30.2° E) and Virunga (1.3° – 1.6° S, 29.1° – 29.7° E) mountain ranges] block all near-surface atmospheric circulation and thereby constrain the influence of Lake Albert, Lake Edward, and Lake Kivu to their direct surroundings. Likewise, the steep topography surrounding Lake Tanganyika [e.g., Itombwe (2.5° – 4.5° S, 28.5° – 29.1° E), Kibira (2.2° – 3.8° S, 29.1° – 29.6° E), and Mahale (6.0° – 6.5° S, 29.7° – 30.1° E) Mountains] limits its cooling influence to the lower inland (Figs. 1, 8). The central plateau south of Lake Victoria is also not influenced by the lake presence, given the predominantly southeasterly flow in this part of the domain. These elements highlight that distance from the lake is not the only decisive factor determining the lake influence on T_{2m} but that topography and atmospheric circulation also play a major role.

The lake influence on T_{2m} is characterized by a clear seasonal pattern, with stronger cooling in the months following the main dry season (August–October: -1.4 K

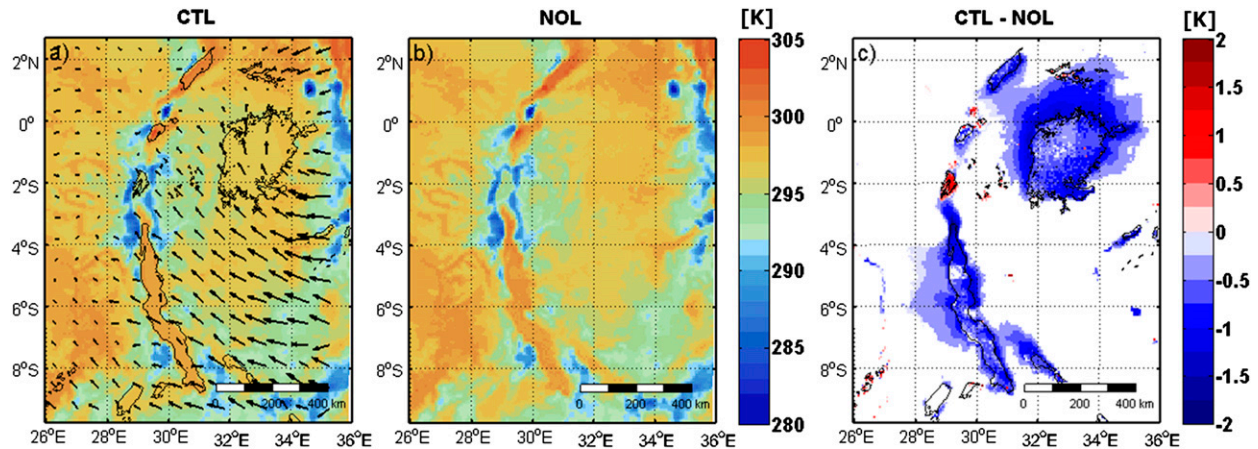


FIG. 8. Impact of the AGL on 2-m air temperature T_{2m} . Shown are annual mean T_{2m} (K) for the (a) CTL and (b) NOL simulations; (c) statistically significant changes at the 5% significance level (CTL – NOL; two-tailed t test) over the period 1999–2008. Temporally averaged 10-m wind vectors from the control simulation are shown in (a).

over the AGL vs -0.3 K during the remaining months; Figs. 10a,d), caused by seasonally variable land–water temperature contrasts. Near-surface water temperature variability in the AGL is primarily governed by LHF, for which the lake-induced change peaks during the main dry season (JJA; Figs. 10c,f) as near-surface relative humidity drops and induces the evaporative cooling of the lake surfaces (Savijärvi and Järvenoja 2000; MacIntyre 2012; Schmid and Wüest 2012; Thiery et al. 2014a). Land temperatures follow a similar seasonal pattern, but increase more rapidly at the end of the dry season because of their relatively low heat capacity. Hence, the largest land–lake temperature contrast and associated lake cooling effect is found from August to October. For similar reasons, the strongest AGL cooling occurs during daytime (0700–1600 UTC), because at

night lakes have a warming effect (1800–0500 UTC; Figs. 10g,j).

2) PRECIPITATION

As a result of the lakes' presence, modeled precipitation is enhanced by 59 mm yr^{-1} (+5%) on average over the model domain, by 713 mm yr^{-1} (+79%) over all lake pixels, and by 732 mm yr^{-1} (+87%) over the four major AGL (Table 3; Fig. 9). The largest increase is noted over Lake Kivu ($+1373 \text{ mm yr}^{-1}$ or +145%), whereas the three other major AGL induce similar absolute increases over their surface [$+706 \text{ mm yr}^{-1}$ (+85%), $+745 \text{ mm yr}^{-1}$ (+82%), and $+647 \text{ mm yr}^{-1}$ (+112%) over Lake Victoria, Lake Tanganyika, and Lake Albert, respectively]. The smaller lakes within the model domain generate similar increases, except for

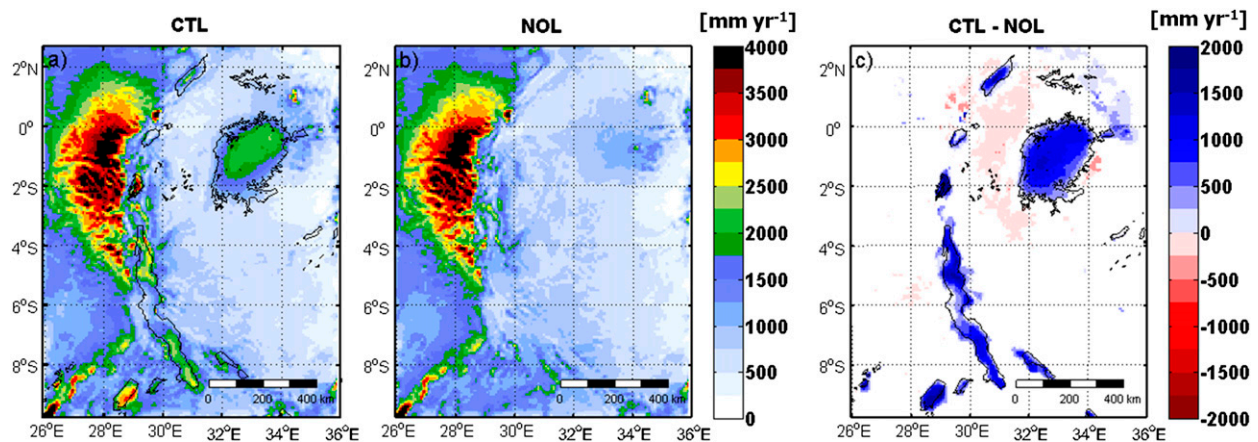


FIG. 9. Impact of the AGL on precipitation. Shown are annual mean P (mm yr^{-1}) for the (a) CTL and (b) NOL simulations; (c) statistically significant changes at the 5% significance level (CTL – NOL; two-tailed t test) over the period 1999–2008.

Lake Edward, which does not produce any additional precipitation according to COSMO-CLM².

In contrast to the influence of the lakes on T_{2m} , the precipitation impact is very localized and mostly limited to the lake itself (Fig. 9c). Over Lake Victoria, lake-induced precipitation increases from southeast to northwest, demonstrating the nonuniform response of the atmospheric column to the presence of the lake, in line with Anyah and Semazzi (2004). Over Lake Tanganyika, the increase in precipitation over the central part is absent or weak compared to the northern and southern sectors. In this part of the lake, a narrow corridor induces relatively strong dry season winds (see also Savijärvi and Järvenoja 2000), which transport over-lake air masses westward into the Congo basin (see also Fig. 8a). The differential spatial impact patterns confirm that next to changes in evapotranspiration, temporal patterns and changes in circulation induced by the AGL also play a dominant role in redistributing precipitation (Datta 1981; Savijärvi 1997; Savijärvi and Järvenoja 2000; Song et al. 2004; Anyah and Semazzi 2004; Anyah et al. 2006; Anyah and Semazzi 2007, 2009; Williams et al. 2015). Our findings furthermore suggest that onshore pluviometer measurements will never fully capture precipitation effects induced by the AGL. The dynamical response to lake presence is further investigated in section 3d.

Precipitation over the AGL displays a distinct diurnal cycle, with precipitation occurring mostly at night and morning hours over the lakes (0000–0900 UTC). This is in general agreement with observations from a pluviometer representative of the central Lake Victoria (Datta 1981). For the surrounding land, in contrast, the precipitation maximum occurs around local noon (0700–1200 UTC; Figs. 10h,k). The nighttime precipitation maximum is enabled by the sustained evaporation from the lakes throughout the whole day. This is not the case for the land evapotranspiration, which displays a clear maximum during the local afternoon and slightly lags the precipitation peak (Figs. 10i,l). Overall, the AGL generate a total moisture input into the atmosphere of $222 \text{ km}^3 \text{ yr}^{-1}$, which is $134 \text{ km}^3 \text{ yr}^{-1}$ more than the equivalent land surface (+151%). This increase is more than sufficient to explain the enhanced over-lake precipitation production ($+99 \text{ km}^3 \text{ yr}^{-1}$), both on daily and subdaily time scales. On seasonal scales, the impact on precipitation is lowest during the main dry season (JJA: $+7 \text{ mm month}^{-1}$ over the AGL vs $+77 \text{ mm month}^{-1}$ during the remaining months).

c. Decomposing the lake-induced surface temperature change

An overview of the net changes in the main components of the surface energy balance induced by the lake

presence, for all pixels and lake pixels only, is provided in Figs. 11a and 11c, respectively. The increase in net shortwave radiation ($\delta \text{SW}_{\text{net}}$) is caused by the lower albedo of water relative to the surrounding land (-0.12) and reduced cloud cover during daytime. Furthermore, as lakes evaporate at the potential evaporation rate, they enhance evapotranspiration (LHF) relative to the surrounding land, while SHF is reduced (Table 3).

The seven factors contributing to a change in surface temperature are described in Eq. (2) and are expressed in Kelvin. The parameters and flux components responsible for these forcings are shown with their corresponding forcing in Figs. 11b,d. Note that the temperature imbalance is only 0.005 and 0.002 K for the all-pixels and lake-pixels case, respectively, demonstrating balance closure for the depicted components.

Lakes are darker and therefore reflect less incoming radiation, resulting in a positive contribution to δT_s from changing albedo of $+0.51 \text{ K}$ over the whole domain and $+4.91 \text{ K}$ over the lakes (Figs. 11b,d: α). On the other hand, the contribution to δT_s caused by the higher surface longwave emissivity of water relative to the surrounding vegetation is negligible (Figs. 11b,d: ϵ). A strong increase in evaporation from the lakes contributes to a lower δT_s by -1.30 K over the whole domain and up to -12.21 K over the lakes and forms the largest individual contribution to δT_s (Figs. 11b,d: LHF). Note that, since the change in evapotranspiration is influenced by the latent heat of vaporization and air saturation (in turn, depending on temperature), it is impossible to distinguish between direct and indirect components in the case of LHF (Akkermans et al. 2014). The lower roughness length of the lake surface relative to vegetated land increases aerodynamic resistance and therefore slows down the turbulent heat transfer from the surface to the atmosphere. The upward SHF is also modified by a changing temperature gradient within the atmospheric surface layer. Together, both processes induce a warming of the surface by $+0.81 \text{ K}$ over the whole domain, and $+8.64 \text{ K}$ over the AGL, thereby presenting the strongest positive impact of T_s (Figs. 11b,d: SHF). Furthermore, since daytime cloud cover over the AGL is not significantly modified ($+2\%$), the contribution of changing incoming shortwave radiation to δT_s is negligible over the AGL (Figs. 11b,d: SW_{in}). The same can be said for the contribution from changing incoming longwave radiation, a feedback depending both on cloud cover and atmospheric temperature (Figs. 11b,d: LW_{in}). Finally, the impact of a changing subsurface heat flux represents a small positive contribution to δT_s (Figs. 11b,d: G).

As expected, the temperature impact of lake presence is much larger over the AGL compared to the rest of the

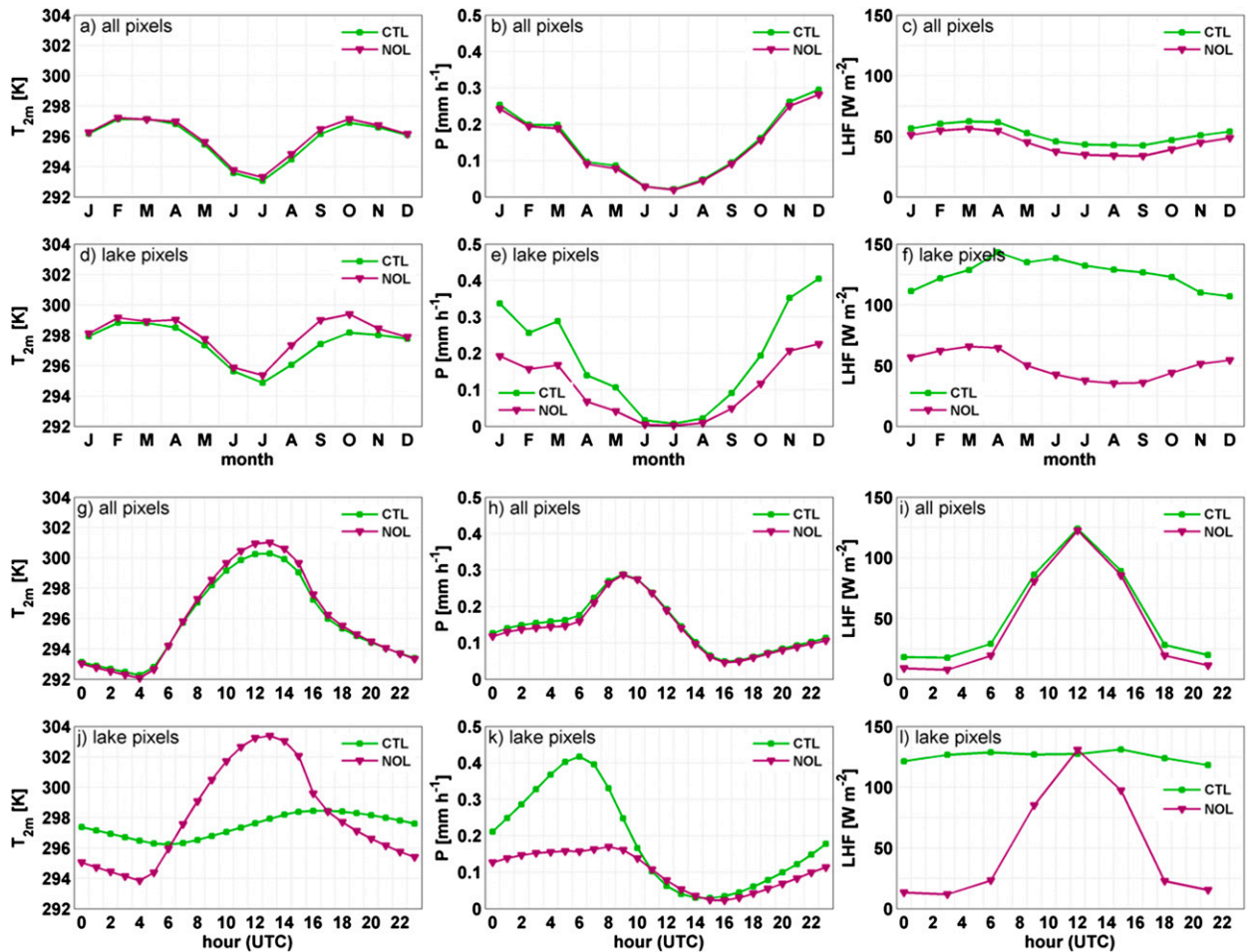


FIG. 10. Domain-averaged seasonal cycle over the period 1999–2008 for (a) T_{2m} (K), (b) P (mm h^{-1}), and (c) LHF (W m^{-2}) from the CTL and NOL simulations (green and purple lines, respectively). (d)–(f) As in (a)–(c), but considering only lake pixels in CTL and the corresponding pixels in NOL. (g)–(l) As in (a)–(f), but for the diurnal cycle.

domain (Table 3). However, due to the dynamical changes induced by the AGL and associated changes in near-surface temperature and moisture (see section 3d for a detailed description), some components are altered over land as well. For instance, the warming effect caused by the enhanced daytime incoming solar radiation (SW_{in}) becomes slightly more important when considering the whole domain, while the influence of a change in incoming longwave radiation (LW_{in}) switches sign (Figs. 11b,d).

Altogether, individual contributions to δT_s result in surface temperature increases of 0.26 and 3.02 K over the whole domain and the AGL, respectively (Figs. 11b,d; Table 3). This seems to be in contradiction with the simulated change in T_{2m} , which was shown to decrease on average (Figs. 8, 11b,d; Table 3). This apparent contradiction is, however, solved when comparing the forcing components separately during daytime (0900, 1200, 1500, and 1800 UTC) and nighttime (2100, 0000, 0300, and

0600 UTC; Fig. 12a). Note that the full surface energy balance decomposition method cannot be applied on subdaily time scales due to the lag effect of the heat storage component; hence, δG is computed from Eq. (2) in this case.

Although δT_s and δT_{2m} depict the same sign on subdaily time scales, their magnitudes vary. During daytime, both T_s and T_{2m} are lower in CTL relative to NOL, as a large fraction of the solar energy penetrates the lakes rather than being absorbed at the surface (Fig. 12a: G). At night, when this heat is released again from the mixed layer to the surface, the opposite effect is seen. The contribution of G to δT_s is only partly offset by reduced SHF during daytime and enhanced LHF during nighttime in CTL relative to NOL (Fig. 12a: SHF and LHF). Furthermore, the lake influence on vertical turbulent heat transport explains the differences in magnitude between δT_s and δT_{2m} : during daytime, the strong decrease in SHF over the lakes (shown by the strong

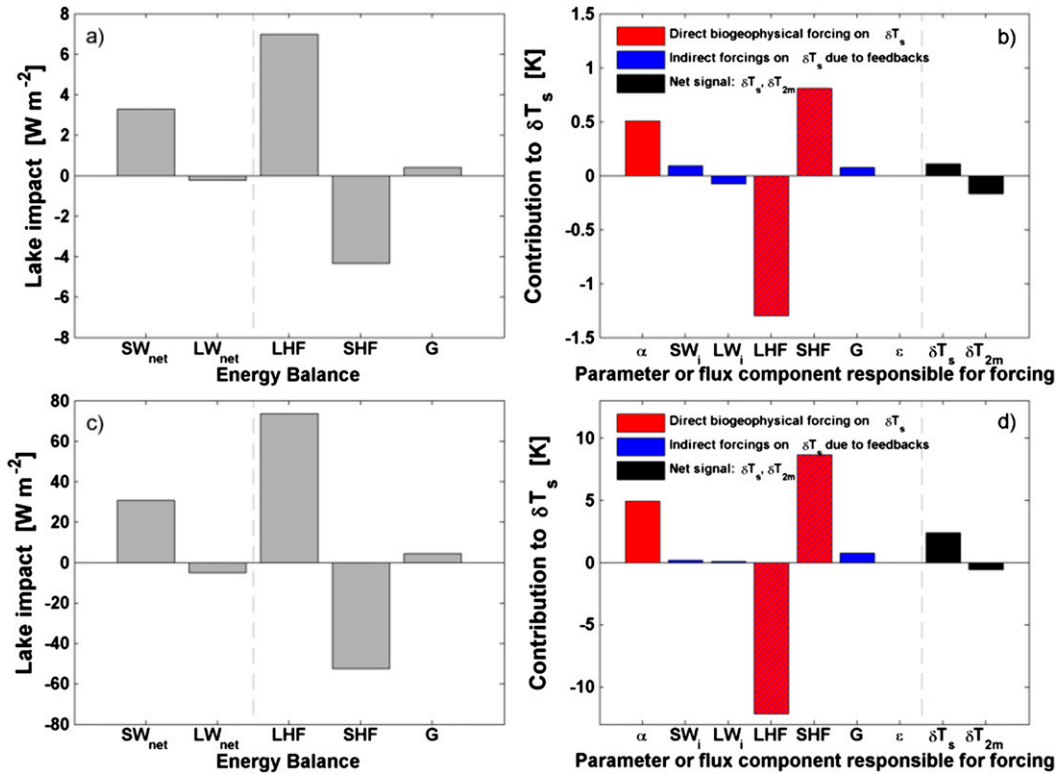


FIG. 11. Lake-induced change in the surface energy balance components SW_{net}, LW_{net}, LHF, SHF, and G for (a) the whole domain and (c) lake pixels only (all units W m⁻²). Individual direct (red), indirect (blue), and mixed (hatched) contributions to δT_s described in Eq. (2) are shown for (b) the whole domain and (d) lake pixels only (all units K). Each contributing factor is indicated by its corresponding responsible parameter or flux component, with α denoting the change in T_s caused by a modified albedo, SW_i by changing incoming shortwave radiation, LW_i by changing incoming longwave radiation, LHF by changing evapotranspiration, SHF_{res} by changing sensible heat flux due to modified aerodynamic resistance, SHF_{imp} by changing sensible heat flux due to temperature gradient, G by changing subsurface heat flux, and ϵ by changing emissivity. Finally, the AGL impact on T_{2m} is also shown.

positive contribution of SHF to δT_s in Fig. 12a) effectively inhibits heat transfer away from the surface—hence, the more pronounced decrease in T_{2m} relative to T_s . At night, the relative contribution to δT_s vanishes as

SHF drops over land while remaining more or less constant over lake surfaces (Fig. 12a), but again low SHF limits warming at 2 meters (see also Fig. 7i). Hence, when considering the whole day, the nighttime warming

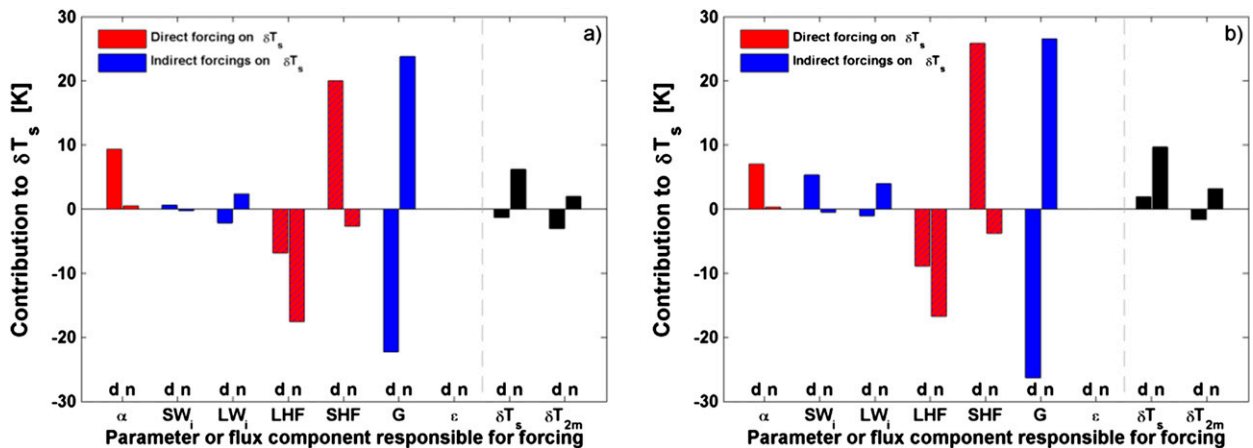


FIG. 12. (a) As in Fig. 11d, but now separately for 0900–1800 UTC (daytime; shown as d) and 2100–0600 UTC (nighttime; shown as n). (b) As in (a), but for Lake Kivu only.

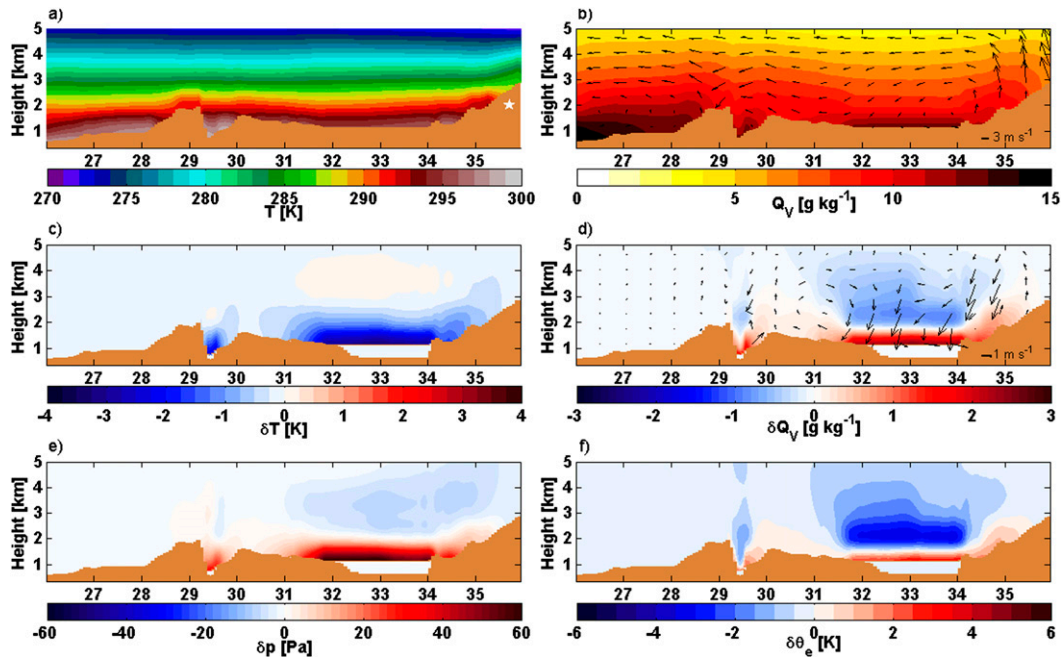


FIG. 13. Vertical cross sections along the transect indicated in Fig. 1 for the 10-yr reference climatologies (CTL, 1999–2008) from 0900–1800 UTC (daytime) of (a) T (K) and (b) Q_V (g kg^{-1}), including longitudinal circulation climatology, and for the mean change due to lake presence (CTL – NOL) in (c) δT (K); (d) δQ_V (g kg^{-1}) due to heat low-induced net convergence at lower levels, as indicated by arrows; (e) δp (Pa); and (f) $e \delta \theta_e$ (K). Lake depth and vertical wind velocity were height exaggerated by factor 10 and 200, respectively. The white star in (a) denotes the Kenyan Rift Valley mountains.

dominates δT_s , whereas the daytime cooling dominates δT_{2m} (Figs. 11d, 12a).

Lake Kivu constitutes an interesting exception, as argued in sections 3b(1) and 3b(2), given the positive T_{2m} anomaly and strong precipitation increase generated by its presence (Figs. 8, 9). The reasons for this behavior become apparent when applying the surface energy balance decomposition method to this lake alone. Over Lake Kivu, daytime T_s increases as SHF is strongly dampened during this time (+25.81 K contribution to δT_s ; Fig. 12b). Furthermore, the lake presence lowers daytime cloud cover and therefore enhances solar radiation input. Both effects are only partly offset by changes in other contributions to δT_s (Fig. 12b: G , α , and LHF). At night, the heat release from Lake Kivu is modeled to be more effective relative to the other AGL, further strengthening the nighttime warming influence. The different response of the various surface energy balance components is likely caused by the high altitude of Lake Kivu (1463 m MSL) relative to other AGL. In our simulation, the surface layer over Lake Kivu is predicted to be very unstable, with an average 3.4-K temperature difference between the lake surface and 2-m level (relative to 1.7, 1.7, and 1.2 K over Lake Victoria, Lake Tanganyika, and Lake Albert, respectively).

Overall, the absence of daytime T_s cooling and strong nighttime T_s warming in CTL relative to NOL causes Lake Kivu to display a general warming influence upon the near-surface air. In addition, the strong nighttime warming intensifies the dynamical response to lake presence (see also section 3d), leading to enhanced atmospheric column destabilization (Fig. 15b) and associated precipitation production.

d. Dynamical response to lake presence

The dynamical response of the atmosphere to lake presence is further investigated using a set of vertical cross sections along a transect covering the northern sector of Lake Victoria (Fig. 1). Based on the diurnal variability of lake impact on T_{2m} and precipitation (Figs. 10g–l), we construct two composites of the 1999–2008 3-hourly mean model output, with a first composite averaging output during daytime (0900, 1200, 1500, and 1800 UTC; Fig. 13) and a second during nighttime (2100, 0000, 0300, and 0600 UTC; Fig. 14).

During daytime, the atmospheric temperature decrease induced by the lake extends well beyond its shores and up to ~ 2 -km height above the surface (Fig. 13c). At 2 km MSL, annual average daytime temperature still decreases by around -0.14 K over the

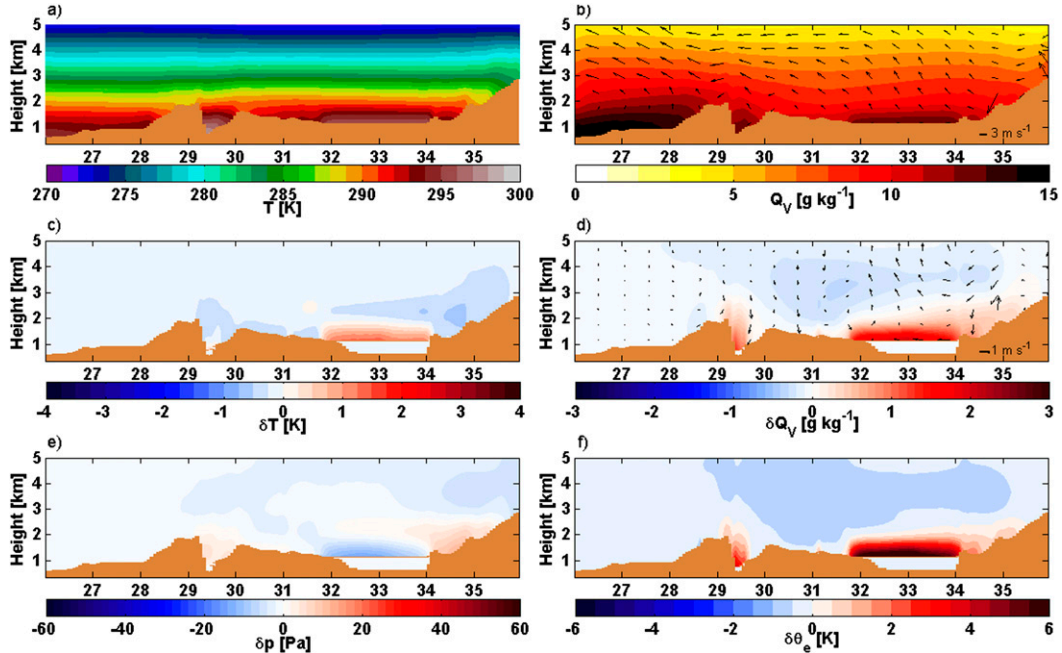


FIG. 14. As in Fig. 13, but from 2100–0600 UTC (nighttime).

whole model domain and by -0.40 K over lake surfaces (both changes statistically significant at the 5% significance level). The pressure increase resulting from this cooling (in excess of $+0.60$ hPa; Fig. 13e) generates a lake breeze between ~ 1 – 2 km MSL across the lake shore towards the western rift valley (Fig. 13d). The lake breeze is offset by updrafts over land and with westerlies at ~ 3 – 5 km MSL and an over-lake, drying subsidence flow closing the secondary circulation cell over Lake Victoria’s western sector (Fig. 13d). Although the moisture buildup in the persistently unstable surface layer (Verburg and Antenucci 2010) tends to destabilize the atmospheric column, the clockwise circulation induces a stabilization of the atmospheric column, especially over the western sector of the lake, as reflected by an increased equivalent potential temperature (θ_e) above ~ 1.5 km MSL and extending up to ~ 6 km MSL (Fig. 13f):

$$\theta_e = \left(T + \frac{L_v}{c_p} q_v \right) \left(\frac{p_0}{p} \right), \quad (3)$$

where L_v is the latent heat of evaporation (2.50×10^6 J kg $^{-1}$), c_p is the specific heat capacity of air at constant pressure (1005 J kg $^{-1}$ K $^{-1}$), q_v is the specific humidity (kg kg $^{-1}$), p_0 is the standard reference pressure (1000×10^2 Pa), and p is the surface air pressure (Pa). The θ_e at lower levels enhances as the effect of increased humidity (Fig. 13d) overcompensates the effect of lower temperatures and higher air pressure (Figs. 13c,d). The

stabilization of the air results in a decrease in upward convective mass flux density (i.e. the vertical mass transport per unit area at cloud-base height due to convection; Fig. 15a), less intense convection, and consequently, less rainfall during daytime over the lake. In contrast, the lake presence enhances the convective mass flux density during daytime around the lake (Fig. 15a) and therefore daytime precipitation.

In the eastern lake sector, the vicinity of the Kenyan Rift Valley mountains (Fig. 13a) modifies the classic lake-breeze circulation as observed over the western sector. Here, the primary daytime circulation is one of orographically induced convection (Fig. 13b), associated with an anabatic wind advecting the over-lake moisture upslope up to ~ 3 km MSL, confirming the conclusion from Anyah et al. (2006) that the anabatic daytime circulation is enhanced by the lake breeze. The strengthening of the anabatic component induces near-surface divergence and associated downward secondary flow aloft from ~ 2 to 5 km (Fig. 13d). Consequently, the primary upward motion is already suppressed on-shore, causing less intense stabilization over the eastern sector relative to the western part (Figs. 13d,f) and consequently a more limited decrease in convective mass flux density (Fig. 15a).

At night, the lake surface warms the boundary layer and generates a statistically significant pressure deficit of about -0.12 hPa at the surface (Figs. 14c,e). As a response, the secondary circulation over the western

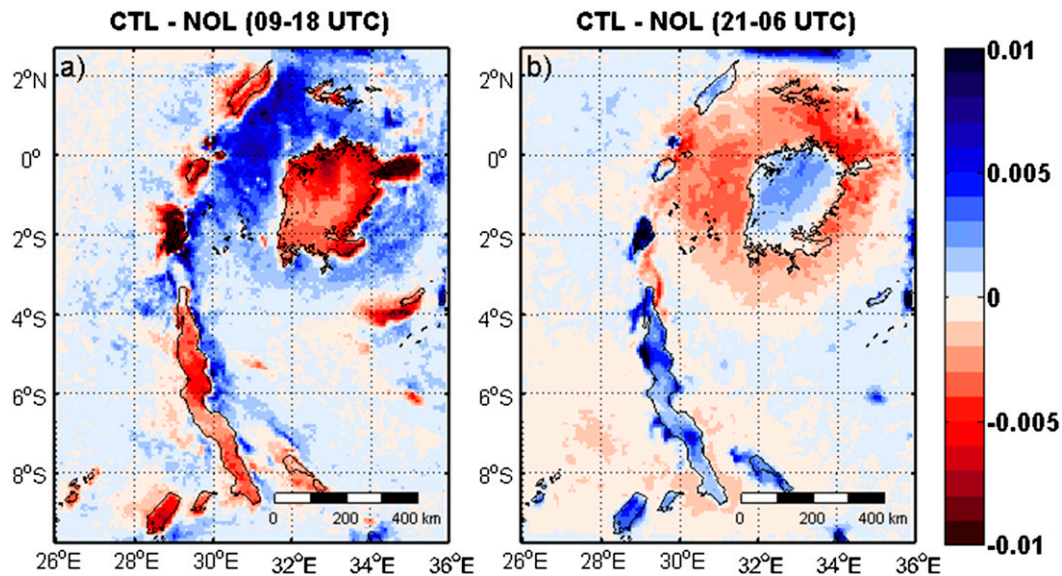


FIG. 15. The 1999–2008 mean change in convective mass flux density at cloud-base height ($\text{kg m}^{-2} \text{s}^{-1}$) induced by lake presence, for (a) 0900–1800 UTC (daytime) and (b) 2100–0600 UTC (nighttime).

sector is effectively reversed, with the lake breeze being replaced by a weak land breeze from the colder land to the warmer lake surface and offset by a counterclockwise motion aloft (Fig. 14d). When advected over the water, the cold air is warmed and moistened by strong evaporation from the lake ($\text{LHF} \sim 100 \text{ W m}^{-2}$ higher than equivalent land points; Fig. 10l). While the near-surface air converges and induces upward motion, the warming signal dissipates more quickly in the vertical due to adiabatic decompression, and the enhanced moisture is efficiently transported aloft (Figs. 14c,d). At 1 km MSL, annual average nighttime specific humidity still increases by around $+0.30 \text{ g kg}^{-1}$ over the whole domain and by $+1.66 \text{ g kg}^{-1}$ over lake surfaces (both changes statistically significant at the 5% significance level). Also note that, again, this is the opposite of the daytime, when downward motion inhibits upward moisture transport building up in the boundary layer and rather transports it horizontally across the lake boundaries (Fig. 13d). At night, higher air temperatures, higher specific humidity, and lower air pressure reinforce each other in destabilizing the first ~ 1 km of the atmospheric column over Lake Victoria [see Eq. (3)], as reflected by the strong increase in θ_e there ($\sim +6 \text{ K}$; Figs. 14c–f). This time, the increase of θ_e in lower levels is not accompanied by a notable decrease at higher levels caused by secondary circulation, pointing to the general destabilization of the nighttime over-lake atmospheric column. This, in turn, causes an increase in upward convective mass flux density (Fig. 15b), more intense convection, and associated precipitation during

nighttime over the lake. Again, the sign is reversed around the lake, where the lake presence reduces convection and, therefore, precipitation.

At night, the difference between the western and eastern sectors is generally less pronounced, although some differences can be noted. Over the eastern sector, the nighttime land breeze enforces katabatic winds flowing down from the eastern mountains (Anyah et al. 2006) and inhibits upslope transport of the warm temperature anomaly (Figs. 14b–d). The enhanced katabatic wind generates near-surface divergence on the eastern mountain slope and associated secondary downward motion aloft from ~ 2 to 4 km MSL, displaying similar secondary circulation over land compared to daytime, although less pronounced (Fig. 14d).

4. Conclusions

The influence of the AGL on the regional climate was studied for the period of 1999–2008 with the regional climate model COSMO-CLM². Efforts were made to enhance the realism of the simulations by accounting for (i) a model setup and land surface model suited for tropical conditions; (ii) a horizontal grid resolution effectively resolving individual lakes and complex topography, unprecedented for climate simulations in this region; and (iii) a state-of-the-art one-dimensional lake model capable of reproducing tropical LSWT.

A comprehensive evaluation of COSMO-CLM², nested within the ERA-Interim-driven CORDEX-Africa simulation (COSMO-CLM), shows an adequate

representation of precipitation and LSWT; the model reproduces the most important spatial patterns, including enhanced over-lake precipitation, absolute LSWT values, and LSWT gradients within and between lakes. The phase and amplitude of the mean annual cycle are also similar to observations, although the amplitude is overestimated for LSWT, and precipitation is underestimated during April and the main dry season. The remaining LSWT biases are ascribed to an underestimation of the mixed layer depth and the absence of three-dimensional circulation in the larger lakes. Furthermore, the mean annual cycles of net shortwave and longwave radiation at the surface, sensible and latent heat flux, and cloud cover are mostly simulated within the margins of observational uncertainty. Finally, we show that our simulation largely outperforms a state-of-the-art reanalysis product (ERA-Interim) for most of the considered variables, especially precipitation and LSWT, whereas the added value relative to a state-of-the-art, continent-scale RCM simulation (COSMO-CLM CORDEX-Africa evaluation simulation) is evident for precipitation, LSWT, and net surface shortwave radiation.

The AGL significantly reduce offshore near-surface air temperature by about -0.57 K , with maxima in excess of -1.50 K . The cooling effect is advected across the lake shores within dynamic and orographic constraints and is found to be strongest at the end of the main dry season, when the land surface warms faster than the water surface and the lake–land temperature contrast reaches a maximum. The four major AGL also enhance precipitation by $+732\text{ mm yr}^{-1}$ ($+87\%$) over their surface and even $+1373\text{ mm yr}^{-1}$ ($+145\%$) over Lake Kivu. All lakes together annually evaporate 222 km^3 of water into the atmosphere. In contrast to the near-surface temperature impact, the precipitation change is highly restricted to the lake areas. Both for temperature and precipitation, the mean effect masks a pronounced diurnal pattern: the temperature signal exhibits strong cooling during daytime and moderate warming during nighttime over the lakes, whereas precipitation is enhanced mostly at night and during early morning.

Decomposition of the lake-induced surface temperature increase over the AGL shows that reduced albedo has a moderate warming influence ($+5.91\text{ K}$), while reduced sensible heating enhances surface temperatures even more ($+8.64\text{ K}$). For the most part, their effect is offset by the enhanced lake evaporation, responsible for -12.21 K cooling. The apparent contradiction between surface and near-surface temperature change is cleared by considering daytime and nighttime separately: daytime heat storage in the lake and reduced upward sensible heat flux dominate the near-surface air temperature

change, whereas the nighttime warming determines the surface temperature signal.

Finally, analysis of the dynamical response using daytime and nighttime cross sections over Lake Victoria highlights the importance of circulation changes induced by the lake–land temperature contrast. During daytime, the lake breeze transports cold air across the lake borders and generates overland updrafts and over-lake subsidence. This secondary circulation stabilizes the atmosphere above $\sim 1.5\text{ km}$ and therefore effectively suppresses convection from the unstable surface layer. At night, the thermal inertia of the lake surface generates a positive temperature anomaly and a pressure deficit and maintains the daytime evaporation rates, inputting large amounts of moisture into the boundary layer. These three effects together cause a strong destabilization of the lower atmosphere. As the land breeze and secondary circulation subsequently induce near-surface convergence and the lifting of these highly unstable air masses, strong convection is triggered, and precipitation is released over the lake. On the eastern shore, complex topography and associated gravity currents superimpose on this pattern, generating a somewhat different response, especially during daytime.

Acknowledgments. We would like to thank the CLM-Community (<http://www.clm-community.eu>) and, in particular, Tom Akkermans and Alessandro Dosio for the helpful discussions on the modelling with COSMO-CLM². François Darchambeau, Pierre-Denis Plisnier, Meteo Rwanda, and Patrick Willems are thanked for supplying observational data, Thomas Antheunis for his thoughts on the surface energy balance decomposition technique, and Sonia Seneviratne for supporting this research. We sincerely thank three anonymous reviewers for their constructive remarks. Wim Thiery, Matthias Demuzere, and Stef Lhermitte are research fellows at the Research Foundation Flanders (FWO). This work was further supported by the Belgian Science Policy Office (BELSPO) through the research projects EAGLES, CLIMLAKE, and CLIMFISH. Parts of the station data were obtained from the FRIEND/NILE project of UNESCO and the Flanders in Trust Fund of the Flemish Government of Belgium. The computational resources and services used in this work were provided by the VSC (Flemish Supercomputer Center), funded by the Hercules Foundation and the Flemish Government department EWI.

REFERENCES

- Akkermans, T., 2013: Modeling land-atmosphere interactions in tropical Africa: The climatic impact of deforestation in the Congo Basin. Ph.D. thesis, KU Leuven, 160 pp.

- , and Coauthors, 2012: Validation and comparison of two soil–vegetation–atmosphere transfer models for tropical Africa. *J. Geophys. Res.*, **117**, G02013, doi:10.1029/2011JG001802.
- , W. Thiery, and N. P. M. Van Lipzig, 2014: The regional climate impact of a realistic future deforestation scenario in the Congo basin. *J. Climate*, **27**, 2714–2734, doi:10.1175/JCLI-D-13-00361.1.
- Anyah, R. O., and F. H. M. Semazzi, 2004: Simulation of the sensitivity of Lake Victoria basin climate to lake surface temperatures. *Theor. Appl. Climatol.*, **79**, 55–69, doi:10.1007/s00704-004-0057-4.
- , and —, 2006: Climate variability over the Greater Horn of Africa based on NCAR AGCM ensemble. *Theor. Appl. Climatol.*, **86**, 39–62, doi:10.1007/s00704-005-0203-7.
- , and —, 2007: Variability of East African rainfall based on multiyear RegCM3 simulations. *Int. J. Climatol.*, **27**, 357–371, doi:10.1002/joc.1401.
- , and —, 2009: Idealized simulation of hydrodynamic characteristics of Lake Victoria that potentially modulate regional climate. *Int. J. Climatol.*, **29**, 971–981, doi:10.1002/joc.1795.
- , —, and L. Xie, 2006: Simulated physical mechanisms associated with climate variability over Lake Victoria basin in East Africa. *Mon. Wea. Rev.*, **134**, 3588–3609, doi:10.1175/MWR3266.1.
- Argent, R., X. Sun, F. H. M. Semazzi, L. Xie, and B. Liu, 2015: The development of a customization framework for the WRF Model over the Lake Victoria basin, Eastern Africa on seasonal timescales. *Adv. Meteorol.*, **2015**, 653473, doi:10.1155/2015/653473.
- Balsamo, G., R. Salgado, E. Dutra, S. Boussetta, T. Stockdale, and M. Potes, 2012: On the contribution of lakes in predicting near-surface temperature in a global weather forecasting model. *Tellus*, **64A**, 15829, doi:10.3402/tellusa.v64i0.15829.
- Bates, G., S. Hostetler, and F. Giorgi, 1995: Two-year simulation of the Great Lakes region with a coupled modeling system. *Mon. Wea. Rev.*, **123**, 1505–1522, doi:10.1175/1520-0493(1995)123<1505:TYSOTG>2.0.CO;2.
- Bennington, V., M. Notaro, and K. D. Holman, 2014: Improving climate sensitivity of deep lakes within a regional climate model and its impact on simulated climate. *J. Climate*, **27**, 2886–2911, doi:10.1175/JCLI-D-13-00110.1.
- Bonan, G. B., 1995: Sensitivity of a GCM simulation to inclusion of inland water surfaces. *J. Climate*, **8**, 2691–2704, doi:10.1175/1520-0442(1995)008<2691:SOAGST>2.0.CO;2.
- , K. W. Oleson, M. Vertenstein, S. Levis, X. Zeng, Y. Dai, R. E. Dickinson, and Z.-L. Yang, 2002: The land surface climatology of the Community Land Model coupled to the NCAR Community Climate Model. *J. Climate*, **15**, 3123–3149, doi:10.1175/1520-0442(2002)015<3123:TLSCOT>2.0.CO;2.
- Bookhagen, B., and D. W. Burbank, 2006: Topography, relief, and TRMM-derived rainfall variations along the Himalaya. *Geophys. Res. Lett.*, **33**, L08405, doi:10.1029/2006GL026037.
- , and M. R. Strecker, 2008: Orographic barriers, high-resolution TRMM rainfall, and relief variations along the eastern Andes. *Geophys. Res. Lett.*, **35**, L06403, doi:10.1029/2007GL032011.
- Burbank, D. W., B. Bookhagen, E. J. Gabet, and J. Putkonen, 2012: Modern climate and erosion in the Himalaya. *C. R. Geosci.*, **344**, 610–626, doi:10.1016/j.crte.2012.10.010.
- Climate Prediction Center, 2011: NOAA CPC Morphing Technique (CMORPH) Global Precipitation Analyses. Research Data Archive at the National Center for Atmospheric Research, Computational and Information Systems Laboratory, accessed 13 June 2014. [Available online at <http://rda.ucar.edu/datasets/ds502.0/>.]
- Coe, M., and G. Bonan, 1997: Feedbacks between climate and surface water in northern Africa during the middle Holocene. *J. Geophys. Res.*, **102**, 11 087–11 101, doi:10.1029/97JD00343.
- Crétat, J., E. K. Vizio, and K. H. Cook, 2014: How well are daily intense rainfall events captured by current climate models over Africa? *Climate Dyn.*, **42**, 2691–2711, doi:10.1007/s00382-013-1796-7.
- Darchambeau, F., H. Sarmiento, and J.-P. Descy, 2014: Primary production in a tropical large lake: The role of phytoplankton composition. *Sci. Total Environ.*, **473–474**, 178–188, doi:10.1016/j.scitotenv.2013.12.036.
- Datta, R. K., 1981: Certain aspects of monsoonal precipitation dynamics over Lake Victoria. *Monsoon Dynamics*, J. Lighthill and R. P. Pearce, Eds., Cambridge University Press, 333–349.
- Davies, H., 1983: Limitations of some common lateral boundary schemes used in regional NWP models. *Mon. Wea. Rev.*, **111**, 1002–1012, doi:10.1175/1520-0493(1983)111<1002:LOSCLB>2.0.CO;2.
- Davin, E. L., and S. I. Seneviratne, 2012: Role of land surface processes and diffuse/direct radiation partitioning in simulating the European climate. *Biogeosciences*, **9**, 1695–1707, doi:10.5194/bg-9-1695-2012.
- , R. Stöckli, E. B. Jaeger, S. Levis, and S. I. Seneviratne, 2011: COSMO-CLM²: A new version of the COSMO-CLM model coupled to the Community Land Model. *Climate Dyn.*, **37**, 1889–1907, doi:10.1007/s00382-011-1019-z.
- , S. I. Seneviratne, P. Ciais, A. Ollio, and T. Wang, 2014: Preferential cooling of hot extremes from cropland albedo management. *Proc. Natl. Acad. Sci. USA*, **111**, 9757–9761, doi:10.1073/pnas.1317323111.
- De Boor, C., 1978: *A Practical Guide to Splines*. Applied Mathematical Sciences, Vol. 27, Springer-Verlag, 348 pp.
- Dee, D. P., and Coauthors, 2011: The ERA-Interim reanalysis: Configuration and performance of the data assimilation system. *Quart. J. Roy. Meteor. Soc.*, **137**, 553–597, doi:10.1002/qj.828.
- Dinku, T., S. Chidzambwa, P. Ceccato, S. J. Connor, and C. F. Ropelewski, 2008: Validation of high-resolution satellite rainfall products over complex terrain. *Int. J. Remote Sens.*, **29**, 4097–4110, doi:10.1080/01431160701772526.
- Doms, G., 2011: A description of the nonhydrostatic regional COSMO-Model. Part I: Dynamics and numerics. COSMO Tech. Rep., 153 pp. [Available online at <http://www.cosmo-model.org/content/model/documentation/core/cosmoDyncsNumcs.pdf>.]
- , and Coauthors, 2011: A description of the nonhydrostatic regional COSMO Model. Part II: Physical parameterization. COSMO Tech. Rep., 161 pp. [Available online at <http://www.cosmo-model.org/content/model/documentation/core/cosmoPhysParamtr.pdf>.]
- Dosio, A., H.-J. Panitz, M. Schubert-Frisius, and D. Lüthi, 2015: Dynamical downscaling of CMIP5 global circulation models over CORDEX-Africa with COSMO-CLM: Evaluation over the present climate and analysis of the added value. *Climate Dyn.*, **44**, 2637–2661, doi:10.1007/s00382-014-2262-x.
- Endris, H. S., and Coauthors, 2013: Assessment of the performance of CORDEX regional climate models in simulating East African rainfall. *J. Climate*, **26**, 8453–8475, doi:10.1175/JCLI-D-12-00708.1.
- Giorgi, F., C. Jones, and G. Asrar, 2009: Addressing climate information needs at the regional level: the CORDEX framework. *WMO Bull.*, **58**, 175–183.

- Gourgue, O., E. Deleersnijder, and L. White, 2007: Toward a generic method for studying water renewal, with application to the epilimnion of Lake Tanganyika. *Estuarine Coastal Shelf Sci.*, **74**, 628–640, doi:10.1016/j.ecss.2007.05.009.
- Goyens, C., D. Lauwaet, M. Schröder, M. Demuzere, and N. P. M. Van Lipzig, 2012: Tracking mesoscale convective systems in the Sahel: Relation between cloud parameters and precipitation. *Int. J. Climatol.*, **32**, 1921–1934, doi:10.1002/joc.2407.
- Goyette, S., N. McFarlane, and G. M. Flato, 2000: Application of the Canadian regional climate model to the Laurentian great lakes region: Implementation of a lake model. *Atmos.–Ocean*, **38**, 481–503, doi:10.1080/07055900.2000.9649657.
- Grasselt, R., D. Schüttemeyer, K. Warrach-Sagi, F. Ament, and C. Simmer, 2008: Validation of TERRA-ML with discharge measurements. *Meteor. Z.*, **17**, 763–773, doi:10.1127/0941-2948/2008/0334.
- Gu, H., J. Jin, Y. Wu, M. B. Ek, and Z. M. Subin, 2015: Calibration and validation of lake surface temperature simulations with the coupled WRF-lake model. *Climatic Change*, **129**, 471–483, doi:10.1007/s10584-013-0978-y.
- Gula, J., and W. R. Peltier, 2012: Dynamical downscaling over the Great Lakes basin of North America using the WRF Regional Climate Model: The impact of the Great Lakes system on regional greenhouse warming. *J. Climate*, **25**, 7723–7742, doi:10.1175/JCLI-D-11-00388.1.
- Hernández-Díaz, L., R. Laprise, L. Sushama, A. Martynov, K. Winger, and B. Dugas, 2013: Climate simulation over CORDEX Africa domain using the fifth-generation Canadian Regional Climate Model (CRCM5). *Climate Dyn.*, **40**, 1415–1433, doi:10.1007/s00382-012-1387-z.
- Hostetler, S. W., and F. Giorgi, 1995: Effects of a $2 \times \text{CO}_2$ climate on two large lake systems: Pyramid Lake, Nevada, and Yellowstone Lake, Wyoming. *Global Planet. Change*, **10**, 43–54, doi:10.1016/0921-8181(94)00019-A.
- , —, G. T. Bates, and P. J. Bartlein, 1994: Lake–atmosphere feedbacks associated with paleolakes Bonneville and Lahontan. *Science*, **263**, 665–668, doi:10.1126/science.263.5147.665.
- Huffman, G., R. Adler, M. Morrissey, D. Bolvin, S. Curtis, R. Joyce, B. McGavock, and J. Susskind, 2001: Global precipitation at one-degree daily resolution from multisatellite observations. *J. Hydrometeorol.*, **2**, 36–50, doi:10.1175/1525-7541(2001)002<0036:GPAODD>2.0.CO;2.
- Jacobs, L., O. Dewitte, J. Poesen, D. Delvaux, W. Thiery, and M. Kervyn, 2015: The Rwenzori Mountains, a landslide-prone region? *Landslides*, in press.
- Joyce, R., J. Janowiak, P. Arkin, and P. Xie, 2004: CMORPH: A method that produces global precipitation estimates from passive microwave and infrared data at high spatial and temporal resolution. *J. Hydrometeorol.*, **5**, 487–503, doi:10.1175/1525-7541(2004)005<0487:CAMTPG>2.0.CO;2.
- Juang, J.-Y., G. Katul, M. Siqueira, P. Stoy, and K. Novick, 2007: Separating the effects of albedo from eco-physiological changes on surface temperature along a successional chronosequence in the southeastern United States. *Geophys. Res. Lett.*, **34**, L21408, doi:10.1029/2007GL031296.
- Jung, M., M. Reichstein, and A. Bondeau, 2009: Towards global empirical upscaling of FLUXNET eddy covariance observations: Validation of a model tree ensemble approach using a biosphere model. *Biogeosciences*, **6**, 2001–2013, doi:10.5194/bg-6-2001-2009.
- , and Coauthors, 2010: Recent decline in the global land evapotranspiration trend due to limited moisture supply. *Nature*, **467**, 951–954, doi:10.1038/nature09396.
- Kitaigorodskii, S. A., and Y. Z. Miropolskii, 1970: On the theory of the open ocean active layer. *Izv., Atmos. Ocean. Phys.*, **6**, 97–102.
- Kourzeneva, E., 2010: External data for lake parameterization in Numerical Weather Prediction and climate modeling. *Boreal Environ. Res.*, **15**, 165–177.
- , H. Asensio, E. Martin, and S. Faroux, 2012: Global gridded dataset of lake coverage and lake depth for use in numerical weather prediction and climate modelling. *Tellus*, **64A**, 15640, doi:10.3402/tellusa.v64i0.15640.
- Kummerow, C., and Coauthors, 2000: The status of the Tropical Rainfall Measuring Mission (TRMM) after two years in orbit. *J. Appl. Meteor.*, **39**, 1965–1982, doi:10.1175/1520-0450(2001)040<1965:TSOTTR>2.0.CO;2.
- Laprise, R., and Coauthors, 2008: Challenging some tenets of regional climate modelling. *Meteor. Atmos. Phys.*, **100**, 3–22, doi:10.1007/s00703-008-0292-9.
- , L. Hernández-Díaz, K. Tete, L. Sushama, L. Šeparović, A. Martynov, K. Winger, and M. Valin, 2013: Climate projections over CORDEX Africa domain using the fifth-generation Canadian Regional Climate Model (CRCM5). *Climate Dyn.*, **41**, 3219–3246, doi:10.1007/s00382-012-1651-2.
- Lauwaet, D., N. P. M. Lipzig, and K. Ridder, 2009: The effect of vegetation changes on precipitation and Mesoscale Convective Systems in the Sahel. *Climate Dyn.*, **33**, 521–534, doi:10.1007/s00382-009-0539-2.
- , N. P. M. van Lipzig, K. Van Weverberg, K. De Ridder, and C. Goyens, 2012: The precipitation response to the desiccation of Lake Chad. *Quart. J. Roy. Meteor. Soc.*, **138**, 707–719, doi:10.1002/qj.942.
- Legates, D., and C. Willmott, 1990: Mean seasonal and spatial variability in gauge-corrected, global precipitation. *Int. J. Climatol.*, **10**, 111–127, doi:10.1002/joc.3370100202.
- Lejeune, Q., E. Davin, B. Guillod, and S. Seneviratne, 2015: Influence of Amazonian deforestation on the future evolution of regional surface fluxes, circulation, surface temperature and precipitation. *Climate Dyn.*, **44**, 2769–2786, doi:10.1007/s00382-014-2203-8.
- Lorenz, R., E. L. Davin, and S. I. Seneviratne, 2012: Modeling land-climate coupling in Europe: Impact of land surface representation on climate variability and extremes. *J. Geophys. Res.*, **117**, D201109, doi:10.1029/2012JD017755.
- Luyssaert, S., and Coauthors, 2014: Land management and land-cover change have impacts of similar magnitude on surface temperature. *Nat. Climate Change*, **4**, 389–393, doi:10.1038/nclimate2196.
- MacCallum, S., and C. Merchant, 2012: Surface water temperature observations of large lakes by optimal estimation. *Can. J. Remote Sens.*, **38**, 25–45, doi:10.5589/m12-010.
- MacIntyre, S., 2012: Climatic variability, mixing dynamics, and ecological consequences in the African Great Lakes. *Climatic Change and Global Warming of Inland Waters: Impacts and Mitigation for Ecosystems and Societies*, C. R. Goldman, M. Kumagai, and R. D. Robarts, Eds., John Wiley & Sons, Inc., 311–337, doi:10.1002/9781118470596.ch18.
- , J. R. Romero, G. M. Silsbe, and B. M. Emery, 2014: Stratification and horizontal exchange in Lake Victoria, East Africa. *Limnol. Oceanogr.*, **59**, 1805–1838, doi:10.4319/lo.2014.59.6.1805.
- Martynov, A., L. Sushama, R. Laprise, K. Winger, and B. Dugas, 2012: Interactive lakes in the Canadian Regional Climate Model, version 5: The role of lakes in the regional climate of North America. *Tellus*, **64A**, 16226, doi:10.3402/tellusa.v64i0.16226.

- Mironov, D. V., 2008: Parameterization of lakes in numerical weather prediction. Part 1: Description of a lake model. COSMO Tech. Rep. 11, 47 pp. [Available online at <http://www.cosmo-model.org/content/model/documentation/techReports/docs/techReport11.pdf>.]
- , E. Heise, E. Kourzeneva, B. Ritter, N. Schneider, and A. Terzhevik, 2010: Implementation of the lake parameterisation scheme FLake into the numerical weather prediction model COSMO. *Boreal Environ. Res.*, **15**, 218–230.
- Mueller, B., and Coauthors, 2013: Benchmark products for land evapotranspiration: LandFlux-EVAL multi-data set synthesis. *Hydrol. Earth Syst. Sci.*, **17**, 3707–3720, doi:10.5194/hess-17-3707-2013.
- Naithani, J., and E. Deleersnijder, 2004: Are there internal Kelvin waves in Lake Tanganyika? *Geophys. Res. Lett.*, **31**, L06303, doi:10.1029/2003GL019156.
- , —, and P.-D. Plisnier, 2002: Origin of intraseasonal variability in Lake Tanganyika. *Geophys. Res. Lett.*, **29**, 2093, doi:10.1029/2002GL015843.
- , —, and —, 2003: Analysis of wind-induced thermocline oscillations of Lake Tanganyika. *Environ. Fluid Mech.*, **3**, 23–39, doi:10.1023/A:1021116727232.
- Nicholson, S., 1996: A review of climate dynamics and climate variability in Eastern Africa. *The Limnology, Climatology and Paleoclimatology of the East African Lakes*, T. Johnson and E. Odada, Eds., CRC Press, 25–56.
- Nikulin, G., and Coauthors, 2012: Precipitation climatology in an ensemble of CORDEX-Africa regional climate simulations. *J. Climate*, **25**, 6057–6078, doi:10.1175/JCLI-D-11-00375.1.
- Notaro, M., K. Holman, A. Zarrin, E. Fluck, S. Vavrus, and V. Bennington, 2013: Influence of the Laurentian Great Lakes on regional climate. *J. Climate*, **26**, 789–804, doi:10.1175/JCLI-D-12-00140.1.
- Nyeko-Ogiramo, P., G. Ngirane-Katashaya, P. Willems, and V. Ntegeka, 2010: Evaluation and inter-comparison of Global Climate Models' performance over Katonga and Ruizi catchments in Lake Victoria basin. *Phys. Chem. Earth*, **35**, 618–633, doi:10.1016/j.pce.2010.07.037.
- , P. Willems, and G. Ngirane-Katashaya, 2013: Trend and variability in observed hydrometeorological extremes in the Lake Victoria basin. *J. Hydrol.*, **489**, 56–73, doi:10.1016/j.jhydrol.2013.02.039.
- Oleson, K. W., and Coauthors, 2004: Technical description of the Community Land Model (CLM). NCAR Tech. Note NCAR/TN-461+STR, 186 pp., doi:10.5065/D6N877R0.
- , and Coauthors, 2008: Improvements to the Community Land Model and their impact on the hydrological cycle. *J. Geophys. Res.*, **113**, G01021, doi:10.1029/2007JG000563.
- Panitz, H.-J., A. Dosio, M. Büchner, D. Lüthi, and K. Keuler, 2014: COSMO-CLM (CCLM) climate simulations over CORDEX-Africa domain: Analysis of the ERA-Interim driven simulations at 0.44° and 0.22° resolution. *Climate Dyn.*, **42**, 3015–3038, doi:10.1007/s00382-013-1834-5.
- Perroud, M., and S. Goyette, 2009: Simulation of multiannual thermal profiles in deep Lake Geneva: A comparison of one-dimensional lake models. *Limnol. Oceanogr.*, **54**, 1574–1594, doi:10.4319/lo.2009.54.5.1574.
- Plisnier, P.-D., S. Serneels, and E. Lambin, 2000: Impact of ENSO on East African ecosystems: A multivariate analysis based on climate and remote sensing data. *Global Ecol. Biogeogr.*, **9**, 481–497, doi:10.1046/j.1365-2699.2000.00208.x.
- , and Coauthors, 2009: Limnological variability and pelagic fish abundance (*Stolothrissa tanganyicae* and *Lates stappersii*) in Lake Tanganyika. *Hydrobiologia*, **625**, 117–134, doi:10.1007/s10750-009-9701-4.
- Raschendorfer, M., 2001: The new turbulence parameterization of LM. *COSMO newsletter*, No. 1, Deutscher Wetterdienst, Offenbach, Germany, 90–98. [Available online at http://cosmo-model.cscs.ch/content/model/documentation/newsLetters/newsLetter01/newsLetter_01.pdf.]
- Read, J. S., and Coauthors, 2012: Lake-size dependency of wind shear and convection as controls on gas exchange. *Geophys. Res. Lett.*, **39**, L09405, doi:10.1029/2012GL051886.
- Ritter, B., and J. Geleyn, 1992: A comprehensive radiation scheme for numerical weather prediction models with potential applications in climate simulations. *Mon. Wea. Rev.*, **120**, 303–325, doi:10.1175/1520-0493(1992)120<0303:ACRSFN>2.0.CO;2.
- Rockel, B., A. Will, and A. Hense, 2008: The Regional Climate Model COSMO-CLM (CCLM). *Meteor. Z.*, **17**, 347–348, doi:10.1127/0941-2948/2008/0309.
- Rooney, G., and F. Bornemann, 2013: The performance of FLake in the Met Office Unified Model. *Tellus*, **1A**, 21363, doi:10.3402/tellusa.v65i0.21363.
- Rossow, W. B., and R. A. Schiffer, 1999: Advances in understanding clouds from ISCCP. *Bull. Amer. Meteor. Soc.*, **80**, 2261–2287, doi:10.1175/1520-0477(1999)080<2261:AIUCFI>2.0.CO;2.
- Rudolf, B., A. Becker, and U. Schneider, 2011: New GPCC full data reanalysis version 5 provides high-quality gridded monthly precipitation data. *GEWEX News*, Vol. 21, No. 2, International GEWEX Project Office, Silver Spring, MD, 4–5.
- Saeed, F., A. Haensler, T. Weber, S. Hagemann, and D. Jacob, 2013: Representation of extreme precipitation events leading to opposite climate change signals over the Congo basin. *Atmosphere*, **4**, 254–271, doi:10.3390/atmos4030254.
- Samuelsson, P., E. Kourzeneva, and D. Mironov, 2010: The impact of lakes on the European climate as simulated by a regional climate model. *Boreal Environ. Res.*, **15**, 113–129.
- Savijärvi, H., 1997: Diurnal winds around Lake Tanganyika. *Quart. J. Roy. Meteor. Soc.*, **123**, 901–918, doi:10.1002/qj.49712354006.
- , and S. Järvenoja, 2000: Aspects of the fine-scale climatology over Lake Tanganyika as resolved by a mesoscale model. *Meteor. Atmos. Phys.*, **73**, 77–88, doi:10.1007/s007030050066.
- Schmid, M., and A. Wüest, 2012: Stratification, mixing and transport processes in Lake Kivu. *Lake Kivu: Limnology and Biogeochemistry of a Tropical Great Lake*, J.-P. Descy, F. Darchambeau, and M. Schmid, Eds., Springer, 13–29, doi:10.1007/978-94-007-4243-7.
- Schneider, U., A. Becker, P. Finger, A. Meyer-Christoffer, M. Ziese, and B. Rudolf, 2014: GPCC's new land surface precipitation climatology based on quality-controlled in situ data and its role in quantifying the global water cycle. *Theor. Appl. Climatol.*, **115**, 15–40, doi:10.1007/s00704-013-0860-x.
- Sellers, P., and Coauthors, 1997: Modeling the exchanges of energy, water, and carbon between continents and the atmosphere. *Science*, **275**, 502–509, doi:10.1126/science.275.5299.502.
- Semazzi, F. H. M., 2011: Enhancing safety of navigation and efficient exploitation of natural resources over Lake Victoria and its basin by strengthening meteorological services on the lake. North Carolina State University Climate Modeling Laboratory Tech. Rep., 104 pp. [Available online at http://climlab02.meas.ncsu.edu/HYVIC/Final_Report_LVBC.pdf.]
- Song, Y., F. H. M. Semazzi, L. Xie, and L. J. Ogallo, 2004: A coupled regional climate model for the Lake Victoria basin of East Africa. *Int. J. Climatol.*, **24**, 57–75, doi:10.1002/joc.983.

- Stackhouse, P. W., S. K. Gupta, S. J. Cox, T. Zhang, J. C. Mikovitz, and L. M. Hinkelman, 2011: 24.5-year surface radiation budget data set released. *GEWEX News*, Vol. 21, No. 1, International GEWEX Project Office, Silver Spring, MD, 10–12.
- Stepanenko, V., S. Goyette, A. Martynov, M. Perroud, X. Fang, and D. Mironov, 2010: First steps of a Lake Model Intercomparison Project: LakeMIP. *Boreal Environ. Res.*, **15**, 191–202.
- , and Coauthors, 2013: A one-dimensional model intercomparison study of thermal regime of a shallow, turbid midlatitude lake. *Geosci. Model Dev.*, **6**, 1337–1352, doi:10.5194/gmd-6-1337-2013.
- , K. Jöhnk, and E. Machulskaya, 2014: Simulation of surface energy fluxes and stratification of a small boreal lake by a set of one-dimensional models. *Tellus*, **66A**, 21389, doi:10.3402/tellusa.v66.21389.
- Stöckli, R., and Coauthors, 2008: Use of FLUXNET in the Community Land Model development. *J. Geophys. Res.*, **113**, G01025, doi:10.1029/2007JG000562.
- Subin, Z. M., L. N. Murphy, F. Li, C. Bonfils, and W. J. Riley, 2012: Boreal lakes moderate seasonal and diurnal temperature variation and perturb atmospheric circulation: Analyses in the Community Earth System Model 1 (CESM1). *Tellus*, **64A**, 15639, doi:10.3402/tellusa.v64i0.15639.
- Sun, L., F. Semazzi, F. Giorgi, and L. Ogallo, 1999: Application of the NCAR regional climate model to eastern Africa: 1. Simulation of the short rains of 1988. *J. Geophys. Res.*, **104**, 6529–6548, doi:10.1029/1998JD200051.
- Sun, X., L. Xie, F. H. M. Semazzi, and B. Liu, 2014a: Effect of lake surface temperature on the spatial distribution and intensity of the precipitation over the Lake Victoria basin. *Mon. Wea. Rev.*, **143**, 1179–1192, doi:10.1175/MWR-D-14-00049.1.
- , —, —, and —, 2014b: A numerical investigation of the precipitation over Lake Victoria basin using a coupled atmosphere-lake limited-area model. *Adv. Meteorol.*, **2014**, 960924, doi:10.1155/2014/960924.
- Sylla, M. B., F. Giorgi, E. Coppola, and L. Mariotti, 2013: Uncertainties in daily rainfall over Africa: assessment of gridded observation products and evaluation of a regional climate model simulation. *Int. J. Climatol.*, **33**, 1805–1817, doi:10.1002/joc.3551.
- Thiery, W., A. Martynov, F. Darchambeau, J.-P. Descy, P.-D. Plisnier, L. Sushama, and N. P. M. van Lipzig, 2014a: Understanding the performance of the FLake model over two African Great Lakes. *Geosci. Model Dev.*, **7**, 317–337, doi:10.5194/gmd-7-317-2014.
- , and Coauthors, 2014b: LakeMIP Kivu: Evaluating the representation of a large, deep tropical lake by a set of one-dimensional lake models. *Tellus*, **66A**, 21390, doi:10.3402/tellusa.v66.21390.
- Tiedtke, M., 1989: A comprehensive mass flux scheme for cumulus parameterization in large-scale models. *Mon. Wea. Rev.*, **117**, 1779–1800, doi:10.1175/1520-0493(1989)117<1779:ACMFSF>2.0.CO;2.
- Vanden Broucke, S., S. Luyssaert, E. Davin, I. Janssens, and N. P. M. van Lipzig, 2015: Temperature decomposition of paired site observations reveals new insights in climate models' capability to simulate the impact of LUC. *J. Geophys. Res.*, in press.
- Verburg, P., and J. P. Antenucci, 2010: Persistent unstable atmospheric boundary layer enhances sensible and latent heat loss in a tropical great lake: Lake Tanganyika. *J. Geophys. Res.*, **115**, 5347, doi:10.1029/2009JD012839.
- , —, and R. E. Hecky, 2011: Differential cooling drives large-scale convective circulation in Lake Tanganyika. *Limnol. Oceanogr.*, **56**, 910–926, doi:10.4319/lo.2011.56.3.0910.
- Vizy, E. K., and K. H. Cook, 2012: Mid-twenty-first-century changes in extreme events over northern and Tropical Africa. *J. Climate*, **25**, 5748–5767, doi:10.1175/JCLI-D-11-00693.1.
- Williams, K., J. Chamberlain, C. Buontempo, and C. Bain, 2015: Regional climate model performance in the Lake Victoria basin. *Climate Dyn.*, **44**, 1699–1713, doi:10.1007/s00382-014-2201-x.

LakeMIP Kivu: evaluating the representation of a large, deep tropical lake by a set of one-dimensional lake models

By WIM THIERY^{1*}, VICTOR M. STEPANENKO², XING FANG³, KLAUS D. JÖHNK⁴, ZHONGSHUN LI⁵, ANDREY MARTYNOV⁶, MARJORIE PERROUD⁷, ZACHARY M. SUBIN⁸, FRANÇOIS DARCHAMBEAU⁹, DMITRII MIRONOV¹⁰ and NICOLE P. M. VAN LIPZIG¹, ¹*Department of Earth and Environmental Sciences, University of Leuven, Leuven, Belgium;* ²*Laboratory for Supercomputing modelling of climate system processes, Moscow State University, Moscow, Russia;* ³*Department of Civil Engineering, Auburn University, Auburn, AL, USA;* ⁴*CSIRO Land and Water, Black Mountain, Canberra, Australia;* ⁵*Department of Hydraulic Engineering, Tsinghua University, Beijing, P.R. China;* ⁶*Institute of Geography and Oeschger Centre for Climate Change Research, University of Bern, Bern, Switzerland;* ⁷*Climate Reporting and Adaptation Section, Swiss Federal Office for the Environment, Bern, Switzerland;* ⁸*Princeton Environmental Institute, Princeton, NJ, USA;* ⁹*Chemical Oceanography Unit, Université de Liège, Liège, Belgium;* ¹⁰*Research & Development Unit, German Weather Service, Offenbach am Main, Germany*

(Manuscript received 12 May 2013; in final form 20 December 2013)

ABSTRACT

The African great lakes are of utmost importance for the local economy (fishing), as well as being essential to the survival of the local people. During the past decades, these lakes experienced fast changes in ecosystem structure and functioning, and their future evolution is a major concern. In this study, for the first time a set of one-dimensional lake models are evaluated for Lake Kivu (2.28°S; 28.98°E), East Africa. The unique limnology of this meromictic lake, with the importance of salinity and subsurface springs in a tropical high-altitude climate, presents a worthy challenge to the seven models involved in the Lake Model Intercomparison Project (LakeMIP). Meteorological observations from two automatic weather stations are used to drive the models, whereas a unique dataset, containing over 150 temperature profiles recorded since 2002, is used to assess the model's performance. Simulations are performed over the freshwater layer only (60 m) and over the average lake depth (240 m), since salinity increases with depth below 60 m in Lake Kivu and some lake models do not account for the influence of salinity upon lake stratification. All models are able to reproduce the mixing seasonality in Lake Kivu, as well as the magnitude and seasonal cycle of the lake enthalpy change. Differences between the models can be ascribed to variations in the treatment of the radiative forcing and the computation of the turbulent heat fluxes. Fluctuations in wind velocity and solar radiation explain inter-annual variability of observed water column temperatures. The good agreement between the deep simulations and the observed meromictic stratification also shows that a subset of models is able to account for the salinity- and geothermal-induced effects upon deep-water stratification. Finally, based on the strengths and weaknesses discerned in this study, an informed choice of a one-dimensional lake model for a given research purpose becomes possible.

Keywords: lake modelling, model intercomparison, surface-atmosphere interactions, tropical lakes, Lake Kivu

1. Introduction

In regions where lakes compose a large fraction of the earth surface, they form an important component of the climate

system. The strong contrasts in albedo, surface roughness and heat capacity between land and water modify the surface-atmosphere exchanges of moisture, heat and momentum over lakes compared to adjacent land (Bonan, 1995). Some reported effects of this modified exchange are the dampened diurnal temperature range over lakes

*Corresponding author.
email: wim.thiery@ees.kuleuven.be

(Subin et al., 2012a), the enhanced evaporation or even a persistent unstable atmospheric boundary layer (Verburg and Antenucci, 2010), the resulting increased precipitation downwind of the lake (Lauwaet et al., 2011), the stronger winds due to higher wind fetch (Subin et al., 2012a), and the formation of local diurnal winds (Savijärvi, 1997; Verburg and Hecky, 2003).

Given the significant impact of lakes on surface-atmosphere interactions, the need for an accurate representation of lake surface temperatures in Numerical Weather Prediction systems (NWP), Regional Climate Models (RCM) and General Circulation Models (GCM) arises. Although a multitude of one-dimensional lake models developed in the past may be a candidate to represent lake-atmosphere exchanges, only a subset of these models has been interactively coupled to atmospheric prediction models so far (Hostetler et al., 1994; Bonan, 1995; Song et al., 2004; Kourzeneva et al., 2008; Mironov et al., 2010; Davin et al., 2011; Balsamo et al., 2012; Goyette and Perroud, 2012; Martynov et al., 2012; Akkermans et al., 2014). Computational efficiency of the lake parameterisation scheme is often decisive for the choice of the scheme. A comparative assessment of different one-dimensional lake models, with emphasis on the strengths and weaknesses with respect to specific research goals, could however favour an informed choice.

From this need, in 2008 the Lake Model Intercomparison Project (LakeMIP) emerged. In a first stage, this project aims at a comparison of the thermodynamic regime of a wide range of climatic conditions and mixing regimes by a number of one-dimensional lake models (Stepanenko et al., 2010). Inspired by a model intercomparison study for the deep lake Geneva (Perroud et al., 2009), LakeMIP focused on a number of test cases such as, for mid-latitudes, the small Lake Sparkling (Stepanenko et al., 2010) and the shallow turbid Lake Kossenblatter (Stepanenko et al., 2012), whereas for a boreal climate, the small Lake Valkea-Kotinen was investigated (Stepanenko et al., 2013).

However, despite the abundance of lakes in tropical regions such as East Africa and Indonesia, up to now a lake model intercomparison study has never been conducted for an equatorial lake. In tropical climates, the limited seasonal cycle of both air temperature and incoming shortwave radiation makes way for other factors to control the mixing regime. With the meteorological controls on a lake's mixing regime and its water temperatures varying between climate zones, the need arose to conduct a model intercomparison experiment for a tropical lake.

Consequently, in this study, for the first time a set of one-dimensional lake models is evaluated over an East African lake: Lake Kivu (2.28°S; 28.98°E). Lake Kivu's meromictic mixing regime clearly differs from lakes previously studied

within the project, that is, monomictic, dimictic or polymictic lakes with seasonal complete or partial ice cover. Furthermore, given the influence of salinity, dissolved gasses and geothermal springs on the characteristics of the hypolimnion, the modelling of Lake Kivu presents a worthy challenge to the one-dimensional lake models currently involved in LakeMIP. Finally, as a consequence of its distinct characteristics, Lake Kivu is among the best-studied lakes in the African Great Lakes region. Anthropogenic influences and recurrent natural hazards call for a close monitoring of the lake's physical and biological characteristics. For instance, when lava flowed into the lake after a major eruption of the near-shore Nyiragongo volcano, no significant impact on the water column stability was recorded (Lorke et al., 2004). In contrast, effects on density stratification of the emerging industrial methane extraction from lake Kivu are expected and will critically depend on the reinjection depth of the deep waters after the methane harvest (Descy et al., 2012; Wüest et al., 2012). To meet these and other challenges, a comprehensive dataset containing observed lake temperatures, Secchi depths and many other variables has been compiled over the last decade.

The two main goals of this study are: (i) the evaluation of the seasonal and inter-annual variability of Lake Kivu's thermal structure as represented by a set of one-dimensional lake models, and (ii) the assessment of the ability of the different models to simulate the effects of salinity, chemical composition and geothermal energy sources upon deep water stratification. This was done by performing two sets of simulations, one including only the freshwater mixed layer and another one for the whole lake including salinity, chemical and geothermal effects in the equation of state.

In the next section, an overview of the participating one-dimensional lake models is provided, together with a description of the observational dataset and the experimental setup. Section 3 describes the results of the intercomparison, with emphasis on the ability of the different models to reproduce Lake Kivu's mixing cycle, the surface energy exchange and the deep-water stratification. Finally, in Section 4, different options to improve individual model performance are discussed, and the validity of the horizontal homogeneity assumption is investigated.

2. Data and methods

2.1. Lake models

Seven one-dimensional lake models participate in the LakeMIP-Kivu experiment (Table 1). Time step, number of horizontal layers and their interspacing used by the different models are listed in Table 1, including the Central Processing Unit (CPU) time needed to conduct a single

Table 1. Participating one-dimensional lake models and numerical model settings used in this study for Kamembe meteorology runs on a 60 and 240 m depth grid

Lake model	No. of layers	Layer thickness (m)	Time step (min)	CPU time (Kamembe 60 m; 2557 d)*
Hostetler	60	1	60	6.1 s
SimStrat	60/240	1	10	20.5 s
LAKEoneD	60/240	1	5	52.5 s
LAKE	40/40	1.5/6	20	226.0 s
FLake	2	/	60	1.7 s
MINLAKE2012	65/80	1/5	60	8.3 s
CLM4-LISSS	25	Irregular	30	150.0 s

Note that MINLAKE2012 includes fine layer spacing in the first 1 m to facilitate the ice formation prediction. *All CPU times were measured on an Intel Core i5 processor (2.27 GHz), except for CLM4-LISSS (2.1 GHz AMD Magny-Cours processor), a model tailored for a supercomputing environment and therefore not easily portable to a single-processor machine.

simulation. All models compute lake water temperatures and heat, water and momentum exchange between the lake surface and the overlying atmosphere from basic meteorological quantities. A short description of the different models is given below; for more extensive overviews, one is referred to Perroud et al. (2009), Stepanenko et al. (2012) and references herein.

The Hostetler model (Hostetler et al., 1993) includes semi-empirical formulations for the buoyant convection and wind-driven eddy turbulence mixing, adding to the thermal conductivity and molecular diffusion in a multi-layered water column. A second model, the Lake, Ice, Snow and Sediment Simulator within the Community Land Model 4 (CLM4-LISSS; Subin et al., 2012b) is originally based on the Hostetler model, but has undergone major improvements since its first inclusion in CLM2 (Bonan et al., 2002). The now comprehensive treatment of lake snow and ice, bottom sediments, lake depth and surface-atmosphere exchange significantly improved the model’s performance, for shallow to medium-depth small lakes as well as for large, deep lakes (Subin et al., 2012b).

Three models belong to the class of k - ϵ turbulence closure models: LAKEoneD (Jöhnk and Umlauf, 2001; Jöhnk, 2013), SimStrat (Goudsmit et al., 2002) and LAKE (Stepanenko and Lykosov, 2005). They encompass a more sophisticated representation of the turbulent diffusivity (D_{turb}) at a certain depth and time through the relation $D_{turb} = ck^2/\epsilon$, where k is the turbulent kinetic energy, ϵ the turbulent dissipation rate and c either a constant or a stability function, depending on the models (Stepanenko et al., 2012). Although k - ϵ models formally employ identical model equations, some differences in water temperature distribution are expected, given the variations in the coefficients used in the k - ϵ equations, and given the model-dependent treatment of the heat exchange with the overlying atmosphere and underlying bottom sediments.

In contrast to other participating models, that are multi-layered finite difference models, FLake (Mironov, 2008) is a two-layer bulk model, employing the concept of self-similarity to parameterise the temperature-depth curve. FLake consists of a mixed layer of constant temperature and an underlying thermocline down to the lake bottom, the latter parameterised through a fourth-order polynomial depending on a shape coefficient. The mixed layer depth is computed depending on convective entrainment and wind-driven mixing.

Next, MINLAKE2012 presents an update of MINLAKE96 (Fang and Stefan, 1996), used in previous intercomparison experiments. The model solves the one-dimensional, unsteady heat transfer equation using empirical formulations for the variable vertical diffusion coefficient and the heat exchange between water and bottom sediments (Fang and Stefan, 1996). The most important upgrades compared to MINLAKE96 are the conversion to a user-friendly spreadsheet environment and the introduction of variable temporal resolution, allowing to run the model at an hourly time step in contrast to the daily time step previously applicable.

2.2. Observations

2.2.1. Study area. Lake Kivu (01°35’S–02°30’S 028°50’E–029°23’E; 2370 km² surface area; 485 m maximum depth; 1463 m a.s.l.) is located on the border between Rwanda and the Democratic Republic of Congo, and is one of the seven African Great Lakes (Fig. 1). It drains into the Ruzizi, which flows south towards Lake Tanganyika. Below an oxic mixolimnion, which deepens to 60–70 m during the dry season, the monimolimnion is found rich in nutrients and dissolved gases, in particular carbon dioxide and methane (Fig. 2; Degens et al., 1973; Borgès et al., 2011; Descy et al., 2012). Due to the input of heat and salts from deep geothermal springs, temperature

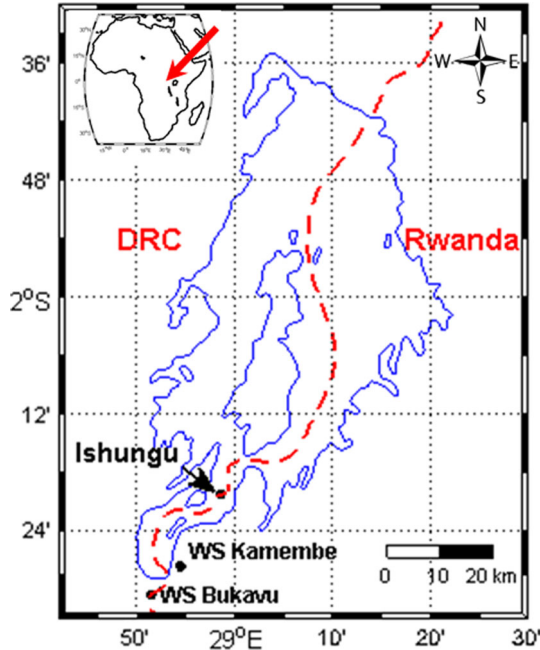


Fig. 1. Lake Kivu with situation of the Ishungu evaluation site and the Kamembe Weather Station (WS Kamembe) and Automatic Weather Station Bukavu (WS Bukavu).

and salinity in the monimolimnion increase with depth (Degens et al., 1973; Spiegel and Coulter, 1996; Schmid et al., 2005). Lake Kivu’s surface water temperatures vary less compared to African Great Lakes located further away from the equator.

2.2.2. Model forcing data. The Kamembe airport Weather Station (WS Kamembe; $02^{\circ}27'31''\text{S}$ – $028^{\circ}54'30''\text{E}$, 1591 m a.s.l.) is used to force the participating lake models. It is situated approximately 1.5 km from the lakeshore and 15 km southwest of the lake monitoring site Ishungu, but is assumed representative for meteorological conditions over this sub-basin. The station records air temperature, T (K); relative humidity, RH (%); air pressure, P (Pa), at three-hourly resolution throughout the whole day; wind velocity, u (m s^{-1}), and direction, WD ($^{\circ}$), at hourly resolution from 6 to 18 UTC (assumed at 4 m height); and precipitation P (mm d^{-1}) at daily resolution. Although it contains only small data gaps during the integration period (January 2002–December 2008), it does not record incoming short-wave radiation SW_{in} (W m^{-2}) and incoming longwave radiation LW_{in} (W m^{-2}), input variables necessary to run the lake models. Hence, both SW_{in} and LW_{in} data were obtained from the ERA-Interim (Dee et al., 2011) grid point closest to the Ishungu evaluation site and converted from six-hourly accumulated values to hourly instanta-

neous values. After linearly interpolating T , RH and p from three-hourly to hourly resolutions, and assuming that the different meteorological variables show only little spatial variability over short distances, data gaps at WS Kamembe were filled with corresponding recordings from an Automatic Weather Station in Bukavu (WS Bukavu, $2^{\circ}30'27''\text{S}$ – $28^{\circ}51'27''\text{E}$), located approximately 8 km southwest of WS Kamembe. After this operation, remaining data gaps were filled by the corresponding, climatological value that was calculated for each hour of the year from available observations. WS Kamembe characteristics and meteorological averages are listed in Table 2.

Furthermore, each simulation was also conducted using the time series of WS Bukavu as forcing (observation height assumed at 10 m). However, since data gaps occur more often at this station, an elaborate gap correction was conducted, whereas comparison to a newly installed, offshore automatic WS led to an upward corrected by 1 m s^{-1} of all measured wind velocities at this station (Thiery et al., 2014). Note that WS Kamembe was chosen as the reference time series since it required less invasive corrections.

2.2.3. Model evaluation data. Model integrations are evaluated using 125 Conductivity–Temperature–Depth (CTD) casts collected at Ishungu ($2^{\circ}20'25''\text{S}$ $28^{\circ}58'36''\text{E}$; Fig. 1) from January 2003 to August 2008. The 125 CTD casts represent a slice of the longest time series of vertical water temperature observations available for a tropical lake (on-going since 2003). Although the CTD casts are primarily representative for the Ishungu sub-basin (101 km²; 180 m maximum depth), the horizontal homogeneity across all sub-basins – except Bukavu and Kabuno bay – allows to assume their representativeness for the whole lake (Section 4). Vertical piecewise cubic Hermite interpolation (increment 1 m; De Boor, 1978) was applied to each cast (original vertical resolution ranging from 0.01 m to 10 m), serving as reference in the evaluation procedure. Note that for visualisation purposes (Fig. 2), an increment of 0.1 m was employed, and the same technique was applied for temporal interpolation (increment 1 d). The model’s ability to reproduce the observed temperature structure was tested using a set of four model efficiency scores: the normalised standard deviation, σ_{norm} ($^{\circ}\text{C}$), the centred Root Mean Square Error $RMSE_c$ ($^{\circ}\text{C}$), the Pearson correlation coefficient r and the Brier Skill Score BSS (Nash and Sutcliffe, 1970; Wilks, 2005). σ_{norm} is computed according to:

$$\sigma_{norm} = \sqrt{\frac{\sum_{i=1}^n (m_i - \bar{m})^2}{\sum_{i=1}^n (o_i - \bar{o})^2}} \quad (1)$$

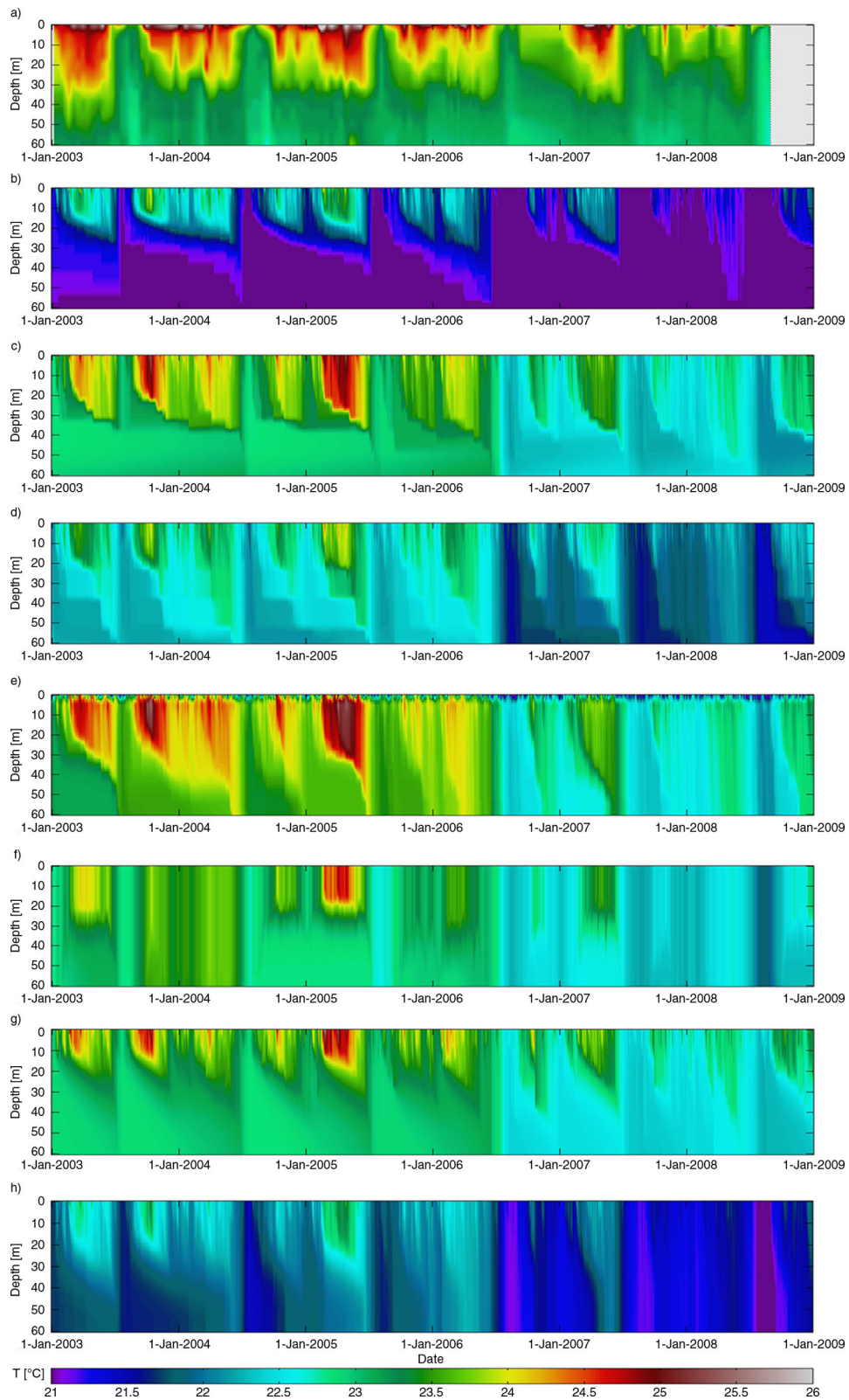


Fig. 2. Lake water temperatures ($^{\circ}\text{C}$) at Ishungu (Lake Kivu), 2003–2008: (a) from observations, and as predicted by the models: (b) Hostetler, (c) LAKEoneD, (d) SimStrat, (e), LAKE, (f) FLake, (g) MINLAKE2012, (h) CLM4-LISSS.

Table 2. Average meteorological conditions at Kamembe Weather Station (WS Kamembe) during the model integration period excluding spin-up (2003–2008)

	Meteorological average*	Measurement frequency	Data gaps (%)	Source
T	19.6°C	3 h	3	WS Kamembe
RH	77%	3 h	4	WS Kamembe
p	842 hPa	3 h	25	WS Kamembe
u	2.7 m s ⁻¹	1 h, 6–18 UTC	47	WS Kamembe
WD	114°	1 h, 6–18 UTC	47	WS Kamembe
P	3.8 mm d ⁻¹	24 h, accumulated	2	WS Kamembe
SW_{in}	193 W m ⁻²	6 h, accumulated	0	ERA-Interim
LW_{in}	361 W m ⁻²	6 h, accumulated	0	ERA-Interim

*Depicted meteorological averages are prior to any correction.

while the $RMSE_c$ is given by:

$$RMSE_c = \sqrt{\frac{1}{n} \sum_{i=1}^n ((m_i - \bar{m}) - (o_i - \bar{o}))^2} \quad (2)$$

with o_i the observed (interpolated) water temperature at time i , \bar{o} the average observed water temperature, and m_i and \bar{m} the corresponding modelled values. Together, σ_{norm} , $RMSE_c$ and r can be visualised in a Taylor diagram (Taylor, 2001). The BSS represents the ratio of the mean square error to the observed variance, and values for BSS range from $-\alpha$, suggesting no relation between observed and predicted value, to $+1$, implying a perfect prediction. Furthermore, while the BSS quickly degrades in the presence of a systematic bias, σ_{norm} , $RMSE_c$ and r are bias-independent model skill scores of the degree of agreement of the variance, the centred pattern of variation and the linear dependence between modelled and observed values, respectively (Taylor, 2001).

2.3. Experimental setup

2.3.1. Parameter and model settings. To obtain a sensible comparison of the treatment of limnological processes within each model, parameter settings have been unified as far as possible in the control and sensitivity experiments. Besides the unifications described hereafter, no additional calibration step was included.

Optical parameters. The light attenuation coefficient of water (k) has a value of 0.27 m⁻¹, computed from the average Secchi depth in Lake Kivu ($Z_{SD} = 5.21$ m; $n = 163$) according to (Poole and Atkins, 1929):

$$k = \frac{-\ln(0.25)}{z_{sd}} \quad (3)$$

where the value 0.25 represents the fraction of the incident solar radiation remaining at the time of the visual disappearance of the Secchi disc used for the measurements. Note

that this fraction was retrieved through 15 simultaneous measurements during 2007 and 2008 of Z_{SD} (using the Secchi disc) and k (using a LI-193SA Spherical Quantum Sensor). Additional lake optical parameters had to be used in the experiments. These are the surface shortwave albedo α_{SW} (0.07), the surface longwave albedo α_{LW} (0.03) and the surface longwave emissivity of the water surface (0.97), the latter serving as input to the Stefan-Boltzmann law. Finally, 35% (β in Table 3) of the incoming solar radiation signal is partitioned to the near-infrared part of the electromagnetic spectrum, while the remainder is attributed to the visible/ultraviolet part. In most models (LAKE, CLM4-LISSS, LAKEoneD, MINLAKE2012 and optionally in FLake), the near-infrared radiation fraction is absorbed directly at the surface, whereas the remaining part (65%) penetrates through the lake water column and is gradually absorbed according to the Beer-Lambert law. The value of β was obtained through integration of the ASTM G-173-03 global reference spectrum (ASTM, 2012) from 280 to 750 nm, and from 750 to 1175 nm and served to determine the visible/ultraviolet and the near-infrared fraction, respectively.

Lake bathymetry. Although a detailed bottom topography of Lake Kivu exists (Lahmeyer and Osaе, 1998), it can only be included in a subset of lake models (LAKEoneD, SimStrat, LAKE and MINLAKE2012). The influence of lake bathymetry was therefore neglected to avoid an additional source of discrepancy among participating models. Since the concerned one-dimensional lake models only implicitly account for the lake bathymetry through the distribution of the geothermal heat – and optionally the exchange with a bottom sediment layer – over the difference in area between two consecutive horizontal layers, this is achieved by equating the surface area of all layers (‘bathtub morphology’).

Surface flux schemes. By unifying the surface flux routines, it would be possible to exclude discrepancies among the participating lake models caused by surface–atmosphere interactions. From the comparison of five stand-alone

Table 3. Net radiation R_{net} (W m^{-2}) calculation used in this study by the different one-dimensional lake models to close the hourly lake energy balance

Lake model	Net radiation calculation
Hostetler	$R_{net} = (1 - \alpha_{SW})SW_{in} + (1 - \alpha_{LW})LW_{in} - LW_{out}$
LAKEoneD	$R_{net} = (1 - \beta)(1 - \alpha_{SW})SW_{in} + \beta SW_{in} + (1 - \alpha_{LW})LW_{in} - LW_{out}$
SimStrat	$R_{net} = (1 - \alpha_{SW})(SW_{in,t-1} + 7/12\Delta SW_{in}) + (LW_{in,t-1} + 7/12\Delta LW_{in}) - LW_{out}$
LAKE	$R_{net} = (1 - \beta)(1 - \alpha_{SW})(SW_{in,t-1} + 2/3\Delta SW_{in}) + \beta(SW_{in,t-1} + 2/3\Delta SW_{in}) + (1 - \alpha_{LW})(LW_{in,t-1} + 2/3\Delta LW_{in}) - LW_{out}$
Flake	$R_{net} = (1 - \alpha_{SW})SW_{in} + LW_{in} - LW_{out}$
MINLAKE2012	$R_{net} = (1 - \beta)(1 - \alpha_{SW})SW_{in,t-1} + \beta SW_{in,t-1} + (1 - \alpha_{LW})LW_{in,t-1} - LW_{out}$
CLM4-LISSS	$R_{net} = (1 - \alpha_{SW})(SW_{in,t-1} + 1/4\Delta SW_{in}) + (LW_{in,t-1} + 1/4\Delta LW_{in}) - LW_{out}$

The terms are: shortwave (longwave) albedo α_{SW} (α_{LW}), incoming shortwave (longwave) radiation SW_{in} (LW_{in}), outgoing longwave radiation LW_{out} , SW_{in} fractioning coefficient $\beta = 0.35$ (35% to near-infrared, 65% to visible/ultraviolet radiation). Formulations are valid for each 1 h output time step (except LAKEoneD where this is for the last time step of each hour), with Δ denoting the change between the previous and current time step. Note that CLM4-LISSS does not account for SW_{in} when the computed zenith angle is at or below the horizon.

surface flux schemes over Lake Kossenblatter, Stepanenko et al. (2013) concluded that differences between these modules indeed impact the lake’s heat budget (from May to November 2003, average LHF and SHF differ up to 19.0 and 3.8 W m^{-2} , respectively). In this study, however, it was chosen to maintain the native surface flux scheme of each participating model. This way, variations in predicted lake water temperatures can be caused both by the representation of lake hydrodynamics and surface-atmosphere interactions. It also makes the comparison more relevant for researchers employing the standard surface fluxes/lake hydrodynamics package available for each model.

Horizontal variability. Horizontal variability of all forcing quantities and external parameters, such as the treatment of the Coriolis effect in LAKEoneD, or the influence of riverine and subsurface groundwater inflows on the thermal structure, are neglected in all the experiments. Meteorological forcing fields of Bukavu and Kamembe are assumed valid at Ishungu. The validity of this assumption is investigated in Section 4.2.

Numerical settings. No stringent requirements are imposed with respect to numerical settings. In particular, the choice of the number of vertical layers, the layer spacing and the model time step was free; an overview is presented in Table 1. However, the evaluation of model output was performed using 5 m layer spacing up to 60 m, and with 20 m layer spacing there below (if applicable), all at a temporal resolution of 1 h. For models using a shorter time step, surface energy balance components are integrated over this period to permit energy balance closure.

Initial conditions. Initial conditions for temperature and salinity in the top 100 m were set by the climatological

vertical profile for January at Ishungu (i.e. the mean profile computed from the 14 CTD casts collected in January). Salinity (S) in g l^{-1} is calculated from measured conductivity (C) in mS cm^{-1} using the relationship $S = 0.4665C^{1.0878}$ derived by Williams (1986). The conditions below this depth, and initial concentrations of dissolved CO_2 and CH_4 are estimated from Schmid et al. (2005).

2.3.2. Control and sensitivity experiments. To assess and understand the ability of different lake models to reproduce both the mixolimnion temperature variability and the deep-water stratification, two control integrations were conducted with each model. In the first simulation, an artificial lake depth of 60 m was imposed to each model. Additionally, effects induced by salinity, aquatic chemistry and geothermal sources were neglected in this simulation, leaving the computation of the water column stability to the native equation of state of the respective models. The calculation of heat conduction through the bottom sediments was switched off in the models explicitly treating this process (FLake, CLM4-LISSS, LAKE and MINLAKE2012). This first experiment is hereafter referred to as the freshwater simulation. The freshwater simulation focuses on the depth range influenced by seasonal variability: given the relatively homogeneous salt content in this layer, water temperatures vary according to meteorological variability (Section 3.2), whereas below ~ 65 m, the stabilizing salinity gradient causes a permanent stratification and therewith inhibits seasonal temperature variability (Schmid and Wüest, 2012).

In the second control integration, set up to investigate deep water stratification, a subset of models was run with

the observed average depth of 240 m. Note that FLake, Hostetler and CLM4-LISSS cannot be applied in this case as they do not account for salinity. FLake, moreover, assumes the extension of the thermocline layer down to the lake bottom. Here, the bottom sediment routine was switched on in the models treating the exchange of the water body with the underlying sediments. Furthermore, following computations by Schmid et al. (2010), an upward bottom heat flux of 0.3 W m^{-2} is introduced in each model, either at the water bottom interface (SimStrat, MINLAKE2012 and LAKEoneD), or at the lowest layer of bottom sediments (LAKE). Finally, the effects of salinity and dissolved gas concentrations upon water column stratification are accounted for in LAKEoneD, LAKE and MINLAKE2012 through implementation of one and the same equation of state for the water density ρ (kg m^{-3} ; Schmid et al., 2004):

$$\begin{aligned} \rho(T, S, CO_2, CH_4) \\ = \rho(T) \left(1 + \beta_S S + \beta_{CO_2} CO_2 + \beta_{CH_4} CH_4 \right) \end{aligned} \quad (4)$$

with $\rho(T)$ water density (kg m^{-3}) depending on water temperature T (K) only, S salinity (g kg^{-1}), CO_2 and CH_4 carbon dioxide and methane mass concentrations, respectively (g kg^{-1}), β_S the coefficient of saline concentration ($0.75 \times 10^{-3} \text{ kg g}^{-1}$; Wüest et al., 1996), β_{CO_2} the coefficient of CO_2 concentration ($0.284 \times 10^{-3} \text{ kg g}^{-1}$; Ohsumi et al., 1992), and β_{CH_4} the coefficient of CH_4 concentration ($-1.25 \times 10^{-3} \text{ kg g}^{-1}$; Lekvam and Bishnoi, 1997). Note that profiles of S , CO_2 and CH_4 are kept constant throughout the simulation period. This second experiment is hereafter referred to as the deep simulation.

To compare the model's computational expense, CPU times needed to conduct the WS Kamembe driven simulation at 60 m depth (2557 d) were recorded for each model (Table 1). CPU times indicate that FLake is the fastest one-dimensional model, followed by Hostetler, which partly explains their success when it comes to coupling with climate and NWP models (e.g. Martynov et al., 2012). The slowest model is LAKE: it requires, for instance, 133 times more computational resources compared to FLake. Although the differences in computation time between one-dimensional models (10^0 – 10^2) are smaller than typical differences between one- and three-dimensional models (10^3 – 10^4 , Jöhnk and Umlauf, 2001) – this issue requires consideration in applications where computational efficiency is critical.

Besides the two control integrations from January 2002 to December 2008, 12 additional sensitivity experiments were designed. In particular, a subset of the models was run at both depths for the highest and lowest observed value of the light attenuation coefficient, while for the deep simulation additional experiments without geothermal heat flux and without bottom sediments were conducted.

Additionally, each control and sensitivity integration was conducted using the WS Bukavu forcing fields from January 2003 to December 2011. Both in the control and sensitivity experiments, the first year was considered as spin-up and removed from the results. Subsequently, the output of the models was vertically interpolated (increment 1 m) using the piecewise cubic hermite interpolation technique (De Boor, 1978).

3. Results

3.1. Model performance over the mixolimnion

While throughout most of the year, Lake Kivu is weakly stratified below 10–30 m, the mixed layer deepens during the dry season to approximately 60 m (Fig. 2a), driven primarily by the significantly reduced RH at that time, which opens up the potential for evaporative-driven cooling of near-surface waters, and secondly by the reduced LW_{in} reaching the lake surface due to lower cloudiness (Thiery et al., 2014). In general, all models succeed in reproducing the enhanced stratification during the rainy season relative to the dry season (Fig. 2). Hostetler, CLM4-LISSS and SimStrat however display clearly lower water temperatures, suggesting an underestimation of heat entering the lake (Fig. 2b, d). Since this affects the whole water column, it cannot be primarily due to differences in the mixing processes, but is likely due to a different surface energy exchange. In Section 3.2., this issue is further investigated. Furthermore, in the top 5 m of the water column, LAKE predicts a slightly unstable stratification (Fig. 2e). This can be ascribed to a numerical precision artefact of the fully implicit time stepping scheme employed in this model. For each iteration, the numerical procedure solves the temperature conductance equation including radiative heating, and using a Dirichlet top boundary condition. The temperature profile will therefore contain its temperature maximum close to the surface – instead of at the surface – with the abundance of this maximum depending on the eddy conductance at the top layers calculated by the k - ϵ scheme. Hence, in LAKE the top boundary conditions of the k - ϵ parameterisation might be inappropriate to successfully simulate the mixing at the top of water column.

From mid-2006 onwards, a sudden temperature decrease appears in all simulated time series, a change hardly visible in the measured data. This apparent cooling is related to a change in the meteorological forcing. During the 2006 dry season, wind velocities attain clearly higher values compared to other years (4.3 m s^{-1} versus 3.6 m s^{-1} for JJA), with the maximum wind velocity measured at this station since 1977 occurring during this period (35 m s^{-1} on 19 June 2006). Especially in the models LAKEoneD, SimStrat and LAKE,

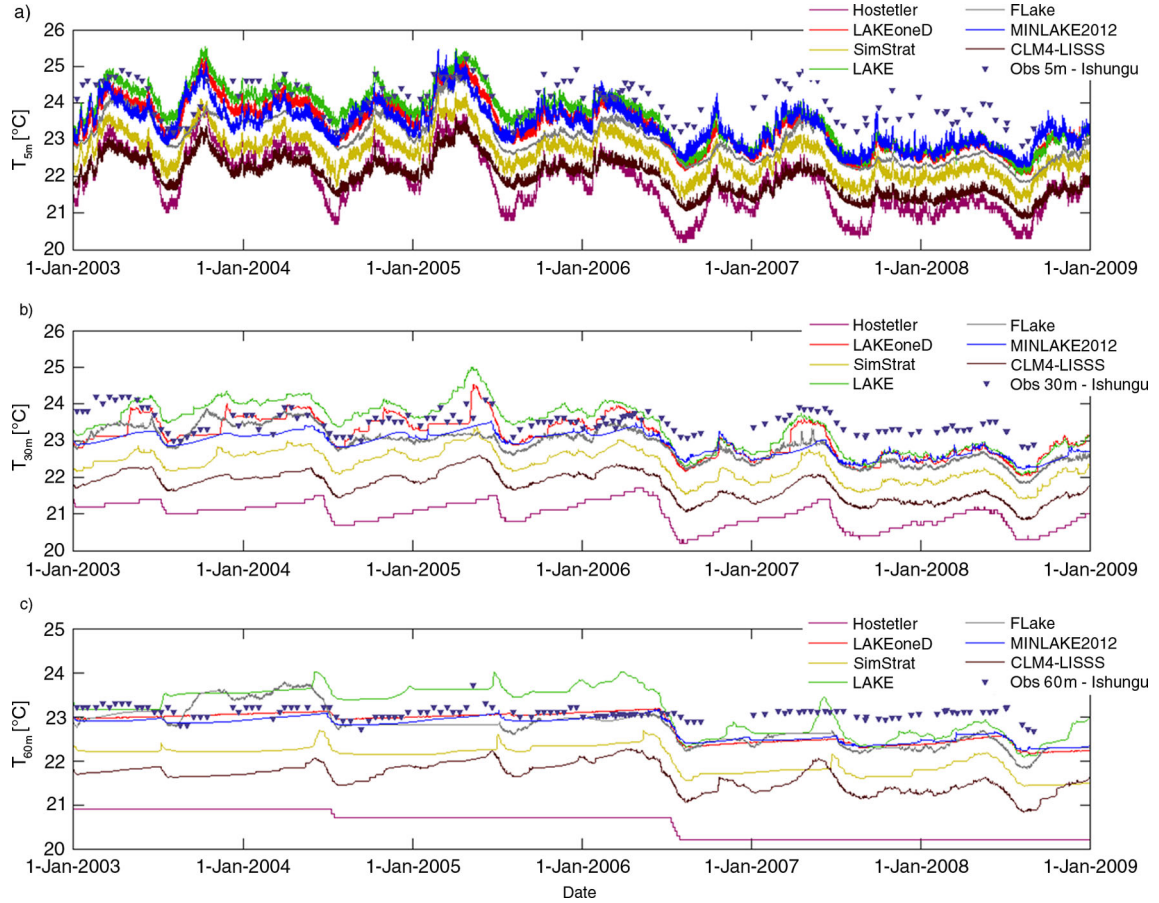


Fig. 3. Modelled and observed temperature evolution at Ishungu (Lake Kivu), 2003–2008, at (a) 5 m, (b) 30 m, and (c) 60 m depth.

but to a lesser extent also in FLake, MINLAKE2012 and CLM4-LISS, the enhanced winds cause a more intense evaporative driven cooling at the start of the dry season relative to previous years. Comparing modelled to observed water temperatures at 5, 30 and 60 m illustrates that this sudden cooling results in a negative bias in all models from mid-2006 onwards (Fig. 3). Before that time, however, nearly all models very closely reproduce observed near-surface water temperatures at Ishungu. Hence, either all models react too strong to the enhanced wind speeds, or wind speeds are overestimated during this period.

Vertical profiles of the BSS (1 m vertical increment, BSS below -20 were set to -20) indicate that models skills decrease with depth in all models (Fig. 4a). Since the BSS accounts for the effect of a systematic bias, BSS for Hostetler, CLM4-LISS and SimStrat quickly reach low values. A Taylor diagram, in contrast, allows us to assess model performance irrespective of a possible systematic bias, given its use of the normalised standard deviation σ ($^{\circ}\text{C}$), the centred Root Mean Square Error, $RMSE_c$ ($^{\circ}\text{C}$), and the Pearson correlation coefficient, r . Here, surprisingly, the best model scores at 5 m are attained by

CLM4-LISS ($\sigma_{norm} = 0.98$; $RMSE_c = 0.36^{\circ}\text{C}$; $r = 0.76$), SimStrat ($\sigma_{norm} = 1.11$; $RMSE_c = 0.39^{\circ}\text{C}$) and Hostetler ($r = 0.78$) (Fig. 5a). Also at 30 and 60 m, all three models depict high skills: at these depths they are only outperformed by MINLAKE2012 in terms of σ_{norm} and $RMSE_c$ (Fig. 5b–c). Hence, although Hostetler and SimStrat both depict a cold bias, they most successfully reproduce seasonal and interannual lake water temperature variability. On the other hand, towards deeper layers both LAKE and, to a lesser extent, FLake depict reducing skill compared to other models (Fig. 5b–c). For LAKE, the overestimation of the observed variance can probably be explained by a higher sensitivity of LAKE to wind velocity relative to other models (Fig. 2), whereas for FLake, this might be ascribed to the fully mixed conditions predicted during the 2003–2004 wet season (Fig. 1f): in both cases this increases the deep water temperature variability during the integration period (Fig. 2c).

The different sensitivity experiments generally show only a small response from the models, except for FLake. This model exhibits a marked sensitivity to its configuration. Setting the light attenuation coefficient k to the highest and

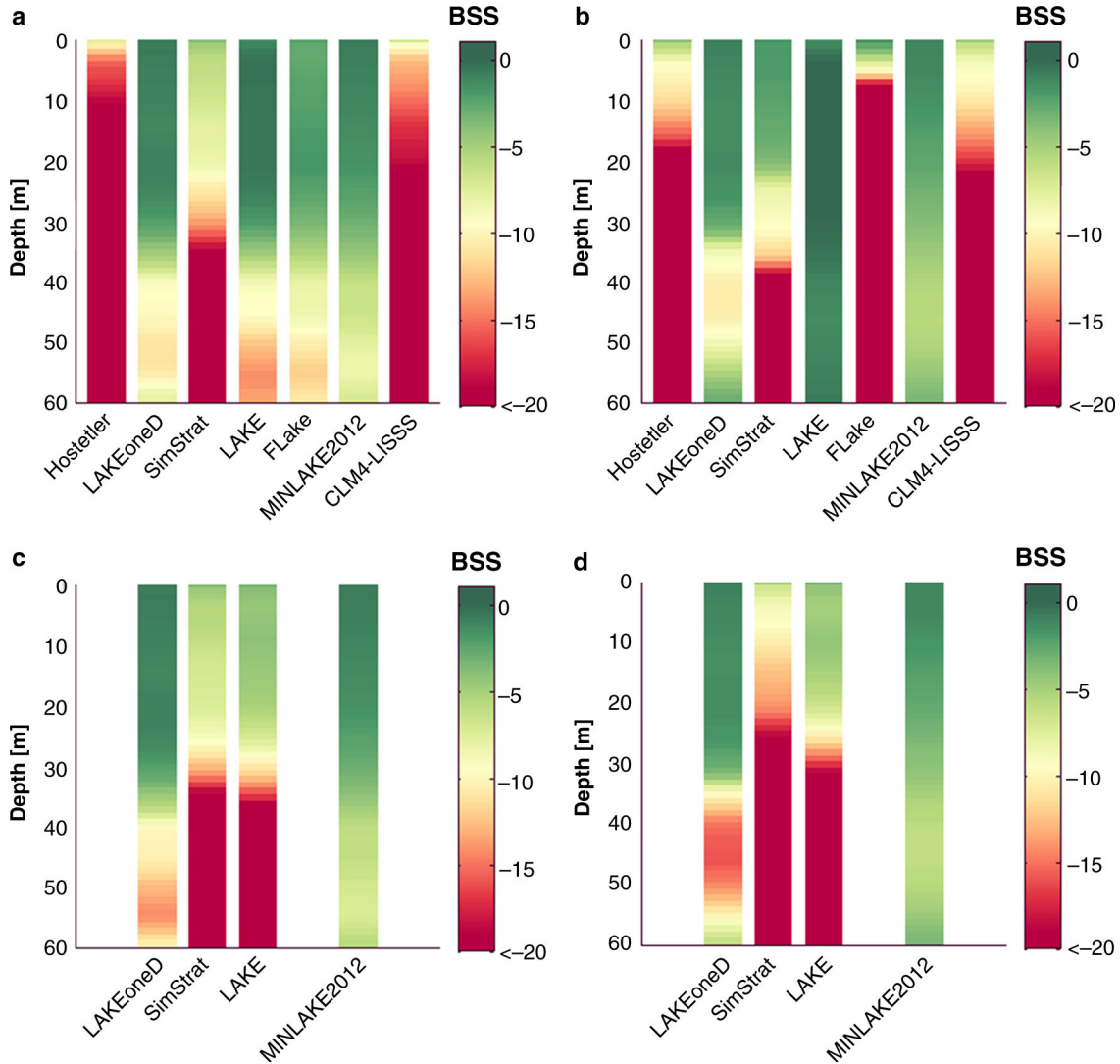


Fig. 4. Brier Skill Score (*BSS*) vertical profiles at Ishungu (Lake Kivu), calculated per 1 m vertical increment over the respective integration period, for (a) the WS Kamembe 60 m, (b) the WS Bukavu 60 m, (c) the WS Kamembe 240 m and (d) the WS Bukavu 240 m integrations. Note that Hostetler, FLake and CLM4-LISSS were not applied in the 240 m depth experiment.

lowest value observed at Ishungu (WS Kamembe forcing), generally has little effect upon the different model's ability to represent water column temperatures. Vertically averaged BSS never change more than 20%, except for FLake in case of increasing k (*BSS* reduces by 60% as average water column temperature values cool by 0.15°C) and MINLAKE2012 when decreasing k (*BSS* increases by 25%). Note that when k is reduced to 0.20 m^{-1} , *BSS* increases for Hostetler, LAKEoneD, FLake and MINLAKE2012.

Each control and sensitivity experiment was also conducted using meteorological measurements at Bukavu (Fig. 1) as forcing. Relative to the WS Kamembe driven control integration, vertically averaged *BSS* of Hostetler, LAKEoneD, SimStrat, MINLAKE2012 and CLM4-LISSS

showed little to no change when forced by the alternative dataset (Fig. 4b). In contrast, LAKE enhances its predictive skill, whereas FLake's predictions deteriorate below $\sim 5\text{ m}$. For LAKE, model predictions improve especially because the observed water temperature variability at depth is well captured when forced by WS Bukavu. When LAKE is forced by WS Kamembe, significant wind velocity increases during the dry season result in too strong mixing. For FLake, the WS Bukavu driven simulation decreases in predictive skill as from mid-2004 onwards, a strong cooling of the thermocline layer sets in, reaching down to the temperature of maximum density (4°C) near the bottom. Note, however that this effect does not influence the good skill of FLake near the surface (Fig. 4a, b).

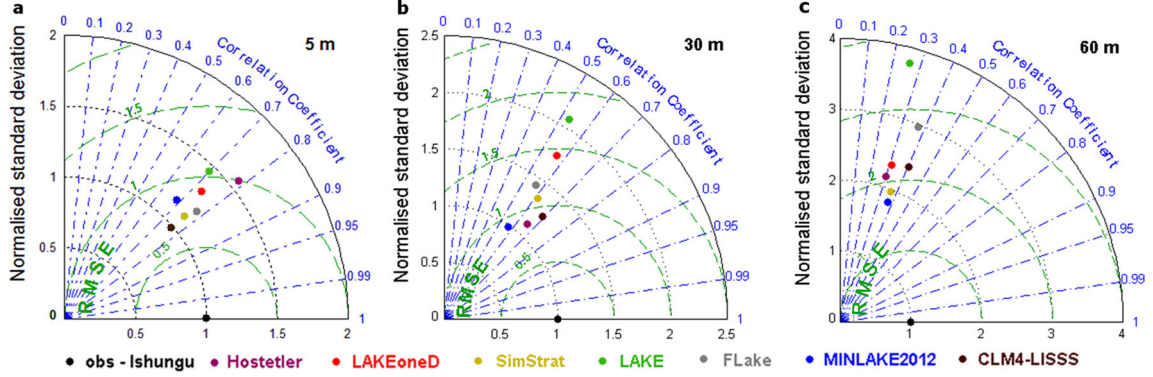


Fig. 5. Taylor diagram indicating model performance for water temperature at (a) 5 m, (b) 30 m and (c) 60 m depths at Ishungu (Lake Kivu), 2003–2008. Standard deviation σ ($^{\circ}\text{C}$; radial distance), centred Root Mean Square Error $RMSE_c$ ($^{\circ}\text{C}$; distance apart) and Pearson correlation coefficient r (azimuthal position of the simulation field) were calculated from the observed temperature profile interpolated to a regular grid (1 m increment) and the corresponding modelled midday profile.

This cooling of the thermocline layer in FLake has been encountered in previous studies (Subin et al., 2012b; Thiery et al., 2014) and during the development of its online version, FLake-Global (Kirillin et al., 2011). The thermal behaviour of dimictic and temperate polymictic lakes, where the average water column temperature approaches the temperature of maximum density twice or several times a year, respectively, can generally be reproduced very closely by FLake (e.g. Kirillin, 2010; Martynov et al., 2010). Lake Kivu’s mixolimnion, in contrast, is characterised by a weak stratification, with a seasonally mixed layer deepening down to ~ 60 m, so the model needs to be able to develop and maintain this weak stratification. Possibly, the observed transition to the shallow, permanent stratification and cold bottom is related to the self-similar representation of the shape factor of the thermocline and its time rate-of-change. When the mixed layer deepens, FLake will respond by changing its thermocline shape towards a more convex shape (Mironov, 2008). However, during aforementioned cooling, the thermocline’s shape factor is permanently at its maximum value, 0.8 (maximum convexity), thus inhibiting any thermocline response to mixed layer deepening. As the small-scale fluctuations of the mixed layer depth are not mirrored by changes in the thermocline shape, they could cause an unphysical loss of heat from the thermocline layer. This effect might be responsible for the observed cooling near the lake bottom which can reach down to 4°C and therewith trigger an irreversible switch to a permanently stratified mixing regime, but further research is necessary to investigate this issue.

3.2. Lake energy balance

Differences in column-integrated water temperatures between the one-dimensional lake models can be understood when comparing their lake energy budget. To this end, we

first employ the relationship describing the enthalpy change H_{obs} of the lake’s top 60 m (assuming constant pressure):

$$H_{obs} = h\rho c_p \frac{d\bar{T}}{dt} \quad (5)$$

with h the water column height (60 m), ρ the lake water density (1000 kg m^{-3}), c_p the specific heat capacity of water at constant pressure ($4.1813 \times 10^3 \text{ J kg}^{-1} \text{ K}^{-1}$) and $d\bar{T}/dt$ the average water column temperature change computed per output time step based on the observed temperature profiles. Since all models switched off the bottom sediment routine and adopted a zero heat flux assumption at the artificial lake bottom, the predicted enthalpy change H_{mod} is given by:

$$H_{mod} = R_{net} - LHF - SHF \quad (6)$$

with R_{net} the net radiation, and with LHF and SHF the turbulent fluxes of latent heat and sensible heat, respectively (all units W m^{-2}). Comparison of monthly average H_{obs} and H_{mod} shows that H_{obs} is well captured by the different models throughout most of the year (Fig. 6a). Although the observed variation is also subject to uncertainty, this given the CTD casts’ low temporal resolution and variable collection hours, the good agreement between model and observation indirectly suggests that the seasonal cycles of the radiative inputs and turbulent fluxes are correctly reproduced.

Besides variations in the computation of LHF and SHF , also different formulations are employed by the models to determine R_{net} , as shown in Table 3. In particular, note that FLake and CLM4-LISSS assume $\alpha_{LM} = 0$, while LAKE and LAKEoneD assume $\alpha_{SM} = 0$ for the near-infrared fraction of SW_{in} , on average responsible for a higher energy input into the lake of 11 W and 5 W m^{-2} , respectively. Also, given the small time step used by LAKE, SimStrat and CLM4-LISSS, SW_{in} and LW_{in} require modification to achieve

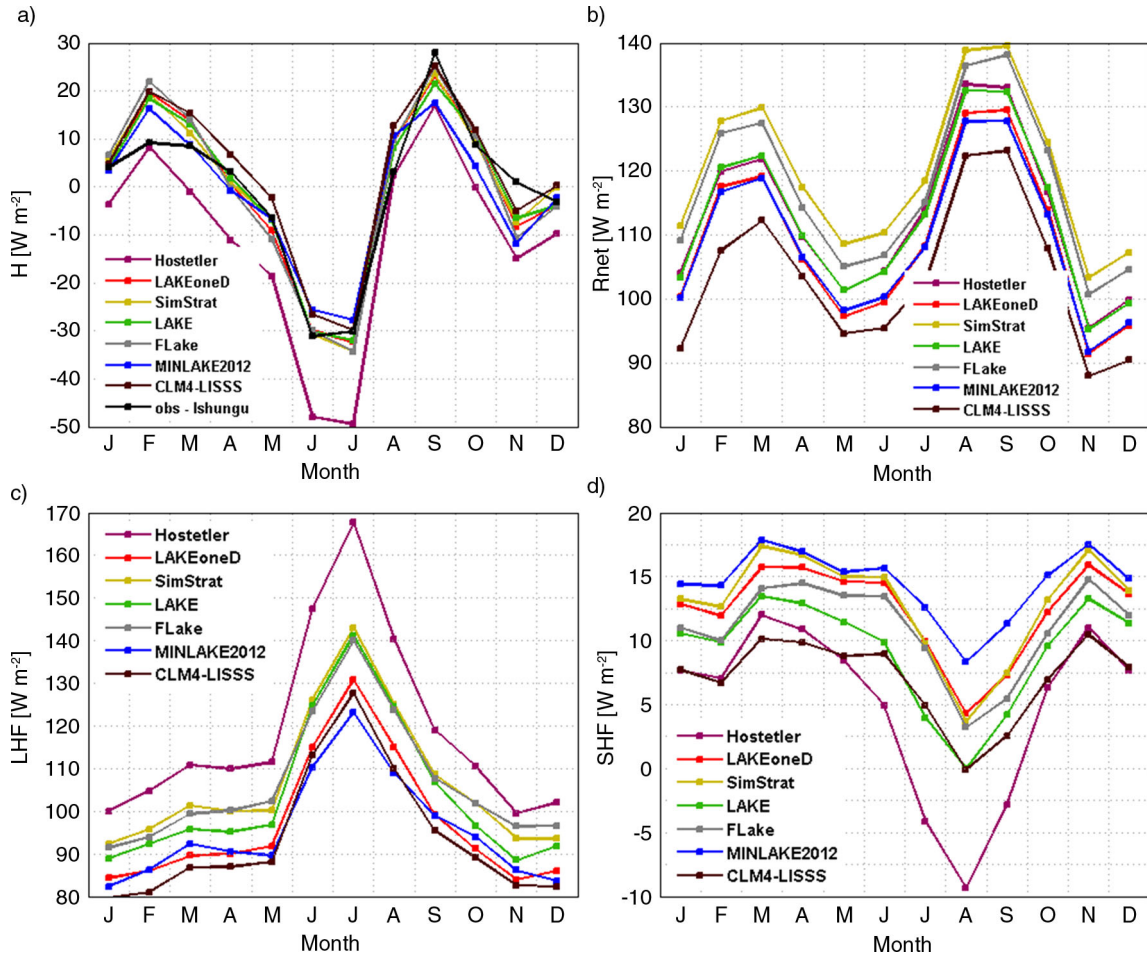


Fig. 6. Monthly average lake energy balance components (W m^{-2}) at Ishungu (Lake Kivu), 2003–2008, calculated by model’s surface flux routines. Components are (a) lake enthalpy change H , (b) net radiation R_{net} , (c) latent heat flux LHF , and (d) sensible heat flux SHF .

surface heat balance closure over each output time step. Finally, MINLAKE2012 employs the input radiative fluxes of the previous time step to compute hourly values. As a consequence of these differences, models predict variable radiative input into the lake: maximum discrepancies of monthly mean R_{net} values range from 13 to 20 W m^{-2} (Fig. 6b). The radiative input into the lake peaks twice a year: once during February–March and again during August–September, in agreement with the two distinct maxima in SW_{net} and the drop in LW_{net} from May to July.

In contrast to the treatment of radiative fluxes, turbulent energy exchanges show more variation among different models. For instance, relative to other participating models, in the Hostetler model, a higher portion of the available heat is consumed by evaporation: the annual mean LHF in the control integration is 14 W m^{-2} higher relative to the multi-model mean LHF (105 W m^{-2} ; Fig. 6c), equivalent to an enhanced total lake evaporation of $0.5 \text{ km}^3 \text{ yr}^{-1}$. Over time, the resulting year-round reduction in net energy

available to heat the lake will therefore enhance the cold bias observed for the Hostetler model (Fig. 6a, c), even though the enhanced evaporative cooling is partly compensated by the limited energy loss through the SHF and the higher radiative input into the lake, equivalent to 6 W m^{-2} lower and 2 W m^{-2} higher compared to multi-model means, respectively (Fig. 6d, b). For SimStrat, in turn, on the one hand slightly higher radiative input into the lake ($+7 \text{ W m}^{-2}$ relative to the multi-model mean) and on the other hand slightly positive LHF ($+4 \text{ W m}^{-2}$) and SHF ($+3 \text{ W m}^{-2}$) anomalies compensate for each other and generate a close reproduction of the observed enthalpy change, hence no change of the cold bias is expected (Fig. 6a, c, d). By analogy, also for CLM4-LISSS the cold bias is not expected to change over time (Fig. 6a). In future intercomparison experiments, wherein lake models will be interactively coupled to atmospheric models, the impact of variations in the turbulent heat fluxes on lake models will require further attention.

Besides differences among the models, also intra- and inter-annual variations in the water column stratification can be attributed to meteorological variability and associated changes in the lake energy balance. Since all models report high to very high correlations between wind velocity and LHF (with correlation coefficients up to 0.95 ($p < 0.01$) in Hostetler and LAKEoneD, for instance), and because stronger winds cause enhanced mechanical mixing, variations in wind speed must certainly be considered in this case. In particular, the increasing annual mean wind velocities explain the generally reducing stratification observed throughout the integration period, as well as the sudden decrease in water temperatures observed mid 2006

(Section 3.1) and the very weak stratification during the first months of 2008 (Fig. 2a). However, variations in wind velocity provide no explanation for the high near-surface water temperatures and relatively strong stratification observed during the first months of 2005 (Fig. 2a). During this period, enhanced solar radiation reaches the lake surface, therewith increasing the amount of energy available to stratify the near-surface layers. In response to this relatively high radiative forcing (Fig. 7c), but normal turbulent heat fluxes (Fig. 7a, b) at the start of 2005, all models show similar variability in the lake's enthalpy change (Fig. 7d), and therewith reproduce the enhanced stratification during this period.

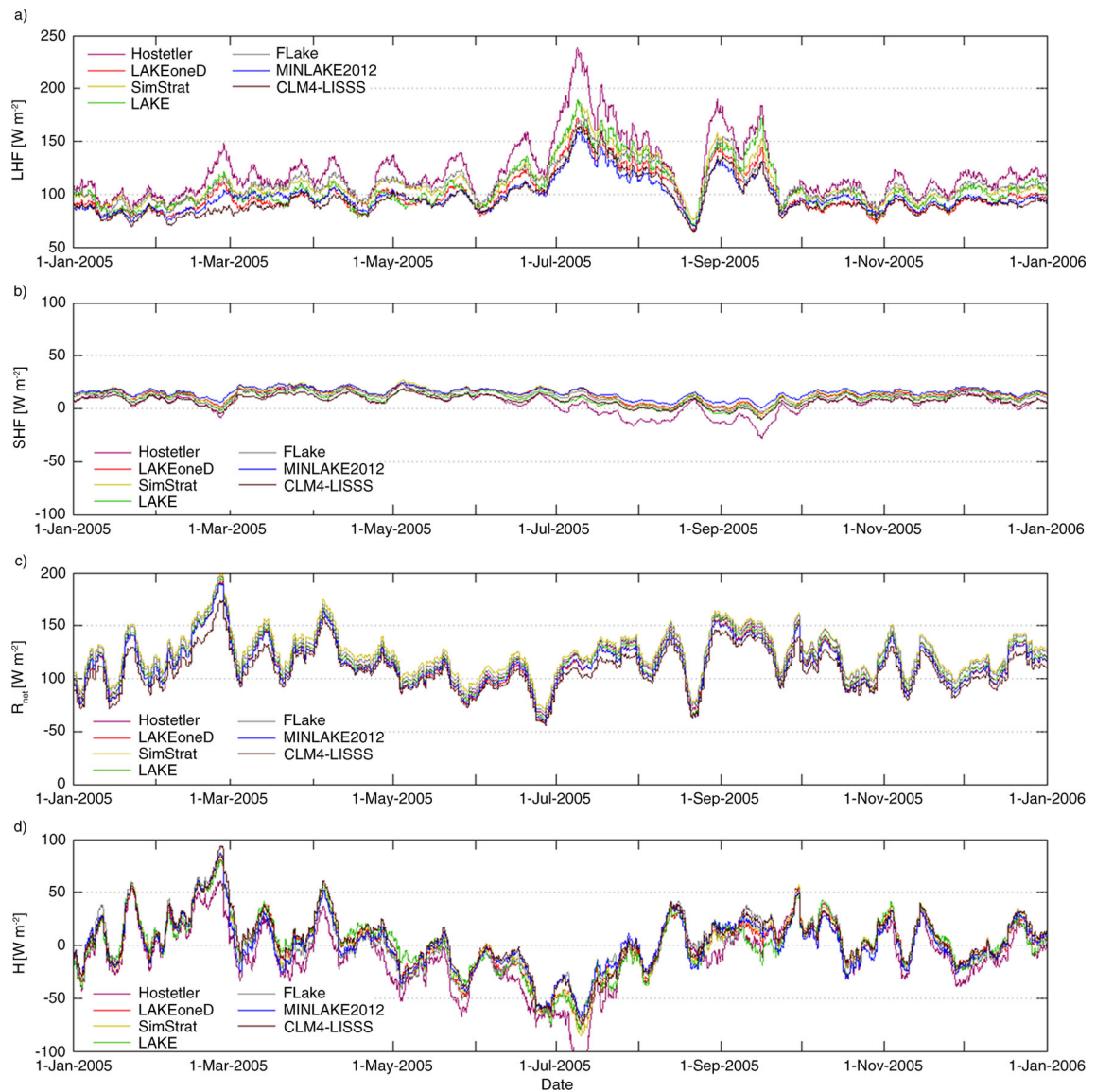


Fig. 7. Running mean lake energy balance components (W m^{-2} ; 7 d averaging window) at Ishungu (Lake Kivu), for 2005. Components are (a) latent heat flux LHF , (b) sensible heat flux SHF , (c) net radiation R_{net} , and (d) the resulting lake enthalpy change H .

3.3. Deep-water stratification

The deep simulations conducted by a subset of models (LAKEoneD, SimStrat, LAKE, MINLAKE2012) all succeed in reproducing Lake Kivu's meromictic state (Fig. 8). Compared to the corresponding freshwater simulation, all models display similar *BSS* for the top 60 m of the water column, except for LAKE, where a cold bias decreases the

BSS towards 60 m (Fig. 4c). Again, it is found that setting the light extinction coefficient to the highest and lowest observed values at Ishungu, or switching off the bottom sediment routine, has little to no impact upon the results of LAKEoneD, LAKE and MINLAKE2012.

Below 60 m, modelled temperature variations are only regulated by thermal diffusion. In the permanently

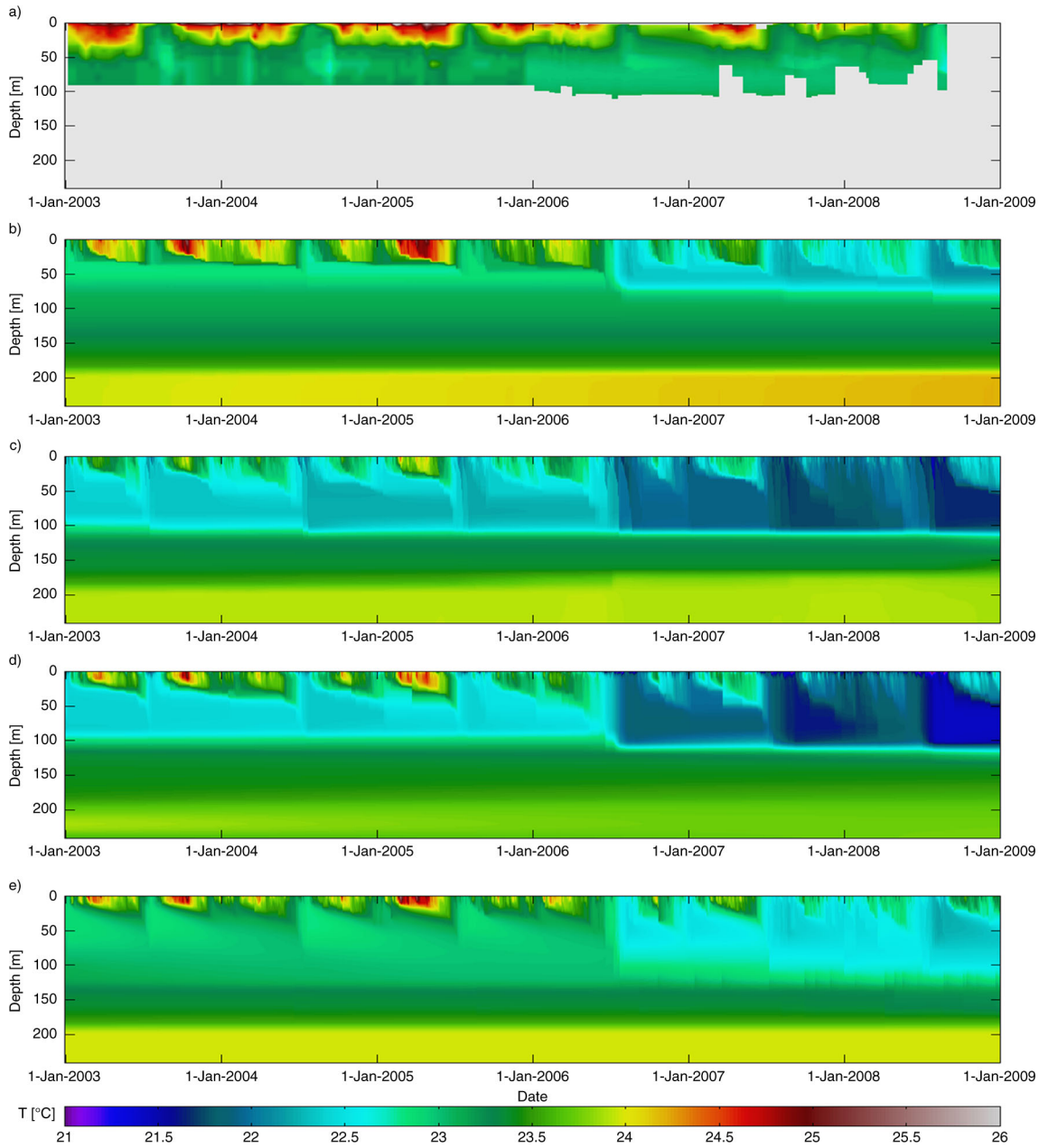


Fig. 8. Lake water temperatures (°C) at Ishungu (Lake Kivu), 2003–2008: (a) as observed, and as predicted by the models: (b) LAKEoneD, (c) SimStrat, (d) LAKE, (e) MINLAKE2012 for the 240 m deep geometry. Note that linear interpolation was applied to the observed Ishungu profiles to avoid spurious extrapolation effects, and grey areas therefore denote depths or longer time periods for which no observations are available.

stratified hypolimnion represented in the deep simulations (Fig. 8), the eddy diffusivity usually vanishes and molecular diffusivity becomes the dominant term. In lake Kivu, both double diffusive convection (Schmid et al., 2010) and subsurface inflows (Schmid et al., 2005), associated with the slow upward motion of the whole water column by about 0.5 m yr^{-1} , additionally influence the deep water temperature structure. However, none of the models involved in this study include mechanisms to account diffusivity generated by these processes. Nevertheless, the predicted temperature profiles still fairly correspond to the observed temperature profile in the main basin during February 2004 (Schmid et al., 2005), that is, 2 yr after being initialised with this profile (Fig. 9).

In the last $\sim 50 \text{ m}$ above ground, the heat input into the deep zone starts to influence water temperatures. At the bottom of Lake Kivu, strong geothermal heating can be expected due to its location on the East African rift. In addition to the geothermal heat flow, some warm, subaquatic springs heat the bottom layers. Together, their magnitude was estimated at $0.1\text{--}0.3 \text{ W m}^{-2}$ by Schmid et al. (2010). The excess heat is removed both by the upward motion and enhanced diffusion through the double-diffusive staircases (Schmid and Wüest, 2012). Relative to the sensitivity experiment wherein the bottom heat flux is neglected, average temperature of the lowest 50 m is $0.02\text{--}0.18^\circ\text{C}$ higher when including the bottom heat flux leads, while the water masses above this depth are almost not affected by the bottom heat flux. Throughout the integration period, LAKEoneD exhibits a warming trend of 0.24°C for the lowest 50 m , while the other comprehensive model show no temperature change for this zone.

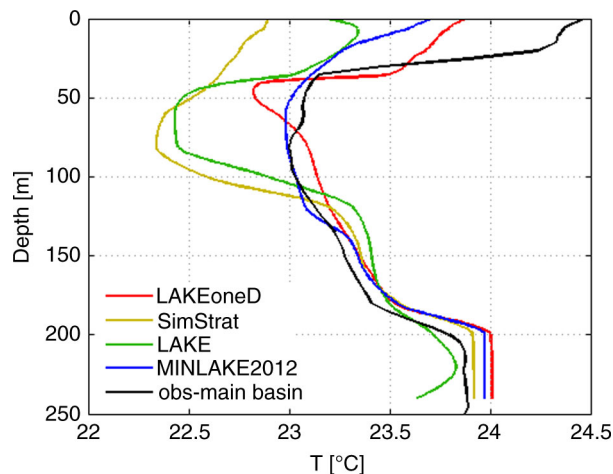


Fig. 9. Comparison of the observed temperature profile representative for the main basin during February 2004, as reported by Schmid et al. (2005; reproduced with permission), and corresponding modelled profiles (February 2004 average).

4. Discussion

4.1. Model improvement

At this point, an interesting question is if, and in which way, the performance of individual models can be improved. For instance, for FLake, which was found sensitive both to its model configuration and forcing fields when applied to a deep, tropical lake, enhancing the robustness of the model would be beneficial. Work is currently underway to meet this need. Therewith, potentially this model will become more applicable to large, deep lakes for which no accurate forcing fields and external parameter values are available.

While for the one-dimensional lake models Hostetler, CLM4-LISSS and SimStrat, a key asset is the ability to capture the observed water temperature variability, a cold bias is observed in each case (Figs. 5, 6). However, the systematic bias can be removed through a calibration step. To illustrate the potential of a bias correction procedure, all simulations with the SimStrat model were also conducted using a modified calibration parameter for the turbulent heat fluxes. In SimStrat, the *SHF* and *LHF* are deduced from an empirical formulation which contains a parameter to calibrate the obtained result within a certain range. Through a much better reproduction of the observed lake enthalpy change, SimStrat predictions significantly improved: for instance, for the WS Kamembe driven freshwater simulation, there is now a very close agreement between modelled and observed water temperatures (Figs. 2, 10). In particular, the vertically averaged *BSS* increased from -23.5 to -2.9 , therewith even obtaining the highest score of all models. In short, the success of the bias correction procedure illustrates

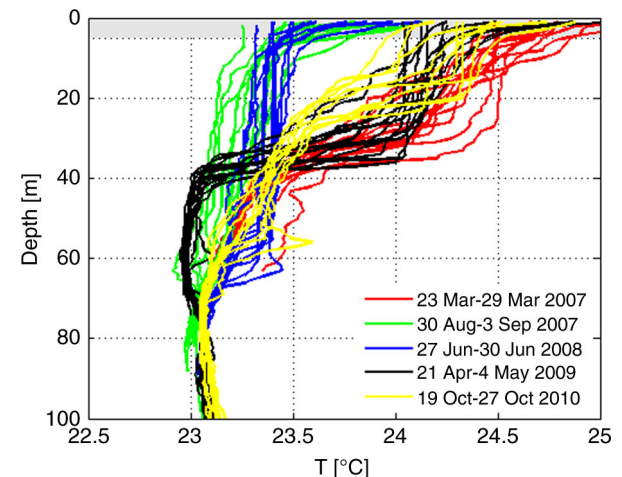


Fig. 10. Temperature profiles collected at 14 different locations in Lake Kivu during five cruises. Profiles collected at Bukavu and Kabuno bay are omitted due to their clear deviation from profiles of the main basin. Differences in the top 5 m (grey shade area) are partly due to daily variations.

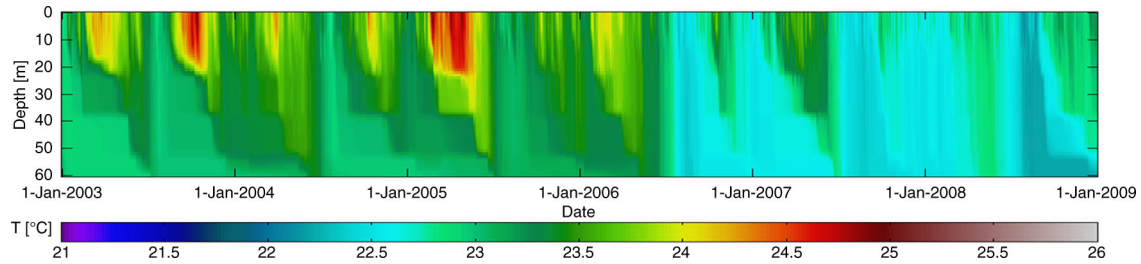


Fig. 11. Lake water temperatures ($^{\circ}\text{C}$) at Ishungu (Lake Kivu), 2003–2008, as predicted by SimStrat, using a modified turbulent heat flux calibration parameter.

the added value of a model outcome containing a systematic bias, but a correct reproduction of the observed variability, over an unbiased prediction that fails to reproduce the observed variability.

4.2. Validity of the horizontal homogeneity assumption

Analysis of 60 temperature profiles collected during five cruises from March 2007 to October 2010 shows that spatial differences are clearly less important than seasonal variations (Fig. 11). Maximum horizontal temperature variations during a single cruise range from 0.3 to 0.6°C (0.5°C on average) at 5 m depth, while maximum temporal temperature fluctuations at one location range from 0.3 to 1.5°C (1.1°C on average) at 5 m . Towards 60 m , vertical temperature profiles converge, both in space and time. In agreement, previous studies report very similar thermal, chemical and biological lake characteristics across all sub-basins except Bukavu and Kabuno bay, and attribute horizontal homogeneity in the monimolimnion to long residence times (Sarmiento et al., 2006; Pasche et al., 2009; Tassi et al., 2009; Pasche et al., 2011; Schmid and Wüest, 2012). The assumption of horizontal homogeneity can thus be considered valid for Lake Kivu.

5. Conclusion

The model intercomparison experiment for Lake Kivu showed that all models succeed in reproducing the timing and magnitude of water temperatures in the mixolimnion and the observed lake enthalpy change. Moreover, during the integration period the models accounting for the effects of salinity and dissolved gasses upon the water column stratification can correctly represent the meromictic state of Lake Kivu. At the same time, this study also revealed a number of strengths and weaknesses for the different groups of models.

First, while FLake is computationally the most efficient and depicts good predictive skill in the control simulation compared to other models, water temperatures towards the bottom of Lake Kivu's mixolimnion are found sensitive to modifications in the forcing fields and model configuration.

Further research is needed to address the ability of FLake to represent weakly stratified lakes. However, since near-surface temperatures, in contrast to near-bottom temperatures, are more robust, the model remains a good candidate in applications where a quick and reliable computation of lake surface temperatures is important.

Second, given their limited computational expense, the Hostetler-based models (Hostetler and CLM4-LISSS) are also attractive candidates to represent lake processes within atmospheric models. Although both models predict colder water temperatures compared to observations, they correctly reproduce the observed variability, and a model calibration can potentially correct for the small systematic bias.

Third, the more comprehensive lake models, that is, MINLAKE2012 and the k - ϵ models SimStrat, LAKE and LAKEoneD, not only capture the variability of Lake Kivu's mixolimnion and therewith the effects of the meteorological controls on mixing, they also succeed in reproducing the effect of salinity and dissolved gases on the stratification. Sometimes, individual models react stronger to a certain forcing than other models, such as the heating in the lowest layers of LAKEoneD in response to the imposed geothermal heat flow (deep simulation), or the marked response to wind stress in LAKE. However, altogether, the considered comprehensive lake models are suited to investigate hydrodynamic processes occurring within large, deep lakes, and therewith make way for further studies of, for instance, biogeochemical cycling within these lakes.

Thanks to this and previous lake model intercomparison studies, the selection of a one-dimensional lake model most appropriate for a certain purpose can now be based on an informed choice. The aforementioned set of strengths and weaknesses may serve as a first indication in this respect. At the same time, this set calls for continuing the development of individual lake models, and for monitoring their progress in future intercomparison experiments.

6. Acknowledgements

We thank Martin Schmid for the helpful discussions on this project. The Institut Supérieur Pédagogique in Bukavu and

Meteo Rwanda are acknowledged for supplying meteorological observations, and Alberto V. Borges for providing the temperature profiles of the CAKI cruises. We sincerely thank two anonymous Reviewers for their constructive remarks. This work was partially funded by the Research Foundation—Flanders (FWO), the Belgian Science Policy Office (BELSPO) through the research project EAGLES, and the Fund for Scientific Research (FNRS) through the research projects CAKI and MICKI, and used resources of the National Energy Research Scientific Computing Center (NERSC).

References

- Akkermans, T., Thiery, W. and van Lipzig, N. 2014. The regional climate impact of a realistic future deforestation scenario in the Congo Basin. *J. Clim.* DOI: JCLI-D-13-00361.1
- ASTM International. 2012. Standard tables for reference solar spectral irradiances: direct normal and hemispherical on 37° tilted surface. Online at: <http://www.astm.org/Standards/G173.htm>
- Balsamo, G., Salgado, R., Dutra, E., Boussetta, S. and Stockdale, T. 2012. On the contribution of lakes in predicting near-surface temperature in a global weather forecasting model. *Tellus A.* **64**, 15829. DOI: 10.3402/tellusa.v64i0.15829.
- Bonan, G. B. 1995. Sensitivity of a GCM Simulation to inclusion of Inland Water surfaces. *J. Clim.* **8**, 2691–2703.
- Bonan, G. B., Oleson, K. W., Vertenstein, M., Levis, S., Zeng, X. and co-authors. 2002. The land surface climatology of the community land model coupled to the NCAR community climate model. *J. Clim.* **15**, 3123–3149. DOI: 10.1175/1520-0442(2002)015<3123:TLSCOT.2.0.CO;2.
- Borgès, A. V., Abril, G., Delille, B., Descy, J.-P. and Darchambeau, F. 2011. Diffusive methane emissions to the atmosphere from Lake Kivu (Eastern Africa). *J. Geophys. Res.* **116**, G03032. DOI: 10.1029/2011JG001673.
- Davin, E. L., Stoeckli, R., Jaeger, E. B., Levis, S. and Seneviratne, S. I. 2011. COSMO-CLM2: A new version of the COSMO-CLM model coupled to the Community Land Model. *Clim. Dyn.* **37**, 1889–1907. DOI: 10.1007/s00382-011-1019-z.
- De Boor, C. 1978. *A Practical Guide to Splines*. Applied Mathematical Sciences series, 27, Springer-Verlag, New York, 346 pp.
- Dee, D. P., Uppala, S. M., Simmons, A. J., Berrisford, P., Poli P. and co-authors. 2011. The ERA-Interim reanalysis: configuration and performance of the data assimilation system, *Q. J. Roy. Meteorol. Soc.* **137**, 553–597.
- Degens, E. T., von Herzen, R. P., Wong, H.-K., Deuser, W. G. and Jannash, H. W. 1973. Lake Kivu: structure, chemistry and biology of an East African Rift Lake. *Geol. Rundsch.* **62**, 245–277. DOI: 10.1007/BF01826830.
- Descy, J.-P., Darchambeau, F. and Schmid, M. 2012. Lake Kivu: past and Present. In: *Lake Kivu: Limnology and Biogeochemistry of a Tropical Great Lake* (eds. J.-P. Descy, F. Darchambeau, and M. Schmid), Springer, Dordrecht, pp. 1–11.
- Fang, X. and Stefan, H. G. 1996. Long-term lake water temperature and ice cover simulations/measurements. *Cold Reg. Sci. Technol.* **24**, 289–304.
- Goudsmit, G.-H., Burchard, H., Peeters, F. and Wüest, A. 2002. Application of k-ε turbulence models to enclosed basins: the role of internal seiches. *J. Geophys. Res.* **107**, 3230–3243.
- Goyette, S. and Perroud, M. 2012. Interfacing a one-dimensional lake model with a single-column atmospheric model: application to the deep Lake Geneva, Switzerland. *Water Resour. Res.* **48**, W04507. DOI: 10.1029/2011WR011223.
- Hostetler, S. W., Bates, G. T. and Giorgi, F. 1993. Interactive coupling of a lake thermal model with a regional climate model. *J. Geophys. Res.* **98**, 5045–5057.
- Hostetler, S. W., Giogri, F., Bates, G. T. and Bartlein, P. J. 1994. Lake-atmosphere feedbacks associated with paleolakes Bonneville and Lahontan. *Science.* **263**, 665–668.
- Jöhnk, K. D. 2013. *Limnophysics – Turbulenz, Meromixis, Sauerstoff*. Institute of Limnophysics, Cottbus, Germany. ISBN 978-1-4475-3387-0.
- Jöhnk, K. D. and Umlauf, L. 2001. Modelling the metalimnetic oxygen minimum in a medium sized alpine lake. *Ecol. Model.* **136**, 67–80.
- Kirillin, G. 2010. Modelling the impact of global warming on water temperature and seasonal mixing regimes in small temperature lakes. *Boreal Environ. Res.* **15**, 279–293.
- Kirillin, G., Hochschild, J., Mironov, D., Terzhevik, A., Golosov, S. and co-authors. 2011. FLake-Global: online lake model with worldwide coverage. *Environ. Model. Software.* **26**, 683–684. DOI: 10.1016/j.envsoft.2010.12.004.
- Kourzeneva, E. V., Samuelsson, P., Ganbat, G. and Mironov, D. 2008. Implementation of Lake Model FLake in HIRLAM. *HIRLAM Newsletter.* **54**, 54–61.
- Lahmeyer and Osaé 1998. Bathymetric survey of Lake Kivu – Final report. Republic of Rwanda, Ministry of Public Work, Directory of Energy and Hydrocarbons, Kigali, 18 pp.
- Lauwaet, D., van Lipzig, N. P. M., Van Weverberg, K., De Ridder, K. and Goyens, C. 2011. The precipitation response to the desiccation of Lake Chad. *Q. J. Roy. Meteorol. Soc.* **138**, 707–719. DOI: 10.1002/qj.942.
- Lekvam, K. and Bishnoi, P. R. 1997. Dissolution of methane in water at low temperatures and intermediate pressures. *Fluid Phase Equil.* **131**, 297–309.
- Lorke, A., Tietze, K., Halbwachs, M. and Wüest, A. 2004. Response of Lake Kivu to lava inflow and climate warming. *Limnol. Oceanogr.* **49**, 778–783.
- Martynov, A., Sushama, L. and Laprise, R. 2010. Simulation of temperate freezing lakes by one-dimensional lake models: performance assessment for interactive coupling with regional climate models. *Boreal Environ. Res.* **15**, 143–164.
- Martynov, A., Sushama, L., Laprise, R., Winger, K. and Dugas, B. 2012. Interactive Lakes in the Canadian Regional Climate Model, version 5: the role of lakes in the regional climate of North America. *Tellus A.* **64**, 16226. DOI: 10.3402/tellusa.v64i0.16226.
- Mironov, D. 2008. Parameterization of Lakes in Numerical Weather Prediction: Description of a Lake Model. COSMO Technical Report No. 11, 47 pp.

- Mironov, D., Heise, E., Kourzeneva, E., Ritter, B., Schneider, N. and co-authors. 2010. Implementation of the lake parameterisation scheme FLake into the numerical weather prediction model COSMO. *Boreal Environ. Res.* **15**, 218–230.
- Nash, J. E. and Sutcliffe, J. V. 1970. River flow forecasting through conceptual models part I – a discussion of principles. *J. Hydrol.* **10**, 282–290.
- Ohsumi, T., Nakashiki, N., Shitashima, K. and Hiram, K. 1992. Density change of water due to dissolution of carbon dioxide and near-field behaviour of CO₂ from a source on deep-sea floor. *Energ. Convers. Manag.* **33**, 685–690.
- Pasche, N., Dinkel, C., Müller, B., Schmid, M., Wüest, A. and co-authors. 2009. Physical and biogeochemical limits to internal nutrient loading of meromictic Lake Kivu. *Limnol. Oceanogr.* **54**, 1863–1873.
- Pasche, N., Schmid, M., Vazquez, F., Schubert, C. J., Wüest, A. and co-authors. 2011. Methane sources and sinks in Lake Kivu. *J. Geophys. Res.* **116**, G03006. DOI: 10.1029/2011JG001690.
- Perroud, M., Goyette, S., Martynov, A., Beniston, M. and Anneville, O. 2009. Simulation of multiannual thermal profiles in deep Lake Geneva: a comparison of one-dimensional lake models. *Limnol. Oceanogr.* **54**, 1574–1594.
- Poole, H. H. and Atkins, W. R. G. 1929. Photo-electric Measurements of Submarine Illumination throughout the Year. *J. Mar. Biol. Assoc. UK.* **16**, 297–324.
- Sarmiento, H., Isumbishu, M. and Descy, J.-P. 2006. Phytoplankton ecology of Lake Kivu (eastern Africa). *J. Plankton Res.* **28**, 815–829. DOI: 10.1029/2004GC000892.
- Savijärvi, H. 1997. Diurnal winds around Lake Tanganyika. *Q. J. Roy. Meteorol. Soc.* **123**, 901–918.
- Schmid, A. and Wüest, A. 2012. Stratification, mixing and transport processes in Lake Kivu. In: *Lake Kivu: Limnology and Biogeochemistry of a Tropical Great Lake* Descy (eds. J.-P. Descy, F. Darchambeau, and M. Schmid). Springer, Dordrecht, pp. 13–29.
- Schmid, M., Busbridge, M. and Wüest, A. 2010. Double-diffusive convection in Lake Kivu. *Limnol. Oceanogr.* **55**, 225–238.
- Schmid, M., Halbwachs, M., Wehrli, B. and Wüest, A. 2005. Weak mixing in Lake Kivu: new insights indicate increasing risk of uncontrolled gas eruption. *Geochem. Geophys. Geosy.* **6**, 1–11. DOI: 10.1029/2004GC000892.
- Schmid, M., Tietze, K., Halbwachs, M., Lorke, A., McGinnis, D. and co-authors. 2004. How hazardous is the gas accumulation in Lake Kivu? Arguments for a risk assessment in light of the Nyiragongo Volcano eruption of 2002. *Acta Vulcanol.* **14/15**, 115–121.
- Song, Y., Semazzi, F. H. M., Xie, L. and Ogallo, L. J. 2004. A coupled regional climate model for the Lake Victoria Basin of East Africa. *Int. J. Climatol.* **24**, 57–75.
- Spigel, R. H. and Coulter, G. W. 1996. Comparison of hydrology and physical limnology of the East African Great Lakes: Tanganyika, Malawi, Victoria, Kivu and Turkana (with references to some North American Great Lakes). In: *The Limnology, Climatology and Paleoclimatology of the East African Lakes* (eds. T. C. Johnson and E. Odada). Gordon and Breach Publishers, Amsterdam, pp. 103–140.
- Stepanenko, V. M., Goyette, S., Martynov, A., Perroud, M., Fang, X. and co-authors. 2010. First steps of a Lake Model Intercomparison Project: LakeMIP. *Boreal Environ. Res.* **15**, 191–202.
- Stepanenko, V. M., Jöhnk, K., Machulskaya, E., Mironov, D., Perroud, D. and co-authors. 2013. Simulation of surface energy fluxes and stratification of a small boreal lake by a set of one-dimensional models. *Tellus A.* (in review). **66**, 1–18.
- Stepanenko, V. M. and Lykosov, V. N. 2005. Numerical simulation of heat and moisture transport in the “lake–soil” system. *Russ. Meteorol. Hydrol.* **3**, 95–104.
- Stepanenko, V. M., Martynov, A., Jöhnk, K. D., Subin, Z. M., Perroud, M. and co-authors. 2012. A one-dimensional model intercomparison study of thermal regime of a shallow turbid midlatitude lake. *Geosci. Model Dev.* **6**, 1337–1352.
- Subin, Z. M., Murphy, L. N., Li, F., Bonfils, C. and Riley, W. J. 2012a. Boreal lakes moderate seasonal and diurnal temperature variation and perturb atmospheric circulation: analyses in the Community Earth System Model 1 (CESM1). *Tellus A.* **64**, 15639. DOI: 10.3402/tellusa.v64i0.15639.
- Subin, Z. M., Riley, W. J. and Mironov, D. 2012b. An improved lake model for climate simulations: model structure, evaluation and sensitivity analyses in CESM1. *J. Adv. Mod. Earth Sys.* **4**, M02001. DOI: 10.1029/2011MS000072.
- Tassi, F., Vaselli, O., Tedesco, D., Montegrossi, G., Darrah, T. and co-authors. 2009. Water and gas chemistry at Lake Kivu (DRC): geochemical evidence of vertical and horizontal heterogeneities in a multibasin structure. *Geochem. Geophys. Geosy.* **10**. DOI: 10.1029/2008GC002191.
- Taylor, K. E. 2001. Summarizing multiple aspects of model performance in a single diagram. *J. Geophys. Res.* **106**, 7183–7192.
- Thiery, W., Martynov, A., Darchambeau, F., Descy, J.-P., Plisnier, P.-D. and co-authors. 2014. Understanding the performance of the FLake model over two African Great Lakes. *Geosci. Model Dev.* in press.
- Verburg, P. and Antenucci, J. P. 2010. Persistent unstable atmospheric boundary layer enhances sensible and latent heat loss in a tropical great lake: lake Tanganyika. *J. Geophys. Res.* **115**, D11109, DOI: 10.1029/2009JD012839.
- Verburg, P. and Hecky, R. E. 2003. Wind patterns, evaporation and related physical variables in lake Tanganyika, East-Africa. *J. Great Lakes Res.* **29**, 48–61.
- Wilks, D. S. 2005. *Statistical Methods in Atmospheric Sciences*. International Geophysics Series, 100, Academic Press, Oxford, 676 pp.
- Williams, W. D. 1986. Conductivity and salinity of Australian salt lakes. *Aust. J. Mar. Fresh. Res.* **37**, 177–182.
- Wüest, A., Jare, L., Bürgmann, H., Pasche, N. and Schmid, M. 2012. Methane formation and Future Extraction in Lake Kivu. In: *Lake Kivu: Limnology and Biogeochemistry of a Tropical Great Lake* (eds. J.-P. Descy, F. Darchambeau, and M. Schmid). Springer, Dordrecht, pp. 165–180.
- Wüest, A., Piepke, G. and Halfman, J. D. 1996. Combined effects of dissolved solids and temperature on the density stratification of lake Malawi. In: *The Limnology, Climatology and Paleoclimatology of the East-African Lakes* (eds. T. C. Johnson and E. O. Odada). Gordon and Breach, Toronto, pp. 183–202.